frontiers | Research Topics

Formation of immunological niches in tumor microenvironments: mechanisms and therapeutic potential

Edited by
Ying Luo, Weiling Li, Qingyu Luo and Xiaosheng Tan

Coordinated by
Yabing Nan

Published in
Frontiers in Immunology
Frontiers in Oncology

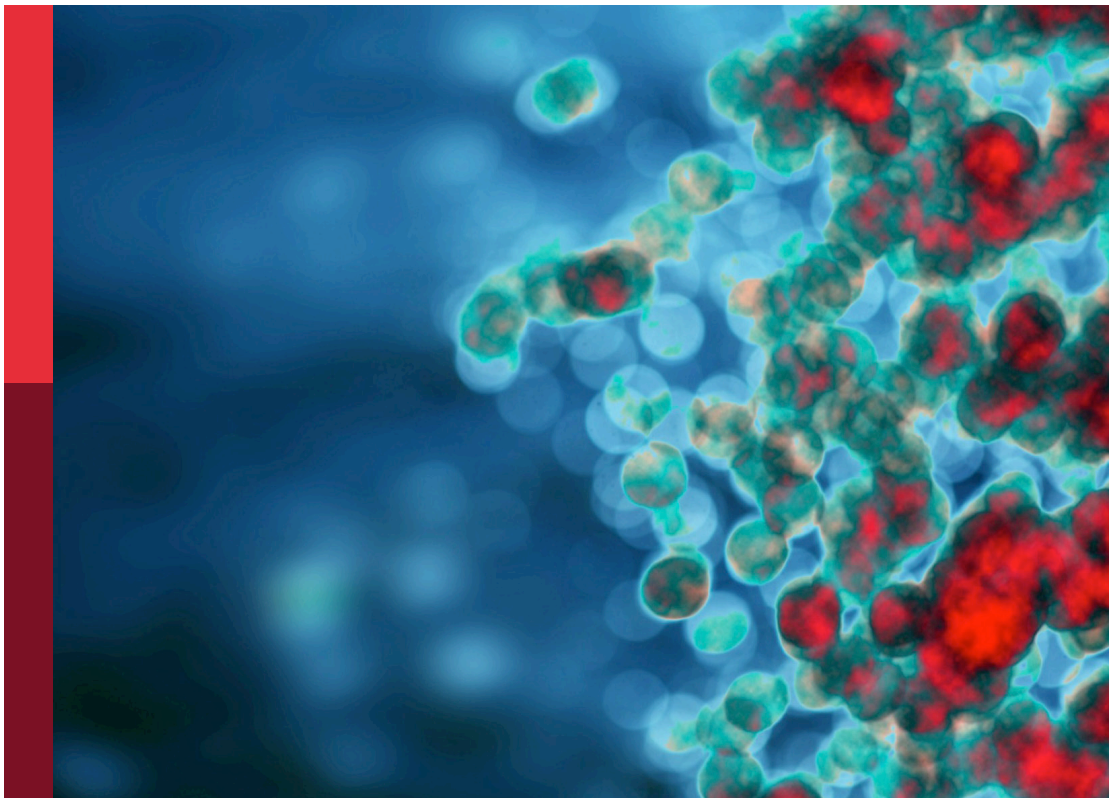

FRONTIERS EBOOK COPYRIGHT STATEMENT

The copyright in the text of individual articles in this ebook is the property of their respective authors or their respective institutions or funders. The copyright in graphics and images within each article may be subject to copyright of other parties. In both cases this is subject to a license granted to Frontiers.

The compilation of articles constituting this ebook is the property of Frontiers.

Each article within this ebook, and the ebook itself, are published under the most recent version of the Creative Commons CC-BY licence. The version current at the date of publication of this ebook is CC-BY 4.0. If the CC-BY licence is updated, the licence granted by Frontiers is automatically updated to the new version.

When exercising any right under the CC-BY licence, Frontiers must be attributed as the original publisher of the article or ebook, as applicable.

Authors have the responsibility of ensuring that any graphics or other materials which are the property of others may be included in the CC-BY licence, but this should be checked before relying on the CC-BY licence to reproduce those materials. Any copyright notices relating to those materials must be complied with.

Copyright and source acknowledgement notices may not be removed and must be displayed in any copy, derivative work or partial copy which includes the elements in question.

All copyright, and all rights therein, are protected by national and international copyright laws. The above represents a summary only. For further information please read Frontiers' Conditions for Website Use and Copyright Statement, and the applicable CC-BY licence.

ISSN 1664-8714
ISBN 978-2-8325-6885-9
DOI 10.3389/978-2-8325-6885-9

Generative AI statement
Any alternative text (Alt text) provided alongside figures in the articles in this ebook has been generated by Frontiers with the support of artificial intelligence and reasonable efforts have been made to ensure accuracy, including review by the authors wherever possible. If you identify any issues, please contact us.

About Frontiers

Frontiers is more than just an open access publisher of scholarly articles: it is a pioneering approach to the world of academia, radically improving the way scholarly research is managed. The grand vision of Frontiers is a world where all people have an equal opportunity to seek, share and generate knowledge. Frontiers provides immediate and permanent online open access to all its publications, but this alone is not enough to realize our grand goals.

Frontiers journal series

The Frontiers journal series is a multi-tier and interdisciplinary set of open-access, online journals, promising a paradigm shift from the current review, selection and dissemination processes in academic publishing. All Frontiers journals are driven by researchers for researchers; therefore, they constitute a service to the scholarly community. At the same time, the *Frontiers journal series* operates on a revolutionary invention, the tiered publishing system, initially addressing specific communities of scholars, and gradually climbing up to broader public understanding, thus serving the interests of the lay society, too.

Dedication to quality

Each Frontiers article is a landmark of the highest quality, thanks to genuinely collaborative interactions between authors and review editors, who include some of the world's best academicians. Research must be certified by peers before entering a stream of knowledge that may eventually reach the public - and shape society; therefore, Frontiers only applies the most rigorous and unbiased reviews. Frontiers revolutionizes research publishing by freely delivering the most outstanding research, evaluated with no bias from both the academic and social point of view. By applying the most advanced information technologies, Frontiers is catapulting scholarly publishing into a new generation.

What are Frontiers Research Topics?

Frontiers Research Topics are very popular trademarks of the *Frontiers journals series*: they are collections of at least ten articles, all centered on a particular subject. With their unique mix of varied contributions from Original Research to Review Articles, Frontiers Research Topics unify the most influential researchers, the latest key findings and historical advances in a hot research area.

Find out more on how to host your own Frontiers Research Topic or contribute to one as an author by contacting the Frontiers editorial office: frontiersin.org/about/contact

Formation of immunological niches in tumor microenvironments: mechanisms and therapeutic potential

Topic editors

Ying Luo — University of Texas Southwestern Medical Center, United States
Weiling Li — Dalian Medical University, China
Qingyu Luo — One Patient One Cure, United States
Xiaosheng Tan — Rutgers, The State University of New Jersey, United States

Topic coordinator

Yabing Nan — Department of Cancer Biology, Dana–Farber Cancer Institute, United States

Citation

Luo, Y., Li, W., Luo, Q., Tan, X., Nan, Y., eds. (2025). *Formation of immunological niches in tumor microenvironments: mechanisms and therapeutic potential*. Lausanne: Frontiers Media SA. doi: 10.3389/978-2-8325-6885-9

Table of contents

07 Editorial: Formation of immunological niches in tumor microenvironments: mechanisms and therapeutic potential
Zilu Chen, Qingyu Luo, Weiling Li, Ying Luo and Xiaosheng Tan

10 Revealing the mechanisms of RAC3 in tumor aggressiveness, the immunotherapy response, and drug resistance in bladder cancer
Hanyuan Gao, Yanru Qiu, Xueqin Zheng, Tianwen Xu and Guangjian Liu

26 Real-world study and prognostic analysis of angioimmunoblastic T-cell lymphoma
Suxiao Li, Xiaoyan Feng, Yunfei Song, Mengke Fan, Qingjiang Chen, Mingzhi Zhang, Xiaolong Wu, Meng Dong, Jieming Zhang, Lijuan Han and Xudong Zhang

36 Characterization of ligand-receptor pair in acute myeloid leukemia: a scoring model for prognosis, therapeutic response, and T cell dysfunction
Chunlan Fu, Di Qiu, Mei Zhou, Shaobo Ni and Xin Jin

55 Comprehensive evaluation of clinical outcomes in hepatic epithelioid hemangioendothelioma subsets: insights from SEER Database and departmental cohort analysis
Bingchen Wang, Xiao Chen, Rongxuan Li, Bolun Ai, Feng Ye, Jianjun Zhao, Yefan Zhang, Zhen Huang, Zhiyu Li, Xinyu Bi, Hong Zhao, Dayong Cao, Jianqiang Cai, Jianguo Zhou and Tao Yan

68 Prognostic significance of systemic pan-immune-inflammation value in locally advanced cervical cancer
Shu Yan, Xin Gong, Rui Liu and Xiaojing Jia

78 Single-cell sequencing unveils mitophagy-related prognostic model for triple-negative breast cancer
Peikai Ding, Shengbin Pei, Zheng Qu, Yazhe Yang, Qiang Liu, Xiangyi Kong, Zhongzhao Wang, Jing Wang and Yi Fang

92 Comparison of treatment models for single primary advanced gallbladder cancer
Rongxuan Li, Xiao Chen, Bingchen Wang, Bolun Ai, Fangdi Min, Dayong Cao, Jianguo Zhou and Tao Yan

109 Expression and clinical significance of Numb and Notch-1 proteins between tissue of colon cancer and regional lymph node metastases
Jingyou Ma, Jinpeng Zhen, Ningbao Yang, Changjuan Meng and Yanjun Lian

116 Gut virome dysbiosis impairs antitumor immunity and reduces 5-fluorouracil treatment efficacy for colorectal cancer
Hui Huang, Ying Yang, Xiaojiao Wang, Biao Wen, Xianglan Yang, Wei Zhong, Qiurong Wang, Feng He and Jun Li

133 Integrating bioinformatics and machine learning to identify AhR-related gene signatures for prognosis and tumor microenvironment modulation in melanoma
Qianru Li and Heli Li

146 Bibliometric analysis of metformin as an immunomodulator (2013–2024)
Tongyi Zhou, Yunfeng Yu, Liu Li, Xiu Liu, Qin Xiang and Rong Yu

164 Combining single-cell analysis and molecular docking techniques to construct a prognostic model for colon adenocarcinoma and uncovering inhibin subunit βb as a novel therapeutic target
Qinqing Wu, Lu Ye, Yuwei Wu, Mengyu Zhao, Jiaxin Lu, Yanping Yu, Yixiao Niu, Luxiao Zhang and Peijun Zuo

181 Targeting NANOS1 in triple-negative breast cancer: synergistic effects of digoxin and PD-1 inhibitors in modulating the tumor immune microenvironment
Tangyi Wang, Yadian Lei, Jingwei Sun, Li Wang, Yuxin Lin, Zhijing Wu, Shoude Zhang, Chengzhu Cao and Haiyan Wang

197 Correction: Targeting NANOS1 in triple-negative breast cancer: synergistic effects of digoxin and PD-1 inhibitors in modulating the tumor immune microenvironment
Tangyi Wang, Yadian Lei, Jingwei Sun, Li Wang, Yuxin Lin, Zhijing Wu, Shoude Zhang, Chengzhu Cao and Haiyan Wang

200 Peripheral blood immunoinflammatory biomarkers: prospective predictors of postoperative long-term survival and chronic postsurgical pain in breast cancer
Baoli Li, Li Che, Huixian Li, Fangdi Min, Bolun Ai, Linxin Wu, Taihang Wang, Peixin Tan, Bingbing Fu, Jiashuo Yang, Yi Fang, Hui Zheng and Tao Yan

216 Correlations between primary tumour location, biomarkers of inflammation and lung injury, and postoperative pulmonary complications in patients underwent laparoscopic colorectomy: a propensity score matched analysis of 300 patients
Hui-xian Li, Li Che, Yuan Li, Tai-hang Wang, Fang-di Min, Lei Xu, Meng Wang, Zhao-xu Zheng, Shi-ning Qu, Fei Wang, Wei Tang, Shi-jing Wei, Yu-lin Sun, Hui Zheng and Tao Yan

231 The clinical significance of T-cell regulation in hypertension treatment
Miaoxin Fu, Mingzhu Lv, Jinyue Guo, Aihua Mei, Hang Qian, Handong Yang, Wenwen Wu, Zhixin Liu, Jixin Zhong, Ying Wei, Xinwen Min, Haiyan Wu and Jun Chen

242 The aggrephagy-related gene TUBA1B influences clinical outcomes in glioma patients by regulating the cell cycle
Zesheng Sun, Pengcheng Huang, Jialiang Lin, Guiping Jiang, Jian Chen and Qianqian Liu

258 Inflammation and cancer: molecular mechanisms and clinical consequences
Hikmet Akkız, Halis Şimşek, Deniz Balcı, Yakup Ülger, Engin Onan, Nevin Akçaer and Anıl Delik

277 Melanocortin-1 receptor expression as a predictive factor for postoperative outcomes in melanoma patients: a retrospective study
Tian Xiang, Haiying Li, Xiaowei Wang and Danke Su

293 Unraveling the triad of immunotherapy, tumor microenvironment, and skeletal muscle biomechanics in oncology
Shuang Ma, Ying Lu, Shang Sui, Jia-shuo Yang, Bing-bing Fu, Pei-xin Tan, Yicheng Chai, Jiaqi Lv, Lingyu Kong, Xiaolin Wu, Yi-bo Gao and Tao Yan

315 Combination of anlotinib with immunotherapy enhanced both anti-angiogenesis and immune response in high-grade serous ovarian cancer
Hongwei Lan, Hui Liu, Helei Hou, Chuantao Zhang, Jingjuan Zhu, Na Zhou and Xiaochun Zhang

336 Cancer-associated fibroblasts gene signature: a novel approach to survival prediction and immunotherapy guidance in colon cancer
Wenbing Zhang, Chi Yang, Ye Lu, Chenling Tang, Mengyu Zhao, Zhaohui Wang, Jidong Gao, Shuangjiu Hu and Zhihua Chen

349 Tumor microenvironment and immune-related myositis: addressing muscle wasting in cancer immunotherapy
Shuang Ma, Guangyu Zhao, Shang Sui, Xiankai Chen, Linxin Wu, Taihang Wang, Wanying Xu, Zhijiao Lu, Andong Wang, Xiaolin Wu, Jiaxuan Wu, Yi Liu and Tao Yan

370 Application and recent advances in conventional biomarkers for the prognosis of papillary thyroid carcinoma
Muzi Li, Qiong Li, Cancan Zou, Qin Huang and Yanlin Chen

384 Multifactorial risk stratification for central lymph node metastasis in papillary thyroid carcinoma: a predictive model integrating clinical and tumor characteristics
Huaiyu Yang, Liyuan Wei, Jiaxin Qian and Wensheng Liu

399 Senescence-associated secretory phenotype in lung cancer: remodeling the tumor microenvironment for metastasis and immune suppression
Chen Chen, Ji Chen, Yanling Zhang, Qijun Zhang and Haixia Shi

412 Research progress on the cross-regulation between ferroptosis and immunogenic cell death in tumor micro-environment
Weitao Liu, Yichen Jing, Yang Chen, Han Sun, Wenbo Xu, Ruihan Liang, Wanglin Liu, Zengyu Zhang and Huiping Liu

439 Impact of postoperative depression and immune-inflammatory biomarkers on the prognosis of patients with esophageal cancer receiving minimally invasive esophagectomy: a retrospective cohort study based on a Chinese population
Pei-xin Tan, Lin-xin Wu, Shuang Ma, Shi-jing Wei, Tai-hang Wang, Bing-chen Wang, Bing-bing Fu, Jia-shuo Yang, Qing Zhao, Li Sun, Yi Liu and Tao Yan

453 Comprehensive analysis of single-cell and bulk RNA sequencing data reveals an EGFR signature for predicting immunotherapy response and prognosis in pan-cancer
Changchun Ye, Xiaoya Chen, Zilu Chen, Shiyuan Liu, Ranran Kong, Wenhao Lin, Minxia Zhu, Xuejun Sun and Zhengshui Xu

473 CHMP6 as a novel prognostic biomarker in bladder cancer: insights from a comprehensive cell death-related gene risk model
Wei Ning, Yan-Ru Yang, Chen-Xu Wu, Yue Hou, Zhi-Wei Liu and Chang-Bin Yang

frontiers | Frontiers in Oncology

TYPE Editorial
PUBLISHED 09 September 2025
DOI 10.3389/fonc.2025.1675697

Check for updates

OPEN ACCESS

EDITED AND REVIEWED BY
Luisa Lanfrancone,
European Institute of Oncology (IEO), Italy

*CORRESPONDENCE
Xiaosheng Tan
txs900416@163.com
Ying Luo
13349917272@163.com
Weiling Li
liweiling2004@163.com
Qingyu Luo
qingyu.luo@onepatientonecure.org

RECEIVED 29 July 2025
ACCEPTED 26 August 2025
PUBLISHED 09 September 2025

CITATION
Chen Z, Luo Q, Li W, Luo Y and Tan X (2025) Editorial: Formation of immunological niches in tumor microenvironments: mechanisms and therapeutic potential. *Front. Oncol.* 15:1675697. doi: 10.3389/fonc.2025.1675697

COPYRIGHT
© 2025 Chen, Luo, Li, Luo and Tan. This is an open-access article distributed under the terms of the Creative Commons Attribution License (CC BY). The use, distribution or reproduction in other forums is permitted, provided the original author(s) and the copyright owner(s) are credited and that the original publication in this journal is cited, in accordance with accepted academic practice. No use, distribution or reproduction is permitted which does not comply with these terms.

Editorial: Formation of immunological niches in tumor microenvironments: mechanisms and therapeutic potential

Zilu Chen[1], Qingyu Luo[2]*, Weiling Li[3]*, Ying Luo[4]* and Xiaosheng Tan[5]*

[1]Department of Medicine, Rutgers Cancer Institute of New Jersey, New Brunswick, NJ, United States, [2]One Patient One Cure, Boston, MA, United States, [3]Department of Biotechnology, College of Basic Medical Sciences, Dalian Medical University, Dalian, Liaoning, China, [4]Department of Immunology, University of Texas (UT) Southwestern Medical Center, Dallas, TX, United States, [5]Child Health Institute of New Jersey, Rutgers Robert Wood Johnson Medical School, New Brunswick, NJ, United States

KEYWORDS

tumor microenvironment, immunological niches, immune evasion, biomarkers, immunotherapy resistance

Editorial on the Research Topic
Formation of immunological niches in tumor microenvironments: mechanisms and therapeutic potential

Introduction

Immunological niches in tumor microenvironments (TMEs) are spatially organized functional units in which tumor cells interact with immune and stromal components via dynamic molecular networks (1). These specialized microdomains exhibit dual functionality: while they are capable of supporting anti-tumor immunity through immune cell activation, they frequently evolve immunosuppressive properties that enable immune evasion and therapy resistance (2). Emerging evidence reveals that niche characteristics significantly influence immunotherapy responses, with distinct spatial architectures associated with treatment sensitivity or resistance across cancer types (3). Understanding these regulatory mechanisms provides critical insights for developing strategies to therapeutically reprogram immunosuppressive niches.

Decoding niche formation: cellular and molecular architects

Immunological niches within tumors emerge through coordinated interactions between three fundamental components: (1) tumor cells displaying antigenic and metabolic heterogeneity, (2) immune populations (CD8+ T cells, tumor-associated macrophages [TAMs], and dendritic cells [DCs]), and (3) stromal elements (cancer-associated fibroblasts [CAFs], the extracellular matrix [ECM], and the vasculature). These components communicate through cytokine-chemokine networks (e.g., IFN-γ-mediated

immune activation versus TGF-β-driven suppression) and direct cell-contact signals (e.g., PD-1/PD-L1 checkpoint interactions) to collectively regulate anti-tumor immunity (2, 4).

At the cellular level, stromal components - particularly CAFs - have been identified as key architectural regulators (5). Single-cell multi-omics approaches have enabled the precise characterization of CAF heterogeneity. For instance, in colon adenocarcinoma, an 11-gene CAF signature effectively stratified patients into high- and low-risk groups, with the high-risk group exhibiting greater immune infiltration yet paradoxically lower drug sensitivity (Zhang et al.). Similarly, in triple-negative breast cancer (TNBC), Ding et al. established a prognostic model in which high-risk patients showed increased stromal CAF and endothelial cell infiltration and poorer clinical outcomes.

At the molecular level, pathway activation analyses reveal critical mediators of niche functionality (6). A pan-cancer study demonstrated that EGFR pathway activation drives immunotherapy resistance through an EGFR-related gene signature (EGFR.Sig), which correlates with elevated exhaustion markers (TIM-3 and LAG-3) and immunosuppressive ligands (PD-L1 and CD47) (Ye et al.). The convergence of these molecular and cellular pathways underscores the need for multidimensional therapeutic approaches targeting niche formation at multiple levels, a strategy that may help overcome therapeutic resistance and improve clinical outcomes.

Biomarkers: from niches to clinical tools

Beyond mechanistic insights, translating immunological niches into clinically actionable biomarkers has become a critical frontier in precision oncology (7). Systemic inflammation indices derived from peripheral blood have demonstrated clinical utility as non-invasive niche proxies. As demonstrated in our Research Topic, these indices provide valuable insights for clinical prognosis and treatment strategies. For example, in esophageal cancer, the systemic immune-inflammation index (SII) was identified as an independent prognostic factor for recurrence-free survival after esophagectomy (Tan et al.). In breast cancer, an elevated preoperative systemic inflammation response index (SIRI) was found to serve as an independent risk factor for disease-free survival (Li et al.). Similarly, in locally advanced cervical cancer, the pan-immune-inflammation value (PIV) was identified as a robust and independent prognostic factor significantly correlated with both overall survival and disease-free survival (Yan et al.).

Niche-informed molecular subtyping is transforming patient stratification. In acute myeloid leukemia, molecular subtyping based on ligand-receptor (LR) pairs has unveiled distinct immune landscapes and prognostic differences. A scoring model termed LR.score was established to stratify patients by survival risk and reflect the degree of T-cell dysfunction, offering insights into niche-driven immune dysregulation and therapy resistance (Fu et al.). In melanoma, aryl hydrocarbon receptor (AhR)-related gene signatures (MAP2K1, PRKACB, KLF5, and PIK3R2) have been identified as potential prognostic tools strongly associated with immune infiltration and tumor progression, providing a robust prognostic framework and potential therapeutic targets (Li et al.).

These advances collectively represent a paradigm shift in cancer management, where niche-derived biomarkers are moving from research tools to clinical implementation. By capturing the complex interplay between tumor cells and their microenvironment, these biomarkers enable more precise patient stratification and treatment selection (8).

Therapeutic strategies: rewriting niche rules

Although biomarkers yield valuable insights into niche dynamics, converting these findings into effective treatments remains a major challenge. To bridge this gap, therapeutic development is increasingly directed at reprogramming the tumor–immune interface by modulating niche biology through diverse approaches (9).

Targeting immune-related molecules remains a well-established and effective therapeutic approach. For example, RAC3 has been shown to drive tumor aggressiveness and immune evasion in bladder cancer, positioning it as a potential dual biomarker and therapeutic target (Gao et al.).

Stromal remodeling strategies are also gaining prominence. Evidence of clinical translation is already seen in the success of anlotinib (an anti-angiogenic agent) combined with anti-PD-L1 therapy in treating high-grade serous ovarian cancer. This combination therapy inhibits angiogenesis and enhances immune infiltration, while simultaneously reinvigorating exhausted T cells (Lan et al.), demonstrating the therapeutic potential of coordinated niche modulation.

Tumor metabolic regulators coordinate immune–tumor cell networks within the TME, and targeting these metabolic vulnerabilities is a promising yet clinically challenging therapeutic avenue (10). Ferroptosis inducers such as erastin enhance immunogenic cell death by releasing damage-associated molecular patterns (DAMPs) which recruit and activate immune cells, while lipid peroxides generated during ferroptosis may potentiate immune cell–mediated tumor killing (Liu et al.). In parallel, repurposing existing drugs such as metformin modulates the immune microenvironment, enhances the efficacy of immunotherapy and radiotherapy, and overcomes resistance in “cold” or refractory tumors, all while maintaining a favorable safety profile (Zhou et al.).

Notably, microbiome-targeted strategies are opening new therapeutic dimensions (11). TLR3 agonists, including Poly(I: C), have been shown to restore immune competence in colorectal cancer models with viral dysbiosis (Huang et al.), offering novel combination approaches.

Together, these diverse strategies demonstrate how targeting niche biology across stromal, metabolic, epigenetic, and microbial axes can help dismantle long-standing therapeutic barriers and expand the efficacy of cancer immunotherapy.

Clinical challenges and future directions

Despite remarkable progress, significant challenges remain in translating niche biology into clinical practice (3). The dynamic nature of immunological niches complicates therapeutic targeting, as exemplified by cellular senescence transitioning from tumor-suppressive (p53/p21/p16-mediated) to pro-tumorigenic SASP states during cancer progression (Chen et al.). This plasticity necessitates precisely timed interventions and robust biomarkers to identify optimal treatment windows.

Unexpected systemic effects further complicate therapeutic development, with immune checkpoint inhibitors causing immune-related adverse events such as myositis in up to 30% of patients (Ma et al.). Emerging monitoring tools, including impedance myography and advanced serum biomarkers (Ma et al.), offer potential mitigation through early detection.

Technological innovations will be crucial for addressing niche complexity. Multiplex immunohistochemistry, spatial transcriptomics, and AI-enhanced image analysis are enabling high-resolution mapping of niche organization and evolution. These tools are particularly valuable in elucidating resistance mechanisms and tailoring personalized therapeutic strategies (12, 13). Integrating these technologies into clinical trials will be vital for translating niche biology into individualized cancer care.

Conclusion

The formation and regulation of immunological niches within the TME represent both challenges and opportunities in cancer therapy. As evidenced throughout this Research Topic, targeting niche components—including immune, stromal, metabolic, and microbial elements—can enhance therapeutic precision and improve patient outcomes. Looking forward, a deeper mechanistic understanding and integrative translational efforts are indispensable to transforming niche biology from conceptual frameworks into clinically actionable strategies for precision oncology.

Author contributions

XT: Writing – review & editing. ZC: Writing – original draft. QL: Writing – review & editing. WL: Writing – review & editing. YL: Writing – review & editing.

Conflict of interest

The authors declare that the research was conducted in the absence of any commercial or financial relationships that could be construed as a potential conflict of interest.

Generative AI statement

The author(s) declare that no Generative AI was used in the creation of this manuscript.

Any alternative text (alt text) provided alongside figures in this article has been generated by Frontiers with the support of artificial intelligence and reasonable efforts have been made to ensure accuracy, including review by the authors wherever possible. If you identify any issues, please contact us.

Publisher's note

All claims expressed in this article are solely those of the authors and do not necessarily represent those of their affiliated organizations, or those of the publisher, the editors and the reviewers. Any product that may be evaluated in this article, or claim that may be made by its manufacturer, is not guaranteed or endorsed by the publisher.

References

1. Binnewies M, Roberts EW, Kersten K, Chan V, Fearon DF, Merad M, et al. Understanding the tumor immune microenvironment (TIME) for effective therapy. *Nat Med*. (2018) 24:541–50. doi: 10.1038/s41591-018-0014-x

2. Chen DS, Mellman I. Elements of cancer immunity and the cancer-immune set point. *Nature*. (2017) 541:321–30. doi: 10.1038/nature21349

3. Hegde PS, Chen DS. Top 10 challenges in cancer immunotherapy. *Immunity*. (2020) 52:17–35. doi: 10.1016/j.immuni.2019.12.011

4. Joyce JA, Fearon DT. T cell exclusion, immune privilege, and the tumor microenvironment. *Science*. (2015) 348:74–80. doi: 10.1126/science.aaa6204

5. Kieffer Y, Hocine HR, Gentric G, Pelon F, Bernard C, Bourachot B, et al. Single-cell analysis reveals fibroblast clusters linked to immunotherapy resistance in cancer. *Cancer Discov*. (2020) 10:1330–51. doi: 10.1158/2159-8290.CD-19-1384

6. de Visser KE, Joyce JA. The evolving tumor microenvironment: From cancer initiation to metastatic outgrowth. *Cancer Cell*. (2023) 41:374–403. doi: 10.1016/j.ccell.2023.02.016

7. Butterfield LH, Najjar YG. Immunotherapy combination approaches: mechanisms, biomarkers and clinical observations. *Nat Rev Immunol*. (2024) 24:399–416. doi: 10.1038/s41577-023-00973-8

8. Fridman WH, Zitvogel L, Sautès-Fridman C, Kroemer G. The immune contexture in cancer prognosis and treatment. *Nat Rev Clin Oncol*. (2017) 14:717–34. doi: 10.1038/nrclinonc.2017.101

9. Galon J, Bruni D. Approaches to treat immune hot, altered and cold tumours with combination immunotherapies. *Nat Rev Drug Discov*. (2019) 18:197–218. doi: 10.1038/s41573-018-0007-y

10. Huang K, Han Y, Chen Y, Shen H, Zeng S, Cai C. Tumor metabolic regulators: key drivers of metabolic reprogramming and the promising targets in cancer therapy. *Mol Cancer*. (2025) 24:7. doi: 10.1186/s12943-024-02205-6

11. Neagu AI, Bostan M, Ionescu VA, Gheorghe G, Hotnog CM, Roman V, et al. The impact of the microbiota on the immune response modulation in colorectal cancer. *Biomolecules*. (2025) 15. doi: 10.3390/biom15071005

12. Pich O, Bailey C, Watkins TBK, Zaccaria S, Jamal-Hanjani M, Swanton C. The translational challenges of precision oncology. *Cancer Cell*. (2022) 40:458–78. doi: 10.1016/j.ccell.2022.04.002

13. Marx V. Method of the Year: spatially resolved transcriptomics. *Nat Methods*. (2021) 18:9–14. doi: 10.1038/s41592-020-01033-y

frontiers | Frontiers in Oncology

TYPE Original Research
PUBLISHED 16 September 2024
DOI 10.3389/fonc.2024.1466319

Check for updates

OPEN ACCESS

EDITED BY
Xiaosheng Tan,
Rutgers, United States

REVIEWED BY
Xin Yu,
Baylor College of Medicine, United States
Yu Yan,
University of North Carolina at Chapel Hill, United States
Jinkai Wan,
Harvard Medical School, United States

*CORRESPONDENCE
Tianwen Xu
xutianwen53@126.com
Guangjian Liu
kentliu321@fjmu.edu.cn

†These authors have contributed equally to this work

RECEIVED 17 July 2024
ACCEPTED 26 August 2024
PUBLISHED 16 September 2024

CITATION
Gao H, Qiu Y, Zheng X, Xu T and Liu G (2024) Revealing the mechanisms of RAC3 in tumor aggressiveness, the immunotherapy response, and drug resistance in bladder cancer. *Front. Oncol.* 14:1466319. doi: 10.3389/fonc.2024.1466319

COPYRIGHT
© 2024 Gao, Qiu, Zheng, Xu and Liu. This is an open-access article distributed under the terms of the Creative Commons Attribution License (CC BY). The use, distribution or reproduction in other forums is permitted, provided the original author(s) and the copyright owner(s) are credited and that the original publication in this journal is cited, in accordance with accepted academic practice. No use, distribution or reproduction is permitted which does not comply with these terms.

Revealing the mechanisms of RAC3 in tumor aggressiveness, the immunotherapy response, and drug resistance in bladder cancer

Hanyuan Gao[1†], Yanru Qiu[2†], Xueqin Zheng[2], Tianwen Xu[2*] and Guangjian Liu[1*]

[1]Department of Nephrology, The Second Affiliated Hospital of Fujian Medical University, Quanzhou, China, [2]Department of Oncology, The Second Affiliated Hospital of Fujian Medical University, Quanzhou, Fujian, China

Background: Bladder cancer (BLCA) is a prevalent urinary tract malignancy with a high propensity for recurrence and chemoresistance. The molecular mechanisms underlying its progression and response to therapy have not been fully elucidated.

Methods: We conducted a multifaceted analysis, integrating immunohistochemical (IHC) staining, bioinformatics evaluation using TCGA and CCLE databases, and *in vitro* assays using the BLCA cell lines 5637 and T24. RAC3 expression was assessed relative to clinical and pathological features. Functional enrichment analyses and gene set enrichment analysis (GSEA) were performed to identify associated biological processes and pathways. The impacts of RAC3 on cell proliferation, migration, invasion, and the immune microenvironment were evaluated using siRNA knockdown, CCK-8, Transwell, wound healing and colony formation assays.

Results: Elevated RAC3 expression was significantly correlated with an advanced tumor stage, lymph node metastasis, and poor prognosis for BLCA patients. The functional enrichment analysis implicated RAC3 in immune cell infiltration and immune checkpoint mechanisms. Notably, RAC3 knockdown significantly reduced the proliferative, migratory, and invasive capabilities of BLCA cells. These effects were reversed by the overexpression of RAC3. Additionally, RAC3 expression was linked to chemoresistance, with high RAC3 expression predicting resistance to certain therapeutic agents. The TIDE algorithm indicated that RAC3 expression could be a predictive biomarker for the immunotherapy response.

Conclusion: RAC3 was identified as a potential therapeutic target and biomarker of BLCA, as its expression significantly influenced tumor progression, the immune response, and chemosensitivity. Targeting RAC3 may provide a novel strategy for the management of BLCA, particularly for patients resistant to

conventional therapies. Further research is essential to elucidate the detailed mechanisms of RAC3 in BLCA and explore its clinical application in precision medicine.

KEYWORDS

bladder cancer, Rac3, tumor aggressiveness, immunotherapy response, drug resistance

Introduction

Bladder cancer, a prevalent urinary tract malignancy, is almost exclusively linked to the urothelium, with 90% of cases stemming from this tissue (1). The prognosis for bladder cancer patients with lung or bone metastases is sobering, typically with a median survival period of approximately 15 months. The 5-year survival rate for such patients is generally between 5% and 10% (2, 3). These findings suggest that the survival prospects for patients with advanced bladder cancer are quite bleak. Identifying more efficacious treatments is of paramount importance to increase the long-term survival of these patients.

Recent research has shown that targeted therapies and immunotherapies might provide benefits to certain patients (4–8). Given its immunogenic nature, bladder cancer may be more likely to provoke a pronounced immune response, offering potential therapeutic advantages (9). However, similar to other types of cancer, drug resistance remains the greatest challenge for these therapeutic approaches (10). Moreover, patients with low PD-L1 expression often find single-agent immunotherapy to be less effective, while combination chemotherapy is more likely to provide clinical advantages. Platinum-based chemotherapy remains the primary treatment option for patients with recurrent and advanced stages of bladder cancer, but its limited effectiveness and the development of drug resistance are significant contributors to disease progression (11, 12). The mechanisms underlying drug resistance are not yet fully understood, and improving treatment outcomes while reducing the incidence of resistance is of critical clinical importance. Research indicates that alterations in the immune microenvironment are linked to the emergence of cisplatin resistance (13, 14). In addition, immunotherapy has the potential to reshape the tumor immune microenvironment. Consequently, the combination of immunotherapy with chemotherapy may synergistically enhance their therapeutic effects and even potentially counteract cisplatin resistance.

The Rho family of guanosine triphosphatases (GTPases) act as indispensable regulators within the intricate network of cell signaling pathways and cytoskeletal dynamics (15, 16). Their influence extends to pivotal cellular processes such as adhesion, morphology, migration, and the cell cycle, underscoring their importance in a diverse array of cell types. These enzymes have the remarkable ability to promote tumor progression (17). RAC3, a Rho subfamily Ras protein, is a gene that encodes a small GTPase with a crucial role in orchestrating the actin cytoskeleton and the complex cascade of intracellular signal transduction (18, 19). The discovery that RAC3 may function as an oncogene highlights its influence on cancer development, suggesting that it could be a key player in the intricate dance of oncogenesis. According to recent findings, a pronounced association between RAC3 expression and immune cell infiltration exists in the tumor microenvironment, suggesting that RAC3 might function as an indicator of the immune status and is capable of influencing the immune microenvironment and tumor immune response (20). Consequently, RAC3 may be a novel target for immunotherapeutic interventions. Additionally, RAC3 contributes to the development of chemoresistance in tumors. Wang et al. (21) revealed that the genetic silencing of RAC3 in bladder cancer cells increased their susceptibility to gemcitabine, suggesting that RAC3 could play a role in the progression of chemotherapy resistance in bladder cancer by modulating the immune microenvironment. The development of an optimal molecular signature, distinguished by its chemical responsiveness and immune attributes, is crucial for an accurate risk analysis and the personalized determination of treatment strategies, potentially leading to improved outcomes and clinical results for high-risk patients with bladder cancer.

Our study demonstrates that RAC3 is highly expressed in bladder cancer and is correlated with the clinical and pathological features of patients, suggesting that RAC3 may facilitate the progression of bladder cancer. Building on these findings, we validated the regulatory role of RAC3 in the clinical and pathological characteristics, immune microenvironment, and chemoresistance of bladder cancer at the bioinformatics level. Furthermore, at the cellular level, we confirmed the impacts of RAC3 on the proliferation, migration, invasion, and chemokine expression of bladder cancer cells. Our research indicates that RAC3 potentially modulates the expression of chemokines, reshaping the immune microenvironment and mediating the development of chemotherapy resistance in bladder cancer.

Materials and methods

Immunohistochemical staining

Sixty sets of bladder urothelial carcinoma (BLCA) tissues and their adjacent normal tissues were collected from patients who underwent surgical resection at The Second Affiliated Hospital of

Fujian Medical University between January 2019 and December 2020. All patients had pathologically confirmed BLCA without any history of other cancers and had not received radiotherapy, chemotherapy, or any other targeted treatments prior to surgery. The study received ethical approval from the hospital's Ethics Committee (No. 2024285). Immunohistochemical (IHC) staining for RAC3 was conducted using a specific monoclonal antibody (Clone: ab124943, Abcam, USA) according to the manufacturer's guidelines. Two independent pathologists assessed the presence of RAC3 in tumor cells and calculated the average percentage of positively stained cells across five randomly selected fields. A staining threshold of ≥1% was established to define a positive RAC3 result.

Bioinformatics analysis

The transcriptome data for our study were obtained from TCGA (22), GTEx (23), and CCLE (24) databases and included samples from both neoplastic and nonneoplastic tissues, as well as various cell lines. We performed a detailed intergroup comparison and survival analysis.

Tumor immune analyses

TCGA-BLCA dataset was employed for assessing various parameters: microsatellite instability (MSI), tumor mutational burden (TMB), the immune context of tumors, and scores reflecting immune cell infiltration. MSI was gauged with the Microsatellite Analysis for Normal Tumor InStability (MANTIS) tool (25). The computation of the TMB was executed with the 'maftools' R package, version 2.2.10 (25). The ESTIMATE algorithm was applied to evaluate the immune microenvironment in relation to RAC3 expression in BLCA (26). The ESTIMATE algorithm was used to investigate the link between RAC3 expression levels and the extent of immune cell infiltration in BLCA, including the immune score, ESTIMATE score, and tumor purity, in BLCA samples. For all analyses involving the calculation of rank correlation coefficients, Spearman's Rho method was the chosen approach.

Immunotherapy evaluation

RNA-sequencing expression profiles and corresponding clinical information for bladder cancer patients were downloaded from TCGA dataset (https://portal.gdc.com). The potential ICB response was predicted with the TIDE algorithm (27). The R programming language, augmented with the "limma" and "ggpubr" libraries, was used to conduct comparative immunotherapy analyses between groups exhibiting different clinical and pathological characteristics.

Functional enrichment analysis

To explore the differential pathway enrichment between groups with high and low RAC3 expression, we utilized the "ggplot2" and "GSVA" R packages for KEGG pathway analysis. The GSVA method, which is unsupervised and nonparametric, offered insights into the variation in gene set enrichment among the samples. Additionally, we conducted Gene Set Enrichment Analysis (GSEA) with the c5.go.v7.5.1 hallmark gene sets (28), applying GSEA software version 4.2.3.

Cell lines and cell culture

Our investigation utilized the bladder cancer cell lines 5637, T24 and the SV-HUC-1 normal uroepithelial cell line, both of which were acquired from Procell Life Science & Technology, Wuhan, China. The cells were cultured in RPMI 1640, McCoy's 5A or Ham's F-12K media from Gibco, USA, supplemented with 10% heat-inactivated FBS and antibiotics (100 U/mL penicillin and streptomycin). The culture was maintained in a humidified incubator at 37°C with an atmosphere containing 5% CO2.

Transfection of small interfering RNAs

RAC3 was targeted by three distinct siRNA constructs, designated siRAC-1, siRAC-2, and siRAC-3, to knockdown its expression, with a nontargeting siRNA serving as the control, all of which were procured from Sangon Biotech in Shanghai, China. The transfection process was facilitated by LipoRNAi reagent, a product from Beyotime, Shanghai, China. Prior to transfection, the 5637 and T24 cells were plated in a 10 cm dish and allowed to grow to 70–80% confluence in complete growth medium. Following transfection, which occurred 18–24 hours after seeding, the cells were cultured in fresh complete medium for 24 additional hours. The experimental group, known as the siRAC group, received siRNAs specific to RAC3, whereas the control group, termed the si-NC group, was transfected with siRNAs targeting a nonspecific sequence. In control group, only the transfection reagent was added without any siRNA. The specific siRNA target sequences are described in detail in Supplementary Table S1.

Establishment of a cotransfection system

We established a cotransfection system in cells by transfecting siRNAs along with an overexpression plasmid (Hanbio, Shanghai, China) to validate the effects of siRNA transfection and perform rescue experiments. The objective was to counteract the effect of siRNA-mediated knockdown on the expression of RAC-3. The specific procedure involved the transfection of the siRNAs with LipoRNAi reagent (Beyotime, Shanghai, China) and the overexpression plasmid with LipoFiter3.0 (Hanbio, Shanghai, China). The 5637 and T24 cells were plated in 10 cm culture dishes and cultured in complete growth medium until they reached 70–80% confluence. Transfection was initiated 24 hours after seeding, and the cells were then further cultured in fresh complete medium for an additional 24 hours. The experimental group, designated the si+ovRAC group, contained a specific

overexpression plasmid, the details of which can be found in Supplementary Figure S1.

Quantitative reverse transcription PCR

Total RNA was extracted from 5637 cells and T24 cells using an RNA extraction kit from Beyotime (Shanghai, China) according to the manufacturer's protocol. The RNA was subsequently reverse transcribed into cDNA using a cDNA synthesis kit from TaKaRa (Tokyo, Japan). For the quantitative gene expression analysis, the cDNA was processed with SYBR Premix Ex Taq reagent from TaKaRa (Tokyo, Japan). The expression of RAC3 was quantified relative to that of the housekeeping gene GAPDH using the $2^{-\Delta\Delta CT}$ method. The sequences of primers used for gene amplification were provided by Sangon Biotech (Shanghai, China) and are listed in Supplementary Table S1.

Western blotting analysis

The cell lysates were meticulously prepared with lysis buffer (Beyotime Biotechnology, Shanghai, China). Protein concentrations were quantified with a BCA kit, which was also provided by Beyotime. The samples were resolved on SDS–PAGE gels and transferred to a PVDF membrane (Millipore, Bedford, MA, USA). The membrane was blocked with Beyotime's rapid sealing solution for 30 minutes, followed by an overnight incubation at 4°C with primary antibodies. After three washes with TBST, the membrane was incubated with an HRP-conjugated goat anti-rabbit IgG antibody (Cat No. AS014; ABclonal, Wuhan, China; 1:4000) for 1 hour at room temperature. The immunoreactive bands were visualized using the Clarity Western ECL substrate (Beyotime Biotechnology, Shanghai, China) and captured on autoradiographic film. The antibodies used included those against GAPDH (Cat No. 10494-1-AP; Proteintech, Wuhan, China; dilution, 1:20000) and RAC3 (Cat No. ab124943; Abcam, USA; dilution, 1:5000).

Cell counting kit-8 assay

The proliferative activity of bladder cancer (BLCA) cells was assessed using the Cell Counting Kit-8 (CCK-8) from Everbright, Inc. (USA). After a 24-hour transfection period, the 5637 and T24 cells were seeded into a 96-well plate at a concentration of 1×10^4 cells/mL. CCK-8 solution was added to the wells, and the plates were incubated at 37°C. At 0, 24, 48, and 72 hours, the optical density (OD) was measured at 450 nm using a spectrophotometer to determine the cell proliferation rate.

Migration and invasion assays

The migratory and invasive properties of the 5637 and T24 cell lines were evaluated using Transwell assays. At 24 hours post transfection, the BLCA cells were detached with trypsin and suspended at a density of 1×10^5 cells/mL in serum-free RPMI 1640 medium. For the migration assay, 2×10^4 cells in 200 µL of medium were added to the upper chamber of the Transwell system, which faced the lower chamber containing 600 µL of medium supplemented with 10% FBS. For invasion assays, the upper surface of the Transwell membrane was coated with 50 µL of Matrigel from BD Bioscience, USA. Following a 24-hour incubation, the cells were fixed with 4% paraformaldehyde for 30 minutes and stained with crystal violet for 20 minutes. The experimental quantification was based on counting the number of cells in the lower compartment across five random fields to determine the average number of migrated or invaded cells.

Wound healing assay

The migratory capacity of the cells was assessed through a wound healing assay. Cells at nearly 90% confluence post transfection growing in 6-well plates were scratched with a 200 µL pipette tip. The detachment of nonadherent cells was facilitated by rinsing with PBS. After a subsequent 24-hour incubation in serum-free medium, cells were monitored by capturing images at 24 and 48 hours using a microscope, with attention to consistent fields of view. The migration rate was determined by calculating the wound closure rate with the following formula: wound closure rate = ((initial scratch area at 24 h)-scratch area at 48 h)/initial area at 24 h) * 100%. These assays were repeated a minimum of three times for reliability.

Colony formation assay

In the experimental setup for the colony formation assay, 1000 cells were plated in each well with 2 mL of RPMI 1640 medium containing 10% FBS and cultured for approximately 7 days at 37°C with 5% CO2 to form colonies. After the incubation period, the cells were washed with PBS, fixed with 4% paraformaldehyde for 15 minutes, and stained with crystal violet for 5 minutes. The colonies were then photographed, and the counts were analyzed statistically to determine the results.

Statistical analysis

IBM SPSS Statistics version 23.0 software, GraphPad Prism version 8.0 software, and R software were used as statistical tools. The chi-square test was used to analyze categorical data. Clinical patient data are presented as the means ± standard deviations (SDs). Spearman's correlation coefficients were calculated for the correlation analysis. For the bioinformatics analysis, the Wilcoxon test was used to compare differences between continuous variables. The Kruskal–Wallis test was used to compare differences between multiple groups. For *in vitro* experiments, since a normal distribution was not expected, a nonparametric two-tailed Student's t test was used to calculate significant results. A p value of <0.05 was considered to indicate statistical significance.

Results

RAC3 was highly expressed in BLCA

The role of RAC3 in bladder cancer (BLCA) was explored through a series of analyses focusing on its expression levels in BLCA tissues and cell lines. An immunohistochemical (IHC) study was performed on tissue sections from human BLCA tumors and corresponding normal tissues (Figures 1A, B). In a cohort of 60 surgically removed BLCA samples, RAC3 was found to be overexpressed (detectable at >1%) in 62% of the cases, with 37 of 60 samples testing positive, and it was under expressed (detectable at <1%) in 38% of the cases, with 23 of 60 samples testing negative (Figure 1C). Our findings indicate a significant increase in RAC3 gene expression within the tumor tissues compared with the surrounding normal tissue samples. We assessed the expression of RAC3 in BLCA cell lines (5637 cells and T24 cells) and a normal uroepithelial cell line (SV-HUC-1 cells) using qRT–PCR and Western blot (Figures 1D–F) analyses to further examine this finding. These results were consistent with those of the IHC analysis, which revealed notably lower expression of RAC3 in normal uroepithelial cells (SV-HUC-1 cells) than in BLCA cells (5637 cells and T24 cells). This study indicates that the level of RAC3 expression in bladder cancer tissues is notably elevated compared with that in normal tissues.

High expression of RAC3 is associated with a poor prognosis and clinicopathological features of BLCA

Data from 432 bladder cancer patients within TCGA database, which included 413 tumor tissues and 19 normal tissue samples, were divided into two groups based on the median expression of the RAC3 mRNA. Kaplan–Meier survival curves confirmed that higher RAC3 expression was associated with poorer patient outcomes, specifically shorter times to disease progression and death (Figures 2A–C). Expanding upon these initial observations, our subsequent analysis aimed to explore the relationship between RAC3 expression and the clinical outcomes of BLCA patients. Notably, increased levels of RAC3 were correlated with several negative prognostic indicators, such as the M stage (M1 vs. M0) and the final N stage (N3 vs. N0/1/2) (Figures 2D–G). Furthermore, predictive models, in the form of nomograms, were developed to estimate the 1-, 3- and 5-year overall survival rates for bladder cancer patients (Figures 2H, I). The survival estimate was derived from the sum of the points allocated to each prognostic factor according to the nomogram's scoring algorithm. The findings underscore the strong correlation between RAC3 expression and the prognosis, including survival rates at the specified time points, for patients with bladder cancer.

The expression level of RAC3 is connected with immune cell infiltration and immune checkpoint mechanisms

RAC3 expression within bladder cancer tissues has been found to be linked to both the density of immune cells within the tumor microenvironment and the expression patterns of genes that are pivotal in the modulation of immune checkpoints. This association suggests that RAC3 may play a role in the interaction of tumors with the immune system, potentially influencing the effectiveness of immune checkpoint therapies. In our quest to understand how RAC3 gene expression correlates with the infiltration of immune cells in BLCA, we categorized the patient data from TCGA database into two groups using the median RAC3 mRNA expression as the dividing criterion. Postsegmentation, we employed CIBERSORT and ESTIMATE computational tools to meticulously assess the degree of immune cell infiltration within the tumor samples of the categorized patient groups. The ESTIMATE algorithm was then applied to determine the relationship between the expression levels of RAC3 and the scores indicative of immune cell infiltration. Furthermore, the MSI, TNB and TIDE algorithms were leveraged to anticipate the response to immunotherapy, particularly the impact of immune checkpoint blocking agents.

Analysis of RAC3 expression, immune cell infiltration and immune pathways

We utilized CIBERSORT to assess the presence of 22 distinct immune cell types, including various T cells, B cells, NK cells, and myeloid cells. Only findings with a significant p value ($p < 0.05$) were selected for the detailed analysis. The results indicated that within the group with elevated RAC3 expression, notable increases in the numbers of M0 macrophages and activated mast cells were observed. Conversely, the group with reduced RAC3 expression presented a greater prevalence of activated memory $CD4^+$ T cells and resting NK cells (Figures 3A–E). Furthermore, patients were stratified into high-risk and low-risk groups based on the expression levels of RAC3. An analysis was conducted to explore the correlation between RAC3 expression and various immune pathways. The findings revealed that variations in RAC3 expression were significantly associated with the presence of HLA molecules, immature dendritic cells (iDCs), NK cells, and regulatory T cells (Tregs), which are often referred to as Th2 cells in some contexts (Figure 3F).

Analysis of immune-related genes

Expanding on our prior explorations, we embarked on a correlation study examining the relationship between RAC3 and a subset of inhibitory checkpoint molecules, all of which are immune-related genes extracted from the IRG database. Spearman correlation analysis was applied to evaluate the correlation, from which we selected the initial 30 genes with the lowest P-values for detailed review. The outcome of this study highlighted a positive correlation between RAC3 and the majority of the immune checkpoints in BLCA, with PSMD4, BIRC5, and TOR2AR standing out as having the most pronounced correlation values (Figure 3G).

Analysis of RAC3 expression and TME scores

Understanding the tumor microenvironment (TME) is essential for advancing cancer research, as it dictates the trajectory of the disease and the effectiveness of treatments (29). Our study aimed to

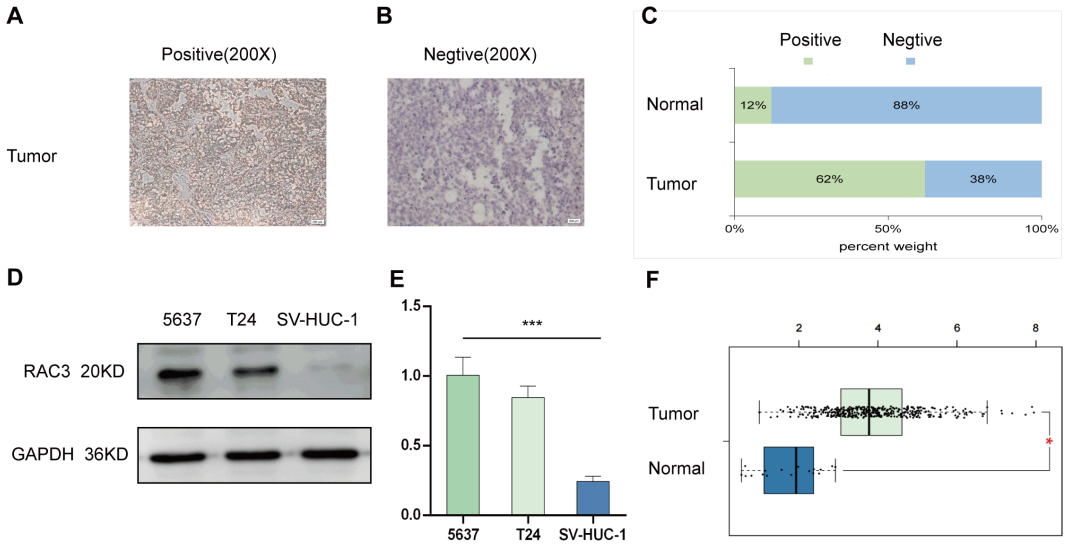

FIGURE 1
RAC3 expression was elevated in bladder cancer (BLCA). **(A, B)** Immunohistochemistry (IHC) was utilized to examine the presence of RAC3 in positive expression **(A)** and negative expression **(B)**. **(C)** A comparison was made to highlight the variations in RAC3 levels between the cancerous and adjacent normal tissues. **(D)** Western blotting was used to determine RAC3 protein levels in the 5637, T24 and SV-HUC-1 cell lines. **(E)** RAC3 mRNA expression was measured in the 5637, T24 and SV-HUC-1 cell lines using qRT–PCR. **(F)** The expression difference of RAC3 in bladder cancer tumor tissues compared to normal tissues from TCGA database. The experiment was repeated at least 3 times. The symbols * and *** indicate statistical significance at the $p<0.05$ and $p<0.001$ levels, respectively.

clarify the interaction between the RAC3 protein and the TME in bladder cancer (BLCA) by quantifying immune cell infiltration with the ESTIMATE algorithm (30). We calculated the stromal scores and immune scores, as well as the overall ESTIMATE score and tumor purity. Notably, the group with increased RAC3 expression had significantly lower scores in all measured categories ($p=0.035$, $p<0.0001$, and $p=0.00031$), and a clear positive correlation between RAC3 levels and tumor purity was observed, indicating a potential role of RAC3 in modulating the TME (Figures 4A–E).

Analysis of RAC3 expression and the response to immunotherapy

The TIDE algorithm serves as a prognostic instrument designed to assess the probable effectiveness of tumor immunotherapy, factoring in the dynamics of dysfunction and exclusion within the tumor microenvironment (TME) (31). In our investigation, the TIDE algorithm was used to predict the impact of immunotherapy mediated by immune checkpoint inhibitors. The findings indicated that female patients under the age of 65 years, with a particular emphasis on those afflicted with low-grade, early-stage cancer, presented a diminished TIDE score (Figures 4H–N). These findings suggest that these patients may have a greater propensity for positive responses to immunotherapy interventions. Accumulated evidence from prior research underscores the importance of the tumor mutation burden (TMB) and microsatellite instability (MSI) as key predictive indicators of a tumor's immunological responsiveness (32). Patients characterized by a high mutational load due to the TMB and those with a high degree of MSI (MSI-H) are more likely to mount a robust immune response. Consequently, the FDA has sanctioned the use of diverse anti-PD-1 and anti-PD-L1 immune checkpoint inhibitors for therapeutic intervention in such patients (33, 34). Our study revealed a significant positive correlation between RAC3 expression and the MSI (Figure 4F) and TMB (Figure 4G) scores. This association suggests that individuals with higher RAC3 expression levels could experience greater benefits from immunotherapy. Additionally, our results introduce RAC3 as a potential novel biomarker for the prediction of the immunotherapy response.

Potential biological functions and pathways of RAC3 in BLCA

Results of the GO enrichment analysis

We conducted a functional enrichment analysis to distinguish the genes that were differentially expressed across the high- and low-RAC3 expression groups, with significance defined as a log2-fold change (FC) ≥ 1 and $p < 0.05$. Gene Ontology (GO) analysis revealed several biological processes pivotal to cell signaling, notably those involving immune functions. The results revealed that the expression of these genes was related to the modulation of chemical synaptic transmission, the regulation of transsynaptic signaling, and nucleosome assembly and organization. Furthermore, the cellular component (CC) analysis provided an in-depth depiction of the subcellular elements implicated in gene expression, offering insights into the underlying cellular machinery associated with the observed expression patterns. We found that the expression of RAC3 was related to the transmembrane transporter complex, transporter complex and monoatomic ion channel complex. Finally, the molecular function (MF) analysis describes the biochemical activities of genes, such as metal ion

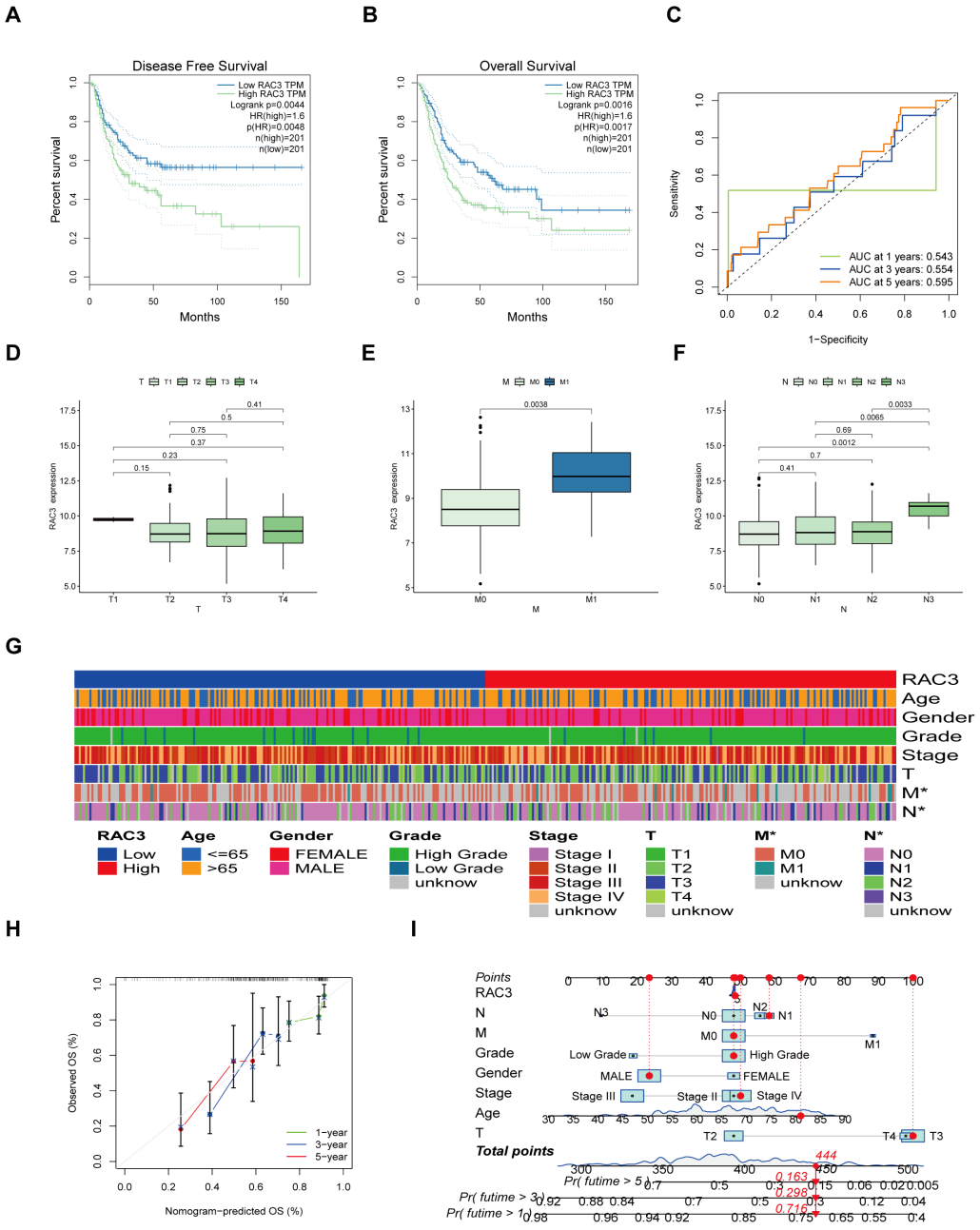

FIGURE 2
Relationships between RAC3 expression levels and patient outcomes. **(A–C)** The effects of RAC3 on disease-free survival **(A)**, overall survival **(B)** and the ROC curves are depicted **(C)**. **(D–G)** The correlation of RAC3 expression with various clinical and pathological characteristics was examined. **(H, I)** By summing the points allocated to different prognostic indicators in the nomogram scoring system, the 1-, 3- and 5-year survival probabilities were predicted.

transmembrane transporter activity, monoatomic ion channel activity and protein heterodimerization activity. This examination delved into the intrinsic functions of gene products at the molecular level, providing essential insights into the core biological mechanisms at play within cellular contexts (Figure 5A). Paralleling our approach, a gene set enrichment analysis (GSEA)-based exploration of KEGG (Figure 5B) and GO (Figure 5C) pathways revealed the enrichment of the immune network for IgA production, the B- and T-cell receptor signaling pathways and the immunoglobulin complex. After synthesizing our observations, the data collectively suggest that increased RAC3 expression in BLCA is correlated with intensified immune responses. This correlation may indicate that RAC3 is a promising adjunctive therapeutic target for patients who have demonstrated resistance to conventional anti-PD-1/PD-L1 treatment modalities.

10.3389/fonc.2024.1466319

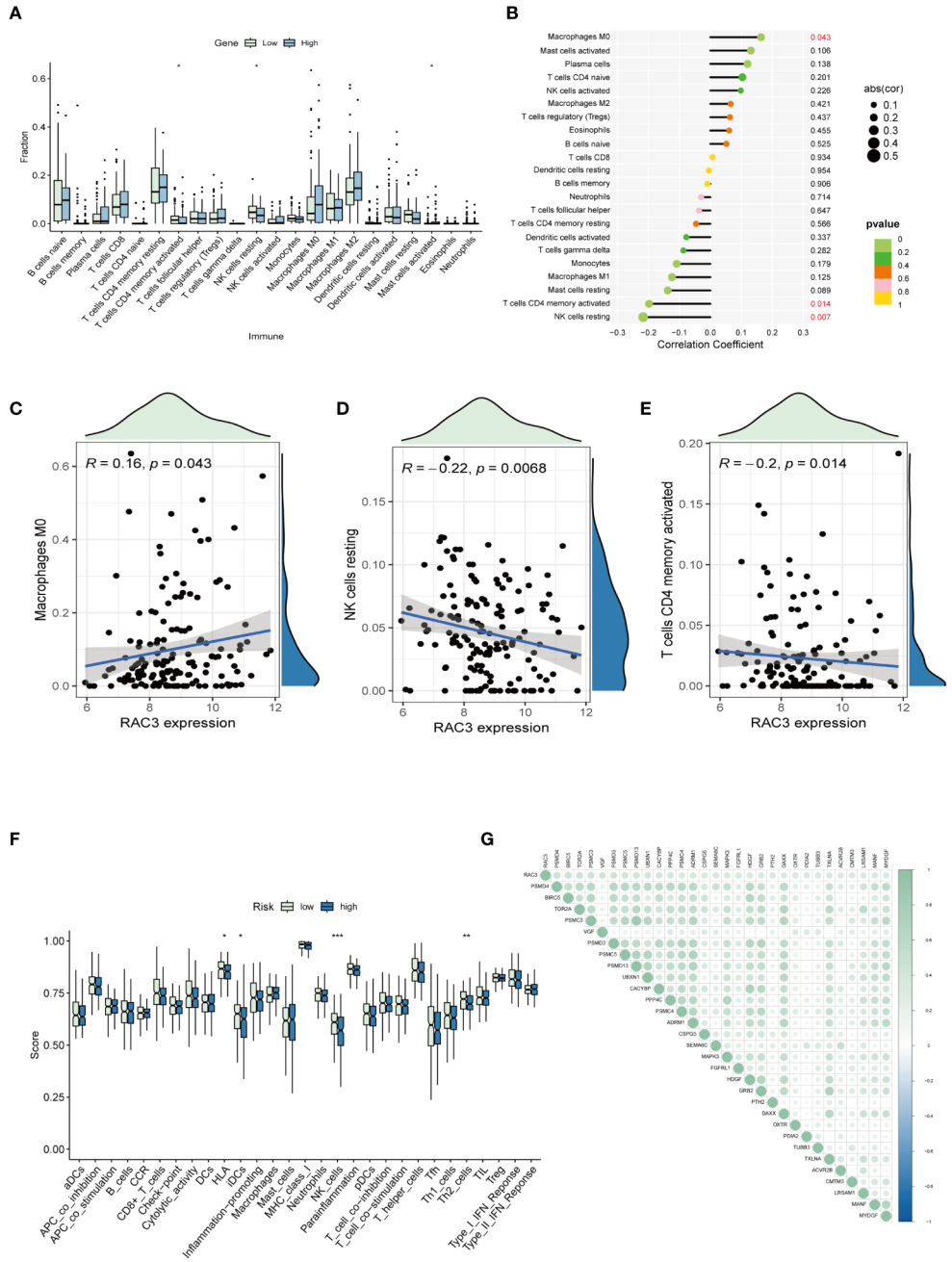

FIGURE 3
The associations of RAC3 with the presence of immune cells and immune checkpoint molecules were explored. **(A–E)** A comparative analysis was conducted to assess the variations in the infiltration levels of 22 distinct immune cell types between groups characterized by high and low levels of RAC3 expression. **(F)** A comparative analysis was conducted to assess the variation in immune pathways between groups characterized by high and low levels of RAC3 expression. **(G)** This study investigated how RAC3 expression correlated with the expression of immune checkpoint inhibitory molecules. Statistical significance is indicated by asterisks: * for p<0.05, ** for p<0.01, and *** for p<0.001.

RAC3 promotes BLCA cell proliferation, migration and invasion

In an effort to decipher the potential interplay between RAC3 expression levels and the aggressive behavior of bladder cancer cells, we strategically utilized siRNAs to silence RAC3 in BLCA 5637 cells and T24 cells. The experimental results revealed the substantial suppression of cancer cell characteristics such as cell proliferation, migratory patterns, invasiveness, and the ability to form colonies upon RAC3 knockdown. This inhibition is theorized to be associated with the reduced capacity of the cells to withstand aggressiveness. We further quantified the clonal potential of the cells using a colony formation assay (Figures 6A, B, 7A, B). Additionally, the CCK-8 assay was utilized to evaluate the influence of RAC3 on cell proliferation (Figures 6C, 7C). The results indicated that the introduction of si-RAC3 markedly decreased the cellular proliferation rate compared with that of

10.3389/fonc.2024.1466319

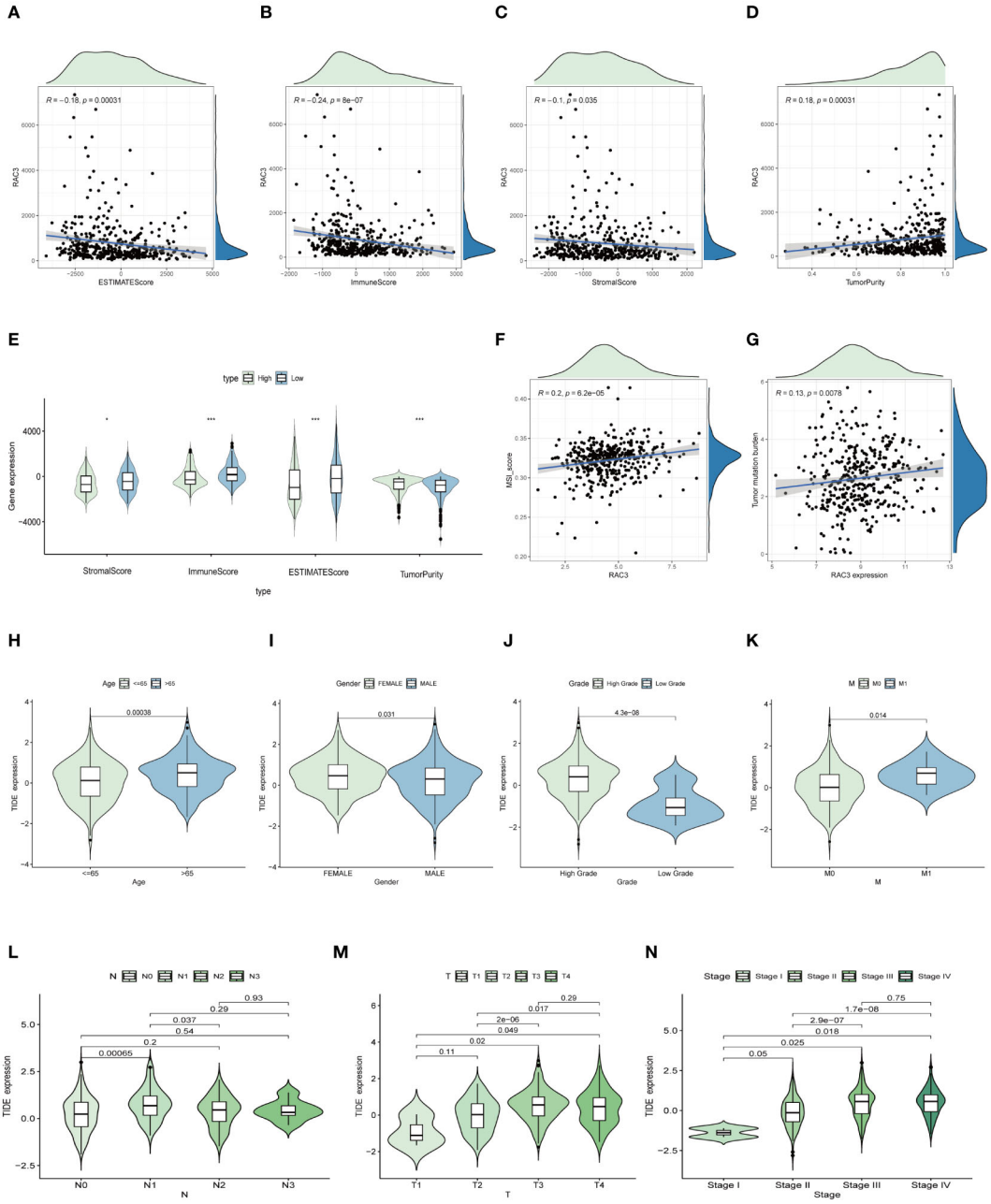

FIGURE 4
The relationship between RAC3 expression and the immune context within tumors. **(A–E)** The study analyzed how RAC3 expression correlated with scores reflecting the characteristics of the tumor microenvironment, such as the immune score and the ESTIMATE score. **(F–N)** The MSI score **(F)**, tumor mutation burden (TNB) score **(G)**, and tumor immunity estimation and direction (TIDE) model were applied to predict the potential efficacy of immunotherapy **(H–N)**. The significance of the findings is denoted by asterisks: * for p<0.05, and *** for p<0.001.

both the si-NC group and the untreated controls. Moreover, we assessed the impact of RAC3 on cell invasiveness and motility using a Transwell assay (Figures 6D, 7D) and a wound healing assay to measure migration capacity (Figures 6E, 7E). Knocking down RAC-3 while simultaneously overexpressing the gene can reversed the reductions in cell proliferation, migration, and invasion capabilities caused by the decreased expression of RAC-3. By restoring RAC-3 expression in cells wherein which it has been knocked down, researchers can determine whether the observed effects on cell behavior are indeed attributable to the manipulation of RAC-3 levels. If the phenotype is reversed upon overexpression, this finding strengthens the evidence that RAC-3 plays a critical role in these cellular processes. Both assays consistently indicated that the attenuation of RAC3 expression substantially compromised the invasive and migratory capabilities of bladder cancer cells. Taken together, these observations highlight the putative role of RAC3 as a

10.3389/fonc.2024.1466319

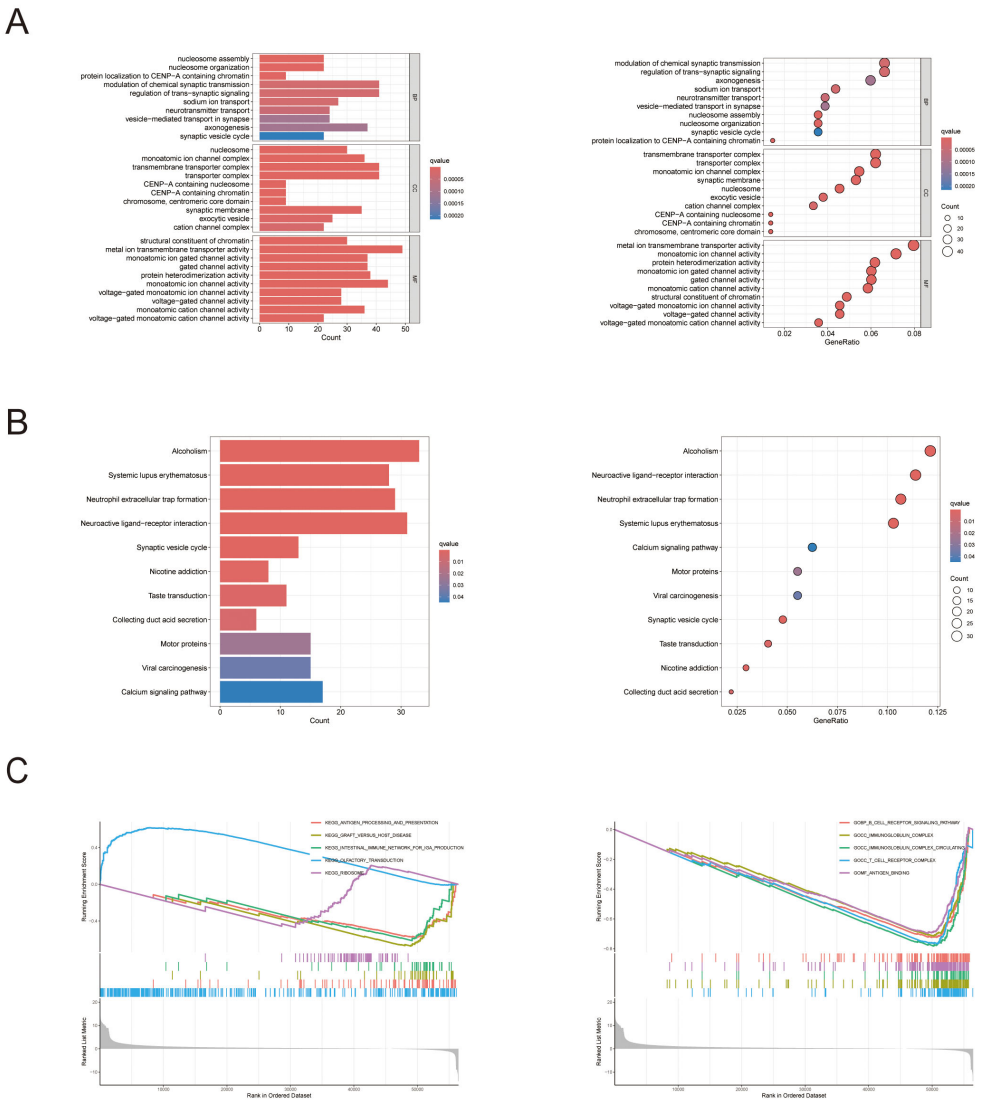

FIGURE 5
The biological functions and pathways associated with RAC3 in bladder cancer (BLCA). **(A)** The figure displays the outcomes of the Gene Ontology (GO) enrichment analysis. **(B)** The results of gene set enrichment analysis (GSEA) are presented, with a focus on the enrichment of KEGG functional pathways and **(C)** GO functional pathways.

central modulator of the proliferative, invasive, and metastatic activities of bladder cancer, suggesting its potential as a novel therapeutic target for BLCA.

Exploring the link between RAC3 and drug resistance in bladder cancer

We stratified patients into high- and low-expression cohorts using the median RAC3 expression level as the cut-off to elucidate the correlation between RAC3 expression and chemoresistance in bladder cancer. The IC50 value, an established metric of drug sensitivity with an inverse relationship to sensitivity, was utilized to assess the drug response. We harnessed the OncoPredict analytical package to evaluate the drug resistance profiles of the patient groups (35). the oncoPredict package, which we utilized for assessing patient sensitivity to 196 chemotherapeutic drugs based on IC50 values, operates on the principle that a higher IC50 value corresponds to a higher sensitivity score. This means that a higher score indicates lower sensitivity, or increased drug resistance, to the respective compound. Our analysis indicated that patients exhibiting elevated RAC3 expression displayed reduced sensitivity to a subset of therapeutic agents, notably mitoxantrone (Figure 8A), SB505124 (Figure 8B), VE-822 (Figure 8C) and PD0325901 (Figure 8D). These findings suggest that increased RAC3 levels may contribute to the acquisition of resistance to a spectrum of treatments, including chemotherapy, targeted therapies, and immunotherapies, within bladder cancer. This refined investigation provides reference value for further exploration into the role of RAC3 as a potential biomarker for chemoresistance and its implications for personalized therapeutic strategies in bladder cancer management.

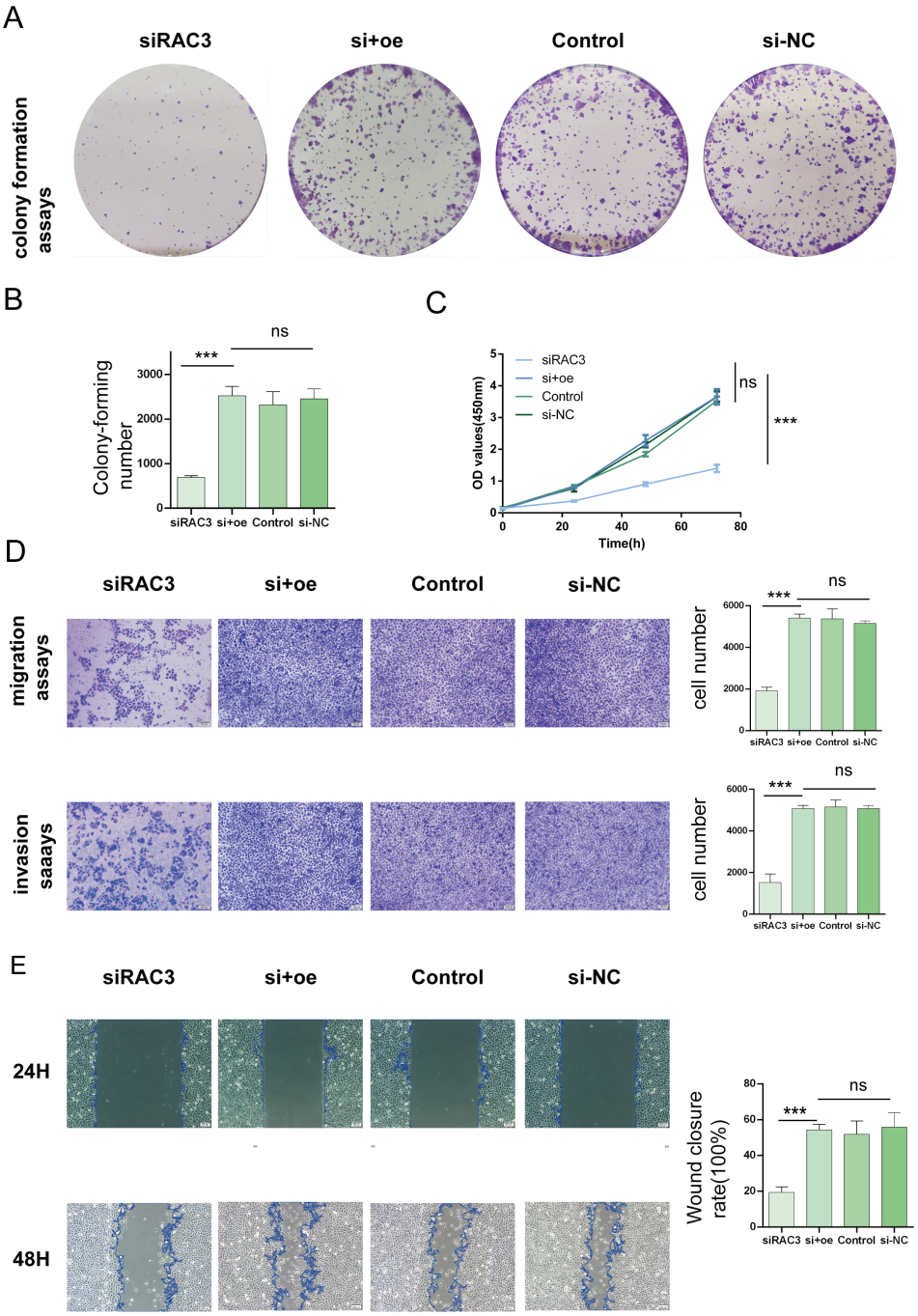

FIGURE 6
Impacts of RAC3 on the proliferation, migration, and invasion of bladder cancer-derived 5637 cells **(A, B)** A colony formation assay was conducted to assess the effect of RAC3 on cell proliferation. **(C)** The CCK-8 assay was also utilized to further analyse the proliferation capabilities of cells with different RAC3 expression levels. **(D)** Transwell assays were used to evaluate the invasive and migratory abilities of the cells under the influence of RAC3. **(E)** A wound healing assay was conducted to measure the migration behavior of the cells, providing additional insights into their motility. The experiment was repeated at least 3 times. The significance of the differences observed is indicated by asterisks: *** for p<0.001. ns for P>0.05.

Discussion

According to the International Agency for Research on Cancer (IARC) report of the World Health Organization in 2020 (36), 570,000 new cases of bladder cancer occurred globally, accounting for 3% of the total incidence of cancer, with 210,000 deaths. In men in particular, it is the sixth most common malignant tumor. Bladder cancer treatments include surgical treatment, chemotherapy, radiotherapy, and targeted therapy. However, due to the lack of early diagnostic methods, patients often present at an advanced

10.3389/fonc.2024.1466319

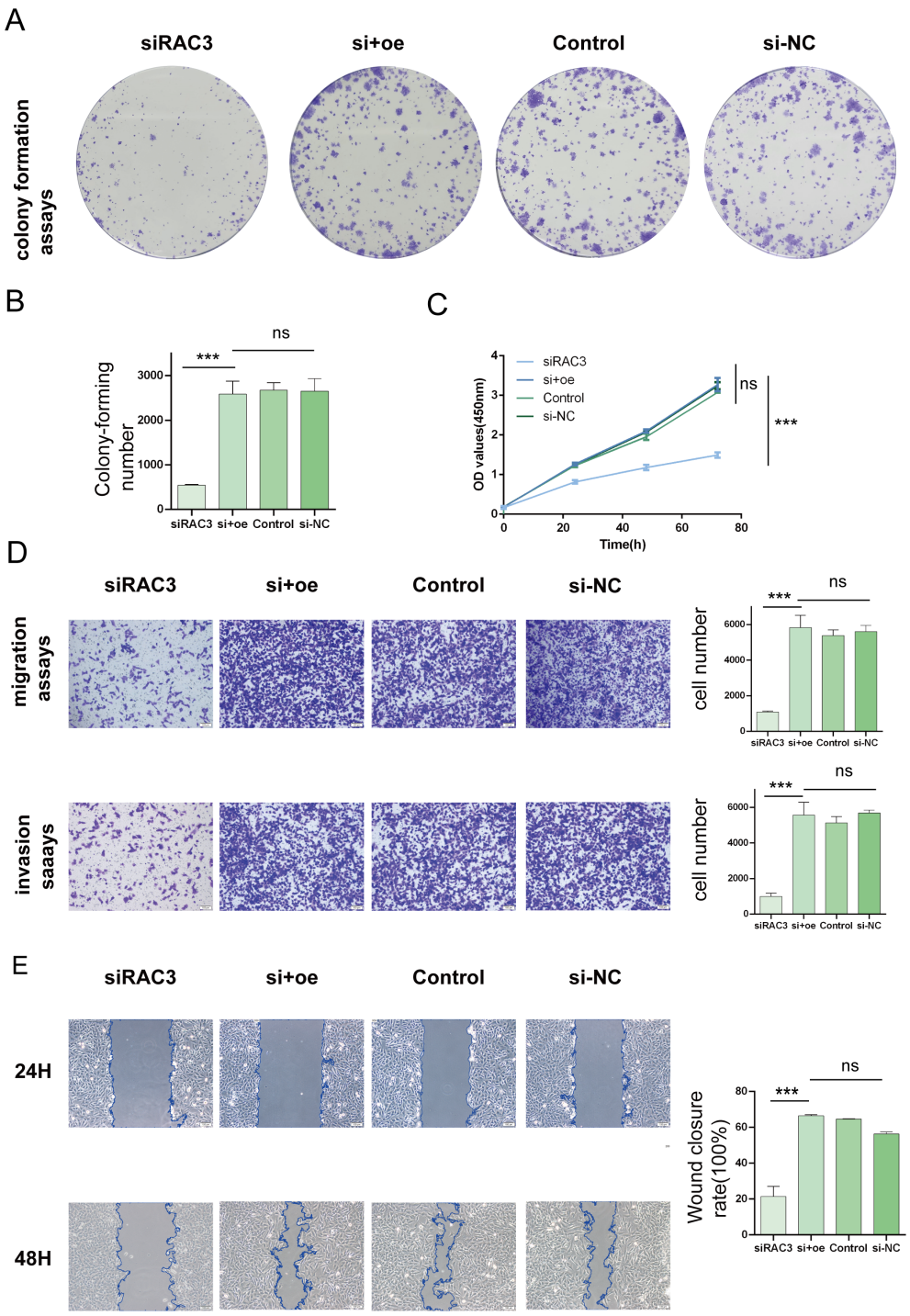

FIGURE 7
Impacts of RAC3 on the proliferation, migration, and invasion of bladder cancer-derived T24 cells. **(A, B)** A colony formation assay was conducted to assess the effect of RAC3 on cell proliferation. **(C)** The CCK-8 assay was also utilized to further analyse the proliferation capabilities of cells with different RAC3 expression levels. **(D)** Transwell assays were used to evaluate the invasive and migratory abilities of the cells under the influence of RAC3. **(E)** A wound healing assay was conducted to measure the migration behavior of the cells, providing additional insights into their motility. The experiment was repeated at least 3 times. The significance of the differences observed is indicated by asterisks: *** for p<0.001. ns for P>0.05.

stage when they seek medical attention due to symptoms. Even after standardized surgical treatment, recurrence and metastasis are still prone to occur. For these patients, platinum-based doublet therapy is the first-line treatment, but drug resistance is common. Patients are insensitive to second-line treatments, and the treatment efficacy is poor. With the advent of the immunotherapy era represented by PD-1/PD-L1 inhibitors, research has shown that immunotherapy can benefit some bladder cancer patients, but it is only effective for a

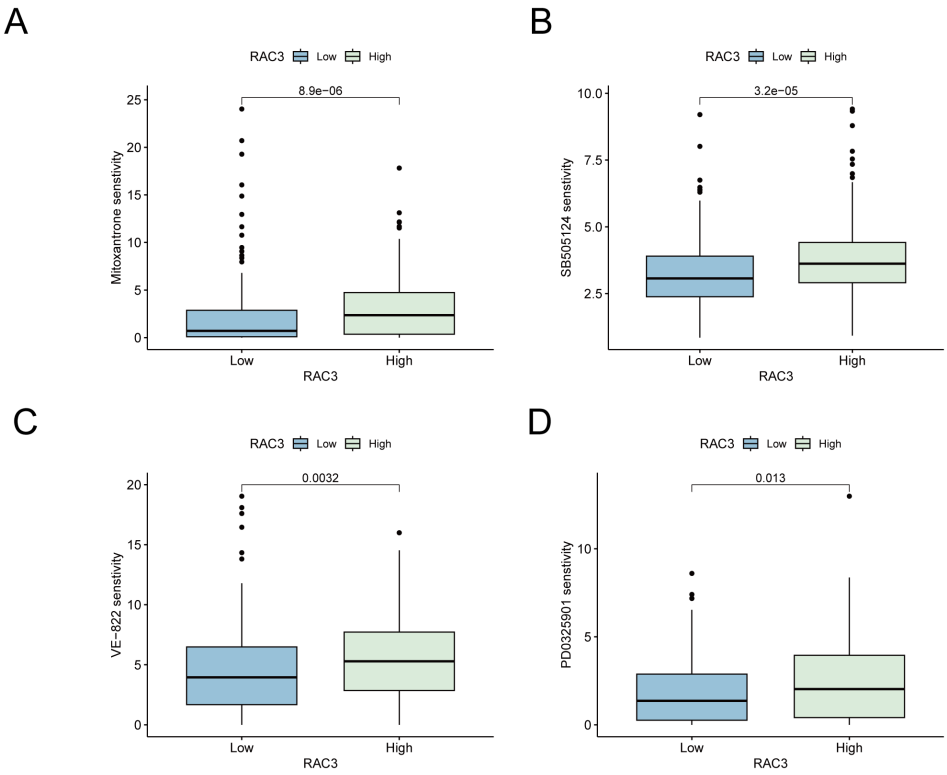

FIGURE 8
The expression of RAC3 is implicated in the development of resistance to chemotherapy and immunotherapy drugs. **(A)** senstivity for drug mitoxantrone. **(B)** senstivity for drug SB505124. **(C)** senstivity for drug VE-822. **(D)** senstivity for drug PD0325901.

small number of patients, especially those with high expression of PD-L1. Therefore, finding more effective immunotherapy targets and therapeutic approaches or reducing the occurrence of resistance to first-line treatments is highly important for improving patients' clinical outcomes. Therefore, our team has identified a novel immunotherapeutic target with potential value, with the aim of achieving this objective.

RAC3, a member of the Ras protein family, significantly influences a range of critical biological processes, such as adhesion, morphology, migration, and the cell cycle, underscoring its importance in a diverse array of cell types. Extensive research has implicated RAC-3 in the genesis of multiple cancers, confirming its classification as a broad-spectrum oncogene (37, 38). However, the precise mechanisms through which it modulates tumor progression, particularly in bladder cancer, are not fully understood and are understudied. Our research revealed that RAC3 is markedly overexpressed in bladder cancer tissues and cells compared with their normal counterparts and that this overexpression is linked to the severity of malignant characteristics and an unfavorable prognosis for patients. By employing RNA interference to knock down RAC3 expression, we observed notable suppression of the proliferative, migratory, and invasive capabilities of bladder cancer cells. The effect of siRNAs on RAC-3 expression and cell malignant progression can be reversed by transfecting an overexpression plasmid. These findings underscore the pivotal role of RAC3 in the malignant progression of bladder cancer. This discovery highlights RAC3 as a promising candidate for targeted therapies, warranting further exploration as a potential therapeutic strategy. The development of drugs aimed at modulating RAC3 activity could offer a novel approach to combat bladder cancer, particularly for patients facing resistance to existing treatments. This avenue of research holds great potential for improving clinical outcomes and providing new hope for individuals battling this aggressive disease. However, the precise mechanisms by which RAC3 contributes to the malignancy of tumor cells remain unclear. Many immune checkpoints regulate the immune microenvironment, thereby controlling the immune evasion of tumor cells and leading to disease progression. Therefore, we will explore whether RAC3 can modulate the immune microenvironment in our next phase of research.

The immune microenvironment is a pivotal determinant of cancer patient outcomes, significantly influencing responses to immunotherapy and potentially contributing to the development of resistance to both chemotherapy and immunotherapy (39, 40). A nuanced understanding of the tumor immune microenvironment, with a particular focus on the patterns of immune cell infiltration, is essential for elucidating the aetiology and progression of bladder cancer. Prior studies have demonstrated that elevated RAC3 levels in epithelial cancer tissues are inversely linked to the infiltration of CD8+T cells, thereby orchestrating a microenvironment that suppresses the immune response and targeting RAC3 offers a strategic approach to reconfigure the immune microenvironment, thereby amplifying the potency of immune cells in combating tumor growth (41). Our research revealed that RAC3 expression

modulates the signaling pathways of B- and T-cell receptors, which are integral to the immune response, in bladder cancer. The presence of immune cells within the tumor microenvironment is a critical determinant of the effectiveness of the immune response. Furthermore, we observed a correlation between RAC3 expression and the IgA-producing immune network, as well as the accumulation of immunoglobulin complexes. Accumulating evidence suggests that IgA and other immunoglobulins play a significant role in the interplay between cancer development and the immune response, potentially influencing the efficacy of immunotherapies and the body's ability to combat tumor growth (42, 43). This insight into the multifaceted role of RAC3 in the immune landscape of bladder cancer may provide novel avenues for therapeutic intervention and a better understanding of the complex dynamics at play in cancer immunology.

We identified an increased immune score in patients with elevated RAC3 expression, which was correlated with the infiltration of diverse immune cells and immune pathways. Intriguingly, our findings suggest that female patients under 65 years of age with low-grade, early-stage cancer exhibit reduced TIDE scores, indicating potential responsiveness to immune checkpoint inhibitors. This insight provides a rationale for the potential therapeutic utility of RAC3 targeting in patients who are refractory to conventional anti-PD-1/PD-L1 therapies. In conclusion, the collective observations from our study underscore the potential of RAC3 as a valuable therapeutic target in bladder cancer, particularly for those who may not benefit from existing immunotherapies. The role of RAC3 in the immune microenvironment represents a promising avenue for the development of novel treatment strategies that could enhance the efficacy of immunotherapy and improve patient outcomes. While immunotherapy alone is effective for only a subset of patients, the exploration of combination therapies remains a mainstream direction in cancer treatment. The conclusion that immunotherapy combined with chemotherapy can enhance therapeutic efficacy has been validated in numerous clinical studies. With this result in mind, we are further investigating whether RAC3 regulates the development of chemoresistance in the hopes of providing a theoretical foundation for combination therapies. Our aim is to elucidate the role of RAC3 in chemotherapy resistance, which could inform more effective treatment strategies that combine the strengths of immunotherapy with the targeted action of chemotherapeutic agents.

Platinum-based chemotherapy regimens are a mainstay in the treatment of bladder cancer; however, the propensity for these tumors to develop resistance presents a formidable clinical obstacle. The mechanisms behind this resistance remain largely elusive. Notably, heightened expression of RAC3 has been identified in BLCA tissues that exhibit drug resistance, where it is implicated in augmenting chemoresistance through the PAK1-ERK1/2 signaling pathway (44). Our research revealed a correlation between elevated RAC3 levels and diminished sensitivity to specific therapeutic agents, such as mitoxantrone, a chemotherapeutic agent for bladder cancer, as well as SB505124 and VE-822. SB505124, when coadministered with cisplatin, can enhance the tumor response to cisplatin, potentially reducing the need for prolonged cisplatin therapy (45). VE-822, an ATM/ATR kinase inhibitor, has been shown to inhibit cell proliferation, colony formation, and migration by suppressing p-ATR expression, thereby disrupting DNA repair mechanisms and potentiating the effects of cisplatin on a nude mouse xenograft model (46). Additionally, PD0325901, an ERK inhibitor, has been shown to augment the efficacy of PD-1 inhibitors (47). These findings suggest that the overexpression of RAC3 is associated with an increased risk of resistance to cisplatin and immune checkpoint inhibitors, potentially accounting for the poor prognosis of patients with high RAC3 expression. Consequently, immunotherapy strategies that target RAC3 could represent a synergistic therapeutic approach when combined with cisplatin chemotherapy, potentially enhancing treatment efficacy. Moreover, for patients who are resistant to cisplatin and PD-1/PD-L1 inhibitors, RAC3-targeted therapies may be promising for reversing drug resistance and improving survival outcomes.

Conclusion

I In this comprehensive study, we explored the intricate role of Ras-related C3 (RAC3), a pivotal member of the Rho subfamily of Ras proteins, in the modulation of bladder cancer (BLCA) progression. Our research highlights the significant association of RAC3 with key biological processes, including the promotion of cell proliferation, migration, invasion, and somatic growth, as well as its influence on the tumor microenvironment (TME) and immune response. Our findings reveal that increased RAC3 expression is linked to an aggressive phenotype of BLCA, with implications for chemoresistance and immune evasion. The molecular mechanisms implicated in these effects suggest that RAC3 modulates the immune landscape within the TME, potentially through its interaction with nuclear receptors and transcription factors, thereby influencing the expression of chemokines and immune cell infiltration patterns. In conclusion, our research identifies RAC3 as a multifaceted regulator in BLCA, with potential as a novel target for immunotherapeutic interventions. The elucidation of the role of RAC3 in the immune microenvironment and chemoresistance mechanisms opens avenues for the development of personalized medicine approaches, which may ultimately enhance the efficacy of therapeutic strategies and improve clinical outcomes for patients with high-risk BLCA. Further in-depth investigations are warranted to dissect the complex interplay of RAC3 in tumor biology and to harness its full potential in bladder cancer management.

Data availability statement

The original contributions presented in the study are included in the article/Supplementary Material. Further inquiries can be directed to the corresponding author/s.

Ethics statement

This study was approved by Ethics Committee of The Second Afliated Hospital of Fujian Medical University. Because of its

retrospective nature, the need for written informed consent was waived by the Ethics Committee of The Second Afliated Hospital of Fujian Medical University. All methods in this study were carried out in accordance with relevant guidelines and regulations.

Author contributions

HG: Writing – original draft, Project administration, Validation. YQ: Funding acquisition, Methodology, Writing – original draft, Validation. XZ: Writing – original draft, Data curation. TX: Formal analysis, Writing – review & editing, Funding acquisition. GL: Conceptualization, Writing – review & editing, Methodology.

Funding

The author(s) declare financial support was received for the research, authorship, and/or publication of this article. The sources of funding are as follows: Startup Fund for scientific research, Fujian Medical University(Grant number : 2023 QH1143).

Conflict of interest

The authors declare that the research was conducted in the absence of any commercial or financial relationships that could be construed as a potential conflict of interest.

Publisher's note

All claims expressed in this article are solely those of the authors and do not necessarily represent those of their affiliated organizations, or those of the publisher, the editors and the reviewers. Any product that may be evaluated in this article, or claim that may be made by its manufacturer, is not guaranteed or endorsed by the publisher.

Supplementary material

The Supplementary Material for this article can be found online at: https://www.frontiersin.org/articles/10.3389/fonc.2024.1466319/full#supplementary-material

References

1. Laurie MA, Zhou SR, Islam MT, Shkolyar E, Xing L, Liao JC. Bladder cancer and artificial intelligence: emerging applications. *Urol Clin North Am*. (2024) 51:63–75. doi: 10.1016/j.ucl.2023.07.002

2. Haoyuan MA, Yanshu LI. Structure, regulatory factors and cancer-related physiological effects of ADAM9. *Cell Adh Migr*. (2020) 14:165–81. doi: 10.1080/19336918.2020.1817251

3. Cheng W, Fu D, Xu F, Zhang Z. Unwrapping the genomic characteristics of urothelial bladder cancer and successes with immune checkpoint blockade therapy. *Oncogenesis*. (2018) 7:2–18. doi: 10.1038/s41389-017-0013-7

4. Li AH, Park SY, Li P, Zhou C, Kluz T, Li J, et al. Transcriptome analysis reveals anti-cancer effects of isorhapontigenin (ISO) on highly invasive human T24 bladder cancer cells. *Int J Mol Sci*. (2024) 25:1783–803. doi: 10.3390/ijms25031783

5. Pappot H, Ullén A. Optimal systemic treatment of advanced bladder cancer-A moving target. *Cancers (Basel)*. (2020) 12:3607–10. doi: 10.3390/cancers12123607

6. Yan H, Zhang L, Li R. Identification of m6A suppressor EIF4A3 as a novel cancer prognostic and immunotherapy biomarker through bladder cancer clinical data validation and pan-cancer analysis. *Sci Rep*. (2023) 13:16457–60. doi: 10.1038/s41598-023-43500-4

7. Larsen ES, Joensen UN, Poulsen AM, Goletti D, Johansen IS. Bacillus Calmette-Guérin immunotherapy for bladder cancer: a review of immunological aspects, clinical effects and BCG infections. *Apmis*. (2020) 128:92–103. doi: 10.1111/apm.13011

8. Lopez-Beltran A, Cookson MS, Guercio BJ, Cheng L. Advances in diagnosis and treatment of bladder cancer. *Bmj*. (2024) 384:e76743–64. doi: 10.1136/bmj-2023-076743

9. Bromwich EJ, McArdle PA, Canna K, McMillan DC, McNicol AM, Brown M, et al. The relationship between T-lymphocyte infiltration, stage, tumor grade and survival in patients undergoing curative surgery for renal cell cancer. *Br J Cancer*. (2003) 89:1906–08. doi: 10.1038/sj.bjc.6601400

10. Pfail JL, Katims AB, Alerasool P, Sfakianos JP. Immunotherapy in non-muscle-invasive bladder cancer: current status and future directions. *World J Urol*. (2021) 39:1319–29. doi: 10.1007/s00345-020-03474-8

11. Okobi TJ, Uhomoibhi TO, Akahara DE, Odoma VA, Sanusi IA, Okobi OE, et al. Immune checkpoint inhibitors as a treatment option for bladder cancer: current evidence. *Cureus*. (2023) 15:e40031–41. doi: 10.7759/cureus.40031

12. Ren X, Tian Y, Wang Z, Wang J, Li X, Yin Y, et al. Tislelizumab in combination with gemcitabine plus cisplatin chemotherapy as first-line adjuvant treatment for locally advanced or metastatic bladder cancer: a retrospective study. *BMC Urol*. (2022) 22:128–39. doi: 10.1186/s12894-022-01083-8

13. Li QY, Guo Q, Luo WM, Luo XY, Ji YM, Xu LQ, et al. Overexpression of MTFR1 promotes cancer progression and drug-resistance on cisplatin and is related to the immune microenvironment in lung adenocarcinoma. *Aging (Albany Ny)*. (2024) 16:66–88. doi: 10.18632/aging.205338

14. Chen SH, Chang JY. New insights into mechanisms of cisplatin resistance: from tumor cell to microenvironment. *Int J Mol Sci*. (2019) 20:23–78. doi: 10.3390/ijms20174136

15. Li H, Peyrollier K, Kilic G, Brakebusch C. Rho GTPases and cancer. *Biofactors*. (2014) 40:226–35. doi: 10.1002/biof.1155

16. Etienne-Manneville S, Hall A. Rho GTPases in cell biology. *Nature*. (2002) 420:629–35. doi: 10.1038/nature01148

17. Bustelo XR. RHO GTPases in cancer: known facts, open questions, and therapeutic challenges. *Biochem Soc Trans*. (2018) 46:741–60. doi: 10.1042/BST20170531

18. Scala M, Nishikawa M, Ito H, Tabata H, Khan T, Accogli A, et al. Variant-specific changes in RAC3 function disrupt corticogenesis in neurodevelopmental phenotypes. *Brain*. (2022) 145:3308–27. doi: 10.1093/brain/awac106

19. Donnelly SK, Cabrera R, Mao S, Christin JR, Wu B, Guo W, et al. Rac3 regulates breast cancer invasion and metastasis by controlling adhesion and matrix degradation. *J Cell Biol*. (2017) 216:4331–49. doi: 10.1083/jcb.201704048

20. Ou-Yang S, Liu JH, Wang QZ. Upregulation of RAC3 in bladder cancer predicts adverse clinical outcome and increased tumor immune response. *Int J Clin Exp Pathol*. (2020) 13:2937–49.

21. Cai T, Feng T, Li G, Wang J, Jin S, Ye D, et al. Deciphering the prognostic features of bladder cancer through gemcitabine resistance and immune-related gene analysis and identifying potential small molecular drug PIK-75. *Cancer Cell Int*. (2024) 24:125–35. doi: 10.1186/s12935-024-03258-9

22. Zhang K, Wang H. Cancer genome atlas pan-cancer analysis project. *Zhongguo Fei Ai Za Zhi*. (2015) 18:219–23. doi: 10.3779/j.issn.1009-3419.2015.04.02

23. Lonsdale J, Thomas J, Salvatore M. The genotype-tissue expression (GTEx) project. *Nat Genet*. (2013) 45:580–85. doi: 10.1038/ng.2653

24. Ghandi M, Huang FW, Jané-Valbuena J, Kryukov GV, Lo CC, McDonald ER, et al. Next-generation characterization of the cancer cell line encyclopedia. *Nature*. (2019) 569:503–08. doi: 10.1038/s41586-019-1186-3

25. Kautto EA, Bonneville R, Miya J, Yu L, Krook MA, Reeser JW, et al. Performance evaluation for rapid detection of pan-cancer microsatellite instability with MANTIS. *Oncotarget*. (2017) 8:7452–63. doi: 10.18632/oncotarget.13918

26. Chen H, Yang W, Ji Z. Machine learning-based identification of tumor-infiltrating immune cell-associated model with appealing implications in improving

prognosis and immunotherapy response in bladder cancer patients. *Front Immunol*. (2023) 14:1171420. doi: 10.3389/fimmu.2023.1171420

27. Zheng J, Cai X, Zhang Y, Wang H, Liu L, Tang F, et al. A comprehensive pan-cancer analysis of necroptosis molecules in four gynecologic cancers. *BMC Cancer*. (2022) 22:1160–81. doi: 10.1186/s12885-022-10166-6

28. Cheng Y, Liu J, Fan H, Liu K, Zou H, You Z. Integrative analyses of a mitophagy-related gene signature for predicting prognosis in patients with uveal melanoma. *Front Genet*. (2022) 13:1050341. doi: 10.3389/fgene.2022.1050341

29. Lee TJ, Nair M, Banasavadi-Siddegowda Y, Liu J, Nallanagulagari T, Jaime-Ramirez AC, et al. Enhancing therapeutic efficacy of oncolytic herpes simplex virus-1 with integrin β1 blocking antibody OS2966. *Mol Cancer Ther*. (2019) 18:1127–36. doi: 10.1158/1535-7163.MCT-18-0953

30. Sturm G, Finotello F, Petitprez F, Zhang JD, Baumbach J, Fridman WH, et al. Comprehensive evaluation of transcriptome-based cell-type quantification methods for immuno-oncology. *Bioinformatics*. (2019) 35:i436–45. doi: 10.1093/bioinformatics/btz363

31. Zheng Q, Gong Z, Li B, Cheng R, Luo W, Huang C, et al. Identification and characterization of CLEC11A and its derived immune signature in gastric cancer. *Front Immunol*. (2024) 15:1324959. doi: 10.3389/fimmu.2024.1324959

32. Luchini C, Bibeau F, Ligtenberg M, Singh N, Nottegar A, Bosse T, et al. ESMO recommendations on microsatellite instability testing for immunotherapy in cancer, and its relationship with PD-1/PD-L1 expression and tumor mutational burden: a systematic review-based approach. *Ann Oncol*. (2019) 30:1232–43. doi: 10.1093/annonc/mdz116

33. Picard E, Verschoor CP, Ma GW, Pawelec G. Relationships between immune landscapes, genetic subtypes and responses to immunotherapy in colorectal cancer. *Front Immunol*. (2020) 11:369. doi: 10.3389/fimmu.2020.00369

34. Palmeri M, Mehnert J, Silk AW, Jabbour SK, Ganesan S, Popli P, et al. Real-world application of tumor mutational burden-high (TMB-high) and microsatellite instability (MSI) confirms their utility as immunotherapy biomarkers. *Esmo Open*. (2022) 7:100336–43. doi: 10.1016/j.esmoop.2021.100336

35. Pan YB, Xu WJ, Huang MS, Lu YD, Zhou YJ, Teng Y, et al. Anoikis-related signature identifies tumor microenvironment landscape and predicts prognosis and drug sensitivity in colorectal cancer. *J Cancer*. (2024) 15:841–57. doi: 10.7150/jca.91627

36. Sung H, Ferlay J, Siegel RL, Laversanne M, Soerjomataram I, Jemal A, et al. Global cancer statistics 2020: GLOBOCAN estimates of incidence and mortality worldwide for 36 cancers in 185 countries. *CA Cancer J Clin*. (2021) 71:209–49. doi: 10.3322/caac.21660

37. de Curtis I. The rac3 GTPase in neuronal development, neurodevelopmental disorders, and cancer. *Cells*. (2019) 8:1–15. doi: 10.3390/cells8091063

38. Liu TQ, Wang GB, Li ZJ, Tong XD, Liu HX. Silencing of Rac3 inhibits proliferation and induces apoptosis of human lung cancer cells. *Asian Pac J Cancer Prev*. (2015) 16:3061–65. doi: 10.7314/apjcp.2015.16.7.3061

39. Sameni M, Tovar EA, Essenburg CJ, Chalasani A, Linklater ES, Borgman A, et al. Cabozantinib (XL184) inhibits growth and invasion of preclinical TNBC models. *Clin Cancer Res*. (2016) 22:923–34. doi: 10.1158/1078-0432.CCR-15-0187

40. Khalaf K, Hana D, Chou JT, Singh C, Mackiewicz A, Kaczmarek M. Aspects of the tumor microenvironment involved in immune resistance and drug resistance. *Front Immunol*. (2021) 12:656364. doi: 10.3389/fimmu.2021.656364

41. Huang P, Qian Y, Xia Y, Wang S, Xu C, Zhu X, et al. Integrated analysis identifies RAC3 as an immune-related prognostic biomarker associated with chemotherapy sensitivity in endometrial cancer. *J Cell Mol Med*. (2023) 27:2385–97. doi: 10.1111/jcmm.17824

42. Ellis JA. Canine IgA and IgA deficiency: Implications for immunization against respiratory pathogens. *Can Vet J*. (2019) 60:1305–11.

43. Hu D, Zheng H, Liu H, Li M, Ren W, Liao W, et al. Immunoglobulin expression and its biological significance in cancer cells. *Cell Mol Immunol*. (2008) 5:319–24. doi: 10.1038/cmi.2008.39

44. Chen Y, Huang M, Lu J, Zhang Q, Wu J, Peng S, et al. Establishment of a prognostic model to predict chemotherapy response and identification of RAC3 as a chemotherapeutic target in bladder cancer. *Environ Toxicol*. (2024) 39:509–28. doi: 10.1002/tox.23860

45. Marini KD, Croucher DR, McCloy RA, Vaghjiani V, Gonzalez-Rajal A, Hastings JF, et al. Inhibition of activin signaling in lung adenocarcinoma increases the therapeutic index of platinum chemotherapy. *Sci Transl Med*. (2018) 10:1–13. doi: 10.1126/scitranslmed.aat3504

46. Chen T, Yang F, Dai X, Yu Y, Sun Y, Wu X, et al. VE-822 enhanced cisplatin chemotherapy effects on head and neck squamous cell carcinoma drug-resistant cells. *Curr Cancer Drug Targets*. (2023) 23:482–95. doi: 10.2174/1568009623666230206143216

47. Luo M, Xia Y, Wang F, Zhang H, Su D, Su C, et al. PD0325901, an ERK inhibitor, enhances the efficacy of PD-1 inhibitor in non-small cell lung carcinoma. *Acta Pharm Sin B*. (2021) 11:3120–33. doi: 10.1016/j.apsb.2021.03.010

frontiers | Frontiers in Immunology

TYPE Original Research
PUBLISHED 14 October 2024
DOI 10.3389/fimmu.2024.1481301

Check for updates

OPEN ACCESS

EDITED BY
Xiaosheng Tan,
Rutgers, United States

REVIEWED BY
Kaikai Lyu,
University of North Carolina at Chapel Hill, United States
Zihan Ma,
Yale University, United States
Yuting Tang,
Cincinnati Children's Hospital Medical Center, United States

*CORRESPONDENCE
Xudong Zhang
fcczhangxd@zzu.edu.cn

†These authors have contributed equally to this work

RECEIVED 15 August 2024
ACCEPTED 24 September 2024
PUBLISHED 14 October 2024

CITATION
Li S, Feng X, Song Y, Fan M, Chen Q, Zhang M, Wu X, Dong M, Zhang J, Han L and Zhang X (2024) Real-world study and prognostic analysis of angioimmunoblastic T-cell lymphoma.
Front. Immunol. 15:1481301.
doi: 10.3389/fimmu.2024.1481301

COPYRIGHT
© 2024 Li, Feng, Song, Fan, Chen, Zhang, Wu, Dong, Zhang, Han and Zhang. This is an open-access article distributed under the terms of the Creative Commons Attribution License (CC BY). The use, distribution or reproduction in other forums is permitted, provided the original author(s) and the copyright owner(s) are credited and that the original publication in this journal is cited, in accordance with accepted academic practice. No use, distribution or reproduction is permitted which does not comply with these terms.

Real-world study and prognostic analysis of angioimmunoblastic T-cell lymphoma

Suxiao Li[1,2†], Xiaoyan Feng[1,2†], Yunfei Song[1,2], Mengke Fan[1,2], Qingjiang Chen[3,4], Mingzhi Zhang[1,2], Xiaolong Wu[1,2], Meng Dong[1,2], Jieming Zhang[1,2], Lijuan Han[1,2] and Xudong Zhang[1,2*]

[1]Department of Oncology, The First Affiliated Hospital of Zhengzhou University, Zhengzhou, Henan, China, [2]Department of Oncology, Lymphoma Diagnosis and Treatment Center of Henan Province, Zhengzhou, Henan, China, [3]Department of Oncology, Xinxiang Medical College, Xinxiang, Henan, China, [4]Henan Academy of Innovations in Medical Science, Zhengzhou, Henan, China

Objective: To analyze the clinical prognostic factors and treatments for angioimmunoblastic T-cell lymphoma (AITL) and develop a novel prognostic model specifically for AITL.

Method: We retrospectively analyzed 231 patients with AITL from the First Affiliated Hospital of Zhengzhou University. Patients were enrolled between January 2014 and July 2023. The primary end points were overall survival (OS) and progression-free survival (PFS).

Result: The patients' median age was 63 years, with 88.3% at an advanced stage (III/IV). The majority of patients (47.6%) received anthracycline-containing regimens, and there was no significant difference in survival compared with those treated with epigenetic-targeting and gemcitabine- containing regimens. The median PFS and OS were 6 and 17 months, respectively. In multivariate analysis, age >60 years, Eastern Cooperative Oncology Group performance status ≥2, elevated LDH, and splenomegaly were associated with inferior OS. Based on these four factors, a novel prognostic model (AITL model) was constructed that stratified patients into low-, intermediate-, and high-risk groups, with 2-year OS estimates of 63.6%, 42.1%, and 18.6%, respectively.

Conclusion: Currently, there is no consensus on the optimal initial therapy for AITL, and the efficacy of anthracycline-containing regimens remains suboptimal. The novel model developed herein demonstrates predictive significance for both OS and PFS, and exhibits better stratification and discrimination capabilities.

KEYWORDS

angioimmunoblastic T-cell lymphoma, prognostic, treatment, prognostic model, outcomes

1 Introduction

Angioimmunoblastic T-cell lymphoma (AITL) is a distinct pathological subtype of peripheral T-cell lymphomas (PTCL), accounting for 15–20% of PTCL (1). AITL typically involves the expression of follicular helper T cell (TFH) markers, with positivity for two or more markers such as those encoded by *BCL6, CD10, CXCL13, PD-1*, or *ICOS*. Most patients are diagnosed at an advanced stage. AITL is characterized by systemic lymphadenomegaly, B symptoms, rash, serous cavity effusion, and splenomegaly. Currently, no standardized treatment exists for AITL; commonly used anthracycline-containing chemotherapy regimens have demonstrated poor long-term efficacy, with 5-year overall survival (OS) and progression-free survival (PFS) estimates of 32–41% and 18–38%, respectively (2). These statistics highlight the high mortality rate and rapid progression associated with AITL. Neoplasms remain the leading cause of death worldwide (3–8).

Few studies have attempted to identify clinicopathological and imaging-related adverse prognostic factors for AITL. Previous studies have found the presence of Epstein-Barr virus (EBV)-positive B cells in 66%–86% of AITL patients; these cells are detectable at an early stage post-diagnosis and potentially play a significant role in disease progression. Nevertheless, whether EBV status affects the prognosis of AITL is controversial (9–11). PET-CT is commonly used for tumor diagnosis and efficacy assessment, and studies have indicated that the tumor load at diagnosis has prognostic significance (12, 13). Spleen involvement has been shown to be an adverse prognostic factor in other lymphoma subtypes (14); however, whether splenomegaly is an independent poor prognostic factor for AITL remains uncertain.

Researchers have proposed several prognostic models for AITL, but their clinical utility remains controversial. For example, the Prognostic Index for PTCL-NOS (PIT) and its modified version (m-PIT) are primarily designed for PTCL-NOS, which exhibits distinct clinical and genetic characteristics from AITL. PIT incorporates age, performance status, lactate dehydrogenase (LDH), and bone marrow involvement, while the m-PIT replaces bone marrow invasion with a Ki-67 index of ≥80%. The Prognostic Index for AITL (PIAI) and AITL score were developed specifically for AITL. PIAI included (15), for the first time, extranodal involvement≥ 2, thrombocytopenia, and B symptoms, in addition to age >60 years and ECOG >2. However, PIAI only categorizes patients into two risk strata. The AITL score, proposed in the T-cell Project (TCP), has been validated in a limited dataset of 96 patients (16). Given the limitations of existing models, there is an urgent need for AITL-specific prognostic models capable of accurately identifying high-risk patients and assisting clinical decision-making. Therefore, the objective of this study was to further characterize the clinical features of AITL and identify critical prognostic factors at the time of diagnosis.

2 Materials and methods

2.1 Patients

For this study, 231 patients diagnosed with AITL between 2014-01-01 and 2023-07-01 at the First Affiliated Hospital of Zhengzhou University were enrolled. Clinical data were retrospectively analyzed, including clinical symptoms, laboratory findings, pathology, bone marrow involvement, treatments, and survival outcomes. The cohort comprised 155 males and 76 females, with a median age of 63 years (range, 26–94 years). Of these, 204 patients (88.3%) were classified as stage III/IV. Inclusion criteria were as follows: (1) pathologically confirmed diagnosis of AITL according to the World Health Organization (WHO) classification and (2) available clinical data, including baseline information for staging, treatment regimens, efficacy evaluation, and follow-up. Exclusion criteria were as follows: (1) acute myocardial infarction or cerebral infarction within 6 months; (2) uncontrolled hypertension and symptomatic arrhythmia; and (3) pregnancy or lactation. This study was approved by the Medical Ethics Committee of the First Affiliated Hospital of Zhengzhou University, Henan Province (2022-KY-0869-001) and patients provided informed consent.

In our cohort, patients were primarily treated with CHOP-like chemotherapy regimens, while other common regimens included those containing gemcitabine or epigenetic drugs. These chemotherapeutic regimens were administered according to standard protocols regarding dose, timing, duration, and cycle (17–19).

2.2 Statistical analysis

A retrospective analysis of the cohort (n=231) was conducted to characterize the clinicopathologic features and identify prognostic factors for proposing a new prognostic model. The primary end points of the study were OS and PFS, which were calculated using the log-rank test and Kaplan–Meier survival curves. ROC analysis was used to determine the ideal critical values for PET/CT metabolic parameters (SUVmax). To identify the prognostic factors, univariate and multivariate analyses were performed using Cox proportional hazards regression models. Significant covariates (with $p < 0.05$) were incorporated into the multivariate analyses.

3 Results

3.1 Clinicopathological features of patients with AITL

Table 1 summarizes the clinical characteristics of 231 patients with AITL. The median age was 63 years (range 26–49). Most patients were male (67.1%). A total of 88.3% (204/231) of patients presented with advanced-stage disease (III/IV), while 58.9% (136/231) and 9.5% (22/231) had splenomegaly and hepatomegaly, respectively. Additionally, extranodal involvement at two or more sites was observed in 19.9% (46/231) of patients, and bone marrow involvement was noted in 27.9% (64/229). Furthermore, rash occurred in 16.9% (39/231), joint pain in 5.2% (12/231), and serous cavity effusion in 51.9% (120/231) of patients. Peripheral blood EBV-DNA ≥500 copies/mL was detected in 42.2% (54/128) patients. EBER- status were detected by ISH in 203 patients, with 65.5% (103/203) expressing EBV-infected B cells (EBER+).

TABLE 1 Clinicopothological features of 231 patients with AITL.

		OS		OS	
		Univariate analysis		Multivariate analysis	
Variables	N(%)	P	HR(95%CI)	P	HR(95%CI)
Age, median (range)	63(26–94)				
Age>60 years	131/231(56.7%)	0.005	1.599(1.151,2.221)	0.024	2.321(1.117,4.825)
Male	155/231(67.1%)	0.137	1.305(0.919,1.854)		
Stage III~IV	204/231(88.3%)	0.127	1.537(0.885,2.670)		
ECOG≥2	79/231(34.2%)	0.000	1.931(1.384,2.694)	0.044	2.443(1.026,5.815)
B symptoms	150/231(64.9%)	0.203	1.248(0.887,1.756)		
WBC<10000/mm^3	42/231(18.2%)	0.496	1.147(0.772,1.705)		
Platelets<100000/mm^3	43/231(18.6%)	0.148	1.357(0.897,2.053)		
Anemia	142/231(61.5%)	0.021	1.459(1.058,2.010)	0.559	0.800(0.378,1.691)
NLR<4.635	119/231(51.5%)	0.029	1.429(1.038,1.967)	0.187	0.597(0.278,1.283)
LDH>ULN	144/221(65.2%)	0.001	1.880(1.295,2.728)	0.049	2.560(1.005,6.516)
Alb<3.5 g/dL	108/230(47.0%)	0.001	1.747(1.263,2.416)	0.261	1.524(0.732,3.173)
Hypergammaglobulinemia	75/228(32.9%)	0.310	1.192(0.849,1.675)		
β2M>ULN	131/207(63.3%)	0.000	1.997(1.372,2.906)	0.317	0.590(0.209,1.660)
Eosinophil<0.02	193/231(83.5%)	0.000	0.487(0.328,0.723)	0.461	1.561(0.478,5.102)
Extranodal sites≥2	46/231(19.9%)	0.460	1.141(0.804,1.619)		
Bone marrow involvement	64/229(27.9%)	0.154	1.304(0.905,1.877)		
Pneumonia	199/231(86.1%)	0.532	1.166(0.720,1.888)		
Splenomegaly	135/231(58.4%)	0.022	1.470(1.057,2.043)	0.013	3.117(1.267,7.664)
Hepatomegaly	22/230(9.6%)	0.331	1.285(0.775,2.132)		
Rash	39/231(16.9%)	0.382	1.199(0.798,1.801)		
Joint pain	12/230(5.2%)	0.434	1.309(0.667,2.571)		
Serous cavity effusion	120/231(52.4%)	0.024	1.453(1.051,2.008)	0.284	1.495(0.717,3.117)
Ki67>45%	55/230(23.9%)	0.005	1.726(1.181,2.522)	0.792	0.894(0.388,2.058)
SUVmax>12	81/138(58.7%)	0.036	1.628(1.032,2.569)	0.183	1.716(0.775,3.801)
CD20+	124/225(55.1%)	0.026	0.686(0.493,0.955)	0.087	0.557(0.285,1.089)
CD30+	102/111(91.9%)	0.987	0.995(0.536,1.845)		
DBIL>6.8	52/231(22.5%)	0.002	1.782(1.236,2.569)	0.346	0.637(0.249,1.628)
EBER-ISH	133/203(65.5%)	0.983	1.004(0.699,1.442)		
EBV-DNA ≥500 copies/mL	54/128(42.2%)	0.011	1.763(1.141,2.726)	0.803	0.899(0.390,2.074)

NLR, neutrophil to lymphocyte ratio; SUVmax: standard uptake value of lymph node in PET-CT. ULN: Upper limit of normal. LDH >ULN: the elevated LDH, LDH >245 IU/L. Splenomegaly: the long diameter of the spleen >12 cm on US or CT, the vertical diameter of spleen >13 cm on PET/CT. β2M: β2 microglobulin.

3.2 Treatment regimens and outcome

Among the cohort, 100 patients (43.2%) received anthracycline-containing chemotherapy (CHOP-like), including CHOP (n = 53), CHOPE (n = 11), and other anthracycline-based regimens. Forty-three patients (18.6%) received GDP-like regimens (e.g., GDP, GDPT), while 40 patients (30.7%) were treated with epigenetic-modifying therapies (PET-like), including PET (n=9) and CPET (n=31) regimens. Compared with CHOP-like regimens, PET-like and GDP-like did not improve the outcomes (all P > 0.05, Table 2). To assess the efficacy of anthracyclines, epigenetic agents, and gemcitabine, we categorized all patients into an anthracyclines (n=100) and non-anthracyclines (n=110) group; epigenetic (n=71) and non-epigenetic (n=139) group; and gemcitabine

10.3389/fimmu.2024.1481301

TABLE 2 Common chemotherapeutic regimens in patients with AITL in the cohort.

Characteristics		N	P value (OS)	P value (PFS)
Category 1	CHOP-like	100	0.589	0.435
	GDP-like	43		
Category 2	CHOP-like	100	0.482	0.754
	PET-like	40		
Category 3	GDP-like	43	0.818	0.708
	PET-like	40		
Category 4	CHOP	53	0.545	0.943
	CHOPE	11		
Category 5	Epigenetics	71	0.743	0.705
	Non-epigenetics	139		
Category 6	Anthracycline	100	0.681	0.891
	Non-anthracycline	110		
Category 7	Gemcitabine	51	0.985	0.941
	Non-gemcitabine	159		

CHOP, Cyclophosphamide + Hydroxydoxorubicin + Oncovin + Prednisone; CHOPE, CHOP + Etoposide; GDP, Gemcitabine + Cisplatin+ Dexamethasone; GDPT, GDP + Thalidomide; PET, Prednisone + Etoposide + Thalidomide; CPET, Cedaramine + Prednisone + Etoposide + Thalidomide.

(n=51) and non-gemcitabine (n=159) group. Additionally, 21 patients (9.1%) received only symptomatic treatment post-diagnosis. Only 9 patients underwent consolidative autologous stem cell transplantation (ASCT).

Among the 231 patients in this study, there were 121 deaths recorded, with 102 of these deaths occurring within the first year after diagnosis. The median follow-up duration was 42 months (range, 1–135 months). The 3- and 5-year OS rates for the entire group were 37.7%, and 26.6%. The 3–, and 5–year PFS rates were 21.1% and 11.9%, respectively. The median PFS and OS were 6 and 17 months, respectively (Figure 1). In patients treated with CHOP-like therapy, the median PFS and OS were 7 and 20 months, respectively, with 5-year PFS and OS rates of 12.3% and 26.2% (Figure 2). For patients who received anthracycline-containing chemotherapy regimens with or without etoposide, there was no significant difference in OS and PFS (Table 2). Notably, there was no significant difference in OS or PFS among patients treated with anthracycline-, gemcitabine- or epigenetic agent- containing regimens (all P>0.05). Additionally, there was no significant difference in OS or PFS between patients treated during the periods 2014-2018 (n=77) and 2019-2023 (n=154; Figure 3).

3.3 Prognostic index

The prognostic value of the PIT, m-PIT, PIAI, and AITL score were assessed in this study. Patients were categorized into 4 risk groups based on PIT, 3 risk groups based on AITL score and m-PIT, and 2 risk groups based on PIAI (Table 3). Patients classified as high-risk based on PIT (27.5%, 60/218), m-PIT (21.2%, 47/222), PIAI (66.2%, 153/231), and AITL scores (42.6%, 75/176) had 4-year PFS estimates of 6.6%, 6.4%,11.5% and 3.9%, respectively, and 4-year OS estimates of 22.3%, 23.8%, 26.2% and 22.3%, respectively (all P < 0.05).

Among the patient groups stratified by PIT (Figures 4A, B), there was no significant difference observed in OS and PFS between the low-risk and low-int risk group (P=0.226 and P=0.770). The m-PIT effectively discriminates only between low-risk groups (Figures 4C, D), with no significant difference found between int-risk and high-risk groups (P=0.955). Patients were stratified into only low- and high-risk groups based on PIAI (Figures 4E, F), with a significant difference observed between the two groups. The 2-year OS showed little numerical difference between the groups (low risk: 50.0% vs. highrisk: 40.7%), as did the 2-year PFS rates (low-risk: 32.7% vs. high-risk: 21.8%). The AITL score was predictive of PFS, although distinguishing the int-risk group from the other two cohorts in terms of OS according to the AITL score was challenging (Figure 4H). Even for PFS (Figure 4G), there was no significant difference between the int-risk and high risk group. These findings underscore the urgent need for a more finely stratified prognostic model capable of predicting both OS and PFS.

In the univariate analysis, factors associated with inferior OS included age >60 years, ECOG performance status ≥ 2, anemia, NLR2 < 4.635, elevated β2M, elevated LDH, Alb < 3.5 g/dL, eosinophil < 0.02, DBIL > 6.8, hepatomegaly, serous cavity effusion, SUVmax > 12, *Ki-67* >45%, and CD20+ and EBV-DNA ≥ 500 copies/mL (Table 1). The multivariate analysis showed that only the following 4 factors retained independent prognostic value for OS: age >60 years, ECOG ≥2, elevated LDH and splenomegaly. Based on these 4 factors, we developed a novel prognostic score (AITL model) that stratified patients into low- (score between 0 and 1), intermediate-(score between 2 and 3), and high -risk (score 4). Patients classified as low-, intermediate-, and high-risk based on the AITL model had 2-year PFS estimates of 42.4%, 23.4%, and 0%, respectively (P<0.05,

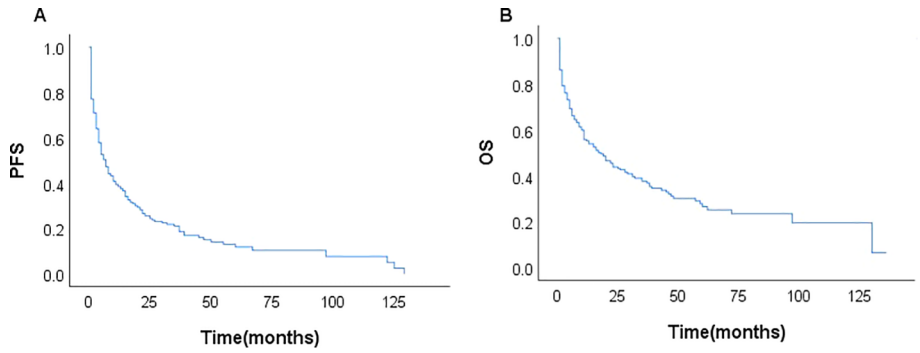

FIGURE 1
Kaplan–Meier curves of the entire study cohort (n=231); PFS **(A)** and OS **(B)**.

Figure 5A) and 2-year OS estimates of 63.6%, 42.1%, and 18.6%, respectively (P<0.05, Figure 5B). The new model (AITL model) therefore demonstrated predictive ability for both OS and PFS, with improved discriminatory power relative to previous models.

We additionally evaluated pathological features and imaging indices as possible prognostic factors, including CD20, CD30+, EBER - ISH, Ki-67 index, and SUVmax of the lymph node. In the univariate analysis, Ki-67 index > 45% (p = 0.005), CD20+ (P=0.026), and SUVmax of lymph node >12 (P=0.036) significantly influenced OS. However, in multivariate analysis, neither factor was found to be independent prognostic factor for OS. Table 4 shows the adverse prognostic factors included in the AITL model and other models.

4 Discussion

AITL, the most common subtype of lymph node TFH lymphoma, is characterized by the specific expression of TFH markers such as CD10, BCL6, PD-1, CXCL13 and ICOS. Patients with AITL frequently harbor alterations in epigenetic genes such as *TET2*, *DNMT3A*, *IDH2*, and *RHOA* (20). The pathogenesis of AITL is complex, involving close interactions between tumor cells, the immune microenvironment, and EBV (21). It is hypothesized that dysregulation of the immune microenvironment and EBV infection contribute to immune escape and promote the survival of infected cells, thereby driving disease progression (11, 22). AITL occurs more frequently in older men, with a median age of 63 years. The majority of patients (88.3%) presented with advanced-stage disease (III/IV) at the time of diagnosis. Patients often present with systemic lymphadenomegaly due to immune dysregulation. Extranodal involvement is not uncommon in AITL, with 19.9% of patients in our cohort having extranodal involvement at more than two extranodal sites. Bone marrow involvement was present in 27.9% of patients, and 58.4% had splenic involvement.

Most patients (43.3%) were treated with CHOP-like regimens, and only 4.8% received CHOPE regimens, likely because of the older age of patients in our cohort. Consistent with prior reports (23), the addition of etoposide in our study did not improve the OS and PFS (P=0.545 and P=0.943, respectively), indicating that intensive regimens may not improve the prognosis of patients with AITL. In recent years, epigenetic-modifying therapies and gemcitabine-based chemotherapy have been explored in several studies for PTCL with the aim of improving clinical outcomes in untreated patients (17, 24, 25). Epigenetic drugs have demonstrated favorable short-term effects and longer duration of response in AITL (26, 27). Furthermore, the efficacy of chidamide in combination with PET regimens (CPET) has been evaluated in several clinical trials (18), further supporting the higher mutation frequency of *TET2* and *DNMT3A* in AITL. In our study, 71 patients with untreated AITL received epigenetic drugs in combination

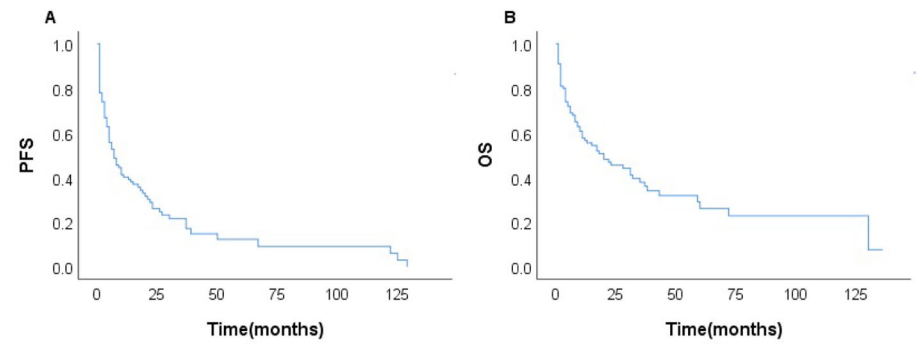

FIGURE 2
Survival of the patients with AITL treated with CHOP-like regimens (n=100); PFS **(A)** and OS **(B)**.

10.3389/fimmu.2024.1481301

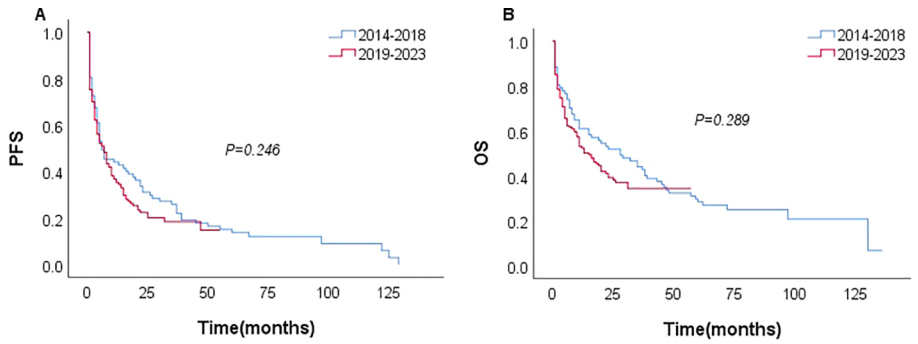

FIGURE 3
Survival at different periods (n=231); PFS **(A)** and OS **(B)**.

with chemotherapy; however, no significant difference in OS and PFS with or without epigenetic drugs (P=0.743 and P=0.704, respectively) was observed. We also found no significant benefit from PET-like regimens compared with CHOP-like regimens in AITL patients. A small proportion of patients (43 cases) were treated with gemcitabine-based chemotherapy. Consistent with previous studies (28, 29), the gemcitabine- based regimen was not superior to CHOP as front-line therapy in patients with untreated AITL in our study. Only 9 patients in our study underwent consolidative ASCT, and no patients were treated with brentuximab vedotin, which may partly reflect the older age and economic constraints of our cohort. Although new therapies, including chidamide, azacitidine, and gemcitabine, offer more treatment options for patients with AITL, we did not observe significant differences in outcomes. The efficacy of CHOP+X and ASCT after first remission for patients with AITL still needs further investigation.

The prognosis of patients with AITL is dismal. Our study analyzed the prognosis of a large retrospective AITL cohort, with 5year OS and PFS estimates of 26.6% and 11.9%, respectively. The outcomes were slightly different to those reported in a large

TABLE 3 Comparison of established prognostic indices.

Prognostic index	N(%)	2-y OS	4-y OS	2-y PFS	4-y PFS
PIT					
Low-risk (0)	24/218 (11.0)	73.7	56.1	45.1	32.9
low-int risk (1)	64/218 (29.4)	60.5	37.2	43.8	28.2
High-int risk (2–3)	70/218 (32.1)	39.6	20.6	20.1	3.3
High-risk (3–4)	60/218 (27.5)	22.3	22.3	6.6	6.6
m-PIT					
Low-risk (0–1)	110/222 (49.5)	57.7	38.5	36.5	23.5
Int-risk (2)	65/222 (29.3)	35.0	21.6	16.8	5.6
High-risk (3–4)	47/222 (21.2)	27.8	23.8	12.8	6.4
PIAI					
Low-risk (0–1)	78/231 (33.8)	50.0	37.3	32.7	21.9
High-risk (2–5)	153/231 (66.2)	40.7	26.2	21.8	11.5
AITL score					
Low-risk (0–1)	42/176 (23.9)	65.9	37.1	39.0	24.8
Int-risk (2)	59/176 (33.5)	45.1	30.1	21.6	13.7
High-risk (3–4)	75/176 (42.6)	34.1	22.3	20.3	3.9
AITL model					
Low-risk (0–1)	68/221 (30.8)	63.6	49.8	42.4	29.8
Int-risk (2–3)	123/221 (55.7)	42.1	25	23.4	10.7
High-risk (4)	30/221 (13.6)	18.6	18.6	0	0

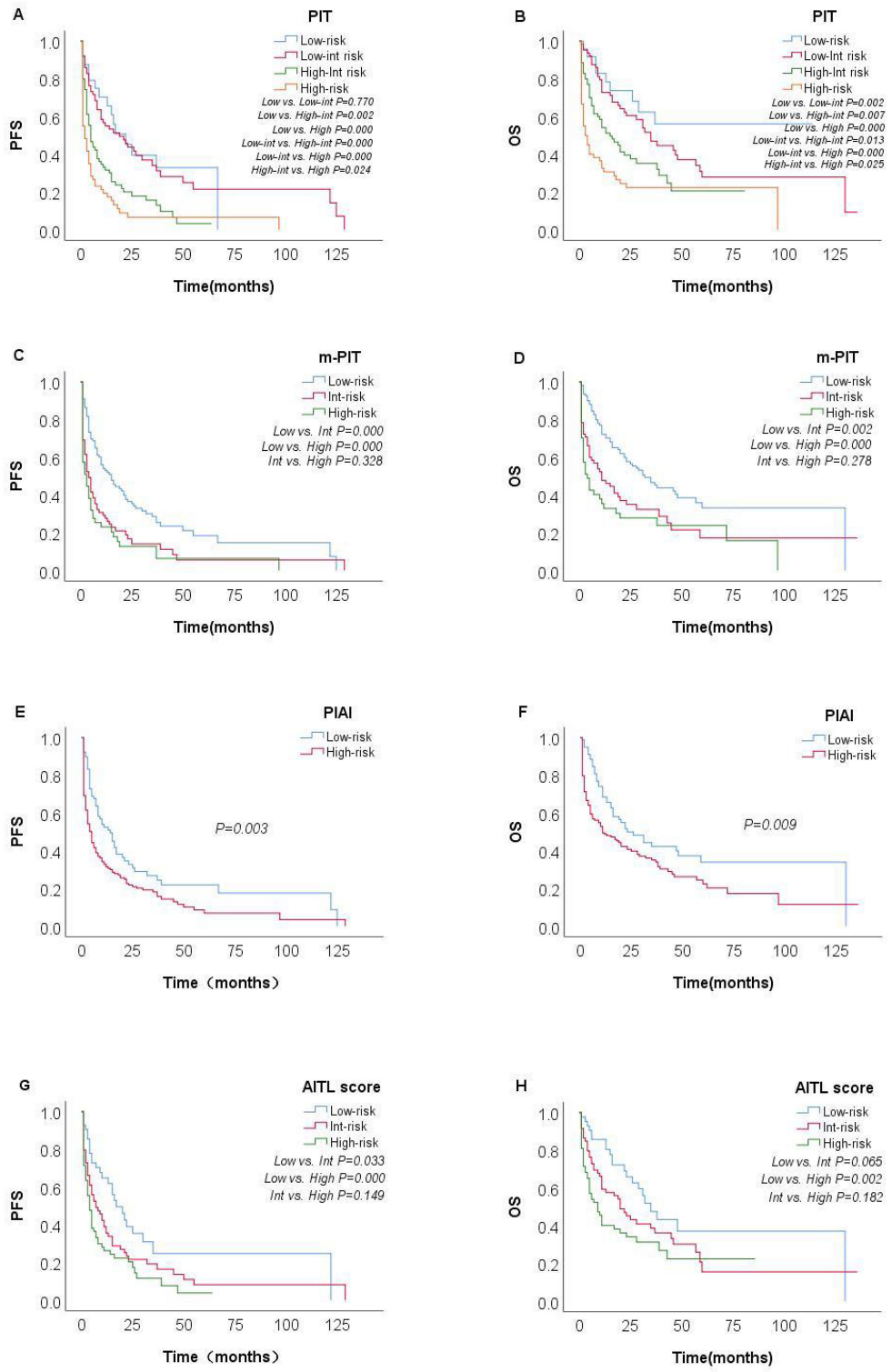

FIGURE 4
Survival probabilities of the overall AITL cohort. Kaplan–Meier curves show PFS and OS in patients with AITL stratified by PIT [**(A, B)** n=218], m-PIT [**(C, D)** n=222], PIAI [**(E, F)** n=231], and AITL score [**(G, H)** n=176].

population-based study from the Swedish Lymphoma Registry (5-year OS and PFS estimates of 32% and 20%, respectively) (30), confirming adverse clinical outcomes. Although the majority of patients with AITL were sensitive to chemotherapy, the response duration was typically brief, and frequent relapses led to a low survival rate. We also found that nearly two-thirds (151 cases) of patients experienced disease progression within 12 months. The identification of reliable prognostic indicators is crucial for selecting appropriate treatment regimens, and there is an urgent need for prognostic models that can specifically stratify AITL.

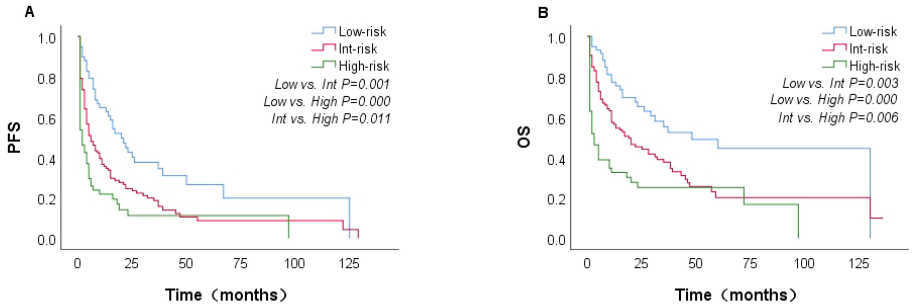

FIGURE 5
Kaplan–Meier curves showing PFS and OS in patients with AITL, stratified by the AITL model (n=221). PFS **(A)** and OS **(B)**.

To date, few studies have explored prognostic factors in AITL. Our study validated the predictive value of the PIT, m-PIT, PIAI, and AITL score. PIT (31)is a prognostic model specific to PTCL-NOS. Went et al. (32) proposed m-PIT after considering pathological factors, and reported that m-PIT outperformed PIT in terms of prognostic prediction. The clinical characteristics and genetic background of AITL differ significantly from those of PTCL-NOS, and the prognostic model developed for PTCL-NOS is not applicable to AITL (33). The PIAI was also validated in our cohort ($P < 0.05$). However, it was only categorized into two groups, namely, low-risk and high-risk, with the 2-year OS (50.0% vs 40.7%) and PFS (32.7% vs 21.8%) between the two groups being numerically close. Moreover, this classification approach exhibited limitations in accurately stratifying high-risk patients based on their risk scores. Ranjana H (16) proposed the AITL score and identified β2M and CRP as independent prognostic factors for PFS in a limited cohort of 96 patients. This model was not well validated in our cohort, and the int-risk group was not significantly different from the other groups. There have been few follow-up studies for PIAI and AITL score, and these have not yet been widely applied in clinical practice. A recent Asian multicenter study (34) found that age > 60 years, bone marrow involvement, total WBC >12 × 10^9/L, and elevated LDH were associated with inferior outcome in AITL; on this basis, they proposed a new model (AITL-PI). Additionally, the AITLI model (35) was developed based on age >60 years, albumin <30 g/L, Ki-67 rate ≥70%, and a positive Coombs test. Some studies (12, 13, 36) have focused on the importance of metabolic parameters in PET/CT, finding that baseline TLG (total lesion glycolysis), SUVmax of spleen, and SUVmax of extranodal lesions are strong predictors of AITL. However, the number of cases included in these studies was relatively small, and the application of these indicators remains controversial. This further highlights the lack of effective prognostic models for patients with AITL.

We identified age >60 years, ECOG≥2, elevated LDH as independent prognostic factors associated with OS; these have also been recognized as strong influencing factor in previous studies (20, 35). The novel model (AITL model) combining four variables (age >60 years, ECOG≥2, elevated LDH and splenomegaly) stratified patients into low-, intermediate-, and high-risk groups. The AITL model demonstrated strong power of classification based on risk score and good predictive value for both PFS and OS. In a large data cohort of 221 patients, we identified novel prognostic factors and developed a new

TABLE 4 Adverse prognostic factors in AITL.

Adverse prognostic factor	PIT	m-PIT	PIAI	AITL score	AITL model
Age ≥60 y	+	+	+	+	+
ECOG>2	+	+	+	+	+*
LDH>ULN	+	+			+
Stage III-IV					
Extranodal sites≥2			+		
Bone marrow involvement	+				
B symptoms			+		
Splenomegaly					+
Thrombocytopenia (<150 000/mm3)			+		
Ki-67≥80%		+			
CRP>ULN				+	
β2M>ULN				+	

*: ECOG≥2 in AITL model and ECOG>2 in the other 4 models; CRP>ULN: C-reactive protein>5; β2M>ULN: β2M>3.

prognostic model. The 2-year OS was 63.6%, 42.1%, and 18.6% for the low-, intermediate-, and high-risk groups, respectively. The 2-year PFS was 42.4%, 23.4%, and 0%, respectively. Patients classified as high-risk according to the AITL model all experienced disease progression within 2 years. In comparison, the 2-year PFS was 6.6% to 21.8% for patients with high-risk PIT, m-PIT, PIAI, and AITL scores. This indicates that the AITL model has a superior ability to identify patients who are insensitive to chemotherapy or have a short duration of response, showing good discriminatory ability. Lymphoma involvement of the spleen is common, and the lymph nodes and spleen are the most common primary sites of PTCL (37), as predominantly characterized by splenomegaly on imaging. This study comprised a higher percentage of patients with splenomegaly—58.4%, compared with 46.8% in previous studies (2, 18). This discrepancy may be attributable to our inclusion of splenomegaly based on imaging reports (US, CT, PET/CT). PET/CT shows sensitivity in detecting splenic involvement in patients with lymphoma, and some studies have suggested that SUVmax of the spleen can be used as a reference index for determining the prognosis of patients with AITL (14, 36). In conclusion, patients with splenomegaly tended to demonstrate worse OS than those without splenomegaly. The four factors identified in our study are common and practical for use in clinical applications. Our findings suggest that the model can effectively identify high-risk patients with AITL and accurately predict survival outcomes.

Few studies have attempted to identify pathological prognostic factors in AITL. This study sought to evaluate the potential prognostic value of CD20, CD30, and the Ki-67 index. We found that CD20 positivity and Ki-67 >45% were associated with poor OS; however, these factors did not show independent prognostic value for OS in the multivariate analysis. We analyzed PET/CT parameters and found that high lymph node SUVmax (SUVmax >12) was indicative of shorter OS, although not statistically significant (P=0.183). Furthermore, a high EBV viral load at diagnosis was associated with shorter OS and emerged as a key marker of poor prognosis, while positive EBER-ISH did not significantly affect survival, consistent with previous studies (38, 39).

The main limitation of this study is that it is a retrospective analysis. Our cohort spanned 10 years, from 2014 to 2023 (all post-2010, i.e., after FDA approval of romidepsin for disease relapse, reflecting an era of increased use of novel medications). Furthermore, owing to the limitations of the retrospective study itself, the new model was only internally validated. The proposed model still requires further evaluation and validation in prospective or multi-center cohorts. Although the first-line therapy varied among the cohort, there was no significant difference in survival at different periods (2014–2018 vs. 2019–2023).

In conclusion, the long-term outcomes for patients with AITL treated with contemporary chemotherapeutic regimens remain unsatisfactory. In terms of therapeutic outcomes, there was no significant difference between anthracycline- or epigenetic- or gemcitabine-based regimens, highlighting the need for further exploration of standardized therapeutic regimens. Splenomegaly at initial diagnosis was identified as an independent poor prognostic factor for OS. The new model (AITL model) demonstrated strong classification and predictive power for both OS and PFS in patients with AITL.

Data availability statement

The original contributions presented in the study are included in the article/supplementary material. Further inquiries can be directed to the corresponding author.

Ethics statement

This study was approved by the Medical Ethics Committee of the First Affiliat-ed Hospital of Zhengzhou University, Henan Province (2022-KY-0869-001) and patients gave their informed consent. The studies were conducted in accordance with the local legislation and institutional requirements. Written informed consent for participation was not required from the participants or the participants' legal guardians/next of kin in accordance with the national legislation and institutional requirements.

Author contributions

SL: Conceptualization, Formal analysis, Investigation, Writing – review & editing. XF: Formal analysis, Investigation, Methodology, Writing – original draft. YS: Data curation, Project administration, Writing – original draft. MF: Investigation, Software, Writing – original draft. QC: Funding acquisition, Resources, Supervision, Writing – review & editing. MZ: Resources, Supervision, Writing – review & editing. XW: Data curation, Software, Writing – original draft. MD: Data curation, Software, Writing – original draft. JZ: Data curation, Software, Writing – original draft. LH: Data curation, Software, Writing – original draft. XZ: Conceptualization, Funding acquisition, Supervision, Writing – review & editing.

Funding

The author(s) declare financial support was received for the research, authorship, and/or publication of this article. The paper is supported by the Major Medical Scientific and Technological Project of Henan Province (Grant No. SBGJ202001008), the Scientific Research Innovation team of the First Affiliated Hospital of Zhengzhou University Excellent innovation team (ZYCXTD2023004), and the Outstanding Youth Item of Henan Health-related Technological and Innovative Talents Project (Grant No.11459).

Acknowledgments

The authors thank the study participants for the generosity of their time in participating in our study.

Conflict of interest

The authors declare that the research was conducted in the absence of any commercial or financial relationships that could be construed as a potential conflict of interest.

Publisher's note

All claims expressed in this article are solely those of the authors and do not necessarily represent those of their affiliated organizations, or those of the publisher, the editors and the reviewers. Any product that may be evaluated in this article, or claim that may be made by its manufacturer, is not guaranteed or endorsed by the publisher.

References

1. Mohammed Saleh MF, Kotb A, Abdallah GEM, Muhsen IN, El Fakih R, Aljurf M. Recent advances in diagnosis and therapy of angioimmunoblastic T cell lymphoma. *Curr Oncol*. (2021) 28:5480–98. doi: 10.3390/curroncol28060456

2. Huang Y, Zeng R, Xue C, Huang Q, Yu D, Shao L, et al. Involvement of spleen is associated with shorter survival in patients with angioimmunoblastic T cell lymphoma. *J Cancer Res Clin Oncol*. (2023) 149:9721–6. doi: 10.1007/s00432-023-04868-y

3. Yang Z, Jiang S, Lu C, Ji T, Yang W, Li T, et al. Sox11: friend or foe in tumor prevention and carcinogenesis? *Ther Adv Med Oncol*. (2019) 11:1758835919853449. doi: 10.1177/1758835919853449

4. Hu W, Yang Y, Fan C, Ma Z, Deng C, Li T, et al. Clinical and pathological significance of N-Myc downstream-regulated gene 2 (Ndrg2) in diverse human cancers. *Apoptosis*. (2016) 21:675–82. doi: 10.1007/s10495-016-1244-3

5. Cheng J, Guo JM, Xiao BX, Miao Y, Jiang Z, Zhou H, et al. Pirna, the new non-coding rna, is aberrantly expressed in human cancer cells. *Clin Chim Acta Int J Clin Chem*. (2011) 412:1621–5. doi: 10.1016/j.cca.2011.05.015

6. Tang Z, Dong H, Li T, Wang N, Wei X, Wu H, et al. The synergistic reducing drug resistance effect of cisplatin and ursolic acid on osteosarcoma through a multistep mechanism involving ferritinophagy. *Oxid Med Cell Longev*. (2021) 2021:5192271. doi: 10.1155/2021/5192271

7. Guo W, Qiao T, Li T. The role of stem cells in small-cell lung cancer: evidence from chemoresistance to immunotherapy. *Semin Cancer Biol*. (2022) 87:160–9. doi: 10.1016/j.semcancer.2022.11.006

8. Zhang X, Yu S, Li X, Wen X, Liu S, Zu R, et al. Research progress on the interaction between oxidative stress and platelets: another avenue for cancer? *Pharmacol Res*. (2023) 191:106777. doi: 10.1016/j.phrs.2023.106777

9. Wei C, Zhang Y, Wang W, Zhang W, Zhou D. Analysis of clinical characteristics of angioimmunoblastic T-cell lymphoma and the prognostic impact of EBV infection. *J Clin Hematol*. (2021) 34:149–55. doi: 10.13201/j.issn.1004-2806.2021.03.002

10. Eladl AE, Shimada K, Suzuki Y, Takahara T, Kato S, Kohno K, et al. Ebv status has prognostic implication among young patients with angioimmunoblastic T-cell lymphoma. *Cancer Med*. (2020) 9:678–88. doi: 10.1002/cam4.2742

11. Bahri R, Boyer F, Halabi MA, Chaunavel A, Feuillard J, Jaccard A, et al. Epstein-Barr virus (Ebv) is mostly latent and clonal in angioimmunoblastic T cell lymphoma (Aitl). *Cancers*. (2022) 14(12). doi: 10.3390/cancers14122899

12. Hu L, Luo N, Li L, Qiu D, Hu X. A preliminary investigation of the relationship between (18)F-Fdg Pet/Ct metabolic parameters and prognosis in angioimmunoblastic T-cell lymphoma. *Front Oncol*. (2023) 13:1171048. doi: 10.3389/fonc.2023.1171048

13. Wang H, Yu W, Wu T, Xue Y, Zhang D, Xu H. The incremental prognostic value of baseline (18)F-Fdg Pet/Ct imaging in angioimmunoblastic T-cell lymphoma. *BioMed Res Int*. (2020) 2020:4502489. doi: 10.1155/2020/4502489

14. St-Pierre F, Broski SM, LaPlant BR, Ristow K, Maurer MJ, Macon WR, et al. Detection of extranodal and spleen involvement by Fdg-Pet imaging predicts adverse survival in untreated follicular lymphoma. *Am J Hematol*. (2019) 94:786–93. doi: 10.1002/ajh.25493

15. Federico M, Rudiger T, Bellei M, Nathwani BN, Luminari S, Coiffier B, et al. Clinicopathologic characteristics of angioimmunoblastic T-cell lymphoma: analysis of the international peripheral T-cell lymphoma project. *J Clin Oncol*. (2013) 31:240–6. doi: 10.1200/JCO.2011.37.3647

16. Advani RH, Skrypets T, Civallero M, Spinner MA, Manni M, Kim WS, et al. Outcomes and prognostic factors in angioimmunoblastic T-cell lymphoma: final report from the international T-cell project. *Blood*. (2021) 138:213–20. doi: 10.1182/blood.2020010387

17. Sun Y, Li L, Li X, Zhang L, Wang X, Fu X, et al. Outcomes of Gdpt (gemcitabine, cisplatin, prednisone, thalidomide) versus chop in newly diagnosed peripheral T-cell lymphoma patients. *Ther Adv Med Oncol*. (2020) 12:1758835920923829. doi: 10.1177/1758835920923829

18. Wang Y, Zhang M, Song W, Cai Q, Zhang L, Sun X, et al. Chidamide plus prednisone, etoposide, and thalidomide for untreated angioimmunoblastic T-cell lymphoma in a Chinese population: a multicenter phase II trial. *Am J Hematol*. (2022) 97:623–9. doi: 10.1002/ajh.26499

19. Zhu J, Ma J, Union for China Lymphoma Investigators of Chinese Society of Clinical Oncology. Chinese Society of Clinical Oncology (CSCO) diagnosis and treatment guidelines for Malignant lymphoma 2021 (English version). *Chin J Cancer Res (English Version)*. (2021) 33:289–301. doi: 10.21147/j.issn.1000-9604.2021.03.01

20. Wei C, Li W, Qin L, Liu S, Xue C, Ren K, et al. Clinicopathologic characteristics, outcomes, and prognostic factors of angioimmunoblastic T-cell lymphoma in China. *Cancer Med*. (2023) 12:3987–98. doi: 10.1002/cam4.5248

21. Lage LAPC, Culler HF, Reichert CO, da Siqueira SAC, Pereira J. Angioimmunoblastic T-cell lymphoma and correlated neoplasms with T-cell follicular helper phenotype: from molecular mechanisms to therapeutic advances. *Front Oncol*. (2023) 13:1177590. doi: 10.3389/fonc.2023.1177590

22. Bayda N, Tilloy V, Chaunavel A, Bahri R, Halabi MA, Feuillard J, et al. Comprehensive Epstein-Barr virus transcriptome by RNA-sequencing in angioimmunoblastic T cell lymphoma (Aitl) and other lymphomas. *Cancers*. (2021) 13(4). doi: 10.3390/cancers13040610

23. Deng S, Lin S, Shen J, Zeng Y. Comparison of chop vs chope for treatment of peripheral T-cell lymphoma: a meta-analysis. *Onco Targets Ther*. (2019) 12:2335–42. doi: 10.2147/OTT.S189825

24. Li L, Duan W, Zhang L, Li X, Fu X, Wang X, et al. The efficacy and safety of gemcitabine, cisplatin, prednisone, thalidomide versus chop in patients with newly diagnosed peripheral T-cell lymphoma with analysis of biomarkers. *Br J Haematol*. (2017) 178:772–80. doi: 10.1111/bjh.14763

25. Rai S, Kim WS, Ando K, Choi I, Izutsu K, Tsukamoto N, et al. Oral HDAC inhibitor tucidinostat in patients with relapsed or refractory peripheral T-cell lymphoma: phase IIb results. *Haematologica*. (2023) 108:811–21. doi: 10.3324/haematol.2022.280996

26. Lemonnier F, Dupuis J, Sujobert P, Tournillhac O, Cheminant M, Sarkozy C, et al. Treatment with 5-azacytidine induces a sustained response in patients with angioimmunoblastic T-cell lymphoma. *Blood*. (2018) 132:2305–9. doi: 10.1182/blood-2018-04-840538

27. Falchi L, Ma H, Klein S, Lue JK, Montanari F, Marchi E, et al. Combined oral 5-azacytidine and Romidepsin are highly effective in patients with PTCL: a multicenter phase 2 study. *Blood*. (2021) 137:2161–70. doi: 10.1182/blood.2020009004

28. Jia B, Hu S, Yang J, Zhou S, Liu P, Qin Y, et al. Comparison of gemcitabin, cisplatin, and dexamethasone (Gdp), chop, and chope in the first-line treatment of peripheral T-cell lymphomas. *Hematology*. (2016) 21:536–41. doi: 10.1080/10245332.2016.1152084

29. Gleeson M, Peckitt C, To YM, Edwards L, Oates J, Wotherspoon A, et al. Chop versus Gem-P in previously untreated patients with peripheral T-cell lymphoma (chemo-T): a phase 2, multicentre, randomised, open-label trial. *Lancet Haematol*. (2018) 5:e190–200. doi: 10.1016/S2352-3026(18)30039-5

30. Ellin F, Landström J, Jerkeman M, Relander T. Real-world data on prognostic factors and treatment in peripheral T-cell lymphomas: a study from the Swedish lymphoma registry. *Blood*. (2014) 124:1570–7. doi: 10.1182/blood-2014-04-573089

31. Gallamini A, Stelitano C, Calvi R, Bellei M, Mattei D, Vitolo U, et al. Peripheral T-cell lymphoma unspecified (Ptcl-U): a new prognostic model from a retrospective multicentric clinical study. *Blood*. (2004) 103:2474–9. doi: 10.1182/blood-2003-09-3080

32. Went P, Agostinelli C, Gallamini A, Piccaluga PP, Ascani S, Sabattini E, et al. Marker expression in peripheral T-cell lymphoma: a proposed clinical-pathologic prognostic score. *J Clin Oncol*. (2006) 24:2472–9. doi: 10.1200/JCO.2005.03.6327

33. Lee YP, Yoon SE, Cho J, Ko YH, Jo H, Kim SJ, et al. Comprehensive comparison of international prognostic indexes for follicular helper T-cell lymphoma. *Ann Hematol*. (2022) 101:1535–43. doi: 10.1007/s00277-022-04805-y

34. Chang EWY, Yang VS, Ong SY, Kang HX, Lim BY, de Mel S, et al. Clinical features and prognostic outcomes of angioimmunoblastic T cell lymphoma in an Asian multicenter study. *Leuk Lymphoma*. (2023) 64:1782–91. doi: 10.1080/10428194.2023.2235043

35. Huang C, Zhang H, Gao Y, Diao L, Liu L. Development of a novel clinical prognostic model for patients with angioimmunoblastic T-cell lymphoma. *Technol Cancer Res Treat*. (2020) 19:1533033820964231. doi: 10.1177/1533033820964231

36. Gong HY, Ding ZY, Hu Y, Tang LJ. Prognostic value of splenic SUVmax in pretreatment angioimmunoblastic T-cell lymphoma (18)F-FDG PET/CT. *J Clin Oncol*. (2021) 26:1004–10. doi: 10.3969/j.issn.1009-0460.2021.11.008

37. Davis O, Truong D, Day S, Pandey M, Ibrahimi S, Khawandanah M, et al. Impact of primary organ site of involvement by peripheral T-cell lymphoma not otherwise specified on survival. *Cancer Med*. (2023) 12:21770–8. doi: 10.1002/cam4.6743

38. Liang JH, Lu L, Zhu HY, Li W, Fan L, Li JY, et al. The prognostic role of circulating Epstein-Barr virus DNA copy number in angioimmunoblastic T-cell lymphoma treated with dose-adjusted epoch. *Cancer Res Treat*. (2019) 51:150–7. doi: 10.4143/crt.2017.476

39. Chen Y, Zheng X, Chen B, Yang X, Zheng J, Zheng Z, et al. The clinical significance of Epstein-Barr virus DNA in peripheral blood mononuclear cells in patients with non-Hodgkin lymphoma. *Leuk Lymphoma*. (2017) 58:2349–55. doi: 10.1080/10428194.2017.1300894

frontiers | Frontiers in Oncology

TYPE Original Research
PUBLISHED 17 October 2024
DOI 10.3389/fonc.2024.1473048

Check for updates

OPEN ACCESS

EDITED BY
Xiaosheng Tan,
Rutgers, United States

REVIEWED BY
Zilu Chen,
Rutgers, The State University of New Jersey, United States
Ying Yang,
Karolinska Institutet (KI), Sweden

*CORRESPONDENCE
Xin Jin
drjinxin1991@outlook.com

RECEIVED 30 July 2024
ACCEPTED 20 September 2024
PUBLISHED 17 October 2024

CITATION
Fu C, Qiu D, Zhou M, Ni S and Jin X (2024) Characterization of ligand-receptor pair in acute myeloid leukemia: a scoring model for prognosis, therapeutic response, and T cell dysfunction. *Front. Oncol.* 14:1473048. doi: 10.3389/fonc.2024.1473048

COPYRIGHT
© 2024 Fu, Qiu, Zhou, Ni and Jin. This is an open-access article distributed under the terms of the Creative Commons Attribution License (CC BY). The use, distribution or reproduction in other forums is permitted, provided the original author(s) and the copyright owner(s) are credited and that the original publication in this journal is cited, in accordance with accepted academic practice. No use, distribution or reproduction is permitted which does not comply with these terms.

Characterization of ligand-receptor pair in acute myeloid leukemia: a scoring model for prognosis, therapeutic response, and T cell dysfunction

Chunlan Fu[1], Di Qiu[1], Mei Zhou[1], Shaobo Ni[1] and Xin Jin[2]*

[1]Department of Hematology, Zhuji Affiliated Hospital of Wenzhou Medical University, Zhuji, Zhejiang, China, [2]Department of Breast Surgery, Zhuji Affiliated Hospital of Wenzhou Medical University, Zhuji, Zhejiang, China

Introduction: The significance of ligand-receptor (LR) pair interactions in the progression of acute myeloid leukemia (AML) has been the focus of numerous studies. However, the relationship between LR pairs and the prognosis of AML, as well as their impact on treatment outcomes, is not fully elucidated.

Methods: Leveraging data from the TCGA-LAML cohort, we mapped out the LR pair interactions and distinguished specific molecular subtypes, with each displaying distinct biological characteristics. These subtypes exhibited varying mutation landscapes, pathway characteristics, and immune infiltration levels. Further insight into the immune microenvironment among these subtypes revealed disparities in immune cell abundance.

Results: Notably, one subtype showed a higher prevalence of CD8 T cells and plasma cells, suggesting increased adaptive immune activities. Leveraging a multivariate Lasso regression, we formulated an LR pair-based scoring model, termed "LR.score," to classify patients based on prognostic risk. Our findings underscored the association between elevated LR scores and T-cell dysfunction in AML. This connection highlights the LR score's potential as both a prognostic marker and a guide for personalized therapeutic interventions. Moreover, our LR.score revealed substantial survival prediction capacities in an independent AML cohort. We highlighted CLEC11A, ICAM4, ITGA4, and AVP as notably AML-specific.

Discussion: qRT-PCR analysis on AML versus normal bone marrow samples confirmed the significant downregulation of CLEC11A, ITGA4, ICAM4, and AVP in AML, suggesting their inverse biomarker potential in AML. In summary, this study illuminates the significance of the LR pair network in predicting AML prognosis, offering avenues for more precise treatment strategies tailored to individual patient profiles.

KEYWORDS

Ligand-receptor, Acute Myeloid Leukemia, prognosis, therapeutic response, T cell

Introduction

Acute Myeloid Leukemia (AML) is a hematological malignancy characterized by the rapid growth of abnormal myeloid progenitor cells in the bone marrow and peripheral blood, accounting for approximately 20% of leukemia cases in adults (1), with a high degree of clinical and molecular heterogeneity. The prognosis for AML varies widely depending on factors such as age, cytogenetic abnormalities, and molecular mutations, with older patients and those experiencing relapse generally having poorer outcomes (2–5).

Recent advances in high-throughput sequencing technologies have significantly enhanced our understanding of the genetic and epigenetic landscapes of AML (6–8). These include mutations in genes such as NPM1, FLT3, DNMT3A, IDH1, and IDH2, which are frequently observed in AML and are associated with distinct clinical outcomes. Molecular classifiers have been developed to categorize AML patients into risk-specific subgroups, including cytogenetically normal AML (CN-AML), core-binding factor AML (CBF-AML), and subgroups defined by specific mutations like FLT3-ITD or IDH mutations (9–13). These classifications have proven valuable in predicting prognosis and guiding therapeutic decisions. Despite these advances, the prognosis for AML remains relatively poor, particularly in older patients and those who relapse post-treatment.

Despite these advances, AML remains a challenging disease to treat, particularly due to its complex tumor microenvironment (TME). The TME in AML is composed of a variety of cell types, including leukemic cells, stromal cells, immune cells, and the extracellular matrix, all of which interact to influence disease progression and response to therapy (14–16). The interactions between leukemic cells and their surrounding stroma are mediated by a network of ligand-receptor (LR) pairs that facilitate cell-cell communication, migration, and survival. While individual LR pairs, such as CXCL12/CXCR4, have been studied extensively in AML, the broader network of LR interactions and its impact on disease biology remains poorly understood.

In this study, we employed advanced computational approaches to map the LR pair interaction network in AML and to correlate these interactions with clinical outcomes. By analyzing transcriptomic data from large AML cohorts, we identified three distinct molecular subtypes characterized by unique LR pair-related gene signatures. These subtypes exhibit different mutation landscapes, pathway activation profiles, and levels of immune cell infiltration. Our LR pair-based scoring system, LR.score, demonstrated significant potential in predicting patient responses to both traditional chemotherapy and emerging targeted therapies, with a particular emphasis on its association with T-cell dysfunction and the downregulation of specific markers such as CLEC11A, ICAM4, ITGA4, and AVP in AML. These findings provide new insights into the complexity of cell-cell communication in AML and offer a robust framework for developing personalized treatment strategies tailored to the molecular characteristics of individual patients.

Materials and methods

Data acquisition and processing

We sourced clinical and RNA-Seq data specific to Acute Myeloid Leukemia (AML) from the TCGA dataset, accessible through the UCSC Xena portal (https://xenabrowser.net). Each tumor's gene expression data was aligned with the human hg38 genome annotation. For subsequent analyses, we converted the gene expression measurements to Transcripts Per Kilobase Million (TPM) followed by log2 transformation ([TPM] + 1). We excluded samples that were missing either gene expression details or clinical annotations, resulting in a primary cohort of 142 AML patients. For our validation efforts, we turned to two public datasets: GSE37642 (17–20) and GSE12417 (21, 22). We incorporated only the primary AML samples with available clinical details and normalized gene expression metrics. We omitted probes without gene annotation, and for genes associated with multiple probes, the median expression was determined. This process led to the creation of validation sets with 417 and 163 AML samples, respectively. Additionally, we integrated 2293 Ligand-Receptor (LR) pairs from the connectome DB2020 database (23) detailed in (Supplementary Table S1). A schematic outline of our research methodology is presented in (Figure 1A).

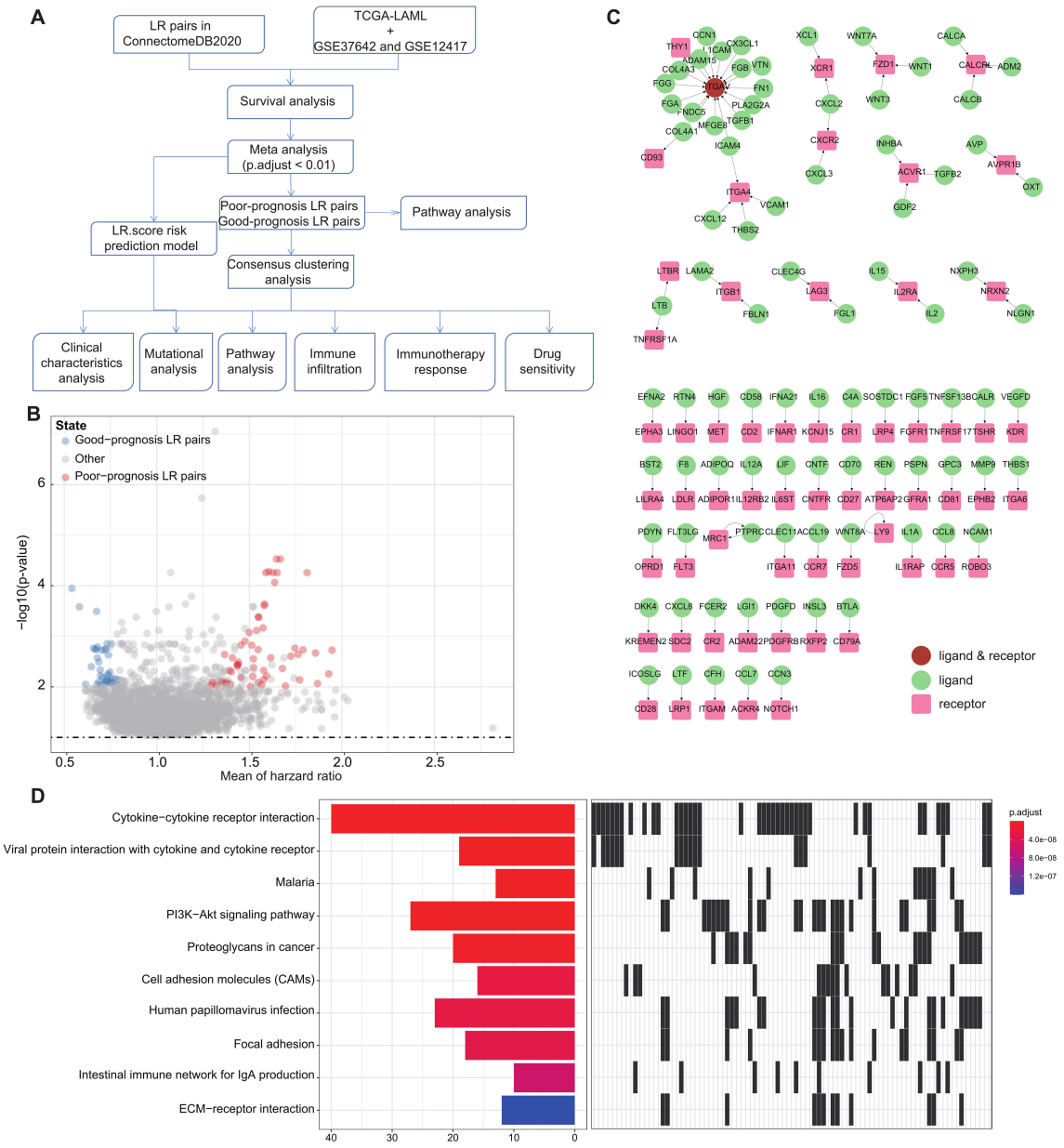

FIGURE 1
LR pairs with prognostic significance **(A)**. Overview of the study's workflow **(B)**. Volcano plot representations highlight LR pairs with significant prognostic implications. LR genes associated with favorable prognosis are denoted in red, while those linked to poor prognosis are illustrated in blue **(C)**. Network visualization of the significant prognostic LR pairs, with receptors showcased in red and ligands in green **(D)**. The top ten enriched KEGG pathways derived from the prognostic-relevant LR pairs are presented.

Stratification and survival analysis of patients based on ligand-receptor pairs

For each set of patient data, individuals were grouped into "high" or "low" categories based on the aggregate expression levels of specific ligand-receptor (LR) gene pairs. A patient was labeled as "high" if their total LR pair gene expression met or exceeded the median value for the entire patient group; otherwise, they were designated as "low." To assess the influence of these classifications on patient outcomes, we utilized R's "Survival" package (version 4.3.2). The log-rank test was employed to establish statistical significance, and hazard ratios (HRs) were derived using Cox regression models. Each patient group's survival outcomes were scrutinized independently. To amalgamate insights from various cohorts, we turned to a meta-analysis approach, deploying the "Edgington" method through the "sump" function in R's "metap" package (version 1.4). We selected the 94 significant LR pairs based on two primary criteria: 1) a Storey-adjusted q-value less than 0.1, ensuring statistical significance across multiple hypothesis tests, and 2) a consistent hazard ratio, either surpassing or falling below 1, across all evaluated cohorts, indicating a robust association with patient survival outcomes. To adjust for multiple hypothesis testing, we adopted Storey's method (24) via the "qvalue" package in R (version 2.18.0).

Samples clustering through consensus clustering

Using consensus clustering, we categorized the samples based on their gene expression patterns. We generated a consistency matrix with the "ConsensusClusterPlus" package in R (25). After narrowing down to significant ligand-receptor (LR) pairs, we used these to ascertain the molecular subtypes of the samples.

For the clustering process, the "pam" algorithm was employed, and the "Canberra" method was chosen as the distance metric. We executed 500 bootstrap replications, with each cycle including 80% of the patients from the training set. We considered a cluster range from 2 to 10. The most stable clustering solution was pinpointed by examining both the consistency matrix and the consensus cumulative distribution function (CDF), as detailed by Senbabaoglu et al. (26).

Functional enrichment analysis

To delve into the distinct gene expression landscapes across various molecular subtypes, we implemented Gene Set Enrichment Analysis (GSEA v4.0) (27, 28). We utilized comprehensive gene sets from the Hallmark database (29) and applied specific criteria for statistical significance, including a normalized p-value less than 0.01 and a False Discovery Rate (FDR) below 0.05. For functional characterization of genes that are either upregulated or downregulated, we employed the "clusterProfiler" package (30) to conduct Kyoto Encyclopedia of Genes and Genomes (KEGG) pathway analyses. This helps to identify the biological pathways that are most impacted by the gene expression differences in each subtype.

Immune cell infiltration analysis

Regarding the immune landscape within the samples, we applied the deconvolution technique known as Cell-type Identification By Estimating Relative Subsets Of RNA Transcripts (CIBERSORT) (31). This enabled us to approximate the proportions of 22 different immune cell types within each sample. Furthermore, we used the ESTIMATE algorithm to assess the relative abundance of immune and stromal cells in the tumor microenvironment.

To evaluate the functionality and presence of T cells within tumors, we utilized the default settings of the TIDE program, which provides scores for T-cell dysfunction and exclusion (32). Additionally, we calculated the single-sample Gene Set Enrichment Analysis (ssGSEA) scores using the GSVA package in R (33), which allowed us to represent the relative enrichment levels of each KEGG pathway. By integrating these multifaceted analyses, we aim to provide a comprehensive overview of the functional roles of genes, the immune cell composition, and their potential implications for patient prognosis and treatment strategies.

Genomic data exploration and visualization

For our analysis of genomic variations, we sourced the Simple Nucleotide Variation (SNV) dataset from the TCGA, specifically the Level 4 data processed via the "MuTect2" algorithm. This data was retrieved from the Genomic Data Commons (GDC) portal (https://portal.gdc.cancer.gov/).

To examine and illustrate the Single Nucleotide Polymorphisms (SNPs), we utilized the "oncplot" function available in the R package "maftools." (34), allowing for comprehensive visualization and analysis of these genomic alterations, aiding in the interpretation of their potential biological significance.

Development of the LR.score prognostic model

To develop a personalized prognostic model, we focused on ligand-receptor (LR) pairs that demonstrated significant relevance for patient outcomes, incorporating them into a penalized Cox regression model using the L1-penalized LASSO (Least Absolute Shrinkage and Selection Operator) methodology, implemented with the R package "glmnet." The optimal λ value, which controls the strength of the penalty applied to the model, was determined using ten-fold cross-validation, where the data was divided into ten subsets, with each subset used as a validation set once. The optimal λ was chosen based on minimizing the partial likelihood deviance, thereby retaining the most important predictor variables by shrinking the coefficients of less relevant ones to zero, ensuring the best predictive performance while avoiding overfitting. After identifying the predictor variables, we further refined the model using stepwise multivariate regression analysis with the Akaike Information Criterion (AIC) via the "stepAIC" function in the "MASS" package in R. This approach iteratively removed variables to minimize the AIC value, achieving an optimal balance between model complexity and goodness of fit. The final set of 10 LR pairs included in the LR.score were those that remained stable across multiple models and consistently contributed to predicting overall survival. The final risk score for each patient, termed the LR.score, was computed as follows:

$$\begin{aligned}\text{LR.score} &= (\beta_1 x_{i1} + \beta_2 x_{i2} + \ldots + \beta_p x_{ip}) \\ &= 0.269 \times \text{CALCA_CALCRL} + 0.213 \\ &\quad \times \text{NCAM1_ROBO3} + 0.160 \times \text{NLGN1_NRXN2} \\ &\quad + 0.125 \times \text{IL2_IL2RA} - 0.121 \times \text{HGF_MET} \\ &\quad - 0.199 \times \text{CXCL12_ITGA4} - 0.262 \\ &\quad \times \text{CLEC11A_ITGA11} - 0.317 \times \text{AVP_AVPR1B} \\ &\quad - 0.491 \times \text{ICAM4_ITGA4} - 0.708 \\ &\quad \times \text{CCL7_ACKR4}\end{aligned}$$

Analysis of drug sensitivity in relation to LR.score

To investigate the relationship between drug responsiveness and the LR.score prognostic model, we obtained drug sensitivity data for nearly a thousand cancer cell lines from the Genomics of Drug Sensitivity in Cancer (GDSC) database. We used the Area Under the Curve (AUC) values for various anti-cancer drugs as indicators of drug efficacy. Spearman's rank correlation analysis was employed to assess the correlation between each drug's sensitivity and the LR.score. We set a significance threshold at an absolute Spearman's correlation coefficient (|ρ|) greater than 0.2 and adjusted for False Discovery Rate (FDR) using the Benjamini-Hochberg method with a significance level set at less than 0.05. To further refine drug response predictions, we utilized the "pRRophetic" R package (35). Additionally, for a more targeted approach, we incorporated transcriptomic and clinical data from the IMvigor210 cohort of patients with metastatic bladder cancer who were treated with the anti-PD-L1 drug Atezolizumab. This data was accessed using the "IMvigor210CoreBiologies" R package (36). The immune checkpoints list waw derived from the HisgAtlas database (37).

Primary AML sample collection and quantitative reverse transcription polymerase chain reaction analysis

Bone marrow specimens were collected from 24 individuals with a primary diagnosis of AML at the Zhuji Affiliated Hospital of Wenzhou Medical University. Additionally, 12 healthy bone marrow samples were donated from individuals undergoing total hip arthroplasty, serving as a control group. All participants provided informed consent, and the study was conducted in line with the Declaration of Helsinki principles. The research was approved from the Ethics Committee of Zhuji People's Hospital Affiliated to Wenzhou Medical University. Diagnosis for AML was made using the French-American-British (FAB) system, alongside tests such as immunophenotyping, cytogenetic analysis, and molecular genetic profiling. A complete response (CR) to treatment was identified by several criteria, including bone marrow blasts below 5%, no Auer rod-positive blasts, no extramedullary leukemia, an absolute neutrophil count above $1.0 \times 10^{\wedge 9}$/L, and a platelet count over $100 \times 10^{\wedge 9}$/L. RNA was extracted from various tissues and cells using Trizol reagent as per the manufacturer's instructions. The reverse transcription step was carried out using the PrimeScript RT reagent Kit. Quantitative real-time PCR (qRT-PCR) was then performed with SYBR Prime Script RT-PCR Kits, following the prescribed procedure. Expression levels of CLEC11A, ICAM4, ITGA4, and AVP were quantified using the $2^{-\Delta\Delta Ct}$ method and normalized against GAPDH mRNA. These expression levels were reported relative to a control level set to a baseline of 1.0. The primer sequences used for amplifying CLEC11A, ICAM4, ITGA4, and AVP genes were as follows: for CLEC11A, forward (5′-GGG CCT CTA CCT CTT CGA AA-3′) and reverse (5′-CAG TTC TCG AGC GTG CCA CC-3′); for ICAM4, forward (5'-GCCTACAGTGAGGGACAGG-3') and reverse (5'-ATCACGGGCTGCCAGAAG-3'); for ITGA4, forward (5′-TTCCAGAGCCAAATCCAAGAGTAA-3′) and reverse (5′-AAGCCAGCCTTCCACATAACAT-3′); and for AVP, forward (5′-GGGCAGGTAGTTCTCCTCCT-3′) and reverse (5′-CACCTCTGCCTGCTACTTCC-3′).

Enzyme-linked immunosorbent assay for protein validation

In addition to the mRNA analysis, protein levels of CLEC11A, ICAM4, ITGA4, and AVP were measured using enzyme-linked immunosorbent assays (ELISAs). Bone marrow plasma was separated by centrifugation at 1500 × g for 10 minutes at 4°C from the same 24 AML patients and 12 healthy controls as described above and stored at -80°C until analysis. ELISA kits specific for human CLEC11A (#ELK6393), ICAM4 (#ELK3048), ITGA4 (#ELK9691), and AVP (#ELK5414) were used according to the manufacturer's protocols. All reagents and samples were brought to room temperature (18-25°C) before use. The 25× Wash Buffer was diluted to 1× with double-distilled water. Standard dilutions were prepared from a stock concentration of 60 ng/mL to create a standard curve with points at 60, 30, 15, 7.5, 3.75, 1.88, and 0.94 ng/mL. 100 µL of each standard, control, or sample was added in duplicate to the appropriate wells of a pre-coated microplate, which was then incubated at 37°C for 80 minutes. After incubation, the wells were washed three times with 200 µL of 1× Wash Buffer, followed by the addition of 100 µL of Biotinylated Antibody Working Solution to each well. The plate was incubated for another 50 minutes at 37°C, and the washing step was repeated. Next, 100 µL of Streptavidin-HRP Working Solution was added to each well, followed by incubation at 37°C for 50 minutes and another washing step repeated five times. The colorimetric reaction was developed by adding 90 µL of TMB Substrate Solution to each well, incubating the plate in the dark at 37°C for 20 minutes. The reaction was stopped by adding 50 µL of Stop Solution, changing the color from blue to yellow. Absorbance was immediately measured at 450 nm using a microplate reader (R&D, MN, USA). The concentration of each protein in the samples was then determined by comparing the corrected absorbance values to the standard curve generated from the known concentrations of the standards.

Statistics

For the evaluation of statistical differences between two continuous and normally distributed variables, we utilized the unpaired Student's t-test. In cases where the variables were not normally distributed, the Wilcoxon rank-sum test was employed instead. For comparisons involving three or more groups with non-parametric distributions, Kruskal-Wallis tests were conducted. For examining relationships between categorical variables, Fisher's exact test was implemented. Correlation analyses were conducted using Spearman's rank correlation test to assess the strength and direction of associations between variables. All visualizations and

statistical computations were carried out using R software, version 4.3.2, provided by the R Foundation for Statistical Computing in Vienna, Austria.

Results

Identification and analysis of prognostic LR pairs in acute myeloid leukemia

To pinpoint Ligand-Receptor (LR) pairs significantly correlated with the survival outcomes in AML, we incorporated data from three distinct AML cohorts: TCGA-LAML, GSE37642, and GSE12417. Initially, survival analysis for these LR pairs was executed separately for each cohort. This was followed by a meta-analysis where we amalgamated the P-values pertaining to the prognostic importance of these LR pairs from all three cohorts (adjust P-value< 0.01). Upon completing multiple hypothesis testing corrections, we isolated 94 LR pairs that demonstrated substantial prognostic relevance. Of these, 56 LR pairs were indicative of a poor prognosis, while 38 suggested a favorable outcome (Figure 1B; Supplementary Table S2). The interactive network involving these LR pairs is depicted in (Figure 1C).

Additionally, we undertook KEGG pathway enrichment analysis targeting the specific ligands and receptors from these pairs. Remarkably, these 94 LR pairs were predominantly enriched in key biological pathways. These include Cytokine–cytokine receptor interaction, Viral protein interaction with cytokine and cytokine receptor, PI3K–Akt signaling pathway, Proteoglycans in cancer, Cell adhesion molecules (CAMs), and ECM–receptor interaction (Figure 1D).

Molecular classification of ligand-receptor pairs

Further, we summed the expression levels of the receptor and ligand genes to represent the expression intensity of each LR pair. We then used the gene expression levels of these LR pairs for molecular subtyping. In this step, we included the 94 LR pairs that

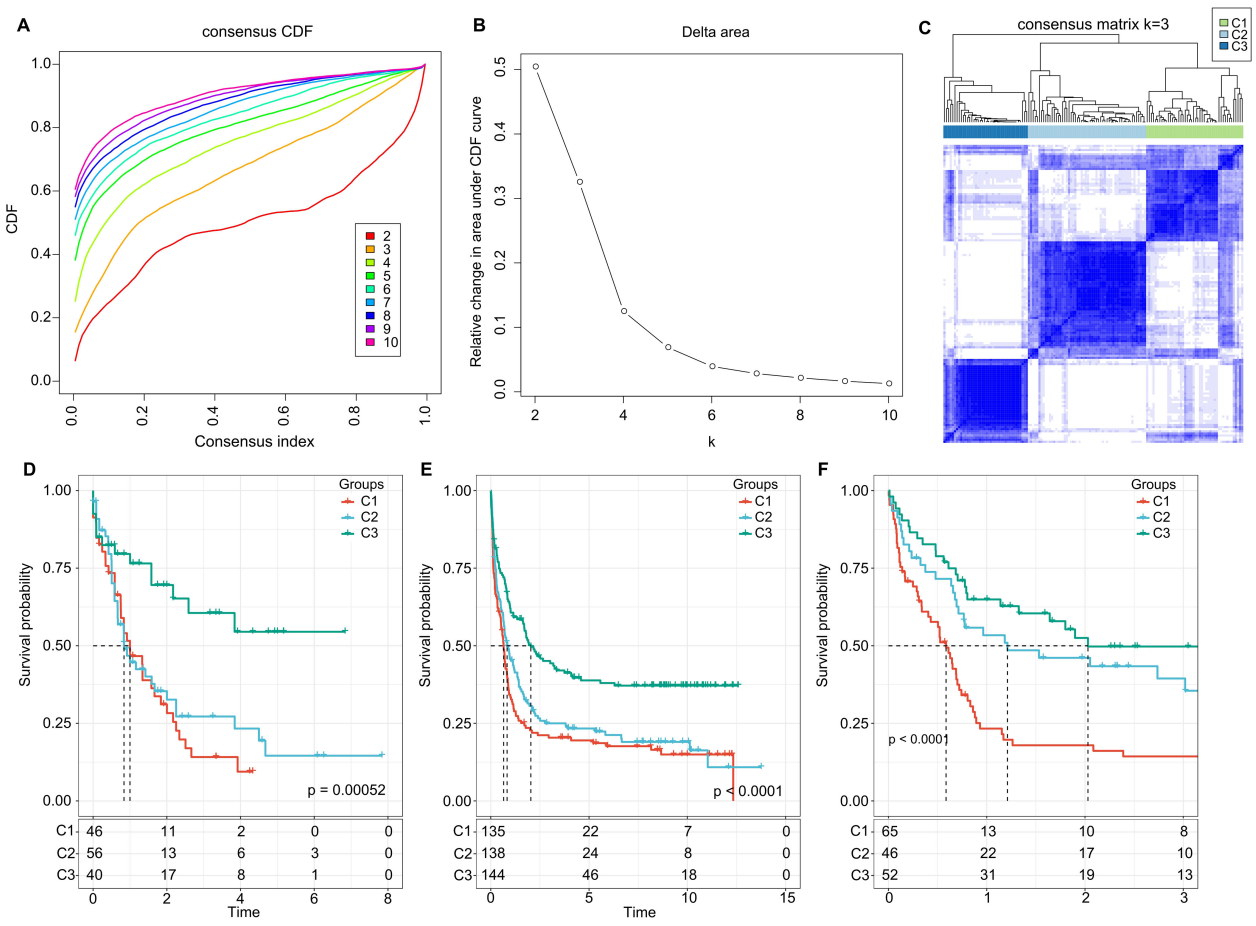

FIGURE 2
Cluster Analysis and Survival Outcomes Based on LR Pairs. **(A)** Consensus clustering using LR pairs and CDF curves from the consensus clustering in the TCGA dataset. **(B)** Delta area plot from the consensus clustering in the TCGA dataset. **(C)** Consensus matrices showcasing the identified clusters (k = 3). **(D)** Overall survival Kaplan-Meier plot for the three subtypes in the TCGA cohort (P = 0.00052, log-rank test). **(E)** Overall survival KaplanMeier plot for the three subtypes in the GSE37642 dataset (P< 0.0001, log-rank test). **(F)** Overall survival Kaplan-Meier plot for the three subtypes in the GSE12417 dataset (P< 0.0001, log-rank test).

FIGURE 3
LR pairs-based clusters and clinical characteristics **(A)**. Distribution of clinical information for molecular subtypes in the TCGA cohort (Fisher's exact test). *P< 0.05. **(B)** Distribution of clinical information for molecular subtypes in the GSE37642 cohort (Fisher's exact test). *P< 0.05. **(C)** Distribution of clinical information for molecular subtypes in the GSE12417 cohort (Fisher's exact test). *P< 0.05.

were identified in the previous analysis as being significantly correlated and prognostically relevant. Using Consensus Clustering, we clustered 142 AML samples from the TCGA cohort. Based on the Cumulative Distribution Function (CDF), we determined the optimal number of clusters. The CDF Delta area curve suggested that choosing three clusters provided the most stable clustering results (as shown in Figures 2A, B). Ultimately, we selected k=3 to obtain three molecular subtypes (Figure 2C). Upon further analysis of the prognostic features of these three subtypes, we observed significant prognostic differences among them. Specifically, subtype C3 showed better prognosis, while subtype C1 had poorer outcomes (P = 0.00052; Figure 2D). Additionally, using the same methodology, we conducted molecular subtyping for the AML patient cohort in GSE37642, and observed similar significant prognostic differences among these three subtypes (P< 0.0001; Figure 2E), consistent with the training set. The same phenomenon was also observed in the GSE12417 cohort (P< 0.0001; Figure 2F).

Additionally, in the TCGA dataset, we compared the distribution of various clinical pathological features across the three molecular subtypes to examine if these features varied among the subtypes. We found that there were differences in

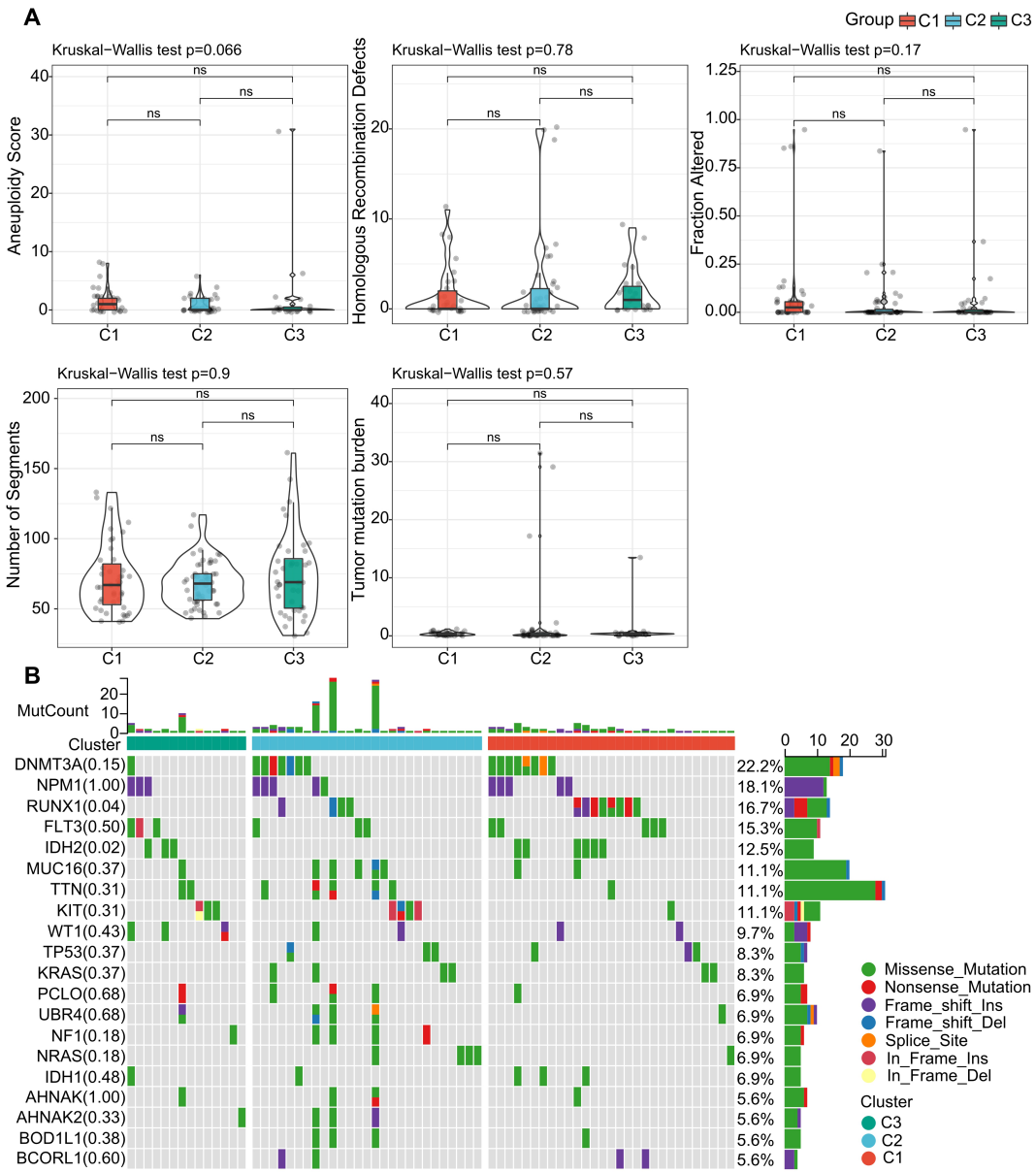

FIGURE 4
Genomic Variation Patterns Across LR Pair-Defined Clusters. **(A)** Analysis of parameters such as aneuploidy score, homologous recombination deficits, segment count, fraction of alterations, and tumor mutation burden within the LR pair-based clusters. Significance levels: ns, P > 0.05; *P < 0.05; **P < 0.01; ***P < 0.001. Kruskal-Wallis test employed. **(B)** Mutation profile showcasing the top 20 prevalent mutations across 142 AML patients. The top panel provides a count of mutations for each individual, whereas the bar chart below denotes the LR pair-defined clusters. An accompanying legend depicts various genetic mutation types and their occurrences.

"age" groups, "CALGB Cytogenetics Risk Category," and "FAB Category" among the three molecular subtypes. Specifically, the C1 subtype had a significantly higher proportion of older patients compared to the C3 subtype (Fisher's exact test, -log10 P-value = 4.74). Most patients in the C3 subtype fell into the "Favorable" (Fisher's exact test, -log10 P-value = 7.53) (Figure 3A). Similarly, we examined differences in clinical information among different molecular subtypes in the GSE37642 and GSE12417 cohorts (Figures 3B, C). We observed that the majority of patients did not have RUNX1 mutations. These analyses further support the notion that these molecular subtypes not only have prognostic value but also correlate with various clinical and pathological features, thereby potentially aiding in more targeted treatment approaches.

Mutation characteristics across different molecular subtypes

We further investigated the differences in genomic alterations among the three molecular subtypes within the TCGA cohort. Our analysis revealed that there were no significant differences among

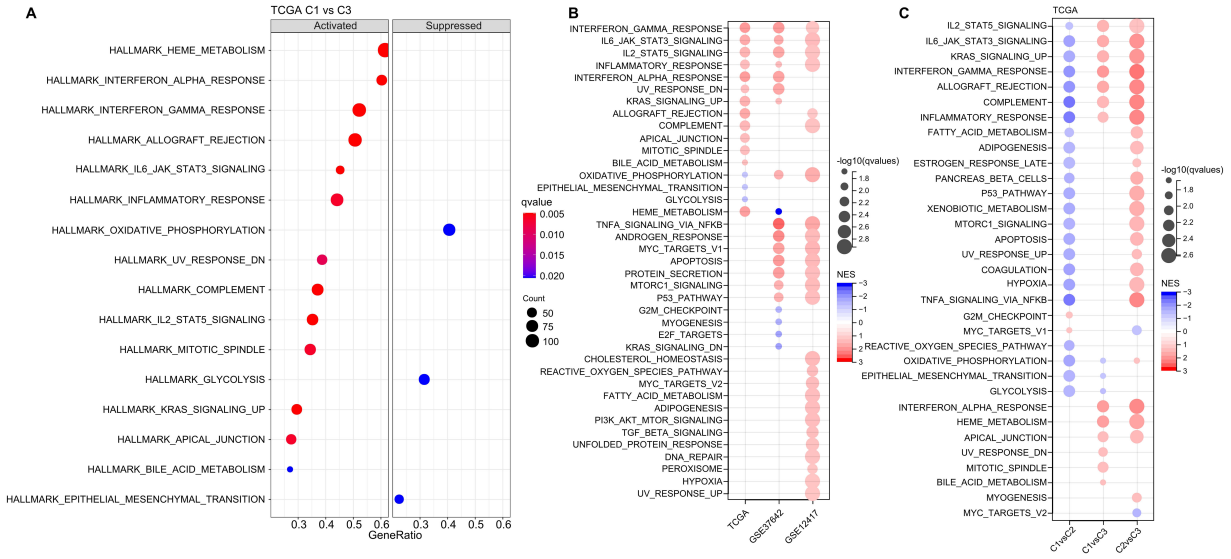

FIGURE 5
Analysis of Pathway Enrichment in LR-Based Clusters. **(A)** GSEA output contrasting C1 vs C3 in the TCGA-LAML dataset. **(B)** Visual representation of GSEA findings when comparing C1 vs C3 subtypes across three AML cohorts: TCGA-LAML, GSE37642, and GSE12417. **(C)** A color-coded bubble chart detailing GSEA results for various molecular subtypes within the TCGA-LAML dataset. Blue bubbles signify downregulated hallmarks, while red bubbles point to upregulated ones.

the molecular subtypes in terms of Aneuploidy Score, Homologous Recombination Defects, Fraction Altered, Number of Segments, and Tumor Mutation Burden (Figure 4A).

Moreover, we scrutinized the variations in gene mutations across the distinct molecular subtypes. We highlighted the top 20 genes that showed substantial differences in their mutation rates (Figure 4B). Of particular interest were genes like DNMT3A, NPM1, and RUNX1, which exhibited noticeable disparities in mutation frequency among the three molecular subgroups. Intriguingly, a higher prevalence of RUNX1 and DNMT3A mutations was observed in subtypes C1 and C2, and these mutations were correlated with unfavorable prognostic outcomes. This observation aligns with existing scientific literature that associates these specific mutations with poorer survival rates in AML (38, 39).

These findings imply that while some genomic features like Aneuploidy Score and Tumor Mutation Burden may not differ significantly among the subtypes, specific genes do show variations in mutation rates. This could have implications for understanding the biological distinctions among the subtypes and potentially for targeted therapeutic strategies.

Functional annotation of ligand-receptor pairs-based clustering

Next, we investigated whether there were differentially activated pathways within the various molecular subgroups. To identify these pathways, we performed Gene Set Enrichment Analysis (GSEA) using all candidate gene sets from the Hallmark database, with FDR threshold less than 0.05 for significant enrichment. In the TCGA cohort, when compared to the C3 subtype, the C1 subtype exhibited activation of 13 pathways and suppression of 3 pathways, as shown in (Figure 5A). These pathways were mainly related to immune responses, such as INTERFERON_GAMMA_RESPONSE, INFLAMMATORY_RESPONSE, INTERFERON_ALPHA_RESPONSE, ALLOGRAFT_REJECTION, and COMPLEMENT. In addition, we analyzed the significant enriched gene sets in the two validation cohorts when comparing the C1 subtype with the C3 subtype. Generally, activated pathways primarily included immune markers, such as INTERFERON_GAMMA_RESPONSE, IL6_JAK_STAT3_SIGNALING, IL2_STAT5_SIGNALING, and INFLAMMATORY_RESPONSE (Figure 5B). Furthermore, we compared differential pathways between C1 and C2, C1 and C3, as well as C2 and C3 in TCGA cohort. As shown in (Figure 5C),

we identified a notable concentration of immune-related pathways among the diverse subtypes. GSEA analysis across these subtypes revealed that individuals in the C1 subtype typically displayed heightened activity in immune regulatory pathways. This leads us to hypothesize that the ligand-receptor pairs utilized for molecular classification might have significant influence in shaping the immune microenvironment.

To delve deeper into the variations in the immune microenvironment across patients from different molecular groups, we assessed the relative proportions of 22 immune cell types across the three AML cohorts using the CIBERSORT algorithm. This revealed pronounced differences in the presence of specific immune cells across the three molecular subtypes (as illustrated in (Figures 6A, C, E). Notably, the C3 subtype exhibited elevated levels of CD8 T cells and plasma cells, suggesting heightened adaptive immune responses. Additionally, we employed the ESTIMATE algorithm to assess immune cell

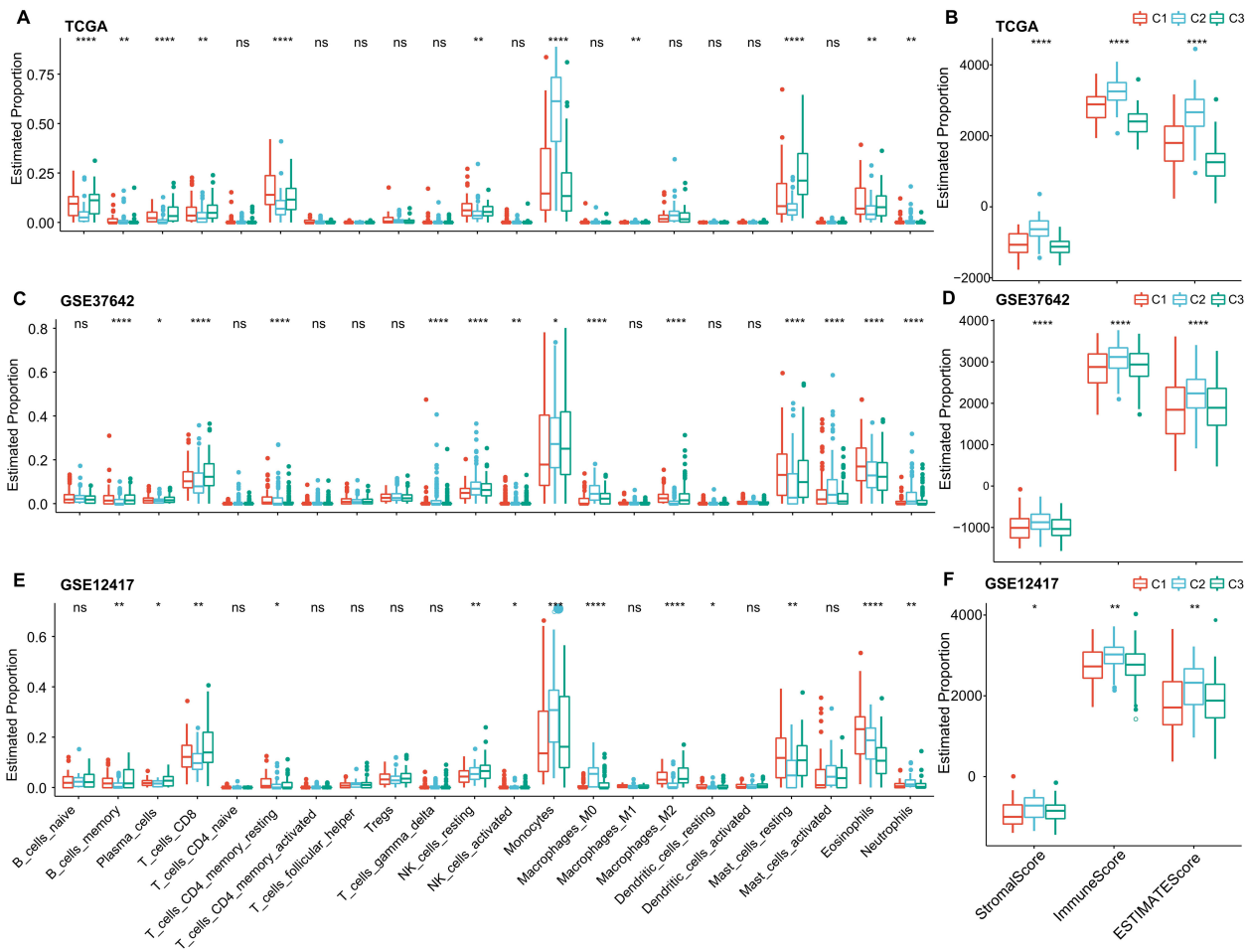

FIGURE 6
Immune Cell Variability Across Different Molecular Subtypes in Three AML Cohorts. **(A–F)** Differences in immune cell infiltration among subtypes, as determined by CIBERSORT and ESTIMATE. Significance levels: ns, P > 0.05; *P > 0.05; **P > 0.01; ***P > 0.001; ****P > 0.0001. Analyzed using the Kruskal-Wallis test.

infiltration, as shown in (Figures 6B, D, F). We found that the "ImmuneScore" was consistently highest in the C2 subtype across the TCGA, GSE37642, and GSE12417 cohorts, indicating a relatively higher level of immune cell infiltration in the C2 subtype, importantly, C2 also has highest myeloid lineage cells compare to C1 and C2.

Development of a scoring model based on ligand-receptor pairs

We found that molecular subtypes based on LR pairs exhibit different mutation landscapes, distinct pathway features, and varying levels of immune infiltration. To further refine our risk model, we employed lasso regression on the 94 significant LR pairs identified from the meta-analysis within the TCGA-LAML cohort. We showed that as the value of lambda increases, the number of coefficients tending towards zero also increases (Supplementary Figure S1A). Using 10-fold cross-validation, we identified an optimal lambda value of 0.0868 and selected 13 LR pairs for further analysis (Supplementary Figure S1B). Subsequently, we used stepwise multivariate regression analysis and employed the Akaike Information Criterion (AIC) to further refine our model, ultimately identifying 10 key LR pairs. These pairs include "AVP->AVPR1B," "CALCA->CALCRL," "CCL7->ACKR4," "CLEC11A->ITGA11," "CXCL12->ITGA4," "HGF->MET," "ICAM4->ITGA4," "IL2->IL2RA," "NCAM1->ROBO3," and "NLGN1->NRXN2" (Supplmentary Figure S1C).

Building on the 10 distinguished ligand-receptor (LR) pairs, we developed an LR scoring system, termed LR.score, to quantifiably gauge the activity patterns of these LR pairs in AML patients. We observed a notably elevated LR.score in patients of the "C1" subtype in comparison to their "C3" counterparts (Figure 7A). Probing the clinical relevance of the LR.score, we categorized patients into high and low LR.score groups, using "0" as the demarcation point. Interestingly, those with a diminished LR.score exhibited a pronounced survival advantage (Figure 7B; log-rank test, P< 0.0001). The receiver operating characteristic (ROC) curve's area

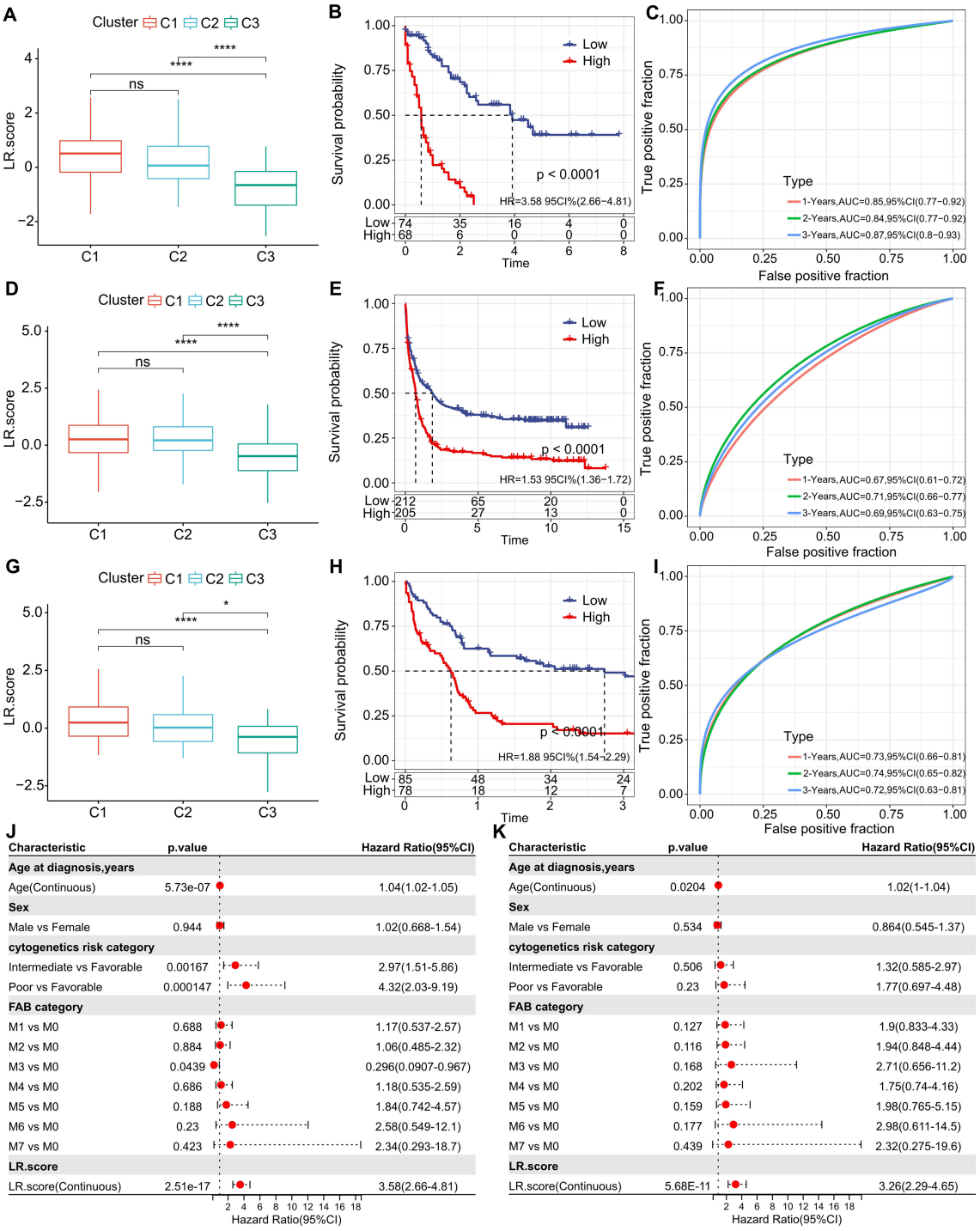

FIGURE 7
Understanding the LR.score Across Cohorts. **(A)** Variability in LR.score among the TCGA-LAML cohort. **(B)** Survival comparison between high and low LR.score groups in TCGA-LAML. **(C)** Predictive accuracy of LR.score in the TCGA-LAML cohort for 1, 2, and 3-year survival. **(D-I)** Similar analyses conducted for GSE37642 and GSE12417 cohorts. **(J, K)** Univariate and multivariate Cox regression model analyses factoring in LR.score, age, gender, cytogenetics risk, FAB category, and outcomes in the TCGA-LAML cohort.

under the curve (AUC) for 1-, 3-, and 5-year overall survival stood at 0.85, 0.84, and 0.87, respectively (Figure 7C). In our validation datasets, GSE37642 and GSE12417, a similar pattern emerged where the LR.score for "C1" was appreciably higher than for "C2" and "C3" (Wilcoxon rank-sum test, P< 0.001) (Figures 7D, G). In alignment with our initial observations, patients with a reduced LR.score in these validation sets also showcased a marked survival benefit (Figures 7E, H; log-rank test, P< 0.0001). The AUC values from the ROC assessments were 0.67, 0.71, and 0.69 for 1-, 3-, and 5-year overall survival in GSE37642, and 0.73, 0.74, and 0.72 in

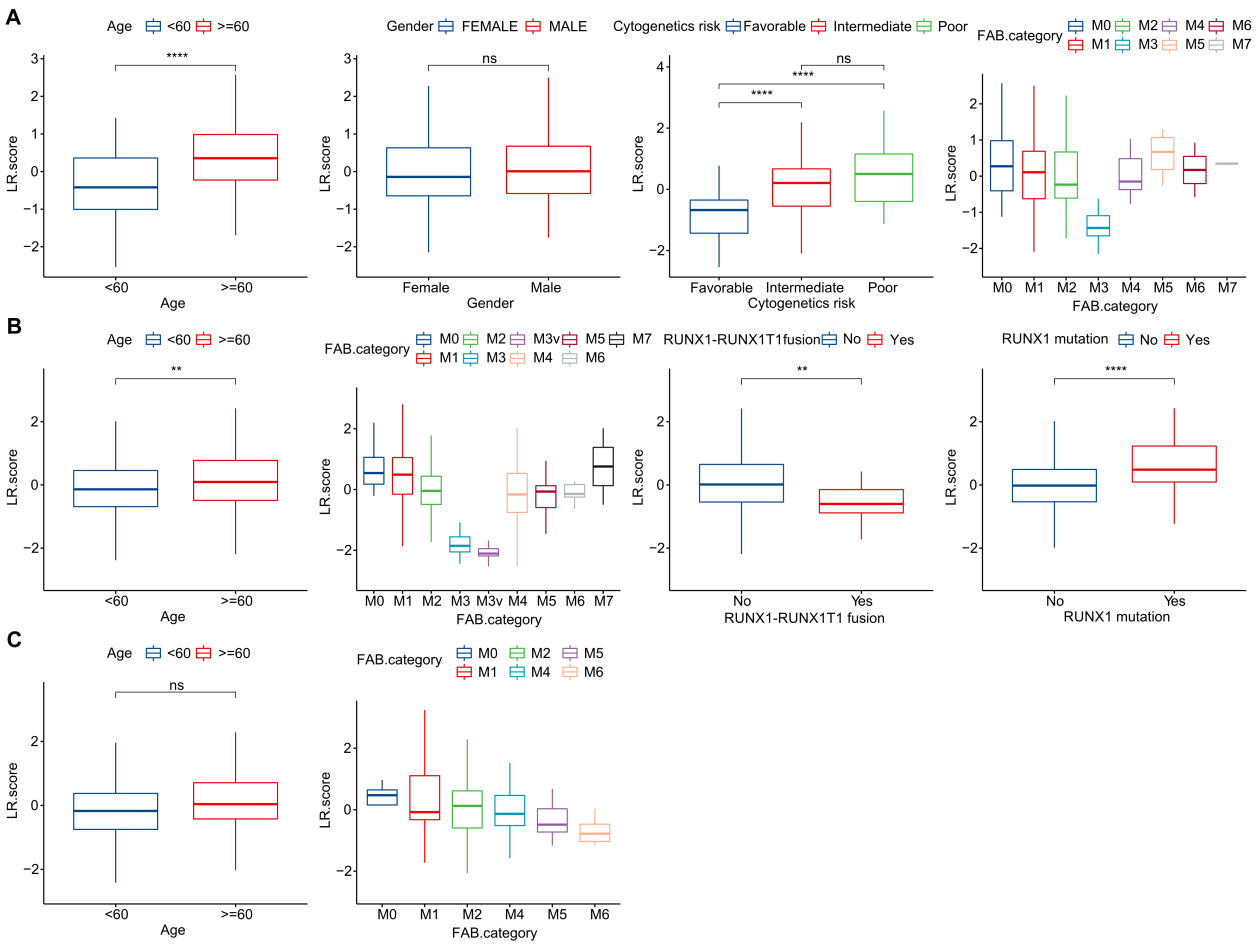

FIGURE 8
Clinical Implications of the LR.score. **(A–C)** Distribution of LR.score concerning various clinical-pathological features across TCGA-LAML, GSE37642, and GSE12417 cohorts. Significance denoted as: ns, $P > 0.05$; ** $P < 0.01$; ****$P < 0.0001$. Analyzed using the Wilcoxon rank-sum test.

GSE12417, respectively. The consistency in AUC values across these intervals underscores the reliability of the model's prognostic potential (Figures 7F, I).

To examine whether the LR.score could serve as an independent prognostic factor, we performed both univariate and multivariate Cox regression analyses using patient clinical features such as age, gender, cytogenetics risk category, and FAB category. We found that the LR.score is a reliable and independent prognostic biomarker (Figures 7J, K; HR=3.26, 95% CI 2.29-4.65, P = 5.68E-11).These results suggest that the LR.score can reflect the LR-pairs patterns in AML patients and predict prognosis.

To investigate the relationship between the LR.score and clinical characteristics of AML, we analyzed the differences in the LR.score based on various clinical-pathological features in the TCG dataset. Our findings indicated that as age increases, the LR.score also rises. Moreover, higher "cytogenetics risk" levels were associated with elevated LR.score values (Figure 8A). We further compared the relationship between patients' LR.score and their clinical-pathological characteristics in the GSE37642 and GSE12417 cohorts (Figures 8B, C). It was observed that older patients tended to have higher LR.score as well as RUNX1 mutation patients. In summary, the higher the clinical staging level of the patient, the greater the LR.score.

LR.score and relevant biological functions

We further delved into the distribution differences of scores for 22 immune cell types across LR.score groupings in the TCGA cohort, as depicted in (Figure 9A). Generally, scores for most immune cells do not display significant disparities between LR.score groups. However, certain cells like T_cells_gamma_delta, NK_cells_activated, and Mast_cells_resting exhibited notable differences. Moreover, when comparing immune infiltration, the ImmuneScore was consistently lower in the low LR.score group than in the high LR.score group (Figure 9B). Additionally, Employing Pearson's correlation coefficient, we evaluated the association between the LR.score and immune cell infiltration, the results of which are shown in (Figure 9C). Interestingly, a strong positive correlation was observed between LR.score and T_cells_regulatory (Tregs), while a significant negative correlation was noted with Mast_cells_resting.

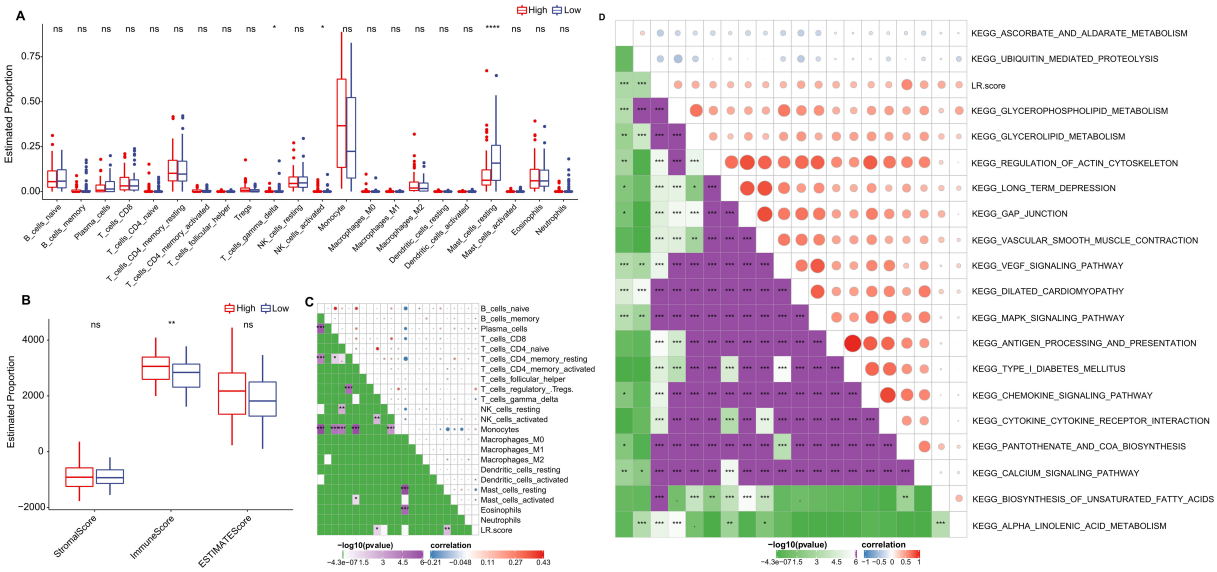

FIGURE 9
Role of LR.score in Immune Infiltration and Pathway Activation. **(A, B)** Distribution of immune cell types and stromal-immune scores between high and low LR.score groups in the TCGA-LAML cohort. **(C, D)** Correlation analyses between immune cell components, KEGG pathways, and the LR.score.

To understand the relationship between LR.score and biological functionality, we employed single-sample GSEA analysis (ssGSEA) on the gene expression profiles of AML samples from the TCGA cohort. This enabled us to compute scores for each sample across various functionalities, leading to ssGSEA scores for each function across individual samples. Further correlation analysis between these functional scores and LR.score revealed functions with correlations greater than 0.35, as shown in (Figure 9D) and (Supplementary Table S3). As a result, 17 pathways positively correlated with the LR.score of samples, while 2 pathways demonstrated a negative correlation. Notably, cancer-related pathways such as KEGG_GLYCEROPHOSPHOLIPID_METABOLISM, KEGG_GLYCEROLIPID_METABOLISM, KEGG_REGULATION_OF_ACTIN_CYTOSKELETON, and KEGG_MAPK_SIGNALING_PATHWAY were positively correlated with LR.score.

LR.score model in immunotherapy/chemotherapy

Furthermore, we investigated if there were disparities between LR.score groupings concerning their responses to treatment. Initially, we compared the expression of immune checkpoints between the LR.score groups. As shown in (Figure 10A), certain immune checkpoint genes exhibited differential expression across the LR.score groups. Specifically, high gene expressions of ARHGEF5, CD274, CD80, CTLA4, LAG3, PDCD1, and VISTA are associated with high LR.score ($P< 0.05$, Wilcoxon rank-sum test).

We subsequently examined the disparities in immunotherapy outcomes between the LR.score categories. Utilizing the TIDE algorithm, we gauged the probable clinical ramifications of immunotherapy among our designated high and low LR.score groups. Notably, a heightened TIDE prediction score implies an augmented propensity for immune evasion, hinting at potentially diminished benefits from immunotherapy for the patient. As illustrated in (Figure 10B) and (Supplementary Table S4), discernible distinctions between high- and low- LR.scores in MDSC, CAF, and TIDE scores were absent. Simultaneously, we contrasted the anticipated T-cell dysfunction and exclusion scores across various metabolic molecular subtypes within the TCGA cohort. The group with elevated LR.score exhibited the most pronounced T-cell dysfunction score ($P< 0.01$, Wilcoxon rank-sum test).

Delving deeper into the ramifications of LR.score on drug responsiveness, we explored its association with reactions in tumor cell lines to drugs. Through Spearman correlation analysis, we discerned four notable associations between LR.score and drug susceptibility in the Genomics of Drug Sensitivity in Cancer (GDSC) database (Figure 10C). Among these, three correlations indicated drug resistance in tandem with the LR.score, encompassing Forentinib, BPD-00008900, and Vinblastine. We also gauged the variances in responses to prevalent chemotherapy agents such as 'Bexarotene', 'Bortezomib', 'Erlotinib', and 'Rapamycin' between the LR.score categories (Figure 10D). Observations revealed that patients with a diminished LR.score manifested heightened sensitivity to drugs, notably Bortezomib ($P = 0.0039$, Wilcoxon rank-sum test) and Erlotinib ($P = 0.028$, Wilcoxon rank-sum test), as compared to their high LR.score counterparts. Collectively, these insights underscore a linkage between LR pairs and drug sensitivity, positing the LR.score as a potential biomarker to inform tailored therapeutic approaches.

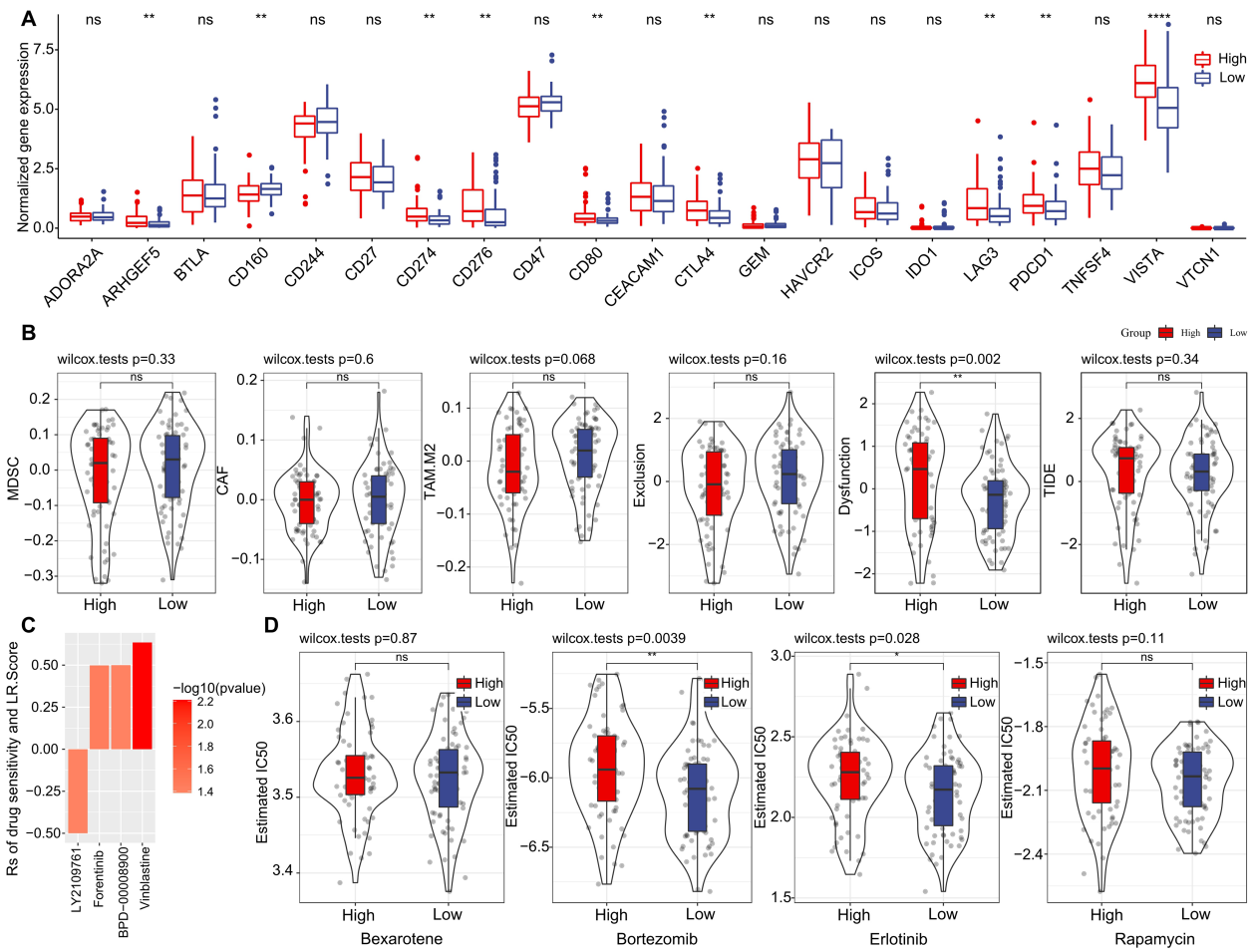

FIGURE 10
Drug Sensitivity Predictions Using the LR.score. **(A)** Immune checkpoint expression differences between LR.score groups in TCGA-LAML. **(B)** Comparing scores related to immune activity between high and low LR.score groups. **(C)** Correlation between drug sensitivity and the LR.score, including the Estimated IC50 values for various drugs. **(D)** Comparing scores related to chemotherapy drugs between high and low LR.score groups. ns, $P > 0.05$; *$P < 0.05$; **$P < 0.01$; ****$P < 0.0001$.

Validation of the LR.score model genes

Considering the LR.score model's proven capability in predicting the risk and treatment outcomes for AML, we aim to validate the individual gene expression profiles to determine whether the model possesses the requisite sensitivity and specificity to be applicable for validation within our patient cohort. First of all, we investigated the cancer specificity of certain gene-protein pairs by checking the cell line database in The Human Protein Atlas (HPA), focusing on the following associations: "AVP->AVPR1B," "CALCA->CALCRL," "CCL7->ACKR4," "CLEC11A->ITGA11," "CXCL12->ITGA4," "HGF->MET," "ICAM4->ITGA4," "IL2->IL2RA," "NCAM1->ROBO3," and "NLGN1->NRXN2". Our analysis revealed that, among the genes studied, CLEC11A, ICAM4, ITGA4, and AVP exhibited the highest specificity to AML when compared to other cancer types. This suggests a strong association between the expression levels of these genes and AML, pointing to their potential role as specific biomarkers for this disease (Figure 11A). Next, we examined the expression of CLEC11A, ICAM4, ITGA4, and AVP in 12 normal and 24 AML bone marrow samples by quantitative reverse-transcription polymerase chain reaction (qRT-PCR). In comparison to the healthy bone marrow (Figure 11B), the levels of CLEC11A, ITGA4, and AVP were notably reduced in samples from AML patients, with a highly significant statistical difference ($P< 0.0001$). The expression of ICAM4 was also found to be slightly diminished ($P< 0.05$). These findings indicate that CLEC11A, ICAM4, ITGA4, and AVP may act as inverse biomarkers in the context of AML. Additionally, we used enzyme-linked immunosorbent assay (ELISA) to further validation these genes in the protein level. As shown in Figure 11C, the protein concentrations of CLEC11A and ITGA4 were significantly higher in normal samples compared to AML ($P< 0.0001$), and the same trend was observed for ICAM4 and AVP ($P< 0.01$). Furthermore, survival analysis reveals that patients with higher levels of CLEC11A has a better prognosis than those with lower expression (Figure 11D, $P< 0.0001$), reinforcing the potential role of CLEC11A as a particularly significant negative biomarker.

10.3389/fonc.2024.1473048

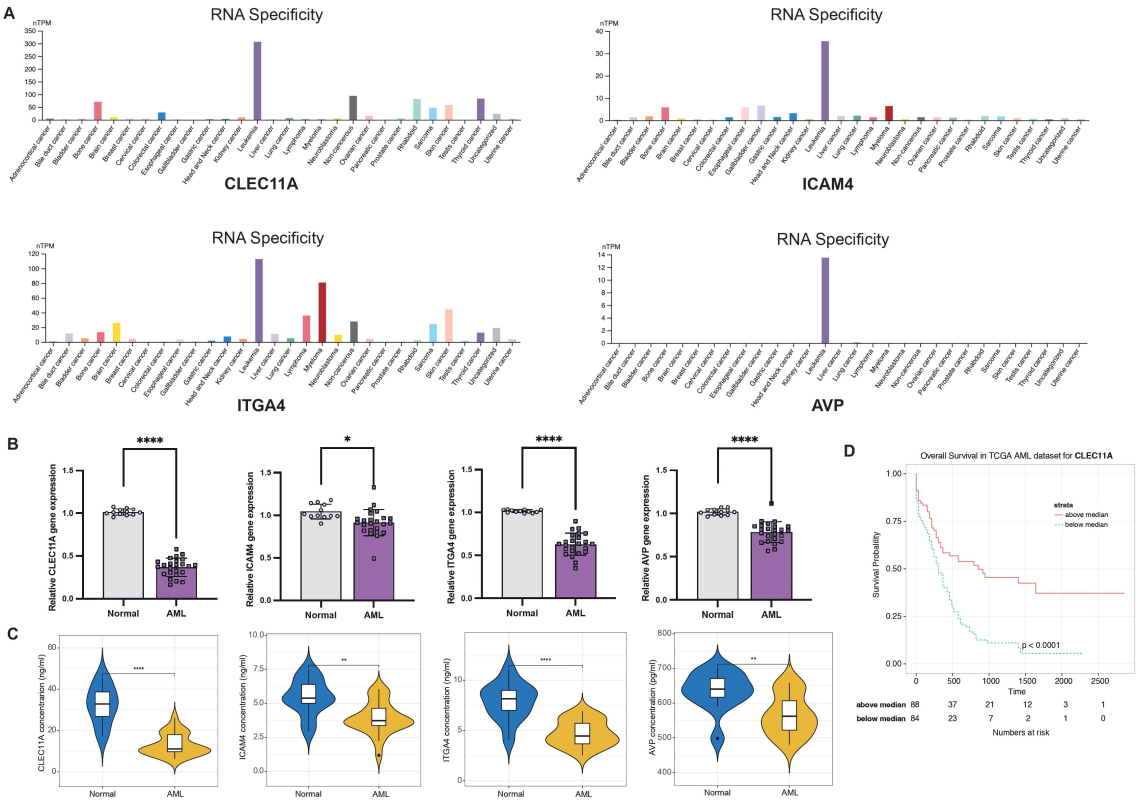

FIGURE 11
LR.score model validation. **(A)** Cancer specificity of CLEC11A, ICAM4, ITGA4, and AVP expressions among pan-cancer. **(B)** qRT-PCR of CLEC11A, ICAM4, ITGA4, and AVP comparing normal and AML bone marrows. Significance denoted as: *P< 0.05; ****P< 0.0001. Analyzed using the unpaired t test. **(C)** ELISA concentration of CLEC11A, ICAM4, ITGA4, and AVP comparing normal and AML bone marrows. Significance denoted as: **0.001< P< 0.01; ****P< 0.0001. Analyzed using the unpaired t test. **(D)** Overall survival Kaplan-Meier plot for high- and low- CLEC11A expressions in the TCGA dataset (P< 0.0001, log-rank test).

Discussion

In our research, we pinpointed 94 prognostic LR pairs that predominantly participate in pathways such as Cytokine-cytokine receptor interactions, PI3K-Akt signaling, and Proteoglycans in cancer. This indicates that specific LR pairs significantly influence AML survival by modulating key oncogenic signaling pathways. Based on these survival-related LR pairs, we delineated three distinct molecular subtypes. Furthermore, we devised a prognostic scoring model anchored on 10 LR pairs, and its predictive efficacy was corroborated in separate cohorts. The LR.score model offers a novel advantage over existing AML prognostic models by focusing on ligand-receptor interactions within the tumor microenvironment, providing insights into the dynamic cell-cell communication that drives disease progression and therapeutic response. This model not only enhances prognostic accuracy by identifying distinct molecular subtypes but also predicts responses to targeted therapies, thereby facilitating more personalized treatment strategies. Notably, this scoring system provided insights into chemotherapy responsiveness and probable outcomes to immune checkpoint blockade treatments in AML patients. Our findings underscore the potential of LR pair-driven gene signatures as prospective biomarkers for both prognosis and therapeutic response prediction in AML.

The C1 subtype was distinguished by its association with the worst prognosis, also demonstrated a notable immune cell infiltration, as evidenced by the higher immune score. The C3 subtype was marked by a more favorable prognosis when compared to the other subtypes. Additionally, patients within the C3 subtype demonstrated higher CD8 T cell and plasma cell levels, indicative of enhanced adaptive immune activities. The C3 subtype, with its lower LR.score, showed potential sensitivity to ICB treatments. This aligns with recent research that has indicated a synergistic therapeutic potential when combining targeted therapies with immunotherapies (40–45).

In our analysis of genomic alterations across the three molecular subtypes within the TCGA cohort, we observed no significant differences in traditional markers of genomic instability, such as Aneuploidy Score, Homologous Recombination Defects, Fraction Altered, Number of Segments, and Tumor Mutation Burden. These predominantly negative results suggest that these conventional genomic features are not the primary drivers of the distinct molecular and clinical characteristics seen in each AML subtype (7, 46). This finding underscores the complexity of AML and highlights the potential importance of other factors, such as epigenetic modifications, microenvironmental influences, or specific signaling pathways

activated by ligand-receptor (LR) pairs, in defining the disease behavior and therapeutic response. The lack of significant differences in these traditional genomic metrics reinforces the need to explore alternative mechanisms beyond standard genomic alterations, emphasizing the critical role of LR interactions in understanding AML heterogeneity and in identifying novel therapeutic targets.

The roles of specific mutations, particularly DNMT3A, RUNX1, NPM1C, and Flt3, in the progression and prognosis of AML have been the focus of several studies. DNMT3A mutations, often found in about a third of AML patients, have been associated with adverse outcomes and are often linked with a more aggressive disease course and shorter overall survival rates (38, 47, 48). Similarly, RUNX1 mutations are known to be recurrent in AML and have been associated with lower complete remission rate and shorter event-free survival (39, 49). Conversely, NPM1C and FLT3 mutations, while prevalent in AML, have a more complex relationship with prognosis, have certain numbers of NPM1C and FLT3 mutations in C1 and C2.

Of particular interest is the observation that DNMT3A and RUNX1 mutations seem to have a more pronounced influence on ligand-receptor (LR) pair interactions and intercellular communication in the AML microenvironment. This suggests that these mutations might be disrupting the cellular crosstalk essential for hematopoiesis, thereby promoting leukemogenesis. On the other hand, NPM1C and FLT3 mutations, although significant, appear to exert a less direct effect on these LR pairs and cellular communications. This differential impact underscores the importance of considering the individual and combined effects of these mutations. It's not just their presence, but their influence on cellular networks and communication that might determine disease progression and therapeutic responses. As we move forward, a comprehensive understanding of these mutations, especially in the context of LR pairs, will be vital for tailoring therapeutic strategies and improving prognosis assessments for AML patients.

The low LR.score group displayed a marked potential for sensitivity to immune checkpoint blockade (ICB) treatments. This observation is further supported by the notably T-cell dysfunction score within this group, suggesting an increased probability of a favorable response to anti-PD1/PD-L1 therapies. Immune checkpoints, such as PD-1 and its ligand PD-L1, are crucial modulators of the immune response, and their dysregulation can be leveraged by cancer cells to evade immune surveillance (50–53). The presence and abundance of specific immune cells, especially CD8 T cells and Tregs, could be pivotal in determining the therapeutic outcome of ICB treatments. CD8 T cells are the primary effectors in antitumor immunity, responsible for recognizing and killing cancer cells. The reinvigoration of these cells through ICB has been linked to improved patient outcomes in multiple studies (54, 55). Considering the low LR.score group's immune cell composition and TIDE score, it is plausible that they would benefit significantly from ICB therapies. Further analysis of the underlying molecular mechanisms revealed that LR pairs such as CXCL12-ITGA4 and HGF-MET, which are significantly downregulated in the low LR.score group, might contribute to the observed T-cell dysfunction. The CXCL12-ITGA4 axis is known to regulate the trafficking and homing of T cells to the bone marrow, and its downregulation could lead to impaired T-cell recruitment and function in the tumor microenvironment (56, 57). Similarly, the HGF-MET pathway has been implicated in promoting T-cell exhaustion through the activation of downstream signaling pathways, such as PI3K/AKT and MAPK/ERK (58, 59), which are involved in maintaining the immunosuppressive tumor microenvironment.

Moreover, the negative correlation between LR.score and T-cell regulatory pathways, including the TGF-beta signaling pathway, suggests that the low LR.score group may have reduced immunosuppressive signaling, further enhancing the potential effectiveness of ICB therapies. TGF-beta is a well-known suppressor of T-cell function, and its downregulation in the low LR.score group could lead to a more favorable immune microenvironment for the activation and expansion of effector T cells in response to ICB.

A higher LR score, indicative of altered ligand-receptor interactions, can potentially impact the finely-tuned signaling pathways that regulate hematopoiesis. These disruptions can further skew the differentiation of hematopoietic stem cells (HSCs) towards the myeloid lineage, leading to an accumulation of blasts and a concomitant decrease in lymphoid cells, especially T cells. The decreased differentiation and maturation of lymphoid progenitors could potentially explain the T-cell dysfunction observed in high LR score patients.

Moreover, the T cell differentiation block, a hallmark of aggressive AML, can be particularly concerning. T cells play a pivotal role in immune surveillance, and their differentiation block can facilitate an immunosuppressive environment, which AML cells exploit for their survival and proliferation. This can lead to a vicious cycle where the increased number of AML blasts further suppresses T cell differentiation, leading to a more aggressive disease phenotype. Considering these intricate biological interactions, it becomes evident that strategies aiming to restore T-cell function and differentiation might be particularly beneficial for AML patients with high LR scores. Immune checkpoint blockade therapies, which have shown promise in rejuvenating exhausted T cells in other malignancies, could potentially rectify the T cell differentiation block and restore the balance in hematopoiesis. This approach, when combined with a deeper understanding of the molecular underpinnings of AML, offers a promising avenue for more targeted and effective therapies for this aggressive malignancy.

Our study also yields with limitations. First and foremost, while our LR.score has shown promise in predicting survival in an independent AML cohort, it is based on retrospective data, which inherently carries potential biases. Prospective validation in diverse patient populations is essential to establish its universal applicability. Moreover, the molecular complexities of AML and its subtypes might not be entirely captured by the LR.score alone. The nuances of individual patient genetics, epigenetics, and the ever-evolving tumor microenvironment might introduce variations not accounted for in our model. Additionally, our study predominantly focuses on T-cell dysfunction and its relationship

with the LR.score, potentially overlooking other critical components influencing AML progression. Lastly, while our findings provide a foundation for therapeutic considerations, actual clinical efficacy requires rigorous testing through controlled clinical trials.

The critical ligand-receptor pairs such as ICAM4-ITGA4, CLEC11A-ITGA11, AVP-AVPR1B, along with CXCL12-ITGA4, HGF-MET, IL2-IL2RA, NCAM1-ROBO3, and NLGN1-NRXN2, sheds light on the complexity of leukemic pathophysiology. These genes, through their respective ligand-receptor interactions, are essential in maintaining normal bone marrow function, facilitating precise communication between cellular and extracellular components, and ensuring proper immune function and stress response. The downregulation of ICAM4 and its receptor ITGA4 compromises not just the physical adhesion of hematopoietic cells to the bone marrow stroma but also interrupts intracellular signaling pathways that guide cell fate decisions, which can be a consequence of the leukemic cells outcompeting their normal counterparts for niche occupancy and resources (60–62). Similarly, the diminished expression of CLEC11A and ITGA11, possibly due to epigenetic phenomena like promoter hypermethylation, disrupts not only the proliferation and differentiation of hematopoietic stem cells but also the integrity of the bone marrow's extracellular matrix—a critical scaffold for cellular interactions and signaling (63, 64). Furthermore, the hormonal regulation of the bone marrow environment, exemplified by the AVP-AVPR1B axis, is crucial in modulating responses to physiological stress and may be disrupted in AML, reflecting a systemic dysregulation of homeostatic mechanisms in response to the leukemic burden (65). Disruptions in cell adhesion molecules like NCAM1 and their interactions with receptors such as ROBO3, along with synaptic adhesion molecules like NLGN1 and their neurexin partners such as NRXN2, suggest a broader disruption of intercellular communication within the bone marrow niche, extending beyond the classical pathways known to be involved in hematopoiesis (66, 67). The downregulation of these critical genes (e.g., CLEC11A, ICAM4, ITGA4, and AVP) and their pathways in AML is not merely indicative of the disease's pathology but may also serve as negative biomarkers, which could provide valuable insights into the disease's severity, progression, and responsiveness to treatment. Their expression levels could potentially inform prognostic stratification and therapeutic targeting, underlining the necessity for continued research and development of interventions that can specifically modulate these dysregulated pathways. The intricate interplay of these gene expressions and their associated signaling cascades represents a sophisticated network that, when altered, contributes to the malignant phenotype of AML, emphasizing the importance of a nuanced understanding of these molecular mechanisms in the quest for more effective treatments.

Conclusion

The high ligand-receptor (LR) scores identified in Acute Myeloid Leukemia (AML) are strongly associated with T-cell dysfunction, underscoring the complex molecular interactions within the disease. Our findings validate the LR.score as a robust prognostic marker that accurately predicts survival outcomes and stratifies patients based on their likely responses to chemotherapy and immunotherapy. Clinically, the LR.score could be instrumental in guiding personalized treatment strategies by identifying patients who may benefit from specific therapies, such as immune checkpoint inhibitors or targeted treatments, based on their LR interaction profiles. This approach not only enhances prognostic precision but also supports the development of tailored therapeutic interventions, paving the way for more effective and individualized management of AML.

Data availability statement

The datasets presented in this study can be found in online repositories. The names of the repository/repositories and accession number(s) can be found in the article/Supplementary Material.

Ethics statement

The studies involving humans were approved by the Ethics Committee of Zhuji People's Hospital Affiliated to Wenzhou Medical University. The studies were conducted in accordance with the local legislation and institutional requirements. The participants provided their written informed consent to participate in this study.

Author contributions

CF: Conceptualization, Formal analysis, Investigation, Methodology, Software, Writing – original draft, Writing – review & editing. DQ: Data curation, Investigation, Validation, Writing – original draft, Writing – review & editing. MZ: Data curation, Resources, Writing – original draft, Writing – review & editing. SN: Formal analysis, Writing – original draft, Writing – review & editing. XJ: Conceptualization, Funding acquisition, Methodology, Project administration, Supervision, Writing – original draft, Writing – review & editing.

Funding

The author(s) declare financial support was received for the research, authorship, and/or publication of this article. This research was supported by the Zhejiang Province Medical and Health Technology Plan Project (Grant Numbers:2023RC293) and the Zhuji Medical and Health Technology Plan Project (Grant Numbers:2023YW095) and the Shaoxing Health Science and Technology Plan Project (Grant Numbers:2023SKY120).

Acknowledgments

We would like to thank the TCGA and UCSC databases for the availability of the data.

Conflict of interest

The authors declare that the research was conducted in the absence of any commercial or financial relationships that could be construed as a potential conflict of interest.

Publisher's note

All claims expressed in this article are solely those of the authors and do not necessarily represent those of their affiliated organizations, or those of the publisher, the editors and the reviewers. Any product that may be evaluated in this article, or claim that may be made by its manufacturer, is not guaranteed or endorsed by the publisher.

Supplementary material

The Supplementary Material for this article can be found online at: https://www.frontiersin.org/articles/10.3389/fonc.2024.1473048/full#supplementary-material

SUPPLEMENTARY FIGURE 1
(A) Trajectory depiction for each LR pair, with the horizontal axis representing the log value of each lambda and the vertical axis showcasing coefficient values. **(B)** Partial likelihood deviance for each ln(lambda) within the LASSO Cox regression model. **(C)** LASSO Cox coefficients for identified risk and protective LR pairs.

References

1. Dohner H, Estey EH, Amadori S, Appelbaum FR, Buchner T, Burnett AK, et al. Diagnosis and management of acute myeloid leukemia in adults: recommendations from an international expert panel, on behalf of the European LeukemiaNet. *Blood.* (2010) 115:453–74. doi: 10.1182/blood-2009-07-235358

2. Dohner H, Weisdorf DJ, Bloomfield CD. Acute myeloid leukemia. *N Engl J Med.* (2015) 373:1136–52. doi: 10.1056/NEJMra1406184

3. Stone RM, Mandrekar SJ, Sanford BL, Laumann K, Geyer S, Bloomfield CD, et al. Midostaurin plus chemotherapy for acute myeloid leukemia with a FLT3 mutation. *N Engl J Med.* (2017) 377:454–64. doi: 10.1056/NEJMoa1614359

4. Strickland SA, Vey N. Diagnosis and treatment of therapy-related acute myeloid leukemia. *Crit Rev Oncol Hematol.* (2022) 171:103607. doi: 10.1016/j.critrevonc.2022.103607

5. Lim JJ, Othus M, Shaw CM, Russell K, Halpern AB, Appelbaum JS, et al. Time independent factors that predict relapse in adults with acute myeloid leukemia. *Blood Cancer J.* (2024) 14:5. doi: 10.1038/s41408-023-00954-z

6. Tyner JW, Tognon CE, Bottomly D, Wilmot B, Kurtz SE, Savage SL, et al. Functional genomic landscape of acute myeloid leukaemia. *Nature.* (2018) 562:526–31. doi: 10.1038/s41586-018-0623-z

7. Cancer Genome Atlas Research N, Ley TJ, Miller C, Ding L, Raphael BJ, Mungall AJ, et al. Genomic and epigenomic landscapes of adult *de novo* acute myeloid leukemia. *N Engl J Med.* (2013) 368:2059–74. doi: 10.1056/NEJMoa1301689

8. Miles LA, Bowman RL, Merlinsky TR, Csete IS, Ooi AT, Durruthy-Durruthy R, et al. Single-cell mutation analysis of clonal evolution in myeloid Malignancies. *Nature.* (2020) 587:477–82. doi: 10.1038/s41586-020-2864-x

9. Papaemmanuil E, Gerstung M, Bullinger L, Gaidzik VI, Paschka P, Roberts ND, et al. Genomic classification and prognosis in acute myeloid leukemia. *N Engl J Med.* (2016) 374:2209–21. doi: 10.1056/NEJMoa1516192

10. Bullinger L, Dohner K, Dohner H. Genomics of acute myeloid leukemia diagnosis and pathways. *J Clin Oncol.* (2017) 35:934–46. doi: 10.1200/JCO.2016.71.2208

11. Narayanan D, Pozdnyakova O, Hasserjian RP, Patel SS, Weinberg OK. Effect of DNMT3A variant allele frequency and double mutation on clinicopathologic features of patients with *de novo* AML. *Blood Adv.* (2021) 5:2539–49. doi: 10.1182/bloodadvances.2021004250

12. Uckelmann HJ, Haarer EL, Takeda R, Wong EM, Hatton C, Marinaccio C, et al. Mutant NPM1 directly regulates oncogenic transcription in acute myeloid leukemia. *Cancer Discovery.* (2023) 13:746–65. doi: 10.1158/2159-8290.CD-22-0366

13. Short NJ, Nguyen D, Ravandi F. Treatment of older adults with FLT3-mutated AML: Emerging paradigms and the role of frontline FLT3 inhibitors. *Blood Cancer J.* (2023) 13:142. doi: 10.1038/s41408-023-00911-w

14. Shafat MS, Oellerich T, Mohr S, Robinson SD, Edwards DR, Marlein CR, et al. Leukemic blasts program bone marrow adipocytes to generate a protumoral microenvironment. *Blood.* (2017) 129:1320–32. doi: 10.1182/blood-2016-08-734798

15. Uy GL, Aldoss I, Foster MC, Sayre PH, Wieduwilt MJ, Advani AS, et al. Flotetuzumab as salvage immunotherapy for refractory acute myeloid leukemia. *Blood.* (2021) 137:751–62. doi: 10.1182/blood.2020007732

16. Vadakekolathu J, Rutella S. Escape from T-cell-targeting immunotherapies in acute myeloid leukemia. *Blood.* (2024) 143:2689–700. doi: 10.1182/blood.2023019961

17. Kuett A, Rieger C, Perathoner D, Herold T, Wagner M, Sironi S, et al. IL-8 as mediator in the microenvironment-leukaemia network in acute myeloid leukaemia. *Sci Rep.* (2015) 5:18411. doi: 10.1038/srep18411

18. Li Z, Herold T, He C, Valk PJ, Chen P, Jurinovic V, et al. Identification of a 24-gene prognostic signature that improves the European LeukemiaNet risk classification of acute myeloid leukemia: an international collaborative study. *J Clin Oncol.* (2013) 31:1172–81. doi: 10.1200/JCO.2012.44.3184

19. Herold T, Metzeler KH, Vosberg S, Hartmann L, Rollig C, Stolzel F, et al. Isolated trisomy 13 defines a homogeneous AML subgroup with high frequency of mutations in spliceosome genes and poor prognosis. *Blood.* (2014) 124:1304–11. doi: 10.1182/blood-2013-12-540716

20. Herold T, Jurinovic V, Batcha AMN, Bamopoulos SA, Rothenberg-Thurley M, Ksienzyk B, et al. A 29-gene and cytogenetic score for the prediction of resistance to induction treatment in acute myeloid leukemia. *Haematologica.* (2018) 103:456–65. doi: 10.3324/haematol.2017.178442

21. Metzeler KH, Hummel M, Bloomfield CD, Spiekermann K, Braess J, Sauerland MC, et al. An 86-probe-set gene-expression signature predicts survival in cytogenetically normal acute myeloid leukemia. *Blood.* (2008) 112:4193–201. doi: 10.1182/blood-2008-02-134411

22. Wang YH, Lin CC, Hsu CL, Hung SY, Yao CY, Lee SH, et al. Distinct clinical and biological characteristics of acute myeloid leukemia with higher expression of long noncoding RNA KIAA0125. *Ann Hematol.* (2021) 100:487–98. doi: 10.1007/s00277-020-04358-y

23. Hou R, Denisenko E, Ong HT, Ramilowski JA, Forrest ARR. Predicting cell-to-cell communication networks using NATMI. *Nat Commun.* (2020) 11:5011. doi: 10.1038/s41467-020-18873-z

24. Storey JD. A direct approach to false discovery rates. *J R Stat Society: Ser B (Statistical Methodology).* (2002) 64:479–98. doi: 10.1111/1467-9868.00346

25. Wilkerson MD, Hayes DN. ConsensusClusterPlus: a class discovery tool with confidence assessments and item tracking. *Bioinformatics.* (2010) 26:1572–3. doi: 10.1093/bioinformatics/btq170

26. Senbabaoglu Y, Michailidis G, Li JZ. Critical limitations of consensus clustering in class discovery. *Sci Rep.* (2014) 4:6207. doi: 10.1038/srep06207

27. Mootha VK, Lindgren CM, Eriksson KF, Subramanian A, Sihag S, Lehar J, et al. PGC-1alpha-responsive genes involved in oxidative phosphorylation are coordinately downregulated in human diabetes. *Nat Genet.* (2003) 34:267–73. doi: 10.1038/ng1180

28. Subramanian A, Tamayo P, Mootha VK, Mukherjee S, Ebert BL, Gillette MA, et al. Gene set enrichment analysis: a knowledge-based approach for interpreting genome-wide expression profiles. *Proc Natl Acad Sci U S A.* (2005) 102:15545–50. doi: 10.1073/pnas.0506580102

29. Liberzon A, Birger C, Thorvaldsdottir H, Ghandi M, Mesirov JP, Tamayo P. The Molecular Signatures Database (MSigDB) hallmark gene set collection. *Cell Syst.* (2015) 1:417–25. doi: 10.1016/j.cels.2015.12.004

30. Yu G, Wang LG, Han Y, He QY. clusterProfiler: an R package for comparing biological themes among gene clusters. *OMICS*. (2012) 16:284–7. doi: 10.1089/omi.2011.0118

31. Newman AM, Liu CL, Green MR, Gentles AJ, Feng W, Xu Y, et al. Robust enumeration of cell subsets from tissue expression profiles. *Nat Methods*. (2015) 12:453–7. doi: 10.1038/nmeth.3337

32. Jiang P, Gu S, Pan D, Fu J, Sahu A, Hu X, et al. Signatures of T cell dysfunction and exclusion predict cancer immunotherapy response. *Nat Med*. (2018) 24:1550–8. doi: 10.1038/s41591-018-0136-1

33. Hanzelmann S, Castelo R, Guinney J. GSVA: gene set variation analysis for microarray and RNA-seq data. *BMC Bioinf*. (2013) 14:7. doi: 10.1186/1471-2105-14-7

34. Mayakonda A, Lin DC, Assenov Y, Plass C, Koeffler HP. Maftools: efficient and comprehensive analysis of somatic variants in cancer. *Genome Res*. (2018) 28:1747–56. doi: 10.1101/gr.239244.118

35. Geeleher P, Cox N, Huang RS. pRRophetic: an R package for prediction of clinical chemotherapeutic response from tumor gene expression levels. *PloS One*. (2014) 9:e107468. doi: 10.1371/journal.pone.0107468

36. Mariathasan S, Turley SJ, Nickles D, Castiglioni A, Yuen K, Wang Y, et al. TGFbeta attenuates tumour response to PD-L1 blockade by contributing to exclusion of T cells. *Nature*. (2018) 554:544–8. doi: 10.1038/nature25501

37. Liu Y, He M, Wang D, Diao L, Liu J, Tang L, et al. HisgAtlas 1.0: a human immunosuppression gene database. *Database (Oxford)*. (2017) 2017:bax094. doi: 10.1093/database/bax094

38. Ley TJ, Ding L, Walter MJ, McLellan MD, Lamprecht T, Larson DE, et al. DNMT3A mutations in acute myeloid leukemia. *N Engl J Med*. (2010) 363:2424–33. doi: 10.1056/NEJMoa1005143

39. Mendler JH, Maharry K, Radmacher MD, Mrozek K, Becker H, Metzeler KH, et al. RUNX1 mutations are associated with poor outcome in younger and older patients with cytogenetically normal acute myeloid leukemia and with distinct gene and MicroRNA expression signatures. *J Clin Oncol*. (2012) 30:3109–18. doi: 10.1200/JCO.2011.40.6652

40. Bohme M, Kayser S. Immune-based therapeutic strategies for acute myeloid leukemia. *Cancers (Basel)*. (2021) 14:105. doi: 10.3390/cancers14010105

41. Witkowski MT, Lasry A, Carroll WL, Aifantis I. Immune-based therapies in acute leukemia. *Trends Cancer*. (2019) 5:604–18. doi: 10.1016/j.trecan.2019.07.009

42. Sun Y, Wang R, Xie S, Wang Y, Liu H. A novel identified necroptosis-related risk signature for prognosis prediction and immune infiltration indication in acute myeloid leukemia patients. *Genes (Basel)*. (2022) 13:1837. doi: 10.3390/genes13101837

43. Chen Y, You S, Li J, Zhang Y, Kokaraki G, Epstein E, et al. Follicular helper T-cell-based classification of endometrial cancer promotes precise checkpoint immunotherapy and provides prognostic stratification. *Front Immunol*. (2021) 12:788959. doi: 10.3389/fimmu.2021.788959

44. Huang X, Chen C, Xu Y, Shen L, Chen Y, Su H. Infiltrating T-cell abundance combined with EMT-related gene expression as a prognostic factor of colon cancer. *Bioengineered*. (2021) 12:2688–701. doi: 10.1080/21655979.2021.1939618

45. Chen Y, Chen D, Wang Q, Xu Y, Huang X, Haglund F, et al. Immunological classification of pancreatic carcinomas to identify immune index and provide a strategy for patient stratification. *Front Immunol*. (2021) 12:719105. doi: 10.3389/fimmu.2021.719105

46. Cheng WY, Li JF, Zhu YM, Lin XJ, Wen LJ, Zhang F, et al. Transcriptome-based molecular subtypes and differentiation hierarchies improve the classification framework of acute myeloid leukemia. *Proc Natl Acad Sci U S A*. (2022) 119:e2211429119. doi: 10.1073/pnas.2211429119

47. Ribeiro AF, Pratcorona M, Erpelinck-Verschueren C, Rockova V, Sanders M, Abbas S, et al. Mutant DNMT3A: a marker of poor prognosis in acute myeloid leukemia. *Blood*. (2012) 119:5824–31. doi: 10.1182/blood-2011-07-367961

48. Gaidzik VI, Schlenk RF, Paschka P, Stolzle A, Spath D, Kuendgen A, et al. Clinical impact of DNMT3A mutations in younger adult patients with acute myeloid leukemia: results of the AML Study Group (AMLSG). *Blood*. (2013) 121:4769–77. doi: 10.1182/blood-2012-10-461624

49. Tang JL, Hou HA, Chen CY, Liu CY, Chou WC, Tseng MH, et al. AML1/RUNX1 mutations in 470 adult patients with *de novo* acute myeloid leukemia: prognostic implication and interaction with other gene alterations. *Blood*. (2009) 114:5352–61. doi: 10.1182/blood-2009-05-223784

50. Topalian SL, Drake CG, Pardoll DM. Immune checkpoint blockade: a common denominator approach to cancer therapy. *Cancer Cell*. (2015) 27:450–61. doi: 10.1016/j.ccell.2015.03.001

51. Pardoll DM. The blockade of immune checkpoints in cancer immunotherapy. *Nat Rev Cancer*. (2012) 12:252–64. doi: 10.1038/nrc3239

52. Zhang Y, Chen Y, Papakonstantinou A, Tsagkozis P, Linder-Stragliotto C, Haglund F. Evaluation of PD-L1 expression in undifferentiated pleomorphic sarcomas, liposarcomas and chondrosarcomas. *Biomolecules*. (2022) 12:292. doi: 10.3390/biom12020292

53. Xu Y, Chen D, Shen L, Huang X, Chen Y, Su H. Identification and mechanism of the PD-1/PD-L1 genomic signature SORL1 as protective factor in bladder cancer. *Front Genet*. (2021) 12:736158. doi: 10.3389/fgene.2021.736158

54. Schreiber RD, Old LJ, Smyth MJ. Cancer immunoediting: integrating immunity's roles in cancer suppression and promotion. *Science*. (2011) 331:1565–70. doi: 10.1126/science.1203486

55. Tumeh PC, Harview CL, Yearley JH, Shintaku IP, Taylor EJ, Robert L, et al. PD-1 blockade induces responses by inhibiting adaptive immune resistance. *Nature*. (2014) 515:568–71. doi: 10.1038/nature13954

56. Ennis S, Conforte A, O'Reilly E, Takanlu JS, Cichocka T, Dhami SP, et al. Cell-cell interactome of the hematopoietic niche and its changes in acute myeloid leukemia. *iScience*. (2023) 26:106943. doi: 10.1016/j.isci.2023.106943

57. Shi Y, Riese DJ 2nd, Shen J. The role of the CXCL12/CXCR4/CXCR7 chemokine axis in cancer. *Front Pharmacol*. (2020) 11:574667. doi: 10.3389/fphar.2020.574667

58. Liu ZL, Chen HH, Zheng LL, Sun LP, Shi L. Angiogenic signaling pathways and anti-angiogenic therapy for cancer. *Signal Transduct Target Ther*. (2023) 8:198. doi: 10.1038/s41392-023-01460-1

59. Kim J, Lee TS, Lee MH, Cho IR, Ryu JK, Kim YT, et al. Pancreatic cancer treatment targeting the HGF/c-MET pathway: the MEK inhibitor trametinib. *Cancers (Basel)*. (2024) 16:1056. doi: 10.3390/cancers16051056

60. Li M, Ye J, Xia Y, Li M, Li G, Hu X, et al. METTL3 mediates chemoresistance by enhancing AML homing and engraftment via ITGA4. *Leukemia*. (2022) 36:2586–95. doi: 10.1038/s41375-022-01696-w

61. Kohnke T, Liu X, Haubner S, Bucklein V, Hanel G, Krupka C, et al. Integrated multiomic approach for identification of novel immunotherapeutic targets in AML. *biomark Res*. (2022) 10:43. doi: 10.1186/s40364-022-00390-4

62. Lee G, Spring FA, Parsons SF, Mankelow TJ, Peters LL, Koury MJ, et al. Novel secreted isoform of adhesion molecule ICAM-4: potential regulator of membrane-associated ICAM-4 interactions. *Blood*. (2003) 101:1790–7. doi: 10.1182/blood-2002-08-2529

63. Swanson AJ, Rogowski VJ, Bishop JA, Walker DM, Roxas GM, Raimondi SL. CLEC11A methylation is correlated to AML subtypes and cytogenetic risk factors but not patient demographics. *PloS One*. (2024) 19:e0300477. doi: 10.1371/journal.pone.0300477

64. Yin C, Zhang J, Guan W, Dou L, Liu Y, Shen M, et al. High expression of CLEC11A predicts favorable prognosis in acute myeloid leukemia. *Front Oncol*. (2021) 11:608932. doi: 10.3389/fonc.2021.608932

65. Freiwan A, Zoine JT, Crawford JC, Vaidya A, Schattgen SA, Myers JA, et al. Engineering naturally occurring CD7- T cells for the immunotherapy of hematological Malignancies. *Blood*. (2022) 140:2684–96. doi: 10.1182/blood.2021015020

66. Cai Z, Wei J, Chen Z, Wang H. High ROBO3 expression predicts poor survival in non-M3 acute myeloid leukemia. *Exp Biol Med (Maywood)*. (2021) 246:1184–97. doi: 10.1177/1535370220988246

67. Sasca D, Szybinski J, Schuler A, Shah V, Heidelberger J, Haehnel PS, et al. NCAM1 (CD56) promotes leukemogenesis and confers drug resistance in AML. *Blood*. (2019) 133:2305–19. doi: 10.1182/blood-2018-12-889725

frontiers | Frontiers in Immunology

TYPE Original Research
PUBLISHED 22 October 2024
DOI 10.3389/fimmu.2024.1491922

Check for updates

OPEN ACCESS

EDITED BY
Weiling Li,
Dalian Medical University, China

REVIEWED BY
Baifeng Li,
The First Affiliated Hospital of China Medical University, China
Li Guosheng,
Ningbo Diagnostic Pathology Center, China
Lei Cai,
Chongqing General Hospital, China

*CORRESPONDENCE
Dayong Cao
caodayongdoctty@163.com
Jianqiang Cai
caijianqiangdoctty@163.com
Jianguo Zhou
zjgtydoct@163.com
Tao Yan
blizzardyt@163.com

†These authors have contributed equally to this work

RECEIVED 05 September 2024
ACCEPTED 07 October 2024
PUBLISHED 22 October 2024

CITATION
Wang B, Chen X, Li R, Ai B, Ye F, Zhao J, Zhang Y, Huang Z, Li Z, Bi X, Zhao H, Cao D, Cai J, Zhou J and Yan T (2024) Comprehensive evaluation of clinical outcomes in hepatic epithelioid hemangioendothelioma subsets: insights from SEER Database and departmental cohort analysis. *Front. Immunol.* 15:1491922. doi: 10.3389/fimmu.2024.1491922

COPYRIGHT
© 2024 Wang, Chen, Li, Ai, Ye, Zhao, Zhang, Huang, Li, Bi, Zhao, Cao, Cai, Zhou and Yan. This is an open-access article distributed under the terms of the Creative Commons Attribution License (CC BY). The use, distribution or reproduction in other forums is permitted, provided the original author(s) and the copyright owner(s) are credited and that the original publication in this journal is cited, in accordance with accepted academic practice. No use, distribution or reproduction is permitted which does not comply with these terms.

Comprehensive evaluation of clinical outcomes in hepatic epithelioid hemangioendothelioma subsets: insights from SEER Database and departmental cohort analysis

Bingchen Wang[1†], Xiao Chen[1†], Rongxuan Li[1†], Bolun Ai[2†], Feng Ye[3], Jianjun Zhao[1], Yefan Zhang[1], Zhen Huang[1], Zhiyu Li[1], Xinyu Bi[1], Hong Zhao[1], Dayong Cao[1*], Jianqiang Cai[1*], Jianguo Zhou[1*] and Tao Yan[4*]

[1]Department of Hepatobiliary Surgery, National Cancer Center/National Clinical Research Center for Cancer/Cancer Hospital, Chinese Academy of Medical Sciences and Peking Union Medical College, Beijing, China, [2]Department of Breast Surgical Oncology, National Cancer Center/National Clinical Research Center for Cancer/Cancer Hospital, Chinese Academy of Medical Sciences and Peking Union Medical College, Beijing, China, [3]Department of Radiology, National Cancer Center/National Clinical Research Center for Cancer/Cancer Hospital, Chinese Academy of Medical Sciences and Peking Union Medical College, Beijing, China, [4]Department of Anesthesiology, National Cancer Center/National Clinical Research Center for Cancer/Cancer Hospital, Chinese Academy of Medical Sciences and Peking Union Medical College, Beijing, China

Background: Epithelioid hemangioendothelioma (EHE), is an uncommon, intermediate-grade malignant vascular tumor that can manifest in diverse organs, including the liver, lungs, and bones. Given its unique malignancy profile and rarity, there lacks a consensus on a standardized treatment protocol for EHE, particularly for hepatic epithelioid hemangioendothelioma (HEHE). This study aims to elucidate factors influencing the clinical prognosis of EHE by analyzing data from the SEER database, complemented with insights from a departmental cohort of 9 HEHE cases. Through this, we hope to shed light on potential clinical outcomes and therapeutic strategies for HEHE.

Methods: Using SEER data from 22 registries, we analyzed 313 liver cancer patients with ICD-O-3 9130 and 9133 histology. Twelve variables were examined using Cox regression and mlr3 machine learning. Significant variables were identified and compared. Clinical data, imaging characteristics, and treatment methods of nine patients from our cohort were also presented.

Result: In univariate and multivariate Cox regression analyses, Age, Sex, Year of diagnosis, Surgery of primary site, Chemotherapy, and Median household income were closely related to survival outcomes. Among the ten survival-related machine learning models, CoxPH, Flexible, Mboost, and Gamboost stood out based on Area Under the Curve(AUC), Decision Curve Analysis(DCA), and Calibration Curve Metrics. In the feature importance analysis of these four selected models, Age and Surgery of primary site were consistently identified as the most critical factors influencing prognosis. Additionally, the clinical data of nine patients from our cohort not only demonstrated unique imaging

characteristics of HEHE but also underscored the importance of surgical intervention.

Conclusion: For patients with resectable HEHE, surgical treatment is currently a highly important therapeutic approach.

KEYWORDS

general surgery, hepatic epithelioid hemangioendothelioma, SEER, Cox regression analyses, machine learning

1 Introduction

Epithelioid hemangioendothelioma (EHE) is a rare vascular tumor, first high-lighted by the seminal studies of Weiss and Enzinger in 1982 (1). This low-grade malignancy is characterized by its unique assembly of predominantly epithelioid endothelial cells. While EHE can be found in various anatomical locations, its presence in the liver, known as hepatic epithelioid hemangioendothelioma (HEHE), often navigates the challenging waters of diagnosis, sometimes being mistaken for other hepatic tumors (2, 3). Intriguingly, epidemiological insights suggest a greater inclination toward females, especially those aged 40-55, though its overall incidence is notably low, less than 0.1 per 100,000 (3–9). A defining characteristic of EHE is its absence of vasoformation, distinguishing it from other vascular tumors (10). Delving into its molecular underpinnings, chromosomal rearrangements involving the WWTR1 and CAMTA1 genes emerge as key players, complemented by the noteworthy YAP-THE3 gene fusion (11–13). Diagnostically, EHE's marked preference for specific endothelial markers is a pivotal feature (14).

Clinical presentations of Hepatic Epithelioid Hemangioendothelioma (HEHE) are diverse. While some patients exhibit no symptoms, others may experience a range of manifestations, including right upper quadrant pain, weight loss, jaundice, nausea, anorexia, fatigue, and hepatomegaly (3, 4, 6, 9). In radiographic evaluations, the nodules of HEHE routinely appear to be multiple and peripheral in the image presentation. HEHE distinctly manifests through three primary characteristics: the Capsular Retraction (15, 16), indicative of liver tissue hypertrophy due to tumor-associated fibrotic changes; the Target Sign on T2W imaging, epitomized by a central high-intensity core, flanked by a low-intensity ring and subtly accentuated by an outer high-intensity halo (17); and the Lollipop Sign in enhanced imaging, where the 'candy' delineates the evident tumor mass, while the 'bar' depicts the occluded vein on T2WI (18). Collectively, these imaging signatures are instrumental in differentiating HEHE from other hepatic metastatic entities.

Due to the rarity of EHE and limited research available, a standardized treatment protocol for HEHE has yet to be established. For 253 diagnosed HEHE patients, survival rates irrespective of the treatment approach were observed to be 83.4% (211 patients) at 1 year, 55.7% (141 patients) at 3 years, and 41.1% (104 patients) at 5 years (9). For HEHE patients, various treatment modalities have been explored in clinical trials and analyses. These include surgical options like hepatectomy and liver transplantation (LT), alternative therapies such as ablation and transcatheter arterial chemoembolization (TACE), as well as systemic treatments encompassing chemotherapy, anti-VEGF therapy, and mTOR inhibitors (19–22). However, one study suggested that the 5-year survival rates across various treatment approaches showed no significant differences, leading to a recommendation for a watchful waiting strategy (23). While the mechanisms and progress in basic research on EHE are continuously advancing, surgical treatments remain the most common and major treatments for patients with EHE at present from a clinical aspect (9).

2 Materials and methods

2.1 The data sources

From the SEER Research data encompassing 22 registries, 313 liver cancer patients diagnosed with histology ICD-O-3 9133 (EHE) and 9130 (HE) were identified for detailed analysis. Key variables such as age, sex, year of diagnosis, race, combined summary stage, surgery of primary site, radiotherapy, chemotherapy, preoperative or postoperative systemic therapy, sequence number, median household income, rural urban continuum code, survival duration, and living status were extracted from their respective fields in the SEER database.

For this study, 9 HEHE patients were selected from our hospital. The inclusion criteria were: 1) patients who underwent liver resection due to hepatic lesions between 2012 and 2022 and were pathologically diagnosed with HEHE post-surgery, and 2) patients aged 18 years or older. Patients were excluded from the study if they met any of the following criteria: 1) Patients who did not undergo surgical resection, and 2) Patients under 18 years of age. Detailed baseline information was compiled, including gender, age, primary diagnosis, tumor ICD, clinical symptoms, underlying conditions, and physical signs. Radiological features covered tumor location, size, multiplicity, peripheral involvement, capsular retraction, target sign, and lollipop sign. Pathological features, including immunohistochemical markers

like CD34, CD31, ERG, and Fli1, were documented, with results presented in an embedded pie chart. Laboratory results included markers such as CA199, AFP, CEA, ALT, AST, and additional tests. All clinical and pathological data were obtained through routine hospital procedures. This study was approved by the Institutional Review Board of the Cancer Hospital, Chinese Academy of Medical Sciences and Peking Union Medical College. All patients provided informed consent.

2.2 Statistical analysis

Statistical analyses were primarily executed in R Studio. Using the autoReg package, we performed univariate and multivariate Cox regression analyses to identify variables related to survival. The dataset was divided into training and validation sets in an 8:2 ratio to prepare for survival-related machine learning and there were no statistically significant differences in baseline characteristics (Supplementary Table 1) or survival information (Supplementary Figure 1) between the training and validation sets. We constructed survival-related machine learning models using the following mlr3 models: "surv.coxph" (a traditional proportional hazards model), "surv.cv_glmnet" (a regularized regression model), "surv.rpart" (a decision tree-based model), "surv.rfsrc" (a random forest model), "surv.gbm" (a gradient boosting model), "surv.flexible" (a flexible parametric spline learner using flexsurv::flexsurvspline()), "surv.blackboost", "surv.gamboost", and "surv.glmboost" (all boosting-based models). For each model, we calculated and plotted the AUC (evaluating discriminatory power), calibration curves (assessing prediction accuracy), and DCA (analyzing clinical utility) for both the training and validation sets. Models with an AUC above 0.75, calibration curves fitting the reference line, and beneficial DCA were selected. Feature importance analysis was conducted on the top-performing models to rank variables influencing survival. The important variables identified by traditional Cox regression and machine learning (especially treatment methods) were further analyzed in different subgroups (Figure 1).

3 Results

3.1 Study population and Cox regression

The baseline characteristics of 313 patients, stratified by the surgery of the primary site, are presented in Table 1. It can be observed that the choice of surgery of the primary site among the various groups shows statistically significant differences only in the preoperative or postoperative systemic therapy group. In all other groups, the surgery of the primary site (including no surgery or unknown, wedge or segmental resection, lobectomy, hepatectomy, and transplant) does not exhibit statistically significant differences.

Table 2 also presents data for the 313 patients, showing that the mean age at diagnosis is 51 years, with a higher proportion of female patients (53.7%). A portion of the patients (34.5%) were diagnosed at the distant stage. Univariate and multivariate Cox regression analyses identified age (Final HR: 1.03 [1.02-1.04], p<.001), gender (Female vs. Male, Final HR: 0.67 [0.48-0.93], p=.017), year of diagnosis (after 2010 vs. before 2010, Final HR: 0.53 [0.37-0.75], p<.001), surgery of the primary site (wedge or segmental resection or lobectomy vs. no surgery or unknown, Final HR: 0.43 [0.25-0.73], p=.002; hepatectomy and/or transplant vs. no surgery or unknown, Final HR: 0.27 [0.11-0.66], p=.004), chemotherapy (yes vs. no or unknown, Final HR: 1.89 [1.32-2.72], p=.001), and median household income (more than $70,000 vs. below $70,000, Final HR: 0.57 [0.41-0.80], p=.001) as significant variables influencing survival prognosis.

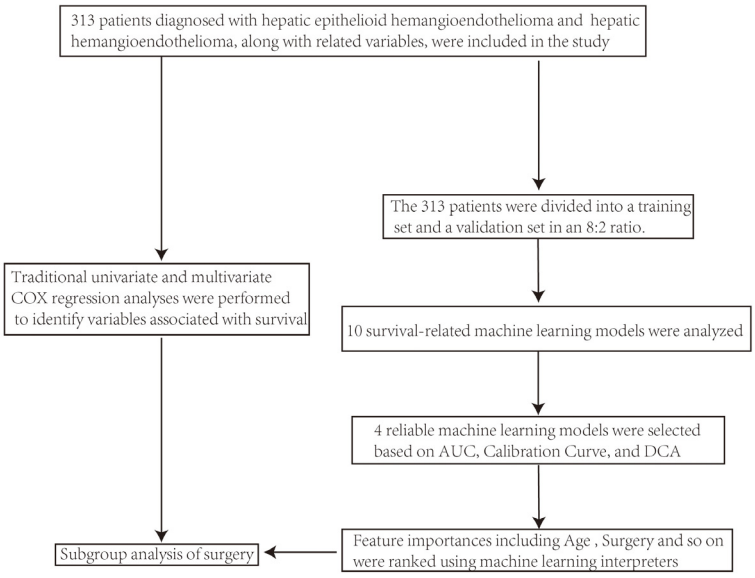

FIGURE 1
Flowchart of analysis using the SEER database.

TABLE 1 Baseline Characteristics of 313 Patients Stratified by Primary Site Surgery

	no surgery or unknown	Wedge or segmental resection or Lobectomy	Hepatectomy and or transplant	p.overall
	N=229	*N=58*	*N=26*	
Age	55.0 [39.0;65.0]	53.5 [37.2;62.8]	45.0 [38.2;54.2]	0.164
Sex:				**0.301**
Male	107 (46.7%)	23 (39.7%)	15 (57.7%)	
Female	122 (53.3%)	35 (60.3%)	11 (42.3%)	
Year of diagnosis:				**0.454**
before and in 2010	106 (46.3%)	23 (39.7%)	14 (53.8%)	
after 2010	123 (53.7%)	35 (60.3%)	12 (46.2%)	
Race:				**0.858**
White	183 (79.9%)	48 (82.8%)	22 (84.6%)	
others	46 (20.1%)	10 (17.2%)	4 (15.4%)	
Combined Summary Stage:				
Localized	49 (21.4%)	34 (58.6%)	6 (23.1%)	
Regional	25 (10.9%)	9 (15.5%)	12 (46.2%)	
Distant	91 (39.7%)	11 (19.0%)	6 (23.1%)	
Unknown/unstaged	64 (27.9%)	4 (6.90%)	2 (7.69%)	
Radiation recode:				**0.450**
None or Unknown	221 (96.5%)	56 (96.6%)	24 (92.3%)	
radiation performed	8 (3.49%)	2 (3.45%)	2 (7.69%)	
Chemotherapy recode:				**0.120**
No or Unknown	161 (70.3%)	48 (82.8%)	17 (65.4%)	
Yes	68 (29.7%)	10 (17.2%)	9 (34.6%)	
Systemic Sur Seq:				**<0.001**
no Systemic therapy after and before surgery	225 (98.3%)	50 (86.2%)	19 (73.1%)	
Systemic therapy after or before surgery	4 (1.75%)	8 (13.8%)	7 (26.9%)	
Sequence number:				**0.806**
One primary only	187 (81.7%)	47 (81.0%)	20 (76.9%)	
Over one	42 (18.3%)	11 (19.0%)	6 (23.1%)	
Median_household_income_inflation_adj_to_2021:				**0.807**
below $70000	113 (49.3%)	26 (44.8%)	12 (46.2%)	
more than $70000	116 (50.7%)	32 (55.2%)	14 (53.8%)	
Rural Urban Continuum Code:				**0.441**
Metropolitan (1 million+)	161 (70.3%)	37 (63.8%)	20 (76.9%)	
Other metropolitan or non-metropolitan	68 (29.7%)	21 (36.2%)	6 (23.1%)	

TABLE 2 Univariate and Multivariate Cox Regression Analyses

	Dependent: Surv(time, status == 1)	all	HR (univariable)	HR (multivariable)	HR (final)
Age	Mean ± SD	51.0 ± 17.9	1.03 (1.02-1.04, p<.001)	1.04 (1.02-1.05, p<.001)	1.03 (1.02-1.04, p<.001)
Sex	Male	145 (46.3%)			
	Female	168 (53.7%)	0.69 (0.49-0.95, p=.025)	0.68 (0.49-0.95, p=.024)	0.67 (0.48-0.93, p=.017)
Year of diagnosis	before and in 2010	143 (45.7%)			
	after 2010	170 (54.3%)	0.68 (0.48-0.96, p=.027)	0.59 (0.41-0.86, p=.006)	0.53 (0.37-0.75, p<.001)
Race	White	253 (80.8%)			
	others	60 (19.2%)	1.12 (0.75-1.69, p=.576)		
Combined Summary Stage	Localized	89 (28.4%)			
	Regional	46 (14.7%)	1.31 (0.72-2.37, p=.374)	1.39 (0.75-2.57, p=.293)	
	Distant	108 (34.5%)	1.86 (1.16-2.96, p=.010)	1.51 (0.90-2.54, p=.116)	
	Unknown/unstaged	70 (22.4%)	2.09 (1.28-3.40, p=.003)	1.88 (1.08-3.30, p=.026)	
Surg Prim Site	no surgery or unknown	229 (73.2%)			
	Wedge or segmental resection or Lobectomy	58 (18.5%)	0.41 (0.24-0.69, p<.001)	0.54 (0.31-0.96, p=.036)	0.43 (0.25-0.73, p=.002)
	Hepatectomy and or transplant	26 (8.3%)	0.26 (0.11-0.64, p=.003)	0.29 (0.12-0.73, p=.009)	0.27 (0.11-0.66, p=.004)
Radiation recode	None or Unknown	301 (96.2%)			
	radiation performed	12 (3.8%)	1.85 (0.90-3.77, p=.092)		
Chemotherapy recode	No or Unknown	226 (72.2%)			
	Yes	87 (27.8%)	1.53 (1.08-2.17, p=.017)	2.00 (1.34-2.99, p=.001)	1.89 (1.32-2.72, p=.001)
Systemic Sur Seq	no Systemic therapy after and before surgery	294 (93.9%)			
	Systemic therapy after or before surgery	19 (6.1%)	0.94 (0.48-1.85, p=.857)		
Sequence number	One primary only	254 (81.2%)			
	Over one	59 (18.8%)	1.40 (0.95-2.06, p=.091)		
Median_household_income_inflation_adj_to_2021	below $70000	151 (48.2%)			
	more than $70000	162 (51.8%)	0.68 (0.49-0.95, p=.023)	0.56 (0.40-0.79, p=.001)	0.57 (0.41-0.80, p=.001)
Rural Urban Continuum Code	Metropolitan (1 million+)	218 (69.6%)			
	Other metropolitan or non-metropolitan	95 (30.4%)	1.37 (0.97-1.93, p=.070)		

n=313, events=143, Likelihood ratio test=95.49 on 10 df(p<.001).

10.3389/fimmu.2024.1491922

3.2 Construction and selection of survival-related machine learning models and presentation of variable importance

Figure 2A presents the AUC values of 10 different machine learning models at 1, 3, and 5-year specific time points in the training set, while Figure 2B shows the AUC values for these models at the same time points in the validation set. It was observed that the AUC values of the CoxPH model, flexible model, gamboost model, mboost model, and gbm model were all greater than 0.75 (Supplementary Figures 2A–J). However, the DCA curve indicated that the performance of the gbm model was not ideal (Figure 2C), whereas the calibration curves for the CoxPH model, flexible model, gamboost model, and mboost model fit the reference line (Figures 2D–G). Consequently, the CoxPH model, flexible model, gamboost model, and mboost model were selected for subsequent variable importance analysis. Figures 3A–D illustrate the feature importance of relevant variables for the CoxPH model, flexible model, gamboost model, and mboost model at 1, 3, and 5 years, while Figure 3E presents the time-dependent variable importance. It can be clearly seen that, across the different time points, Age and surgery of the primary site consistently emerged as the two most significant factors influencing prognosis. Basic sequencing studies have also found that age is associated with rapid tumor progression, and surgical treatment remains a superior option in the absence of effective chemotherapy and targeted therapy.

3.3 Group analyses of surgery and comparison of surgery types

At the aim of further exploring the specific therapeutic role of surgery in HEHE tumors, group analyses of surgery's presence or absence within "Age" group, "Chemotherapy" group, "Stage" group, "Median house income" group, "Race" group, "Radiotherapy" group, "Rural urban continuum" group, "Sequence number" group, "Sex" group, "Systemic therapy and surgery" group and "Year of diagnosis" group, are performed and the forest plot of group analyses is drawn (Figure 4A).

In the forest plot for subgroup analysis, it is evident that surgery has a positive effect across various groups, including the year of diagnosis, presence of preoperative or postoperative adjuvant therapy, gender, sequence number, rural-urban continuum code, and income. Patients with localized or regional stage disease benefit from surgery, whereas those with distant stage disease do not show a significant benefit. Patients undergoing chemotherapy or radiation therapy may not derive a clear benefit from surgery, likely due to their more advanced stage at diagnosis. Interestingly, patients younger than 50 years old do not seem to benefit from surgical treatment, which may be due to the limited sample size leading to the lack of statistical significance for surgical treatment. After performing propensity score matching (PSM) to ensure baseline comparability for surgery performed or not (Supplementary Table 2), surgery remained a significant variable associated with better prognosis in both univariate and multivariate Cox regression analyses (Supplementary Table 3). Overall, it can be concluded that patients with limited tumor stages who meet the surgical criteria should undergo further surgical treatment.

In terms of surgical approaches, no significant differences were observed between resection or lobectomy and hepatectomy or transplant across patient-level variables, apart from tumor staging (Supplementary Table 4). The Sankey diagram further highlights a preference for resection or lobectomy in patients with localized tumors, whereas hepatectomy or transplant was more frequently chosen for those with regional or distant disease (Figure 4B). Nonetheless, no statistically significant differences in survival outcomes were detected between the two surgical strategies (Figure 4C).

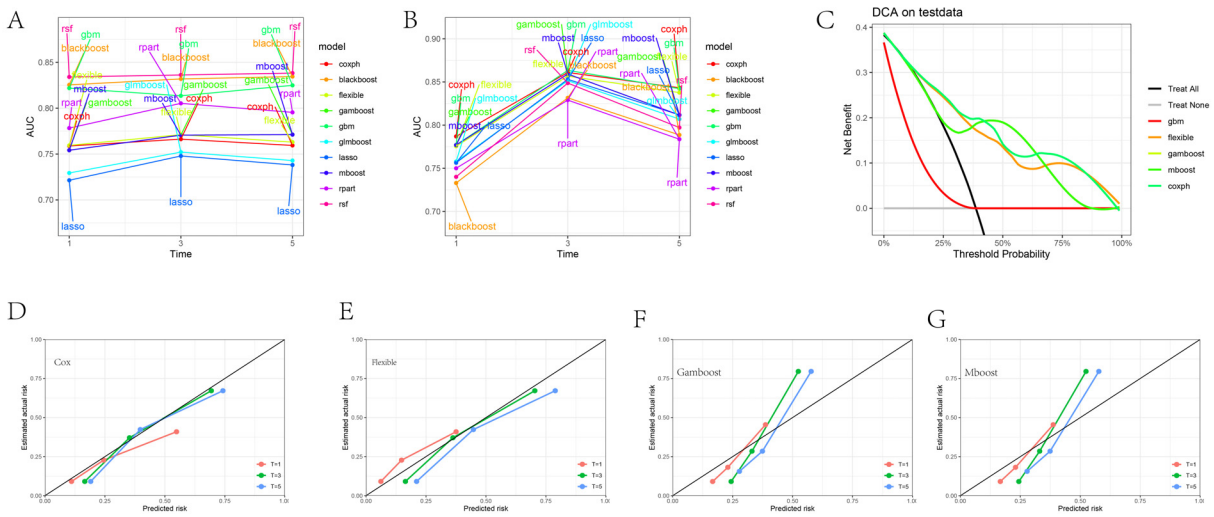

FIGURE 2
Machine Learning Model Evaluation and Display. **(A)** AUC values of 10 different machine learning models at 1, 3, and 5-year specific time points in the training set. **(B)** AUC values of 10 different machine learning models at 1, 3, and 5-year specific time points in the test set. **(C)** DCA plot of selected machine model. **(D–G)** Calibration plot of CoxPH, Flexible, Gamboost, mboost machine model.

10.3389/fimmu.2024.1491922

FIGURE 3
Feature Importance Ranking Display of the Four Selected Models. **(A)** CoxPH model. **(B)** Flexible model. **(C)** Gamboost model **(D)** Mboost model **(E)** Time-dependent feature importance of the four models.

3.4 Clinical information for the nine patients from our departmental cohort

Inset pie charts are used to visualize baseline information, image feature, pathological features about HEHE patients in our cohort (Figure 5). It's evident that the majority of patients are in good overall health, with 66.7% having no concurrent illnesses. Similarly, 66.7% of the patients are asymptomatic, and a significant portion of the cohort is female (Figure 5A). When it comes to imaging information for HEHE patients, the majority of tumor lesions are characterized as multiple (66.7%) and peripheral (88.9%). Capsular retraction is observed in 44.4% of cases, while 'target' and 'lollipop' signs are also significant features, each present in 33.3% of the images (Figures 5B, 6). It can be observed that peripheral 'target' signs in T2 MRI (Figures 6A–C, E, F) and capsular retraction (Figure 6A). 'Lollipop' signs can be clearly detected in which offer the valuable imaging feature (Figure 6D). The pathological features of HEHE samples from our department can be summarized as follows: HEHE tumors exhibit a range of sizes with some showing no cumulative liver involvement. Histologically, these tumors often present with epithelial-like or spindle-shaped cells, some of which have cellular atypia. Notably, features such as fatty degeneration of surrounding liver tissue, vacuoles in the cytoplasmic membrane, and rare nuclear mitoses can be observed. Furthermore, the presence of multinucleated cells and cells arranged in nests are consistent with epithelioid hemangioendothelioma morphology. When it comes to the pathological immunohistochemical features, the majority of specimens show positive staining for CD31 and CD34 (former), as well as for Ki67, Vimentin, and SMA (latter) at rates of 77.8%, 66.7%, 88.9%, 55.6%, and 44.4%, respectively. The former two markers signify endothelial characteristics, while the latter two indicate cytokeratin and smooth muscle actin markers. Ki67, in particular, implies the proliferative nature of the tumor cells (Figure 5C). A small

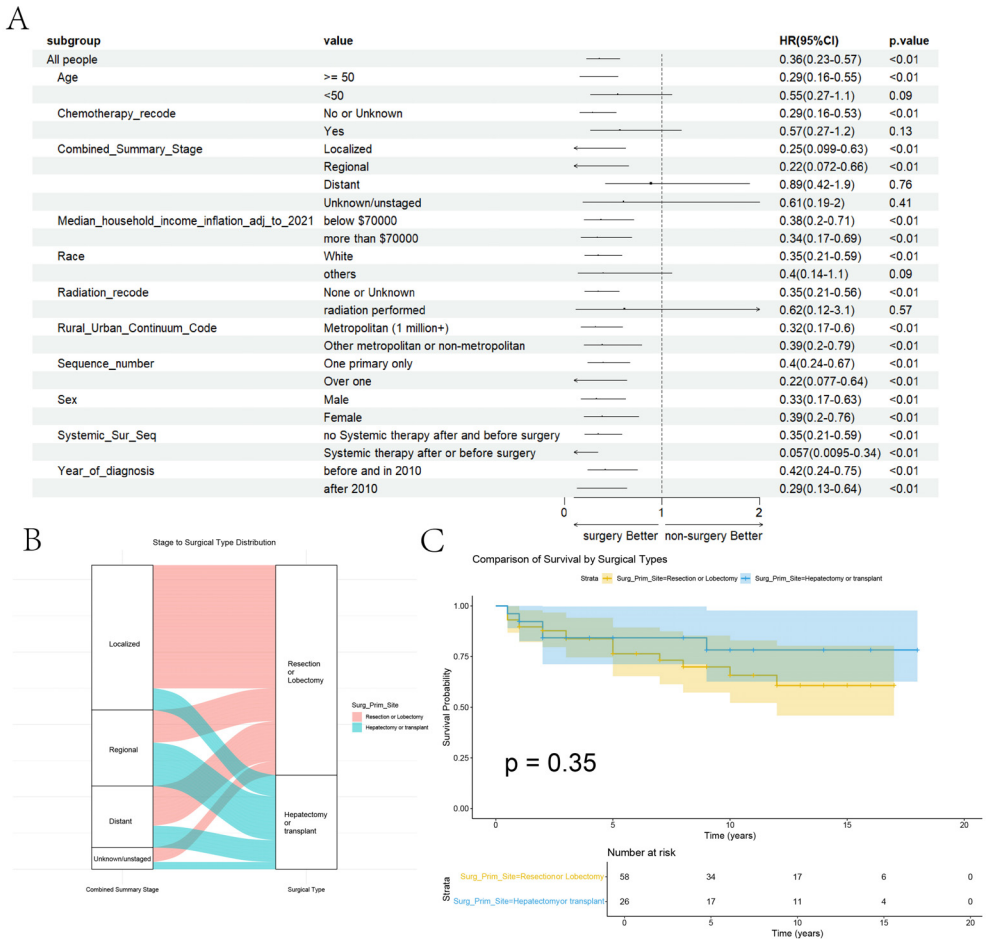

FIGURE 4
Group Analyses of Surgery and Comparison of Surgery Types. **(A)** Group Analyses of Surgery within the related variables. **(B)** The Sankey diagram illustrates the relationship between tumor staging and surgical approaches. **(C)** Comparison of the Kaplan-Meier curves between the two surgical approaches.

portion of them also stains positively for MelanA, HMB 45, Flil, ERG in immunohistochemistry while few of them stains positively for CK18, GPC3, Hepatocyte, Desmin (Figures 5D, E). The laboratory parameters (mainly including liver function and tumor markers) of the 9 patients before and after surgery are mostly within the normal range. All nine EHE patients underwent surgery corresponding to the site of tumor growth and their progression-free survival (PFS) was listed (Figure 7). The HEHE recurrence rate is relatively high (4/9),with nearly all recurrence sites located in adjacent liver tissues. Due to the small sample size, it is not sufficient to draw statistically significant conclusions, and further relevant analysis cannot be conducted.

4 Discussion

Epithelioid hemangioendothelioma (EHE) is a unique vascular tumor, initially identified in 1982. When it appears in the liver, it's termed hepatic epithelioid hemangioendothelioma (HEHE) and often poses diagnostic challenges. Though prevalent in females aged 40-55, its incidence is low. Distinctive molecular markers and its absence of vasoformation set it apart from similar tumors. Clinically, HEHE symptoms vary, with some patients being asymptomatic, while others show signs like pain and weight loss. Radiographically, HEHE is characterized by its peripheral distribution and multifocality. Additionally, distinctive imaging features include capsular retraction, 'target' sign, and 'lollipop' signs. Treatment protocols are diverse and not yet standardized due to its rare occurrence.

Despite the limited dataset in our department, which consists of only 9 cases, the clinical characteristics of HEHE patients exhibit a certain degree of representativeness. Additionally, by combining our departmental data with existing literature, certain clinical features of HEHE can be elucidated. In HEHE patients, a preference for females, non-specific clinical symptoms, and the presence of multiple and peripheral nodular lesions are main manifestations. Capsular retraction, along with the 'target' and 'lollipop' signs, are prominent radiological hallmarks observed in

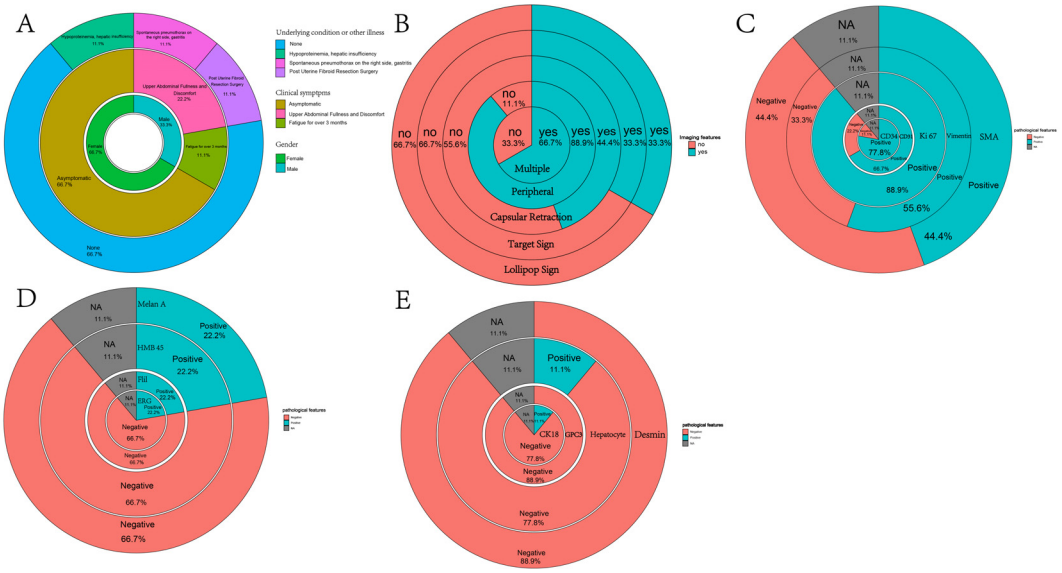

FIGURE 5
Inset pie charts visualizing various types of information about HEHE patients. **(A)** Inset pie chart showing the underlying condition or illness, clinical symptoms, and gender of 9 HEHE patients. **(B)** Inset pie chart showing the imaging features of 9 patients. **(C)** Inset pie chart showing pathological specimens of 9 patients with immunohistochemical information on CD34, CD31, Ki67, Vimentin, SMA. **(D)** Inset pie chart showing pathological specimens of 9 patients with immunohistochemical information on ERG, FliI, HMB45, MelanA. **(E)** Inset pie chart showing pathological specimens of 9 patients with immunohistochemical information on CK18, GPC3, Hepatocyte, Desmin.

HEHE imaging. However, right upper quadrant pain is regarded as the most common clinical manifestation of HEHE (5, 6) and some rare cases had rare syndrome such as Budd-Chiari syndrome (24) and Kasabach–Merrit syndrome (25). On contrast-enhanced study, CT and MRI share common features and the character can be described as three patterns. Some tumors display mild homogeneous enhancement in arterial phase without any change in the delayed or portal vein phase. Some masses show ring like enhancement at first in the arterial phase and full enhancement in the delayed and portal phases, which is called “halo sign”. And the last type is the heterogeneous enhancement which progresses in all phases (26, 27). It has been concisely summarized that lesions smaller than 2 cm predominantly exhibit mild homogeneous enhancement; lesions ranging from 2-3cm display ring-like enhancement transitioning to heterogeneous delayed enhancement; lesions exceeding 3 cm predominantly manifest heterogeneous delayed enhancement (28, 29). The imaging characteristics of our cohort of 9 patients, especially those

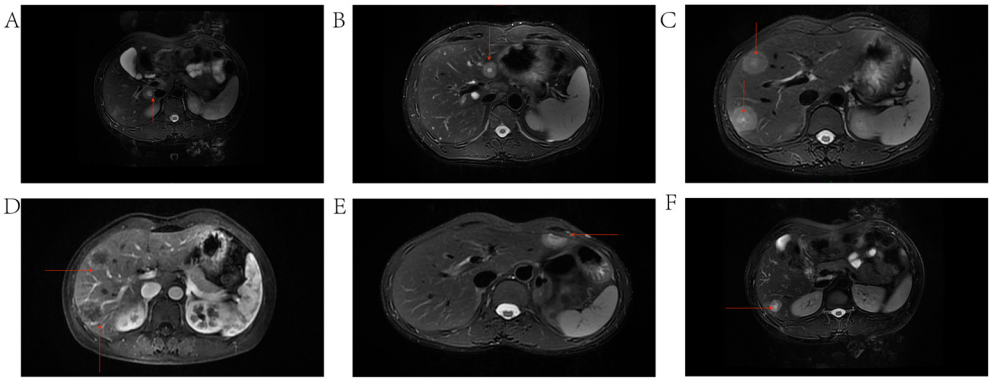

FIGURE 6
Typical imaging features including capsular retraction, ‘target’ and ‘lollipop’ signs on MRI. **(A)** HEHE tumor located in the periphery of the caudate lobe of the liver exhibiting the target sign and capsular retraction. **(B)** HEHE tumor located in the periphery of the left lobe of the liver exhibiting a Target Sign. **(C)** Multiple HEHE tumors located in the peripheral areas of segment VIII of the liver, exhibiting target signs. **(D)** EHE tumors exhibiting the Lollipop sign, where the tumor represents the head of the lollipop, and the tortuous, occluded vessels form the stick of the lollipop. **(E)** HEHE tumor located in the periphery of segment III of the liver, exhibiting a Target Sign. **(F)** HEHE tumor located in the periphery of the right lobe of the liver, exhibiting the target Sign.

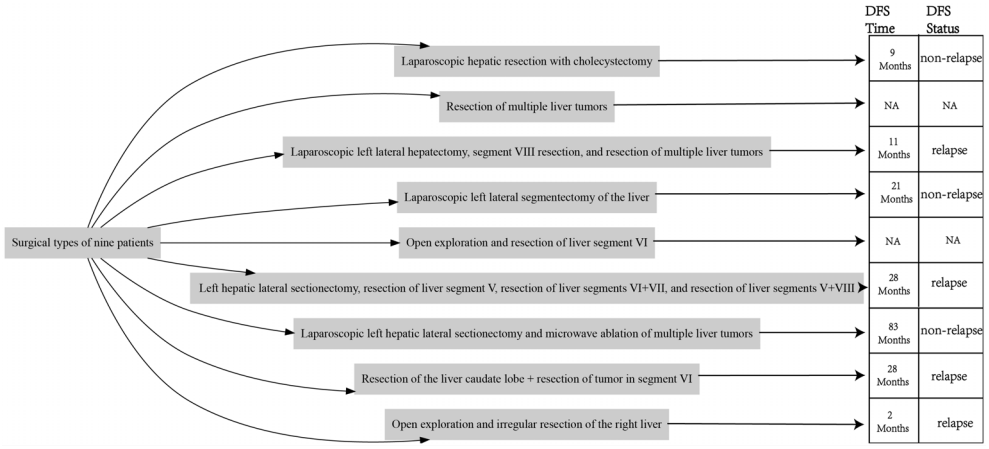

FIGURE 7
Surgery types and corresponding PFS information of the 9 HEHE patients.

discerned from MRI, largely resonate with the imaging findings delineated in the review literature concerning EHE patients. However, the manifestations of enhancement types in HEHE may seem restricted, given the limited sample size. The immunohistochemical staining characteristics of endothelial cells in the pathology of the 9 patients presented in the department align with the pathological features of EHE: epithelioid cells arranged in cords and nests within the stroma but do not exhibit vasoformation. The pathological finding of poorly formed endothelial cells is the primary criterion for identifying EHE, but It is also proved that immunohistochemistry for CAMTA1 expression of nuclear is a significant method to distinguish EHE from other epithelioid vascular tumors including epithelioid angiosarcoma, epithelioid sarcoma which have the mimic histologic features with the expression of TFE3 by immunohistochemistry being another candidate method (30, 31).

In one study aiming at detecting common secondary genomic variants associated with advanced EHE from 49 participants, more than half patients exhibited pathogenic genomic variants in addition to TAZ-CAMTA1 fusion and 18.4% patients in the study showed potentially targetable genomic variants. Importantly, patients who were older were more likely to have clinically targetable variants and the same condition occurred in patients with III/IV stage (32). The aforementioned literature emphasizes that secondary mutations may be the reason for the transition of EHE from indolent to malignant. It also points out that as age increases and disease stage advances, there may be a higher likelihood of secondary mutations occurring, leading to potentially more uncontrollable disease progression. This is consistent with the impact observed in the analysis of the machine results we examined.

It is unknown why the chemotherapy exhibits opposite effect in our Cox Model. Several reasons might hide behind the above question. First of all, the SEER database lacks comprehensive specific information regarding chemotherapy. It is not clear which chemotherapy agent is used for EHE patients. Secondly, the progress of chemotherapy seemed stagnant before the mechanism of EHE was discovered and the oral drug therapy is limited for the rarity of EHE. Conventional chemotherapy such as anthracyclines regimens、pazopanib、paclitaxel and so on exerted restricted effect on treatment of HEHE (33). Thirdly, the information collected in the SEER database spans a wide range of years, and until recent clinical trials have shown significant efficacy of IFN-a 2b (34), Anti-VEGF chemotherapeutic agents such as bevacizumab, pazopanib, sorafenib thalidomide (35–39) and mTOR inhibitor sirolimus(rapamycin) (20, 40–42) for patients, the effectiveness of chemotherapy in treating EHE patients remained uncertain. By the way, it is hard to explain why the sequence numbers which are all reportable neoplasms over the lifetime of the patient have the positive correlation with survival times.

The use of surgical treatment and surgical types should be considered exhaustively according to the tumors location within the liver、the size of the mass、number of nodules、the status of vascular invasion、condition of extrahepatic diseases (22). Patients who underwent surgical treatments had significantly higher survival than those did nothing, and multivariate analysis revealed surgical therapy was only independent prognostic factor for survival (7). Group analysis can provide a new understanding of the suitability for surgical treatment, specifically identifying when surgery is most beneficial. For example, as mentioned earlier, in cases where the tumor is in a more advanced stage the potential benefits of surgery may be limited. Surgical treatments mainly consist of surgical resection and liver transplantation (LT). There had concluded that over half patients benefited from surgical resection and LT also shows excellent 5-year survival outcome in diverse clinical trials (9, 22, 43–47). some articles summarized that surgical resection had better overall survival rates and higher disease-free-survival than LT (9, 20, 48) while others demonstrated that there was no significantly difference between two modalities (5). To sum up, the choice of surgical resection and liver transplantation should be considered

carefully after exact analysis of both benefits and risks and group analysis may offer some valuable insights for surgical decision-making.

There are several limitations in the study. Firstly, in the SEER data, radiation therapy and chemotherapy are all treated as binary variables, and the 'stage' variable is categorized as distant, localized, and regional, which may be somewhat generalized and lack specificity. Additionally, as mentioned earlier, the chemotherapy information is limited and outdated, and the study findings may be influenced by a lag in recording research advancements. Furthermore, some of the subgroup analyses lack convincing power due to small sample sizes. Lastly, the dataset from our department is limited in size. While the clinical symptoms, imaging information, and pathological features are somewhat representative, it lacks the generality of larger sample sizes.

Recent advancements in fundamental research and omics analyses are shedding light on EHE's complexities. One study identified potentially targetable genomic variants in EHE, emphasizing variants like CDKN2A/B, which are notably involved in cell cycle regulation and DNA damage repair (32). Notably, the loss of CDKN2A/B was prevalent in older patients and was linked to more aggressive EHE behavior (49). Investigations also revealed that fusion proteins in EHE can modulate the chromatin environment and hyperactivate a TEAD-based transcriptional program (50). Single-cell RNA sequencing (scRNA-seq) highlighted EHE's cellular heterogeneity, suggesting potential underlying pathways that merit further exploration (51, 52). While anti-VEGF therapies and mTOR inhibitors have clinical implications, MEK inhibitors and YAP/TAZ-TEAD disruptors have shown promise in reducing EHE cell proliferation, although their clinical efficacy remains to be ascertained (53–56).

5 Conclusions

Machine learning and Cox regression models have highlighted the significant importance of surgical treatment for HEHE. Given the limited basic research and the lack of further clinical translation for HEHE, surgical treatment remains a worthwhile and preferred option for consideration.

Data availability statement

The original contributions presented in the study are included in the article/Supplementary Materials, further inquiries can be directed to the corresponding authors.

Ethics statement

This study was approved by the Institutional Review Board of the Cancer Hospital, Chinese Academy of Medical Sciences and Peking Union Medical College. All patients provided informed consent. The studies were conducted in accordance with the local legislation and institutional requirements. Written informed consent was obtained from the individual(s) for the publication of any potentially identifiable images or data included in this article.

Author contributions

BW: Writing – original draft, Conceptualization, Data curation, Methodology, Software, Validation, Visualization. XC: Conceptualization, Data curation, Investigation, Methodology, Supervision, Writing – original draft. RL: Conceptualization, Data curation, Formal analysis, Methodology, Software, Writing – original draft. BA: Data curation, Methodology, Software, Writing – original draft. FY: Data curation, Funding acquisition, Resources, Writing – review & editing. JZ: Investigation, Project administration, Supervision, Writing – review & editing. YZ: Data curation, Investigation, Methodology, Writing – review & editing. ZH: Investigation, Methodology, Project administration, Software, Writing – review & editing. ZL: Conceptualization, Formal analysis, Project administration, Writing – review & editing. XB: Funding acquisition, Project administration, Resources, Validation, Writing – review & editing. HZ: Funding acquisition, Investigation, Methodology, Project administration, Resources, Supervision, Validation, Visualization, Writing – review & editing. DC: Formal analysis, Funding acquisition, Methodology, Project administration, Resources, Supervision, Visualization, Writing – review & editing. JC: Investigation, Methodology, Project administration, Resources, Software, Supervision, Writing – review & editing. JZ: Conceptualization, Data curation, Formal analysis, Funding acquisition, Investigation, Methodology, Project administration, Resources, Software, Supervision, Validation, Visualization, Writing – original draft, Writing – review & editing. TY: Conceptualization, Data curation, Formal analysis, Funding acquisition, Investigation, Methodology, Project administration, Resources, Software, Supervision, Validation, Visualization, Writing – original draft, Writing – review & editing.

Funding

The author(s) declare financial support was received for the research, authorship, and/or publication of this article. This study was supported by the National Key Research and Development Program of China (2023YFC3403800), National Natural Science Foundation of China (82141127), CAMS Innovation Fund for Medical Sciences (CIFMS) (2021-I2M-C&T-B-057).

Acknowledgments

We thank everyone who contributed to this study and the staff of the Department of Radiology in our Cancer Hospital for their assistance.

Conflict of interest

The authors declare that the research was conducted in the absence of any commercial or financial relationships that could be construed as a potential conflict of interest.

Publisher's note

All claims expressed in this article are solely those of the authors and do not necessarily represent those of their affiliated organizations, or those of the publisher, the editors and the reviewers. Any product that may be evaluated in this article, or claim that may be made by its manufacturer, is not guaranteed or endorsed by the publisher.

Supplementary material

The Supplementary Material for this article can be found online at: https://www.frontiersin.org/articles/10.3389/fimmu.2024.1491922/full#supplementary-material

References

1. Weiss S. Epithelioid hemangioendothelioma a vascular tumor often mistaken for a carcinoma. (1982) 50:970–81. doi: 10.1002/1097-0142(19820901)50:5<970::AID-CNCR2820500527>3.0.CO;2-Z

2. Weiss S. Epithelioid hemangioendothelioma and related lesions. *Semin Diagn Pathol.* (1986) 3:259–87.

3. Ishak KG, Sesterhenn IA, Goodman MZD, Rabin L, Stromeyer FW. Epithelioid hemangioendothelioma of the liver: a clinicopathologic and follow-up study of 32 cases. *Hum Pathol.* (1984) 15:839–52. doi: 10.1016/S0046-8177(84)80145-8

4. Remiszewski P. Epithelioid hemangioendothelioma of the liver as a rare indication for liver transplantation. *WJG.* (2014) 20:11333. doi: 10.3748/wjg.v20.i32.11333

5. Ajay PS, Tsagkalidis V, Casabianca A, Burchard PR, Melucci AD, Chacon A, et al. A review of hepatic epithelioid hemangioendotheliomaAnalyzing patient characteristics and treatment strategies. *J Surg Oncol.* (2022) 126:1423–9. doi: 10.1002/jso.27066

6. Chahrour MA, Khachfe HH, Habib JR, El-Asmar R, Saifi O, Jamali FR. Treatment and prognosis of hepatic epithelioid hemangioendothelioma: A SEER database analysis. *World J Surg.* (2021) 45:2886–94. doi: 10.1007/s00268-021-06165-6

7. Noh OK, Kim SS, Yang MJ, Lim SG, Hwang JC, Cho HJ, et al. Treatment and prognosis of hepatic epithelioid hemangioendothelioma based on SEER data analysis from 1973 to 2014. *Hepatobiliary Pancreatic Dis Int.* (2020) 19:29–35. doi: 10.1016/j.hbpd.2019.11.006

8. Sanduzzi-Zamparelli M, Rimola J, Montironi C, Nunes V, Alves VAF, Sapena V, et al. Hepatic epithelioid hemangioendothelioma: An international multicenter study. *Digestive Liver Dis.* (2020) 52:1041–6. doi: 10.1016/j.dld.2020.05.003

9. Mehrabi A, Kashfi A, Fonouni H, Schemmer P, Schmied BM, Hallscheidt P, et al. Primary Malignant hepatic epithelioid hemangioendothelioma: A comprehensive review of the literature with emphasis on the surgical therapy. *Cancer.* (2006) 107:2108–21. doi: 10.1002/cncr.22225

10. Antonescu C. Malignant vascular tumors—an update. *Modern Pathol.* (2014) 27: S30–8. doi: 10.1038/modpathol.2013.176

11. Errani C. A novel WWTR1-CAMTA1 gene fusion is a consistent abnormality in epithelioid hemangioendothelioma of different anatomic sites. *Genes, chromosomes & cancer* (2011) 50:644–53. doi: 10.1002/gcc.20886

12. Tanas MR, Sboner A, Oliveira AM, Erickson-Johnson MR, Hespelt J, Hanwright PJ, et al. Identification of a disease-defining gene fusion in epithelioid hemangioendothelioma. *Sci Transl Med.* (2011) 3:98ra82. doi: 10.1126/scitranslmed.3002409

13. Antonescu CR, Le Loarer F, Mosquera J-M, Sboner A, Zhang L, Chen C-L, et al. Novel YAP1-TFE3 fusion defines a distinct subset of epithelioid hemangioendothelioma. *Genes Chromosomes Cancer.* (2013) 52:775–84. doi: 10.1002/gcc.22073

14. Kuo F-Y, Huang H-Y, Chen C-L, Eng H-L, Huang C-C. *TFE3*- rearranged hepatic epithelioid hemangioendothelioma-a case report with immunohistochemical and molecular study. *APMIS.* (2017) 125:849–53. doi: 10.1111/apm.12716

15. Soyer P. Capsular retraction of the liver in Malignant tumor of the biliary tract MRI findings. *Clin Imaging.* (1994) 18:255–7. doi: 10.1016/0899-7071(94)90003-5

16. Sans N, Fajadet P, Galy-Fourcade D, Trocart J, Jarlaud T, Chiavassa H, et al. Is capsular retraction a specific CT sign of Malignant liver tumor? *Eur Radiol.* (1999) 9:1543–5. doi: 10.1007/s003300050880

17. Mamone G, Miraglia R. The "Target sign" and the "Lollipop sign" in hepatic epithelioid hemangioendothelioma. *Abdom Radiol.* (2019) 44:1617–20. doi: 10.1007/s00261-018-1820-9

18. Alomari AI. The lollipop sign: A new cross-sectional sign of hepatic epithelioid hemangioendothelioma. *Eur J Radiol.* (2006) 59:460–4. doi: 10.1016/j.ejrad.2006.03.022

19. Weitz J, Klimstra DS, Cymes K, Jarnagin WR, D'Angelica M, La Quaglia MP, et al. Management of primary liver sarcomas. *Cancer.* (2007) 109:1391–6. doi: 10.1002/cncr.22530

20. Kou K, Chen Y-G, Zhou J-P, Sun X-D, Sun D-W, Li S-X, et al. Hepatic epithelioid hemangioendothelioma: Update on diagnosis and therapy. *WJCC.* (2020) 8:3978–87. doi: 10.12998/wjcc.v8.i18.3978

21. Cardinal J. Treatment of hepatic epithelioid hemangioendothelioma: A single-institution experience with 25 cases. *Arch Surg.* (2009) 144:1035. doi: 10.1001/archsurg.2009.121

22. Stacchiotti S, Miah AB, Frezza AM, Messiou C, Morosi C, Caraceni A, et al. Epithelioid hemangioendothelioma, an ultra-rare cancer: a consensus paper from the community of experts. *ESMO Open.* (2021) 6:100170. doi: 10.1016/j.esmoop.2021.100170

23. Thomas RM, Aloia TA, Truty MJ, Tseng WH, Choi EA, Curley SA, et al. Treatment sequencing strategy for hepatic epithelioid haemangioendothelioma. *HPB.* (2014) 16:677–85. doi: 10.1111/hpb.12202

24. Hayashi Y, Inagaki K, Hirota S, Yoshikawa T, Ikawa H. Epithelioid hemangioendothelioma with marked liver deformity and secondary Budd-Chiari syndrome: Pathological and radiological correlation. *Pathol Int.* (1999) 49:547–52. doi: 10.1046/j.1440-1827.1999.00906.x

25. Frider B, Bruno A, Selser J, Vanesa R, Pascual P, Bistoletti R. Kasabach–Merrit syndrome and adult hepatic epithelioid hemangioendothelioma an unusual association. *J Hepatol.* (2005) 42:282–3. doi: 10.1016/j.jhep.2004.09.007

26. Studer LL, Selby DM. Hepatic epithelioid hemangioendothelioma. *Arch Pathol Lab Med.* (2018) 142:263–7. doi: 10.5858/arpa.2016-0171-RS

27. Epelboym Y, Engelkemier DR, Thomas-Chausse F, Alomari AI, Al-Ibraheemi A, Trenor CC, et al. Imaging findings in epithelioid hemangioendothelioma. *Clin Imaging.* (2019) 58:59–65. doi: 10.1016/j.clinimag.2019.06.002

28. Zhou L, Cui M-Y, Xiong J, Dong Z, Luo Y, Xiao H, et al. Spectrum of appearances on CT and MRI of hepatic epithelioid hemangioendothelioma. *BMC Gastroenterol.* (2015) 15:69. doi: 10.1186/s12876-015-0299-x

29. Liu X, Yu H, Zhang Z, Si S, Huang J, Tan H, et al. MRI appearances of hepatic epithelioid hemangioendothelioma: a retrospective study of 57 patients. *Insights Imaging.* (2022) 13:65. doi: 10.1186/s13244-022-01213-8

30. Doyle LA, Fletcher CDM, Hornick JL. Nuclear expression of CAMTA1 distinguishes epithelioid hemangioendothelioma from histologic mimics. *Am J Surg Pathol.* (2016) 40:94–102. doi: 10.1097/PAS.0000000000000511

31. Jung H, Kim H-N, Jang Y, Park C-K, Ha S-Y. CAMTA-1 expression in 24 cases of hepatic epithelioid hemangioendothelioma in a single institute: diagnostic utility for differential diagnosis from hepatic angiosarcoma. *In Vivo.* (2019) 33:2293–7. doi: 10.21873/invivo.11736

32. Seligson ND, Awasthi A, Millis SZ, Turpin BK, Meyer CF, Grand'Maison A, et al. Common secondary genomic variants associated with advanced epithelioid hemangioendothelioma. *JAMA Netw Open.* (2019) 2:e1912416. doi: 10.1001/jamanetworkopen.2019.12416

33. Frezza AM, Ravi V, Lo Vullo S, Vincenzi B, Tolomeo F, Chen TW, et al. Systemic therapies in advanced epithelioid haemangioendothelioma: A retrospective international case series from the World Sarcoma Network and a review of literature. *Cancer Med.* (2021) 10:2645–59. doi: 10.1002/cam4.3807

34. Liu X, Zhang Z, Huang J, Tan H, Yang Z. Efficacy and safety of interferon-alpha 2b for patients with hepatic epithelioid hemangioendothelioma: outcomes of a case-series analysis. *CMAR.* (2021) 13:8273–9. doi: 10.2147/CMAR.S334171

35. Chevreau C, Le Cesne A, Ray-Coquard I, Italiano A, Cioffi A, Isambert N, et al. Sorafenib in patients with progressive epithelioid hemangioendothelioma: A phase 2 study by the French Sarcoma Group (GSF/GETO). *Cancer.* (2013) 119:2639–44. doi: 10.1002/cncr.28109

36. Agulnik M, Yarber JL, Okuno SH, von Mehren M, Jovanovic BD, Brockstein BE, et al. An open-label, multicenter, phase II study of bevacizumab for the treatment of angiosarcoma and epithelioid hemangioendotheliomas. *Ann Oncol*. (2013) 24:257–63. doi: 10.1093/annonc/mds237

37. Telli TA, Okten IN, Tuylu TB, Demircan NC, Arikan R, Alan O, et al. VEGF-VEGFR pathway seems to be the best target in hepatic epithelioid hemangioendothelioma: A case series with review of the literature. *Curr Problems Cancer*. (2020) 44:100568. doi: 10.1016/j.currproblcancer.2020.100568

38. Bally O, Tassy L, Richioud B, Decouvelaere A-V, Blay J-Y, Derbel O. Eight years tumor control with pazopanib for a metastatic resistant epithelioid hemangioendothelioma. *Clin Sarcoma Res*. (2015) 5:12. doi: 10.1186/s13569-014-0018-3

39. Lau A, Malangone S, Green M, Badari A, Clarke K, Elquza E. Combination capecitabine and bevacizumab in the treatment of metastatic hepatic epithelioid hemangioendothelioma. *Ther Adv Med Oncol*. (2015) 7:229–36. doi: 10.1177/1758834015582206

40. Stacchiotti S, Simeone N, Lo Vullo S, Baldi GG, Brunello A, Vincenzi B, et al. Activity of sirolimus in patients with progressive epithelioid hemangioendothelioma: A case-series analysis within the Italian Rare Cancer Network. *Cancer*. (2021) 127:569–76. doi: 10.1002/cncr.33247

41. Fukuhara S, Tahara H, Hirata Y, Ono K, Hamaoka M, Shimizu S, et al. Hepatic epithelioid hemangioendothelioma successfully treated with living donor liver transplantation: A case report and literature review. *Clin Case Rep*. (2020) 8:108–15. doi: 10.1002/ccr3.2558

42. Stacchiotti S, Provenzano S, Dagrada G, Negri T, Brich S, Basso U, et al. Sirolimus in advanced epithelioid hemangioendothelioma: A retrospective case-series analysis from the italian rare cancer network database. *Ann Surg Oncol*. (2016) 23:2735–44. doi: 10.1245/s10434-016-5331-z

43. Brahmbhatt M, Prenner S, Bittermann T. Liver transplantation for hepatic epithelioid hemangioendothelioma is facilitated by exception points with acceptable long-term outcomes. *Transplantation*. (2020) 104:1187–92. doi: 10.1097/TP.0000000000002982

44. Lai Q, Feys E, Karam V, Adam R, Klempnauer J, Oliverius M, et al. Hepatic epithelioid hemangioendothelioma and adult liver transplantation: proposal for a prognostic score based on the analysis of the ELTR-ELITA registry. *Transplantation*. (2017) 101:555–64. doi: 10.1097/TP.0000000000001603

45. Konstantinidis IT, Nota C, Jutric Z, Ituarte P, Chow W, Chu P, et al. Primary liver sarcomas in the modern era: Resection or transplantation? *J Surg Oncol*. (2018) 117:886–91. doi: 10.1002/jso.24979

46. Lerut JP, Orlando G, Adam R, Schiavo M, Klempnauer J, Mirza D, et al. The place of liver transplantation in the treatment of hepatic epitheloid hemangioendothelioma: report of the european liver transplant registry. *Ann Surg*. (2007) 246:949–57. doi: 10.1097/SLA.0b013e31815c2a70

47. Rodriguez JA, Becker NS, O'Mahony CA, Goss JA, Aloia TA. Long-term outcomes following liver transplantation for hepatic hemangioendothelioma: the UNOS experience from 1987 to 2005. *J Gastrointest Surg*. (2008) 12:110–6. doi: 10.1007/s11605-007-0247-3

48. Grotz TE, Nagorney D, Donohue J, Que F, Kendrick M, Farnell M, et al. Hepatic epithelioid haemangioendothelioma: is transplantation the only treatment option? *HPB*. (2010) 12:546–53. doi: 10.1111/j.1477-2574.2010.00213.x

49. Seavey CN, Hallett A, Li S, Che K, Pobbati AV, Ma S, et al. Loss of CDKN2A cooperates with WWTR1(TAZ)-CAMTA1 gene fusion to promote tumor progression in epithelioid hemangioendothelioma. *Clin Cancer Res*. (2023) 29:2480–93. doi: 10.1158/1078-0432.CCR-22-2497

50. Merritt N, Garcia K, Rajendran D, Lin Z-Y, Zhang X, Mitchell KA, et al. TAZ-CAMTA1 and YAP-TFE3 alter the TAZ/YAP transcriptome by recruiting the ATAC histone acetyltransferase complex. *eLife*. (2021) 10:e62857. doi: 10.7554/eLife.62857

51. Driskill JH, Zheng Y, Wu B-K, Wang L, Cai J, Rakheja D, et al. WWTR1(TAZ)-CAMTA1 reprograms endothelial cells to drive epithelioid hemangioendothelioma. *Genes Dev*. (2021) 35:495–511. doi: 10.1101/gad.348221.120

52. Seavey CN, Pobbati AV, Hallett A, Ma S, Reynolds JP, Kanai R, et al. *WWTR1* (TAZ)- *CAMTA1* gene fusion is sufficient to dysregulate YAP/TAZ signaling and drive epithelioid hemangioendothelioma tumorigenesis. *Genes Dev*. (2021) 35:512–27. doi: 10.1101/gad.348220.120

53. Ma S, Kanai R, Pobbati AV, Li S, Che K, Seavey CN, et al. The TAZ-CAMTA1 fusion protein promotes tumorigenesis via connective tissue growth factor and ras–MAPK signaling in epithelioid hemangioendothelioma. *Clin Cancer Res*. (2022) 28:3116–26. doi: 10.1158/1078-0432.CCR-22-0421

54. Pobbati AV, Rubin BP. Protein-protein interaction disruptors of the YAP/TAZ-TEAD transcriptional complex. *Molecules*. (2020) 25:6001. doi: 10.3390/molecules25246001

55. Li Q, Sun Y, Jarugumilli GK, Liu S, Dang K, Cotton JL, et al. Lats1/2 sustain intestinal stem cells and wnt activation through TEAD-dependent and independent transcription. *Cell Stem Cell*. (2020) 26:675–692.e8. doi: 10.1016/j.stem.2020.03.002

56. Pobbati AV, Han X, Hung AW, Weiguang S, Huda N, Chen G-Y, et al. Targeting the central pocket in human transcription factor TEAD as a potential cancer therapeutic strategy. *Structure*. (2015) 23:2076–86. doi: 10.1016/j.str.2015.09.009

frontiers | Frontiers in Oncology

TYPE Original Research
PUBLISHED 28 October 2024
DOI 10.3389/fonc.2024.1492251

Check for updates

OPEN ACCESS

EDITED BY
Xiaosheng Tan,
Rutgers, United States

REVIEWED BY
Kang Yu,
National Institute of Arthritis and Musculoskeletal and Skin Diseases (NIH), United States
Xiaodong Zou,
Memorial Sloan Kettering Cancer Center, United States
Zishuo Yu,
Harvard University, United States
Ruiling Wu,
Generate Biomedicines. Inc, United States

*CORRESPONDENCE
Xiaojing Jia
jaixj@mails.jlu.edu.cn

RECEIVED 06 September 2024
ACCEPTED 04 October 2024
PUBLISHED 28 October 2024

CITATION
Yan S, Gong X, Liu R and Jia X (2024) Prognostic significance of systemic pan-immune-inflammation value in locally advanced cervical cancer.
Front. Oncol. 14:1492251.
doi: 10.3389/fonc.2024.1492251

COPYRIGHT
© 2024 Yan, Gong, Liu and Jia. This is an open-access article distributed under the terms of the Creative Commons Attribution License (CC BY). The use, distribution or reproduction in other forums is permitted, provided the original author(s) and the copyright owner(s) are credited and that the original publication in this journal is cited, in accordance with accepted academic practice. No use, distribution or reproduction is permitted which does not comply with these terms.

Prognostic significance of systemic pan-immune-inflammation value in locally advanced cervical cancer

Shu Yan, Xin Gong, Rui Liu and Xiaojing Jia*

Department of Tumor Radiotherapy, The Second Hospital of Jilin University, Changchun, China

Objective: This study investigates the significance of systemic pan-immune inflammation value (PIV) prior to concurrent chemoradiotherapy (CCRT) in predicting the therapeutic efficacy as well as prognosis of patients with locally advanced cervical squamous cell carcinoma.

Methods: A retrospective analysis was conducted on the clinical data of 847 patients with locally advanced cervical cancer (LACC) treated at the Second Hospital of Jilin University between 2016 and 2020. All patients underwent radical CCRT, including platinum-based sensitizing chemotherapy. The PIV was measured as given by: (platelet count × neutrophil count × monocyte count)/ lymphocyte count. Logistic regression analysis was utilized to study the effect of PIV on therapeutic response in LACC patients and Kaplan–Meier survival together with Cox proportional hazard model to assess its impact on prognosis.

Results: With the therapeutic effect as the endpoint, the optimal cutoff of PIV (356.0099) was signified via the receiver operating characteristics curve, and patients were grouped and compared based on this value. PIV was determined as an independent predictor of the therapeutic effect in CCRT for LACC (hazard ratio (HR) 1.696, 95% confidence interval (CI) 1.111–2.590). PIV was also an independent predictor of overall survival (OS) (HR 0.540, 95% CI 0.409–0.713, p<0.001) as well as disease-free survival (DFS) (HR 0.680, 95% CI 0.528–0.876, p=0.003). Compared to the low-PIV group, it was noted that individuals with a high PIV exhibited a poorer therapeutic effect and shorter OS and DFS.

Conclusion: Patients with LACC and high PIV had poorer therapeutic outcomes and shorter OS and DFS. Our results may provide PIV as a new prognostic biomarker for LACC, if future prospective studies with large patient numbers support our findings.

KEYWORDS

pan immune inflammation value, locally advanced cervical cancer, prognostic prediction, concurrent chemoradiotherapy, immune-inflammatory biomarkers

Introduction

Cervical cancer is globally recognized as the fourth most well-known death caused by cancers among women, presenting a substantial risk to their overall health and longevity across the globe (1). The conventional treatment protocol for locally advanced cervical cancer (LACC) typically includes a synergistic application of localized radiotherapy and systemic chemotherapy. However, the efficacy of such treatments often faces significant challenges, including issues, such as local relapse and the occurrence of distant metastasis (2–5). This necessitates the rational prediction of patient survival times to formulate more personalized treatment plans at an early stage, with such a wide range of factors affecting these predictions being layered (6, 7). Although the staging criteria defined by the International Federation of Gynecology and Obstetrics (FIGO) provide an important reference for clinical management in LACC, experience from practice suggests that patients with similar stages can have markedly different responses to treatment. This demonstrated that patient-specific factors play a vital role in determining the effectiveness of interventions (8).

The link between inflammation and cancer has been thoroughly explored in recent years to offer new insights into treating oncological diseases (9, 10). Previous clinical studies have indicated that chronic inflammation can induce malignant cell proliferation, promoting the formation of malignant tumors and affecting patient prognosis (11). Furthermore, the inflammatory microenvironment within tumors significantly impacts their response to anti-cancer therapies (12). A growing body of evidence indicates that certain specific immuno-inflammatory biomarkers (IIBs), such as neutrophil, lymphocyte, and monocyte levels, reflect the equilibrium of the host's immunoinflammatory environment, these biomarkers are crucial for predicting cancer prognosis and are associated with carcinogenesis and tumor progression (13, 14). Additionally, the neutrophil-to-lymphocyte ratio (NLR), platelet-to-lymphocyte ratio (PLR), lymphocyte-to-monocyte ratio (LMR), and systemic inflammatory index have demonstrated significant predictive value in the clinical prognosis of a wide range of cancer types, especially in malignant tumors where patients exhibit chemoresistance (15–19). As a solid malignant tumor, cervical cancer prognosis is similarly influenced by these IIBs, prior research has indicated that certain hematological indicators including prognostic nutritional index (PNI), PLR, and LMR can serve as significant prognostic factors for cervical cancer outcomes (20). The Pan-Immune-Inflammation Value (PIV), first introduced in a 2020 study, is a calculated metric derived from four blood parameters: platelets, neutrophils, monocytes, and lymphocytes (21). This value reflects the balance between host immunity and inflammation, it serves as an accessible indicator for evaluating cancer outcomes and has been identified as an independent predictor of prognosis in metastatic colorectal cancer patients (22). It was also proven in different other malignancies like oral, esophageal, and head & neck tumors (23–26). Nevertheless, an exhaustive investigation of the correlation between the PIV and the clinical traits, along with its prognostic significance, in the context of LACC remains to be conducted.

Consequently, this research's goal to explore the relationship the PIV with the clinical profile of patients diagnosed with LACC. Additionally, we sought to assess the prognostic predictive efficacy of PIV for CCRT in LACC, using both uni- and multivariate survival analyses. It is anticipated that our findings will yield novel theoretical insights and offer practical directives, thereby enhancing the precision and personalization of therapeutic approaches for LACC.

Methods and materials

Patients

In this research, we retrospectively examined the clinical records of 847 patients with LACC, all of whom received treatment at the Department of Radiotherapy in our hospital from 2016 to 2020. The inclusion criteria include: (1) diagnosis of cervical squamous cell carcinoma by histopathology, (2) staging as IB3-IVA according to the 2018 FIGO staging, and (3) serum laboratory results from our hospital's automatic blood analyzer within 5 days prior to treatment. The exclusion criteria include: (1) the occurrence of other primary malignant tumors; (2) previous radiotherapy, chemotherapy, or radical surgery before treatment; (3) acute or chronic infections; (4) hematological or other autoimmune diseases; (5) incomplete clinical data; and (6) loss to follow-up. The flowchart of the recruitment process is shown in Supplementary Figure S1.

All patients provided informed consent and the study obtain approval from the Declaration of Helsinki. This study protocol was approved by the Ethics Committee of the Second Hospital of Jilin University (2024-030). The PIV was calculated using the formula: (neutrophil count [109/L] × platelet count [109/L] × monocyte count [109/L])/lymphocyte count [109/L] (22), derived from the results of the automatic blood analyzer within 5 days prior to treatment.

All patients with LACC were untreated prior to receiving CCRT. The clinical data collected included medical history, laboratory data, physical examination, imaging examinations (pelvic CT or MRI), bone scans, positron emission tomography-CT, as well as lymph node ultrasonography. Older adult patients were defined as those aged >65 years. The clinical characteristic parameters included in the study were patient age, comorbidities, gravidity and parity, lymph node metastasis status, histopathological results, tumor size before and after treatment, degree of change, parametrial invasion, and lymph node metastasis status. Given that patient recruitment started in 2016 and ended in 2020, all included patients' FIGO staging was adjusted to the 2018 FIGO staging. All patients underwent radical CCRT (45–50.4 Gy) and concurrently received platinum-based sensitizing chemotherapy. The effectiveness of tumor therapy was gauged by the levels of sensitivity, categorized as complete and partial responses (CR&PR), and by the tolerance, which included stable and progressive diseases (SD&PD), according to the Response Evaluation Criteria in Solid Tumors (RECIST). These assessments were made by reviewing the patient outcomes during a 6-month post-treatment surveillance period. After treatment, a structured follow-up plan was initiated which required patients to be checked every three months within first year after which checking was to be relative with time in

between six to twelve months intervals. Each follow-up entailed a review of the imaging materials and laboratory work done while still in our hospital. The final follow-up deadline was December 30, 2023, or the patient's death. The primary endpoint of the study was 3-year OS of the patients.

Data analysis

We employed the SPSS software (version 26; IBM Corp., Armonk, NY) for all statistical analyses. For descriptive statistics, categorical data are presented as numbers as well as percentages meanwhile continuous data are denoted as interquartile range (IQR) and median. PIV-associated optimal threshold was determined by the receiver operating characteristic (ROC) curve as well as Youden's J statistic with tumor response as a binary outcome. Logistic regression analysis was used to assess the factors that predicted sensitivity of tumors to chemoradiotherapy based on OR and 95% CI. Kaplan-Meier plots were constructed for overall survival and tested using log rank test. OS and disease-free survival (DFS) were measured using the Cox proportional hazards model, adjusting for integer age at diagnosis; the hazard ratios (HRs), with their 95% CIs, are presented. The threshold for statistical significance was represented as a p-value of less than 0.05.

Findings

Patient characteristics

In this research, from a pool of 1,194 patients extracted from our hospital's medical records spanning 2016 to 2020, a total of 847 patients diagnosed with LACC (classified according to FIGO 2018 as stages IB3-IVA) were selected based on the study's eligibility criteria. The patients' mean age at diagnosis was 55 (IQR, 49–62) years. Predominantly, the study enrolled patients with stage IIB LACC, constituting 55.4% of the study's cohort. Each patient underwent pelvic irradiation along with chemotherapy regimens based on platinum, with 471 (55.6%) undergoing less than five cycles of chemotherapy, whereas 376 (44.4%) completed five or more cycles of concurrent chemotherapy. A total of 808 patients (95.4%) underwent brachytherapy. The total treatment time was 8 weeks (56 days) in 448 cases (52.9%) and <8 weeks in 399 cases (47.1%). Detailed clinical and pathological characteristics and baseline hematological indicators of the patients with LACC are shown in Table 1. The detailed distribution of PIV, platelets, lymphocytes, monocytes, and neutrophils is illustrated in Supplementary Figure S2.

TABLE 1 Patient characteristics (n=847).

Variable	Characteristics
Median age (IQR)	55 (49–62)
Complication	
Hypertension	110 (13%)
Diabetes	40 (4.7%)
Cardiovascular disease	38 (4.5%)
Others	16 (1.9%)
Tumor size	
≤4 cm	310 (36.6%)
>4 cm	537 (63.4%)
Staging (FIGO 2018)	
IB3-IIA	57 (6.7%)
IIB	469 (55.4%)
IIIA-IIIB	197 (23.3%)
IIIC-IVA	124 (14.6%)
Parauterine	779 (92%)
Vagina	48 (5.7%)
Lymph node (yes/no)	
Pelvic lymph	88 (10.4%)
Inguinal lymph	259 (30.6%)
Paravascular iliac lymph	387 (45.7%)
Paraaortic lymph	14 (1.7%)
Supraclavicular lymph	11 (1.3%)
Brachytherapy	808 (95.4%)
EQD2 (point A)	
<80 Gy	283 (33.4%)
≥80 Gy	564 (66.6%)
Chemotherapy cycle	
<5th	471 (55.6%)
≥5th	376 (44.4%)
Overall treatment time (d)	
<56	399 (47.1%)
≥56	448 (52.9%)
Platelets ($\times10^3$ μL^{-1})	255.00 (205.9–309.0)
Lymphocyte ($\times10^3$ μL^{-1})	1.50 (0.90–2.00)
Neutrophil ($\times10^3$ μL^{-1})	4.10 (2.88–5.40)
Monocyte ($\times10^3$ μL^{-1})	0.40 (2.88–5.40)
Albumin (g/L)	42.5 (40.20–44.45)
HB (g/L)	127.00 (113.00–136.00)
NLR	2.91 (2.00–4.48)

(Continued)

Comparison of PIV with other IIBs

To assess the efficacy of the pre-treatment PIV in predicting the responsiveness of patients with LACC to CCRT, we conducted a comparative analysis using the ROC curve. This analysis pitted PIV against traditional inflammatory markers, such as the PLR and NLR, as well as the individual components necessary for PIV

TABLE 1 Continued

Variable	Characteristics
Overall treatment time (d)	
PLR	178.00 (131.50–270.00)
LMR	0.34 (0.22–0.50)
PIV	278.73 (163.53–489.19)

FIGO, International Federation of Gynecology and Obstetrics; EQD2, 2-Gy equivalent dose; HB, hemoglobin; NLR, neutrophil-to-lymphocyte ratio; PLR, platelet-to-lymphocyte ratio; LMR, lymphocyte-to-monocyte ratio; PIV, pan-immune-inflammation value.

computation, namely neutrophil and platelet counts. The outcomes of the ROC curve analysis indicated that PIV demonstrated superior predictive accuracy for the sensitivity of the patients to concurrent chemoradiotherapy (CCRT), with an area under the curve (AUC) of 0.593 (Figure 1A). This AUC was significantly higher than that of the PLR, NLR, neutrophil count and platelet count.

Moreover, the efficacy of these indicators in predicting OS and DFS was compared (Figures 1B, C). PIV was also superior to other comparative indicators in OS and DFS which were 0.645 and 0.543, accordingly. These results could have significant implications for the assessment of LACC patients' sensitivity to CCRT in PIV.

Relationship between PIV and patient characteristics

An ROC curve was generated Using tumor regression following LACC treatment as the endpoint, with PIV as the test variable. The coordinate points representing sensitivity and 1-specificity on the ROC curve were identified. Utilizing the formula: Youden index (J) = sensitivity + specificity - 1, we calculated the Youden index (J) for each coordinate point. The coordinate point corresponding to the maximum value of the Youden index (J) represents the optimal cutoff point for PIV. Using this aforesaid threshold value of 356.0099, patients were then classified into high- and low-PIV groups Table 2 presents the association between clinical characteristics and PIV-based classification. Notable differences were observed between the high-PIV (PIV ≥356) and low-PIV (PIV <356) groups in terms of tumor dimensions (p less than 0.001), FIGO stage classification (p less than 0.001), parametrial invasion (p = 0.027), pelvic lymph node metastasis (p = 0.003), lower vaginal wall invasion (p = 0.020), para-aortic lymph node involvement (p = 0.027), and pre-treatment serum albumin levels (p < 0.001).

Predictors of therapeutic effect

PIV was closely related to the therapeutic effect, with fewer patients in the high-PIV group being more sensitive to treatment than those in the low-PIV group (90.34% vs. 82.08%, p=0.001). Following the outcomes of uni- and multivariate logistic regression analyses, PIV was an independent predictor of the therapeutic effect of CCRT for LACC (HR 1.696, 95% CI 1.111–2.590, p=0.014). In addition, FIGO staging, para-aortic lymph node metastasis, and total treatment time were independent predictors of therapeutic effects (Table 3).

Predictors of OS and DFS

Employing the Kaplan-Meier method for survival analysis, we scrutinized the variance in OS and DFS among patients with LACC, distinguishing between the high and low PIV cohorts. Utilizing a critical PIV value of 356 as the threshold, the findings indicated that patients with elevated PIV scores notably experienced reduced OS and DFS in comparison to those with lower PIV scores, with the difference being statistically significant (p less than 0.001). This difference was confirmed via the log-rank test (Figure 2).

Furthermore, uni- and multivariate Cox proportional hazards models were utilised to analyse the data (Tables 4, 5). Following the preliminary screening of variables via univariate analysis, a multivariate analysis was conducted. The data analysis

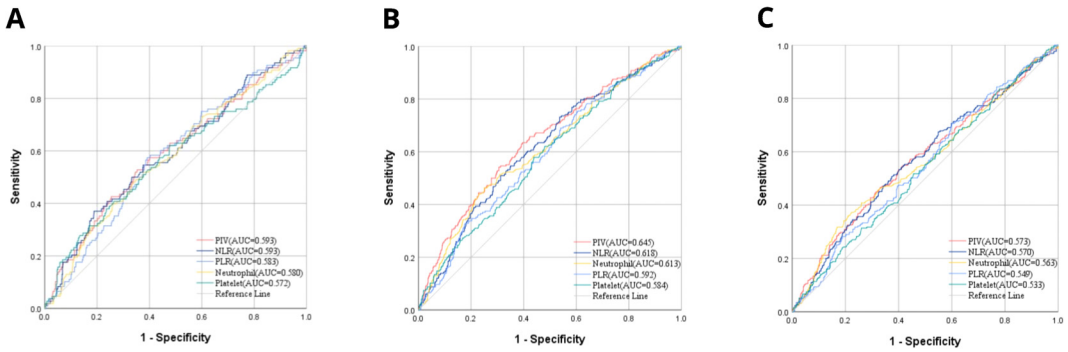

FIGURE 1
(A) AUC comparisons for CCRT responsiveness between PIV and other IIBs by ROC; **(B)** AUC comparisons for OS between PIV and other IIBs by ROC; **(C)** AUC comparisons for DFS between PIV and other IIBs by ROC.

TABLE 2 Baseline clinical characteristics according to the PIV.

Variable	Low-PIV (n=529)	High-PIV (n=318)	P-Value
Age, years			
<65	437 (82.6%)	276 (86.8%)	0.120
≥65	92 (17.4%)	42 (13.2%)	
Complication (yes, no)			
Hypertension	74 (14%)/455 (86%)	36 (11.3%)/282 (88.7%)	0.292
Diabetes	29 (5.5%)/500 (94.5%)	11 (3.5%)/307 (96.5%)	0.241
Cardiovascular disease	25 (4.7%)/504 (95.3%)	13 (4.1%)/305 (95.9%)	0.734
Others	11 (2.1%)/518 (97.9%)	5 (1.6%)/313 (98.4%)	0.796
Diameter			
≤4 cm	231 (43.7%)	79 (24.8%)	<0.001
>4 cm	298 (56.3%)	239 (75.2%)	
FIGO			
IB3-IIA	44 (8.3%)	13 (4.1%)	<0.001
IIB	317 (59.9%)	152 (47.8%)	
IIIA-IIIB	108 (20.4%)	89 (28.0%)	
IIIC-IVA	60 (11.3%)	64 (20.144%)	
Parauterine	478 (90.4%)/51 (9.6%)	301 (94.7%)/17 (5.3%)	0.027
Vagina	22 (4.2%)/507 (95.8%)	26 (8.2%)/292 (91.8%)	0.020
Lymph node (yes/no)			
Pelvic lymph	42 (7.9%)/487 (92.1%)	46 (14.5%)/272 (85.5%)	0.003
Inguinal lymph	156 (29.5%)/373 (70.5%)	103 (32.4%)/215 (67.6%)	0.397
Paravascular iliac lymph	226 (42.7%)/303 (57.3%)	161 (50.6%)/157 (49.4%)	0.027
Para-aortic lymph	8 (1.5%)/521 (98.5%)	6 (1.9%)/312 (98.1%)	0.782
Supraclavicular lymph	6 (1.1%)/523 (98.9%)	5 (1.6%)/313 (98.4%)	0.755
Albumin (g/L)	42.90 (40.90–44.70)	41.70 (39.18–43.83)	<0.001
HB (g/L)	129.00 (119.00–137.00)	122.00 (103.00–132.25)	<0.001

FIGO, International Federation of Gynecology and Obstetrics; HB, haemoglobin.

demonstrated a strong and statistically significant association between the PIV score and both OS (HR 0.540, 95% CI 0.409–0.713, p<0.001) and DFS (HR 0.680, 95% CI 0.528–0.876, p=0.003). The research outcomes highlight that, in contrast to the group with lower PIV levels, the high-PIV group exhibited a respective 54% and 68% escalation in the risks of mortality and disease advancement. Consequently, PIV can be deemed an independent predictor of DFS as well as OS in patients with LACC.

In the present research, tumor size and stage were established as significant, independent prognostic factors for OS as well as DFS in patients with LACC. Furthermore, 2-Gy equivalent dose (EQD2) and the cumulative duration of therapy were validated as independent predictors specifically for OS. These results highlight the importance of PIV in informing clinical management plans and predicting the prognosis with respect to patients with LACC.

Discussion

In this research, we evaluated the predictive value of the PIV for therapeutic findings and prognosis in patients having LACC before initiating CCRT. By applying Cox proportional hazards model and Kaplan–Meier survival analysis, we identified PIV as a robust and independent prognostic factor significantly correlated with patient therapeutic outcomes and survival prognosis. High PIV often implies a poor prognosis. This is, to our knowledge the first study where we have demonstrated that PIV has a particular significance in patients with LACC.

Our findings indicate that elevated PIV serves not only as a reliable predictor of poor OS and DFS, but also as a significant independent marker for unfavorable treatment responses in patients with LACC. Compared to traditional indicators such as neutrophil counts, platelet levels, NLR, and PLR, PIV demonstrates superior

TABLE 3 Logistic regression analyses for clinical characteristics.

Variable	Univariate analysis		Multivariate analysis	
	OR (95% CI)	P-value	OR (95% CI0	P-value
Age				
(years, ≥65 vs.<65)	0.993 (0.571–1.729)	0.981		
Complication				
Hypertension	1.193 (0.673–2.117)	0.546		
Diabetes	1.220 (0.500–2.977)	0.663		
Cardiovascular disease	0.575 (0.174–1.902)	0.364		
Others	0.977 (0.219–4.360)	0.976		
Diameter	1.297 (0.842–2.000)	0.238		
FIGO (2018)				
IB3-IIA	Reference		Reference	
IIB	11.250 (2.604–48.597)	0.001	7.796 (1.634–37.198)	0.010
IIIA-IIIB	3.855 (2.350–6.322)	<0.001	3.017 (1.466–6.206)	0.003
IIIC-IVA	2.815 (1.590–4.983)	<0.001	2.544 (1.191–5.473)	0.016
Para-uterine	1.557 (0.657–3.692)	0.315		
Vagina	1.632 (0.767–3.471)	0.204		
Lymph node (yes/no)				
Pelvic lymph	3.232 (1.929–5.416)	0.000	1.093 (0.501–2.383)	0.823
Inguinal lymph	1.397 (0.917–2.128)	0.120		
Paravascular iliac lymph	1.873 (1.243–2.824)	0.003	1.577 (1.030–2.413)	0.036
Para-aortic lymph	1.891 (0.519–6.889)	0.334		
Supraclavicular lymph	1.530 (0.326–7.179)	0.589		
Brachytherapy	1.827 (0.817–4.086)	0.142		
EQD2	0.760 (0.502–1.153)	0.197		
Chemotherapy	1.046 (0.697–1.570)	0.827		
Time	1.681 (1.106–2.533)	0.015	1.555 (1.010–2.389)	0.045
PIV (high vs. low)	2.047 (1.363–3.074)	0.001	1.696 (1.111–2.590)	0.014

FIGO, International Federation of Gynecology and Obstetrics; EQD2, 2-Gy equivalent dose; PIV, Pan-immune-inflammation value.

predictive capability. Furthermore, its calculation relies on readily obtainable and cost-effective clinical parameters, establishing it as a prognostic indicator of considerable clinical relevance. The correlation between PIV and adverse treatment outcomes may be attributed to the immunosuppressive and pro-inflammatory states associated with elevated PIV levels. Such conditions could potentially facilitate tumor evasion, progression, and resistance to therapeutic interventions (27). An immunosuppressed milieu characterized by heightened neutrophil counts coupled with diminished lymphocyte levels may contribute to more aggressive tumor growth and metastasis (28, 29). Additionally, the pro-inflammatory state may enhance angiogenesis, invasion, and metastasis—factors indicative of poor cancer prognosis (30). Our results further underscore the necessity of integrating PIV alongside conventional clinical and pathological factors when forecasting treatment outcomes in LACC cases. Incorporating PIV into predictive models can augment prediction accuracy while informing the development of personalized therapeutic strategies.

The relationship between inflammation and the progression of cancer, as well as its correlation with an unfavorable prognosis, has been widely reported (23–26). In LACC treatment, the immune-inflammatory response is a critical prognostic factor that should not be overlooked. Previous studies have reported the significance of various immune-inflammatory cells, which include neutrophils, thrombocytes, lymphocytes, and monocytes, in predicting cancer prognosis (31). Subsequently, ratios involving immune cells have been widely proposed and used for cancer prognosis prediction, including the LMR, NLR, PLR, and other predictive factors (32). Based on these studies, PIV, a novel indicator, has been used in several disease prediction studies. Several studies have demonstrated

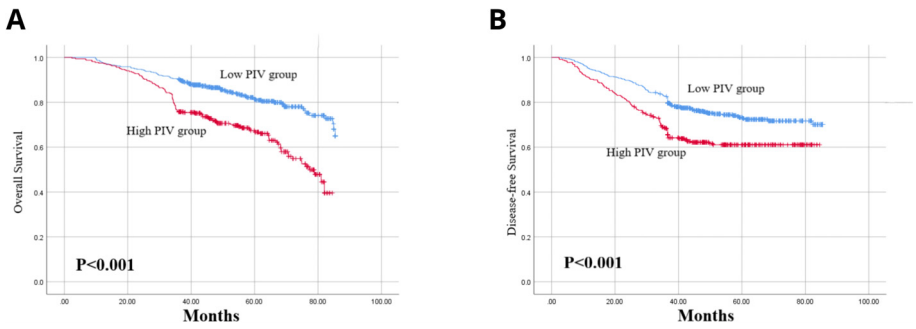

FIGURE 2
(A) Kaplan–Meier curves regarding OS; **(B)** Kaplan–Meier curves regarding DFS.

that PIV is linked to the prognosis of various solid tumors, including oral malignant tumors, head and neck tumors, and other malignant tumors. Although the design of these studies varies, the potential of PIV as a predictive tool has gradually emerged, and its predictive value has been widely recognized.

Currently, there is a scarcity of studies examining the prognostic significance with respect to the PIV in cervical cancer. Nevertheless, previous studies indicated an increased PLR and NLR are related to worse survival in patients having cervical cancer (16, 33–37). Similarly, a decrease in the LMR and PNI is also linked to poorer clinical outcomes (38–40). Consistent with these results, the present research compared the significance of PIV with several conventional inflammatory indicators, including PLR, NLR, neutrophil count, and platelet count, to predict the therapeutic efficacy using the ROC curve

TABLE 4 Univariate analysis.

Variable	OS		DFS	
	OR (95% CI)	P-value	OR (95% CI)	P-value
Age				
(years, ≥65 vs.<65)	0.945 (0.652–1.370)	0.765	0.993 (0.981–1.006)	0.280
Diameter	0.532 (0.388–0.728)	<0.001	0.611 (0.464–0.803)	<0.001
FIGO (2018)				
IB3	Reference		Reference	
II	0.182 (0.078–0.424)	<0.001	0.370 (0.188–0.731)	0.004
III	0.316 (0.224–0.446)	<0.001	0.557 (0.600–0.774)	0.001
IVA	0.591 (0.413–0.848)	0.004	0.892 (0.622–1.279)	0.532
Parauterine	0.442 (0.218–0.896)	0.023	0.632 (0.369–1.084)	0.096
Vagina	0.554 (0.353–0.869)	0.010	0.730 (0.452–1.179)	0.198
Lymph node (yes/no)				
Pelvic lymph	0.526 (0.361–0.768)	0.001	0.841 (0.571–1.238)	0.381
Inguinal lymph	0.751 (0.569–0.992)	0.043	0.791 (0.612–1.024)	0.075
Paravascular iliac lymph	0.764 (0.585–0.997)	0.048	0.879 (0.687–1.124)	0.303
Para-aortic lymph	1.121 (0.416–3.019)	0.821	1.148 (0.428–3.084)	0.784
Supraclavicular lymph	0.722 (0.268–1.944)	0.520	1.076 (0.345–3.360)	0.899
Brachytherapy	1.320 (0.753–2.314)	0.332	1.018 (0.570–1.817)	0.953
EQD2	1.341 (1.018–1.766)	0.037	1.135 (0.878–1.466)	0.334
Chemotherapy	1.136 (0.866–1.489)	0.356	1.156 (0.901–1.483)	0.253
Time	0.691 (0.525–0.909)	0.008	0.772 (0.602–0.990)	0.041
PIV (high vs. low)	0.439 (0.335–0.575)	<0.001	0.598 (0.467–0.765)	<0.001

FIGO, International Federation of Gynecology and Obstetrics; EQD2, 2-Gy equivalent dose; PIV, Pan-immune-inflammation value.

TABLE 5 Multivariate analysis.

Variable	OS		DFS	
	OR (95% CI)	P-value	OR (95% CI)	P-value
Diameter	0.697 (0.503–0.966)	0.030	0.731 (0.550–0.971)	0.031
FIGO (2018)				
IB3	Reference		Reference	
II	0.276 (0.117–0.653)	0.003	0.465 (0.234–0.926)	0.029
III	0.404 (0.284–0.575)	<0.001	0.634 (0.453–0.886)	0.008
IVA	0.633 (0.441–0.910)	0.014	0.909 (0.633–1.305)	0.604
EQD2	1.274 (0.963–1.685)	0.090		
Time	0.730 (0.553–0.963)	0.026		
PIV (high vs. low)	0.540 (0.409–0.713)	<0.001	0.680 (0.528–0.876)	0.003

FIGO, International Federation of Gynecology and Obstetrics; EQD2, 2-Gy equivalent dose; PIV, Pan-immune-inflammation value.

and AUC. While PIV demonstrated an equivalent AUC to NLR in predicting treatment efficacy, it exhibited superior predictive performance for OS and DFS, underscoring its robust combined predictive capability. Furthermore, PIV emerged not only as an independent prognostic factor for LACC but also significantly correlated with poor therapeutic effects and shorter DFS and OS in patients with higher PIV.

It has been demonstrated that an increased neutrophil and platelet count and a decreased lymphocyte count is related to poorer prognoses of cancer patients in previously published studies (41–43). Therefore, as a ratio combining multiple immune factors, it is predictable that a high PIV is linked to a decreased OS. Changes in PIV not only provide comprehensive information about the tumor immune microenvironment but also reveal the immune status and body function, especially in its interaction with the tumor. Specifically, the PIV may indicate the intensity and efficiency of the patient's immune surveillance. A higher PIV might reflect an immunosuppressive or inflammatory state, which is associated with tumor evasion and progression. In contrast, a lower PIV may reflect how well the antitumor immune response is working.

It is furthermore known that PIV has a close connection with tumor immunotherapy. The increased PIV change may reflect an intricate balance of inflammation and immunity responsible for determining the best tumor treatment options, prognosis prediction, and therapeutic response. Recently, studies have also identified PIV as an important prognostic factor in patients with recurrent or metastatic squamous cell carcinoma of the head and neck when treated with an immune checkpoint inhibitor. A multivariable PIV-based prognostic model incorporating Programmed Death Ligand 1 may provide a useful tool for future risk stratification and prognosis assessment (44). In addition, the studies showed a higher PIV correlated positively with worse survival among cancer patients post-immunotherapy treatment (45). This suggests that PIV is not just highly correlated with cancer progression, but can also influence the response of cancers to treatment include chemotherapy, radiotherapy and immunotherapy. Therefore, PIV may serve as a piece of creditable evidence for patient survival prognosis and disease progression detection.

In addition to the preliminary evidence of this study with respect to PIV in CCRT for LACC, some limitations are to be acknowledged. First and foremost, since it was a single-center, retrospective study the findings may not be generalizable. Secondly, all patients received platinum-based chemo- and radiotherapy, but potential heterogeneity with respect to the specific treatment plan may have impacted the results of this study. Moreover, the hospital adjuvant therapy could be another factor to affect the survival outcome. Third, despite the quite strict criteria for inclusion and exclusion in our study, confounding factors cannot be completely removed since all indicators were derived from peripheral blood samples of patients. Fourth, only patients with inflammation and hematological diseases or abnormal liver and kidney function or autoimmune diseases were excluded during data collection. However, individual differences in human beings are complex. This may explain why there is some variation among the study results. In the end, as this study was retrospective, data collection mainly focused on baseline characteristics, treatment responses, and prognostic data of patients. Detailed recording of side effects, toxic reactions, and other inflammatory markers during treatment was not conducted. Additionally, the follow-up time was relatively short in this study and additional surveillance for therapeutic efficacy-indexes during initial treatment improvement needs to be verified by longer duration of survival.

This study has some limitations, however it does suggest that PIV may be a promising candidate for evaluation of prognosis prior to CCRT in LACC patients. Future studies must be validated in a greater multi-center cohort to confirm the prognostic value of PIV, and are needed for exploring its potential applications as part of personalized medical strategies. Moreover, an in-depth study of the molecular biological mechanism underlying the interaction between PIV and CCRT is likely to establish more reliable treatment approaches. In addition, examination of the joint effects between PIV and these traditional biomarkers might help improve prognosis more accurately. Overall, the present study emphasizes the potential application of PIV in the prognostic assessment of LACC and highlights a new direction for future clinical practice and scientific research.

Conclusion

We highlight the prognostic significance of PIV for patients with LACC. Our findings demonstrate that elevated PIV is related with unfavorable disease progression in LACC patients and identify PIV as an independent predictor of OS and DFS. The strategic application of PIV could improve the predictive accuracy of treatment responses and post-treatment survival durations in cervical cancer patients. We recommend that future studies should further validate the predictive value of PIV through prospective clinical trials and explore its potential application in personalized medicine. At the same time, we advocate for more in-depth mechanism studies of the interaction between PIV and the tumor microenvironment, as well as long-term follow-up studies to assess the impact of PIV on long-term survival and recurrence risk. Through these efforts, we expect to increase the clinical value of PIV as a prognostic tool, resulting in substantial improvements in treatment strategies and survival outcomes for patients with LACC.

Data availability statement

The raw data supporting the conclusions of this article will be made available by the authors, without undue reservation.

Ethics statement

The studies involving humans were approved by Ethics Committee of the Second Norman Bethune Hospital of Jilin University, The Second Norman Bethune Hospital of Jilin University, Chang Chun. The studies were conducted in accordance with the local legislation and institutional requirements. The ethics committee/institutional review board waived the requirement of written informed consent for participation from the participants or the participants' legal guardians/next of kin because The pathological data, tests, imaging data and basic information used in this study came from previous outpatients/inpatients in our hospital. Since the biological information and data have been de-identified, they are not individually identifiable and cannot be traced. Moreover, the research project does not involve personal privacy and commercial interests, and informed consent of the subjects cannot be objectively obtained, we hereby apply for exemption.

Author contributions

SY: Data curation, Writing – original draft, Writing – review & editing. XG: Investigation, Writing – review & editing. RL: Investigation, Writing – review & editing. XJ: Methodology, Writing – review & editing.

Funding

The author(s) declare that no financial support was received for the research, authorship, and/or publication of this article.

Acknowledgments

We are grateful to our colleagues for their extraordinary effort and adherence in conducting this study.

Conflict of interest

The authors declare that the research was conducted in the absence of any commercial or financial relationships that could be construed as a potential conflict of interest.

Publisher's note

All claims expressed in this article are solely those of the authors and do not necessarily represent those of their affiliated organizations, or those of the publisher, the editors and the reviewers. Any product that may be evaluated in this article, or claim that may be made by its manufacturer, is not guaranteed or endorsed by the publisher.

Supplementary material

The Supplementary Material for this article can be found online at: https://www.frontiersin.org/articles/10.3389/fonc.2024.1492251/full#supplementary-material

SUPPLEMENTARY FIGURE 1
Flowchart of recruitment process.

SUPPLEMENTARY FIGURE 2
Distribution of PIV, Platelet, Lymphocyte, Monocyte, and Neutrophil. (PLT, Platelet; LYM, Lymphocyte; MON, Monocyte; NEU, Neutrophil).

References

1. Sung H, Ferlay J, Siegel RL, Laversanne M, Soerjomataram I, Jemal A, et al. Global cancer statistics 2020: GLOBOCAN estimates of incidence and mortality worldwide for 36 cancers in 185 countries. *CA: A Cancer J Clin*. (2021) 71:209–49. doi: 10.3322/caac.21660

2. Peiretti M, Zapardiel I, Zanagnolo V, Landoni F, Morrow CP, Maggioni A. Management of recurrent cervical cancer: A review of the literature. *Surg Oncol*. (2012) 21:e59–66. doi: 10.1016/j.suronc.2011.12.008

3. Boussios S, Seraj E, Zarkavelis G, Petrakis D, Kollas A, Kafantari A, et al. Management of patients with recurrent/advanced cervical cancer beyond first line platinum regimens: Where do we stand? A literature review. *Crit Rev Oncol/Hematol*. (2016) 108:164–74. doi: 10.1016/j.critrevonc.2016.11.006

4. Zhao K, Yi Y, Ma Z, Zhang W. INHBA is a prognostic biomarker and correlated with immune cell infiltration in cervical cancer. *Front Genet*. (2021) 12:705512. doi: 10.3389/fgene.2021.705512

5. Zhao K, Ma Z, Zhang W. Comprehensive analysis to identify SPP1 as a prognostic biomarker in cervical cancer. *Front Genet*. (2021) 12:732822. doi: 10.3389/fgene.2021.732822

6. Chen L, Liu Q, Tan C, Wu T, Wu M, Tan X, et al. The age-male-albumin-bilirubin-platelets (aMAP) risk score predicts liver metastasis following surgery for breast cancer in Chinese population: A retrospective study. *Immunotargets Ther*. (2024) 13:75–94. doi: 10.2147/ITT.S446545

7. Chen L, Tan C, Li Q, Ma Z, Wu M, Tan X, et al. Assessment of the albumin-bilirubin score in breast cancer patients with liver metastasis after surgery. *Heliyon*. (2023) 9:e21772. doi: 10.1016/j.heliyon.2023.e21772

8. Qiang S, Fu F, Wang J, Dong C. Definition of immune molecular subtypes with distinct immune microenvironment, recurrence, and PANoptosis features to aid clinical therapeutic decision-making. *Front Genet*. (2022) 13:1007108. doi: 10.3389/fgene.2022.1007108

9. Zhou ZW, Long HZ, Xu SG, Li FJ, Cheng Y, Luo HY, et al. Therapeutic effects of natural products on cervical cancer: based on inflammatory pathways. *Front Pharmacol*. (2022) 13:899208. doi: 10.3389/fphar.2022.899208

10. Zhou ZW, Long HZ, Cheng Y, Luo HY, Wen DD, Gao LC. From microbiome to inflammation: the key drivers of cervical cancer. *Front Microbiol*. (2021) 12:767931. doi: 10.3389/fmicb.2021.767931

11. Singh N, Baby D, Rajguru J, Patil P, Thakkannavar S, Pujari V. Inflammation and cancer. *Ann Afr Med*. (2019) 18:121–6. doi: 10.4103/aam.aam_56_18

12. Winarno GNA, Mulyantari AI, Kurniadi A, Suardi D, Zulvayanti Z, Trianasari N. Predicting chemotherapy resistance in gestational trophoblastic neoplasia: ratio of neutrophils, lymphocytes, monocytes, and platelets. *Med Sci Monit*. (2022) 28:e938499. doi: 10.12659/MSM.938499

13. Olive KP. Fanning the flames of cancer chemoresistance: inflammation and anticancer therapy. *J Oncol Pract*. (2017) 13:181–3. doi: 10.1200/JOP.2017.021154

14. Gong J, Jiang H, Shu C, Hu MQ, Huang Y, Liu Q, et al. Prognostic value of lymphocyte-to-monocyte ratio in ovarian cancer: a meta-analysis. *J Ovarian Res*. (2019) 12:51. doi: 10.1186/s13048-019-0527-z

15. Gao Y, Guo W, Cai S, Zhang F, Shao F, Zhang G, et al. Systemic immune-inflammation index (SII) is useful to predict survival outcomes in patients with surgically resected esophageal squamous cell carcinoma. *J Cancer*. (2019) 10:3188–96. doi: 10.7150/jca.30281

16. Chen J-H, Zhai E-T, Yuan Y-J, Wu K-M, Xu J-B, Peng J-J, et al. Systemic immune-inflammation index for predicting prognosis of colorectal cancer. *World J Gastroenterol*. (2017) 23:6261–72. doi: 10.3748/wjg.v23.i34.6261

17. Tomita M, Ayabe T, Maeda R, Nakamura K. Systemic immune-inflammation index predicts survival of patients after curative resection for non-small cell lung cancer. *In Vivo*. (2018) 32:663–7. doi: 10.21873/invivo.11291

18. Huang H, Liu Q, Zhu L, Zhang Y, Lu X, Wu Y, et al. Prognostic value of preoperative systemic immune-inflammation index in patients with cervical cancer. *Sci Rep*. (2019) 9:3284. doi: 10.1038/s41598-019-39150-0

19. Hu B, Yang X-R, Xu Y, Sun Y-F, Sun C, Guo W, et al. Systemic immune-inflammation index predicts prognosis of patients after curative resection for hepatocellular carcinoma. *Clin Cancer Res*. (2014) 20:6212–22. doi: 10.1158/1078-0432.CCR-14-0442

20. Kumar A, Gurram L, Naga Ch P, Nayak P, Mulye G, Chopra S, et al. Correlation of hematological parameters with clinical outcomes in cervical cancer patients treated with radical radio(chemo)therapy: A retrospective study. *Int J Radiat Oncol Biol Phys*. (2024) 118:182–91. doi: 10.1016/j.ijrobp.2023.07.022

21. Guven DC, Sahin TK, Erul E, Kilickap S, Gambichler T, Aksoy S. The association between the pan-immune-inflammation value and cancer prognosis: A systematic review and meta-analysis. *Cancers (Basel)*. (2022) 14:2675. doi: 10.3390/cancers14112675

22. Fucà G, Guarini V, Antoniotti C, Morano F, Moretto R, Corallo S, et al. The Pan-Immune-Inflammation Value is a new prognostic biomarker in metastatic colorectal cancer: results from a pooled-analysis of the Valentino and TRIBE first-line trials. *Br J Cancer*. (2020) 123:403–9. doi: 10.1038/s41416-020-0894-7

23. Yeh C-C, Kao H-K, Huang Y, Tsai T-Y, Young C-K, Hung S-Y, et al. Discovering the clinical and prognostic role of pan-immune-inflammation values on oral cavity squamous cell carcinoma. *Cancers*. (2023) 15:322. doi: 10.3390/cancers15010322

24. Feng J, Wang L, Yang X, Chen Q, Cheng X. Pretreatment pan-immune-inflammation value (PIV) in predicting therapeutic response and clinical outcomes of neoadjuvant immunochemotherapy for esophageal squamous cell carcinoma. *Ann Surg Oncol*. (2023) 31:272–83. doi: 10.1245/s10434-023-14430-2

25. Guven DC, Erul E, Yilmaz F, Yasar S, Yildirim HC, Ercan F, et al. The association between pan-immune-inflammation value and survival in head and neck squamous cell carcinoma. *Eur Arch Oto Rhino Laryngol*. (2022) 280:2471–8. doi: 10.1007/s00405-022-07804-x

26. Wang Z, Ren D, Chen S, Duan G. Pan-immune-inflammation value is an independent prognostic factor in patients with non-small cell lung cancer with an established nomogram prognostic model. *Asian J Surg*. (2023) 46:4999–5000. doi: 10.1016/j.asjsur.2023.06.042

27. Topkan E, Selek U, Kucuk A, Pehlivan B. Low pre-chemoradiotherapyPan-immune-inflammation value (PIV) measures predict better survival outcomes in locally advanced pancreatic adenocarcinomas. *J Inflammation Res*. (2022) 15:5413–23. doi: 10.2147/JIR.S385328

28. Shaul ME, Fridlender ZG. Neutrophils as active regulators of the immune system in the tumor microenvironment. *J Leukoc Biol*. (2017) 102:343–9. doi: 10.1189/jlb.5MR1216-508R

29. Basu A, Ramamoorthi G, Albert G, Gallen C, Beyer A, Snyder C, et al. Differentiation and regulation of T(H) cells: A balancing act for cancer immunotherapy. *Front Immunol*. (2021) 12:669474. doi: 10.3389/fimmu.2021.669474

30. Colotta F, Allavena P, Sica A, Garlanda C, Mantovani A. Cancer-related inflammation, the seventh hallmark of cancer: links to genetic instability. *Carcinogenesis*. (2009) 30:1073–81. doi: 10.1093/carcin/bgp127

31. Dolan RD, McSorley ST, Horgan PG, Laird B, McMillan DC. The role of the systemic inflammatory response in predicting outcomes in patients with advanced inoperable cancer: Systematic review and meta -analysis. *Crit Rev Oncol/Hematol*. (2017) 116:134–46. doi: 10.1016/j.critrevonc.2017.06.002

32. Dupré A, Malik HZ. Inflammation and cancer: What a surgical oncologist should know. *Eur J Surg Oncol*. (2018) 44:566–70. doi: 10.1016/j.ejso.2018.02.209

33. Wang D, Wu M, Feng F-Z, Huang H-F, Yang J-X, Shen K, et al. Pretreatment neutrophil-to-lymphocyte and platelet-to-lymphocyte ratios do not predict survival in patients with cervical cancer treated with neoadjuvant chemotherapy and radical hysterectomy. *Chin Med J*. (2013) 126:1464–8. doi: 10.3760/cma.j.issn.0366-6999.20122672

34. Zhang Y, Wang L, Liu Y, Wang S, Shang P, Gao Y, et al. Preoperative neutrophil-lymphocyte ratio before platelet-lymphocyte ratio predicts clinical outcome in patients with cervical cancer treated with initial radical surgery. *Int J Gynecol Cancer*. (2014) 24:1319–25. doi: 10.1097/IGC.0000000000000219

35. Chen L, Zhang F, Sheng X-G, Zhang S-Q, Chen Y-T, Liu B-W. Peripheral platelet/lymphocyte ratio predicts lymph node metastasis and acts as a superior prognostic factor for cervical cancer when combined with neutrophil. *Medicine*. (2016) 95:e4381. doi: 10.1097/MD.0000000000004381

36. Jonska-Gmyrek J, Gmyrek L, Zolciak-Siwinska A, Kowalska M, Fuksiewicz M, Kotowicz B. Pretreatment neutrophil to lymphocyte and platelet to lymphocyte ratios as predictive factors for the survival of cervical adenocarcinoma patients. *Cancer Manage Res*. (2018) 10:6029–38. doi: 10.2147/CMAR.S178745

37. Wu J, Chen M, Liang C, Su W. Prognostic value of the pretreatment neutrophil-to-lymphocyte ratio in cervical cancer: a meta-analysis and systematic review. *Oncotarget*. (2017) 8:13400–12. doi: 10.18632/oncotarget.14541

38. Zhang S-Q, Zhang F, Sheng X-G, Chen L. Decreased pretreatment lymphocyte/monocyte ratio is associated with poor prognosis in stage Ib1–IIa cervical cancer patients who undergo radical surgery. *OncoTargets Ther*. (2015) 8:1355–62. doi: 10.2147/OTT.S82174

39. Gangopadhyay A. Prognostic nutritional index and clinical response in locally advanced cervical cancer. *Nutr Cancer*. (2020) 72:1438–42. doi: 10.1080/01635581.2020.1729820

40. Haraga J, Nakamura K, Omichi C, Nishida T, Haruma T, Kusumoto T, et al. Pretreatment prognostic nutritional index is a significant predictor of prognosis in patients with cervical cancer treated with concurrent chemoradiotherapy. *Mol Clin Oncol*. (2016) 5:567–74. doi: 10.3892/mco.2016.1028

41. Teramukai S, Kitano T, Kishida Y, Kawahara M, Kubota K, Komuta K, et al. Pretreatment neutrophil count as an independent prognostic factor in advanced non-small-cell lung cancer: an analysis of Japan Multinational Trial Organisation LC00-03. *Eur J Cancer*. (2009) 45:1950–8. doi: 10.1016/j.ejca.2009.01.023

42. Li L, Wang J, Meng S, Li Z, Huang Z, Sun J, et al. Peripheral blood leukocytes and platelets serve as prognostic factors in breast cancer. *Cancer Biother Radiopharm*. (2021) 36:167–73. doi: 10.1089/cbr.2019.3032

43. Quigley DA, Kristensen V. Predicting prognosis and therapeutic response from interactions between lymphocytes and tumor cells. *Mol Oncol*. (2015) 9:2054–62. doi: 10.1016/j.molonc.2015.10.003

44. Lien M-Y, Hwang T-Z, Wang C-C, Hsieh C-Y, Yang C-C, Wang C-C, et al. A novel prognostic model using pan-immune-inflammation value and programmed death ligand 1 in patients with recurrent or metastatic head and neck squamous cell carcinoma receiving immune checkpoint inhibitors: A retrospective multicenter analysis. *Target Oncol*. (2024) 19:71–9. doi: 10.1007/s11523-023-01018-9

45. Kuang T, Qiu Z, Wang K, Zhang L, Dong K, Wang W. Pan-immune inflammation value as a prognostic biomarker for cancer patients treated with immune checkpoint inhibitors. *Front Immunol*. (2024) 15:1326083. doi: 10.3389/fimmu.2024.1326083

frontiers | Frontiers in Immunology

TYPE Original Research
PUBLISHED 04 November 2024
DOI 10.3389/fimmu.2024.1489444

Check for updates

OPEN ACCESS

EDITED BY
Qingyu Luo,
Dana–Farber Cancer Institute, United States

REVIEWED BY
Lijuan Wang,
Shandong University, China
Shun Gong,
Northern Theater Command General Hospital, China
Liang Ji,
Harbin Medical University, China

*CORRESPONDENCE
Jing Wang
wangjing@cicams.ac.cn
Yi Fang
fangyi@cicams.ac.cn

†These authors have contributed equally to this work

RECEIVED 01 September 2024
ACCEPTED 11 October 2024
PUBLISHED 04 November 2024

CITATION
Ding P, Pei S, Qu Z, Yang Y, Liu Q, Kong X, Wang Z, Wang J and Fang Y (2024) Single-cell sequencing unveils mitophagy-related prognostic model for triple-negative breast cancer.
Front. Immunol. 15:1489444.
doi: 10.3389/fimmu.2024.1489444

COPYRIGHT
© 2024 Ding, Pei, Qu, Yang, Liu, Kong, Wang, Wang and Fang. This is an open-access article distributed under the terms of the Creative Commons Attribution License (CC BY). The use, distribution or reproduction in other forums is permitted, provided the original author(s) and the copyright owner(s) are credited and that the original publication in this journal is cited, in accordance with accepted academic practice. No use, distribution or reproduction is permitted which does not comply with these terms.

Single-cell sequencing unveils mitophagy-related prognostic model for triple-negative breast cancer

Peikai Ding†, Shengbin Pei†, Zheng Qu†, Yazhe Yang†, Qiang Liu, Xiangyi Kong, Zhongzhao Wang, Jing Wang* and Yi Fang*

Department of Breast Surgical Oncology, National Cancer Center/National Clinical Research Center for Cancer/Cancer Hospital, Chinese Academy of Medical Sciences and Peking Union Medical College, Beijing, China

Background: Triple-negative breast cancer (TNBC) is an aggressive subtype of breast cancer lacking hormone receptors and HER2 expression, leading to limited treatment options and poor prognosis. Mitophagy, a selective autophagy process targeting damaged mitochondria, plays a complex role in cancer progression, yet its prognostic significance in TNBC is not well understood.

Methods: This study utilized single-cell RNA sequencing data from the TCGA and GEO databases to identify mitophagy-related genes (MRGs) associated with TNBC. A prognostic model was developed using univariate Cox analysis and LASSO regression. The model was validated across multiple independent cohorts, and correlations between MRG expression, immune infiltration, and drug sensitivity were explored.

Results: Nine key MRGs were identified and used to stratify TNBC patients into high-risk and low-risk groups, with the high-risk group showing significantly worse survival outcomes. The model demonstrated strong predictive accuracy across various datasets. Additionally, the study revealed a correlation between higher MRG expression levels and increased immune cell infiltration, as well as potential responsiveness to specific chemotherapeutic agents.

Conclusion: The mitophagy-related prognostic model offers a novel method for predicting outcomes in TNBC patients and highlights the role of mitophagy in influencing the tumor microenvironment, with potential applications in personalized treatment strategies.

KEYWORDS

triple-negative breast cancer, mitophagy, single-cell sequencing, prognostic model, immunoassay

1 Introduction

In recent times, breast cancer has established itself as the most prevalent malignant tumor in women across the globe. The Global Cancer Statistics 2022 report indicates that breast cancer ranks first among newly diagnosed cancers worldwide. It caused approximately 685,000 deaths, accounting for 6.9% of all cancer-related deaths. Despite a decline in mortality rates resulting from advances in early detection and treatment, the prevalence of breast cancer is on the rise globally, particularly in rapidly developing regions (1). Triple-negative breast cancer (TNBC) represents a highly malignant variant of the disease, accounting for approximately 10-20% of all diagnosed cases of breast cancer (2). Patients diagnosed with TNBC tend to have a less favorable prognosis, with a five-year survival rate that is considerably lower than that observed in other breast cancer subtypes. Additionally, they exhibit a higher incidence of recurrence and metastasis. The prevalence of TNBC is notably elevated among younger women and those of African descent, who also exhibit a proclivity for inferior outcomes. Consequently, there is a strong imperative to develop new prognostic models for breast cancer and to identify novel biomarkers.

Mitophagy represents a vital cellular mechanism that enables the selective degradation of damaged mitochondria, thereby maintaining mitochondrial function and cellular homeostasis. It is instrumental in cellular energy metabolism, oxidative stress responses, and programmed cell death (apoptosis) (3). More and more studies have shown that mitophagy plays a complex role in the development and progression of cancer (4). PINK1, a kinase of the mitochondria, is recruited to the outer membrane of the mitochondria and is responsible for Parkin activation. Parkin is an E3 ubiquitin ligase that facilitates the ubiquitination of damaged mitochondria, marking them for subsequent autophagic degradation (5). This mechanism plays a key role in the maintenance of mitochondrial function and the regulation of cancer cell survival as well as death. The aberrant expression levels of PINK1 and Parkin have been observed in lung and breast cancers, which points towards a potential involvement in the processes of tumorigenesis and progression (6, 7). The available evidence suggests that elevated mitophagy activity may contribute to the enhanced resilience of cancer cells to chemotherapy and radiotherapy (8). The clearance of damaged mitochondria enables cancer cells to survive the stress induced by treatment. Consequently, the inhibition of mitophagy may represent a promising avenue for enhancing the efficacy of cancer therapies.

Although TNBC is a highly invasive disease with a poor prognosis, and although mitophagy plays an essential role in cellular metabolism and apoptosis, prognostic studies targeting mitophagy-related genes in TNBC remain scarce. The majority of extant prognostic models are predicated on traditional molecular markers or gene expression profiles and thus lack a comprehensive examination of this crucial cellular process. Accordingly, the construction of a prognostic model based on mitophagy-related genes (MRGs) has the potential to address this research gap, as well as to provide new biomarkers for the personalized treatment of TNBC patients.

The advent of single-cell sequencing technology has afforded researchers a previously unattainable level of cellular resolution in the field of cancer research. This has enabled scientists to conduct in-depth investigations into the heterogeneous nature of tumors and the intricate interactions within the tumor microenvironment (9). Single-cell sequencing allows for a comprehensive analysis of gene expression, genomic variations, and epigenetic states at the individual cellular level, thereby elucidating differences among tumor cells and their responses to therapeutic interventions. In the field of malignant tumor research, single-cell sequencing has emerged as a pivotal technique for identifying novel molecular subtypes, pinpointing prospective therapeutic targets, and characterizing prognostic biomarkers.

In this study, we obtained publicly available data on triple-negative breast cancer (TNBC) from the TCGA and GEO databases. A novel prognostic model was developed through comprehensive bioinformatics analysis, utilizing nine MRGs. Patients with TNBC were stratified according to their risk profiles, resulting in the formation of two distinct groups: high-risk and low-risk. Moreover, the expression of mitophagy-related genes enabled the detection of alterations in immune infiltration and immune checkpoints in TNBC patients. The findings of our research may provide a novel perspective for the diagnosis and management of TNBC.

2 Methods

2.1 Data acquisition and preprocessing for model construction and validation in TNBC

The RNA expression profiles, gene mutation information, and clinical data for TNBC patients were sourced from the TCGA database. To build the model, the training set was utilized, while the validation set was employed to evaluate the model's stability and accuracy. Additionally, expression profiles were retrieved from the Gene Expression Omnibus datasets GSE21653, GSE58812, and GSE65194, along with data from the Molecular Taxonomy of Breast Cancer database, to serve as external, independently validated cohorts. All datasets were formatted in TPM and log-transformed for subsequent analysis. To address potential batch effects across datasets, the "sva" package was utilized.

2.2 Acquisition and processing of scRNA-seq data

The single-cell RNA sequencing (scRNA-seq) dataset GSE161529, consisting of ten TNBC samples, was obtained from the Gene Expression Omnibus (GEO) database. The quality of the scRNA-seq data was evaluated using the "Seurat" and "SingleR" R packages. To maintain the integrity of the scRNA-seq data, cells with less than 10% mitochondrial gene content, more than 200 total genes, or those expressed in fewer than three cells with expression levels between 200 and 7,000 were excluded. Given the diverse sample origins, the "FindIntegrationAnchors" function from canonical correlation analysis (CCA) was utilized to eliminate any potential batch effects that could impact downstream analyses.

Subsequently, the "IntegrateData" and "ScaleData" functions were used to ensure comprehensive data integration and scaling. Principal component analysis (PCA) was then employed to determine the anchors for dimensionality reduction, and the t-distributed stochastic neighbor embedding (t-SNE) method was used to examine the first 20 principal components (PCs) to identify meaningful clusters. The variability in the cell cycle among clusters was assessed using cell cycle markers integrated within the "Seurat" package.

2.3 Acquisition of mitophagy-related genes

MRGs were identified from the GeneCards database, with a relevance score exceeding 1.5 employed as the criterion for selecting MRGs for subsequent investigation (see Supplementary Table).

2.4 Using AUCell

The most relevant genes impacting mitophagy were identified from the single-cell RNA-sequencing data using the AUCell R package. AUCell is a computational tool that assesses the activity status of gene sets within single-cell RNA sequencing data, assigning a mitophagy activity score to each cell. The area under the curve (AUC) values for the selected MRGs were used to determine the proportion of highly expressed gene sets within each cell based on the gene expression rankings. Cells with a higher number of selected genes exhibited higher AUC values. The "AUCell explore thresholds" function was employed to identify cells actively participating in mitophagy. The cells were then categorized into two groups—high mitophagy AUC and low mitophagy AUC—based on the median AUC value. The results were graphically represented using the "ggplot2" R package.

2.5 Single-sample gene set enrichment analysis

ssGSEA is a frequently utilized method for calculating precise scores for enriched gene sets within a given sample. In this study, the ssGSEA method was employed to ascertain the mitophagy score (MM score) for each TNBC patient within the TCGA cohort.

2.6 Construction of mitophagy-related risk signatures

The process began with univariate Cox analysis to identify MRGs that had prognostic significance. These MRGs were further refined using Lasso regression, leading to the creation of a prognostic model. Each TNBC patient was then assigned a risk score based on the algorithm. The TCGA-TNBC cohort was divided into high-risk and low-risk groups according to the median value. The differences in prognosis between these two groups were then analyzed, and the model's accuracy was evaluated.

2.7 Evaluation of the independence and validity of the prognostic model

To estimate the one-year, three-year, and five-year overall survival (OS) probabilities, a nomogram was constructed using risk scores, age, gender, pathological stage, and other clinical parameters as independent prognostic factors. Kaplan-Meier survival curves were generated to assess the prognostic implications, with their statistical significance evaluated using the log-rank test. The accuracy of the nomogram was further validated through calibration curves and receiver operating characteristic (ROC) curves. Additionally, a decision curve analysis (DCA) was performed to assess the net benefit of the nomogram alongside individual clinical features. A stratified analysis was also conducted to evaluate the prognostic relevance of the risk score concerning various clinical characteristics, including age, gender, clinical stage, and pathological T stage.

2.8 Correlation analysis of the prognostic model with tumor immunity and immunotherapy

We assessed the extent of immune infiltration in TNBC patients using data from the TCGA database, specifically from the TIMER 2.0 database, which includes results from seven distinct assessment methods. This data was utilized to generate heatmaps that illustrate the relative levels of immune cell infiltration within the tumor stroma. Following this, the genes in the prognostic risk assessment model were analyzed using ssGSEA via the GSEABase R package, which is related to immune-associated attributes. The "estimate" R package was then employed to calculate the relative abundance of stromal cells, immune cells, and tumor cells, and these values were compared across various risk categories.

2.9 Genomic mutation profile and drug sensitivity

The genomic mutation profiles of TNBC patients were obtained from the TCGA database and visualized using the "maftools" R package. These comprehensive gene mutation data were then integrated with the risk scores. Additionally, the "pRRophetic" R package was utilized to calculate the half-maximal inhibitory concentration (IC50) of commonly used chemotherapy drugs, allowing for an evaluation of the correlation between risk scores and drug sensitivity. The Wilcoxon signed-rank test was used to determine if there were any statistically significant differences in IC50 values between the two risk groups.

3 Results

3.1 Single-cell sequencing data analysis

Using dimensionality reduction algorithms (tSNE), we identified 18 distinct cell clusters characterized by different gene

10.3389/fimmu.2024.1489444

expression profiles (Figure 1A). Through cell annotation, nine different cell types were identified, including fibroblasts, myeloid cells, and tumor cells (Figure 1B). To explore the expression characteristics of MRGs, we evaluated the MM activity of each cell using the AUCell R package. An AUC score was attributed to all cells corresponding to the MRGs to categorize them into high- and low-AUC expression groups based on the established AUC score thresholds. Cells with elevated gene expression demonstrated elevated AUC values, a phenomenon predominantly observed in the orange-colored myeloid cells, fibroblasts, and tumor cells (Figure 1C). To ascertain the biological mechanisms that may be responsible for the observed differences in AUC scores, we conducted a differential expression and functional analysis. The differential expression analysis revealed that these genes were primarily associated with oxidative phosphorylation, mTORC1 signaling, fatty acid metabolism, PI3K-AKT-mTOR signaling, apoptosis, and the P53 pathway (Figure 1D). To further elucidate the association between MRGs and the outcome of TNBC patients, we performed an in-depth analysis of the most relevant genes affecting the activity of mitophagy obtained from single-cell data. We constructed a prognostic model using the TCGA-BC training set and identified 63 prognostic genes by univariate analysis ($P < 0.01$). Subsequently, we utilized LASSO Cox regression analysis to construct the prognostic model. Under the optimal regularization parameter, nine model genes were selected: MRPS5, C20orf27, PSMB5, PYCR1, HEBP1, CBR1, PTMS, LSM2, and NDUFS3 (Figure 1E). The calculation method for the prognostic model is as follows:

$$risk\ \ score = \sum_{n=i}^{k}(Coef_i \exp i)$$

Coefi represents the coefficient of each model gene and Expi represents the expression level of each model gene. Accordingly, a risk score was calculated for each sample and categorized into high-risk and low-risk groups. Of the nine genes used to construct

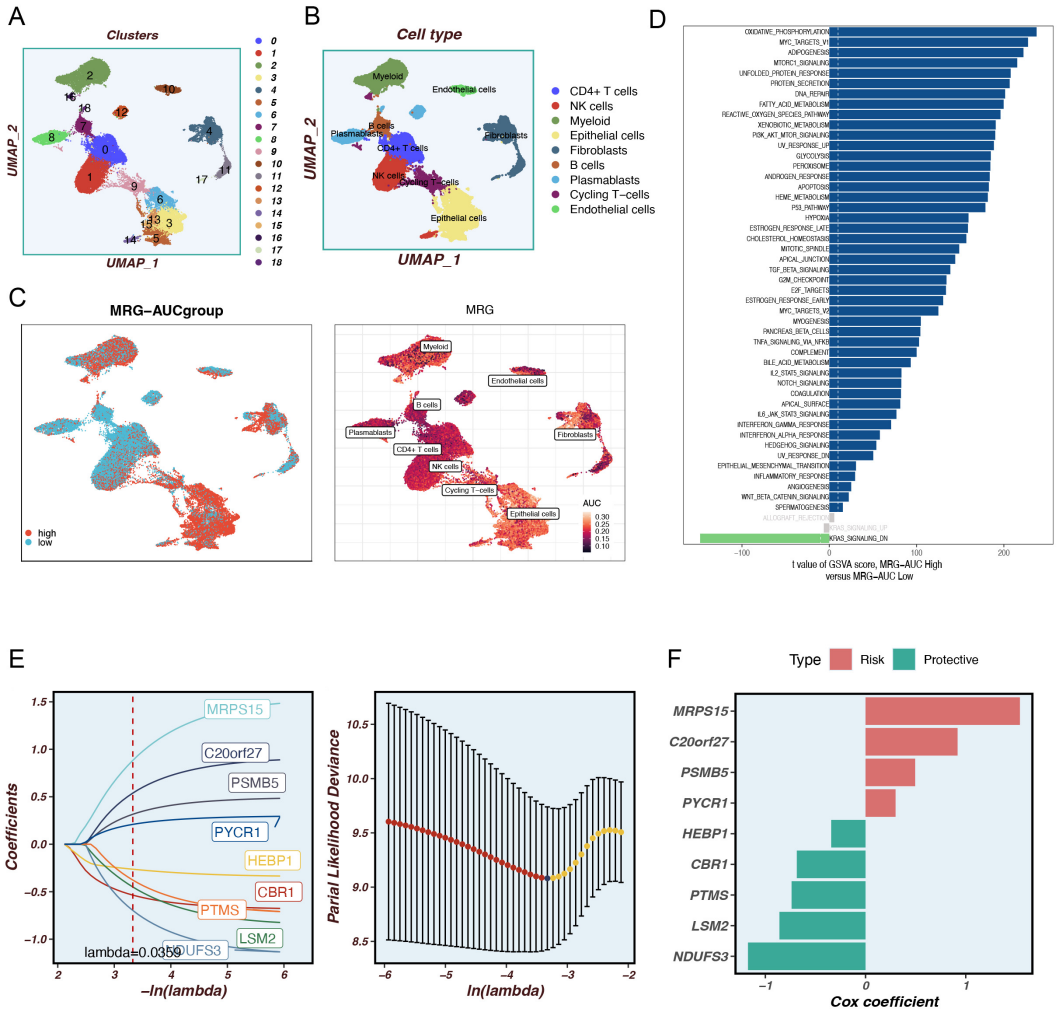

FIGURE 1
Identify differentially expressed genes and annotate cell subsets. **(A)** The tSNE plot shows the results of the dimension reduction cluster analysis. **(B)** The cells have been annotated into 9 different types of cells. **(C)** All cells were scored into high and low groups according to mitophagy-related genes (MRGs). **(D)** Analyze differentially expressed genes between high and low groups. **(E)** LASSO Cox regression analysis to develop the prognostic model. **(C)** The role of seven model genes. **(F)** The role of nine model genes.

the model, four were risk factors and five were protective factors (Figure 1F).

3.2 Construction and validation of the mitophagy-related prognostic model

Principal component analysis (PCA) of the nine model genes across the TCGA, MetaBric, GSE58812, GSE2653, and GSE65194 datasets revealed that the model effectively stratified TNBC patients into two risk groups. To ascertain the precision of the MRGs in prognosticating the outcome of TNBC patients, we conducted a receiver operating characteristic (ROC) curve analysis on both the training and testing datasets. In the training set TCGA database, TNBC patients can be effectively categorized into two risk groups (Figure 2A). Meanwhile, there was a significant difference in the prognosis of patients in the two groups (P=0.0017, Figure 2B). In the MetaBric test set, it was possible to distinguish well between the two groups of patients while there was a significant difference in prognosis between the two groups (P=0.00028, Figures 2C, D). In the GSE58812 test set, the AUC was consistently above 0.8, indicating the high accuracy of the model in assessing patient prognosis (Figures 2E, F). In the GSE2653 test set, PCA did a good job of separating patients into high-risk and low-risk groups (Figure 2G), and a similar pattern was observed for both patient survival and AUC (Figure 2H). Although the PCA in the GSE65194 cohort effectively stratified patients into high- and low-risk groups (Figure 2I), and a trend of poorer prognosis was observed in the high-risk group, the difference in prognosis between the two groups did not reach statistical significance (P=0.056, Figure 3J). This result suggests that the relatively small sample size or cohort-specific variability may have limited the ability to detect a statistically significant difference. Further validation with larger cohorts may help confirm these findings. In conclusion, the prognostic model based on MRGs demonstrated high predictive accuracy in all four independent cohorts.

3.3 Prognostic value of mitophagy-related genes in triple-negative breast cancer: correlations with survival and risk scores

The aim of this research is to analyze the potential association of expression levels of nine MRGs with survival outcomes and risk scores in TNBC patients. Kaplan-Meier survival analysis showed a difference in overall outcome between individuals with high and low expression of these genes. In particular, elevated expression of genes such as CBR1, HEBP1, and PTMS was markedly linked to diminished survival rates, with P-values of 0.002, 0.006, and 0.018, respectively. This suggests that these genes may serve as crucial prognostic predictors for TNBC. Although the P-values for some genes, such as MRPS15 and PYCR1, were slightly above the traditional significance level ($p<0.05$), they still exhibited a general trend associated with poor prognosis (Figure 3A).

In addition, scatterplot analysis showed the association between the expression level of each gene and the risk score. Expression of CBR1 and HEBP1 was significantly negatively correlated with risk scores, with Pearson correlation coefficients of -0.42 ($q = 5.8e-15$) and -0.53 ($q = 0$), respectively. This indicates that high level of these gene expression may be associated with lower risk scores, further supporting their potential protective role in prognosis. Conversely, the expression of LSM2 and MRPS15 showed a positive correlation with risk scores, with correlation coefficients of 0.14 ($q = 0.016$) and 0.48 ($q = 0$), respectively. These results indicate that high expression levels of these genes may be linked to increased risk scores and poorer prognosis (Figure 3B).

The results indicate that the analysis of mitophagy-related gene expression patterns may serve as an effective stratification method for TNBC patients into distinct risk groups and for predicting their survival outcomes. The findings suggest that these genes may be critical in the progression of TNBC and provide new potential targets for personalized therapy.

3.4 Construction of a nomogram model and drug sensitivity analysis

Based on the TCGA data, we selected several key variables (such as risk score, age, and cancer stage) and constructed a nomogram model to more precisely quantify the risk for breast cancer patients (Figure 4A). As an intuitive and practical tool, the nomogram plays an important role in cancer prognosis prediction and personalized treatment (10). By integrating multiple predictive variables, the nomogram provides accurate assessments of survival probability and recurrence risk, thereby aiding clinicians in making more optimized treatment decisions, which in turn enhances patient outcomes and quality of life. To ascertain the veracity and predictive efficacy of the nomogram model, we conducted a calibration curve analysis, which demonstrated that the predicted values of the model were highly consistent with observed values at different time points, indicating high predictive accuracy.

Furthermore, a clinical heatmap was generated using the prognostic model genes to evaluate the associations among the model genes and clinicopathologic features (such as lymph node positivity, recurrence status, tumor size, etc.) (Figure 4B). The results showed significant differences between the two groups, especially in terms of tumor size and recurrence status ($p < 0.05$).

A notable meaningful positivity was detected between multidrug sensitivity (IC50) and TNBC risk score. This suggests that an elevated risk score is indicative of heightened sensitivity among patients to these pharmaceutical agents. The drugs in question are Dasatinib, AP-24534, AZD7762, Cisplatin, BEZ235, and Talazoparib (Figure 4C). These findings are of considerable clinical significance. Patients with higher risk scores may exhibit greater sensitivity to these drugs, thereby warranting their prioritization in the treatment regimen. Of the drugs under consideration, talazoparib demonstrated the highest correlation ($R = 0.39$), indicating its potential efficacy in high-risk TNBC patients.

3.5 Impact of tumor mutational burden: a comprehensive study of risk scores and survival analysis

TMB is a biomarker that has been widely accepted as an essential factor in cancer research and treatment, particularly in

the setting of immunotherapy. This metric is increasingly being acknowledged as a potential indicator of responsiveness to immune checkpoint inhibitors (ICIs) (11). A high TMB is associated with an elevated number of mutations, which has the potential to generate an enhanced generation of neoantigens that can be recognized by the immune system, thereby improving ICIs' efficacy (12). Our study found that in the MetaBric database, the high-risk group exhibited a higher mutation frequency, which was statistically significant (P = 0.0042, Figure 5A). Correlation analysis revealed a positive relationship between risk score and mutation frequency, with higher risk scores associated with higher mutation frequencies (Figure 5B). Previous studies have shown that tumors with a high mutational burden generally have a worse prognosis. This view has also been confirmed in breast cancer research. A study by Barroso-Sousa et al. found that high TMB is not only common in breast cancer, especially TNBC, but is also associated with worse survival (13). Our results provide further evidence to support the hypothesis that high mutational load may serve as a negative prognostic indicator. In terms of survival analysis, the low-risk and high-TMB groups had the most favorable prognosis for survival, whereas the high-risk and low-TMB groups had the worst prognosis, with a statistically significant difference between them (Figure 5C). Similar prognostic differences were observed in the TCGA database, although no statistical difference was found between TMB and risk rating in this database (Figures 5D–F).

3.6 Analysis of tumor microenvironment and immune cell infiltration

The level of immune cell infiltration in each test specimen was assessed according to seven different methods to gain a deeper understanding of the distribution and correlation of 18 types of tumor-infiltrating immune cells (TICs) in the TCGA-BC cohort. The high-risk group showed increased levels of immune cell infiltration compared to the low-hazard group (Figure 6A). In particular, the high-risk group showed increased amounts of immune cell infiltration, particularly macrophages, neutrophils, and cancer-associated fibroblasts. The low-risk group had significantly enhanced stromal, immune, and ESTIMATE scores, suggesting increased general immune status and the immunogenicity of the tumor microenvironment (TME) ($P < 0.05$). Additionally, a positive correlation with tumor purity was observed (Figure 6B). The expression levels of 29 immune cells were further analyzed in the training and validation sets, and the box plot results demonstrated that two types of cells in the training set exhibited high infiltration in the high-risk group: CD8+ T cells and Tfh (Figure 6C). The cytolytic activity represents a crucial mechanism through which the immune system can control and eliminate harmful cells within the body. Our findings revealed elevated cytolytic activity in the high-risk group (Figure 6E). In the validation set (Metabric), macrophages, neutrophils, and Treg exhibited high infiltration in the high-risk group (Figure 6D). Additionally, they demonstrated heightened activity in CCR, HLA, and other biological processes (Figure 6F).

3.7 Insights into immune therapy efficacy through checkpoint analysis

Tumors have two distinct immune escape mechanisms: on the one hand, some immunosuppressive factors prevent T-cell infiltration; on the other hand, some tumors are functionally inactivated despite high levels of cytotoxic T-cell infiltration. TIDE (Tumor Immune Dysfunction and Exclusion) is a computational tool for evaluating the tumor immune escape mechanism and a computational tool for predicting immune checkpoint inhibitor (ICI) treatment response. Tumor immune escape is predicted by a combined assessment of the activity of these two mechanisms. Higher TIDE scores were associated with poorer immune checkpoint inhibition therapy. The results of the violin plot showed higher TIDE scores in the high-risk group than in the low-risk group, which was consistent but not statistically significant and may be related to the small sample size (Figure 7A). Meanwhile, the bubble plot showed the model genes correlated with immune checkpoints, in which PYCR1 was significantly negatively correlated with immune checkpoints (Figure 7B). We further analyzed the expression levels of immune checkpoints in high and low-risk groups, in which TNFSF15, ADORA2A, TNFSF4 and CD160 were expressed at higher levels in high-risk groups (Figure 7C).

3.8 Differential pathway enrichment in high- and low-risk TNBC patients: insights from GSEA and GSVA analysis

Gene Set Enrichment Analysis (GSEA) was employed to categorize TNBC patients into high-risk and low-risk groups based on the risk model constructed from mitophagy-related genes. The results demonstrated notable discrepancies in numerous signaling pathways between the two groups. The high-risk group exhibited enrichment of the TGF-β signaling pathway. The transforming growth factor-beta (TGF-β) signaling pathway plays a pivotal role in regulating a multitude of cellular processes, including proliferation, differentiation, and apoptosis. Additionally, it plays a pivotal role in the tumor microenvironment, influencing processes such as tumor cell proliferation, immune evasion, and metastasis (14). The upregulation of the TGF-β signaling pathway in the high-risk group may facilitate tumor cell invasion and metastasis while simultaneously impeding the immune system's anti-tumor response. The high-risk group exhibited an enrichment of epithelial-mesenchymal transition (EMT), which suggests an elevated propensity for tumor cell invasion and metastasis. Epithelial-mesenchymal transition (EMT) is a process by which epithelial cells gain a mesenchymal phenotype, a transformation that is closely associated with cancer metastasis (15). The PI3K/AKT/mTOR signaling pathway, which plays a pivotal role in cell growth, proliferation, and survival, was also found to be upregulated in the high-risk group. The aberrant activation of the PI3K/AKT/mTOR pathway is a common occurrence in a multitude of cancers, and it serves to promote tumor growth and drug resistance (16).

10.3389/fimmu.2024.1489444

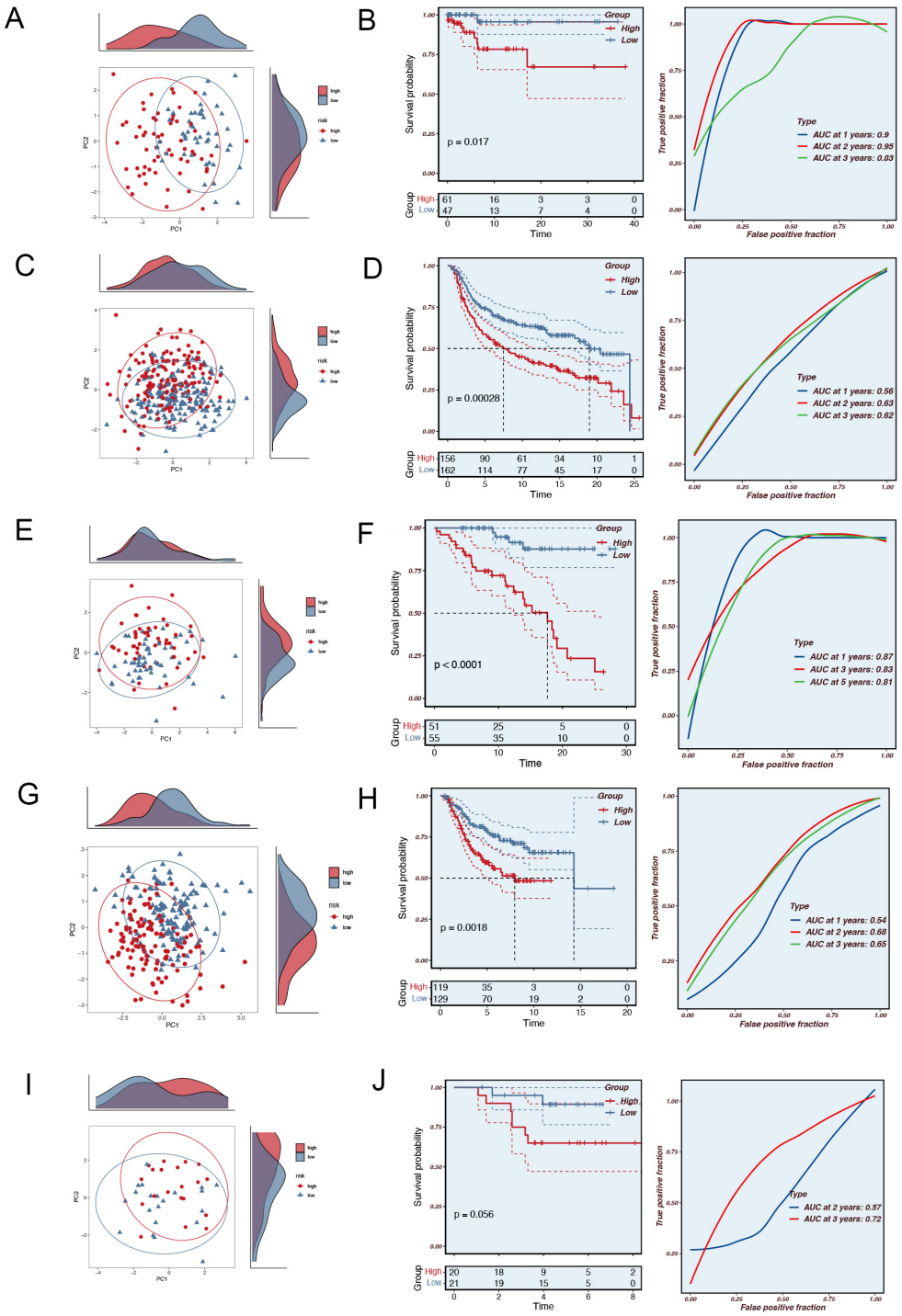

FIGURE 2
The validation of the Mitophagy-related Prognostic Model. **(A)** PCA analysis in the TCGA training set. **(B)** The area under the curve (AUC) values for the TCGA train cohort. **(C)** PCA analysis in the MetaBric validation set. **(D)** The areas under the curve at 1, 3, and 5 years for the MetaBric test group. **(E)** PCA analysis in the GSE58812 validation set. **(F)** The areas under the curve at 1, 3, and 5 years for the GSE58812 test group. **(G)** PCA analysis in the GSE2653 validation set. **(H)** The areas under the curve at 1, 3, and 5 years for the GSE2653 test group. **(I)** PCA analysis in the GSE65194 validation set. **(J)** The areas under the curve at 1, 3, and 5 years for the GSE65194 test group.

The observed upregulation of this pathway in the high-risk group may contribute to the rapid proliferation of tumor cells and their anti-apoptotic capabilities, thereby increasing tumor aggressiveness and resistance to therapy. In contrast, the DNA repair pathway was found to be more active in the low-risk group, indicating that the DNA repair capacity may be compromised in the high-risk group, which could result in increased genomic instability. The results demonstrate a notable enrichment of multiple critical biological pathways in triple-negative breast cancer. Among these pathways are those associated with cell cycle regulation, genomic stability,

10.3389/fimmu.2024.1489444

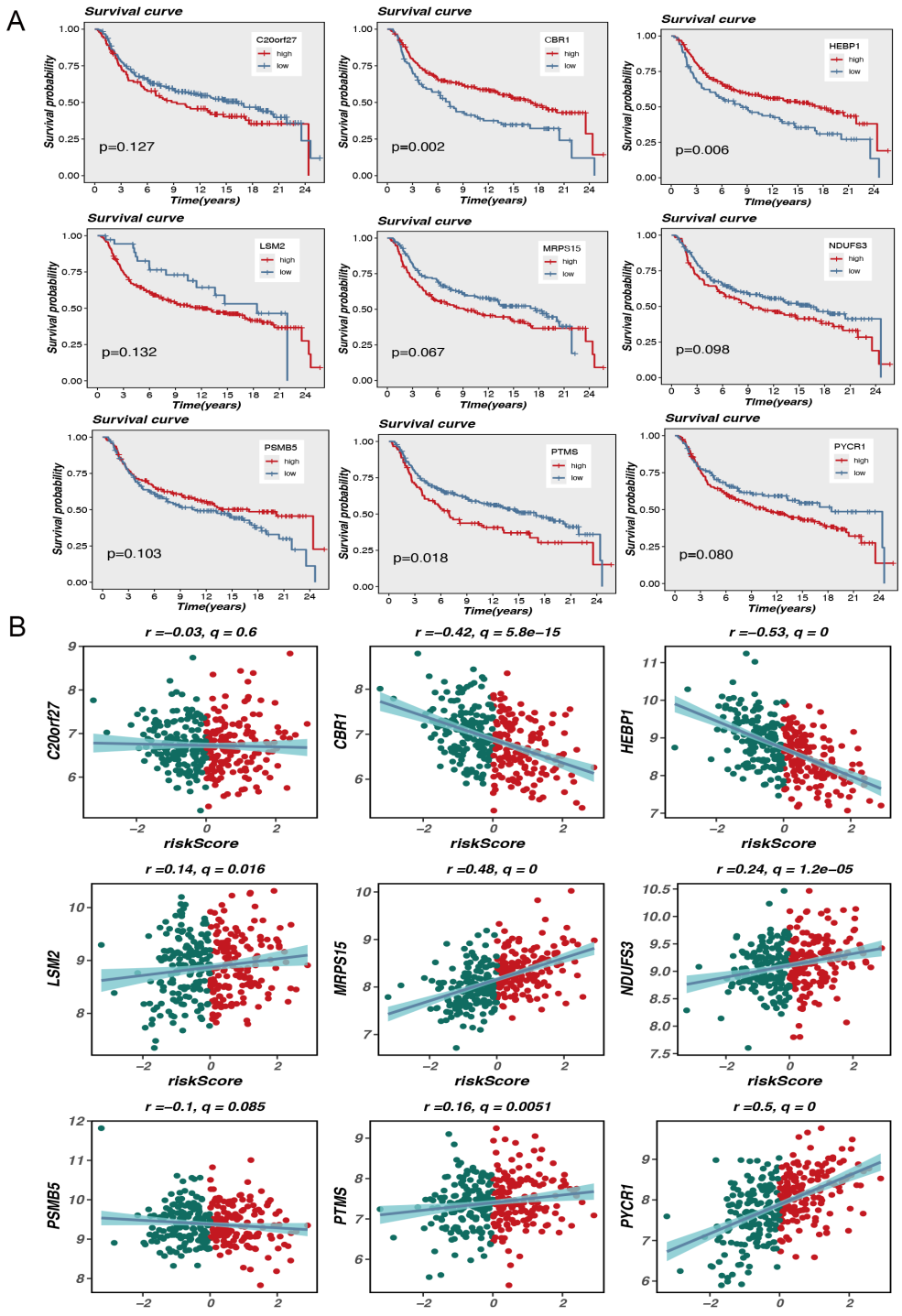

FIGURE 3
Model gene survival and risk assessment. **(A)** Model gene survival analysis. **(B)** Model genes correlate with risk scores.

cellular metabolism, tumor invasion, and metastasis (Figure 8A). To validate these results, we conducted further analysis using gene set variation analysis (GSVA). The results of GSVA were also consistent, with the high-risk group being enriched in pathways such as the TGF-β signaling, PI3K/AKT/mTOR signaling, and others, further supporting the conclusions drawn by GSEA (Figure 8B).

4 Discussion

TNBC is distinguished by its high degree of heterogeneity and intricate molecular composition, which collectively contribute to its generally poor prognosis. Conventional classification techniques frequently prove inadequate for encompassing the full spectrum of

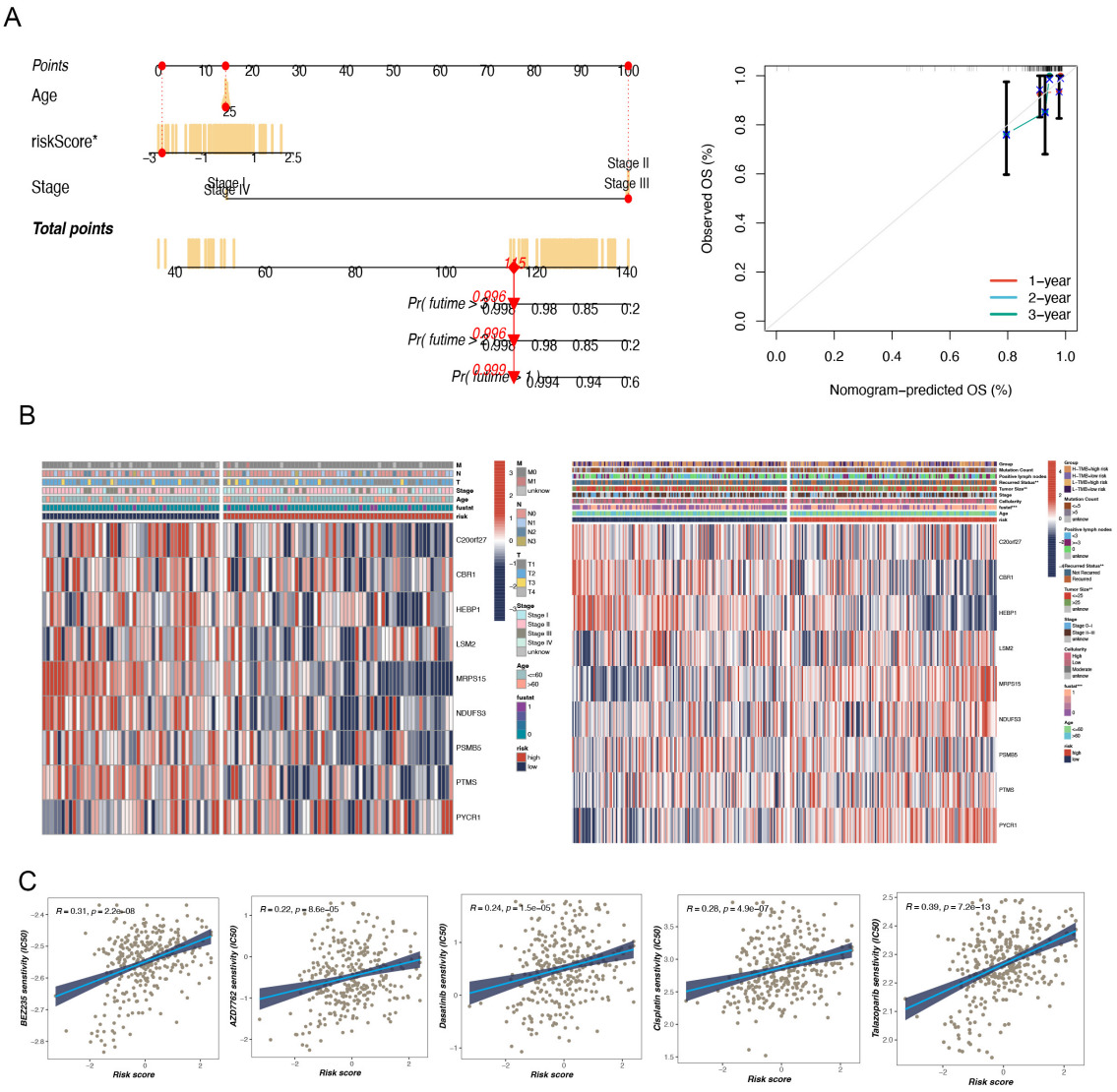

FIGURE 4
The construction of a nomogram and clinical correlation analysis. **(A)** Nomogram to assess the risk of BC patients. **(B)** There were significant differences in tumor size and recurrence status between high and low-risk groups. **(C)** Potential drug screening in high-risk patients.

TNBC, resulting in considerable obstacles in clinical management and a significant burden on patients and society alike. The heterogeneous nature of TNBC is evident not only in its molecular characteristics, but also in the significant variability observed in its clinical presentation and response to treatment (17). The current classification methods are inadequate for capturing the full spectrum of molecular diversity observed in TNBC, leading to considerable uncertainty in patient prognosis. Consequently, reliance on a single classification standard is inadequate for the effective prediction of TNBC treatment response and survival outcomes. In light of these considerations, we proposed a novel perspective based on the analysis of mitophagy-related gene expression as a means of evaluating TNBC prognosis, thereby providing a more reliable foundation for personalized treatment. This approach not only enhances patient prognosis but also offers guidance for the development of novel therapeutic strategies.

Mitophagy is a selective form of autophagy, a process by which cells degrade mitochondria. It is a vital mechanism for maintaining cellular health and function, playing a pivotal role in processes such as cellular stress, aging, and cancer (18). Mitophagy has been demonstrated to play a complex and dual role in cancer, with the potential to either promote cancer cell survival or to inhibit cancer initiation and progression (4). Despite the growing body of research on mitophagy in breast cancer in recent years, with notable advances in TNBC, the majority of these studies remain confined to fundamental mechanistic investigation (19). The precise role of mitophagy in TNBC and its clinical applications remain to be fully elucidated through rigorous scientific inquiry. Notably, there is a significant deficit in the construction of prognostic models based on mitophagy. This is the first instance in which a prognostic model for TNBC has been constructed using mitophagy-related genes. Our study not only addresses this gap in the literature but also

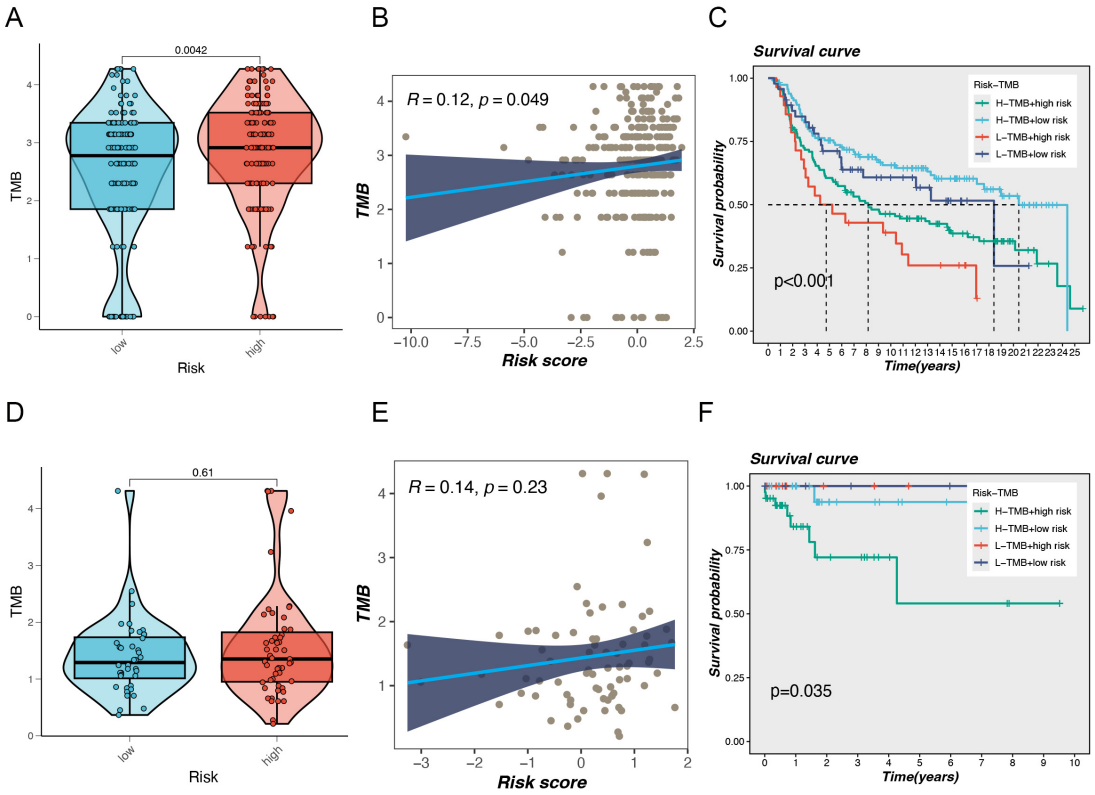

FIGURE 5
Gene mutation analysis. **(A)** Differences in Tumor Mutational Burden (TMB) levels between the two risk groups in the MetaBric database. **(B)** The correlation between TMB and risk score. **(C)** Correlation analysis between TMB and prognosis. **(D)** Differences in Tumor Mutational Burden (TMB) levels between the two risk groups in the TCGA database. **(E)** The correlation between TMB and risk score. **(F)** Correlation analysis between TMB and prognosis.

establishes a foundation for further, more in-depth research in the future.

The study employed single-cell sequencing to examine the function of MRGs in TNBC. Through Cox and Lasso regression analyses, nine MRGs were identified and used to construct a TNBC prognostic model. This model was validated in four independent datasets (METABRIC, GSE58812, GSE2653, and GSE65194) and exhibited strong predictive accuracy and robustness. While current prognostic models like MammaPrint®, Breast Cancer Index (BCI), and Oncotype DX are effective for certain breast cancer subtypes, they lack optimization for TNBC. As a result, their predictions for TNBC patients are not as reliable (20–22). Existing TNBC-specific models frequently fail to consider the pivotal function of mitophagy, which is essential for cellular metabolism, stress response, and tumor survival. A prognostic model based on MRGs thus offers greater biological and clinical relevance. Our study represents an innovative application of single-cell sequencing, which has been instrumental in uncovering the heterogeneity of TNBC and in the development of a more precise prognostic model. Our findings indicate that patients classified as high-risk by our model are more likely to develop larger tumors and experience recurrence, thereby demonstrating the model's utility in predicting outcomes in TNBC.

TNBC is characterized by the absence of specific hormone receptors and HER2 expression, which restricts the range of available treatment options and renders chemotherapy the most commonly employed systemic therapy. To further validate the clinical utility of our model, we conducted an analysis of chemotherapy drugs. Five drugs were identified as particularly effective in the high-risk group: BEZ235, AZD7762, dasatinib, cisplatin, and talazoparib. AZD7762, a Chk1 inhibitor, has demonstrated considerable promise in the treatment of breast cancer, particularly in cases where p53 mutations and TNBC are present. This is due to its ability to enhance the efficacy of radiotherapy and chemotherapy (23, 24). Dasatinib has also been shown to possess notable therapeutic potential in the treatment of breast cancer, particularly in the TNBC and HER2-positive subtypes. This is achieved by targeting breast cancer stem cells and enhancing the sensitivity of cancer cells to chemotherapy (25, 26). Cisplatin, a traditional platinum-based chemotherapy drug, has demonstrated efficacy against TNBC by inhibiting the EMT process. Furthermore, it has been shown to enhance the efficacy of other drugs, such as paclitaxel, in treating TNBC (27). Talazoparib, a recently developed PARP inhibitor, has demonstrated remarkable efficacy in patients with HER2-negative advanced breast cancer and BRCA mutations. This treatment has demonstrated marked

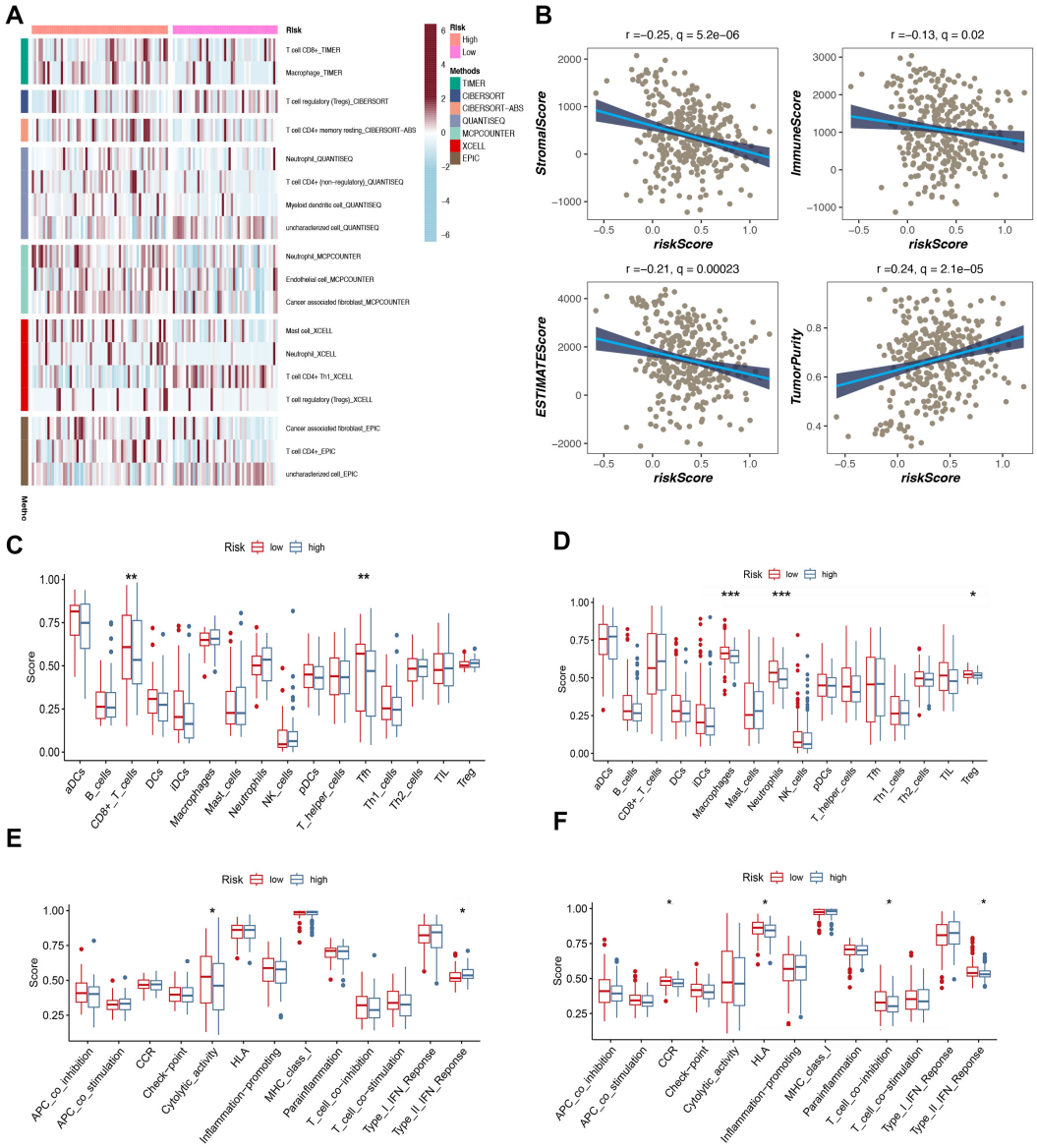

FIGURE 6
Analysis of immune microenvironment. **(A)** The distribution and association of tumor-infiltrating immune cells (TICs) in two risk groups. **(B)** Correlation analysis of immune score and risk score, ESTIMATE score and risk score, Stromal score and risk score, tumor purity and risk score. **(C, D)** Analysis of immune cell infiltration. **(E, F)** Analysis of the immunization process.

improvements in both OS and PFS, as well as quality of life (28, 29). Therefore, Talazoparib may become a crucial element in personalized treatment plans for high-risk patients. Clinicians may consider integrating Talazoparib into treatment regimens based on the patient's BRCA mutation status, to optimize therapeutic outcomes while reducing adverse effects. For other drugs (such as dasatinib, AZD7762, and cisplatin), it is recommended that clinicians personalize drug selection based on the patient's molecular characteristics (such as gene mutations or expression profiles).

In cancer research, immune infiltration is a key concept as it involves the immune system's response to tumors or lesions. The degree and type of immune infiltration can significantly influence disease progression, patient prognosis, and treatment response (30). In recent years, immunotherapy, particularly immune checkpoint inhibitors, has made remarkable progress in various types of tumors (31). However, triple-negative breast cancer (TNBC), due to its high aggressiveness and lack of effective targeted therapies, often does not respond well to traditional treatments. In this context, immunotherapy has become a critical research focus for TNBC treatment. Currently, the application of immunotherapy in TNBC has shown some efficacy. Clinical trials such as KEYNOTE-355 and IMpassion130 have found that PD-L1-positive TNBC patients respond better to immune checkpoint inhibitors combined with chemotherapy, significantly prolonging PFS and OS (32, 33). However, the efficacy of immunotherapy varies among

10.3389/fimmu.2024.1489444

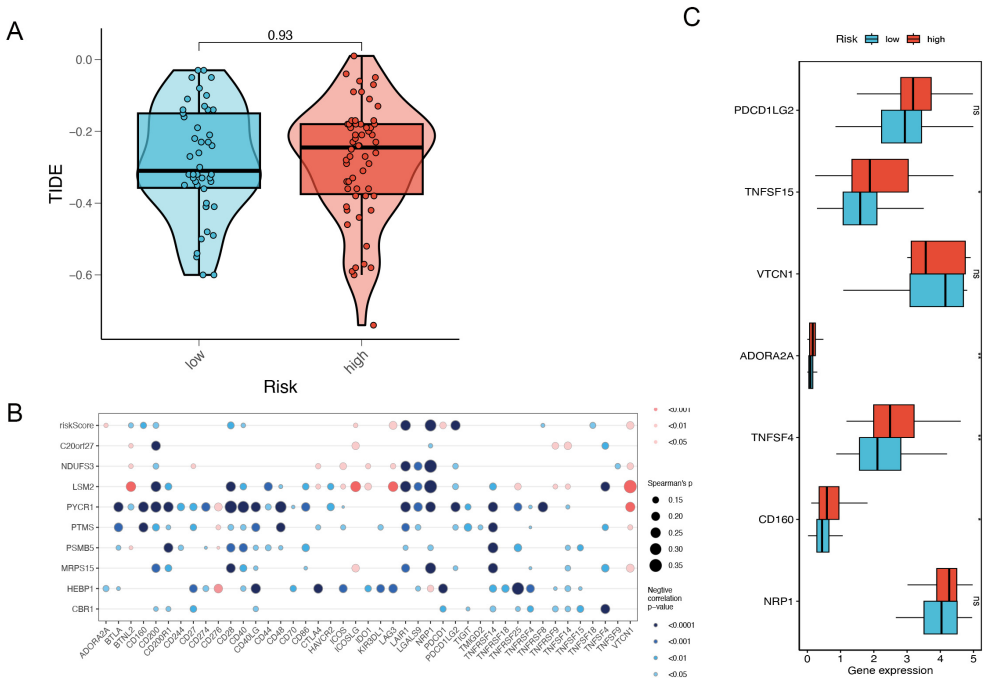

FIGURE 7
Risk gene and immune checkpoint analysis. **(A)** The difference in TIDE scores between high and low-risk groups. **(B)** Risk gene and immune checkpoint correlation. **(C)** Differences in the abundance of immune-checkpoint-related genes between high and low-risk groups. *P<0.05, **P< 0.01, ***P<0.001, ns indicates No significance.

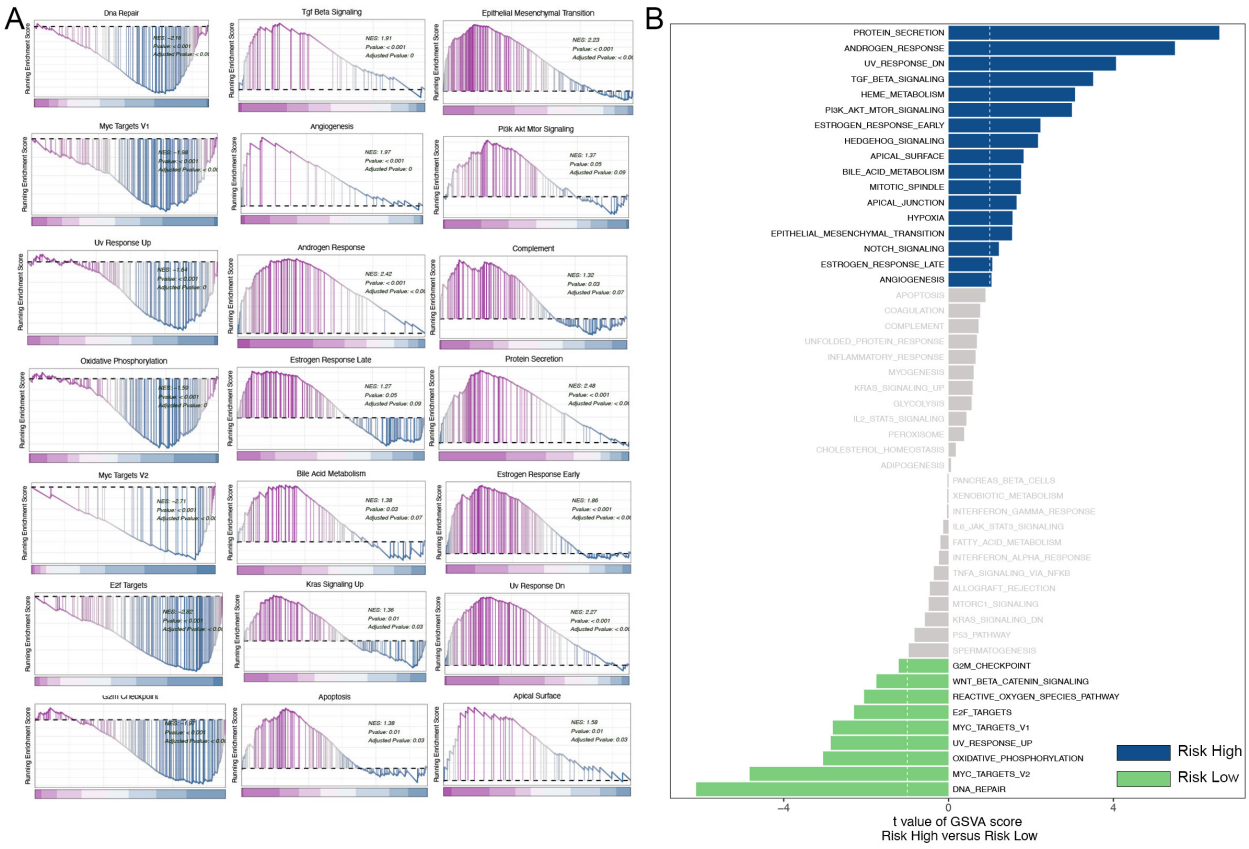

FIGURE 8
Analysis of GSEA and GSVA. **(A)** GSEA pathway enrichment analysis. **(B)** GSVA pathway enrichment analysis.

individuals, and not all patients benefit (34). Additionally, the occurrence of immune-related adverse events presents a significant challenge, requiring further optimization of treatment strategies.

In this study, we found that the infiltration levels of cancer-associated fibroblasts (CAFs) and endothelial cells were significantly higher in the high-risk group compared to the low-risk group. This finding is consistent with existing literature and further validates the critical role these cells play in tumor progression and patient prognosis. Specifically, CAFs not only promote tumor growth and metastasis by secreting growth factors and cytokines, but they also interact with immune cells, altering the tumor microenvironment and thereby enhancing the malignancy of the tumor (34). Additionally, endothelial cells significantly facilitate breast cancer cell invasion and metastasis through metabolic reprogramming and the secretion of specific factors (35). These mechanisms may elucidate the association between higher endothelial cell infiltration in the high-risk group and a poorer prognosis. Furthermore, we conducted a comprehensive investigation into the composition of immune cells, immune infiltration, and immune scoring in TNBC. These studies provide crucial theoretical support and potential therapeutic targets for immunotherapy in TNBC. These findings not only enhance our comprehension of the immune microenvironment in TNBC but also provide direction for prospective treatment strategies.

This study employed TIDE analysis to further elucidate the impact of immune escape mechanisms on immunotherapy in high-risk TNBC patients. Although the TIDE scores were higher in the high-risk group, indicating that these patients may respond poorly to immune checkpoint inhibitors (ICI), the difference in TIDE scores was not statistically significant, likely due to the small sample size or data heterogeneity. Nevertheless, the observed trend in TIDE scores suggests that immune escape mechanisms may be more active in high-risk patients. It is recommended that future research should aim to increase the sample size or incorporate additional immune marker analysis to improve the ability to predict responses to immunotherapy. Furthermore, the model gene PYCR1 was found to be negatively correlated with immune checkpoints, indicating that PYCR1 may play a pivotal role in immune escape. The elevated expression of immune checkpoints, including TNFSF15, ADORA2A, TNFSF4, and CD160, in the high-risk group indicates that these checkpoints may represent promising therapeutic targets in the future.

While this study makes a notable contribution to the understanding of the immune microenvironment in TNBC, it is not without limitations. First, due to the limitations of the experimental design, we were unable to conduct *in vivo* and *in vitro* experiments to validate these findings. Instead, we relied on data analysis. Although our results were validated using multiple external datasets, the lack of our dataset may limit the generalizability of the findings. It is therefore recommended that future research should include experimental validation to solidify these findings and explore more precise immunotherapy strategies.

5 Conclusion

This study developed a mitophagy-related prognostic model for TNBC using single-cell sequencing data, effectively stratifying patients into high- and low-risk groups. Patients at high risk exhibited diminished survival, increased tumor size, and elevated recurrence rates. A drug sensitivity analysis identified chemotherapeutic agents, including talazoparib, as potentially more effective in high-risk patients. The immune analysis revealed an increased infiltration of macrophages, neutrophils, and cancer-associated fibroblasts in patients at high risk, which has been linked to tumor progression. The correlation between PYCR1 and immune checkpoints indicates its involvement in immune evasion, thereby offering potential targets for immunotherapy. The model offers insights into TNBC prognosis and provides a foundation for personalized treatment strategies.

Data availability statement

The original contributions presented in the study are included in the article/Supplementary Material. Further inquiries can be directed to the corresponding authors.

Author contributions

PD: Data curation, Methodology, Writing – original draft, Writing – review & editing. SP: Formal Analysis, Validation, Writing – original draft, Writing – review & editing. ZQ: Methodology, Writing – original draft, Writing – review & editing. YY: Software, Writing – original draft, Writing – review & editing. QL: Conceptualization, Supervision, Writing – original draft, Writing – review & editing. XK: Data curation, Methodology, Writing – original draft, Writing – review & editing. ZW: Investigation, Writing – original draft, Writing – review & editing. JW: Funding acquisition, Methodology, Writing – original draft, Writing – review & editing. YF: Funding acquisition, Resources, Supervision, Writing – original draft, Writing – review & editing.

Funding

The author(s) declare financial support was received for the research, authorship, and/or publication of this article. This work was supported by the Natural Science Foundation of China (No. 82072940) and the Beijing Hope Run Special Fund of Cancer Foundation of China (No. LC2019L07).

Acknowledgments

We extend our gratitude to the TCGA and GEO databases for providing the data used in this study. We also thank the reviewers and editors for their valuable comments.

Conflict of interest

The authors declare that the research was conducted in the absence of any commercial or financial relationships that could be construed as a potential conflict of interest.

Publisher's note

All claims expressed in this article are solely those of the authors and do not necessarily represent those of their affiliated organizations, or those of the publisher, the editors and the reviewers. Any product that may be evaluated in this article, or claim that may be made by its manufacturer, is not guaranteed or endorsed by the publisher.

Supplementary material

The Supplementary Material for this article can be found online at: https://www.frontiersin.org/articles/10.3389/fimmu.2024.1489444/full#supplementary-material

References

1. Bray F, Laversanne M, Sung H, Ferlay J, Siegel RL, Soerjomataram I, et al. Global cancer statistics 2022: GLOBOCAN estimates of incidence and mortality worldwide for 36 cancers in 185 countries. *CA Cancer J Clin*. (2024) 74:229–63. doi: 10.3322/caac.21834

2. Liu L, Wang Y, Miao L, Liu Q, Musetti S, Li J, et al. Combination immunotherapy of MUC1 mRNA nano-vaccine and CTLA-4 blockade effectively inhibits growth of triple negative breast cancer. *Mol Ther*. (2018) 26:45–55. doi: 10.1016/j.ymthe.2017.10.020

3. Vara-Perez M, Felipe-Abrio B, Agostinis P. Mitophagy in cancer: A tale of adaptation. *Cells*. (2019) 8. doi: 10.3390/cells8050493

4. Kubli DA, Gustafsson ÅB. Mitochondria and mitophagy: the yin and yang of cell death control. *Circ Res*. (2012) 111:1208–21. doi: 10.1161/CIRCRESAHA.112.265819

5. Eiyama A, Okamoto K. PINK1/Parkin-mediated mitophagy in mammalian cells. *Curr Opin Cell Biol*. (2015) 33:95–101. doi: 10.1016/j.ceb.2015.01.002

6. Li J, Xu X, Huang H, Li L, Chen J, Ding Y, et al. Pink1 promotes cell proliferation and affects glycolysis in breast cancer. *Exp Biol Med (Maywood)*. (2022) 247:985–95. doi: 10.1177/15353702221082613

7. Lu X, Liu QX, Zhang J, Zhou D, Yang GX, Li MY, et al. PINK1 overexpression promotes cell migration and proliferation via regulation of autophagy and predicts a poor prognosis in lung cancer cases. *Cancer Manag Res*. (2020) 12:7703–14. doi: 10.2147/CMAR.S262466

8. Panigrahi DP, Praharaj PP, Bhol CS, Mahapatra KK, Patra S, Behera BP, et al. The emerging, multifaceted role of mitophagy in cancer and cancer therapeutics. *Semin Cancer Biol*. (2020) 66:45–58. doi: 10.1016/j.semcancer.2019.07.015

9. Kinker GS, Greenwald AC, Tal R, Orlova Z, Cuoco MS, McFarland JM, et al. Pan-cancer single-cell RNA-seq identifies recurring programs of cellular heterogeneity. *Nat Genet*. (2020) 52:1208–18. doi: 10.1038/s41588-020-00726-6

10. Balachandran VP, Gonen M, Smith JJ, DeMatteo RP. Nomograms in oncology: more than meets the eye. *Lancet Oncol*. (2015) 16:e173–80. doi: 10.1016/S1470-2045(14)71116-7

11. Samstein RM, Lee CH, Shoushtari AN, Hellmann MD, Shen R, Janjigian YY, et al. Tumor mutational load predicts survival after immunotherapy across multiple cancer types. *Nat Genet*. (2019) 51:202–6. doi: 10.1038/s41588-018-0312-8

12. Yarchoan M, Hopkins A, Jaffee EM. Tumor mutational burden and response rate to PD-1 inhibition. *N Engl J Med*. (2017) 377:2500–1. doi: 10.1056/NEJMc1713444

13. Barroso-Sousa R, Jain E, Cohen O, Kim D, Buendia-Buendia J, Winer E, et al. Prevalence and mutational determinants of high tumor mutation burden in breast cancer. *Ann Oncol*. (2020) 31:387–94. doi: 10.1016/j.annonc.2019.11.010

14. Giarratana AO, Prendergast CM, Salvatore MM, Capaccione KM. TGF-β signaling: critical nexus of fibrogenesis and cancer. *J Transl Med*. (2024) 22:594. doi: 10.1186/s12967-024-05411-4

15. Huang Y, Hong W, Wei X. The molecular mechanisms and therapeutic strategies of EMT in tumor progression and metastasis. *J Hematol Oncol*. (2022) 15:129. doi: 10.1186/s13045-022-01347-8

16. Glaviano A, Foo ASC, Lam HY, Yap KCH, Jacot W, Jones RH, et al. PI3K/AKT/mTOR signaling transduction pathway and targeted therapies in cancer. *Mol Cancer*. (2023) 22:138. doi: 10.1186/s12943-023-01827-6

17. Hu XE, Yang P, Chen S, Wei G, Yuan L, Yang Z, et al. Clinical and biological heterogeneities in triple-negative breast cancer reveals a non-negligible role of HER2-low. *Breast Cancer Res*. (2023) 25:34. doi: 10.1186/s13058-023-01639-y

18. Gustafsson ÅB, Dorn GW 2nd. Evolving and expanding the roles of mitophagy as a homeostatic and pathogenic process. *Physiol Rev*. (2019) 99:853–92. doi: 10.1152/physrev.00005.2018

19. Xie XQ, Yang Y, Wang Q, Liu HF, Fang XY, Li CL, et al. Targeting ATAD3A-PINK1-mitophagy axis overcomes chemoimmunotherapy resistance by redirecting PD-L1 to mitochondria. *Cell Res*. (2023) 33:215–28. doi: 10.1038/s41422-022-00766-z

20. Cardoso F, van't Veer LJ, Bogaerts J, Slaets L, Viale G, Delaloge S, et al70-Gene Signature as an Aid to Treatment Decisions in Early-Stage Breast Cancer. *N Engl J Med*. (2016) 375(8):717–29. doi: 10.1056/NEJMoa1602253

21. Bartlett JMS, Sgroi DC, Treuner K, Zhang Y, Ahmed I, Piper T, et al. Breast Cancer Index and prediction of benefit from extended endocrine therapy in breast cancer patients treated in the Adjuvant Tamoxifen-To Offer More? (aTTom) trial. *Ann Oncol*. (2019) 30:1776–83. doi: 10.1093/annonc/mdz289

22. Zhang S, Fitzsimmons KC, Hurvitz SA. Oncotype DX Recurrence Score in premenopausal women. *Ther Adv Med Oncol*. (2022) 14:17588359221081077. doi: 10.1177/17588359221081077

23. Ma Z, Yao G, Zhou B, Fan Y, Gao S, Feng X. The Chk1 inhibitor AZD7762 sensitises p53 mutant breast cancer cells to radiation in *vitro* and in vivo. *Mol Med Rep*. (2012) 6:897–903. doi: 10.3892/mmr.2012.999

24. Zhu H, Rao Z, Yuan S, You J, Hong C, He Q, et al. One therapeutic approach for triple-negative breast cancer: Checkpoint kinase 1 inhibitor AZD7762 combination with neoadjuvant carboplatin. *Eur J Pharmacol*. (2021) 908:174366. doi: 10.1016/j.ejphar.2021.174366

25. Tian J, Raffa FA, Dai M, Moamer A, Khadang B, Hachim IY, et al. Dasatinib sensitises triple negative breast cancer cells to chemotherapy by targeting breast cancer stem cells. *Br J Cancer*. (2018) 119:1495–507. doi: 10.1038/s41416-018-0287-3

26. Kheraldine H, Gupta I, Cyprian FS, Vranic S, Al-Farsi HF, Merhi M, et al. Targeting HER2-positive breast cancer cells by a combination of dasatinib and BMS-202: Insight into the molecular pathways. *Cancer Cell Int*. (2024) 24:94. doi: 10.1186/s12935-023-03195-z

27. Wang H, Guo S, Kim SJ, Shao F, Ho JWK, Wong KU, et al. Cisplatin prevents breast cancer metastasis through blocking early EMT and retards cancer growth together with paclitaxel. *Theranostics*. (2021) 11:2442–59. doi: 10.7150/thno.46460

28. Litton JK, Rugo HS, Ettl J, Hurvitz SA, Gonçalves A, Lee KH, et al. Talazoparib in patients with advanced breast cancer and a germline BRCA mutation. *N Engl J Med*. (2018) 379:753–63. doi: 10.1056/NEJMoa1802905

29. Litton JK, Hurvitz SA, Mina LA, Rugo HS, Lee KH, Gonçalves A, et al. Talazoparib versus chemotherapy in patients with germline BRCA1/2-mutated HER2-negative advanced breast cancer: final overall survival results from the EMBRACA trial. *Ann Oncol*. (2020) 31:1526–35. doi: 10.1016/j.annonc.2020.08.2098

30. Petitprez F, Meylan M, de Reyniès A, Sautès-Fridman C, Fridman WH. The tumor microenvironment in the response to immune checkpoint blockade therapies. *Front Immunol*. (2020) 11:784. doi: 10.3389/fimmu.2020.00784

31. Wang Y, Zhang H, Liu C, Wang Z, Wu W, Zhang N, et al. Immune checkpoint modulators in cancer immunotherapy: recent advances and emerging concepts. *J Hematol Oncol*. (2022) 15:111. doi: 10.1186/s13045-022-01325-0

32. Cortes J, Cescon DW, Rugo HS, Nowecki Z, Im SA, Yusof MM, et al. Pembrolizumab plus chemotherapy versus placebo plus chemotherapy for previously untreated locally recurrent inoperable or metastatic triple-negative breast cancer (KEYNOTE-355): a randomised, placebo-controlled, double-blind, phase 3 clinical trial. *Lancet*. (2020) 396:1817–28. doi: 10.1016/S0140-6736(20)32531-9

33. Schmid P, Adams S, Rugo HS, Schneeweiss A, Barrios CH, Iwata H, et al. Atezolizumab and nab-paclitaxel in advanced triple-negative breast cancer. *N Engl J Med*. (2018) 379:2108–21. doi: 10.1056/NEJMoa1809615

34. Sharma P, Hu-Lieskovan S, Wargo JA, Ribas A. Primary, adaptive, and acquired resistance to cancer immunotherapy. *Cell*. (2017) 168:707–23. doi: 10.1016/j.cell.2017.01.017

35. Tan ML, Jenkins-Johnston N, Huang S, Schutrum B, Vadhin S, Adhikari A, et al. Endothelial cells metabolically regulate breast cancer invasion toward a microvessel. *APL Bioeng*. (2023) 7:046116. doi: 10.1063/5.0171109

frontiers | Frontiers in Immunology

TYPE Original Research
PUBLISHED 13 November 2024
DOI 10.3389/fimmu.2024.1500091

Check for updates

OPEN ACCESS

EDITED BY
Xiaosheng Tan,
Rutgers, United States

REVIEWED BY
Chengshuo Zhang,
China Medical University, China
Zilu Chen,
Rutgers, The State University of New Jersey, United States
Chunliang Liu,
Indiana University Indianapolis, United States
Yu Li,
Duke University, United States

*CORRESPONDENCE
Tao Yan
blizzardyt@163.com
Jianguo Zhou
zjgtydoct@163.com
Dayong Cao
caodayongdoctty@tom.com

†These authors have contributed equally to this work and share first authorship

RECEIVED 22 September 2024
ACCEPTED 21 October 2024
PUBLISHED 13 November 2024

CITATION
Li R, Chen X, Wang B, Ai B, Min F, Cao D, Zhou J and Yan T (2024) Comparison of treatment models for single primary advanced gallbladder cancer.
Front. Immunol. 15:1500091.
doi: 10.3389/fimmu.2024.1500091

COPYRIGHT
© 2024 Li, Chen, Wang, Ai, Min, Cao, Zhou and Yan. This is an open-access article distributed under the terms of the Creative Commons Attribution License (CC BY). The use, distribution or reproduction in other forums is permitted, provided the original author(s) and the copyright owner(s) are credited and that the original publication in this journal is cited, in accordance with accepted academic practice. No use, distribution or reproduction is permitted which does not comply with these terms.

Comparison of treatment models for single primary advanced gallbladder cancer

Rongxuan Li[1†], Xiao Chen[1†], Bingchen Wang[1†], Bolun Ai[2†], Fangdi Min[3†], Dayong Cao[1*], Jianguo Zhou[1*] and Tao Yan[3*]

[1]Department of Hepatobiliary Surgery, National Cancer Center/National Clinical Research Center for Cancer/Cancer Hospital, Chinese Academy of Medical Sciences and Peking Union Medical College, Beijing, China, [2]Department of Breast Surgical Oncology, National Cancer Center/National Clinical Research Center for Cancer/Cancer Hospital, Chinese Academy of Medical Sciences and Peking Union Medical College, Beijing, China, [3]Department of Anesthesiology, National Cancer Center/National Clinical Research Center for Cancer/Cancer Hospital, Chinese Academy of Medical Sciences and Peking Union Medical College, Beijing, China

Purpose: Treatment for advanced gallbladder cancer (GBC) remains controversial, with various recommendations regarding the choice and combination of surgery and adjuvant therapy. The present article is targeting for the exploration of optimal treatment models for advanced GBC.

Methods: AJCC (American Joint Committee on Cancer, 8th edition) stage III and stage IV GBC, were defined as advanced GBC. Patients with advanced GBC were identified using the Surveillance, Epidemiology, and End Results (SEER) database and departmental cohort. Because of the most representative, only gallbladder adenocarcinoma (GBAC) patients were selected. Based on their surgical status (No, Non-radical and Radical surgery), chemotherapy status (Chemotherapy, No chemotherapy), and radiotherapy status (Radiotherapy, No radiotherapy), treatment models were categorized. For the purposes of evaluating the treatment outcomes of various treatment models and determining the risk element for cancer-specific survival (CSS), Cox regression analysis was applied. Kaplan-Meier curves were used before and after adjusting for covariates, with log-rank tests used to analyze discrepancies between curves. Immunotherapy was analyzed using clinical data from departmental cohort. Finally, to compensate for the limitations of the database, a review examines the progress in treatment models for advanced GBC.

Results: 5,154 patients aged over 18 years with solitary primary advanced GBC were identified from the SEER database. In advanced GBC patients, the treatment model has emerged as a significant prognostic factor. "Radical surgery + Chemotherapy + Radiotherapy" models maximally improved the CSS of advanced GBC before and after adjusting for covariates, while "No surgery + No chemotherapy + No radiotherapy" model had the lowest CSS. The present conclusions were supported even after subgroup analysis by AJCC stage. The

efficacy of immunotherapy was demonstrated in the departmental cohort analysis. Additionally, this article provides a comprehensive overview of recent advancements in various emerging treatment strategies.

Conclusion: Even when optimal treatment model cannot be pursued, providing comprehensive combinations of treatments to advanced GBC patients whenever possible is always beneficial for their survival.

KEYWORDS

advanced gallbladder cancer, surgery, chemotherapy, radiotherapy, immunotherapy, SEER, cancer-specific survival

1 Introduction

As the most familiar cancer from biliary tract, GBC ranks 23rd among all tumors and 6th among digestive system tumors (1). The global morbidity and mortality of GBC have been increasing annually, Eastern Asia, South America, and Melanesia were the regions with highest ranking (2, 3), the latest global incidence and mortality data for GBC are visualized in Supplementary Figure 1. Moreover, the etiology of GBC varies across different countries (4). GBC is one of the few cancers that shows a gender difference (5), with the morbidity in females nearly three times that of males (6), and is the only digestive system tumor that is predominantly female (7). As early symptoms are rare and lymph nodes and distant metastases often occur early, three-quarters of GBC patients are diagnosed with advanced stages or metastases, which results in poor prognoses (5, 8). In fact, symptomatic gallstones lead to cholecystectomy in most cases of GBC (9, 10). Additionally, among the biliary tract cancers, GBC has the shortest median survival rate. Despite improvements in diagnosis and treatment over the years, its 5-year survival rate remains lower than 20% (3). Therefore, addressing the treatment of GBC, a highly lethal tumor, is a significant challenge worldwide, and there is still considerable controversy surrounding the treatment of advanced GBC patients. Given that adenocarcinoma is the most prevalent and representative pathological type of GBC (11), and that treatment research has primarily centered on gallbladder adenocarcinoma (GBAC) (12, 13), the present study specifically addresses GBAC to ensure homogeneity, as other histological types exhibit different biological behaviors and treatment responses (14). Currently, among all treatment options for gallbladder cancer (GBC), only surgical intervention has demonstrated clear effectiveness, while other options, including radiotherapy, chemotherapy, and immunotherapy, remain in the exploratory stage (15). In the present article the SEER database, departmental cohort and the PubMed database were utilized to investigate treatment models for patients with advanced GBC, while also summarizing alternative treatment options.

2 Patients and methods

2.1 Patients selection

Information on demographic, cancer, treatment and follow-up is provided by the SEER database. To retrospectively collect GBC patient data, SEERStat (version 8.4.3) was used. 19,417 patients diagnosed with GBC from 2000 to 2019 were identified. Inclusion criteria were defined as Site recode ICD-O-3/WHO 2008 registered as gallbladder. Only those with AJCC stage III and stage IV GBC were selected. As per the AJCC, 8th edition, stage IIIA, IIIB, IVA and IVB were defined as "T3 + N0 + M0", "T1-3 + N1 + M0", "T4 + N0-1 + M0" and "Any T + N2 + M0" or "Any T + Any N + M1", respectively. Exclusion criteria were as follows: not adenocarcinoma, not single primary cancer, patients diagnosed before 2004 (without tumor grade), unknown surgical information, without chemotherapy or radiotherapy information, less than 18 years old, AJCC stage I or stage II, unknown survival status, and death or alive within 1 month of diagnosis. Ultimately, 5,154 eligible patients with advanced GBC diagnosis remained. The detailed flowchart is illustrated in Figure 1. Given that immunotherapy is a novel treatment option, we selected only patients who underwent treatment in our department in 2022 for this study, with follow-up completed by July 30, 2023. CSS was recorded. The inclusion and exclusion criteria were identical to those used in SEER database cases. A total of 15 patients with complete data were included in the cohort, with demographic and clinical information presented in Supplementary Table 1.

2.2 Study covariates

The definitions and information on covariates such as age, gender, race, marital status, size, grade, T staging, N staging, M staging, surgical information, radiotherapy information, chemotherapy information and survival status were obtained in the SEER database. Deaths from GBC were taken as events, and survivors were censored based on CSS. For age at diagnosis, according to the WHO elderly

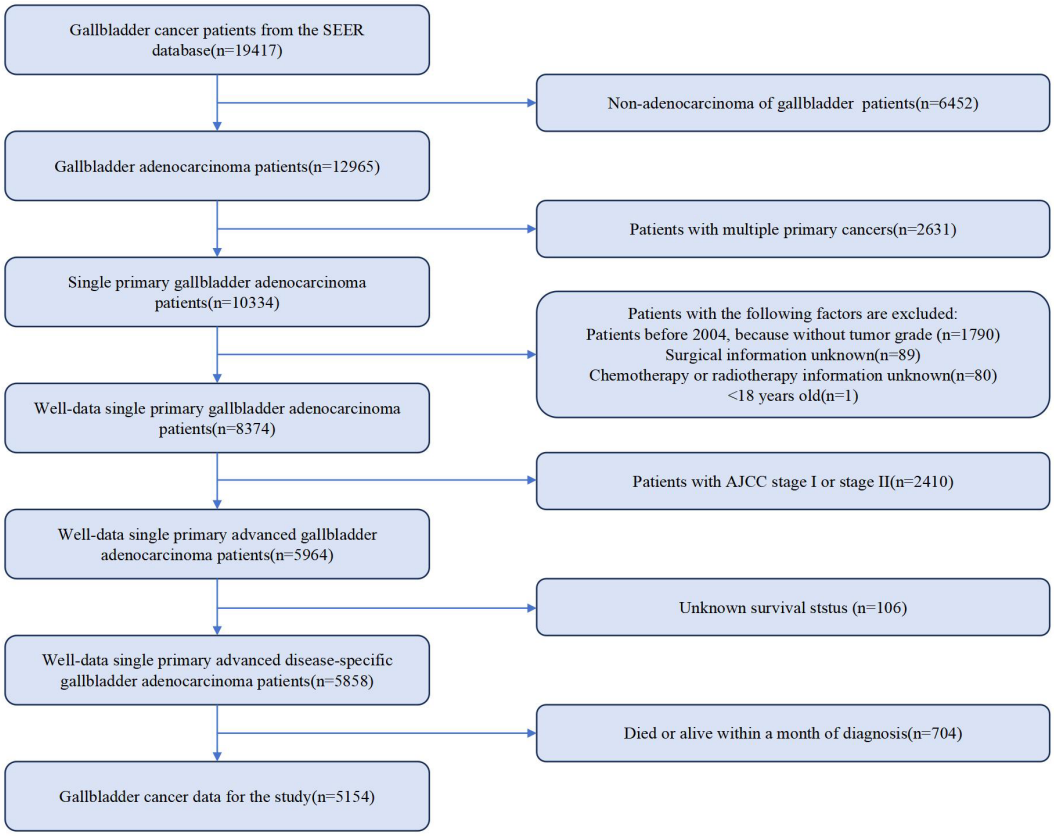

FIGURE 1
Flowchart of patient enrollment.

classification standards, patients were classified into under 65 years old group and group for 65 years old and above. Gender included female and male. Races of patients were categorized as White, Black, Asian or Pacific Islander, American Indian or Alaska Native, and unknown. On the basis of marital status, patients were classified into groups with partners (Yes), without partners (No), and unknown marital status (Unknown). The without partners group includes single (never married), separated, divorced, and widowed, while for the with partners group, both same-sex and heterosexual couples were included. Tumor grades were classified as well, moderately, poorly and un- differentiated, corresponding to Grades I to IV, respectively, with the remaining patients labeled as Unknown grade. The optimal cutoff points determined by the X-tile software (version 3.6.1) were used to sort the tumors into groups of size <39, 40-60, ≥61, and unknown groups, with measurements in millimeters (mm). A screenshot of the software is presented as Supplementary Figure 2. T, N, and M staging were corrected based on the AJCC, 8th edition, and AJCC stages were generated. In surgical types, besides radical surgery, all other types of surgery were defined as non-radical surgery, with a separate group for no surgery performed. In the radiotherapy status, "None/Unknown" and "Refused" were considered as not received radiotherapy, while the rest were considered as received radiotherapy. In the chemotherapy status, "No/Unknown" was considered as not received chemotherapy, and "yes" was considered as received chemotherapy. Survival status included alive and dead. The data in the departmental cohort were categorized in the same manner.

2.3 Statistical analysis

The quantity (percentage (%)) was used to specify the categorical variables. Pearson's Chi-squared test and Fisher's exact test were employed to describe baseline characteristics. Cox proportional hazards models were used to evaluate the impact of covariates on the risk of CSS, and calculate the hazard ratios (HR) and 95% confidence intervals (CI) for advanced GBC. CSS was predicted using Kaplan-Meier curves before and after adjusting for covariates in different models, with log-rank tests used to analyze discrepancies between curves. Cramér's V analysis was applied to assess the correlation between covariates. Propensity score matching (PSM) was used to match demographic baseline statistical characteristics. P-values < 0.05 is considered statistically significant. By using MSTATA software (https://www.mstata.com/), all analyses were carried out utilizing the R software (version 4.2.2) for statistical computing. Ultimately, through a comprehensive search of the literature database, we supplemented the treatment options not addressed in the SEER database and synthesized these findings to enhance the interpretation of our conclusions.

3 Results

3.1 Demographic and clinical characteristics

Altogether 5,154 eligible GBC patients were involved in the study cohort from 2000 to 2019. Among them, there were 849 cases with "No surgery + No chemotherapy + No radiotherapy" (NSNCNR) model, 1109 cases with "No surgery + Chemotherapy + No radiotherapy" (NSCNR) model, 45 cases with "No surgery + No chemotherapy + Radiotherapy" (NSNCR) model, 132 cases with "No surgery + Chemotherapy + Radiotherapy" (NSCR) model, 1185 cases with "Non-radical surgery + No chemotherapy + No radiotherapy" (NrSNCNR) model, 882 cases with "Non-radical surgery + Chemotherapy + No radiotherapy" (NrSCNR) model, 83 cases with "Non-radical surgery + No chemotherapy + Radiotherapy" (NrSNCR) model, 411 cases with "Non-radical surgery + Chemotherapy + Radiotherapy" (NrSCR) model, 190 cases with "Radical surgery + No chemotherapy + No radiotherapy" (RSNCNR) model, 131 cases with "Radical surgery + Chemotherapy + No radiotherapy" (RSCNR) model, 12 cases with "Radical surgery + No chemotherapy + Radiotherapy" (RSNCR) model, and 125 cases with "Radical surgery + Chemotherapy + Radiotherapy" (RSCR) model. For ease of reading, these treatment models are clearly designated by the letters A to L in the tables and figures. According to Table 1, the overall and different treatment models for GBC patients differ in demographics and clinical characteristics. Most patients were aged 65 or older (61.37%), and the distribution by gender was skewed toward females (70.70%). The racial composition was predominantly White (75.07%), followed by Black (12.44%) and Asian or Pacific Islander (11.08%). Over half of the participants were married (51.96%). The distribution by tumor size varied, with 27.90% having a tumor size of 39 or less, 14.82% between 40-60, and 11.91% greater than or equal to 61, with measurements in millimeters (mm). Grade I, II, III, IV, and grade Unknown accounted for 4.89%, 24.64%, 27.69%, 0.91%, and 41.87%, respectively. For AJCC stage perspective, stage IVB held the highest percentage of participants (56.67%). Various treatment models were administered, with the most common being "NrSNCNR" (23.00%), "NSCNR" (21.52%), "NrSCNR" (17.11%), and "NSNCNR" (16.47%). 81.99% of participants were dead when assessment. The line chart illustrating the selection of various treatment models over time is presented in Supplementary Figure 3.

3.2 Identification of risk factors

Univariate Cox regression analysis indicated that age, gender, marital status, tumor size, tumor grade, AJCC stage, and treatment model significantly influenced CSS in advanced GBC patients, while race did not show a significant impact. After removing covariates with nonsignificant ($p > 0.05$) effects on survival time from the univariate Cox regression analysis, Table 2 presents the results for the remaining covariates by multivariate Cox regression analysis. In our analysis, the covariates did not exhibit significant collinearity, as detailed in Supplementary Figure 4.

In line with the Cox regression analysis, the following treatment models had significantly lower hazard ratios (HR) for CSS than "NSNCNR": "NSCNR" (HR = 0.43, 95% CI 0.39-0.48, $p < 0.001$), "NSNCR" (HR = 0.83, 95% CI 0.61-1.14, $p = 0.256$), "NSCR" (HR = 0.42, 95% CI 0.35-0.51, $p < 0.001$), "NrSNCNR" (HR = 0.49, 95% CI 0.44-0.55, $p < 0.001$), "NrSCNR" (HR = 0.30, 95% CI 0.27-0.34, $p < 0.001$), "NrSNCR" (HR = 0.38, 95% CI 0.30-0.50, $p < 0.001$), "NrSCR" (HR = 0.25, 95% CI 0.21-0.29, $p < 0.001$), "RSNCNR" (HR = 0.38, 95% CI 0.31-0.46, $p < 0.001$), "RSCNR" (HR = 0.25, 95% CI 0.20-0.32, $p < 0.001$), "RSNCR" (HR = 0.37, 95% CI 0.20-0.68, $p = 0.001$), and "RSCR" (HR = 0.24, 95% CI 0.19-0.31, $p < 0.001$). The forest plot was shown in Figure 2. As a supplement, the results of univariate and multivariate analyses for the remaining treatment models, after excluding those with insufficient sample sizes (<1%), have been added to Supplementary Table 2. Additionally, to eliminate baseline differences between groups, PSM was applied based on whether patients received radical or non-radical surgery. The resulting baseline table and the Cox regression analysis have been designated as Supplementary Tables 3, 4, respectively. Due to missing data and a large number of "Unknown" entries, Supplementary Table 5 was created based on patients with complete data. The findings indicated that the results presented in the Supplementary Material showed trends that are nearly identical to those from the original analysis. Therefore, we opted to present the results from the original cohort, which includes a larger number of patients, in the main text.

3.3 Survival curve of each treatment group

The unadjusted survival curves for advanced GBC patients as a whole and for each treatment model were shown in Figure 3. After adjusting the covariates that were significant in multivariate Cox regression analysis, the CSS curves with advanced GBC and each treatment model were shown in Figure 4. The adjusted survival curves were calculated and plotted using the "conditional" method, which was based on the Cox proportional hazards models (16). This method involves creating multiple copies of the data to balance covariate differences across groups, resulting in a more accurate assessment of the effect of group membership on survival outcomes.

3.4 Subgroup analysis

To better demonstrate the impact of different treatment models on CSS for advanced GBC patients, we grouped all patients based on AJCC stage in addition to the multivariate Cox regression analysis. It was noticed that for advanced GBC patients, treatment model remained an independent prognostic factor in Table 3 and Figure 5. "RSCR" was regarded as the most effective treatment models for CSS in AJCC stage IIIA, "RSCR" and "RSCNR" were identified as the most effective treatment models for CSS in AJCC stage IIIB, while "RSCNR" was found to be the most effective for AJCC stage IVA, "NrSCR" and "RSCR" were noticed as the most effective for AJCC stage IVB. Based on these speculations, patients were combined into AJCC stage III and stage

TABLE 1 Demographic and clinical characteristics of advanced GBC patients receiving twelve treatment models.

Characteristic	Treatment Model												
	All, N = 5,154	A, N = 849[1]	B, N = 1,109[1]	C, N = 45[1]	D, N = 132[1]	E, N = 1,185[1]	F, N = 882[1]	G, N = 83[1]	H, N = 411[1]	I, N = 190[1]	J, N = 131[1]	K, N = 12[1]	L, N = 125[1]
Age													
<65	1,991 (38.63%)	235 (27.68%)	532 (47.97%)	15 (33.33%)	58 (43.94%)	283 (23.88%)	438 (49.66%)	26 (31.33%)	201 (48.91%)	61 (32.11%)	65 (49.62%)	5 (41.67%)	72 (57.60%)
≥65	3,163 (61.37%)	614 (72.32%)	577 (52.03%)	30 (66.67%)	74 (56.06%)	902 (76.12%)	444 (50.34%)	57 (68.67%)	210 (51.09%)	129 (67.89%)	66 (50.38%)	7 (58.33%)	53 (42.40%)
Gender													
Female	3,644 (70.70%)	596 (70.20%)	735 (66.28%)	34 (75.56%)	88 (66.67%)	882 (74.43%)	642 (72.79%)	63 (75.90%)	295 (71.78%)	127 (66.84%)	94 (71.76%)	9 (75.00%)	79 (63.20%)
Male	1,510 (29.30%)	253 (29.80%)	374 (33.72%)	11 (24.44%)	44 (33.33%)	303 (25.57%)	240 (27.21%)	20 (24.10%)	116 (28.22%)	63 (33.16%)	37 (28.24%)	3 (25.00%)	46 (36.80%)
Race													
White	3,869 (75.07%)	611 (71.97%)	794 (71.60%)	26 (57.78%)	95 (71.97%)	945 (79.75%)	702 (79.59%)	58 (69.88%)	304 (73.97%)	138 (72.63%)	91 (69.47%)	9 (75.00%)	96 (76.80%)
Black	641 (12.44%)	129 (15.19%)	170 (15.33%)	8 (17.78%)	18 (13.64%)	102 (8.61%)	99 (11.22%)	11 (13.25%)	48 (11.68%)	25 (13.16%)	16 (12.21%)	2 (16.67%)	13 (10.40%)
Asian or Pacific Islander	571 (11.08%)	94 (11.07%)	130 (11.72%)	9 (20.00%)	17 (12.88%)	123 (10.38%)	73 (8.28%)	14 (16.87%)	54 (13.14%)	20 (10.53%)	23 (17.56%)	1 (8.33%)	13 (10.40%)
American Indian/ Alaska Native	59 (1.14%)	12 (1.41%)	11 (0.99%)	2 (4.44%)	2 (1.52%)	13 (1.10%)	6 (0.68%)	0 (0.00%)	4 (0.97%)	6 (3.16%)	1 (0.76%)	0 (0.00%)	2 (1.60%)
Unknown	14 (0.27%)	3 (0.35%)	4 (0.36%)	0 (0.00%)	0 (0.00%)	2 (0.17%)	2 (0.23%)	0 (0.00%)	1 (0.24%)	1 (0.53%)	0 (0.00%)	0 (0.00%)	1 (0.80%)
Marital													
Yes	2,678 (51.96%)	349 (41.11%)	651 (58.70%)	23 (51.11%)	74 (56.06%)	504 (42.53%)	508 (57.60%)	51 (61.45%)	256 (62.29%)	91 (47.89%)	78 (59.54%)	6 (50.00%)	87 (69.60%)
No	2,305 (44.72%)	461 (54.30%)	431 (38.86%)	20 (44.44%)	57 (43.18%)	640 (54.01%)	337 (38.21%)	30 (36.14%)	141 (34.31%)	95 (50.00%)	52 (39.69%)	5 (41.67%)	36 (28.80%)
Unknown	171 (3.32%)	39 (4.59%)	27 (2.43%)	2 (4.44%)	1 (0.76%)	41 (3.46%)	37 (4.20%)	2 (2.41%)	14 (3.41%)	4 (2.11%)	1 (0.76%)	1 (8.33%)	2 (1.60%)
Size													
≤39	1,438 (27.90%)	122 (14.37%)	163 (14.70%)	5 (11.11%)	18 (13.64%)	435 (36.71%)	347 (39.34%)	28 (33.73%)	171 (41.61%)	57 (30.00%)	33 (25.19%)	7 (58.33%)	52 (41.60%)
40-60	764 (14.82%)	90 (10.60%)	131 (11.81%)	9 (20.00%)	27 (20.45%)	174 (14.68%)	133 (15.08%)	14 (16.87%)	76 (18.49%)	34 (17.89%)	41 (31.30%)	1 (8.33%)	34 (27.20%)
≥61	614 (11.91%)	128 (15.08%)	155 (13.98%)	5 (11.11%)	20 (15.15%)	115 (9.70%)	79 (8.96%)	2 (2.41%)	31 (7.54%)	42 (22.11%)	21 (16.03%)	2 (16.67%)	14 (11.20%)
Unknown	2,338 (45.36%)	509 (59.95%)	660 (59.51%)	26 (57.78%)	67 (50.76%)	461 (38.90%)	323 (36.62%)	39 (46.99%)	133 (32.36%)	57 (30.00%)	36 (27.48%)	2 (16.67%)	25 (20.00%)

(Continued)

10.3389/fimmu.2024.1500091

TABLE 1 Continued

Characteristic	Treatment Model												
	All, N = 5,154	A, N = 849[1]	B, N = 1,109[1]	C, N = 45[1]	D, N = 132[1]	E, N = 1,185[1]	F, N = 882[1]	G, N = 83[1]	H, N = 411[1]	I, N = 190[1]	J, N = 131[1]	K, N = 12[1]	L, N = 125[1]
Grade													
Grade I	252 (4.89%)	14 (1.65%)	12 (1.08%)	2 (4.44%)	2 (1.52%)	103 (8.69%)	47 (5.33%)	8 (9.64%)	38 (9.25%)	12 (6.32%)	6 (4.58%)	2 (16.67%)	6 (4.80%)
Grade II	1,270 (24.64%)	69 (8.13%)	91 (8.21%)	1 (2.22%)	12 (9.09%)	431 (36.37%)	279 (31.63%)	25 (30.12%)	181 (44.04%)	70 (36.84%)	48 (36.64%)	5 (41.67%)	58 (46.40%)
Grade III	1,427 (27.69%)	106 (12.49%)	132 (11.90%)	9 (20.00%)	23 (17.42%)	462 (38.99%)	348 (39.46%)	43 (51.81%)	137 (33.33%)	77 (40.53%)	47 (35.88%)	5 (41.67%)	38 (30.40%)
Grade IV	47 (0.91%)	2 (0.24%)	6 (0.54%)	0 (0.00%)	0 (0.00%)	15 (1.27%)	9 (1.02%)	2 (2.41%)	6 (1.46%)	3 (1.58%)	3 (2.29%)	0 (0.00%)	1 (0.80%)
Unknown	2,158 (41.87%)	658 (77.50%)	868 (78.27%)	33 (73.33%)	95 (71.97%)	174 (14.68%)	199 (22.56%)	5 (6.02%)	49 (11.92%)	28 (14.74%)	27 (20.61%)	0 (0.00%)	22 (17.60%)
Stage													
IIIA	1,260 (24.45%)	160 (18.85%)	135 (12.17%)	10 (22.22%)	35 (26.52%)	472 (39.83%)	184 (20.86%)	32 (38.55%)	108 (26.28%)	57 (30.00%)	26 (19.85%)	5 (41.67%)	36 (28.80%)
IIIB	809 (15.70%)	6 (0.71%)	8 (0.72%)	1 (2.22%)	1 (0.76%)	241 (20.34%)	193 (21.88%)	26 (31.33%)	191 (46.47%)	51 (26.84%)	31 (23.66%)	6 (50.00%)	54 (43.20%)
IVA	164 (3.18%)	34 (4.00%)	38 (3.43%)	1 (2.22%)	15 (11.36%)	23 (1.94%)	15 (1.70%)	2 (2.41%)	8 (1.95%)	10 (5.26%)	10 (7.63%)	0 (0.00%)	8 (6.40%)
IVB	2,921 (56.67%)	649 (76.44%)	928 (83.68%)	33 (73.33%)	81 (61.36%)	449 (37.89%)	490 (55.56%)	23 (27.71%)	104 (25.30%)	72 (37.89%)	64 (48.85%)	1 (8.33%)	27 (21.60%)
Status													
Dead	4,226 (81.99%)	765 (90.11%)	968 (87.29%)	41 (91.11%)	117 (88.64%)	955 (80.59%)	677 (76.76%)	69 (83.13%)	299 (72.75%)	141 (74.21%)	93 (70.99%)	11 (91.67%)	90 (72.00%)
Alive	928 (18.01%)	84 (9.89%)	141 (12.71%)	4 (8.89%)	15 (11.36%)	230 (19.41%)	205 (23.24%)	14 (16.87%)	112 (27.25%)	49 (25.79%)	38 (29.01%)	1 (8.33%)	35 (28.00%)

[1]n (%).

A:No surgery + No chemotherapy + No radiotherapy; B:No surgery + Chemotherapy + No radiotherapy; C:No surgery + No chemotherapy + Radiotherapy; D:No surgery + Chemotherapy + Radiotherapy; E:Non-radical surgery + No chemotherapy + No radiotherapy; F: Non-radical surgery + Chemotherapy + No radiotherapy; G:Non-radical surgery + No chemotherapy + Radiotherapy; H:Non-radical surgery + Chemotherapy + Radiotherapy; I:Radical surgery + No chemotherapy + No radiotherapy; J:Radical surgery + Chemotherapy + No radiotherapy; K:Radical surgery + No chemotherapy + Radiotherapy; L:Radical surgery + Chemotherapy + Radiotherapy.

10.3389/fimmu.2024.1500091

10.3389/fimmu.2024.1500091

TABLE 2 Univariate and multivariate Cox proportional hazards models of CSS for advanced GBC patients in twelve treatment models.

Characteristic	Univariable					Multivariable				
	N	Event N	HR[1]	95% CI[1]	p-value	N	Event N	HR[1]	95% CI[1]	p-value
Age										
<65	1,991	1,608	reference	reference		1,991	1,608	reference	reference	
≥65	3,163	2,618	1.22	1.14, 1.29	<0.001	3,163	2,618	1.14	1.07, 1.21	<0.001
Gender										
Female	3,644	2,959	reference	reference		3,644	2,959	reference	reference	
Male	1,510	1,267	1.1	1.03, 1.17	0.006	1,510	1,267	1.11	1.04, 1.19	0.002
Race										
White	3,869	3,162	reference	reference						
Black	641	536	1.08	0.99, 1.19	0.084					
Asian or Pacific Islander	571	473	1	0.91, 1.10	0.985					
American Indian/Alaska Native	59	49	1.32	1.00, 1.76	0.051					
Unknown	14	6	0.53	0.24, 1.19	0.123					
Marital										
Yes	2,678	2,189	reference	reference		2,678	2,189	reference	reference	
No	2,305	1,898	1.17	1.10, 1.24	<0.001	2,305	1,898	1.1	1.03, 1.17	0.005
Unknown	171	139	1.11	0.93, 1.31	0.242	171	139	1.19	1.00, 1.42	0.046
Size										
≤39	1,438	1,094	reference	reference		1,438	1,094	reference	reference	
40-60	764	603	1.21	1.10, 1.34	<0.001	764	603	1.12	1.01, 1.24	0.031
≥61	614	514	1.67	1.51, 1.86	<0.001	614	514	1.39	1.25, 1.54	<0.001
Unknown	2,338	2,015	1.65	1.53, 1.78	<0.001	2,338	2,015	1.23	1.14, 1.33	<0.001
Grade										
Grade I	252	196	reference	reference		252	196	reference	reference	
Grade II	1,270	1,042	1.17	1.00, 1.36	0.045	1,270	1,042	1.26	1.08, 1.47	0.003
Grade III	1,427	1,240	1.68	1.45, 1.96	<0.001	1,427	1,240	1.74	1.50, 2.03	<0.001
Grade IV	47	40	1.97	1.40, 2.77	<0.001	47	40	2.3	1.63, 3.24	<0.001
Unknown	2,158	1,708	2.23	1.92, 2.59	<0.001	2,158	1,708	1.43	1.22, 1.67	<0.001
Stage										
IIIA	1,260	993	reference	reference		1,260	993	reference	reference	
IIIB	809	520	0.57	0.51, 0.63	<0.001	809	520	0.74	0.66, 0.82	<0.001
IVA	164	141	1.34	1.13, 1.60	0.001	164	141	1.31	1.10, 1.57	0.003
IVB	2,921	2,572	1.78	1.65, 1.92	<0.001	2,921	2,572	1.75	1.62, 1.90	<0.001
Treatment										
A	849	765	reference	reference		849	765	reference	reference	
B	1,109	968	0.46	0.41, 0.50	<0.001	1,109	968	0.43	0.39, 0.48	<0.001
C	45	41	0.75	0.55, 1.03	0.077	45	41	0.83	0.61, 1.14	0.256
D	132	117	0.4	0.33, 0.48	<0.001	132	117	0.42	0.35, 0.51	<0.001

(Continued)

TABLE 2 Continued

Characteristic	Univariable					Multivariable				
	N	Event N	HR[1]	95% CI[1]	p-value	N	Event N	HR[1]	95% CI[1]	p-value
Treatment										
E	1,185	955	0.34	0.31, 0.38	<0.001	1,185	955	0.49	0.44, 0.55	<0.001
F	882	677	0.24	0.22, 0.27	<0.001	882	677	0.3	0.27, 0.34	<0.001
G	83	69	0.26	0.20, 0.33	<0.001	83	69	0.38	0.30, 0.50	<0.001
H	411	299	0.16	0.14, 0.18	<0.001	411	299	0.25	0.21, 0.29	<0.001
I	190	141	0.28	0.23, 0.33	<0.001	190	141	0.38	0.31, 0.46	<0.001
J	131	93	0.21	0.17, 0.26	<0.001	131	93	0.25	0.20, 0.32	<0.001
K	12	11	0.21	0.12, 0.39	<0.001	12	11	0.37	0.20, 0.68	0.001
L	125	90	0.15	0.12, 0.19	<0.001	125	90	0.24	0.19, 0.31	<0.001

[1]HR, Hazard Ratio; CI, Confidence Interval.

IV to mitigate differences in patient numbers between different stages, and the results obtained were generally consistent with the previous findings in Table 4 and Figure 6. It was noteworthy that regardless of being in AJCC stage III or stage IV, "RSCR" model exhibited the best HR values, followed by "NrSCR" and "RSCNR".

3.5 Departmental cohort analysis

Patients were divided into two groups based on whether they received immunotherapy: 5 in the "Immunotherapy" group and 10 in the "No immunotherapy" group. Data such as age, gender, and tumor size were included in the analysis, and the demographic and clinical characteristics are displayed in Supplementary Table 6. Statistical analysis revealed no significant differences between the groups for any measured variables, with all p-values greater than 0.05. Additionally, in the present study, we conducted Kaplan-Meier survival analysis, as shown in Figure 7, to compare CSS between patients who received immunotherapy and those who did not. The survival curves suggested a trend toward improved prognosis in the immunotherapy group, but the p-value from the log-rank test was 0.23.

4 Discussion

Currently, treatment options for advanced GBC patients remain uncertain. Surgery continues to be the preferred treatment option for advanced GBC. Radical surgical is the only potential curative method for advanced GBC patients. Unfortunately, due to lymph node and distant metastases in advanced GBC, which limit the opportunity for radical surgery, non-radical surgery, as an alternative, including procedures aimed at relieving jaundice or pain, simple cholecystectomy, and tumor debulking surgeries, are often adopted. However, the efficacy of single surgical treatment is unsatisfactory. Therefore, adjuvant therapies, including chemotherapy and radiotherapy, as well as more advanced immunotherapy and targeted therapy, are also frequently used in the comprehensive management of advanced GBC patients to improve their survival time (17).

There is currently a controversy regarding whether radical surgery should be performed for advanced GBC patients. The scope of radical surgery for advanced GBC typically includes the removal of the gallbladder, adjacent liver tissue, lymph node(s), and affected organ (s). More aggressive procedures involve pancreaticoduodenectomy (PD) and hepatopancreaticoduodenectomy (HPD) (18, 19). Some scholars argue that aggressive surgery is beneficial for patient survival (10, 20–24). A multicenter cohort study analyzed the effects of extended resection surgery on locally advanced GBC patients, confirming the role of radical resection, resulting in some patients achieving a survival time of over two years (25). Even in AJCC stage IV GBC patients, the survival rate after radical surgery has been shown to be significantly higher than that of no surgery (26, 27). Conversely, some physicians question the benefits of radical surgery, considering routine or prophylactic extended surgery to have no significant survival advantage, and non-radical surgery is more recommended (18, 28). In one report, although HPD could eradicate locally advanced GBC, it did not show superiority over non-radical surgery in terms of overall survival, complication morbidity, and mortality (28–30). Therefore, in light of the above perspectives and the findings of this study, as an alternative, non-radical surgery is adopted, as it has also been proven effective for survival in advanced GBC (19, 28, 29).

Chemotherapy is widely used in gastrointestinal tumors, and although the progression-free survival of advanced GBC is relatively short due to its particularity, it still has a positive impact (31). Currently, the gemcitabine and cisplatin (GS) regimen is the most widely accepted chemotherapy regimen for GBC (32–35). With the emergence of neoadjuvant chemotherapy, it has also created opportunities for radical surgery and longer survival time (36–40). Recently, with the use of new drugs and the conduct of more clinical trials, more chemotherapy regimens have emerged, such as FOLFOX, modified FOLFIRINOX (mFOLFIRINOX), and GEMOX regimens (35, 41). Additionally, hepatic arterial infusion chemotherapy (HAIC) is also a choice (36, 42). It is worth

10.3389/fimmu.2024.1500091

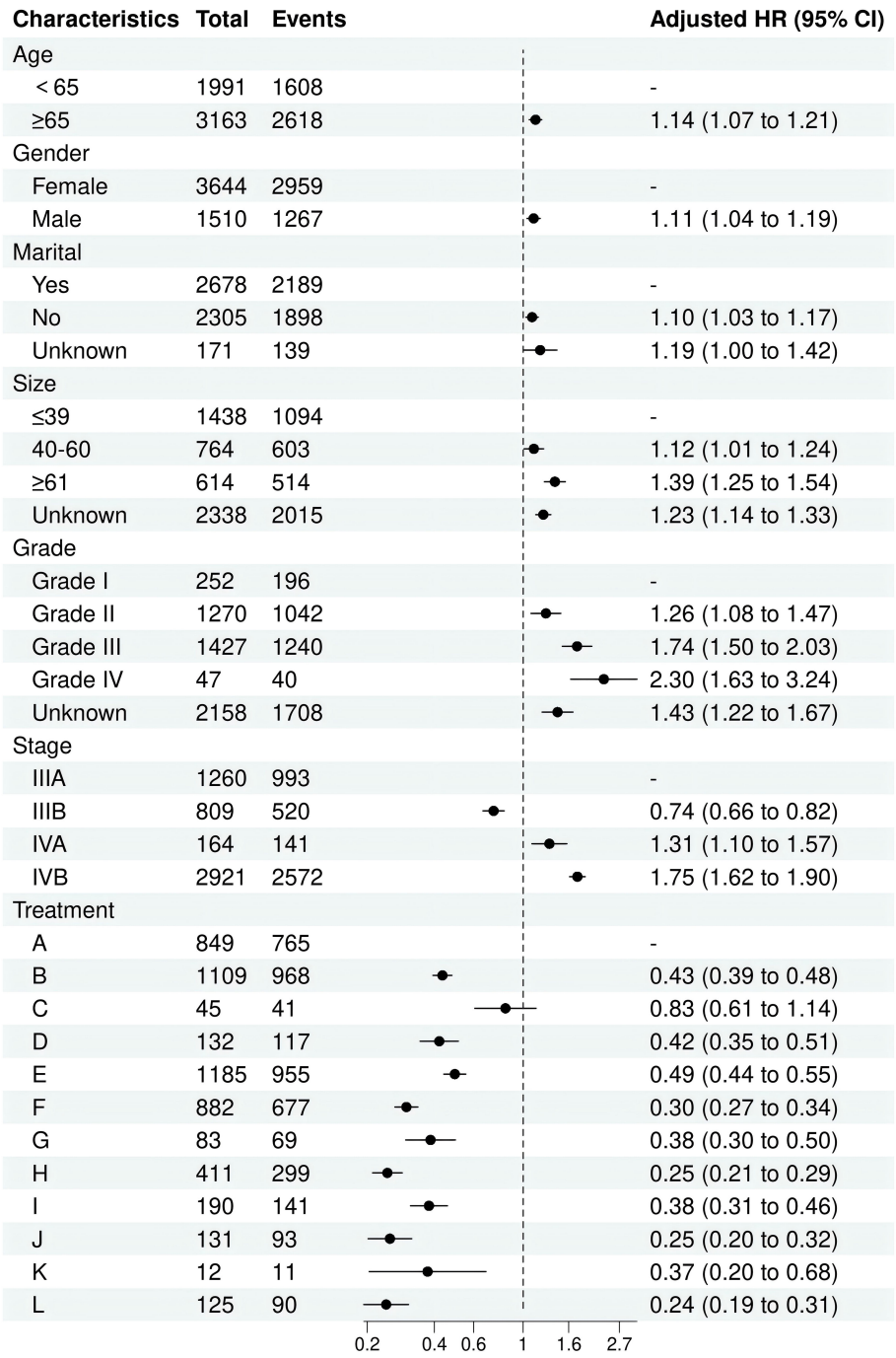

FIGURE 2
The forest plot for multivariate Cox proportional hazards models for CSS in twelve treatment models.

mentioning that even without surgery, palliative chemotherapy is beneficial for the survival of advanced GBC (43, 44).

Radiotherapy, as a treatment option, is not widely used in advanced GBC, but still has a positive role (45). Currently, radiotherapy mainly includes four forms: preoperative radiotherapy (neoadjuvant radiotherapy), intraoperative radiotherapy, postoperative radiotherapy (adjuvant radiotherapy), and palliative radiotherapy, with doses mostly concentrated in the range of 45-54 Gy (46, 47). Some scholars have pointed out that after surgery for advanced GBC, not using radiotherapy or chemoradiotherapy can increase the risk of local recurrence (47, 48). In advanced GBC, radiotherapy is usually jointly used with chemotherapy for effect enhancement, including adjuvant chemoradiotherapy and neoadjuvant chemoradiotherapy (49, 50). It is worth mentioning that for unresectable advanced GBC, both radiotherapy and chemoradiotherapy can bring survival benefits to patients and create opportunities for radical surgery (50, 51).

Immunotherapy and targeted therapy also boost the survival of advanced GBC patients (34, 52). The term immunotherapy refers

10.3389/fimmu.2024.1500091

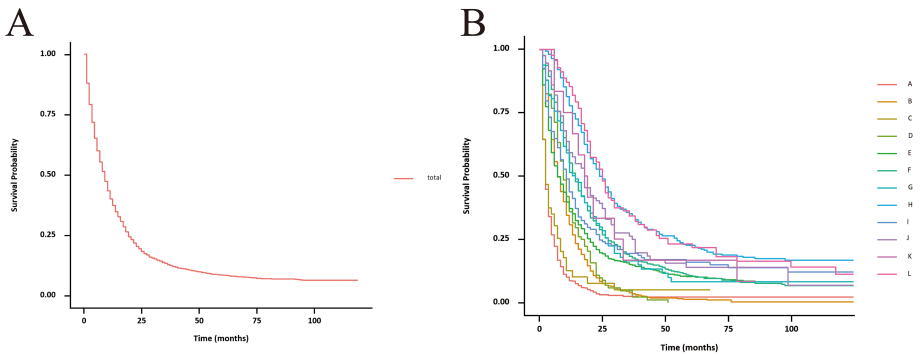

FIGURE 3
Unadjusted CSS curves for advanced GBC patients. **(A)**, total patients; **(B)**, twelve treatment models.

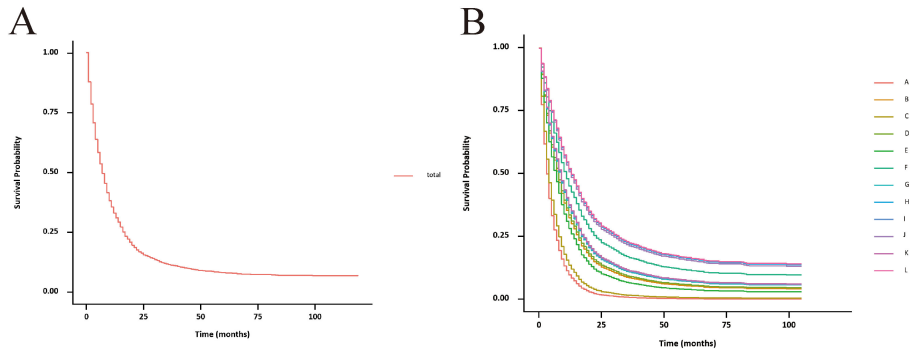

FIGURE 4
Adjusted CSS curves for advanced GBC patients. **(A)**, total patients; **(B)**, twelve treatment models.

TABLE 3 Multivariate Cox proportional hazards models of CSS for advanced GBC in twelve treatment models at different pathological stages, reported separately for stage IIIA, IIIB, IVA and IVB.

Characteristic	IIIA				IIIB				IVA				IVB			
	N	HR[1]	95% CI[1]	p-value	N	HR[1]	95% CI[1]	p-value	N	HR[1]	95% CI[1]	p-value	N	HR[1]	95% CI[1]	p-value
Age																
<65	398	reference	reference		294	reference	reference		65	reference	reference		1,234	reference	reference	
≥65	862	1.33	1.15, 1.54	<0.001	515	1.19	0.98, 1.44	0.08	99	1.38	0.89, 2.13	0.152	1,687	1.09	1.01, 1.18	0.035
Gender																
Female	878	reference	reference		591	reference	reference		114	reference	reference		2,061	reference	reference	
Male	382	1.11	0.96, 1.28	0.16	218	1.42	1.17, 1.74	<0.001	50	0.72	0.47, 1.12	0.145	860	1.1	1.00, 1.19	0.038
Marital																
Yes	607	reference	reference		445	reference	reference		85	reference	reference		1,541	reference	reference	
No	602	1.31	1.14, 1.50	<0.001	334	1.08	0.88, 1.31	0.458	73	1.08	0.74, 1.59	0.678	1,296	1.04	0.96, 1.13	0.298
Unknown	51	1.26	0.90, 1.76	0.183	30	1.12	0.71, 1.77	0.618	6	0.87	0.33, 2.28	0.782	84	1.26	0.99, 1.59	0.056
Size																
≤39	385	reference	reference		373	reference	reference		31	reference	reference		649	reference	reference	

(Continued)

TABLE 3 Continued

Characteristic	IIIA				IIIB				IVA				IVB			
	N	HR[1]	95% CI[1]	p-value	N	HR[1]	95% CI[1]	p-value	N	HR[1]	95% CI[1]	p-value	N	HR[1]	95% CI[1]	p-value
Size																
40-60	204	1.19	0.97, 1.46	0.087	138	1.18	0.91, 1.53	0.206	35	1.11	0.61, 2.01	0.73	387	1.09	0.95, 1.26	0.2
≥61	184	1.6	1.30, 1.98	<0.001	71	2.14	1.58, 2.88	<0.001	25	1.05	0.55, 2.03	0.873	334	1.18	1.02, 1.36	0.025
Unknown	487	1.22	1.04, 1.43	0.015	227	1.26	1.02, 1.56	0.029	73	1.17	0.71, 1.94	0.538	1,551	1.18	1.07, 1.31	0.001
Grade																
Grade I	81	reference	reference		68	reference	reference		8	reference	reference		95	reference	reference	
Grade II	393	1.35	1.02, 1.78	0.039	301	1.21	0.87, 1.69	0.253	45	1.1	0.46, 2.66	0.83	531	1.21	0.96, 1.53	0.105
Grade III	401	1.87	1.41, 2.48	<0.001	272	1.62	1.16, 2.26	0.004	45	2.43	1.03, 5.71	0.042	709	1.62	1.29, 2.04	<0.001
Grade IV	11	2.97	1.49, 5.89	0.002	11	1.83	0.81, 4.13	0.144	1	0.51	0.06, 4.51	0.543	24	2.27	1.42, 3.64	<0.001
Unknown	374	1.54	1.14, 2.09	0.005	157	1.38	0.92, 2.08	0.124	65	1.32	0.52, 3.39	0.562	1,562	1.34	1.06, 1.68	0.013
Treatment																
A	160	reference	reference		6	reference	reference		34	reference	reference		649	reference	reference	
B	135	0.54	0.42, 0.70	<0.001	8	0.7	0.20, 2.44	0.581	38	0.63	0.35, 1.12	0.113	928	0.42	0.37, 0.46	<0.001
C	10	0.46	0.22, 0.95	0.037	1	0	0.00, Inf	0.991	1	0.82	0.11, 6.31	0.85	33	1.03	0.72, 1.48	0.853
D	35	0.46	0.31, 0.68	<0.001	1	0.34	0.04, 3.10	0.34	15	0.39	0.19, 0.81	0.011	81	0.42	0.33, 0.54	<0.001
E	472	0.42	0.33, 0.52	<0.001	241	0.43	0.16, 1.20	0.109	23	0.96	0.50, 1.84	0.896	449	0.57	0.49, 0.65	<0.001
F	184	0.39	0.30, 0.50	<0.001	193	0.25	0.09, 0.70	0.008	15	0.29	0.13, 0.65	0.003	490	0.28	0.24, 0.32	<0.001
G	32	0.31	0.20, 0.49	<0.001	26	0.53	0.18, 1.59	0.259	2	0.26	0.03, 2.06	0.203	23	0.37	0.24, 0.57	<0.001
H	108	0.24	0.18, 0.33	<0.001	191	0.25	0.09, 0.69	0.008	8	0.35	0.13, 0.91	0.032	104	0.21	0.16, 0.26	<0.001
I	57	0.29	0.20, 0.43	<0.001	51	0.37	0.13, 1.06	0.065	10	0.75	0.31, 1.85	0.537	72	0.41	0.31, 0.54	<0.001
J	26	0.25	0.14, 0.42	<0.001	31	0.24	0.08, 0.76	0.015	10	0.16	0.06, 0.42	<0.001	64	0.25	0.19, 0.34	<0.001
K	5	0.29	0.11, 0.80	0.016	6	0.47	0.13, 1.74	0.261					1	0.26	0.04, 1.89	0.184
L	36	0.22	0.14, 0.35	<0.001	54	0.24	0.08, 0.71	0.01	8	0.25	0.10, 0.61	0.003	27	0.21	0.14, 0.33	<0.001

[1]HR, Hazard Ratio; CI, Confidence Interval.

mainly to immune checkpoint inhibitors, such as PD-1, PD-L1, TMB-H, and MSI/MMRd (53–56). In the phase III TOPAZ-1 trial in 2022 and the KEYNOTE-966 trial in 2023, the combination of durvalumab or pembrolizumab with gemcitabine-cisplatin demonstrated improved survival compared to treatment with gemcitabine-cisplatin alone (57–59). Additionally, several phase II clinical trials have provided evidence supporting the effectiveness of other immunotherapy regimens, such as stereotactic body radiotherapy (SBRT) combined with nivolumab and ipilimumab, camrelizumab plus FOLFOX4 or GEMOX, and nab-paclitaxel combined with sintilimab (60–64). Targeted drugs include trastuzumab, erdafitinib, lenvatinib, and so on, mainly targeting specific molecular pathways such as Hedgehog, PI3K/AKT/mTOR, Notch, ErbB, MAPK/ERK, and Angiogenesis (53, 65–67). Additionally, patient-derived tumor organoid and patient-derived tumor xenograft models can facilitate personalized treatment for patients with advanced GBC (68).

The SEER database was utilized to compare treatment models for advanced GBC patients in this study. Among all patients, through Cox regression analyses, it was observed that the "RSCR" model

10.3389/fimmu.2024.1500091

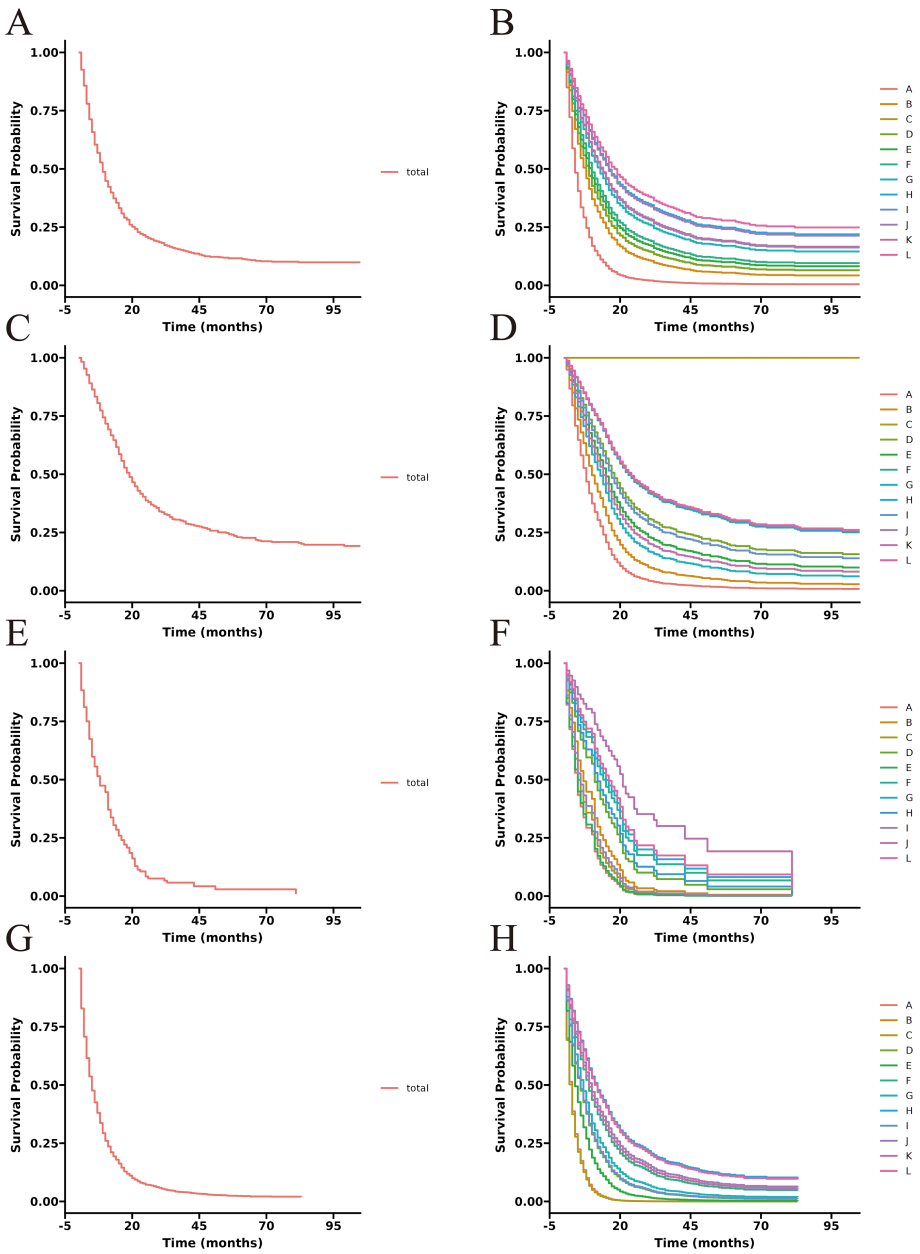

FIGURE 5
Adjusted CSS curves for advanced GBC patients at different pathological stages. Stage IIIA: **(A)**, total patients; **(B)**, twelve treatment models. Stage IIIB: **(C)**, total patients; **(D)**, twelve treatment models. Stage IVA: **(E)**, total patients; **(F)**, twelve treatment models. Stage IVB: **(G)**, total patients; **(H)**, twelve treatment models.

exhibited the most significant improvement in CSS compared to the "NSNCNR" model, with other models also showing varying degrees of improvement. After excluding treatment models with insufficient sample sizes and analyzing the post-PSM data, or after conducting analysis using only cases with complete data, the results remained robust. These results consistent with the current understanding. After subgroup analysis by AJCC stage, the efficacy of the "RSCR" model remained significant. Some discordant results observed in subgroup analyses may stem from variations in the underlying patient profiles at each AJCC stage, or from the relatively small sample sizes in certain treatment models and stage categories. It is noteworthy that the extension effect of the "NrSCR" model on CSS was also considerable, often ranking second only to the "RSCR" model. Considering the difficulty of achieving radical surgery in advanced GBC, non-radical surgery is also a treatment option for patients who cannot undergo radical surgery, of course, in conjunction with other treatment options as much as possible. Additionally, it was found that the use of radical or non-radical surgery, chemotherapy, and radiotherapy

10.3389/fimmu.2024.1500091

TABLE 4 Multivariate Cox proportional hazards models of CSS for advanced GBC in twelve treatment models at different pathological stages, reported separately for stage III and IV.

Characteristic	III				IV			
	N	HR[1]	95% CI[1]	p-value	N	HR[1]	95% CI[1]	p-value
Age								
<65	692	reference	reference		1,299	reference	reference	
≥65	1,377	1.28	1.14, 1.43	<0.001	1,786	1.09	1.01, 1.18	0.034
Gender								
Female	1,469	reference	reference		2,175	reference	reference	
Male	600	1.21	1.08, 1.36	0.001	910	1.07	0.98, 1.16	0.109
Marital								
Yes	1,052	reference	reference		1,626	reference	reference	
No	936	1.22	1.10, 1.37	<0.001	1,369	1.05	0.97, 1.13	0.254
Unknown	81	1.2	0.92, 1.57	0.177	90	1.21	0.97, 1.52	0.093
Size								
≤39	758	reference	reference		680	reference	reference	
40-60	342	1.2	1.03, 1.41	0.019	422	1.07	0.94, 1.22	0.322
≥61	255	1.8	1.52, 2.14	<0.001	359	1.17	1.01, 1.34	0.032
Unknown	714	1.28	1.13, 1.45	<0.001	1,624	1.19	1.07, 1.31	<0.001
Grade								
Grade I	149	reference	reference		103	reference	reference	
Grade II	694	1.29	1.04, 1.60	0.02	576	1.21	0.97, 1.51	0.094
Grade III	673	1.76	1.42, 2.18	<0.001	754	1.68	1.35, 2.09	<0.001
Grade IV	22	2.21	1.32, 3.71	0.003	25	2.11	1.33, 3.34	0.001
Unknown	531	1.42	1.12, 1.81	0.004	1,627	1.36	1.09, 1.70	0.006
Treatment								
A	166	reference	reference		683	reference	reference	
B	143	0.54	0.42, 0.69	<0.001	966	0.43	0.38, 0.48	<0.001
C	11	0.43	0.21, 0.88	0.021	34	1.04	0.73, 1.48	0.831
D	36	0.45	0.31, 0.67	<0.001	96	0.4	0.32, 0.50	<0.001
E	713	0.38	0.31, 0.46	<0.001	472	0.58	0.51, 0.67	<0.001
F	377	0.27	0.22, 0.34	<0.001	505	0.29	0.25, 0.33	<0.001
G	58	0.35	0.25, 0.49	<0.001	25	0.35	0.23, 0.55	<0.001
H	299	0.21	0.17, 0.27	<0.001	112	0.22	0.17, 0.28	<0.001
I	108	0.28	0.21, 0.38	<0.001	82	0.43	0.33, 0.56	<0.001
J	57	0.21	0.14, 0.31	<0.001	74	0.24	0.19, 0.32	<0.001
K	11	0.32	0.16, 0.61	<0.001	1	0.27	0.04, 1.92	0.19
L	90	0.21	0.15, 0.28	<0.001	35	0.21	0.15, 0.31	<0.001

[1]HR, Hazard Ratio; CI, Confidence Interval.

10.3389/fimmu.2024.1500091

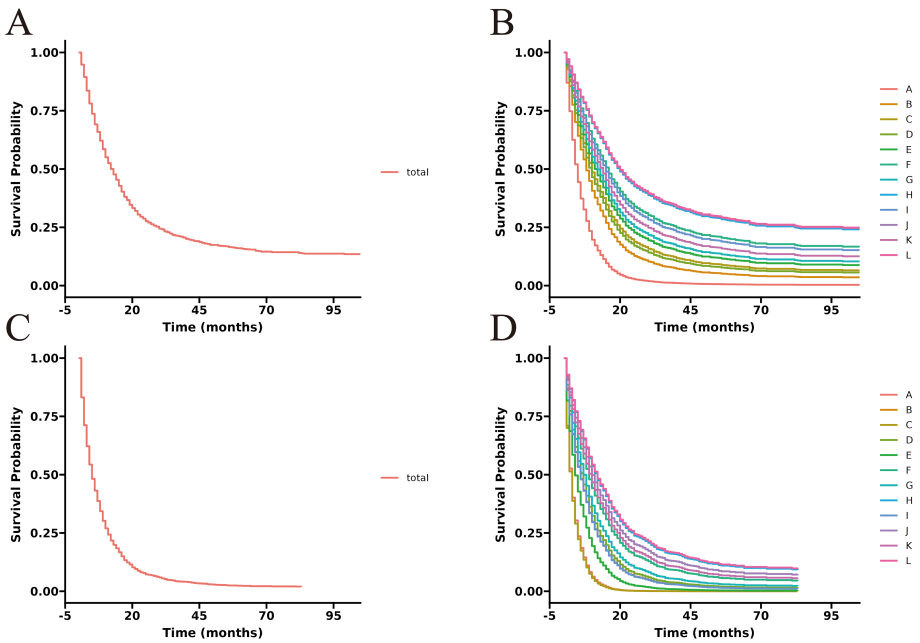

FIGURE 6
Adjusted CSS curves for advanced GBC patients at different pathological stages. Stage III: **(A)**, total patients; **(B)**, twelve treatment models. Stage IV: **(C)**, total patients; **(D)**, twelve treatment models.

provided significant benefits to patients compared to no surgery, no chemotherapy, and no radiotherapy, and the survival time was prolonged to varying degrees after the combination of treatment options.

In our departmental cohort analysis, the absence of significant differences in clinical and demographic characteristics between the two groups ($p > 0.05$) indicates that the patients were comparable in terms of baseline factors at the time of treatment assignment. This comparability is crucial as it reduces the likelihood of confounding bias, allowing any observed differences in survival outcomes to be more confidently attributed to the effect of immunotherapy rather than baseline imbalances. In the KM analysis, the lack of statistical

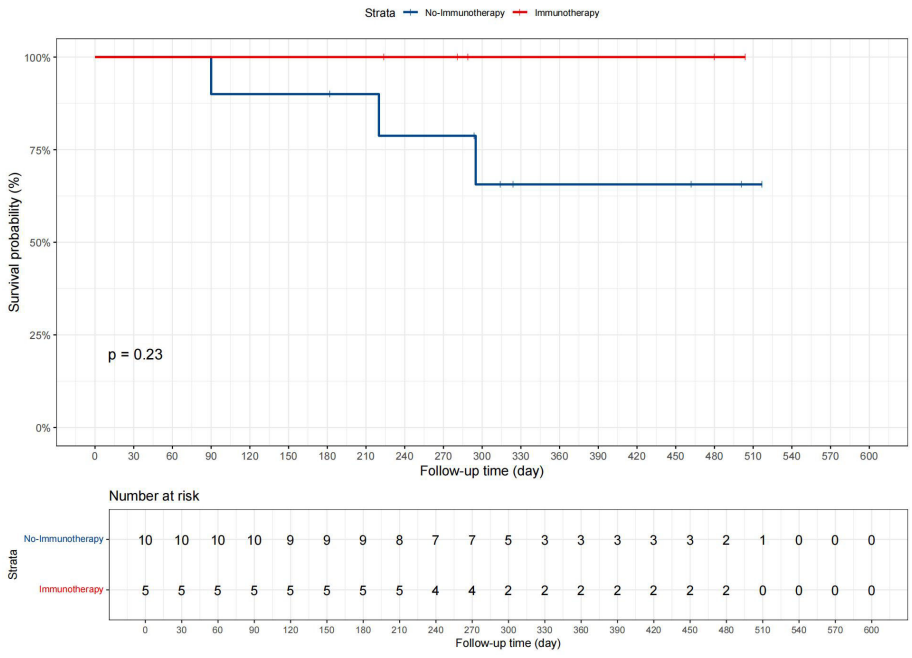

FIGURE 7
The CSS curves for advanced GBC patients in the departmental cohort.

significance (p = 0.23) may be attributed to the limited sample size in our cohort, particularly with only 5 patients receiving immunotherapy. Small sample sizes often reduce the power of statistical tests, making it more difficult to detect significant differences even if a true effect exists. While the trend observed in the Kaplan-Meier curves suggests a potential benefit of immunotherapy, further studies with larger patient cohorts are needed to confirm this finding and achieve adequate statistical power. It is believed that these results can provide new insights to clinicians, indicating that when conditions permit, comprehensive treatment including surgery, chemotherapy, radiotherapy, as well as immunotherapy and targeted therapy should be provided to patients with advanced GBC, rather than limiting treatment to one or two options.

However, several limitations still exist in this innovative study. Firstly, the SEER database is a retrospective database, and data such as vital signs, nutritional status, underlying diseases of patients are not reflected in the database. Secondly, the specific location of the tumor, tumor burden, and surgical procedures were not mentioned. Additionally, the specific modes, doses, and durations of chemotherapy and radiotherapy, as well as the sequence and intervals of surgery, chemotherapy, and radiotherapy, were not within the scope of the study, and treatment options such as targeted therapy and immunotherapy were not embraced. Despite these limitations, the SEER database is still useful in terms of providing the most comprehensive data on treatment patterns and survival status in the United States to date. Additionally, to address the limitations of the database, we conducted a review of our departmental cohort and literature from the PubMed database to enhance our understanding of immunotherapy and related treatments. Based on our knowledge, a comprehensive study of all twelve treatment models selected from the SEER database is being conducted for the first time, while several studies have utilized the database to analyze GBC, none have combined such a broad range of treatment models and ranked them accordingly (69). Additionally, this study is one of the few that focuses on advanced GBC. Previous researchers have often overlooked this patient group, as advanced GBC has traditionally been considered unsuitable for surgical intervention (70). Given that the SEER database analysis is retrospective in nature, future research should incorporate more detailed clinical data, including specific surgical approaches, chemotherapy regimens, radiation doses, and the sequencing of various treatment options. Moreover, larger departmental cohorts should be established to enhance the reliability of the findings. Furthermore, we recommend that prospective studies explore these aspects in greater depth and assess their applications in clinical practice.

5 Conclusion

For the SEER database, the "Radical surgery + Chemotherapy + Radiotherapy" models provide the greatest survival benefit for advanced GBC patients. At the same time, the departmental cohort analysis suggests that incorporating immunotherapy may offer further advantages to patients. Providing patients with the most comprehensive treatment possible, even if the optimal treatment effect is not achieved, is a way to extend the survival of patients. As long as treatment options are taken, it is always beneficial for patient survival. This innovative finding requires more comprehensive data and prospective studies for validation.

Data availability statement

The original contributions presented in the study are included in the article/Supplementary Material. Further inquiries can be directed to the corresponding authors.

Ethics statement

The studies involving humans were approved by Ethics Committee of National Cancer Center/Cancer Hospital, Chinese Academy of Medical Sciences and Peking Union Medical College. The studies were conducted in accordance with the local legislation and institutional requirements. Written informed consent for participation was not required from the participants or the participants' legal guardians/next of kin in accordance with the national legislation and institutional requirements.

Author contributions

RL: Conceptualization, Formal analysis, Investigation, Methodology, Software, Writing – original draft, Writing – review & editing. XC: Conceptualization, Investigation, Methodology, Writing – review & editing. BW: Conceptualization, Formal analysis, Software, Writing – review & editing. BA: Conceptualization, Formal analysis, Investigation, Writing – review & editing. FM: Conceptualization, Writing – review & editing. DC: Supervision, Validation, Writing – review & editing. JZ: Supervision, Validation, Writing – review & editing. TY: Supervision, Validation, Writing – review & editing.

Funding

The author(s) declare that no financial support was received for the research, authorship, and/or publication of this article.

Acknowledgments

We extend our sincere gratitude to all participants involved in this study.

Conflict of interest

The authors declare that the research was conducted in the absence of any commercial or financial relationships that could be construed as a potential conflict of interest.

Publisher's note

All claims expressed in this article are solely those of the authors and do not necessarily represent those of their affiliated organizations, or those of the publisher, the editors and the reviewers. Any product that may be evaluated in this article, or claim that may be made by its manufacturer, is not guaranteed or endorsed by the publisher.

Supplementary material

The Supplementary Material for this article can be found online at: https://www.frontiersin.org/articles/10.3389/fimmu.2024.1500091/full#supplementary-material

References

1. Sung H, Ferlay J, Siegel RL, Laversanne M, Soerjomataram I, Jemal A, et al. Global cancer statistics 2020: GLOBOCAN estimates of incidence and mortality worldwide for 36 cancers in 185 countries. *CA: Cancer J Clin*. (2021) 71:209–49. doi: 10.3322/caac.21660

2. Vuthaluru S, Sharma P, Chowdhury S, Are C. Global epidemiological trends and variations in the burden of gallbladder cancer. *J Surg Oncol*. (2023) 128:980–8. doi: 10.1002/jso.27450

3. Huang J, Patel HK, Boakye D, Chandrasekar VT, Koulaouzidis A, Lucero-Prisno Iii DE, et al. Worldwide distribution, associated factors, and trends of gallbladder cancer: A global country-level analysis. *Cancer Lett*. (2021) 521:238–51. doi: 10.1016/j.canlet.2021.09.004

4. Narayan RR, Creasy JM, Goldman DA, Gönen M, Kandoth C, Kundra R, et al. Regional differences in gallbladder cancer pathogenesis: Insights from a multi-institutional comparison of tumor mutations. *Cancer*. (2019) 125:575–85. doi: 10.1002/cncr.31850

5. Schmidt MA, Marcano-Bonilla L, Roberts LR. Gallbladder cancer: epidemiology and genetic risk associations. *Chin Clin Oncol*. (2019) 8:31. doi: 10.21037/cco.2019.08.13

6. Randi G, Franceschi S, La Vecchia C. Gallbladder cancer worldwide: geographical distribution and risk factors. *Int J Cancer*. (2006) 118:1591–602. doi: 10.1002/ijc.21683

7. Bray F, Ferlay J, Soerjomataram I, Siegel RL, Torre LA, Jemal A. Global cancer statistics 2018: GLOBOCAN estimates of incidence and mortality worldwide for 36 cancers in 185 countries. *CA: Cancer J Clin*. (2018) 68:394–424. doi: 10.3322/caac.21492

8. Rawla P, Sunkara T, Thandra KC, Barsouk A. Epidemiology of gallbladder cancer. *Clin Exp Hepatol*. (2019) 5:93–102. doi: 10.5114/ceh.2019.85166

9. Piehler JM, Crichlow RW. Primary carcinoma of the gallbladder. *Surgery gynecology obstetrics*. (1978) 147:929–42.

10. de Savornin Lohman E, de Bitter T, Verhoeven R, van der Geest L, Hagendoorn J, Haj Mohammad N, et al. Trends in treatment and survival of gallbladder cancer in the Netherlands; identifying gaps and opportunities from a nation-wide cohort. *Cancers*. (2020) 12. doi: 10.3390/cancers12040918

11. Wernberg JA, Lucarelli DD. Gallbladder cancer. *Surg Clinics North America*. (2014) 94:343–60. doi: 10.1016/j.suc.2014.01.009

12. Wang Y, Kong Y, Yang Q, Zhong C, Zhou D, Wang W. Survival benefit of adjuvant chemotherapy in patients with resected gallbladder adenocarcinoma: An updated retrospective cohort analysis. *Eur J Surg Oncol*. (2024) 50:108047. doi: 10.1016/j.ejso.2024.108047

13. Jh L RA, Lw G, Tr H. Immunotherapy in biliary tract cancers: current standard-of-care and emerging strategies. *Cancers*. (2023) 15. doi: 10.3390/cancers15133312

14. Ayabe RI, Wach MM, Ruff SM, Diggs LP, Martin SP, Wiemken T, et al. Gallbladder squamous cell carcinoma: An analysis of 1084 cases from the National Cancer Database. *J Surg Oncol*. (2020) 122:716–22. doi: 10.1002/jso.26066

15. Roa JC, García P, Kapoor VK, Maithel SK, Javle M, Koshiol J. Gallbladder cancer. *Nat Rev Dis Primers*. (2022) 8:69. doi: 10.1038/s41572-022-00398-y

16. Terry M, Crowson CS, Atkinson EJ. "Adjusted survival curves". *The R Project for Statistical Computing*. (2015). Available at: https://cran.r-project.org/web/packages/survival//vignettes/adjcurve.pdf.

17. Zhou Y, Yuan K, Yang Y, Ji Z, Zhou D, Ouyang J, et al. Gallbladder cancer: current and future treatment options. *Front Pharmacol*. (2023) 14:1183619. doi: 10.3389/fphar.2023.1183619

18. Krell RW, Wei AC. Gallbladder cancer: surgical management. *Chin Clin Oncol*. (2019) 8:36. doi: 10.21037/cco.2019.06.06

19. Todoroki T, Takahashi H, Koike N, Kawamoto T, Kondo T, Yoshida S, et al. Outcomes of aggressive treatment of stage IV gallbladder cancer and predictors of survival. *Hepato-gastroenterology*. (1999) 46:2114–21.

20. Feo CF, Ginesu GC, Fancellu A, Perra T, Ninniri C, Deiana G, et al. Current management of incidental gallbladder cancer: A review. *Int J Surg (London England)*. (2022) 98:106234. doi: 10.1016/j.ijsu.2022.106234

21. Chan SY, Poon RT, Lo CM, Ng KK, Fan ST. Management of carcinoma of the gallbladder: a single-institution experience in 16 years. *J Surg Oncol*. (2008) 97:156–64. doi: 10.1002/jso.20885

22. Patkar S, Patel S, Kazi M, Goel M. Radical surgery for stage IV gallbladder cancers: Treatment strategies in patients with limited metastatic burden. *Ann hepato-biliary-pancreatic Surg*. (2023) 27:180–8. doi: 10.14701/ahbps.22-111

23. Coburn NG, Cleary SP, Tan JC, Law CH. Surgery for gallbladder cancer: a population-based analysis. *J Am Coll Surgeons*. (2008) 207:371–82. doi: 10.1016/j.jamcollsurg.2008.02.031

24. Chen C, Wang L, Zhang R, Li Q, Zhao YL, Zhang GJ, et al. Who benefits from R0 resection? A single-center analysis of patients with stage IV gallbladder cancer. *Chronic Dis Trans Med*. (2019) 5:188–96. doi: 10.1016/j.cdtm.2019.08.004

25. Kuipers H, de Savornin Lohman EAJ, van Dooren M, Braat AE, Daams F, van Dam R, et al. Extended resections for advanced gallbladder cancer: results from a nationwide cohort study. *Ann Surg Oncol*. (2021) 28:835–43. doi: 10.1245/s10434-020-08858-z

26. Kang MJ, Song Y, Jang JY, Han IW, Kim SW. Role of radical surgery in patients with stage IV gallbladder cancer. *HPB : Off J Int Hepato Pancreato Biliary Assoc*. (2012) 14:805–11. doi: 10.1111/j.1477-2574.2012.00544.x

27. Nekarakanti P KS, Nag H. Surgery versus no surgery in stage IV gallbladder carcinoma: A propensity score-matched analysis. *Turkish J Surg*. (2023) 39:153–61. doi: 10.47717/turkjsurg.2023.5975

28. Mizuno T, Ebata T, Yokoyama Y, Igami T, Yamaguchi J, Onoe S, et al. Major hepatectomy with or without pancreatoduodenectomy for advanced gallbladder cancer. *Br J Surg*. (2019) 106:626–35. doi: 10.1002/bjs.11088

29. Chang Y, Li Q, Wu Q, Chi L, Bi X, Zeng Q, et al. Impact of surgical strategies on the survival of gallbladder cancer patients: analysis of 715 cases. *World J Surg Oncol*. (2020) 18:142. doi: 10.1186/s12957-020-01915-7

30. Higuchi R, Ota T, Araida T, Kajiyama H, Yazawa T, Furukawa T, et al. Surgical approaches to advanced gallbladder cancer : a 40-year single-institution study of prognostic factors and resectability. *Ann Surg Oncol*. (2014) 21:4308–16. doi: 10.1245/s10434-014-3885-1

31. Azizi AA, Lamarca A, McNamara MG, Valle JW. Chemotherapy for advanced gallbladder cancer (GBC): A systematic review and meta-analysis. *Crit Rev oncology/hematology*. (2021) 163:103328. doi: 10.1016/j.critrevonc.2021.103328

32. Valle J, Wasan H, Palmer DH, Cunningham D, Anthoney A, Maraveyas A, et al. Cisplatin plus gemcitabine versus gemcitabine for biliary tract cancer. *New Engl J Med*. (2010) 362:1273–81. doi: 10.1056/NEJMoa0908721

33. Ramaswamy A, Ostwal V, Pinninti R, Kannan S, Bhargava P, Nashikkar C, et al. Gemcitabine-cisplatin versus gemcitabine-oxaliplatin doublet chemotherapy in advanced gallbladder cancers: a match pair analysis. *J hepato-biliary-pancreatic Sci*. (2017) 24:262–7. doi: 10.1002/jhbp.439

34. Lamarca A, Edeline J, Goyal L. How I treat biliary tract cancer. *ESMO Open*. (2022) 7:100378. doi: 10.1016/j.esmoop.2021.100378

35. Javle M, Zhao H, Abou-Alfa GK. Systemic therapy for gallbladder cancer. *Chin Clin Oncol*. (2019) 8:44. doi: 10.21037/cco.2019.08.14

36. Singh S, Goel S, Aggarwal A, Iqbal A, Hazarika D, Talwar V. Combination of portal vein embolization and neoadjuvant chemotherapy for locally advanced gallbladder cancer requiring extended hepatectomy - A novel approach. *Indian J gastroenterology : Off J Indian Soc Gastroenterol*. (2021) 40:580–9. doi: 10.1007/s12664-021-01182-8

37. Inoue M, Hakoda K, Sawada H, Hotta R, Ohmori I, Miyamoto K, et al. Locally advanced gallbladder cancer treated with effective chemotherapy and subsequent

curative resection: a case report. *J Med Case Rep*. (2022) 16:30. doi: 10.1186/s13256-021-03248-9

38. Sirohi B, Mitra A, Jagannath P, Singh A, Ramadvar M, Kulkarni S, et al. Neoadjuvant chemotherapy in patients with locally advanced gallbladder cancer. *Future Oncol (London England)*. (2015) 11:1501–9. doi: 10.2217/fon.14.308

39. Ozer M, Goksu SY, Sanford NN, Porembka M, Khurshid H, Ahn C, et al. A propensity score analysis of chemotherapy use in patients with resectable gallbladder cancer. *JAMA network Open*. (2022) 5:e2146912. doi: 10.1001/jamanetworkopen.2021.46912

40. Yang Z, Wu Z, Xiong Y, Liu S, Cai C, Shao Z, et al. Successful conversion surgery for locally advanced gallbladder cancer after gemcitabine and nab-paclitaxel chemotherapy. *Front Oncol*. (2022) 12:977963. doi: 10.3389/fonc.2022.977963

41. Cui XY, Li XC, Cui JJ, Wu XS, Zou L, Song XL, et al. Modified FOLFIRINOX for unresectable locally advanced or metastatic gallbladder cancer, a comparison with GEMOX regimen. *Hepatobiliary Surg Nutr*. (2021) 10:498–506. doi: 10.21037/hbsn-20-846

42. Zheng K, Wang X, Cao G, Xu L, Zhu X, Fu L, et al. Hepatic arterial infusion chemotherapy with oxaliplatin and 5-fluorouracil for advanced gallbladder cancer. *Cardiovasc interventional Radiol*. (2021) 44:271–80. doi: 10.1007/s00270-020-02661-9

43. Bravo-Soto GA, Brañes R, Peña J, Nervi B. Palliative chemotherapy for advanced gallbladder cancer. *Medwave*. (2021) 21:e8045. doi: 10.5867/medwave.2021.03.8046

44. Dierks J, Gaspersz MP, Belkouz A, van Vugt JLA, Coelen RJS, de Groot JWB, et al. Translating the ABC-02 trial into daily practice: outcome of palliative treatment in patients with unresectable biliary tract cancer treated with gemcitabine and cisplatin. *Acta Oncol (Stockholm Sweden)*. (2018) 57:807–12. doi: 10.1080/0284186x.2017.1418532

45. Kamarajah SK, Al-Rawashdeh W, White SA, Abu Hilal M, Salti GI, Dahdaleh FS. Adjuvant radiotherapy improves long-term survival after resection for gallbladder cancer A population-based cohort study. *Eur J Surg oncology : J Eur Soc Surg Oncol Br Assoc Surg Oncol*. (2022) 48:425–34. doi: 10.1016/j.ejso.2021.09.002

46. Alam MN, Agrawal S, Rastogi N, Maria Das KJ. Consolidation chemoradiation (cCTRT) improves survival in responders to first-line chemotherapy (CT) in locally advanced gallbladder cancer (LA-GBC): A new standard of care? *Indian J Cancer*. (2022) 59:577–83. doi: 10.4103/ijc.IJC_1145_20

47. Verma V, Crane CH. Contemporary perspectives on the use of radiation therapy for locally advanced gallbladder cancer. *Chin Clin Oncol*. (2019) 8:41. doi: 10.21037/cco.2019.08.12

48. Kim TG. Patterns of initial failure after resection for gallbladder cancer: implications for adjuvant radiotherapy. *Radiat Oncol J*. (2017) 35:359–67. doi: 10.3857/roj.2017.00388

49. Engineer R, Patkar S, Lewis SC, Sharma AD, Shetty N, Ostwal V, et al. A phase III randomised clinical trial of perioperative therapy (neoadjuvant chemotherapy versus chemoradiotherapy) in locally advanced gallbladder cancers (POLCAGB): study protocol. *BMJ Open*. (2019) 9:e028147. doi: 10.1136/bmjopen-2018-028147

50. Sinha S, Engineer R, Ostwal V, Ramaswamy A, Chopra S, Shetty N. Radiotherapy for locally advanced unresectable gallbladder cancer - A way forward: Comparative study of chemotherapy versus chemoradiotherapy. *J Cancer Res Ther*. (2022) 18:147–51. doi: 10.4103/jcrt.JCRT_1568_20

51. Song J, Kang X, Di Y, Ren G, Wang Y. Associations between external beam radiotherapy and overall survival in patients with gallbladder cancer: A population-based study. *Front Public Health*. (2022) 10:1012142. doi: 10.3389/fpubh.2022.1012142

52. Harding JJ, Khalil DN, Fabris L, Abou-Alfa GK. Rational development of combination therapies for biliary tract cancers. *J Hepatol*. (2023) 78:217–28. doi: 10.1016/j.jhep.2022.09.004

53. Wu T, Pu C, Wang Q, Zhang K. Comparison of efficacy and safety of anti-programmed cell death-1 antibody plus lenvatinib and chemotherapy as first-line therapy for patients with stage IV gallbladder cancer: A real-world study in a chinese population. *Biomedicines*. (2023) 11. doi: 10.3390/biomedicines11112933

54. Sturm N, Schuhbaur JS, Hüttner F, Perkhofer L, Ettrich TJ. Gallbladder cancer: current multimodality treatment concepts and future directions. *Cancers*. (2022) 14. doi: 10.3390/cancers14225580

55. Frega G, Cossio FP, Banales JM, Cardinale V, Macias RIR, Braconi C, et al. Lacking immunotherapy biomarkers for biliary tract cancer: A comprehensive systematic literature review and meta-analysis. *Cells*. (2023) 12. doi: 10.3390/cells12162098

56. Zuo B, Yang X, Yang X, Bian J, Long J, Wang D, et al. A real-world study of the efficacy and safety of anti-PD-1 antibodies plus lenvatinib in patients with advanced gallbladder cancer. *Cancer immunology immunotherapy : CII*. (2022) 71:1889–96. doi: 10.1007/s00262-021-03121-0

57. Oh D-Y, Ruth He A, Qin S, Chen L-T, Okusaka T, Vogel A, et al. Durvalumab plus gemcitabine and cisplatin in advanced biliary tract cancer. *NEJM Evid*. (2022) 1: EVIDoa2200015. doi: 10.1056/EVIDoa2200015

58. Oh D-Y, He AR, Bouattour M, Okusaka T, Qin S, Chen L-T, et al. Durvalumab or placebo plus gemcitabine and cisplatin in participants with advanced biliary tract cancer (TOPAZ-1): updated overall survival from a randomised phase 3 study. *Lancet Gastroenterol Hepatol*. (2024) 9:694–704. doi: 10.1016/S2468-1253(24)00095-5

59. Kelley RK, Ueno M, Yoo C, Finn RS, Furuse J, Ren Z, et al. Pembrolizumab in combination with gemcitabine and cisplatin compared with gemcitabine and cisplatin alone for patients with advanced biliary tract cancer (KEYNOTE-966): a randomised, double-blind, placebo-controlled, phase 3 trial. *Lancet*. (2023) 401:1853–65. doi: 10.1016/S0140-6736(23)00727-4

60. Klein O, Kee D, Nagrial A, Markman B, Underhill C, Michael M, et al. Evaluation of combination nivolumab and ipilimumab immunotherapy in patients with advanced biliary tract cancers: subgroup analysis of a phase 2 nonrandomized clinical trial. *JAMA Oncol*. (2020) 6:1405–9. doi: 10.1001/jamaoncol.2020.2814

61. Sahai V, Griffith KA, Beg MS, Shaib WL, Mahalingam D, Zhen DB, et al. A randomized phase 2 trial of nivolumab, gemcitabine, and cisplatin or nivolumab and ipilimumab in previously untreated advanced biliary cancer: BilT-01. *Cancer*. (2022) 128:3523–30. doi: 10.1002/cncr.34394

62. Markussen A, Johansen JS, Larsen FO, Theile S, Hasselby JP, Willemoe GL, et al. Nivolumab with or without ipilimumab combined with stereotactic body radiotherapy in patients with metastatic biliary tract cancer: A randomized phase 2 study. *Clin Cancer Res*. (2024) 30:3428–37. doi: 10.1158/1078-0432.CCR-24-0286

63. Chen X, Qin S, Gu S, Ren Z, Chen Z, Xiong J, et al. Camrelizumab plus oxaliplatin-based chemotherapy as first-line therapy for advanced biliary tract cancer: A multicenter, phase 2 trial. *Int J Cancer*. (2021) 149:1944–54. doi: 10.1002/ijc.33751

64. Li X, Zhou N, Yang Y, Lu Z, Gou H. Efficacy and biomarker analysis of second-line nab-paclitaxel plus sintilimab in patients with advanced biliary tract cancer. *Cancer Sci*. (2024) 115:2371–83. doi: 10.1111/cas.16179

65. Bizama C, García P, Espinoza JA, Weber H, Leal P, Nervi B, et al. Targeting specific molecular pathways holds promise for advanced gallbladder cancer therapy. *Cancer Treat Rev*. (2015) 41:222–34. doi: 10.1016/j.ctrv.2015.01.003

66. Lee CK, Chon HJ, Cheon J, Lee MA, Im HS, Jang JS, et al. Trastuzumab plus FOLFOX for HER2-positive biliary tract cancer refractory to gemcitabine and cisplatin: a multi-institutional phase 2 trial of the Korean Cancer Study Group (KCSG-HB19-14). *Lancet Gastroenterol Hepatol*. (2023) 8:56–65. doi: 10.1016/s2468-1253(22)00335-1

67. Feng Y, Su W, Oh D, Shen L, Kim L, Liu X, et al. Updated analysis with longer follow up of a phase 2a study evaluating erdafitinib in Asian patients (pts) with advanced cholangiocarcinoma (CCA) and fibroblast growth factor receptor (FGFR) alterations. *J Clin Oncol*. (2022) 40:430–0. doi: 10.1200/JCO.2022.40.4_suppl.430

68. Tan D, An J, Gong M, Wang H, Li H, Meng H, et al. Screening of an individualized treatment strategy for an advanced gallbladder cancer using patient-derived tumor xenograft and organoid models. *Front Oncol*. (2022) 12:1043479. doi: 10.3389/fonc.2022.1043479

69. Mao W, Deng F, Wang D, Gao L, Shi X. Treatment of advanced gallbladder cancer: A SEER-based study. *Cancer Med*. (2020) 9:141–50. doi: 10.1002/cam4.2679

70. Zhu J, Wu Y, Xiao W, Li Y. Survival predictors of resectable gallbladder carcinoma: an analysis of the surveillance, epidemiology, and end results database. *Am surgeon*. (2023) 89. doi: 10.1177/00031348221074238

frontiers | Frontiers in Oncology

TYPE Study Protocol
PUBLISHED 03 December 2024
DOI 10.3389/fonc.2024.1467517

Check for updates

OPEN ACCESS

EDITED BY
Qingyu Luo,
Dana–Farber Cancer Institute, United States

REVIEWED BY
Armel Hervé Nwabo Kamdje,
Université de Garou, Cameroon
Hong Yu,
The University of Texas Health Science Center at San Antonio, United States

*CORRESPONDENCE
Yanjun Lian
lianalian@163.com

RECEIVED 20 July 2024
ACCEPTED 28 October 2024
PUBLISHED 03 December 2024

CITATION
Ma J, Zhen J, Yang N, Meng C and Lian Y (2024) Expression and clinical significance of Numb and Notch-1 proteins between tissue of colon cancer and regional lymph node metastases.
Front. Oncol. 14:1467517.
doi: 10.3389/fonc.2024.1467517

COPYRIGHT
© 2024 Ma, Zhen, Yang, Meng and Lian. This is an open-access article distributed under the terms of the Creative Commons Attribution License (CC BY). The use, distribution or reproduction in other forums is permitted, provided the original author(s) and the copyright owner(s) are credited and that the original publication in this journal is cited, in accordance with accepted academic practice. No use, distribution or reproduction is permitted which does not comply with these terms.

Expression and clinical significance of Numb and Notch-1 proteins between tissue of colon cancer and regional lymph node metastases

Jingyou Ma, Jinpeng Zhen, Ningbao Yang, Changjuan Meng and Yanjun Lian*

The Gastrointestinal Surgery of Xingtai Central Hospital, Xingtai, Hebei, China

Objective: To investigate the expression and clinical significance of Notch-1 and Numb protein in colon cancer tissues and regional lymph node metastases.

Methods: Immunohistochemical method was used to detect the expression of Notch-1 protein and Numb protein in 110 cases of colon cancer tissues, along with tumor adjacent tissues and 56 cases of MLN tissues, and to analyze its role in colon cancer and MLN tissue.

Results: Comparing colon cancer tissue or lymph node metastases with tumor adjacent tissue, the positive expression rate of Numb was significantly decreased, while the positive expression of Notch-1 was significantly increased in colon cancer tissue or lymph node metastases (both $p<0.05$). The expression of Notch-1 and Numb was correlated with the lymph node metastasis, TNM stage, and degree of differentiation ($p<0.05$). The expression between Numb and Notch-1 showed negative correlation in colon cancer tissues ($r=-0.261$, $p<0.05$). There was no relationship between the expression of Numb and Notch-1 protein in colon cancer and metastatic lymph node tissue ($p>0.05$).

Conclusion: Numb expression is decreased and Notch-1 expression is increased in colon cancer tissue and metastatic lymph node tissue, suggesting that the interaction between the two proteins may play a promote role in the development, invasion, and metastasis of colon cancer. There was no relationship between the expression of Numb and Notch-1 protein in colon cancer and metastatic lymph node tissue, suggesting that there is no obvious enhancement of the cancer cells; in the process of lymph node metastasis, the degree of malignant biological behavior remains relatively stable.

KEYWORDS

colon cancer tissue, metastatic lymph node tissue, tumor adjacent tissue, Notch-1 protein, Numb protein

Introduction

In recent years, the incidence of colon cancer is increasing gradually, and colon cancer has heterogeneity, which requires individualized treatment plan, so personalized treatment has become a new trend in the field of cancer treatment. The key of personalized therapy lies in the high selectivity of tumor targets, and the selection of targeted drugs with good effect and light side effects has become a research hotspot. Molecular targeted therapy can effectively improve the prognosis of cancer patients, improve the survival rate of patients, and become another new method in addition to surgical resection, radiotherapy, and chemotherapy, providing a new treatment for colon cancer patients. Notch-1 protein is involved in cell proliferation, differentiation, apoptosis, etc. (1, 2). The abnormal transmission of Notch-1 signaling pathway may be related to the occurrence of tumors (3). Numb is known as the fate determinant of cell differentiation and can influence cell differentiation in a variety of ways. The role of Numb in the Notch signaling pathway has become the focus of current research (4, 5). It has been suggested that Numb may inhibit the invasion and metastasis of melanoma by regulating NOTCH-CCNE axis, and upregulation Numb inhibitors may play a role in the treatment of melanoma (6). By detecting the expression of Notch-1 protein and Numb protein in colon cancer and MLN, this study provides a possible theoretical basis for the occurrence, development, and metastasis of colon cancer. At the same time, Notch-1 and Numb are targeted to provide a possible molecular basis for the targeted therapy and prognosis of colon cancer.

Data and methods

General information

A total of 110 carcinoma tissues and adjacent carcinoma tissues of patients with colon cancer who had surgery in the gastrointestinal surgery of Xingtai Central Hospital in China during October 2019–October 2022 were selected. A total of 56 regional lymph node metastases tissues were selected as samples among the above cases. Of the 110 cases of colon cancer patients, 57 cases were men, 53 cases were women, ages were 41–83 years old, with an average age of 67 years old, and 44 cases were in stage I+II and 66 cases were in stage III+IV. There were 68 cases with tumor diameter ≤5 cm and 42 cases with tumor diameter >5 cm. None of the selected cases received neoadjuvant therapy before surgery and had no intestinal obstruction before surgery. All specimens were treated with radical resection of colon cancer and were pathologically diagnosed as colonic adenocarcinoma.

Reagent

Numb polyclonal antibody and Notch-1 polyclonal antibody are bought from Proteintech Group, Inc. (Wuhan, Hubei, China).; the kit and citric acid antigen repair reagents were bought from Beijing Zhong Shan -Golden Bridge Biological Technology CO., LTD (Beijing, China).

Method

Using the immunohistochemical SP method, the specimens were made of biopsies that were 4 μm, fully hydrated after conventional xylene dewaxing, and repaired by citric acid antigen. Peroxidase is blocked by 3% hydrogen peroxide in each biopsy and incubated for 10 min at room temperature, and the serum was removed; Numb or Notch-1 primary polyclonal antibody is added to each biopsy as a fight and incubated for 90 min at room temperature. Each biopsy was incubated for 30 min at room temperature with the second antibody, added by streptomyces avidin peroxidase reagents, and colored in DAB microscope.

The result judgment standard

Numb is mainly expressed in the cytoplasm and cell membrane; the yellow particles mean positive cells. Notch-l protein is mainly expressed in the cytoplasm and the nucleus in tan particles; the color intensity of positive cell and the number of positive cells were judged based on the integral semi-quantitative method. Colorless, pale yellow, tan, and brown were marked by 0, 1, 2, and 3, respectively, according to positive staining intensity. Each biopsy was marked by the number of positive cells (0, 1, 2, 3, and 4 points mean <10%, 10%–10%, 26%–50%, 51%–70%, and >70%, respectively). Comprehensive score is equal to the product of two grades, 0 means negative, 1–4 means weakly positive, 5–8 means moderate positive, and >8 means strong positive. Negative and weakly positive scores are viewed as a negative expression; moderate positive and strong positive are viewed as positive expression.

Statistical processing

The SPSS 21.0 software was used for data analysis, where the significance of count data was compared by χ^2 test, and the expression correlation of Numb and Notch-1 proteins was analyzed by Spearman rank correlation. p-value <0.05 was considered to be statistically significant.

Results

The Numb and Notch-1 expression in different tissues

As shown in Table 1, in colon cancer and metastasis lymph node tissues, the positive expression rate of Numb was significantly lower than those in the adjacent normal tissue; the positive expression rate of Notch-1 was significantly higher than that in the adjacent normal tissue (Figure 1). The difference was statistically significant ($p < 0.05$). The positive expression rate of Numb or Notch-1 has no statistically significant difference between cancer and metastasis lymph node tissues ($p > 0.05$).

TABLE 1 The Numb and Notch-1 expression in different tissues.

group	*n*	Notch-1		Numb	
		positive	positive rate (%)	positive	positive rate (%)
Cancer tissues	110	71	64.55①	34	30.91④
Carcinoma Adjacent normal tissue	110	26	23.64②	69	62.73⑤
Metastatic lymph node tissue	56	39	69.64③	14	25.00⑥

comparison of each two in different organizations.
①and②: χ^2=37.340 p= 0.000 ①and③: χ^2=0.431 p= 0.511.
②and③: χ^2=32.968 p=0.000: ④and⑤: χ^2=22.363 p=0.000.
④and⑥: χ^2=0.630 p=0.427: ⑤and⑥: χ^2=21.127 p=0.000.

Clinicopathological factors according to the expression of Numb and Notch-1 protein in 110 patients with colon cancer

As shown in Table 2, the expression of Numb was significantly associated in colon cancer with the lymph node metastasis, TNM stage, and degree of differentiation ($p < 0.05$), not with age, gender, serous membrane invasion, and tumor size ($p > 0.05$). The expression of Notch-1 was significantly associated in colon cancer with the lymph node metastasis, TNM stage, and degree of differentiation ($p < 0.05$), not with age, gender, serous membrane invasion,and tumor size ($p > 0.05$).

Discussion

After the Notch ligand binds to corresponding receptors in the Notch signaling pathway, it causes the division and release of the Notch Intracellular Domain (NICD), acts on downstream target genes, and regulates cell development, proliferation, differentiation, and other activities (7, 8). Notch-1 signaling pathway is related to the occurrence, development, invasion, and metastasis of tumors. However, there are many unexplained factors that affect the Notch signaling pathway. Notch-1, as one of the important members of the Notch family, has gradually become a new trend in the study of colon cancer (9, 10). The most important feature of Numb is the regulation of cell differentiation through asymmetric allocation during mitosis and is therefore known as a determinant of cell fate, and these properties have important implications for the role of Numb in cell physiological development and various diseases (11, 12). Numb and Notch are antagonistic proteins in many literatures (13, 14). Studies have shown that in colorectal cancer, loss of Numb expression leads to abnormal activation of Notch signaling pathway, which is closely related to the occurrence and development of colon cancer (3). However, it has been suggested that different subtypes of Numb have different roles in tumors, with NUMB exon 12 (E12) hop isomer p65/p66 promoting

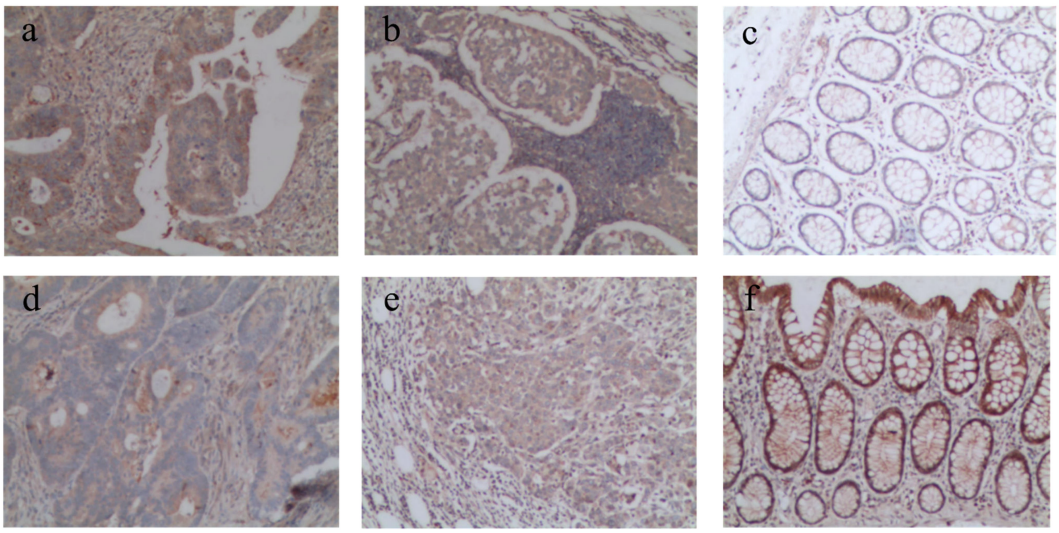

FIGURE 1
Immunohistochemical detection of Notch-1 protein and Numb protein expression in different tissues (SP × 100). **(A)** Notch-1 is highly expressed in cancer tissues; **(B)** Notch-1 is highly expressed in lymph node metastatic tissues; **(C)** Notch-1 is lowly expressed in tumor adjacent tissues; **(D)** Numb is lowly expressed in cancer tissues; **(E)** Numb is lowly expressed in lymph node metastatic tissues; **(F)** Numb is highly expressed in tumor adjacent tissues.

TABLE 2 Clinicopathological factors according to the expression of Numb and Notch-1 protein in 110 patients with colon cancer tissues.

Characteristics	*n*	Notch-1			Numb		
		positive	positive rate(%)	*p*	positive	Positive rate(%)	*p*
Age (years)							
≥65岁	87	52	59.77	0.212	26	29.89	0.651
<65岁	23	17	73.91		8	34.78	
Gender							
Male	57	39	68.42	0.378	16	28.07	0.504
Female	53	32	60.38		18	33.96	
Tumor size (cm)							
≤5 cm	68	40	58.82	0.110	24	35.29	0.205
>5 cm	42	31	73.81		10	23.81	
Serous membrane invasion							
Positive	67	46	68.66	0.261	17	25.37	0.117
Negative	43	25	58.14		17	39.53	
Lymph node metastasis							
Positive	66	52	78.79	<0.001	13	19.70	0.002
Negative	44	19	43.18		21	47.73	
TNM stage							
I–II	44	48	72.73	0.028	15	22.73	0.023
III–IV	66	23	52.27		19	43.18	
Differentiation							
Medium–high	61	46	75.41	0.008	12	19.67	0.004
Poor	49	25	51.02		22	44.90	

epithelial-to-mesenchymal transformation (EMT) and cancer cell migration *in vitro* and promoting cancer metastasis in mice; the p71/p72 isomer acts as a negative regulator of Notch-1 by ubiquitinating the Notch-1 intracellular domain (N1ICD) and promoting its degradation, and the NUMB isoform is considered to be a key regulator of EMT and cancer cell migration (15). In this study, the expression of Notch-1 protein and Numb protein in colon cancer tissues and MLN tissues was detected to analyze the relationship between the two proteins and clinical case factors, so as to provide a possible theoretical basis for finding molecular targets for colon cancer and predicting lymph node metastasis.

Notch signaling pathway promotes the occurrence and development of tumors in most cases but inhibits tumors in some cases. This opposite result may be caused by the different expression levels of Notch-1 protein in different tumor cells and different stages of tumor development (16, 17). This study showed that the expression of Notch-1 protein in colon cancer tissues was significantly higher than that in adjacent tissues ($p < 0.05$), suggesting that the high expression of Notch-1 leads to abnormal activation of Notch signaling pathway, which may be involved in the occurrence and development of colon cancer and play a role in promoting cancer, which is consistent with Xu et al. (18, 19). Many downstream target genes regulated by Notch-1 (such as *CyclinD1*, *Hes1*, *Bcl-2*, *NF-κB*, and *Hey-1*) are closely related to cell proliferation cycle and self-renewal (20, 21). Some studies have found that in mouse intestinal epithelial cells, the lack of Golgi membrane protein 1 causes abnormal activation of Notch, thus affecting the differentiation and maturation of intestinal epithelial cells, leading to the occurrence and development of malignant tumors. Inhibition of Notch abnormal expression by drugs can inhibit the tumor progression of intestinal epithelial cells lacking Golgi membrane protein-1, suggesting that Golgi membrane protein-1 prevents colon tumorigenesis by regulating Notch signaling pathway (22). The Schmidt EM study found that blocking Notch and MAPK signaling pathways by targeted drugs plays a regulatory role in the proliferation and plasticity of different colon cancer cell subsets (23). Pu described the role of newly developed drugs in the regulation of colon cancer by affecting the Notch signaling pathway (24). Therefore, the abnormal activation of Notch may affect the occurrence and development of tumors and also provide a certain theoretical basis for the targeted therapy of colon cancer.

In many cancer types, Numb acts as a tumor suppressor, and its downregulation leads to the development of tumors (3, 25). In this study, it was found that the expression of Numb in para-cancerous tissues was significantly higher than that in cancerous tissues and metastatic lymph nodes ($p<0.05$) and was related to the degree of tissue differentiation, presence or absence of lymph node metastasis, and TNM stage ($p<0.05$), but not related to tumor size and presence or absence of envelope invasion ($p>0.05$). It is suggested that Numb plays a cancer-suppressing role in colon cancer, which is consistent with Zhang et al. (26). Cheng et al. (27) showed that Numb can negatively regulate epithelial–mesenchymal transformation through Wnt signaling pathway, thus inhibiting the development of colorectal cancer, which is consistent with the results of this study. However, the downregulation of Numb expression is negatively correlated with the depth of invasion and tumor size, which is different from the results of this study. It is considered that Numb may be affected by multiple factors or play a role in the development of tumor through multiple signaling pathways. In lung adenocarcinoma, Numb inhibits Notch pathway and epithelial–mesenchymal transformation, inhibiting tumor growth, while in lung squamous cell carcinoma, Numb may promote tumor proliferation (28). Saha et al. (29) found in colon cancer that NUMB may play an important role in the bias effect of Wnt/Notch signaling crosstalk through KRT19. Zhang analyzed the role of Numb in tumor by searching literature with various software, suggesting that in colorectal cancer, NUMBL inhibits Notch pathway in colorectal tumor with unchanged NUMB expression, and the decrease in NUMBL expression leads to increased malignancies and poor prognosis (30). Because Numb has different subtypes and contains different domains, it may play a different role in different tumor tissues and play a cancer suppressor role in colorectal cancer.

Abnormal expression of Notch signaling pathway can affect cell differentiation and induce undifferentiated cells to turn to malignant cells, resulting in the occurrence of tumors, and the degree of differentiation of malignant tumors affects the prognosis of patients (31). In this study, it was found that the positive expression rate of Notch-1 was higher in colon cancer tissues with poor differentiation types ($p < 0.05$), suggesting that the expression of Notch-1 is related to the differentiation types of colon cancer and may be involved in cell differentiation, which is closely related to the occurrence and development of colon cancer.

Lymphatic duct metastasis is the main way of colon cancer recurrence and metastasis and also the key factor of postoperative recurrence of colon cancer (32, 33). The presence of regional lymph node metastasis and the number of metastatic lymph nodes are important determinants of prognosis in patients with colon cancer, so preoperative evaluation of lymph node metastasis is crucial (34). Jepsen used pT1 colorectal cancer with regional lymph node metastasis to investigate the association between the presence of miR-17/92 cluster and LNM, and the results suggested that early regional lymph node metastasis of colon cancer was associated with the high expression level of miR-17/92 cluster members (miR-17-3p, miR-92a) (35). Jiang (36) established a new cell line FDOVL from metastatic lymph nodes of patients with primary platinum-resistant ovarian cancer and found that NOTCH1-pC702fs mutation was only highly expressed in FDOVL cell lines and metastatic lymph nodes, and this mutation promoted the migration and invasion of tumor cells. These effects were significantly inhibited by NOTCH inhibitor LY3039478, suggesting that NOTCH1 mutation may be a driver of lymph node metastasis in ovarian cancer. This study found that the expression of Notch-1 protein in colon cancer tissues with lymph node metastasis was higher than that in colon cancer tissues without lymph node metastasis, suggesting that the overexpression of Notch-1 protein may promote lymph node metastasis of colon cancer. Gonulcu et al. (6) found that the expression status and expression level of Numb and lymph node metastasis and stage are significantly correlated with the survival of colorectal cancer patients. Cox regression analysis showed that lymph node metastasis and downregulation of Numb are independent prognostic factors of colon cancer. In this study, the downregulation of Numb expression is associated with lymph node metastasis in colon cancer tissues, suggesting that the downregulation of Numb expression may promote lymph node metastasis in colon cancer. Yang et al. (37) suggest the following: Numb controls the migration of epithelial cells by regulating intercellular connectivity, and the inhibition of the expression of Numb can promote the migration and invasion of colon cancer cells induced by TGF-β, upregulate the expression of EMT-related molecule Snail, inhibit the expression of E-cadherin, resulting in the destruction of intercellular links, and participate in the invasion and metastasis of colon cancer cells. Ulintz et al. (38) found that both the primary tumor region and the corresponding lymph node metastasis were polyclonal, and the clonal population of each lymph node was different. In some patients, clusters of cancer cells in specific lymph nodes originate from multiple different regions of the tumor. However, there was no significant difference in the expression of Notch-1 protein and Numb protein between colon cancer tissues and MLN tissues ($p>0.05$), suggesting that the malignancy degree of cancer cells did not improve significantly during lymph node metastasis and the biological behavior remained relatively stable. The study also found that poorly differentiated colon cancer patients had a high rate of lymph node metastasis, suggesting that poorly differentiated cancer cells were at high risk of lymph node metastasis. Therefore, in patients with colon cancer, no definite metastatic lymph nodes were found on preoperative imaging, while patients with poor tissue differentiation indicated by preoperative colonoscopy biopsy may be predicted to have a greater potential risk of lymph node metastasis, providing a possible theoretical basis for clinical preoperative staging and follow-up treatment.

The abnormal expression of Notch-1 protein and Numb protein may affect the differentiation degree of tumor cells and lymph node metastasis, thus promoting the occurrence, development, recurrence, and metastasis of colon cancer, providing a possible theoretical basis for exploring the biological behavior of colon cancer cells and targeted therapy. However, the mechanism of Notch-1 and Numb in the lymph node metastasis of colon cancer needs further study.

Author contributions

JM: Conceptualization, Data curation, Formal analysis, Investigation, Methodology, Project administration, Resources, Software, Supervision, Validation, Visualization, Writing – original draft, Writing – review & editing. JZ: Data curation, Formal analysis,

Resources, Writing – review & editing. NY: Conceptualization, Data curation, Resources, Writing – review & editing. CM: Data curation, Project administration, Resources, Software, Writing – original draft, Formal analysis, Writing – review & editing. YL: Funding acquisition, Investigation, Writing – review & editing, Project administration.

Funding

The author(s) declare financial support was received for the research, authorship, and/or publication of this article. This work was supported by the Xingtai City key research and development plan self-raised project (grant number: 2022ZC191).

Conflict of interest

The authors declare that the research was conducted in the absence of any commercial or financial relationships that could be construed as a potential conflict of interest.

Publisher's note

All claims expressed in this article are solely those of the authors and do not necessarily represent those of their affiliated organizations, or those of the publisher, the editors and the reviewers. Any product that may be evaluated in this article, or claim that may be made by its manufacturer, is not guaranteed or endorsed by the publisher.

References

1. Katoh M, Katoh M. Precision medicine for human cancers with Notch signaling dysregulation (Review). *Int J Mol Med*. (2020) 45:279–97. doi: 10.3892/ijmm.2019.4418

2. Pennarubia F, Ito A, Takeuchi M, Haltiwanger RS. Cancer-associated Notch receptor variants lead to O-fucosylation defects that deregulate Notch signaling. *J Biol Chem*. (2022) 298:102616. doi: 10.1016/j.jbc.2022.102616

3. Gonulcu SC, Unal B, Bassorgun IC, Ozcan M, Coskun HS, Elpek GO, et al. Expression of Notch pathway components (Numb, Itch, and Siah-1) in colorectal tumors: A clinicopathological study. *World J Gastroenterol*. (2020) 26:3814–33. doi: 10.3748/wjg.v26.i26.3814

4. Ortega-Campos SM, García-Heredia JM. The multitasker protein: A look at the multiple capabilities of NUMB. *Cells*. (2023) 12:333. doi: 10.3390/cells12020333

5. Zhu D, Xia J, Liu C, Fang C. Numb/Notch/PLK1 signaling pathway mediated hyperglycemic memory in pancreatic cancer cell radioresistance and the therapeutic effects of metformin. *Cell Signal*. (2022) 93:110268. doi: 10.1016/j.cellsig.2022.110268

6. Hristova DM, Fukumoto T, Takemori C, Gao L, Hua X, Wang JX, et al. NUMB as a therapeutic target for melanoma. *J Invest Dermatol*. (2022) 142:1882–92. doi: 10.1016/j.jid.2021.11.027

7. Shi F, Sun MH, Zhou Z, Wu L, Zhu Z, Xia SJ, et al. Tumor-associated macrophages in direct contact with prostate cancer cells promote Malignant proliferation and metastasis through NOTCH1 pathway. *Int J Biol Sci*. (2022) 18:5994–6007. doi: 10.7150/ijbs.73141

8. Mohamed SY, Kaf RM, Ahmed MM, Elwan A, Ashour HR, Ibrahim A, et al. The prognostic value of cancer stem cell markers (Notch1, ALDH1, and CD44) in primary colorectal carcinoma. *J Gastrointest Cancer*. (2019) 50:824–37. doi: 10.1007/s12029-018-0156-6

9. Dunkin D, Iuga AC, Mimouna S, Harris CL, Haure-Mirande JV, Bozec D, et al. Intestinal epithelial Notch-1 protects from colorectal mucinous adenocarcinoma. *Oncotarget*. (2018) 9:33536–48. doi: 10.18632/oncotarget.26086

10. Liao W, Li G, You Y, Wan H, Wu Q, Wang C, et al. Antitumor activity of Notch-1 inhibition in human colorectal carcinoma cells. *Oncol Rep*. (2018) 39:1063–71. doi: 10.3892/or.2017.6176

11. Choi HY, Seok J, Kang GH, Lim KM, Cho SG. The role of NUMB/NUMB isoforms in cancer stem cells. *BMB Rep*. (2021) 54:335–43. doi: 10.5483/BMBRep.2021.54.7.048

12. Huang C, Ji C, Wang J. Current thoughts on cellular functions of numb-associated kinases. *Mol Biol Rep*. (2023) 50:4645–52. doi: 10.1007/s11033-023-08372-x

13. Luo Z, Mu L, Zheng Y, Shen W, Li J, Xu L, et al. NUMB enhances Notch signaling by repressing ubiquitination of NOTCH1 intracellular domain. *J Mol Cell Biol*. (2020) 12:345–58. doi: 10.1093/jmcb/mjz088

14. Kim H, Ronai ZA. Rewired Notch/p53 by Numb'ing Mdm2. *J Cell Biol*. (2018) 217:445–6. doi: 10.1083/jcb.201712007

15. Zhan Z, Yuan N, You X, Meng K, Sha R, Wang Z, et al. Exclusion of NUMB exon12 controls cancer cell migration through regulation of notch1-SMAD3 crosstalk. *Int J Mol Sci*. (2022) 23:4363. doi: 10.3390/ijms23084363

16. Singh AK, Shuaib M, Prajapati KS, Prajapati KS, Kumar S. Rutin potentially binds the gamma secretase catalytic site, down regulates the notch signaling pathway and reduces sphere formation in colonospheres. *Metabolites*. (2022) 12:926. doi: 10.3390/metabo12100926

17. Aster JC, Pear WS, Blacklow SC. The varied roles of notch in cancer. *Annu Rev Pathol*. (2017) 12:245–75. doi: 10.1146/annurev-pathol-052016-100127

18. Xu K, Shen K, Liang X, Li Y, Nagao N, Li J, et al. MiR-139-5p reverses CD44+/CD133+-associated multidrug resistance by downregulating NOTCH1 in colorectal carcinoma cells. *Oncotarget*. (2016) 7:75118–29. doi: 10.18632/oncotarget.12611

19. Tyagi A, Sharma AK, Damodaran C. A review on notch signaling and colorectal cancer. *Cells*. (2020) 9:1549. doi: 10.3390/cells9061549

20. Emam O, Wasfey EF, Hamdy NM. Notch-associated lncRNAs profiling circuiting epigenetic modification in colorectal cancer. *Cancer Cell Int*. (2022) 22:316. doi: 10.1186/s12935-022-02736-2

21. Xia R, Xu M, Yang J, Ma X. The role of Hedgehog and Notch signaling pathway in cancer. *Mol Biomed*. (2022) 3:44. doi: 10.1186/s43556-022-00099-8

22. Pu Y, Song Y, Zhang M, Long CF, Li J, Wang Y, et al. GOLM1 restricts colitis and colon tumorigenesis by ensuring Notch signaling equilibrium in intestinal homeostasis. *Signal Transduct Target Ther*. (2021) 6:148. doi: 10.1038/s41392-021-00535-1

23. Schmidt EM, Lamprecht S, Blaj C, Schaaf C, Krebs S, Blum H, et al. Targeting tumor cell plasticity by combined inhibition of NOTCH and MAPK signaling in colon cancer. *J Exp Med*. (2018) 215:1693–708. doi: 10.1084/jem.20171455

24. Pu Z, Yang F, Wang L, Diao Y, Chen D. Advancements of compounds targeting Wnt and Notch signalling pathways in the treatment of inflammatory bowel disease and colon cancer. *J Drug Targeting*. (2021) 29:507–19. doi: 10.1080/1061186X.2020.1864741

25. Zhang H, Qi S, Liu Z, Li CY, Li MJ, Zhao XB. Melatonin inhibits 17β-estradiol-induced epithelial-mesenchymal transition in endometrial adenocarcinoma cells via upregulating numb expression. *Gynecol Obstet Invest*. (2022) 87:89–99. doi: 10.1159/000522170

26. Zhang H, Ye Y, Zhou J. Relationship between p53 gene mutation and Numb protein expression and clinicopathological features and prognosis of colorectal cancer. *Chin J Gen Surg*. (2022) 37:122–6. doi: 10.3760/cma.j.cn113855-20210920-00561

27. Cheng C, Huang Z, Zhou R, An H, Cao G, Ye J, et al. Numb negatively regulates the epithelial-to-mesenchymal transition in colorectal cancer through the Wnt signaling pathway. *Am J Physiol Gastrointest Liver Physiol*. (2020) 318:G841–53. doi: 10.1152/ajpgi.00178.2019

28. Kikuchi H, Sakakibara-Konishi J, Furuta M, Kikuchi E, Kikuchi J, Oizumi S, et al. Numb has distinct function in lung adenocarcinoma and squamous cell carcinoma. *Oncotarget*. (2018) 9:29379–91. doi: 10.18632/oncotarget.25585

29. Saha SK, Yin Y, Chae HS, Cho SG. Opposing regulation of cancer properties via KRT19-mediated differential modulation of wnt/β-catenin/notch signaling in breast and colon cancers. *Cancers (Basel)*. (2019) 11:99. doi: 10.3390/cancers11010099

30. Zhang Y, Yang H, Liu W, Song Q, Li Y, Zhang JJ. Comprehensive pan-cancer analysis of expression profiles and prognostic significance for NUMB and NUMBL in human tumors. *Med (Baltimore)*. (2023) 102:e34717. doi: 10.1097/MD.0000000000034717

31. Misiorek JO, Przybyszewska-Podstawka A, Kałafut J, Paziewska B, Rolle K, Rivero-Müller A, et al. Context matters: NOTCH signatures and pathway in cancer progression and metastasis. *Cells*. (2021) 10:94. doi: 10.3390/cells10010094

32. Kudo SE, Ichimasa K, Villard B, Mori Y, Misawa M, Saito S, et al. Artificial intelligence system to determine risk of T1 colorectal cancer metastasis to lymph node. *Gastroenterology*. (2021) 160:1075–84. doi: 10.1053/j.gastro.2020.09.027

33. Hartwig MF, Slumstrup L, Fiehn AK, Gögenur I. The risk of lymph node metastasis in patients with T2 colon cancer. *Colorectal Dis*. (2023) 25:853–60. doi: 10.1111/codi.16485

34. Polack M, Hagenaars SC, Couwenberg A, Kool W, Tollenaar RAEM, Vogel WV, et al. Characteristics of tumour stroma in regional lymph node metastases in colorectal cancer patients: a theoretical framework for future diagnostic imaging with FAPI PET/CT. *Clin Transl Oncol*. (2022) 24:1776–84. doi: 10.1007/s12094-022-02832-9

35. Jepsen RK, Novotny GW, Klarskov LL. et al.Early metastatic colorectal cancers show increased tissue expression of miR-17/92 cluster members in the invasive tumor front. *Hum Pathol*. (2018) 80:231–8. doi: 10.1016/j.humpath.2018.05.027

36. Jiang W, Ouyang X, Jiang C, Yin L, Yao Q, Pei X, et al. A NOTCH1 mutation found in a newly established ovarian cancer cell line (FDOVL) promotes lymph node metastasis in ovarian cancer. *Int J Mol Sci*. (2023) 24:5091. doi: 10.3390/ijms24065091

37. Yang Y, Li L, He H, Shi M, He L, Liang S, et al. Numb inhibits migration and promotes proliferation of colon cancer cells via RhoA/ROCK signaling pathway repression. *Exp Cell Res*. (2022) 411:113004. doi: 10.1016/j.yexcr.2021.113004

38. Ulintz PJ, Greenson JK, Wu R, Fearon ER, Hardiman KM. Lymph node metastases in colon cancer are polyclonal. *Clin Cancer Res*. (2018) 24:2214–24. doi: 10.1158/1078-0432.CCR-17-1425

frontiers | Frontiers in Oncology

TYPE Original Research
PUBLISHED 19 December 2024
DOI 10.3389/fonc.2024.1501981

Check for updates

OPEN ACCESS

EDITED BY
Qingyu Luo,
Dana–Farber Cancer Institute, United States

REVIEWED BY
Yang Li,
Baylor College of Medicine, United States
Xiaowei Wu,
Dana–Farber Cancer Institute, United States
Hong Yu,
The University of Texas Health Science Center at San Antonio, United States

*CORRESPONDENCE
Feng He
85453001@qq.com
Jun Li
84183967@qq.com

†These authors have contributed equally to this work

RECEIVED 26 September 2024
ACCEPTED 25 November 2024
PUBLISHED 19 December 2024

CITATION
Huang H, Yang Y, Wang X, Wen B, Yang X, Zhong W, Wang Q, He F and Li J (2024) Gut virome dysbiosis impairs antitumor immunity and reduces 5-fluorouracil treatment efficacy for colorectal cancer. *Front. Oncol.* 14:1501981. doi: 10.3389/fonc.2024.1501981

COPYRIGHT
© 2024 Huang, Yang, Wang, Wen, Yang, Zhong, Wang, He and Li. This is an open-access article distributed under the terms of the Creative Commons Attribution License (CC BY). The use, distribution or reproduction in other forums is permitted, provided the original author(s) and the copyright owner(s) are credited and that the original publication in this journal is cited, in accordance with accepted academic practice. No use, distribution or reproduction is permitted which does not comply with these terms.

Gut virome dysbiosis impairs antitumor immunity and reduces 5-fluorouracil treatment efficacy for colorectal cancer

Hui Huang[1,2†], Ying Yang[3†], Xiaojiao Wang[1,2], Biao Wen[1,2], Xianglan Yang[4], Wei Zhong[1,2], Qiurong Wang[1,2], Feng He[1,2*] and Jun Li[1,2*]

[1]Department of Clinical Medicine, Chengdu Medical College, Chengdu, Sichuan, China, [2]Department of Gastroenterology, First Affiliated Hospital of Chengdu Medical College, Chengdu, Sichuan, China, [3]Department of Gastroenterology, Fifth People's Hospital of Sichuan Province, Chengdu, Sichuan, China, [4]First Affiliated Hospital of Chengdu Medical College, Pengzhou Second People's Hospital, Chengdu, China

Introduction: Despite the established influence of gut bacteria, the role of the gut virome in modulating colorectal cancer (CRC) patient chemotherapy response remains poorly understood. In this study, we investigated the impact of antiviral (AV) drug-induced gut virome dysbiosis on the efficacy of 5-FU in CRC treatment.

Methods: Using a subcutaneous CRC mouse model, we assessed tumor growth and immune responses following AV treatment, fecal microbiota transplantation (FMT), and 5-FU administration.

Results: AV therapy reduced the abundance of gut DNA and RNA viruses, leading to accelerated tumor growth, shortened survival, and diminished chemotherapy efficacy. FMT restored the gut virome, improving tumor suppression and extending the survival of 5-FU-treated mice. Metagenomic sequencing revealed significant changes in virome composition, AV treatment expanded *Kahnovirus*, *Petivirales*, and *Enterogokushovirus*, whereas FMT enriched *Peduovirus STYP1*, *Mahlunavirus rarus*, and *Jouyvirus ev207*. AV treatment reduced the number of dendritic cells and CD8+ T cells in peripheral blood and tumor tissues, impairing antitumor immunity, FMT reversed these deficiencies. To further investigate the underlying mechanisms, we examined the TLR3-IRF3-IFN-β pathway, essential for recognizing viral RNA and triggering immune responses. AV treatment downregulated this pathway, impairing immune cell recruitment and reducing chemotherapy efficacy, while activation of TLR3 with Poly(I:C) restored pathway function and enhanced the effectiveness of 5-FU.

Discussion: These findings suggest the importance of maintaining gut virome integrity or activating TLR3 as adjunct strategies to enhance chemotherapy outcomes in CRC patients.

KEYWORDS

colorectal cancer, 5-fluorouracil, gut virome, fecal microbiota transplantation, immune response

1 Introduction

Colorectal cancer (CRC) is one of the most common malignant tumors of the digestive tract. According to statistics, over 1.9 million new cases of colorectal cancer arise worldwide each year and approximately 935,000 deaths occur, accounting for one-tenth of all cancer-related deaths (1). Surgical resection is curative for most early-stage patients, but chemotherapy remains the most common treatment modality for patients with advanced-stage colon cancer. The first-line clinical chemotherapy regimen is traditional 5-fluorouracil (5-FU)-based therapy. 5-FU is a cytotoxic drug that targets thymidylate synthase, thereby inducing double-stranded RNA and DNA breaks, causing cell cycle arrest and apoptosis and subsequently inhibiting cancer cell growth (2). However, the treatment efficacy of 5-FU in advanced colon cancer patients is only 10% to 15%, and recurrence rates of up to 30% in stage I-III patients and up to 65% in stage IV patients occur after chemotherapy (3, 4). Therefore, improving the efficacy of chemotherapy for treating CRC has become a critical clinical issue.

The human gut microbiome comprises bacteria, viruses, fungi, archaea, and parasites, and the total number of these cells usually exceeds that of the host cells (5). Homeostasis of the gut microbiome is considered beneficial for health; however, gut microbiota dysbiosis poses a threat to host health and can lead to various diseases, including inflammatory bowel disease, chronic liver disease, obesity, diabetes, hypertension, etc. (6). Studies have shown that gut bacteria are closely related to the occurrence and development of CRC and can modulate the antitumor response to chemotherapeutic drugs. In animal experiments, administration of a mixture of antibiotics, including vancomycin, imipenem, and neomycin, to deplete the gut microbiota impaired the anticancer effects of the cytotoxic drugs oxaliplatin and cisplatin in CT26 subcutaneous tumor-bearing mice (7). Furthermore, the use of antibiotics in patients with metastatic CRC before starting 5-FU-based chemotherapy is associated with shorter progression-free survival and overall survival (8).

In addition to gut bacteria, gut viruses are also important components of the gut microbiome. The human gut virome is primarily composed of bacteriophages, eukaryotic viruses, archaeal viruses, and endogenous retroviruses. Given that commensal viruses participate in host immune development and maturation, dysbiosis of these viruses may be closely associated with CRC (9). Studies have revealed that the gut viromes of CRC patients are altered compared with those of healthy subjects, with enrichment of several genera, including *Orthobunyavirus*, *Inovirus*, and *Tunalikevirus*, and that the composition of the gut virome is closely related to CRC stage and prognosis (10). In addition, multiple studies have shown that human papillomavirus (HPV), cytomegalovirus (CMV), and human polyomavirus 2 (JCV) may be associated with an increased incidence of CRC (11). Gogokhia et al. reported that a tail-shaped bacteriophage isolated from patients with active ulcerative colitis inhibited the growth of carcinogenic adherent-invasive *Escherichia coli* and suppressed intestinal tumor growth in a mouse model (12). To date, no consistent conclusion has been reached regarding the role of gut viruses in the occurrence and development of CRC. Moreover, studies regarding whether gut viruses affect the efficacy of chemotherapy for CRC treatment have not been reported. Therefore, in this study we aimed to investigate the impact of gut viruses in conjunction with 5-FU treatment on antitumor efficacy in patients with CRC.

Our study revealed that administration of an antiviral cocktail therapy including ribavirin (10 mg/kg), lamivudine (30 mg/kg), and acyclovir (20 mg/kg) induced gut virome dysbiosis, which promoted CRC growth in mice and reduced the antitumor effects of 5-FU. Furthermore, depletion of the gut virome significantly reduced the number of dendritic cells (DCs) and CD8+ T cells in peripheral blood and tumor tissues, whereas no significant difference was observed in the number of CD4+ T cells. The restoration of the gut microbiota through fecal microbiota transplantation (FMT) inhibited the progression of CRC and reversed the weakened antitumor effect of 5-FU. Moreover, the numbers of DCs and CD8+ T cells in the peripheral blood and tumor tissues were significantly increased. To further investigate the mechanistic underpinnings of gut virome involvement, we analyzed the TLR3-IRF3-IFN-β signaling pathway, which plays a crucial role in innate immunity by recognizing viral RNA and initiating an immune response. We hypothesized that antiviral treatment would downregulate this pathway, thus impairing immune cell recruitment and weakening the efficacy of 5-FU chemotherapy. In addition, we explored whether the TLR3 agonist Poly(I:C) could restore this pathway's activity and enhance the therapeutic effects of 5-FU. This work helps to fill the research gap regarding the effects of gut viruses on the efficacy of chemotherapy for CRC treatment and further enhances our understanding of the relationship between the gut microbiome and tumor treatment, thereby improving the efficacy of antitumor drugs to benefit CRC patients.

2 Materials and methods

2.1 Subjects and sample collection

This study was approved by the Ethics Committee of the First Affiliated Hospital of Chengdu Medical College (2024CYFYIRB-BA-Jul17), and informed consent was obtained from all participants prior to their inclusion in the study. A total of 10 CRC patients meeting the inclusion criteria were recruited between January 2023 and June 2024, including 4 males and 6 females, aged 45 to 64. Fresh fecal samples were collected before and after 2 cycles of chemotherapy (The chemotherapy regimen consists of oxaliplatin combined with leucovorin and fluorouracil), stored at -80°C, and subsequently analyzed via metagenomic sequencing. Tumor size was assessed by imaging (CT or MRI) before and after chemotherapy according to RECIST 1.1 criteria, and its correlation with changes in the gut virome was analyzed.

2.2 Drugs and cell lines

5-FU, ribavirin, lamivudine, and acyclovir were purchased from MedChemExpress (USA). MC38 mouse colon cancer cells were obtained from West China Hospital, Sichuan University (China).

2.3 Experimental design and grouping

Throughout the experiment, internationally recognized animal experimentation guidelines were followed, and all animal experiments were approved by the Animal Experiment Ethics Committee of Chengdu Medical College (2022CYA-003). A total of 40 female C57BL/6 mice, aged 6-8 weeks and weighing 19.7 ± 2 g, were purchased from Chengdu Dashuo Experimental Animal Co., Ltd. The mice were housed under specific pathogen-free (SPF) conditions with a 12-h light/dark cycle and were allowed free access to food and water. The mice were divided into different treatment groups: 1) Antiviral group (AV): received oral antiviral cocktail therapy including ribavirin (10 mg/kg), lamivudine (30 mg/kg), and acyclovir (20 mg/kg) for 10 consecutive days (13); 2) Nonantiviral group (V): received oral PBS for 10 consecutive days; 3) Antiviral + 5-FU group (AV+FU): received antiviral cocktail therapy combined with intraperitoneal injection of 5-FU (25 mg/kg) for 5 consecutive days; 4) Nonantiviral + 5-FU group (V+FU): received oral PBS combined with intraperitoneal injection of 5-FU (25 mg/kg); 5) Antiviral + FMT group (AV+FMT): received antiviral cocktail therapy combined with 200 μl of fresh fecal suspension orally; and 6) Antiviral + PBS group (AV+PBS): received antiviral cocktail therapy combined with 200 μl of PBS orally; 7) Antiviral + FMT + 5-FU group (AV+FMT+FU): received antiviral cocktail therapy, 200 μl of fresh fecal suspension orally, and intraperitoneal injection of 5-FU (25 mg/kg); 8) Antiviral + PBS + 5-FU group (AV+PBS+FU): received antiviral cocktail therapy, 200 μl of PBS orally, and intraperitoneal injection of 5-FU (25 mg/kg); 9) Poly group: received antiviral cocktail therapy, followed by intraperitoneal injections of 5-FU (25 mg/kg for 5 consecutive days) and the TLR3 agonist Poly(I:C) [10 μg/mouse, administered twice every 5 days until the endpoint (14)] after tumor appearance; and 10) no-Poly group: received antiviral cocktail therapy, followed by intraperitoneal injections of 5-FU (25 mg/kg for 5 consecutive days) and an equivalent volume of PBS (administered twice every 5 days until the endpoint) after tumor appearance. MC38 colon cancer cells were cultured in a humidified atmosphere of 5% CO2 at 37°C. To establish a mouse model of subcutaneous CRC tumors, tumor cells were diluted to 5×10^6 cells/ml and injected subcutaneously into the right axillae of C57BL/6 mice. Tumor size was monitored every 3 days, and the tumor volume (mm^3) was calculated as follows: (longest diameter) × (shortest diameter)^2/2. Tumor growth curves and survival curves were plotted. At the study endpoint, the mice were anesthetized with isoflurane via a gas anesthesia machine. Fecal, peripheral blood, and tumor tissue samples were collected, and the mice were euthanized.

2.4 Fecal microbiota transplantation

Fresh feces were collected from healthy donor mice. Approximately 1 g feces was placed in a 15 ml centrifuge tube, and 5 ml sterile 0.9% NaCl solution (37°C) was added. The mixture was homogenized, and the homogenate was centrifuged at 800 × g for 2 min. The supernatant was collected for FMT. FMT was performed every other day, with each mouse receiving 200 μl of fresh fecal suspension orally for 2 weeks.

2.5 VLP staining of fecal samples

Fresh fecal samples were collected from the mice after antiviral cocktail therapy or FMT treatment. A 0.5 g fecal sample was suspended in 10 ml 0.02 μm-filtered sterile magnesium salt buffer solution. The suspension was centrifuged at 2500 rpm for 10 min at 4°C, and the supernatant was filtered through 0.45 μm and 0.22 μm syringe filters to remove the cells. The filtrate was then diluted 10-fold and filtered through a 0.02 μm filter. The filter was stained with 10X SYBR Gold (Thermo, USA) and 10X SYBR Green II (Thermo, USA) for 15 min. After washing, the fluorescence was visualized under a microscope, and images were captured and quantified.

2.6 Metagenomic sequencing of fecal samples

Genomic DNA was extracted from the fecal samples using a HiPure Fecal DNA Kit (Magen, catalog number D3141) according to the manufacturer's instructions. The steps were as follows: (1) extraction and quality control of the fecal microbial metagenome, (2) random fragmentation of DNA, (3) construction of a standard DNA-seq library, (4) library quality control and quantification, and (5) HiSeq platform sequencing to obtain FastQ data.

2.7 Flow cytometry analysis of peripheral blood DC cells

Five microliters of anti-mouse CD11c antibody (Elabscience, catalog number AF10866) and 5 μL of anti-mouse MHC II antibody (Elabscience, catalog number AF11357) were added to 100 μL of noncoagulated mouse blood in a flow cytometry tube, mixed, and incubated on ice for 30 min. Red blood cells were lysed with 2 ml lysis buffer on ice for 10 min, and the suspension was subsequently centrifuged at 300 × g for 5 min. The supernatant was discarded, and the cells were washed with 2 ml PBS and centrifuged at 300 × g for 5 min. The cells were resuspended in 500 μl 1× flow cytometry staining buffer and analyzed by flow cytometry.

2.8 Flow cytometry analysis of peripheral blood CD4+ and CD8+ T cells

One hundred microliters of single-cell suspension was added to a flow cytometry tube, along with 5 μl anti-mouse CD4 antibody (Elabscience, catalog number AF15231) and 5 μl anti-mouse CD8a antibody (Elabscience, catalog number AF13226). The mixture was vortexed, incubated on ice for 30–60 min, and lysed with 2 ml 1× red blood cell lysis buffer. The cells were subsequently centrifuged at

300 × g for 5 min, washed with 2 ml PBS, and resuspended in 500 µl 1× flow cytometry staining buffer for flow cytometry analysis.

2.9 Immunohistochemistry

To assess immune cell infiltration in tumor tissues, IHC was performed to detect CD4, CD8, and CD11c expression. Frozen slides were placed in a 37°C oven for 10-20 min, fixed in paraformaldehyde for 30 min, and subjected to antigen retrieval in EDTA antigen retrieval buffer. The slides were blocked with 3% BSA, incubated overnight at 4°C with primary antibodies against CD4 (Cell Signaling Technology, catalog number 25229S), CD8α (Cell Signaling Technology, catalog number 98941S), and CD11c (Cell Signaling Technology, catalog number 97585), and then labeled with horseradish peroxidase (HRP) for visualization. Staining scores were determined based on the intensity and percentage of positively stained cells. The percentage of positive cells was categorized into four levels: 0 (<5% positive), 1 (<25% positive), 2 (25–50% positive), 3 (51–75% positive), and 4 (>75% positive). Staining intensity was rated as follows: 0 (no staining), 1 (weak staining), 2 (moderate staining), and 3 (strong staining). To ensure accurate representation, 10 fields per slide were randomly selected and examined at ×100 magnification, with an average score calculated to provide an overall expression level (15).

2.10 Western blot analysis

To evaluate the expression levels of TLR3, IRF3, p-IRF3, and IFN-β proteins, we performed Western blotting on tumor tissue samples. Protein was extracted using RIPA lysis buffer (Thermo Fisher Scientific, Cat# 89900), and protein concentration was determined with the BCA Protein Assay Kit (Beyotime, Cat# P0012). Equal amounts of protein were separated by SDS-PAGE and transferred onto a PVDF membrane (Millipore, Cat# IPVH00010). The membranes were blocked with 5% non-fat milk for 1 hour at room temperature. Primary antibodies used were TLR3 (Abcam, Cat# ab62566), IRF3 (Cell Signaling Technology, Cat# 4302), p-IRF3 (Cell Signaling Technology, Cat# 4947), and IFN-β (Thermo Fisher Scientific, Cat# PA5-20390), with β-Actin (Abcam, Cat# ab8226) as the loading control. Membranes were incubated with primary antibodies overnight at 4°C, followed by incubation with HRP-conjugated secondary antibodies (Abcam, Cat# ab97051) for 1 hour at room temperature. Bands were visualized using an ECL detection kit (Thermo Fisher Scientific, Cat# 32106), and band intensities were analyzed with ImageJ software.

2.11 Immunofluorescence analysis

Immunofluorescence staining was performed to assess the localization and expression of TLR3, p-IRF3, and IFN-β in tumor tissues. Tumor samples were fixed in 4% paraformaldehyde and embedded in paraffin. Following deparaffinization and rehydration, the sections were permeabilized with 0.3% Triton X-100 for 10 minutes, then blocked with 10% goat serum (Sigma-Aldrich, Cat# G9023) for 1 hour at room temperature. The sections were incubated overnight with primary antibodies for TLR3 (Abcam, Cat# ab62566), p-IRF3 (Thermo Fisher Scientific, Cat# PA5-105648), and IFN-β (Thermo Fisher Scientific, Cat# PA5-20390). The next day, sections were incubated with Alexa Fluor 488- or Alexa Fluor 594-conjugated secondary antibodies (Thermo Fisher Scientific, Cat# A-11001 for Alexa Fluor 488 and Cat# A-11012 for Alexa Fluor 594) for 1 hour at room temperature. DAPI (Beyotime, Cat# C1002) was used for nuclear staining. Images were captured with a fluorescence microscope, and fluorescence intensity was quantified using ImageJ software.

2.12 Statistical analysis

Statistical analysis was performed via GraphPad Prism 8.0.2 software. Quantitative data with a normal distribution are expressed as the means ± standard deviations (x ± s), and comparisons among three groups were performed via one-way ANOVA. Nonnormally distributed data were analyzed via the Kruskal-Wallis test. Chi-square tests were used to compare qualitative data between groups. Statistical significance was defined as $P<0.05$.

3 Results

3.1 Associations between the gut virome and chemotherapy efficacy in CRC patients

To investigate the association between the gut virome and chemotherapy efficacy in CRC patients, we collected fecal samples from 10 CRC patients before and after chemotherapy. The baseline characteristics of the patients are shown in Table 1. According to the RECIST 1.1 criteria for tumor assessment, these patients were divided into responders (stable disease in 4 patients, partial response in 1 patient) and nonresponders (disease progression in 5 patients). The sample groups were as follows: prechemotherapy nonresponders (P-NR), prechemotherapy responders (P-R), postchemotherapy nonresponders (Po-NR), and postchemotherapy responders (Po-R). The PLS-DA plot was generated based on the relative abundances of viral genera identified from fecal metagenomic sequencing data. The viral abundance matrix was normalized, log-transformed, and used as input for PLS-DA analysis to visualize the differences in gut virome composition among the sample groups. Figure 1A shows distinct clustering of viral communities among the sample groups. The P-R and P-NR groups clustered separately from the Po-R and Po-NR groups, indicating significant differences in viral composition before and after chemotherapy. Additionally, the viral communities in the P-R and Po-R groups were similar, indicating that the viral communities of the responders were relatively stable. The ACE index (Figure 1B) shows the α diversity across different sample groups. We found that the viral diversity of nonresponders before and after chemotherapy was greater than that of responders,

TABLE 1 Basic information of colorectal cancer patients.

Patient ID	Gender	Age	Cancer Stage	Chemotherapy Regimen	Comorbidities	ECOG Score
1	Male	55	III	FOLFOX (5-FU + Oxaliplatin)	Hypertension, Diabetes	1
2	Female	53	II	FOLFIRI (5-FU + Irinotecan)	None	0
3	Male	48	III	FOLFOX (5-FU + Oxaliplatin)	Coronary artery disease, Stroke	2
4	Male	60	III	FOLFOX (5-FU + Oxaliplatin)	Hyperlipidemia	1
5	Female	56	II	FOLFIRI (5-FU + Irinotecan)	None	0
6	Female	52	III	FOLFIRI (5-FU + Irinotecan) + Bevacizumab	Hyperthyroidism, Asthma	1
7	Male	64	IV	FOLFIRI (5-FU + Irinotecan) + Cetuximab	Hypertension, Chronic kidney disease	2
8	Female	58	II	FOLFOX (5-FU + Oxaliplatin)	Asthma, Osteoporosis	0
9	Female	45	III	FOLFOX (5-FU + Oxaliplatin)	None	0
10	Female	62	IV	FOLFOX (5-FU + Oxaliplatin) + Bevacizumab	Osteoporosis, Diabetes	2

ECOG, Eastern Cooperative Oncology Group performance status score was used to evaluate each patient's performance status at enrollment, ranging from 0 to 5. A score of 0 indicates the patient is fully active and can carry out all normal activities without restriction. 1 means the patient is ambulatory but restricted in strenuous activity, able to perform light work. 2 signifies the patient can perform all self-care tasks but is unable to engage in work activities and is up for more than 50% of their waking hours. 3 indicates the patient has limited self-care ability and is confined to a bed or chair for more than 50% of the day. 4 represents a completely disabled patient who cannot perform any self-care and is totally confined to a bed or chair. Finally, 5 represents death.

although the difference was not statistically significant. Additionally, there was no significant difference in viral diversity among CRC patients before and after chemotherapy, suggesting that chemotherapy has no significant impact on gut viral diversity.

Figure 1C illustrates the relative abundance of various viral taxa in different sample groups. There were notable differences in the viral taxon composition among the groups. The viral community in the P-NR group was highly diverse and was composed of genera

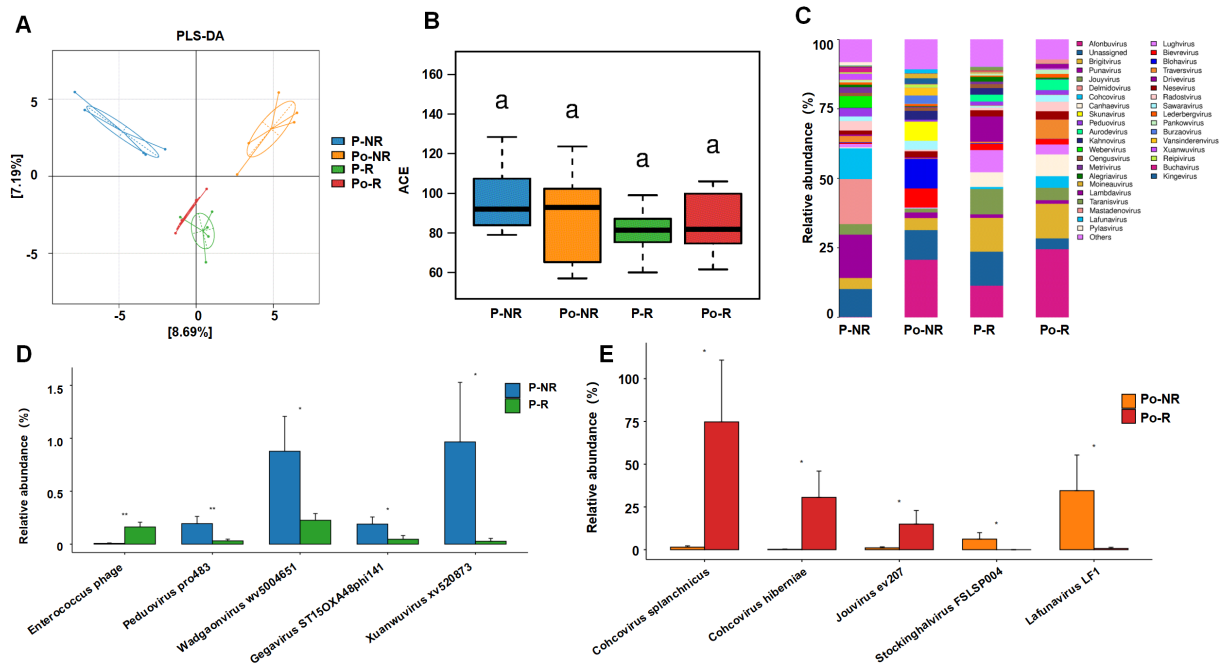

FIGURE 1
Associations between the gut virome and chemotherapy efficacy in CRC patients. **(A)** PLS-DA plot showing the clustering of viral communities in different sample groups (P-NR, Po-NR, P-R, and Po-R). **(B)** Box plot of ACE indices representing α diversity across different sample groups. Statistical significance is indicated by letters (a). **(C)** Stacked bar charts showing the relative abundance of various viral taxa in different sample groups. **(D)** Bar graphs comparing the relative abundance of specific viral species between the P-NR and P-R groups. **(E)** Bar graphs comparing the relative abundance of specific viral species between the Po-NR and Po-R groups. *, $P < 0.05$; **, $P < 0.01$.

such as *Punavirus*, *Delmidovirus*, and *Cohcovirus*. In the Po-NR group, the relative abundances of *Afonbuvirus* and *Brigitvirus* increased, whereas the abundance of *Punavirus* decreased, suggesting that chemotherapy may have promoted the expansion of certain viral genera. Compared with those in the P-NR group, the viral genera in the P-R group were dominated by *Afonbuvirus* and *Brigitvirus*, with lower abundances of *Punavirus* and *Delmidovirus*. In the Po-R group, the abundance of *Brightvirus* and *Ardovirus* increased, but the overall viral community structure changed little, indicating that the abundances of these viral genera remained relatively stable after chemotherapy. Further analysis of the significantly differentially abundant viral taxa before and after chemotherapy in nonresponders and responders revealed that, before chemotherapy, *Enterococcus phage* was significantly enriched in the P-R group, whereas *Peduovirus pro483*, *Wadgaonvirus wv5004651*, *Gegavirus ST15OXA48phi141*, and *Xuanwuvirus xv520873* were significantly enriched in the P-NR group (Figure 1D). After chemotherapy, *Cohcovirus splanchnicus*, *Cohcovirus hiberniae*, and *Jouyvirus ev207* were significantly enriched in the Po-R group, whereas *Stockinghalvirus FSLSP004* and *Lafunavirus LF1* were significantly enriched in the Po-NR group (Figure 1E). These findings suggest that certain viral taxa may be associated with differences in chemotherapy outcomes in patients with CRC. Observed variations in viral enrichment between responders and nonresponders, both before and after treatment, could offer preliminary insights into potential biomarkers for predicting chemotherapy responses. However, further investigation is needed to establish a direct relationship between these viral taxa and chemotherapy effectiveness.

3.2 Antiviral treatment impairs the efficacy of 5-FU treatment against colorectal tumors

To further investigate the impact of gut viruses on 5-FU treatment for CRC, we employed an antiviral cocktail therapy (ribavirin, lamivudine, and acyclovir) to eliminate gut viruses in mice. After establishing a subcutaneous xenograft model using MC38 mouse colon cancer cells, we treated the mice with 5-FU and observed tumor growth (Figure 2A). SYBR Gold staining (for DNA viruses) and SYBR Green II staining (for RNA viruses) were used to detect virus-like particles in feces to assess gut viral abundance. We observed a significant reduction in numbers of both DNA and RNA viruses after antiviral treatment compared with before treatment (Figure 2B). By comparing the tumor volumes and survival times between the antiviral group and the nonantiviral group, we found that by day 22, the tumor volumes in the antiviral group (AV) were significantly greater than those in the nonantiviral group (V) (Figure 2C), and the survival time in the antiviral group was significantly shorter than that in the nonantiviral group (Figure 2F). There were no significant differences in body weight changes among the groups throughout the experimental period (Figure 2D). These results indicate that antiviral treatment promotes colorectal tumor growth and decreases survival time in mice. Additionally, we assessed the effect of antiviral treatment on the chemotherapeutic efficacy of 5-FU treatment by comparing tumor size and survival time between mice in the AV+FU and V+FU groups. The tumor volume in the V+FU group was significantly smaller than that in the nonantiviral

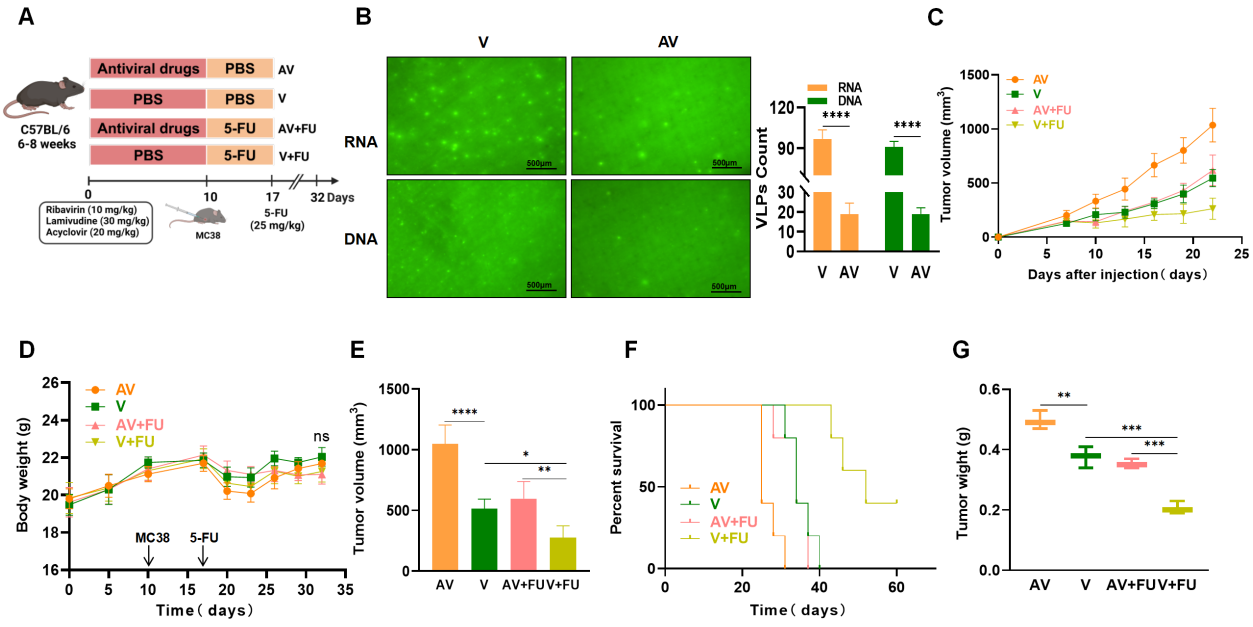

FIGURE 2
Antiviral (AV) treatment impairs the efficacy of 5-FU treatment against colorectal tumors. **(A)** Experimental design. **(B)** Fluorogram of DNA and RNA virus-like particle staining of mouse feces before and after AV treatment and quantification. Scale bar=500 μm. **(C)** Tumor volume progression over time in different treatment groups. **(D)** Changes in body weight over time in different treatment groups. **(E)** Comparison of final tumor volumes after 22 days among the different groups. **(F)** Survival rates of the mice in each treatment group over time. **(G)** Comparison of tumor weights among the groups. n=5. *, P < 0.05; **, P < 0.01; ***, P < 0.001; ****, P < 0.0001.

group by day 22 (Figures 2C, E), and the survival time was extended (Figure 2F), suggesting that 5-FU effectively inhibited colorectal tumor growth. However, the therapeutic effect of 5-FU was reduced following antiviral treatment. The tumor volume in the AV+FU group was significantly greater than that in the V+FU group by day 22 (Figure 2E), and the survival time was shorter (Figure 2F), indicating that antiviral treatment diminishes the inhibitory effect of 5-FU on colorectal tumor growth. Furthermore, the tumor weight in the V+FU group was significantly lower than that in the AV+FU group (Figure 2G). These findings further support that antiviral treatment promotes colorectal tumor growth in mice and diminishes the efficacy of 5-FU treatment.

3.3 FMT enhances the efficacy of 5-FU treatment against colorectal tumors

To verify whether AV treatment affects the efficacy of 5-FU by modulating the gut microbiota, all the mice were subjected to AV drug treatment to eliminate gut viruses. The mice in the AV + FMT + 5-FU group received FMT followed by that with 5-FU, whereas the mice in the AV + PBS + 5-FU group received PBS treatment followed by that with 5-FU (Figure 3A). We observed a significant increase in numbers of both intestinal DNA and RNA viruses following FMT compared with those in the AV group (Figure 3B). We compared the tumor volumes and survival times among the various treatment groups. The tumor volumes in the AV+PBS group mice were significantly greater than those in the AV+FMT group mice by day 22 (Figures 3C, E), suggesting that FMT can inhibit tumor growth. No significant differences in body weight changes were observed among the groups throughout the experimental period (Figure 3D). When 5-FU was administered, the tumor volumes in the AV+PBS+5-FU group mice were significantly greater than those in the AV+FMT+5-FU group mice (Figure 3E), indicating that FMT enhances the efficacy of 5-FU treatment. Survival analysis revealed that mice in the AV+FMT +5-FU group had longer survival times than those in the AV+PBS +5-FU group did (Figure 3F). Furthermore, the tumor weights in the AV+PBS group mice were significantly greater than those in the AV+FMT group mice, and the tumor weights in the AV+PBS+5-FU group mice were significantly greater than those in the AV +FMT+5-FU group mice (Figure 3G). These findings indicate that FMT enhances the inhibitory effect of 5-FU treatment on colorectal tumor growth in mice and extends survival time, suggesting that modulation of the gut microbiota can improve the efficacy of chemotherapy.

3.4 Impact of AV drugs on the gut microbiota

To study the impact of AV drugs and FMT on the gut virome, we conducted metagenomic sequencing analysis on fecal samples from mice after gut virus depletion or FMT. The PLS-DA plot (Figure 4A) shows distinct clustering of viral communities among the V+FU, AV+FU, AV+FMT+FU, and AV+PBS+FU groups, indicating significant differences in gut virome composition. α diversity analysis via the Chao1 index (Figure 4B) revealed that

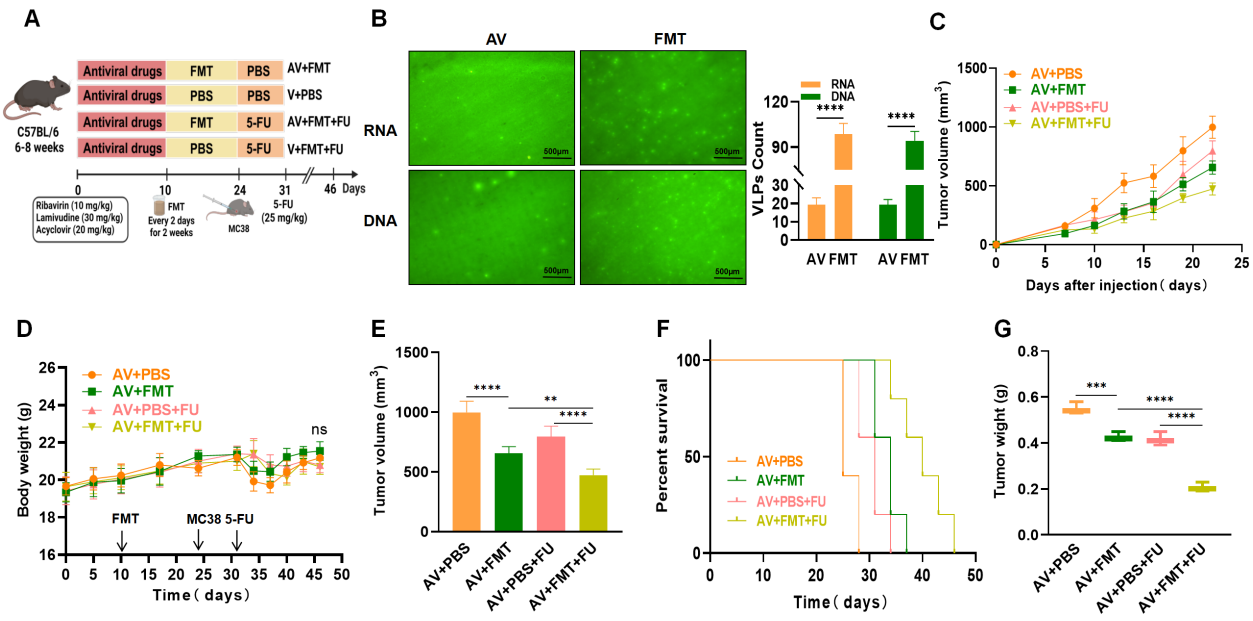

FIGURE 3
Fecal microbiota transplantation (FMT) enhances the efficacy of 5-FU treatment against colorectal tumors. **(A)** Experimental design. **(B)** Fluorogram of DNA and RNA virus-like particle staining of mouse feces before and after FMT and quantification. Scale bar=500 μm. **(C)** Tumor volume progression over time in different treatment groups. **(D)** Changes in body weight over time in different treatment groups. **(E)** Comparison of final tumor volume after 22 days among the different groups. **(F)** Survival rates of the mice in each treatment group over time. **(G)** Comparison of tumor weights among the groups. n=5. **, P < 0.01; ***, P < 0.001; ****, P < 0.0001.

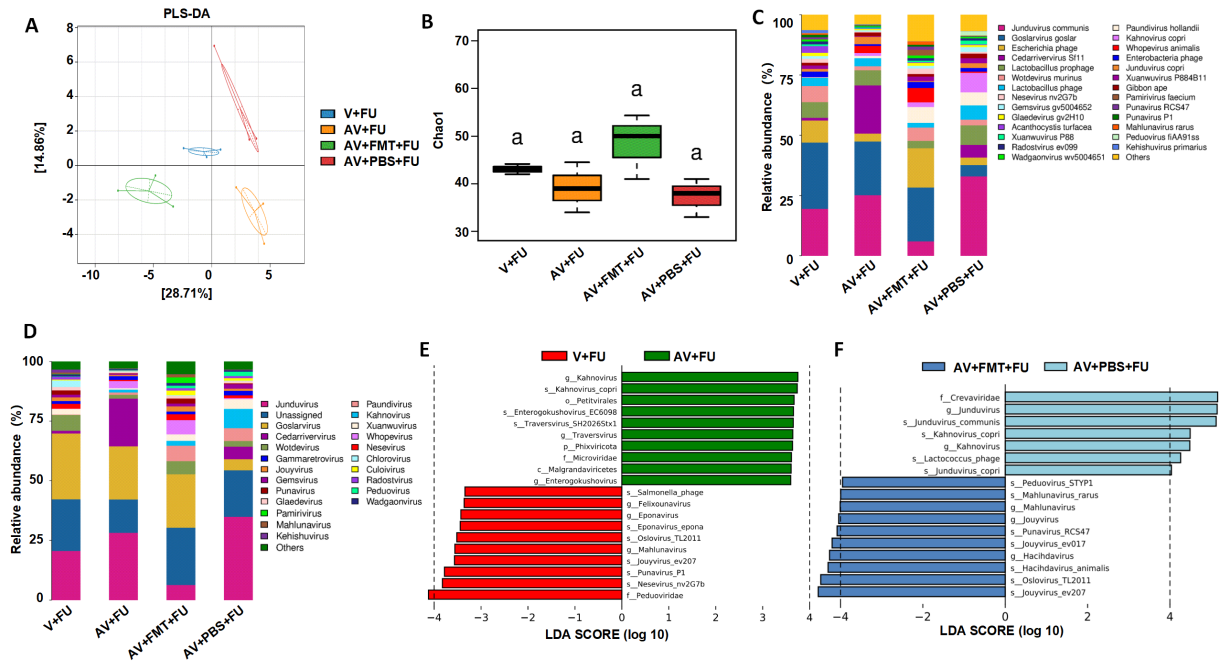

FIGURE 4
Impact of AV drugs on the gut virome. **(A)** PLS-DA plot showing the clustering of different treatment groups on the basis of viral community composition. **(B)** Chao1 index of gut viruses in different treatment groups. Statistical significance is indicated by letters (a). **(C)** Relative abundance of viral taxa across different treatment groups. **(D)** Relative abundance of specific viral families in each treatment group. **(E)** LEfSe analysis showing significantly differentially abundant viral taxa between the V+FU and AV+FU groups. **(F)** LEfSe analysis showing significantly differentially abundant viral taxa between the AV+FMT+FU and AV+PBS+FU groups.

the AV+FMT+FU group and the V+FU group presented higher median Chao1 indices than the AV+FU group and AV+PBS+FU group did, indicating greater viral richness in both groups, although the differences were not statistically significant. The analysis of intestinal viruses at the genus level (Figure 4C) revealed that the genera with the highest relative abundance across all groups were *Jundivirus communis*, *Goslarvirus goslar*, *Escherichia phage*, and *Cedarvirus Sf11*. The viral genus structures in the V+FU group and the AV+FMT+FU group were similar. Compared with those in the V+FU group and the AV+FMT+FU group, the relative abundances of *Jundivirus communis* and *Cedarvirus Sf11* increased in the AV +FU group and the AV+PBS+FU group, whereas the relative abundances of *Goslarvirus goslar* and *Escherichia phage* decreased. Figure 4D shows the changes in the relative abundances of specific viral species across the different groups. *Jundivirus*, *Goslarvirus*, and *Cedarvirus* included the species with the highest relative abundances in all the groups, collectively accounting for more than 50% of the total. The relative abundances of these genera varied under different treatment conditions. Compared with those in the V+FU group and the AV+FMT+FU group, the relative abundance of *Jundivirus* increased in the AV+FU and AV+PBS +FU groups, whereas the relative abundance of *Goslarvirus* decreased. Fecal microbiota transplantation (AV+FMT+FU) resulted in a species structure similar to that of the V+FU group.

LEfSe analysis (Figure 4E) revealed significant differences in viral taxa between the V+FU and AV+FU groups. In the V+FU group, taxa such as *Salmonella phage*, *Felixounavirus*, and *Eponavirus* were enriched, indicating that these viruses dominated the environment prior to AV treatment. In the AV +FU group, viral taxa such as *Kahnovirus*, *Petivirales*, *Enterogokushovirus*, *Traversvirus*, and *Phixviricota* were significantly enriched, reflecting the promoting effect of AV treatment on these viruses. Similarly, LEfSe analysis (Figure 4F) revealed significant differences between the AV+FMT+FU and AV +PBS+FU groups. In the AV+PBS+FU group, viral taxa such as the family *Crevaviridae*, the genera *Jundivirus* and *Kahnovirus*, and *Lactococcus phage* were significantly enriched. The combination of AV treatment and PBS may have promoted the expansion of these viruses, rendering them dominant in this group. In the AV+FMT +FU group, taxa such as *Peduovirus STYP1*, *Mahlunavirus rarus*, *Mahlunavirus*, *Jouyvirus*, *Punavirus RCS47*, *Hachidavirus*, *Oslovirus TL2011*, and *Jouyvirus ev207* were significantly enriched. These findings indicate that these viruses had high relative abundances in the environment following FMT, potentially rendering them dominant in this group. These findings suggest that FMT can modulate the gut virome composition and potentially restore a more beneficial viral community that enhances the efficacy of 5-FU chemotherapy in treating CRC.

Through metagenomic analysis of the gut bacterial and fungal communities, we found that the bacterial and fungal communities in the V+FU, AV+FU, AV+FMT+FU, and AV+PBS+FU groups clustered distinctly, indicating significant differences in their composition (Figures 5A, D). α diversity analysis using the Chao1 index (Figures 5B, E) revealed no significant differences in bacterial or fungal diversity across the groups. The relative abundances of

10.3389/fonc.2024.1501981

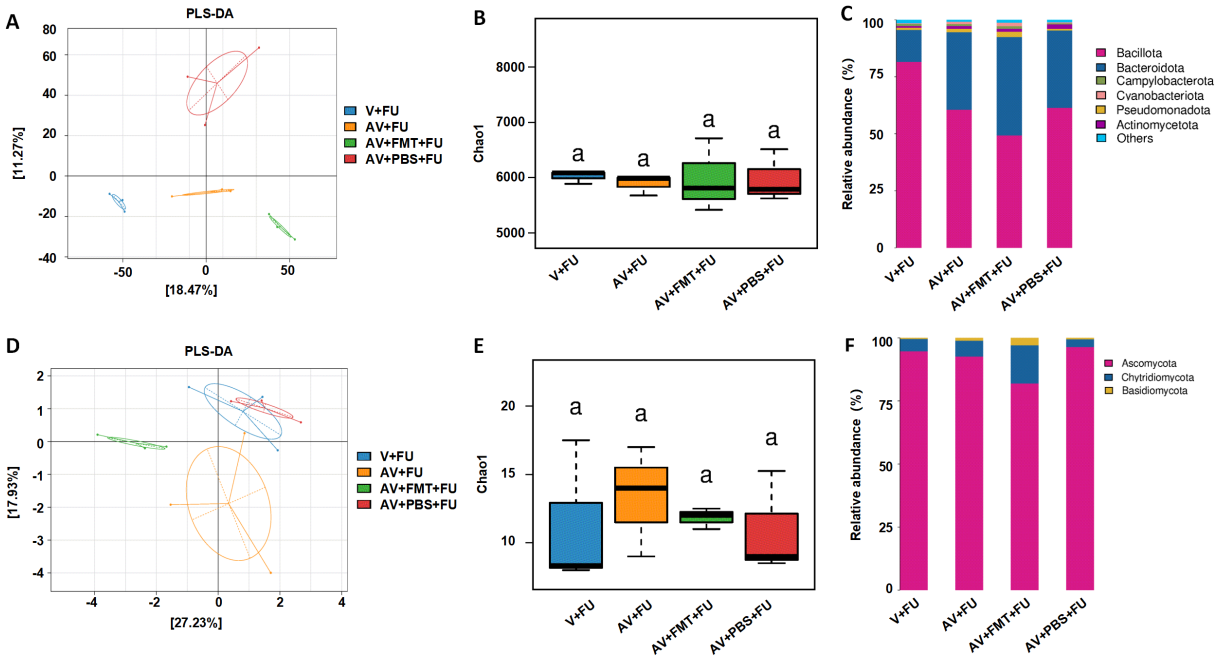

FIGURE 5
Impact of AV drugs on gut bacteria and the mycobiome. **(A)** PLS-DA plot showing the clustering of different treatment groups on the basis of bacterial community composition. **(B)** Chao1 indices of gut bacteria in different treatment groups. **(C)** Relative abundance of bacterial phyla across different treatment groups. **(D)** PLS-DA plot showing the clustering of different treatment groups on the basis of fungal community composition. **(E)** Chao1 indices of gut fungi in different treatment groups. **(F)** Relative abundance of fungal phyla across different treatment groups.

bacterial and fungal phyla (Figures 5C, F) highlighted changes in composition across the treatment groups. In the V+FU group, the gut microbiota was predominantly composed of *Bacillota* and *Bacteroidota*, with lower proportions of other phyla, such as *Cyanobacteria* and *Actinomycetota*. The AV+FU group exhibited an increased abundance of *Bacteroidota* and *Cyanobacteria*, indicating that AV treatment significantly altered the gut bacterial composition. In contrast, the AV+FMT+FU group displayed a more distinct microbial profile, with greater differences in bacterial communities compared to both the AV+FU and V+FU groups. This group showed higher proportions of *Bacteroidota* and *Pseudomonadota*, suggesting that FMT had a significant impact on these bacterial populations. Regarding fungal communities, the microbiota in the V+FU, AV+FU, AV+FMT+FU, and AV+PBS +FU groups was predominantly composed of *Ascomycota*, with minor contributions from *Basidiomycota* and *Chytridiomycota*. The AV+FMT+FU group showed a higher proportion of *Basidiomycota* and *Chytridiomycota* compared to the AV+PBS+FU group, suggesting that FMT supports the growth of these fungal communities.

3.5 The dysbiosis of the gut microbiota induced by AV drugs reduces DCs and CD8+ T cells

To examine the impact of AV drug-induced gut microbiota dysbiosis on immune cells, we conducted flow cytometry to assess the cell number proportions of immune cells in peripheral blood and immunohistochemistry to evaluate immune cell infiltration in tumor tissues, based on the experimental design in Figure 2A. The results revealed that the number of DCs was significantly greater in the V+FU group than in the AV group or the AV+FU group (Figure 6A). The cell number proportion of CD8+ T cells in the V +FU group was also significantly higher than in the AV+FU group (Figure 6B). The cell number proportion of CD4+ T cells in the V group was lower compared to the AV group, and the cell number proportion of CD4+ T cells in the V+FU group was lower than in the AV+FU group, although these differences were not statistically significant (Figure 6B). Immunohistochemical staining of tumor tissues (Figures 6C, D) revealed greater numbers of DCs and CD8+ T cells in the V and V+FU groups than in the AV and AV+FU groups. There was no significant difference in the number of CD4+ T cells in any of the treatment groups (Figure 6E). These results suggest that AV treatment-induced gut microbiota dysbiosis reduces the numbers of DCs and CD8+ T cells in both peripheral blood (Figures 6A, B) and tumor tissues (Figures 6C, D), potentially impairing the immune response and the efficacy of 5-FU chemotherapy for treating CRC.

3.6 FMT restores the gut microbiota and increases DCs and CD8+ T cells

To explore the effects of FMT on gut microbiota restoration and immune cell populations, we performed flow cytometry to assess the cell number proportions of immune cells in peripheral blood and immunohistochemistry to evaluate immune cell infiltration in

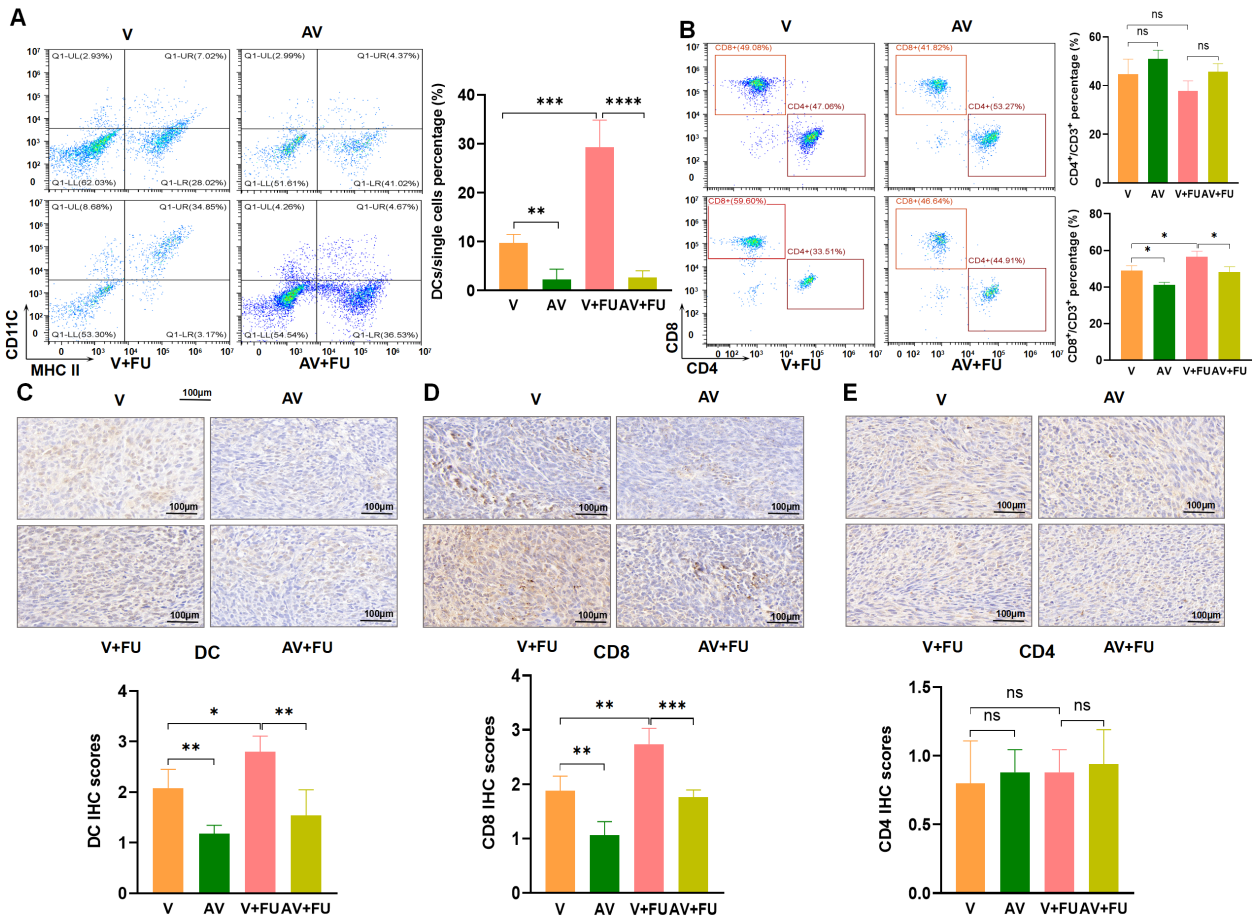

FIGURE 6
The dysbiosis of the gut microbiota induced by AV drugs reduces DCs and CD8+ T cells. **(A)** Flow cytometry analysis of DCs in different treatment groups (V, AV, V+FU, AV+FU). The bar chart illustrates the percentage of DCs among the total single cell population in each group. **(B)** Flow cytometry analysis of CD4+ and CD8+ T cells in different treatment groups. The bar chart shows the percentages of CD4+ and CD8+ T cells within the total CD3+ T cell population for each group. **(C)** Immunohistochemical staining and scoring of DCs in tumor tissues from different treatment groups. **(D)** Immunohistochemical staining and scoring of CD8+ T cells in tumor tissues from different treatment groups. **(E)** Immunohistochemical staining and scoring of CD4+ T cells in tumor tissues from different treatment groups. n=3. *, $P < 0.05$; ***, $P < 0.001$; ****, $P < 0.0001$.

tumor tissues, based on the experimental design in Figure 3A. Flow cytometry analysis revealed that the number of DCs was significantly greater in the AV+FMT+FU group than in the AV +PBS group and the AV+PBS+FU group (Figure 7A), indicating that FMT increases the number of DCs in the presence of 5-FU. The cell number proportion of CD8+ T cells in the AV+FMT+FU group was also significantly greater than that in the AV+PBS+FU group. The cell number proportion of CD4+ T cells in the V group was lower than in the AV group, and the cell number proportion of CD4 + T cells in the V+FU group was lower than in the AV+FU group, although these differences were not statistically significant (Figure 7B). Immunohistochemical staining of tumor tissues revealed that more DCs and CD8+ T cells were present in the AV+FMT group than in the AV+PBS group (Figures 7C, D). Additionally, the AV+FMT+FU group had more DCs and CD8+ T cells than did the AV+PBS+FU group. There was no significant difference in CD4+ T cell infiltration in all treatment groups (Figure 7E). These results suggest that FMT helps restore the gut microbiota and increases the numbers of DCs and CD8+ T cells in both peripheral blood (Figures 7A, B) and tumor tissues (Figures 7C, D), potentially improving the immune response and the efficacy of 5-FU chemotherapy for treating CRC.

3.7 Modulation of the TLR3-IRF3-IFN-β pathway by gut virome influences the efficacy of 5-FU chemotherapy in CRC

The TLR3-IRF3-IFN-β pathway is known to play a key role in detecting viral RNA and inducing antiviral immune responses, including type I interferon production, which is critical for enhancing immune cell functions like dendritic cell maturation and CD8+ T cell activation (16, 17). Given that the gut virome, composed of various viruses residing in the gut, can interact with host immune pathways like TLR3, there is potential for these viral communities to influence cancer immune responses and treatment efficacy. To explore whether modulation of the TLR3 pathway by the gut virome could impact CRC treatment, we investigated how antiviral-induced virome depletion and TLR3 activation through the agonist Poly(I:C) affect immune cell recruitment and the efficacy

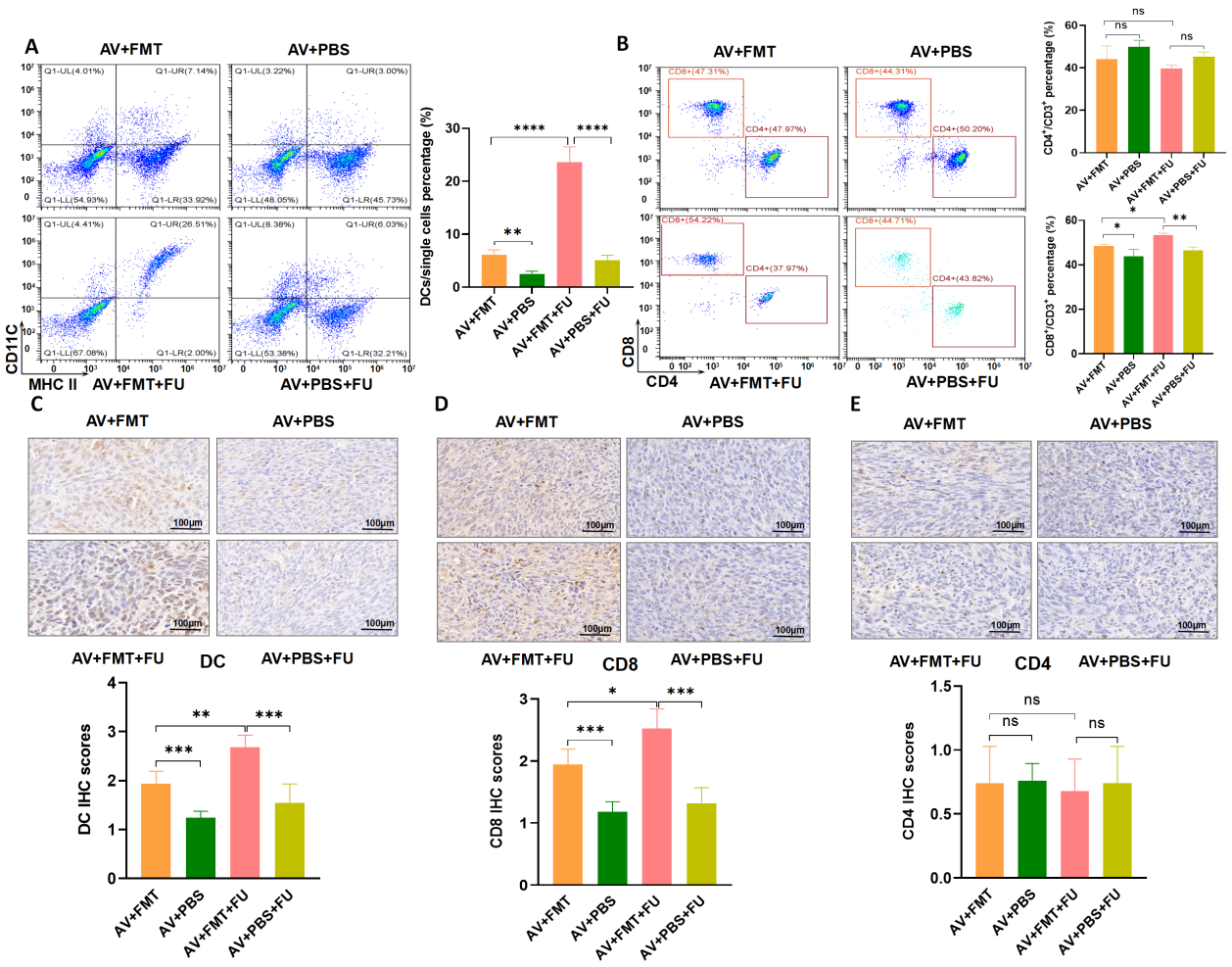

FIGURE 7
Fecal microbiota transplantation (FMT) restores the gut microbiota and increases DCs and CD8+ T cells. **(A)** Flow cytometry analysis of DCs in different treatment groups (AV+FMT, AV+PBS, AV+FMT+FU, AV+PBS+FU). The bar chart illustrates the percentage of DCs among the total single cell population in each group. **(B)** Flow cytometry analysis of CD4+ and CD8+ T cells in different treatment groups. The bar chart shows the percentages of CD4+ and CD8+ T cells within the total CD3+ T cell population for each group. **(C)** Immunohistochemical staining and scoring of DCs in tumor tissues from different treatment groups. **(D)** Immunohistochemical staining and scoring of CD8+ T cells in tumor tissues from different treatment groups. **(E)** Immunohistochemical staining and scoring of CD4+ T cells in tumor tissues from different treatment groups. n=3. *, $P < 0.05$; **, $P < 0.01$; ****, $P < 0.0001$.

of 5-FU chemotherapy. Western blot analysis (Figure 8A) revealed that in the AV+FU group, expression of TLR3, p-IRF3, and IFN-β was reduced compared to the V+FU group, suggesting that antiviral treatment diminished TLR3 pathway activation. This finding was supported by immunofluorescence staining, which showed lower fluorescence intensities of TLR3, p-IRF3, and IFN-β in the AV+FU group compared to the V+FU group (Figure 8B), indicating that the presence of gut viruses may influence TLR3 activation levels.

We further explored whether TLR3 activation could restore immune responses and enhance the efficacy of 5-FU by treating mice with the TLR3 agonist Poly(I:C) in combination with 5-FU (experimental design shown in Figure 8C). Tumor measurements over time showed that Poly(I:C) treatment significantly inhibited tumor growth in the Poly group compared to the no-Poly group (Figure 8D), with both final tumor volumes and tumor weights lower in the Poly group (Figures 8E, F), indicating enhanced antitumor efficacy. Flow cytometry analysis of peripheral blood revealed that DC percentages were higher in the Poly group than in the no-Poly group, indicating increased recruitment of DCs following TLR3 activation (Figure 8G). Additionally, CD8+ T cell levels were elevated in the Poly group, while CD4+ T cell levels showed a downward trend in the Poly group compared to the no-Poly group, though this difference was not statistically significant (Figure 8H). Immunohistochemical staining of tumor tissues further confirmed increased infiltration of DCs and CD8+ T cells in the Poly group compared to the no-Poly group (Figure 8I). CD4+ T cell infiltration also showed a slight decrease in the Poly group, which aligned with the peripheral blood trends, but the difference was not statistically significant. Further validation through Western blot and immunofluorescence analyses demonstrated that Poly(I:C) treatment increased expression of TLR3, p-IRF3, and IFN-β in tumor tissues in the Poly group compared to the no-Poly group, confirming successful activation of the TLR3-IRF3-IFN-β pathway (Figures 8J, K). These findings collectively suggest that gut virome

10.3389/fonc.2024.1501981

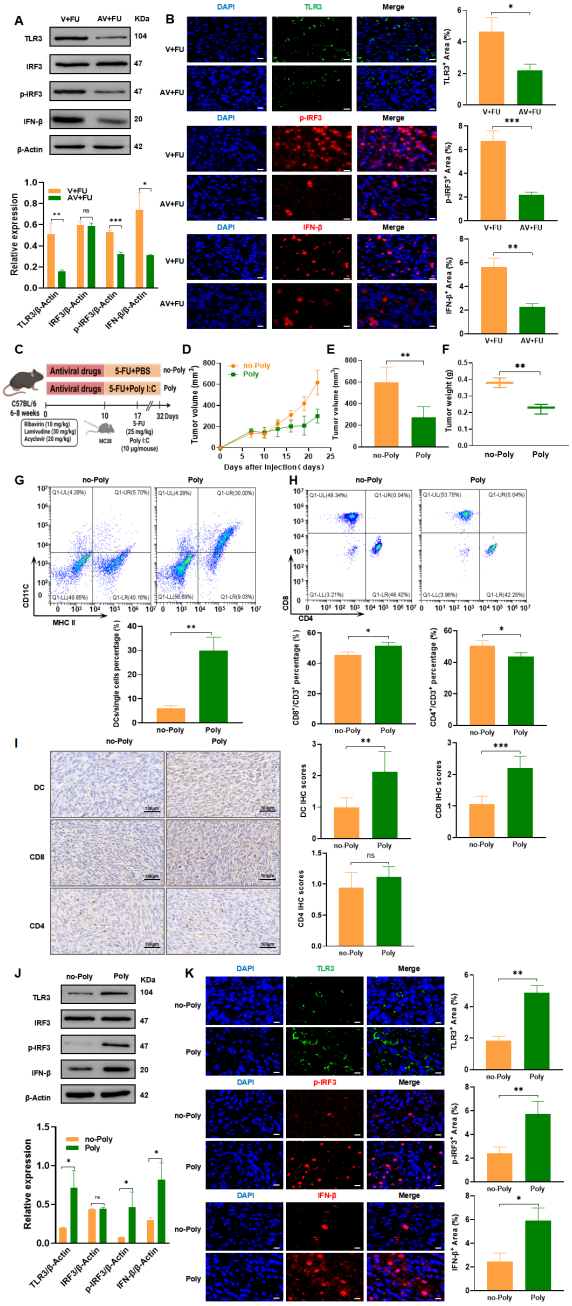

FIGURE 8
TLR3-IRF3-IFN-β pathway modulation by gut virome influences 5-FU efficacy in CRC treatment. **(A)** Western blot analysis of TLR3, IRF3, phosphorylated IRF3 (p-IRF3), and IFN-β expression in tumor tissues from the V+FU and AV+FU groups. β-Actin is used as a loading control. Quantification of band intensity is shown in the bar graph. **(B)** Immunofluorescence staining of TLR3, p-IRF3, and IFN-β in tumor sections from the V+FU and AV+FU groups. DAPI (blue) marks nuclei, while green and red fluorescence indicates TLR3, p-IRF3, and IFN-β expression, respectively. Quantitative analysis of fluorescence intensity is shown on the right. Scale bar=50 μm. **(C)** Schematic of experimental design: C57BL/6 mice were treated with antiviral drugs followed by 5-FU chemotherapy and the TLR3 agonist Poly(I:C). **(D)** Tumor volume measurements over time in Poly and no-Poly groups. **(E)** Comparison of final tumor volume on day 22 between Poly and no-Poly groups. **(F)** Comparison of tumor weights at the end of the experiment between Poly and no-Poly groups. **(G)** Flow cytometry analysis of DCs in different treatment groups (Poly and no-Poly). The bar chart illustrates the percentage of DCs among the total single cell population in each group. **(H)** Flow cytometry analysis of CD4+ and CD8+ T cells in different treatment groups (Poly and no-Poly). The bar chart shows the percentages of CD4+ and CD8+ T cells within the total CD3+ T cell population for each group. **(I)** Immunohistochemical staining of DCs, CD8+, and CD4+ T cells in tumor tissues from Poly and no-Poly groups. Scale bars=100 μm. Quantification of immunohistochemical scores for each cell type is shown to the right. **(J)** Western blot analysis of TLR3, IRF3, p-IRF3, and IFN-β expression in tumor tissues from Poly and no-Poly groups. β-Actin serves as the loading control. Quantification of protein expression levels is displayed in the bar graph. **(K)** Immunofluorescence staining of TLR3, p-IRF3, and IFN-β in tumor sections from Poly and no-Poly groups. DAPI (blue) highlights nuclei, while TLR3 (green), p-IRF3 (red), and IFN-β (red) are visualized in fluorescence channels. Quantitative analysis of each protein's expression area is shown to the right. Scale bar=50 μm. n=3. *, P < 0.05; **, P < 0.01; ***, P < 0.001.

depletion reduces TLR3 pathway activation, subsequently limiting immune cell recruitment and potentially impairing 5-FU efficacy. Conversely, activating TLR3 with Poly(I:C) restores immune cell functions, enhancing the antitumor effects of 5-FU, thereby underscoring the potential role of gut virome interactions in optimizing CRC chemotherapy outcomes.

4 Discussion

CRC is one of the most prevalent malignancies worldwide, and chemotherapy remains an important treatment option, especially for patients with advanced-stage disease. However, responses to chemotherapy vary significantly among patients, with only 15–27% achieving complete remission, while 20–40% show minimal or no response to treatment (18). Therefore, there is an urgent need to better understand the factors affecting chemotherapy efficacy and to develop strategies to improve treatment outcomes for CRC patients. Recent studies have shown that the gut microbiome plays a crucial role in modulating the efficacy of chemotherapeutic drugs. The impact of antibiotics on gut bacteria and subsequent chemotherapy response has received considerable attention (8), but the role of the gut virome remains unclear. Therefore, in this study, we aimed to investigate how AV drug-induced gut virome dysbiosis affects the efficacy of 5-FU for treating CRC and to explore the underlying mechanisms involved.

Previous studies have focused mainly on the bacterial components of the gut microbiota, with limited attention given to the role of the gut virome. To investigate the relationship between the gut virome and chemotherapy efficacy in CRC patients, we collected fecal samples from 10 CRC patients before and after chemotherapy for metagenomic analysis. Based on the RECIST 1.1 tumor assessment criteria, these patients were divided into responders (4 patients with stable disease, 1 patient with partial response) and nonresponders (5 patients with disease progression). Our analysis revealed that the prechemotherapy responder (P-R) and nonresponder (P-NR) groups clustered separately from the postchemotherapy responder (Po-R) and nonresponder (Po-NR) groups, indicating that the gut virome structures differed between patients with different characteristics. However, the similarity of the viral communities between the P-R and Po-R groups suggests that responder viromes remained relatively stable despite chemotherapy, which may be one reason for their positive treatment response. The ACE index revealed that the viral diversity of nonresponders before and after chemotherapy was greater than that of responders, but the difference was not statistically significant. This observation suggests that a more diverse gut virome may be associated with a poor chemotherapy response. Analysis of the viral compositions of the different groups revealed that the gut viromes of the prechemotherapy nonresponder (P-NR) group were highly diverse, and genera such as *Punavirus*, *Delmidovirus*, and *Cohcovirus* were predominant. After chemotherapy, the relative abundances of *Afonbuvirus* and *Brigitvirus* increased in the postchemotherapy nonresponder (Po-NR) group, whereas the abundance of *Punavirus* decreased. These changes suggest that chemotherapy selectively promotes the expansion of certain viral genera while inhibiting others, which may contribute to poor chemotherapy outcomes. In contrast, the gut viromes of the prechemotherapy responder (P-R) group were dominated by *Afonbuvirus* and *Brigitvirus*, with lower abundances of *Punavirus* and *Delmidovirus*. In the postchemotherapy responder (Po-R) group, the abundances of *Brigitvirus* and *Ardovirus* increased, but the overall viral community structure remained relatively stable. This stable virome compositions of the responders may indicate that certain viral genera, such as *Brightvirus* and *Ardovirus*, play a protective role or support a gut environment favorable for the chemotherapeutic response. Further analysis of significantly differentially abundant viral taxa between pre- and postchemotherapy nonresponders and responders revealed key viral species whose abundances were associated with treatment outcomes. Before chemotherapy, *Enterococcus phage* was significantly enriched in the P-R group, suggesting that this phage may play a role in enhancing the chemotherapy response. In contrast, the P-NR group was significantly enriched in *Peduovirus pro483*, *Wadgaonvirus wv5004651*, *Gegavirus ST15OXA48phi141*, and *Xuanwuvirus xv520873*, indicating that these viruses may be associated with poor chemotherapy efficacy. After chemotherapy, *Cohcovirus splanchnicus*, *Cohcovirus hiberniae*, and *Jouyvirus ev207* were significantly enriched in the Po-R group, whereas *Stockinghalvirus FSLSP004* and *Lafunavirus LF1* were significantly enriched in the Po-NR group. These postchemotherapy changes suggest that certain viral species may support a continued positive response in responders or contribute to persistent poor treatment efficacy in nonresponders. The results of this study highlight the potential significance of the gut virome for influencing chemotherapy outcomes in CRC patients. The differences in the enrichment of specific viral taxa between responders and nonresponders suggest that the gut virome could serve as a biomarker for predicting chemotherapy efficacy. Identifying and understanding the roles of these viral taxa may help develop microbiome-based targeted therapies that enhance chemotherapy outcomes by modulating the gut virome. Additionally, the stability of the virome in responders despite chemotherapy treatment suggests that maintaining or restoring a specific viral community structure is critical for achieving better treatment outcomes. These findings demonstrate the possibility of using FMT to manipulate the gut virome to support the response to chemotherapy.

To further investigate the impact of gut viruses on 5-FU treatment for CRC, we employed an AV cocktail therapy (ribavirin, lamivudine, and acyclovir) to eliminate gut viruses in mice. After establishing a subcutaneous xenograft model with MC38 mouse colon cancer cells, we treated the mice with 5-FU and observed tumor growth. Our results showed that AV cocktail therapy significantly reduced the abundance of gut DNA and RNA viruses in mice. This is consistent with the findings of Yang et al. (13). Additionally, mice treated with AV drugs had larger tumor volumes and shorter survival times, indicating that AV drugs promote colorectal tumor growth. In mice treated with 5-FU, colorectal tumor growth was inhibited, and survival time was extended; however, in the AV-treated group, the antitumor effect of 5-FU was reduced. The potential antagonistic interaction between AV treatment and chemotherapy may be mediated by

AV drug-induced gut microbiota dysbiosis. Previous studies have reported similar phenomena in animal models treated with antibiotics. Lu et al. reported that the combination of 5-FU and antibiotics significantly reduced the antitumor effect of 5-FU in a mouse CRC model (19). The potential mechanism may be that antibiotic-induced gut microbiota dysbiosis reduces the antitumor effect of 5-FU. In our study, we found that the reduction in viral abundance was consistent with increased tumor volume and shortened survival time, suggesting that AV drug-induced microbiota dysbiosis creates a gut environment favorable for tumor progression. Therefore, we hypothesize that the effects of AV drugs on colorectal tumor growth and 5-FU chemotherapy efficacy may be due to AV drug-induced gut microbiota dysbiosis. To verify this hypothesis, we performed FMT with healthy donor feces on recipient mice after AV drug treatment. We found that FMT restored the abundance of gut DNA and RNA viruses in mice treated with AV drugs. The tumor volumes of these mice were significantly reduced, and the survival time was significantly extended in FMT-treated mice compared with those not subjected to FMT. Additionally, colorectal tumor growth was inhibited, and survival time was extended in FMT-treated mice receiving 5-FU chemotherapy. These results suggest that restoring a healthy gut virome through FMT can enhance the therapeutic effect of 5-FU, possibly by reconstructing a gut environment that supports antitumor immunity. This finding is consistent with previous studies showing that FMT has the potential to restore the gut microbiota balance and improve CRC treatment outcomes. Previous studies have shown that transplanting healthy donor gut microbiota into patients to restore gut microbiota homeostasis may improve various gastrointestinal diseases, including irritable bowel syndrome, *Clostridioides difficile* infection, and CRC (20). John et al. reported that during CRC treatment, modulating the gut microbiota through FMT could restore chemotherapy-induced gut dysbiosis (21). These results suggest that the gut microbiota is closely related to colorectal tumor growth and chemotherapy efficacy.

To further study the effects of the gut microbiota on colorectal tumor growth and 5-FU chemotherapy efficacy, we performed metagenomic analysis on fecal samples from mice after gut virus depletion or FMT. Our results revealed distinct clustering of viral communities among the different treatment groups, indicating significant differences in the gut virome composition. The AV +FMT+FU and V+FU groups presented greater viral richness than the AV treatment groups did (AV+FMT+FU, AV+PBS +FU), although the differences were not statistically significant. Consistent with the findings of Li et al., the gut viromes of colorectal tumor-bearing mice exhibited significantly reduced α diversity and altered viral spectra (22), suggesting that AV treatment may reduce gut viral diversity, thereby affecting the gut environment and CRC progression. At the genus level, *Jundivirus communis*, *Goslarvirus goslar*, *Escherichia phage*, and *Cedarvirus Sf11* were the most abundant viral taxa across all groups. Notably, the viral community structures in the AV+FMT+FU group mice were similar to those in the V+FU group mice, suggesting that FMT may help restore a viral composition that is more conducive to inhibiting tumor growth. In contrast, AV treatment (AV+FU and AV+PBS+FU) led to increased relative abundances of *Jundivirus communis* and *Cedarvirus Sf11*, whereas the relative abundances of *Goslarvirus goslar* and *Escherichia phage* decreased. These changes suggest that AV treatment selectively promotes the development of certain viral taxa while inhibiting that of others, which may lead to a gut environment that supports CRC progression. LEfSe analysis further confirmed these findings by revealing significant differences in abundances of viral taxa between the V+FU and AV+FU groups. In the V+FU group, viruses such as *Salmonella phage*, *Felixounavirus*, and *Eponavirus* were enriched, indicating their dominance in the gut environment prior to AV treatment. In contrast, the AV+FU group was characterized by an enrichment of viral taxa such as *Kahnovirus*, *Petivirales*, and *Enterogokushovirus*, suggesting that AV treatment promotes the expansion of these viruses, which may negatively impact the efficacy of 5-FU treatment. In the AV+FMT+FU group, viral species such as *Peduovirus STYP1*, *Mahlunavirus rarus*, and *Jouyvirus ev207* were significantly enriched, indicating that FMT may create an environment that supports the proliferation of beneficial viral communities. Studies have shown that viruses, in addition to bacteria, play an important role in FMT; Zuo et al. reported that the therapeutic response to FMT in patients with *C. difficile* infection is associated with high colonization levels in the recipient of donor-derived tail-shaped bacteriophages (23). These findings suggest that FMT can modulate the gut virome composition, potentially restoring a more balanced and beneficial viral community that enhances the efficacy of 5-FU chemotherapy for treating CRC.

Our metagenomic analysis also revealed distinct clustering of bacterial and fungal communities among the different treatment groups, indicating compositional differences. However, α diversity analysis revealed no significant differences in bacterial or fungal diversity across the groups, suggesting that while the overall diversity remained stable, the specific compositions of these communities were altered by the treatments. Consistent with the findings of Yuan et al., AV drugs affected only a few specific bacterial taxa in the gut microbiome, with minimal effects on bacterial diversity. In the V+FU group, the gut bacterial community was predominantly composed of *Bacillota* and *Bacteroidota*, with lower proportions of other phyla, such as *Cyanobacteria* and *Actinomycetota*. The AV+FU group presented an increased abundance of *Bacteroidota* and *Cyanobacteria*, indicating that AV treatment alters the gut bacterial community in a manner that may disrupt the balance between beneficial and harmful bacteria. This disruption could contribute to the reduced efficacy of 5-FU treatment observed in the AV+FU group. In contrast, the AV+FMT+FU group exhibited a more distinct microbial profile, with greater differences in bacterial communities compared to both the AV+FU and V+FU groups. This group showed higher proportions of *Bacteroidota* and *Pseudomonadota*, suggesting that FMT had a significant impact on these bacterial populations. Such changes may contribute to creating a gut environment that is more favorable for enhancing the efficacy of 5-FU chemotherapy. Studies have revealed dysbiosis of the gut mycobiome in CRC patients, with an increased ratio of *Basidiomycota/Ascomycota* (24). In our study, the mycobiomes of all the groups were predominantly composed of *Ascomycota*, with

minor contributions from *Basidiomycota* and *Chytridiomycota*. Notably, compared to the AV+PBS+FU group, the AV+FMT+FU group had higher proportions of *Basidiomycota* and *Chytridiomycota*, indicating that FMT supports the growth of these fungal communities. This shift may help improve 5-FU efficacy by promoting a gut environment that supports anti-tumor immunity and inhibits tumor progression. These results suggest that the gut microbiota is closely related to colorectal tumor growth and chemotherapy efficacy and that the role of gut viruses is particularly important compared with that of bacteria and fungi.

Cellular immunity plays a crucial role in tumor treatment, and immune cells exert antitumor immune responses through direct or indirect actions (25). Some studies have shown that chemotherapy-induced damage to living cells is a major determinant of T cell immunity (26). Other studies have reported a trend toward increased T cell proportions in tumors after chemotherapy, and traditional chemotherapeutic drugs may reshape the tumor immune microenvironment in some gastric cancer patients by recomposing T cell components and activating innate immune cells (27). Nakamura et al. reported that anthracycline drugs promote an increase in DC cells in tumor lesions through the chemokine CCL2 (28). Our results revealed that the number of DCs in the V+FU group was significantly greater than that in the AV group and AV+FU group. Similarly, the number of CD8+ T cells in the V+FU group was significantly greater than that in the AV+FU group. These results suggest that AV treatment induces gut microbiota dysbiosis, thereby reducing the numbers of DCs and CD8+ T cells in peripheral blood and tumor tissues. DCs are important antigen-presenting cells that play a key role in initiating and regulating immune responses, especially in activating CD8+ T cells (29). CD8+ T cells, also known as cytotoxic T cells, are key players in the directly killing of tumor cells (30). The reduced numbers of these cells suggest that AV treatment may impair the host's ability to mount an effective immune response against CRC. Without a strong immune response, the ability of chemotherapy to target and destroy tumor cells is likely to be diminished. In contrast, we found that FMT restored the numbers of DCs and CD8+ T cells in the peripheral blood and tumor tissues. The numbers of these immune cells were significantly greater in the AV+FMT+FU group than in the AV +PBS and AV+PBS+FU groups. These findings suggest that FMT not only helps restore the gut microbiota but also enhances immune responses, thereby improving the antitumor effects of chemotherapy. The increase in DCs and CD8+ T cells following FMT indicates that restoring a balanced gut microbiota may reconstruct a more favorable immune environment. This is especially important in cancer treatment because a strong immune response is necessary for effectively eradicating tumors. We hypothesize that AV drug-induced gut microbiota dysbiosis may reduce the antitumor effect of 5-FU by suppressing the antitumor immune responses of DC and CD8+ T cells. However, the specific mechanisms involved remain to be further investigated.

The TLR3-IRF3-IFN-β signaling pathway is a critical component of innate immunity, recognized for its role in detecting viral infections and triggering antiviral responses. TLR3, a pattern recognition receptor, binds double-stranded RNA—a common feature of viral genomes—which initiates a signaling cascade through IRF3 (interferon regulatory factor 3) that ultimately leads to the production of IFN-β (16). IFN-β, a type I interferon, exerts several immunomodulatory effects, including enhancing dendritic cell maturation and promoting CD8+ T cell activation, both of which are crucial for mounting an effective antitumor immune response (17). Recently, studies have revealed that the gut virome can influence the host immune system by interacting with TLR3 signaling (13). This interaction may be essential in maintaining immune homeostasis and could influence cancer treatment outcomes. Thus, we hypothesized that modulating the gut virome could impact TLR3 pathway activation, potentially affecting immune cell dynamics and the efficacy of 5-FU chemotherapy in CRC. To test this hypothesis, we used antiviral treatment to deplete the gut virome in tumor-bearing mice and examined its impact on the TLR3-IRF3-IFN-β pathway activation and immune cell populations. We also explored whether activating TLR3 with the agonist Poly(I:C) could counteract the effects of virome depletion and improve the efficacy of 5-FU chemotherapy.

In this study, antiviral treatment aimed at depleting the gut virome reduced TLR3 pathway activation, as evidenced by decreased expression of TLR3, p-IRF3, and IFN-β in the AV+FU group. This downregulation in the TLR3-IRF3-IFN-β pathway coincided with lower levels of DC and CD8+ T cell populations, suggesting that the absence of viral components in the gut microbiome reduces the activation signals necessary for maintaining a robust antitumor immune response. Since DCs and CD8+ T cells are essential in detecting and eliminating tumor cells, the reduction in these cell populations likely compromised the effectiveness of 5-FU, as indicated by larger tumor volumes and weights in the AV+FU group. Conversely, activating the TLR3 pathway using the agonist Poly(I:C) restored TLR3 signaling and promoted the expression of IFN-β and downstream immune responses. The Poly+5-FU combination treatment led to increased DC and CD8+ T cell infiltration in tumor tissues, supporting the hypothesis that TLR3 activation can counterbalance the immunosuppressive effects of virome depletion. This observation suggests that TLR3 pathway activation facilitates the recruitment and function of immune cells within the tumor microenvironment, enhancing the overall efficacy of 5-FU chemotherapy. The role of TLR3 in boosting IFN-β levels is particularly relevant, as IFN-β not only aids in viral clearance but also supports an immune-permissive tumor environment by increasing antigen presentation and stimulating CD8+ T cell responses, which are essential for effective chemotherapy. The observed differences in CD4+ T cell dynamics between the treatment groups add further nuance to the interpretation of TLR3's role in CRC. While CD4+ T cell levels exhibited a trend of reduction in the Poly group compared to the no-Poly group, this difference was not statistically significant. The slight decrease in CD4+ T cells suggests that TLR3 activation may selectively enhance cytotoxic CD8+ T cell responses. This selective recruitment of CD8+ T cells over CD4+ T cells may be an advantageous mechanism in CRC, where increased cytotoxic activity can directly limit tumor progression.

The findings of this study emphasize the importance of the gut virome as an immunomodulatory element, capable of enhancing chemotherapy efficacy through TLR3-mediated signaling. Gut viral

communities, by interacting with host immune receptors like TLR3, may act as natural adjuvants, triggering innate immune responses that potentiate antitumor activity. Thus, the depletion of these viral components through antiviral treatments could inadvertently suppress beneficial immune pathways, underscoring the complexity of gut microbiota and virome interactions in cancer therapy. Targeting the gut virome or employing TLR3 agonists like Poly(I:C) could be strategic for enhancing immune responses, particularly in cases where patients have undergone antiviral treatments that may reduce gut microbial diversity and function. Future research could further investigate the precise viral components within the gut virome that are essential for TLR3 pathway activation, which may lead to the development of tailored microbial therapies or TLR3-based immunomodulatory strategies for CRC patients.

Although this study reveals the impact of AV drug-induced gut microbiota dysbiosis on the efficacy of chemotherapy for treatment of CRC, several limitations remain. First, the clinical study had a small sample size of 10 CRC patients, limiting the generalizability of the findings. A larger cohort would provide more robust data and help validate the observed associations between the abundance of specific viral taxa and chemotherapy outcomes. Second, this study focused primarily on changes in the gut virome and their impact on chemotherapy efficacy, with limited investigations into the combined effects of other microbiota, such as gut bacteria, fungi, and archaea. Since these microbiota may play important roles in host immunity and tumor progression, future research should aim to elucidate these complex interactions to better understand the mechanisms by which the gut microbiota influences CRC treatment outcomes.

5 Conclusion

This study reveals that AV drug-induced gut virome dysbiosis impairs the TLR3-IRF3-IFN-β pathway, reducing the numbers of immune cells, such as DCs and CD8+ T cells, which are crucial for an effective antitumor response in CRC. This impairment diminishes the efficacy of 5-FU chemotherapy, as shown by increased tumor growth and reduced survival in AV-treated mice. Conversely, activation of the TLR3 pathway through Poly(I:C) enhances immune function, restores DC and CD8+ T cell populations, and improves the antitumor effects of 5-FU, suggesting a potential strategy to counteract the negative impact of virome depletion on chemotherapy. These findings underscore the importance of maintaining gut virome integrity or activating TLR3 as adjunct strategies to enhance chemotherapy outcomes in CRC patients.

Data availability statement

The metagenomic sequencing data generated in this study have been deposited in the Sequence Read Archive (SRA) of the National Center for Biotechnology Information (NCBI) and can be accessed via the following URL: https://www.ncbi.nlm.nih.gov/sra/ PRJNA1195998; https://www.ncbi.nlm.nih.gov/sra/ PRJNA1196101.

Ethics statement

The animal study was approved by Animal Ethics Committee of Chengdu Medical College (2022CYA-003). The study was conducted in accordance with the local legislation and institutional requirements. The studies involving humans were approved by First Affiliated Hospital of Chengdu Medical College (2024CYFYIRB-BA-Jul17). The studies were conducted in accordance with the local legislation and institutional requirements. The participants provided their written informed consent to participate in this study.

Author contributions

HH: Investigation, Methodology, Writing – original draft. YY: Investigation, Writing – original draft. XW: Writing – original draft. WZ: Writing – original draft. BW: Writing – original draft. XY: Writing – original draft. QW: Writing – original draft. FH: Conceptualization, Writing – review & editing. JL: Conceptualization, Writing – original draft, Writing – review & editing.

Funding

The author(s) declare financial support was received for the research, authorship, and/or publication of this article. This research was supported by the Natural Science Foundation of Sichuan Province (Grant No. 2022NSFSC0766), the Health Commission of Sichuan Province Medical Science and Technology Program (Grant No. 24QNMP087), the Central Government-Directed Project for Local Science and Technology Development (Grant No. 2024ZYD0146), the Medical Science and Technology Project of Chengdu Municipal Health Commission (Grant No. 2024404), and the Sichuan Provincial Department of Science and Technology (Grant No. 2023YFS0280).

Acknowledgments

We would like to express our special thanks to the members of the Department of Gastroenterology at the First Affiliated Hospital of Chengdu Medical College.

Conflict of interest

The authors declare that the research was conducted in the absence of any commercial or financial relationships that could be construed as a potential conflict of interest.

Generative AI statement

The author(s) declare that no Generative AI was used in the creation of this manuscript.

Publisher's note

All claims expressed in this article are solely those of the authors and do not necessarily represent those of their affiliated organizations, or those of the publisher, the editors and the reviewers. Any product that may be evaluated in this article, or claim that may be made by its manufacturer, is not guaranteed or endorsed by the publisher.

References

1. Patel SG, Karlitz JJ, Yen T, Lieu CH, Boland CR. The rising tide of early-onset colorectal cancer: a comprehensive review of epidemiology, clinical features, biology, risk factors, prevention, and early detection. *Lancet Gastroenterol Hepatol.*. (2022) 7:262–74. doi: 10.1016/S2468-1253(21)00426-X

2. Wilson PM, Danenberg PV, Johnston PG, Lenz H-J, Ladner RD. Standing the test of time: targeting thymidylate biosynthesis in cancer therapy. *Nat Rev Clin Oncol.*. (2014) 11:282–98. doi: 10.1038/nrclinonc.2014.51

3. Wang W, Guo W, Li L, Fu Z, Liu W, Gao J, et al. Andrographolide reversed 5-FU resistance in human colorectal cancer by elevating BAX expression. *Biochem Pharmacol*. (2016) 121:8–17. doi: 10.1016/j.bcp.2016.09.024

4. Marjaneh RM, Khazaei M, Ferns GA, Avan A, Aghaee-Bakhtiari SH. The role of microRNAs in 5-FU resistance of colorectal cancer: Possible mechanisms. *J Cell Physiol.*. (2019) 234:2306–16. doi: 10.1002/jcp.v234.3

5. Villéger R, Lopès A, Carrier G, Veziant J, Billard E, Barnich N, et al. Intestinal microbiota: a novel target to improve anti-tumor treatment? *Int J Mol Sci.*. (2019) 20:4584. doi: 10.3390/ijms20184584

6. Carding S, Verbeke K, Vipond DT, Corfe BM, Owen LJ. Dysbiosis of the gut microbiota in disease. *Microb Ecol Health Dis.*. (2015) 26:26191. doi: 10.3402/mehd.v26.26191

7. Iida N, Dzutsev A, Stewart CA, Smith L, Bouladoux N, Weingarten RA, et al. Commensal bacteria control cancer response to therapy by modulating the tumor microenvironment. *Science*. (2013) 342:967–70. doi: 10.1126/science.1240527

8. Abdel-Rahman O, Ghosh S, Walker J. Outcomes of metastatic colorectal cancer patients in relationship to prior and concurrent antibiotics use; individual patient data analysis of three clinical trials. *Clin Transl Onco.*. (2020) 22:1651–6. doi: 10.1007/s12094-020-02301-1

9. Hannigan GD, Duhaime MB, Ruffin MT IV, Koumpouras CC, Schloss PD. Diagnostic potential and interactive dynamics of the colorectal cancer virome. *mBio*. (2018) 9:. doi: 10.1128/mbio.02248-02218

10. Nakatsu G, Zhou H, Wu WKK, Wong SH, Coker OO, Dai Z, et al. Alterations in enteric virome are associated with colorectal cancer and survival outcomes. *Gastroenterology*. (2018) 155:529–541. e525. doi: 10.1053/j.gastro.2018.04.018

11. Wang Z, Guo K, Liu Y, Huang C, Wu M. Dynamic impact of virome on colitis and colorectal cancer: immunity, inflammation, prevention and treatment. *Semin Cancer Biol*. (2022) 943–54. doi: 10.1016/j.semcancer.2021.10.004

12. Gogokhia L, Buhrke K, Bell R, Hoffman B, Brown DG, Hanke-Gogokhia C, et al. Expansion of bacteriophages is linked to aggravated intestinal inflammation and colitis. *Cell Host Microbe*. (2019) 25:285–99. e288. doi: 10.1016/j.chom.2019.01.008

13. Yang JY, Kim MS, Kim E, Cheon JH, Lee YS, Kim Y, et al. Enteric viruses ameliorate gut inflammation via toll-like receptor 3 and toll-like receptor 7-mediated interferon-β Production. *Immunity*. (2016) 44:889–900. doi: 10.1016/j.immuni.2016.03.009

14. Forte G, Rega A, Morello S, Luciano A, Arra C, Pinto A, et al. Polyinosinic-polycytidylic acid limits tumor outgrowth in a mouse mode l of metastatic lung cancer. *J Immunol*. (2012) 188:5357–64. doi: 10.4049/jimmunol.1103811

15. Jiang X, Li Y, Feng J-l, Nik Nabil WN, Wu R, Lu Y, et al. Safrana l Prevents Prostate Cancer Recurrence by Blocking the Re-activ ation of Quiescent Cancer Cells via Downregulation of S-Phase Kinase-A ssociated Protein 2. *Front Cell Dev Biol*. (2020) 8. doi: 10.3389/fcell.2020.598620

16. Honda K, Takaoka A, Taniguchi T. Type I inteferon gene induction by the interferon regulatory factor family of transcription factors. *Immunity*. (2006) 25:349–60. doi: 10.1016/j.immuni.2006.08.009

17. Audsley KM, Wagner T, Ta C, Newnes HV, Buzzai AC, Barnes SA, et al. IFNβ Is a potent adjuvant for cancer vaccination strategies. *Front Immunol*. (2021) 12. doi: 10.3389/fimmu.2021.735133

18. Sebag-Montefiore D, Stephens RJ, Steele R, Monson J, Grieve R, Khanna S, et al. Myint AS et al: Preoperative radiotherapy versus selective postoperative chemoradiothe rapy in patients with rectal cancer (MRC CR07 and NCIC-CTG C016): a mu lticentre, randomised trial. *Lancet*. (9666) 373:811–20. doi: 10.1016/S0140-6736(09)60484-0

19. Yuan L, Zhang S, Li H, Yang F, Mushtaq N, Ullah S, et al. The influence of gut microbiota dysbiosis to the efficacy of 5-Fluorouracil treatment on colorectal cancer. *Biomed Pharmacother*. (2018) 108:184–93. doi: 10.1016/j.biopha.2018.08.165

20. Ooijevaar RE, Terveer EM, Verspaget HW, Kuijper EJ, Keller JJ. Clinical application and potential of fecal microbiota transplantation. *Annu Rev Med.*. (2019) 70:335–51. doi: 10.1146/annurev-med-111717-122956

21. Kenneth MJ, Tsai H-C, Fang C-Y, Hussain B, Chiu Y-C, Hsu B-M. Diet-mediated gut microbial community modulation and signature metabolites as potential biomarkers for early diagnosis, prognosis, prevention and stage-specific treatment of colorectal cancer. *J Adv Res.*. (2023) 52:45–57. doi: 10.1016/j.jare.2022.12.015

22. Li Y, Zhang F, Zheng H, Kalasabail S, Hicks C, Fung KY, et al. Fecal DNA virome is associated with the development of colorectal neoplasia in a murine model of colorectal cancer. *Pathogens*. (2022) 11:457. doi: 10.3390/pathogens11040457

23. Zuo T, Wong SH, Lam K, Lui R, Cheung K, Tang W, et al. Bacteriophage transfer during faecal microbiota transplantation in Clostridium difficile infection is associated with treatment outcome. *Gut*. (2018) 67:634–43. doi: 10.1136/gutjnl-2017-313952

24. Iliev ID, Leonardi I. Fungal dysbiosis: immunity and interactions at mucosal barriers. *Nat Rev Immunol*. (2017) 17:635–46. doi: 10.1038/nri.2017.55

25. Kumar A, Taghi Khani A, Sanchez Ortiz A, Swaminathan S. GM-CSF: A double-edged sword in cancer immunotherapy. *Front Immunol*. (2022) 13:901277. doi: 10.3389/fimmu.2022.901277

26. Sriram G, Milling LE, Chen J-K, Kong YW, Joughin BA, Abraham W, et al. The injury response to DNA damage in live tumor cells promotes antitumor immunity. *Science Signaling*. (2021) 14. doi: 10.1126/scisignal.abc4764

27. Kim R, An M, Lee H, Mehta A, Heo YJ, Kim K-M, et al. Early tumor–immune microenvironmental remodeling and response to first-line fluoropyrimidine and platinum chemotherapy in advanced gastric cancer. *Cancer Discov*. (2022) 12:984–1001. doi: 10.1158/2159-8290.CD-21-0888

28. Nakamura K, Smyth MJ. Myeloid immunosuppression and immune checkpoints in the tumor microenvironment. *Cell Mol Immunol.*. (2020) 17:1–12. doi: 10.1038/s41423-019-0306-1

29. Randolph GJ. Dendritic cells: The first step. *J Exp Med.*. (2021) 218:e20202077. doi: 10.1084/jem.20202077

30. Tanaka A, Sakaguchi S. Regulatory T cells in cancer immunotherapy. *Cell Research*. (2017) 27:109–18. doi: 10.1038/cr.2016.151

frontiers | Frontiers in Immunology

TYPE Original Research
PUBLISHED 06 January 2025
DOI 10.3389/fimmu.2024.1519345

Check for updates

OPEN ACCESS

EDITED BY
Qingyu Luo,
Dana–Farber Cancer Institute, United States

REVIEWED BY
Xiaowei Wu,
Dana–Farber Cancer Institute, United States
Hao Song,
St. Jude Children's Research Hospital, United States
Shunian Xiang,
Admera Health, United States
Haili Ma,
Dana–Farber Cancer Institute, United States

*CORRESPONDENCE
Heli Li
liheli@hust.edu.cn

RECEIVED 29 October 2024
ACCEPTED 12 December 2024
PUBLISHED 06 January 2025

CITATION
Li Q and Li H (2025) Integrating bioinformatics and machine learning to identify AhR-related gene signatures for prognosis and tumor microenvironment modulation in melanoma.
Front. Immunol. 15:1519345.
doi: 10.3389/fimmu.2024.1519345

COPYRIGHT
© 2025 Li and Li. This is an open-access article distributed under the terms of the Creative Commons Attribution License (CC BY). The use, distribution or reproduction in other forums is permitted, provided the original author(s) and the copyright owner(s) are credited and that the original publication in this journal is cited, in accordance with accepted academic practice. No use, distribution or reproduction is permitted which does not comply with these terms.

Integrating bioinformatics and machine learning to identify AhR-related gene signatures for prognosis and tumor microenvironment modulation in melanoma

Qianru Li[1,2] and Heli Li[3]*

[1]Department of Dermatology, Wuhan No.1 Hospital, Wuhan, Hubei, China, [2]Hubei Province & Key Laboratory of Skin Infection and Immunity, Wuhan, Hubei, China, [3]Division of Child Healthcare, Department of Pediatrics, Tongji Hospital, Tongji Medical College, Huazhong University of Science and Technology, Wuhan, China

Background: The Aryl Hydrocarbon Receptor (AhR) pathway significantly influences immune cell regulation, impacting the effectiveness of immunotherapy and patient outcomes in melanoma. However, the specific downstream targets and mechanisms by which AhR influences melanoma remain insufficiently understood.

Methods: Melanoma samples from The Cancer Genome Atlas (TCGA) and normal skin tissues from the Genotype-Tissue Expression (GTEx) database were analyzed to identify differentially expressed genes, which were intersected with a curated list of AhR-related pathway genes. Prognostic models were subsequently developed, and feature genes were identified. Advanced methodologies, including Gene Set Enrichment Analysis (GSEA) and immune cell infiltration analysis, were employed to explore the biological significance of these genes. The stability of the machine learning models and the relationship between gene expression and immune infiltrating cells were validated using three independent melanoma datasets. A mouse melanoma model was used to validate the dynamic changes of the feature genes during tumor progression. The relationship between the selected genes and drug sensitivity, as well as non-coding RNA interactions, was thoroughly investigated.

Results: Our analysis identified a robust prognostic model, with four AhR-related genes (MAP2K1, PRKACB, KLF5, and PIK3R2) emerging as key contributors to melanoma progression. GSEA revealed that these genes are involved in primary immunodeficiency. Immune cell infiltration analysis demonstrated enrichment of $CD4^+$ naïve and memory T cells, macrophages (M0 and M2), and $CD8^+$ T cells in melanoma, all of which were associated with the expression of the four feature genes. Importantly, the diagnostic power of the prognostic model and the relevance of the feature genes were validated in three additional independent

melanoma datasets. In the mouse melanoma model, Map2k1 and Prkacb mRNA levels exhibited a progressive increase with tumor progression, supporting their role in melanoma advancement.

Conclusions: This study presents a comprehensive analysis of AhR-related genes in melanoma, highlighting MAP2K1, PRKACB, KLF5, and PIK3R2 as key prognostic markers and potential therapeutic targets. The integration of bioinformatics and machine learning provides a robust framework for enhancing prognostic evaluation in melanoma patients and offers new avenues for the development of treatments, particularly for those resistant to current immunotherapies.

KEYWORDS

Aryl Hydrocarbon Receptor, melanoma, prognostic model, immune cell infiltration, machine learning models

1 Introduction

Melanoma, a highly aggressive skin cancer type, accounts for around 4% of skin tumor cases but is responsible for approximately 80% of skin cancer-related deaths (1). Immunotherapy, especially through immune checkpoint inhibitors, has transformed the treatment landscape for melanoma, providing substantial benefits to certain patient groups (2). However, many patients exhibit variable responses or develop resistance to these therapies, highlighting the need for more precise therapeutic strategies. Recent oncology research has increasingly focused on the aryl hydrocarbon receptor (AhR), historically known for its role in xenobiotic metabolism (3). Environmental carcinogens, such as polycyclic aromatic hydrocarbons and polychlorinated biphenyls, act as ligands that bind to and activate AhR (4). In melanoma, AhR is implicated in multiple chemical carcinogenic signaling pathways and exhibits a dual role, functioning as both a promoter and suppressor of tumorigenesis (5). It has also emerged as a key modulator within the tumor microenvironment (TME) (6).

Studies suggest that AhR activation triggers the expression of various cytokines and immune-modulating factors, shaping the TME in distinct ways (7). In melanoma, AhR activation has been linked to the recruitment and activity of regulatory T cells (Tregs), which suppress anti-tumor immunity (8). Conversely, AhR signaling has also been shown to enhance anti-tumor immune responses by promoting Th17 cell differentiation (9), highlighting its complex role. Additionally, AhR activation can drive macrophages to acquire an immunosuppressive phenotype, which can mediate chemotherapy resistance in tumor (10, 11). AhR is notably present in various crucial immune cells, both innate and adaptive immunity, but comprehensive analyses of the relevant pathway are lacking (4). This gap in knowledge presents a significant hurdle in harnessing AhR's potential in therapeutic strategies.

While several studies have associated AhR with melanoma prognosis and resistance to immune checkpoint inhibitors (12), significant gaps persist. For instance, although AHR is implicated in the recruitment of immunosuppressive cells (3), the key downstream targets of the AhR pathway in melanoma, their roles in shaping the tumor microenvironment, and their potential as reliable prognostic markers have yet to be fully characterized. This study addresses these gaps by leveraging bioinformatics tools to systematically analyze AhR-related genes and their associations with melanoma. Through robust machine learning models, it identifies novel prognostic markers and potential therapeutic targets. By enhancing our understanding of the AhR pathway, this research provides a foundation for identifying new treatment strategies and clarifying the biological mechanisms driving melanoma progression.

2 Materials and methods

2.1 Raw data acquisition

Figure 1 was created to show the flowchart of our data analysis process. The study utilized public datasets from TCGA (www.cancer.gov) for melanoma samples and GTEx (www.gtexportal.org) as controls. The combined data enabled the comparison of melanoma-specific gene expression patterns. Gene expression and single-cell RNA sequencing (scRNA-seq) data for melanoma were obtained from the Gene Expression Omnibus (www.ncbi.nlm.nih.gov/geo/). The GSE19234 dataset (GPL570) includes data from 38 melanoma patients (13). The GSE65904 dataset (GPL10558) consists of data from 214 melanoma patients, with only cutaneous melanoma samples that have available disease-specific survival information and survival duration selected (n=21) (14). The GSE72056 dataset (GPL18573) contains single-cell RNA-seq data from 4645 cells isolated from 19 melanoma patients (15). Gene expression across different cell types was processed and analyzed using the Seurat and SingleR R packages (16, 17).

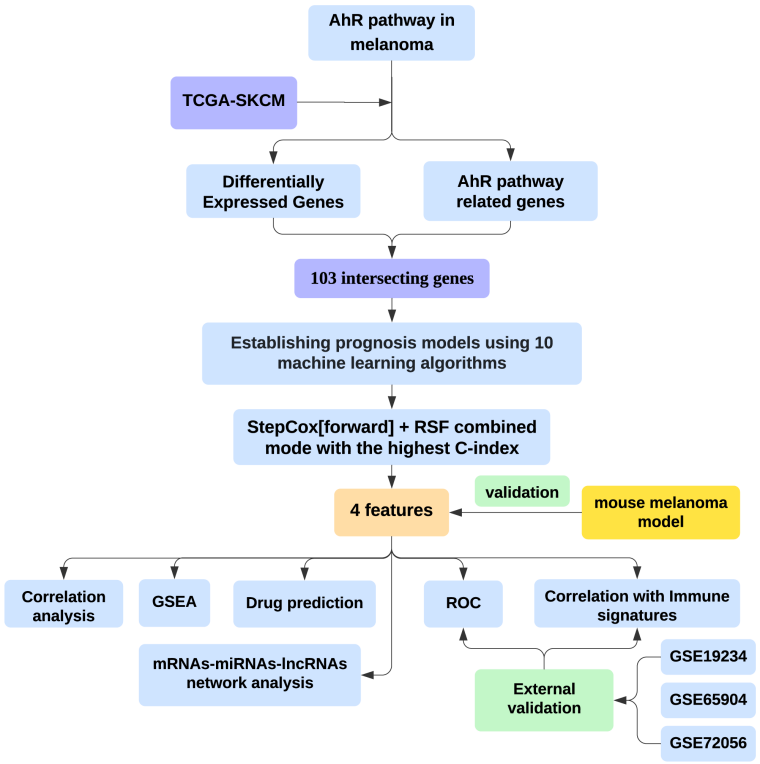

FIGURE 1
Integrating bioinformatics and machine learning to identify AhR-related gene signatures for prognosis and tumor microenvironment modulation in melanoma.

2.2 Differentially expressed genes

Using the limma package (18), DEGs were screened according to the threshold parameters ($|logFC| > 0.5$ and adjusted $p < 0.05$). Volcano plots and heatmaps were generated to show the gene expression changes by R. The analysis focused on genes within the chemical carcinogenesis receptor activation signaling pathway (hsa05207) involving AhR pathway, identifying 103 intersecting genes. Network of 103 intersecting genes were conducted by igraph package with $p < 0.5$, $r > 0.3$. The skin-specific coexpression network were conducted by NetworkAnalyst, which have human tissue-specific gene coexpression from the iNetModels database (19).

2.3 Construction of prognostic model and immune cell infiltration analysis in melanoma

The melanoma dataset from TCGA was split into training (75%) and testing (25%) sets. Using the R software and the Mime package, we constructed an optimal prognostic model and identified feature genes (20). Mime, a machine learning framework, integrates ten classic algorithms: Lasso, Enet, Boruta, CoxBoost, Random Forests (RSF), eXtreme Gradient Boosting (Xgboost), StepCox, plsRcox, Generalized Boosted Regression Model (GBM), and Support Vector Machine Recursive Feature Elimination (SVM-REF). A total of 117 combinations were applied with K-fold cross-validation for model training. The model's performance, assessed using the C-index, demonstrated its capability to stratify patients into high- and low-risk survival groups. Immune cell infiltration was analyzed using xCell, Epic, abis, estimate, and Cibersort via the Mime and immunedeconv packages (21).

2.4 Gene set enrichment and variation analyses

GSEA was used to investigate the functional enrichment of the feature genes. We divided each feature gene into high expression and low expression groups based on its expression level, and conducted differential analysis with a p-valuecutoff value of 0.05. Using R software along with the enrichplot packages, KEGG pathways were identified to explore the roles of feature genes in TCGA melanoma samples (22).

2.5 Ear injection model in mice

C57BL/6 mice were purchased from HFK Bioscience (Beijing, China) and housed in a specific pathogen-free environment. For the ear injection model, B16-F10 cells (2×10^5) were injected intradermally into the ears of mice (8-week-old) in 25 µl of HBSS buffer.

2.6 RNA extraction and quantitative real-time PCR

Total RNA from tumor or normal tissue was obtained. qRT-PCR mixtures were prepared by a SYBR green real-time PCR kit (Toyobo, Osaka, Japan). mRNA levels were normalized to GAPDH, and fold changes were determined using the $2^{-\Delta\Delta Ct}$ method. Primer pairs: 5'-TCTCCACACCTATGGTGCAA -3' and 5'- CAAGAAACAG GGGAGCTGAG -3' (Gapdh); 5'- AACGGTGGAGTG GTCTTCAAG -3' and 5'- CGGATTGCGGGTTTGATCTC -3' (Map2k1); 5'- AGGGCAGGACATGGACATTG -3' and 5'-CGCCTTATTGTAACCCTTGCTG -3' (Prkacb); 5'- CAGGC CACCTACTTTCCCC -3' and 5'- GAATCGCCAGTT TGGAAGCAA -3' (Klf5); 5'- ACCTAAGCCCTCTAAGGCAAA -3' and 5'- TCCCGGAGTCTCTCATTCACC-3' (Pik3r2).

2.7 Drug sensitivity

To explore the therapeutic implications, drug-gene interactions were predicted for the identified hub genes using Gene Set Cancer Analysis (GSCA). GSCA integrates over 750 small molecule drugs from Cancer Therapeutics Response Portal (CTRP) and Genomics of Drug Sensitivity in Cancer (GDSC) databases (23). This analysis is crucial for identifying potential compounds that could reverse resistance to immunotherapy.

2.8 mRNA-miRNA-lncRNA network

A comprehensive mRNA-miRNA-lncRNA network was constructed to explore the post-transcriptional regulation of the feature genes. Using the miRDB database (24) for miRNA prediction (target score ≥ 95) and ENCORI database (25) for lncRNA prediction.

3 Results

3.1 DEGs identification and correlation analysis

We conducted a differential gene expression analysis between melanoma samples from TCGA and normal control tissues from GTEx, identifying 12891 differentially expressed genes (DEGs) (Figure 2A). From the human chemical carcinogenesis receptor activation signaling pathway (hsa05207), which is closely associated with the AHR pathway, we identified 215 related genes (Supplementary Figure S1). Of these, 103 genes overlapped with the DEGs (Figure 2B), with 52 genes being upregulated and 51 downregulated in melanoma (Figure 2C). Correlation analysis further demonstrated strong interrelationships among these 103 genes (Figure 2D). Additionally, we constructed the skin-specific coexpression network of these 103 genes using NetworkAnalyst (Supplementary Figure S2).

3.2 Construction of prognostic models

The TCGA melanoma dataset (n = 456) was divided into a training subset (75%, n = 342) and a testing subset (25%, n = 114). A set of 103 overlapping genes was utilized with both subsets to build prognostic models, applying 10 machine learning algorithms via Mime. Out of the 117 models developed, the StepCox[forward] + RSF combined model achieved the highest C-index mean across both the training and testing datasets (Figure 3A). Both the StepCox[forward] + RSF combined model and the RSF model yielded the same mean C-index across training and testing datasets. Since the combined model selected the same feature genes as both methods, which are deemed more significant, we chose the StepCox[forward] + RSF combined model for further analysis. Based on the median risk score calculated by Mime from the combined mode, patients were categorized into high-risk and low-risk groups. The survival probability for each cohort was assessed, showing that individuals in the high-risk group had significantly poorer outcomes in both datasets (Figure 3B). Notably, the 3- and 5-year AUC of the combined model reached 1 in the test set and >0.96 in the training set, indicating the model's exceptional precision and stability (Figure 3C).

3.3 Selection of significant feature genes

We analyzed the top 10 genes from the StepCox and RSF models, respectively (Figure 4A). Using a Venn diagram, we identified MAP2K1, PRKACB, KLF5, and PIK3R2 as significant features common to both models (Figure 4B). Based on the expression of the feature genes, patients were stratified into high-risk and low-risk groups using Mime, and survival probabilities were calculated for each cohort. Notably, higher expression levels of PRKACB and MAP2K1 were associated with better survival outcomes, while elevated expression of KLF5 and PIK3R2 correlated with poorer prognosis (Figure 4C). An examination of the expression profiles of melanoma patients from the TCGA database, compared to normal controls from the GTEx database, revealed that AHR, MAP2K1, and PRKACB were upregulated in melanoma, whereas KLF5 and PIK3R2 were downregulated (Figure 4D). Correlation analysis demonstrated a significant positive correlation between AHR and MAP2K1, as well as PRKACB, and a significant negative correlation with PIK3R2. No significant correlation was observed between KLF5 and the other genes (Figure 4E). AHR also co-expressed with these feature genes in a skin tissue coexpression network (Supplementary Figure S2). These results suggest that these genes are not only key prognostic markers but may also play essential roles in melanoma progression, positioning them as promising targets for therapy.

To assess the robustness and predictive accuracy of the prognostic model, we used external datasets, GSE19234 and

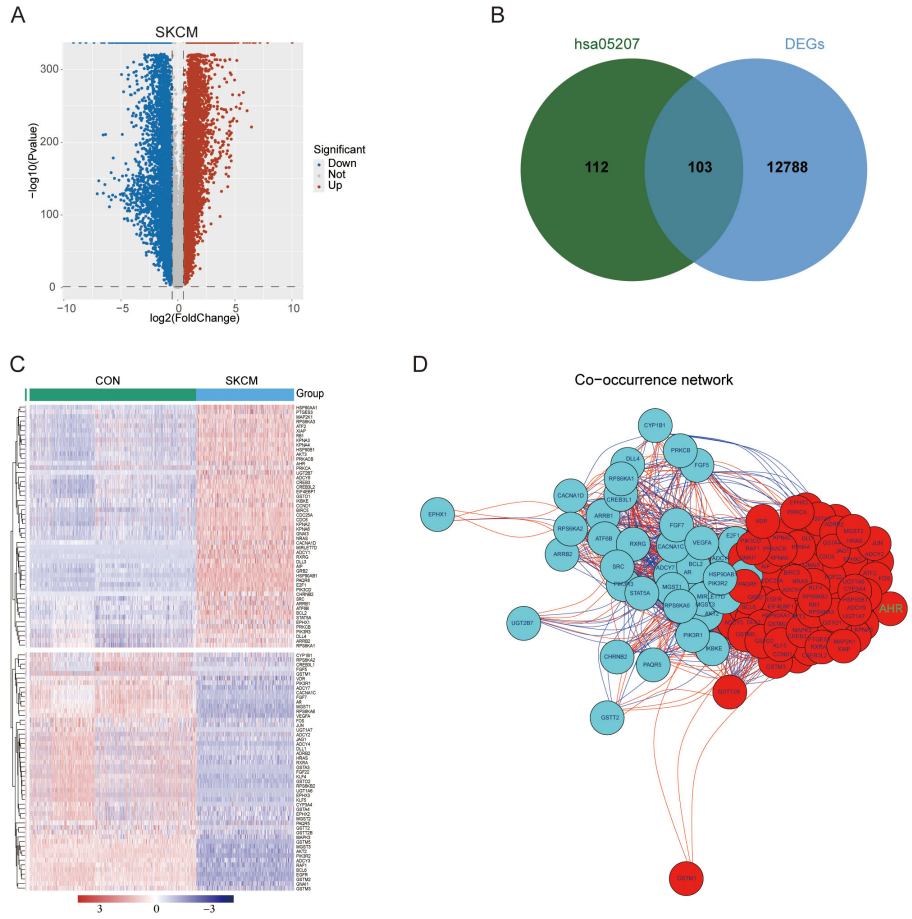

FIGURE 2
DEGs identification and correlation analysis. **(A)** Volcano plot of DEGs between melanoma samples from TCGA-SKCM and control tissues from GTEx. **(B)** 103 intersecting genes of DEGs and genes from the hsa05207 pathway. **(C)** Heat map depicting the expression patterns of DEGs across the two groups. **(D)** Network of 103 intersecting genes. Red nodes represent upregulated genes and blue nodes representing downregulated genes. Red lines indicate positive correlations, while blue lines denote negative correlations between the genes.

GSE65904, as independent test sets. The combined StepCox [forward] + RSF model showed strong consistency across these datasets (Supplementary Figures S3A, C). Notably, melanoma patients in GSE65904 with high MAP2K1 expression exhibited better outcomes (Supplementary Figures S3B, D). Additionally, we conducted a correlation analysis of MAP2K1, KLF5, PRKACB, and PIK3R2 with immune signatures across both datasets (Supplementary Figures S3E, F). However, due to the limited sample size, survival differences between the low-risk and high-risk groups were not statistically significant for other genes, and their correlations with immune signatures varied between the datasets.

3.4 GSEA analysis of selected feature genes

Beyond their prognostic significance, the four feature genes are implicated in key biological pathways. GSEA revealed that MAP2K1 is predominantly associated with the metabolism of xenobiotics by cytochrome P450, primary immunodeficiency and tyrosine metabolism (Figure 5A). KLF5 is linked to the metabolism of xenobiotics by cytochrome P450 and tyrosine metabolism (Figure 5B). PRKACB is primarily involved in primary immunodeficiency (Figure 5C). PIK3R2 plays a role in the metabolism of xenobiotics by cytochrome P450, tyrosine metabolism and oxidative phosphorylation (Figure 5D).

3.5 Correlation between feature genes and immune signatures

The immunological environment plays a critical role in the progression of melanoma. To explore this, we enriched immune infiltration and tumor microenvironment signatures using Mime. Immune scores obtained through various tools, including xCell and ESTIMATE, while specific immune cell populations such as $CD4^+$ T cells (via EPIC), $CD4^+$ naïve and memory T cells (via ABIS), $CD8^+$ T cells, and macrophages (M0 and M2 types) were assessed using CIBERSORT and CIBERSORT_abs, showing high expression in melanoma samples from the TCGA dataset (Figure 6A).

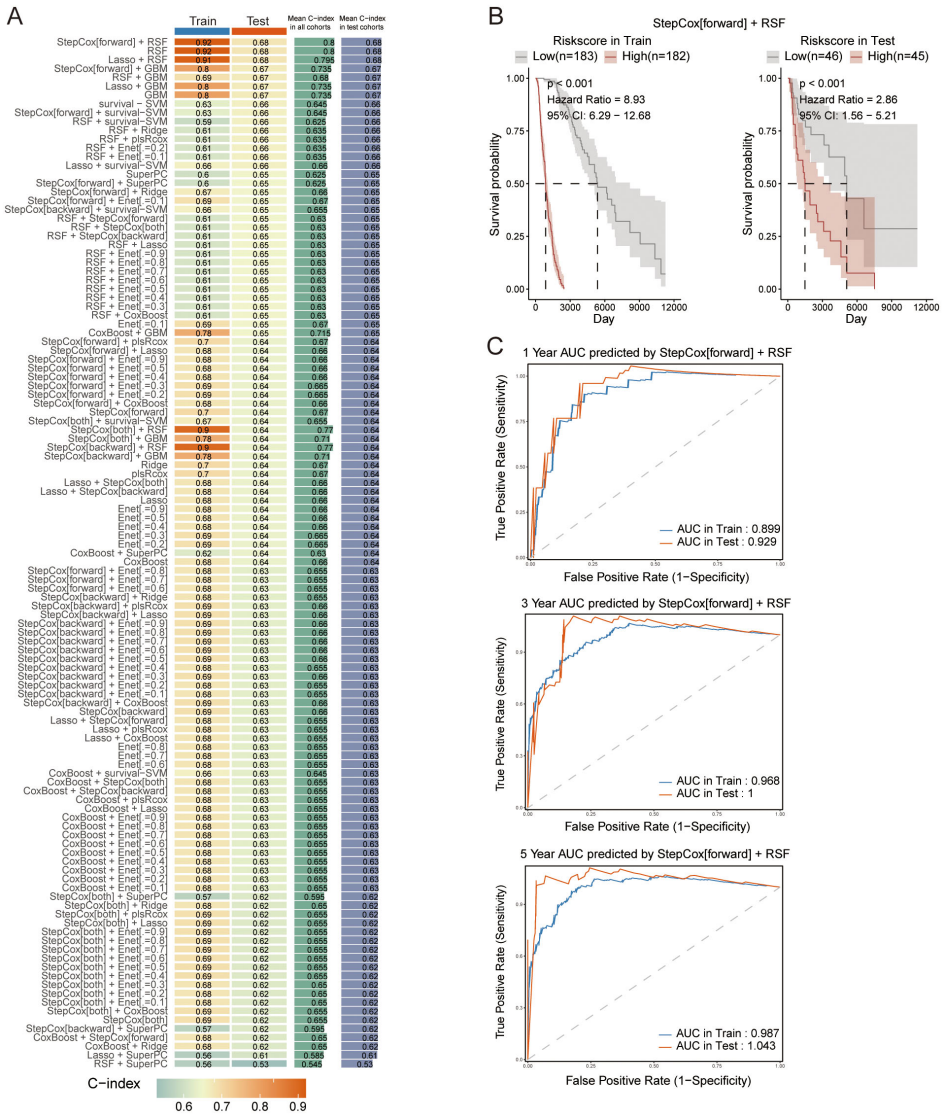

FIGURE 3
Construction of prognostic models. **(A)** C-index values for each model across both the training and testing datasets, highlighting model performance. **(B)** Survival curves for patients stratified by risk scores, calculated using the StepCox[forward] + RSF combined model across different datasets. **(C)** ROC curves for the 1-, 3-, and 5-year survival predictions, demonstrating the performance of the StepCox[forward] + RSF combined model in both the training and testing datasets.

Correlation analysis between the feature genes and immune cell signatures revealed that MAP2K1 and PRKACB are positively correlated with $CD4^+$ T cells and immune score, both of which are crucial for anti-tumor immunity. KLF5 and PIK3R2 were associated with the $CD4^+$ naïve T cells and immunosuppressive macrophages (M2 type) (Figure 6B). These findings highlight the diverse roles of AHR-related genes in melanoma and emphasize their potential as key modulators of the immune landscape.

3.6 Validation of the relationships between feature genes and immune cells

We analyzed the expression of the feature genes in different immune cells using single-cell sequencing data from melanoma (GSE72056). First, we grouped the cells based on their expression profiles (Figure 7A) and examined the expression of the feature genes across different cell types (Figure 7B). Notably, AHR and the four feature genes were expressed in T cells and macrophages (Figures 7C, D). These results further confirm that the feature genes are involved in immune responses within the melanoma microenvironment. The expression of these genes in T cells and macrophages, key immune cell types, supports the hypothesis that they play crucial roles in regulating immune responses and may influence the tumor's ability to evade immune surveillance.

3.7 Validation of the feature genes in mouse melanoma model

To further validate the dynamic changes in the feature genes during melanoma progression, we established a melanoma model in

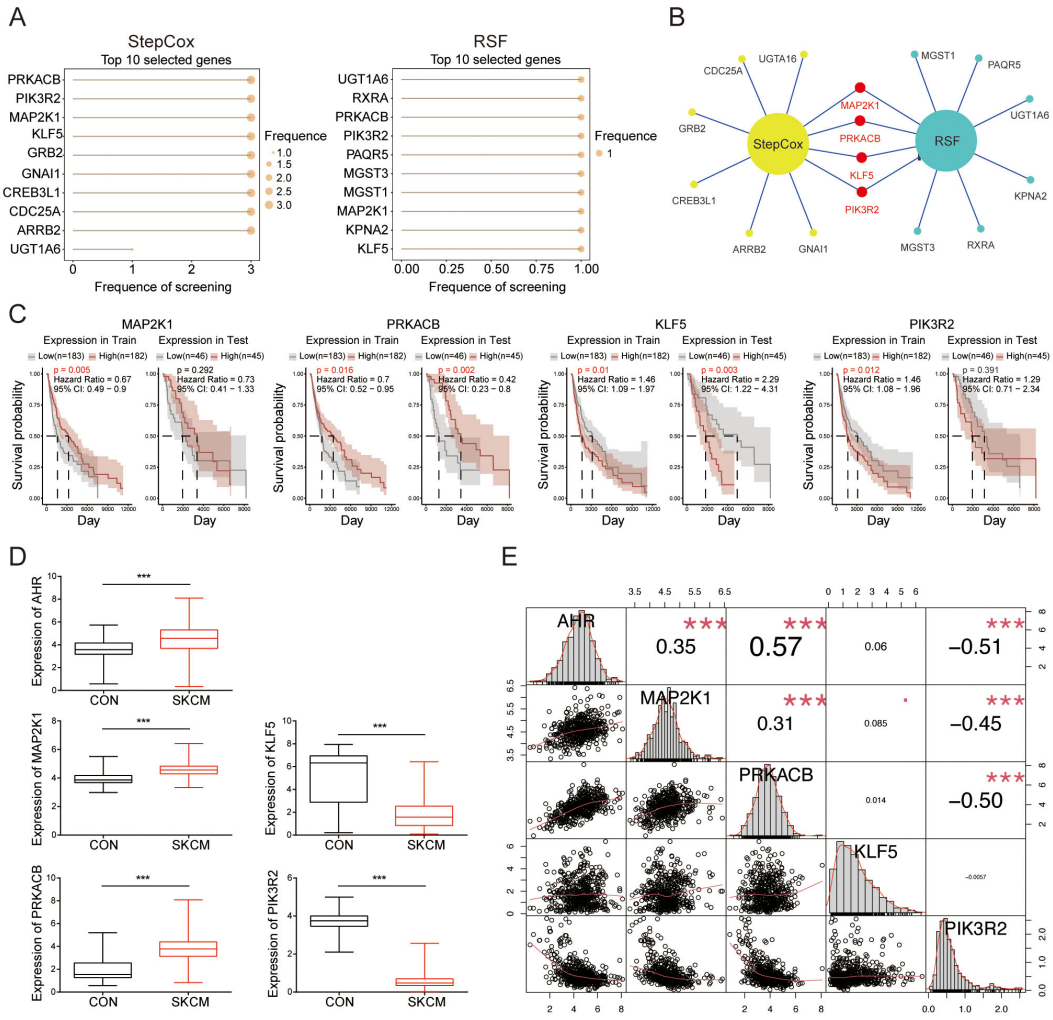

FIGURE 4
Selection of significant feature genes. **(A)** Top 10 features selected by the StepCox (left) and Random Forest (right) algorithms. **(B)** Venn diagram showing the intersection of four feature genes derived from both the StepCox and Random Forest models. **(C)** Survival curves of patients stratified by the median expression levels of each gene across different datasets. **(D)** Comparison of the expression levels of the identified feature genes in melanoma patients from the TCGA database against normal controls from the GTEx database. **(E)** A correlation heatmap illustrating the relationships among the selected genes. ***P < 0.001.

the mouse ear (Figure 8A), which is considered more clinically relevant for studying the progression and metastasis of human melanoma (26). In this model, the mRNA levels of Map2k1 and Prkacb increased significantly on days 21 and 14, respectively, whereas the expression of Klf5 and Pik3r2 showed no significant changes (Figures 8B).

3.8 Construction of mRNA-miRNAs-lncRNAs network and Drug-gene interactions

We predicted the drugs correlated with AHR, MAP2K1, KLF5, PRKACB and PIK3R2 using data from the CTRP and GDSC databases. Additionally, the drug-gene interactions were visualized using the GSCA platform (Supplementary Figures S4A, B). To further explore regulatory mechanisms, we searched the miRDB database to identify miRNAs with a target score of ≥ 95 that are linked to the mRNAs of these feature genes. We then used the ENCORI database to identify lncRNAs associated with these miRNAs. A comprehensive mRNA-miRNA-lncRNA network was constructed by intersecting the identified miRNAs and lncRNAs (Supplementary Figure S5). These analyses aim to uncover potential therapeutic strategies for melanoma by targeting key molecules in the AHR, MAP2K1, KLF5, PRKACB, and PIK3R2 signaling pathways. These analyses aim to identify therapeutic strategies for melanoma by targeting key genes (AHR, MAP2K1, KLF5, PRKACB, PIK3R2) and their regulatory RNA networks, offering

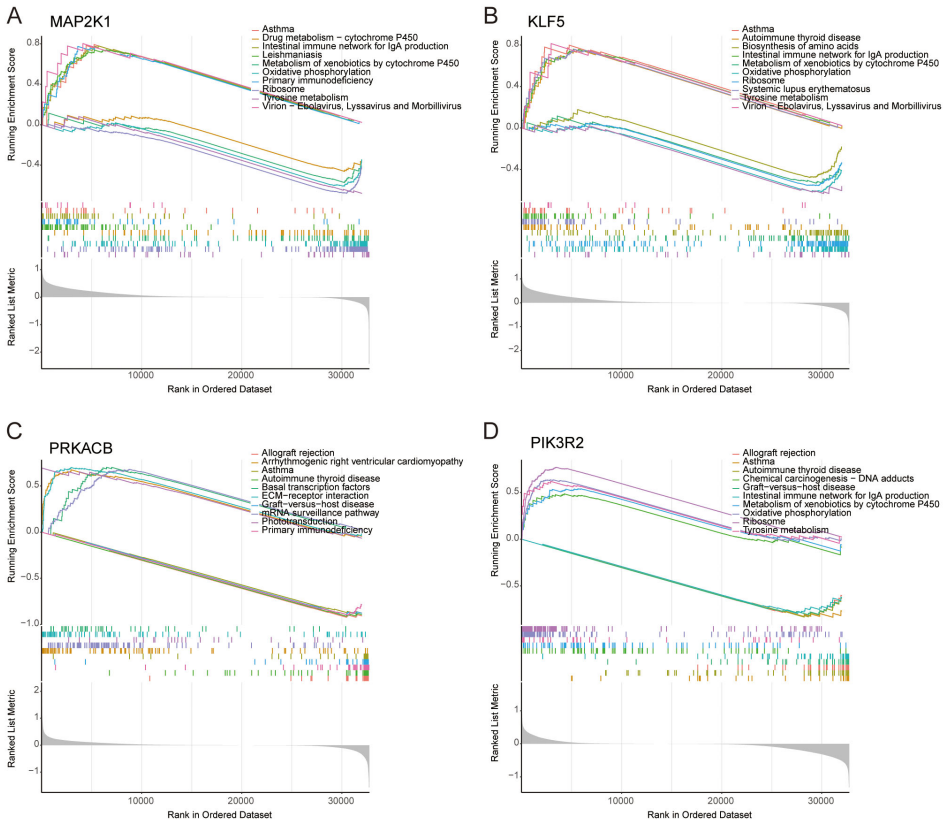

FIGURE 5
GSEA analysis of selected feature genes. In terms of KEGG pathway analysis, the top five upregulated and downregulated pathways were identified for **(A)** MAP2K1, **(B)** KLF5, **(C)** PRKACB, and **(D)** PIK3R2.

potential for personalized treatments and novel biomarkers to improve clinical outcomes.

4 Discussion

4.1 Overview of findings

This study provides significant insights into the role of the AhR pathway in melanoma, particularly in relation to tumor progression and immune modulation. Previous research has highlighted the dualistic nature of AhR signaling in cancer, where it can either suppress or promote tumorigenesis depending on the context (5, 27). Recent evidences in melanoma, where AhR appears to promote macrophage polarization towards immunosuppressive phenotype (11) and widely suppress immune cell function (28), complicating its utility as a straightforward therapeutic target. By integrating bioinformatics and machine learning, we identified four key AhR-associated genes—MAP2K1, PRKACB, KLF5, and PIK3R2—that serve as both prognostic markers and potential therapeutic targets. These genes were systematically analyzed for their biological roles and correlations with immune infiltration and patient outcomes.

4.2 Biological and clinical implications of key genes

MAP2K1, also referred to as MEK1, is a crucial element of the mitogen-activated protein kinase (MAPK) signaling pathway, which plays a pivotal role in controlling cell proliferation, differentiation, and survival (29, 30). MEK1/2 can activated AhR, resulting in a transient inhibition of cytochrome P450 family 1 subfamily A member 1 (CYP1A1) (31). AHR introduces the transcriptional activation of CYP1A1, which facilitates the biotransformation of environmental toxins and carcinogenic substances into highly reactive and carcinogenic diol epoxide intermediates (32). Additionally, AhR can influence MAPK signaling, thereby affecting cellular processes such as dysfunction and apoptosis (33). In melanoma, dysregulation of MAPK signaling, often through mutations in upstream effectors like

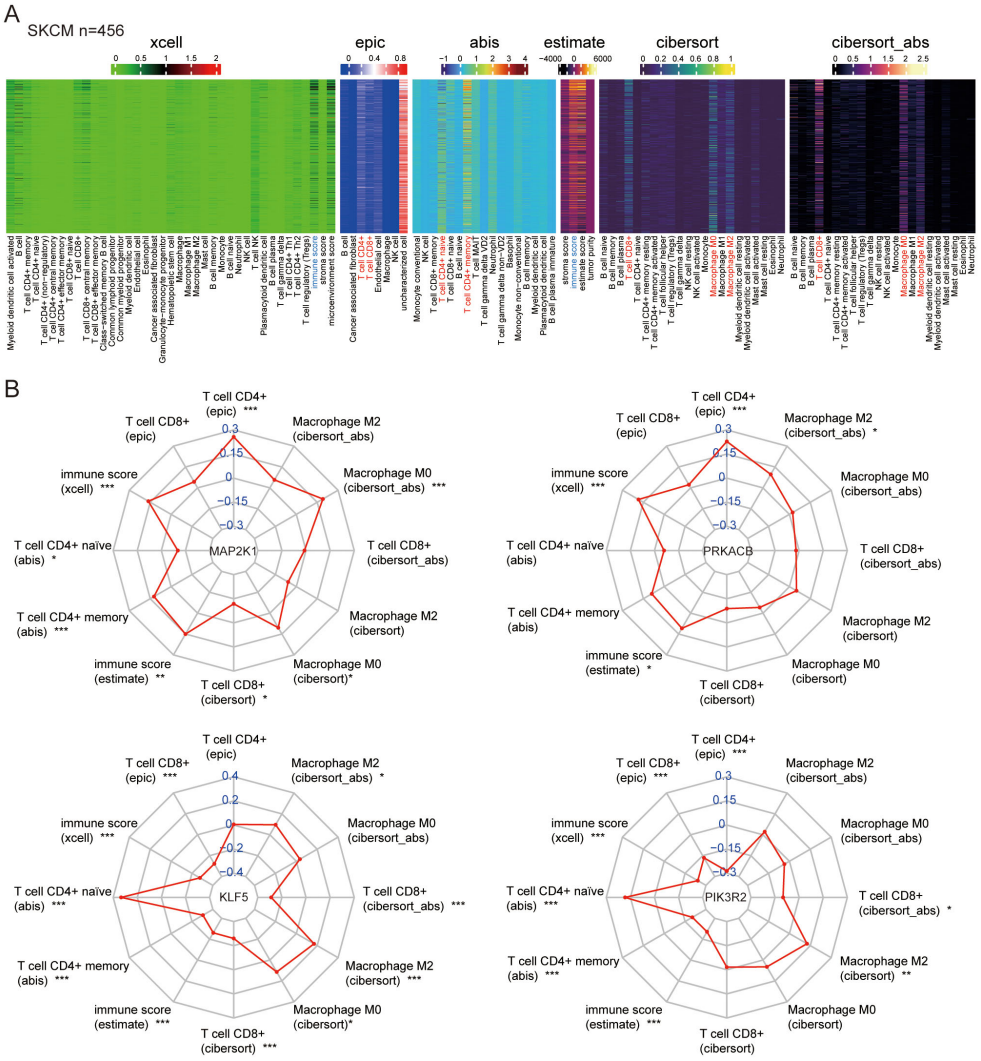

FIGURE 6
Correlation between feature genes and immune signatures. **(A)** Immune signatures in melanoma samples from TCGA were deconvoluted using various methods. **(B)** Correlations were analyzed between the feature genes (MAP2K1, KLF5, PRKACB, PIK3R2) and the immune signatures. *P < 0.05, **P < 0.01, ***P < 0.001.

BRAF, leads to unchecked tumor growth and resistance to therapy (34). Our results demonstrate a positive association between MAP2K1 expression and T cell infiltration in the TME and better outcomes. This finding is significant because it underscores the complex role of MAP2K1, which could potentially be exploited to enhance the efficacy of immunotherapies.

PRKACB, a gene encoding the catalytic subunit of protein kinase A (PKA), is involved in the regulation of metabolism, transcription, and immune response (35). Studies show that AhR can activate PKA signaling, thereby regulating the activation of cancer stemness (36). In melanoma, PKA can enhance the migration and metastasis of melanoma cells (37) and impair T cell infiltration into the tumor microenvironment (38). Recent evidence indicated that PKA mediates the growth inhibition of melanoma cells (39). In our study, the positive correlation between PRKACB expression and immune score, suggests that PRKACB may facilitate anti-tumor immunity in melanoma. PKA has been shown to modulate can phosphorylate the NF-κB subunit p65, promoting T cell activation and survival (40, 41), which may explain the association between high PRKACB expression and better survival outcomes observed in this study. Interestingly, PRKACB is also associated with inhibiting the proliferation and invasion of tumor cells (42), making it a promising therapeutic target in combination with existing immunotherapies.

KLF5 (Kruppel-like factor 5) is a transcription factor known for its role in cell proliferation, differentiation, and apoptosis (43). Studies indicate that KLF5 can enhance the expression of CYP1A1, which are involved in inducing the expression of proinflammatory

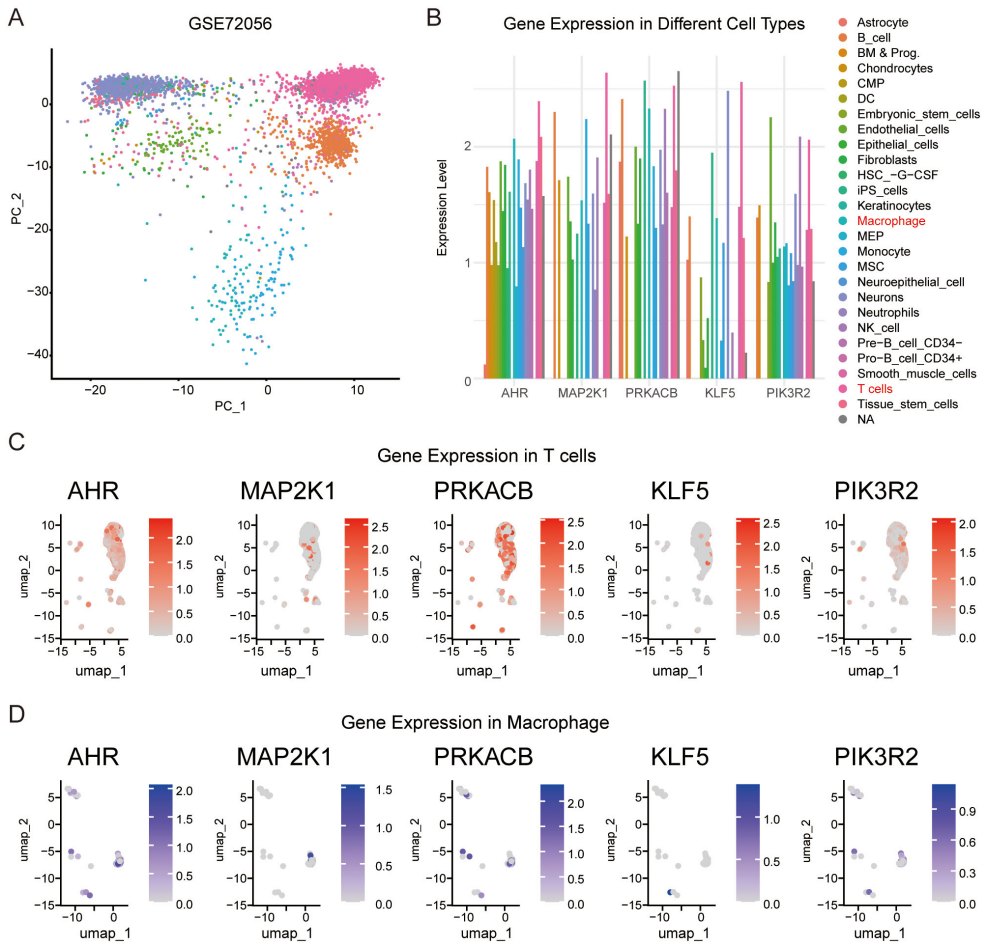

FIGURE 7
Validation of the relationships between feature genes and immune cells. **(A)** Single cell expression profiles were clustered into different cell types using the SingleR R package. **(B)** Expression levels of AHR and the four feature genes across various cell types. **(C)** Expression of AHR, MAP2K1, KLF5, PRKACB, and PIK3R2 in T cells. **(D)** Expression of AHR, MAP2K1, KLF5, PRKACB, and PIK3R2 in macrophage.

cytokines (such as TNF) that can influence melanoma progression (44, 45). KLF5 can promote the epithelial-mesenchymal transition (EMT) (46), a process crucial for melanoma invasion and metastasis (47), making it a potential target for therapeutic interventions aimed at disrupting these pathways. Moreover, KLF5 can promote the podosome formation in macrophages and enhance the tissue infiltration ability of macrophages (48). KLF5 promotes malignant phenotype of melanoma cells and inhibits autophagy, leading to poor prognosis (49). Targeting KLF5 could, therefore, be a potential strategy to reverse EMT and reduce immunosuppression in the TME.

PIK3R2, encoding the regulatory subunit of phosphoinositide-3-kinase (PI3K), is frequently activated in various cancers, including melanoma (50). Activation of AHR has been shown to lead to the phosphorylation of AKT, a downstream effector of the PI3K pathway, thereby promoting tumor cell proliferation and chemotherapy drug resistance (32). PIK3R2 is identified to promote malignant progression of melanoma by activating the PI3K/AKT/NF - κ B pathway (51). Here, we indicate a negative correlation between PIK3R2 expression and T cell infiltration, alongside a positive association with M2 macrophages. This dual association highlights the immunosuppressive role of PIK3R2 in the TME. Additionally, several bioinformatics analyses based on melanoma transcriptome have indicated that PIK3R2 leads to poor prognosis and low immune cell infiltration in melanoma (52, 53). Targeting PIK3R2 in combination with therapies that reprogram macrophages could potentially enhance anti-tumor immunity and improve patient outcomes.

The upregulation of AHR, MAP2K1, and PRKACB, alongside the downregulation of KLF5 and PIK3R2 (Figure 4D), suggests that these genes play critical roles in melanoma progression through various signaling pathways. AHR promotes immune evasion and tumor progression, influencing MAP2K1 and PRKACB, which regulate key pathways like MAPK and NF-κB signaling, respectively. Conversely, the downregulation of KLF5 and PIK3R2 may facilitate a more aggressive, proliferative melanoma phenotype

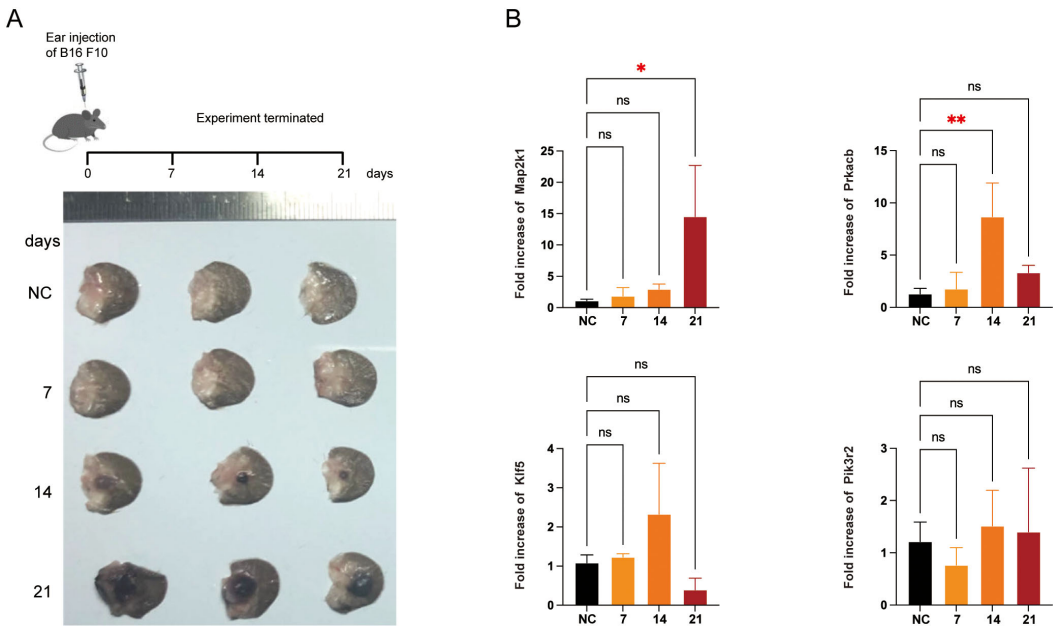

FIGURE 8
Validation of the feature genes in mice melanoma model. **(A)** Schematic representation for the mice model. B16 F10 cells were injected into right ears of C57BL/6 mice (n = 3). Representative tumor images from three independent experiments were shown. **(B)** qRT-PCR for the feature genes in the tumor or normal tissue. *P < 0.05, **P < 0.01.

by affecting cell differentiation and metabolism (Figure 5). In the mouse model, the differential expression of these genes over time reflects their roles in tumor progression, with the immune microenvironment possibly influencing gene expression. These findings highlight the importance of these genes as potential therapeutic targets and the need for further investigation into their roles in immune modulation and melanoma progression.

4.3 Integration of bioinformatics and machine learning

The extensive application of high-throughput sequencing technologies and machine learning has significantly advanced our comprehension of biological processes and cancer heterogeneity (54). Increasingly, researchers have been able to identify distinct molecular characteristics associated with disease progression, patient outcomes, and responses to treatment using sequencing data (55). By leveraging diverse feature selection algorithms, the study achieved high C-index values, validating the reliability of these genes in predicting patient survival outcomes. This integration underscores the growing potential of computational tools in uncovering complex molecular interactions and identifying actionable therapeutic targets. Additionally, Drug sensitivity analyses further support the feasibility of these approaches, providing a foundation for preclinical and clinical investigations.

4.4 Limitations and future directions

However, our study has certain limitations. A more profound understanding of the molecular mechanisms linking AHR with melanoma is evidently required. Both *in vivo* and *in vitro* experiments hold great potential to clarify these complexities, indicating numerous opportunities for future research. This inquiry is anticipated to expand our knowledge and introduce new therapeutic possibilities for managing melanoma, paving the way for enhanced understanding and future innovations in treatment.

4.5 Conclusion

This study provides an integrated approach to understanding the AhR pathway's role in melanoma, identifying MAP2K1, PRKACB, KLF5, and PIK3R2 as critical prognostic markers and therapeutic targets. By employing bioinformatic tools and machine learning techniques, a more detailed understanding of the AHR pathway's involvement in immune regulation and tumor development has been achieved. The use of bioinformatics and machine learning not only enhances our understanding of melanoma biology but also paves the way for more effective therapeutic strategies.

Data availability statement

The original contributions presented in the study are included in the article/Supplementary Material. Further inquiries can be directed to the corresponding author.

Ethics statement

The animal study was approved by the Ethics Committee of Tongji Medical College of Huazhong University of Science and Technology. This study was conducted in accordance with the recommendations of the Guide for the Care and Use of Laboratory Animals of Hubei Provincial Animal Care and Use Committee.

Author contributions

QL: Conceptualization, Data curation, Investigation, Methodology, Writing – review & editing. HL: Conceptualization, Data curation, Project administration, Software, Writing – original draft, Writing – review & editing.

Funding

The author(s) declare financial support was received for the research, authorship, and/or publication of this article. This work was supported by the Scientific Research Fund Cultivation Project of Tongji Hospital (<grant number 2023B14>).

Conflict of interest

The authors declare that the research was conducted in the absence of any commercial or financial relationships that could be construed as a potential conflict of interest.

Generative AI statement

The author(s) declare that no Generative AI was used in the creation of this manuscript.

Publisher's note

All claims expressed in this article are solely those of the authors and do not necessarily represent those of their affiliated organizations, or those of the publisher, the editors and the reviewers. Any product that may be evaluated in this article, or claim that may be made by its manufacturer, is not guaranteed or endorsed by the publisher.

Supplementary material

The Supplementary Material for this article can be found online at: https://www.frontiersin.org/articles/10.3389/fimmu.2024.1519345/full#supplementary-material

References

1. Splendiani E, Besharat ZM, Covre A, Maio M, Di Giacomo AM, Ferretti E. Immunotherapy in melanoma: Can we predict response to treatment with circulating biomarkers? *Pharmacol Ther*. (2024) 256:108613. doi: 10.1016/j.pharmthera.2024.108613

2. Holder AM, Dedeilia A, Sierra-Davidson K, Cohen S, Liu D, Parikh A, et al. Defining clinically useful biomarkers of immune checkpoint inhibitors in solid tumours. *Nat Rev Cancer*. (2024) 24:498–512. doi: 10.1038/s41568-024-00705-7

3. Hezaveh K, Shinde RS, Klötgen A, Halaby MJ, Lamorte S, Ciudad MT, et al. Tryptophan-derived microbial metabolites activate the aryl hydrocarbon receptor in tumor-associated macrophages to suppress anti-tumor immunity. *Immunity*. (2022) 55:324–340.e8. doi: 10.1016/j.immuni.2022.01.006

4. Bahman F, Choudhry K, Al-Rashed F, Al-Mulla F, Sindhu S, Ahmad R. Aryl hydrocarbon receptor: current perspectives on key signaling partners and immunoregulatory role in inflammatory diseases. *Front Immunol*. (2024) 15:1421346. doi: 10.3389/fimmu.2024.1421346

5. Elson DJ, Kolluri SK. Tumor-suppressive functions of the aryl hydrocarbon receptor (AhR) and ahR as a therapeutic target in cancer. *Biol (Basel)*. (2023) 12:526. doi: 10.3390/biology12040526

6. Bender MJ, McPherson AC, Phelps CM, Pandey SP, Laughlin CR, Shapira JH, et al. Dietary tryptophan metabolite released by intratumoral Lactobacillus reuteri facilitates immune checkpoint inhibitor treatment. *Cell*. (2023) 186(9):1846–18.e26. doi: 10.1016/j.cell.2023.03.011

7. Griffith BD, Frankel TL. The aryl hydrocarbon receptor: impact on the tumor immune microenvironment and modulation as a potential therapy. *Cancers*. (2024) 16:472. doi: 10.3390/cancers16030472

8. Mascanfroni ID, Takenaka MC, Yeste A, Patel B, Wu Y, Kenison JE, et al. Metabolic control of type 1 regulatory (Tr1) cell differentiation by AHR and HIF1-α. *Nat Med*. (2015) 21:638. doi: 10.1038/nm.3868

9. Veldhoen M, Hirota K, Westendorf AM, Buer J, Dumoutier L, Renauld J-C, et al. The aryl hydrocarbon receptor links TH17-cell-mediated autoimmunity to environmental toxins. *Nature*. (2008) 453:106–9. doi: 10.1038/nature06881

10. Halbrook CJ, Pontious C, Kovalenko I, Lapienyte L, Dreyer S, Lee H-J, et al. Macrophage-released pyrimidines inhibit gemcitabine therapy in pancreatic cancer. *Cell Metab*. (2019) 29:1390–1399.e6. doi: 10.1016/j.cmet.2019.02.001

11. Wu N, Li J, Li L, Yang L, Dong L, Shen C, et al. MerTK+ macrophages promote melanoma progression and immunotherapy resistance through AhR-ALKAL1 activation. *Sci Adv*. (2024) 10:eado8366. doi: 10.1126/sciadv.ado8366

12. Labadie BW, Bao R, Luke JJ. Reimagining IDO pathway inhibition in cancer immunotherapy via downstream focus on the tryptophan-kynurenine-aryl hydrocarbon axis. *Clin Cancer Res*. (2019) 25:1462–71. doi: 10.1158/1078-0432.CCR-18-2882

13. Bogunovic D, O'Neill DW, Belitskaya-Levy I, Vacic V, Yu Y-L, Adams S, et al. Immune profile and mitotic index of metastatic melanoma lesions enhance clinical staging in predicting patient survival. *Proc Natl Acad Sci U.S.A*. (2009) 106:20429–34. doi: 10.1073/pnas.0905139106

14. Cabrita R, Lauss M, Sanna A, Donia M, Skaarup Larsen M, Mitra S, et al. Tertiary lymphoid structures improve immunotherapy and survival in melanoma. *Nature*. (2020) 577:561–5. doi: 10.1038/s41586-019-1914-8

15. Tirosh I, Izar B, Prakadan SM, Wadsworth MH, Treacy D, Trombetta JJ, et al. Dissecting the multicellular ecosystem of metastatic melanoma by single-cell RNA-seq. *Science*. (2016) 352:189–96. doi: 10.1126/science.aad0501

16. Aran D, Looney AP, Liu L, Wu E, Fong V, Hsu A, et al. Reference-based analysis of lung single-cell sequencing reveals a transitional profibrotic macrophage. *Nat Immunol*. (2019) 20:163–72. doi: 10.1038/s41590-018-0276-y

17. Hao Y, Stuart T, Kowalski MH, Choudhary S, Hoffman P, Hartman A, et al. Dictionary learning for integrative, multimodal and scalable single-cell analysis. *Nat Biotechnol*. (2024) 42:293–304. doi: 10.1038/s41587-023-01767-y

18. Ritchie ME, Phipson B, Wu D, Hu Y, Law CW, Shi W, et al. limma powers differential expression analyses for RNA-sequencing and microarray studies. *Nucleic Acids Res*. (2015) 43:e47. doi: 10.1093/nar/gkv007

19. Zhou G, Soufan O, Ewald J, Hancock REW, Basu N, Xia J. NetworkAnalyst 3.0: a visual analytics platform for comprehensive gene expression profiling and meta-analysis. *Nucleic Acids Res*. (2019) 47:W234–41. doi: 10.1093/nar/gkz240

20. Liu H, Zhang W, Zhang Y, Adegboro AA, Fasoranti DO, Dai L, et al. Mime: A flexible machine-learning framework to construct and visualize models for clinical characteristics prediction and feature selection. *Comput Struct Biotechnol J*. (2024) 23:2798–810. doi: 10.1016/j.csbj.2024.06.035

21. Sturm G, Finotello F, Petitprez F, Zhang JD, Baumbach J, Fridman WH, et al. Comprehensive evaluation of transcriptome-based cell-type quantification methods for immuno-oncology. *Bioinformatics*. (2019) 35:i436–45. doi: 10.1093/bioinformatics/btz363

22. Wu T, Hu E, Xu S, Chen M, Guo P, Dai Z, et al. clusterProfiler 4.0: A universal enrichment tool for interpreting omics data. *Innovation (Camb)*. (2021) 2:100141. doi: 10.1016/j.xinn.2021.100141

23. Liu C-J, Hu F-F, Xie G-Y, Miao Y-R, Li X-W, Zeng Y, et al. GSCA: an integrated platform for gene set cancer analysis at genomic, pharmacogenomic and immunogenomic levels. *Brief Bioinform*. (2023) 24:bbac558. doi: 10.1093/bib/bbac558

24. Chen Y, Wang X. miRDB: an online database for prediction of functional microRNA targets. *Nucleic Acids Res*. (2020) 48:D127-D131. doi: 10.1093/nar/gkz757

25. Li J-H, Liu S, Zhou H, Qu L-H, Yang J-H. starBase v2.0: decoding miRNA-ceRNA, miRNA-ncRNA and protein-RNA interaction networks from large-scale CLIP-Seq data. *Nucleic Acids Res*. (2014) 42:D92–97. doi: 10.1093/nar/gkt1248

26. Hwang B-J, Zhang Y, Brozowski JM, Liu Z, Burette S, Lough K, et al. The dysfunction of BP180/collagen XVII in keratinocytes promotes melanoma progression. *Oncogene*. (2019) 38:7491. doi: 10.1038/s41388-019-0961-9

27. Xue P, Fu J, Zhou Y. The aryl hydrocarbon receptor and tumor immunity. *Front Immunol*. (2018) 9:286. doi: 10.3389/fimmu.2018.00286

28. Kober C, Roewe J, Schmees N, Roese L, Roehn U, Bader B, et al. Targeting the aryl hydrocarbon receptor (AhR) with BAY 2416964: a selective small molecule inhibitor for cancer immunotherapy. *J Immunother Cancer*. (2023) 11:e007495. doi: 10.1136/jitc-2023-007495

29. Truong A, Yoo JH, Scherzer MT, Sanchez JMS, Dale KJ, Kinsey CG, et al. Chloroquine sensitizes GNAQ/11-mutated melanoma to MEK1/2 inhibition. *Clin Cancer Res*. (2020) 26:6374–86. doi: 10.1158/1078-0432.CCR-20-1675

30. Xie S, Tan X, Liu Y, Duan Y, Chen G, Feng H, et al. Hypersonins A-D, polycyclic polyprenylated acylphloroglucinols with a 1,2-seco-homoadamantane architecture from hypericum wilsonii. *J Nat Prod*. (2020) 83:1804–9. doi: 10.1021/acs.jnatprod.9b01187

31. Lee Y-H, Lin C-H, Hsu P-C, Sun Y-Y, Huang Y-J, Zhuo J-H, et al. Aryl hydrocarbon receptor mediates both proinflammatory and anti-inflammatory effects in lipopolysaccharide-activated microglia. *Glia*. (2015) 63:1138–54. doi: 10.1002/glia.22805

32. Akhtar S, Hourani S, Therachiyil L, Al-Dhfyan A, Agouni A, Zeidan A, et al. Epigenetic regulation of cancer stem cells by the aryl hydrocarbon receptor pathway. *Semin Cancer Biol*. (2022) 83:177–96. doi: 10.1016/j.semcancer.2020.08.014

33. Gong S, Zheng J, Zhang J, Han J. Arabinogalactan ameliorates benzo[a]pyrene-induced intestinal epithelial barrier dysfunction via AhR/MAPK signaling pathway. *Int J Biol Macromol*. (2023) 242:124866. doi: 10.1016/j.ijbiomac.2023.124866

34. Schreuer M, Jansen Y, Planken S, Chevolet I, Seremet T, Kruse V, et al. Combination of dabrafenib plus trametinib for BRAF and MEK inhibitor pretreated patients with advanced BRAFV600-mutant melanoma: an open-label, single arm, dual-centre, phase 2 clinical trial. *Lancet Oncol*. (2017) 18:464–72. doi: 10.1016/S1470-2045(17)30171-7

35. Taylor SS, Wallbott M, Machal EMF, Søberg K, Ahmed F, Bruystens J, et al. PKA Cβ: a forgotten catalytic subunit of cAMP-dependent protein kinase opens new windows for PKA signaling and disease pathologies. *Biochem J*. (2021) 478:2101–19. doi: 10.1042/BCJ20200867

36. Ni H, Tang S, Yuan X, Xu J, Zheng F, Chen K, et al. Prolonged exposure of environmental concentration benzo[a]pyrene promoted cancer stemness through AhR/PKA/SOX2 dependent pathway in small cell lung cancer. *Sci Total Environ*. (2024) 906:167824. doi: 10.1016/j.scitotenv.2023.167824

37. Finger EC, Castellini L, Rankin EB, Vilalta M, Krieg AJ, Jiang D, et al. Hypoxic induction of AKAP12 variant 2 shifts PKA-mediated protein phosphorylation to enhance migration and metastasis of melanoma cells. *Proc Natl Acad Sci U.S.A*. (2015) 112:4441–6. doi: 10.1073/pnas.1418164112

38. Cui Y, Miao Y, Cao L, Guo L, Cui Y, Yan C, et al. Activation of melanocortin-1 receptor signaling in melanoma cells impairs T cell infiltration to dampen antitumor immunity. *Nat Commun*. (2023) 14:5740. doi: 10.1038/s41467-023-41101-3

39. Bae J, Kumazoe M, Lee K-W, Fujimura Y, Tachibana H. 67-kDa laminin receptor mediates oolonghomobisflavan B-induced cell growth inhibition in melanoma. *Phytomedicine*. (2023) 118:154970. doi: 10.1016/j.phymed.2023.154970

40. Postler TS. A most versatile kinase: The catalytic subunit of PKA in T-cell biology. *Int Rev Cell Mol Biol*. (2021) 361:301–18. doi: 10.1016/bs.ircmb.2021.01.005

41. Tan X, Qi C, Zhao X, Sun L, Wu M, Sun W, et al. ERK inhibition promotes engraftment of allografts by reprogramming T-cell metabolism. *Adv Sci (Weinh)*. (2023) 10:e2206768. doi: 10.1002/advs.202206768

42. Chen Y, Gao Y, Tian Y, Tian D-L. PRKACB is downregulated in non-small cell lung cancer and exogenous PRKACB inhibits proliferation and invasion of LTEP-A2 cells. *Oncol Lett*. (2013) 5:1803–8. doi: 10.3892/ol.2013.1294

43. Zeng L, Zhu Y, Moreno CS, Wan Y. New insights into KLFs and SOXs in cancer pathogenesis, stemness, and therapy. *Semin Cancer Biol*. (2023) 90:29–44. doi: 10.1016/j.semcancer.2023.02.003

44. Hawerkamp HC, Kislat A, Gerber PA, Pollet M, Rolfes KM, Soshilov AA, et al. Vemurafenib acts as an aryl hydrocarbon receptor antagonist: Implications for inflammatory cutaneous adverse events. *Allergy*. (2019) 74:2437–48. doi: 10.1111/all.13972

45. Qi C, Tan X, Shi Z, Feng H, Sun L, Hu Z, et al. Discovery of an oxepine-containing diketopiperazine derivative active against concanavalin A-induced hepatitis. *J Nat Prod*. (2020) 83:2672–8. doi: 10.1021/acs.jnatprod.0c00558

46. Zhang X, Chen J, Lin R, Huang Y, Wang Z, Xu S, et al. Lactate drives epithelial-mesenchymal transition in diabetic kidney disease via the H3K14la/KLF5 pathway. *Redox Biol*. (2024) 75:103246. doi: 10.1016/j.redox.2024.103246

47. Liu H, Gao J, Feng M, Cheng J, Tang Y, Cao Q, et al. Integrative molecular and spatial analysis reveals evolutionary dynamics and tumor-immune interplay of in *situ* and invasive acral melanoma. *Cancer Cell*. (2024) 42:1067–1085.e11. doi: 10.1016/j.ccell.2024.04.012

48. Ma D, Zheng B, Suzuki T, Zhang R, Jiang C, Bai D, et al. Inhibition of KLF5-myo9b-rhoA pathway-mediated podosome formation in macrophages ameliorates abdominal aortic aneurysm. *Circ Res*. (2017) 120:799–815. doi: 10.1161/CIRCRESAHA.116.310367

49. Jia X, Chen H, Ren Y, Dejizhuoga, Gesangyuzhen, Gao N, et al. BAP1 antagonizes WWP1-mediated transcription factor KLF5 ubiquitination and inhibits autophagy to promote melanoma progression. *Exp Cell Res*. (2021) 402:112506. doi: 10.1016/j.yexcr.2021.112506

50. Vallejo-Díaz J, Chagoyen M, Olazabal-Morán M, González-García A, Carrera AC. The opposing roles of PIK3R1/p85α and PIK3R2/p85β in cancer. *Trends Cancer*. (2019) 5:233–44. doi: 10.1016/j.trecan.2019.02.009

51. Wang J, Cai S, Xiong Q, Weng D, Wang Q, Ma Z. PIK3R2 predicts poor outcomes for patients with melanoma and contributes to the Malignant progression via PI3K/AKT/NF-κB axis. *Clin Transl Oncol*. (2023) 25:1402–12. doi: 10.1007/s12094-022-03036-x

52. Liu J, Ma R, Chen S, Lai Y, Liu G. Anoikis patterns via machine learning strategy and experimental verification exhibit distinct prognostic and immune landscapes in melanoma. *Clin Transl Oncol*. (2024) 26:1170–86. doi: 10.1007/s12094-023-03336-w

53. Tian M, Yang J, Han J, He J, Liao W. A novel immune checkpoint-related seven-gene signature for predicting prognosis and immunotherapy response in melanoma. *Int Immunopharmacol*. (2020) 87:106821. doi: 10.1016/j.intimp.2020.106821

54. Kourou K, Exarchos TP, Exarchos KP, Karamouzis MV, Fotiadis DI. Machine learning applications in cancer prognosis and prediction. *Comput Struct Biotechnol J*. (2015) 13:8–17. doi: 10.1016/j.csbj.2014.11.005

55. Ding L, Bailey MH, Porta-Pardo E, Thorsson V, Colaprico A, Bertrand D, et al. Perspective on oncogenic processes at the end of the beginning of cancer genomics. *Cell*. (2018) 173:305–320.e10. doi: 10.1016/j.cell.2018.03.033

frontiers | Frontiers in Immunology

TYPE Systematic Review
PUBLISHED 08 January 2025
DOI 10.3389/fimmu.2024.1526481

Check for updates

OPEN ACCESS

EDITED BY
Qingyu Luo,
Dana–Farber Cancer Institute, United States

REVIEWED BY
Xiaowei Wu,
Dana–Farber Cancer Institute, United States
Haili Ma,
Dana–Farber Cancer Institute, United States

*CORRESPONDENCE
Rong Yu
yurong196905@163.com

†These authors have contributed equally to this work

RECEIVED 11 November 2024
ACCEPTED 13 December 2024
PUBLISHED 08 January 2025

CITATION
Zhou T, Yu Y, Li L, Liu X, Xiang Q and Yu R (2025) Bibliometric analysis of metformin as an immunomodulator (2013–2024). *Front. Immunol.* 15:1526481. doi: 10.3389/fimmu.2024.1526481

COPYRIGHT
© 2025 Zhou, Yu, Li, Liu, Xiang and Yu. This is an open-access article distributed under the terms of the Creative Commons Attribution License (CC BY). The use, distribution or reproduction in other forums is permitted, provided the original author(s) and the copyright owner(s) are credited and that the original publication in this journal is cited, in accordance with accepted academic practice. No use, distribution or reproduction is permitted which does not comply with these terms.

Bibliometric analysis of metformin as an immunomodulator (2013–2024)

Tongyi Zhou[1†], Yunfeng Yu[1†], Liu Li[1], Xiu Liu[1,2], Qin Xiang[1] and Rong Yu[1,2*]

[1]School of Traditional Chinese Medicine, Hunan University of Chinese Medicine, Changsha, China, [2]Hunan Key Laboratory of Traditional Chinese Medicine Prescription and Syndromes Translational Medicine, Hunan University of Chinese Medicine, Changsha, China

Background: Metformin, the frontline treatment for diabetes, has considerable potential as an immunomodulator; however, detailed bibliometric analyses on this subject are limited.

Methods: This study extracted 640 relevant articles from the Web of Science (WOS) Core Collection and conducted visual analyses using Microsoft Excel, VOSviewer, and CiteSpace.

Results: The findings showed that research on the immunomodulatory function of metformin has grown steadily since 2017, with China and the United States being the leading contributors. These studies have mostly been published in journals such as *the International Journal of Molecular Sciences, Cancers, Frontiers in Immunology, and Scientific Reports*. Keyword co-occurrence analysis highlighted metformin's role as an immunomodulator, particularly in the context of the tumor immune microenvironment, immunosuppressive checkpoints, and metformin derivatives. Recent research has highlighted metformin's application in aging, autoimmune diseases, COVID-19, and tuberculosis. Additionally, its role in regulating inflammation and gut microbiota is also being investigated.

Conclusion: Overall, the immunomodulatory effects of metformin were investigated in anti-tumor, antiviral, anti-aging, and autoimmune disease research. This highlights the scope of metformin use in these fields, while also significantly enhancing its clinical value as a repurposed drug.

KEYWORDS

metformin, immunomodulator, tumor immune microenvironment, immune checkpoint inhibition, aging, inflammation, bibliometric analysis

1 Introduction

Metformin, a guanidine derivative of herbal goat bean, has long been the primary oral hypoglycemic agent used to treat type 2 diabetes (T2DM). It is recognized for its high-efficiency hypoglycemic and cardiovascular protective effects, without increasing body weight or the risk of hypoglycemia (1). This drug has garnered significant attention due to its extensive clinical application and potential health benefits. Preclinical and observational studies have demonstrated the promising potential of metformin in treating conditions such as obesity, metabolic syndrome, osteoporosis, rheumatoid arthritis, aging, periodontitis, cancer, liver disease, kidney disease, inflammatory bowel disease, tuberculosis, coronavirus disease 2019 (COVID-19), osteoarthritis, and other autoimmune inflammatory rheumatic diseases (2–4). However, the specific mechanisms and clinical efficacy of these effects requires further investigation.

Over the past decade, research has displayed that in addition to its hypoglycemic effects, metformin can regulate cell energy metabolism, proliferation, growth, inflammation, endoplasmic reticulum stress (ERS), and autophagy, as well as improve intestinal flora (5–8). Mounting evidence shows that metformin is an effective immune system activator (9). It not only regulates the host immune function but also demonstrates an enhanced therapeutic efficacy in treating the aforementioned diseases and overcomes immunotherapy resistance, although the molecular mechanisms of these effects are not completely understood (10, 11). The unexpected immunomodulatory benefits of metformin were initially identified by Pearceet al. (12), who demonstrated that metformin enhances the generation and persistence of memory CD8+ T cells by activating fatty acid oxidation in T cells, revealing a novel mechanism for improving immune function. This finding was later supported by Finisguerra et al. (13). Many experimental and clinical studies have demonstrated that metformin can regulate tumor-infiltrating effector immune cells and inhibit immunosuppressive cells in various tumor models of breast, liver, lung, head and neck, and colorectal cancer (14–18). Metformin also exhibits an anti-tumor effect by regulating programmed death-1 (PD-1)/programmed death-ligand 1(PD-L1) immunosuppressive checkpoints, which may involve ERS and adenosine monophosphate-activated protein kinase (AMPK) pathways (19, 20). Other studies have shown that metformin prevents age-related ovarian fibrosis by balancing the number of fibroblasts, myofibroblasts and immune cells (21). Furthermore, metformin exerts its anti-inflammatory and immunosuppressive effects by regulating the macrophage expression of the plasticity factor, zinc finger e-box binding homeobox 1(ZEB1) (22). However, in cases of obesity (23), atherosclerosis (24), and bone-related lesions (25), metformin induces M2 polarization. Rodriguez's team found that supformin, a metformin dimer, disrupts the plasticity of human immune cells, dendritic cells (DCs) and macrophages. Thus, opening avenues for the development of innovative treatments (26). Given its considerable potential, metformin as an immunomodulator is increasingly featured in scientific publications. However, an integration of data and visual analysis is essential to better understand the developments in this domain.

This bibliometric study focuses on the direct relationship between metformin and its immunomodulatory effects. Bibliometric analysis is widely used to quantitatively evaluate published studies and predict future trends. This type of research is based on existing literature involving different countries, institutions, authors, journals, and keywords. It uses mathematical and statistical tools to quantify and predict the status quo of scientific research to objectively evaluate the knowledge framework and identify research hotspots. Recently, the number of research publications in this field has increased rapidly. Nonetheless, bibliometric analyses of metformin as an immunomodulator remain limited. This study evaluated published research on metformin's role as an immunomodulator over the past decade and aimed to provide new insights for academic dynamics, drug development, and disease treatment, offering a broad perspective and roadmap for future research.

2 Materials and methods

2.1 Search strategy

This study collected research on metformin and immune regulation published from January 1, 2013, to October 1, 2024, from the WOS core collection database. Data collection was completed on October 8, 2024. The search utilized the following keywords ((TS=(Metformin OR Dimethylbiguanidine OR Dimethylguanylguanidine OR Glucophage)) AND (TS=(Immunity OR Immunization OR Immunological OR Immune))).

2.2 Data collection

To ensure the authenticity and reliability of the study, two researchers collaborated closely in retrieving and thoroughly screening the data. By excluding irrelevant literature individually, a total of 640 papers were analyzed. The detailed data screening process is illustrated in Figure 1. All retrieved literature that met the established criteria were used in the bibliometric analysis. The complete records and reference lists were extracted and saved as "txt" files, which served as the data source for the analysis.

2.3 Data analysis and visualization

We used CiteSpace (version 6.4.R1), VOSviewer (version 1.6.20), and Microsoft Excel 365 for analyzing and presenting data. VOSviewer (27) was used to extract detailed information of countries, institutions, journals, authors, citations, and keywords, as well as to construct a network visualization map. Each node in VOSviewer represented an entity, and its size was related to its weight. The thickness of the connection between the nodes was closely related to the strength of cooperation, co-citation and co-occurrence. We used CiteSpace (version 6.4.R1) (28) to calculate the burst of references, timeline of keywords, and burst of keywords to visualize the data. Microsoft Excel 365 was utilized to visualize the

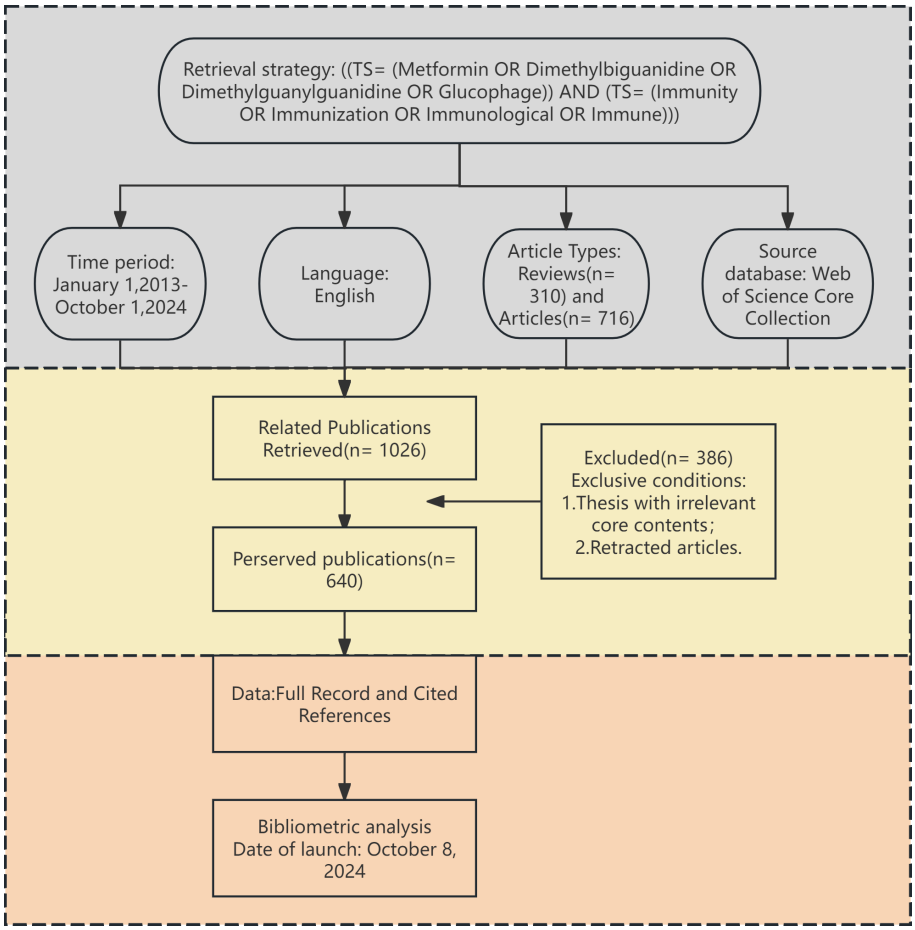

FIGURE 1
Flow diagram presenting the selection process for studies on metformin as an immunomodulator. This diagram depicts the screening of 640 publications published between January 2013 and October 2024.

annual count of literature, countries, institutions, authors, journals, and the most cited local references.

3 Results

3.1 Quantitative analysis of publications output

This study retrieved and reviewed effective literature from 2013 to 2024 in the WOS core database, screening 640 papers from 4,354 authors across 77 countries and 1,246 institutions. Figure 2 demonstrates a steady increase in the number of articles related to metformin and immune regulation over time. This trend indicated that researchers paid little attention to the immunomodulatory mechanism of metformin between 2013 and 2016, with fewer than 20 articles published annually. As the potential therapeutic value of metformin's immune regulation was better understood, there was a rapid increase on its research over the following eight years. By 2021, the annual number of publications exceeded 100, which was nearly ten times the previous number. This demonstrated that metformin as an immunomodulator has garnered significant interest from researchers.

3.2 Country and institutional analysis

3.2.1 Inter-country research cooperation network

A total of 77 countries are conducting research on the immunomodulating properties of metformin. Table 1 highlights the top 10 countries based on published articles, with China (n=217) and United States of America (USA) (n=158) accounting for 58.60% of the total number of published articles. This highlights the dominance of these two countries in this field. Notably, although USA has fewer publications than China, the average citation per article (47.95 times) and h-index (47) are higher, indicating greater research quality and influence. Additionally, the size of each node in Figure 3 and the thickness of the connections between adjacent nodes reflect the degree of cooperation between countries. For example, in addition to its deep cooperation with China, USA also has positive cooperative relationships with Germany, Italy, Canada, Japan, and France.

FIGURE 2
Publication trends of metformin as an immunomodulator. The orange bar chart shows the cumulative number of publications, and the blue line chart represents the annual number of publications. The horizontal axis marks the years, the left vertical axis indicates the cumulative publication count, and the right vertical axis denotes the annual publication count.

3.2.2 Inter-agency cooperation network

The studies were performed 1,246 institutions. Table 2 shows the top 14 institutions with more than 7 related publications, including 10 from China, 2 from USA, and 1 from Japan and Austria. Shanghai Jiao Tong Univ (n=17) published the most papers, followed by Okayama Univ (n=15), and Harvard Med School (n=15). Notably, China Med Univ (average citation rate 82.14) and Northwestern Univ (average citation rate 72.14) achieved higher average citation rates. Additionally, the visual map in Figure 4 shows a close cluster effect among different institutions. Specifically, Harvard Med School (Total link strength [TLS]=45), Chinese Acad Sci [TLS=26] exhibit extensive collaborations with other institutions.

3.2.3 Cooperation network among authors

Through screening, a total of 4,353 authors and 28,209 co-cited authors were identified. Table 3 gathers the top 10 most prolific and most frequently co-cited authors. Heiichiro Udono (n=13) emerged as the most prolific author, followed by Mikako Nishida (n=6) and Shingo Eikawa (n=5). Notably, Shingo Eikawa stood out with the highest average citation count of 129.6, highlighting substantial academic influence. Figure 5A illustrates a close collaborative relationships among these cited authors. Furthermore, Figure 5B showcases authors with more than 20 co-citations, with the top three being Shingo Eikawa (113 citations), Marc Foretz (97 citations), and Jeong-Heon Cha (91 citations), indicating the important contributions of these authors in these relevant research fields.

3.2.4 Cooperation network among journals

The 640 articles included in this study are from 380 journals and 4,438 co-cited journals. The top 10 cited and co-cited journals that published metformin and immunotherapy-related papers are listed in Table 4. Based on the collaboration network of cited journals shown in

TABLE 1 Top 10 countries in the field of Metformin as an immunomodulator.

Rank	Country	Documents	Percent (%)	Total citations	Average citations	H-index
1	China	217	33.91	5942	27.38	42
2	USA	158	24.69	7576	47.95	47
3	Italy	36	5.63	1182	32.83	22
4	Japan	35	5.47	1349	38.54	19
5	France	28	4.38	1171	41.82	20
6	Germany	26	4.06	622	23.92	18
7	England	24	3.75	1179	49.13	21
8	Egypt	22	3.44	198	9.00	10
9	Canada	21	3.28	745	35.48	19
10	South Korea	20	3.13	2246	112.30	17

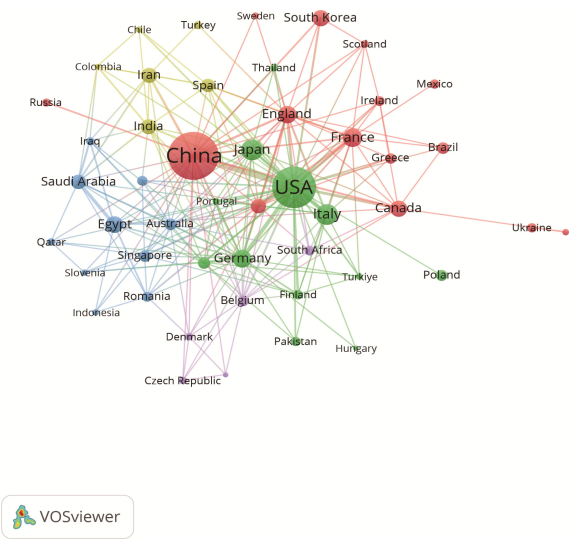

FIGURE 3
Associations between countries with more than two articles. Each circle represents a node, with larger nodes indicating greater influence of a country. The thickness of the lines denotes the strength of collaboration between two countries.

Figure 6A and the 2024 *Journal Citation Report (JCR)*, *International Journal of Molecular Sciences* has published the most papers (n=22, IF=4.9), followed by *Cancers* (n=6, IF=4.5), *Frontiers in Immunology* (n=16, IF=5.7), *Scientific Reports* (n=16, IF=3.8), *International Immunopharmacology* (n=10, IF=4.8), and *Journal for Immunotherapy of Cancer* (n=10, IF=10.3). The VOSviewer co-occurrence analysis showed that *Nature* (IF=50.5), *Plos One* (IF=2.9), and *Proceedings of the National Academy of Sciences of the United States of America (PNAS)* (IF=9.4) had higher co-citation rates (Figure 6B).

3.2.5 Citation and co-citation literature network analysis

An analysis of the top 10 cited and co-cited references using VOSviewer is presented in Tables 5 and 6, with their collaborative networks illustrated in Figures 7A and B. Among the top-cited references, the leading three are Cheng SC. et al. (2014, *Science*, 1,432 citations); Shin NR et al. (2014, *Gut*, 1,176 citations); and Jin MZ. et al. (2020, *Signal Transduction and Targeted Therapy*, 657 citations). These are followed by Cha JH et al. (2018, *Nature Immunology*, 522 citations) and Eikawa S. et al. (2015, *PNAS*, 415 citations). For co-cited references, the top three are by Eikawa S. et al. (2015, *PNAS*, 111 citations); Cha JH et al. (2018, *Molecular Cell*, 87 citations); and Scharping NE. et al. (2017, *Cancer Immunology Research*, 63 citations). Figure 8 highlights the top 15 references with the most significant increase in citations since 2013. Notably, the study by Eikawa S. et al., published in 2015, on the anti-tumor immunotherapy effects of metformin, demonstrates the highest citation burst intensity. Moreover, many references continue to show increasing citation rates, indicating that research into the immune mechanisms of metformin remains a prominent and active area of investigation.

3.3 Keywords and hotspots

Keyword analysis showed the dynamic progress of metformin's immune regulation. Using the "author keywords" mode in VOSviewer, a total of 1,615 keywords were obtained. After merging synonyms, 1,537 keywords were analyzed. Table 7 lists the top 20 keywords with the highest frequency, and Figure 9A displays the co-occurring keyword analysis on metformin and immune regulation research showing the evolution of research focus from 2013 to 2024. The top three core keywords were "metformin" (293 occurrences),

TABLE 2 Top 14 institutions in the field of Metformin as an immunomodulator.

Rank	Institution	Documents	Country	Total citations	Average citations
1	Shanghai Jiao Tong Univ	17	China	1017	59.82
2	Harvard Med School	15	USA	830	55.33
3	Okayama Univ	15	Japan	871	58.07
4	Chinese Acad Sci	14	China	274	19.57
5	Chinese Acad Med Sci & Peking Union Med Coll	13	China	304	23.38
6	Cent South Univ	11	China	230	20.91
7	Huazhong Univ Sci & Technol	11	China	311	28.27
8	Fudan Univ	8	China	200	25.00
9	Med Univ Vienna	7	Austria	195	27.86
10	Northwestern Univ	7	USA	505	72.14
11	China Med Univ	7	China	575	82.14
12	Nanjing Univ	7	China	433	61.86
13	Sun Yat Sen Univ	7	China	215	30.71
14	Zhejiang Univ	7	China	82	11.71

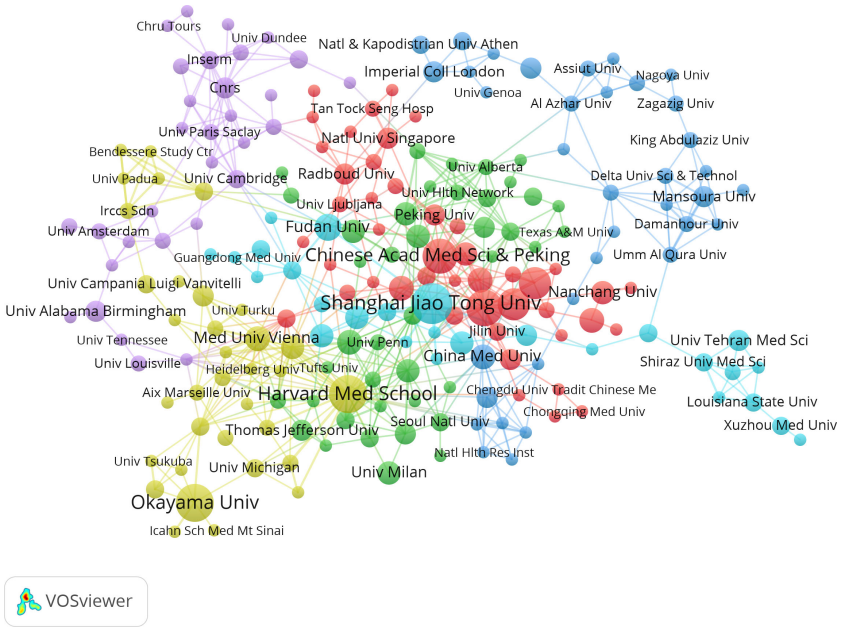

FIGURE 4
Correlations between institutions with more than two articles. In the network, larger nodes indicate greater importance of an institution and thicker lines show a higher frequency of collaborations between institutions.

"diabetes" (78 occurrences), and "immunotherapy" (44 occurrences), followed by "inflammation" (37 occurrences) and "tumor microenvironment" (30 occurrences). These topics have consistently attracted significant interest. Using the density view (Figure 9B) and timeline diagram (Figure 10A) of time evolution, it was observed that since the year 2013, the focus on metformin's immune regulatory properties gradually shifted from metabolic diseases and insulin resistance to tumor immunity, autoimmune diseases, COVID-19, and aging. The mechanisms broadly involve oxidative stress, inflammation, intestinal flora, immunosuppressive checkpoints, the tumor immune microenvironment, and oxidative glycolysis.

From the keyword bursts, the top 20 keywords with the highest burst intensity are shown in Figure 10B. Over the past decade, the focus of metformin immunotherapy has shifted from metabolic and diabetic diseases to the treatment outcomes and mechanisms of tumors. Currently, research is predominantly focused on metformin as an immunomodulator in tumor immunity; however, other mechanisms such as inflammation and intestinal flora are also being explored.

TABLE 3 Top 10 most prolific authors and the 10 most frequently co-cited authors with the highest citation counts.

Author	Documents	Citations	Average citations	Co-cited author	Citations
Heiichiro Udono	13	843	64.85	Shingo Eikawa	113
Mikako Nishida	6	589	98.17	Marc Foretz	97
Shingo Eikawa	5	648	129.60	Jeong-Heon Cha	91
Jenna M. Bartley	4	38	9.50	Nicole E Scharping	70
Mi-La Cho	4	180	45.00	Clifford J Bailey	68
Iryna Kamyshna	4	27	6.75	Jungeun Kim	63
Xin Li	4	236	59.00	D Grahame Hardie	59
Yang Li	4	207	51.75	Gu-Cheng Zhou	57
Ubaldo Martinez-Outschoorn	4	92	23.00	Erika L Pearce	56
Sung-Hwan Park	4	182	45.50	Josie M M Evans	52

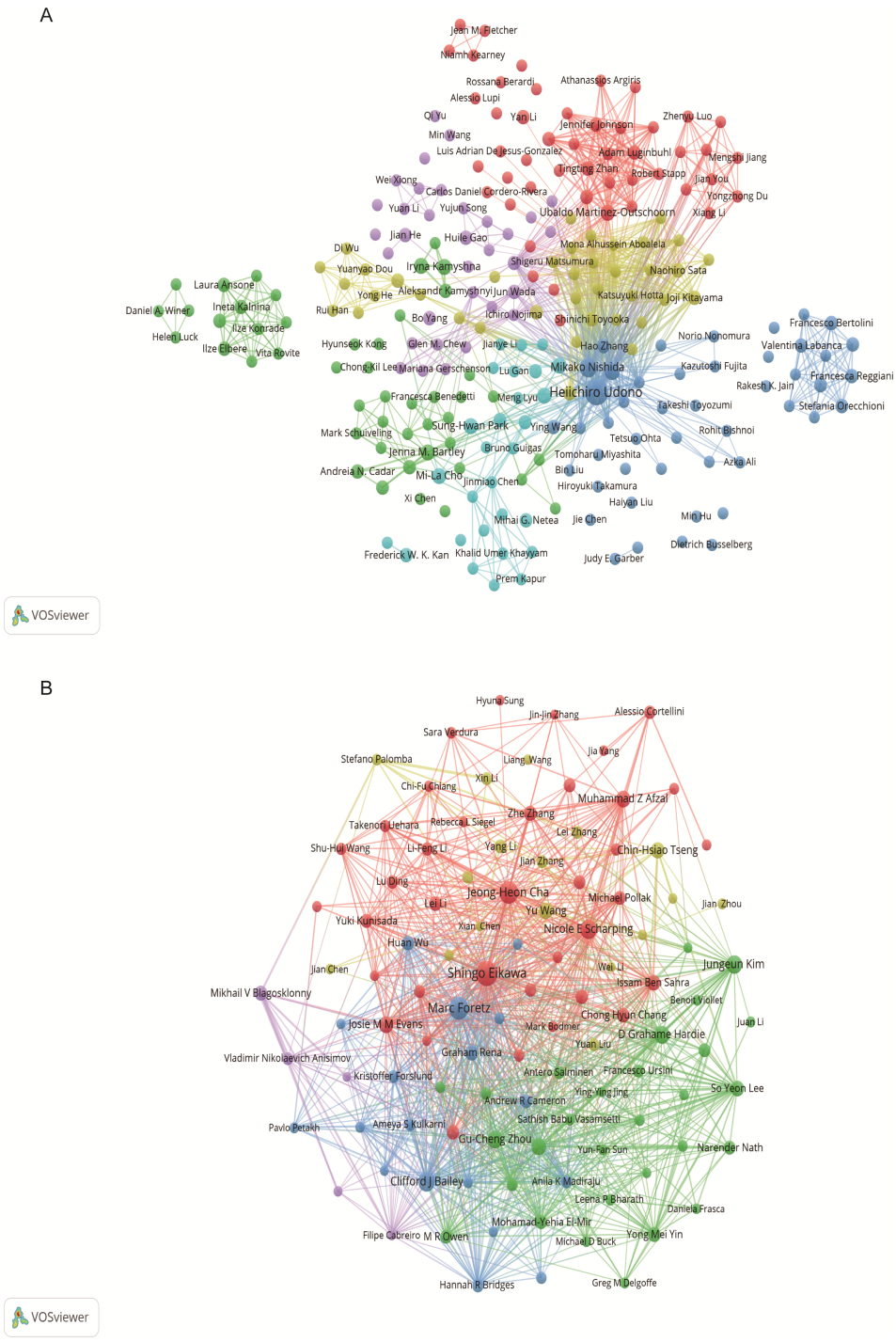

FIGURE 5
Author visualization in metformin as an immunomodulator. **(A)** Cited Author Map: This map includes authors cited in at least two studies. Larger nodes indicate higher citation frequencies, and thicker lines denote closer collaborations in the field of metformin and immunology research. **(B)** Co-cited Author Co-occurrence Map: This map features authors with more than 20 co-citations. Node size and line thickness reflect the frequency of co-citations and the strength of collaborations, respectively. Node colors represent distinct co-cited author collaboration networks.

4 Discussion

4.1 General information

This study conducted a visual analysis on data from 640 publications obtained from WOS, using CiteSpace and VOSviewer. The results depict trends in annual publication volume, geographical and institutional cooperation, journal distribution, author co-occurrence, literature cross-citation, and research hotspots. In 2013, this field was in its infancy; however, the academic output increased significantly from 2017 to 2023, with a publication peak observed in 2020. It is expected that the number

TABLE 4 Top 10 cited journals and co-cited journals that published literatures on metformin as an immunomodulator.

Journal	Articles Counts	IF	Co-cited Journal	Cocitation	IF
International Journal of Molecular Sciences	22	4.9	*Nature*	829	50.5
Cancers	16	4.5	*Plos One*	768	2.9
Frontiers in Immunology	16	5.7	*Proceedings of the National Academy of Sciences of the United States of America*	664	9.4
Scientific Reports	16	3.8	*Journal of Immunology*	653	3.6
International Immunopharmacology	10	4.8	*Cell*	616	45.5
Journal for Immunotherapy of Cancer	10	10.3	*Cell Metabolism*	597	27.7
Frontiers In Oncology	9	3.5	*Frontiers in Immunology*	588	5.7
Plos One	9	2.9	*Cancer Research*	575	12.5
Nature Communications	8	14.7	*Science*	470	44.7
Frontiers in Pharmacology	7	5.6	*Journal of Clinical Investigation*	467	13.3

of articles will continue to grow in 2024 and beyond suggesting of increased interest and focus in this field.

In modern research, the immune response is a crucial factor for understanding the therapeutic mechanism of metformin. Data from various countries and academic institutions showed that most research with high publication volume and h-index has been published from the USA, which has a well-established cooperation network with other countries. Strengthening overall communication would benefit academic development in this field. Analysis of institutional cooperation showed that Chinese institutions dominate research related to metformin immunomodulatory therapy. Domestic institutions frequently cooperate and exhibit regional collection characteristics. The top 3 institutions according to literatures are Shanghai Jiao Tong Univ (17 papers), Okayama Univ (15 papers), and Harvard Med School (15 papers). Regarding journal distribution, the *International Journal of Molecular Sciences* leads in publication frequency with 22 papers, highlighting its exemplary role in this area of research. The hierarchical structure of journals showed that *Cancers, Frontiers in Immunology*, and *Scientific Reports* were the key publishers of this research. Additionally, *Nature* (co-citation = 829) was the most frequently co-cited journal, with the highest impact factor of 50.5. Heiichiro Udono from Okayama University in Japan was a prolific author in this domain (n=13). He collaborated with Shingo Eikawa on studies investigating the enhanced effect of cancer immunotherapy through metabolic intervention with metformin, and has published several highly cited articles (29, 30). These research results provided new perspectives and potential therapeutic strategies for the application of metformin in cancer immunotherapy, deepening the understanding of its immunoregulatory mechanisms (31–33). The top 10 references mainly focus on tumor immunity, tumor hypoxia, the tumor microenvironment, immune checkpoint inhibition, anti-inflammatory effects, tuberculosis, polycystic ovary syndrome, gut microbiota, and the endoplasmic reticulum pathway. This highlights the immunomodulatory role of metformin in various diseases, etiologies, and pathological mechanisms. Its wide application offers significant guidance for both basic and clinical research.

4.2 Hotspots and frontiers

4.2.1 Metformin-mediated tumor immunity

The study of high-frequency keywords can clarify the hot spot distribution and trajectory on research elated to metformin and host immunity research over the recent years. Previously, researchers have demonstrated promising anticancer effects of metformin on prostate, breast, lung, liver, colon, ovarian, head and neck, glioblastoma cancers (34). Metformin is a highly effective and promising anti-tumor inhibitor. Targeted tumor immunity is an attractive research topic. As shown in the Figure 9A, keyword clusters such as ″tumor immunotherapy″, ″tumor microenvironment″, ″immune checkpoint inhibitors″, ″immunotherapy″, ″drug repurposing″, ″tumor-associated macrophages″, ″CD8(+) T cell″, ″lung cancer″, ″breast cancer″, ″photodynamic therapy″, ″chemoprevention″, and ″survival″ highlight the prominence of metformin's immune-mediated effects in tumor research. These indicate that the immune-mediated role of metformin in tumor diseases is a current topic of interest. Its detailed mechanism of action involves many aspects of tumor pathogenesis, such as the tumor immune microenvironment, immune checkpoint inhibition, and the application of metformin derivatives.

Firstly, metformin significantly influences the regulation of the tumor immune microenvironment, covering a variety of immune cells and their interactions, inhibiting tumor metastasis, progression, and angiogenesis. It enhances the anti-tumor immune function of CD8+ T cells by regulating glucose metabolism, activating fatty acid oxidation, and targeting oxidative phosphorylation (35). Metformin can promote the maturation of dendritic cells by depressing mitochondrial complex I, enhance the co-stimulatory ability of CD4+ T cells, and further stimulate the immune response (36). Through the p38

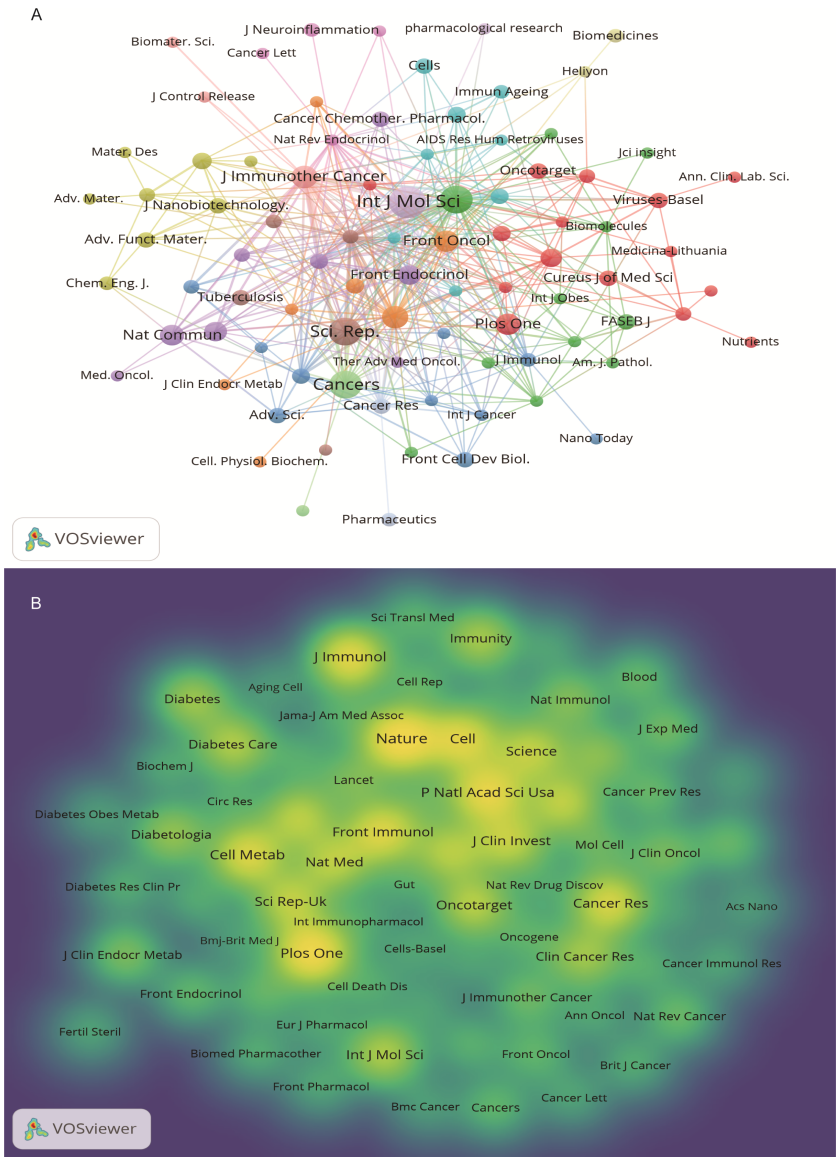

FIGURE 6
Journal visualization of metformin as an immunomodulator. **(A)** Cited Journal Co-occurrence Network: Node size represents the influence of journals within the network. Nodes of the same color indicate journal groups with close research connections. **(B)** Co-cited Journal Density Map: Brightly colored and high-density areas represent journals with high citation frequency, indicating the importance in the field.

TABLE 5 Top 10 most cited references of Metformin as an immunomodulator.

Author	Title	Journal	Citation	Year
Cheng SC. et al.	Mtor- and hif-1α-mediated aerobic glycolysis as metabolic basis for trained immunity	*Science*	1432	2014
Shin NR. et al.	An increase in the akkermansia spp. population induced by metformin treatment improves glucose homeostasis in diet-induced obese mice	*Gut*	1176	2014
Jin MZ. et al.	The updated landscape of tumor microenvironment and drug repurposing	*Signal Transduction And Targeted Therapy*	657	2020
Cha JH. et al.	Metformin promotes antitumor immunity via endoplasmic-reticulum-associated degradation of pd-L1	*Molecular Cell*	522	2018
Eikawa S. et al.	Immune-mediated antitumor effect by type 2 diabetes drug, metformin	*PNAS*	415	2015

(Continued)

TABLE 5 Continued

Author	Title	Journal	Citation	Year
Foretz M. et al.	Understanding the glucoregulatory mechanisms of metformin in type 2 diabetes mellitus	*Nature Reviews Endocrinology*	376	2019
Scharping NE. et al.	Efficacy of pd-1 blockade is potentiated by metformin-induced reduction of tumor hypoxia	*Cancer Immunology Research*	373	2017
Singhal A. et al.	Metformin as adjunct antituberculosis therapy	*Science Translational Medicine*	360	2014
Li L. et al.	Metformin-induced reduction of cd39 and cd73 blocks myeloid-derived suppressor cell activity in patients with ovarian cancer	*Cancer Research*	204	2018
Song M. et al.	Environmental factors, gut microbiota, and colorectal cancer prevention	*Clinical Gastroenterology And Hepatology*	194	2019

mitogen-activated protein kinase pathway, metformin enhances the anti-tumor activity of natural killer cells and increases their toxicity to cancer cells (37). It also inhibits tumor infiltration of Treg and myeloid-derived suppressor cells (38), stimulates the proliferation of natural killer T and T cells (14), and delays cancer growth. Studies have shown that metformin regulates macrophage function, increases tumor-infiltrating T cells, and significantly heightened the anti-tumor effect of cancer vaccines (39, 40). When combined with antitumor drugs such as pazopanib and cyclophosphamide, metformin improves the immune microenvironment. This could be achieved by inhibiting phosphorylated protein kinase B/nuclear factor kappa-light-chain-enhancer of activated B cell/signal transducer and activator of transcription 3 (STAT3p-Akt/NF-κB/STAT3)/PD-L1 pathway (41, 42). In addition, metformin causes immunogenic death of ovarian cancer cells and inhibits tumor growth by activating AMPK (43). It improves prognosis and prolongs survival in patients with pancreatic and breast cancer by reducing the abundance of M2 macrophages and increasing tumor-infiltrating lymphocytes (TIL) (44, 45). In summary, metformin shows a wide range of anticancer potential by modulating anti-tumor immune cells, reducing immunosuppression, and significantly improving the tumor immune microenvironment.

Secondly, immune checkpoint molecules, such as PD-L1 and cytotoxic T-lymphocyte associated protein 4(CTLA4), have been extensively investigated as a cancer therapy, with this immunotherapy notably enhancing the survival rates of patients with certain types of cancer (46). Metformin, as a small molecule immune checkpoint inhibitor, decreases PD-L1 expression on tumor cell surfaces and boosts the cytotoxic T cells ability to kill (20). By activating AMPK, metformin phosphorylates PD-L1, induces endoplasmic reticulum stress, and enhances anti-tumor immunity (47). Concurrently, metformin restrains the expression of mechanistic target of

TABLE 6 Top 10 most co-cited references concerning Metformin as an immunomodulator.

Author	Title	Journal	Citation	Year
Eikawa S. et al.	Immune-mediated antitumor effect by type 2 diabetes drug, metformin	*PNAS*	111	2015
Cha JH. et al.	Metformin promotes antitumor immunity via endoplasmic-reticulum-associated degradation of PD-L1	*Molecular Cell*	87	2018
Scharping NE. et al.	Efficacy of PD-1 blockade is potentiated by metformin-induced reduction of tumor hypoxia	*Cancer Immunology Research*	63	2017
Evans JMM. et al.	Metformin and reduced risk of cancer in diabetic patients	*BMJ (British Medical Journal)*	48	2005
Foretz M. et al.	Metformin: from mechanisms of action to therapies	*Cell Metabolism*	45	2014
Pearce EL. et al.	Enhancing CD8 T-cell memory by modulating fatty acid metabolism	*Nature*	45	2009
Rena G. et al.	The mechanisms of action of metformin	*Diabetologia*	40	2017
Wheaton WW. et al.	Metformin inhibits mitochondrial complex I of cancer cells to reduce tumorigenesis	*eLife*	38	2014
Owen MR. et al.	Evidence that metformin exerts its anti-diabetic effects through inhibition of complex 1 of the mitochondrial respiratory chain	*Biochemical Journal*	37	2000
Kunisada Y. et al.	Attenuation of CD4+CD25+ Regulatory T Cells in the Tumor Microenvironment by Metformin, a Type 2 Diabetes Drug	*EBioMedicine*	36	2017

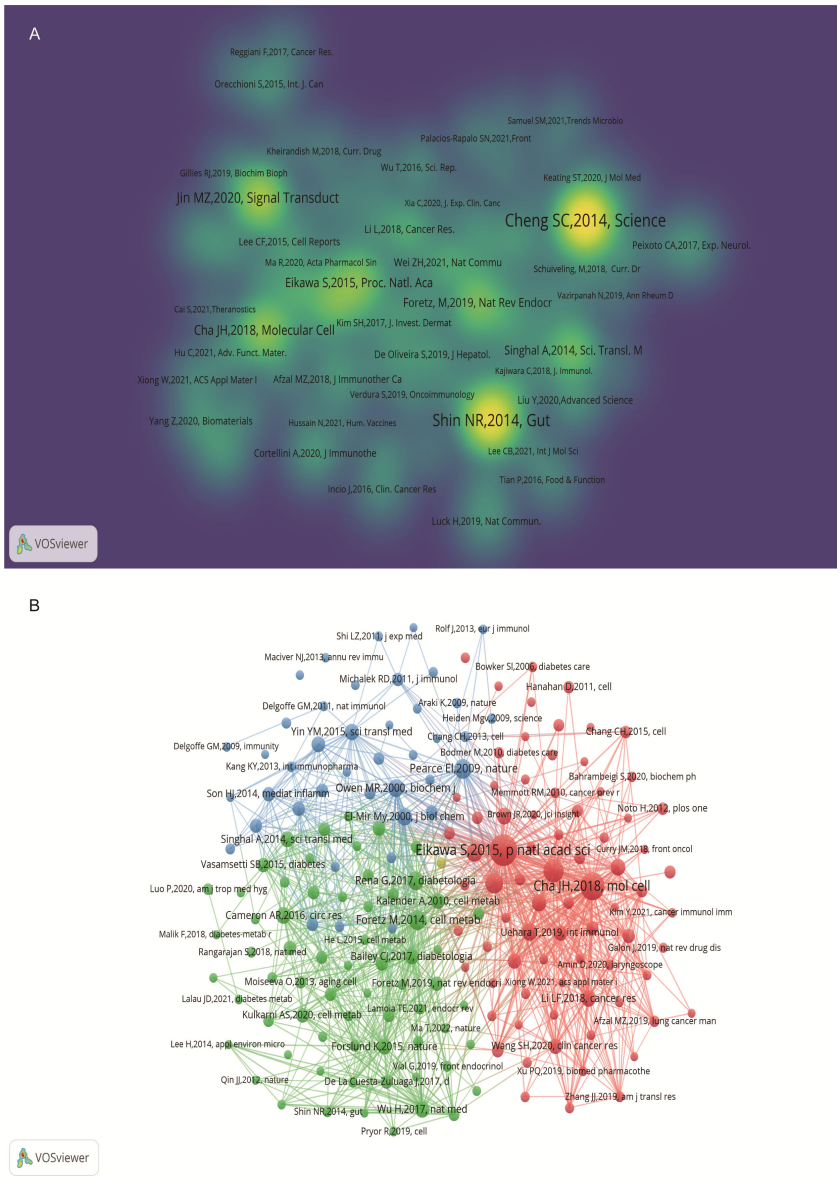

FIGURE 7
Visualization of cited references on metformin as an immunomodulator. **(A)** Cited Literature Cluster Analysis: The size of each node is proportional to the citation frequency in literature. Larger nodes indicate higher influence within the network. **(B)** Co-cited Literature Density Map: Brightly colored and concentrated areas represent literature with higher co-citation frequency, indicating greater importance in the field.

rapamycin (mTOR) signaling and hypoxia-inducible factor 1-alpha (HIF-1α), decreases oxygen consumption, strengthens the efficacy of PD-1 blockade therapy, and diminishes immune escape (48, 49). In addition, metformin combined with anti-PD-1 therapy promotes the normalization of tumor blood vessels, increases the expression of vascular endothelial cadherin (VE-cadherin) and vascular cell adhesion molecule 1(VCAM-1), and infiltration of CD8+ T cells, and slows tumor growth (32). Studies have shown that metformin significantly prolonged overall survival (OS) and progression-free survival (PFS) in patients with non-small cell lung cancer (NSCLC) treated with immune checkpoint inhibitors (50). This combination therapy not only enhances the effectiveness of immunotherapy but enhances the prognosis of cancer patients.

Further, reuse of metformin has gained momentum. Due to its clear anti-cancer effect, good safety, and tolerance, but low drug concentration, researchers have developed a variety of metformin derivatives to enhance its efficacy in anti-tumor immunotherapy. The platinum-metformin conjugate promotes the degradation of PD-L1 through the AMPK/transcription factor EB (TFEB) pathway and enhances the anti-tumor immune effect in NSCLC (51). Researchers have further enhanced the therapeutic effects on cold tumors and drug-resistant tumors by using nanotechnology delivery systems combined with photodynamic therapy, radiotherapy, and immune checkpoint blockade therapy (52–54). For example, MET-HMME/CAT-HMME@Nlip (55) and Mn-MSN@Met-M NPs (56) improves tumor hypoxia, activates the

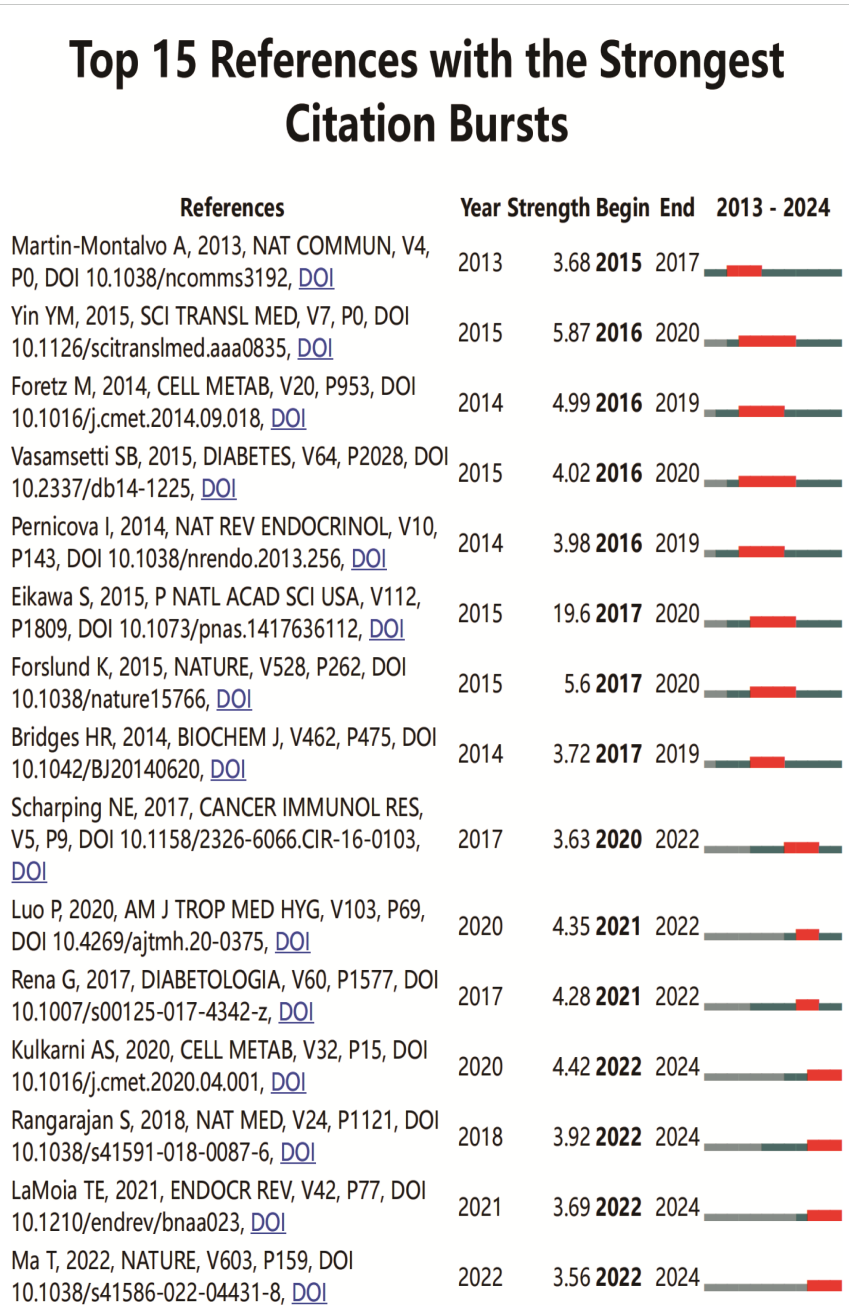

FIGURE 8
Top 15 co-cited references on metformin as an immunomodulator. Blue line segments represent the timeline from 2013 to 2024, and red markers indicate the specific period and duration of reference bursts.

TABLE 7 Top 20 keywords related to metformin as an immunomodulator.

Rank	Keyword	Occurrences	Rank	Keyword	Occurrences
1	metformin	293	11	cancer	21
2	diabetes	78	12	mitochondrial dysfunction	21
3	immunotherapy	44	13	T cells	19
4	inflammation	37	14	macrophages	17
5	tumor microenvironment	30	15	metabolism	17

(Continued)

TABLE 7 Continued

Rank	Keyword	Occurrences	Rank	Keyword	Occurrences
6	immune system	29	16	obesity	16
7	AMPK	25	17	PD-1	16
8	COVID-19	24	18	breast cancer	15
9	immune checkpoint inhibitors	24	19	immunometabolism	13
10	aging	21	20	tumor immunotherapy	13

stimulator of interferon genes (STING) pathway, and improves efficacy of PD-1 inhibitors. Tpp-Met@MnO2@Alb nano-adjuvant enhances the sensitivity of tumors to radiotherapy by regulating PD-L1 and transforming growth factor beta 1(TGF-β1) and provides a long-term immune memory effect (52). Nanogels (D@HPMNG) (57) significantly inhibits the growth and recurrence of melanoma by reprogramming tumor-associated macrophages (58), whereas HMMDN-Met@PM enhances tumor inhibition by promoting the transformation of M2 to M1 (59). Through these mechanisms, metformin derivatives not only improve the tumor microenvironment but also inhibit tumor growth and metastasis, providing a long-term anti-tumor immune effect.

In summary, the interplay between metformin and the immune response is a complex and dynamic research area with exciting implications. These results might have important applications in controlling cancer progression and prognosis, opening avenues for the development of innovative treatments.

4.2.2 Application of metformin immunotherapy in other diseases

In addition to anti-tumor immunity, metformin has a broad application in several diseases because of its ability to regulate the immune system. Keywords clusters such as ″diabetes″, ″metabolism″, ″autoimmune diseases″, ″polycystic ovary syndrome″, ″multiple sclerosis″, ″SARS-COV-2″, ″aging″, ″obesity″, etc., are all recent research topics. Metformin improves type 1 diabetes (T1DM), autoimmune diseases, and metabolic syndrome by activating AMPK pathway, inhibiting pro-inflammatory Th1 and Th17 cells, and promoting Tregs development (60, 61). Metformin has been shown to regulate differentiation of immune complexes and B cells and reduce the inflammatory response of diseases such as systemic lupus erythematosus (62). It also improves Sjogren's syndrome by restoring Ca2+ signaling and inhibiting ERS (63), and enhances immune recognition and lowers viral replication in human immunodeficiency virus type 1(HIV-1) infection (64) and Helicobacter pylori infection. Metformin exhibits anti-inflammatory and antiviral effects in COVID-19 infections likely improving immune response and prognosis (65). Surprisingly, it can also promote osteogenic differentiation of bone marrow mesenchymal stem cells by regulating the macrophage phenotype (66) and enhancing innate immunity in tuberculosis (67, 68). In addition, metformin exhibits anti-aging and anti-fibrosis effects by reducing the number of senescent T cells and improving T cell function (69) and exhibits immunomodulatory effects in diseases such as polycystic ovary syndrome, pregnancy, and liver disease (70).

4.2.3 Research hotspots on the basic mechanism of metformin immunotherapy

A clustered analysis of existing keywords showed that metformin regulated direct immune cells and also regulated immunity through other pathways involving ″fibrosis″, ″oxidative stress″, ″inflammation″, ″apoptosis″, ″ROS″, ″mTOR″, ″AMPK″, ″mitochondrial dysfunction″, ″gut microbiota″, and ″OXPHOS″, and ″mTOR″ signaling (71, 72). In addition, metformin can inhibit the differentiation of pro-inflammatory macrophages (M1) and reduce the production of reactive oxygen species (ROS) showing a strong anti-inflammatory effect (73, 74). By regulating reactive oxygen/nitrogen levels and immune metabolism, metformin may help prevent age-related diseases and provide a new direction for clinical treatment (75). It improves diabetic complications and T cell function in patients with COVID-19 by reprogramming dendritic cell metabolism, inducing tolerance, and reducing pro-inflammatory factors such as IL-2 and tumor necrosis factor alpha (76). Metformin also reduces inflammation caused by obesity and insulin resistance by regulating Th17/Treg balance, intestinal flora, and NF-κB signaling pathway (77, 78). Furthermore, it improves efficacy of anti-PD-L1 antibodies by affecting the intestinal microbiota, promotes anti-tumor immunity (79), and shows antiviral potential for COVID-19 treatment (80). In short, the relationship between anti-inflammatory, intestinal flora, and metformin immune regulation is an emerging research field. Although some studies have reported on alterations in the gut microbiome after the use of metformin (78), the exact mechanism by which metformin regulates the gut microbiome and the impact of these changes on the efficacy of metformin immunotherapy is not known. Further research is required to understand these effects.

4.3 Advantages and limitations

This study for the first time systematically used VOSviewer and CiteSpace to analyze the bibliometrics of research related to metformin and immune regulation, providing an overview of the cooperation network and research trends. However, there are some limitations to this study. In this study, the data was sourced from only the core collection of WOS, excluding other databases and non-English publications. Further, reference delays and database updates might have also affected the accuracy of trend analysis. Nevertheless, by combining published literature, this study offered valuable insights into the clinical application of metformin as an

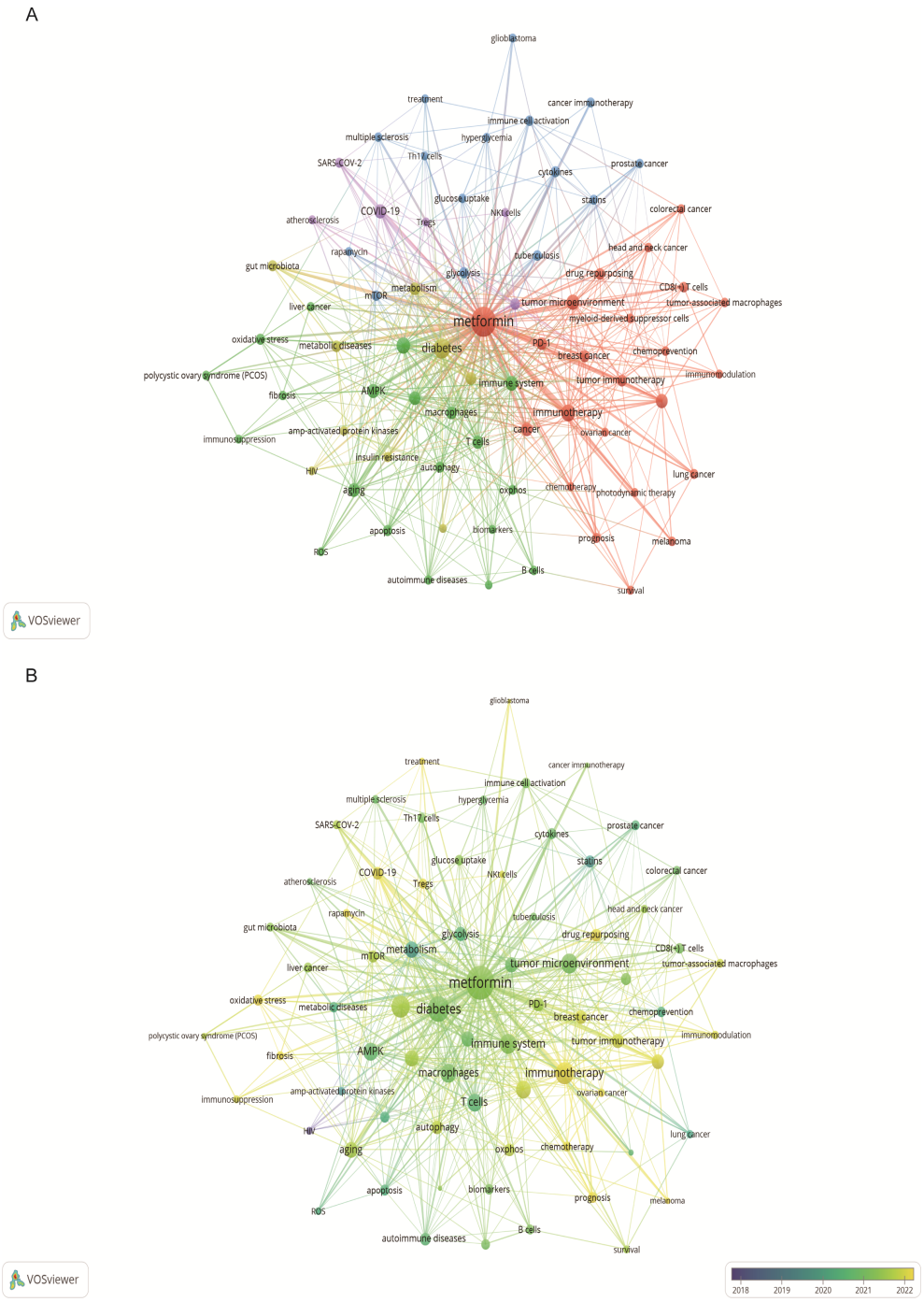

FIGURE 9
Keyword co-occurrence and annual analysis related to metformin as an immunomodulator. **(A)** Keyword Co-occurrence Network: Node size corresponds to the frequency of keyword occurrences, and the lines between nodes indicate the strength of the association. Larger nodes denote higher frequencies, and thicker lines represent stronger relationships between keywords. **(B)** Annual Analysis of Keyword Occurrence: Each node represents a keyword, with its color indicating the average year of occurrence. This visualization shows the research intensity of keywords over specific periods, highlighting the research focus in different time frames.

immunomodulator. Although current *in vivo* and *in vitro* studies have identified important mechanisms underlying the inhibitory effect of metformin on cancer immunity and other diseases, systematic and large-center clinical research studies are warranted.

5 Conclusion

This study used bibliometric analysis to review the dynamics and developments in the immunomodulatory effects of metformin.

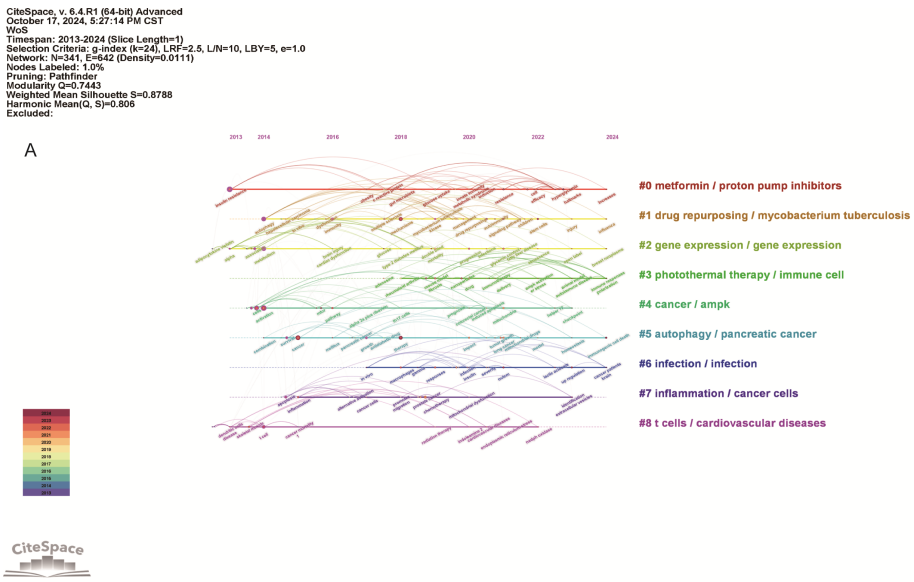

B

Top 20 Keywords with the Strongest Citation Bursts

Keywords	Year	Strength	Begin	End	2013 - 2024
protein kinase	2013	2.79	2013	2017	
alpha	2013	2.34	2013	2017	
activated protein kinase	2013	2.26	2013	2014	
metabolism	2014	4.4	2014	2018	
pancreatic cancer	2017	2.71	2017	2019	
cholesterol	2017	2.66	2017	2019	
growth	2017	2.21	2017	2020	
th17 cells	2018	2.64	2018	2020	
rheumatoid arthritis	2018	2.27	2018	2019	
receptor	2019	3.6	2019	2021	
mortality	2019	3.16	2019	2021	
suppressor cells	2019	2.98	2019	2020	
insulin resistance	2013	2.71	2019	2020	
gut microbiome	2020	2.79	2020	2021	
drug	2020	2.43	2020	2021	
infection	2020	2.2	2020	2021	
lung cancer	2021	2.95	2021	2022	
tumor growth	2021	2.58	2021	2022	
natural killer cells	2021	2.21	2021	2022	
nf kappa b	2017	2.55	2022	2024	

FIGURE 10
Keyword timeline and burst word analysis of metformin's role as an Immunomodulator. **(A)** Keyword Cluster Timeline: Keywords within the same cluster are aligned on the same horizontal line. This visualization shows the number of keywords in each cluster and the time span, indicating the temporal evolution of various research directions. **(B)** Top 20 Keyword Burst Analysis: Red line segments indicate the start and end of a keyword burst. The "strength" metric represents the intensity of research on a keyword during a specific period, with higher values indicating greater research focus and attention.

With the rapid growth of research on the role of metformin and its derivatives in cancer immunotherapy, the prospects of metformin use are expanding. Notably, as an immunomodulator, metformin not only improves the tumor immune microenvironment and enhances the efficacy of immune checkpoint inhibitors but also boosts the treatment effects of radiotherapy, cold tumors, and drug-resistant tumors, along with minimizing its side effects. Beyond tumor immunity, the immunomodulatory effects of metformin in aging, tuberculosis, viral infections, and autoimmune diseases, and its potential in gut microbiota and anti-inflammatory treatments, are important for future research. Further exploration of the detailed mechanisms of metformin as an immunomodulator and its biological distribution in tissues is crucial for optimizing its clinical application.

Data availability statement

The raw data supporting the conclusions of this article will be made available by the authors, without undue reservation.

Author contributions

TZ: Conceptualization, Writing – original draft, Writing – review & editing. YY: Methodology, Writing – original draft. LL: Formal analysis, Writing – original draft. XL: Data curation, Writing – original draft. QX: Visualization, Writing – original draft. RY: Conceptualization, Supervision, Writing – review & editing.

Funding

The author(s) declare financial support was received for the research, authorship, and/or publication of this article. This study was supported by key projects supported by the National Natural Science Foundation of China and Joint Fund for Regional Innovation and Development (U21A20411); Hunan Provincial Natural Science Foundation Project (2024JJ5303); Hunan Provincial Traditional Chinese Medicine Research Project (B2024003); Graduate Innovation Project of Hunan University of Chinese Medicine(2023CX06).

Conflict of interest

The authors declare that the research was conducted in the absence of any commercial or financial relationships that could be construed as a potential conflict of interest.

Generative AI statement

The author(s) declare that no Generative AI was used in the creation of this manuscript.

Publisher's note

All claims expressed in this article are solely those of the authors and do not necessarily represent those of their affiliated organizations, or those of the publisher, the editors and the reviewers. Any product that may be evaluated in this article, or claim that may be made by its manufacturer, is not guaranteed or endorsed by the publisher.

References

1. Ahmad E, Sargeant JA, Zaccardi F, Khunti K, Webb DR, Davies MJ. Where does metformin stand in modern day management of type 2 diabetes? *Pharm (Basel)*. (2020) 13:427. doi: 10.3390/ph13120427

2. Foretz M, Guigas B, Viollet B. Metformin: update on mechanisms of action and repurposing potential. *Nat Rev Endocrinol*. (2023) 19:460–76. doi: 10.1038/s41574-023-00833-4

3. Salvatore T, Pafundi PC, Morgillo F, Di Liello R, Galiero R, Nevola R, et al. Metformin: An old drug against old age and associated morbidities. *Diabetes Res Clin Pract*. (2020) 160:108025. doi: 10.1016/j.diabres.2020.108025

4. Dutta S, Shah RB, Singhal S, Dutta SB, Bansal S, Sinha S, et al. Metformin: A review of potential mechanism and therapeutic utility beyond diabetes. *Drug Des Devel Ther*. (2023) 17:1907–32. doi: 10.2147/DDDT.S409373

5. He L. Metformin and systemic metabolism. *Trends Pharmacol Sci*. (2020) 41:868–81. doi: 10.1016/j.tips.2020.09.001

6. Bharath LP, Nikolajczyk BS. The intersection of metformin and inflammation. *Am J Physiol Cell Physiol*. (2021) 320:C873–9. doi: 10.1152/ajpcell.00604.2020

7. Lu G, Wu Z, Shang J, Xie Z, Chen C, Zhang C. The effects of metformin on autophagy. *BioMed Pharmacother*. (2021) 137:111286. doi: 10.1016/j.biopha.2021.111286

8. Pavlo P, Kamyshna I, Kamyshnyi A. Effects of metformin on the gut microbiota: A systematic review. *Mol Metab*. (2023) 77:101805. doi: 10.1016/j.molmet.2023.101805

9. Panaampon J, Zhou Y, Saengboonmee C. Metformin as a booster of cancer immunotherapy. *Int Immunopharmacol*. (2023) 121:110528. doi: 10.1016/j.intimp.2023.110528

10. Chen GG, Woo PYM, Ng SCP, Wong GKC, Chan DTM, Van Hasselt C A, et al. Impact of metformin on immunological markers: Implication in its anti-tumor mechanism. *Pharmacol Ther*. (2020) 213:107585. doi: 10.1016/j.pharmthera.2020.107585

11. Abdelmoneim M, Aboalela MA, Naoe Y, Matsumura S, Eissa IR, Bustos-Villalobos I, et al. The impact of metformin on tumor-infiltrated immune cells: preclinical and clinical studies. *Int J Mol Sci*. (2023) 24:13353. doi: 10.3390/ijms241713353

12. Pearce EL, Walsh MC, Cejas PJ, Harms GM, Shen H, Wang L S, et al. Enhancing CD8 T-cell memory by modulating fatty acid metabolism. *Nature*. (2009) 460:103–7. doi: 10.1038/nature08097

13. Finisguerra V, Dvorakova T, Formenti M, Van Meerbeeck P, Mignion L, Gallez B, et al. Metformin improves cancer immunotherapy by directly rescuing tumor-infiltrating CD8 T lymphocytes from hypoxia-induced immunosuppression. *J Immunother Cancer*. (2023) 11:e005719. doi: 10.1136/jitc-2022-005719

14. Petrovic A, Jovanovic I, Stojanovic B, Dimitrijevic Stojanovic M, Stojanovic BS, Jurisevic M, et al. Harnessing metformin's immunomodulatory effects on immune cells to combat breast cancer. *Int J Mol Sci*. (2024) 25:5869. doi: 10.3390/ijms25115869

15. Huang X, Sun T, Wang J, Hong X, Chen H, Yan T, et al. Metformin reprograms tryptophan metabolism to stimulate CD8+ T-cell function in colorectal cancer. *Cancer Res*. (2023) 83:2358–71. doi: 10.1158/0008-5472.CAN-22-3042

16. Crist M, Yaniv B, Palackdharry S, Lehn MA, Medvedovic M, Stone T, et al. Metformin increases natural killer cell functions in head and neck squamous cell carcinoma through CXCL1 inhibition. *J Immunother Cancer*. (2022) 10:e005632. doi: 10.1136/jitc-2022-005632

17. Abd El-Fattah EE, Zakaria AY. Metformin modulate immune fitness in hepatocellular carcinoma: Molecular and cellular approach. *Int Immunopharmacol*. (2022) 109:108889. doi: 10.1016/j.intimp.2022.108889

18. Levy A, Doyen J. Metformin for non-small cell lung cancer patients: Opportunities and pitfalls. *Crit Rev Oncol Hematol*. (2018) 125:41–7. doi: 10.1016/j.critrevonc.2018.03.001

19. Chen S, Zhou X, Yang X, Li W, Li S, Hu Z, et al. Dual blockade of lactate/GPR81 and PD-1/PD-L1 pathways enhances the anti-tumor effects of metformin. *Biomolecules*. (2021) 11:1373. doi: 10.3390/biom11091373

20. Park SH, Lee J, Yun HJ, Kim SH, Lee JH. Metformin suppresses both PD-L1 expression in cancer cells and cancer-induced PD-1 expression in immune cells to promote antitumor immunity. *Ann Lab Med*. (2024) 44:426–36. doi: 10.3343/alm.2023.0443

21. Landry DA, Yakubovich E, Cook DP, Fasih S, Upham J, Vanderhyden BC. Metformin prevents age-associated ovarian fibrosis by modulating the immune landscape in female mice. *Sci Adv*. (2022) 8:eabq1475. doi: 10.1126/sciadv.abq1475

22. Cortes M, Brischetto A, Martinez-Campanario MC, Ninfali C, Dominguez V, Fernandez S, et al. Inflammatory macrophages reprogram to immunosuppression by reducing mitochondrial translation. *Nat Commun*. (2023) 14:7471. doi: 10.1038/s41467-023-42277-4

23. Jing Y, Wu F, Li D, Yang L, Li Q, Li R. Metformin improves obesity-associated inflammation by altering macrophages polarization. *Mol Cell Endocrinol*. (2018) 461:256–64. doi: 10.1016/j.mce.2017.09.025

24. Vasamsetti SB, Karnewar S, Kanugula AK, Thatipalli AR, Kumar JM, Kotamraju S. Metformin inhibits monocyte-to-macrophage differentiation via AMPK-mediated inhibition of STAT3 activation: potential role in atherosclerosis. *Diabetes*. (2015) 64:2028–41. doi: 10.2337/db14-1225

25. Yan Z, Tian X, Zhu J, Lu Z, Yu L, Zhang D, et al. Metformin suppresses UHMWPE particle-induced osteolysis in the mouse calvaria by promoting polarization of macrophages to an anti-inflammatory phenotype. *Mol Med*. (2018) 24:20. doi: 10.1186/s10020-018-0013-x

26. Solier S, Muller S, Caneque T, Versini A, Mansart A, Sindikubwabo F, et al. A druggable copper-signalling pathway that drives inflammation. *Nature*. (2023) 617:386–94. doi: 10.1038/s41586-023-06017-4

27. Van Eck NJ, Waltman L. Software survey: VOSviewer, a computer program for bibliometric mapping. *Scientometrics*. (2010) 84:523–38. doi: 10.1007/s11192-009-0146-3

28. Chen C. Searching for intellectual turning points: progressive knowledge domain visualization. *Proc Natl Acad Sci U.S.A*. (2004) 101 Suppl 1:5303–10. doi: 10.1073/pnas.0307513100

29. Nojima I, Eikawa S, Tomonobu N, Hada Y, Kajitani N, Teshigawara S, et al. Dysfunction of CD8 + PD-1 + T cells in type 2 diabetes caused by the impairment of metabolism-immune axis. *Sci Rep*. (2020) 10:14928. doi: 10.1038/s41598-020-71946-3

30. Kunisada Y, Eikawa S, Tomonobu N, Domae S, Uehara T, Hori S, et al. Attenuation of CD4(+)CD25(+) regulatory T cells in the tumor microenvironment by metformin, a type 2 diabetes drug. *EBioMedicine*. (2017) 25:154–64. doi: 10.1016/j.ebiom.2017.10.009

31. Nishida M, Yamashita N, Ogawa T, Koseki K, Warabi E, Ohue T, et al. Mitochondrial reactive oxygen species trigger metformin-dependent antitumor immunity via activation of Nrf2/mTORC1/p62 axis in tumor-infiltrating CD8T lymphocytes. *J Immunother Cancer*. (2021) 9:e002954. doi: 10.1136/jitc-2021-002954

32. Tokumasu M, Nishida M, Zhao W, Chao R, Imano N, Yamashita N, et al. Metformin synergizes with PD-1 blockade to promote normalization of tumor vessels via CD8T cells and IFNgamma. *Proc Natl Acad Sci U.S.A*. (2024) 121:e2404778121. doi: 10.1073/pnas.2404778121

33. Uehara T, Eikawa S, Nishida M, Kunisada Y, Yoshida A, Fujiwara T, et al. Metformin induces CD11b+-cell-mediated growth inhibition of an osteosarcoma: implications for metabolic reprogramming of myeloid cells and anti-tumor effects. *Int Immunol*. (2019) 31:187–98. doi: 10.1093/intimm/dxy079

34. Ma R, Yi B, Riker AI, Xi Y. Metformin and cancer immunity. *Acta Pharmacol Sin*. (2020) 41:1403–9. doi: 10.1038/s41401-020-00508-0

35. Pujalte-Martin M, Belaid A, Bost S, Kahi M, Peraldi P, Rouleau M, et al. Targeting cancer and immune cell metabolism with the complex I inhibitors metformin and IACS-010759. *Mol Oncol*. (2024) 18:1719–38. doi: 10.1002/1878-0261.13583

36. Turpin R, Liu R, Munne PM, Peura A, Rannikko JH, Philips G, et al. Respiratory complex I regulates dendritic cell maturation in explant model of human tumor immune microenvironment. *J Immunother Cancer*. (2024) 12:e008053. doi: 10.1136/jitc-2023-008053

37. Xia W, Qi X, Li M, Wu Y, Sun L, Fan X, et al. Metformin promotes anticancer activity of NK cells in a p38 MAPK dependent manner. *Oncoimmunology*. (2021) 10:1995999. doi: 10.1080/2162402X.2021.1995999

38. Kang J, Lee D, Lee KJ, Yoon JE, Kwon JH, Seo Y, et al. Tumor-suppressive effect of metformin via the regulation of M2 macrophages and myeloid-derived suppressor cells in the tumor microenvironment of colorectal cancer. *Cancers (Basel)*. (2022) 14:2881. doi: 10.3390/cancers14122881

39. Scafidi A, Lind-Holm Mogensen F, Campus E, Pailas A, Neumann K, Legrave N, et al. Metformin impacts the differentiation of mouse bone marrow cells into macrophages affecting tumour immunity. *Heliyon*. (2024) 10:e37792. doi: 10.1016/j.heliyon.2024.e37792

40. Guo Q, Wang L, Wuriqimuge, Dong L, Feng M, Bao X, et al. Metformin improved a heterologous prime-boost of dual-targeting cancer vaccines to inhibit tumor growth in a melanoma mouse model. *Int Immunopharmacol*. (2024) 128:111431. doi: 10.1016/j.intimp.2023.111431

41. Abdallah FM, Ghoneim AI, Abd-Alhaseeb MM, Abdel-Raheem IT, Helmy MW. Unveiling the antitumor synergy between pazopanib and metformin on lung cancer through suppressing p-Akt/NF-kappaB/STAT3/PD-L1 signal pathway. *BioMed Pharmacother*. (2024) 180:117468. doi: 10.1016/j.biopha.2024.117468

42. Zaki HM, Ali KM, Abd Allah MYY, Abouelnaga AM, Abdraboh ME, Hussein O. Metronomic cyclophosphamide and metformin inhibited tumor growth and repopulated tumor-infiltrating lymphocytes in an experimental carcinoma model. *BMC Res Notes*. (2024) 17:4. doi: 10.1186/s13104-023-06651-1

43. Chen Y, Wang L, Chen N, Tang G. Metformin induces tumor immunogenic cell death in ovarian cancer by activating AMPK pathway. *Transl Oncol*. (2024) 47:102052. doi: 10.1016/j.tranon.2024.102052

44. Van Eijck CWF, Vadgama D, Van Eijck CHJ, Wilmink JW, Dutch Pancreatic Cancer G. Metformin boosts antitumor immunity and improves prognosis in upfront resected pancreatic cancer: an observational study. *J Natl Cancer Inst*. (2024) 116:1374–83. doi: 10.1093/jnci/djae070

45. Shiba S, Harao M, Saito A, Sakuragi M, Kitayama J, Sata N. Metformin alters tumor immune microenvironment, improving the outcomes of breast cancer patients with type 2 diabetes mellitus. *J Breast Cancer*. (2024) 27:121–9. doi: 10.4048/jbc.2023.0285

46. Leong SP. Immune responses and immunotherapeutic approaches in the treatment against cancer. *Clin Exp Metast*. (2024) 41:473–93. doi: 10.1007/s10585-024-10300-7

47. Cha JH, Yang WH, Xia W, Wei Y, Chan LC, Lim S O, et al. Metformin promotes antitumor immunity via endoplasmic-reticulum-associated degradation of PD-L1. *Mol Cell*. (2018) 71:606–620 e607. doi: 10.1016/j.molcel.2018.07.030

48. Cao Y, Wo M, Xu C, Fei X, Jin J, Shan Z. An AMPK agonist suppresses the progress of colorectal cancer by regulating the polarization of TAM to M1 through inhibition of HIF-1alpha and mTOR signal pathway. *J Cancer Res Ther*. (2023) 19:1560–7. doi: 10.4103/jcrt.jcrt_2670_22

49. Song CW, Kim H, Cho H, Kim MS, Paek SH, Park H J, et al. HIF-1alpha inhibition improves anti-tumor immunity and promotes the efficacy of stereotactic ablative radiotherapy (SABR). *Cancers (Basel)*. (2022) 14:3273. doi: 10.3390/cancers14133273

50. Wang J, Lin J, Guo H, Wu W, Yang J, Mao J, et al. Prognostic impact of metformin in solid cancer patients receiving immune checkpoint inhibitors: novel evidences from a multicenter retrospective study. *Front Pharmacol*. (2024) 15:1419498. doi: 10.3389/fphar.2024.1419498

51. Liu B, Liang BB, Cao WD, Su XX, Cao Q, Mao ZW. Platinum-metformin conjugates acting as promising PD-L1 inhibitors through the AMP-activated protein kinase mediated lysosomal degradation pathway. *Angew Chem Int Ed Engl*. (2024) 63:e202410586. doi: 10.1002/anie.202410586

52. Yi L, Jiang X, Zhou Z, Xiong W, Xue F, Liu Y, et al. A hybrid nanoadjuvant simultaneously depresses PD-L1/TGF-beta1 and activates cGAS-STING pathway to overcome radio-immunotherapy resistance. *Adv Mater*. (2024) 36:e2304328. doi: 10.1002/adma.202304328

53. Yang J, Zhang C, Chen X, Zhou D, Sun Z, Niu R, et al. Ultra-efficient radio-immunotherapy for reprogramming the hypoxic and immunosuppressive tumor microenvironment with durable innate immune memory. *Biomaterials*. (2023) 302:122303. doi: 10.1016/j.biomaterials.2023.122303

54. Zhao Y, Lv B, Xue G, Sun Y, Cao J. Smart nanosystem-mediated inhibition of mitochondrial respiration for enhanced phototherapy-induced antitumor immunity. *Int J Nanomed*. (2023) 18:3443–57. doi: 10.2147/IJN.S413204

55. Wang T, Chen S, Sun J, Li K. Functional co-delivery nanoliposomes based on improving hypoxia for increasing photoimmunotherapy efficacy of cold tumors. *Int J Pharm*. (2024) 663:124581. doi: 10.1016/j.ijpharm.2024.124581

56. Dou Y, Zheng J, Kang J, Wang L, Huang D, Liu Y, et al. Mesoporous manganese nanocarrier target delivery metformin for the co-activation STING pathway to overcome immunotherapy resistance. *iScience*. (2024) 27:110150. doi: 10.1016/j.isci.2024.110150

57. Tian H, Li W, Wang G, Tian Y, Yan J, Zhou S, et al. Self-degradable nanogels reshape immunosuppressive tumor microenvironment via drug repurposing strategy to reactivate cytotoxic CD8(+) T cells. *Adv Sci (Weinh)*. (2023) 10:e2301661. doi: 10.1002/advs.202301661

58. Tang L, Fu C, Liu H, Yin Y, Cao Y, Feng J, et al. Chemoimmunotherapeutic nanogel for pre- and postsurgical treatment of Malignant melanoma by reprogramming tumor-associated macrophages. *Nano Lett*. (2024) 24:1717–28. doi: 10.1021/acs.nanolett.3c04563

59. Chong L, Jiang YW, Wang D, Chang P, Xu K, Li J. Targeting and repolarizing M2-like tumor-associated macrophage-mediated MR imaging and tumor immunotherapy by biomimetic nanoparticles. *J Nanobiotechnol*. (2023) 21:401. doi: 10.1186/s12951-023-02122-8

60. Rajeev D, Maciver NJ. Metformin as a therapeutic agent for obesity-associated immune dysfunction. *J Nutr*. (2024) 154:2534–42. doi: 10.1016/j.tjnut.2024.07.001

61. Halfon M, Tankeu AT, Ribi C. Mitochondrial dysfunction in systemic lupus erythematosus with a focus on lupus nephritis. *Int J Mol Sci*. (2024) 25:6162. doi: 10.3390/ijms25116162

62. Sumikawa MH, Iwata S, Zhang M, Miyata H, Ueno M, Todoroki Y, et al. An enhanced mitochondrial function through glutamine metabolism in plasmablast differentiation in systemic lupus erythematosus. *Rheumatol (Oxford)*. (2022) 61:3049–59. doi: 10.1093/rheumatology/keab824

63. Nascimento Da Conceicao V, Sun Y, Chai X, Ambrus JL, Mishra BB, Singh BB. Metformin-induced activation of Ca(2+) signaling prevents immune infiltration/pathology in Sjogren's syndrome-prone mouse models. *J Transl Autoimmun*. (2023) 7:100210. doi: 10.1016/j.jtauto.2023.100210

64. Fert A, Richard J, Raymond Marchand L, Planas D, Routy JP, Chomont N, et al. Metformin facilitates viral reservoir reactivation and their recognition by anti-HIV-1 envelope antibodies. *iScience*. (2024) 27:110670. doi: 10.1016/j.isci.2024.110670

65. Martin DE, Cadar AN, Bartley JM. Old drug, new tricks: the utility of metformin in infection and vaccination responses to influenza and SARS-CoV-2 in older adults. *Front Aging*. (2023) 4:1272336. doi: 10.3389/fragi.2023.1272336

66. Fan S, Zhang C, Sun X, Su C, Xue Y, Song X, et al. Metformin enhances osteogenic differentiation of BMSC by modulating macrophage M2 polarization. *Sci Rep*. (2024) 14:20267. doi: 10.1038/s41598-024-71318-1

67. Gonzalez-Muniz OE, Rodriguez-Carlos A, Santos-Mena A, Jacobo-Delgado YM, Gonzalez-Curiel I, Rivas-Santiago C, et al. Metformin modulates corticosteroids hormones in adrenals cells promoting Mycobacterium tuberculosis elimination in human macrophages. *Tubercul (Edinb)*. (2024) 148:102548. doi: 10.1016/j.tube.2024.102548

68. Pavan Kumar N, Padmapriyadarsini C, Nancy A, Tamizhselvan M, Mohan A, Reddy D, et al. Effect of Metformin on systemic chemokine responses during anti-tuberculosis chemotherapy. *Tubercul (Edinb)*. (2024) 148:102523. doi: 10.1016/j.tube.2024.102523

69. Yang J, Liu HC, Zhang JQ, Zou JY, Zhang X, Chen W M, et al. The effect of metformin on senescence of T lymphocytes. *Immun Ageing*. (2023) 20:73. doi: 10.1186/s12979-023-00394-0

70. Ryssdal M, Vanky E, Stokkeland LMT, Jarmund AH, Steinkjer B, Lovvik T S, et al. Immunomodulatory effects of metformin treatment in pregnant women with PCOS. *J Clin Endocrinol Metab*. (2023) 108:e743–53. doi: 10.1210/clinem/dgad145

71. Petrasca A, Hambly R, Kearney N, Smith CM, Pender EK, Mac Mahon J, et al. Metformin has anti-inflammatory effects and induces immunometabolic reprogramming via multiple mechanisms in hidradenitis suppurativa. *Br J Dermatol*. (2023) 189:730–40. doi: 10.1093/bjd/ljad305

72. Sorrenti V, Benedetti F, Buriani A, Fortinguerra S, Caudullo G, Davinelli S, et al. Immunomodulatory and antiaging mechanisms of resveratrol, rapamycin, and metformin: focus on mTOR and AMPK signaling networks. *Pharm (Basel)*. (2022) 15:912. doi: 10.3390/ph15080912

73. Wang Z, Wang M, Lin M, Wei P. The immunomodulatory effects of metformin in LPS-induced macrophages: an *in vitro* study. *Inflammation Res*. (2024) 73:175–81. doi: 10.1007/s00011-023-01827-8

74. Nassif RM, Chalhoub E, Chedid P, Hurtado-Nedelec M, Raya E, Dang P M, et al. Metformin inhibits ROS production by human M2 macrophages via the activation of AMPK. *Biomedicines*. (2022) 10:319. doi: 10.3390/biomedicines10020319

75. Hartwig J, Loebel M, Steiner S, Bauer S, Karadeniz Z, Roeger C, et al. Metformin attenuates ROS via FOXO3 activation in immune cells. *Front Immunol*. (2021) 12:581799. doi: 10.3389/fimmu.2021.581799

76. Ali A, Shaheen S, Imran MZ, Memon Z, Zahid N, Ahmad F, et al. Modulation of altered immune parameters IL-2 and TNF-alpha in diabetic animal models: A therapeutic insinuation of metformin beyond diabetes. *Cureus*. (2023) 15:e45216. doi: 10.7759/cureus.45216

77. Son HJ, Lee J, Lee SY, Kim EK, Park MJ, Kim K W, et al. Metformin attenuates experimental autoimmune arthritis through reciprocal regulation of Th17/Treg balance and osteoclastogenesis. *Mediators Inflammation*. (2014) 2014:973986. doi: 10.1155/2014/973986

78. Briviba M, Silamikele L, Kalnina I, Silamikelis I, Birzniece L, Ansone L, et al. Metformin targets intestinal immune system signaling pathways in a high-fat diet-induced mouse model of obesity and insulin resistance. *Front Endocrinol (Lausanne)*. (2023) 14:1232143. doi: 10.3389/fendo.2023.1232143

79. Zhao X, Liu C, Peng L, Wang H. Metformin facilitates anti-PD-L1 efficacy through the regulation of intestinal microbiota. *Genes Immun*. (2024) 25:7–13. doi: 10.1038/s41435-023-00234-7

80. Petakh P, Kamyshna I, Oksenych V, Kamyshnyi O. Metformin alters mRNA expression of FOXP3, RORC, and TBX21 and modulates gut microbiota in COVID-19 patients with type 2 diabetes. *Viruses*. (2024) 16:281. doi: 10.3390/v16020281

frontiers | Frontiers in Immunology

TYPE Original Research
PUBLISHED 09 January 2025
DOI 10.3389/fimmu.2024.1524560

Check for updates

OPEN ACCESS

EDITED BY
Qingyu Luo,
Dana–Farber Cancer Institute, United States

REVIEWED BY
Xiaowei Wu,
Dana–Farber Cancer Institute, United States
Shunian Xiang,
Admera Health, United States

*CORRESPONDENCE
Peijun Zuo
peijunzuo@hotmail.com
Luxiao Zhang
fantuantuan0207@163.com

†These authors have contributed equally to this work and share first authorship

RECEIVED 07 November 2024
ACCEPTED 18 December 2024
PUBLISHED 09 January 2025

CITATION
Wu Q, Ye L, Wu Y, Zhao M, Lu J, Yu Y, Niu Y, Zhang L and Zuo P (2025) Combining single-cell analysis and molecular docking techniques to construct a prognostic model for colon adenocarcinoma and uncovering inhibin subunit βb as a novel therapeutic target. *Front. Immunol.* 15:1524560. doi: 10.3389/fimmu.2024.1524560

COPYRIGHT
© 2025 Wu, Ye, Wu, Zhao, Lu, Yu, Niu, Zhang and Zuo. This is an open-access article distributed under the terms of the Creative Commons Attribution License (CC BY). The use, distribution or reproduction in other forums is permitted, provided the original author(s) and the copyright owner(s) are credited and that the original publication in this journal is cited, in accordance with accepted academic practice. No use, distribution or reproduction is permitted which does not comply with these terms.

Combining single-cell analysis and molecular docking techniques to construct a prognostic model for colon adenocarcinoma and uncovering inhibin subunit βb as a novel therapeutic target

Qinqing Wu[1,2†], Lu Ye[3†], Yuwei Wu[4†], Mengyu Zhao[1,5†], Jiaxin Lu[3], Yanping Yu[1,2], Yixiao Niu[1,2], Luxiao Zhang[3*] and Peijun Zuo[1,2*]

[1]Department of Preventive Medicine, Shantou University Medical College, Shantou, China, [2]School of Public Health, Shantou University, Shantou, China, [3]Department of Breast Surgical Oncology, National Cancer Center/National Clinical Research Center for Cancer/Cancer Hospital, Chinese Academy of Medical Sciences and Peking Union Medical College, Beijing, China, [4]Department of General Surgery, Union Hospital affiliated to Fujian Medical University, Fuzhou, China, [5]Department of Neurosurgery, First Affiliated Hospital of Anhui Medical University, Hefei, China

Background: Colon adenocarcinoma (COAD) is a malignancy with a high mortality rate and complex biological characteristics and heterogeneity, which poses challenges for clinical treatment. Anoikis is a type of programmed cell death that occurs when cells lose their attachment to the extracellular matrix (ECM), and it plays a crucial role in tumor metastasis. However, the specific biological link between anoikis and COAD, as well as its mechanisms in tumor progression, remains unclear, making it a potential new direction for therapeutic strategy research.

Methods: We employed transcriptomic data and clinical information from The Cancer Genome Atlas (TCGA) and Gene Expression Omnibus (GEO) to pinpoint differentially expressed anoikis-related genes (ARGs) in COAD. Using Cox proportional hazards models and Lasso regression analysis, we developed a prognostic signature derived from these ARGs. We also investigated the roles and interactions of these genes in the tumor microenvironment by analyzing single-cell RNA sequencing data. Additionally, we employed molecular docking techniques to evaluate the potential of inhibin subunit beta B (INHBB) as therapeutic targets and to assess the binding affinity of candidate drugs. Finally, we used gene knockout techniques to silence the key gene INHBB and explored its biological functions *in vitro*.

Results: In our study, by analyzing the expression differences of ARGs, we successfully classified patients with COAD. Kaplan-Meier survival analysis demonstrated that patients with elevated risk scores experienced poorer prognosis, a finding that was confirmed in both the training and validation cohorts. Additionally, immune infiltration analysis revealed a notable increase in

immune cell presence within the tumor microenvironment of high-risk patients. Molecular docking identified potential drug candidates with high binding affinity to INHBB, including risperidone. Furthermore, *in vitro* experiments with INHBB showed that downregulation of its expression in COAD cell lines significantly reduced cellular viability and migration capacity.

Conclusion: In summary, our research, based on the expression characteristics of ARGs, provides new insights into the precise classification, prognosis assessment, and identification of potential therapeutic targets in COAD. It also validates the key role of INHBB in the progression of COAD, establishing the foundation for future personalized treatment strategies.

KEYWORDS

anoikis, colon adenocarcinoma, single-cell analysis, molecular docking, INHBB 1

1 Introduction

Colorectal cancer (CC) ranks among the most prevalent cancers globally. According to the 2022 cancer statistics from the World Health Organization, CC ranks third in incidence among all cancer types, with 1,926,425 new cases reported; it also ranks second in mortality, with 904,019 new deaths attributable to CC (1–3). This poses a significant challenge to healthcare systems globally. Among all histopathological types, colon adenocarcinoma (COAD) comprises the majority (4). Currently, surgical resection remains the predominant curative approach; Nonetheless, progress in chemotherapy, targeted therapies, and immunotherapy has introduced new treatment alternatives for patients with COAD (5). Despite these advancements, issues such as tumor specificity, treatment resistance, and the potential for local recurrence or metastasis still negatively impact patient outcomes. Consequently, it is crucial to explore the molecular mechanisms driving COAD progression, investigate early diagnostic techniques, and assess the importance of prognostic biomarkers.

Anoikis is a specific form of apoptosis initiated when cells lose their usual attachment to the extracellular matrix (ECM) (6, 7). This self-destructive process is activated when cells detach from their supportive matrix or surrounding tissues, preventing them from proliferating in inappropriate locations and thereby avoiding the formation of abnormal tissues or cancer. Cancer cells often evade anoikis through various mechanisms, allowing them to survive after detaching from their primary site and metastasize to other tissues or organs, contributing to tumor spread. Recent studies have indicated that anoikis serves as a mechanism by which tumor cells evade apoptosis, closely correlating with tumor aggressiveness, metastatic potential, and prognosis (8, 9). Breast cancer cells exhibit a heightened ability to evade anoikis, particularly pronounced in triple-negative breast cancer (TNBC). These cells promote their survival upon detachment from the ECM by increasing the expression of anti-apoptotic factors (such as Bcl-2) and activating the PI3K/Akt signaling pathway, which enhances their invasive and metastatic potential (10–12). In non-small cell lung cancer (NSCLC) cells, anoikis is also linked to metastatic potential. Some studies suggest that by modulating the expression of integrins and E-cadherin, tumor cells can adjust their dependency on the ECM, allowing them to escape immune detection and apoptosis, thus facilitating their colonization and growth in distant tissues (13). However, comprehensive analyses of the impact of anoikis in COAD remain scarce. Therefore, identifying anoikis-related genes (ARGs) with prognostic significance in COAD is crucial.

Single-cell sequencing is a technique that enables the analysis of genetic information, including genomics, transcriptomics, and epigenomics, at the level of individual cells (14). Unlike traditional bulk sequencing, single-cell sequencing reveals critical details of heterogeneity within cellular populations, such as gene expression differences among various cell types, functional states of specific cell subpopulations, and dynamic changes in cells during developmental processes. Molecular docking is a computational simulation method used to predict the binding modes of small molecules, such as drug compounds, with target proteins. This technique estimates the interactions and energy between molecules to predict the optimal binding conformations and sites of small molecules with receptor proteins, thereby inferring potential drug targets or aiding in the design of novel therapeutics (15).

In this research, we seek to reveal the molecular features and clinical significance of ARGs in COAD by integrating extensive transcriptomic data from The Cancer Genome Atlas (TCGA) and Gene Expression Omnibus (GEO) alongside clinical information, with the goal of developing a prognostic gene model for COAD (16). Utilizing single-cell analysis techniques, we further investigate the roles of these genes within the tumor microenvironment and their interactions with the tumor immune microenvironment (17). Additionally, through molecular docking studies, we will explore the potential of these genes as therapeutic targets and assess the binding affinities of candidate drugs to these targets. *In vitro* experiments will further confirm the expression levels and functions of critical genes

identified in the model (18). This research offers fresh perspectives and a foundational framework for the early diagnosis, targeted therapy, and prognostic evaluation of COAD.

2 Materials and methods

2.1 Data acquisition and preprocessing

RNA-seq data and clinical details for COAD patients were sourced from TCGA database (https://portal.gdc.cancer.gov/). A total of 585 transcriptomic datasets, clinical data (GSE40967), and single-cell datasets from 13 COAD samples (GSE110009) were acquired from the GEO database (https://www.ncbi.nlm.nih.gov/geo/). A total of 576 ARGs were sourced from the GeneCards database (https://www.genecards.org/) and the Harmonizome database (https://maayanlab.cloud/Harmonizome/) (19). To maintain the accuracy and reliability of the analyses, only ARGs with a correlation coefficient exceeding 0.4 were chosen for further examination.

2.2 Exploration of Anoikis-related prognostic genes

In this research, we obtained transcriptomic and clinical data from COAD samples within TCGA database. Differential expression analysis was performed using the R package "DESeq2" to identify differentially expressed genes (DEGs) with a fold change of at least 2 and a p-value of less than 0.01. By intersecting these DEGs with ARGs, we identified 134 significantly different genes in COAD. Standardized merging with GEO data led to further prognostic analysis, revealing 37 genes associated with overall survival (OS). Gene copy number variations were assessed using data obtained from the UCSC Xena website (https://xena.ucsc.edu/), while a protein-protein interaction (PPI) network was generated using the online tool STRING to investigate co-expression relationships and potential molecular interactions among the genes (20, 21).

2.3 Consistency cluster analysis

We performed an in-depth clustering analysis of samples using the K-means clustering algorithm from the "ConsensusClusterPlus" package, setting the maximum number of clusters to 9 (maxK = 9). Through detailed analysis of the consistency matrix of clustering results, we successfully determined the optimal number of clusters to be 2, which was validated using principal component analysis (PCA) (22). Heatmap analysis demonstrated relationships between alterations in gene expression and clinical characteristics, while survival curve analysis showed that Cluster A had a better prognosis than Cluster B, revealing notable differences in immune cell expression between the two clusters. Gene Set Variation Analysis (GSVA) and Gene Set Enrichment Analysis (GSEA) were utilized to further investigate biological functions and pathway activity differences across the various subtypes.

2.4 Construction of prognostic model

We utilized the "createDataPartition" function in R to randomly partition the dataset into training and testing subsets. Univariate Cox regression analysis was performed to identify significant genes, followed by Lasso regression and cross-validation to optimize a multivariate Cox model (23). The "glmnet" package facilitated the calculation of risk scores for COAD patients based on the refined model. Patients were categorized into high-risk and low-risk groups based on the median risk score. The risk score was calculated using the formula: Risk score = Σ(expi * βi), where expi represents the expression level of each gene and βi denotes the corresponding regression coefficient. Kaplan-Meier survival curves were plotted using the "survival" package, and time-dependent receiver operating characteristic (tROC) curves were generated with the "timeROC" package to evaluate the model's predictive accuracy regarding patient survival.

2.5 Construction of nomograms

Nomograms were developed using the "rms" and "regplot" packages in R to forecast survival in COAD patients, taking into account factors such as age, sex, and stage. Calibration curves validated the precision of the nomogram's predictions for survival rates at 1 year, 3 years, and 5 years (24). Decision curve analysis revealed that the nomogram's predictive ability was superior to that of individual clinical factors. Performance assessment of the risk score showed that its accuracy in prediction surpassed that of conventional clinical indicators.

2.6 Risk score correlation with clinical variables

Both univariate and multivariate Cox regression analyses indicated a significant association between age, stage, and risk scores with the survival duration of patients with COAD. The risk score model constructed using these variables demonstrated significant differences in survival times across patients of varying gender, age, and stage.

2.7 Enrichment analysis

Using R packages "clusterProfiler" and "org.Hs.eg.db," we conducted Gene Ontology (GO) and Kyoto Encyclopedia of Genes and Genomes (KEGG) enrichment analysis on differentially expressed genes across different risk groups. GO enrichment analysis revealed distinct patterns in the distribution of differentially expressed genes between high-risk and low-risk groups, spanning biological processes (BP), molecular functions (MF), and cellular components (CC) (25). Additionally, KEGG pathway analysis highlighted the key pathways enriched by these differentially expressed genes.

2.8 Immune cell infiltration

We employed the CIBERSORT algorithm for precise calculation of immune cell infiltration proportions (26). A heatmap was utilized to visually represent the strength and directionality of correlations among different immune cell types. Specific immune cell subpopulations exhibited significant expression differences across risk groups. Furthermore, we employed the "estimate" package to calculate tumor microenvironment scores (TME scores) to evaluate the infiltration levels of immune and stromal cells within the tumor microenvironment (27).

2.9 Single-cell analysis

We performed thorough quality control and filtering of scRNA-seq data utilizing the "Seurat" and "SingleR" R packages. Each gene was required to be expressed in a minimum of three cells and to have an expression level of at least 50 genes. The "subset" function was applied to filter cells based on the criteria of having more than 50 genes and less than 5% mitochondrial gene expression. Data normalization was carried out using the "NormalizeData" function with a scaling factor of 10,000. The "FindVariableFeatures" function was then employed to identify genes exhibiting high variability, selecting the 1,500 genes with the most significant expression fluctuations for further analysis. Through PCA dimensionality reduction and t-SNE clustering analysis, we successfully identified multiple distinct cell clusters and recognized several marker genes (28). We used the SingleR algorithm in R to annotate cell types in our single-cell dataset by comparing it to a reference dataset. The results were visualized using t-SNE, which provided a clear representation of the cellular landscape. Additionally, we applied the Monocle algorithm to infer the developmental trajectories of the cells and construct dynamic models of cellular differentiation.

2.10 Candidate drug prediction and molecular docking

We conducted an extensive drug screening utilizing the gene prediction drug online resource (https://maayanlab.cloud/Enrichr/), selecting drugs based on an adjusted p-value of less than 0.05. The 2D structures of these drugs were retrieved from the PubChem database (https://pubchem.ncbi.nlm.nih.gov/) and converted into 3D models using "Chem3D." Protein structure data for the relevant genes were sourced from the PDB database (http://www.rcsb.org/). The receptor was prepared using "PyMol," removing water molecules and small ligand compounds. Molecular docking was conducted to identify active pockets using "Autodock Vina v.1.5.7" (29).

2.11 Cell transfection

The cell lines present in this study were obtained from The Cell Resource Center of Shanghai Life Sciences Institute. Firstly, lipo3000 transfection reagent was mixed with siRNA to form transfection complex. These complexes are then added to cells in a petri dish to bind to the cell membrane and enter the cell. After transfection, the cells were cultured for 24 hours under suitable culture conditions so that the foreign nucleic acid could be expressed or function. Finally, PCR was used to detect the transfection effect and the knockdown of exogenous genes. Primer information and siRNA sequence are Supplementary Table 1.

2.12 Western blotting

Total protein from the cells was extracted using RIPA Lysis Buffer (Beyotime, P0013B), and its concentration was determined using the Enhanced BCA Protein Assay Kit (Beyotime, P0010). The results were measured by ImageJ software.

2.13 Colony

After diluting the cells to an appropriate concentration, they are evenly seeded into sterile 6-well plates and then cultured in an incubator for 10-14 days until visible cell colonies form. Next, the cells are fixed with formaldehyde and stained with crystal violet.

2.14 Wound healing

Cultivate the cells to near confluence and then gently create a straight line scratch in the cell layer at the bottom of the culture dish using a sterile pipette. Subsequently, remove any cell debris from the scratch area and rinse once with fresh medium to eliminate floating cells. After that, place the cells back in the incubator and observe and capture images of the scratch healing at 0 and 48 hours to assess the rate and capacity of cell migration.

2.15 Statistical analysis

In this study, we performed logarithmic transformation and batch correction to standardize the data. All data analyses and graphical visualizations were performed using R software (version 4.3.3). To explore the co-expression relationships among genes, we employed Pearson correlation analysis. Furthermore, Spearman correlation analysis was performed to assess the association between risk scores and levels of immune cell infiltration. A comprehensive predictive model was established by combining univariate, Lasso, and multivariate Cox regression analyses. For comparative evaluations, t-tests were utilized to determine differences between two groups, while one-way ANOVA was applied to examine statistical variations across multiple groups. A p-value of less than 0.05 was deemed significant, with * denoting $P < 0.05$, ** indicating $P < 0.01$, and *** representing $P < 0.001$.

3 Results

3.1 Prognostic genes and subtype classification based on anoikis-related genes in COAD

Our research workflow is clearly illustrated (Figure 1). We collected transcriptomic data and clinical details from 483 COAD samples and 41 adjacent normal samples via TCGA database. After data organization, we merged the samples and converted probe IDs into gene IDs. We then compared gene expression levels between tumor and normal tissues, performing differential analysis using the "DESeq2" package (fold change = 2, p-value = 0.01). The intersection with ARGs yielded 134 significantly different genes in COAD (Figure 2A). We then standardized and merged the transcriptomic dataset of 585 samples and corresponding clinical data from the GEO database with TCGA dataset, extracting the expression levels of DEGs. Employing survival status and OS as outcome measures, univariate Cox regression analysis identified 37 prognostic genes, which are depicted in a forest plot (Figure 2B). The prognostic network diagram depicted in Supplementary Figure 1A illustrates the co-expression relationships among 29 high-risk and 8 low-risk genes. We subsequently displayed

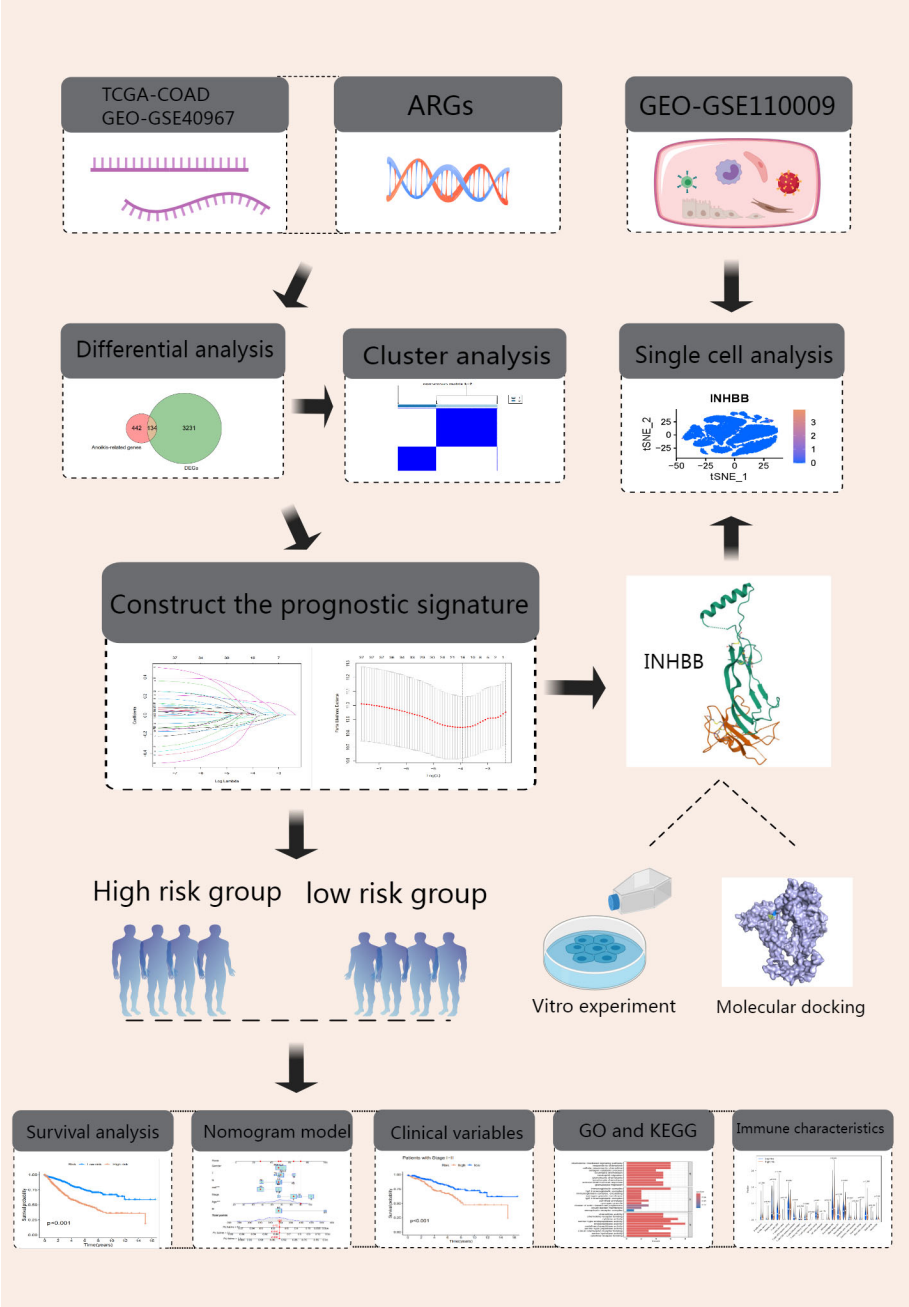

FIGURE 1
Experimental Design Flowchart.

10.3389/fimmu.2024.1524560

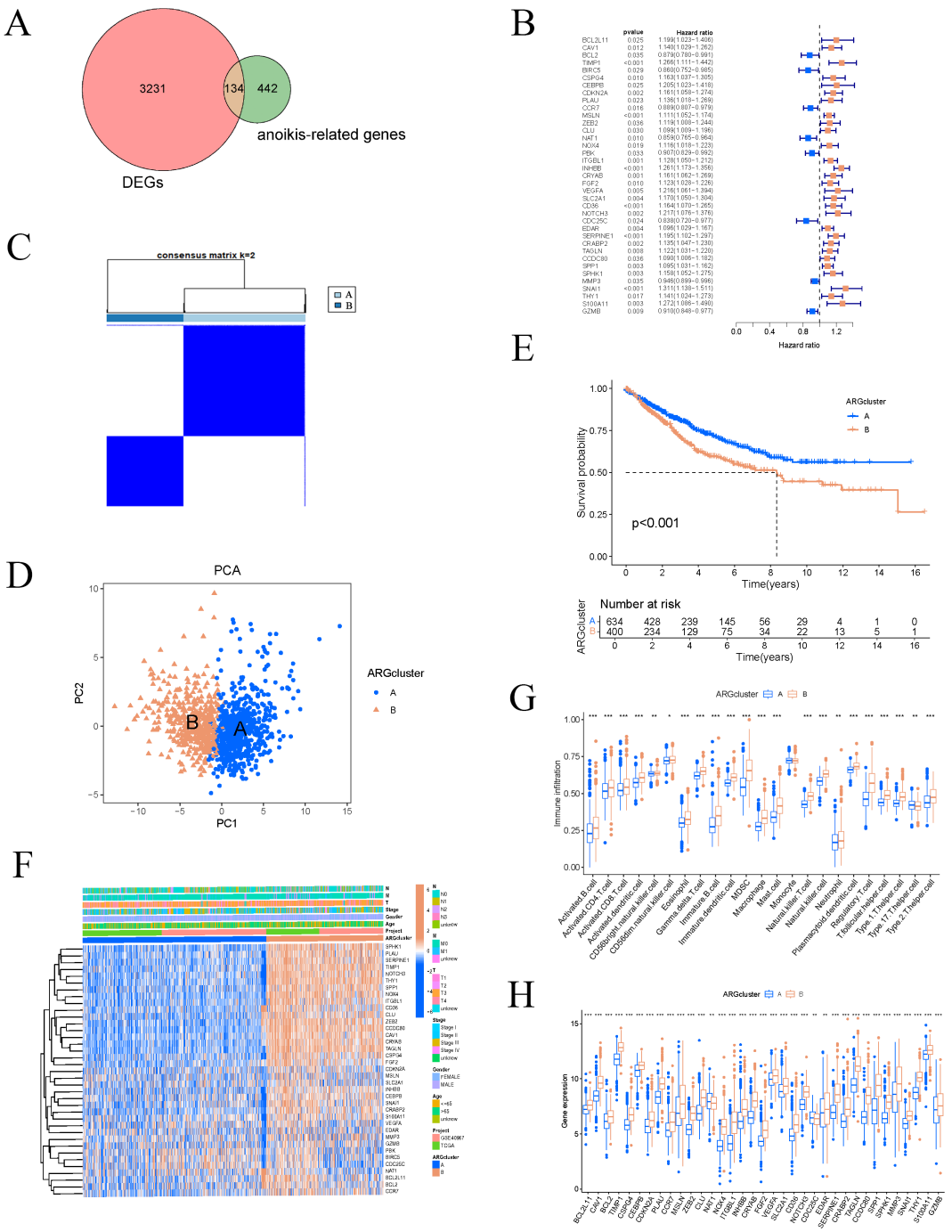

FIGURE 2
Consensus clustering analysis of ARGs. **(A)** Differential expression between COAD and ARGs. **(B)** Univariate Cox regression forest plot. **(C)** Divide COAD patients into two subgroups through consensus clustering analysis. **(D)** PCA for classification. **(E)** Survival analysis based on classification. **(F)** Thermogram combining typing with clinical characteristics of samples. **(G–H)** Differences in ARGs and immune cells across different clusters. These symbols (* for P < 0.05, ** for P < 0.01, *** for P < 0.001) are used to denote the significance levels of statistical results.

the frequency of copy number increases or decreases for specific genes within the samples, indicating the prevalence of gene variations across the samples, as shown in Supplementary Figure 1B. A copy number circle plot depicted in Supplementary Figure 1C shows the frequency of gene copy numbers at corresponding chromosomal positions. We constructed a PPI network for the anoikis-related DEGs, as shown in Supplementary Figure 1D, identifying genes with protein interaction relationships through connecting lines. The correlation network diagram in Supplementary Figure 1E illustrated the strength of correlations among different genes.

Based on the expression levels of ARGs, the samples were classified into two subtypes, A and B (Figure 2C). PCA demonstrated that the subtyping effectively separated the samples into distinct groups (Figure 2D). To further investigate the differences between subtypes A and B, survival curves confirmed a significant disparity in patient survival ($p < 0.001$), with subtype A exhibiting superior prognosis

compared to subtype B (Figure 2E). The subtype heatmap integrated subtype classifications with clinical characteristics, providing a detailed analysis of the distribution of upregulated and downregulated genes (Figure 2F). We also examined the differential expression of ARGs and immune cells between subtypes A and B (Figures 2G, H). Subsequently, GSVA and GSEA analyses were performed to investigate the biological functions and pathways associated with the different subtypes, emphasizing the discrepancies in biological pathway activities (Figure 3A). The findings indicated that cell adhesion molecules (CAMs), cytokine-cytokine receptor interactions, ECM receptor interactions, focal adhesion, and neuroactive ligand-receptor interactions were significantly reduced in subtype A (Figure 3B). Conversely, subtype B exhibited increased expression of CAMs, cytokine-cytokine receptor interactions, ECM receptor interactions, neuroactive ligand-receptor interactions, and systemic lupus erythematosus (Figure 3C).

3.2 Construction of a nine-gene prognostic model

We integrated a transcriptome dataset of 1,034 samples with survival data from TCGA and GEO databases, randomly partitioning it into a training cohort (n=517) and a test cohort (n=517). We employed the Least Absolute Shrinkage and Selection Operator (LASSO) to construct a regression model, identifying the point of minimal error through cross-validation (Figures 4A, B). Subsequently, we performed multivariate Cox regression analysis to enhance the model, selecting nine genes as risk features: NAT1, INHBB, FGF2, CD36, CCDC80, SPP1, MMP3, S100A11, and GZMB (Figure 4C). The risk score for COAD patients was computed using the following formula: Risk Score (RS)=(−0.25374×NAT1 expression)+(0.19775×INHBB expression)+(0.14497×FGF2 expression)+(0.23801×CD36 expression)+(−0.34139×CCDC80

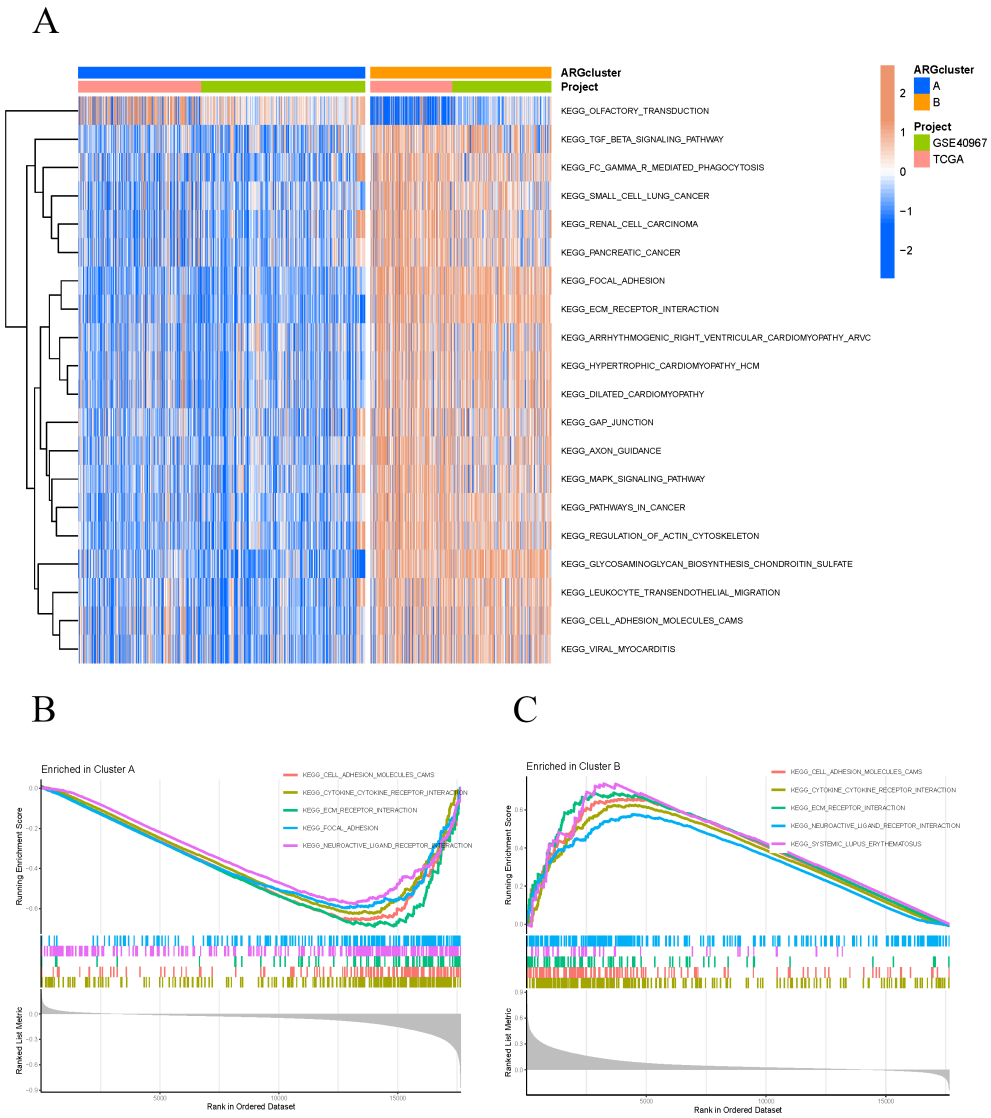

FIGURE 3
GSVA and GSEA analysis. **(A)** Differential expression of multiple biological pathways in different clusters and projects. **(B, C)** The GSEA pathways significantly enriched in clusters A and B.

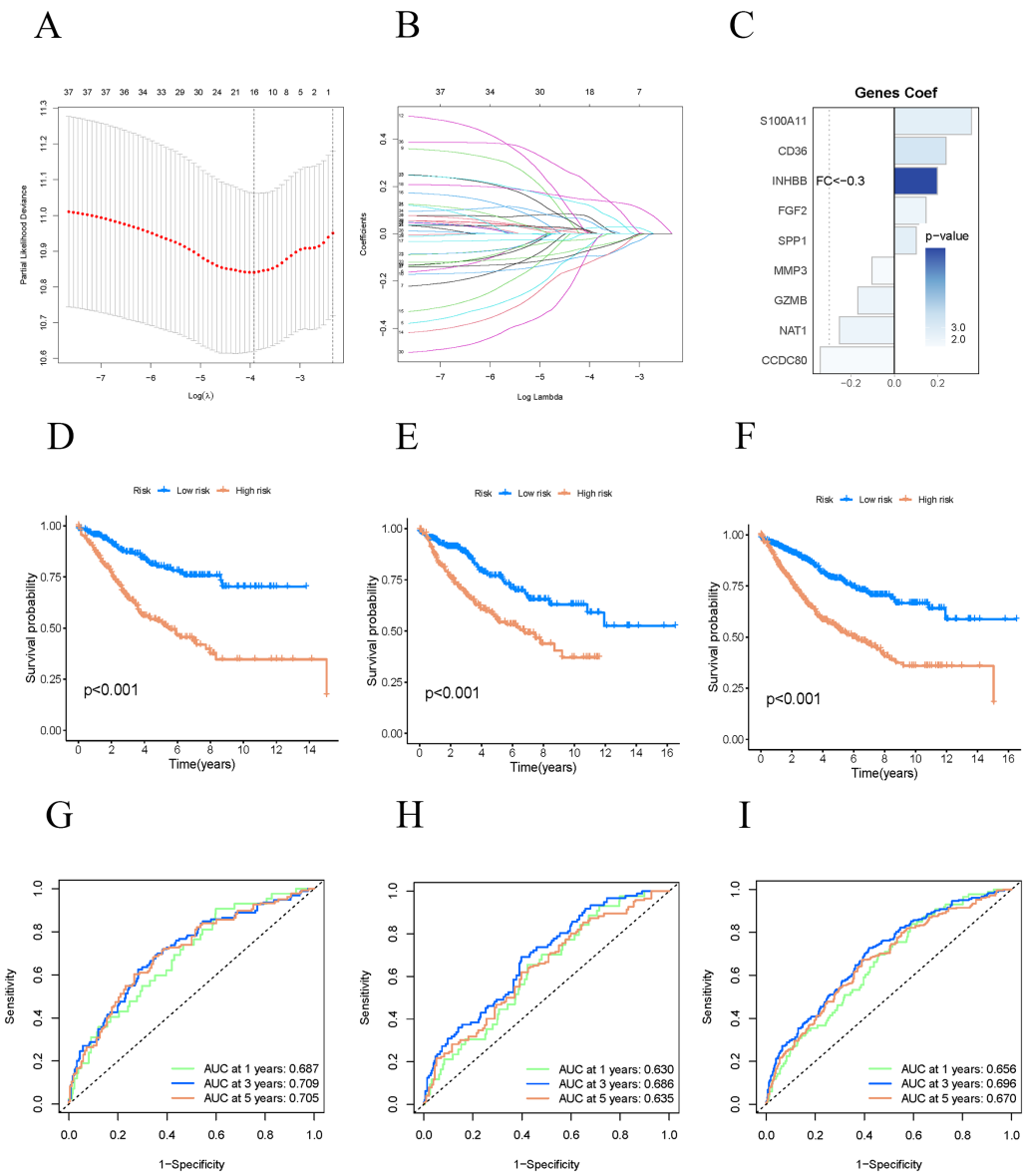

FIGURE 4
Constructing a prognostic model. **(A–C)** Constructing prognostic related model genes using Lasso regression. **(D–F)** The K-M curves of the training group, validation group, and all groups show the prognosis of COAD patients in high-risk and low-risk groups. **(G–I)** ROC curves of three groups of queues for one year, three years, and five years.

expression)+(0.09980×SPP1 expression)+(−0.10291×MMP3 expression)+(0.35502×S100A11 expression)+(−0.16830×GZMB expression) Using the median risk score, we stratified the samples into high-risk and low-risk groups within both the training and test cohorts. We evaluated our model's predictive efficacy for OS in COAD patients across all cohorts. Kaplan-Meier survival analysis revealed that high-risk COAD patients experienced significantly poorer OS in all three cohorts (Figures 4D–F). The ROC curves for the three cohorts showed AUC values exceeding 0.6, specifically 0.687, 0.709, and 0.705 for 1-year, 3-year, and 5-year survival, respectively (Figures 4G–I). These results indicate that our model is highly accurate in predicting survival outcomes for COAD patients at 1, 3, and 5 years.

3.3 Construction and validation of a prognostic nomogram for COAD survival (clinical and molecular features)

We constructed a nomogram (Figure 5A) that aggregates scores from each clinical characteristic (age, sex, stage) to predict patient survival. To assess the predictive performance of the nomogram, we generated calibration curves and decision curves. The calibration curves showed high accuracy in forecasting 1-year, 3-year, and 5-year survival using the nomogram (Figure 5B). The decision curves for 1 year, 3 years, and 5 years indicated that the nomogram's predictive power significantly exceeded that of other clinical factors (Figures 5C–E). In analyzing the survival rates of COAD patients,

10.3389/fimmu.2024.1524560

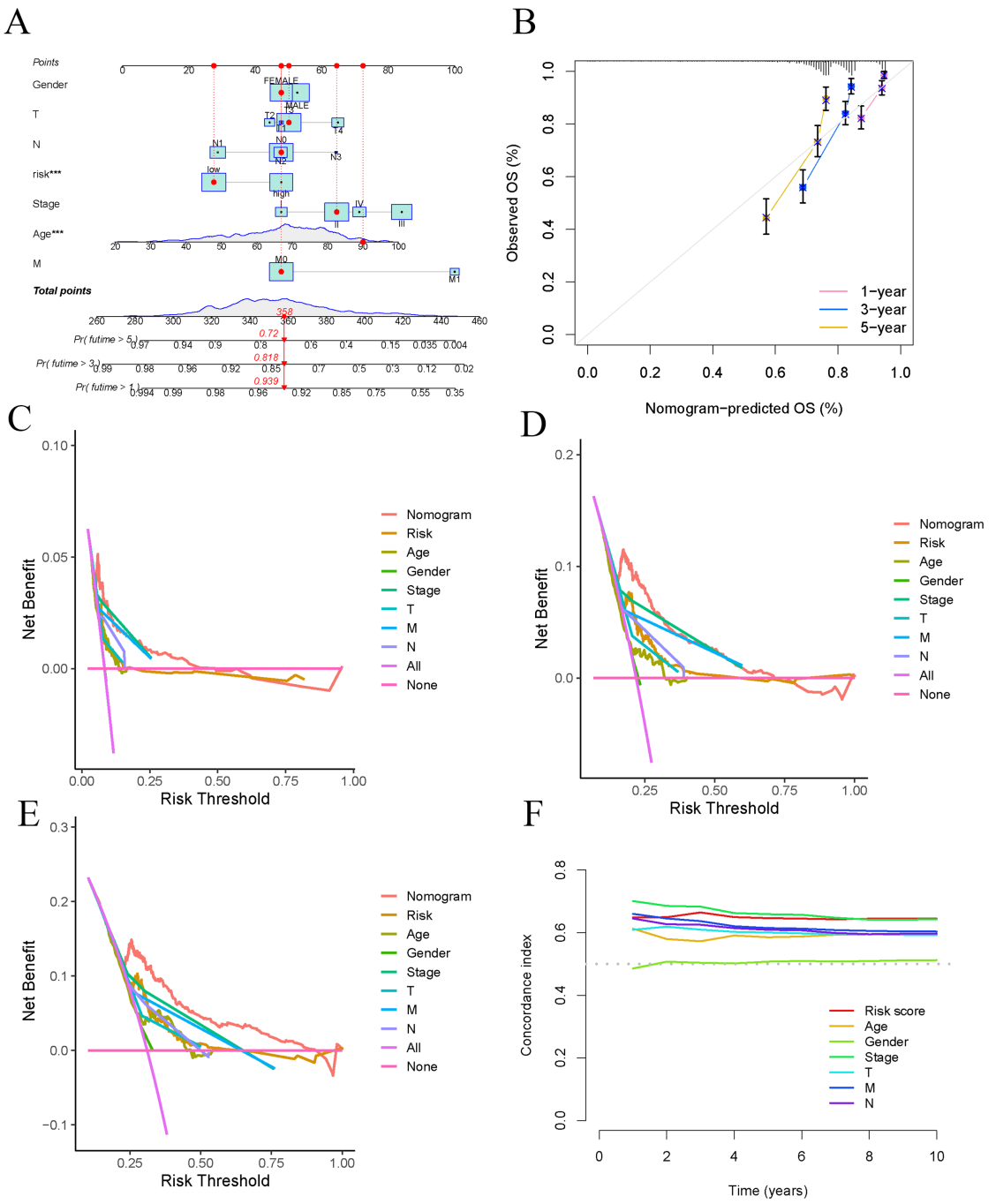

FIGURE 5
Establish and validate prognostic Nomogram. **(A)** Nomogram validation of OS in COAD patients. **(B)** Verify the predictive ability of Nomogram through calibration curves. **(C–E)** DCA curves for risk scores and clinical characteristics (1 year, 3 years, and 5 years). **(F)** C-index used to evaluate the performance of predictive models.

we compared the effectiveness of ARG features. Our findings revealed that the risk score exhibited the highest C-index, affirming its predictive accuracy and surpassing traditional clinical indicators, including pathological stage, age, and sex (Figure 5F).

Univariate Cox regression analysis was conducted to generate a forest plot (Figure 6A), showing significant associations between survival time and age, stage, and risk score. Multivariate Cox regression analysis further demonstrated statistical relationships between survival time and age, T, M, N stages, and risk score, as illustrated in a forest plot (Figure 6B). Consequently, the risk score calculated based on the nine ARGs can predict the survival rate of COAD patients. Stratification by age, sex, and stage demonstrated significant differences in survival times between high-risk and low-risk groups across all categories ($p < 0.01$). High-risk patients showed reduced survival durations compared to those classified as low-risk (Figures 6C–H).

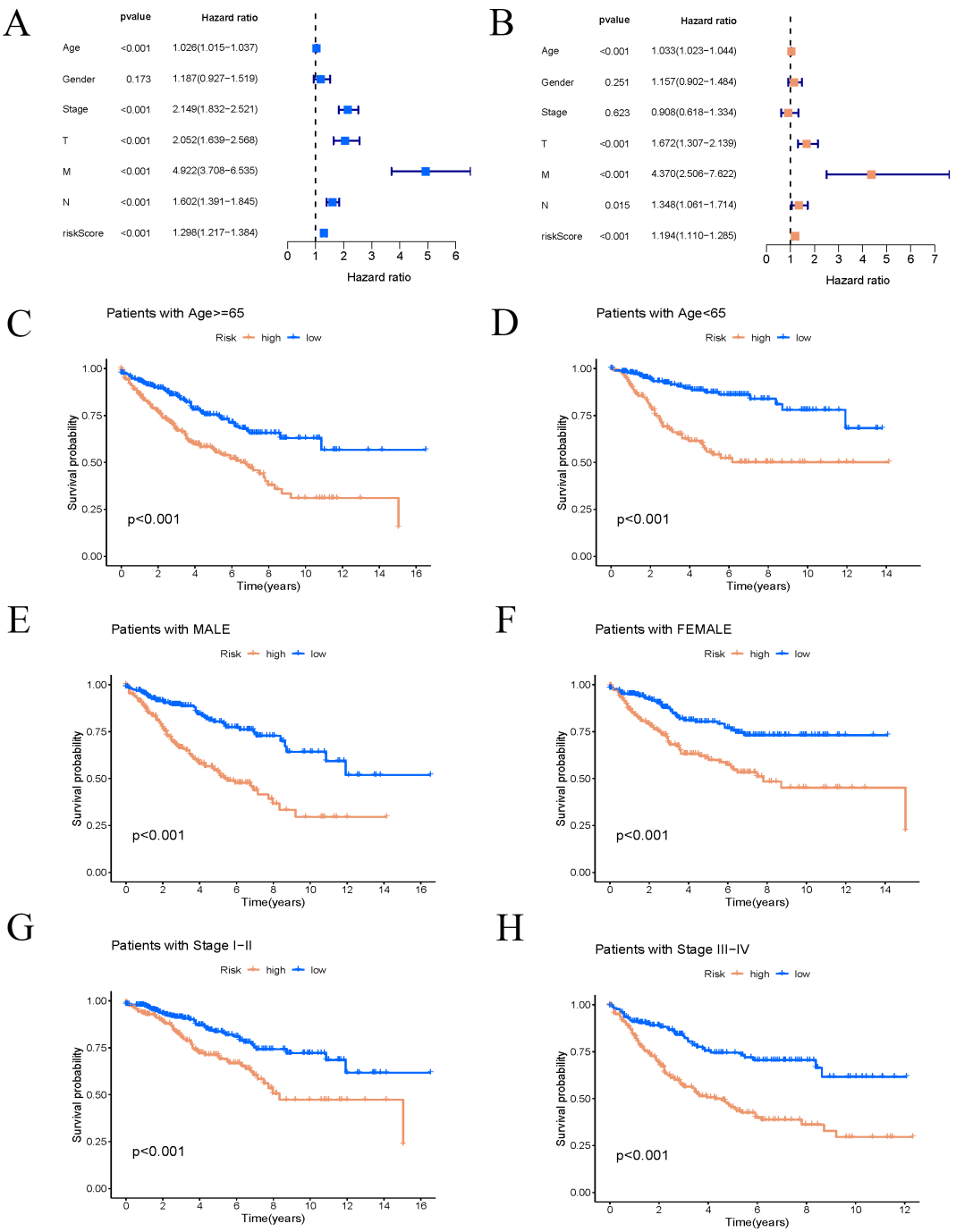

FIGURE 6
Risk score is highly correlated with clinical variables. **(A, B)** Univariate and multivariate Cox regression forest plots of risk score and clinical features. **(C–H)** K–M survival curves of patients stratified by different clinical pathological factors.

3.4 Enrichment analysis and immune microenvironment analysis reveal biological mechanisms and clinical relevance

To examine the distribution patterns of gene sets across BP, MF, and CC, we conducted GO enrichment analysis using differentially expressed genes from the high and low-risk groups. GO analysis indicated significant enrichment in cellular response to chemokine, endopeptidase activity, and immunoglobulin complex (Figures 7A). KEGG pathway analysis revealed that the differentially expressed genes were mainly enriched in pathways including cytokine-cytokine receptor interaction, IL-17 signaling pathway, viral protein interactions with cytokines and receptors, chemokine signaling pathway, and rheumatoid arthritis (Figures 7B). Notable differences in expression levels were found for plasma cells, activated CD4 memory T cells, resting NK cells, monocytes, M1 macrophages, and M2 macrophages across the different risk

10.3389/fimmu.2024.1524560

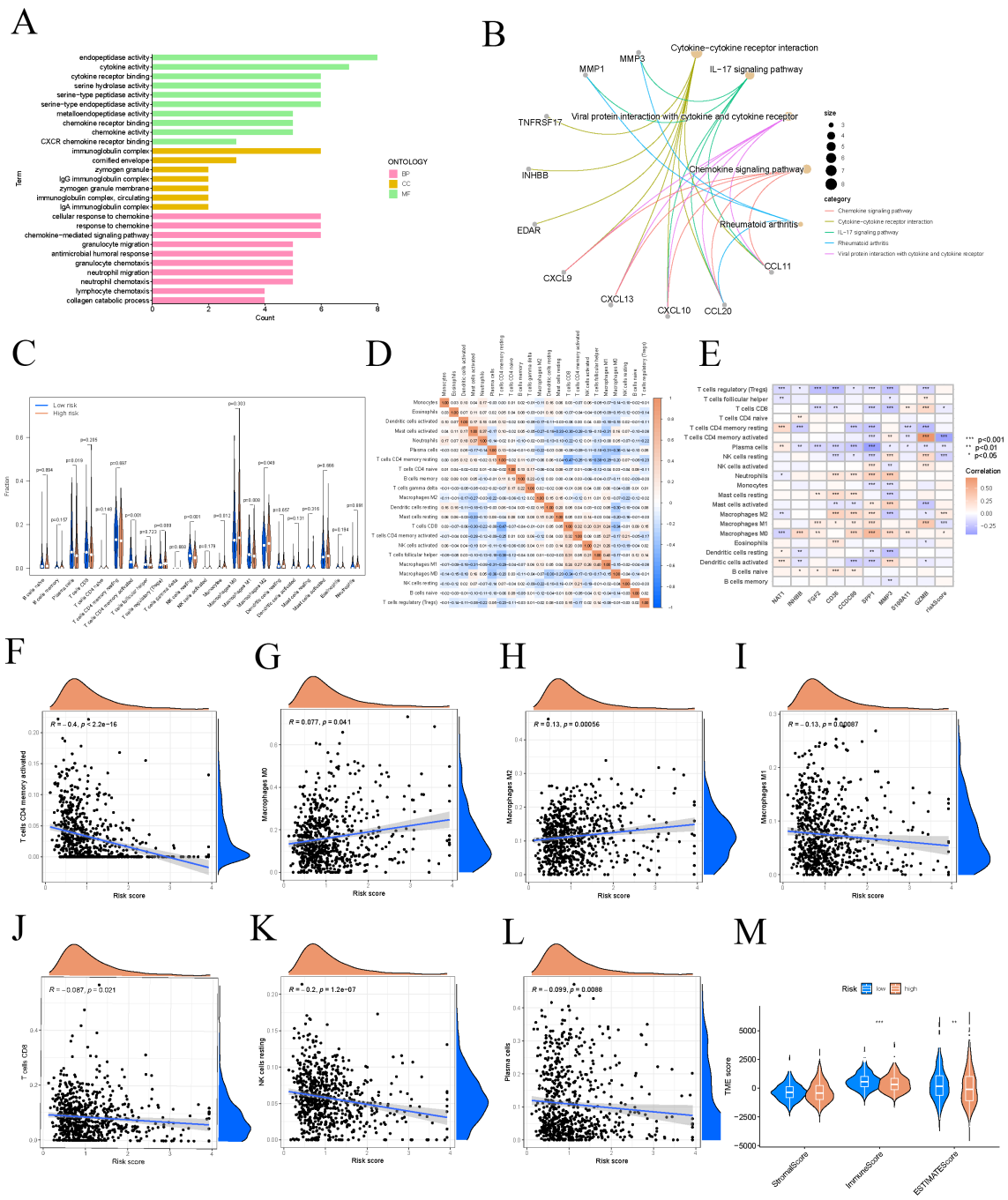

FIGURE 7
Different risk groups have different immune characteristics. **(A)** The GO signaling pathway involves biological processes in BP, MF, and CC. **(B)** Pathways significantly enriched in KEGG. **(C)** Differential analysis of immune cells in different risk groups. **(D)** Correlation heatmap of immune cells. **(E)** The correlation strength between model genes and immune cell types. **(F–L)** Immune cells significantly correlated with risk scores. **(M)** Differential assessment of TME scores. These symbols (* for P < 0.05, ** for P < 0.01, *** for P < 0.001) are used to denote the significance levels of statistical results.

categories (Figure 7C). We conducted a differential analysis of immune cells between high-risk and low-risk groups, illustrated by a heatmap that shows the correlation strength and direction among various immune cell types, such as monocytes, eosinophils, and activated dendritic cells (Figure 7D). A heatmap illustrating the correlations between immune cells, model genes, and risk scores was also presented (Figure 7E). Notably, risk scores exhibited significant expression differences with M0 macrophages, M1 macrophages, M2 macrophages, resting NK cells, plasma cells, activated CD4 memory T cells, and CD8 T cells, with the strongest correlation identified with activated CD4 memory T cells (R = -0.4, p < 2.2e−16) (Figures 7F–L). Patients in the low-risk group generally exhibit higher TME scores, which may be associated with stronger immune responses and lower tumor purity, thereby potentially having a positive impact on patient treatment responses and survival outcomes. The violin plot demonstrated

statistically significant differences in tumor TME scores, including immunescore and estimatescore, between high and low-risk groups (Figure 7M).

3.5 Single-cell analysis identifies key gene expression and cell types

We retrieved single-cell datasets for COAD from the GEO database, utilizing gene expression profiles from 13 COAD samples for further analysis. Initial quality control and filtering were performed, isolating the 1,500 most variably expressed genes, with the top ten most variable genes highlighted (Figure 8A). PCA was employed to reduce dimensionality on these 1,500 genes (Figure 8B), and expression levels of PC1-PC4 feature genes were visualized in a heatmap (Figure 8C). TSNE clustering analysis of 15 principal components identified 17 distinct clusters (Figure 8D). The differential analysis for each cluster has identified 5,933 marker genes, which are detailed in Supplementary Table 2. We conducted a detailed examination of the expression patterns for the nine key genes within the constructed model. Notably, the INHBB gene exhibited significantly elevated expression in cluster 15, while CCDC80 showed higher expression in cluster 13, and S100A11 was notably expressed in cluster 12 (Figures 8E, F). Analysis of cell types within each cluster revealed diverse populations, including T cells, B cells, epithelial cells, monocytes, macrophages, fibroblasts, tissue stem cells, and natural killer cells (Figure 8G). Further annotation revealed specific gene-cell type associations: INHBB was most highly expressed in endothelial cells, CCDC80 in fibroblasts, and S100A11 in epithelial cells. These findings provide crucial molecular evidence for understanding the roles of different cell types in biological processes. The cells were primarily derived from hematopoietic stem cells and differentiated along two distinct pathways: one pathway leading to the formation of epithelial-like cells, and the other leading to the generation of monocytes (Figure 8H).

3.6 Candidate drug prediction and molecular docking

In the prognostic model, the INHBB gene was identified as the most significant biomarker affecting OS in COAD patients, as shown in Supplementary Figure 2. To explore potential therapeutic strategies targeting this key gene, we conducted a comprehensive drug screening using a gene-drug prediction database. By considering adjusted p-values, we successfully identified 22 compounds with potential therapeutic relevance in Supplementary Table 3. To further assess the binding affinity of these candidate drugs with their targets, we performed molecular docking for the top four compounds. Using AutoDock Vina v.1.5.7, we analyzed the binding sites and interactions of these candidates with the INHBB protein, calculating binding energies for each interaction. The docking results indicated that INHBB had the lowest binding energy with risperidone at -9.5 kcal/mol, suggesting a stable interaction. Visualize the docking results of four drugs with INHBB using Pymol software (Figures 9A–D). This analysis not only allows us to predict potentially effective drugs but also provides critical insights into drug-target interactions, informing drug development and optimization efforts.

3.7 Impact of INHBB knockdown on proliferation and survival

Further analysis revealed that patients with high INHBB expression in COAD had worse OS and disease-free survival (DFS) (Figures 10A, B). In RKO and SW620 cell lines, INHBB knockdown resulted in significant changes in INHBB expression levels (Figure 10C). The verification of the low efficiency protein level is shown in the Supplementary Figure 3. In the wound healing assay, we observed a significant decrease in the proliferation activity of RKO and SW620 cells post-INHBB knockdown compared to control cells (Figures 10D, E). To further validate the impact of INHBB on the proliferative capacity of colorectal cancer cells, we conducted colony formation assays. The results showed that after INHBB gene knockdown, both cell lines exhibited reduced colony number and size (Figure 10F, G).

4 Discussion

Anoikis was first described in 1994 and refers to the programmed cell death of normally adherent cells when they remain in a suspended state for an extended period, leading to their demise due to “homelessness” (6). This form of apoptosis, characterized as a type of cellular “suicide,” is induced by the loss of contact with the ECM. Anoikis serves to eliminate cells that fail to attach properly to the matrix, thereby preventing their excessive proliferation (30). This mechanism is crucial for immune surveillance, helping to avoid the survival and dissemination of potential tumor or infected cells within the body. Tumor cells often evade immune attacks by suppressing anoikis; they may upregulate anti-apoptotic proteins (such as Bcl-2 family proteins) to inhibit apoptosis, thereby surviving even in the absence of matrix attachment, which provides a selective advantage for tumor progression. In the tumor microenvironment, anoikis may also impact the infiltration and functionality of immune cells (31). Damaged or unstable matrices can enable tumor cells to escape immune surveillance, adversely affecting the efficacy of immunotherapy. COAD cells frequently escape normal death signals through anoikis, thereby acquiring the ability to grow at distant sites (32). Understanding the mechanisms underlying anoikis is essential for elucidating how tumor cells survive during the metastatic process.

Due to the high heterogeneity of tumors, traditional molecular subtyping still exhibits significant variability in treatment outcomes for COAD patients. Precision therapy is crucial in the management of various solid tumors and represents a key direction for future cancer treatment. In this study, we leveraged COAD samples from TCGA database and GEO database to explore and identify a series of ARGs. Leveraging these genes, we established a prognostic model comprising nine key genes (NAT1, INHBB, FGF2, CD36, CCDC80,

10.3389/fimmu.2024.1524560

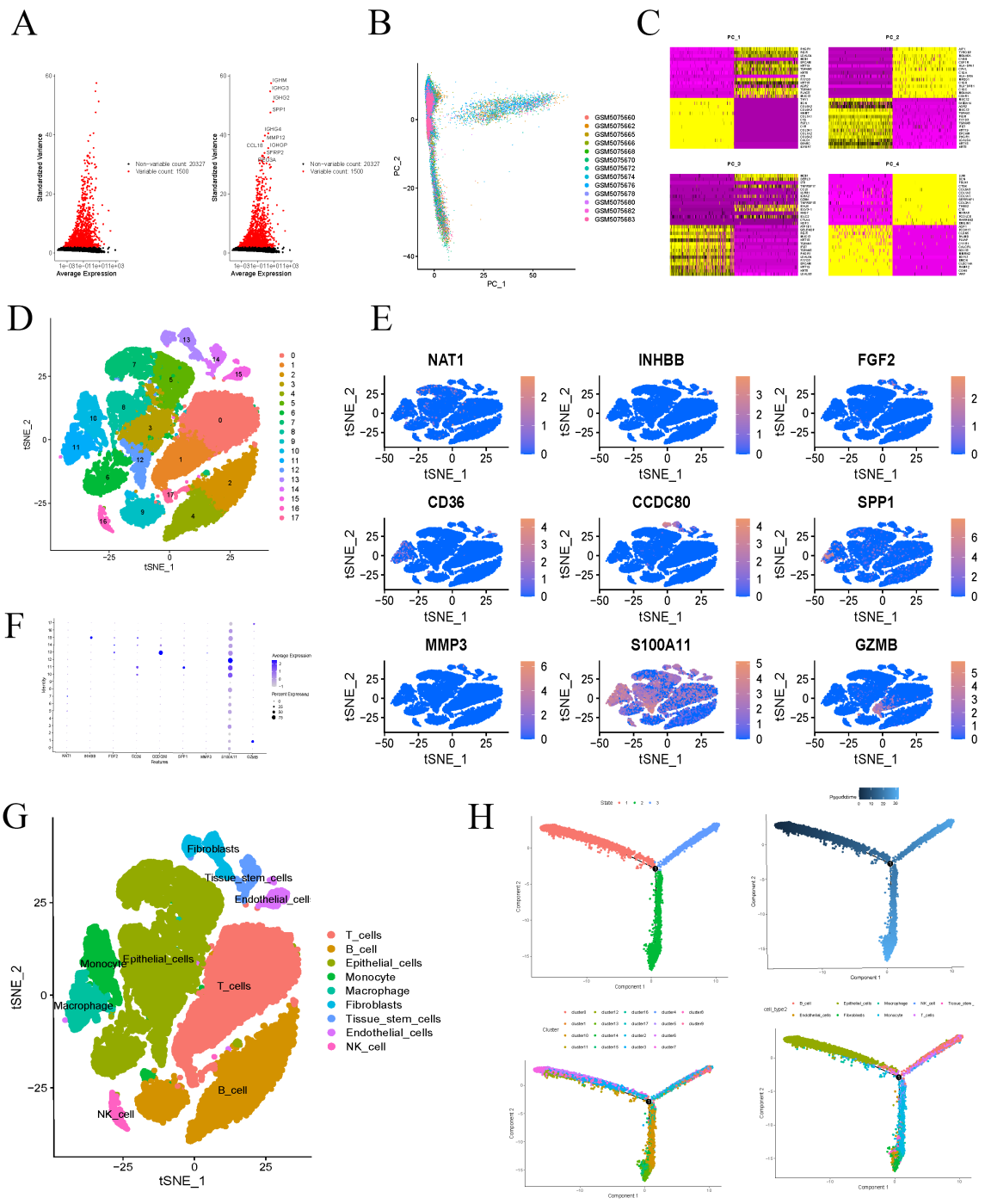

FIGURE 8
Single-cell analysis. **(A)** Select the top 1500 genes with the largest fluctuations and mark the top 10 genes for ranking. **(B)** Using PCA to reduce the dimensionality of the top 1500 genes in the ranking. **(C)** Heatmap displays the characteristic genes of PC1-PC4. **(D)** Divide all cells into 17 clusters using t-SNE algorithm. **(E, F)** Expression of model genes in 17 clusters. **(G)** After dimensionality reduction using t-SNE algorithm, the classification of cells was demonstrated. **(H)** Cell differentiation trajectory diagram.

SPP1, MMP3, S100A11, and GZMB) (33, 34). This model stratified COAD patients into high-risk and low-risk groups based on risk scores, revealing significant disparities in survival outcomes, mutation patterns, immune cell infiltration, and chemotherapy responses between the two groups.

GO and KEGG enrichment analyses conducted on the differentially expressed genes across the risk categories indicated their participation in cellular responses to chemokines. This suggests these genes could have significant roles in inflammation and immune response mechanisms. KEGG pathway enrichment further suggests active inflammatory responses and intercellular signaling among the differentially expressed genes, which could significantly impact tumor progression and metastasis. Significant differences were observed in the expression levels of various

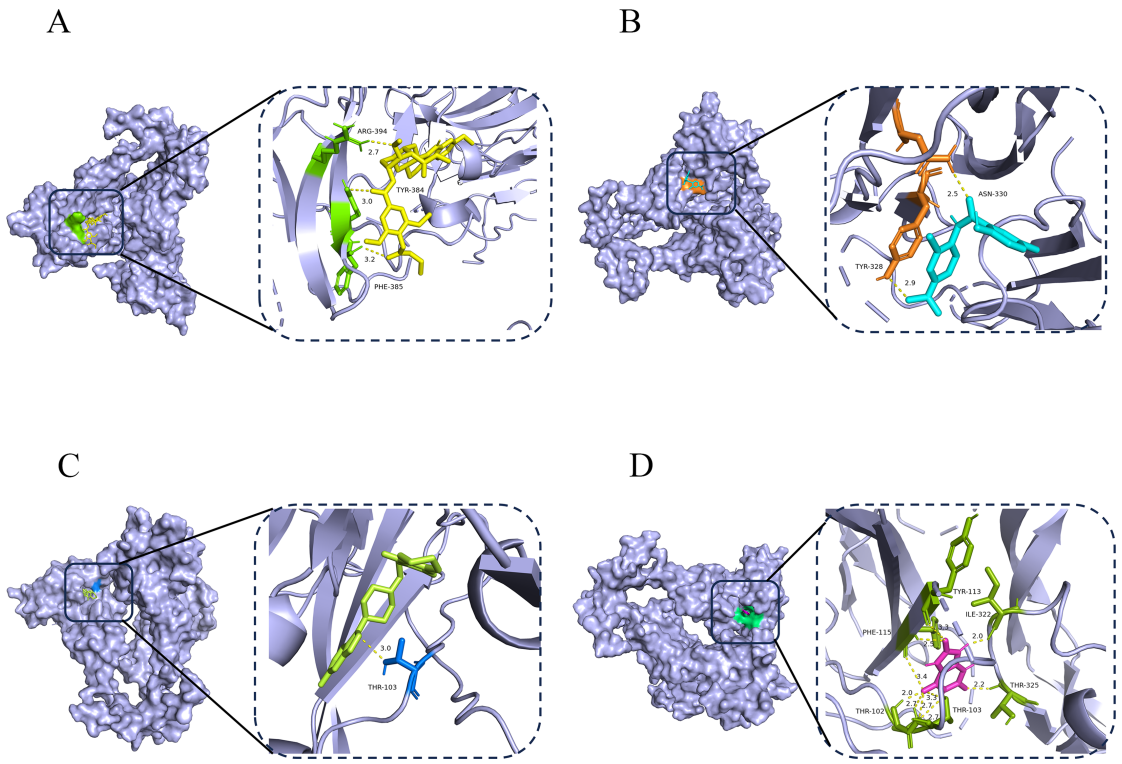

FIGURE 9
Potential therapeutic compounds and molecular docking analysis of INHBB. **(A–D)** Molecular docking technology was applied to the top four drugs (syrosingopine, niclosamide, risperidone and uric acid) ranked.

immune cell populations, such as plasma cells, activated CD4 memory T cells, resting NK cells, monocytes, and M1 and M2 macrophages across the risk groups. The notable decrease in plasma cell expression within the high-risk group may suggest a compromised ability to produce antibodies, which could diminish the immune system's capacity to combat tumor cells. Additionally, lower NK cell infiltration in the high-risk group may facilitate immune evasion by tumor cells, as NK cells are critical for directly killing tumor cells. M1 macrophages are typically associated with anti-tumor immune responses, while M2 macrophages may promote tumor development and metastasis, suggesting a potential strong immune evasion mechanism in the high-risk group. Notable differences in immune scores and tumor microenvironment scores reinforce the link between immune cell infiltration and tumor progression. Single-cell analysis uncovered unique expression patterns of different cell types and their associated genes within the COAD microenvironment, offering valuable insights into the biological mechanisms driving tumor behavior.

Elevated levels of crucial genes such as INHBB, CCDC80, and S100A11 could be significantly linked to tumor development, progression, and the modulation of the tumor microenvironment. INHBB is a member of the transforming growth factor-beta (TGF-β) superfamily, primarily encoded by the INHBB gene, and is part of the inhibin family, functioning alongside inhibin subunit beta A (INHBA) and inhibin subunit beta C (INHBC) to play important physiological roles (35). INHBB is involved in various biological processes, including cell proliferation and apoptosis, making it an important candidate in cancer research. Previous studies have shown that INHBB exhibits a complex dual role in different types of cancer. It not only promotes the proliferation and invasion of various cancers, such as clear cell renal carcinoma (36), hepatocellular carcinoma (37), endometrial carcinoma (38), and prostate cancer (39), but also, in some cases, suppresses the metastasis of nasopharyngeal carcinoma (40) and induces apoptosis. For example, INHBB expression is significantly elevated in endometrial carcinoma tissues and enhances cancer cell invasion by activating the SMAD2/3 and integrin β3 signaling pathways. INHBB promotes gastric cancer (GC) by reprogramming fibroblasts into cancer-associated fibroblasts (CAFs) and activating the NF-κB pathway, which enhances gastric cancer cell proliferation, migration, and invasion (41). However, research on the mechanisms of INHBB in colon cancer is relatively limited. Some studies suggest that increased INHBB expression may promote epithelial-mesenchymal transition (EMT) in cancer cells, thereby enhancing their metastatic potential (42). In our study, we observed a negative correlation between INHBB levels and OS in high-risk COAD patients. We also validated the expression level and functional role of INHBB in COAD, finding that knocking down INHBB significantly reduced cell proliferation, further supporting its potential as a prognostic biomarker (43). We also explored the therapeutic potential of INHBB and used molecular docking technology to identify risperidone as the

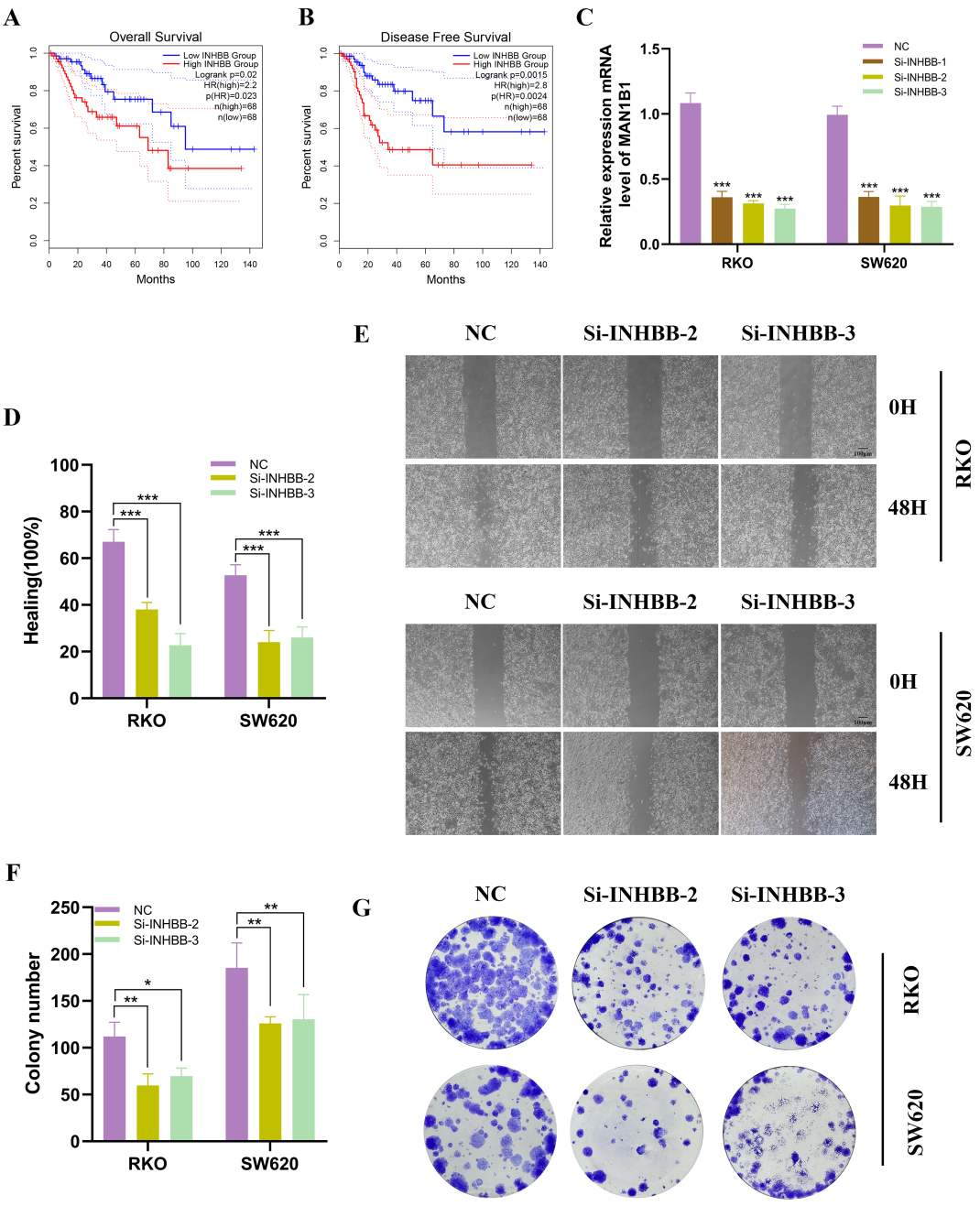

FIGURE 10
Analysis and experimental validation of INHBB expression. **(A, B)** Investigating INHBB's impact on COAD OS and DFS in TCGA dataset. **(C)** INHBB was knocked down in RKO and SW620. **(D, E)** Scratch assays demonstrated that the migratory activity of cells with INHBB knockdown was significantly reduced. **(F, G)** Colony formation assays showed that the proliferative activity of cells with INHBB knockdown was significantly decreased. These symbols (* for P < 0.05, ** for P < 0.01, *** for P < 0.001) are used to denote the significance levels of statistical results.

compound with the lowest binding energy to INHBB. Risperidone may indirectly affect COAD cell proliferation by regulating dopamine and serotonin receptor signaling pathways. On the other hand, CCDC80 has been shown to reduce COAD cell proliferation by negatively regulating the ERK1/2 signaling pathway, thereby inhibiting tumor progression (44). SPP1 is overexpressed in COAD, significantly enhancing tumor cell invasion and metastasis, and is associated with poor prognosis (45). GZMB plays a key role in the immune system, and studies have shown that it participates in regulating cancer cell apoptosis during COAD immune responses, indicating its potential application in immunotherapy (46).

This study, however, does have certain limitations. Our analysis relies on transcriptomic data from public databases, which may introduce selection bias, as these datasets may not fully represent the diversity of all COAD patients. The predictive capability of this model requires further assessment and validation in independent, diverse patient cohorts through prospective studies.

5 Conclusions

In conclusion, our research, based on the features of ARGs, offers novel perspectives on the molecular subtyping and prognostic evaluation of COAD, as well as highlighting potential targets for future therapeutic interventions and drug development. The findings of this research hold promise for advancing the field of personalized treatment for COAD, offering patients more precise and effective therapeutic options.

Data availability statement

The datasets presented in this study can be found in online repositories. The names of the repository/repositories and accession number(s) can be found in the article/Supplementary Material.

Ethics statement

Ethical approval was not required for the studies on humans in accordance with the local legislation and institutional requirements because only commercially available established cell lines were used.

Author contributions

QW: Conceptualization, Data curation, Writing – original draft, Writing – review & editing. LY: Methodology, Software, Writing – original draft, Writing – review & editing. YW: Formal analysis, Visualization, Writing – original draft, Writing – review & editing. MZ: Software, Supervision, Writing – original draft, Writing – review & editing. JL: Methodology, Validation, Writing – original draft, Writing – review & editing. YY: Data curation, Formal analysis, Writing – original draft, Writing – review & editing. YN: Conceptualization, Formal analysis, Writing – original draft, Writing – review & editing. LZ: Conceptualization, Supervision, Writing – original draft, Writing – review & editing. PZ: Supervision, Validation, Writing – original draft, Writing – review & editing.

Funding

The author(s) declare that no financial support was received for the research, authorship, and/or publication of this article.

Acknowledgments

We are very grateful for data provided by databases such as TCGA, GEO. Thanks to reviewers and editors for their sincere comments.

Conflict of interest

The authors declare that the research was conducted in the absence of any commercial or financial relationships that could be construed as a potential conflict of interest.

Generative AI statement

The author(s) declare that no Generative AI was used in the creation of this manuscript.

Publisher's note

All claims expressed in this article are solely those of the authors and do not necessarily represent those of their affiliated organizations, or those of the publisher, the editors and the reviewers. Any product that may be evaluated in this article, or claim that may be made by its manufacturer, is not guaranteed or endorsed by the publisher.

Supplementary material

The Supplementary Material for this article can be found online at: https://www.frontiersin.org/articles/10.3389/fimmu.2024.1524560/full#supplementary-material

SUPPLEMENTARY FIGURE 1
Exploration of Anoikis-Related Prognostic Genes. **(A)** Correlation network diagram of ARGs. **(B)** The histogram displays the gain or loss of CNV. **(C)** Copy loop diagram showing the position of ARGs on chromosomes. **(D)** The PPI network of ARGs. **(E)** The correlation network diagram shows the correlation between ARGs.

SUPPLEMENTARY FIGURE 2
The impact of expression levels of six genes on OS in COAD patients, as compared by ROC curves and survival analysis.

SUPPLEMENTARY FIGURE 3
The WB blot of INHBB after siRNA transfection to indicate its knockdown efficiency.

References

1. Morgan E, Arnold M, Gini A, Lorenzoni V, Cabasag CJ, Laversanne M, et al. Global burden of colorectal cancer in 2020 and 2040: incidence and mortality estimates from globocan. *Gut*. (2023) 72:338–44. doi: 10.1136/gutjnl-2022-327736

2. Siegel RL, Wagle NS, Cercek A, Smith RA, Jemal A. Colorectal cancer statistics, 2023. *CA Cancer J Clin*. (2023) 73:233–54. doi: 10.3322/caac.21772

3. Sung H, Ferlay J, Siegel RL, Laversanne M, Soerjomataram I, Jemal A, et al. Global cancer statistics 2020: globocan estimates of incidence and mortality worldwide for 36 cancers in 185 countries. *CA Cancer J Clin*. (2021) 71:209–49. doi: 10.3322/caac.21660

4. Di Nicolantonio F, Vitiello PP, Marsoni S, Siena S, Tabernero J, Trusolino L, et al. Precision oncology in metastatic colorectal cancer - from biology to medicine. *Nat Rev Clin Oncol*. (2021) 18:506–25. doi: 10.1038/s41571-021-00495-z

5. Al-Joufi FA, Setia A, Salem-Bekhit MM, Sahu RK, Alqahtani FY, Widyowati R, et al. Molecular pathogenesis of colorectal cancer with an emphasis on recent advances

in biomarkers, as well as nanotechnology-based diagnostic and therapeutic approaches. *Nanomaterials (Basel)*. (2022) 12(1):169. doi: 10.3390/nano12010169

6. Mei J, Jiang XY, Tian HX, Rong DC, Song JN, Wang L, et al. Anoikis in cell fate, physiopathology, and therapeutic interventions. *MedComm (2020)*. (2024) 5:e718. doi: 10.1002/mco2.718

7. Yuan Z, Li Y, Zhang S, Wang X, Dou H, Yu X, et al. Extracellular matrix remodeling in tumor progression and immune escape: from mechanisms to treatments. *Mol Cancer*. (2023) 22:48. doi: 10.1186/s12943-023-01744-8

8. Wang Y, Cheng S, Fleishman JS, Chen J, Tang H, Chen ZS, et al. Targeting anoikis resistance as a strategy for cancer therapy. *Drug Resist Update*. (2024) 75:101099. doi: 10.1016/j.drup.2024.101099

9. Fanfone D, Wu Z, Mammi J, Berthenet K, Neves D, Weber K, et al. Confined migration promotes cancer metastasis through resistance to anoikis and increased invasiveness. *Elife*. (2022) 11:e73150. doi: 10.7554/eLife.73150

10. Li W, Huang M, Wu Z, Zhang Y, Cai Y, Su J, et al. Mrna-lipid nanoparticle-mediated restoration of ptpn14 exhibits antitumor effects by overcoming anoikis resistance in triple-negative breast cancer. *Adv Sci (Weinh)*. (2024) 11:e2309988. doi: 10.1002/advs.202309988

11. Long WB, Pu X, Tang Y, Li M, Liu Y, She Q, et al. Arginine adp-ribosyltransferase 1 regulates glycolysis in colorectal cancer via the pi3k/akt/hif1α Pathway. *Curr Med Sci*. (2022) 42:733–41. doi: 10.1007/s11596-022-2606-4

12. Narayanankutty A. Pi3k/akt/mtor pathway as a therapeutic target for colorectal cancer: A review of preclinical and clinical evidence. *Curr Drug Targets*. (2019) 20:1217–26. doi: 10.2174/1389450120666190618123846

13. Yao X, Gray S, Pham T, Delgardo M, Nguyen A, Do S, et al. Downregulation of bit1 expression promotes growth, anoikis resistance, and transformation of immortalized human bronchial epithelial cells via erk activation-dependent suppression of E-cadherin. *Biochem Biophys Res Commun*. (2018) 495:1240–8. doi: 10.1016/j.bbrc.2017.11.126

14. Wang X, Liu Y, Liu H, Pan W, Ren J, Zheng X, et al. Recent advances and application of whole genome amplification in molecular diagnosis and medicine. *MedComm (2020)*. (2022) 3:e116. doi: 10.1002/mco2.116

15. Paggi JM, Pandit A, Dror RO. The art and science of molecular docking. *Annu Rev Biochem*. (2024) 93:389–410. doi: 10.1146/annurev-biochem-030222-120000

16. Ding G, Ma T, Zhang K, Chen G, Shen J, Zhang S, et al. A pan-cancer analysis of the role of wdfy2 in human tumors. *Biotechnol Genet Eng Rev*. (2024) 40:1456–71. doi: 10.1080/02648725.2023.2194077

17. Li N, Chen S, Xu X, Wang H, Zheng P, Fei X, et al. Single-cell transcriptomic profiling uncovers cellular complexity and microenvironment in gastric tumorigenesis associated with helicobacter pylori. *J Adv Res*. (2024) S2090-1232(24)00466-1. doi: 10.1016/j.jare.2024.10.012

18. Jiang Z, Yang G, Wang G, Wan J, Zhang Y, Song W, et al. Sec14l3 knockdown inhibited clear cell renal cell carcinoma proliferation, metastasis and sunitinib resistance through an sec14l3/rps3/nfκb positive feedback loop. *J Exp Clin Cancer Res*. (2024) 43:288. doi: 10.1186/s13046-024-03206-5

19. Xie R, Li C, Yun J, Zhang S, Zhong A, Cen Y, et al. Identifying the pattern characteristics of anoikis-related genes in keloid. *Adv Wound Care (New Rochelle)*. (2024). doi: 10.1089/wound.2024.0027

20. Zhang Z, Liu X, Chu C, Zhang Y, Li W, Yu X, et al. Mir937 amplification potentiates ovarian cancer progression by attenuating fbxo16 inhibition on ulk1-mediated autophagy. *Cell Death Dis*. (2024) 15:735. doi: 10.1038/s41419-024-07120-8

21. Feng Q, Su C, Yang C, Wu M, Li X, Lin X, et al. Rxrα/mr signaling promotes diabetic kidney disease by facilitating renal tubular epithelial cells senescence and metabolic reprogramming. *Transl Res*. (2024) 274:101–17. doi: 10.1016/j.trsl.2024.10.001

22. Sulleyx S, Zhou Y, Ndanga M, Saka A. Integrating aging biomarkers and immune function to predict kidney health: insights from the future of families and child wellbeing study. *Geroscience*. (2024). doi: 10.1007/s11357-024-01402-x

23. Li Z, Pei S, Wang Y, Zhang G, Lin H, Dong S. Advancing predictive markers in lung adenocarcinoma: A machine learning-based immunotherapy prognostic prediction signature. *Environ Toxicol*. (2024) 39(10):4581–93. doi: 10.1002/tox.24284

24. Skarping I, Bendahl PO, Szulkin R, Alkner S, Andersson Y, Bergkvist L, et al. Prediction of high nodal burden in patients with sentinel node-positive luminal erbb2-negative breast cancer. *JAMA Surg*. (2024) 159(12):1393–403. doi: 10.1001/jamasurg.2024.3944

25. de Lima J, Leite JA, Basso PJ, Ghirotto B, Martins da Silva E, Menezes-Silva L, et al. Sirtuin 1 regulates the phenotype and functions of dendritic cells through ido1 pathway in obesity. *Cell Death Dis*. (2024) 15:757. doi: 10.1038/s41419-024-07125-3

26. Kang Y, Zhong R, Gan Y, You J, Chen J, Chen F, et al. Fanca promotes lung adenocarcinoma progression and is a potential target for epitope vaccine immunotherapy. *J Transl Med*. (2024) 22:911. doi: 10.1186/s12967-024-05675-w

27. Skubleny D, Purich K, McLean DR, Martins-Filho SN, Buttenschoen K, Haase E, et al. The tumour immune microenvironment drives survival outcomes and therapeutic response in an integrated molecular analysis of gastric adenocarcinoma. *Clin Cancer Res*. (2024) 30(23):5385–98. doi: 10.1158/1078-0432.Ccr-23-3523

28. Xie J, Chen L, Wu D, Liu S, Pei S, Tang Q, et al. Significance of liquid-liquid phase separation (Llps)-related genes in breast cancer: A multi-omics analysis. *Aging (Albany NY)*. (2023) 15:5592–610. doi: 10.18632/aging.204812

29. Cao Y, Yang Y, Hu Q, Wei G. Identification of potential drug targets for rheumatoid arthritis from genetic insights: A mendelian randomization study. *J Transl Med*. (2023) 21:616. doi: 10.1186/s12967-023-04474-z

30. Liu Y, Ding L, Chen G, Wang P, Wang X. A thermo-sensitive hydrogel with prominent hemostatic effect prevents tumor recurrence via anti-anoikis-resistance. *J Nanobiotechnology*. (2024) 22:496. doi: 10.1186/s12951-024-02739-3

31. Li X, Gao L, Wang B, Hu J, Yu Y, Gu B, et al. Fxa-mediated par-2 promotes the efficacy of immunotherapy for hepatocellular carcinoma through immune escape and anoikis resistance by inducing pd-L1 transcription. *J Immunother Cancer*. (2024) 12(7):e009565. doi: 10.1136/jitc-2024-009565

32. Yang T, Liu YL, Guo HL, Peng XF, Zhang B, Wang D, et al. Unveiling an anoikis-related risk model and the role of rad9a in colon cancer. *Int Immunopharmacol*. (2024) 140:112874. doi: 10.1016/j.intimp.2024.112874

33. Chen W, Kang Y, Sheng W, Huang Q, Cheng J, Pei S, et al. A new 4-gene-based prognostic model accurately predicts breast cancer prognosis and immunotherapy response by integrating wgcna and bioinformatics analysis. *Front Immunol*. (2024) 15:1331841. doi: 10.3389/fimmu.2024.1331841

34. Dong X, Liao P, Liu X, Yang Z, Wang Y, Zhong W, et al. Construction and validation of a reliable disulfidptosis-related lncrnas signature of the subtype, prognostic, and immune landscape in colon cancer. *Int J Mol Sci*. (2023) 24(16):12915. doi: 10.3390/ijms241612915

35. Wijayarathna R, de Kretser DM. Activins in reproductive biology and beyond. *Hum Reprod Update*. (2016) 22:342–57. doi: 10.1093/humupd/dmv058

36. Sun Y, Cai H, Ge J, Shao F, Huang Z, Ding Z, et al. Tubule-derived inhbb promotes interstitial fibroblast activation and renal fibrosis. *J Pathol*. (2022) 256:25–37. doi: 10.1002/path.5798

37. Chen Y, Qian B, Sun X, Kang Z, Huang Z, Ding Z, et al. Sox9/inhbb axis-mediated crosstalk between the hepatoma and hepatic stellate cells promotes the metastasis of hepatocellular carcinoma. *Cancer Lett*. (2021) 499:243–54. doi: 10.1016/j.canlet.2020.11.025

38. Xiong S, Klausen C, Cheng JC, Zhu H, Leung PC. Activin B induces human endometrial cancer cell adhesion, migration and invasion by up-regulating integrin B3 via smad2/3 signaling. *Oncotarget*. (2015) 6:31659–73. doi: 10.18632/oncotarget.5229

39. Hofland J, van Weerden WM, Steenbergen J, Dits NF, Jenster G, de Jong FH. Activin a stimulates akr1c3 expression and growth in human prostate cancer. *Endocrinology*. (2012) 153:5726–34. doi: 10.1210/en.2011-2065

40. Zou G, Ren B, Liu Y, Fu Y, Chen P, Li X, et al. Inhibin B suppresses anoikis resistance and migration through the transforming growth factor-B Signaling pathway in nasopharyngeal carcinoma. *Cancer Sci*. (2018) 109:3416–27. doi: 10.1111/cas.13780

41. Jin Y, Cai Q, Wang L, Ji J, Sun Y, Jiang J, et al. Paracrine activin B-nf-Bb signaling shapes an inflammatory tumor microenvironment in gastric cancer via fibroblast reprogramming. *J Exp Clin Cancer Res*. (2023) 42:269. doi: 10.1186/s13046-023-02861-4

42. Yuan J, Xie A, Cao Q, Li X, Chen J. Inhbb is a novel prognostic biomarker associated with cancer-promoting pathways in colorectal cancer. *BioMed Res Int*. (2020) 2020:6909672. doi: 10.1155/2020/6909672

43. Li Y, Cai H, Yang J, Xie X, Pei S, Wu Y, et al. Decoding tumor heterogeneity in uveal melanoma: basement membrane genes as novel biomarkers and therapeutic targets revealed by multi-omics approaches for cancer immunotherapy. *Front Pharmacol*. (2023) 14:1264345. doi: 10.3389/fphar.2023.1264345

44. Wang W, Xu C, Ren Y, Wang S, Liao C, Fu X, et al. A novel cancer stemness-related signature for predicting prognosis in patients with colon adenocarcinoma. *Stem Cells Int*. (2021) 2021:7036059. doi: 10.1155/2021/7036059

45. Wei T, Bi G, Bian Y, Ruan S, Yuan G, Xie H, et al. The significance of secreted phosphoprotein 1 in multiple human cancers. *Front Mol Biosci*. (2020) 7:565383. doi: 10.3389/fmolb.2020.565383

46. Cao Y, Jiao N, Sun T, Ma Y, Zhang X, Chen H, et al. Cxcl11 correlates with antitumor immunity and an improved prognosis in colon cancer. *Front Cell Dev Biol*. (2021) 9:646252. doi: 10.3389/fcell.2021.646252

frontiers | Frontiers in Oncology

TYPE Original Research
PUBLISHED 24 January 2025
DOI 10.3389/fonc.2024.1536406

Check for updates

OPEN ACCESS

EDITED BY
Xiaosheng Tan,
Rutgers, United States

REVIEWED BY
Yuhao Xie,
St. John's University, United States
Jin-Ming Zhang,
University of Texas Health Science Center at Houston, United States
Chenxu Guo,
Massachusetts General Hospital Cancer Center, United States
Xutong Xue,
Boston Children's Hospital and Harvard Medical School, United States
Xiaoyu Yang,
Rice University, United States

*CORRESPONDENCE
Haiyan Wang
wanghaiyan@qhu.edu.cn

†These authors have contributed equally to this work and share first authorship

RECEIVED 28 November 2024
ACCEPTED 31 December 2024
PUBLISHED 24 January 2025
CORRECTED 02 September 2025

CITATION
Wang T, Lei Y, Sun J, Wang L, Lin Y, Wu Z, Zhang S, Cao C and Wang H (2025) Targeting NANOS1 in triple-negative breast cancer: synergistic effects of digoxin and PD-1 inhibitors in modulating the tumor immune microenvironment. *Front. Oncol.* 14:1536406. doi: 10.3389/fonc.2024.1536406

COPYRIGHT
© 2025 Wang, Lei, Sun, Wang, Lin, Wu, Zhang, Cao and Wang. This is an open-access article distributed under the terms of the Creative Commons Attribution License (CC BY). The use, distribution or reproduction in other forums is permitted, provided the original author(s) and the copyright owner(s) are credited and that the original publication in this journal is cited, in accordance with accepted academic practice. No use, distribution or reproduction is permitted which does not comply with these terms.

Targeting NANOS1 in triple-negative breast cancer: synergistic effects of digoxin and PD-1 inhibitors in modulating the tumor immune microenvironment

Tangyi Wang[1†], Yadian Lei[1†], Jingwei Sun[2], Li Wang[1], Yuxin Lin[1], Zhijing Wu[1], Shoude Zhang[3], Chengzhu Cao[1,4,5] and Haiyan Wang[1,4,5*]

[1]Department of Basic Medical Sciences, Qinghai University Medical College, Xining, Qinghai, China, [2]Department of Medical Laboratory, Qinghai Provincial People's Hospital, Xining, Qinghai, China, [3]State Key Laboratory of Plateau Ecology and Agriculture, Qinghai University, Xining, Qinghai, China, [4]Research Center for High Altitude Medicine, Qinghai University, Xining, Qinghai, China, [5]Key Laboratory of the Ministry of High Altitude Medicine, Qinghai University, Xining, Qinghai, China

Introduction: Triple-negative breast cancer (TNBC) is an aggressive subtype of breast cancer resistant to endocrine and targeted therapies. Immune checkpoint inhibitors (ICIs) have shown significant efficacy in various cancers. *Taraxacum officinale*, commonly known as dandelion, has traditionally been used to treat breast-related diseases and is recognized for its beneficial composition and low side effects. FDA-approved drugs, having undergone rigorous validation for their safety, efficacy, and quality, provide a foundation for drug repurposing research. Researchers may explore FDA-approved drugs targeting the potential target NANOS1 for TOE (*Taraxacum officinale* extract) treatment to develop innovative therapeutic strategies. In this context, Dig (Digoxin) and AA (Algestone acetophenide) have been identified as potential drug candidates for further exploration of their therapeutic effects and application potential in targeting NANOS1.

Methods: RNA sequencing (RNA-seq) was employed to identify potential targets for triple-negative breast cancer (TNBC) from TOE. Bioinformatics tools, including bc-GenExMiner v4.8, the Human Protein Atlas, and the TIMER database, were utilized for target identification. Molecular docking studies assessed FDA-approved drugs interacting with these targets, with Dig and AA selected as candidate drugs. The therapeutic efficacy of Dig and AA in combination with PD-1 inhibitors was evaluated using the 4T1 mouse model. Flow cytometry was applied to assess lymphocyte infiltration in the tumor immune microenvironment. RNA-seq analysis after target silencing by small interfering RNA (siRNA) was performed, followed by Gene Ontology (GO) and Kyoto Encyclopedia of Genes and Genomes (KEGG) pathway analysis. Validation of findings was conducted through quantitative PCR and Western blot analysis.

Results: TOE inhibited TNBC cell growth, migration, and invasion, as assessed by CCK-8 and transwell assays. RNA-seq indicated the effects may be due to *NANOS1* down-regulation. Survival analysis showed lower *NANOS1* expression correlated with better prognosis. Immunoinfiltration analysis indicated a negative correlation between *NANOS1* levels and activated NK cells. Molecular docking identified Dig and AA as high-affinity binders of *NANOS1*. Animal experiments showed Dig and PD-1 inhibitor combination enhanced immunotherapy efficacy for TNBC.

Discussion: The findings from this study suggest that TOE may offer a novel therapeutic approach for TNBC by targeting *NANOS1*, a protein whose down-regulation is associated with improved patient outcomes. The negative correlation between *NANOS1* and activated NK cells highlights the potential role of the immune system in TNBC pathogenesis and response to treatment. The identification of Dig as potential drugs targeting *NANOS1* provides a new direction for drug repurposing in TNBC. The synergistic effect of Dig and PD-1 inhibition observed in animal models is promising and warrants further investigation into the role of immunotherapy in TNBC treatment. Overall, this study identifies *NANOS1* as a new target for TNBC therapy and suggests a combination therapy approach that could enhance immunotherapy effectiveness and improve patient outcomes.

KEYWORDS

immune checkpoint blockade, triple-negative breast cancer, malignant phenotype, nanos1, PD-1 inhibitors, tumor microenvironments

1 Introduction

Breast cancer is among the most prevalent and aggressive malignancies globally. In women, breast cancer remains the leading cause of both morbidity and mortality according to the latest data, with triple-negative breast cancer (TNBC) being one of the most challenging subtypes to treat (1). TNBC is characterized by the absence of progesterone receptors (PR), estrogen receptors (ER), and human epidermal growth factor receptor 2 (HER-2), rendering it unresponsive to endocrine and targeted molecular therapies (2). As a result, chemotherapy continues to be the mainstay of treatment for TNBC, despite its associated adverse effects and long-term regimens, which significantly impair patients' quality of life (3).

These limitations highlight the urgent need for alternative therapeutic strategies for TNBC. Traditional Chinese medicine (TCM), with its multi-component, multi-target, and synergistic effects, offers promising advantages, including fewer adverse effects compared to conventional treatments. In recent years, the exploration of natural active ingredients from TCM has become a prominent research focus, with many compounds showing promise in cancer treatment (4–8). Among these, *Taraxacum officinale*, commonly known as dandelion, has attracted attention as a traditional herbal remedy with promising potential in breast cancer treatment. Studies have shown that extracts from *T. mongolicum* and *T. formosanum* induce apoptosis in breast cancer cells, reduce cell proliferation, disrupt mitochondrial membrane potential, and affect cell migration *in vitro* (9). *In vivo*, *T. mongolicum* administration in breast cancer-bearing mice has been shown to reduce tumor volume and weight, further supporting its potential as an effective therapeutic agent in breast cancer treatment (10).

Despite these promising findings, the molecular mechanisms underlying TOE's therapeutic effects remain poorly understood. Previous studies have highlighted the interaction between NANOS1 and PUMILIO2 proteins in human germ cells, suggesting that their interplay plays a significant role in controlling mRNA stability and translation during germ cell development (11). Recent studies have suggested that NANOS1 expression, a key factor in epithelial-mesenchymal transition (EMT), plays a pivotal role in the invasiveness, migratory potential, and stem cell-like properties of breast cancer cells (12). Thus, NANOS1 is not only a potential

Abbreviations: ANOVA, analysis of variance; DEGs, differentially expressed genes; IC50, 50% inhibitory concentration; ICIs, immune checkpoint inhibitors; PMSF, phenylmethylsulfonyl fluoride; PVDF, polyvinylidene fluoride; TNBC, triple-negative breast cancer; TAM, tumor-associated macrophage; TOE, *Taraxacum officinale* extract; GO, Gene Ontology; KEGG, Kyoto Encyclopedia of Genes and Genomes.

regulatory factor in the onset and progression of breast cancer but also represents a novel therapeutic target.

Considering the limitations of current therapies for TNBC and the emerging therapeutic potential of targeting NANOS1, this study investigates the repurposing of FDA-approved drugs, specifically Dig and AA, for synergistic use with PD-1 inhibitors. Digoxin, a cardiac glycoside, is widely used for managing heart failure and arrhythmias due to its inhibition of Na+/K+-ATPase, which increases intracellular calcium levels (13). Beyond its cardiovascular applications, digoxin has demonstrated anticancer properties by inducing apoptosis, reducing tumor cell proliferation, and modulating the tumor microenvironment (14–16). These effects are linked to the role of Na+/K+-ATPase in cancer cell signaling and survival (17). Algestone acetophenide, a synthetic progestin commonly used for hormone regulation and anti-inflammatory therapy, exhibits molecular activity by binding to progesterone receptors and modulating downstream pathways, which may suppress inflammatory responses and inhibit cancer cell migration and proliferation (18, 19). The distinct mechanisms of these drugs make them promising candidates for repurposing in TNBC, particularly in targeting NANOS1 and enhancing the efficacy of immune checkpoint inhibitors. This study employed MDA-MB-231 human breast cancer cells and 4T1 murine breast cancer cells as *in vitro* models to investigate the effects of *Taraxacum officinale* extract (TOE) on triple-negative breast cancer (TNBC), focusing on its potential to suppress tumor growth and invasiveness. The findings identified NANOS1 as a potential prognostic marker for breast cancer. Furthermore, the potential of digoxin and algestone acetophenide to modulate NANOS1-mediated pathways was investigated, providing a novel approach for targeting TNBC pathways regulated by NANOS1. By combining these FDA-approved drugs with PD-1 inhibitors, this study seeks to advance understanding of combination therapies for TNBC, thereby addressing the critical need for more effective treatment options.

2 Materials and methods

2.1 Preparation of TOE

Taraxacum officinale (Product Standard No. GHT1091), was purchased from Liaoning Senkangyuan Ecological Agriculture Co. The plant material was refluxed with 75% ethanol for 3 hours at 60°C, followed by filtration and concentration. This process was repeated three times, and the combined extract was purified using a D-101 macroporous resin column, where sugars were removed by water elution. The ethanol leaching fraction was collected, evaporated, and spray-dried to obtain *Taraxacum officinale* extract (TOE).

2.2 Chemicals

PD-1inhibitor (PD-1) and Digoxin (Dig) were purchased from Selleckchem. Algestone acetophenide (AA) was purchased from TOPSCIENCE. All chemicals were dissolved in DMSO for the *in vivo* and *in vitro* studies.

2.3 Animal model construction

Dissolve 10 g of tribromoethanol (Sigma) in 10 mL of tert-amyl alcohol (Sigma) at room temperature to prepare a crystal-free stock solution. Filter the stock solution using a 0.22 μm filter (Millex-GP SLGPR33RB, Millipore), then dilute it with physiological saline (National Drug Approval No. H11021190; 0.9 g/100 mL) to prepare a 19.2 mg/mL (2.5% avertin) working solution. Incubate the working solution at 37°C for 4 hours, mix thoroughly by shaking, and store at 4°C protected from light. To establish a mammary fat pad tumor model in mice, intraperitoneally inject 2.5% avertin at a dose of 160 μL/10 g body weight (307 mg/kg) for anesthesia. Once fully anesthetized, the mice were placed in a supine position on a sterile workbench, and their skin was disinfected with povidone-iodine. Make a small incision (~0.5 cm) above the fourth right mammary gland using ophthalmic scissors. Carefully lift the skin with a cotton swab to expose the mammary fat pad, then inject 40 μL of serum-free suspension containing 5 × 10^5 4T1 cells into the fat pad. Mice in the monotherapy groups received intraperitoneal injections of Dig (5 mg/kg) daily or AA (10 mg/kg) every two days, and the combination group also received a 5 mg/kg PD-1 inhibitor every two days for 14 days. Tumor volume was measured using calipers, and the formula used was: volume (mm^3) = [width^2 (mm^2) × length (mm)]/2. On the 15th day of treatment, the mice were euthanized with 2.5% avertin anesthesia. Freshly isolated tumors were rapidly dissociated to obtain viable single cells. Tumor-infiltrating cells were analyzed by fluorescence-activated cell sorting (FACS) to assess antitumor immune responses.

2.4 Cell culture

The 4T1 and MDA-MB-231 cell lines were obtained from the Procell Life Science & Technology Co., Ltd. MDA-MB-231 cells were cultured in DMEM supplemented with 10% fetal bovine serum and 1% penicillin/streptomycin (Procell). 4T1 cells were cultured in RPMI-1640 supplemented with 10% fetal bovine serum and 1% penicillin/streptomycin (Procell). Cells were cultured at 37° C with a 5% CO2 atmosphere.

2.5 CCK8 assays

MDA-MB-231 or 4T1 cells were seeded in a 96-well plate at 2.0×10^5 cells/mL and cultured in medium at 37°C with a 5% CO2 atmosphere for 24 h. After that, the cells were pretreated with various concentrations of TOE for 24 h. At the end of the stimulation, the medium was removed, and 20 μL of CCK-8 reagent (Elabscience, China) was added to each well, and the incubation was continued for 1 h. The absorbance of each well was measured at 450 nm.

2.6 Transwell assay

The migration and invasion abilities of cells were assessed using Transwell chambers (Corning). For invasion assays, 30 μg of Matrigel matrix (Corning) was added to the upper chamber and incubated at 37°C for 1 hour. For migration assays, no Matrigel was added. A total of 200 μL of cells (2.5×10^5/mL, treated with TOE, Dig, or AA at IC50 concentration in serum-free medium) was added to the upper chamber, and 750 μL of serum-containing medium was added to the lower chamber. The cells were incubated for 20 hours at 37°C in a 5% CO2 atmosphere. After incubation, the medium was removed, and the chambers were washed twice with PBS. The cells were fixed with 3.7% formaldehyde in PBS for 15 minutes, washed twice with PBS, stained with Giemsa dye for 10 minutes, and the remaining cells on the upper surface of the membrane were gently wiped away using a cotton swab. The number of migrated cells was then counted.

2.7 Transcriptome sequencing

MDA-MB-231 cells were seeded in 10 cm dishes and grown to 90% confluency. 9 mL of complete media or TOE (at a concentration of IC50) were added to the control and treatment groups, respectively. After incubated at 37°C with a 5% CO2 atmosphere for 24 h, the medium was removed and washed twice with PBS. Cells were collected in Trizol (Invitrogen). RNA quality control, library construction, and sequencing were performed by Biomarker Technologies.

MDA-MB-231 cells were seeded into 10 cm culture dishes and incubated until they reached 90% confluence. The knockdown efficiency of siNANOS1#1 was validated by qPCR. The control and treatment groups were transfected with either siNC or siNANOS1#1, respectively, using Lipofectamine 3000 (Thermo Fisher). The cells were incubated at 37°C in a 5% CO2 atmosphere for 48 hours, after which the medium was removed, and the cells were washed twice with PBS. Cells were harvested in TRIzol (Invitrogen). RNA quality control, library construction, and sequencing were performed by GeneWiz Inc.

2.8 *NANOS1* expression in breast cancer

Gene expression data were analyzed using the bc-GenExMiner v4.8 platform (http://bcgenex.ico.unicancer.fr/) (20), which integrates publicly available breast cancer transcriptomic data, including 11,359 DNA microarray samples and 4,421 RNA-seq samples. These datasets include healthy breast tissue, adjacent normal tissue, tumor tissue, and various subtypes of breast cancer. The expression of the NANOS1 gene was compared across these tissue types, including healthy tissue, tumor tissue, and triple-negative breast cancer (TNBC) subtypes. Statistical analysis was performed using t-tests or ANOVA to assess the significance of gene expression differences, with a p-value of less than 0.05 considered statistically significant. Gene expression variations were visualized using box plots to provide a clearer representation of differences between groups. Additionally, the platform enables correlation analysis between gene expression data and clinical characteristics, further exploring potential associations between gene expression and clinical outcomes in breast cancer.

2.9 Survival analysis

The Human Protein Atlas (THPA, https://www.proteinatlas.org/) (21) provided protein expression from the Tissue Atlas and Pathology Atlas. This platform combines gene expression, protein data, and clinical outcomes to investigate the relationship between NANOS1 expression levels and prognosis in breast cancer patients. The relationship between the *NANOS1* gene and the prognosis of breast cancer patients was analyzed using the Kaplan-Meier Plotter online analysis tool (https://kmplot.com/analysis/) (22) which sources its databases from GEO, EGA, and TCGA. Kaplan-Meier survival analysis was performed to classify patients into high-expression and low-expression groups based on NANOS1 protein levels. Survival curves were generated and compared to evaluate the association between NANOS1 expression and patient survival. The log-rank test was used to assess statistical significance, with a p-value of less than 0.05 considered statistically significant. Through this analysis, The Human Protein Atlas provides valuable insights into the potential of NANOS1 as a prognostic biomarker in breast cancer.

2.10 Assessment of immune cell infiltration in TNBC

TIMER2.0 (http://timer.cistrome.org/) was used to assess immune cell infiltration in various cancer types based on deconvolution algorithms (23). The platform allows for the evaluation of the infiltration levels of different immune cells in the tumor microenvironment and correlates these with gene expression and clinical data. In this study, we analyzed the correlation between the expression of the NANOS1 gene and immune cell infiltration in tumor samples from The Cancer Genome Atlas (TCGA). Additionally, TIMER2.0 was used to explore the relationship between immune infiltration and clinical outcomes, such as patient survival and tumor stage. The tool supports analysis across multiple cancer types, providing insights into immune response patterns and the potential role of NANOS1 in immune evasion and immunotherapy.

2.11 High-throughput virtual molecular docking screening

The structure of NANOS1 protein was obtained from the PDB database with PDB number 4CQO (24). Hydrogen atoms were added using UCSF Chimera software and protonated states were

assigned using the H++3.0 program (25). SiteMap (26) was then used to predict the optimal small molecule binding site.

AutoDock Vina1.2.0 software (27) was used for high-throughput virtual screening, and the active site predicted by SiteMap was set as a docking center with docking center coordinates X,Y and Z of 14.25, -5.6, and 50.11, respectively, and the box size was set as a square with a side length of 22.5 Å. The conformation is sampled and scored using a genetic algorithm, and the best conformation is selected by ranking the conformations according to the docking score.

2.12 Virtual screening

3177 molecules from the ZINC database were used as screening targets in this study, and they are all drug molecules approved for various applications. Some potential drug molecules that may bind to the NANOS1 protein were obtained after virtual screening by AutoDock Vina1.2.0 software using the above binding pocket as the docking site.

2.13 H&E staining

Hematoxylin and eosin (H&E) staining was performed to evaluate tissue morphology. Briefly, tumor tissues were collected and fixed in 4% paraformaldehyde overnight at 4°C. The samples were then dehydrated through a graded series of ethanol (70%, 85%, 95%, and 100%) and embedded in paraffin. Thin tissue sections (5 μm) were cut and mounted onto glass slides. The sections were deparaffinized and rehydrated before staining with hematoxylin for 5 minutes and eosin for 3 minutes. After washing and dehydration, the slides were mounted with neutral balsam and observed under a light microscope.

2.14 Tumor dissociation

The tumor dissociation procedure was performed to obtain a single-cell suspension for subsequent flow cytometry analysis. Mouse tumor tissues were first excised and placed into a culture dish containing PBS (Procell). The tissues were minced using scissors and transferred into a new culture dish containing enzymatic digestion solution [Collagenase IV 2 mg/mL, DNase I 0.1 mg/mL, RPMI-1640 medium (Procell)] and incubated at 37°C for 1 hour, with gentle shaking every 15 minutes to facilitate complete digestion. Collagenase IV (Thermo Fisher Scientific) assisted in the breakdown of the extracellular matrix, while DNase I (Thermo Fisher Scientific) aided in the removal of nuclear debris. After digestion, the tissue was filtered through a 70 μm cell strainer to eliminate undigested tissue chunks and impurities. The filtered cell suspension was centrifuged (300×g for 5 minutes) to collect the cell pellet. The pellet was resuspended in red blood cell lysis solution (Biyuntian Biotechnology) and incubated at room temperature for 5 minutes with gentle shaking to ensure uniform lysis. The suspension was washed twice with PBS (Procell) to remove any residual lysis solution and cell debris. Finally, the cell pellet was resuspended in PBS, resulting in a single-cell suspension suitable for flow cytometry analysis.

2.15 RNA interference

Small interfering RNA (siRNA) oligonucleotides targeting *NANOS1* were provided by Xianghong Biotech Co., Ltd. (Beijing, China) (Supplementary Table S1). Each siRNA was transfected using Lipofectamine 3000 (Invitrogen). The specific sequences of the target gene are provided in the supplementary information.

2.16 Quantitative real-time PCR analysis

Total RNA was extracted using Trizol reagent (Invitrogen) and reverse transcribed using the PrimeScript™ RT reagent kit (Takara). Quantitative real-time PCR (qRT-PCR) was performed in triplicate using TB Green Premix Ex Taq (Takara). The primer sequences used for qRT-PCR of the target genes are listed in Supplementary Table S1.

2.17 Flow cytometry

Flow cytometry was used to analyze the immune cell populations within the tumor microenvironment. The single-cell suspension was aliquoted into two tubes for different fluorescent antibody labeling. One tube was labeled with F4/80, CD11b, CD45.2 antibodies, while the other tube was labeled with CD3e, CD4, CD8a, CD279 (PD-1), CD223 (LAG-3), and CD366 (TIM3) antibodies, all obtained from Thermo Fisher Scientific. The cells were incubated on ice for 30 minutes, allowing surface antigens on the cell membranes to bind to the respective fluorescently labeled antibodies. Following incubation, the cells were washed twice with PBS (Procell) to remove unbound antibodies. The cells were then fixed with 4% paraformaldehyde for 15 minutes, followed by two PBS washes. After all staining and fixation steps, the cells were washed again and resuspended in PBS for flow cytometry analysis. Antibodies were purchased from Thermo Fisher Scientific, and their specific details are provided in Supplementary Table S2.

Flow cytometry data were acquired using a BD FACSCalibur flow cytometer. Initial gating was performed using forward scatter (FSC) and side scatter (SSC) plots. Immune phenotype analysis was conducted using multiple fluorescence channels. The flow cytometry data were analyzed with FlowJo software, and FSC and SSC gating were used to select the appropriate cell populations. Immune phenotype analysis was based on distinct fluorescence markers. The gating strategy is outlined in Supplementary Figure S1.

2.18 Western blot assay

Cells were treated with Dig and AA for 48 hours, then lysed on ice using RIPA buffer (Solarbio) containing 1% PMSF. Protein

concentration was determined using the Pierce BCA Protein Assay Kit (Thermo Fisher Scientific). Equal amounts of protein (20 μg) were separated by 10% SDS-PAGE (Vazyme), transferred to a PVDF membrane (Millipore), and blocked with 5% nonfat milk at room temperature. The membrane was incubated overnight with primary antibody at 4°C, washed with TBST, and incubated with secondary antibody at room temperature. Protein signals were detected using a high-sensitivity ECL chemiluminescent detection kit (Proteintech) on the BG-gdsAUTO730. Anti-NOS-1 was purchased from abcam (working concentration: 2 μg/mL), Beta Actin Polyclonal antibody from ProteinTech Group, Inc. (1:2000 dilution), and Multi-rAb HRP-Goat Anti-Rabbit Recombinant Secondary Antibody (H+L) from ProteinTech Group, Inc. (1:5000 dilution).

2.19 Statistical analysis

Data were collected from independent experiments and expressed as the mean ± SEM. All graphs and analyses were generated using GraphPad Prism software. The significance among multiple (three or more) groups was compared using one-way ANOVA analysis, and differences between the different groups were analyzed by a Student's *t*-test.

3 Results

3.1 Inhibition of growth, migration and invasion of TNBC by TOE

As shown in Figure 1A, TOE significantly inhibited the growth of MDA-MB-231 and 4T1 cells, with the inhibitory effect increasing in a concentration-dependent manner. Additionally, TOE reduced the migration and invasion abilities of these cells (Figure 1B). MDA-MB-231 cells were treated with an IC50 dose of TOE (635.4 μg/ml), and RNA sequencing (RNA-seq) was performed to assess their transcriptomes. A total of 8451 differentially expressed genes (DEGs) were identified following 24 hours of treatment with TOE, with 2,020 genes upregulated and 2,048 genes downregulated (Figure 1C). The top 600 upregulated and downregulated genes were selected for KEGG pathway enrichment analysis based on the |log2(FC)| values, and the top 20 pathways with the lowest p-values are shown in Figure 1D. The five most significantly enriched pathways included pathways in cancer, the MAPK signaling pathway, transcriptional misregulation in cancer, microRNA in cancer, and the cell cycle.

3.2 Correlation of NANOS1 protein with prognosis and immune cell infiltration in TNBC

Kaplan-Meier survival analysis was performed to assess the prognostic significance of the top 600 upregulated and downregulated differentially expressed genes (DEGs). Genes positively correlated with survival were identified, focusing on the low expression of downregulated genes and the high expression of upregulated genes. A total of 132, 269, and 179 genes were found to be positively associated with overall survival (OS), relapse-free survival (RFS), and distant metastasis-free survival (DMFS), respectively. Subsequently, 640 prognostic genes were selected based on TCGA data and antibody-based protein data. Of these, 209 genes were associated with an unfavorable prognosis, while 431 genes were linked to a favorable prognosis for breast cancer at the protein level. Ultimately, 8 genes were identified as being associated with prognosis at both the transcript and protein levels (Figure 2A, Table 1). Among these, NANOS1, a less studied and the only downregulated gene, was chosen for further analysis. The prognostic value of NANOS1 protein expression in breast cancer was evaluated using the online tool available at www.proteinatlas.org, and the results demonstrated that lower expression of NANOS1 was associated with better prognosis ($p < 0.001$) (Figure 2B). At the mRNA level, reduced NANOS1 expression was also positively correlated with OS ($p < 0.001$), RFS ($p < 0.001$), and DMFS ($p < 0.001$) in breast cancer patients (Figures 2C–E).

The correlation between NANOS1 expression and immune cell infiltration levels in BRCA-BASAL was assessed, given the association of immune infiltration with cancer development and treatment outcomes. Based on deconvolutional procedure, *NANOS1* expression was positively associated with Macrophage (*P*=8.20e-04), CD4+ T cell (non-regulatory) (*P*=2.30e-04) and Endothelial cell (*P*=3.09e-02), meanwhile, *NANOS1* expression was negatively associated with B cell (*P*=7.14e-03),Myeloid dendritic cell (*P*=3.72e-02), activated NK cell (*P*=5.44e-03), and T cell follicular helper (*P*=2.35e-03) (Figure 2F). Among these immune cells, NK cell infiltration was associated with a reduced risk of TNBC, and survival analysis revealed that high NK cell infiltration correlated with better prognosis in patients with low NANOS1 expression (*P*=0.0216) (Figure 2G). Furthermore, the level of NK cell infiltration in the somatic copy number amplifications (sCNA-Amplifications) state of *NANOS1* was demonstrated by violin plots. As shown in Figure 2H, a significant difference in NK cell infiltration was observed between high amplification samples and normal samples (*p*=0.032).

3.3 FDA-approved drugs virtual screening to NANOS1 proteins

Typically, targetable proteins need to have a typical binding pocket, so the first step in this study was to use the SimteMap tool to analyze the targetable binding pocket on the surface of the NANOS1 protein. By calculation, SiteMap found a large potential ligand binding pocket consisting of the following amino acids: ALA2076, PRO2077, ARG2080, CYS2118, ASP2119, VAL2120, ILE2121, PRO2122, PRO2123, ASN2124, ARG2129, GLY2207, ASN2208, ARG2209, TYR2210, ASN2211, LEU2212, GLN2213, ASN2216, GLU2261, LEU2265, ASN2268, ALA2269, ASN2272,

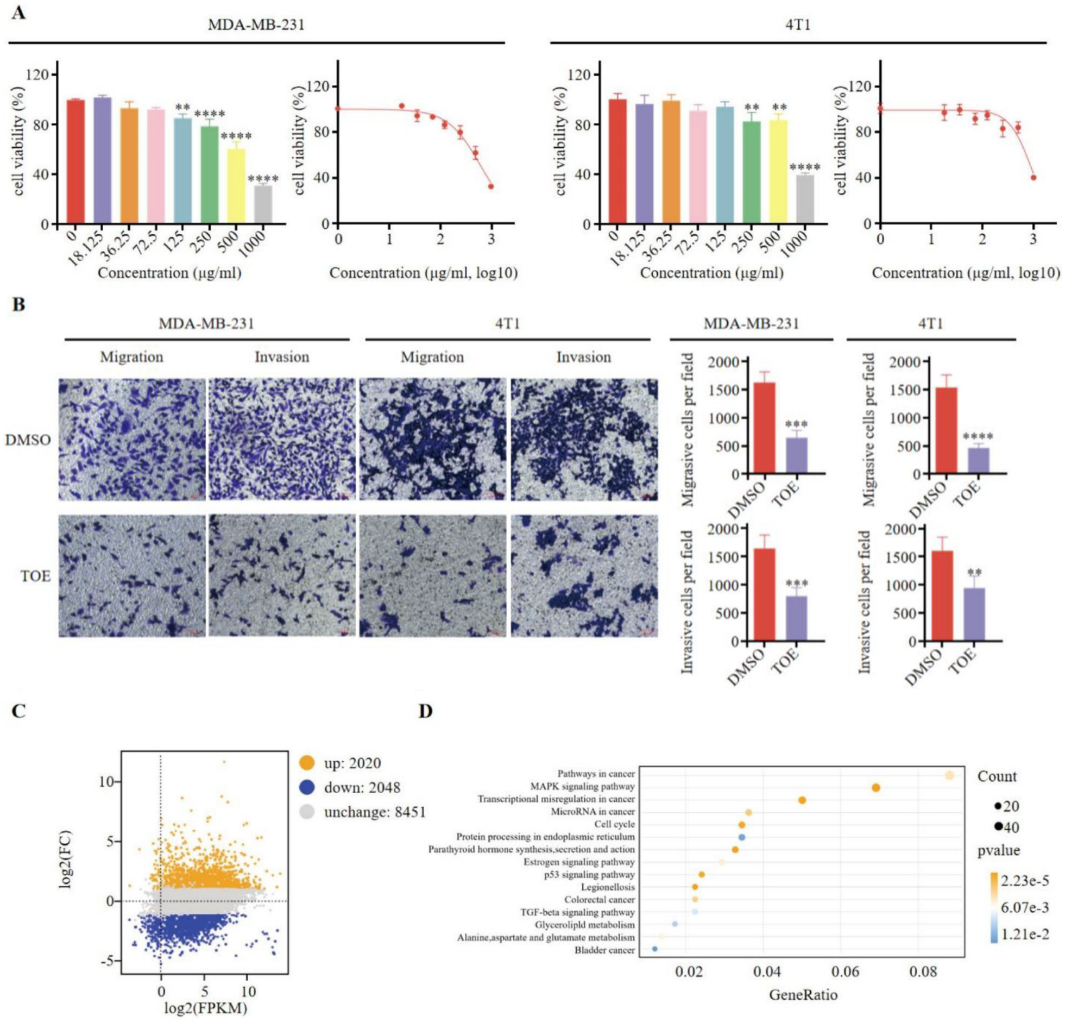

FIGURE 1
TOE suppresses malignant phenotype of triple negative breast cancer cells. **(A)** The effect of TOE on cell proliferation in MDA-MB-231 and 4T1 cells. Cells were treated with varying concentrations of TOE for 24 hours, and cell proliferation was assessed using the CCK-8 assay. Data are expressed as the mean ± SEM (n = 3). Statistical significances were calculated via Student's t-test. **p < 0.01 and ***p < 0.001 and ****p < 0.0001. **(B)** Transwell migration and invasion assay of MDA-MB-231 and 4T1 cells after treatment with TOE for 24 hours. Representative images of the migrated and invaded cells from randomly selected fields of Transwell inserts are shown on the left, while quantitative data for cell numbers are presented on the right. Cell numbers were calculated and expressed as the mean ± SEM of three independent experiments. Statistical significance was determined by t-test, with $^{**}p < 0.01$ and $^{***}p < 0.001$ and $^{****}p < 0.0001$ indicating significant differences between TOE-treated and DMSO-treated cells. Scale bar = 100 μm. **(C)** MA plot of DGEs in MDA-MB-231 treated with TOE. **(D)** Enrichment and scatter map of KEGG pathway of DGEs.

ARG2311. This indicates the presence of a targetable binding pocket for NANOS1 (Figures 3A, B). To explore potential interactions between approved drugs and the NANOS1 protein, we specifically selected drugs from the ZINC database for virtual docking simulations. The ZINC database was chosen due to its extensive collection of commercially available, drug-like molecules, as well as its provision of detailed compound information, including structural data and molecular properties, which are essential for accurate molecular docking. This approach allowed us to identify candidate drugs that may bind effectively to NANOS1. Next, the binding affinity of FDA-approved drugs was predicted using AutoDock Vina. A total of 3177 drug molecules were ranked based on their docking scores, from highest to lowest. The results indicated that Dig and AA both achieved the highest scores, with a docking score of -9.9 kcal/mol for each drug (a larger absolute value indicates stronger binding affinity) (Table 2). The binding modes were then visualized. Figures 3C, D show the interaction between Dig and the NANOS1 protein, where Dig forms five hydrogen bonds with the protein. This interaction involves hydroxyl groups as hydrogen bond donors and acceptors, and a hydrogen bond is formed between the carbonyl group of the terminal cyclic ether and Arg2209. No π-stacking or salt bridge interactions were observed. Additionally, Dig exhibits significant hydrophobic interactions with the protein due to its hydrophobic backbone. Figures 3E, F illustrate the interaction between AA and the NANOS1 protein. AA forms two hydrogen bonds, one H-π stacking interaction, and hydrophobic interactions with the protein. The hydrogen bonds occur between the side chain of Arg2080 and the oxygen atom on

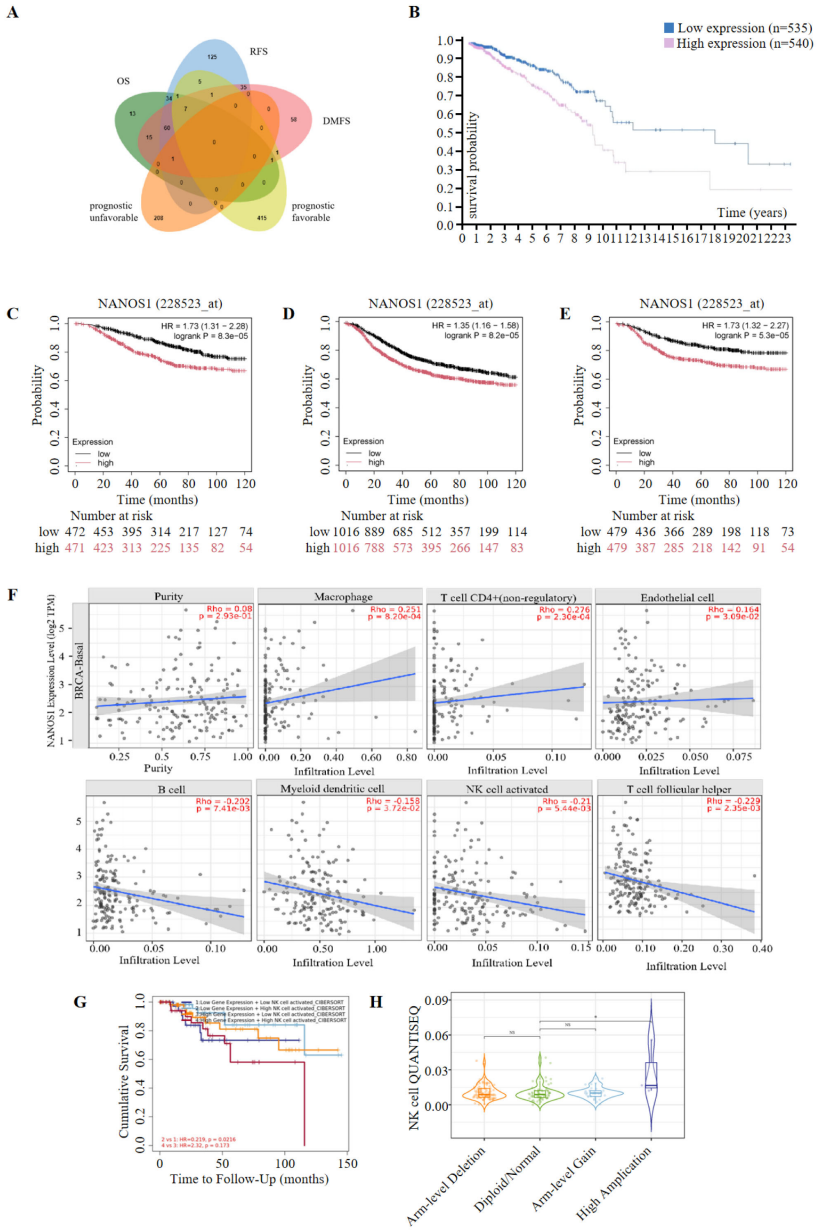

FIGURE 2
Prognostic significance of *NANOS1* and its association with immune infiltration in breast cancer. **(A)** Venn diagram of prognostic genes. Genes were selected based on RNA-Seq data (top 600 upregulated and 600 downregulated genes). Prognostic evaluation was conducted using the Kaplan-Meier Plotter tool (https://kmplot.com/analysis/), which integrates data from GEO, EGA, and TCGA. Statistical significance was determined using the log-rank test ($p < 0.05$). Genes were further validated using protein expression data from the Human Protein Atlas (HPA, https://www.proteinatlas.org/). The Venn diagram was created using the EVenn online tool (http://www.ehbio.com/test/venn/#/). **(B)** Survival curves in breast cancer at the protein level (n=1075) (www.proteinatlas.org). Data were obtained from the Human Protein Atlas (www.proteinatlas.org), and Kaplan-Meier survival curves were constructed based on protein expression levels of NANOS1. The statistical significance of survival curves was calculated using the log-rank test. **(C–E)** Survival curves of overall survival (OS), relapse-free survival (RFS), and distant metastasis-free survival (DMFS) in breast cancer at the mRNA level. Data were obtained from the Kaplan-Meier Plotter database (n = 943 for OS, n = 2032 for RFS, n = 958 for DMFS) (www.kmplot.com). Kaplan-Meier survival analysis was performed to evaluate the prognostic significance of NANOS1 expression at the mRNA level, with log-rank p-values shown for each curve. **(F)** Correlation between *NANOS1* expression and the level of immune infiltration. **(G)** The correlation between clinical outcomes and NK cell infiltration with NANOS1 expression in the BRCA-BASAL. The clinical relevance of tumor immune subtypes was explored using TIMER2.0 (http://timer.cistrome.org/), which shows NK cell immune infiltration levels and Kaplan-Meier survival curves based on NANOS1 expression. NK cell infiltration levels were categorized as low or high. The hazard ratios and p-values from the Cox proportional hazards model, along with the log-rank p-value from the Kaplan-Meier analysis, are displayed on the survival curves. Data source: TIMER2.0 database, using gene expression profiles and clinical data. **(H)** Violin plot showing NK cell infiltration levels in relation to sCNA amplifications of NANOS1 in BRCA-Basal. The immune infiltration distribution was analyzed using TIMER2.0 (http://timer.cistrome.org/) based on the sCNA (somatic copy number alteration) status of the gene NANOS1. The sCNA data were obtained from gene-level copy number segmentation, including "arm-level deletion," "diploid/normal," "arm-level gain," and "high amplification" categories defined by GISTIC2.0. NK cell infiltration levels were assessed using the QUANTISEQ method. Significant differences in NK cell infiltration were observed between the "high amplification" and "normal" samples ($p = 0.032$).

TABLE 1 DGEs associated with prognosis in breast cancer.

ID	Symbol	log2FC	FDR	Regulated	Prognostics
ENSG00000188613	NANOS1	-2.099116259	5.3654288157e-26	down	unfavorable
ENSG00000159388	BTG2	3.827077677	1.4953679154e-91	up	favorable
ENSG00000121104	FAM117A	2.05076956	3.0029034189e-31	up	favorable
ENSG00000152804	HHEX	3.401245139	1.0481947934e-253	up	favorable
ENSG00000164128	NPY1R	3.055241553	1.1667617660e-09	up	favorable
ENSG00000181788	SIAH2	2.694286398	8.4419828317e-207	up	favorable
ENSG00000163659	TIPARP	2.650981515	0	up	favorable
ENSG00000160908	ZNF394	2.047360395	2.2696551915e-113	up	favorable

the furan ring, as well as between the oxygen atom on the carbonyl group and the amide backbone of Asn2124. The π-stacking interaction occurs between the charge center of Asn2208 and the phenyl ring at the terminal end of AA. Additionally, AA interacts with several hydrophobic amino acids such as Pro2122, Pro2123, Leu2265, and Leu2212.

3.4 Dig and AA inhibit tumor growth in TNBC mouse models and suppress malignant cellular phenotypes

Dig and AA were selected for *in vitro* validation. CCK-8 assays showed that both drugs significantly reduced cell viability, inhibited proliferation, and slowed growth (Figure 4A). The 24-hour IC50 values for Dig were 0.6806 μM and 1.162 μM for MDA-MB-231 and 4T1 cells, respectively, and for AA, 23.25 μM and 21.63 μM. Transwell assays demonstrated that Dig and AA significantly reduced the migration and invasion of MDA-MB-231 and 4T1 cells (Figures 4B, C). To assess the potential of Dig and AA in inhibiting TNBC tumor growth *in vivo*, a 4T1 mouse tumor model was established. Mice were randomly divided into six groups, receiving different treatments: PD-1 inhibitor monotherapy (5 mg/kg), Dig (5 mg/kg), AA (10 mg/kg), Dig + PD-1 inhibitor combination, AA + PD-1 inhibitor combination, and a saline control. Both Dig and AA significantly inhibited tumor growth compared to the control group (Figure 4D). Moreover, the combination of Dig and PD-1 inhibitor showed superior tumor suppression compared to PD-1 inhibitor alone, highlighting the potential of this combination as a therapeutic strategy for TNBC (Figure 4E). No significant weight changes were observed in the combination treatment groups (Figure 4F).

3.5 Combination therapy of Dig with PD-1 inhibitor enhances antitumor immune response

Freshly excised tumor tissues were harvested; one portion was used for flow cytometry analysis to assess immune cell populations, while the remaining portion was processed for H&E staining to examine tissue morphology and immune cell infiltration (Figure 5A). To evaluate the potential of combination therapy in promoting tumor lymphocyte infiltration and modulating the immunosuppressive environment within 4T1 tumors, several parameters were assessed. The combination of Dig and PD-1 significantly increased the frequency of tumor-associated macrophages compared to the control group (Figures 5B, G). Evaluation of effector T cells revealed that the combination therapy of Dig and PD-1 resulted in a significant increase in the frequency of effector CD8+ T cells compared to the saline group, and this effect was superior to the PD-1 monotherapy group. AA enhances the proportion of CD8+ T cells. However, although the AA + PD-1 inhibitor combination showed a more pronounced increase in CD8+ T cells, the lack of statistical significance (adjusted p value = 0.2576) indicates that the effect of the AA and PD-1 inhibitor combination is less effective than that of the Dig and PD-1 inhibitor combination (Figures 5C, H). These findings indicate that the combination therapy involving Dig effectively enhances the immune response to immune checkpoint blockade (ICB) therapy.

This study also investigated the effects of Dig and AA, either as monotherapies or in combination with PD-1 inhibitors, on exhausted T cells. The results showed that Dig, either alone or in combination with PD-1 inhibitors, effectively reduced the frequency of LAG-3-expressing exhausted T cells (Figures 5D, I). The combination of Dig and PD-1 exhibited synergistic effects in reducing TIM-3 expression levels (Figures 5E, J). Dig monotherapy also effectively reduced the frequency of PD-1-positive exhausted T cells (Figures 5F, K). The analysis of exhausted T cells revealed a concerning trend in the AA + PD-1 inhibitor group, where the proportions of LAG-3+, TIM-3+, and PD-1+ exhausted T cells were higher than those in the AA alone group. The adjusted p-values of 0.5676, 0.8546, and 0.9632 indicate an increase in T cell exhaustion with the AA + PD-1 combination, which may account for the diminished efficacy observed with this combination. This suggests that while AA alone exhibits significant antitumor activity, its combination with PD-1 inhibitors may induce a state of T cell exhaustion, potentially limiting the overall therapeutic benefit. These findings provide strong experimental evidence for the development of novel tumor immunotherapy strategies. The "drug repurposing" approach has emerged as a

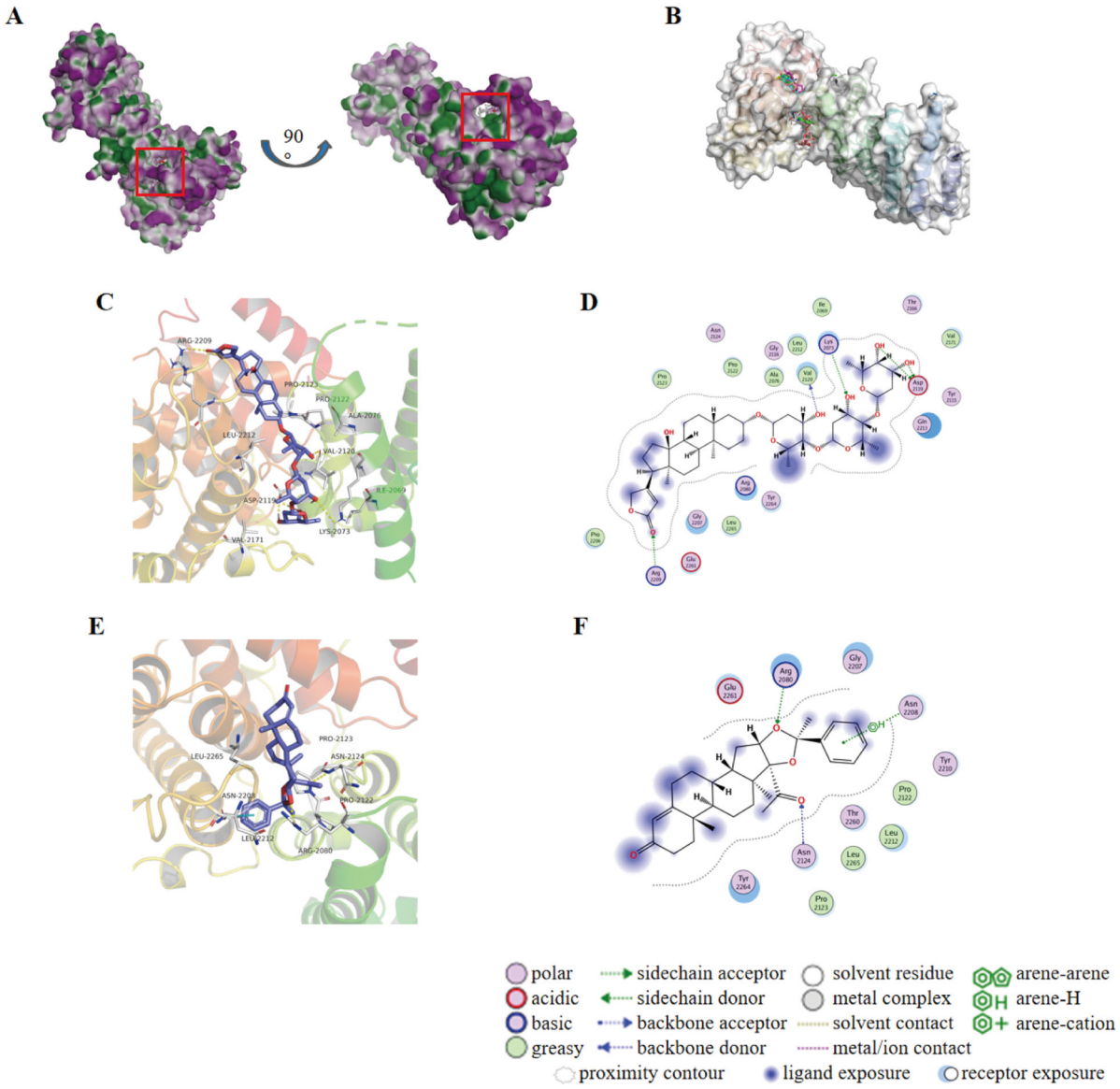

FIGURE 3
Molecular docking results of Dig and AA against NANOS1 protein. **(A)** Target binding pockets on the NANOS1 protein. The SimteMap tool analyzes the surface of the NANOS1 protein, highlighting potential binding pockets that could serve as targets for therapeutic intervention. **(B)** An overview of the binding modes of the six top-ranked compounds with distinct scaffolds. The figure presents the interaction patterns of each compound with the NANOS1 protein. The binding modes are visually represented in 3D molecular models, illustrating the orientation and interactions with the protein's active site. **(C)** 3D diagram of the interaction between Dig and the NANOS1 protein. Dig forms five hydrogen bonds, primarily involving hydroxyl groups as hydrogen bond donors and acceptors, with one hydrogen bond formed between the carbonyl group of the terminal cyclic ether and Arg2209. There are no π-stacking or salt bridge interactions. Hydrophobic interactions are also observed due to the hydrophobic backbone of Dig. The interacting amino acids are shown as stick models in gray, with O atoms in red, N atoms in blue, and C atoms in gray. Yellow and cyan dotted lines indicate intermolecular hydrogen bonds and π-stacking interactions. **(D)** 2D diagrams of the docked structure of Dig in the active domain of NANOS1. **(E)** 3D diagram of the interaction between AA and the NANOS1 protein. AA forms two hydrogen bonds, one H-π stacking interaction, and several hydrophobic interactions with the protein. The hydrogen bonds are formed between Arg2080 and the oxygen on the furan ring, and between the oxygen on the carbonyl group and Asn2124. **(F)** 2D diagrams of the docked structure of AA in the active domain of NANOS1.

new paradigm in antitumor drug discovery, offering the advantage of bypassing established toxicological and pharmacokinetic evaluations. Furthermore, this study demonstrates that modulating the tumor microenvironment, as evidenced by increased immune cell infiltration in the tumor, can enhance the efficacy of existing immunotherapies, significantly reducing development time and research costs.

3.6 Dig and AA inhibit tumor progression by regulating *NANOS1* to suppress TNF-α expression

To investigate the role of NANOS1, we silenced its expression using siNANOS1#1 in MDA-MB-231. The silencing of NANOS1 was confirmed by quantitative PCR analysis. Differential gene

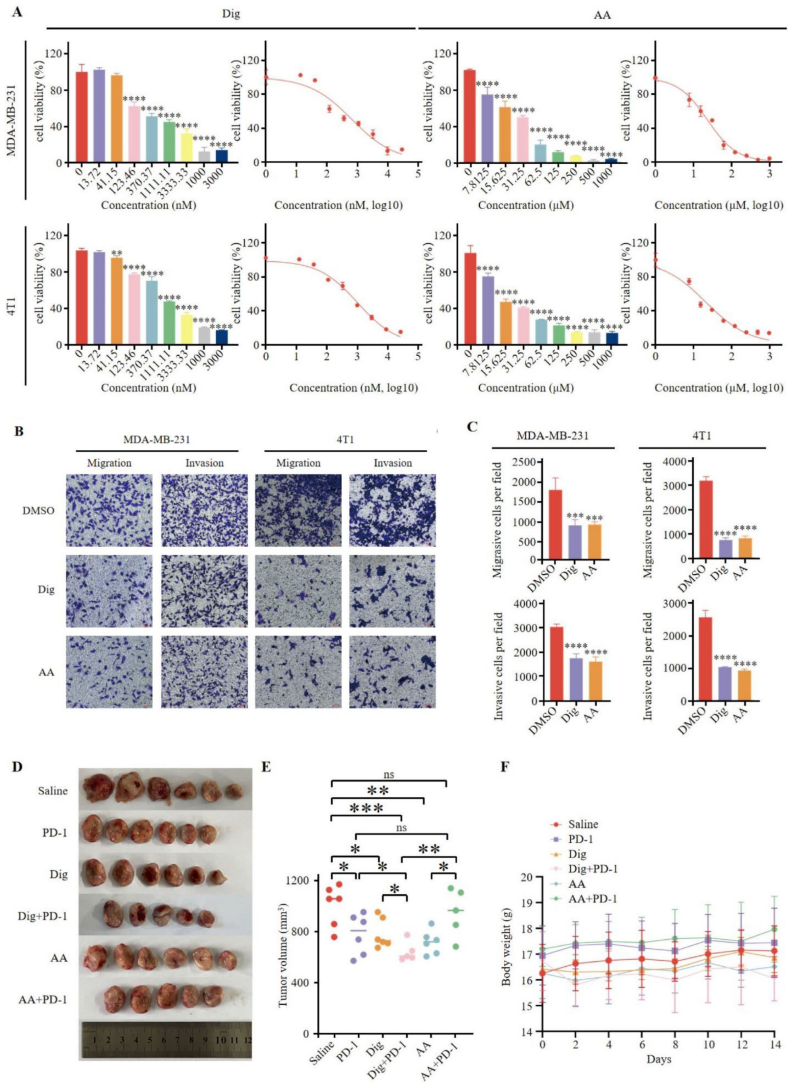

FIGURE 4
Dig and AA inhibited tumor growth in breast cancer mouse models. **(A)** Inhibition of growth by Dig and AA in MDA-MB-231 and 4T1 cells for 24 h. MDA-MB-231 and 4T1 cells were treated with Dig and AA (at various concentration) for 24 hours, and cell proliferation was assessed using the CCK-8 assay. Data are presented as the mean ± SEM from three independent experiments (n = 3). Statistical significance was determined using unpaired *t*-tests, with *$p < 0.05$, **$p < 0.01$, ***$p < 0.001$, and ****$p < 0.0001$ indicating significant differences compared to the DMSO control. **(B)** Transwell migration and invasion assay of MDA-MB-231 and 4T1 cells with Dig and AA treatment for 24 h. Representative images from randomly selected fields of transwell inserts, and Scalebar = 100 μm. **(C)** Quantitative data from the Transwell migration and invasion assays. Cell numbers were calculated and are expressed as the mean ± SEM of three independent experiments. * $p < 0.05$,** $p < 0.01$, *** $p < 0.001$ and ****$p < 0.0001$, as determined by unpaired *t*-tests. **(D)** Diagrammatic representation of tumor volume measurement. The diagram illustrates the measurement method, including caliper-based measurements of length and width used to calculate tumor volume (Volume = 1/2 × length × width^2). **(E)** Tumor sizes at day 14. **(F)** The body weight changes of mice in the period of 14 days after different treatments. The body weight of mice was monitored every 2 days after Dig and AA treatment. Data are expressed as the mean ± SEM. No significant changes in body weight were observed, suggesting that the treatments did not cause overt toxicity in mice.

expression analyses identified a notable number of genes exhibiting upregulation and downregulation (Figure 6A). Among these, IL6 was identified as the most significantly differential gene, with an adjusted p-value of 4.67E-191. A differential gene expression heatmap was generated to visualize these changes (Figure 6B). These 77 differentially expressed genes were then subjected to GO and KEGG pathway analyses to explore their biological functions and relevant pathways (Figures 6C, D). KEGG biological pathway analysis showed gene enrichment on pathways such as the TNF-signal pathway. In the triple-negative breast cancer cell lines MDA-MB-231 and 4T1, siRNA interference, Dig, and AA treatments effectively downregulated the expression of NANOS1 (Figure 6E). Furthermore, Dig and AA treatments reduced the protein expression of NANOS1 in TNBC cell lines (Figure 6F). We discuss the role of TNF-α in promoting tumor cell vascular adhesion and supporting angiogenesis. Previous studies have shown that TNF-α enhances tumor metastasis by upregulating the expression of adhesion molecules and stimulating the expression of angiogenesis factors (28–30). Our experimental results indicate that siRNA interference, Dig, and AA treatments

10.3389/fonc.2024.1536406

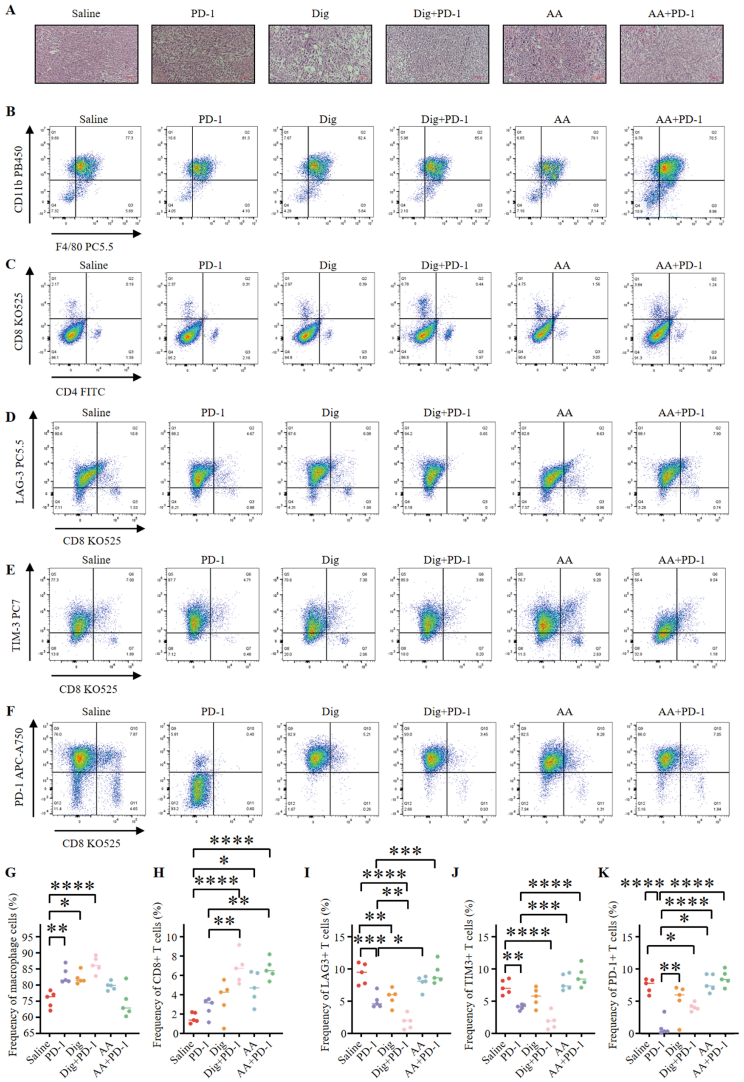

FIGURE 5
Dig combined with PD-1 immunotherapy can promote immune stimulation of *in situ* 4T1 breast tumors. **(A)** HE staining of mouse tumor tissues (scale bar = 100 μm). **(B)** Representative flow cytometry plots showing tumor-associated macrophages (TAMs) (CD45.2+, CD11b+, F4/80+) were obtained after different treatments. **(C)** Representative flow cytometry plots showing tumor immune cells after different treatments, including CTLs (CD45+, CD3+, CD8+) and Th cells (CD45+, CD3+, CD4+). **(D)** Representative flow cytometry plots demonstrating tumor-infiltrating LAG-3+ exhausted T cells (CD3+, CD8+, LAG-3+) after different treatments. **(E)** Representative flow cytometry plots demonstrating tumor-infiltrating TIM-3+ exhausted T cells (CD3+, CD8+, TIM-3+) after different treatments. **(F)** Representative flow cytometry plots demonstrating tumor-infiltrating PD-1+ exhausted T cells (CD3+, CD8 +, PD-1+) after different treatments. **(G)** The levels of TAMs were quantified through flow cytometry analysis (n = 5). Statistical analysis was performed using Tukey's multiple comparison test. The following adjusted p-values were obtained for each comparison: Saline vs PD-1: 0.0033; Saline vs Dig: 0.0106; Saline vs Dig+PD-1: <0.0001; Saline vs AA: 0.2039; Saline vs AA+PD-1: 0.9935; PD-1 vs Dig: 0.9961; PD-1 vs Dig+PD-1: 0.4395; PD-1 vs AA: 0.4330; PD-1 vs AA+PD-1: 0.0009; Dig vs Dig+PD-1: 0.2080; Dig vs AA: 0.7273; Dig vs AA+PD-1: 0.0028; Dig+PD-1 vs AA: 0.0109; Dig+PD-1 vs AA +PD-1: <0.0001; AA vs AA+PD-1: 0.0715. **(H)** The levels of CTLs were quantified by flow cytometry analysis (n = 5). The following adjusted p-values were obtained for each comparison: Saline vs PD-1: 0.7941; Saline vs Dig: 0.2550; Saline vs Dig+PD-1: <0.0001; Saline vs AA: 0.0161; Saline vs AA+PD-1: <0.0001; PD-1 vs Dig: 0.9237; PD-1 vs Dig+PD-1: 0.0013; PD-1 vs AA: 0.2253; PD-1 vs AA+PD-1: 0.0016; Dig vs Dig+PD-1: 0.0136; Dig vs AA: 0.7542; Dig vs AA+PD-1: 0.0164; Dig+PD-1 vs AA: 0.2253; Dig+PD-1 vs AA+PD-1: >0.9999; AA vs AA+PD-1: 0.2576. **(I)** Flow cytometry analysis quantified the levels of LAG-3+ exhausted T cells (n = 5). Statistical analysis was performed using Tukey's multiple comparison test. Flow cytometry analysis quantified the levels of LAG-3+ exhausted T cells (n = 5). Statistical analysis was performed using Tukey's multiple comparison test. The following adjusted p-values were obtained for each comparison: Saline vs PD-1: 0.0006; Saline vs Dig: 0.0030; Saline vs Dig+PD-1: <0.0001; Saline vs AA: 0.5950; Saline vs AA+PD-1: >0.9999; PD-1 vs Dig: 0.9841; PD-1 vs Dig+PD-1: 0.0094; PD-1 vs AA: 0.0282; PD-1 vs AA+PD-1: 0.0005; Dig vs Dig+PD-1: 0.0019; Dig vs AA: 0.1152; Dig vs AA+PD-1: 0.0027; Dig+PD-1 vs AA: <0.0001; Dig+PD-1 vs AA+PD-1: <0.0001; AA vs AA+PD-1: 0.5676. **(J)** Flow cytometry analysis quantified the levels of TIM-3+ exhausted T cells (n = 5). Statistical analysis was performed using Tukey's multiple comparison test. The following adjusted p-values were obtained for each comparison: Saline vs PD-1: 0.0073; Saline vs Dig: 0.3784; Saline vs Dig+PD-1: <0.0001; Saline vs AA: 0.9296; Saline vs AA+PD-1: 0.3206; PD-1 vs Dig: 0.4016; PD-1 vs Dig+PD-1: 0.0959; PD-1 vs AA: 0.0007; PD-1 vs AA+PD-1: <0.0001; Dig vs Dig+PD-1: 0.0011; Dig vs AA: 0.0698; Dig vs AA+PD-1: 0.0050; Dig+PD-1 vs AA: <0.0001; Dig+PD-1 vs AA+PD-1: <0.0001; AA vs AA+PD-1: 0.8546. **(K)** Flow cytometry analysis quantified the levels of PD-1+ exhausted T cells (n = 5). Statistical analysis was performed using Tukey's multiple comparison test. The following adjusted p-values were obtained for each comparison: Saline vs PD-1: <0.0001; Saline vs Dig: 0.2205; Saline vs Dig+PD-1: 0.0276; Saline vs AA: 0.9984; Saline vs AA+PD-1: 0.8260; PD-1 vs Dig: 0.0043; PD-1 vs Dig+PD-1: 0.0469; PD-1 vs AA: <0.0001; PD-1 vs AA+PD-1: <0.0001; Dig vs Dig+PD-1: 0.9030; Dig vs AA: 0.1042; Dig vs AA+PD-1: 0.0181; Dig+PD-1 vs AA: 0.0108; Dig+PD-1 vs AA+PD-1: 0.0015; AA vs AA+PD-1: 0.9632. Data are expressed as the mean ± SEM. *$p < 0.05$, **$p < 0.01$, ***$p < 0.001$ and ****$p < 0.0001$ vs. Saline.

10.3389/fonc.2024.1536406

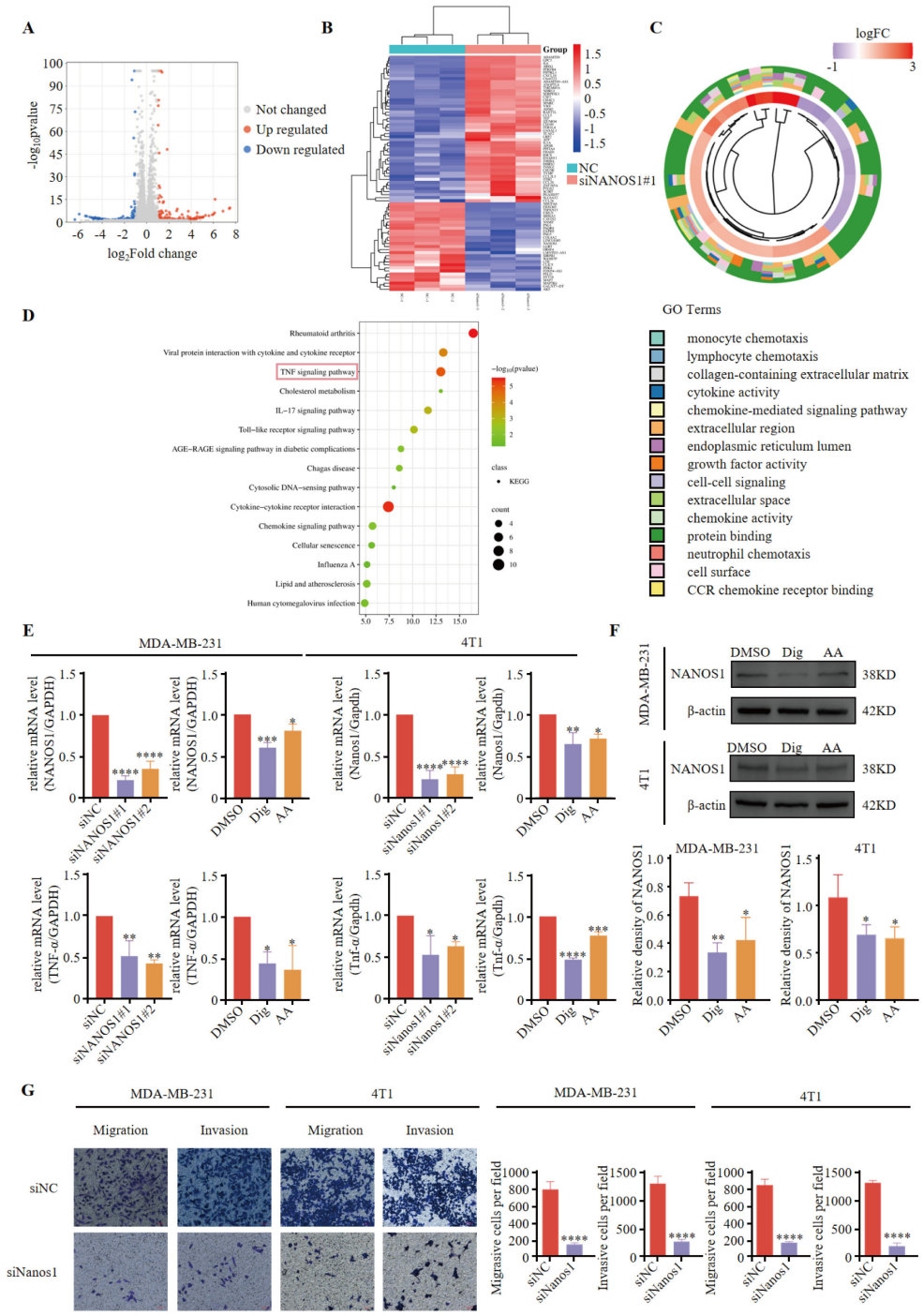

FIGURE 6
NANOS1 Silencing Reduces TNF-α Expression and Cell Invasiveness. **(A)** Volcano plots of RNA-seq. Differential gene expression analysis was performed using RNA sequencing data from MDA-MB-231 cells with siNANOS1#1 silencing. The volcano plot shows the distribution of genes based on log-fold change versus the negative log-transformed p-value. Significant upregulated and downregulated genes are indicated with colored dots. Genes that meet the threshold of log-fold change (|logFC| > 2) and adjusted p-value < 0.05 are considered differentially expressed. **(B)** Heatmap of differential gene expression. **(C)** Chord diagram of GO enrichment results and related genes. **(D)** Top 15 KEGG pathways. The x-axis represents the gene ratio ($p < 0.05$), and the y-axis represents the enriched terms. **(E)** The knockdown efficiency of siRNA and the expression of NANOS1 and TNF-α following Dig and AA treatment were quantified by qPCR. MDA-MB-231 and 4T1 cells were transfected with siRNA targeting NANOS1, followed by treatment with Dig and AA. Quantitative PCR was performed to assess the expression levels of NANOS1 and TNF-α. The data are expressed as the mean ± SEM, with statistical significance calculated using one-way ANOVA. **(F)** Dig and AA decreased the expression of NANOS1 protein (n = 3). Data are expressed as the mean ± SEM. Statistical significances were calculated via one-way ANOVA, *$p < 0.05$, **$p < 0.010$, ***$p < 0.001$ and ****$p < 0.0001$ vs. DMSO. **(G)** Perforation migration and invasion assays of MDA-MB-231 and 4T1 cells after 24 h of siRNA treatment, scale bar = 100 mm. Cell numbers were calculated and are expressed as the mean ± SEM of three independent experiments. *$p < 0.05$, **$p < 0.01$, ***$p < 0.001$ and ****$p < 0.0001$, as determined by unpaired t-tests, were regarded as significant.

TABLE 2 Docking scores and drug information of Top6 molecules.

ZIN No.	Docking score	Drugs
ZINC08101076	-9.9	Digoxin
ZINC03830650	-9.9	Algestone acetophenide
ZINC03831193	-9.7	Nandrolone phenylpropionate (NPP)
ZINC11592964	-9.6	Daunorubicin
ZINC01482077	-9.5	Gliquidone
ZINC03830767	-9.5	Estradiol Benzoate

all suppress TNF-α gene expression, which is consistent with previous findings. Transwell assays revealed that siRNA-mediated silencing of *NANOS1* expression significantly reduced the migration and invasion abilities of MDA-MB-231 and 4T1 cells (Figure 6G).

4 Discussion

TNBC is an aggressive, recurring and poorly prognosed malignancy. Compared to other breast cancer subtypes, the mortality rate within 5 years of diagnosis is approximately 40% (31) and is more prone to distant metastases to visceral and brain (32, 33). Since TNBC tumors lack ER, PR and HER2, it is not sensitive to either endocrine therapy or molecular targeted therapy, and chemotherapy remains the standard approach to treatment (34). However, drug resistance of tumor cells and side effects of chemotherapy greatly limit the application of chemotherapy in the treatment of TNBC. Therefore, there is still an urgent need for new drugs with high efficiency and low toxicity for the treatment of TNBC.

Recent studies have demonstrated that *Taraxacum officinale* exhibits promising effects in the treatment of TNBC, with a low risk of treatment-related adverse effects, increasing its appeal. Nassan (35) observed that administering TOE to breast cancer-bearing mice for 4 weeks reduced the serum marker CA15-3, which is commonly used to monitor breast cancer progression. This effect was linked to the inhibition of the PI3K/Akt pathway, a signaling cascade often abnormally activated in tumorigenesis, drug resistance, and cancer progression. Furthermore, TOE may regulate endoplasmic reticulum stress and apoptosis by activating the PERK/p-eIF2α/ATF4/CHOP signaling pathway, leading to suppressed TNBC cell growth (36). In our study, TOE inhibited the growth, migration, and invasion of two TNBC cell lines, suggesting its potential therapeutic value. To explore the targets of TOE, we performed RNA sequencing analysis of MDA-MB-231 cells, followed by KEGG pathway enrichment analysis of the top 600 up-regulated and 600 down-regulated genes. The top five significantly enriched pathways were: pathways in cancer, MAPK signaling pathway, transcriptional misregulation in cancer, microRNAs in cancer, and the cell cycle. Among them, several MAPK signaling pathways have been shown to be closely associated with TNBC (37, 38), while some microRNAs members also play roles in carcinogenesis, metastasis, diagnosis, treatment and prognosis of TNBC (39). Transcriptional misregulation of breast cancer-related genes can likewise promote tumor development (40). This result provides confidence for *Taraxacum officinale* to treat breast cancer. Among the 1,200 differentially expressed genes, NANOS1 is the only gene whose protein levels are associated with breast cancer prognosis and are downregulated. Interestingly, the biological function of NANOS1 remains unannotated, highlighting the importance of our investigation into this gene.

NANOS1 is a member of the *NANOS* gene family which encodes a CCHC-type zinc finger protein (41). It has been shown to promote tumor cell migration, dissemination, and invasion by displacing linker proteins and disrupting E-cadherin–dependent cell-cell adhesion (42). In this study, we analyzed the expression of NANOS1 in breast cancer and found that lower NANOS1 expression in breast cancer patients was associated with a better prognosis. Given that immune infiltration levels are linked to cancer progression and treatment outcomes, we further explored the correlation between NANOS1 expression and immune infiltration. Specifically, NANOS1 expression was negatively correlated with activated NK cells, and survival analysis revealed that high NK cell infiltration was associated with a better prognosis when NANOS1 expression was low.

Additionally, we investigated whether any approved drugs could target *NANOS1* to suppress the malignant phenotype of TNBC cells. Among the top six ranked drugs, nandrolone phenylpropionate (43) and daunorubicin (44) have been previously shown to be effective in treating breast cancer, suggesting that *NANOS1* is a novel target for these drugs. Notably, digoxin, a commonly used medication for heart disease, was also identified as a potential candidate targeting *NANOS1*. Its efficacy in treating breast cancer requires further validation, which presents an opportunity to explore its novel therapeutic applications.

This study demonstrated that the combination of Dig and PD-1 inhibitors significantly suppresses the growth of triple-negative breast cancer (TNBC) in an allograft mouse model. The combined therapy not only enhanced tumor infiltration of macrophages and CD8+ T cells but also reduced the proportion of exhausted T cells in the tumor microenvironment (TME), indicating its potential as a novel immunotherapeutic strategy. Our findings highlight the potential of combining FDA-approved drugs with PD-1 inhibitors as a strategy to enhance the efficacy of immune checkpoint blockade (ICB) in TNBC. By leveraging the synergistic effects of FDA-approved drugs and modern immunotherapies, this study provides a new perspective for exploring effective cancer combination therapies.

Digoxin is a commonly used cardiac glycoside for the treatment of heart failure and atrial fibrillation, but its narrow therapeutic index significantly increases the risk of toxicity. The recommended therapeutic plasma concentration of digoxin is 0.5 to 2 ng/mL, and concentrations exceeding this range can lead to severe adverse effects, including gastrointestinal symptoms, central nervous system disturbances, and life-threatening arrhythmias (45). Renal function plays a crucial role in the elimination of digoxin, and impaired renal function can result in drug accumulation, further increasing the risk of toxicity (46). In this experiment, we assessed the effects of digoxin monotherapy and combination therapy on

mouse body weight, kidney and liver indices, with no significant differences compared to the saline control group. These preliminary findings suggest the safety of the combination therapy with digoxin. Therefore, close monitoring of serum digoxin concentrations, renal function, and electrolyte levels in subjects receiving the drug is essential to prevent toxicity and enhance the clinical translational value of this combination therapy.

The limited response of TNBC to immune checkpoint blockade (ICB) remains poorly understood, with one critical factor being the lack of activated immune cells within the tumor microenvironment (TME). This deficiency renders many TNBC tumors "cold," resulting in poor responses to immunotherapy. Previous studies have shown that targeting the JAK1/STAT3 pathway with Aurora kinase inhibitors can promote the expression of Th1 chemokines such as CXCL10 and CXCL11, facilitating the conversion of "cold" tumors to "hot" tumors and thereby improving the efficacy of ICB (47). Similarly, our findings suggest that Dig can remodel the TME by promoting immune cell recruitment and antitumor immune responses, supporting its potential role as an adjuvant to ICB therapy. While our *in vivo* results are promising, further studies are required to elucidate the precise molecular targets and mechanisms of these compounds. Future research should focus on optimizing their dosage and combinations to maximize therapeutic potential.

Data availability statement

The datasets used in this study have been uploaded to the NCBI database with the accession number PRJNA1209407. Further inquiries can be directed to the corresponding authors.

Ethics statement

Ethical approval was not required for the studies on humans in accordance with the local legislation and institutional requirements because only commercially available established cell lines were used. The animal study was approved by Medical College of Qinghai University (2022-01). The study was conducted in accordance with the local legislation and institutional requirements.

Author contributions

TW: Formal analysis, Validation, Writing – original draft, Writing – review & editing. YDL: Conceptualization, Formal analysis, Methodology, Writing – review & editing. JS: Data curation, Visualization, Writing – review & editing. LW: Formal analysis, Investigation, Writing – review & editing. YXL: Investigation, Writing – review & editing. ZW: Investigation, Writing – review & editing. SZ: Investigation, Writing – review & editing. CC: Resources, Writing – review & editing. HW: Conceptualization, Data curation, Funding acquisition, Methodology, Project administration, Resources, Supervision, Validation, Writing – review & editing.

Funding

The author(s) declare financial support was received for the research, authorship, and/or publication of this article. This work was supported by research funding from the National Natural Science Foundation of China (32260187 to HW), the Applied Basic Research Project Fund of the Qinghai Provincial Department of Science and Technology (2023-ZJ-729 to HW), and the Qinghai University Team Research Project Fund (2023-QYY-6 to HW).

Conflict of interest

The authors declare that the research was conducted in the absence of any commercial or financial relationships that could be construed as a potential conflict of interest.

Correction note

A correction has been made to this article. Details can be found at: 10.3389/fonc.2025.1654169.

Generative AI statement

The author(s) declare that no Generative AI was used in the creation of this manuscript.

Publisher's note

All claims expressed in this article are solely those of the authors and do not necessarily represent those of their affiliated organizations, or those of the publisher, the editors and the reviewers. Any product that may be evaluated in this article, or claim that may be made by its manufacturer, is not guaranteed or endorsed by the publisher.

Supplementary material

The Supplementary Material for this article can be found online at: https://www.frontiersin.org/articles/10.3389/fonc.2024.1536406/full#supplementary-material

References

1. Sung H, Ferlay J, Siegel RL, Laversanne M, Soerjomataram I, Jemal A, et al. Global cancer statistics 2020: GLOBOCAN estimates of incidence and mortality worldwide for 36 cancers in 185 countries. *CA Cancer J Clin*. (2021) 71(3):209–49. doi: 10.3322/caac.21660

2. Wolff AC, Hammond MEH, Allison KH, Harvey BE, Mangu PB, Bartlett JMS, et al. Human epidermal growth factor receptor 2 testing in breast cancer: american society of clinical oncology/college of american pathologists clinical practice guideline focused update. *J Clin Oncol*. (2018) 36(20):2105–22. doi: 10.1200/JCO.18.00149

3. Yin L, Duan JJ, Bian XW, Yu SC. Triple-negative breast cancer molecular subtyping and treatment progress. *Breast Cancer Res*. (2020) 22(1):61. doi: 10.1186/s13058-020-01277-5

4. Wang CY, Bai XY, Wang CH. Traditional Chinese medicine: a treasured natural resource of anticancer drug research and development. *Am J Chin Med*. (2014) 42 (3):543–59. doi: 10.1142/S0192415X14500359

5. Yang Y, Guo Z, Zhu P, Chen J, Huang Y. Traditional Chinese medicine as a cancer treatment: Modern perspectives of ancient but advanced science. *Cancer Med*. (2019) 8 (5):1958–75. doi: 10.1002/cam4.2019.8.issue-5

6. Chen D, Zhao J, Cong W. Chinese herbal medicines facilitate the control of chemotherapy-induced side effects in colorectal cancer: progress and perspective. *Front Pharmacol*. (2018) 9:1442. doi: 10.3389/fphar.2018.01442

7. Zhang X, Wei X, Shi L, Jiang H, Ma F, Li Y, et al. The latest research progress: active components of Traditional Chinese medicine as promising candidates for ovarian cancer therapy. *J Ethnopharmacology*. (2024) 337:118811. doi: 10.1016/j.jep.2024.118811

8. Jia L, Ma S, Hou X, Wang X, Qased AB, Sun X, et al. The synergistic effects of traditional Chinese herbs and radiotherapy for cancer treatment. *Oncol Letters*. (2013) 5:1439–47. doi: 10.3892/ol.2013.1245

9. Lin CJ, Chen JT, Yeh LJ, Yang RC, Huang SM, Chen TW, et al. Characteristics of the Cytotoxicity of Taraxacum mongolicum and Taraxacum formosanum in Human Breast Cancer Cells. *Int J Mol Sci*. (2022) 23:11918. doi: 10.3390/ijms23191918

10. Qu J, Ke F, Liu Z, Yang X, Li X, Xu H, et al. Uncovering the mechanisms of dandelion against triple-negative breast cancer using a combined network pharmacology, molecular pharmacology and metabolomics approach. *Phytomedicine*. (2022) 99:153986. doi: 10.1016/j.phymed.2022.153986

11. Maschi D, Fernández-Alvarez AJ, Boccaccio GL. The RNA-binding protein NANOS1 controls hippocampal synaptogenesis. *PloS One*. (2023) 18(4):e0284589. doi: 10.1371/journal.pone.0284589

12. Ilaslan E, Sajek MP, Jaruzelska J, Kusz-Zamelczyk K. Emerging roles of NANOS RNA-binding proteins in cancer. *Int J Mol Sci*. (2022) 23(16):9408. doi: 10.3390/ijms23169408

13. Ren Y, Anderson AT, Meyer G, Lauber KM, Gallucci JC, Kinghorn AD. Digoxin and its Na+/K+-ATPase-targeted actions on cardiovascular diseases and cancer. *Bioorganic Medicinal Chem*. (2024) 114:117939. doi: 10.1016/j.bmc.2024.117939

14. Smith TW, Antman EM. Digitalis: Mechanisms of action and clinical use. *N Engl J Med*. (1992) 318(6):358–65. doi: 10.1056/NEJM198802113180606

15. McConkey DJ, Lin Y, Nutt LK. Cardiac glycosides: From molecular targets to immunogenic cell death. *Trends Pharmacol Sci*. (2011) 32:146–53. doi: 10.1016/j.bcp.2016.08.017

16. Askari A. The sodium pump and digitalis drugs: Dogmas and fallacies. *Pharmacol Res Perspectives*. (2019) 7:e00505. doi: 10.1002/prp2.2019.7.issue-4

17. Newman RA, Yang P, Pawlus AD, Block KI. Cardiac glycosides as novel cancer therapeutic agents. *Mol Interv*. (2008) 8(1):36–49. doi: 10.1124/mi.8.1.8

18. Mijatovic T, Van Quaquebeke E, Delest B, Debeir O, Darro F, Kiss R. Cardiotonic steroids on the road to anti-cancer therapy. *Biochim Biophys Acta Rev Cancer*. (2007) 1776(1):32–57. doi: 10.1016/j.bbcan.2007.06.002

19. Sitruk-Ware R. Pharmacological profile of progestins. *Maturitas*. (2004) 47 (4):277–83. doi: 10.1016/j.maturitas.2004.01.001

20. Jézéquel P, Gouraud W, Ben Azzouz F, Guérin-Charbonnel C, Juin PP, Lasla H, et al. bc-GenExMiner 4.5: new mining module computes breast cancer differential gene expression analyses. *Database (Oxford)*. (2021) 2021:baab007. doi: 10.1093/database/baab007

21. Karlsson M, Zhang C, Méar L, Zhong W, Digre A, Katona B, et al. A single-cell type transcriptomics map of human tissues. *Sci Adv*. (2021) 7(31):eabh2169. doi: 10.1126/sciadv.abh2169

22. Lanczky A, Gyorffy B. Web-based survival analysis tool tailored for medical research (KMplot): development and implementation. *J Med Internet Res*. (2021) 23(7): e27633. doi: 10.2196/27633

23. Li T, Fu J, Zeng Z, Cohen D, Li J, Chen Q, et al. TIMER2.0 for analysis of tumor-infiltrating immune cells. *Nucleic Acids Res*. (2020) 48(W1):W509–14. doi: 10.1093/nar/gkaa562

24. Pettersen EF, Goddard TD, Huang CC, Couch GS, Greenblatt DM, Meng EC, et al. UCSF Chimera—a visualization system for exploratory research and analysis. *J Comput Chem*. (2004) 25(13):1605–12. doi: 10.1002/jcc.20067

25. Anandakrishnan R, Aguilar B, Onufriev AV. H++ 3.0: automating p K prediction and the preparation of biomolecular structures for atomistic molecular modeling and simulations. *Nucleic Acids Res*. (2012) 40:W537–41. doi: 10.1093/nar/gks401

26. Halgren T. New method for fast and accurate binding-site identification and analysis. *Chem Biol Drug design*. (2007) 69(2):146–8. doi: 10.1111/j.1747-0285.2006.00540.x

27. Goodsell DS, Morris GM, Olson AJ. Automated docking of flexible ligands: applications of AutoDock. *J Mol Recognit*. (1996) 9(1):1–5. doi: 10.1002/jmr.5500090103

28. Bates RC, Mercurio AM. Tumor necrosis factor-alpha stimulates the epithelial-to-mesenchymal transition of human colonic organoids. *Mol Biol Cell*. (2003) 14 (5):1790–800. doi: 10.1091/mbc.e02-09-0583

29. Zhu Y, Cheng Y, Guo Y, Chen J, Chen F, Luo R, et al. Protein kinase D2 contributes to TNF-alpha-induced epithelial mesenchymal transition and invasion via the PI3K/GSK-3beta/beta-catenin pathway in hepatocellular carcinoma. *Oncotarget*. (2016) 7(5):5327–41. doi: 10.18632/oncotarget.6633

30. Soria G, Ofri-Shahak M, Haas I, Yaal-Hahoshen N, Leider-Trejo L, Leibovich-Rivkin T, et al. Inflammatory mediators in breast cancer: coordinated expression of TNFalpha & IL-1beta with CCL2 & CCL5 and effects on epithelial-to-mesenchymal transition. *BMC Cancer*. (2011) 11:130. doi: 10.1186/1471-2407-11-130

31. Dent R, Trudeau M, Pritchard KI, Hanna WM, Kahn HK, Sawka CA, et al. Triple-negative breast cancer: clinical features and patterns of recurrence. *Clin Cancer Res*. (2007) 13:4429–34. doi: 10.1158/1078-0432.CCR-06-3045

32. Reda A, Refaat A, Abd-Rabou AA, Mahmoud AM, Adel M, Sabet S, et al. Role of mitochondria in rescuing glycolytically inhibited subpopulation of triple negative but not hormone-responsive breast cancer cells. *Sci Rep*. (2019) 9(1):13748. doi: 10.1038/s41598-019-49970-6

33. Lin NU, Claus E, Sohl J, Razzak AR, Arnaout A, Winer EP. Sites of distant recurrence and clinical outcomes in patients with metastatic triple-negative breast cancer: high incidence of central nervous system metastases. *Cancer*. (2008) 113 (10):2638–45. doi: 10.1002/cncr.23775

34. Fabbri F, Salvi S, Bravaccini S. Know your enemy: Genetics, aging, exposomic and inflammation in the war against triple negative breast cancer. *Semin Cancer Biol*. (2020) 60:285–93. doi: 10.1016/j.semcancer.2019.12.002

35. Nassan MA, Soliman MM, Ismail SA, El-Shazly S. Effect of Taraxacum officinale extract on PI3K/Akt pathway in DMBA-induced breast cancer in albino rats. *Biosci Rep*. (2018) 38(6):BSR20180334. doi: 10.1042/BSR20180334

36. Li XH, He XR, Zhou YY, Zhao HY, Zheng WX, Jiang ST, et al. Taraxacum mongolicum extract induced endoplasmic reticulum stress associated-apoptosis in triple-negative breast cancer cells. *J Ethnopharmacol*. (2017) 206:55–64. doi: 10.1016/j.jep.2017.06.042

37. Chen MS, Yeh HT, Li YZ, Lin WC, Lee YR, Tseng YS, et al. Flavopereirine inhibits autophagy via the AKT/p38 MAPK signaling pathway in MDA-MB-231 cells. *Int J Mol Sci*. (2020) 21(15):5362. doi: 10.3390/ijms21155362

38. Loi S, Dushyanthen S, Beavis PA, Salgado R, Denkert C, Savas P, et al. RAS/MAPK activation is associated with reduced tumor-infiltrating lymphocytes in triple-negative breast cancer: therapeutic cooperation between MEK and PD-1/PD-L1 immune checkpoint inhibitors. *Clin Cancer Res*. (2016) 22:1499–509. doi: 10.1158/1078-0432.CCR-15-1167

39. Sabit H, Cevik E, Tombuloglu H, Abdel-Ghany S, Tombuloglu G, Esteller M. Triple negative breast cancer in the era of miRNA. *Crit Rev Oncol Hematol*. (2021) 157 (6):103196. doi: 10.1016/j.critrevonc.2021.103196

40. Lee TI, Young RA. Transcriptional regulation and its misregulation in disease. *Cell*. (2013) 152(6):1237–51. doi: 10.1016/j.cell.2013.02.009

41. Ilaslan E, Kwiatkowska K, Smialek MJ, Sajek MP, Lemanska Z, Alla M, et al. Distinct roles of NANOS1 and NANOS3 in the cell cycle and NANOS3-PUM1-FOXM1 axis to control G2/M phase in a human primordial germ cell model. *Int J Mol Sci*. (2022) 23(12). doi: 10.3390/ijms23124929

42. Strumane K, Bonnomet A, Stove C, Vandenbroucke R, Nawrocki-Raby B, Bruyneel E, et al. E-cadherin regulates human Nanos1, which interacts with p120ctn and induces tumor cell migration and invasion. *Cancer Res*. (2006) 66(20):10007–15. doi: 10.1158/0008-5472.CAN-06-0947

43. Szujewski HA. Nandrolone phenpropionate: a new palliative agent in the management of mammary carcinoma. *Am Pract Dig Treat*. (1959) 10:2157–9.

44. Ju RJ, Cheng L, Peng XM, Wang T, Li CQ, Song XL, et al. Octreotide-modified liposomes containing daunorubicin and dihydroartemisinin for treatment of invasive breast cancer. *Artif Cells Nanomed Biotechnol*. 46(sup1):616–28. doi: 10.1080/21691401.2018.1433187

45. Patocka J, Nepovimova E, Wu W, Kuca K. Digoxin: Pharmacology and toxicology—A review. *Environ Toxicol Pharmacol*. (2020) 79:103400. doi: 10.1016/j.etap.2020.103400

46. Shlipak MG, Smith GL, Rathore SS, Massie BM, Krumholz HM. Renal function, digoxin therapy, and heart failure outcomes: evidence from the digoxin intervention group trial. *J Am Soc Nephrol*. (2004) 15(8):2195–203. doi: 10.1097/01.ASN.0000135121.81744.75

47. Wang H, Li S, Wang Q, Jin Z, Shao W, Gao Y, et al. High-throughput screening for the discovery of combination immunotherapy compounds based on tumor immunological phenotype signature. *Sci Adv*. (2021) 7:eabd7851. doi: 10.1126/sciadv.abd7851

frontiers | Frontiers in Oncology

TYPE Correction
PUBLISHED 02 September 2025
DOI 10.3389/fonc.2025.1654169

Check for updates

OPEN ACCESS

APPROVED BY
Frontiers Editorial Office,
Frontiers Media SA, Switzerland

*CORRESPONDENCE
Haiyan Wang
wanghaiyan@qhu.edu.cn

†These authors have contributed equally to this work and share first authorship

RECEIVED 26 June 2025
ACCEPTED 19 August 2025
PUBLISHED 02 September 2025

CITATION
Wang T, Lei Y, Sun J, Wang L, Lin Y, Wu Z, Zhang S, Cao C and Wang H (2025) Correction: Targeting NANOS1 in triple-negative breast cancer: synergistic effects of digoxin and PD-1 inhibitors in modulating the tumor immune microenvironment. *Front. Oncol.* 15:1654169. doi: 10.3389/fonc.2025.1654169

COPYRIGHT
© 2025 Wang, Lei, Sun, Wang, Lin, Wu, Zhang, Cao and Wang. This is an open-access article distributed under the terms of the Creative Commons Attribution License (CC BY). The use, distribution or reproduction in other forums is permitted, provided the original author(s) and the copyright owner(s) are credited and that the original publication in this journal is cited, in accordance with accepted academic practice. No use, distribution or reproduction is permitted which does not comply with these terms.

Correction: Targeting NANOS1 in triple-negative breast cancer: synergistic effects of digoxin and PD-1 inhibitors in modulating the tumor immune microenvironment

Tangyi Wang[1†], Yadian Lei[1†], Jingwei Sun[2], Li Wang[1], Yuxin Lin[1], Zhijing Wu[1], Shoude Zhang[3], Chengzhu Cao[1,4,5] and Haiyan Wang[1,4,5*]

[1]Department of Basic Medical Sciences, Qinghai University Medical College, Xining, Qinghai, China, [2]Department of Medical Laboratory, Qinghai Provincial People's Hospital, Xining, Qinghai, China, [3]State Key Laboratory of Plateau Ecology and Agriculture, Qinghai University, Xining, Qinghai, China, [4]Research Center for High Altitude Medicine, Qinghai University, Xining, Qinghai, China, [5]Key Laboratory of the Ministry of High Altitude Medicine, Qinghai University, Xining, Qinghai, China

KEYWORDS

immune checkpoint blockade, triple-negative breast cancer, malignant phenotype, nanos1, PD-1 inhibitors, tumor microenvironments

A Correction on

Targeting NANOS1 in triple-negative breast cancer: synergistic effects of digoxin and PD-1 inhibitors in modulating the tumor immune microenvironment

By Wang T, Lei Y, Sun J, Wang L, Lin Y, Wu Z, Zhang S, Cao C and Wang H (2025) *Front. Oncol.* 14:1536406. doi: 10.3389/fonc.2024.1536406

There was a mistake in **Figure 1B** as published. The figure contains an error caused by an unintentional assembly mistake: while adjusting the layout to keep the spacing and formatting uniform, we duplicated a placeholder image that inadvertently overwrote the correct panel, resulting in incorrect image usage. The corrected **Figure 1** and its caption appear below.

There was a mistake in **Figure 4B** as published. The figure contains an error due to an unintentional mistake during assembly, where the "4T1-Invasion-Dig" image was overwritten by the "MDA-MB-231-Invasion-AA" image, resulting in incorrect image usage. The corrected **Figure 4** and its caption appear below.

The original version of this article has been updated.

Publisher's note

All claims expressed in this article are solely those of the authors and do not necessarily represent those of their affiliated organizations, or those of the publisher, the editors and the reviewers. Any product that may be evaluated in this article, or claim that may be made by its manufacturer, is not guaranteed or endorsed by the publisher.

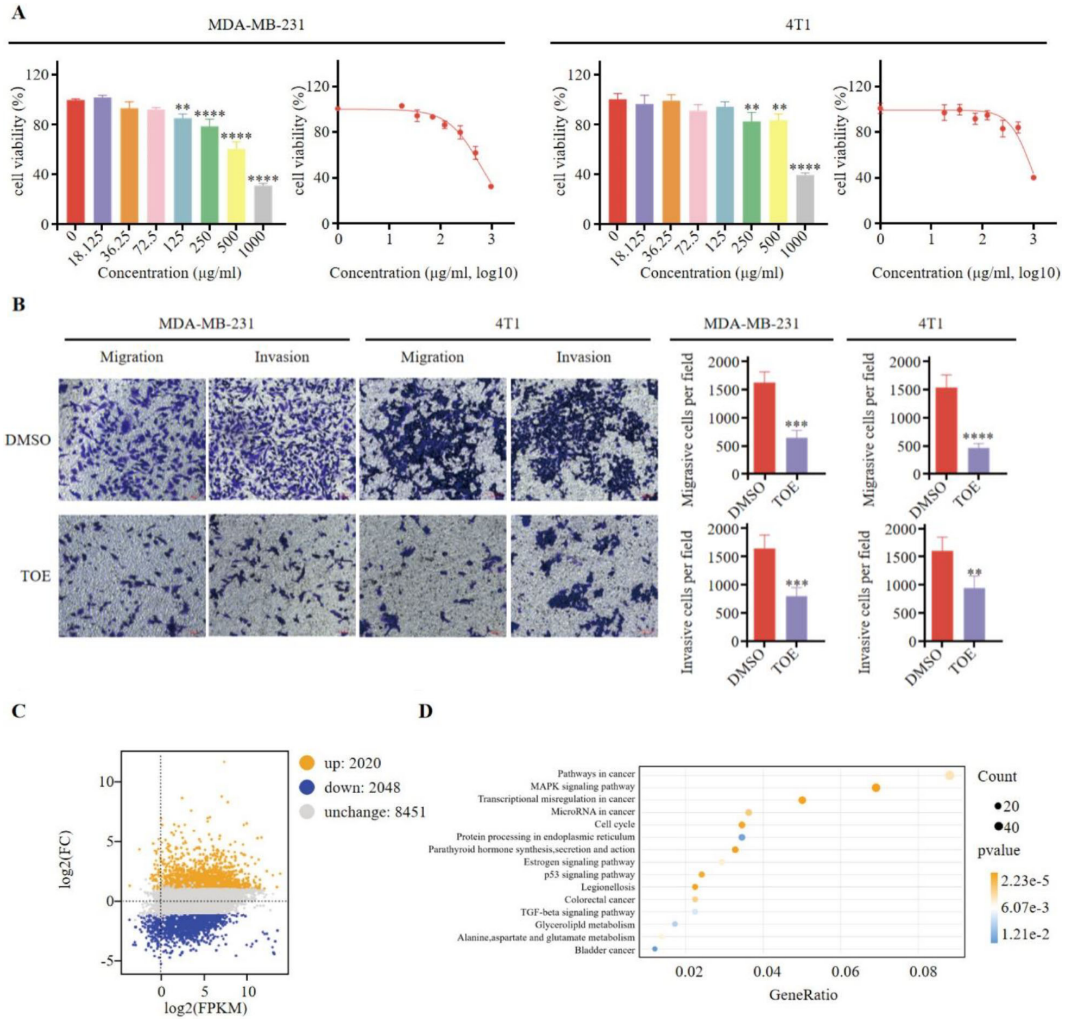

FIGURE 1
TOE suppresses malignant phenotype of triple negative breast cancer cells. **(A)** The effect of TOE on cell proliferation in MDA-MB-231 and 4T1 cells. Cells were treated with varying concentrations of TOE for 24 hours, and cell proliferation was assessed using the CCK-8 assay. Data are expressed as the mean ± SEM (n = 3). Statistical significances were calculated via Student's t-test. **p < 0.01 and ***p < 0.001 and ****p < 0.0001. **(B)** Transwell migration and invasion assay of MDA-MB-231 and 4T1 cells after treatment with TOE for 24 hours. Representative images of the migrated and invaded cells from randomly selected fields of Transwell inserts are shown on the left, while quantitative data for cell numbers are presented on the right. Cell numbers were calculated and expressed as the mean ± SEM of three independent experiments. Statistical significance was determined by t-test, with **p < 0.01 and ***p < 0.001 and ****p < 0.0001 indicating significant differences between TOE-treated and DMSO-treated cells. Scale bar = 100 μm. **(C)** MA plot of DGEs in MDA-MB-231 treated with TOE. **(D)** Enrichment and scatter map of KEGG pathway of DGEs.

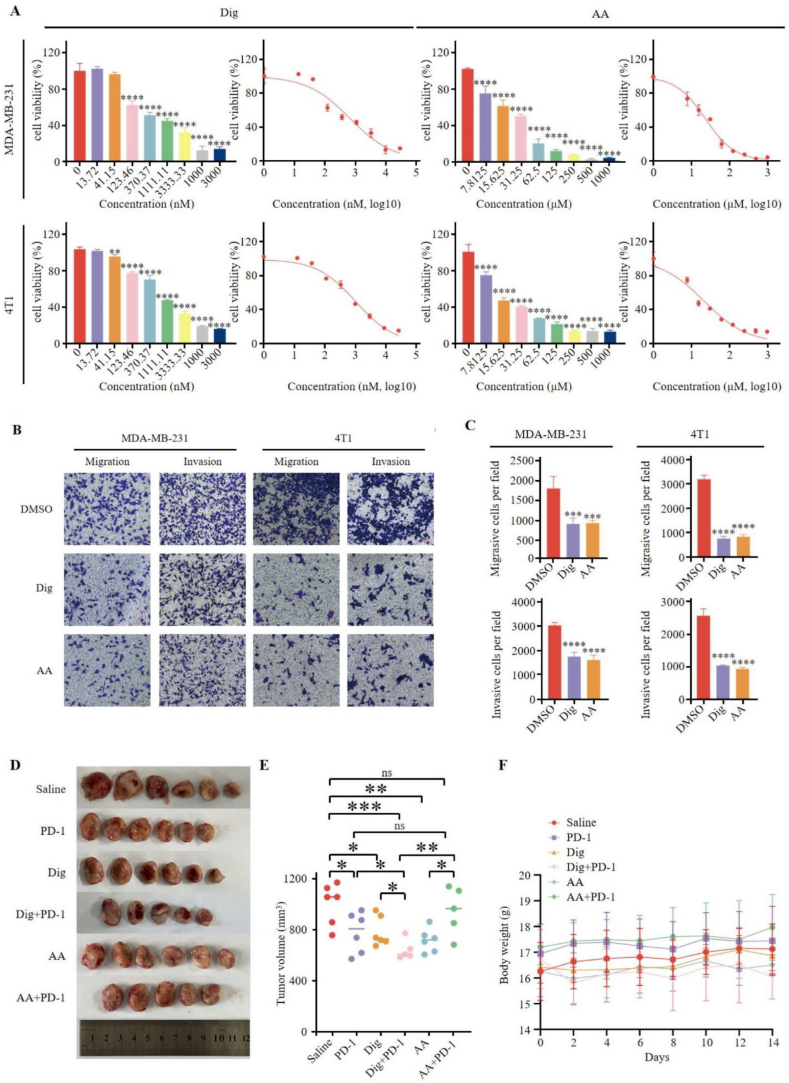

FIGURE 4
Dig and AA inhibited tumor growth in breast cancer mouse models. **(A)** Inhibition of growth by Dig and AA in MDA-MB-231 and 4T1 cells for 24 h. MDA-MB-231 and 4T1 cells were treated with Dig and AA (at various concentration) for 24 hours, and cell proliferation was assessed using the CCK-8 assay. Data are presented as the mean ± SEM from three independent experiments (n = 3). Statistical significance was determined using unpaired *t*-tests, with *$p < 0.05$, **$p < 0.01$, ***$p < 0.001$, and ****$p < 0.0001$ indicating significant differences compared to the DMSO control. **(B)** Transwell migration and invasion assay of MDA-MB-231 and 4T1 cells with Dig and AA treatment for 24 h. Representative images from randomly selected fields of transwell inserts, and Scalebar = 100 μm. **(C)** Quantitative data from the Transwell migration and invasion assays. Cell numbers were calculated and are expressed as the mean ± SEM of three independent experiments. * $p < 0.05$,** $p < 0.01$, *** $p < 0.001$ and ****$p < 0.0001$, as determined by unpaired *t*-tests. **(D)** Diagrammatic representation of tumor volume measurement. The diagram illustrates the measurement method, including caliper-based measurements of length and width used to calculate tumor volume (Volume = 1/2 × length × width^2). **(E)** Tumor sizes at day 14. **(F)** The body weight changes of mice in the period of 14 days after different treatments. The body weight of mice was monitored every 2 days after Dig and AA treatment. Data are expressed as the mean ± SEM. No significant changes in body weight were observed, suggesting that the treatments did not cause overt toxicity in mice.

frontiers | Frontiers in Immunology

TYPE Original Research
PUBLISHED 29 January 2025
DOI 10.3389/fimmu.2025.1531639

Check for updates

OPEN ACCESS

EDITED BY
Qingyu Luo,
Dana–Farber Cancer Institute, United States

REVIEWED BY
Xiaosheng Tan,
Rutgers, United States
Xiaowei Wu,
Dana–Farber Cancer Institute, United States
Yunchang Mo,
First Affiliated Hospital of Wenzhou Medical University, China
Haili Ma,
Dana–Farber Cancer Institute, United States

*CORRESPONDENCE
Tao Yan
blizzardyt@163.com
Hui Zheng
zhenghui@cicams.ac.cn
Yi Fang
fangyi@cicams.ac.cn

†These authors have contributed equally to this work

RECEIVED 20 November 2024
ACCEPTED 13 January 2025
PUBLISHED 29 January 2025

CITATION
Li B, Che L, Li H, Min F, Ai B, Wu L, Wang T, Tan P, Fu B, Yang J, Fang Y, Zheng H and Yan T (2025) Peripheral blood immunoinflammatory biomarkers: prospective predictors of postoperative long-term survival and chronic postsurgical pain in breast cancer. *Front. Immunol.* 16:1531639. doi: 10.3389/fimmu.2025.1531639

COPYRIGHT
© 2025 Li, Che, Li, Min, Ai, Wu, Wang, Tan, Fu, Yang, Fang, Zheng and Yan. This is an open-access article distributed under the terms of the Creative Commons Attribution License (CC BY). The use, distribution or reproduction in other forums is permitted, provided the original author(s) and the copyright owner(s) are credited and that the original publication in this journal is cited, in accordance with accepted academic practice. No use, distribution or reproduction is permitted which does not comply with these terms.

Peripheral blood immunoinflammatory biomarkers: prospective predictors of postoperative long-term survival and chronic postsurgical pain in breast cancer

Baoli Li[1†], Li Che[2†], Huixian Li[1†], Fangdi Min[1†], Bolun Ai[3†], Linxin Wu[1†], Taihang Wang[1], Peixin Tan[1], Bingbing Fu[1], Jiashuo Yang[1], Yi Fang[3*], Hui Zheng[1*] and Tao Yan[1*]

[1]Department of Anesthesiology, National Cancer Center/National Clinical Research Center for Cancer/Cancer Hospital, Chinese Academy of Medical Sciences and Peking Union Medical College, Beijing, China, [2]Department of Cardiology, Central Hospital of Dalian University of Technology, Dalian, China, [3]Department of Breast Surgical Oncology, National Cancer Center/National Clinical Research Center for Cancer/Cancer Hospital, Chinese Academy of Medical Sciences and Peking Union Medical College, Beijing, China

Background: Tumor progression and chronic postsurgical pain (CPSP) in patients with breast cancer are both significantly influenced by inflammation. The associations between immunoinflammatory biomarkers and long-term survival, as well as CPSP, remain ambiguous. This study examined the predictive value of immunoinflammatory biomarkers for both long-term survival and CPSP.

Methods: Data on the clinicopathological characteristics and perioperative peripheral blood immunoinflammatory biomarkers of 80 patients who underwent breast cancer surgery were retrospectively collected. Optimal cut-off values for preoperative immunoinflammatory biomarkers, including the preoperative systemic immune-inflammation index (SII), systemic inflammation response index (SIRI), neutrophil-to-lymphocyte ratio (NLR), and pan-immune-inflammation value (PIV), were established via receiver operating characteristic (ROC) curves. Kaplan–Meier curves and Cox regression analysis were used to evaluate the relationships between preoperative immunoinflammatory biomarkers and long-term survival. The relationships among the perioperative neutrophil count (NEU), monocyte count (MONO), lymphocyte count (LYM), platelet count (PLT), SII, SIRI, NLR, PIV, dynamic changes in peripheral blood cell counts, and CPSP were further assessed using logistic regression analysis.

Results: Kaplan–Meier curves revealed a considerable prolongation of disease-free survival (DFS) and overall survival (OS) in the low preoperative SII, SIRI, NLR, and PIV groups. Multivariate Cox regression analysis revealed that only an elevated preoperative SIRI was an independent risk factor for postoperative DFS (HR=8.890, P=0.038). The incidence of CPSP was 28.75%. Univariate logistic regression analysis revealed that body mass index (BMI), postoperative

NEU, MONO, SIRI, and PIV were negatively correlated with the occurrence of CPSP, whereas subsequent multivariate logistic regression analysis revealed that only BMI was independently associated with CPSP (OR=0.262, P=0.023).

Conclusion: Elevated preoperative SIRI was an independent risk factor for poor DFS in breast cancer patients after surgery. In contrast, perioperative immunoinflammatory biomarkers had limited potential for predicting CPSP in patients who underwent breast cancer surgery.

KEYWORDS

breast cancer, disease-free survival, overall survival, chronic postsurgical pain, immunoinflammatory biomarkers

1 Introduction

According to the latest data released by GLOBOCAN in 2024, breast cancer topped the list of female cancers worldwide in 2022 and significantly contributed to cancer-related mortality among women globally (1). The primary treatment strategy for breast cancer focuses on early surgical surgery, frequently accompanied by adjuvant therapies, including chemotherapy, radiotherapy, and endocrine therapy. Despite advancements in treatment, tumor recurrence and metastasis remain significant challenges for patient prognosis and long-term survival (2, 3). Consequently, identifying reliable prognostic biomarkers is crucial for optimizing treatment options and enhancing patient survival.

Inflammation is intricately associated with tumor advancement and survival (4, 5). Although protective inflammation helps the immune system eliminate stimuli and reestablish homeostasis, long-term chronic inflammation can facilitate tumor progression by stimulating tumor angiogenesis, promoting immune evasion, and causing DNA damage (6). Classic inflammatory and immune cells, such as neutrophils, monocytes, lymphocytes, and platelets, are correlated with the prognosis of numerous tumors (7). Immunoinflammatory biomarkers in peripheral blood represent the condition of the overall immunoinflammatory system in humans and have been recommended as prognostic indicators for a number of malignancies (8, 9). However, there remains insufficient support from long-term studies regarding the predictive value of immunoinflammatory biomarkers for breast cancer prognosis.

Postsurgical pain is a prevalent complication following breast cancer surgery. It has been reported that as many as 68% of patients endure moderate to severe acute pain within the first 72 hours after surgery (10). A meta-analysis indicated that almost 50% of female breast cancer patients who underwent surgery may develop chronic postsurgical pain (CPSP). Among those affected, up to 50% report moderate to severe pain, which significantly compromises their quality of life and may influence their subsequent treatments (11). Inflammation is a significant cause of acute pain, and persistent inflammation-mediated peripheral and central sensitization is an essential mechanism for facilitating the chronicity of acute postoperative pain (12–14). The relationship between perioperative immunoinflammatory biomarkers and CPSP in breast cancer patients has not been extensively studied. Hence, it is essential to explore the predictive significance and potential therapeutic applications of these markers in CPSP.

Eight commonly used inflammation indicators were included in this study, including the systemic immune-inflammation index (SII), systemic inflammation response index (SIRI), neutrophil-to-lymphocyte ratio (NLR), pan-immune-inflammation value (PIV), neutrophil count (NEU), monocyte count (MONO), lymphocyte count (LYM), and platelet count (PLT). The predictive significance of immunoinflammatory biomarkers for long-term survival and CPSP in patients who underwent breast cancer surgery with approximately 8 years of regular follow-up was assessed.

2 Research materials and procedures

2.1 Research design

This study constituted a secondary analysis of breast cancer patients who had previously participated in a prospective clinical trial and received regular follow-ups for approximately eight years. This prospective study was officially recorded in the Chictr.org.cn database on August 21, 2018 (ChiCTR1800017910). The previous enrollment was from February 2016 to February 2017 at the Cancer Hospital of the Chinese Academy of Medical Sciences. The inclusion criteria for patients were as follows (1): underwent mastectomy or breast-conserving surgery along with sentinel lymph node biopsy or axillary lymph node dissection and (2) received adjuvant therapy according to the guidelines after surgery. The exclusion criteria were as follows: (1) distant metastasis at diagnosis; (2) preoperative adjuvant radiotherapy, chemotherapy, or surgery; (3) history of other malignancies; (4) concomitant hematological or autoimmune diseases; (5) concomitant acute or chronic infections; (6) concomitant severe

cardiovascular, endocrine, or neurological diseases; and (7) incomplete clinical or follow-up information.

2.2 Clinical data collection

Data regarding patient demographics and clinical characteristics, including age at surgery, body mass index (BMI), menstrual status, American Society of Anesthesiologists (ASA) classification, type of anesthesia, type of surgery, tumor size, type of tumor, TNM stage, histological grade, carcinoma cell embolus, nerve infiltration, estrogen receptor (ER), progesterone receptor (PR), human epidermal growth factor receptor 2 (HER2), Ki-67 expression, postoperative adjuvant therapies and other relevant clinical information, were extracted from the clinical electronic medical record system. Additionally, peripheral blood cell counts, including the NEU, MONO, LYM, and PLT, were obtained from the clinical laboratory within one week preceding and one week following surgery. The immunoinflammatory biomarkers of the patients were calculated using the following formulas: (1) SII=PLT×NEU/LYM; (2) SIRI=NEU×MONO/LYM; (3) NLR=NEU/LYM; and (4) PIV=NEU×MONO×PLT/LYM.

The preoperative SII, SIRI, NLR, and PIV were used in this study to evaluate the prognostic value of preoperative immunoinflammatory biomarkers for long-term survival, including disease-free survival (DFS) and overall survival (OS). Additionally, perioperative NEU, MONO, LYM, PLT, SII, SIRI, NLR, PIV, and dynamic changes in peripheral blood cell counts were utilized to explore the predictive significance of perioperative immunoinflammatory markers for CPSP.

2.3 Postoperative follow-up

The follow-up was conducted by outpatient review and telephone re-examination with a deadline of September 30, 2024. Routine follow-up occurred biannually for five years post-surgery and then annually. Recurrence or metastasis was confirmed by pathological examination following puncture/resection of the lesion or diagnostic imaging reports, including computed tomography, magnetic resonance imaging, or nuclear medicine bone scans. Information regarding the recurrence, metastasis, or death of patients was obtained from patients and their families, inpatient and outpatient records, and the local security census. CPSP was defined as (1) the emergence of postsurgical pain persisting for ≥3 months; (2) pain localized to or associated with the area of surgery, including the chest wall, axilla, or upper limb on the surgical side; and (3) the exclusion of alternate etiologies for the pain, including infection, tumor recurrence, and preexisting pain conditions (15).

2.4 Statistical analysis

SPSS 27.0 and GraphPad Prism 10.0 were used to conduct the statistical evaluations. To describe the data, quantitative parameters adhering to a normal distribution are presented as the means ± standard deviations (SDs), those deviating from a normal distribution are presented as the medians (P25, P75), and categorical variables are presented as numbers (proportions). For group comparisons, continuous variables following a normal distribution were analyzed using the Student's t-test, deviations from this norm were assessed via the Mann–Whitney U test, and qualitative variables were examined via Pearson's chi-square test or Fisher's exact test. The optimal cut-off values of preoperative immunoinflammatory biomarkers were identified by receiver operating characteristic (ROC) curves. Kaplan–Meier curves and log-rank tests were employed to evaluate the associations between immunoinflammatory biomarkers and long-term survival. Prognostic risk factors for breast cancer patients were ascertained through univariate and multivariate Cox regression analysis, whereas factors influencing CPSP were identified via univariate and multivariate logistic regression analysis. $P < 0.05$ was considered a sign of a notable statistical discrepancy.

3 Results

3.1 Clinicopathological features

The study included 80 female breast cancer patients who satisfied the selection criteria, as shown in the flowchart (Figure 1). The clinicopathological properties of the participants are presented in Table 1. Forty patients were under 50 years of age, 41 had a BMI below 22 kg/m^2, and 37 were postmenopausal. Among the patients, 48 were ASA I, 26 were ASA II, and 6 were ASA III. The surgery types included breast-conserving surgery (31 patients) and mastectomy (49 patients). The anesthesia types included total intravenous anesthesia (TIVA) for 42 patients and combined intravenous–inhalation anesthesia (CIVIA) for 38 patients. Among the tumor classifications, 3 cases were identified as carcinoma *in situ*, with the remaining 77 categorized as invasive. With respect to TNM staging, 29 patients were in stages Tis and I, whereas 51 patients were classified into stages II and III. Histological grades were distributed as follows: 9 patients were classified as grade I, 45 as grade II, and 26 as grade III. Evidence of carcinoma cell embolus was present in 24 patients, nerve infiltration in 10 patients, and lymph node metastasis in 28 patients. In terms of receptor status, 59 patients were ER-positive (ER+), 57 were PR-positive (PR+), and 17 were HER2-positive (HER2+). Postoperative interventions included chemotherapy for 63 patients, radiotherapy for 35 patients, endocrine therapy for 59 patients, and targeted therapy for 17 patients.

3.2 Optimal cut-off values of preoperative immunoinflammatory biomarkers

Given the low mortality at the end of the follow-up, which was also affected by causes of death unrelated to tumor progression, we constructed ROC curves on the basis of recurrence and metastasis, as illustrated in Figure 2. The optimal cut-off values for the preoperative SII, SIRI, NLR, and PIV, ascertained through the maximal Youden's index, were 757.00, 0.79, 2.50, and 172.33,

10.3389/fimmu.2025.1531639

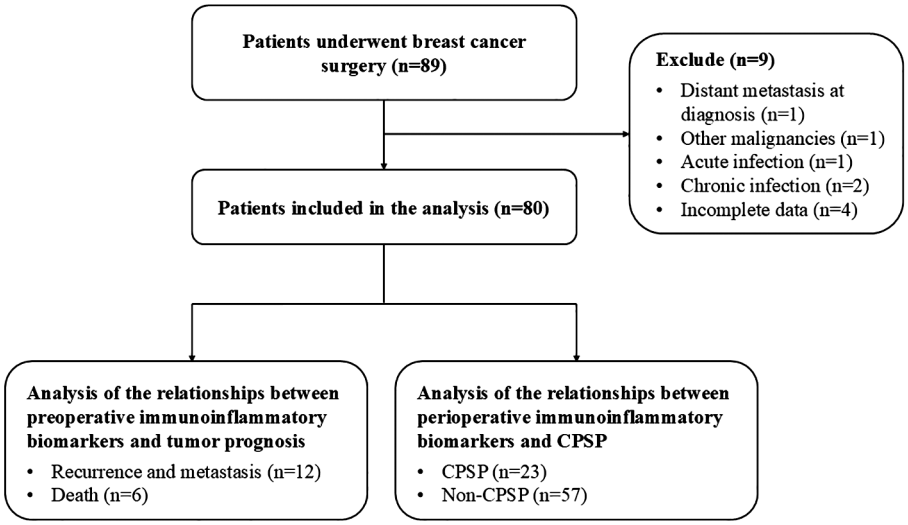

FIGURE 1
Flowchart of the study cohort. CPSP, chronic postsurgical pain.

TABLE 1 Clinicopathological features of eighty patients.

Characteristic	Number	Percentage (%)	Characteristic	Number	Percentage (%)
Total	80	100	Lymph node metastasis		
Age	49.73 ± 10.70		No	52	65.0
< 50 years	40	50.0	Yes	28	35.0
≥ 50 years	40	50.0	ER		
BMI	21.67 (20.92,22.63)		–	21	26.2
< 22 kg/m^2	41	51.2	+	59	73.8
≥ 22 kg/m^2	39	48.8	PR		
Menopausal			–	23	28.7
Premenopausal	43	53.8	+	57	71.3
Postmenopausal	37	46.2	HER2		
ASA classification			–	63	78.8
I	48	60.0	+	17	21.2
II	26	32.5	Ki-67		
III	6	7.5	≤ 20%	33	41.2
Anesthesia			> 20%	47	58.8
CIVIA	38	47.5	Postoperative chemotherapy		
TIVA	42	52.5	No	17	21.2
Surgery			Yes	63	78.8
Mastectomy	49	61.2	Postoperative radiotherapy		
Breast conserving surgery	31	38.8	No	45	56.2
Tumor size			Yes	35	43.8

(Continued)

TABLE 1 Continued

Characteristic	Number	Percentage (%)	Characteristic	Number	Percentage (%)
< 2 cm	37	46.2	Endocrine therapy		
≥ 2 cm	43	53.8	No	21	26.2
Tumor type			Yes	59	73.8
Carcinoma in situ	3	3.8	Targeted therapy		
Invasive carcinoma	77	96.2	No	63	78.8
TNM stage			Yes	17	21.2
Tis + I	29	36.3	Recurrence/Metastasis		
II + III	51	63.7	No	68	85.0
Histological grade			Yes	12	15.0
I	9	11.2	Death		
II	45	56.3	No	74	92.5
III	26	32.5	Yes	6	7.5
Carcinoma cell embolus			CPSP		
No	56	70.0	No	57	71.3
Yes	24	30.0	Yes	23	28.7
Nerve infiltration					
No	70	87.5			
Yes	10	12.5			

BMI, body mass index; ASA, American Society of Anesthesiologists; CIVIA, combined intravenous–inhalation anesthesia; TIVA, total intravenous anesthesia; TNM, tumor node metastasis; ER, estrogen receptor; PR, progesterone receptor; HER2, human epidermal growth factor receptor 2; CPSP, chronic postsurgical pain. Continuous variables are summarized as the means ± SDs or medians (P25, P75). Categorical variables are summarized as the number of subjects and percentage.

respectively, as presented in Table 2. Patients were subsequently categorized into two corresponding groups according to these cut-off values: for the SII, a low group (<757.00, N=68) and a high group (≥757.00, N=12); for the SIRI, a low group (<0.79, N=52) and a high group (≥0.79, N=28); for the NLR, a low group (<2.50, N=60) and a high group (≥2.50, N=20); and for the PIV, a low group (<172.33, N=54) and a high group (≥172.33, N=26).

3.3 Correlations between preoperative immunoinflammatory biomarkers and clinicopathological characteristics

The correlations between preoperative immunoinflammatory biomarkers and clinicopathological characteristics are shown in Table 3. The chi-square test revealed that patients classified in the high preoperative NLR group were substantially younger at the time of surgery (P=0.009) and presented a greater prevalence of premenopausal status (P=0.007). Additionally, a significant decrease in the incidence of HER2+ breast cancer patients was observed in the high preoperative PIV group compared to the low PIV group (P=0.008). No statistically significant differences were identified between the high and low preoperative SII groups regarding any clinicopathological characteristics, a finding that was consistent across the high and low preoperative SIRI groups.

3.4 Survival analysis

The median follow-up time was 94 months, ranging from 19 to 101 months. During the follow-up, 12 patients experienced recurrence or metastasis, and six patients died. The Kaplan–Meier curves indicated that elevated preoperative SII, SIRI, NLR, and PIV values were significantly associated with poor DFS and OS (P<0.05) (refer to Figure 3). Supplementary Figure 1 shows the Kaplan–Meier curves stratified by the clinicopathologic features of the patients. The results indicated that patients with high Ki-67 expression and those with positive carcinoma cell embolus had significantly shorter DFS than their counterparts with low Ki-67 expression and negative carcinoma cell embolus (P=0.012 and P=0.017, respectively). While not statistically significant, there was a trend toward decreased OS in patients with axillary sentinel lymph node metastasis (P=0.061). Analysis of additional clinicopathologic variables through Kaplan–Meier curves and log-rank tests did not reveal any statistically significant differences.

3.5 Factors affecting long-term prognosis

Cox regression analysis was conducted to explore the factors influencing DFS and OS (refer to Tables 4, 5). Univariate Cox regression analysis indicated that positive carcinoma cell embolus

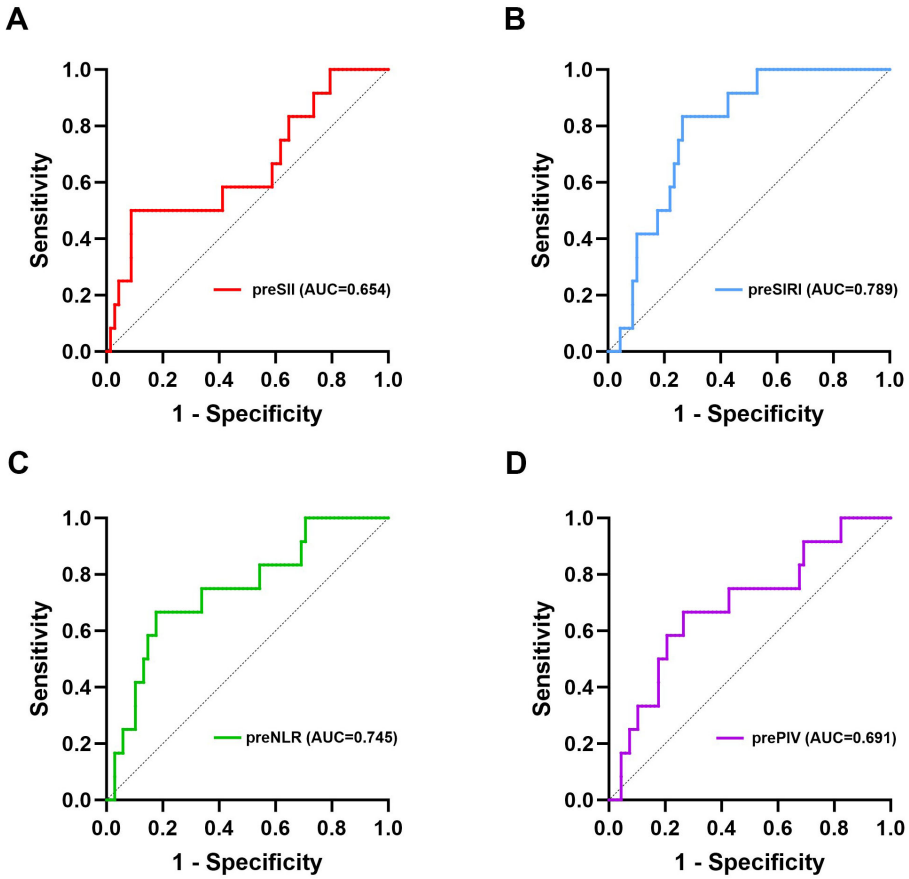

FIGURE 2
ROC curves of the preoperative SII, SIRI, NLR, and PIV for predicting long-term survival. **(A)** ROC curve of the preoperative SII for DFS; **(B)** ROC curve of the preoperative SIRI for DFS; **(C)** ROC curve of the preoperative NLR for DFS; **(D)** ROC curve of the preoperative PIV for DFS. pre, preoperative; SII, systemic immune-inflammation index; SIRI, systemic inflammation response index; NLR, neutrophil-to-lymphocyte ratio; PIV, pan-immune-inflammation value; DFS, disease-free survival.

(HR=3.677, P=0.026) and high Ki-67 expression (HR=8.820, P=0.037) were related factors for DFS. Additionally, the preoperative SII (HR=6.437, P=0.001), preoperative SIRI (HR=10.574, P=0.002), preoperative NLR (HR=6.712, P=0.002), and preoperative PIV (HR=4.398, P=0.016) were negatively associated with DFS. Notably, multivariate Cox regression analysis revealed that only an elevated preoperative SIRI was an independent risk factor for decreased DFS (HR=8.890, P=0.038). In terms of OS, univariate Cox regression analysis indicated that the preoperative SII (HR=6.168, P=0.026), preoperative NLR (HR=6.393, P=0.032), and preoperative PIV (HR=11.215, P=0.027) were negatively associated with OS. However, multivariate Cox regression analysis revealed that none of these variables independently predicted OS.

3.6 Characteristics of patients with and without CPSP

The clinicopathological characteristics associated with the presence or absence of CPSP are summarized in Table 6. The

TABLE 2 The cut-off values of the preoperative SII, SIRI, NLR, and PIV for predicting long-term survival.

Variables	AUC	95% CI	Sensitivity	Specificity	Youden's index	Cut-off value
pre SII	0.654	0.474-0.835	0.500	0.912	0.412	757.00
pre SIRI	0.789	0.681-0.897	0.833	0.735	0.568	0.79
pre NLR	0.745	0.595-0.896	0.667	0.824	0.491	2.50
pre PIV	0.691	0.527-0.855	0.667	0.735	0.402	172.33

AUC, area under the curve; CI, confidence interval; pre, preoperative; SII, systemic immune-inflammation index; SIRI, systemic inflammation response index; NLR, neutrophil-to-lymphocyte ratio; PIV, pan-immune-inflammation value.

10.3389/fimmu.2025.1531639

TABLE 3 Relationships between the preoperative SII, SIRI, NLR, and PIV and clinicopathological characteristics.

Characteristic	pre SII			pre SIRI			pre NLR			pre PIV		
	Low (%)	High (%)	*p*	Low (%)	High (%)	*p*	Low (%)	High (%)	*p*	Low (%)	High (%)	*p*
Total	68	12		52	28		60	20		54	26	
Age (years)	50.15 ± 10.74	47.33 ± 10.59	0.404	50.38 ± 10.79	48.50 ± 10.62	0.456	51.50 ± 10.38	44.40 ± 10.08	**0.009**	50.06 ± 10.95	49.04 ± 10.34	0.693
BMI			0.178			0.761			0.897			0.747
< 22 kg/m^2	37(54.4)	4(33.3)		26(50.0)	15(53.6)		31(51.7)	10(50.0)		27(50.0)	14(53.8)	
≥ 22 kg/m^2	31(45.6)	8(66.7)		26(50.0)	13(46.4)		29(48.3)	10(50.0)		27(50.0)	12(46.2)	
Menopausal			0.109			0.063			**0.007**			0.148
Premenopausal	34(50.0)	9(75.0)		24(46.2)	19(67.9)		27(45.0)	16(80.0)		26(48.1)	17(65.4)	
Postmenopausal	34(50.0)	3(25.0)		28(53.8)	9(32.1)		33(55.0)	4(20.0)		28(51.9)	9(34.6)	
ASA classification			1.000			1.000			0.656			0.931
I	41(60.3)	7(58.3)		31(59.6)	17(60.7)		34(56.7)	14(70.0)		33(61.1)	15(57.7)	
II	22(32.4)	4(33.3)		17(32.7)	9(32.1)		21(35.0)	5(25.0)		17(31.5)	9(34.6)	
III	5(7.3)	1(8.4)		4(7.7)	2(7.2)		5(8.3)	1(5.0)		4(7.4)	2(7.7)	
Anesthesia			0.661			0.121			0.438			0.579
CIVIA	33(48.5)	5(41.7)		28(53.8)	10(35.7)		30(50.0)	8(40.0)		27(50.0)	11(42.3)	
TIVA	35(51.5)	7(58.3)		24(46.2)	18(64.3)		30(50.0)	12(60.0)		27(50.0)	15(57.7)	
Surgery			1.000			0.683			0.508			0.971
Mastectomy	42(61.8)	7(58.3)		31(59.6)	18(64.3)		38(63.3)	11(55.0)		33(61.1)	16(61.5)	
Breast conserving surgery	26(38.2)	5(41.7)		21(40.4)	10(35.7)		22(36.7)	9(45.0)		21(38.9)	10(38.5)	
Tumor size			0.330			0.655			0.244			0.641
< 2 cm	33(48.5)	4(33.3)		25(48.1)	12(42.9)		30(50.0)	7(35.0)		24(44.4)	13(50.0)	
≥ 2 cm	35(51.5)	8(66.7)		27(51.9)	16(57.1)		30(50.0)	13(65.0)		30(55.6)	13(50.0)	
Tumor type			0.390			1.000			1.000			1.000
Carcinoma in situ	2(2.9)	1(8.3)		2(3.8)	1(3.6)		2(3.3)	1(5.0)		2(96.3)	1(3.8)	
Invasive carcinoma	66(97.1)	11(91.7)		50(96.2)	27(96.4)		58(96.7)	19(95.0)		52(3.7)	25(96.2)	
TNM stage			0.922			0.575			0.893			0.833
Tis + I	24(35.3)	5(41.7)		20(38.5)	9(32.1)		22(36.7)	7(35.0)		20(37.0)	9(34.6)	
II + III	44(64.7)	7(58.3)		32(61.5)	19(67.9)		38(63.3)	13(65.0)		34(63.0)	17(65.4)	
Histological grade			0.356			0.588			0.368			0.941
I	7(10.3)	2(16.7)		7(13.5)	2(7.1)		6(10.0)	3(15.0)		6(11.1)	3(11.5)	
II	37(54.4)	8(66.6)		27(51.9)	18(64.3)		32(53.3)	13(65.0)		31(57.4)	14(53.8)	
III	24(35.3)	2(16.7)		18(34.6)	8(28.6)		22(36.7)	4(20.0)		17(31.5)	9(34.7)	
Carcinoma cell embolus			0.539			0.413			0.091			0.917
No	49(72.1)	7(58.3)		38(73.1)	18(64.3)		45(75.0)	11(55.0)		38(70.4)	18(69.2)	
Yes	19(27.9)	5(41.7)		14(26.9)	10(35.7)		15(25.0)	9(45.0)		16(29.6)	8(30.8)	
Nerve infiltration			0.058			1.000			0.435			0.367

(Continued)

TABLE 3 Continued

Characteristic	pre SII			pre SIRI			pre NLR			pre PIV		
	Low (%)	High (%)	*p*	Low (%)	High (%)	*p*	Low (%)	High (%)	*p*	Low (%)	High (%)	*p*
No	62(91.2)	8(66.7)		46(88.5)	24(85.7)		54(90.0)	16(80.0)		49(90.7)	21(80.8)	
Yes	6(8.8)	4(33.3)		6(11.5)	4(14.3)		6(10.0)	4(20.0)		5(9.3)	5(19.2)	
Lymph node metastasis			0.646			0.694			1.000			0.293
No	43(63.2)	9(75.0)		33(63.5)	19(67.9)		39(65.0)	13(65.0)		33(61.1)	19(73.1)	
Yes	25(36.8)	3(25.0)		19(36.5)	9(32.1)		21(35.0)	7(35.0)		21(38.9)	7(26.9)	
ER			0.240			0.211			0.187			0.654
–	20(29.4)	1(8.3)		16(30.8)	5(17.9)		18(30.0)	3(15.0)		15(27.8)	6(23.1)	
+	48(70.6)	11(91.7)		36(69.2)	23(82.1)		42(70.0)	17(85.0)		39(72.2)	20(76.9)	
PR			0.177			0.114			0.117			0.437
–	22(32.4)	1(8.3)		18(34.6)	5(17.9)		20(33.3)	3(15.0)		17(31.5)	6(23.1)	
+	46(67.6)	11(91.7)		34(65.4)	23(82.1)		40(66.7)	17(85.0)		37(68.5)	20(76.9)	
HER2			0.422			0.264			1.000			**0.008**
–	52(76.5)	11(91.7)		39(75.0)	24(85.7)		47(78.3)	16(80.0)		38(70.4)	25(96.2)	
+	16(23.5)	1(8.3)		13(25.0)	4(14.3)		13(21.7)	4(20.0)		16(29.6)	1(3.8)	
Ki-67			0.775			0.091			0.088			0.725
≤ 20%	29(42.6)	4(33.3)		25(48.1)	8(28.6)		28(46.7)	5(25.0)		23(42.6)	10(38.5)	
> 20%	39(57.4)	8(66.7)		27(51.9)	20(71.4)		32(53.3)	15(75.0)		31(57.4)	16(61.5)	

pre, preoperative; SII, systemic immune-inflammation index; SIRI, systemic inflammation response index; NLR, neutrophil-to-lymphocyte ratio; PIV, pan-immune-inflammation value; BMI, body mass index; ASA, American Society of Anesthesiologists; CIVIA, combined intravenous–inhalation anesthesia; TIVA, total intravenous anesthesia; TNM, tumor node metastasis; ER, estrogen receptor; PR, progesterone receptor; HER2, human epidermal growth factor receptor 2. Continuous variables are summarized as the means ± SDs or medians (P25, P75). Categorical variables are summarized as the number of subjects and percentage. The values in bold represent P <0.05.

incidence of CPSP was 28.75%. The chi-square test results indicated that the CPSP group presented a greater percentage of patients with a BMI <22 kg/m² (P=0.010). Patients in the CPSP group demonstrated lower levels of postoperative NEU (P=0.004), postoperative MONO (P=0.014), and postoperative SIRI (P=0.021) than those in the non-CPSP group. Additionally, as indicated in Supplementary Table 1, we conducted an analysis of the relationship between CPSP and dynamic changes in peripheral blood cell counts, including the differences and ratios between the postoperative and preoperative levels of each cell type. The results indicated that patients in the CPSP group exhibited a smaller change in NEU (calculated as the postoperative NEU minus the preoperative NEU) (P=0.026). Other characteristics, such as age at surgery, menstrual status, type of anesthesia, type of surgery, and preoperative immunoinflammatory markers, did not significantly correlate with the occurrence of CPSP.

3.7 Factors affecting CPSP

This study investigated the factors affecting CPSP using logistic regression models (refer to Table 7). Univariate logistic regression analysis revealed several factors associated with CPSP, including BMI (OR=0.257, P=0.013), postoperative NEU (OR=0.739, P=0.013), postoperative MONO (OR=0.025, P=0.020), postoperative SIRI (OR=0.757, P=0.017), and postoperative PIV (OR=0.999, P=0.035). However, dynamic changes in any peripheral blood cell count were not found to be correlated with CPSP, as detailed in Supplementary Table 2. Although not statistically significant, the change in NEU (calculated as the postoperative NEU minus the preoperative NEU) appeared to influence CPSP (P=0.051). According to the results of multivariate logistic regression analysis, BMI (OR=0.262, P=0.023) was independently associated with CPSP. Specifically, patients with a BMI <22 kg/m^2 were found to be at a greater risk of developing CPSP than those with a BMI ≥22 kg/m^2.

4 Discussion

Breast cancer remains a leading cause of morbidity and mortality among women globally. Established prognostic biomarkers, such as TNM stage, histologic grade, and molecular markers in tumor pathology, including ER, PR, HER2, and Ki-67, have received extensive clinical attention. However, the complexity of testing methodologies, high costs, and time demands

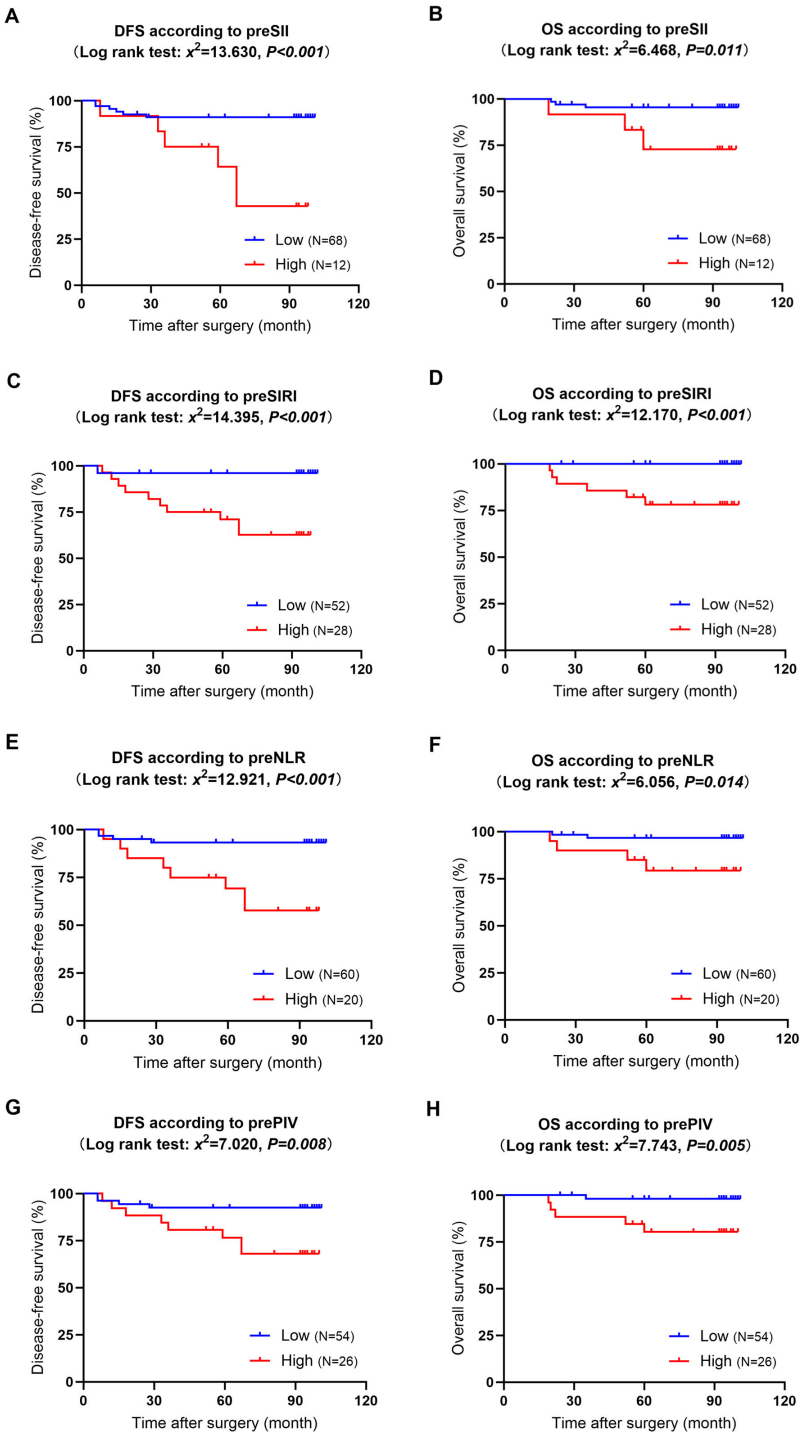

FIGURE 3
Kaplan–Meier curves and log-rank tests for the relationships between preoperative immunoinflammatory biomarkers and long-term survival. **(A)**: DFS in patients with high versus low preoperative SII; **(B)**: OS in patients with high versus low preoperative SII; **(C)**: DFS in patients with high versus low preoperative SIRI; **(D)**: OS in patients with high versus low preoperative SIRI; **(E)**: DFS in patients with high versus low preoperative NLR; **(F)**: OS in patients with high versus low preoperative NLR; **(G)**: DFS in patients with high versus low preoperative PIV;**(H)**: OS in patients with high versus low preoperative PIV. DFS, disease-free survival; OS, overall survival; pre, preoperative; SII, systemic immune-inflammation index; SIRI, systemic inflammation response index; NLR, neutrophil-to-lymphocyte ratio; PIV, pan-immune-inflammation value.

considerably limit their clinical applications, particularly for patients diagnosed with early-stage breast cancer (16–18).

Inflammation plays a vital role in tumor progression (19, 20). Chronic inflammation has been shown to accelerate tumor proliferation, facilitate angiogenesis, and promote tumor metastasis, all of which are closely associated with the prognosis of breast cancer patients (21). Notably, peripheral blood immunoinflammatory biomarkers can not only reflect systemic

10.3389/fimmu.2025.1531639

TABLE 4 Univariate and multivariate Cox regression analysis for DFS.

Characteristic	Univariate analysis			Multivariate analysis		
	HR	95% CI	*P*	HR	95% CI	*P*
Carcinoma cell embolus						
No	1			1		
Yes	3.677	1.166-11.595	**0.026**	3.203	0.980-10.466	0.054
Ki-67						
≤ 20%	1			1		
> 20%	8.820	1.138-68.355	**0.037**	6.693	0.826-54.220	0.075
pre SII						
< 757.00	1			1		
≥ 757.00	6.437	2.064-20.077	**0.001**	2.552	0.435-14.969	0.299
pre SIRI						
< 0.79	1			1		
≥ 0.79	10.574	2.312-48.370	**0.002**	8.890	1.123-70.350	**0.038**
pre NLR						
< 2.50	1			1		
≥ 2.50	6.712	2.016-22.346	**0.002**	0.847	0.111-6.487	0.873
pre PIV						
< 172.33	1			1		
≥ 172.33	4.398	1.323-14.617	**0.016**	0.565	0.073-4.375	0.585

HR, hazard ratio; CI, confidence interval; SII, systemic immune-inflammation index; SIRI, systemic inflammation response index; NLR, neutrophil-to-lymphocyte ratio; PIV, pan-immune-inflammation value. The values in bold represent P <0.05.

immunoinflammatory conditions but also provide advantages in terms of simplicity, cost-effectiveness, and dependability, making them valuable for predicting survival in breast cancer patients. Nevertheless, the specific relationships between these immunoinflammatory biomarkers and the long-term survival of breast cancer patients remain largely unexplored.

This study investigated the predictive significance of preoperative immunoinflammatory biomarkers for the long-term survival of patients who participated in a previous clinical trial and underwent breast cancer surgery, with regular follow-ups lasting approximately eight years. The Kaplan–Meier curves indicated that patients with elevated preoperative NLR, SII, SIRI, and PIV values

TABLE 5 Univariate and multivariate Cox regression analysis for OS.

Characteristic	Univariate analysis			Multivariate analysis		
	HR	95% CI	*P*	HR	95% CI	*P*
pre SII						
< 757.00	1			1		
≥ 757.00	6.168	1.242-30.628	**0.026**	1.149	0.116-11.386	0.905
pre NLR						
< 2.50	1			1		
≥ 2.50	6.393	1.170-34.932	**0.032**	2.014	0.164-24.678	0.584
pre PIV						
< 172.33	1			1		
≥ 172.33	11.215	1.310-96.039	**0.027**	6.928	0.566-84.845	0.130

HR, hazard ratio; CI, confidence interval; SII, systemic immune-inflammation index; NLR, neutrophil-to-lymphocyte ratio; PIV, pan-immune-inflammation value. The values in bold represent P <0.05.

TABLE 6 Characteristics of patients with and without CPSP.

Characteristic	Non-CPSP (N=57)	CPSP (N=23)	*P*	Characteristic	Non-CPSP (N=57)	CPSP (N=23)	*P*
Age (years)	48.77 ± 10.64	52.09 ± 10.72	0.212	**Nerve infiltration**			0.076
BMI			**0.010**	No	47(82.5)	23(100.0)	
< 22 kg/m^2	24(42.1)	17(73.9)		Yes	10(17.5)	0(0.0)	
≥ 22 kg/m^2	33(57.9)	6(26.1)		**Lymph node metastasis**			0.979
Menopausal			0.500	No	37(64.9)	15(65.2)	
Premenopausal	32(56.1)	11(47.8)		Yes	20(35.1)	8(34.8)	
Postmenopausal	25(43.9)	12(52.2)		**Postoperative chemotherapy**			0.815
ASA classification			0.627	No	13(22.8)	4(17.4)	
I	36(63.2)	12(52.2)		Yes	44(77.2)	19(82.6)	
II	17(29.8)	9(39.1)		**Postoperative radiotherapy**			0.975
III	4(7.0)	2(8.7)		No	32(56.1)	13(56.5)	
Anesthesia			0.595	Yes	25(43.9)	10(43.5)	
CIVIA	26(45.6)	12(52.2)		**Endocrine therapy**			0.983
TIVA	31(54.4)	11(47.8)		No	15(26.3)	6(26.1)	
Surgery			0.117	Yes	42(73.7)	17(73.9)	
Mastectomy	38(66.7)	11(47.8)		**Targeted therapy**			0.330
Breast conserving surgery	19(33.3)	12(52.2)		No	47(82.5)	16(69.6)	
Tumor size			0.096	Yes	10(17.5)	7(30.4)	
< 2 cm	23(40.4)	14(60.9)		**pre NEU (×10^9/L)**	3.40(3.09,4.17)	3.08(2.82,3.73)	0.088
≥ 2 cm	34(59.6)	9(39.1)		**pre MONO (×10^9/L)**	0.39(0.30,0.49)	0.34(0.30,0.43)	0.292
Tumor type			1.000	**pre LYM (×10^9/L)**	1.82(1.36,2.33)	1.78(1.61,2.33)	0.774
Carcinoma in situ	2(3.5)	1(4.3)		**pre PLT (×10^9/L)**	235.00(203.00,267.00)	240.00(218.50,266.50)	0.636
Invasive carcinoma	55(96.5)	22(95.7)		**pre SII**	437.88(278.78,667.43)	416.43(309.37,509.02)	0.675
TNM stage			0.393	**pre SIRI**	0.70(0.49,1.14)	0.60(0.41,0.74)	0.169
Tis + I	19(33.3)	10(43.5)		**pre NLR**	2.04(1.34,2.71)	1.72(1.32,2.14)	0.197
II + III	38(66.7)	13(56.5)		**pre PIV**	153.86(105.07,249.26)	154.08(120.81,165.04)	0.473
Histological grade			0.329	**post NEU (×10^9/L)**	7.50(5.76,8.88)	6.04(5.08,6.89)	**0.004**

(Continued)

10.3389/fimmu.2025.1531639

10.3389/fimmu.2025.1531639

TABLE 6 Continued

Characteristic	Non-CPSP (N=57)	CPSP (N=23)	*P*	Characteristic	Non-CPSP (N=57)	CPSP (N=23)	*P*
I	6(10.5)	3(13.0)		**post MONO ($\times10^9$/L)**	0.63(0.49,0.71)	0.48(0.41,0.55)	**0.014**
II	35(61.4)	10(43.5)		**post LYM ($\times10^9$/L)**	0.88(0.62,1.35)	0.93(0.66,1.31)	0.898
III	16(28.1)	10(43.5)		**post PLT ($\times10^9$/L)**	227.00(181.00,262.00)	236.00(210.00,255.00)	0.702
Carcinoma cell embolus			0.628	**post SII**	1808.74(1095.64,2479.03)	1378.67(1138.47,2175.72)	0.262
No	39(68.4)	17(73.9)		**post SIRI**	4.51(3.24,8.15)	3.50(2.34,4.64)	**0.021**
Yes	18(31.6)	6(26.1)		**post NLR**	8.41(5.36,11.90)	6.53(4.41,9.20)	0.138
				post PIV	993.55((598.17,1777.21)	912.47(549.45,1063.33)	0.055

CPSP, chronic postsurgical pain; BMI, body mass index; ASA, American Society of Anesthesiologists; CIVIA, combined intravenous–inhalation anesthesia; TIVA, total intravenous anesthesia; TNM, tumor node metastasis; ER, estrogen receptor; PR, progesterone receptor; HER2, human epidermal growth factor receptor 2; pre, preoperative; post, postoperative; NEU, neutrophil count; MONO, monocyte count; LYM, lymphocyte count; PLT, platelet count; SII, systemic immune-inflammation index; SIRI, systemic inflammation response index; NLR, neutrophil-to-lymphocyte ratio; PIV, pan-immune-inflammation value. Continuous variables are summarized as the means ± SDs or medians (P25, P75). Categorical variables are summarized as the number of subjects and percentage. The values in bold represent P <0.05.

had significantly decreased DFS and OS. This finding aligns with the literature, suggesting that elevated immunoinflammatory biomarkers are associated with poorer survival across various malignancies (22–30).

Recent studies have reported that the NLR is a more reliable marker of systemic immunological status than inflammatory cell counts alone, effectively predicting outcomes in various solid tumors, especially breast cancer (31). A meta-analysis encompassing 31 studies explored the relationship between the preoperative NLR and the prognosis of operable breast cancer patients, confirming a significant association between an elevated preoperative NLR and increased rates of ER+ tumors, as well as shorter DFS and OS (8). Two clinical trials focusing on Asian breast cancer patients, which used NLR cut-off values of 2.57 and 2.50, corroborated the finding that an elevated NLR correlates with a worse prognosis, even in patients with triple-negative and luminal A breast cancer subtypes (32, 33). The SII, derived from peripheral blood neutrophils, platelets, and lymphocytes, provides a comprehensive overview of immunological and inflammatory conditions. A meta-analysis involving 2,642 breast cancer patients from eight studies demonstrated that those with an elevated SII experienced poorer survival (34). According to a study utilizing 758.0 as a cut-off value, a lower SII was linked to improved survival in patients with HER2+ metastatic breast cancer receiving chemotherapy in combination with trastuzumab (35). The SIRI, which integrates peripheral blood monocyte, neutrophil, and lymphocyte counts, has emerged as a robust prognostic marker associated with adverse outcomes across multiple malignancies. Zhu et al. demonstrated that the SIRI serves as an independent prognostic factor for breast cancer patients, with an optimal cut-off value of 0.80, which closely matches the cut-off value of 0.79 established in this study (36). A meta-analysis encompassing eight trials with a total of 2997 patients confirmed that an elevated SIRI is associated with a larger tumor size, more advanced stages, and worse OS (37). The PIV has been recognized as a promising prognostic biomarker across various malignancies based on combinations of peripheral blood neutrophils, monocytes, platelets, and lymphocytes (38). Previous studies have indicated that breast cancer patients with lower preoperative PIV tend to show better responses to neoadjuvant chemotherapy and experience longer DFS and OS (39, 40). Although variability exists in PIV cut-off values across studies, recent investigations have consistently supported its prognostic relevance in breast cancer (41–43). This variability may be attributable to the early stage of PIV research and the small number of studies.

Notably, the univariate Cox regression analysis conducted in this study identified several predictors of DFS, including both preoperative immunoinflammatory markers and tumor characteristics such as carcinoma cell emboli and Ki-67 expression. These findings underscore the importance of breast cancer tumor pathology in prognostic assessments. According to the multivariate Cox regression analysis, compared to the other three immunoinflammatory biomarkers, only an elevated preoperative SIRI emerged as an independent risk factor for decreased DFS. This finding aligns with previous research that indicated the lack of independence of the preoperative NLR as a

TABLE 7 Univariate and multivariate logistic regression analysis for CPSP.

Characteristic	Univariate analysis			Multivariate analysis		
	OR	95% CI	*P*	OR	95% CI	*P*
BMI						
< 22 kg/m^2	1			1		
≥ 22 kg/m^2	0.257	0.088-0.748	**0.013**	0.262	0.082-0.833	**0.023**
post NEU (×10^9/L)	0.739	0.582-0.938	**0.013**	0.823	0.599-1.130	0.228
post MONO (×10^9/L)	0.025	0.001-0.562	**0.020**	0.146	0.004-5.537	0.299
post SIRI	0.757	0.602-0.952	**0.017**	0.762	0.444-1.307	0.324
post PIV	0.999	0.998-1.000	**0.035**	1.001	0.999-1.003	0.495

CPSP, chronic postsurgical pain; OR, odds ratio; CI, confidence interval; BMI, body mass index; post, postoperative; NEU, neutrophil count; MONO, monocyte count; SIRI, systemic inflammation response index; PIV, pan-immune-inflammation value. The values in bold represent P <0.05.

prognostic biomarker, particularly in specific subtypes, such as ER+ HER2- early breast cancer, where other clinical prognostic factors may exert a significant influence (44, 45). In conclusion, identifying preoperative immunoinflammatory biomarkers as predictive tools facilitates the improvement of patient stratification and management strategies. For example, clinicians may consider adopting a more aggressive adjuvant treatment and follow-up strategy for patients exhibiting elevated preoperative SIRI, potentially involving early comprehensive adjuvant therapy, enhanced recurrence surveillance, or additional imaging.

This study further investigated the correlation between perioperative immunoinflammatory markers and CPSP. Univariate logistic regression analysis demonstrated that postoperative NEU, MONO, SIRI, and PIV were significantly correlated with CPSP, indicating that these immunoinflammatory markers may reflect the underlying inflammatory processes contributing to chronic pain. The current literature theoretically supports this observation by highlighting the significant role of inflammation in postoperative pain. The influence of inflammation on acute pain is attributed primarily to the extensive activation of immunoinflammatory cells and the subsequent release of several proinflammatory cytokines induced by surgical tissue injury (12, 46). The continuous release of inflammatory mediators progressively activates microglia, increasing neuronal sensitivity and ultimately leading to central sensitization (47, 48). Notable inflammatory mediators, including prostaglandins and substance P, intensify nociceptive signaling and substantially affect the modulation of both central and peripheral pain pathways (49, 50). Consequently, the peripheral and central sensitization induced by chronic inflammation collectively contributes to the transition from acute postoperative pain to CPSP (13, 14).

The interaction between immunoinflammatory cells and the central nervous system in the modulation of pain underscores the importance of further exploration of the connections between immunoinflammatory biomarkers and CPSP. Regrettably, relevant clinical studies are exceedingly scarce. A single retrospective study evaluated the relationship between CPSP and peripheral blood immunoinflammatory markers in a cohort of 968 individuals following abdominal surgery. This study revealed that preoperative NEU and the changed ratio of NLR were significantly associated with CPSP. Patients in the group with a changed ratio of NLR ≥5 presented a greater incidence of CPSP, an elevated maximum numeric rating scale score post-discharge, an increased prevalence of moderate-to-severe pain, and a more significant impact on quality of life (51). These findings indicate that the care pathways for breast cancer patients should incorporate systematic assessments of immunoinflammatory status and the identification of potential CPSP alongside the implementation of individualized pain management strategies.

Importantly, the subsequent multivariate logistic regression analysis in this study indicated that only BMI independently correlated with CPSP. Although numerous studies have suggested that a high BMI may serve as an independent risk factor for CPSP, considerable high-quality evidence suggests a lack of association between BMI and CPSP, highlighting the complexity of this condition (52–56). Our results indicated that patients with a BMI <22 kg/m^2 may be at increased risk for developing CPSP. This association may be influenced by the selection criteria for grouping, the limited sample size, and the heterogeneity among studies. In summary, our findings reveal the limited ability of perioperative immunoinflammatory markers to predict CPSP, indicating the influence of additional physiological, psychological, and sociobiological factors on pain outcomes. Therefore, a more comprehensive approach is essential when studying CPSP in breast cancer patients. This approach should evaluate not only immunoinflammatory markers but also physical health, psychological status, and pain history.

While our findings clarify the predictive significance of immunoinflammatory markers for long-term survival and CPSP, it is essential to acknowledge certain limitations. First, the limited sample size may limit the generalizability of our results. Second, the immunoinflammatory biomarker data were obtained from a single center, which may introduce potential biases related to demographic factors such as sex, race, and geographic variations. Finally, patient-specific factors, including preoperative physical condition, psychological status, and perioperative medication regimens, may also impact the incidence of CPSP. Nevertheless, our study offers notable strengths that enhance its contribution to

the literature. We conducted regular follow-ups with participants originating from a previous prospective clinical trial over approximately eight years, resulting in reliable data on prognosis outcomes that significantly inform our findings. Moving forward, there is an urgent need for prospective multicenter studies that include larger participant cohorts, comprehensive evaluations of various clinical variables, and more detailed subgroup analysis, especially regarding tumor pathology. Such efforts will deepen our understanding of this promising area of research.

5 Conclusion

In summary, this study highlights the predictive significance of preoperative immunoinflammatory biomarkers for long-term survival in patients who underwent breast cancer surgery. The finding that an elevated preoperative SIRI serves as an independent risk factor for DFS emphasizes the necessity of integrating inflammatory evaluation into clinical practice. The correlation between perioperative immunoinflammatory biomarkers and CPSP warrants further investigation to elucidate the intricacies of postoperative pain. Integrating a comprehensive understanding of inflammation, tumors, and pain will help to enhance individualized medical strategies, resulting in improved outcomes and quality of life for breast cancer patients.

Data availability statement

The original contributions presented in the study are included in the article/Supplementary Material. Further inquiries can be directed to the corresponding authors.

Ethics statement

The studies involving humans were approved by the Ethics Committee of the Cancer Hospital of the Chinese Academy of Medical Sciences. The studies were conducted in accordance with the local legislation and institutional requirements. The participants provided their written informed consent to participate in this study.

Author contributions

BL: Data curation, Formal analysis, Methodology, Software, Visualization, Writing – original draft, Writing – review & editing. LC: Methodology, Formal analysis, Visualization, Writing – review & editing. HL: Methodology, Software, Validation, Writing – review & editing. FM: Data curation, Investigation, Methodology, Writing – review & editing. BA: Investigation, Methodology, Software, Writing – review & editing. LW: Data curation, Methodology, Software, Writing – review & editing. TW: Investigation, Software, Validation, Writing – review & editing. PT: Data curation, Investigation, Writing – review & editing. BF: Investigation, Validation, Writing – review & editing. JY: Investigation, Validation, Writing – review & editing. YF: Project administration, Supervision, Writing – review & editing. HZ: Conceptualization, Funding acquisition, Project administration, Supervision, Writing – review & editing. TY: Conceptualization, Funding acquisition, Project administration, Supervision, Writing – review & editing.

Funding

The author(s) declare financial support was received for the research, authorship, and/or publication of this article. Support for this work was received from the Beijing Hope Run Special Fund of the Cancer Foundation of China (LC2021A18, LC2022B06), the National Natural Science Foundation of China (82073327), and the Bethune Charitable Foundation (BCF, kqxs-2024-A-02).

Acknowledgments

We thank the enrolled breast cancer patients and all the medical staff in our study.

Conflict of interest

The authors declare that the research was conducted in the absence of any commercial or financial relationships that could be construed as a potential conflict of interest.

Generative AI statement

The author(s) declare that no Generative AI was used in the creation of this manuscript.

Publisher's note

All claims expressed in this article are solely those of the authors and do not necessarily represent those of their affiliated organizations, or those of the publisher, the editors and the reviewers. Any product that may be evaluated in this article, or claim that may be made by its manufacturer, is not guaranteed or endorsed by the publisher.

Supplementary material

The Supplementary Material for this article can be found online at: https://www.frontiersin.org/articles/10.3389/fimmu.2025.1531639/full#supplementary-material

References

1. Bray F, Laversanne M, Sung H, Ferlay J, Siegel RL, Soerjomataram I, et al. Global cancer statistics 2022: GLOBOCAN estimates of incidence and mortality worldwide for 36 cancers in 185 countries. *CA Cancer J Clin*. (2024) 74:229–63. doi: 10.3322/caac.21834

2. Hong R, Xu B. Breast cancer: an up-to-date review and future perspectives. *Cancer Commun (Lond)*. (2022) 42:913–36. doi: 10.1002/cac2.12358

3. Liang Y, Zhang H, Song X, Yang Q. Metastatic heterogeneity of breast cancer: Molecular mechanism and potential therapeutic targets. *Semin Cancer Biol*. (2020) 60:14–27. doi: 10.1016/j.semcancer.2019.08.012

4. Zhao H, Wu L, Yan G, Chen Y, Zhou M, Wu Y, et al. Inflammation and tumor progression: signaling pathways and targeted intervention. *Signal Transduct Target Ther*. (2021) 6:263. doi: 10.1038/s41392-021-00658-5

5. Diakos CI, Charles KA, McMillan DC, Clarke SJ. Cancer-related inflammation and treatment effectiveness. *Lancet Oncol*. (2014) 15:e493–503. doi: 10.1016/S1470-2045(14)70263-3

6. Greten FR, Grivennikov SI. Inflammation and cancer: triggers, mechanisms, and consequences. *Immunity*. (2019) 51:27–41. doi: 10.1016/j.immuni.2019.06.025

7. Galdiero MR, Marone G, Mantovani A. Cancer inflammation and cytokines. *Cold Spring Harb Perspect Biol*. (2018) 10:a028662. doi: 10.1101/cshperspect.a028662

8. Savioli F, Morrow ES, Dolan RD, Romics L, Lannigan A, Edwards J, et al. Prognostic role of preoperative circulating systemic inflammatory response markers in primary breast cancer: meta-analysis. *Br J Surg* (2022) 109(12):1206–15. doi: 10.1093/bjs/znac319

9. Bian Z, Xu L, Wang Y, Tsai M-K, Chu DT-W, Tu H, et al. Association of the systemic inflammation and anthropometric measurements with cancer risk: a prospective study in MJ cohort. *Front Oncol*. (2024) 14:1400893. doi: 10.3389/fonc.2024.1400893

10. Habib AS, Kertai MD, Cooter M, Greenup RA, Hwang S. Risk factors for severe acute pain and persistent pain after surgery for breast cancer: a prospective observational study. *Reg Anesth Pain Med*. (2019) 44:192–99. doi: 10.1136/rapm-2018-000040

11. Wang L, Cohen JC, Devasenapathy N, Hong BY, Kheyson S, Lu D, et al. Prevalence and intensity of persistent post-surgical pain following breast cancer surgery: a systematic review and meta-analysis of observational studies. *Br J Anaesth*. (2020) 125:346–57. doi: 10.1016/j.bja.2020.04.088

12. Margraf A, Ludwig N, Zarbock A, Rossaint J. Systemic inflammatory response syndrome after surgery: mechanisms and protection. *Anesth Analg*. (2020) 131:1693–707. doi: 10.1213/ANE.0000000000005175

13. Richebé P, Capdevila X, Rivat C. Persistent postsurgical pain: pathophysiology and preventative pharmacologic considerations. *Anesthesiology*. (2018) 129:590–607. doi: 10.1097/ALN.0000000000002238

14. Pak DJ, Yong RJ, Kaye AD, Urman RD. Chronification of pain: mechanisms, current understanding, and clinical implications. *Curr Pain Headache Rep*. (2018) 22 (2):9. doi: 10.1007/s11916-018-0666-8

15. Schug SA, Lavand'homme P, Barke A, Korwisi B, Rief W, Treede R-D. The IASP classification of chronic pain for ICD-11: chronic postsurgical or posttraumatic pain. *Pain*. (2019) 160:45–52. doi: 10.1097/j.pain.0000000000001413

16. Sestak I, Buus R, Cuzick J, Dubsky P, Kronenwett R, Denkert C, et al. Comparison of the performance of 6 prognostic signatures for estrogen receptor-positive breast cancer: A secondary analysis of a randomized clinical trial. *JAMA Oncol*. (2018) 4:545–53. doi: 10.1001/jamaoncol.2017.5524

17. Sparano JA, Gray RJ, Ravdin PM, Makower DF, Pritchard KI, Albain KS, et al. Clinical and genomic risk to guide the use of adjuvant therapy for breast cancer. *N Engl J Med*. (2019) 380:2395–405. doi: 10.1056/NEJMoa1904819

18. Tarighati E, Keivan H, Mahani H. A review of prognostic and predictive biomarkers in breast cancer. *Clin Exp Med*. (2023) 23:1-16. doi: 10.1007/s10238-021-00781-1

19. Grivennikov SI, Greten FR, Karin M. Immunity, inflammation, and cancer. *Cell*. (2010) 140:883–99. doi: 10.1016/j.cell.2010.01.025

20. Maiorino L, Daßler-Plenker J, Sun L, Egeblad M. Innate immunity and cancer pathophysiology. *Annu Rev Pathol*. (2022) 17:425–57. doi: 10.1146/annurev-pathmechdis-032221-115501

21. Faria SS, Costantini S, de Lima VCC, de Andrade VP, Rialland M, Cedric R, et al. NLRP3 inflammasome-mediated cytokine production and pyroptosis cell death in breast cancer. *J BioMed Sci*. (2021) 28(1):26. doi: 10.1186/s12929-021-00724-8

22. Feier CVI, Muntean C, Faur AM, Gaborean V, Petrache IA, Cozma GV. Exploring inflammatory parameters in lung cancer patients: A retrospective analysis. *J Pers Med*. (2024) 14:552. doi: 10.3390/jpm14060552

23. Meng L, Yang Y, Hu X, Zhang R, Li X. Prognostic value of the pretreatment systemic immune-inflammation index in patients with prostate cancer: a systematic review and meta-analysis. *J Transl Med*. (2023) 21:79. doi: 10.1186/s12967-023-03924-y

24. Topkan E, Selek U, Kucuk A, Pehlivan B. Low pre-chemoradiotherapyPan-immune-inflammation value (PIV) measures predict better survival outcomes in locally advanced pancreatic adenocarcinomas. *J Inflammation Res*. (2022) 15:5413–23. doi: 10.2147/JIR.S385328

25. Yang X-C, Liu H, Liu D-C, Tong C, Liang X-W, Chen R-H. Prognostic value of pan-immune-inflammation value in colorectal cancer patients: A systematic review and meta-analysis. *Front Oncol*. (2022) 12:1036890. doi: 10.3389/fonc.2022.1036890

26. Fucà G, Guarini V, Antoniotti C, Morano F, Moretto R, Corallo S, et al. The Pan-Immune-Inflammation Value is a new prognostic biomarker in metastatic colorectal cancer: results from a pooled-analysis of the Valentino and TRIBE first-line trials. *Br J Cancer*. (2020) 123:403–09. doi: 10.1038/s41416-020-0894-7

27. Huang Y, Gao Y, Wu Y, Lin H. Prognostic value of systemic immune-inflammation index in patients with urologic cancers: a meta-analysis. *Cancer Cell Int*. (2020) 20:499. doi: 10.1186/s12935-020-01590-4

28. Mao H, Yang F. Prognostic significance of systemic immune-inflammation index in patients with ovarian cancer: a meta-analysis. *Front Oncol*. (2023) 13:1193962. doi: 10.3389/fonc.2023.1193962

29. Zheng J, Peng L, Zhang S, Liao H, Hao J, Wu S, et al. Preoperative systemic immune-inflammation index as a prognostic indicator for patients with urothelial carcinoma. *Front Immunol*. (2023) 14:1275033. doi: 10.3389/fimmu.2023.1275033

30. Yan S, Gong X, Liu R, Jia X. Prognostic significance of systemic pan-immune-inflammation value in locally advanced cervical cancer. *Front Oncol*. (2024) 14:1492251. doi: 10.3389/fonc.2024.1492251

31. Templeton AJ, McNamara MG, Šeruga B, Vera-Badillo FE, Aneja P, Ocaña A, et al. Prognostic role of neutrophil-to-lymphocyte ratio in solid tumors: a systematic review and meta-analysis. *J Natl Cancer Inst*. (2014) 106:dju124. doi: 10.1093/jnci/dju124

32. Yao M, Liu Y, Jin H, Liu X, Lv K, Wei H, et al. Prognostic value of preoperative inflammatory markers in Chinese patients with breast cancer. *Onco Targets Ther*. (2014) 7:1743–52. doi: 10.2147/OTT.S69657

33. Noh H, Eomm M, Han A. Usefulness of pretreatment neutrophil to lymphocyte ratio in predicting disease-specific survival in breast cancer patients. *J Breast Cancer*. (2013) 16:55–9. doi: 10.4048/jbc.2013.16.1.55

34. Zhang Y, Sun Y, Zhang Q. Prognostic value of the systemic immune-inflammation index in patients with breast cancer: a meta-analysis. *Cancer Cell Int*. (2020) 20:224. doi: 10.1186/s12935-020-01308-6

35. Pang J, Ding N, Liu X, He X, Zhou W, Xie H, et al. Prognostic value of the baseline systemic immune-inflammation index in HER2-positive metastatic breast cancer: exploratory analysis of two prospective trials. *Ann Surg Oncol*. (2025) 32 (2):750–9. doi: 10.1245/s10434-024-16454-8

36. Zhu M, Chen L, Kong X, Wang X, Fang Y, Li X, et al. The systemic inflammation response index as an independent predictor of survival in breast cancer patients: A retrospective study. *Front Mol Biosci*. (2022) 9:856064. doi: 10.3389/fmolb.2022.856064

37. Zhang S, Cheng T. Prognostic and clinicopathological value of systemic inflammation response index (SIRI) in patients with breast cancer: a meta-analysis. *Ann Med*. (2024) 56:2337729. doi: 10.1080/07853890.2024.2337729

38. Hai-Jing Y, Shan R, Jie-Qiong X. Prognostic significance of the pretreatment pan-immune-inflammation value in cancer patients: an updated meta-analysis of 30 studies. *Front Nutr*. (2023) 10:1259929. doi: 10.3389/fnut.2023.1259929

39. Şahin AB, Cubukcu E, Ocak B, Deligonul A, Oyucu Orhan S, Tolunay S, et al. Low pan-immune-inflammation-value predicts better chemotherapy response and survival in breast cancer patients treated with neoadjuvant chemotherapy. *Sci Rep*. (2021) 11:14662. doi: 10.1038/s41598-021-94184-7

40. Li F, Wang Y, Dou H, Chen X, Wang J, Xiao M. Association of immune inflammatory biomarkers with pathological complete response and clinical prognosis in young breast cancer patients undergoing neoadjuvant chemotherapy. *Front Oncol*. (2024) 14:1349021. doi: 10.3389/fonc.2024.1349021

41. Qi X, Qiao B, Song T, Huang D, Zhang H, Liu Y, et al. Clinical utility of the pan-immune-inflammation value in breast cancer patients. *Front Oncol*. (2023) 13:1223786. doi: 10.3389/fonc.2023.1223786

42. Guven DC, Sahin TK, Erul E, Kilickap S, Gambichler T, Aksoy S. The association between the pan-immune-inflammation value and cancer prognosis: A systematic review and meta-analysis. *Cancers (Basel)*. (2022) 14:2675. doi: 10.3390/cancers14112675

43. Tong L, Wang S, Zhang R, Wu Y, Xu D, Chen L. High levels of SII and PIV are the risk factors of axillary lymph node metastases in breast cancer: A retrospective study. *Int J Gen Med*. (2023) 16:2211–18. doi: 10.2147/IJGM.S411592

44. Ivars Rubio A, Yufera JC, de la Morena P, Fernández Sánchez A, Navarro Manzano E, García Garre E, et al. Neutrophil-lymphocyte ratio in metastatic breast cancer is not an independent predictor of survival, but depends on other variables. *Sci Rep*. (2019) 9:16979. doi: 10.1038/s41598-019-53606-3

45. Truffi M, Piccotti F, Albasini S, Tibollo V, Morasso CF, Sottotetti F, et al. Preoperative systemic inflammatory biomarkers are independent predictors of disease recurrence in ER+ HER2- early breast cancer. *Front Oncol*. (2021) 11:773078. doi: 10.3389/fonc.2021.773078

46. Murphy J, Pak S, Shteynman L, Winkeler I, Jin Z, Kaczocha M, et al. Mechanisms and preventative strategies for persistent pain following knee and hip joint replacement surgery: A narrative review. *Int J Mol Sci*. (2024) 25:4722. doi: 10.3390/ijms25094722

47. Chapman CR, Vierck CJ. The transition of acute postoperative pain to chronic pain: an integrative overview of research on mechanisms. *J Pain*. (2017), 18(4):359.e1-359.e38. doi: 10.1016/j.jpain.2016.11.004

48. Wijayanti IAS, Adnyana IMO, Widyadharma IPE, Wiratnaya IGE, Mahadewa TGB, Astawa INM. Neuroinflammation mechanism underlying neuropathic pain: the role of mesenchymal stem cell in neuroglia. *AIMS Neurosci*. (2024) 11:226–43. doi: 10.3934/Neuroscience.2024015

49. Pergolizzi JV, LeQuang JA, Magnusson P, Varrassi G. Identifying risk factors for chronic postsurgical pain and preventive measures: a comprehensive update. *Expert Rev Neurother*. (2023) 23:1297–310. doi: 10.1080/14737175.2023.2284872

50. Voscopoulos C, Lema M. When does acute pain become chronic. *Br J Anaesth*. (2010) 105 Suppl 1:i69–85. doi: 10.1093/bja/aeq323

51. Shu B, Xu F, Zheng X, Zhang Y, Liu Q, Li S, et al. Change in perioperative neutrophil-lymphocyte ratio as a potential predictive biomarker for chronic postsurgical pain and quality of life: an ambispective observational cohort study. *Front Immunol*. (2023) 14:1177285. doi: 10.3389/fimmu.2023.1177285

52. van Helmond N, Timmerman H, van Dasselaar NT, van de Pol CC, Olesen SS, Drewes AM, et al. High body mass index is a potential risk factor for persistent postoperative pain after breast cancer treatment. *Pain Physician*. (2017) 20:E661–E71.

53. Strijbos BTM, Janssen L, Voogd AC, Zwaans WAR, Roumen RMH, Maaskant-Braat AJG. Persistent pain after breast cancer treatment, an underreported burden for breast cancer survivors. *Ann Surg Oncol*. (2024) 31:6753–63. doi: 10.1245/s10434-024-15682-2

54. Wang L, Guyatt GH, Kennedy SA, Romerosa B, Kwon HY, Kaushal A, et al. Predictors of persistent pain after breast cancer surgery: a systematic review and meta-analysis of observational studies. *CMAJ*. (2016) 188:E352–E61. doi: 10.1503/cmaj.151276

55. Tan HS, Plichta JK, Kong A, Tan CW, Hwang S, Sultana R, et al. Risk factors for persistent pain after breast cancer surgery: a multicentre prospective cohort study. *Anaesthesia*. (2023) 78:432–41. doi: 10.1111/anae.15958

56. Shanthanna H. Risk factors and prediction modelling for chronic post-surgical pain after breast cancer surgery. *Anaesthesia*. (2023) 78:811–15. doi: 10.1111/anae.16011

frontiers | Frontiers in Immunology

TYPE Original Research
PUBLISHED 30 January 2025
DOI 10.3389/fimmu.2025.1546167

Check for updates

OPEN ACCESS

EDITED BY
Xiaosheng Tan,
Rutgers, United States

REVIEWED BY
Xiaowei Wu,
Dana–Farber Cancer Institute, United States
Xiaozhou Yu,
Northwestern University, United States
Yabing Nan,
Dana–Farber Cancer Institute, United States
Mingyan Hao,
Duke University, United States

*CORRESPONDENCE
Tao Yan
yantao@cicams.ac.cn;
blizzardyt@163.com
Hui Zheng
zhenghui@cicams.ac.cn
Yu-lin Sun
ylsun@cicams.ac.cn

†These authors have contributed equally to this work and share first authorship

RECEIVED 16 December 2024
ACCEPTED 06 January 2025
PUBLISHED 30 January 2025

CITATION
Li H-x, Che L, Li Y, Wang T-h, Min F-d, Xu L, Wang M, Zheng Z-x, Qu S-n, Wang F, Tang W, Wei S-j, Sun Y-l, Zheng H and Yan T (2025) Correlations between primary tumour location, biomarkers of inflammation and lung injury, and postoperative pulmonary complications in patients underwent laparoscopic colorectomy: a propensity score matched analysis of 300 patients. *Front. Immunol.* 16:1546167. doi: 10.3389/fimmu.2025.1546167

COPYRIGHT
© 2025 Li, Che, Li, Wang, Min, Xu, Wang, Zheng, Qu, Wang, Tang, Wei, Sun, Zheng and Yan. This is an open-access article distributed under the terms of the Creative Commons Attribution License (CC BY). The use, distribution or reproduction in other forums is permitted, provided the original author(s) and the copyright owner(s) are credited and that the original publication in this journal is cited, in accordance with accepted academic practice. No use, distribution or reproduction is permitted which does not comply with these terms.

Correlations between primary tumour location, biomarkers of inflammation and lung injury, and postoperative pulmonary complications in patients underwent laparoscopic colorectomy: a propensity score matched analysis of 300 patients

Hui-xian Li[1†], Li Che[2†], Yuan Li[3†], Tai-hang Wang[1†], Fang-di Min[1†], Lei Xu[1], Meng Wang[1], Zhao-xu Zheng[4], Shi-ning Qu[5], Fei Wang[6], Wei Tang[7], Shi-jing Wei[1], Yu-lin Sun[8*], Hui Zheng[1*] and Tao Yan[1*]

[1]Department of Anesthesiology, National Cancer Center/National Clinical Research Center for Cancer/Cancer Hospital, Chinese Academy of Medical Sciences and Peking Union Medical College, Beijing, China, [2]Department of Cardiology, Central Hospital of Dalian University of Technology, Dalian, China, [3]Department of Colorectal Surgery, Sun Yat-Sen University Cancer Center, Guangzhou, China, [4]Department of Colorectal Surgery, National Cancer Center/National Clinical Research Center for Cancer/Cancer Hospital, Chinese Academy of Medical Sciences and Peking Union Medical College, Beijing, China, [5]Department of Intensive Care Unit, National Cancer Center/National Clinical Research Center for Cancer/Cancer Hospital, Chinese Academy of Medical Sciences and Peking Union Medical College, Beijing, China, [6]Office of Cancer Screening, National Cancer Center/National Clinical Research Center for Cancer/Cancer Hospital, Chinese Academy of Medical Sciences and Peking Union Medical College, Beijing, China, [7]Department of Diagnostic Radiology, National Cancer Center/National Clinical Research Center for Cancer/Cancer Hospital, Chinese Academy of Medical Sciences and Peking Union Medical College, Beijing, China, [8]State Key Laboratory of Molecular Oncology, National Cancer Center/National Clinical Research Center for Cancer/Cancer Hospital, Chinese Academy of Medical Sciences and Peking Union Medical College, Beijing, China

Introduction: The impact of distinct primary colorectal cancer (CRC) sites on lung injury and complications remains largely unexplored, despite the palpable differences in surgical positions, procedures, and the resulting mechanically induced respiratory pressures at each site.

Materials and methods: This study employed a forwards-looking approach utilising the propensity score matching (PSM) method; 300 patients with pathological CRC after laparoscopic surgery from April 2019 to May 2023 were enrolled. Two categories were bifurcated based on their surgical locations: the rectosigmoid colon (RSC) group and the descending/ascending colon (DAC) group, with a 2:1 ratio. The occurrence of postoperative pulmonary complications (PPCs) within a 30-day postoperative period was meticulously evaluated. Additionally, assessments have been performed for plasma biomarkers of immune response dynamics and lung injury (plasma soluble

advanced glycation end-product receptor [sRAGE], angiopoietin-2 [ANG-2], interleukin-1β/6 [IL-1β/IL-6]) and other parameters.

Results: Although the increase in postoperative lung epithelial damage, as indicated by the plasma sRAGE levels, was significant in the RSC group (DAC vs. RSC; 1029.6 [576.8–1365.2] vs. 1271.6 [896.3–1587.6]; odds ratio=0.999; 95% CI: 0.998 to 1.000; P=0.007), a significantly increased percentage of PPCs was observed in the DAC group (DAC vs. RSC; hazard ratio=1.669; 95% CI, 1.141 to 2.439; P=0.008). A univariate Cox proportional hazards model revealed that sRAGE, ANG-2, IL-1β, and IL-6 levels were not correlated with the incidence of time-to-PPCs across the two cohorts (P>0.05). Propensity score-weighted Cox regression and causal mediation analysis further demonstrated that the DAC site directly affected the incidence of PPCs, regardless of the other baseline confounders and clinical covariates related to the tumour site and PPCs.

Conclusion: The primary site of CRC is an independent predictor of the development of PPCs. Despite the steep Trendelenburg position of the RSC group inciting more pulmonary stress, inflammation and lung epithelial injury, as indicated by higher sRAGE, it demonstrated a lower PPCs occurrence relative to its DAC counterpart, with a slightly inclined or reversed Trendelenburg position. None of the plasma biomarkers of inflammation or lung injury indicated sufficient prognostic value for PPCs.

KEYWORDS

colorectal cancer, Trendelenburg position, inflammatory biomarker, lung injury, postoperative pulmonary complications

1 Introduction

Postoperative pulmonary complications (PPCs), the second most recurrent complication in general surgical operations (1, 2), are intrinsically associated with perioperative morbidity and mortality (3–5). These complications are particularly predisposed to manifest during major abdominal surgeries (both laparotomy and laparoscopy) (6), with incidence rates ranging from 3–30% (3, 7, 8). This variability in incidence primarily arises from the heterogeneity in the definitions of PPCs (9), surgical/anaesthetic methodologies, and patient populations enrolled. A comprehensive review of the American College of Physicians demonstrated that a composite of pneumonia and respiratory failure defined PPCs in nearly 60% of the 16 preceding publications spanning over a quarter of a century (10). However, the European Perioperative Clinical Outcome (EPCO) consortium proposed that PPCs encompass respiratory failure, acute respiratory distress syndrome (ARDS), aspiration pneumonitis, pneumonia, respiratory infection, atelectasis, pleural effusion, pneumothorax, bronchospasm, and pulmonary embolus (11). Several studies have also incorporated lung injury and the subclinical stage of microatelectasis as PPCs (12–14).

Colorectal cancer (CRC), the most frequently observed type of abdominal tumour, represents the second highest incidence rate of 1,926,118 new cases (9.6% morbidity) and 903,859 deaths (9.3% mortality) globally in 2022 (15). CRC has a diverse global geographical distribution, with the majority of CRCs in Asia manifesting as rectal cancers, constituting more than 50% of the total cases. In contrast, in Europe and North America, rectal cancers represent less than 40% of all (16, 17). Given that the overwhelming majority of CRC patients are treated with laparoscopic procedures, the pneumoperitoneum pressure may amplify the skew in the ventilation–perfusion ratio and the generation of pulmonary atelectasis via enhanced transpulmonary pressure and worsened lung compliance, which can promote lung injury and PPCs even in patients with otherwise healthy lungs (18–20).

Notably, CRC can occur in disparate anatomical locations, including the ascending, transverse, descending and sigmoid colon, and rectum (inclusive of the anus). Thus, the surgical positions utilised in treating CRC are contingent upon the specific site of the disease. Rectosigmoid colectomy (RSC) necessitates a steep Trendelenburg position, whereas ascending and descending colectomy (DAC) merely requires a slightly inclined or reverse Trendelenburg position. Notably, the steep Trendelenburg position may induce substantial diaphragm displacement, haemodynamic compromise, reduced functional residual capacity, augmented pulmonary stress facilitating atelectasis, and compromised

oxygenation (21–23). The integration of a large-angle Trendelenburg position along with pneumoperitoneum has also been verified to exacerbate more deterioration of the respiratory system, which can facilitate atelectasis and obstruct oxygenation and related inflammation and lung injury (24). In light of these factors, the primary CRC site, which involves different surgical positions, appears to be a crucial determinant of lung injury and subsequent PPCs incidence.

Despite extensive studies on predictive risk factors for preventing PPCs, including age, surgery type, preoperative spirometry gases, preoperative pulmonary comorbidities, smoking, surgical and anaesthetic strategies (6, 8, 9, 25–29), as well as various predictive risk models (30), research directly exploring how primary CRC sites influence lung injury and whether it correlates with the development of PPCs is limited. This study was designed meticulously to ascertain whether a causal correlation exists between these two variables, utilising propensity score matching to eradicate the bias introduced by other factors.

2 Materials and methods

2.1 Ethical compliance and clinical trial registry

This retrospective study was rigorously conducted at the Cancer Hospital, Chinese Academy of Medical Sciences (Beijing, China). The experimental protocol was thoroughly reviewed and approved by the institutional ethics committee (Approval No. 22/519-3721). Patients enrolled in the initial clinical trial provided informed written consent before commencing treatment. Both treatment protocols and the collation of clinical data were reserved for future scholarly analysis. Patient follow-up was maintained throughout the patients' hospital stay and was sustained postdischarge via telecommunication and outpatient records. The inclusion criteria were as follows: (1) patients who underwent radical laparoscopic resection for colorectal cancer; (2) male and female patients aged between 18 and 80 years; (3) American Society of Anaesthesiologists (ASA) physical status ≤ III; (4) body mass index (BMI) < 40 kg/m^2; (5) elective laparoscopic colorectal surgery that is expected to last for at least 2 h; and (6) intermediate or high risk of postoperative pulmonary complications (PPCs) as defined by the Assess Respiratory Risk in Surgical Patients in Catalonia (ARISCAT) score (a score of 26–44 is defined as intermediate risk and a score of > 44 is defined as high risk). The exclusion criteria were as follows: (1) aged < 18 years or > 80 years; (2) pregnant or breast-feeding status; (3) ASA physical status of IV or higher; (4) had a history of recent pulmonary infection/prior lung or abdominal surgery; (5) pneumothorax/giant bullae/chronic obstructive pulmonary disease; (6) severe cerebral and cardiovascular dysfunction/chronic renal failure with dialysis/hepatic dysfunction (Child–Pugh grade B or C)/immunologic or neuromuscular disease; (7) emergency or unplanned surgery; (8) expected prolonged mechanical ventilation after surgery; (9) allergies or contraindications to sevoflurane, propofol, or nonsteroidal anti-inflammatory drugs (NSAIDs); (10) participation in other drug trials within 1 preoperative month; and (11) distant metastasis.

2.2 Selection of participants

A total of 340 patients who underwent laparoscopic procedures at the National Cancer Center between April 2019 and May 2023 and were subsequently pathologically diagnosed with CRC were selected for this study. Comprehensive clinical information, including demographic and baseline data, intraoperative procedures, and follow-up outcomes, was recorded. The patient cohort was segmented into two separate categories according to the surgical position: the rectosigmoid colon group (RSC group), with the steep Trendelenburg position, and the descending/ascending colon group (DAC group), with a slightly inclined or reversed Trendelenburg position. Propensity score matching (PSM) was subsequently applied to achieve equilibrium in clinicopathological features.

2.3 Methodologies and interventions

Standard clinical practice guided the preoperative preparation and intraoperative monitoring. A lung-protective ventilation approach was utilised for all patients during anaesthesia, maintaining a tidal volume (TV) of 6–8 ml/kg predicted body weight (PBW) (31), accompanied by the same alveolar recruitment manoeuvres (ARMs, every 30 minutes) and positive end-expiratory pressure (PEEP=5 cmH_2O).

2.4 Measurement of outcomes

PPCs were systematically categorised from 1–4 by the criteria delineated by Kroenke et al. (Table 1) (32). The clinical diagnosis of PPCs was substantiated by an independent radiologist utilising a routine low-dose computed tomography (CT) scan of the chest on postoperative day (POD) 3-4. The diagnosis and grading of PPCs were performed independently by a multidisciplinary team comprising medical oncologists, attending surgeons, and intensivists with senior clinical experience. Patients were assessed daily (9:00 to 10:00 a.m.) during the first postoperative week and subsequently weekly from the second to the fourth postoperative week. The plasma soluble forms of the receptor for advanced glycation end products (sRAGE), angiopoietin-2 (ANG-2) and interleukin-1β/6 [IL-1β/IL-6] levels were determined at three time points: preoperatively, on POD 1, and POD 3. In addition, systemic inflammatory markers (interleukin-6, interleukin-1β) and postoperative recovery in the two groups were also analysed for comparison. Furthermore, surgical rating scales (SRS) for the assessment of surgical operating conditions (5 score for optimal; 4 score for good; 3 score for acceptable; 2 score for poor; and 1 score for extremely poor) were administered by experienced surgeons (33), who were blinded to the PnP level to maintain interrater and intrarater agreement.

TABLE 1 Operational definitions of postoperative pulmonary complications [a].

Grade	Definition
1	Cough, dry Microatelectasis: abnormal lung findings and temperature > 37.5°C without other documented cause; results of chest radiograph either normal or unavailable Dyspnoea, not due to other documented cause
2	Cough, productive, not due to other documented cause Bronchospasm: new wheezing or pre-existent wheezing resulting in change therapy Hypoxemia: alveolar-arterial gradient > 29 and symptoms of dyspnoea or wheezing Atelectasis: radiological confirmation plus either temperature > 37.5 °C or abnormal lung findings Hypercarbia, transient, requiring treatment, such as naloxone or increased manual or mechanical ventilation Adverse reaction to pulmonary medication
3	Pleural effusion, resulting in thoracentesis Pneumonia, suspected: radiological evidence without bacteriological confirmation Pneumonia, proved: radiological evidence and documentation of pathological organism by Gram stain or culture Pneumothorax Reintubation postoperative or intubation, period of ventilator dependence (noninvasive or invasive ventilation) ≤ 48 h
4	Ventilatory failure: postoperative ventilator dependence ≥ 48 h, or reintubation with subsequent period of ventilator dependence ≥ 48 h

[a] Source: Kroenke et al. (32).

2.5 Statistical analyses

The process of PSM incorporated factors such as respiratory comorbidity (chronic obstructive pulmonary disease/chronic bronchitis vs. no relevant history), smoking status (either current/former smoker vs. nonsmoker), and age (younger than 60 years vs. 60 years or older), and a 1:2 matching ratio and a calliper of 0.05 were applied via the "MatchIt" R package. The absolute standardised difference (ASD) method, facilitated by the "stddiff" R package, was utilised to juxtapose the characteristics of the two groups and establish a balance, with an ASD value exceeding 0.2 indicating imbalance.

A logistic regression model was used to compare intraoperative procedures and follow-up outcomes between the two groups, and the results are expressed as odds ratios (ORs) and 95% CIs. Kaplan–Meier analysis, along with log-rank tests, was employed to assess the relationship between PPCs incidence and postoperative onset. Univariable or multivariable Cox proportional hazard models were applied to compare the incidence of PPCs within 30 days postoperatively, yielding hazard ratios (HRs) and 95% CIs. The overlap weight-based propensity score weighting method implemented via the R package "WeightIt" was used to eliminate bias by equalizing the distributions of covariates on the basis of the multivariable Cox proportional hazards model.

To determine the valid causal roles of variables of interest in the incidence of PPCs, a causal mediation analysis based on an accelerated failure time (AFT) survival regression model was performed using the R packages "mediation" and "survival". The primary CRC site was designated as the exposure, the incidence and time of PPCs were the outcomes. A Poisson regression framework was employed to characterise the impact of exposure on postoperative gastrointestinal recovery time (mediator, ordered categorical variable), while age (binary, ≥60 years old and <60 years old) and anaesthetic duration (binary, more than and less than 3 hours), which are associated with PPCs incidence in the univariable Cox proportional hazards model, were included in the analysis as covariates. Additionally, a logistic regression approach was used to analyse the effects of exposure on age (mediator) when postoperative gastrointestinal recovery time and anaesthetic duration were included as covariates. Furthermore, the causal mediation analysis was adjusted for the following baseline and clinical confounders related to the primary CRC site: TNM stage (categorical, Tis-stage I, stage II, and stage III-IV), history of neoadjuvant therapy (binary, yes and no), preoperative haemoglobin levels (continuous), blood product transfusion (binary, yes and no) and duration of surgery (continuous). The average causal mediation effects (ACME) were calculated to measure the mediating impact of gastrointestinal recovery time or age on PPCs incidence. The average direct effects (ADE) were the estimation of exposure on the outcome that mediators cannot explain. The results of the AFT models are described in terms of acceleration regression coefficients, in which a negative coefficient indicates a shorter occurrence time of PPCs.

Quantitative variables were analysed with Student's t test or the Mann–Whitney U test, whereas categorical data were evaluated via the chi–square test or Fisher's exact test. A two-sided P value < 0.05 was considered statistically significant. Data analyses were performed using SPSS 25 (IBM SPSS Inc., USA) or R software.

3 Results

3.1 Characteristics and treatment of the patients

Three hundred forty CRC patients matched the criteria for inclusion in the study database. Following PSM, 300 patients were divided into two groups, comprising 200 patients in the RSC group and 100 patients in the DAC group. The median ages were 63.0 and 61.0 years for the two groups. Most characteristics at baseline were comparable across the two groups, with the exception of a greater prevalence of tumour stage II - IV (RSC vs. DAC; 75.0% [150 of 200] vs. 85.0% [85 of 100], ASD=0.253) and a subsequent lower proportion of neoadjuvant therapy (RSC vs. DAC; 14.5% [29 of 200] vs. 5.0% [5 of 100], ASD=0.324), lower haemoglobin levels (g/L; RSC vs. DAC; 137.5 [127.0-152.8] vs. 130.0 [107.5-144.8], ASD=0.570), an enhanced proportion of anaemia (RSC vs. DAC; 21.0% [42 of 200] vs. 41% [41 of 100], ASD=0.443) and more blood product transfusions (RSC vs. DAC; 5.0% [10 of 200] vs. 15.0% [15 of 100], P=0.003) in the DAC group than in the RSC group (Tables 2, 3). Moreover, the DAC group required extended anaesthetic (min; median [interquartile range, IQR]; RSC vs. DAC; 170.0 (145.0–207.8) vs. 199.5 (162.5–221.8), P<0.001) and surgical duration (RSC vs. DAC; 145.0 (112.0–180.0) vs. 165.0 (132.5–193.0), P=0.002) (Table 3). In a predefined subgroup

10.3389/fimmu.2025.1546167

TABLE 2 Demographic and baseline data.

Characteristic	Rectosigmoid colon Group (RSC, N=200)	De/Ascending colon Group (DAC, N=100)	ASD
Age, yr	63.0 (54.0-68.0)	61.0 (52.0-68.8)	0.083
Gender, Male	123 (61.5%)	62 (62.0%)	0.010
Body mass index (BMI), kg/m^2	24.7 ± 3.5	24.9 ± 3.5	0.062
Obesity (Chinese standard*)	33 (16.5%)	22 (22.0%)	0.140
Alcoholism**	33 (16.5%)	16 (16.0%)	0.014
Allergic history	21 (10.5%)	10 (10.0%)	0.016
Smoking status			0.057
Nonsmoker	142 (71.0%)	71 (71.0%)	
Former smoker#	33 (16.5%)	18 (18.0%)	
Current smoker	25 (12.5%)	11 (11.0%)	
Dry cough/ Expectoration	21 (10.5%)	8 (8.1%)	0.083
Respiratory comorbidity			0.177
No relevant history	150 (75%)	75 (75%)	
COPD/ Chronic bronchitis	47 (23.5%)	25 (25.0%)	
Asthma	3 (1.5%)	0 (0.0%)	
Hypertension	86 (43.0%)	45 (45.0%)	0.040
Coronary heart disease	14 (7.0%)	7 (7.0%)	<0.001
Cerebrovascular disease	14 (7.0%)	4 (4.0%)	0.132
Diabetes mellitus	37 (18.5%)	12 (12.0%)	0.182
ASA status			0.057
I	8 (4.0%)	3 (3.0%)	
II	179 (89.5%)	90 (90.0%)	
III	13 (6.5%)	7 (7.0%)	
TNM staging†			0.253
Tis -Stage I	50 (25.0%)	15 (15.0%)	
Stage II	65 (32.5%)	36 (36.0%)	
Stage III- IV	85 (42.5%)	49 (49.0%)	
Adjuvant Chemo/ Radiotherapy	29 (14.5%)	5 (5.0%)	0.324
Anaemia††	42 (21.0%)	41 (41.0%)	0.443
Preoperative routine blood test			
Haemoglobin, g/L	137.5 (127.0-152.8)	130.0 (107.5-144.8)	0.570
White blood cell, 10^9/L	6.0 (5.1-7.1)	6.3 (5.0-7.5)	0.121
Neutrophils, 10^9/L	3.8 (3.0-4.6)	3.8 (2.9-5.0)	0.060

All data are presented as the means ± SDs, n (%), or medians (interquartile ranges). An imbalance between two groups was defined as an absolute standardised difference (ASD) value greater than 0.200. *Chinese standard for obesity: underweight (< 18.5 kg/m^2), normal weight (18.5-23.9 kg/m^2), overweight (24.0-27.9 kg/m^2), or obese (≥ 28.0 kg/m^2). **Alcoholism: daily consumption of the equivalent of 80 g of alcohol for at least 5 years. # Former smoker: weaning more than 4 weeks. †TNM staging was defined by the NCCN guidelines (Colon/Rectal Cancer) Version 1.2022 (www.nccn.org/patients). ††Anaemia was defined as haemoglobin levels of < 13.0 g/dL and 12.0 g/dL for males and females, respectively.
BMI, body mass index; COPD, chronic obstructive pulmonary disease; ASA, American Society of Anaesthesiologists; Tis, tumour *in situ*.

TABLE 3 Intraoperative procedures.

	Rectosigmoid colon Group (RSC, N=200)	De/Ascending colon Group (DAC, N=100)	*P* value
Intraoperative ventilation index			
Tidal volume (ml/kg of predicted body weight)	6-8	6-8	—
Inspired oxygen fraction, (FiO_2, %)	40-60	40-60	—
Intraoperative PEEP (cmH_2O)	5	5	—
Anaesthetic strategy (%)			0.695
Inhalation	177 (88.5)	90 (90.0)	
TIVA	23 (11.5)	10 (10.0)	
Medication			
Propofol (Intubation, mg)	140.0 (120.0-180.0)	150.0 (120.0-180.0)	0.081
Sufentanil (ug)	35.0 (35.0-40.0)	35.0 (35.0-40.0)	0.907
Remifentanil (ug)	960.0 (700.0-1225.0)	850.0 (642.5-1150.0)	0.967
Rocuronium (Intubation, mg)	50.0 (40.0-50.0)	50.0 (45.0-50.0)	0.347
Rocuronium (Maintenance, mg)	40.0 (20.0-60.0)	30.0 (20.0-50.0)	0.593
Duration (min)			
Anaesthesia	170.0 (145.0-207.8)	199.5 (162.5-221.8)	<0.001
Surgery	145.0 (112.0-180.0)	165.0 (132.5-193.0)	0.002

(Continued)

TABLE 3 Continued

	Rectosigmoid colon Group (RSC, N=200)	De/Ascending colon Group (DAC, N=100)	*P* value
Duration (min)			
Category of anaesthetic duration (%)			<0.001
≤ 3 hours	130 (65.0)	35 (35.0)	
> 3 hours	70 (35.0)	65 (65.0)	
Assessment of surgical condition			
SRS Score	5 (5-5)	5 (4-5)	0.003
Volume of fluids administered (ml)			
Crystalloid	1100.0 (1000.0-1500.0)	1100.0 (1000.0-1237.5)	0.192
Colloid	500.0 (0-500.0)	500.0 (500.0-500.0)	0.161
Blood products transfusion (%)	10 (5.0)	15 (15.0)	0.003
Estimated blood loss (ml)	37.5 (20.0-80.0)	50.0 (20.0-100.0)	0.254
Urine volume (ml)	300.0 (200.0-300.0)	300.0 (300.0-300.0)	0.185

All data are presented as the means ± SDs, n (%), or medians (interquartile ranges). FiO_2, fraction of inspired oxygen; PEEP, positive end expiratory pressure; TIVA, total intravenous anaesthesia; SRS, surgical rating scale.

analysis, there was a notable increase in the duration of anaesthesia from the sigmoid (median, 160.0 min; IQR, 127.3-192.0 min), rectal (median, 170.0 min; IQR, 150.0-225.0 min), and ascending (median, 190.5 min; IQR, 160.0-216.3 min) to the descending colon (median, 212.0 min; IQR, 174.5-235.3 min). Similarly, the surgical duration showed a trend comparable to that of the sigmoid (median, 126.5 min; IQR, 100.0–152.5 min), rectal (median, 150.0 min; IQR, 131.0–200.0 min), ascending (median, 163.5 min; IQR, 131.5–187.0 min), and descending colon (median, 175.0 min; IQR, 149.3–208.8 min).

In addition, the Mann–Whitney rank test revealed that the surgical conditions, as evaluated by the surgical rating scale (SRS), were poorer in the DAC group than in the RSC group (RSC vs. DAC; 5 [5.0–5.0] vs. 5.0 [4.0–5.0]; P=0.003, Table 3). Details of the mechanical parameters of pulmonary compliance and peak and plateau airway pressures at different surgical positions at the tumour sites are provided in Table 4.

3.2 Outcomes with respect to efficacy

First, among the indicators related to postoperative recovery, there was no significant difference in postanaesthesia care unit (PACU) recovery time or postoperative hospitalisation days between the DAC and RSC groups. However, a greater protracted gastrointestinal recovery time (defined as the period of first flatus or stool through the anus after surgery) was observed in the DAC group (DAC vs. RSC; 3.0 [2.0–3.0] vs. 3.0 [2.0–3.0]; OR=1.698; 95% CI, 1.098 to 2.684; P=0.020; Table 5). Moreover, the gastrointestinal recovery time was longer in patients with PPCs than in those without (with PPCs vs. without PPCs; 3.0 [2.0–3.0] vs. 2.5 [2.0–3.0]; OR=2.114; 95% CI, 1.361 to 3.362; P=0.001).

Next, the plasma levels of sRAGE on POD1 were greater in the patients in the RSC group than in those in the DAC group (DAC vs. RSC; 1029.6 [576.8–1365.2] vs. 1271.6 [896.3–1587.6]; OR=0.999; 95% CI, 0.998 to 1.000; P=0.007), which also indicated marginal significance for the two groups on POD3 (DAC vs. RSC; 881.1 [510.4–1060.4] vs. 1063.3 [618.4–1335.4]; OR=0.999; 95% CI, 0.998 to 1.000; P=0.077; Table 5). However, the levels of the endothelial injury indicator ANG-2 and the systemic inflammatory indicators interleukin-1β (IL-1β)/IL-6 remained unchanged across the two cohorts (P>0.05, Table 5). In addition, no significant relationship was detected between the plasma biomarkers sRAGE, ANG-2, IL-1β, or IL-6 and the PPCs incidence (P>0.05).

Furthermore, an unexpected finding was that the DAC group exhibited a significantly greater occurrence of PPCs within a span of 30 days postsurgery. The hazard ratio (HR) was 1.669 (95% CI, 1.141 to 2.439; P=0.008; Table 5), with a 48% incidence (48/100) in the DAC group and a 30.0% incidence (60/200) in the RSC group (Figure 1A). Moreover, the DAC group also had a significantly greater incidence of atelectasis (P=0.002) and pleural effusion (P=0.007; Table 5). Notably, in a preplanned subgroup analysis, a significant increase in the incidence of PPCs in the sigmoid colon, rectum, ascending colon, and descending colon was detected (HR=1.218; 95% CI, 1.019 to 1.457; P=0.031; Figure 1B). Among the observed incidents, microatelectasis was the most prevalent, occurring in 21.7% (65 out of 300) of the cases.

3.3 Tumour occurrence in the descending/ascending colon was an independent risk factor for PPCs outcomes

The univariable Cox proportional hazards model identified four PPCs-related factors with statistical significance. These factors included an anaesthetic duration exceeding 3 hours (HR=1.508; 95% CI, 1.033 to 2.202; P=0.033), an age of 60 years or more (HR=1.708; 95% CI, 1.126 to 2.593; P=0.012), a primary CRC site in the DAC (HR=1.669; 95% CI, 1.141 to 2.439; P=0.008) and a gastrointestinal recovery time (HR=1.775; 95% CI, 1.219 to 2.584; P=0.003). The time-to-PPCs were subsequently analysed using these high-risk factors through a multivariable Cox proportional hazards regression model. The findings revealed that gastrointestinal recovery time (HR=1.750; 95% CI, 1.198 to 2.555; P=0.004), age (60 years and above vs. under 60 years, HR=1.678; 95% CI, 1.103 to 2.552; P=0.016) and primary CRC site (DAC vs. RSC; HR=1.470; 95% CI, 0.9847 to 2.194; P=0.059) were significant or marginal independent risk factors for PPCs incidence. To acquire unbiased estimates of the influence of these factors on PPCs, the adjusted HRs of the primary CRC site, age and gastrointestinal recovery time were 1.634 (95% CI, 1.115 to 2.396; P=0.012), 1.745 (95% CI, 1.131 to 2.692; P=0.012) and 1.750 (95% CI, 1.159 to 2.644;

TABLE 4 Mechanical ventilation parameters for different anaesthetic methods.

Characteristic	Rectosigmoid colon Group (RSC, N=200)	De/Ascending colon Group (DAC, N=100)		*P* value*	*P* value#
	25-30° Trendelenburg	10-15° Reverse Trendelenburg	10-15°Trendelenburg		
Ppeak, cmH_2O	27.0 (24.0-32.0)	22.0 (21.0-23.5)	25.0 (24.0-28.5)	<0.001	0.120
Pplate, cmH_2O	23.0 (21.0-27.0)	18.0 (17.0-20.0)	23.0 (21.5-26.5)	<0.001	0.391
Respiratory rate, min	14.0 (13.0-16.0)	13.0 (12.0-15.0)	13.0 (12.0-16.0)	0.006	0.029
$EtCO_2$, mmHg	39.0 (36.0-42.0)	30.0 (28.0-33.0)	32.0 (29.0-34.0)	<0.001	<0.001
Dynamic C_{RS}, ml/cmH_2O	21.1 (20.4-21.6)	26.7 (24.7-29.1)	22.6 (21.3-26.0)	<0.001	<0.001
Static C_{RS}, ml/cmH_2O	25.5 (24.4-26.5)	34.2 (31.6-37.6)	25.3 (23.3-27.8)	<0.001	0.817

The data are shown as n (%) or medians (interquartile ranges).
The quantitative data were compared via the Mann–Whitney rank test.
*Comparison between the Trendelenburg position (25–30°) and the reverse Trendelenburg position (10–15°). # Comparison between the Trendelenburg position (25–30°) and the Trendelenburg position (10–15°).
Ppeak, peak airway pressure; Pplat, plateau pressure; EtCO2, end-tidal carbon dioxide; C_{RS}, respiratory system compliance.

P=0.008), respectively, according to propensity score weighting via overlap weights. In summary, even when adjustments were made in populations with significant differences in other covariates, such as age and gastrointestinal recovery time, the primary CRC site emerged as a stand-alone risk factor for PPCs.

3.4 The impact of the primary CRC site in the DAC on PPCs occurrence cannot be attributed to the other established clinical and baseline variables

The aforementioned analyses demonstrated that the primary CRC site was associated with several baseline and clinical characteristics and PPCs incidence. To address whether the primary CRC site is impacted by other clinical characteristics and, in turn, influences the incidence of PPCs, causal mediation analysis using the AFT survival regression model with the quasi-Bayesian Monte Carlo method was performed (Figure 2A). First, when the gastrointestinal recovery time was designated as a mediator, the primary CRC site had a significant average direct effect (ADE; effect=-1.769 [95% CI, -3.742 to -0.49]; P=0.004) and total effect (effect=-2.072 [95% CI, -4.380 to 0.54]; P=0.004) on increasing the incidence of PPCs, whereas the average causal mediation effect (ACME) was not significant (effect=-0.303 [95% CI, -1.512 to 0.58]; P=0.474; Figure 2B). Even after adjusting for the other confounders associated with the primary CRC site, the mediation effect estimates did not significantly change (Figure 2B). When age was considered a mediator, the ACME, ADE, and total effects were 0.063 (95% CI, -0.164 to 0.34; P=0.596), -1.228 (95% CI, -2.218 to -0.37; P=0.002) and -1.165 (95% CI, -2.125 to -0.29; P=0.004), respectively (Figure 2C). Similarly, the tendency was not significantly altered after adjusting for confounders (Figure 2C). Therefore, compared with those in the RSC group, the occurrence of tumours in the descending/ascending colon (DAC group) directly resulted in an increased incidence of PPCs, and other clinical characteristics, such as the gastrointestinal recovery time and age of patients, did not mediate this effect.

4 Discussion

In the laparoscopic procedure for CRC, anterior resection of rectal cancer and sigmoidectomy necessitate the sustained steep Trendelenburg position, where the patient's head is positioned lower than the feet at an angle of approximately 25–30°. In contrast, ascending and descending colectomies require intermittent transformations of the Trendelenburg position of ±10–15°. Research has indicated that rapid atelectasis involvement can develop in lung areas with high pressure within 10 minutes in the Trendelenburg position (23). The significant discrepancy in peak and plateau airway pressures and pulmonary compliance between these two surgical positions (Table 4) may precipitate various pulmonary stresses and lung injuries (21–23, 29). This process is further complicated by carbon dioxide pneumoperitoneum, which exacerbates atelectasis, inflammation and lung injury via hypercapnia and respiratory acidosis. Consequently, the airway pressure (barotrauma) resulting from laparoscopy may surpass the elastic limits of the lung parenchyma, generating transpulmonary pressures that damage the alveolar epithelium (34, 35). Our results in Table 4 show that patients in the Trendelenburg position (25–30°) had higher peak airway pressure (Ppeak) and plateau airway pressure (Pplat) and lower pulmonary compliance than patients in the reverse Trendelenburg position did (P<0.001, Table 4). The abdominal contents move upwards towards the diaphragm in the Trendelenburg position, increasing intrathoracic cavity pressure and airway pressure and decreasing lung compliance. Once a threshold is overcome, excessive airway pressure and lung strain deform epithelial and endothelial cells (known as barotrauma), resulting in secondary stress fatigue, microcapillary rupture and inflammation (35, 36). Inflammation triggered by damage can be perpetuated by the activation of various signalling pathways, resulting in further biotrauma to the lung. Hence, patients with worse dynamic ventilation parameters can suffer worse lung injuries.

To characterise the magnitude of intraoperative general and pulmonary inflammation and lung injury, our research applied

TABLE 5 Effectiveness outcomes.

	Rectosigmoid colon Group (RSC, N=200)	De/Ascending colon Group (DAC, N=100)	OR (95% CI)	*P* value*
Postoperative recovery				
PACU time, min	20.0 (15.0-30.0)	20.0 (15.0-29.5)	0.996 (0.978-1.014)	0.700
Gastrointestinal recovery time, days	3.0 (2.0-3.0)	3.0 (2.0-3.0)	1.698 (1.098-2.684)	0.020
Postoperative hospitalisation, day	6.0 (6.0-8.0)	7.0 (6.0-8.0)	1.044 (0.934-1.165)	0.439
Mechanical lung injury				
sRAGE, pg/ml				
Preoperation	497.4 (329.7-862.2)	474.5 (348.2-659.3)	1.000 (0.998-1.001)	0.452
POD 1	1271.6 (896.3-1587.6)	1029.6 (576.8-1365.2)	0.999 (0.998-1.000)	0.007
POD 3	1063.3 (618.4-1335.4)	881.1 (510.4-1060.4)	0.999 (0.998-1.000)	0.077
ANG-2, ng/ml				
Preoperation	4.3 (2.3-7.4)	3.6 (2.1-8.1)	1.050 (0.981-1.127)	0.155
POD 1	11.3 (7.6-15.3)	9.9 (4.7-13.4)	0.993 (0.928-1.054)	0.816
POD 3	8.7 (5.6-12.3)	8.2 (4.3-10.9)	1.009 (0.939-1.080)	0.792
Systemic inflammatory index				
IL-1β, pg/ml				
Preoperation	2.9 (2.4-3.3)	2.6 (2.4-3.1)	0.765 (0.470-1.048)	0.170
POD 1	3.7 (3.0-5.0)	4.4 (3.1-6.4)	1.024 (0.983-1.076)	0.249
POD 3	3.1 (2.6-3.6)	3.2 (2.7-4.0)	0.990 (0.905-1.039)	0.740
IL-6, pg/ml				
Preoperation	2.1 (1.6-2.3)	2.1 (1.6-2.3)	0.820 (0.348-1.803)	0.633
POD 1	2.5 (2.1-3.0)	2.6 (2.3-4.4)	1.073 (0.977-1.214)	0.171
POD 3	2.2 (1.7-2.4)	2.2 (1.7-2.5)	1.155 (0.755-1.735)	0.478
Incidence of PPCs within 30 days, cases (%)	60 (30.0)	48 (48.0)	1.669 (1.141-2.439)	0.008#
Kroenke grade				
1	43 (21.5)	23 (23.0)	1.111 (0.669-1.844)	0.684#
2-3	17 (8.5)	25 (25.0)	0.875 (0.465-1.647)	0.679#
Radiographic diagnosis				
Microatelectasis	41 (20.5)	24 (24.0)	1.211 (0.732-2.005)	0.456#
Atelectasis	10 (5.0)	17 (17.0)	3.526 (1.614-7.703)	0.002#
Pleural Effusion	12 (6.0)	16 (16.0)	2.787 (1.318-5.895)	0.007#
Pneumonia	7 (3.5)	7 (7.0)	2.171 (0.761-6.197)	0.147#

The data are shown as n (%) or medians (interquartile ranges).
*Except specifically note that the odds ratios (95% CI) and their relative *P* values were calculated by the logistic regression model.
#Hazard ratios (95% CIs) and their relative *P* values were calculated by the univariate Cox proportional hazards model.
sRAGE, soluble form of the receptor for advanced glycation end products; ANG-2, angiopoietin-2; PPCs, postoperative pulmonary complications; IL-1β, interleukin-1β; IL-6, interleukin-6; PACU, postanaesthesia care unit; POD, postoperative day.

several biological biomarkers. Receptors for advanced glycation end products (RAGE), especially sRAGE, are widely studied as indicators of pulmonary injury because of their high expression in type I pneumocytes (37–39). To the best of our knowledge, plasma sRAGE is the only biomarker that has been correlated with a functional readout of epithelial barrier function and alveolar fluid clearance (40, 41). sRAGE has been extensively implicated in the process of inflammation and lung injury to alveolar epithelial cells (42, 43), particularly in the context of mechanical high tidal volume-induced alveolar overdistension or acute respiratory

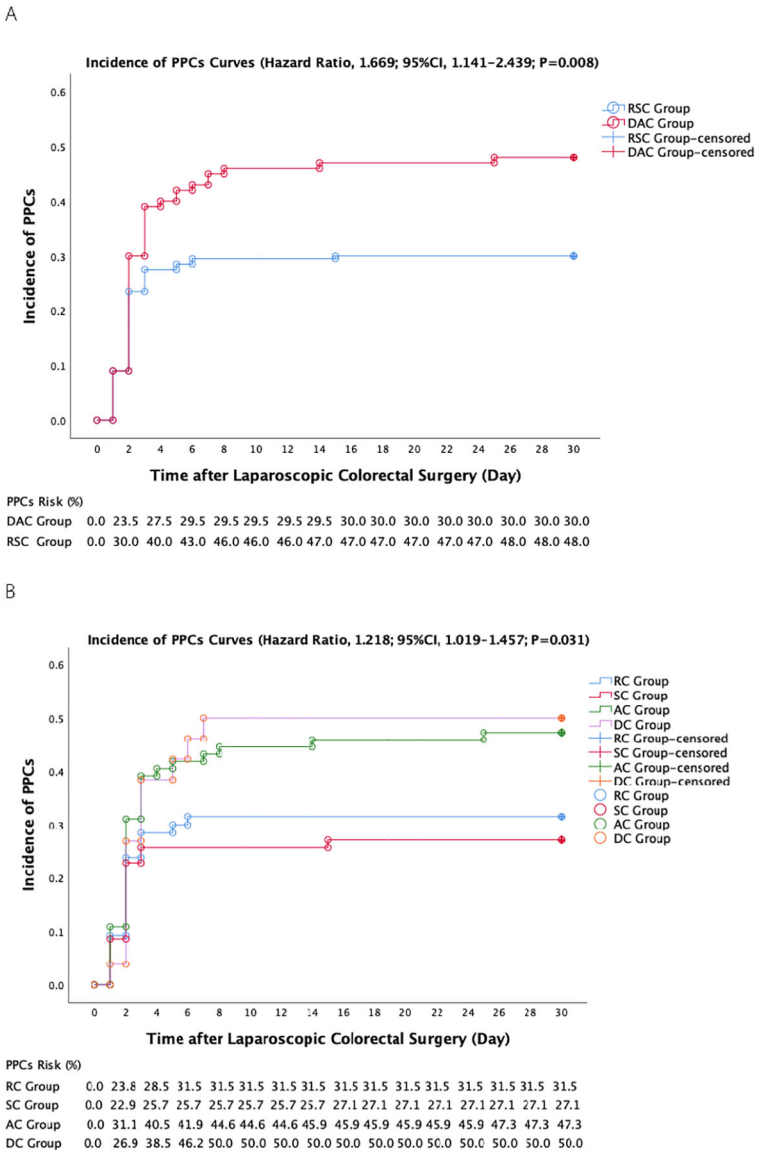

FIGURE 1
Curves representing the incidence of postoperative time-to-PPCs within a 30-day postoperative period (univariate Cox proportional hazards regression analysis). **(A)** Incidence of PPCs in the descending/ascending colon (DAC) group and the rectosigmoid colon (RSC) group. **(B)** Incidence of PPCs in subgroups of various colorectal positions. DC, descending colon; AC, ascending colon; SC, sigmoid colon; RC, rectum of the colon.

distress syndrome (ARDS) (44, 45). Previous study demonstrated that sRAGE is strongly linked to the duration of ventilation for POD 1, with a 25% multiplicative increase in hours of ventilation (95% CI, 2% to 52%, P = 0.03) observed for every 50 pg/ml increase in sRAGE (46). In addition to sRAGE, another major form of RAGE is anchored to the cell membrane (mRAGE) (39, 47). mRAGE is capable of binding proinflammatory ligands in the immune microenvironment, such as AGEs, S100 proteins and high mobility group box 1 (HMGB1), and consequently activates downstream inflammatory pathways, such as nuclear factor kappa-light-chain enhancer of activated B cells (NF-κB) and signal transducer and activator of transcription 3 (STAT3). Stimulation of these pathways can lead to cytokine release, cell migration and upregulated RAGE expression, which in turn perpetuates the inflammatory cascade, resulting in the occurrence and progression of many pathological processes and diseases, including airway inflammation and acute lung injury (ALI) (48). Moreover, the extracellular part of mRAGE is cleaved from the membrane upon lung injury and becomes sRAGE, which can be detected in blood and bronchial lavage fluid. sRAGE functions as a "decoy", as it attaches to ligands of RAGE without activating intracellular pathways and therefore prevents excessive cell injury and airway inflammation by decreasing the expression and release of downstream cytokines, such as tumour necrosis factor-alpha (TNF-α), IL-1β and IL-6 (47, 49). The interactions between RAGE and certain ligands and sequential pathways constitute the RAGE axis. Since the RAGE axis effectively modulates inflammation, several benign and malignant diseases that are strongly associated

10.3389/fimmu.2025.1546167

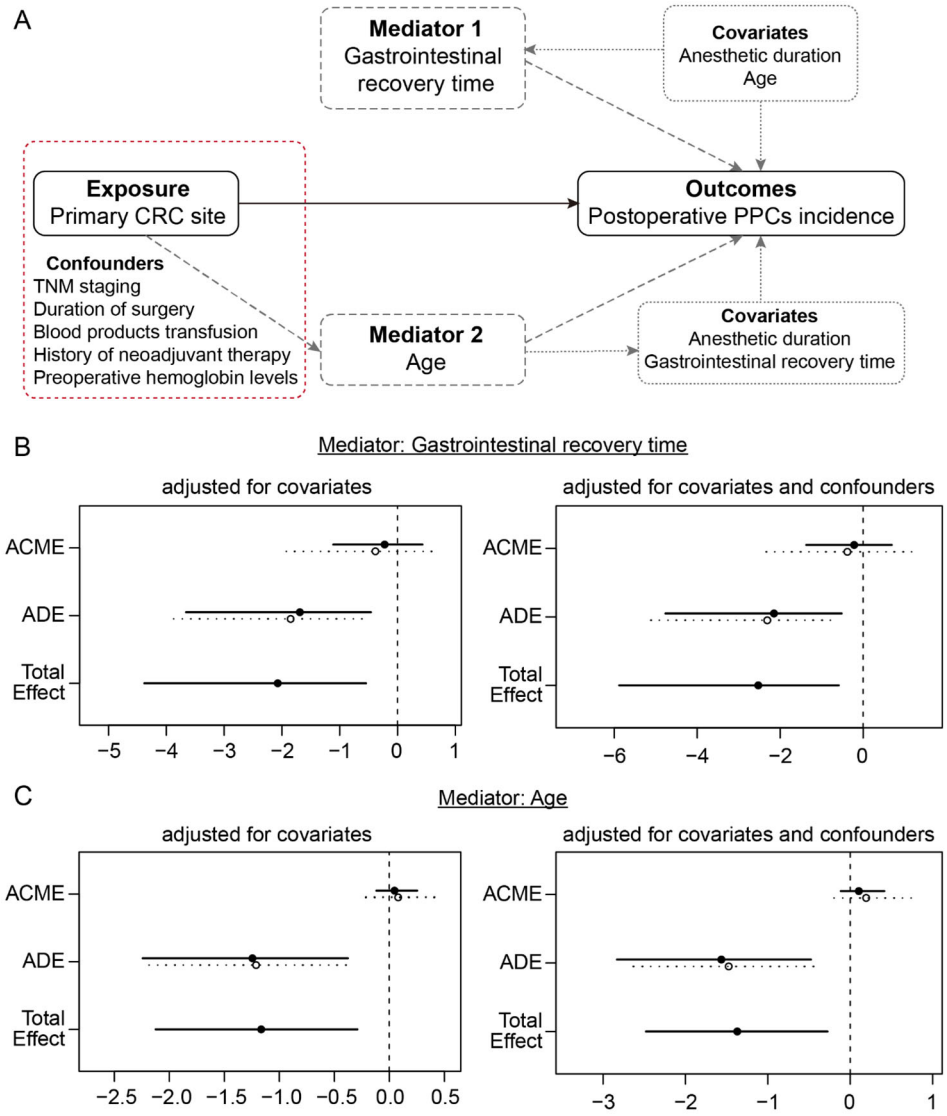

FIGURE 2
Causal mediation analysis of the primary CRC site (exposure), gastrointestinal recovery time (mediator 1), age (mediator 2) and incidence of PPCs (outcome). **(A)** Directed acyclic graph of the mediation model. The measured covariates are included as fixed effects in each model, in the absence or presence of the confounders that are associated with the primary CRC site. **(B)** Mediation analysis of the models with mediator 1 (gastrointestinal recovery time) in the absence or presence of confounders. **(C)** Mediation analysis of the models with mediator 2 (age) in the absence or presence of confounders.

with the immune microenvironment can be affected by the function of RAGE (50). The extant literature provides substantial support for the proposition that endogenous plasma sRAGE plays a mechanistic role in the pathophysiology of ARDS in models of lung injury that involve acid and hyperoxia (37, 51, 52). Additionally, existing studies further corroborate the pivotal function of endogenous plasma sRAGE within the AGE-RAGE axis as a prospective catalyst of lung injury, indicating that there is potential for reducing plasma sRAGE levels or targeting the AGER/sRAGE axis to have a preventative or therapeutic effect on inflammation-related lung disease (53–55). Notably, sRAGE is also regarded as a promising biomarker for colon carcinoma. Aglago et al. reported an inverse association between prediagnostic sRAGE levels and colorectal risk in men (56).

ANG-2 is another potential candidate for endothelial inflammation and injury caused primarily by ARDS and sepsis (57, 58). ANG-2 originates primarily from endothelial cells and acts as a key factor in the modulation of vascular permeability as an antagonist against ANG-1, which promotes endothelial permeability by preserving cellular junctions and signalling the reduction in certain surface-adhesion molecules through tyrosine kinases with immunoglobulin-like and EGF-like domain 2 (Tie-2) signalling pathways (59). As the highest Tie-2 expression in adult tissues is observed in the lung, disruption of the pathway caused by ANG-2 can lead to pulmonary disorders (60). Environmental factors related to pathogenesis, such as hypoxia and increased levels of cytokines, can lead to the production and release of ANG-2 (61), and existing studies have shown that ANG-2 is an

essential biomarker of ALI/ARDS (62, 63). Moreover, ANG-2 has been shown to enhance tumour metastasis and immunosuppression by regulating cytokine levels in the tumour microenvironment, suggesting that ANG-2 is a potential target for cancer treatment therapy (64, 65). ANG-2 and vascular endothelial growth factor (VEGF) may promote the formation of new blood vessels through a synergistic effect, leading to liver metastasis of colorectal cancer (66). ANG-2-targeted comprehensive treatment has sparked new ideas in cancer treatment (67, 68).

Furthermore, IL-1β and IL-6 are major proinflammatory cytokines released by diverse immune and nonimmune cells upon stimulation, such as infection, injury, and stress. IL-1β originates primarily from macrophages, dendritic cells, and neutrophils, although it can also be secreted by epithelial cells and fibroblasts. Canonically, it is synthesised as an inactive precursor, which is cleaved and activated by caspase-1 upon environmental stimulation (69). However, the production of IL-6 is initiated by pathogen-associated molecular patterns (PAMPs) and damage-associated molecular patterns (DAMPs) (70). Various types of cells, including T cells, macrophages, and fibroblasts, are involved in the synthesis and secretion of IL-6. Both cytokines are essential for adjusting the immune microenvironment by triggering the activation of various immune cells, stimulating the differentiation of T helper cells, and contributing to the synthesis and secretion of acute-phase reactants in the liver. Owing to their pivotal roles in inflammation, IL-1β and IL-6 have been proposed as biomarkers of lung injury and airway inflammation, particularly in diseases such as chronic obstructive pulmonary disease (COPD), ALI and ARDS (62). In addition, during general anaesthesia, the expression and release of these cytokines can be stimulated by lung impairment caused by mechanical ventilation and the activation of pathways related to RAGE (47). The presence of these cytokines serves as indicators of ongoing immune activation and the extent of airway remodelling, making them useful for monitoring the magnitude and progression of lung injuries.

Inflammation has been demonstrated to play a critical role in the pathogenesis of PPCs following noncardiac surgery (46). Nevertheless, no correlation between the above inflammatory indicators and the incidence of PPCs was found by the analysis of the univariate Cox proportional hazards model in this study. This result is similar to those of many investigations. Aaron et al. identified sRAGE as a potential indicator of acute lung injury, with no significant correlation with PPCs (46); Neto et al. identified none of the plasma biomarkers expressed for inflammation or lung injury (TNF-α, IL-6 and IL-8; sRAGE, surfactant protein [SP]-D, Clara cell protein [CC]-16 and Krebs von den Lungen 6 [KL6]) is related to PPCs (71); Jabaudon et al. compared the sRAGE levels between patients who received protective ventilation and those who did not and concluded that patients with at least one hypoxemia episode presented elevated sRAGE levels during mechanical ventilation, but no association was observed between intraoperative changes in sRAGE and PPCs within 30 days postsurgery (72). The ambiguity of the correlation between plasma sRAGE and PPCs may be ascribed to the inflammatory consumption of sRAGE, as it works by attaching to ligands. Recent studies have demonstrated that postoperative sRAGE rapidly decreases to or below preoperative levels within 24 hours following cardiac surgery. Consequently, it is plausible that by the time samples were collected on POD 1, sRAGE values may have already returned to normal (46). Additionally, as the heterogeneity of patients and definitions of PPCs vary, not all lung injuries ultimately lead to PPCs.

Notably, patients who undergo proctosigmoidectomy (RSC group) with more pulmonary stress and injury are theoretically more susceptible to PPCs incidence. Our findings revealed a consistent correlation between the RSC group with the steep Trendelenburg position and lung epithelium injury, with higher sRAGE levels in the RSC group on the postoperative day (POD, P=0.007 for POD 1 and P=0.077 for POD 3 [marginal significance]; Table 5). This may be attributed to the greater degree of lung injury in patients in the RSC group suffered from steeper Trendelenburg position than that in the counterpart, as we expected. However, contrary to expectations, univariate and multivariate Cox regression analyses revealed a negative correlation between the primary CRC site and PPCs, with a significantly decreased incidence of PPCs in the RSC group (DAC vs. RSC; HR=1.669; 95% CI, 1.141 to 2.439; P=0.008). Our propensity score weighting method using overlap weights in a Cox proportional hazards regression analysis demonstrated that tumours occurring in the descending/ascending colon (DAC group) indeed increased the risk of PPCs (adjusted HR=1.634; 95% CI, 1.115 to 2.396; P=0.012). The subsequent causal mediation analysis demonstrated that this factor remains a direct effect on the incidence of PPCs when adjusted for several baseline confounders and clinical covariates related to the primary CRC site and PPCs.

The causes of DAC for the high incidence of PPCs are worthy of attention. Postoperative gastrointestinal recovery time, age and anaesthetic duration exceeding 3 hours were also unfavourable factors for the incidence of PPCs according to the univariate Cox proportional hazards model. It is well known that enhanced recovery is essential for reducing postoperative complications (73), especially for PPCs (28, 74). The literature indicates that right hemicolectomy is associated with inferior intestinal function and an elevated prevalence of metabolic syndrome due to factors such as bile acid malabsorption, impaired water reabsorption, small intestinal bacterial overgrowth, and gut microbial dysbiosis, which potentially deteriorates gastrointestinal recovery and facilitates inflammation and PPCs (75–77). In the present study, a greater gastrointestinal recovery time was indeed observed in the DAC group (P=0.020, Table 5), and patients with PPCs exhibited longer gastrointestinal recovery times (patients with PPCs vs. those without PPCs; 3.0 [2.0–3.0] vs. 2.5 [2.0–3.0]; OR=2.114; 95% CI, 1.361 to 3.362; P=0.001). Additionally, age serves as a robust marker for PPCs, even in healthy older patients at elevated risk of PPCs (8, 28). Previous studies have indicated that age over 60 years or 65 years is a risk factor for PPCs development (8, 78). Stratification analysis suggested that the risk of PPCs significantly increased with age, which may be related to the frailty of elderly patients with weakened respiratory muscle function (10, 27, 79). In terms of duration, the literature substantiates that a surgical or anaesthesia duration surpassing two hours independently contributes to PPCs, revealing a significant association between operative duration and

PPCs. This association has odds ratios (and confidence intervals) of 4.9 (2.4 to 10.1) and 9.7 (4.7 to 19.9) for operative periods exceeding 2 and 3 hours, respectively (9, 27). Here, we identified an obvious correlation between primary tumour location and surgical/anaesthesia duration, as shown in Table 3 (P<0.001 for anaesthetic duration, P=0.002 for surgical duration). For subgroup analysis, the median anaesthetic durations for the sigmoid (160.0 min), rectal (170.0 min), ascending (190.5 min) and descending (212.0 min) colon regions also showed apparent relevance to the corresponding time-to-PPCs incidence (P=0.031, Figure 1B).

In addition, three other potential explanations were also considered for the high prevalence of PPCs in the DAC group. First, complex surgical interventions inherently involve a greater degree of trauma and an extended period of anaesthesia and surgery, which consequently fosters an environment conducive to the development of PPCs. Compared with sigmoidectomy, ascending and descending colectomies entail intricate vascular trajectories, neighbouring organ interactions, and complex intestinal anastomosis techniques. Moreover, in comparison with the pelvic support surrounding the rectosigmoid colon, the absence of bony support in the DAC group further constrained the surgical field, thereby increasing procedural difficulty and correlating with a lower SRS score for evaluating surgical conditions in laparoscopic procedures in the presence of identical degrees of neuromuscular blockade (Table 3). Consequently, our study revealed that the surgical and anaesthetic times required for ascending and descending colectomy procedures are longer than those for rectosigmoidectomy. As reported in the literature, the incidence of PPCs is notably elevated in patients receiving extended anaesthesia and surgical procedures (8, 27, 78). Second, the surgical incision pathways for different CRC segments notably influence the development of PPCs (28). The ascending and descending colectomies typically necessitate paramedian or transrectal incisions (Figure 3); as a consequence, structures such as the anterior branches of the intercostal nerve, the rectus sheath (both anterior and posterior), and the rectus abdominis muscle are affected. In conjunction with compromised abdominal respiration, this impairment of rectus abdominis muscle function may accelerate the development of concomitant atelectasis and pneumonia. In contrast, procedures within the RSC group generally require a midline incision of the linea alba, exerting less impact on abdominal autonomy and breathing. Finally, as previously indicated, preoperative anaemia is an independent risk factor for PPCs (25, 27, 80). Likewise, relevant transfusions also promote the onset of this complication (81–83). Owing to the clinical characteristics of patients with DAC symptoms appearing later than those with RSC symptoms, anaemia (ASD=0.443) and transfusion (P=0.003) constitute a substantial proportion of patients with DAC symptoms (Tables 2, 3); hence, anaemia is also a major cause of this postoperative complication.

Notably, cancer and inflammation are mutually reinforcing factors. CRC has been reported to induce inflammation through several mechanisms, with the expression of IL-1 being a mediator. Moreover, once the growth of a tumour exceeds its blood and nutrient supply, necrotic cell death in the tumour results in the release of various DAMPs, including IL-1 and HMGB1, both of which are related to lung inflammation (84). On the other hand, the immune microenvironment in the lung parenchyma can be altered by these DAMPs and establish a premetastatic niche for CRC (85). In summary, CRC patients may be at increased risk of developing lung injuries and PPCs because tumours elicit inflammation, and inflammation in the lungs promotes the metastasis of CRC.

Our investigation is subject to certain limitations. We endeavoured to curtail potential imbalances and limit the influence of clinical characteristics on PPCs by performing PSM for factors such as respiratory comorbidities, smoking status, and age. However, given the inherent peculiarities of these clinical

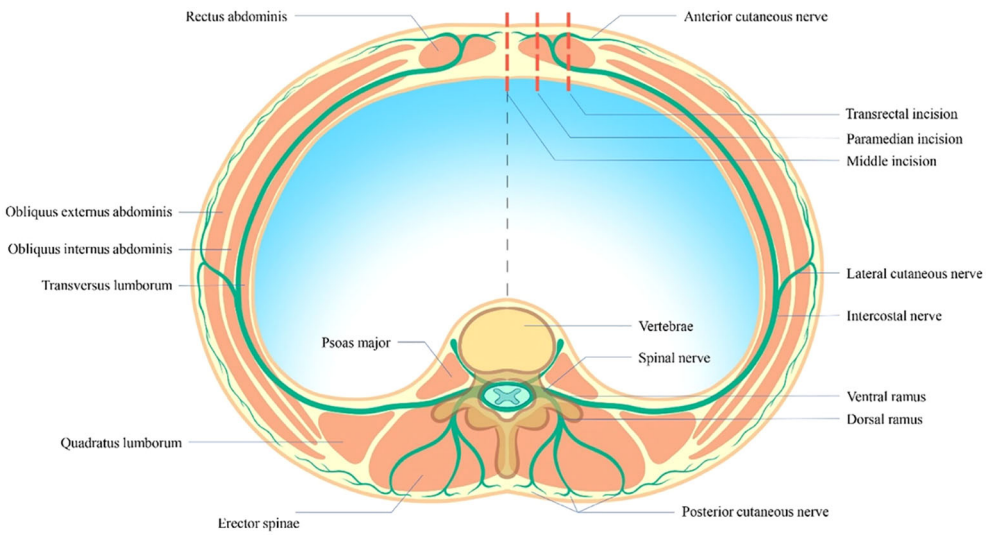

FIGURE 3
Various surgical incision paths cause distinct neuromuscular injuries.

variables in demographic and baseline data, achieving absolute balance remains an unrealistic expectation. Furthermore, although this study is based on the hypothesis that the steep Trendelenburg position induces more lung stress in the pathogenesis of pulmonary injury and PPCs, maintaining a sustained surgical position at one angle is impractical clinically because of the variety of surgical procedures performed, not even with prospective randomised controlled trials. Additionally, as a single-centre study with a population limited to a high-resource cancer centre, the generalisability of the results to other settings remains limited; hence, a larger sample size is needed. Despite these limitations, this study signifies progress in assessing the correlation between primary CRC sites, lung injury and the incidence of PPCs in patients who have received colorectal laparoscopy. Subsequent research could explore the impact of disparate surgical positions on the dynamic distribution of pulmonary ventilation, such as leveraging electrical impedance tomography (EIT) imaging. This approach could further elucidate the correlation between inclined surgical position, the distinct ventral and dorsal redistribution of tidal ventilation, and PPCs.

In summary, CRC patients display diverse surgical positions, procedures, and postoperative recovery patterns (75–77). Although the rectosigmoid colon with the Trendelenburg position in laparoscopy triggers epithelial lung injury, as indicated by elevated postoperative sRAGE levels, a lower PPCs incidence was unexpectedly observed than in those with tumours in the descending/ascending colon. Subsequent analyses confirmed that the primary CRC site was an independent risk factor influencing the onset of PPCs. The other baseline, clinical, and postoperative recovery characteristics cannot explain this effect. Therefore, not the Trendelenburg position and the resulting lung injury but rather the primary tumour site occurring in the descending/ascending colon directly affect the incidence of PPCs.

Data availability statement

The datasets contain identifiable contents of patients. The datasets studied in this research can be obtained from the corresponding authors upon reasonable request. Requests to access these datasets should be directed to TY, blizzardyt@163.com.

Ethics statement

The studies involving humans were approved by National Cancer Center/Cancer Hospital, Chinese Academy of Medical Sciences and Peking Union Medical College, National GCP Center for Anticancer Drugs, The Independent Ethics Committee. The studies were conducted in accordance with the local legislation and institutional requirements. The human samples used in this study were acquired from primarily isolated as part of our previous study for which ethical approval was obtained. Written informed consent for participation was not required from the participants or the participants' legal guardians/next of kin in accordance with the national legislation and institutional requirements.

Author contributions

H-XL: Data curation, Formal analysis, Funding acquisition, Methodology, Writing – original draft, Writing – review & editing. LC: Data curation, Formal analysis, Methodology, Writing – review & editing. YL: Data curation, Formal analysis, Methodology, Writing – review & editing. T-HW: Writing – review & editing, Data curation, Formal analysis, Methodology. F-DM: Data curation, Formal analysis, Methodology, Writing – review & editing. LX: Investigation, Software, Validation, Writing – review & editing. MW: Investigation, Software, Validation, Writing – review & editing. Z-XZ: Investigation, Software, Validation, Writing – review & editing. S-NQ: Investigation, Software, Validation, Writing – review & editing. FW: Resources, Software, Visualization, Writing – review & editing. WT: Investigation, Software, Validation, Writing – review & editing. S-JW: Investigation, Software, Validation, Writing – review & editing. Y-LS: Conceptualization, Funding acquisition, Project administration, Resources, Software, Supervision, Visualization, Writing – original draft, Writing – review & editing. HZ: Conceptualization, Project administration, Supervision, Writing – review & editing. TY: Conceptualization, Funding acquisition, Project administration, Supervision, Writing – original draft, Writing – review & editing.

Funding

The author(s) declare financial support was received for the research, authorship, and/or publication of this article. Support for this work was received from the CAMS Innovation Fund for Medical Sciences (CIFMS, 2022-I2M-C&T-B-061 and 2021-I2M-1-066), the Beijing Hope Run Special Fund for the Cancer Foundation of China (LC2021A18, LC2022B06), and the National Natural Science Foundation of China (82073327).

Conflict of interest

The authors declare that the research was conducted in the absence of any commercial or financial relationships that could be construed as a potential conflict of interest.

Generative AI statement

The author(s) declare that no Generative AI was used in the creation of this manuscript.

Publisher's note

All claims expressed in this article are solely those of the authors and do not necessarily represent those of their affiliated organizations, or those of the publisher, the editors and the reviewers. Any product that may be evaluated in this article, or claim that may be made by its manufacturer, is not guaranteed or endorsed by the publisher.

References

1. Ladha K, Vidal Melo MF, McLean DJ, Wanderer JP, Grabitz SD, Kurth T, et al. Intraoperative protective mechanical ventilation and risk of postoperative respiratory complications: hospital based registry study. *Bmj*. (2015) 351:h3646. doi: 10.1136/bmj.h3646

2. Le LM, Chaiyakunapruk N. Urgent need to take action on reducing postoperative respiratory complications. *Lancet Reg Health West Pac*. (2021) 10:100136. doi: 10.1016/j.lanwpc.2021.100136

3. Abbott TEF, Fowler AJ, Pelosi P, Gama de Abreu M, Moller AM, Canet J, et al. A systematic review and consensus definitions for standardised end-points in perioperative medicine: pulmonary complications. *Br J Anaesth*. (2018) 120:1066–79. doi: 10.1016/j.bja.2018.02.007

4. Serpa Neto A, Hemmes SN, Barbas CS, Beiderlinden M, Fernandez-Bustamante A, Futier E, et al. Incidence of mortality and morbidity related to postoperative lung injury in patients who have undergone abdominal or thoracic surgery: a systematic review and meta-analysis. *Lancet Respir Med*. (2014) 2:1007–15. doi: 10.1016/S2213-2600(14)70228-0

5. Schuijt MTU, Hol L, Nijbroek SG, Ahuja S, van Meenen D, Mazzinari G, et al. Associations of dynamic driving pressure and mechanical power with postoperative pulmonary complications-posthoc analysis of two randomised clinical trials in open abdominal surgery. *EClinicalMedicine*. (2022) 47:101397. doi: 10.1016/j.eclinm.2022.101397

6. Ferrando C, Soro M, Unzueta C, Suarez-Sipmann F, Canet J, Librero J, et al. Individualised perioperative open-lung approach versus standard protective ventilation in abdominal surgery (iPROVE): a randomised controlled trial. *Lancet Respir Med*. (2018) 6:193–203. doi: 10.1016/S2213-2600(18)30024-9

7. Kirmeier E, Eriksson LI, Lewald H, Jonsson Fagerlund M, Hoeft A, Hollmann M, et al. Post-anaesthesia pulmonary complications after use of muscle relaxants (POPULAR): a multicentre, prospective observational study. *Lancet Respir Med*. (2019) 7:129–40. doi: 10.1016/S2213-2600(18)30294-7

8. Miskovic A, Lumb AB. Postoperative pulmonary complications. *Br J Anaesth*. (2017) 118:317–34. doi: 10.1093/bja/aex002

9. Güldner A, Kiss T, Serpa Neto A, Hemmes SN, Canet J, Spieth PM, et al. Intraoperative protective mechanical ventilation for prevention of postoperative pulmonary complications: a comprehensive review of the role of tidal volume, positive end-expiratory pressure, and lung recruitment maneuvers. *Anesthesiology*. (2015) 123:692–713. doi: 10.1097/ALN.0000000000000754

10. Smetana GW, Lawrence VA, Cornell JE, American College of P. Preoperative pulmonary risk stratification for noncardiothoracic surgery: systematic review for the American College of Physicians. *Ann Intern Med*. (2006) 144:581–95. doi: 10.7326/0003-4819-144-8-200604180-00009

11. Jammer I, Wickboldt N, Sander M, Smith A, Schultz MJ, Pelosi P, et al. Standards for definitions and use of outcome measures for clinical effectiveness research in perioperative medicine: European Perioperative Clinical Outcome (EPCO) definitions: a statement from the ESA-ESICM joint taskforce on perioperative outcome measures. *Eur J Anaesthesiol*. (2015) 32:88–105. doi: 10.1097/EJA.0000000000000118

12. Hulzebos EH, Helders PJ, Favié NJ, De Bie RA, Brutel de la Riviere A, Van Meeteren NL. Preoperative intensive inspiratory muscle training to prevent postoperative pulmonary complications in high-risk patients undergoing CABG surgery: a randomized clinical trial. *Jama*. (2006) 296:1851–7. doi: 10.1001/jama.296.15.1851

13. Huang D, Zhou S, Yu Z, Chen J, Xie H. Lung protective ventilation strategy to reduce postoperative pulmonary complications (PPCs) in patients undergoing robot-assisted laparoscopic radical cystectomy for bladder cancer: A randomized double blinded clinical trial. *J Clin Anesth*. (2021) 71:110156. doi: 10.1016/j.jclinane.2020.110156

14. Neto AS, Hemmes SN, Barbas CS, Beiderlinden M, Fernandez-Bustamante A, Futier E, et al. Association between driving pressure and development of postoperative pulmonary complications in patients undergoing mechanical ventilation for general anaesthesia: a meta-analysis of individual patient data. *Lancet Respir Med*. (2016) 4:272–80. doi: 10.1016/S2213-2600(16)00057-6

15. Bray F, Laversanne M, Sung H, Ferlay J, Siegel RL, Soerjomataram I, et al. Global cancer statistics 2022: GLOBOCAN estimates of incidence and mortality worldwide for 36 cancers in 185 countries. *CA Cancer J Clin*. (2024) 74:229–63. doi: 10.3322/caac.21834

16. Yang Y, Wang HY, Chen YK, Chen JJ, Song C, Gu J. Current status of surgical treatment of rectal cancer in China. *Chin Med J (Engl)*. (2020) 133:2703–11. doi: 10.1097/CM9.0000000000001076

17. Devesa SS, Chow WH. Variation in colorectal cancer incidence in the United States by subsite of origin. *Cancer*. (1993) 71:3819–26. doi: 10.1002/1097-0142(19930615)71:12<3819::AID-CNCR2820711206>3.0.CO;2-L

18. Nunn JF, Payne JP. Hypoxaemia after general anaesthesia. *Lancet*. (1962) 2:631–2. doi: 10.1016/S0140-6736(62)92541-2

19. Bendixen HH, Hedley-Whyte J, Laver MB. Impaired oxygenation in surgical patients during general anesthesia with controlled ventilation. A concept of atelectasis. *N Engl J Med*. (1963) 269:991–6. doi: 10.1056/NEJM196311072691901

20. Wang Y, Wang H, Wang H, Zhao X, Li S, Chen L. Exploring the intraoperative lung protective ventilation of different positive end-expiratory pressure levels during abdominal laparoscopic surgery with Trendelenburg position. *Ann Transl Med*. (2019) 7:171. doi: 10.21037/atm.2019.03.45

21. Yu J, Park JY, Kim DH, Kim S, Hwang JH, Seo H, et al. Incidence and Risk Factors of Pulmonary Complications after Robot-Assisted Laparoscopic Prostatectomy: A Retrospective Observational Analysis of 2208 Patients at a Large Single Center. *J Clin Med*. (2019) 8:1509. doi: 10.3390/jcm8101509

22. Awad H, Walker CM, Shaikh M, Dimitrova GT, Abaza R, O'Hara J. Anesthetic considerations for robotic prostatectomy: a review of the literature. *J Clin Anesth*. (2012) 24:494–504. doi: 10.1016/j.jclinane.2012.03.003

23. Girrbach F, Petroff D, Schulz S, Hempel G, Lange M, Klotz C, et al. Individualised positive end-expiratory pressure guided by electrical impedance tomography for robot-assisted laparoscopic radical prostatectomy: a prospective, randomised controlled clinical trial. *Br J Anaesth*. (2020) 125:373–82. doi: 10.1016/j.bja.2020.05.041

24. Andersson LE, Baath M, Thorne A, Aspelin P, Odeberg-Wernerman S. Effect of carbon dioxide pneumoperitoneum on development of atelectasis during anesthesia, examined by spiral computed tomography. *Anesthesiology*. (2005) 102:293–9. doi: 10.1097/00000542-200502000-00009

25. Mazo V, Sabaté S, Canet J, Gallart L, de Abreu MG, Belda J, et al. Prospective external validation of a predictive score for postoperative pulmonary complications. *Anesthesiology*. (2014) 121:219–31. doi: 10.1097/ALN.0000000000000334

26. Brooks-Brunn JA. Predictors of postoperative pulmonary complications following abdominal surgery. *Chest*. (1997) 111:564–71. doi: 10.1378/chest.111.3.564

27. Canet J, Gallart L, Gomar C, Paluzie G, Valles J, Castillo J, et al. Prediction of postoperative pulmonary complications in a population-based surgical cohort. *Anesthesiology*. (2010) 113:1338–50. doi: 10.1097/ALN.0b013e3181fc6e0a

28. Odor PM, Bampoe S, Gilhooly D, Creagh-Brown B, Moonesinghe SR. Perioperative interventions for prevention of postoperative pulmonary complications: systematic review and meta-analysis. *Bmj*. (2020) 368:m540. doi: 10.1136/bmj.m540

29. Grieco DL, Russo A, Anzellotti GM, Romano B, Bongiovanni F, Dell'Anna AM, et al. Lung-protective ventilation during Trendelenburg pneumoperitoneum surgery: A randomized clinical trial. *J Clin Anesth*. (2023) 85:111037. doi: 10.1016/j.jclinane.2022.111037

30. Collaborative ST and Collaborative T. Evaluation of prognostic risk models for postoperative pulmonary complications in adult patients undergoing major abdominal surgery: a systematic review and international external validation cohort study. *Lancet Digit Health*. (2022) 4:e520–31. doi: 10.1016/S2589-7500(22)00069-3

31. Linares-Perdomo O, East TD, Brower R, Morris AH. Standardizing predicted body weight equations for mechanical ventilation tidal volume settings. *Chest*. (2015) 148:73–8. doi: 10.1378/chest.14-2843

32. Kroenke K, Lawrence VA, Theroux JF, Tuley MR. Operative risk in patients with severe obstructive pulmonary disease. *Arch Internal Med*. (1992) 152:967–71. doi: 10.1001/archinte.1992.00400170057011

33. Boon M, Martini CH, Aarts L, Dahan A. The use of surgical rating scales for the evaluation of surgical working conditions during laparoscopic surgery: a scoping review. *Surg Endosc*. (2019) 33:19–25. doi: 10.1007/s00464-018-6424-5

34. Chiumello D, Carlesso E, Cadringher P, Caironi P, Valenza F, Polli F, et al. Lung stress and strain during mechanical ventilation for acute respiratory distress syndrome. *Am J Respir Crit Care Med*. (2008) 178:346–55. doi: 10.1164/rccm.200710-1589OC

35. Protti A, Cressoni M, Santini A, Langer T, Mietto C, Febres D, et al. Lung stress and strain during mechanical ventilation: any safe threshold? *Am J Respir Crit Care Med*. (2011) 183:1354–62. doi: 10.1164/rccm.201010-1757O

36. Marini JJ, Rocco PRM, Gattinoni L. Static and dynamic contributors to ventilator-induced lung injury in clinical practice. Pressure, energy, and power. *Am J Respir Crit Care Med*. (2020) 201:767–74. doi: 10.1164/rccm.201908-1545CI

37. Uchida T, Shirasawa M, Ware LB, Kojima K, Hata Y, Makita K, et al. Receptor for advanced glycation end-products is a marker of type I cell injury in acute lung injury. *Am J Respir Crit Care Med*. (2006) 173:1008–15. doi: 10.1164/rccm.200509-1477OC

38. Shirasawa M, Fujiwara N, Hirabayashi S, Ohno H, Iida J, Makita K, et al. Receptor for advanced glycation endcationhiw is a marker of type I lung alveolar cells. *Genes to Cells*. (2004) 9:165–74. doi: 10.1111/j.1356-9597.2004.00712.x

39. Sierra-Colomina M, Garcia-Salido A, Leoz-Gordillo I, Martinez de Azagra-Garde A, Melen G, Garcia-Teresa MA, et al. sRAGE as severe acute bronchiolitis biomarker, prospective observational study. *Pediatr Pulmonol*. (2020) 55:3429–36. doi: 10.1002/ppul.v55.12

40. Jabaudon M, Blondonnet R, Roszyk L, Bouvier D, Audard J, Clairefond G, et al. Soluble receptor for advanced glycation end-products predicts impaired alveolar fluid clearance in acute respiratory distress syndrome. *Am J Respir Crit Care Med*. (2015) 192:191–9. doi: 10.1164/rccm.201501-0020OC

41. Ware LB, Matthay MA. Alveolar fluid clearance is impaired in the majority of patients with acute lung injury and the acute respiratory distress syndrome. *Am J Respir Crit Care Med*. (2001) 163:1376–83. doi: 10.1164/ajrccm.163.6.2004035

42. Jabaudon M, Hamroun N, Roszyk L, Guerin R, Bazin JE, Sapin V, et al. Effects of a recruitment maneuver on plasma levels of soluble RAGE in patients with diffuse acute respiratory distress syndrome: a prospective randomized crossover study. *Intensive Care Med*. (2015) 41:846–55. doi: 10.1007/s00134-015-3726-0

43. Yehya N, Thomas NJ, Meyer NJ, Christie JD, Berg RA, Margulies SS. Circulating markers of endothelial and alveolar epithelial dysfunction are associated with mortality in pediatric acute respiratory distress syndrome. *Intensive Care Med*. (2016) 42:1137–45. doi: 10.1007/s00134-016-4352-1

44. Kuipers MT, Aslami H, Tuinman PR, Tuip-de Boer AM, Jongsma G, van der Sluijs KF, et al. The receptor for advanced glycation end products in ventilator-induced lung injury. *Intensive Care Med Exp*. (2014) 2:22. doi: 10.1186/s40635-014-0022-1

45. Jabaudon M, Berthelin P, Pranal T, Roszyk L, Godet T, Faure JS, et al. Receptor for advanced glycation end-products and ARDS prediction: a multicentre observational study. *Sci Rep*. (2018) 8:2603. doi: 10.1038/s41598-018-20994-x

46. Mittel A, Drubin C, Hua M, Nitta S, Wagener G, Vidal Melo MF. Association of acute systemic inflammation with patient-centric postoperative pulmonary complications after elective cardiac surgery. *Anesth Analg*. (2024). doi: 10.1213/ANE.0000000000007122

47. Sparvero LJ, Asafu-Adjei D, Kang R, Tang D, Amin N, Im J, et al. RAGE (Receptor for Advanced Glycation Endproducts), RAGE ligands, and their role in cancer and inflammation. *J Transl Med*. (2009) 7:17. doi: 10.1186/1479-5876-7-17

48. Hudson BI, Lippman ME. Targeting RAGE signaling in inflammatory disease. *Annu Rev Med*. (2018) 69:349–64. doi: 10.1146/annurev-med-041316-085215

49. Lin L, Li J, Song Q, Cheng W, Chen P. The role of HMGB1/RAGE/TLR4 signaling pathways in cigarette smoke-induced inflammation in chronic obstructive pulmonary disease. *Immun Inflammation Dis*. (2022) 10:e711. doi: 10.1002/iid3.v10.11

50. Rojas A, Lindner C, Schneider I, Gonzalez I, Uribarri J. The RAGE axis: A relevant inflammatory hub in human diseases. *Biomolecules*. (2024) 14:412. doi: 10.3390/biom14040412

51. Reynolds PR, Schmitt RE, Kasteler SD, Sturrock A, Sanders K, Bierhaus A, et al. Receptors for advanced glycation end-products targeting protect against hyperoxia-induced lung injury in mice. *Am J Respir Cell Mol Biol*. (2010) 42:545–51. doi: 10.1165/rcmb.2008-0265OC

52. Su X, Looney MR, Gupta N, Matthay MA. Receptor for advanced glycation end-products (RAGE) is an indicator of direct lung injury in models of experimental lung injury. *Am J Physiol Lung Cell Mol Physiol*. (2009) 297:L1–5. doi: 10.1152/ajplung.90546.2008

53. Jones TK, Feng R, Kerchberger VE, Reilly JP, Anderson BJ, Shashaty MGS, et al. Plasma sRAGE acts as a genetically regulated causal intermediate in sepsis-associated acute respiratory distress syndrome. *Am J Respir Crit Care Med*. (2020) 201:47–56. doi: 10.1164/rccm.201810-2033OC

54. Keefe J, Yao C, Hwang SJ, Courchesne P, Lee GY, Dupuis J, et al. An integrative genomic strategy identifies sRAGE as a causal and protective biomarker of lung function. *Chest*. (2022) 161:76–84. doi: 10.1016/j.chest.2021.06.053

55. Yonchuk JG, Silverman EK, Bowler RP, Agustí A, Lomas DA, Miller BE, et al. Circulating soluble receptor for advanced glycation end products (sRAGE) as a biomarker of emphysema and the RAGE axis in the lung. *Am J Respir Crit Care Med*. (2015) 192:785–92. doi: 10.1164/rccm.201501-0137PP

56. Aglago EK, Rinaldi S, Freisling H, Jiao L, Hughes DJ, Fedirko V, et al. Soluble receptor for advanced glycation end-products (sRAGE) and colorectal cancer risk: A case-control study nested within a european prospective cohort. *Cancer Epidemiol Biomarkers Prev*. (2021) 30:182–92. doi: 10.1158/1055-9965.EPI-20-0855

57. Calfee CS, Gallagher D, Abbott J, Thompson BT, Matthay MA, Network NA. Plasma angiopoietin-2 in clinical acute lung injury: prognostic and pathogenetic significance. *Crit Care Med*. (2012) 40:1731–7. doi: 10.1097/CCM.0b013e3182451c87

58. Orfanos SE, Kotanidou A, Glynos C, Athanasiou C, Tsigkos S, Dimopoulou I, et al. Angiopoietin-2 is increased in severe sepsis: correlation with inflammatory mediators. *Crit Care Med*. (2007) 35:199–206. doi: 10.1097/01.CCM.0000251640.77679.D7

59. Parikh SM, Mammoto T, Schultz A, Yuan HT, Christiani D, Karumanchi SA, et al. Excess circulating angiopoietin-2 may contribute to pulmonary vascular leak in sepsis in humans. *PloS Med*. (2006) 3:e46. doi: 10.1371/journal.pmed.0030046

60. van der Heijden M, van Nieuw Amerongen GP, van Hinsbergh VW, Groeneveld AB. The interaction of soluble Tie2 with angiopoietins and pulmonary vascular permeability in septic and nonseptic critically ill patients. *Shock*. (2010) 33:263–8. doi: 10.1097/SHK.0b013e3181b2f978

61. Leong A, Kim M. The angiopoietin-2 and TIE pathway as a therapeutic target for enhancing antiangiogenic therapy and immunotherapy in patients with advanced cancer. *Int J Mol Sci*. (2020) 21:8689. doi: 10.3390/ijms21228689

62. Terpstra ML, Aman J, van Nieuw Amerongen GP, Groeneveld AB. Plasma biomarkers for acute respiratory distress syndrome: a systematic review and meta-analysis*. *Crit Care Med*. (2014) 42:691–700. doi: 10.1097/01.ccm.0000435669.60811.24

63. Agrawal A, Matthay MA, Kangelaris KN, Stein J, Chu JC, Imp BM, et al. Plasma angiopoietin-2 predicts the onset of acute lung injury in critically ill patients. *Am J Respir Crit Care Med*. (2013) 187:736–42. doi: 10.1164/rccm.201208-1460OC

64. Khan KA, Wu FT, Cruz-Munoz W, Kerbel RS. Ang2 inhibitors and Tie2 activators: potential therapeutics in perioperative treatment of early stage cancer. *EMBO Mol Med*. (2021) 13:e08253. doi: 10.15252/emmm.201708253

65. Fukumura D, Kloepper J, Amoozgar Z, Duda DG, Jain RK. Enhancing cancer immunotherapy using antiangiogenics: opportunities and challenges. *Nat Rev Clin Oncol*. (2018) 15:325–40. doi: 10.1038/nrclinonc.2018.29

66. Ogawa M, Yamamoto H, Nagano H, Miyake Y, Sugita Y, Hata T, et al. Hepatic expression of ANG2 RNA in metastatic colorectal cancer. *Hepatology*. (2004) 39:528–39. doi: 10.1002/hep.20048

67. Liu N, Liu M, Fu S, Wang J, Tang H, Isah AD, et al. Ang2-targeted combination therapy for cancer treatment. *Front Immunol*. (2022) 13:949553. doi: 10.3389/fimmu.2022.949553

68. Gengenbacher N, Singhal M, Mogler C, Hai L, Milde L, Pari AAA, et al. Timed ang2-targeted therapy identifies the angiopoietin-tie pathway as key regulator of fatal lymphogenous metastasis. *Cancer Discovery*. (2021) 11:424–45. doi: 10.1158/2159-8290.CD-20-0122

69. Pyrillou K, Burzynski LC, Clarke MCH. Alternative pathways of IL-1 activation, and its role in health and disease. *Front Immunol*. (2020) 11:613170. doi: 10.3389/fimmu.2020.613170

70. Tanaka T, Narazaki M, Kishimoto T. IL-6 in inflammation, immunity, and disease. *Cold Spring Harb Perspect Biol*. (2014) 6:a016295. doi: 10.1101/cshperspect.a016295

71. Serpa Neto A, Campos PP, Hemmes SN, Bos LD, Bluth T, Ferner M, et al. Kinetics of plasma biomarkers of inflammation and lung injury in surgical patients with or without postoperative pulmonary complications. *Eur J Anaesthesiol*. (2017) 34:229–38. doi: 10.1097/EJA.0000000000000614

72. Jabaudon M, Futier E, Roszyk L, Sapin V, Pereira B, Constantin JM. Association between intraoperative ventilator settings and plasma levels of soluble receptor for advanced glycation end-products in patients without pre-existing lung injury. *Respirology*. (2015) 20:1131–8. doi: 10.1111/resp.2015.20.issue-7

73. Ljungqvist O, Scott M, Fearon KC. Enhanced recovery after surgery: A review. *JAMA Surg*. (2017) 152:292–8. doi: 10.1001/jamasurg.2016.4952

74. Zheng Y, Mao M, Li F, Wang L, Zhang X, Zhang X, et al. Effects of enhanced recovery after surgery plus pulmonary rehabilitation on complications after video-assisted lung cancer surgery: a multicentre randomised controlled trial. *Thorax*. (2022) 78(6):574–86. doi: 10.1136/thoraxjnl-2021-218183

75. Lin XH, Jiang JK, Luo JC, Lin CC, Ting PH, Yang UC, et al. The long term microbiota and metabolic status in patients with colorectal cancer after curative colon surgery. *PloS One*. (2019) 14:e0218436. doi: 10.1371/journal.pone.0218436

76. Rao SSC, Tan G, Abdulla H, Yu S, Larion S, Leelasinjaroen P. Does colectomy predispose to small intestinal bacterial (SIBO) and fungal overgrowth (SIFO)? *Clin Transl Gastroenterol*. (2018) 9:146. doi: 10.1038/s41424-018-0011-x

77. Hope C, Reilly J, Lund J, Andreyev H. Systematic review: the effect of right hemicolectomy for cancer on postoperative bowel function. *Support Care Cancer*. (2020) 28:4549–59. doi: 10.1007/s00520-020-05519-5

78. McAlister FA, Bertsch K, Man J, Bradley J, Jacka M. Incidence of and risk factors for pulmonary complications after nonthoracic surgery. *Am J Respir Crit Care Med*. (2005) 171:514–7. doi: 10.1164/rccm.200408-1069OC

79. Robinson TN, Wu DS, Pointer L, Dunn CL, Cleveland JC Jr., Moss M. Simple frailty score predicts postoperative complications across surgical specialties. *Am J Surg*. (2013) 206:544–50. doi: 10.1016/j.amjsurg.2013.03.012

80. Hao J, Pang P, Liu X, Chi W, Luo Z, Cai W, et al. Can the lung ultrasound score predict pulmonary complications after non-thoracic surgery in patients with blunt thoracic trauma: A single-center observational study. *J Clin Anesth*. (2024) 99:111675. doi: 10.1016/j.jclinane.2024.111675

81. Raphael J, Chae A, Feng X, Shotwell MS, Mazzeffi MA, Bollen BA, et al. Red blood cell transfusion and pulmonary complications: the society of thoracic surgeons adult cardiac surgery database analysis. *Ann Thorac Surg*. (2024) 117:839–46. doi: 10.1016/j.athoracsur.2023.12.012

82. Yokota S, Koizumi M, Togashi K, Morimoto M, Yasuda Y, Sata N, et al. Preoperative pulmonary function tests do not predict the development of pulmonary complications after elective major abdominal surgery: A prospective cohort study. *Int J Surg*. (2020) 73:65–71. doi: 10.1016/j.ijsu.2019.11.032

83. Lukannek C, Shaefi S, Platzbecker K, Raub D, Santer P, Nabel S, et al. The development and validation of the Score for the Prediction of Postoperative Respiratory Complications (SPORC-2) to predict the requirement for early postoperative tracheal re-intubation: a hospital registry study. *Anaesthesia*. (2019) 74:1165–74. doi: 10.1111/anae.14742

84. Schmitt M, Greten FR. The inflammatory pathogenesis of colorectal cancer. *Nat Rev Immunol*. (2021) 21:653–67. doi: 10.1038/s41577-021-00534-x

85. Chandra R, Karalis JD, Liu C, Murimwa GZ, Voth Park J, Heid CA, et al. The colorectal cancer tumor microenvironment and its impact on liver and lung metastasis. *Cancers (Basel)*. (2021) 13:6206. doi: 10.3390/cancers13246206

frontiers | Frontiers in Immunology

TYPE Review
PUBLISHED 26 February 2025
DOI 10.3389/fimmu.2025.1550206

Check for updates

OPEN ACCESS

EDITED BY
Qingyu Luo,
Dana–Farber Cancer Institute, United States

REVIEWED BY
Kezhi Yan,
Cystic Fibrosis Foundation, United States
Xiaowei Wu,
Dana–Farber Cancer Institute, United States
Haili Ma,
Dana–Farber Cancer Institute, United States

*CORRESPONDENCE
Jun Chen
chenjun0121@126.com
Haiyan Wu
keki027@sina.com
Xinwen Min
minxinwen@163.com

†These authors have contributed equally to this work

RECEIVED 09 January 2025
ACCEPTED 10 February 2025
PUBLISHED 26 February 2025

CITATION
Fu M, Lv M, Guo J, Mei A, Qian H, Yang H, Wu W, Liu Z, Zhong J, Wei Y, Min X, Wu H and Chen J (2025) The clinical significance of T-cell regulation in hypertension treatment. *Front. Immunol.* 16:1550206. doi: 10.3389/fimmu.2025.1550206

COPYRIGHT
© 2025 Fu, Lv, Guo, Mei, Qian, Yang, Wu, Liu, Zhong, Wei, Min, Wu and Chen. This is an open-access article distributed under the terms of the Creative Commons Attribution License (CC BY). The use, distribution or reproduction in other forums is permitted, provided the original author(s) and the copyright owner(s) are credited and that the original publication in this journal is cited, in accordance with accepted academic practice. No use, distribution or reproduction is permitted which does not comply with these terms.

The clinical significance of T-cell regulation in hypertension treatment

Miaoxin Fu[1†], Mingzhu Lv[1†], Jinyue Guo[1†], Aihua Mei[1], Hang Qian[1], Handong Yang[1], Wenwen Wu[2,3], Zhixin Liu[2], Jixin Zhong[4], Ying Wei[1], Xinwen Min[1*], Haiyan Wu[1*] and Jun Chen[1,2*]

[1]Sinopharm Dongfeng General Hospital (Hubei Clinical Research Center of Hypertension), Hubei Key Laboratory of Wudang Local Chinese Medicine Research, Hubei University of Medicine, Shiyan, Hubei, China, [2]Shiyan Key Laboratory of Virology, Hubei University of Medicine, Shiyan, China, [3]School of Public Health, Hubei University of Medicine, Shiyan, Hubei, China, [4]Department of Rheumatology and Immunology, Tongji Hospital, Huazhong University of Science and Technology, Wuhan, Hubei, China

Hypertension, a globally prevalent condition, is closely associated with T cell-mediated inflammatory responses. Studies have shown that T cells, by secreting pro-inflammatory cytokines such as interferon-gamma (IFN-γ), Interleukin-17 (IL-17), and Tumor necrosis factor-alpha (TNF-α), directly lead to vascular dysfunction and elevated blood pressure. The activation of Th1 and Th17 cell subsets, along with the dysfunction of regulatory T cells (Tregs), is a critical mechanism in the onset and progression of hypertension. This review explores the role of T cells in the pathophysiology of hypertension and discusses potential therapeutic strategies targeting T cell regulation, such as immunotherapy and gene-editing technologies. These emerging treatments hold promise for providing personalized therapeutic options for hypertensive patients, reducing inflammatory complications, and improving treatment outcomes.

KEYWORDS

hypertension, regulatory T cells, inflammation, immunotherapy, gene editing

1 Introduction

1.1 Background and importance

Hypertension is a globally prevalent cardiovascular disease and one of the leading causes of cardiovascular events and death. As shown in the chart below, the world's top 25 countries for hypertension mortality in 2021 demonstrate a significant variation in the estimated annual death rates attributed to hypertension (1). This highlights the global burden of the disease and the disparities in hypertension management and control across different regions (Figure 1)

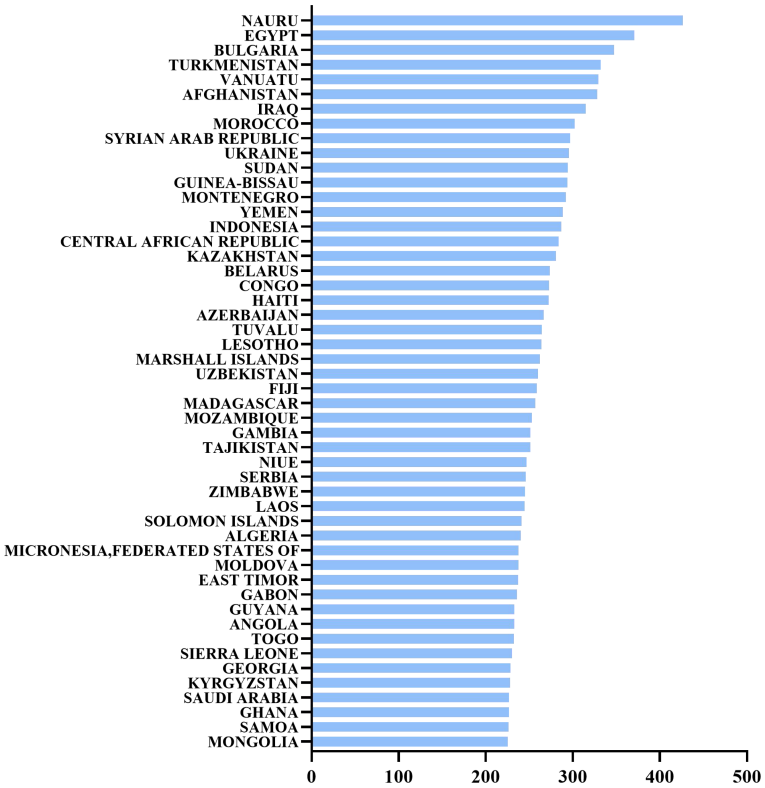

FIGURE 1
The world's top 25 countries for hypertension mortality in 2021. Estimated annual death rate attributed to hypertension, also known as high blood pressure, per 100,000 people.

According to the latest data from the World Health Organization (WHO), over 1.1 billion adults worldwide have hypertension, with 78% residing in low- and middle-income countries, contributing to approximately 7.5 million deaths annually, accounting for 12.8% of global mortality. In high-income countries, the control rate of hypertension is 44%, while in low- and middle-income countries, it is only 21% (2, 3).In this context, numerous studies suggest that adopting stricter blood pressure classification standards, such as the new diagnostic threshold of 130/80 mmHg, could increase awareness of early screening and intervention (3). This new standard advances hypertension diagnosis earlier than the previously lenient threshold of 140/90 mmHg, aiming to prevent severe cardiovascular complications later in life through earlier lifestyle modifications and pharmacological interventions. Additionally, hypertension prevalence varies significantly across age, gender, and regions. Among younger adults (20-45 years), men have a higher prevalence of hypertension than women, whereas in the elderly population (65 years and older), the prevalence in women slightly surpasses that in men (4). The higher hypertension control rate in high-income countries contrasts with the lower rate in low- and middle-income countries, reflecting disparities in hypertension management globally (2). Hypertension not only poses a major risk for cardiovascular events but is also closely related to various organ system disorders, including stroke, myocardial infarction, and renal failure (3).

In recent years, growing evidence has highlighted the connection between the immune system and the pathogenesis of hypertension, particularly the crucial role of T cells in hypertension pathophysiology. T cells, traditionally recognized for their role in immune responses, directly participate in hypertension development by influencing vascular endothelial cells and triggering chronic inflammatory responses. Studies indicate that T cells, through the release of multiple cytokines and chemokines, can induce endothelial damage and vascular dysfunction, leading to elevated blood pressure (5–7). RANTES (Regulated on Activation, Normal T Cell Expressed and Secreted), an important chemokine, plays a pivotal role in the inflammatory response and T-cell accumulation associated with hypertension. By promoting T-cell migration to inflammatory sites, RANTES enhances local immune responses and exacerbates vascular dysfunction (8). This discovery provides new possibilities for immune-regulatory targets in hypertension treatment. In summary, modulating T-cell-mediated inflammatory responses and balancing T-cell subtypes could represent potential therapeutic targets for hypertension, promoting the development of personalized and innovative treatment strategies.

1.2 The clinical status of hypertension and its health impact

Hypertension is a common chronic disease with a complex pathogenesis. Long-term hypertension can lead to severe

complications, particularly affecting the cardiovascular, renal, and ocular systems, posing significant threats to patient health and survival. According to WHO statistics, approximately 12.5 million cardiovascular disease-related deaths each year are associated with hypertension, including 3.5 million cases of myocardial infarction and 9.5 million strokes (2). Cardiovascular complications, such as stroke and myocardial infarction, are particularly prominent; about 54% of strokes are associated with hypertension, and myocardial infarction is the leading cause of death in cardiovascular patients, with hypertension increasing its risk by 2-3 times (3). Additionally, the incidence of chronic kidney disease (CKD) is significantly higher in hypertensive patients, with hypertension being the primary cause of 25-30% of end-stage renal disease (ESRD) (9). Hypertension can also cause retinal damage, impacting vision.

Despite the availability of multiple antihypertensive drugs, including ACE inhibitors, beta-blockers, and calcium channel blockers, drug resistance remains a major challenge. Studies indicate that 15-30% of hypertensive patients develop resistance to one or more antihypertensive drugs, leading to suboptimal blood pressure control (10). This resistance may be linked to genetic differences, metabolic abnormalities, and lifestyle factors such as high salt intake and lack of exercise (5). Furthermore, patient compliance is an issue, with about 50% of hypertensive patients failing to consistently adhere to prescribed medications due to side effects, adverse reactions, and insufficient understanding of the disease and treatment. To address this issue, regular blood pressure monitoring, comprehensive treatments combining medication and lifestyle interventions, and research into novel antihypertensive drugs and personalized treatment strategies are crucial. These measures can enhance hypertension management and improve patient quality of life (11).

2 Immunological basis of hypertension

2.1 Interaction between hypertension and the immune system

Hypertension is a chronic condition, and recent research suggests a complex interplay between hypertension and the immune system. Immune cells, which include lymphocytes (such as T cells and B cells), macrophages, and natural killer (NK) cells, are responsible for immune surveillance, defense, and homeostasis, playing key roles in infection defense and tissue repair. During the pathogenesis of hypertension, immune cell activation and functional alterations can trigger vascular inflammation and remodeling.

The interaction between macrophages and T cells is a critical regulatory mechanism. Macrophages contribute significantly to endothelial cell damage and inflammation by secreting pro-inflammatory cytokines like IL-6 and TNF-α, which activate T cells, thereby exacerbating vascular inflammation (12). This interaction depends on the macrophage's functional phenotype, which ranges from pro-inflammatory M1 to anti-inflammatory M2 (13). This creates a vicious cycle wherein macrophage and T cell activation synergistically enhance inflammation, further damaging the endothelium and worsening hypertension. Activated T cells also release IFN-γ, which amplifies macrophage inflammatory responses, further damaging the endothelium and promoting vascular hardening, ultimately driving hypertension progression (14). Additionally, T cells interact with B cells through CD40 signaling, leading to the production of pro-inflammatory antibodies (especially IgG) by B cells, which enhance macrophage-driven inflammation (15–18). Meanwhile, B cells secrete IL-10 to modulate T cell function and maintain the balance of T cell subsets (19). For instance, B cells help maintain the balance between Th1 and Th17 cells, preventing the differentiation of naïve T cells into these pro-inflammatory subsets, while promoting Treg expansion to suppress pathological Th1/Th17 responses (20, 21). This interplay of immune cells highlights the potential for targeting T cell, B cell, and macrophage functions as novel therapeutic strategies for hypertension. By further understanding these interactions, researchers can explore new therapeutic targets for better managing hypertension and its complications.

2.2 Role of T cells in hypertension

T cells, as a subset of lymphocytes, play an essential role in the immune response and have garnered significant attention in the context of hypertension pathophysiology. T-cell-mediated inflammation contributes to the progression of hypertension, with different T cell subsets and their secreted cytokines playing crucial roles in both the onset and progression of the disease.

Th1 cells, for example, release pro-inflammatory cytokines such as IFN-γ, which are implicated in vascular smooth muscle cell (VSMC) proliferation and vascular inflammation. Recent studies have demonstrated that Th1 cells activate the angiotensin II (Ang II) signaling pathway, promoting VSMC proliferation and triggering vascular inflammation, which can elevate blood pressure (14). Th1-mediated inflammation contributes to the hypertensive pathological process through immune responses that promote vascular damage.

Similarly, Th17 cells secrete IL-17, which has been shown to play a significant role in Ang II-induced hypertension. IL-17 exacerbates vascular inflammation, increases vasoconstriction, and promotes endothelial dysfunction, directly driving the pathological processes of hypertension (6). Additionally, RANTES (Regulated upon Activation, Normal T cell Expressed and Secreted), a key chemokine, not only attracts T cells to inflammatory sites but also intensifies vascular inflammation, worsening the progression of hypertension (8).

The imbalance between T-cell subsets is another critical factor contributing to hypertension. A reduction in regulatory T cells (Tregs) weakens their inhibitory effect on pro-inflammatory T cells, such as Th1 and Th17 cells, leading to uncontrolled inflammation that exacerbates hypertension. This imbalance is particularly prominent in vascular stiffening, where a lack of Tregs leads to endothelial dysfunction and inflammatory dysregulation, further aggravating hypertension (22). Moreover, studies suggest that T

cells can maintain immune balance in hypertension by regulating Th1 and Th17 cell activity, especially in vascular lesions where the immune balance is disturbed (23).

Recent research has also highlighted the importance of epigenetic modifications in regulating T-cell function, particularly in hypertension. Mechanisms such as DNA methylation and histone modifications alter the activation state of T cells, suggesting that gene regulation may contribute significantly to the role of T cells in hypertension beyond just inflammatory responses (24, 25). This highlights the complex regulatory network that influences T cell activity and its contribution to hypertension pathogenesis.

Pro-inflammatory cytokines, such as TNF-α, IL-6, and MCP-1, also play critical roles in T-cell mediated hypertension (26, 27). TNF-α is linked to chronic inflammation, promoting VSMC proliferation, vascular hardening, and the activation of the NF-κB pathway in T cells, further driving vascular damage (28–30). IL-6 and MCP-1, secreted by T cells, activate inflammatory signaling pathways such as the JAK/STAT pathway, contributing to the chronic inflammation that exacerbates hypertension (27, 31, 32).

Although these preclinical studies highlight the critical role of T cells in hypertension, relevant clinical trials are still ongoing. Further clinical data will help validate these findings and guide clinical treatment strategies.

3 Molecular mechanisms of T cell regulation

3.1 Signaling pathways of T cell activation and differentiation

T cell activation is the cornerstone of immune response, involving the proliferation and differentiation of T cells into effector cells. This process requires two signals: the first is delivered through the T-cell receptor (TCR) and is enhanced by adhesion molecules; the second is a co-stimulatory signal, provided by the interaction between co-stimulatory molecules on antigen-presenting cells (APCs) and receptors on T cells, which amplifies the TCR signal (33, 34). The first signal alone cannot induce a full immune response in T cells. Without the second signal, T cells enter a state of anergy, immune tolerance, or undergo programmed cell death, likely due to limited activation of the major histocompatibility complex (MHC)-peptide-TCR complex and internalization of the TCR-CD3 complex. Co-stimulatory complexes like B7-CD28 can prevent such outcomes (35). The first signal determines the specificity of T cell activation, while the co-stimulatory signal directs the functional outcome (36).

Different T cell subsets and their secreted cytokines regulate inflammation through multiple signaling pathways, which play critical roles in the pathogenesis of hypertension. T cell activation and differentiation not only rely on antigen recognition but also involve intricate signaling cascades, including the TCR, NF-κB, JAK/STAT, mTOR, and Notch pathways.

The TCR signaling pathway is central to T cell activation. Upon TCR binding to its antigen, downstream signals such as NF-κB and MAPK are triggered, promoting T cell proliferation and functional differentiation (33). TCR activation induces specific T cell subsets (e.g., Th1 cells) to secrete large amounts of pro-inflammatory cytokines, including IFN-γ and TNF-α (33, 37). These cytokines exacerbate immune responses in hypertension and, through various signaling pathways, stimulate vascular smooth muscle cell proliferation and vascular remodeling, leading to further elevation in blood pressure.

The NF-κB signaling pathway plays a crucial role in T cell-mediated inflammatory responses. Activated by TCR and cytokine signals, NF-κB regulates the expression of various pro-inflammatory cytokines, such as TNF-α and IL-6 (37). Sustained activation of the NF-κB pathway in chronic inflammation accelerates vascular damage, contributing to endothelial dysfunction and arterial stiffening (38–40). NF-κB signaling pathway, activated via Angiotensin II binding to the Angiotensin II type 1 receptor (AT1R), is involved in pro-inflammatory responses, promoting vascular smooth muscle cell proliferation and vascular remodeling, indirectly leading to elevated blood pressure (40–43). The JAK/STAT signaling pathway is closely related to T cell differentiation, particularly in the differentiation of Th17 cells (44). IL-6 activates the JAK/STAT3 pathway, inducing Th17 differentiation and promoting IL-17 secretion (31, 45–47). IL-17 amplifies vascular inflammation and endothelial dysfunction, exacerbating hypertension. Inhibiting the IL-6/JAK/STAT3 pathway reduces Th17 activity, alleviating vascular inflammation and damage in hypertension (6, 31, 48, 49). The mTOR pathway, which regulates T cell metabolism, influences T cell differentiation as well. In hypertension, excessive mTOR activation enhances the proliferation of pro-inflammatory T cell subsets, such as Th1 and Th17, aggravating inflammatory responses. Studies in animal models have shown that mTOR inhibitors can reduce inflammatory T cell numbers and lower blood pressure (50–52). The Notch signaling pathway also plays a pivotal role in T cell differentiation, particularly in regulating Th1 and Th17 differentiation (53). While Notch signaling is linked to pro-inflammatory T cell activation and its role in vascular inflammation, whether direct inhibition of Notch can significantly lower blood pressure in hypertensive patients remains insufficiently supported. Animal studies suggest that inhibiting Notch signaling can reduce inflammation, but its effect on lowering blood pressure alone has not been conclusively demonstrated.

In summary, T cell activation and differentiation signaling pathways regulate the expression of pro-inflammatory and anti-inflammatory cytokines, playing an important role in the pathophysiology of hypertension. Interventions targeting these signaling pathways offer new avenues for future immunotherapy in hypertension, particularly in reducing inflammation and controlling blood pressure (Figure 2)

3.2 Role of epigenetic and post-transcriptional modifications in T cell function

Recent studies have increasingly focused on the role of epigenetic and post-transcriptional modifications in regulating T cell function. These regulatory mechanisms are crucial not only for T cell activation, proliferation, differentiation, and maintenance of

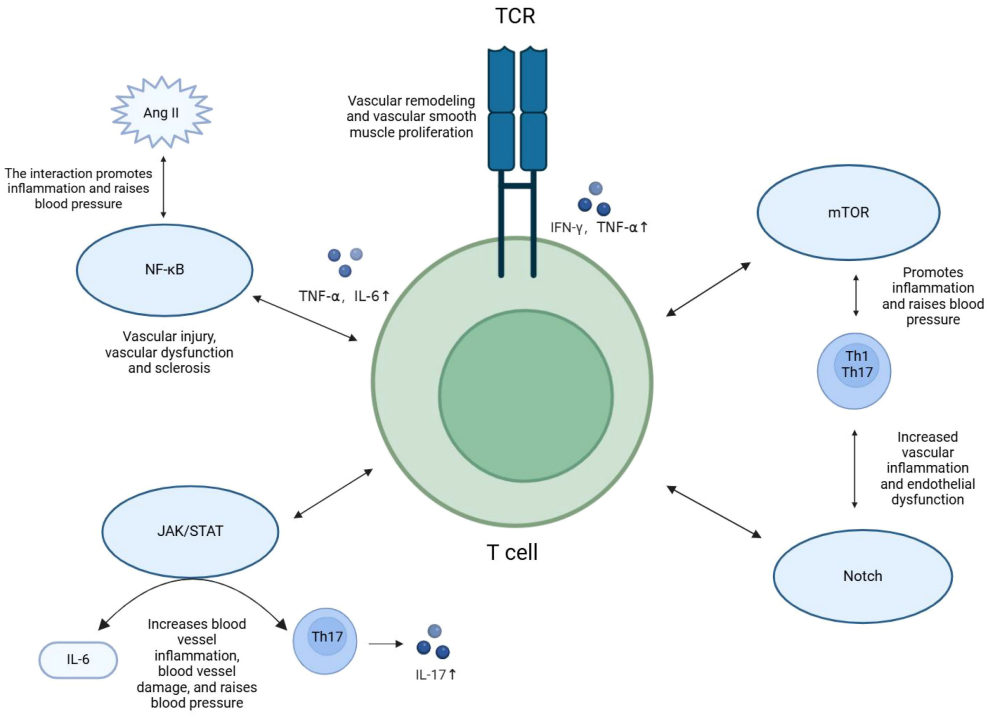

FIGURE 2
Signaling pathways for T cell activation and differentiation. T cell subsets and their secreted cytokines regulate inflammation through signaling pathways such as TCR, NF-kB, JAK/STAT, mTOR, and Notch, playing a role in the pathogenesis of hypertension.

function but are also closely linked to the development and progression of inflammatory diseases like hypertension.

DNA methylation is a classic form of epigenetic regulation, catalyzed by DNA methyltransferases (DNMTs), which add methyl groups to CpG islands within genes, thereby modulating gene expression. In T cells, DNA methylation plays a key role in determining their differentiation and functional status (24). For instance, the Foxp3 gene, which is essential for the differentiation of regulatory T cells (Tregs), is influenced by its DNA methylation status (54). Elevated methylation of the Foxp3 gene in hypertensive patients weakens Treg function, exacerbating immune inflammation and vascular damage. Research has shown that reducing the methylation of Foxp3 can restore Treg function, potentially alleviating hypertension-associated immune inflammation (55–57).

Not only Tregs, but pro-inflammatory T cell subsets like Th1 and Th17 also rely on DNA methylation for their differentiation. DNMTs suppress excessive activation of these cells by methylating key genes (58–61). Studies have shown that inhibiting DNMT activity can significantly reduce the proliferation of Th1 and Th17 cells and suppress the secretion of pro-inflammatory cytokines, such as IFN-γ and IL-17, thereby alleviating chronic inflammation in hypertension (61). This mechanism presents new possibilities for controlling pro-inflammatory immune responses through epigenetic regulation.

MicroRNAs (miRNAs), as key post-transcriptional gene regulators, modulate T cell function by binding to target mRNAs, inhibiting their translation or inducing their degradation (62). miRNAs finely regulate T cell activation, differentiation, and cytokine secretion. For instance, miR-21 is upregulated in hypertensive patients and regulates Treg function, mitigating inflammation and improving vascular function (63–65). In contrast, miR-155 is highly expressed in pro-inflammatory T cells (e.g., Th1 and Th17 cells), enhancing their inflammatory activity and promoting the secretion of IFN-γ and IL-17, thereby aggravating vascular inflammation (66, 67). Targeting miR-155 may reduce the secretion of pro-inflammatory cytokines, alleviating hypertension-related vascular dysfunction (67, 68).

Notably, epigenetic and post-transcriptional modifications are not isolated processes; they interact to co-regulate T cell fate and function. For example, miRNAs can influence DNA methylation by regulating DNMT expression, while also modulating other epigenetic factors, thus extending the regulatory network of T cell functions (69). This interaction increases the complexity of T cell regulation and plays a key role in inflammatory diseases like hypertension.

In conclusion, epigenetic modifications (such as DNA methylation) and post-transcriptional modifications (such as miRNAs) regulate T cell differentiation and function through multiple layers and pathways, driving the immune pathology of hypertension. Future research can further explore these regulatory mechanisms as potential therapeutic targets in hypertension, with broad clinical applications in reducing vascular inflammation and improving vascular function.

3.3 T cells and hypertension-related molecular markers

Recent research has revealed that T cells and their secreted pro-inflammatory cytokines play a central role in the pathogenesis of hypertension. Th1 and Th17 cells, along with their products, such as IFN-γ, TNF-α, and IL-17, significantly contribute to vascular inflammation and dysfunction (70). For example, IL-17 induces local inflammatory responses by activating endothelial cells, eventually leading to vascular remodeling and hypertension. Clinical data have shown that IL-17 expression in hypertensive patients correlates positively with blood pressure levels and cardiovascular risk (6, 71). IFN-γ, by activating the Angiotensin II signaling pathway, promotes vascular smooth muscle cell proliferation and exacerbates inflammation, worsening the condition (72). TNF-α is closely linked to chronic inflammation and vascular stiffening, activating the NF-kB signaling pathway, which enhances T cell activation and the release of pro-inflammatory cytokines, accelerating vascular damage and remodeling associated with hypertension (73–75).

Targeted interventions against these molecular markers have become a focus in immunotherapy research for hypertension. For instance, IL-17 inhibitors have demonstrated significant therapeutic effects in animal models, not only reducing blood pressure but also mitigating vascular inflammatory damage (76, 77). Similarly, blocking IFN-γ and TNF-α signaling pathways can reduce vascular inflammation and remodeling, thereby lowering cardiovascular risk.

Furthermore, epigenetic regulation, such as the methylation level of the Foxp3 gene, directly affects the anti-inflammatory function of regulatory T cells (Tregs). Studies have shown that modulating the methylation state of the Foxp3 gene can enhance Tregs' anti-inflammatory activity, potentially alleviating hypertension-related immune inflammation (78). These findings underscore the critical role of T cells in hypertension and provide promising directions for immunotherapy targeting T cell-related molecular markers, advancing personalized treatment strategies.

4 Clinical review of hypertension treatments

4.1 Effects of current hypertension treatments on T cells

4.1.1 Pharmacological treatment

Current hypertension medications influence T cell function through various mechanisms, thus modulating immune responses related to inflammation. Common antihypertensive drugs (such as ACE inhibitors [ACEI] and angiotensin receptor blockers [ARBs]) inhibit Th1 and Th17 cell activity, reducing the secretion of pro-inflammatory cytokines like IFN-γ and IL-17, which significantly lowers vascular inflammation and improves blood pressure control (79–82). Calcium channel blockers (CCBs) and diuretics reduce Angiotensin II levels, indirectly inhibiting T cell activation and pro-inflammatory cytokine release, thereby preserving vascular function (83–85). Beta-blockers not only modulate regulatory T cell (Treg) function through metabolic and epigenetic pathways but also promote Treg activation, modulating immune responses and alleviating chronic inflammation in hypertension (86–88). Additionally, Tocilizumab, an anti-inflammatory drug targeting IL-6, is primarily used to treat immune-mediated inflammatory diseases like rheumatoid arthritis. While its mechanism of inhibiting Th17 cell activation and reducing inflammatory cytokines through the IL-6/JAK/STAT pathway has been validated in other diseases, its application in hypertension remains in the exploratory phase. Current research has yet to establish the widespread clinical use of Tocilizumab in managing immune inflammation in hypertension (89–92). Therefore, Tocilizumab's potential role in hypertension warrants further investigation, though its immunomodulatory mechanism offers new possibilities for personalized hypertension treatment.

These studies highlight the potential of improving hypertension treatment outcomes by regulating T cell function, suggesting that immune modulation not only effectively controls blood pressure but also reduces hypertension-related inflammation and vascular damage.

4.1.2 Lifestyle interventions

Lifestyle changes also play a significant role in regulating T cell-mediated inflammatory responses in non-pharmacological treatments. Research has shown that the Mediterranean diet, rich in polyunsaturated fatty acids and antioxidants, effectively inhibits pro-inflammatory T cell subsets (e.g., Th1, Th17), while increasing the proportion of regulatory T cells (Tregs), potentially reducing immune inflammation in hypertensive patients (93, 94). A clinical study demonstrated that the Mediterranean diet significantly lowered IL-6 and TNF-α levels in the blood, reducing the risk of developing hypertension (94–101). Additionally, low-sodium diets and regular aerobic exercise reduce Th17 cell activation and increase Treg proportions, significantly lowering blood pressure and reducing vascular inflammation (94, 102). Exercise interventions also have important benefits for improving T cell function. Regular aerobic exercise not only inhibits pro-inflammatory T cell activation and reduces IL-17 secretion but also promotes the recovery of Treg function, alleviating vascular inflammation and immune imbalance (103–108). Exercise also improves obesity-related metabolic disorders, indirectly modulating T cell activity, further enhancing vascular function and lowering blood pressure (109, 110).

Thus, lifestyle interventions provide an effective non-pharmacological treatment strategy for correcting T cell dysfunction, offering long-term vascular protection for hypertensive patients, and providing essential evidence for the development of personalized management plans.

4.2 T cell regulation in novel therapeutic strategies

4.2.1 Gene therapy

Recent advancements in gene therapy technology have made significant progress in research on immune regulation related to hypertension. T cells, particularly regulatory T cells (Tregs), play a

crucial role in the chronic inflammation associated with hypertension. Thus, restoring and enhancing Treg function has emerged as a promising new strategy in hypertension treatment. CRISPR/Cas9 gene-editing technology has shown great potential for modulating Treg function, particularly by targeting the expression of the Foxp3 gene to restore its immunosuppressive function (111, 112). Foxp3 acts as the central regulator of Treg function, and hypermethylation of Foxp3 is closely associated with Treg dysfunction (113, 114). By precisely regulating Foxp3 expression using CRISPR/Cas9 technology, it is possible to restore the anti-inflammatory properties of Tregs while also reducing the excessive activation of pro-inflammatory T cells, such as Th1 and Th17 cells, thus mitigating endothelial damage (111, 115, 116). Recent studies have further demonstrated that modulating the methylation status of the Foxp3 gene can enhance Treg-mediated immunoregulation, which in turn helps alleviate chronic inflammation in hypertension (114, 117–121).

Despite these promising findings in animal models, the clinical application of gene therapy for hypertension in humans still faces significant challenges. These include concerns over the long-term safety, specificity, and potential off-target effects of gene editing. Therefore, future research must focus on optimizing the precision of gene-editing tools like CRISPR/Cas9 and exploring their individualized application in hypertensive patients to ensure efficacy and safety under specific pathological conditions.

4.2.2 Cell therapy

Cell therapy, particularly Treg (regulatory T cell)-based therapy, has shown great potential in the treatment of hypertension. Studies have demonstrated that the number and function of Tregs are significantly reduced in hypertensive patients, while the proportion of pro-inflammatory T cells (e.g., Th17 cells) is elevated, exacerbating inflammatory responses and subsequently increasing blood pressure (22, 122–124). Tregs play a key role in immune regulation by suppressing the release of pro-inflammatory cytokines such as IL-17 and IFN-γ, effectively alleviating hypertension-related chronic inflammation (125, 126). Therefore, expanding and reinfusing autologous Tregs to restore their immunosuppressive abilities has emerged as a promising strategy for improving hypertension treatment (122, 127).

Moreover, researchers are exploring the genetic modification of Tregs to further enhance their immunosuppressive function. For example, using CRISPR/Cas9 technology to modify key regulatory genes in Tregs, such as Foxp3, can significantly improve Treg function and stability. Studies have found that genetically modified Tregs can maintain a longer-lasting anti-inflammatory effect *in vivo*, enhancing their ability to control chronic inflammation caused by hypertension (113, 124).

As technology advances, the application of Treg cell therapy in the immunoregulatory treatment of hypertension holds even greater promise. Future research will focus on improving the stability and safety of Treg cell therapies, particularly in terms of clinical operability. With further basic research and clinical trials, Treg cell therapy could become an important therapeutic approach, offering personalized and effective treatment options for hypertensive patients.

5 Challenges and future research directions

Research on T cell regulation in hypertension faces several significant limitations. A major issue is the small sample sizes in many studies, which reduce the statistical power of the results and hinder a comprehensive understanding of hypertension and its immune mechanisms. Additionally, existing studies tend to focus on isolated T cell subsets or specific pro-inflammatory factors, often overlooking the broader, systemic mechanisms that contribute to the pathogenesis of hypertension. This narrow focus impedes a holistic understanding of how T cells influence hypertension at a molecular and physiological level.

Recent advancements in genetics and gene editing technologies, particularly CRISPR/Cas9, present promising opportunities to address these challenges (128). One notable development is the identification of phosphodiesterase 3A (PDE3A) gene mutations that enhance enzyme activity and are associated with hypertension with brachydactyly (HTNB) (129, 130). This discovery opens new avenues for targeted therapeutic interventions, emphasizing the critical role of genetics in understanding hypertension. However, it also highlights several hurdles. A primary challenge is the need for more *in vivo* models to confirm the involvement of mutated PDE3A in hypertension development. Existing animal models often fail to replicate the immune responses observed in humans, which limits their utility in fully understanding the genetic-immune interactions that underlie hypertension (128, 130).

A significant barrier in hypertension research lies in the inadequacy of current animal models to faithfully simulate human hypertension, particularly in terms of immune system involvement. While advanced technologies like CRISPR/Cas9 have been used to generate PDE3A-mutant animal models, these models do not yet fully capture the immune dynamics of human hypertension (129, 130). For example, while overexpression of PDE3A in smooth muscle cells leads to increased vascular resistance and hypertension, the interaction between these genetic alterations and immune cells—especially T cell subsets—remains poorly understood. Further investigation into this aspect is needed to explore how these mutations impact immune cell function and contribute to hypertension pathogenesis.

To address these challenges, future research should focus on developing more refined animal models that better simulate human immune dynamics, with particular emphasis on T cell regulation. The interaction between PDE3A mutations and immune cells such as T cells and macrophages is a critical area of research. Understanding how PDE3A mutations influence T cell activation and proliferation could reveal novel gene-targeted therapies for hypertension. These insights may also help identify new pathways for modulating immune responses to reduce vascular damage and improve blood pressure regulation (131).

While these findings provide a solid foundation for future therapeutic strategies, it is important to explore how T cell-related discoveries can be translated into clinical applications. For instance, identifying specific T cell subtypes and their functional alterations in hypertensive patients may guide patient stratification, risk

prediction, and individualized treatment strategies, such as the use of immunomodulatory agents. Furthermore, integrating immune and genomic data may lead to more precise treatments, improving patient outcomes and reducing complications. By bridging basic research to clinical practice, we anticipate that personalized treatment strategies will become more precise and tailored, offering new insights into individualized therapy.

Collaboration between genetics, immunology, and cardiology is essential for advancing this field. By integrating gene editing technologies with immune modulation strategies, researchers can create more accurate models of human hypertension, which will provide a clearer picture of the disease's underlying mechanisms. Such integrated research approaches could uncover novel signaling pathways and mechanisms through which PDE3A mutations influence vascular changes and contribute to hypertension (131).

In the long term, gene therapy and immunotherapy could provide exciting new treatment options for hypertension. Future research should aim to translate findings from animal models into clinical applications. This includes using gene editing technologies to precisely target PDE3A mutations or modulate immune responses to alleviate hypertension (129–131). Overcoming challenges related to the safety, efficiency, and long-term effects of gene therapy will be key to bringing these novel approaches into clinical practice.

In conclusion, while PDE3A mutations represent a promising therapeutic target for hypertension, much work remains to be done. The integration of genetic research and immune regulation, coupled with the development of more precise animal models, will be crucial for advancing our understanding of hypertension and improving treatment strategies.

6 Future outlook

In the future, precision medicine and personalized treatment will become increasingly important in the management of hypertension. With the rapid development of genomics and immunology, scientists are expected to gain deeper insights into the role of T cells in hypertension, enabling tailored treatment plans for individual patients. Specifically, genomics research can identify genetic variations related to hypertension, particularly those affecting T cell function. This will provide a crucial basis for developing more precise treatment strategies. Moreover, immune phenotyping can reveal changes in T cell subsets within patients, helping clinicians select appropriate immunomodulatory drugs and adjust dosages to optimize therapeutic outcomes.

In this context, interdisciplinary collaboration and technological innovation will be key drivers of progress. By integrating knowledge from fields such as cardiology, immunology, and genomics, researchers can develop novel immunomodulatory drugs and gene therapies aimed at improving the prognosis of hypertensive patients. Overall, future research will continue to explore the role of T cells in hypertension, promote the development of new immunotherapies, and strive for significant progress in improving patients' quality of life.

7 Conclusion

In conclusion, hypertension remains a global health crisis with significant mortality rates (102, 132, 133).Recent studies highlight the critical role of T cells in hypertension pathogenesis, particularly in immune regulation and inflammatory responses. Dysregulation of Tregs and the imbalance with pro-inflammatory T cells are central to hypertension-induced inflammation (134). Targeted T cell regulation through immunomodulatory drugs, gene therapy, and cell therapy offers new therapeutic possibilities.

Future research should focus on the interactions between T cells and other immune cells, exploring new regulatory molecules and refining animal models. Integrating immune and genomic data could lead to more precise, personalized treatments, improving patient outcomes and reducing complications. T cell regulation holds great potential for advancing hypertension therapy, offering new insights into individualized treatment strategies.

Author contributions

MF: Writing – original draft. ML: Writing – original draft. JG: Writing – original draft. AM: Writing – review & editing. HQ: Writing – review & editing. HY: Writing – review & editing. WW: Writing – review & editing. ZL: Writing – review & editing. JZ: Writing – review & editing. YW: Writing – review & editing. XM: Writing – review & editing. HW: Writing – review & editing. JC: Writing – original draft, Writing – review & editing.

Funding

The author(s) declare that financial support was received for the research, authorship, and/or publication of this article. This work was supported by Hubei Provincial Natural Science Foundation (2022CFB453), Foundation of Health Commission of Hubei (WJ2021M061), Natural Science Foundation of the Bureau of Science and Technology of Shiyan City (grant no. 21Y71), Faculty Development Grants from Hubei University of Medicine (2018QDJZR04), Hubei Key Laboratory of Wudang Local Chinese Medicine Research (Hubei University of Medicine) (Grant No. WDCM2024020, WDCM2024023), and Advantages Discipline Group (Medicine) Project in Higher Education of Hubei Province (2021-2025) (Grant No. 2024XKQT41).

Conflict of interest

The authors declare that the research was conducted in the absence of any commercial or financial relationships that could be construed as a potential conflict of interest.

Generative AI statement

The author(s) declare that no Generative AI was used in the creation of this manuscript.

Publisher's note

All claims expressed in this article are solely those of the authors and do not necessarily represent those of their affiliated organizations, or those of the publisher, the editors and the reviewers. Any product that may be evaluated in this article, or claim that may be made by its manufacturer, is not guaranteed or endorsed by the publisher.

References

1. IHME. *Global Burden of Disease (2024) – with minor processing by Our World in Data. "Child deaths linked to child and maternal malnutrition" [dataset]. IHME, Global Burden of Disease, "Global Burden of Disease - Risk Factors" [original data]*. (2024). Retrieved February 19, 2025 from https://ourworldindata.org/grapher/number-child-deaths-malnutrition.

2. Rukunuzzaman M, Khatun N, Nessa A, Wahed F, Sharmin A, Meherubin I, et al. Study on body mass index, serum total cholesterol and serum triglycerides in adult male hypertensive patients. *Mymensingh Med Journal: Mmj*. (2023) 32(1):44–8.

3. Whelton PK, Carey RM, Aronow WS, Casey DE Jr, Collins KJ, Dennison Himmelfarb C, et al. 2017 ACC/AHA/AAPA/ABC/ACPM/AGS/APHA/ASH/ASPC/NMA/PCNA guideline for the prevention, detection, evaluation, and management of high blood pressure in adults: A report of the american college of cardiology/american heart association task force on clinical practice guidelines. *Circulation*. (2018) 138(17): e484–e594. doi: 10.1016/j.jacc.2017.11.006

4. Amini M, Moradinazar M, Rajati F, Soofi M, Sepanlou SG, Poustchi H, et al. Socioeconomic inequalities in prevalence, awareness, treatment and control of hypertension: evidence from the persian cohort study. *BMC Public Health*. (2022) 22 (1):1401. doi: 10.1186/s12889-022-13444-x

5. Harrison DG, Guzik TJ, Lob HE, Madhur MS, Marvar PJ, Thabet SR, et al. Inflammation, immunity, and hypertension. *Hypertension (Dallas Tex: 1979)*. (2011) 57 (2):132–40. doi: 10.1161/HYPERTENSIONAHA.110.163576

6. Madhur MS, Lob HE, Mccann LA, Iwakura Y, Blinder Y, Guzik TJ, et al. Interleukin 17 promotes angiotensin ii-induced hypertension and vascular dysfunction. *Hypertension (Dallas Tex: 1979)*. (2010) 55(2):500–7. doi: 10.1161/HYPERTENSIONAHA.109.145094

7. Wu J, Thabet SR, Kirabo A, Trott DW, Saleh MA, Xiao L, et al. Inflammation and mechanical stretch promote aortic stiffening in hypertension through activation of P38 mitogen-activated protein kinase. *Circ Res*. (2014) 114(4):616–25. doi: 10.1161/CIRCRESAHA.114.302157

8. Marino AP, Da Silva A, Dos Santos P, Pinto LM, Gazzinelli RT, Teixeira MM, et al. Regulated on activation, normal T cell expressed and secreted (Rantes) antagonist (Met-rantes) controls the early phase of trypanosoma cruzi-elicited myocarditis. *Circulation*. (2004) 110(11):1443–9. doi: 10.1161/01.CIR.0000141561.15939.EC

9. Johansen KL, Chertow GM, Gilbertson DT, Ishani A, Israni A, Ku E, et al. Us renal data system 2022 annual data report: epidemiology of kidney disease in the United States. *Am J Of Kidney Diseases: Off J Of Natl Kidney Foundation*. (2023) 81(3 Suppl1):A8–A11. doi: 10.1053/j.ajkd.2022.12.001

10. Burnier M, Egan BM. Adherence in hypertension. *Circ Res*. (2019) 124:1124–40. doi: 10.1161/CIRCRESAHA.118.313220

11. Vrijens B, Vincze G, Kristanto P, Urquhart J, Burnier M. Adherence to prescribed antihypertensive drug treatments: longitudinal study of electronically compiled dosing histories. *BMJ (Clinical Res Ed)*. (2008) 336(7653):1114–7. doi: 10.1136/bmj.39553.670231.25

12. Chen S, Saeed A, Liu Q, Jiang Q, Xu H, Xiao GG, et al. Macrophages in immunoregulation and therapeutics. *Signal Transduction And Targeted Ther*. (2023) 8 (1):207. doi: 10.1038/s41392-023-01452-1

13. Jackaman C, Tomay F, Duong L, Abdol Razak NB, Pixley FJ, Metharom P, et al. Aging and cancer: the role of macrophages and neutrophils. *Ageing Res Rev*. (2017) 36:105–16. doi: 10.1016/j.arr.2017.03.008

14. Guzik TJ, Hoch NE, Brown KA, McCann LA, Rahman A, Dikalov S, et al. Role of the T cell in the genesis of angiotensin ii induced hypertension and vascular dysfunction. *J Of Exp Med*. (2007) 204(10):2449–60. doi: 10.1084/jem.20070657

15. Owens T. T-cell costimulation: T cells themselves call the shots. *Curr Biol*. (1996) 6:32–5. doi: 10.1016/S0960-9822(02)00415-3

16. Yamano T, Steinert M, Klein L. Thymic B cells and central T cell tolerance. *Front In Immunol*. (2015) 6:376. doi: 10.3389/fimmu.2015.00376

17. Dustin ML. Help to go: T cells transfer cd40l to antigen-presenting B cells. *Eur J Of Immunol*. (2017) 47:31–4. doi: 10.1002/eji.201646786

18. Elgueta R, Benson MJ, De Vries VC, Wasiuk A, Guo Y, Noelle RJ. Molecular mechanism and function of cd40/cd40l engagement in the immune system. *Immunol Rev*. (2009) 229(1):152–72. doi: 10.1111/j.1600-065X.2009.00782.x

19. Radomir L, Kramer MP, Perpinial M, Schottlender N, Rabani S, David K, et al. The survival and function of IL-10-producing regulatory B cells are negatively controlled by slamf5. *Nat Commun*. (2021) 12(1):1893. doi: 10.1038/s41467-021-22230-z

20. Ray A, Basu S, Williams CB, Salzman NH, Dittel BN. A novel IL-10-independent regulatory role for B cells in suppressing autoimmunity by maintenance of regulatory T cells via gitr ligand. *J Of Immunol (Baltimore Md: 1950)*. (2012) 188(7):3188–98. doi: 10.4049/jimmunol.1103354

21. Flores-Borja F, Bosma A, Ng D, Reddy V, Ehrenstein MR, Isenberg DA, et al. CD19+CD24HICD38HI B cells maintain regulatory T cells while limiting th1 and th17 differentiation. *Sci Trans Med*. (2013) 5(173):173ra23. doi: 10.1126/scitranslmed.3005407

22. Barhoumi T, Kasal DA, Li MW, Shbat L, Laurant P, Neves MF, et al. T regulatory lymphocytes prevent angiotensin II-induced hypertension and vascular injury. *Hypertension (Dallas Tex: 1979)*. (2011) 57(3):469–76. doi: 10.1161/HYPERTENSIONAHA.110.162941

23. Matrougui K, Abd Elmageed Z, Kassan M, Choi S, Nair D, Gonzalez-Villalobos RA, et al. Natural regulatory T cells control coronary arteriolar endothelial dysfunction in hypertensive mice. *Am J Of Pathol*. (2011) 178(9):434–41. doi: 10.1016/j.ajpath.2010.11.034

24. Bai L, Hao X, Keith J, Feng Y. Dna methylation in regulatory T cell differentiation and function: challenges and opportunities. *Biomolecules*. (2022) 12 (9):1282. doi: 10.3390/biom12091282

25. Bellanti JA, Li D. Treg cells and epigenetic regulation. *Adv In Exp Med And Biol*. (2021) 1278:95–114. doi: 10.1007/978-981-15-6407-9_6

26. Ridker PM, Rane M. Interleukin-6 signaling and anti-interleukin-6 therapeutics in cardiovascular disease. *Circ Res*. (2021) 128:1728–46. doi: 10.1161/CIRCRESAHA.121.319077

27. Tanaka T, Narazaki M, Kishimoto T. IL-6 in inflammation, immunity, and disease. *Cold Spring Harbor Perspect In Biol*. (2014) 6:A016295. doi: 10.1101/cshperspect.a016295

28. Selzman CH, Shames BD, Reznikov LL, Miller SA, Meng X, Barton HA, et al. Liposomal delivery of purified inhibitory-kappabalpha inhibits tumor necrosis factor-alpha-induced human vascular smooth muscle proliferation. *Circ Res*. (1999) 84 (8):867–75. doi: 10.1161/01.RES.84.8.867

29. Rastogi S, Rizwani W, Joshi B, Kunigal S, Chellappan SP. TNF-α Response of vascular endothelial and vascular smooth muscle cells involve differential utilization of ask1 kinase and P73. *Cell Death And Differentiation*. (2012) 19:274–83. doi: 10.1038/cdd.2011.93

30. Jang DI, Lee AH, Shin HY, Song HR, Park JH, Kang TB, et al. The role of tumor necrosis factor alpha (TNF-α) in autoimmune disease and current TNF-α Inhibitors in therapeutics. *Int J Mol Sci*. (2021) 22(5):2719. doi: 10.3390/ijms22052719

31. Yao X, Huang J, Zhong H, Shen N, Faggioni R, Fung M, et al. Targeting interleukin-6 in inflammatory autoimmune diseases and cancers. *Pharmacol Ther*. (2014) 141(2):125–39. doi: 10.1016/j.pharmthera.2013.09.004

32. Singh S, Anshita D, Ravichandiran V. Mcp-1: function, regulation, and involvement in disease. *Int Immunopharmacol*. (2021) 101:107598. doi: 10.1016/j.intimp.2021.107598

33. Shah K, Al-Haidari A, Sun J, Kazi JU. T cell receptor (TCR) signaling in health and disease. *Signal Transduction And Targeted Ther*. (2021) 6(1):412. doi: 10.1038/s41392-021-00823-w

34. Wilfahrt D, Delgoffe GM. Metabolic waypoints during T cell differentiation. *Nat Immunol*. (2024) 25:206–17. doi: 10.1038/s41590-023-01733-5

35. Szeto C, Zareie P, Wirasinha RC, Zhang JB, Nguyen AT, Riboldi-Tunnicliffe A, et al. Covalent tcr-peptide-mhc interactions induce T cell activation and redirect T cell fate in the thymus. *Nat Commun*. (2022) 13(1):4951. doi: 10.1038/s41467-022-32692-4

36. Hwang JR, Byeon Y, Kim D, Park SG. Recent insights of T cell receptor-mediated signaling pathways for T cell activation and development. *Exp Mol Med*. (2020) 52:750–61. doi: 10.1038/s12276-020-0435-8

37. Castro-Sanchez P, Teagle AR, Prade S, Zamoyska R. Modulation of tcr signaling by tyrosine phosphatases: from autoimmunity to immunotherapy. *Front In Cell And Dev Biol*. (2020) 8:608747. doi: 10.3389/fcell.2020.608747

38. Taniguchi K, Karin M. NF-κB, inflammation, immunity and cancer: coming of age. *Nat Rev Immunol*. (2018) 18:309–24. doi: 10.1038/nri.2017.142

39. Yu H, Lin L, Zhang Z, Zhang H, Hu H. Targeting NF-κB pathway for the therapy of diseases: mechanism and clinical study. *Signal Transduction And Targeted Ther*. (2020) 5(1):209. doi: 10.1038/s41392-020-00312-6

40. Lawrence T. The nuclear factor nf-kappab pathway in inflammation. *Cold Spring Harbor Perspect In Biol*. (2009) 1:A001651. doi: 10.1007/978-981-15-6407-9_6

41. Barnabei L, Laplantine E, Mbongo W, Rieux-Laucat F, Weil R. NF-κB: at the borders of autoimmunity and inflammation. *Front In Immunol.* (2021) 12:716469. doi: 10.3389/fimmu.2021.716469

42. Wolf G, Wenzel U, Burns KD, Harris RC, Stahl RA, Thaiss F. Angiotensin ii activates nuclear transcription factor-kappab through at1 and at2 receptors. *Kidney Int.* (2002) 61(6):1986–95. doi: 10.1046/j.1523-1755.2002.00365.x

43. Esteban V, Ruperez M, Sánchez-López E, Rodríguez-Vita J, Lorenzo O, Demaegdt H, et al. Angiotensin iv activates the nuclear transcription factor-kappab and related proinflammatory genes in vascular smooth muscle cells. *Circ Res.* (2005) 96 (9):965–73. doi: 10.1161/01.RES.0000166326.91395.74

44. Fortelny N, Farlik M, Fife V, Gorki AD, Lassnig C, Maurer B, et al. Jak-stat signaling maintains homeostasis in T cells and macrophages. *Nat Immunol.* (2024) 25 (5):847–59. doi: 10.1038/s41590-024-01804-1

45. Fujimoto M, Serada S, Mihara M, Uchiyama Y, Yoshida H, Koike N, et al. Interleukin-6 blockade suppresses autoimmune arthritis in mice by the inhibition of inflammatory th17 responses. *Arthritis And Rheumatism.* (2008) 58(12):3710–9. doi: 10.1002/art.v58:12

46. Yu H, Lee H, Herrmann A, Buettner R, Jove R. Revisiting stat3 signalling in cancer: new and unexpected biological functions. *Nat Rev Cancer.* (2014) 14(11):736–46. doi: 10.1038/nrc3818

47. Wang SW, Sun YM. The IL-6/jak/stat3 pathway: potential therapeutic strategies in treating colorectal cancer (Review). *Int J Of Oncol.* (2014) 44:1032–40. doi: 10.3892/ijo.2014.2259

48. Gabay C. Interleukin-6 and chronic inflammation. *Arthritis Res Ther.* (2006) 8 Suppl 2:S3. doi: 10.1186/ar1917

49. Johnson DE, O'keefe RA, Grandis JR. Targeting the IL-6/jak/stat3 signalling axis in cancer. *Nat Rev Clin Oncol.* (2018) 15:234–48. doi: 10.1038/nrclinonc.2018.8

50. Huang H, Long L, Zhou P, Chapman NM, Chi H. mTOR signaling at the crossroads of environmental signals and T-cell fate decisions. *Immunol Rev.* (2020) 295 (1):15–38. doi: 10.1111/imr.v295.1

51. Zeng H, Chi H. Mtor signaling in the differentiation and function of regulatory and effector T cells. *Curr Opin In Immunol.* (2017) 46:103–11. doi: 10.1016/j.coi.2017.04.005

52. Zeng H, Yang K, Cloer C, Neale G, Vogel P, Chi H. mTORC1 couples immune signals and metabolic programming to establish T(Reg)-cell function. *Nature.* (2013) 499(7459):485–90. doi: 10.1038/nature12297

53. Amsen D, Helbig C, Backer RA. Notch in T cell differentiation: all things considered. *Trends In Immunol.* (2015) 36(10):802–14. doi: 10.1016/j.it.2015.10.007

54. Huehn J, Polansky JK, Hamann A. Epigenetic control of FOXP3 expression: the key to A stable regulatory T-cell lineage? *Nat Rev Immunol.* (2009) 9:83–9. doi: 10.1038/nri2474

55. Sakaguchi S, Wing K, Onishi Y, Prieto-Martin P, Yamaguchi T. Regulatory T cells: how do they suppress immune responses? *Int Immunol.* (2009) 21:1105–11. doi: 10.1093/intimm/dxp095

56. Sumida TS, Cheru NT, Hafler DA. The regulation and differentiation of regulatory T cells and their dysfunction in autoimmune diseases. *Nat Rev Immunol.* (2024) 24:503–17. doi: 10.1038/s41577-024-00994-x

57. Floess S, Freyer J, Siewert C, Baron U, Olek S, Polansky J, et al. Epigenetic control of the FOXP3 locus in regulatory T cells. *PloS Biol.* (2007) 5(2):E38. doi: 10.1371/journal.pbio.0050038

58. Xia Y, Yang J, Wang G, Li C, Li Q. Age-related changes in dna methylation associated with shifting th1/th2 balance. *Inflammation.* (2016) 39(6):1892–903. doi: 10.1007/s10753-016-0425-0

59. Brand S, Kesper DA, Teich R, Kilic-Niebergall E, Pinkenburg O, Bothur E, et al. Dna methylation of th1/th2 cytokine genes affects sensitization and progress of experimental asthma. *J Of Allergy And Clin Immunol.* (2012) 129(6):1602–10.E6. doi: 10.1016/j.jaci.2011.12.963

60. Guan H, Nagarkatti PS, Nagarkatti M. Cd44 reciprocally regulates the differentiation of encephalitogenic th1/th17 and th2/regulatory T cells through epigenetic modulation involving dna methylation of cytokine gene promoters, thereby controlling the development of experimental autoimmune encephalomyelitis. *J Of Immunol (Baltimore Md: 1950).* (2011) 186:6955–64. doi: 10.4049/jimmunol.1004043

61. Qiu Y, Zhu Y, Yu H, Zhou C, Kijlstra A, Yang P. Dynamic dna methylation changes of tbx21 and rorc during experimental autoimmune uveitis in mice. *Mediators Of Inflammation.* (2018) 2018:9129163. doi: 10.1155/2018/9129163

62. Lu TX, Rothenberg ME. MicroRNA. *J Of Allergy And Clin Immunol.* (2018) 141:1202–7. doi: 10.1016/j.jaci.2017.08.034

63. Lu Q, Wu R, Zhao M, Garcia-Gomez A, Ballestar E. Mirnas as therapeutic targets in inflammatory disease. *Trends In Pharmacol Sci.* (2019) 40(11):853–65. doi: 10.1016/j.tips.2019.09.007

64. Li X, Wei Y, Wang Z. MicroRNA-21 and hypertension. *Hypertension Research: Off J Of Japanese Soc Of Hypertension.* (2018) 41:649–61. doi: 10.1038/s41440-018-0071-z

65. Sekar D, Shilpa BR, Das AJ. Relevance of microRNA 21 in different types of hypertension. *Curr Hypertension Rep.* (2017) 19:57. doi: 10.1007/s11906-017-0752-z

66. Hu J, Huang S, Liu X, Zhang Y, Wei S, Hu X. Mir-155: an important role in inflammation response. *J Of Immunol Res.* (2022) 2022:7437281. doi: 10.1155/2022/7437281

67. Zhang A, Wang K, Zhou C, Gan Z, Ma D, Ye P, et al. Knockout of microRNA-155 ameliorates the th1/th17 immune response and tissue injury in chronic rejection. *J Of Heart And Lung Transplantation: Off Publ Of Int Soc For Heart Transplant.* (2017) 36(2):175–84. doi: 10.1016/j.healun.2016.04.018

68. Eshraghi R, Rafiei M, Hadian Jazi Z, Shafie D, Raisi A, Mirzaei H. MicroRNA-155 and exosomal microRNA-155: small pieces in the cardiovascular diseases puzzle. *Pathology Res Pract.* (2024) 257:155274. doi: 10.1016/j.prp.2024.155274

69. Sato F, Tsuchiya S, Meltzer SJ, Shimizu K. MicroRNAs and epigenetics. *FEBS J.* (2011) 278(10):1598–609. doi: 10.1111/j.1742-4658.2011.08089.x

70. Navaneethabalakrishnan S, Smith HL, Arenaz CM, Goodlett BL, McDermott JG, Mitchell BM. Update on immune mechanisms in hypertension. *Am J Of Hypertension.* (2022) 35(10):842–51. doi: 10.1093/ajh/hpac077

71. Liu XH, Ji QW, Huang Y, Zeng QT. Th17 response promotes angiotensin ii-induced atherosclerosis. *Med Hypotheses.* (2011) 76(4):593–5. doi: 10.1016/j.mehy.2011.01.008

72. Small HY, Migliarino S, Czesnikiewicz-Guzik M, Guzik TJ. Hypertension: focus on autoimmunity and oxidative stress. *Free Radical Biol Med.* (2018) 125:104–15. doi: 10.1016/j.freeradbiomed.2018.05.085

73. Gwon WG, Joung EJ, Kwon MS, Lim SJ, Utsuki T, Kim HR. Sargachromenol protects against vascular inflammation by preventing TNF-α-induced monocyte adhesion to primary endothelial cells via inhibition of NF-κB activation. *Int Immunopharmacol.* (2017) 42:81–9. doi: 10.1016/j.intimp.2016.11.014

74. Nallasamy P, Si H, Babu PV, Pan D, Fu Y, Brooke EA, et al. Sulforaphane reduces vascular inflammation in mice and prevents TNF-α-induced monocyte adhesion to primary endothelial cells through interfering with the NF-κB pathway. *J Of Nutr Biochem.* (2014) 25(8):824–33. doi: 10.1016/j.jnutbio.2014.03.011

75. Jia Z, Nallasamy P, Liu D, Shah H, Li JZ, Chitrakar R, et al. Luteolin protects against vascular inflammation in mice and TNF-alpha-induced monocyte adhesion to endothelial cells via suppressing IKBA/NF-κB signaling pathway. *J Of Nutr Biochem.* (2015) 26(3):293–302. doi: 10.1016/j.jnutbio.2014.11.008

76. Santisteban MM, Schaeffer S, Anfray A, Faraco G, Brea D, Wang G, et al. Meningeal interleukin-17-producing T cells mediate cognitive impairment in A mouse model of salt-sensitive hypertension. *Nat Neurosci.* (2024) 27(1):63–77. doi: 10.1038/s41593-023-01497-z

77. Guzik TJ, Nosalski R, Maffia P, Drummond GR. Immune and inflammatory mechanisms in hypertension. *Nat Rev Cardiol.* (2024) 21(6):396–416. doi: 10.1038/s41569-023-00964-1

78. Chen CN, Hajji N, Yeh FC, Rahman S, Ali S, Wharton J, et al. Restoration of FOXP3(+) regulatory T cells by hdac-dependent epigenetic modulation plays A pivotal role in resolving pulmonary arterial hypertension pathology. *Am J Of Respir And Crit Care Med.* (2023) 208(8):879–95. doi: 10.1164/rccm.202301-0181OC

79. Phoksawat W, Jumnainsong A, Sornkayasit K, Srisak K, Komanasin N, Leelayuwat C. IL-17 and IFN-Γ Productions by CD4+ T cells and T cell subsets expressing nkg2d associated with the number of risk factors for cardiovascular diseases. *Mol Immunol.* (2020) 122:193–9. doi: 10.1016/j.molimm.2020.04.003

80. Toussirot E, Gallais-Sérézal I, Aubin F. The cardiometabolic conditions of psoriatic disease. *Front In Immunol.* (2022) 13:970371. doi: 10.3389/fimmu.2022.970371

81. Nosalski R, Guzik TJ. Perivascular adipose tissue inflammation in vascular disease. *Br J Of Pharmacol.* (2017) 174:3496–513. doi: 10.1111/bph.v174.20

82. Guzik TJ, Mohiddin SA, Dimarco A, Patel V, Savvatis K, Marelli-Berg FM, et al. Covid-19 and the cardiovascular system: implications for risk assessment, diagnosis, and treatment options. *Cardiovasc Res.* (2020) 116(10):1666–87. doi: 10.1093/cvr/cvaa106

83. Yeh JL, Hsu JH, Liang JC, Chen IJ, Liou SF. Lercanidipine and labedipinedilol–A attenuate lipopolysaccharide/interferon-Γ-induced inflammation in rat vascular smooth muscle cells through inhibition of hmgb1 release and mmp-2, 9 activities. *Atherosclerosis.* (2013) 226(2):364–72. doi: 10.1016/j.atherosclerosis.2012.12.005

84. Qi J, Zheng JB, Ai WT, Yao XW, Liang L, Cheng G, et al. Felodipine inhibits ox-LDL-induced reactive oxygen species production and inflammation in human umbilical vein endothelial cells. *Mol Med Rep.* (2017) 16(4):4871–8. doi: 10.3892/mmr.2017.7181

85. Jukema JW, van der Hoorn JW. Amlodipine and atorvastatin in atherosclerosis: A review of the potential of combination therapy. *Expert Opin On Pharmacotherapy.* (2004) 5:459–68. doi: 10.1517/14656566.5.2.459

86. Fumagalli C, Maurizi N, Marchionni N, Fornasari D. β-blockers: their new life from hypertension to cancer and migraine. *Pharmacol Res.* (2020) 151:104587. doi: 10.1016/j.phrs.2019.104587

87. Argulian E, Bangalore S, Messerli FH. Misconceptions and facts about beta-blockers. *Am J Of Med.* (2019) 132:816–9. doi: 10.1016/j.amjmed.2019.01.039

88. Ogrodowczyk M, Dettlaff K, Jelinska A. Beta-blockers: current state of knowledge and perspectives. *Mini Rev In Medicinal Chem.* (2016) 16:40–54. doi: 10.2174/1389557515666151016125948

89. Liu X, Yang J, Deng W. The inflammatory cytokine IL-22 promotes murine gliomas via proliferation. *Exp And Ther Med.* (2017) 13:1087–92. doi: 10.3892/etm.2017.4059

90. Guevara M, Kollipara CS. Recent advances in giant cell arteritis. *Curr Rheumatol Rep.* (2018) 20:25. doi: 10.1007/s11926-018-0737-1

91. Zhang SX, Chen HR, Wang J, Shao HF, Cheng T, Pei RM, et al. The efficacy and safety of short-term and low-dose IL-2 combined with tocilizumab to treat rheumatoid arthritis. *Front In Immunol*. (2024) 15:1359041. doi: 10.3389/fimmu.2024.1359041

92. Fang Y, Chen M, Li G, Yang Y, He P, Chen J, et al. Cancer-associated fibroblast-like fibroblasts in vocal fold leukoplakia suppress cd8(+)T cell functions by inducing IL-6 autocrine loop and interacting with th17 cells. *Cancer Lett*. (2022) 546:215839. doi: 10.1016/j.canlet.2022.215839

93. Whelton PK, Carey RM, Aronow WS, Casey DE Jr, Collins KJ, Dennison Himmelfarb C, et al. 2017 aACC/AHA/AAPA/ABC/ACPM/AGS/APhA/ASH/ASPC/NMA/PCNA guideline for the prevention, detection, evaluation, and management of high blood pressure in adults: A report of the american college of cardiology/american heart association task force on clinical practice guidelines. *Circulation*. (2018) 138(17): e484–594. doi: 10.1161/CIR.0000000000000596

94. Luo T, Ji WJ, Yuan F, Guo ZZ, Li YX, Dong Y, et al. Th17/treg imbalance induced by dietary salt variation indicates inflammation of target organs in humans. *Sci Rep*. (2016) 6:26767. doi: 10.1038/srep26767

95. Andreo-López MC, Contreras-Bolívar V, Muñoz-Torres M, García-Fontana B, García-Fontana C. Influence of the mediterranean diet on healthy aging. *Int J Of Mol Sci*. (2023) 24(5):4491. doi: 10.3390/ijms24054491

96. Mentella MC, Scaldaferri F, Ricci C, Gasbarrini A, Miggiano GAD. Cancer and mediterranean diet: A review. *Nutrients*. (2019) 11(9):2059. doi: 10.3390/nu11092059

97. Ros E, Martínez-González MA, Estruch R, Salas-Salvadó J, Fitó M, Martínez JA, et al. Mediterranean diet and cardiovascular health: teachings of the predimed study. *Adv Nutr (Bethesda Md)*. (2014) 5(3):330s–6s. doi: 10.3945/an.113.005389

98. Panagiotakis SH, Simos P, Basta M, Zaganas I, Perysinaki GS, Akoumianakis I, et al. Interactions of mediterranean diet, obesity, polypharmacy, depression and systemic inflammation with frailty status. *Maedica*. (2022) 17(1):20–7. doi: 10.26574/maedica.2022.17.1.20

99. Di Giosia P, Stamerra CA, Giorgini P, Jamialahamdi T, Butler AE, Sahebkar A. The role of nutrition in inflammaging. *Ageing Res Rev*. (2022) 77:101596. doi: 10.1016/j.arr.2022.101596

100. Kenđel Jovanović G, Mrakovcic-Sutic I, Pavičić Žeželj S, Šuša B, Rahelić D, Klobučar Majanović S. The efficacy of an energy-restricted anti-inflammatory diet for the management of obesity in younger adults. *Nutrients*. (2020) 12(11):3583. doi: 10.3390/nu12113583

101. Nani A, Murtaza B, Sayed Khan A, Khan NA, Hichami A. Antioxidant and anti-inflammatory potential of polyphenols contained in mediterranean diet in obesity: molecular mechanisms. *Molecules*. (2021) 26(4):985. doi: 10.3390/molecules26040985

102. Neal B, Wu Y, Feng X, Zhang R, Zhang Y, Shi J, et al. Effect of salt substitution on cardiovascular events and death. *New Engl J Of Med*. (2021) 385(12):1067–77. doi: 10.1056/NEJMoa2105675

103. Sugama K, Suzuki K, Yoshitani K, Shiraishi K, Kometani T. IL-17, neutrophil activation and muscle damage following endurance exercise. *Exercise Immunol Rev*. (2012) 18:116–27.

104. MaChado OAS, Diniz VLS, Passos MEP, de Oliveira HH, Santos-Oliveira LC, Alecrim AL, et al. Physical exercise increases global and gene-specific (Interleukin-17 and interferon-Γ) dna methylation in lymphocytes from aged women. *Exp Physiol*. (2021) 106(9):1878–85. doi: 10.1113/eph.v106.9

105. Golzari Z, Shabkhiz F, Soudi S, Kordi MR, Hashemi SM. Combined exercise training reduces IFN-Γ And IL-17 levels in the plasma and the supernatant of peripheral blood mononuclear cells in women with multiple sclerosis. *Int Immunopharmacol*. (2010) 10(11):1415–9. doi: 10.1016/j.intimp.2010.08.008

106. Jin F, Li Y, Gao X, Yang X, Li T, Liu S, et al. Exercise training inhibits macrophage-derived IL-17a-cxcl5-cxcr2 inflammatory axis to attenuate pulmonary fibrosis in mice exposed to silica. *Sci Of Total Environ*. (2023) 902:166443. doi: 10.1016/j.scitotenv.2023.166443

107. Chen Z, Yan W, Mao Y, Ni Y, Zhou L, Song H, et al. Effect of aerobic exercise on treg and th17 of rats with ischemic cardiomyopathy. *J Of Cardiovasc Trans Res*. (2018) 11(3):230–5. doi: 10.1007/s12265-018-9794-0

108. Duzova H, Karakoc Y, Emre MH, Dogan ZY, Kilinc E. Effects of acute moderate and strenuous exercise bouts on IL-17 production and inflammatory response in trained rats. *J Of Sports Sci Med*. (2009) 8(2):219–24.

109. Russo A, Bartolini D, Mensà E, Torquato P, Albertini MC, Olivieri F, et al. Physical activity modulates the overexpression of the inflammatory mir-146a-5p in obese patients. *IUBMB Life*. (2018) 70(10):1012–22. doi: 10.1002/iub.v70.10

110. Villareal DT, Aguirre L, Gurney AB, Waters DL, Sinacore DR, Colombo E, et al. Aerobic or resistance exercise, or both, in dieting obese older adults. *New Engl J Of Med*. (2017) 376(20):1943–55. doi: 10.1056/NEJMoa1616338

111. Henschel P, Landwehr-Kenzel S, Engels N, Schienke A, Kremer J, Riet T, et al. Supraphysiological FOXP3 expression in human car-tregs results in improved stability, efficacy, and safety of car-treg products for clinical application. *J Of Autoimmun*. (2023) 138:103057. doi: 10.1016/j.jaut.2023.103057

112. Nguyen DN, Roth TL, Li PJ, Chen PA, Apathy R, Mamedov MR, et al. Polymer-stabilized cas9 nanoparticles and modified repair templates increase genome editing efficiency. *Nat Biotechnol*. (2020) 38(1):44–9. doi: 10.1038/s41587-019-0325-6

113. Alvarez Salazar EK, Cortés-Hernández A, Alemán-Muench GR, Alberú J, Rodríguez-Aguilera JR, Recillas-Targa F, et al. Methylation of FOXP3 tsdr underlies the impaired suppressive function of tregs from long-term belatacept-treated kidney transplant patients. *Front In Immunol*. (2017) 8:219. doi: 10.3389/fimmu.2017.00219

114. Piotrowska M, Gliwiński M, Trzonkowski P, Iwaszkiewicz-Grzes D. Regulatory T cells-related genes are under dna methylation influence. *Int J Of Mol Sci*. (2021) 22 (13):7144. doi: 10.3390/ijms22137144

115. Revenko A, Carnevalli LS, Sinclair C, Johnson B, Peter A, Taylor M, et al. Direct targeting of FOXP3 in tregs with AZD8701, A novel antisense oligonucleotide to relieve immunosuppression in cancer. *J For Immunotherapy Of Cancer*. (2022) 10(4):e003892. doi: 10.1136/jitc-2021-003892

116. Cortez JT, Montauti E, Shifrut E, Gatchalian J, Zhang Y, Shaked O, et al. CRISPR screen in regulatory T cells reveals modulators of FOXP3. *Nature*. (2020) 582 (7812):416–20. doi: 10.1038/s41586-020-2246-4

117. Bézie S, Freuchet A, Sérazin C, Salama A, Vimond N, Anegon I, et al. IL-34 actions on FOXP3(+) tregs and CD14(+) monocytes control human graft rejection. *Front In Immunol*. (2020) 11:1496. doi: 10.3389/fimmu.2020.01496

118. Zhao H, Liao X, Kang Y. Tregs: where we are and what comes next? *Front In Immunol*. (2017) 8:1578. doi: 10.3389/fimmu.2017.01578

119. Wang J, Gong R, Zhao C, Lei K, Sun X, Ren H. Human FOXP3 and tumour microenvironment. *Immunology*. (2023) 168(2):248–55. doi: 10.1111/imm.v168.2

120. Borna Š, Lee E, Nideffer J, Ramachandran A, Wang B, Baker J, et al. Identification of unstable regulatory and autoreactive effector T cells that are expanded in patients with FOXP3 mutations. *Sci Trans Med*. (2023) 15(727): eadg6822. doi: 10.1126/scitranslmed.adg6822

121. Piotrowska M, Gliwiński M, Trzonkowski P, Iwaszkiewicz-Grzes D. Regulatory T cells-related genes are under dna methylation influence. *Int J Of Mol Sci*. (2021) 22 (13):7144. doi: 10.3390/ijms22137144

122. Wang G, Yan Y, Xu N, Yin D, Hui Y. Treatment of type 1 diabetes by regulatory T-cell infusion via regulating the expression of inflammatory cytokines. *J Of Cell Biochem*. (2019) 120(12):19338–44. doi: 10.1002/jcb.v120.12

123. Dall'era M, Pauli ML, Remedios K, Taravati K, Sandova PM, Putnam AL, et al. Adoptive treg cell therapy in A patient with systemic lupus erythematosus. *Arthritis Rheumatol (Hoboken NJ)*. (2019) 71(3):431–40. doi: 10.1002/art.2019.71.issue-3

124. Kvakan H, Kleinewietfeld M, Qadri F, Park JK, Fischer R, Schwarz I, et al. Regulatory T cells ameliorate angiotensin ii-induced cardiac damage. *Circulation*. (2009) 119(22):2904–12. doi: 10.1161/CIRCULATIONAHA.108.832782

125. Wilck N, Matus MG, Kearney SM, Olesen SW, Forslund K, Bartolomaeus H, et al. Salt-responsive gut commensal modulates T(H)17 axis and disease. *Nature*. (2017) 551(7682):585–9. doi: 10.1038/nature24628

126. Bartolomaeus H, Balogh A, Yakoub M, Homann S, Markó L, Höges S, et al. Short-chain fatty acid propionate protects from hypertensive cardiovascular damage. *Circulation*. (2019) 139(11):1407–21. doi: 10.1161/CIRCULATIONAHA.118.036652

127. Singh TP, Farias Amorim C, Lovins VM, Bradley CW, Carvalho LP, Carvalho EM, et al. Regulatory T cells control staphylococcus aureus and disease severity of cutaneous leishmaniasis. *J Of Exp Med*. (2023) 220(12):e20230558. doi: 10.1084/jem.20230558

128. Li ZH, Wang J, Xu JP, Wang J, Yang X. Recent advances in CRISPR-based genome editing technology and its applications in cardiovascular research. *Military Med Res*. (2023) 10(1):12. doi: 10.1186/s40779-023-00447-x

129. Ercu M, Markó L, Schächterle C, Tsvetkov D, Cui Y, Maghsodi S, et al. Phosphodiesterase 3A and arterial hypertension. *Circulation*. (2020) 142(2):133–49. doi: 10.1161/CIRCULATIONAHA.119.043061

130. Ercu M, Walter S, Klussmann E. Mutations in phosphodiesterase 3A (PDE3A) cause hypertension without cardiac damage. *Hypertension (Dallas Tex: 1979)*. (2023) 80:1171–9. doi: 10.1161/HYPERTENSIONAHA.122.19433

131. Ercu M, Mücke MB, Pallien T, Markó L, Sholokh A, Schächterle C, et al. Mutant phosphodiesterase 3A protects from hypertension-induced cardiac damage. *Circulation*. (2022) 146(23):1758–78. doi: 10.1161/CIRCULATIONAHA.122.060210

132. Burnier M, Damianaki A. Hypertension as cardiovascular risk factor in chronic kidney disease. *Circ Res*. (2023) 132(23):1050–63. doi: 10.1161/CIRCRESAHA.122.321762

133. Wang C, Yuan Y, Zheng M, Pan A, Wang M, Zhao M, et al. Association of age of onset of hypertension with cardiovascular diseases and mortality. *J Of Am Coll Of Cardiol*. (2020) 75(23):2921–30. doi: 10.1016/j.jacc.2020.04.038

134. Gan L, Ye D, Feng Y, Pan H, Lu X, Wan J, et al. Immune cells and hypertension. *Immunologic Res*. (2024) 72:1–13. doi: 10.1007/s12026-023-09414-z

frontiers | Frontiers in Oncology

TYPE Original Research
PUBLISHED 28 February 2025
DOI 10.3389/fonc.2025.1531465

Check for updates

OPEN ACCESS

EDITED BY
Weiling Li,
Dalian Medical University, China

REVIEWED BY
Ren Li,
Shanxi Medical University, China
Zijun Zhao,
Capital Medical University, China

*CORRESPONDENCE
Qianqian Liu
ntfyliuqiangian@163.com

†These authors have contributed equally to this work

RECEIVED 20 November 2024
ACCEPTED 04 February 2025
PUBLISHED 28 February 2025

CITATION
Sun Z, Huang P, Lin J, Jiang G, Chen J and Liu Q (2025) The aggrephagy-related gene TUBA1B influences clinical outcomes in glioma patients by regulating the cell cycle. *Front. Oncol.* 15:1531465. doi: 10.3389/fonc.2025.1531465

COPYRIGHT
© 2025 Sun, Huang, Lin, Jiang, Chen and Liu. This is an open-access article distributed under the terms of the Creative Commons Attribution License (CC BY). The use, distribution or reproduction in other forums is permitted, provided the original author(s) and the copyright owner(s) are credited and that the original publication in this journal is cited, in accordance with accepted academic practice. No use, distribution or reproduction is permitted which does not comply with these terms.

The aggrephagy-related gene TUBA1B influences clinical outcomes in glioma patients by regulating the cell cycle

Zesheng Sun[1†], Pengcheng Huang[2†], Jialiang Lin[1†], Guiping Jiang[1], Jian Chen[1] and Qianqian Liu[1*]

[1]Department of Neurosurgery, Affiliated Hospital of Nantong University, Medical School of Nantong University, Nantong, Jiangsu, China, [2]Tianjin Medical University, General Hospital, Tianjin, China

Background: Gliomas are common primary malignant brain tumors, with glioblastoma (GBM) being the most aggressive subtype. GBM is characterized by high recurrence rates and treatment resistance, leading to poor patient outcomes. Current prognostic models have limited predictive power, underscoring the need to elucidate underlying mechanisms and identify novel biomarkers to improve therapeutic strategies and prognostic models.

Methods: Gene expression and clinical data for GBM and LGG were obtained from the TCGA and CGGA database, while single-cell sequencing data from GSE167960 were selected from the GEO database. Molecular characteristics of gliomas were revealed through normalization, consensus clustering analysis, immune scoring, cell infiltration analysis, and pathway analysis. TUBA1B, identified as a key gene through machine learning, was incorporated into a nomogram model using multivariate Cox regression. Its functions were validated through qRT-PCR, *in vitro* functional assays, and mouse xenograft models. All data analyses and statistics were performed using R software.

Results: Consensus clustering of the TCGA glioma dataset identified two aggrephagy subtypes (C1 and C2), with C2 showing worse survival outcomes and higher immune infiltration. TUBA1B was identified as an independent prognostic marker, with high expression associated with upregulated cell cycle pathways and alterations in the immune microenvironment. TUBA1B was shown to influence glioma cell proliferation, migration, invasion, and autophagy, impacting tumor progression and treatment response through intercellular communication and metabolic pathways.

Conclusion: The study demonstrates that high TUBA1B expression is closely associated with glioma malignancy and poor prognosis, making it a potential therapeutic target.

KEYWORDS

glioma, aggrephagy, TUBA1B, prognostic marker, immune microenvironment

1 Introduction

An estimated 40% of all brain tumors are gliomas, which are the most common primary malignant brain tumors (1). Among them, glioblastoma (GBM) is the most aggressive subtype. According to the World Health Organization (WHO) classification, gliomas are categorized into four histopathological grades: I, II, III, and IV. GBM (WHO grade IV) is the most invasive subtype, characterized by neovascularization, and WHO grades II and III are considered lower-grade gliomas (LGG) (2, 3). Histologically, gliomas exhibit high cellular density, active mitosis, vascular proliferation, and necrosis (4). Due to the aggressive nature of the tumor and resistance to chemotherapy and radiotherapy, patients often face high recurrence rates and functional impairments (5). Gliomas are currently treated with surgical resection, adjuvant chemotherapy, and radiotherapy. The median survival for LGG patients can range from five to ten years with combination therapies, while GBM patients typically have a median survival of only one to two years (6, 7). The prognosis of glioma patients varies significantly and is influenced by factors such as tumor grade, isocitrate dehydrogenase (IDH) mutation (8), and epidermal growth factor receptor (EGFR) amplification (9). Current glioma prognosis models are mainly based on clinical factors, but their predictive capacity is limited (10–13). Therefore, it is urgently needed to discover the mechanisms underlying glioma genesis and to identify biomarkers for improving therapeutic strategies and prognostic models.

Aggrephagy is a selective form of autophagy responsible for degrading misfolded or aggregated proteins (e.g., those generated by genetic mutations or cellular stress), which are typically recognized as damaged or misfolded within cells and need to be eliminated to prevent their accumulation (14). Aggrephagy plays a crucial role in cellular homeostasis by removing protein aggregates that might otherwise accumulate and disrupt cellular function. These misfolded proteins may arise continuously within cells due to genetic mutations, incomplete mRNA translation, post-translational misfolding, improper protein modifications, and oxidative stress (15). While these misfolded proteins are typically degraded via the ubiquitin-proteasome system (UPS), in certain cases (such as during protein aggregation), UPS may fail to degrade the target proteins effectively (16). Under these circumstances, aggrephagy becomes an alternative pathway for protein degradation. Aggrephagy is important in maintaining cellular homeostasis and is implicated in various human diseases, including neurodegenerative disorders, cataracts, and type II diabetes (17, 18).

Autophagy plays a dual role in tumorigenesis: at low levels, autophagy can facilitate the initial stages of cancer progression by providing energy and promoting cellular adaptation to stress. However, at elevated levels, autophagy enables tumor cells to survive under nutrient-scarce conditions by maintaining cellular homeostasis and removing damaged components, such as aggregated proteins, thus contributing to tumor cell survival in the later stages of cancer progression (18). Despite high autophagy-related gene expression and activity in glioma tissues and cells (16, 19, 20), whether aggrephagy exerts a similar regulatory role in glioma remains largely uninvestigated. As a result, the study of aggrephagy in gliomas is of considerable academic and clinical interest.

In this study, we explore the role of aggrephagy and its key gene, TUBA1B, in glioma, uncovering its multiple impacts on the tumor microenvironment. Through clustering analysis of The Cancer Genome Atlas (TCGA) dataset, we found that a high level of TUBA1B expression in gliomas indicates a poor prognosis and a rapid progression of the disease. Elevated TUBA1B expression promotes cell proliferation and migration and significantly affects the cell cycle, autophagy, and apoptosis. Immunological analysis indicates that TUBA1B is linked to cancer-associated fibroblasts and various immune cell infiltrations, implying its involvement in modulating the tumor microenvironment and intercellular communication. Furthermore, high TUBA1B expression is correlated with enhanced tumor stemness and decreased sensitivity to immunotherapy in glioma. These findings not only enhance our understanding of aggrephagy in glioma but also provide potential directions for developing new therapeutic targets with important clinical implications.

2 Methods

2.1 Processing and collection of data

In this study, we obtained data on glioblastoma and lower-grade gliomas (GBM and LGG) from the TCGA database. The gene expression data underwent $\log_2$(TPM+1) transformation to standardize the data and mitigate the effects of sequencing depth and gene length. Additionally, corresponding clinical data were acquired. During data curation, samples lacking survival data were excluded, resulting in a final cohort of 660 samples with complete expression profiles and clinical information.

Additionally, we incorporated glioma data from the Chinese Glioma Genome Atlas (CGGA) database to further validate our findings. The CGGA database includes three mRNAseq data (mRNAseq_301, mRNAseq_325 and mRNAseq_693). Gene expression data from these cohorts were processed similarly to the TCGA and GEO datasets, with $\log_2$(TPM+1) transformation to standardize the data. The clinical data for these samples were also curated, and only samples with complete survival and clinical information were included.

For single-cell sequencing results, we selected the single-cell sequencing dataset GSE167960 from the Gene Expression Omnibus (GEO) database, which includes six samples. We performed data normalization and quality control to remove outliers or samples with low cell counts, as well as annotated cell types based on gene expression characteristics.

Subsequently, we integrated the multi-sample data from TCGA with the single-cell data from GEO. Through survival analysis, differential gene expression analysis, and cellular heterogeneity analysis, we systematically explored the molecular characteristics of gliomas to identify potential prognostic biomarkers and key molecular pathways. These analyses provide an essential foundation

for elucidating the relationships between different molecular subtypes and their roles within the tumor microenvironment.

2.2 Consensus clustering analysis

To assess the differential expression of autophagy-related genes across glioma patients, we applied consensus clustering (CC) to classify the patients (21). Initially, we divided all samples based on a range of cluster numbers (k = 2-9). We then calculated the consensus score matrix and plotted CDF curves along with Delta area plots to determine the optimal number of clusters. The optimal k value was then selected for further analysis.

2.3 Immune scoring and immune checkpoint analysis

For immune infiltration analysis, we used multiple algorithms, including TIMER, CIBERSORT, MCP-counter, and xCell. These bioinformatics tools apply different algorithms to infer and quantify the relative proportions of various immune cell types in tumor samples based on gene expression data. TIMER is a tool for estimating the abundance of immune cells from RNA-seq data, while CIBERSORT uses a deconvolution algorithm to estimate the fraction of immune cells in a mixed tissue sample.

2.4 Cell infiltration analysis

To comprehensively analyze the cell types within the tumor microenvironment, we employed multiple bioinformatics tools, including TIMER, CIBERSORT, MCP-counter, and xCell. Each tool applies distinct algorithmic principles to infer and quantify the relative proportions of various immune cell types within tumor samples. The analysis involved importing gene expression data, running the "IOBR" package, and organizing the output to reveal the infiltration characteristics of different cell types. These insights provide a detailed understanding of the cellular composition of the tumor microenvironment.

2.5 Pathway analysis

In the pathway analysis, we utilized Gene Ontology (GO) and Kyoto Encyclopedia of Genes and Genomes (KEGG) to explore the functions and pathways associated with differentially expressed genes. Additionally, Gene Set Enrichment Analysis (GSEA) was employed to investigate the enrichment of differentially expressed genes within known pathways, aiding in the identification of functional and significant pathways. During the analysis, we input a filtered set of genes with differential expression (criteria: adjusted $P < 0.05$, $\log_2FC > 1$) and compared them against reference pathway sets from the Reactome or KEGG databases to identify highly correlated pathways. The activity levels of various biological pathways were assessed by calculating enrichment scores and conducting statistical tests, which helped elucidate these pathways' potential roles in tumor biology.

2.6 Selection of TUBA1B

To identify the key gene TUBA1B, the study employed three machine learning methods: LASSO regression, random forest, and support vector machine (SVM). LASSO regression is a method that applies a penalty to reduce the number of candidate genes, effectively narrowing down the gene list. Random forest, a decision tree-based algorithm, evaluates gene importance scores by constructing multiple decision trees and selecting the most influential genes based on their contribution to the classification. SVM is used to classify candidate genes and validate their classification performance. By cross-analyzing the results from these methods, TUBA1B was identified as a key gene associated with autophagy in gliomas.

2.7 The construction and evaluation of the nomogram

Our nomogram was constructed using univariate and multivariate Cox regression analyses to identify independent prognostic factors significantly associated with survival. A nomogram provides a visual representation of patient survival probabilities, helping clinicians predict survival rates at 1 year, 3 years, and 5 years based on multiple factors. To assess the predictive performance of the nomogram, several statistical methods were used. Receiver Operating Characteristic (ROC) curves were plotted to evaluate the model's ability to discriminate between patients with different survival outcomes. The area under the curve (AUC) was calculated at 1-year, 3-year, and 5-year intervals to measure the accuracy of the model. Calibration curves were then constructed to compare the predicted survival probabilities with the actual observed outcomes, evaluating the degree of agreement between them. A closer alignment between predicted and observed survival indicates a better model performance. Finally, Decision Curve Analysis (DCA) was performed to assess the clinical net benefit of the nomogram. DCA evaluates whether the model provides a net benefit compared to a strategy of treating all patients or treating none. This method helps to identify the most clinically relevant thresholds for the model's decision-making. These comprehensive evaluations demonstrated the nomogram's superiority in survival prediction, supporting its clinical application.

2.8 RNA extraction and quantitative RT-PCR

TRIzol reagent (Invitrogen, Carlsbad, CA) was used to isolate total RNA from transfected and control cell samples. The qRT-PCR reactions were performed in triplicate using Taq Pro Universal SYBR qPCR Master Mix (Vazyme Biotech Co., Ltd., Nanjing, Jiangsu, China) as directed by the manufacturer. The experiment utilized TUBA1B-

specific primers, including the forward primer 5′-GAGCAGCTCATCACAGGCATT-3′ and reverse primer 5′-TGCCTGTGATGAGCTGCTCTT-3′. A $2^{-\Delta\Delta Ct}$ method, normalized to GAPDH as an internal control, was used to determine the relative expression of TUBA1B following qRT-PCR.

2.9 Culturing and transfecting cells

Human glioma U251 and U87 cell lines were cultured and maintained in DMEM (Gibco, Grand Island, NY, USA) supplemented with 10% fetal bovine serum (FBS, Gibco, USA) and 1% penicillin-streptomycin solution in an incubator at 37°C with 5% CO_2. To explore the functional complexity of TUBA1B in GBM, TUBA1B was knocked down in U251 and U87 cells using negative control shRNA (shNC) and shTUBA1B. The transfection was performed using Lipofectamine 3000 reagent (Invitrogen, Carlsbad, CA, USA) strictly according to the manufacturer's protocol. Transfection was initiated when U251 and U87 cells reached approximately 70%-80% density in 6-well plates. Transfected cells were incubated under standard conditions for 48-72 hours to ensure effective knockdown of TUBA1B.

2.10 *In vitro* functional experiments

2.10.1 Cell proliferation

Following TUB1B knockdown, glioma cell proliferation was assessed using the CCK-8 assay. Following transfection with TUBA1B-specific shRNA for 48 hours, cells were harvested and counted. In 96-well plates, cells were seeded at a density of 2×10^3 per well. At 37°C, 10 μL of CCK-8 reagent (Dojindo, Japan) was added every 24 hours and incubated for 2 hours. The proliferation of cells was evaluated by measuring absorbance at 450 nm using a microplate reader.

2.10.2 Migration and invasion

The Transwell assay assessed cell migration and invasion after TUBA1B knockdown. After 48 hours post-transfection, cells were harvested and counted, then seeded at a density of 5×10^4 per well in the upper chamber of 24-well Transwell inserts (8 μm pore size, without Matrigel, Corning, USA). The lower chamber was filled with a complete medium supplemented with 20% FBS. The upper chamber was swabbed with cotton swabs after 24 hours, and the cells were stained with crystal violet and fixed with 4% paraformaldehyde. Invasion assays followed similar procedures, utilizing Matrigel-coated inserts, seeding 8×10^4 cells per well, and incubating for 48 hours to assess the number of invasive cells.

2.10.3 Cell cycle analysis

Flow cytometry analyzed cell cycle distribution following TUBA1B knockdown. We harvested the cells 48 hours post-transfection, washed them with PBS, and incubated them for 15 minutes in RNase-containing PBS containing PI reagent (BD Biosciences, USA). Cells were analyzed using a flow cytometer, and data were processed with ModFit LT software.

2.11 Western blot analysis

Using RIPA lysis buffer (containing protease inhibitors, Beyotime, China), total protein was extracted from treated cells. Protein concentrations were determined via the BCA method. To conduct electrophoresis, 30-50 μg of protein were loaded onto 6% or 10% SDS-polyacrylamide gels. Separated proteins were transferred to methanol activated PVDF membranes (Millipore, USA). Membranes were blocked with 5% BSA (Sigma-Aldrich, USA) in TBST at room temperature for 1 hour. An overnight incubation at 4°C with primary antibodies was performed on membranes: anti-LC3B (1:1000, Cell Signaling Technology, USA), anti-p62 (1:1000, Proteintech, USA), anti-Bcl-2 (1:1000, Cell Signaling Technology, USA), anti-Cyclin D1 (1:1000, Cell Signaling Technology, USA), and loading control anti-Tubulin 1 (1:5000, Proteintech, USA). Following three 10-minute TBST washes, membranes were incubated for 1 hour at room temperature with HRP-conjugated secondary antibodies (anti-rabbit or anti-mouse IgG, 1:5000, Cell Signaling Technology, USA), followed by three additional 10-minute TBST washes. Protein bands were developed with ECL-plus™ chemiluminescent kit (Thermo Fisher, USA) and visualized using a chemiluminescence imaging system.

2.12 *In vivo* xenograft mouse experiments

We obtained female BALB/c nude mice from the Animal Laboratory at Nantong University Medical College, aged 4 weeks. Well-growing U251 cells were prepared and transiently transfected with control and TUBA1B knockdown siRNA. Trypsinization and PBS washing were performed after 24 hours. The cells were counted and diluted to a concentration of 5×10^6 cells/100 μL. Under respiratory anesthesia, 100 μL of control/TUBA1B knockdown cells were subcutaneously injected into the mice. The growth of subcutaneous tumors was monitored. After 28 days, *in vivo* imaging experiments were conducted to measure tumor size. In accordance with animal welfare guidelines, this animal study was approved by the Animal Ethics Committee of Nantong University Medical College (S20240116-009).

2.13 Tumor stemness and immunotherapy benefit analysis

Six tumor stemness indices were utilized: DMPss (differentially methylated probes), DNAss (DNA methylation), ENHss (enhancer elements/DNA methylation), EREG.EXPss (epigenetically regulated RNA expression), EREG-METHss (epigenetically regulated DNA methylation), and RNAss (RNA expression). Spearman analysis was performed to explore the correlation between stemness characteristics and TUBA1B expression (22). Tumor Immune

Dysfunction and Exclusion (TIDE) was applied to predict the response to immune checkpoint blockade therapy (23).

2.14 Analyses of single-cell sequencing

Single cell sequencing data from multiple samples were collected and processed using the "Seurat" package for quality control and normalization. UMAP dimensional reduction was applied to perform clustering analysis, identifying different cell groups. Known cell markers were used to classify cells into eight groups: Oligodendrocytes, Macrophages, Glioma cells, Endothelial cells, Monocytes, T cells, Pericytes, and B cells. The "AddModuleScore" package was employed for gene set variation analysis to evaluate the autophagy-related gene expression levels in different cell groups. The expression of TUBA1B was analyzed across these cell groups, focusing on its distribution in Oligodendrocytes, Macrophages, Glioma cells, and Pericytes. Using the "CellChat" package, cell communication analysis was performed to explore communication patterns among cell groups with high TUBA1B expression, with particular attention to interactions with other cell groups. Signal pathway enrichment analysis was conducted using "cellchat" to identify the main input and output signaling pathways. Additionally, the "scMetabolism" package was used for in-depth analysis of metabolism pathways related to Glioma cells, identifying associations with starch and sucrose metabolism, propionate metabolism, oxidative phosphorylation, fatty acid degradation, and butyrate metabolism. These steps helped reveal the potential mechanisms by which TUBA1B regulates glioma cell biological behavior through intercellular communication and metabolic pathways in the tumor microenvironment.

2.15 Statistical analysis

The research data was analyzed statistically using R software (version 4.3.1). Data were evaluated using the Shapiro-Wilk test to determine whether they were normally distributed. Students' t-tests and one-way ANOVAs were conducted to compare two groups and multiple groups of normally distributed variables. The Wilcoxon test was used for comparisons between two groups of non-normally distributed data, and the Kruskal-Walli test was used for comparisons among multiple groups. Survival analysis was performed using the Kaplan-Meier method, which estimates the probability of survival over time. Log-rank tests were used to compare the survival distributions between groups. The Kaplan-Meier method generates survival curves, and the log-rank test assesses whether there are statistically significant differences between these curves. To ensure the robustness of the findings, the Cox proportional hazards regression model was applied for multivariate analysis, adjusting for potential confounders such as age, gender, and clinical features. The hazard ratio (HR) and corresponding 95% confidence interval (CI) were calculated to evaluate the risk of death associated with each variable. A statistically significant difference was considered when $P < 0.05$.

3 Results

3.1 Biological characteristics and clinical significance of aggrephagy subtypes in glioma

In order to investigate aggrephagy's potential role in glioma, we performed aggrephagy subtype classification using the ConsensusClusterPlus algorithm on the TCGA dataset (GBM +LGG). All samples were divided into k (k = 2–9) clusters. By analyzing the cumulative distribution function (CDF) curve, and Delta area plot, we identified k = 2 as the optimal number of subtypes (Figures 1A–C). Aggrephagy scores were significantly different between the two clusters, with patients in the C2 cluster showing worse survival outcomes (Figures 1D, E). To further understand the immunological differences between the two clusters, we employed multiple algorithms to assess immune infiltration, including TIMER, CIBERSORT, MCP-counter, xCell, Immune checkpoints, and ESTIMATE. The results revealed that overall immune infiltration was notably greater in the C2 cluster (Figures 1F, G, Supplementary Figure 1). Based on this, we defined the C1 cluster as "immune-cold" tumors and the C2 cluster as "immune-hot" tumors. Further analysis of key differentially expressed genes revealed that multiple tubulin-related genes (such as TUBA1A, TUBA1B, TUBA1C, TUBA3C, TUBA4B, TUBA3E, TUBA3D, TUBA4A, and TUBA8) were significantly altered in the C2 cluster compared to the C1 cluster. In addition, genes associated with protein degradation and stress response (such as UBB, UBC, UBA52, RPS27A, VCP, and HSF1) also showed significant changes (Figure 1H). Pathway and functional analysis of these differentially expressed genes indicated their involvement in cell adhesion molecules and trans-synaptic signaling regulation. Specifically, the "immune-hot" tumors exhibited significant upregulation in several pathways, including cell cycle, proliferation, metabolism, signaling, immune regulation, and stress response pathways, such as MYC Targets, E2F Targets, G2M Checkpoint, Interferon Alpha/Gamma Response, Inflammatory Response, TNFA Signaling via NFKB, PI3K/AKT/mTOR Signaling, IL6 JAK/STAT3 Signaling, and Glycolysis (Figures 1I–K). These results suggest that the C2 cluster not only Contributes significantly to maintaining cellular functions and responding to external stimuli but also that its extensive pathway activity may have significant implications for glioma progression.

3.2 TUBA1B as a key aggrephagy gene and independent prognostic marker for glioma patients

To identify key genes associated with aggrephagy in glioma, we employed three machine learning methods: LASSO regression, random forest, and support vector machine, to narrow down candidate genes (Figures 2A–C). Through cross-analysis, we identified seven aggrephagy-related common genes: TUBA1C, VIM, TUBA1B, DYNC1H1, TUBA1A, PRKN, and DYNLL2 (Figure 2D). A subsequent univariate and multivariate Cox regression analysis found

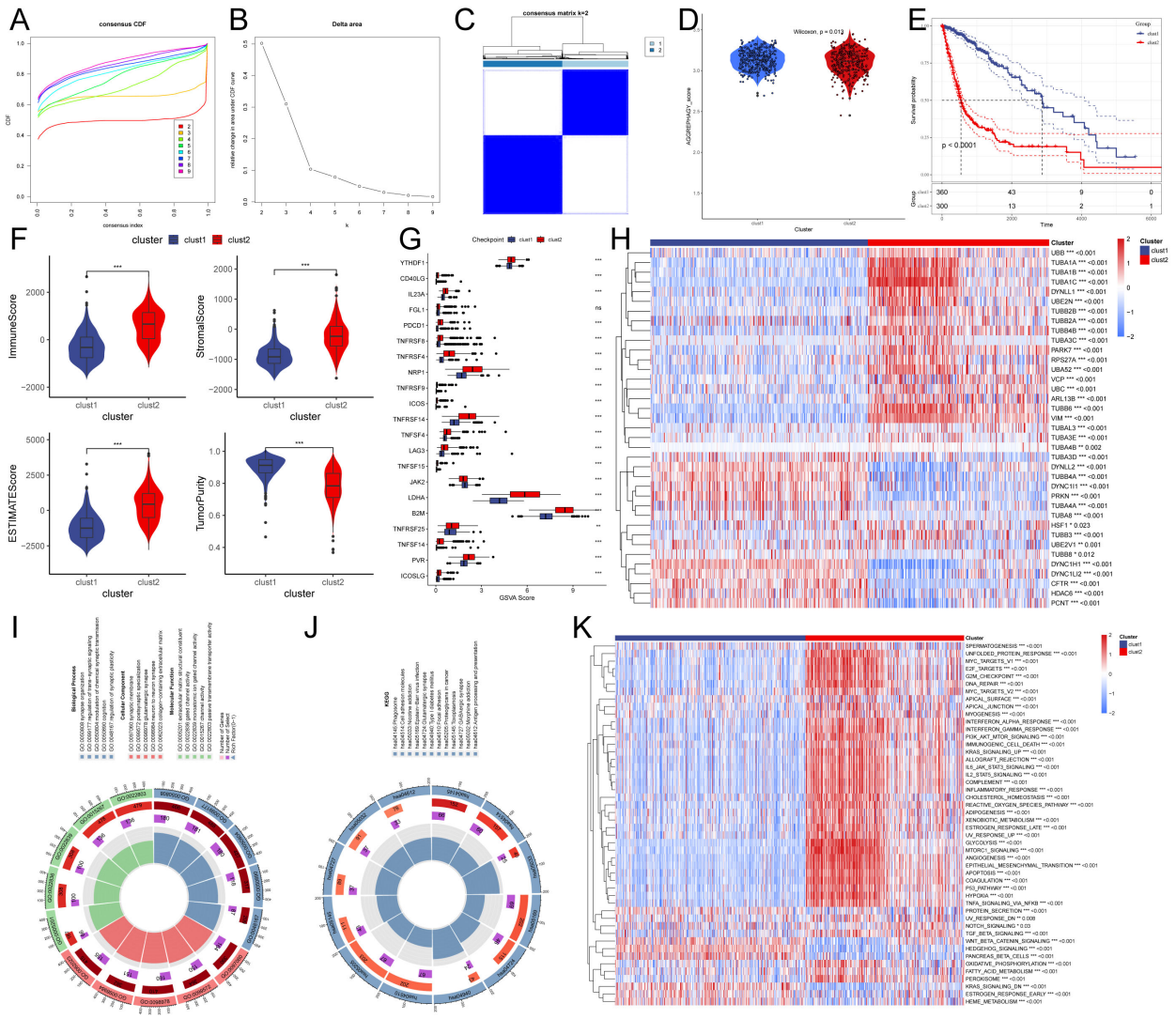

FIGURE 1
Characteristics of autophagy subtypes in glioma. **(A, B)** Cumulative distribution function (CDF) curves and Delta area plots for consensus scores of autophagy subtypes in the TCGA (GBM+LGG) dataset. **(C)** Consensus score matrix for all samples when k = 2. A higher consensus score between two samples indicates a higher likelihood of their co-clustering in different iterations. **(D)** Autophagy scores of the two clusters. **(E)** Kaplan-Meier survival curves for the two clusters. **(F)** Comparison of Immune score, Estimate score, Stromal score, and Tumor purity between the two clusters. **(G)** Expression of immune checkpoint genes between the two clusters. **(H)** Heatmap showing differentially expressed genes between the two clusters. **(I, J)** Gene Ontology (GO) and Kyoto Encyclopedia of Genes and Genomes (KEGG) pathway analysis of differentially expressed genes between the two groups. **(K)** Heatmap of Gene Set Enrichment Analysis (GSEA) for differentially expressed genes between the two groups.

that, except for PRKN, all of the remaining genes played independent prognostic roles. Among them, TUBA1C, VIM, TUBA1B, and TUBA1A were confirmed as risk factors, while DYNC1H1 and DYNLL2 were considered protective factors (Figures 2E, F). We identified TUBA1B and TUBA1C as the most significant prognostic genes in glioma by integrating results from random forest, univariate, and multivariate Cox regression analyses, highlighting their high weights. It has been shown that TUBA1C regulates the cell cycle and is associated with poor prognoses in glioma cells (24). Therefore, we chose to investigate the other gene, TUBA1B. In the TCGA database, Kaplan-Meier curve analysis showed that patients with low TUBA1B expression had significantly better prognoses than those with high expression. The low-expression group exhibited a significantly longer survival time compared to the high-expression group, suggesting that elevated TUBA1B expression may correlate with poor prognosis (Figure 2G). In addition to the TCGA and GEO datasets, we further validated our findings using data from the CGGA database, which includes a broader data of glioma samples. As shown in Supplementary Figure 2, our analysis of CGGA data confirmed the significant association between TUBA1B expression and poor prognosis in glioma patients. These results, consistent with our findings from the TCGA and GEO datasets, reinforce the robustness and relevance of TUBA1B as a potential prognostic biomarker in glioma. According to the ROC curve analysis, TUBA1B has AUC values of 0.812, 0.806, and 0.801 for predicting 1-year, 3-year, and 5-year survival, respectively (Figure 2H). To facilitate the clinical application of TUBA1B as a prognostic marker, we constructed a nomogram incorporating various clinicopathological factors, including TUBA1B expression, to better

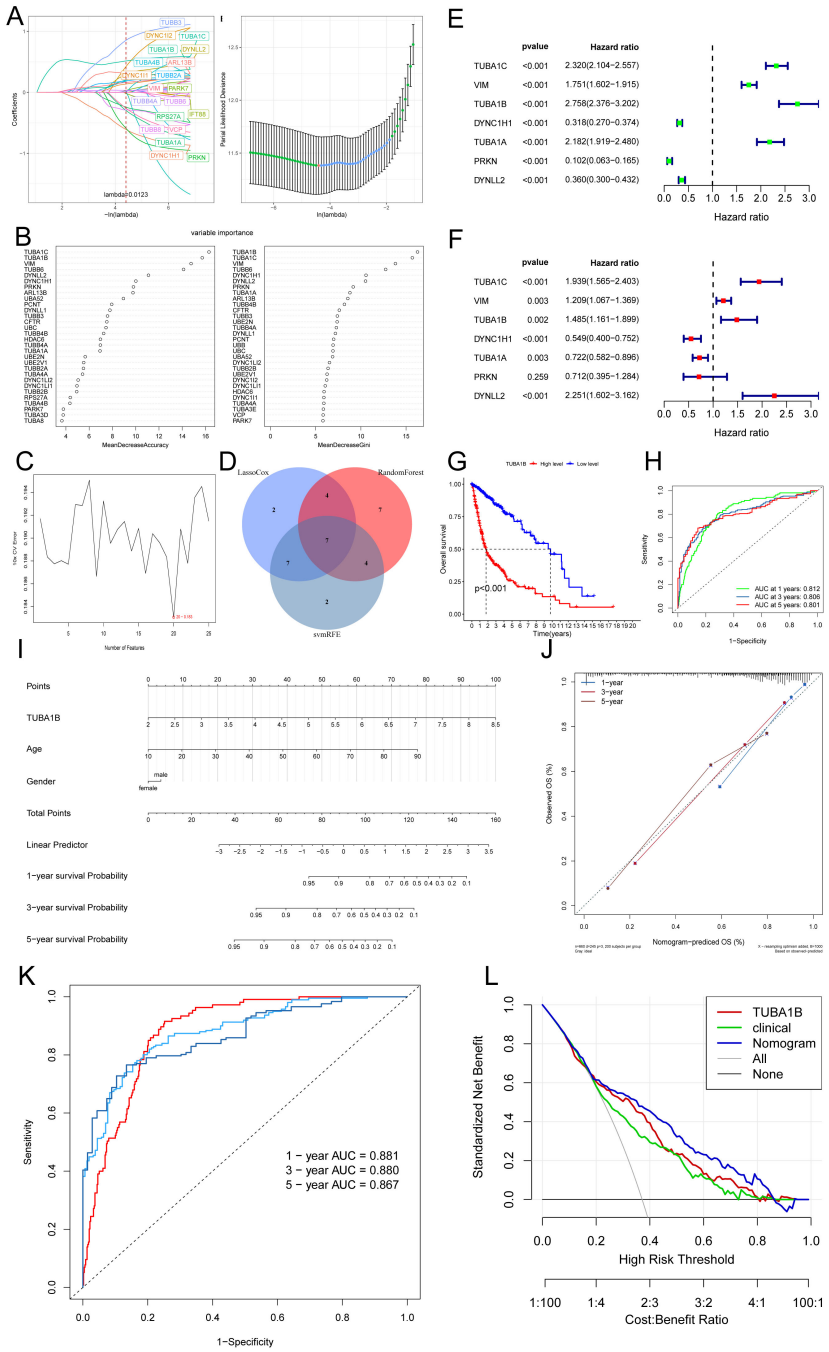

FIGURE 2
TUBA1B as an independent prognostic marker in glioma patients. **(A)** The relationship between partial likelihood deviance and log(λ) in the LASSO Cox regression model. The lambda parameter represents the coefficient of a feature. The x-axis shows the influence of lambda on the independent variables, while the y-axis represents the coefficient of the independent variables. **(B)** Random Forest results. **(C)** Support vector machine (SVM) curve results. **(D)** Venn diagram of key genes identified through the intersection of three machine learning methods. **(E, F)** Univariate and multivariate Cox regression analysis of seven key genes. **(G)** Kaplan-Meier survival analysis of glioma patients stratified by high and low TUBA1B expression. **(H)** Receiver operating characteristic (ROC) curves predicting 1-, 3-, and 5-year prognosis of glioma patients based on TUBA1B expression. **(I)** Nomogram constructed using TUBA1B expression and various clinical characteristics. **(J)** Calibration curves of the nomogram for 1-, 3-, and 5-year overall survival probabilities. **(K)** ROC curves demonstrating the predictive value of the nomogram for 1-, 3-, and 5-year survival in glioma patients. **(L)** Decision curve analysis (DCA) curves comparing the predictive performance of the nomogram.

predict overall survival rates for glioma patients (Figure 2I). Calibration curves, ROC curves, and DCA were used to evaluate this model. Calibration curves showed that the nomogram's predictions of survival after a year, three years, and five years were very close to the actual outcomes (Figure 2J). Based on the ROC curve analysis, the nomogram's AUC values for predicting 1-year, 3-year, and 5-year survival were 0.881, 0.880, and 0.867, respectively (Figure 2K). A DCA revealed that the nomogram had a higher clinical net benefit between

20% and 80% (Figure 2L). Based on these findings, the nomogram is more accurate in predicting glioma patient survival than any single diagnostic feature, highlighting the potential of TUBA1B as a valuable prognostic biomarker.

3.3 Pathway analysis of TUBA1B-related genes

We divided the TCGA database into high and low TUBA1B expression groups based on the median expression level in order to examine TUBA1B's role in gliomas. We identified differentially expressed genes between the two groups and concentrated on those upregulated in the high-expression group for functional and pathway analysis. The KEGG analysis showed that these upregulated genes were mainly involved in several key pathways, including the cell cycle, the AGE-RAGE signaling pathway, ECM-receptor interactions, complement and coagulation cascades, as well as p53 signaling. GO analysis indicated that these genes significantly influenced several biological processes, such as mitotic cell cycle phase transition, chromosome segregation, and nuclear chromosome segregation (Figures 3A–C). These findings suggest a strong association between many genes and the cell cycle. Key genes involved include PTTG1, CCNB1, CCNB2, CDKN2C, AURKB, CDK1, CCNA2, TGFB2, CDCA5, NDC80, CDC45, BUB1, WEE1, and MCM2 (Figure 3C). Additionally, we performed GSEA on the upregulated genes in the TUBA1B high-expression group, which again highlighted the cell cycle as a major pathway of interest (Figure 3D).

3.4 TUBA1B mediates malignant progression of glioblastoma by regulating the cell cycle

The pathway analysis results suggest that TUBA1B may be associated with the cell cycle. Therefore, we performed a correlation analysis and found that the expression of TUBA1B was significantly positively correlated with the cell cycle score (Figure 4A). This finding prompted us to conduct a series of *in vitro* experiments to explore the role of TUBA1B in regulating cell cycle progression and its effect on glioma cell proliferation. First, we successfully knocked down TUBA1B expression in U251 and U87 cells (Figure 4B). Next, flow cytometry was used to analyze the cell cycle, and the results showed that knockdown of TUBA1B led to significant changes in the cell cycle distribution, particularly in the proportion of cells in the G1 and S phases. The percentage of cells in the G1 phase was significantly increased, while the proportion of cells in the S phase was significantly decreased (Figures 4C, D). These results suggest that TUBA1B may regulate cell proliferation by affecting the progression of the cell cycle. Furthermore, we evaluated cell proliferation using the CCK-8 assay. Knockdown of TUBA1B significantly reduced the proliferation rate of U251 and U87 cells (Figure 4E). Additionally, migration and invasion assays showed that TUBA1B knockdown significantly inhibited the migration and invasion capabilities of U251 and U87 cells (Figures 4F, G). However, the addition of the cell cycle activator Cyclin D1 partially restored the inhibitory effect of TUBA1B knockdown on cell migration and invasion, further validating that TUBA1B regulates glioma cell behavior through the cell cycle. Next, we

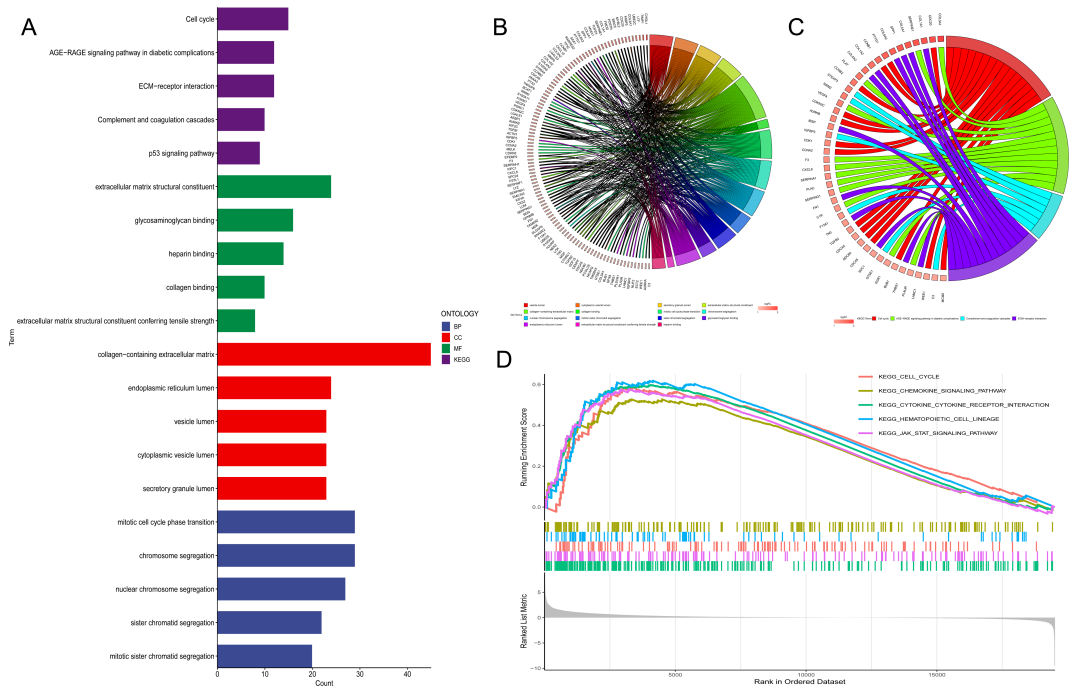

FIGURE 3
Pathway analysis of genes associated with TUBA1B expression. **(A–C)** Gene Ontology (GO) and KEGG pathway analysis of upregulated differentially expressed genes (DEGs) in the high and low TUBA1B expression groups. **(D)** Gene Set Enrichment Analysis (GSEA) of upregulated DEGs in the high and low TUBA1B expression groups.

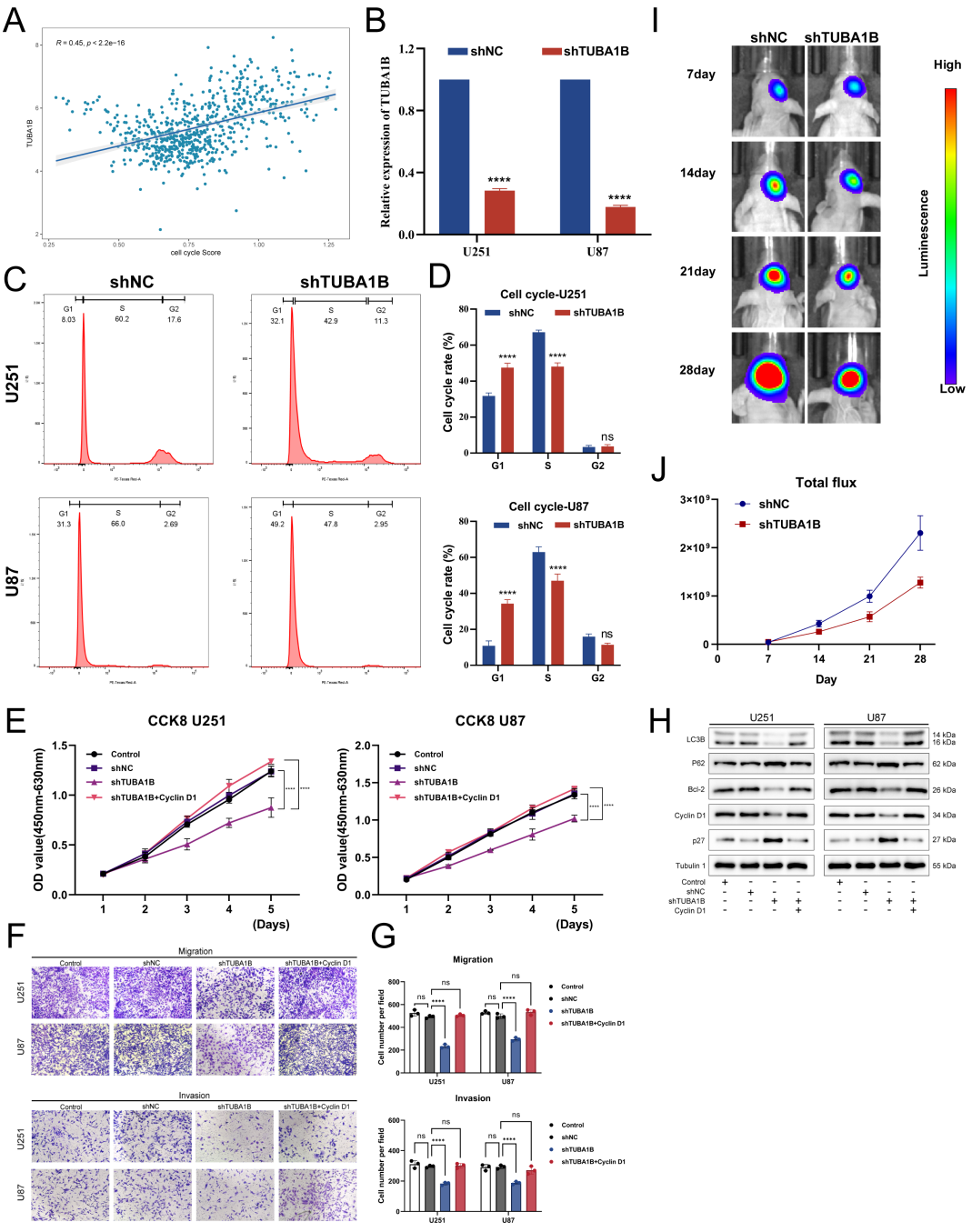

FIGURE 4
TUBA1B influences tumor malignancy progression. **(A)** Correlation analysis between TUBA1B expression and cell cycle score in glioma samples from the TCGA database. **(B)** qPCR analysis confirming the successful knockdown of TUBA1B in U251 and U87 cells. **(C, D)** Flow cytometry analysis of the cell cycle in U251 cells with TUBA1B knockdown. **(E)** CCK-8 assay showing the effect of TUBA1B knockdown on cell proliferation in U251 and U87 cells. **(F, G)** Migration and invasion assay in U251 and U87 cells with TUBA1B knockdown. **(H)** Western blot analysis showing the expression of Cyclin D1, p27, LC3B, and Bcl-2 in U251 and U87 cells with TUBA1B knockdown. **(I)** *In vivo* tumor growth analysis using a mouse xenograft model. **(J)** Statistical analysis of the total fluorescence intensity from the *in vivo* imaging.

performed Western blot analysis, which revealed that knockdown of TUBA1B led to a significant decrease in Cyclin D1 levels, while p27 protein levels were significantly increased (Figure 4H). This result further confirms the regulatory role of TUBA1B on key cell cycle proteins. Additionally, autophagy-related proteins such as LC3B and Bcl-2 also showed changes in expression, indicating that TUBA1B may also be involved in autophagy regulation. These effects were also partially reversed by Cyclin D1, supporting the involvement of the cell cycle in the regulation of TUBA1B's role in glioma. Finally, we further validated the impact of TUBA1B on tumor progression using a mouse xenograft model. Fluorescence imaging results showed that tumor growth was significantly inhibited in the TUBA1B knockdown group (Figure 4I). Statistical analysis (Figure 4J) indicated that the total fluorescence

intensity of the tumor in the TUBA1B knockdown group was significantly lower than that in the control group, further proving the oncogenic role of TUBA1B in glioma. In conclusion, TUBA1B regulates cell cycle progression and associated pathways, significantly affecting glioma cell proliferation, migration, and invasion. It also promotes tumor growth in the mouse xenograft model, suggesting that TUBA1B plays a crucial role in the progression of glioma.

3.5 TUBA1B affects the immune microenvironment of glioblastoma

Based on correlation analyses and immune infiltration assessments, we investigated how TUBA1B affects the immune microenvironment in glioblastoma. First, we evaluated the correlation between TUBA1B expression and EstimateScore, ImmuneScore, StromalScore, and TumorPurity. In the high-expression TUBA1B group, the EstimateScore, ImmuneScore, and StromalScore were significantly elevated and positively correlated with TUBA1B expression (Figure 5A). The higher the expression of TUBA1B, the lower the TumorPurity, while there was a negative correlation between TUBA1B expression and TumorPurity (Figure 5A). Next, we used multiple algorithms (XCELL, QUANTISEQ, MCPCOUNTER, TIMER, CIBERSORT-ABS, EPIC, and CIBERSORT) to assess differences in immune infiltration between the high and low TUBA1B expression groups (Figure 5B). Our analysis focused on results with correlation coefficients greater than 0.3 to determine whether TUBA1B expression correlated with specific immune cell subtypes (Supplementary Figure 3). According to EPIC and MCPCOUNTER algorithms, TUBA1B expression and CAF infiltration are significantly correlated (R = 0.45, P < 2.2e-16). In the XCELL algorithm, the immune infiltration of T helper type 2 cells (CD4+Th2) also exhibited a strong positive correlation with TUBA1B expression (R = 0.56, P < 2.2e-16). The TIMER algorithm demonstrated that $CD8^{+}$T cell infiltration was

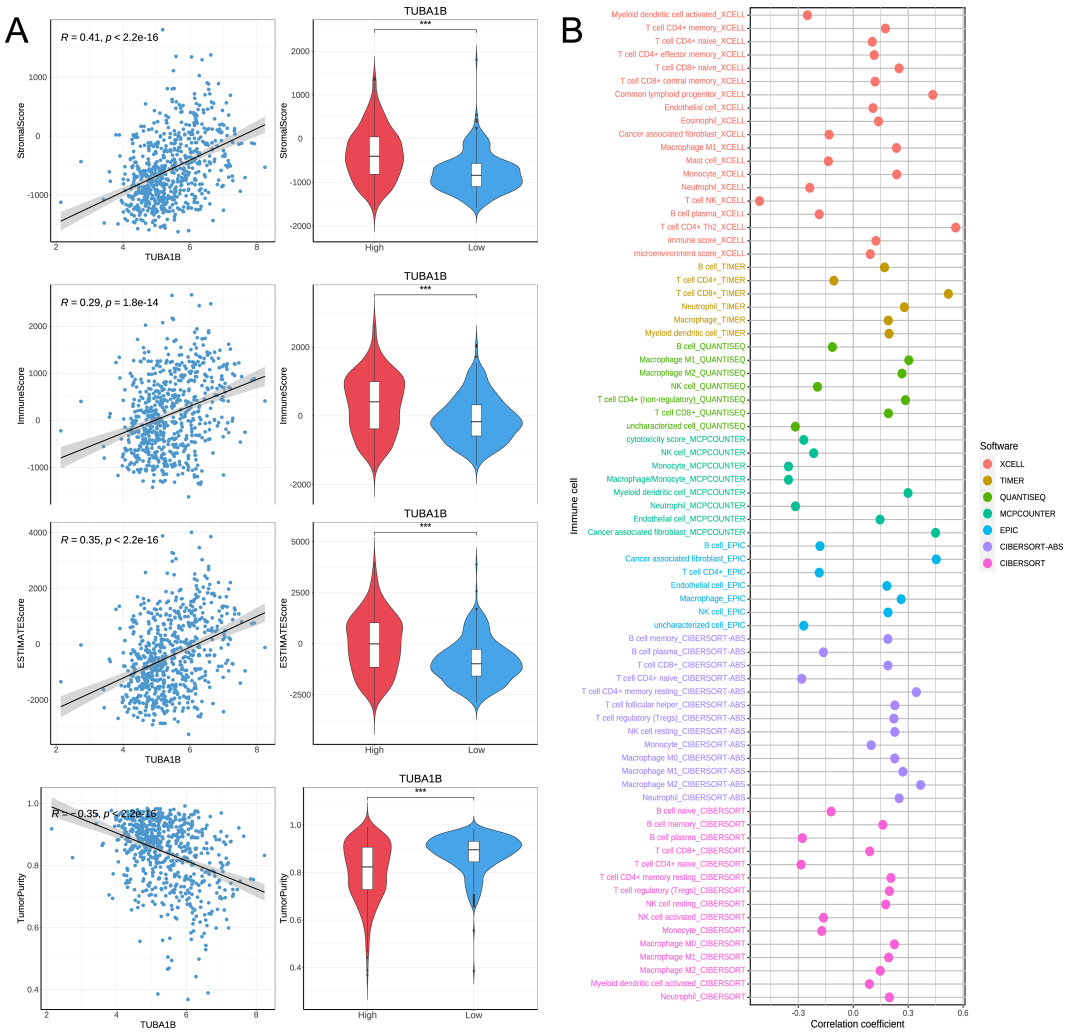

FIGURE 5
TUBA1B affects immune microenvironment in glioblastoma. **(A)** Comparison of Immune score, Estimate score, Stromal score, and Tumor purity between high and low TUBA1B expression groups. **(B)** Heatmap depicting significant differential immune responses between high and low TUBA1B expression groups using TIMER, CIBERSORT, CIBERSORT-ABS, QUANTISEQ, MCPCOUNTER, XCELL, and EPIC algorithms.

significantly positively correlated with TUBA1B expression (R = 0.52, P < 2.2e-16). Additionally, the QUANTISEQ algorithm revealed a positive correlation between M1-type macrophage infiltration and TUBA1B expression (R = 0.3, P = 1.8e-15), while the CIBERSORT-ABS algorithm showed a positive correlation between M2-type macrophage infiltration and TUBA1B expression (R = 0.37, P < 2.2e-16). By contrast, the MCPCOUNTER algorithm found that monocyte infiltration was significantly correlated with TUBA1B expression (R = -0.35, P < 2.2e-16), and in the XCELL algorithm, NK cell (natural killer cell) infiltration was also negatively correlated with TUBA1B expression (R = -0.51, P < 2.2e-16). The results indicate that TUBA1B potentially modulates tumor biology in human gliomas by affecting the immune microenvironment, especially through its impact on fibroblast infiltration and diverse immune cell types.

3.6 TUBA1B influences stemness and therapy response in glioma

To explore the impact of TUBA1B expression on tumor stemness in glioma, we conducted a Spearman correlation analysis. The results demonstrated that TUBA1B expression was significantly positively correlated with four tumor stemness indices (DNAss, EREG-METHss, DMPss, and ENHss), while it was significantly negatively correlated with RNAss and EREG.EXPss, all showing statistical significance (Figures 6A–F). Next, we used the TIDE (Tumor Immune Dysfunction and Exclusion) algorithm to assess the predictive ability of TUBA1B expression for immunotherapy benefits. High-expression TUBA1B had higher TIDE and Exclusion scores than low-expression TUBA1B, suggesting a higher immune escape potential. A lower MSI (Microsatellite Instability) score was also observed in the high-expression group, whereas no significant change was seen in the Dysfunction score. The results of a correlation analysis confirmed these findings, showing a significant positive correlation between TUBA1B expression, TIDE, and Exclusion, as well as a significant negative correlation with MSI (Figures 6G–J). These results suggest that high TUBA1B expression may promote tumor stemness and decrease sensitivity to immunotherapy in gliomas, highlighting the potential importance of TUBA1B in glioma progression and treatment response.

3.7 Intercellular crosstalk disrupts glioblastoma progression

From six samples, we analyzed single cell sequencing data to understand TUBA1B's role in the tumor microenvironment. After the initial screening, 23,520 cells were collected. Using the UMAP method for dimensionality reduction and unsupervised clustering, and with the help of known markers, the cells were classified into eight groups: Oligodendrocytes, Macrophages, Glioma cells, Endothelial cells, Monocytes, T cells, Pericytes, and B cells (Figure 7A; Supplementary Figure 4). We then calculated autophagy scores based on gene expression levels across these cell groups. As shown in Figure 7B, the results indicated that Oligodendrocytes and Glioma cells exhibited relatively high autophagy scores, suggesting that these cell groups may have high autophagic activity within the tumor microenvironment. Analysis of TUBA1B expression across different cell groups revealed that TUBA1B was predominantly expressed in Oligodendrocytes, Macrophages, Glioma cells, and Pericytes (Figure 7C). Based on this, we conducted a cell-cell communication analysis to clarify the interactions between TUBA1B-high-expressing cell groups. As expected, TUBA1B-high-expressing Oligodendrocytes, Macrophages, and Glioma cells displayed strong communication abilities (Figure 7D). Specifically, in Glioma cells, regardless of TUBA1B expression levels, these cells mainly interacted with Macrophages, Glioma cells, and Pericytes (Figure 7D). We then analyzed the main input and output signaling pathways of Glioma cells. For TUBA1B-high-expressing Glioma cells, signal output was primarily through the PTN, ANNEXIN, VEGF, PROS, and BMP pathways, while signal input occurred via the PTN, SPP1, and MK pathways. In contrast, TUBA1B-low-expressing Glioma cells mainly transmitted signals through the PTN pathway and received signals via the PTN, MK, EGF, and CALCR pathways (Figure 7E). Finally, we explored the metabolic pathways associated with Glioma cells. Both TUBA1B-high and TUBA1B-low Glioma cell groups were found to be involved in pathways related to starch and sucrose metabolism, propionate metabolism, oxidative phosphorylation, fatty acid degradation, and butyrate metabolism (Figure 7F). These findings suggest that TUBA1B may regulate glioma cell behavior by affecting intercellular communication and metabolic pathways within the tumor microenvironment.

4 Discussion

In glioma research, autophagy is regarded as a "double-edged sword." On one hand, autophagy exacerbates tumor malignancy by promoting the maintenance and differentiation of glioma stem cells. This function can be attributed to the role of autophagy in protein degradation and cellular energy homeostasis (25). On the other hand, tumor development could be inhibited by autophagy via degrading waste, such as aggregated proteins (26). This dual role makes the regulation of autophagy a critical target for glioma therapy (27, 28). The cross-regulation between autophagy and the ubiquitin-proteasome system also plays a significant role in the growth and chemoresistance of glioma cells (19, 25). Aggrephagy, a selective form of autophagy that targets aggregated proteins for degradation, is pivotal in tumorigenesis and progression (29). Recent studies, particularly by Zhang et al. (30), have identified five aggrephagy-related genes (ARPS) and constructed prognostic signatures, validating their clinical relevance. These findings underline the importance of aggrephagy in gliomas, especially regarding the tumor microenvironment and prognosis.

In this comprehensive study, we have, for the first time, revealed the molecular subtypes of aggrephagy in gliomas and their complex interactions with the immune microenvironment and tumor

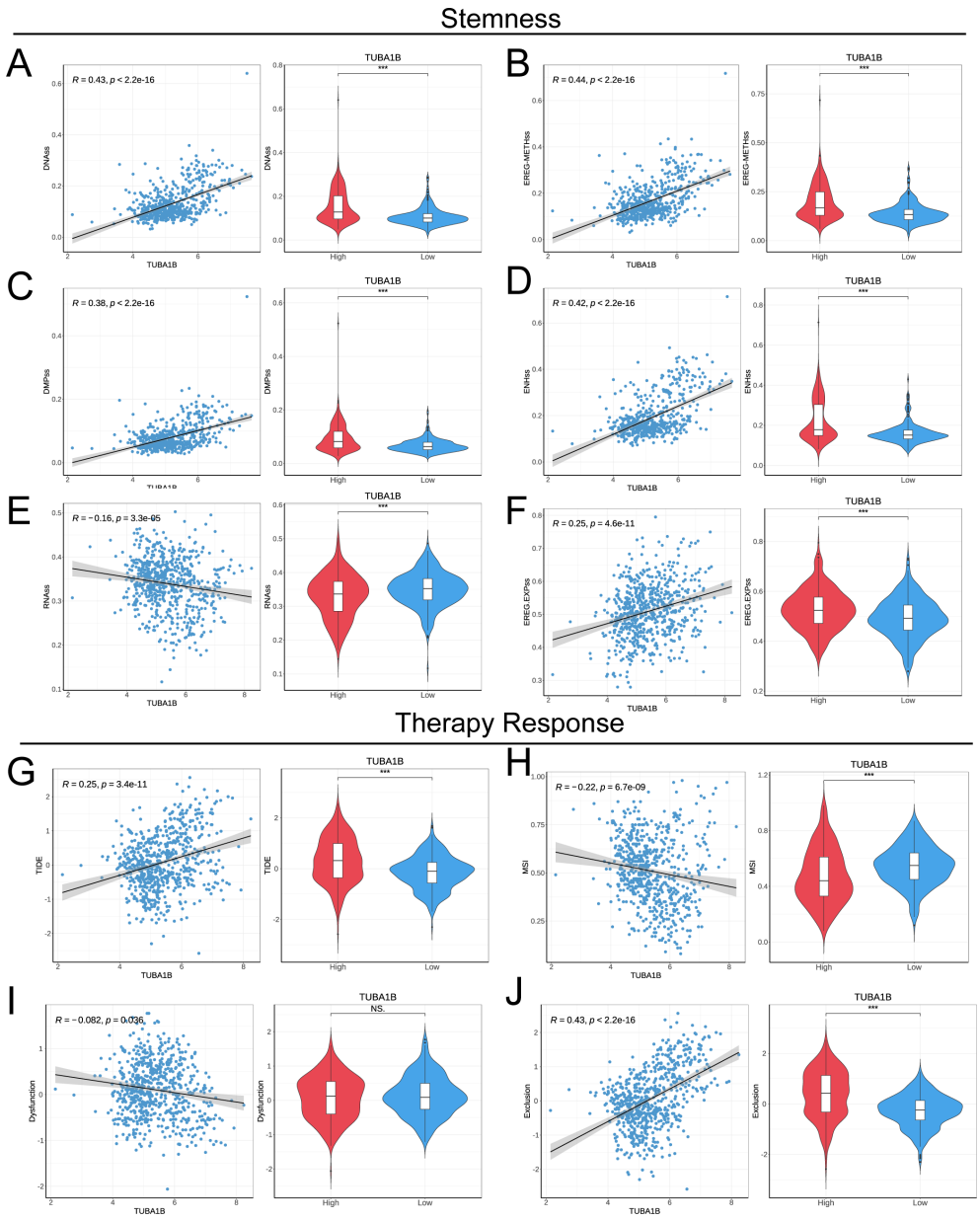

FIGURE 6
TUBA1B influences stemness and treatment response in glioma. **(A–F)** Correlation of tumor stemness with TUBA1B levels analyzed using DNAss, EREG-METHss, DMPss, ENHss, RNAss, and EREG.EXPss. **(G)** TIDE prediction scores between high and low TUBA1B expression groups in the TCGA dataset. **(H–J)** Comparison of responses to immunotherapy between high and low TUBA1B expression groups in the TCGA dataset.

progression. Through an integrated analysis of the TCGA database, two aggrephagy subtypes were identified: "immune-cold" and "immune-hot." The latter is associated with poor survival outcomes, suggesting that aggrephagy may modulate tumor progression by influencing the immune microenvironment. Extensive immune cell infiltration in the "immune-hot" subtype may correspond with a pro-inflammatory state of the tumor, aligning with the intricate immune landscape of gliomas and indicating the potential influence of aggrephagy on immune evasion. However, it is important to note that while the "immune-hot" subtype shows significant immune infiltration, it may also be indicative of immune evasion mechanisms, and future studies should explore the precise immune modulatory role of aggrephagy and its interaction with immune checkpoints.

TUBA1B, a member of the tubulin family, is involved in cytoskeletal formation and cell division (31). In this study, TUBA1B was identified as a core gene of aggrephagy, showing potential as an independent prognostic marker. Machine learning analysis indicates that TUBA1B is a key driver of glioma progression, with high expression correlating with poor prognosis and aggressive

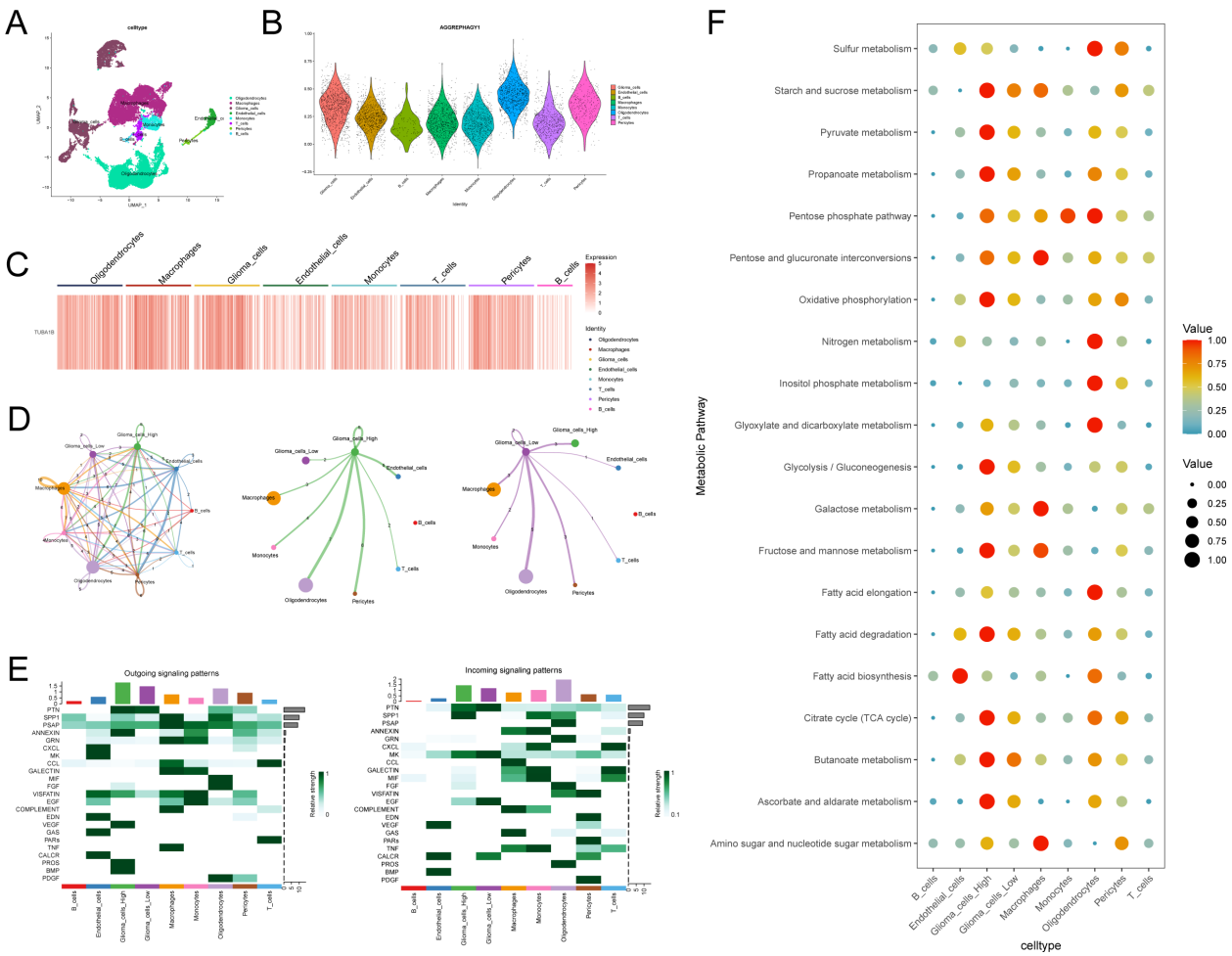

FIGURE 7
Analysis of TUBA1B in regulating glioma cell communication and metabolism within the tumor microenvironment. **(A)** UMAP plot used for cell type annotation in glioma and control samples. **(B)** Autophagy scores in different subsets of cells. **(C)** Heatmap of TUBA1B expression across different cell clusters. **(D)** Communication networks among different cell clusters and between high and low TUBA1B expression groups in gliomas. **(E)** Input and output signaling patterns of glioma cell communication in high and low TUBA1B expression groups. **(F)** Dot plot displaying activity of metabolic signaling pathways in different cell populations.

tumor behavior. Moreover, TUBA1B has been implicated in poor prognosis and chemoresistance in various cancer types (32, 33). Our findings support these observations and suggest that TUBA1B's role in glioma may be multifaceted, affecting not only tumor growth but also the tumor microenvironment, potentially enhancing immune evasion. Transcriptomic and functional analyses revealed a close association between TUBA1B overexpression and cell cycle regulatory genes such as Cyclin D1. Additionally, TUBA1B overexpression modulates various signaling pathways, including AGE-RAGE, ECM-receptor interactions, and complement and coagulation cascades. These pathways are associated with tumor growth, metastasis, and immune evasion in other cancer types (34–37), supporting the multifaceted role of TUBA1B in tumor biology. Studies have shown that a protein encoded by a short open reading frame in the TUBA1B gene plays a role in regulating tumor cell proliferation (38). Our *in vitro* experiments further validated the multifaceted role of TUBA1B in promoting cell proliferation and migration and inhibiting autophagy and apoptosis in gliomas, suggesting its potential as a therapeutic target. These findings underscore TUBA1B's oncogenic potential and its critical role in glioma malignancy. However, future research should focus on developing specific inhibitors targeting TUBA1B, as well as understanding the broader molecular network through which it operates, including potential interactions with autophagy and immune pathways. Some studies have found that TUBA1B and its homolog TUBA1C are involved in regulating immune cell infiltration within the tumor microenvironment (39, 40). Our research reveals that high TUBA1B expression correlates significantly with decreased tumor purity and increased immune and stromal scores, possibly regulating tumor behavior by influencing immune infiltration. Notably, TUBA1B expression was found to correlate with a shift in immune cell composition, particularly in terms of macrophage

infiltration, which may contribute to immune evasion mechanisms in gliomas. This highlights the need for future studies to investigate the interplay between TUBA1B and immune cell subsets in more detail. Finally, single-cell sequencing analysis provides new insights into the role of TUBA1B in cell-cell communication and metabolic pathways. TUBA1B is highly expressed in specific cell populations, such as oligodendrocytes and glioma cells, and is associated with extensive communication networks, indicating its potential collaborative regulatory role in gliomas.

Despite the compelling findings of our study, there are several limitations that must be addressed. First, the primary data used in this study, including TCGA, GEO, and CGGA datasets, are publicly available databases. Although these datasets are robust and widely used in glioma research, they are not exhaustive and may not fully represent the diversity of glioma patients in clinical settings. For example, the lack of detailed treatment regimens and patient follow-up data in some of these datasets may introduce bias in the survival analysis and clinical correlation. Additionally, our study primarily relied on bioinformatic analyses and computational tools to identify molecular signatures and relationships. While these methods are powerful, they cannot replace experimental validation, and we acknowledge that the predictive value of TUBA1B as a biomarker or therapeutic target must be further confirmed through *in vitro* and *in vivo* experiments. Furthermore, the retrospective nature of the data used in our analysis may limit the generalizability of our findings, and prospective studies are necessary to validate the clinical relevance of TUBA1B in glioma patients.

TUBA1B has shown promising potential as a prognostic biomarker for glioma patients, with higher expression levels correlating with poor survival outcomes. These findings suggest that TUBA1B could be an effective therapeutic target for glioma, providing a new avenue for glioma treatment. However, translating these findings into clinical practice will require further validation in preclinical and clinical settings. Combining TUBA1B inhibition with other therapeutic strategies, such as chemotherapy, radiation therapy, or immunotherapy, could also hold promise for improving treatment efficacy.

Furthermore, TUBA1B expression levels could be used to stratify glioma patients based on their risk of progression, enabling more personalized treatment approaches. Patients with high TUBA1B expression could benefit from more aggressive treatment regimens or experimental therapies targeting cell cycle regulators. Moreover, as TUBA1B is implicated in modulating the tumor microenvironment, future research could explore the synergy between TUBA1B inhibition and immunotherapy, which might enhance the immune response against glioma.

In summary, this study delineates the complex mechanisms of TUBA1B in gliomas, offering a new perspective on the role of aggrephagy in malignant tumors. Future in-depth experimental validation of the functions of TUBA1B, as well as its application in diverse clinical conditions, may propel the development of precision medicine and targeted therapies in gliomas.

5 Conclusion

This study deeply explores the biological characteristics and clinical significance of aggrephagy in gliomas. By analyzing the TCGA dataset, we identified two aggrephagy subtypes and revealed their differences within the tumor microenvironment through immune infiltration analysis. Among the highlighted genes, TUBA1B emerged as a key gene, demonstrating potential as an independent prognostic marker. *In vitro* functional experiments further confirmed that TUBA1B promotes the proliferation, migration, and invasion of glioma cells and is related to dynamic changes in the immune microenvironment. Single-cell sequencing analysis indicates that high TUBA1B expression is associated with specific intercellular communications and metabolic pathways, impacting tumor progression. Collectively, these findings underscore the vital role of TUBA1B in the occurrence, development, and treatment of gliomas, suggesting its potential as a clinical target. This provides a possible direction for precision medicine and new therapeutic strategies for gliomas.

Data availability statement

The data presented in this study are deposited in the following repositories: The TCGA data are available through the Genomic Data Commons (GDC) portal (https://portal.gdc.cancer.gov/), under the TCGA-GBMLGG cohort. The GEO dataset (GSE167960) can be accessed through the NCBI GEO database (https://www.ncbi.nlm.nih.gov/geo/). The CGGA data, including the mRNAseq_693, mRNAseq_325, and mRNA-array_301 datasets, are accessible through the CGGA database website (http://www.cgga.org.cn/).

Ethics statement

The animal study was approved by the Animal Ethics Committee of Nantong University Medical College (The ethical approval number was S20240116-009). The study was conducted in accordance with the local legislation and institutional requirements.

Author contributions

ZS: Conceptualization, Data curation, Formal analysis, Investigation, Methodology, Software, Writing – original draft. PH: Data curation, Investigation, Methodology, Software, Writing – review & editing. JL: Data curation, Formal analysis, Methodology, Writing – review & editing. GJ: Conceptualization, Methodology, Software, Supervision, Writing – review & editing. JC: Conceptualization, Methodology, Project administration, Writing – review & editing. QL: Conceptualization, Investigation, Methodology, Project administration, Resources, Software, Validation, Writing – review & editing.

Funding

The author(s) declare financial support was received for the research, authorship, and/or publication of this article. This work was supported by Nantong Science and Technology Plan Project (MS22020017, JC2020060); Nantong "Fourteenth Five Year Plan" Science and Education Strong Health Engineering Medical Innovation Team.

Acknowledgments

We thank the Research Center of Clinical Medicine, Affiliated Hospital of Nantong University for technical assistance and equipment support.

Conflict of interest

The authors declare that the research was conducted in the absence of any commercial or financial relationships that could be construed as a potential conflict of interest.

Generative AI statement

The author(s) declare that no Generative AI was used in the creation of this manuscript.

Publisher's note

All claims expressed in this article are solely those of the authors and do not necessarily represent those of their affiliated organizations, or those of the publisher, the editors and the reviewers. Any product that may be evaluated in this article, or claim that may be made by its manufacturer, is not guaranteed or endorsed by the publisher.

Supplementary material

The Supplementary Material for this article can be found online at: https://www.frontiersin.org/articles/10.3389/fonc.2025.1531465/full#supplementary-material.

References

1. Gusyatiner O, Hegi ME. Glioma epigenetics: From subclassification to novel treatment options. *Semin Cancer Biol*. (2018) 51:50–8. doi: 10.1016/j.semcancer.2017.11.010

2. Samioti SE, Benos LT, Sarris IE. Effect of fractal-shaped outer boundary of glioblastoma multiforme on drug delivery. *Comput Methods Programs BioMed*. (2019) 178:191–9. doi: 10.1016/j.cmpb.2019.06.031

3. Polivka J Jr., Polivka J, Holubec L, Kubikova T, Priban V, Hes O, et al. Advances in experimental targeted therapy and immunotherapy for patients with glioblastoma multiforme. *Anticancer Res*. (2017) 37:21–33. doi: 10.21873/anticanres.11285

4. Ostrom QT, Patil N, Cioffi G, Waite K, Kruchko C, Barnholtz-Sloan JS. CBTRUS statistical report: primary brain and other central nervous system tumors diagnosed in the United States in 2013-2017. *Neuro Oncol*. (2020) 22:iv1–iv96. doi: 10.1093/neuonc/noaa200

5. Louis DN, Perry A, Reifenberger G, von Deimling A, Figarella-Branger D, Cavenee WK, et al. The 2016 world health organization classification of tumors of the central nervous system: a summary. *Acta Neuropathol*. (2016) 131:803–20. doi: 10.1007/s00401-016-1545-1

6. Lapointe S, Perry A, Butowski NA. Primary brain tumours in adults. *Lancet*. (2018) 392:432–46. doi: 10.1016/S0140-6736(18)30990-5

7. Garcia CR, Slone SA, Dolecek TA, Huang B, Neltner JH, Villano JL. Primary central nervous system tumor treatment and survival in the United States, 2004-2015. *J Neurooncol*. (2019) 144:179–91. doi: 10.1007/s11060-019-03218-8

8. Eckel-Passow JE, Lachance DH, Molinaro AM, Walsh KM, Decker PA, Sicotte H, et al. Glioma groups based on 1p/19q, IDH, and TERT promoter mutations in tumors. *N Engl J Med*. (2015) 372:2499–508. doi: 10.1056/NEJMoa1407279

9. Eskilsson E, Røsland GV, Solecki G, Wang Q, Harter PN, Graziani G, et al. EGFR heterogeneity and implications for therapeutic intervention in glioblastoma. *Neuro Oncol*. (2018) 20:743–52. doi: 10.1093/neuonc/nox191

10. Zhao YY, Chen SH, Hao Z, Zhu HX, Xing ZL, Li MH. A nomogram for predicting individual prognosis of patients with low-grade glioma. *World Neurosurg*. (2019) 130:e605–12. doi: 10.1016/j.wneu.2019.06.169

11. Kiran M, Chatrath A, Tang X, Keenan DM, Dutta A. A prognostic signature for lower grade gliomas based on expression of long non-coding RNAs. *Mol Neurobiol*. (2019) 56:4786–98. doi: 10.1007/s12035-018-1416-y

12. Razzak M. Genetics: new molecular classification of gastric adenocarcinoma proposed by The Cancer Genome Atlas. *Nat Rev Clin Oncol*. (2014) 11:499. doi: 10.1038/nrclinonc.2014.138

13. Deng S, Li Y, Yi G, Lei B, Guo M, Xiang W, et al. Overexpression of COX7A2 is associated with a good prognosis in patients with glioma. *J Neurooncol*. (2018) 136:41–50. doi: 10.1007/s11060-017-2637-z

14. Sun D, Wu R, Li P, Yu L. Phase separation in regulation of aggrephagy. *J Mol Biol*. (2020) 432:160–9. doi: 10.1016/j.jmb.2019.06.026

15. Dobson CM. Protein folding and misfolding. *Nature*. (2003) 426:884–90. doi: 10.1038/nature02261

16. Ciechanover A, Kwon YT. Degradation of misfolded proteins in neurodegenerative diseases: therapeutic targets and strategies. *Exp Mol Med*. (2015) 47:e147. doi: 10.1038/emm.2014.117

17. Mathieu C, Pappu RV, Taylor JP. Beyond aggregation: Pathological phase transitions in neurodegenerative disease. *Science*. (2020) 370:56–60. doi: 10.1126/science.abb8032

18. Moreau KL, King JA. Protein misfolding and aggregation in cataract disease and prospects for prevention. *Trends Mol Med*. (2012) 18:273–82. doi: 10.1016/j.molmed.2012.03.005

19. Hombach-Klonisch S, Mehrpour M, Shojaei S, Harlos C, Pitz M, Hamai A, et al. Glioblastoma and chemoresistance to alkylating agents: Involvement of apoptosis, autophagy, and unfolded protein response. *Pharmacol Ther*. (2018) 184:13–41. doi: 10.1016/j.pharmthera.2017.10.017

20. Kundu M, Das S, Dey A, Mandal M. Dual perspective on autophagy in glioma: Detangling the dichotomous mechanisms of signaling pathways for therapeutic insights. *Biochim Biophys Acta Rev Cancer*. (2024) 1879:189168. doi: 10.1016/j.bbcan.2024.189168

21. Coleman S, Kirk PDW, Wallace C. Consensus clustering for Bayesian mixture models. *BMC Bioinf*. (2022) 23:290. doi: 10.1186/s12859-022-04830-8

22. Malta TM, Sokolov A, Gentles AJ, Burzykowski T, Poisson L, Weinstein JN, et al. Machine learning identifies stemness features associated with oncogenic dedifferentiation. *Cell*. (2018) 173:338–354.e315. doi: 10.1016/j.cell.2018.03.034

23. Jiang P, Gu S, Pan D, Fu J, Sahu A, Hu X, et al. Signatures of T cell dysfunction and exclusion predict cancer immunotherapy response. *Nat Med*. (2018) 24:1550–8. doi: 10.1038/s41591-018-0136-1

24. Gui S, Chen P, Liu Y, Chen Q, Cheng T, Lv S, et al. TUBA1C expression promotes proliferation by regulating the cell cycle and indicates poor prognosis in glioma. *Biochem Biophys Res Commun*. (2021) 577:130–8. doi: 10.1016/j.bbrc.2021.08.079

25. Visintin R, Ray SK. Intersections of ubiquitin-proteosome system and autophagy in promoting growth of glioblastoma multiforme: challenges and opportunities. *Cells*. (2022) 11(24):4063. doi: 10.3390/cells11244063

26. Zhang C, Huang C, Xia H, Xu H, Tang Q, Bi F. Autophagic sequestration of SQSTM1 disrupts the aggresome formation of ubiquitinated proteins during proteasome inhibition. *Cell Death Dis*. (2022) 13:615. doi: 10.1038/s41419-022-05061-8

27. Feng F, Zhang M, Yang C, Heng X, Wu X. The dual roles of autophagy in gliomagenesis and clinical therapy strategies based on autophagic regulation mechanisms. *BioMed Pharmacother*. (2019) 120:109441. doi: 10.1016/j.biopha.2019.109441

28. Batara DCR, Choi MC, Shin HU, Kim H, Kim SH. Friend or foe: paradoxical roles of autophagy in gliomagenesis. *Cells*. (2021) 10(6):1411. doi: 10.3390/cells10061411

29. Huang X, Chi H, Gou S, Guo X, Li L, Peng G, et al. An aggrephagy-related lncRNA signature for the prognosis of pancreatic adenocarcinoma. *Genes (Basel)*. (2023) 14(1):124. doi: 10.3390/genes14010124

30. Zhang X, Tan J, Zhang X, Pandey K, Zhong Y, Wu G, et al. Aggrephagy-related gene signature correlates with survival and tumor-associated macrophages in glioma: Insights from single-cell and bulk RNA sequencing. *Math Biosci Eng*. (2024) 21:2407–31. doi: 10.3934/mbe.2024106

31. Martinez-Lage M, Lynch TM, Bi Y, Cocito C, Way GP, Pal S, et al. Immune landscapes associated with different glioblastoma molecular subtypes. *Acta Neuropathol Commun*. (2019) 7:203. doi: 10.1186/s40478-019-0803-6

32. Wu S, Yang W, Zhang H, Ren Y, Fang Z, Yuan C, et al. The prognostic landscape of tumor-infiltrating immune cells and immune checkpoints in glioblastoma. *Technol Cancer Res Treat*. (2019) 18:1533033819869949. doi: 10.1177/1533033819869949

33. Trisciuoglio D, Degrassi F. The tubulin code and tubulin-modifying enzymes in autophagy and cancer. *Cancers (Basel)*. (2021) 14(1):6. doi: 10.3390/cancers14010006

34. Zoroddu S, Sanna L, Bordoni V, Weidong L, Gadau SD, Carta A, et al. Identification of 3-aryl-1-benzotriazole-1-yl-acrylonitrile as a microtubule-targeting agent (MTA) in solid tumors. *Int J Mol Sci*. (2024) 25(11):5704. doi: 10.3390/ijms25115704

35. Zou Y, Wang G, Fan M. Comprehensive multiomic analysis identified TUBA1C as a potential prognostic biological marker of immune-related therapy in pan-cancer. *Comput Math Methods Med*. (2022) 2022:9493115. doi: 10.1155/2022/9493115

36. Wang Y, Li Y, Jing Y, Yang Y, Wang H, Ismtula D, et al. Tubulin alpha-1b chain was identified as a prognosis and immune biomarker in pan-cancer combing with experimental validation in breast cancer. *Sci Rep*. (2024) 14:8201. doi: 10.1038/s41598-024-58982-z

37. Pang XL, Du HF, Nie F, Yang XG, Xu Y. Tubulin alpha-1b as a potential biomarker for lung adenocarcinoma diagnosis and prognosis. *Technol Cancer Res Treat*. (2023) 22:15330338231178391. doi: 10.1177/15330338231178391

38. Tao Y, Bai X, Zhou Y, Zhao Y, Yang L, Zhang S, et al. The translation of a short open reading frame product within the human TUBA1B gene regulates cancer cell proliferation by importin-β. *bioRxiv*. (2023) 2023.08.26.554759. doi: 10.1101/2023.08.26.554759

39. Bian T, Zheng M, Jiang D, Liu J, Sun H, Li X, et al. Prognostic biomarker TUBA1C is correlated to immune cell infiltration in the tumor microenvironment of lung adenocarcinoma. *Cancer Cell Int*. (2021) 21:144. doi: 10.1186/s12935-021-01849-4

40. Alhammad R. Bioinformatics identification of TUBB as potential prognostic biomarker for worse prognosis in ERα-positive and better prognosis in ERα-negative breast cancer. *Diagnostics (Basel)*. (2022) 12(9):2067. doi: 10.3390/diagnostics12092067

frontiers | Frontiers in Oncology

TYPE Review
PUBLISHED 17 March 2025
DOI 10.3389/fonc.2025.1564572

Check for updates

OPEN ACCESS

EDITED BY
Ying Luo,
UT Southwestern Medical Center,
United States

REVIEWED BY
Ziang Zhu,
University of Texas Southwestern Medical Center, United States
Zizheng Li,
University of California, San Francisco, United States
Li Meng,
University of Texas Southwestern Medical Center, United States
Xin Li,
University of North Carolina at Chapel Hill, United States

*CORRESPONDENCE
Hikmet Akkız
hakkiz@superonline.com

RECEIVED 21 January 2025
ACCEPTED 27 February 2025
PUBLISHED 17 March 2025

CITATION
Akkız H, Şimşek H, Balcı D, Ülger Y, Onan E, Akçaer N and Delik A (2025) Inflammation and cancer: molecular mechanisms and clinical consequences.
Front. Oncol. 15:1564572.
doi: 10.3389/fonc.2025.1564572

COPYRIGHT
© 2025 Akkız, Şimşek, Balcı, Ülger, Onan, Akçaer and Delik. This is an open-access article distributed under the terms of the Creative Commons Attribution License (CC BY). The use, distribution or reproduction in other forums is permitted, provided the original author(s) and the copyright owner(s) are credited and that the original publication in this journal is cited, in accordance with accepted academic practice. No use, distribution or reproduction is permitted which does not comply with these terms.

Inflammation and cancer: molecular mechanisms and clinical consequences

Hikmet Akkız[1]*, Halis Şimşek[2], Deniz Balcı[1], Yakup Ülger[3], Engin Onan[4], Nevin Akçaer[5] and Anıl Delik[3,6]

[1]Department of Gastroenterology, Medical Faculty, Bahçeşehir University, İstanbul, Türkiye, [2]Department of Gastroenterology, Medical Faculty, Hacettepe University, Ankara, Türkiye, [3]Department of Gastroenterology, Medical Faculty, Cukurova University, Adana, Türkiye, [4]Department of Nephrology, Medical Faculty, Baskent University, Adana, Türkiye, [5]Department of Gastroenterology, Medical Faculty, Health Sciences University, Adana, Türkiye, [6]Department of Biology, Science and Literature Faculty, Cukurova University, Adana, Türkiye

Inflammation, a hallmark of cancer, has been associated with tumor progression, transition into malignant phenotype and efficacy of anticancer treatments in cancer. It affects all stages of cancer, from the initiation of carcinogenesis to metastasis. Chronic inflammation induces immunosup-pression, providing an environment conducive to carcinogenesis, whereas acute inflammation induces an antitumor immune response, leading to tumor suppression. Solid tumors have an inflammatory tumor microenvironment (TME) containing cancer cells, immune cells, stromal cells, and soluble molecules, which plays a key role in tumor progression and therapy response. Both cancer cells and stromal cells in the TME are highly plastic and constantly change their phenotypic and functional properties. Cancer-associated inflammation, the majority of which consists of innate immune cells, plays an important role in cancer cell plasticity, cancer progression and the development of anticancer drug resistance. Today, with the combined used of advanced technologies, such as single-cell RNA sequencing and spatial molecular imaging analysis, the pathways linking chronic inflammation to cancer have been largely elucidated. In this review article, we highlighted the molecular and cellular mechanisms involved in cancer-associated inflammation and its effects on cancer progression and treatment response. We also comprehensively review the mechanisms linking chronic inflammation to cancer in the setting of GI cancers.

KEYWORDS

tumor microenvironment, cancer-associated inflammation, cancer-associated fibroblasts, gastro-intestinal cancer, innate immunity, adaptive immunity

1 Introduction

Inflammation is an evolutionary process involving the recruitment, activation and action innate and adaptive immune cells (1–4). In addition to its role in host defense against pathogens, inflammation plays a critical role in tissue repair, regeneration, and remodeling, and mild inflammation is necessary to maintain tissue homeostasis (5–8). The canonical inflammatory process is characterized by a series of vascular changes, the release of inflammatory mediators, and recruitment of inflammatory immune cells in inflammatory sites (8–11). In addition to developing in tissue damage and infection, chronic inflammation also occurs in other serious diseases, such as diabetes, atherosclerosis, and cancer (10, 11). The association between cancer and inflammation has been known for a long time. In 1863, the German pathologist Rudolph Virchow observed the presence of inflammatory infiltrates in solid tumors and hypothesized that cancer develops at sites of chronic inflammation (12). Around the same time, William Cooley, pioneer of cancer immunotherapy, showed that some patients displayed tumor regression after being injected with immune stimulatory Streptococcus pyogenes cultures (8, 10). In solid tumors, including gastrointestinal (GI) cancers, molecular features of cancer cell, such as genetic aberrations, epigenetic modifications, signaling pathway deregulation and high metabolic stress, play key roles in shaping an inflammatory tumor microenvironment (TME) that is a major determinant of the biological behavior of tumor cells, and thus tumor progression and clinical outcome (1, 8, 11, 13–17). Inflammation, regardless of diseases from which it originates, has an important effect on the formation of the cellular composition of the TME (8, 10, 11, 17).

During cancer progression, cancer cells develop strategies to evade immune surveillance, such as downregulation of antigen presentation mechanism and induction of immune checkpoint molecules (5, 6, 8, 10, 11, 17). Concurrently, cancer cells hijack immune cells such as neutrophils, macrophages and regulatory T cells (Treg) to regulate an inflammatory TME that promotes immune escape (5, 6, 8, 10, 11, 17). Cancer-associated inflammation is the chronic inflammatory component of the TME and is emerged at all stages of tumor from the onset of carcinogenesis to advanced stage (8, 11, 17–21). It plays a key role in the recruitment of innate immune cells, such as macrophages and neutrophils, and immunosuppressive cells, such as myeloid-derived immunosuppressive cells (MDSCs) and regulatory T (Tregs) cells in the TME, contributing significantly to the shapping the inflammatory and immunosuppressive TME (1, 19, 21). Cancer-associated inflammation plays a critical role in the plasticity of cancer cells and stromal cells as well as shapping the cellular composition of the TME (8, 11, 16, 17, 21, 22). Additionally, it may also contribute to the recruitment of oncogenic mutations and predispose to the development of metastatic lesions (21, 22). Because of all these impacts, cancer-associated inflammation is an important driver of the malignant biological behavior of the tumor (1, 8, 10, 11, 17, 21, 22). Therapy-induced inflammation, which occurs in response to various anti-cancer therapies, including chemotherapy, radiotherapy, and immunotherapy, promotes drug resistance and cancer progression (8–11). Acute inflammation in solid tumors caused by various factors displays anti-cancer function through inducing the activation of dendritic cells (DCs) and $CD8^+$ T cells (1, 8, 10, 11). Unlike the inflammatory response following infection and tissue injury, cancer-associated inflammation is unresolved in character (19–21). Additionally, cancer-extrinsic inflammation induced by environmental factors, such as obesity, smoking, and excessive alcohol consumption has been shown to increases cancer risk and accelerates tumor progression (8, 10, 11). In this review article, we focus on the molecular and cellular mechanisms involved in the pathogenesis of cancer-associated inflammation, as well as the dynamic and complex interactions between cancer-associated inflammation, cancer cells, and immune system. Understanding all aspects of this crosstalk will pave the way for the way for the development of more effective molecular targeted therapies for cancer treatment.

2 Initiation of inflammation and general description

Inflammation is a fundamental immune response that follows tissue injury and infection (10, 11). Many soluble molecules released from damaged tissues and activated immune cells participate in the inflammatory response, such as cytokines, chemokines and growth factors (8, 10, 11). The initial phase of inflammation is triggered by an inter-action between pattern recognition receptors (PRRs) and pathogen-associated molecular patterns (PAMPs) (8, 10, 11). In this stage, PAMPs are recognized by tissue macrophages or other innate immune cells, such as neutrophils, and dendritic cells (DCs), promoting the expression of pro-inflammatory mediators, accentuating the immune response (10, 11, 22). Additionally, damaged tissue secretes a variety of signaling molecules, such as cytokines, chemokines and adhesion molecules, leading to the accumulation of innate immune cells in the inflammatory field (3, 8, 10, 22–26). In the second stage of the inflammatory cascade, inflammatory cells undergo apoptosis and are phagocyted by macrophages (11, 27–30). Tissue-resident macrophages respond to tissue changes by several mechanisms, such as eliminating dying cells, expressing chemotactic molecules, orchestrating immune mechanisms, and contributing to the recruitment of stem cells (8, 10, 29). In the first two stages of inflammatory cascade, inflammation exerts a significant immunostimulatory effects (8, 10, 11). The resolution phase, which is the 3rd phase of inflammation cascade, is characterized by the secretion of anti-inflammatory mediators, such as specialized proresolving lipid mediators (SPMs, e.g., lipoxin A4 (LXA4) and resolving D1 (RVD1), cytokines such as IL-10 and growth factors including TGFβ and epidermal growth factor (EGF) (3, 8, 9, 11). SPMs play an important role in the resolution of inflammation by impeding neutrophil recruitment in damaged tissue, attenuating the secretion of inflammatory cytokines, and fostering the capacity of macrophages to phagocyte apoptotic neutrophils (30–33). These mediators augment the production of Tregs and B cells to suppress

excessive activation of adaptive immunity (30, 32). In the final phase of the inflammatory cascade, the tissue repair process modifies the inflammatory process, weakens the inflammatory responses, and rebuilds tissue homeostasis (3, 8, 10, 11).

Inflammation can be defined as acute and chronic inflammation depending on the duration of the disease (8, 10, 11). Acute inflammation is the initial response to infection or tissue injury; the majority of cells involved in acute inflammation being granulocytes (11). Chronic inflammation is one of the main drivers in the development and progression of cancer (3, 8, 10, 11). Clinical and experimental studies have shown that activation of inflammatory pathways leads to destructive inflammation in the TME, which causes phenotypic and functional changes contributing to cancer progression (8, 10, 22, 34). The immune cell types and mediators secreted by them that participate in chronic inflammation are quite different from those in acute inflammation (1, 7, 8, 10, 35). The majority of cells involved in chronic inflammation belong to the adaptive arm of immune system (11, 22). In contrast to the acute inflammatory response, chronic inflammation is typically activated by DAMPs in the absence of activation of PAMPs (8, 10, 22). Chronic inflammation is regulated by specific signaling pathways that act as suppressors or activators (24–26). Molecular features of cancer cells, such as activation of oncogenes, inactivation of tumor suppressor genes and epigenetic modifications, promote the activation of various transcription factors in the TME, such as NF-κB, STAT3, and HIF-1α, which induce the production soluble molecules by the cancer cells, creating an inflammatory TME (8, 9, 11, 35). NF-κB activated by oxidative stress and pro-inflammatory cytokines initiates inflammation-associated cellular transformation through the expression of various genes, including anti-apoptotic proteins (BCL-XL, BCL-2), cytokines (TNF-α, IL-1β, IL-6, IL-8), inflammatory enzymes (iNOS, and COX-2), active molecules in metastasis, such as adhesion molecules and matrix metalloproteases (MMPs), cell cycle molecules (c-MYC and cylin D1), and angiogenic factors (VEGF and angiopoetin) (11, 35). Therefore, inflammation plays a critical role in all stages of cancer progression (11, 35). Several studies have shown that the combination chemotherapy with anti-inflammatory therapy has a favorable effect on treatment responses and patient survival (11, 35).

3 Molecular mechanisms linking chronic inflammation to cancer in the setting of GI cancers

Epidemiological studies have demonstrated that inflammation is closely related to cancer initiation and development. Approximately 25% of cancers arise from a chronic inflammatory microenvironment (1, 3, 8, 10, 11). Gastrointestinal (GI) cancers, such as colorectal cancer (CRC), stomach cancer, pancreatic cancer and liver cancer, are a leading cause of new cancer cases and cancer-related death, representing 26% of the global cancer incidence and 35% of all cancer-related deaths (1).

3.1 Gastric cancer-inducing inflammation

Gastric cancer is a major global health problem with >1,1 million new cases and >750,000 deaths each year (36). Gastric cancer is a prime example of chronic inflammation-associated cancer, which usually develops from chronic gastritis (36). Gastric cancer has two major subtypes: diffuse and intestinal type (37). Intestinal-type gastric carcinoma is more common than diffuse-type tumors and its main cause is Helicobacter pylori infection (37). Helicobacter pylori infection causes chronic gastritis that is associated with the generation of reactive oxygen species (ROS) and nitric oxide metabolites and a reduction of vitamin C levels, which can lead to peptic ulcer, gastric cancer, and gastric mucosa-associated lymphoid tissue lymphoma (17, 36, 38). In Asian and Eastern European countries, where gastric cancer incidence and mortality are high, the lifetime risk of developing gastric cancer in H. pylori-positive individuals is 1-5% (17). Additionally, in these geographic regions, high salt intake, smoking habits, low iron levels, and pickled foods contribute to the development of gastric cancer (17). Chronic inflammation damages parietal cells and these cells lose their acid-producing properties, resulting in hypochlorhydria or achlorhydria (17). The hypochlorhydric stomach creates a favorable microenvironment for the colonization of proinflammatory microorganisms, leading to the production of genotoxic metabolites and carcinogens, which are directly effective on malignant epithelial cell transformation (17, 37, 38). The etiology of diffuse-type gastric cancer remains unclear, although its incidence continues to increase globally (36).

3.2 Pancreatic cancer-driving inflammation

Pancreatic ductal adenocarcinoma (PDAC) is one of the most lethal cancers, with a 5-year survival rate of below 10% (39). Stromal desmoplasia and persistent activation of the immune system are the main features of PDAC and play a key role in cancer initiation and progression (3, 39). Inflammation, in which activated immune cells secrete a variety of proinflammatory molecules, plays an important role in pancreatic carcinogenesis (3, 39, 40). The continuous interaction between progenitor cells and innate and adaptive immune cells promotes cancer initiation by converting normal progenitor cells into cancer stem cells (3, 40). During this interaction, soluble molecules secreted by immune cells regulate cell migration, proliferation and survival (3, 39, 40). Pancreatic intra-epithelial neoplasia (PanIN) is developed through different stages of PDAC (3, 40). The PanIN lesion microenvironment contains macrophages, neutrophils and fibroblasts (3, 39, 40). As PanIN progresses, CXCL17-secreting macrophages and neutrophils recruit immature DCs (39, 40). Downregulation of CXCL17 develops immune tolerance toward tumor cells. IL-6 is essential for the maintenance of PanIN lesions and activates the MAPK and P13K/AKT pathways in these lesions (3, 41). Acinar cells with KRAS mutation have been indicated to trigger inflammation. Chronic inflammation may lead to PDAC in the absence of p53

(41). In a recently published study, researchers showed that upregulated expression of IKK2 or COX-2 in the absence of p53 leads to chronic inflammation-induced DNA mutations in the KRAS gene and PDAC via various signaling pathways (42). Chronic pancreatitis is the most common risk factor for PDAC, and the relative risk of PDAC in patients with chronic pancreatitis has been reported to be as high as 7.6-68.1 times (40). In studies conducted in Western countries, the incidence of PDAC in patients with chronic pancreatitis has been reported as 1.0-2.6% (40). PDAC has a highly stromal TME that contributes to its poor prognosis (39, 41).

3.3 Chronic inflammation-related colorectal cancer

Another well-known example of chronic inflammation-derived cancer is colitis-associated colorectal cancer (CAC) (13, 14). Persistent chronic inflammation of the colon caused by inflammatory bowel diseases (IBDs), such as Crohn's colitis and ulcerative colitis, is associated with an increased incidence of CAC (13, 14, 43, 44). The risk of CAC is high in patients with long-standing colitis, a large diseased colon segment and concomitant inflammatory diseases, such as primary sclerosing cholangitis (13, 14, 43, 44). Chronic inflammation itself is independent driver in the development of CAC in IBD (13, 14). Chronic inflammation-associated CAC is thought to arise as a result of the expansion of pro-tumorigenic clones (14). Somatic driver mutations can be detected in non-dysplastic inflamed colon years before the diagnosis of CAC (13). Multiple studies using whole exome sequencing have identified TCGA point mutation in the KRAS, BRAF, ERBB2, ERBB3, TP53, and FBXW7 genes in non-dysplastic colon mucosa (43). Local tissue damage leads to inflammation, which cooperates with driver mutations in the KRAS and p53 genes for malignant transformation of the cell (13, 43). Mutations may not be the initial event that triggers carcinogenesis in IBD (43). While p53 mutation is not detected in the colon mucosa, it is detected in approximately 50% of the dysplastic mucosa, and the frequency of p53 mutations gradually increases towards the dysplastic-carcinoma cascade (13, 44). P53 protein exerts transcriptional antagonism to NF-κB, a key regulator of inflammation, in cancer (13, 14, 43, 44). Additionally, copy number alterations accumulate progressively from low-grade dysplasia to high-grade dysplasia and cancer (13, 43, 44). Chatila et al. showed that cancer development in IBD predominantly arises from independent genetic events (14). Two important differences have been detected between CAC and sporadic CRC in terms of genomic landscapes (14). The first is that p53 alterations are early and highly recurrent events in CACs, which occur in half of dysplasia, while it is a late event in sporadic CRC (14). Secondly, while APC mutations are detected at a rate of 81% in sporadic microsatellite stable (MSS) CRC, they are detected at a rate of 11-22% in CAC (14). Studies in mouse models have demonstrated that SMAD4 is also an important player in the regulation of inflammation and loss of SMAD4 leads to the upregulation of some inflammatory signaling pathways, including IL-6/STAT3 and NF-κB (45). Many studies have shown that immunotherapy prevents cancer recurrence and improves overall survival in patients with MSI-H/dMMR (Microsatellite instability-high/mismatch re-pair-deficiency) colorectal cancer (46). Figure 1.

3.4 Link chronic inflammation and liver cancer

Chronic liver diseases are characterized by persistent inflammation and subsequent liver fibrosis, leading to liver cirrhosis and hepatocellular carcinoma (HCC) (47). HCC represents the most common type of liver cancer, which usually arises in the inflamed liver microenvironment caused by HBV and HCV infection, alcohol abuse and metabolic dysfunction-associated steatotic liver disease (MASLD) (47). MASLD is a spectrum of chronic liver disease that ranges from simple steatosis to metabolic dysfunction-associated steatohepatitis (MASH) and is strongly associated with metabolic syndrome (47). MASH is an emerging risk factor for HCC (47). Accumulating evidence has indicated that pre-cirrhotic MASLD might provide an increased risk of HCC, independent of cirrhosis (48). A range of single nucleotide polymorphisms, such as patatin-like phospholipase domain containing 3 (PNPLA3; rs 738409) and transmembrane superfamily member 2 (TM6SF2; rs 58542926) have been associated with the presence of MASLD and disease progression to advanced fibrosis and HCC (49, 50). Many research groups from different countries have shown that HCC is 3 times higher in patients carrying the PNPLA3 polymorphism (46, 49). Genomic analyses have indicated key pathways altered in HCC, including Wnt/β-catenin, P13K/Ras, and cell-cycle pathways (51, 52). The most frequently mutated genes in MASH-associated HCCs are TERT, CTNNB1, TP53 and ACVR2A genes (52). MASH-associated HCC samples have significantly higher rates of ACVR2A mutations than samples of other etiologies (52). The Wnt/TGF-β proliferation subclass is more frequent in MASH-driven HCC than in HCCs of other etiologies (53). Another molecular landscape of MASH-driven HCC is that it has an immunosuppressive pro-carcinogenic and inflammatory tumor microenvironment (52, 53).

In homeostasis, immune cells, particularly KCs are densely populated in the liver, which rapidly sense hepatocyte stress and injury signals, and lead to the activation of pro-inflammatory pathways (51). Metabolic stress induced by several factors causes metabolic disturbance in hepatocytes, increasing reactive oxygen species (ROS), endoplasmic reticulum (ER) stress and oxidative stress and resulting in hepatic metabolic reprogramming (47, 48, 51). These processes result in hepatocyte death of apoptotic or necroptotic type (48, 51). In the liver, dying or damaged hepatocytes release soluble mediators that act as damage-associated molecular patterns (DAMPs) (51). Preclinical studies have revealed that dying hepatocytes release P2Y14 ligands, such as uridine 5'-diphosphate (UDP)-glucose and UDP-galactose, that bind to the P2Y14 receptor on hepatic stellate cell (HSC) and induce activation in both mouse

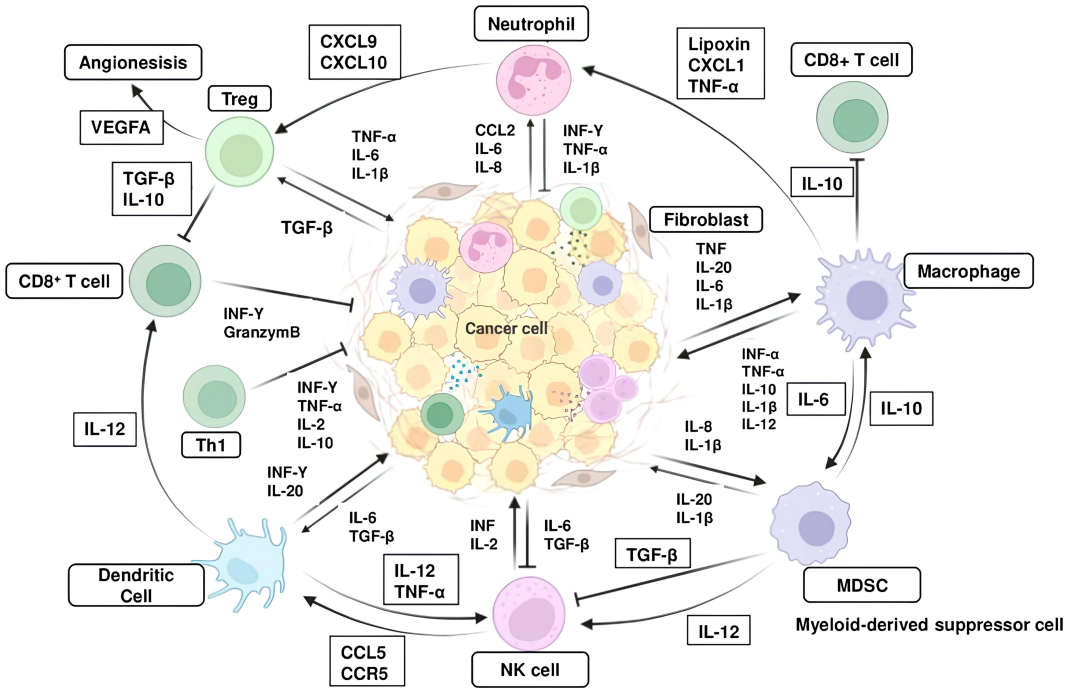

FIGURE 1
Interaction between inflammatory cells and inflammatory molecules in the tumor microenvironment. The major inflammatory cells include T helper cell (Th1), regulatory T cells (Tregs), Cytotoxic CD8$^+$ T cells, macrophages, myeloid-derived suppressor cells (MDSCs), naturel killer (NK) cells and dendritic cells (DCs). Abbreviations: CXCR, CXC-Chemokine receptor; CXCL, Chemokine (C-X-C motif) ligand, TGF-β, transforming growth factor-β; TNF, tumor necrosis factor; IL, interleukin; IFN, interferon.

and human HSCs (54). Liver parenchymal and non-parenchymal cells, including HSCs, KCs, and liver sinusoidal endothelial cells (LSECs) perceive these dangerous signals released from the dying hepatocytes via PRRs and form inflammasome as the first response (55). Inflammasome, a protein complex, initiates the inflammatory response by producing IL-1β, releasing IL-18, and ultimately promoting inflammatory cell death (55). Pro-inflammatory cytokine-producing Innate and adaptive immune cells rapidly accumulate in the inflammatory microenvironment and disrupt hepatocyte metabolism by promoting hepatic metabolic reprogramming, thereby promoting hepatocyte injury and death, DNA damage, and hepatocyte proliferation (56). Inflammatory molecules promote the activation of HSCs, and inflammatory mediators secreted by activated HSCs contribute to the expansion of chronic inflammation and hepatocarcinogenesis (49, 51). Mounting evidence indicates that chronic liver inflammation damages hepatic epithelial cells, including hepatocytes and biliary epithelial cells (51). Simultaneously, chronic inflammation in-duces ROS production and DNA damage, increasing the frequency of genomic alterations (49). Furthermore, chronic liver inflammation induces phenotypic changes in hepatocytes and hepatic immune cells, especially macrophages (16, 49, 51). Chronic inflammation initiates hepatocarcinogenesis through the transformation of hepatocytes into liver progenitor cells and the differentiation of macrophages into tumor-associated macrophages (M2 phenotype) (16). TNFα and IL-6 produced by macrophages in the cirrhotic liver, as well as TNF receptor 1 (TNFR1) signaling expressed by hepatocytes play critical roles in the development and progression of HCC (16). TNFα is one of the protumorigenic cytokines, that activates both NF-κB and JNK signaling pathways (16, 51). Many studies demonstrate that activation of innate immune receptors, such as Toll-like 4 receptors (TLRs), plays a role in HCC development (16, 57).

The gut microbiome, which harbors more than 100 trillion microorganisms including bacteria, viruses, fungi and archaea, plays a critical role in the development and progression of HCC by contributing to the establishment and growth of chronic liver inflammation (58, 59). The liver regulates the intestinal microbiota with bile containing bile acids, IgA and antibacterial metabolites (60). Environmental factors, such as high-fat diets and alcohol consumption, can disrupt microbial compositions, leading to gut dysbiosis, which induces intestinal inflammation, which contributes to intestinal barrier dysfunction and translocation of microorganism-associated molecular patterns (MAMPs), such as lipopolysaccharide (LPS), to the liver and systemic circulation (61). In diet-induced NASH mouse models, a positive correlation between serum LPS levels and liver injury has been demonstrated (62). Cholestasis due to liver tissue remodeling in cirrhosis leads to intestinal dysbiosis (58). Cirrhosis patients display increased bacterial abundance in hepatic tissue, which induces pronounced transcriptional changes, including activation of fibro-inflammatory pathways as well as circuits mediating cancer immunosuppression (63). Increased intestinal permeability in cirrhotic patients allows the translocation of MAMPs and contributes to increased systemic and local

inflammation in the liver (63). Dysbiosis changes the metabolism of intestinal bile acids, with less conversion of primary to secondary bile acids (64). Several studies have indicated that fecal microbial diversity is decreased in patients with cirrhosis compared with healthy controls, however, diversity increases as one progresses from cirrhosis to HCC (65). Preclinical studies have shown that MYC-transgenic mice capable of developing HCC arise lower numbers and sizes of HCC when given antibiotics (66). Another key finding of this study is that primary bile acids increase the accumulation of hepatic NK cells, whereas secondary bile acids reverse this situation (66). Several mouse model trials have revealed a link between the activation of inflammatory signals caused by intestinal permeability, the translocation of MAMPs, and the development of HCC (67). Rats with diethylnitrosamine-induced HCC have increased serum LPS, and administration of antibiotics decreased the tumor size and numbers (67). Another remarkable finding of this study was that tumor size was significantly reduced in TLR4-knock-out mice treated with diethylnitrosamine compared to wild-type mice (67).

4 Main drivers involved in the generation of cancer-association inflammation

Cancer-associated inflammation is characterized by the presence of inflammatory cells and inflammatory mediators, such as chemokines, cytokines and prostaglandins, tissue remodeling and angiogenesis in the TME (8–11, 18, 20, 22, 34, 35).

4.1 Genetic aberrations in oncogenes and tumor suppressor genes

The cancer genome somatic alterations, such as point mutations, genomic amplifications and rearrangements, play an important role in the development of cancer and in shaping of the inflammatory TME (18, 21). Tumor-derived cytokines and chemokines, tumor oncogenes and mutational burden determine the composition of the TME (18, 35). Emerging evidence has shown that there is a strong relationship between both tumor genotype/phenotype and immunological composition of the TME (35, 68). Oncogene-driven expression of cytokines critical for the recruitment and phenotype of immune cells, particularly cells of the myeloid lineage, has been reported (35). The effects of oncogenic pathways on the immune system, especially on inflammatory cells in cancer, vary according to the type, location and stage of cancer (69). KRAS mutations frequently occur in multiple cancers including CRC and PDAC, functioning as a ‘‘molecule switch’’ determining the activation of various oncogenic signaling pathways (35). In addition to its pro-tumorigenic role, KRAS also plays a key role in shaping an inflammatory and immunosuppressive TME through downstream effector activation and secreting various cytokines and chemokines (35). These soluble mediators promote the accumulation of suppressive immune cells into the TME while inhibiting the infiltration of T, B, and NK cells into the TME, thus facilitating unlimited proliferation of tumor cells. KRAS mutations can drive the secretion of anti-inflammatory cytokines, such as IL-10, TGF-β, and GM-CSF, as well as pro-inflammatory cytokines, such as ICAM-1, TNF-α, IL-1β, IL-6, and IL-18 (35, 69, 70). $KRAS^{G12D}$ -driven PDAC secretes high levels of growth factor GM-CSF, which is associated with an increase in tumor-associated Gr+ CD11b+ myeloid cells and suppression of CD8+ T cells (71). Interestingly, genetic ablation of GM-CSF in mice results in decrease myeloid cell infiltration, improved $CD8^+$ T cell infiltration into tumor, and substantially smaller lesion size (35). Another study found that $KRAS^{G12D}$ expression is associated with infiltration of Treg cells in pancreatic cancer tissue (35, 72). In a mouse colorectal cancer model, $KRAS^{G12D}$ expression inhibits T cell infiltration and interferon regulatory factor 2 (IRF2) production and, promotes the migration of $CXCR2^+$ MDSCs into the TME (73). In experimental cancer models, multiple mutant KRAS variants led to increased IL-8, which promoted tumor-associated inflammation, angiogenesis, and tumor growth (21).

Another oncogene with strong immunoregulatory features is MYC, that play a critical role in proliferation, differentiation, metabolism and apoptosis (35, 74). Oncogenic MYC inhibits antitumor immunity by enhancing CD47 and PD-L1 expression to impair macrophage and T cell recruitment, production of IL-1β, and inhibiting the infiltration of CD8+ T cells, NK cells and DCs (21, 35). $BRAF^{V600E}$ has been shown to induce Wnt/β-catenin signaling pathway, which in turn decrease production of CCL4, a chemokine important for the recruitment of $CD103^+$ DCs (21). Additionally, $BRAF^{V600E}$ has been revealed to promote production of factors such as IL-10 and IL-1α, which can induce tolerogenic forms of DC and CAFs (21). Notch signaling can activate monocytes and macrophages by driving CCL2 and IL-1β production, while promoting anti-tumor immunity by regulating TGFβ receptor and uPA production (18, 35, 74). Dysregulation of this pathway promotes epithelial-mesenchymal transition and angiogenesis (18, 35, 74). Oncogenic alterations in ERBB family members, including epidermal growth factor (EGF) and epidermal growth factor receptor 2 (EGFR2), promote cancer cell evasion of immune surveillance, thereby indirectly leading to an increase in the number of inflammatory cells in the TME (75). Mutant EGFR mediates cancer cell evasion of immune control by reducing PD-L1 expression, inhibiting $CD8^+$ T cell recruitment, and promoting Treg infiltration (75). In GI cancers, human epidermal growth factor receptor (HER2) amplification downregulates MHC-1, promoting cancer cell immune evasion (76). Furthermore, HER2 amplification impedes antitumor immunity by inhibiting cGAS-STING pathway (76). Monoclonal antibodies targeting HER2, when combined with chemotherapy, improved patient survival with $HER2^+$ cancer (77).

Inactivation or loss of tumor suppressor genes (TSGs) contributes significantly to cancer-associated inflammation (18, 35). P53 is a key regulator of cell cycle, DNA repair, senescence and apoptosis (78). Loss of p53 in cancer cells promotes secretion of WNT ligands, which in turn induces IL-1β production in TAMs in the TME. IL-1β enhanced accumulation of neutrophils, which

accelerates tumor progression (79). In a $KRAS^{G12D}$ -driven PDAC model, loss of p53 promoted tumor progression through increased expression of chemokines, such as CCL3, CCL11, CXCL5, and macrophage colony-stimulating factor (M-CSF), and the accumulation of macrophages and Treg cells within the TME (79). The p53 pathway can modulate the immunological composition of the tumor tissue by regulating NF-κB signaling, which is generally activated by the loss of p53 (8, 18, 21, 33, 35). NF-κB orchestrates cell survival and proliferation, but also the production of inflammatory cytokines (8, 9, 18, 21, 80). In experimental models, concomitant loss of E-cadherin and p53 promotes NF-κB activation, which is accompanied by increased macrophage recruitment and proinflammatory mediator production (21, 35, 80). Loss of p53 activates NF-κB, and induce the production of the inflammatory soluble molecules from cancer cells, which in turn alters the immune context through paracrine interactions (18, 80). Furthermore, studies in p53 knockout mouse models have revealed that NF-κB-mediated inflammatory response is a driving force of carcinogenesis (18, 80, 81). p53 missense mutations may enhance the malignant properties of cancer cells as well as the loss of p53 function (80, 82). Studies have shown that mutant p53 leads to the release of miR-1246-rich exomes, causing M1 macrophages to polarize into tumor-promoting M2 phenotype, thereby contributing to the establishment of an immunosuppressive and inflammatory TME (82–85). Loss of tumor suppressor gene LKB1 can promote the production of G-CSF, CXCL7, and IL-6, which induces neutrophil accumulation and can prevent the recruitment of immune cells that exhibit antitumor activity (18, 35). PTEN can inhibit NF-κB signaling, as such, loss of PTEN increases NF-κB-mediated expression of soluble molecules, which promotes the recruitment of inflammatory and immunosuppressive cells in the TME, such as neutrophil, macrophage, and Treg (81, 85). Furthermore, the mutational landscape of cancer cells, which directly reflects the immunogenicity of the tumor, may determine the extent and phenotype of the immune infiltrate, i.e. inflammation, in the TME (3, 18, 35, 80) Figure 1.

4.2 Crosstalk between tumor metabolism and inflammation

During tumor development and progression, cancer cells and their TME are continuously exposed to metabolic stress (86). To survive and growth, cellular adaptation and metabolic reprogramming are required (86). Tumor cells consume an enormous amount of glucose through enhanced aerobic glycolysis, resulting in decreased glucose levels in the tumor interstitial fluid (86). Aerobic glycolysis in cancer cells results in the production of large amounts of lactate that accumulate in the TME (35, 86). Lactate acts in an immunosuppressive manner in the TME and decreases cytotoxic activity in NK cells, and enhances proliferation, PD1 expression and the immunosuppressive capacity of Treg cells (1, 35, 86). Additionally, lactate increase MDSCs frequencies in the TME and induces an M2-like polarization in TAMs (1). In glucose deprivation, T cells may be forced to engage in strong oxidative stress, which is characterized by the production of reactive oxygen species (ROS) within cells, plays a critical role in the development of cancer and cancer-related inflammation (1, 35, 86). Excessive production of ROS can trigger chronic inflammation by activating the number of transcription factors such as NF-κB, AP-1, Wnt/β-catenin, p53, PPAR-γ, HIF-1α, and Nrf2 (86). The activation of these transcription factors leads to altered expression of various genes and proteins including growth factors, cell cycle regulatory molecules, oncogenes, tumor suppressor genes, pro-inflammatory cytokines, and chemokines (1, 82, 86). Lactate metabolism is a potential therapeutic target in GI tumors. Recent studies indicate that inhibition of lactate dehydrogenase A leads to the regression of tumor growth in preclinical models (86). The lipids can be taken up by immune cells, such as DCs and TAMs, resulting in enhanced lipid metabolism, high oxidative stress and ROS production (1, 86). Elevated levels of ROS are often associated with chronic inflammation (1, 86).

Tumor hypoxia develops as a result of the rapid consumption of oxygen by tumor cells and quick angiogenesis within the tumor (86, 87). Hypoxia leads to hypoxia-inducible factor (HIF)-1α induction, CAF and TAM activation, and the secretion of various chemokines, which in turn result in the accumulation of proinflammatory myeloid cells, particularly macrophages, in the TME (88). Hypoxia inhibits glycolysis and may promote the angiogenic activity of TAMs (86). In response to hypoxia, HIF-1α potentiates the polarization and suppression of the effect of M2 (89, 90). Hypoxia also promotes the progression of T cells to exhaustion status (90). It promotes the production of immune checkpoint molecules, such as PD1, PD-L1, CTLA-4, LAG-3, and TIM-3, contributing to the TME becoming more inflammatory and immunosuppressive (91). Although hypoxia affects all cells within the tumor tissue, two recent studies have shown that it specifically affects cells with an inflammatory phenotype (87, 88). Macrophages are effector immune cells that undergo significant changes when entering tumors or infected wounds (86–88). Hypoxia generates distinct responses from macrophages depending on the activation state (89). Hypoxia induces transcriptome turnover in macrophages, but inflammatory macrophages exhibit significantly increased mRNA destabilization compared to resting macrophages (87, 91, 92). In another study investigating the relationship between hypoxia and inflammation, Mello et al. found that hypoxia promotes the induction of inflammatory phenotype cancer-associated fibroblasts (iCAFs) by modulating their interaction with tumor cells and that hypoxic regulation of the iCAF phenotype is independent of tumor HIF1α (88). The drivers of tumor-associated inflammation are different in microbial-rich tumors and sterile tumors (8, 20). For example, in CRC, disruption of the intestinal barrier by oncogene in the mucosa where cancer originates leads to translocation of commensal bacteria and their metabolites, to promote IL-23 production and IL-23-mediated cancer-related inflammation (93, 94). In contrast, in tumors not originating in the mucosa genomic and metabolic changes, cell death and hypoxia may be initial inflammatory stimuli (94).

4.3 Key inflammatory cells and inflammatory molecules

Stromal cells, such as cancer-associated fibroblasts (CAFs), tumor-associated macrophages (TAMs), and tumor-associated neutrophils (TANs), are pivotal players in the generation and expansion of tumor-associated inflammation.

CAFs are one of the major components of the TME (1, 21, 95). Recent studies have demonstrated that CAFs display plasticity in response to cues from the TME and can have both tumor-promoting and tumor-limiting activities (1, 95). Studies using single-cell RNA sequencing broadly divided CAFs into 2 distinct subpopulations: inflammatory and growth factor-enriched CAF (iCAF) and myofibroblastic CAF (myCAF) (1, 95). Furthermore, additional CAF subpopulations have been identified in tumors such as HCC and CCA (1, 21, 95). CAFs critically modulate cancer progression through various mechanisms, including production of growth factors, inflammatory ligands and exosomes as well as ECM remodeling, angiogenesis, tumor mechanics and treatment responses (95). CAF-secreted inflammatory ligands and chemokines promote inflammation and tumor cell proliferation (8, 18, 95). Interaction between CAFs and cancer cells is mediated with a complex signaling network that consists of signaling pathways for TGFβ, mitogen-activated protein kinase (MAPK), Wnt/β-catenin pathway, JAK/STAT pathway, epidermal growth factor receptor (EGFR), and NF-κB (95). CAFs also secrete various molecules, such as platelet-derived growth factor (PDGF), human growth factor (HGF), vascular endothelial growth factor (VEGF), TNFα, and stromal cell-derived factor, to enhance tumor progression and inflammation (11, 21, 95). Additionally, these molecules reduce the tumor immunosurveillance and chemotherapy activity of drugs. During carcinogenesis, experimental trials have reported that cancer-derived CAFs modulate immune system through recruiting immune cells, such as neutrophils, monocytes and dendritic cells, and promote these cells to acquire immunosuppressive phenotypes that boost immune evasion (11, 95). The majority of ECM components expressed in the TME are produced by activated CAFs, which provides mechanical stability to the tumor (1, 95). Currently, CAF-targeted therapies aim to specifically deplete CAFs, impede their inflammation-promoting and immunosuppressive effects, or reprogram CAFs to a more quiescent state (1, 95).

Macrophages exert multifaced roles in cancer, a reflection of their plasticity in response to environmental stimuli (96, 97). Macrophages can be divided into two subtypes: proinflammatory M1 and anti-inflammatory M2 macrophages (97, 98). Tumor-associated macrophages (TAMs) are an important component of the TME and have an important role in the regulating of inflammation, angiogenesis, ECM remodeling, cancer cell proliferation, metastasis and immunosuppression and as well as resistance to cancer therapy (1, 2, 7, 18, 21, 98). M1 TAMs can be activated by TNF-α and GM-CSF and promote the recruitment and antitumor activities of $CD8^+$ T cells and NK cells (98, 99). In the inflammatory TME, macrophages account for 30%-50% of cell populations (98–100). M1 TAMs exert a pro-inflammatory effect and play a critical role in the development and progression of tumors by expressing high levels of pro-inflammatory mediators, such as such as TNF-α, IL-1β, IL-6, IL-12, CXCL9 (98, 100, 101). TNF-α expression is increased aberrantly in many tumors, such as liver, breast and ovarian cancer, suggesting this cytokine is an important player in resistance to anticancer treatment (98). TNF-α exerts its antitumor effect by promoting apoptosis of tumor cells, polarizing TAMs to the M1 phenotype, and promoting EMT of tumor cells (102, 103). TNF-α displays its immunosuppressive effect by promoting the survival and function of Tregs (98). IL-6 triggers tumor progression by promoting tumor cell proliferation, survival, EMT, angiogenesis, and chemoresistance (98). In the early stage of cancer, proinflammatory cytokines, such as IL-6, IL-8, and TGF-β secreted from cancer cells, immune cells and stromal cells promote the recruitment of macrophages in the inflammatory TME and their polarization to the M2 phenotype (99, 100, 102–105). M1 macrophages kill tumor cells by secreting cytotoxic molecules, such as ROS and NO, or by antibody-dependent cell-mediated cytotoxicity (ADCC) (1, 98). In contrast, M2 macrophages are protumoral cells and function to suppress the activities of immune effector cells (98). For tumor healing, the proinflammatory M1 macrophages repolarize into anti-inflammatory M2 TAMs to control inflammation. M1 TAMs promote tumor-associated inflammation by producing pro-inflammatory mediators (2, 4, 7, 8, 10, 11, 14, 18, 19, 96, 97). M2 TAMs increase angiogenesis by upregulating angiogenesis-associated genes such as VEGF, PDGF, and PGE2, or via molecules CXCL12, IL-1β, IL-8 and Sema4d, leading to tumor progression (98, 102).

Neutrophils, the most dominant immune cells, play a complex and significant role in cancer initiation, progression and metastasis (1, 11, 98, 106). The N1 and N2 polarization of tumor-associated neutrophils (TANs) can be induced by IFN I and TGF-β, respectively (106). Tumor-released molecules drive a shift of infiltrating neutrophils toward an antitumor phenotype (98, 106). Neutrophils dominate the early phase of inflammation and pave the way for tissue damage to be repair by macrophages (98, 106). These functions are regulated by various cytokines and the production of their receptors (98, 106). TANs may inhibit antitumor immunity by secreting a variety of proinflammatory and immunosuppressive mediators, such as IL-1β, IL-17, TNF-α, TGF-β, VEGF, CCL4, matrix metallo-peptidase (MMP)-9, C-X-C motif chemokine ligand 8 (CXCL8) and angiopoletin-1 (ANG1) (106). Tumor-derived TGF-β promotes the accumulation of N2 neutrophils which then contribute to the formation of immunosuppressive and inflammatory TME (98, 106). Aberrant expression of TGF-β has been found in many tumor types, such as HCC, breast and colon cancer. TGF-β inhibits tumor cell growth and proliferation in the early stage, while promoting cancer cell proliferation, growth, invasion, and angiogenesis in more advanced stages (98, 106). N2 TAN can form NETs, which can promote carcinogenesis in the context of chronic inflammation (2–4, 96). The IL-8/CXCL8 autocrine signaling in tumor cells can induce the formation of NETs (98).

Dendritic cells (DCs) are antigen-presenting cells (APCs) that play crucial roles in bridging innate and adaptive immune responses

(11, 106). DCs are considered main components of the TME and can promote anti-tumor T cell response. However, an immunosuppressive TME can affect DC effector functions, altering DC phenotype and promoting dysfunction and toleragenicity (106). In the TME, tumor-infiltrating DCs are frequently suppressed by tumor cells, leading to T cell tolerance rather than anti-tumor immune response (11, 35, 98). Tumor-derived factors trigger inflammation that promotes tumor growth by regulating the maturation of DCs (98, 106). For example, tumor-derived IL-6 and M-CSF convert immature DCs into macrophages and prevent the priming of tumor-specific T cells. Additionally, PD-L1 and PD-L2 expressed on DCs may also suppress the proliferation and cytokine expression of activated T cells (11, 98, 107)). Immunogenic cell death (ICD) is a unique pattern of programmed cell death that begins with the induction of cellular stress and results in cell death through the active secretion of DAMPs (108). During ICD, DAMPs interact with PRR produced by immune cells, particularly DCs, to activate innate and adaptive immune responses. ICD may provide novel strategy to increase the effectiveness of anticancer treatment since chronic exposure to TME-associated DAMPs may favor the activation of long-lasting anti-tumor immunity (98, 108). The role of DCs in the immune response induced by cancer cells undergoing ICD has been demonstrated in many studies (108). The findings indicate that the ability of different ICD inducers to initiate an efficient anti-tumor T cell response may depend DC activation in the TME (108). DCs, an important member of the innate immune system, have been reported to control the development of CAC through the production of IL-22BP, which neutralizes IL-22 (13, 14). However, cancer cells can hijack DCs to promote chronic inflammation and mitigate TAA presentation, thus accelerating carcinogenesis (13, 14, 98, 107). Different DC subsets have distinct mobilization capacities and exhibit different immunological functions (7, 8, 18, 99, 100). CCR7 is the most important chemotactic mediator of DC migration which recognizes the chemokine ligands CCL19 and CCL21 and it is the main guide in the migration of DCs to lymphoid tissue (107). The presence of inflammatory cells in some tumors, such as eosinophils in CRC and TAMs in breast and pancreatic cancer, is associated with a favorable prognosis (98, 107).

Myeloid-Derived Suppressor Cells (MDSCs): MDSCs are pathologically activated neutrophils and monocytes with potent immune suppressive activity (11, 98). These cells play an important role in accelerating tumor progression and undermining the efficacy of anti-cancer therapies (11, 98). MDSCs are divided into monocyte-myeloid-derived suppressor cells (M-MDSCs) with surface expression of $CD11b^+$ $Ly6G^+$ $Ly6C^-$ high and polymorphonuclear-myeloid-derived suppressor cells (PMN-MDSCs) with $CD11b^+$ $LyG6^+$ $LyG6^-$ low (98). The majority of MDSCs are PMN-MDSCs, accounting for more than 75%, with M-MDSCs accounting for only 10-20% (11, 98, 109). M-MDSCs have a greater capacity for immunosuppression than PMN-MDSCs (109). While PMN-MDSCs use ROS and arginase 1 (ARG1) to mediate immunosuppression, M-MDSC-mediated inhibition relies on nitric oxide (NO) and the suppressive cytokines IL-10 and TGF-β (98, 109). M-MDSCs are quickly accumulated to the inflammatory TME upon exposure to chemokines such as CCL2, CCL5, CXCL8, and CXCL12 and produce multiple immunosuppressive cytokines such as ARG1, NO, TGF-β, and IL-10 (109). The upregulation of ARG1 in MDSCs causes L-arginine deprivation that results in T cell dysfunction by inhibiting T cell receptor (98, 109). Tumor-derived factors such as VEGF, IL-6, and IL-10 accumulate MDSCs which in turn secrete more VEGF via STAT3 signaling, thus augments angiogenesis (98, 109). In addition, MDSC-derived MMPs function as a secondary angiogenic signals (11, 109). Considering that high M-MDSC numbers correlate with decreased tumor-specific T cell expansion and activation, MDSCs may be used as a novel marker to predict response to immune checkpoint inhibitors (ICIs) (11, 98, 109). On the other hand, blockade of MDSC-mediated CSF/CSF-1R signaling decreased MDSCs in the TME and converted immunosuppressive MDSCs to an antitumor phenotype, suggesting that MDSCs are targeted by inhibition of this signal (109). Figure 2.

The core function of innate immune system is to recognize and present tumor-associated antigens (TAAs) to cytotoxic anti-tumor effectors (5, 6). Anti-tumor effector cells can kill cancer cells directly or eliminate them by sensitizing them to biological molecules such as Fas ligand, perforin or granzyme (110–112). $CD8^+$ T cells are pivotal mediators in the elimination of cancer cells, which harbor distinct T cell receptors (TCRs) (21, 113). Growing evidence indicates that several key transcriptional factors (T-bet vs Bcl-6, STAT4 vs STAT3), epigenetic mechanisms (DNA methylation and histone modification) and metabolic reprogramming are involved in the differentiation of naïve T cells into effector cells (113–115). During cancer, naive $CD8^+$ T cells differentiate into $CD8^+$ CTLs producing a range of chemokine receptors and effector molecules (98, 115). Factors within the TME can drive $CD8^+$ T cells to exhausted T cells, which account for unique cellular phenotype, heterogeneity, and functional capacity (21, 114, 115). During exhaustion, $CD8^+$ T cells gradually lose expression of IL-2 and TNF-α, and cytotoxic function (116). Terminal exhausted $CD8^+$ T cells also lose IFN-α expression (116). Experimental trials have reported that terminal exhausted $CD8^+$ T cells can maintain their capacity to produce molecules such as MIP1α, MIP1β, RANTES, and IL-10 (116). Immune checkpoint molecule expression of terminal exhausted $CD8^+$ T cells is high and response to immunotherapies is quite low in these patients (110–112). B cells can inhibit carcinogenesis by expressing tumor-reactive antibodies, promoting tumor killing by NK cells, phagocytosis by macrophages and priming cytotoxic effector cells (111, 112). Tumor-infiltrating-B-lymphocytes (TIL-B) exert cytotoxic effect on HCC cells by producing granzyme and TRAIL (117). The majority of studies investigating the functions of TIL-B cells report that $CD20^+$ TIL-B cells have positive prognostic effects (115). The prognostic power of TIL-B cells is compatible with the density of $CD3^+$ and $CD8^+$ T cells and T cells exert stronger anti-tumor activity in the presence of TIL-B cells (7, 8, 14, 98, 117). Table 1.

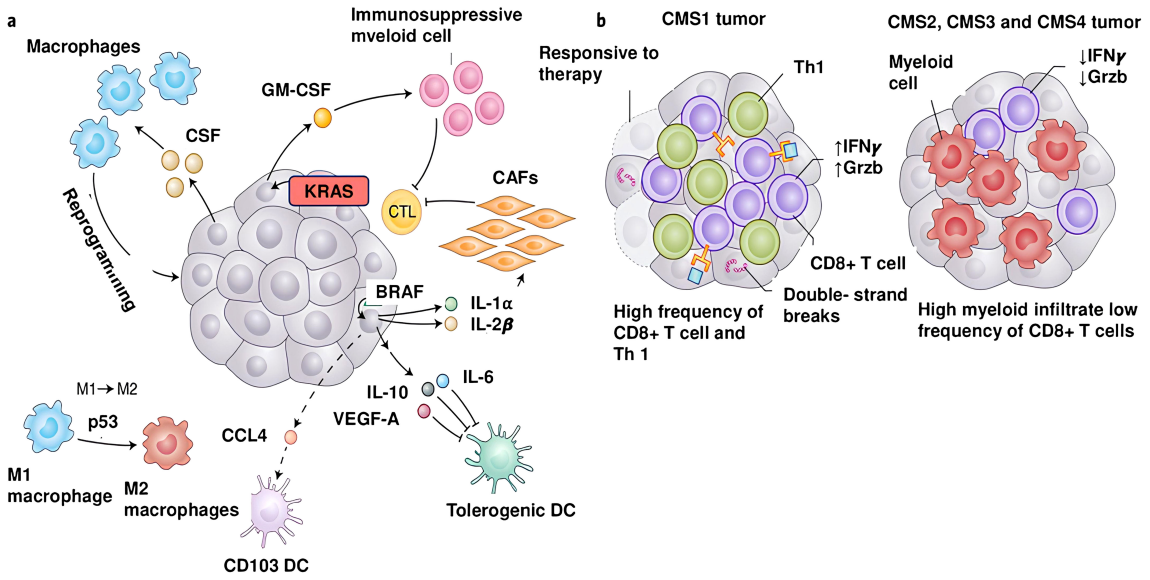

FIGURE 2
Genetic aberrations and molecules generating the inflammatory tumor microenvironment. **(a)** Oncogenes and aberrant signaling signals are key players in the development of inflammatory TME, leading to the production of inflammatory cytokines and chemokines. $BRAF^{V600D}$ activates Wnt/β-catenin signaling, which in turn decreases production of CCL4, a chemokine important for the recruitment of $CD103^{+}$ DCs. Additionally, $BRAF^{V600D}$ evokes the production of IL-10 and IL-1α molecules, leading to tolerogenic DCs and CAFs in the TME. The $KRAS^{G12D}$ mutation induces GM-CSF expression, which leads to accumulation of immunosuppressive $CD11b^{+}$ myeloid cells in the TME. Inactivation of p53 activates signaling pathways that lead to polarization of the immunoactivating M1 phenotype to the immunosuppressive M2 phenotype. Many tumors secrete high levels of the monocyte/macrophage-promoting cytokine CSF-1. **(b)** A high mutational burden is associated with potent expression of tumor neoantigens and extensive infiltration of $CD8^{+}$ T cells into the TME.

4.4 Main inflammatory pathways in cancer

4.4.1 Cyclooxygenase (COX) signaling

Chronic inflammation triggers the production of inflammatory mediators and activates signaling pathways that promote tumor growth, metastasis, and angiogenesis (11, 98). Among these mediators, prostaglandins (PGs) play a crucial role in the initiation and progression of inflammation and cancer (118). The expression of PGs is regulated by COX, which consists of three isoenzymes, namely COX-1, COX-2 and COX-3 (118). Recent studies have shown that COX-2 is upregulated in many tumors, including CRC, HCC, breast, PDAC and gastric cancer and COX-2 overexpression is associated with an unfavorable prognosis (119). Among the 5 key PGs derived via COX pathway, PGE2 is the most important PG in cancer and its upregulation is associated with advanced tumor stage. PGE2 orchestrates IFN-γ synthesis of NK cells, which is a significant inflammatory process (98, 119). PGE2 potentiates M-MDSCs and impairs the proliferation capacity of T cells (98, 119, 120). Furthermore, tumor-derived PGE2 induces NF-κB which epigenetically reprograms monocytes toward an immunosuppressive phenotype (11, 118–120). PGD2, another COX-2 metabolite, may play dual roles in in chronic inflammation and cancer. PGD2 can promote or inhibit tumor cell growth and metastasis depending on the stage of the tumor (119, 120). COX2/PGE2 signaling promotes the accumulation of MDSCs, leading to a decrease in the number of activated $CD8^{+}$ T cells in the TME (98, 118, 120). PGE2 also affects the polarization of macrophage by triggering monocyte differentiation into the M2-TAMs (98). Considering the contribution of the COX2/PGE2 pathway to the formation of immunosuppressive TME, inhibiting this pathway may increase the effectiveness of immunotherapies (11, 118–120).

4.4.2 Lipoxygenase (LOX) signaling

The LOX signaling mainly includes 5-LOX, 12-LOX, and 15-LOX (11). While 5-LOX ve 12-LOX display angiogenic and protumorigenic activity, 15-LOX exhibits both protumorigenic and antitumorigenic impacts (98, 121, 122). Given that 5-LOX and COX2 are upregulated in inflammation-associated tumors, suppression of these two molecules together may lead to more potent tumor suppression (98). The 12-LOX enzyme induces the forming of 12-HETE which promotes tumor growth by activating the integrin-linked kinase/NF-κB pathway (121). 15-LOX-1 may be secreted in Hodgkin lymphoma cells, and its metabolites boosts tumor-associated inflammation (121, 122). A recent study has indicated that 15-LOX levels are lower in doxorubicin (DOX)-resistant cells than DOX-sensitive cells (123). The overexpression of 15-LOX may trigger DOX recruitment in DOX-resistance cancer cells and induce their apoptosis (123). An experimental study demonstrated that 15-LOX promotes the resolution of inflammation in lymphedema developing in breast cancer mouse models by controlling Treg via IFN-β (122). The LOX pathways regulate the metabolism of arachidonic acid to leukotrienes such as leukotriene A4 (LTA4) and leukotriene B4 (LTB4) (121). 5-LOX is a central enzyme in LT biosynthesis, a potent arachidonic acid-derived lipid mediators released by innate immune cells, that

10.3389/fonc.2025.1564572

TABLE 1 Inflammatory cells that exhibit protumor or antitumor activity in cancer.

Cell type	Protumor activation	Antitumor activation
Dendritic cells (DCs)		
	-Promote T cell tolerance	-Provide signal for $CD8^+$ cells
	-Suppress proliferation and cytokine production T cells by secreting PD-L1, PD-L2	-Support anti-tumor T cell response caused by immunogenic cell death -Prevent carcinogenesis by the production of IL-22B
Tumor-associated macrophages (TAMs)		
	-M2 TAMs cause angiogenesis by upregulation of VEGF - degradate ECM - activate the response of endothelial cell to growth F - upregulate TGFβ that promotes EMT	- M1 TAMs promote anti-tumor activities of cytotoxic $CD8^+$ T cells and NK cells
Tumor-associated neutrophils (TANs)		
	-Induce tumor angiogenesis by promoting release of VEGF -Inhibit anti-tumor immunity by the expression proinflammatory mediators -Generate immunosuppressive TME -Promote the remodeling of TME that induces tumor cell extravasation	-N1 TANs display an anti-tumor activity by direct or indirect cytotoxicity
Myeloid-derived suppressor cells (MDSCs)		
	-Inhibit anti-tumor immunity by secreting immunosuppressive molecules -Induce tumor angiogenesis via VEGF and matrix metallopeptidase -Decrease the proliferation and activation of tumor-specific T cells by production colony-stimulating factor-1 receptor	
Vascular endothelial cells		
	-Induce migration of tumor cells due to weakened vascular endothelial junctions upon inflammation	-Form a barrier for blood components including tumor cells to infiltrate tissues under physiological conditions

control inflammatory processes (121). In addition, the enzyme is involved in the generation of omega-3 fatty acid-based oxylipins which promote the resolution of inflammation (121). LTB4 promotes the progression of inflammatory-derived tumors and inhibition of the LTBB4 receptor can suppress the progression of these tumors (121). The leukotriene D4 (LTD4) is upregulated in patients with HCC and chronic hepatitis B (121). Currently, the benefits of combining leukotriene receptor antagonists with multi-kinase inhibitors in the treatment of HCC are being investigated in many studies (98, 121).

4.4.3 JAK-STAT Signaling Pathway

The Janus kinase (JAK) signal transducer and activator of transcription (JAK-STAT) pathway is an evolutionary conserved signaling pathway that functions in several crucial physiological processes, including hematopoiesis, differentiation, metabolism, and inflammation (124, 125). The JAK protein family contains four members: JAK1, JAK2, JAK3, and TYK2. The STAT family involves seven members: STAT1, STAT2, STAT3, STAT4, STAT5A, STAT5B, and STAT6 (124, 125). More than 50 types of cytokines, including IFNs, ILs, and growth factors, have been indicated to play roles in JAK-STAT signaling to fulfill regulatory functions in cell differentiation, metabolism, survival, homeostasis, and immune response (124, 125). Once receptors bind to an extracellular ligand, JAKs induce tyrosine phosphorylation of the receptors and accumulate corresponding STATs. The phosphorylated STATs then dimerize and enter the nucleus to orchestrate specific gene transcription (124, 126). STAT3, the core member of the STAT protein family, plays multifaced roles in the inflammatory responses and tumor progression (124, 126). The dysregulated STAT3 pathway has been indicated to play a role in the development of many inflammatory diseases such as rheumatoid arthritis, and IBD (124–126). Furthermore, persistent activation of STAT3 signaling can induces carcinogenesis (126). Cytokines promoting the activation of STAT3 are upregulated in IBD, such as IL-1β, IL-6, IL-12, IFN, and TNF-α (124). The IL-6/STAT3 pathway, a critical regulator of the inflammatory process, plays a role in the pathogenesis of CAC (124, 126). In addition, CAFs secrete IL-6 which upregulates the production of metastasis-associated markers such as leucine Rich Alpha-Glycoprotein 1 (LRG1) via the JAK/STAT3 signaling (98, 126). In CRC, disruption of the intestinal epithelial barrier integrity and sensing of PAMPs by PRR activates the STAT3 pathway, thereby initiating the inflammatory response (124, 126).

4.4.4 Non-coding small RNA

Over the last two decades, many studies have highlighted the functional and therapeutic relevance of small non-coding microRNAs (miRNAs) in inflammation and cancer (127, 128). Quite recently, a new class of such RNAs have been identified, termed circular RNAs (circRNAs), that have been identified to play critical role in inflammatory diseases (127). The physiological and pathological functions of circRNAs occur through miRNA sponging, interaction with circRNA-binding proteins (cRBPs), protein-translation, or transcriptional regulation. circRNA regulate tumor-associated inflammatory signaling pathways mainly through miRNA sponging, circRNA-binding proteins (cRBBP) binding, and protein translation (127). The signaling pathways, such as Akt, E-cadherin, EGFR, MAPK, NF-κB, STAT, TGF-β, VEGF, and Wnt/β-catenin have been found to involved in tumor-associated inflammation (127, 128). NF-κB is involved in recruiting inflammatory cells and mediating the release of inflammatory chemokines, thus creating an inflammatory TME that promotes tumor progression (11). circRNA can form circRNA-protein complex to modulate signaling pathways in tumor-

associated inflammation (127). Some of the proteins encoded by circRNA participate in signaling pathways to modulate the development and progression of inflammation and cancer (127, 128). Many studies have indicated that circRNAs regulate DC- and neutrophil-mediated immune response, as well as the activation of TAN, TAM, and CAF (127). Inflammasome formation is the relevant mechanism that drives inflammation in immune cells by activating cysteine protease caspase-1, which subsequently induces pyroptosis through the secretion of inflammatory cytokines. circRNAs may play a role in tumor-mediated regulation of the immune system (127).

5 Cancer therapy-induced inflammation

Anti-cancer therapy is associated with an inflammatory response in tumor tissue, which either drives an anti-tumor immune response or, conversely, promotes tumor growth (129). Recent studies have demonstrated the impact of cancer therapy-induced inflammation on both tumor recurrence and clinical outcomes (129–132). Death of cancer cells elicits an anti-tumor immune response and that lipid mediators such as prostaglandin 2 (PG2) and platelet activation factor (PAF), play a role in the clearance of dead cells in the TME (129, 132, 133). Anti-cancer treatments are very effective in destroying cancer cells, but the main challenge in cancer treatment is that some cancer cells cannot be eliminated and they proliferate, causing tumor recurrence (132–134). Chemotherapy and radiotherapy often cause apoptotic cell death (129, 131, 132). In fact, apoptosis is a physiological process in which apoptotic cells are cleared by phagocytes such as macrophages and DCs, which prevents the emergence of inflammation by inhibiting the release of proinflammatory cytokines such as IL-10 and TGF-β, from phagocytes (102, 103). However, during the anticancer therapy, delayed clearance of apoptotic cells can lead to secondary necrosis, which can result in the release of proinflammatory cytokines and thus inflammation (103, 132).

Another type of cell death caused by anti-cancer treatments, including chemotherapy and radiotherapy, is necrosis (129, 132–134). The main landscape of necrotic cell death is the rupture of the cancer cell membrane and the release of DAMPs, which engage distinct receptors present on the innate immune cells (129, 132, 133). Upon recognition, DAMPs activate DCs and promotes the engulfment of dying cells, thereby improving anti-tumor response and clinical consequences (129, 132, 134). Conversely, DAMPs released from dying cancer cells accumulate macrophages to promote cancer cell clearance and polarize them to a M2 phenotype, which may contribute to immunosuppression and cancer cell resistance to anti-cancer therapy (102, 103). Dying cancer cells also express lipid mediators, such as PGE2 and PAF, promoting the proliferation and survival of remaining cancer cells (102, 103, 129, 132). Experimental trials have revealed that DAMPs are not only released from necrotic cells, but certain forms of programmed cell death can induce DAMPs release and lead to immunogenic cell death (129, 132, 134). Distinct chemotherapeutic agents, such as anthracyclines, oxaliplatin, cyclophosphamide, mitochontrone, bortezomid and radiotherapy result in immunogenic cell death (ICD) of cancer cells, and stimulate the release of DAMPs from dying cells (129–133). Following ICD, DAMPs promote the activation of cytotoxic effectors, which play a crucial role in the therapy response (130–132). Chemotherapeutic agents exert anti-cancer influences by influencing main cellular biological processes, which are indispensable for the robust proliferation of tumor cells (132). In addition, anti-cancer drugs modulate the immune cell profile of the TME, by triggering immune reactions and promoting cytotoxic effectors (135, 136). A few anti-cancer agents, such as cisplatin, can cause chronic inflammation through the release of some pro-inflammatory mediators, leading to angiogenesis, tumor progression and resistance to treatment (136, 137).

Currently, radiotherapy has established an important part of conventional cancer treatments, as high dose of radiation kills cancer cells and reduces tumor size (138, 139). Radiotherapy activates transcription factors, including NF-κB and STAT, which generate multiple radioresistance signals through modulating anti-apoptotic pathways (138, 139). Radiotherapy-induced NF-κB activation contributes to the prevention of apoptosis and cell cycle arrest (139) Additionally, NF-κB activation also orchestrate the transcription of a myriad of genes regulating immunity, proliferation, invasion, and angiogenesis, which favor radiotherapy resistance (133, 138, 139). Experimental trials in some types of cancer have reported that drugs that suppress the biological effects of NF-κB, such as indomethacin and curcimin, enhance the radiosensitivity of cancer cells by accentuating radiotherapy-induced apoptosis (133, 139). Irradiated tumor cells secrete many soluble molecules, including proinflammatory cytokines, that also have biological effects on non-irradiated cells (138, 139). In addition, radiotherapy promotes the formation of a proinflammatory TME, by inducing the network between inflammatory pathways, ultimately leading to tumor cell death (133, 139). Radiation-induced inflammation accentuates the adaptive antigen-specific immune response and tumor-host interaction is reshaped during radiotherapy, which contributes to the favorable clinical outcomes (133, 139). Additionally, chronic inflammation induced by radiotherapy in the TME promotes to recruitment of immunosuppressive cells (TAMs, myeloid-derived cells, and regulatory T cells) (133, 139). Radio-therapy can foster proliferation of cancer cell and tumor progression, thus paving the way for treatment resistance (133, 139).

In some solid tumors, such as HCC, immune checkpoint inhibitors (ICIs) have been shown to significantly improve overall survival (140, 141). However, immune-related tissue injury is common in patients with cancer receiving ICIs, adversely affecting clinical outcomes (141, 142). Although immune-related

tissue injury can affect any organ, it is most commonly observed in the skin, endocrine system, gastrointestinal system and liver (142). In randomized controlled trials (RCTs), the incidence of immune-related tissue injury has been reported to be between 1% and 15% (141, 142). In particular, in patients with HCC receiving ICIs, the incidence of immune-related liver damage is directly related to the degree of underlying liver disease and the combined administration of molecularly targeted drugs (141–143). ICIs may cause inflammation due to lysis of tumor cells, especially in patients who achieve an objective radiological response (142, 143). ICIs also led to increased T cell infiltration within the TME, resulting in overproduction of proinflammatory cytokines by these cells, thereby enhancing the inflammatory response (141–143). Cytokine release syndrome (CRS) is one of the most serious clinical toxicities of immunotherapies (143). Many studies have shown that CRS can develop not only during the use of immunotherapies in patients with cancer but also during the treatment of other dis-eases, where CRS is accompanied by severe inflammation (143). Recently, two prospective studies of patients with advanced HCC who received ICIs reported that patients with high baseline AFP levels had a higher frequency of immune-related liver injury and significantly higher levels of inflammation markers than patients with normal AFP levels (142). Although ICIs have provided significant progress in cancer treatment, they fail in a relevant proportion of cancer patients due to their side effects and the development of treatment resistance (142, 143). The main reason for resistance to immunotherapies is the inflammatory TME, where chronic inflammation is the fundamental driver of cancer cell proliferation, angiogenesis, and recruitment of immunosuppressive cell populations (141–143) Figure 3.

6 Targeting tumor-associated inflammation: leveraging precision medicine

Tumor-associated inflammation, which contains complex crosstalk between epithelial and stromal cells, can lead to epigenetic alterations that drive malignant progression and even initiate tumorigenesis (1, 11, 35). In addition, chronic inflammation triggers the production of growth factors that support the newly emergent tumor (98, 144, 145). Additionally, tumor-associated inflammation alters the effectiveness of anti-cancer drugs through modulation of the production of multidrug efflux transporters (e.g., ABCG2, ABCB1, and ABCC1) and drug-metabolizing enzymes

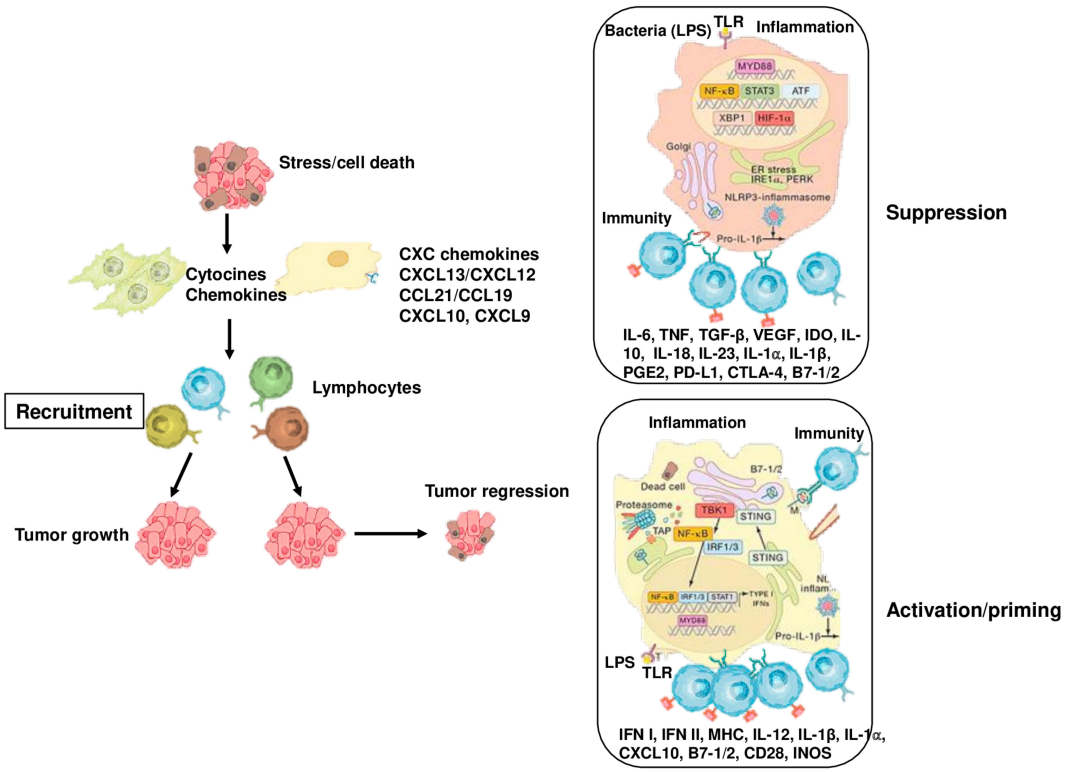

FIGURE 3
Cancer-associated inflammation that affects tumor growth and progression. Stress, cell death, obesity and bacterial infection and its components trigger the activation of innate immune cells and increase the expression of inflammatory mediators, which induce the recruitment of adaptive immune cells to damaged tissue. Myeloid cells, such as DCs, take up antigens and present them T cells, activating to $CD8^+$ T cells. On the other hand, cell death may exert immunosuppressive and tolerogenic effects, thus inhibiting CD8+ T cell activation. Similarly, monocytes and macrophages can impede the anti-tumor activity of CD8+ T cells by producing IL-10, ARG1, IDO, and TGF. In the early stages of cancer, inflammation leads to the production of cytokines, such as IL-1, TNF, and IL-6, that promote tumor growth, as well as VEGF that supports neo-angiogenesis.

(e.g., CYP1A2 and CYP3A4) (146). Furthermore, inflammation can protect cancer cells from drug-mediated cell death by regulating DNA damage repair, downstream adaptive response (e.g., apoptosis, autophagy, and oncogenic bypass signaling), and TME (144, 146). Inflammation-reducing chemopreventive treatments that inhibit either the initiation or propagation of persistent inflammation may therefore prevent or delay cancer (98, 144, 146). Many studies have reported that anti-infective agents, non-steroidal anti-inflammatory drugs (NSAIDs), and other drugs capable of reducing inflammation, such as statins and metformin, reduce the risk and incidence of cancer (98, 144).

6.1 Non-steroidal anti-inflammatory drugs (NSAIDs).

COX2/PGE2 signaling pathway can provide epithelial cells with protumorigenic properties, thereby promoting the development of inflammation-related cancer (98, 144, 146). COX2 can activate the AKT, mTOR, and NF-κB pathways to support cancer cell proliferation either directly or via PGE2 signaling (144, 146). Aspirin and selective COX-2 inhibitors have pro-apoptotic and antiproliferative effects on COX2- overexpressing cancer cells (98). In addition, PGE2 silences TSGs by reinforcing their promoter methylation through a EP4-DNA methytransferase pathway (146). In mice, celexoxib treatment limits intestinal tumor growth and can reverse the silencing of TSGs and activation of oncogenes in COX2 overexpression-induced HCC (144). NSAID treatments prevent colorectal carcinogenesis by blocking the senescence-associated inflammatory response. PEG2 evokes colorectal carcinogenesis via YAP1, a transcriptional regulator in mice, and administration of NSAID indomethacin impedes colon tumorigenesis (146).

NSAIDS exhibit their anti-inflammatory effects by inhibiting cyclooxygenase activity (98). Aspirin can inhibit the nuclear translocation of NF-κB, thereby inhibiting the P13 kinase/Akt-mediated cell survival pathway and promoting cell apoptosis (144, 146, 147). In some types of cancer, aspirin inhibits tumor cell proliferation and evokes apoptosis by upregulating Bax and downregulating Bcl-2, changing the ratio of Bax/Bcl-2 (98). In a systematic review and meta-analysis of observational studies, the risk of CRC was found to be 27% lower in individuals who regularly used aspirin compared to non-users, the risk of esophageal and gastric cardia cancer was 39% lower, the risk of stomach cancer was 36% lower, the risk of hepatobiliary cancer was 38% lower, and the risk of PDAC was 22% lower (148). However, some studies reported that aspirin use did not reduce the risk of PDAC (144). Additionally, studies conducted in Sweden and Taiwan revealed that aspirin use reduce the risk of HCC in patients with chronic viral hepatitis (149, 150). Post-diagnostic aspirin administration reduces overall mortality in GI tumors, and the survival benefit is better in PIK3CA-mutant and COX-2-positive tumors or tumors with low PD-L1 levels (151). As a selective COX-2 inhibitor that inhibits prostaglandin production, celecoxib can induce apoptosis by activating transcriptional regulators of ER stress in hepatoma cells (152). Dexamethasone can evoke apoptosis in multiple myeloma mediated by miR-125b expression (144).

6.2 Antiviral therapies

In addition to the direct oncogenic effects, HBV and HCV infections can cause cancer-promoting inflammation. In infected individuals, antiviral therapies that inhibit HBV and HCv replication, such as interferon-based therapies, nucleoside or nucleotide analogues, and direct antiviral agents, reduce the risk of HCC by 50-80% (153). Antiviral therapies are also effective in reducing disease recurrence and improving postoperative survival outcomes in patients with HCC (153). Similarly, more than 90% of cervical cancers are associated with human papillomavirus (HPV). Many RCTs have indicated that HPV vaccines are highly effective in preventing cervical precancerous lesions (154). Today, HPV vaccination has been implementing for cervical cancer prophylaxis in multiple age groups across different countries (154). Unfortunately, drugs to treat Epstein-Barr virus (EBV), the first tumor virus identified in humans and associated with stomach cancer and lymphoma, have not yet been identified (144). Helicobacter pylori is the strongest risk factor for gastric cancer, and its eradication with broad-spectrum antibiotics not only prevents gastric cancer, but also reduces the rate of developing metachronous gastric cancer in patients with early gastric cancer (17).

6.3 Cytokine- and chemokine-directed therapies.

The elimination of MDSCs in the TME by inhibiting IL-1 pathway is a potential strategy to overcome tumor resistance to immunotherapies (144). Anti-IL-1β monoclonal antibodies (mAbs) can boost the efficacy of PD-L1 inhibition in some types of cancer (144). In CANTOS study, canakinumab, an anti-IL-1β mAb, dose-dependent reduced IL-6 and C-reactive protein (CRP) in atherosclerotic patients with prior myocardial infection and elevated CRP levels (155). IL-2 is a key growth factor for $CD4^+$ T cells and NK cells, which displays antitumor activity. IL-2 treatment can confer durable response in melanoma and renal cell carcinoma (RCC) patients (98). IL-6 is one of the most pivotal cytokines linking cancer-promoting inflammation and immunosuppression (144). Drugs targeting IL-6 exhibit limited activity in patients with cancer when used as monotherapy (144). Galunisertib, a small molecule inhibitor of the TGFβR1 kinase, has been indicated to be safe in patients with various cancers (156). Galunisertib provides modest therapeutic activity when combined with gemcitabine in patients with unresectable PDAC or with sorafenib in advanced HCC (156). Monoclonal antibody therapies targeting TNF have been applied to patients with advanced stage, and modest therapeutic effects have been observed (157).

Can precision medicine contribute to the management of tumor- associated inflammation? Each patient has a unique genome, proteome, epigenome, microbiome, lifestyle, diet, and other characteristics that all interact to influence oncogenes, disease progression, effective treatment options, drug tolerance, remission, and recurrence (145). Molecular characterization of tumors has shifted cancer treatment strategies away from nonspecific cytotoxic treatment of histology-specific tumors toward targeting of actionable mutations that can be found across multiple cancer types (145). Precision oncology provides individualized treatment of cancer on a per-patient basis, based on the unique DNA fingerprint of a patient's cancer (145). Recent studies have identified prognostic and predictive molecular markers that could improve diagnosis, treatment planning, and clinical outcomes (158–165). However, as highlighted in detail in this review article, although the inflammatory cells, soluble molecules, genetic and epigenetic mechanisms involved in the formation of tumor-associated inflammation have been largely elucidated, there is no molecular marker for tumor-associated inflammation yet used in clinical practice.

7 Conclusions and future perspectives

In recent years, technological advances, including single-cell multi-omics and spatial technologies, artificial intelligence-based systems biology approaches have led to a breakthrough in our knowledge of how cancer cell-intrinsic features regulate immune cell composition, spatial distribution and functional status of the TME. These tremendous advances have allowed us to understand more about the interactions between cancer cells, immune cells and stromal cells. Chronic inflammation is thought to be a fundamental feature of cancer, which plays a key role in establishing TME. TME consists of cancer cells, immune cells, stromal cells, ECM proteins, intratumor microbioma and soluble molecules, such as proinflammatory cytokines, chemokines, growth factors and immune checkpoint molecules. TME determines the biological behavior of cancer cells and is therefore an important driver in tumor progression, suppression of antitumor immunity and resistance to anticancer therapy. The immune cell composition, activation status, and spatial distribution of the TME vary among tumor types. Cancer cell molecular characteristics, including genetic and epigenetic alterations, signaling pathway deregulation and altered metabolism play a critical role in governing the composition and functional status of immunological landscape and affect the efficacy of immunomodulatory therapies. Immune cells, like cancer cells, have multifaced functions in the TME, their activities ranging from protumorigenic to antitumorigenic.

Inflammation in the tumor tissue can be induced at different times and stages, i.e. before or after carcinogenesis. In cancer, inflammatory pathways that evolved to elicit immunity against infection and maintain tissue homeostasis are hijacked by cancer cells. Chronic inflammation acts as a tumor promoter by boosting cell survival, proliferation, and angiogenesis during tumorigenesis and tumor progression. In addition, chronic inflammation is involved in carcinogenesis by activating NF-KB and STAT signaling pathways. In the vast majority of tumors, inflammation exerts dual effects; normally, immune cells inhibit tumor growth by eradicating tumor cells, on the other hand, in inflammatory tumors, some immune cells, inflammatory cells and molecules promote cancer growth by boosting cancer cell proliferation and prolonging its survival. A significant number of cancer patients receiving ICIs emerge primary or acquired drug resistance. The interaction between cancer cells and stromal cells in the TME can alter the cellular composition and soluble molecule landscape of the TME and may predispose to the development of drug resistance. Therefore, it is necessary to elucidate this complex crosstalk between cancer cells and immune cells, particularly inflammatory cells to develop effective anti-cancer drugs and improve the overall survival of cancer patients. Considering all of these advances, it can be suggested that treatment of cancer-associated inflammation, elimination of immunosuppressive landscape of the TME and repolarization of terminal exhausted CD8+ T cells into effector CD8+ T cells are necessary for the anti-cancer therapies to be successful in GI cancers. Cancer cell molecular features can be therapeutic targeted to transform the cancer-promoting immune landscape into a tumor-suppressing immune landscape.

Author contributions

HA: Writing – original draft, Writing – review & editing. HŞ: Writing – original draft. DB: Writing – original draft. YÜ: Writing – original draft. EO: Writing – original draft. NA: Writing – original draft. AD: Writing – original draft.

Funding

The author(s) declare that no financial support was received for the research and/or publication of this article.

Acknowledgments

This is a review article to acknowledge the contributions of specific colleagues, institutions, or agencies that aided the efforts of the authors.

Conflict of interest

The authors declare that the research was conducted in the absence of any commercial or financial relationships that could be construed as a potential conflict of interest.

Generative AI statement

The author(s) declare that no Generative AI was used in the creation of this manuscript.

Publisher's note

All claims expressed in this article are solely those of the authors and do not necessarily represent those of their affiliated organizations, or those of the publisher, the editors and the reviewers. Any product that may be evaluated in this article, or claim that may be made by its manufacturer, is not guaranteed or endorsed by the publisher.

References

1. Rauth S, Malafa M, Ponnusamy MP, Batra SK. Emerging trends in gastrointestinal cancer targeted therapies: harnessing tumor microenvironment, immune factors, and metabolomics insights. *Gastroenterology*. (2024) 167:867–84. doi: 10.1053/j.gastro.2024.05.005

2. Sohrab SS, Raj R, Nagar A, Hawthorne S, Paiva-Santos AC, Kamal MA, et al. Chronic inflammation's transformation to cancer: A nanotherapeutic paradigm. *Molecules*. (2023) 28:1–19. doi: 10.3390/molecules28114413

3. Afify SM, Hassan G, Seno A, Seno M. Cancer-inducing niche: the force of chronic inflammation. *Br J Cancer*. (2022) 127:193–201. doi: 10.1038/s41416-022-01775-w

4. Feng H, Zhuo Y, Zhang X, Li Y, Li Y, Duan X, et al. Tumor microenvironment in hepatocellular carcinoma: key players for immunotherapy. *J Hepatocell Carcinoma*. (2022) 9:1109–25. doi: 10.2147/JHC.S381764

5. Baker DJ, Arany Z, Baur JA, Epstein JA, June CH. CAR T therapy beyond cancer: evolution of a living drug. *Nature*. (2023) 619:707–15. doi: 10.1038/s41586-023-06243-w

6. Albelda SM. CAR T cell therapy for patients with solid tumours: key lessons to learn and unlearn. *Nat Rev Clin Oncol*. (2024) 21:47–66. doi: 10.1038/s41571-023-00832-4

7. Wen Y, Zhu Y, Zhang C, Yang X, Gao Y, Li M, et al. Chronic inflammation, cancer development and immunotherapy. *Front Pharma*. (2022) 1-14. doi: 10.3389/fphar.2022.1040163

8. Greten FR, Grivennikov SI. Inflammation and cancer: triggers, mechanisms, and consequences. *Cell*. (2019) 51:27–43. doi: 10.1016/j.immuni.2019.06.025

9. Diakos CI, Charles KA, McMillan DC, Clarke SJ. Cancer-related inflammation and treatment effectiveness. *Lancet Oncol*. (2014) 15:493–503. doi: 10.1016/S1470-2045(14)70263-3

10. Shalapour S, Karin M. Pas de deux: control of anti-tumor immunity by cancer-associated inflammation. *Cell*. (2019) 51:15–25. doi: 10.1016/j.immuni.2019.06.021

11. Zhao H, Yan G, Chen Y, Zhou M, Wu Y, Li Y. Inflammation and tumor progression: signaling pathways and targeted intervention. *Sig Transduct Target Ther*. (2021) 6(1):263. doi: 10.1038/s41392-021-00658-5

12. Balkwill F, Mantovani A. Inflammation and cancer: back to Virchow? *Lancet*. (2001) 357:539–45. doi: 10.1016/S0140-6736(00)04046-0

13. Zhou RW, Harpaz N, Itzkowitz SH, Parsons RE. Molecular mechanisms in colitis-associated colorectal cancer. *Oncogenesis*. (2023) 12:48. doi: 10.1038/s41389-023-00492-0

14. Chatila WK, Walch H, Hechtman JF, Moyer SM, Sgambati V, Faleck DM, et al. Integrated clinical and genomic analysis identifies driver events and molecular evolution of colitis-associated cancers. *Nat Commun*. (2023) 14:110. doi: 10.1038/s41467-022-35592-9

15. Yu L-X, Ling Y, Wang H-Y. Role of unresolving inflammation in hepatocellular carcinoma development and progression. *Precis Oncol*. (2018) 2:1–12. doi: 10.1038/s41698-018-0048-z

16. Galun E. Liver inflammation and cancer: the role of tissue microenvironment in generating the tumor- promoting niche (TPN) in the development of hepatocellular carcinoma. *Hepatology*. (2016) 63:354–6. doi: 10.1002/hep.28344

17. Malfertheiner P, Camorgo MC, El-Omar E, Lio J-M, Peek R, Schulz C, et al. Helicobacter *pylori* infection. *Nat Rev Dis Primers*. (2023) 9:19. doi: 10.1038/s41572-023-00431-8

18. Wellenstein MD, de Visser K. Cancer cell-intrinsic mechanisms shaping the tumor immune landscape. *Cell*. (2018) 48:396–416. doi: 10.1016/j.immuni.2018.03.004

19. Ramirez CFA, Taranto D, Ando-Kuri M, de Groot MHP, Tsouri E, Huang Z, et al. Cancer cell genetics shaping of the tumor microenvironment reveals myeloid cell-centric exploitable vulnerabilities in hepatocellular carcinoma. *Nat Commun*. (2024) 15:2581. doi: 10.1038/s41467-024-46835-2

20. Mantovani A, Allavena P, Sica A, Balkwill F. Cancer-related inflammation. *Nature*. (2018) 454:436–44. doi: 10.1038/nature07205

21. Binnewies M, Roberts EW, Kersten K, Chan V, Faron DF, Merad M, et al. Understanding the tumor immune microenvironment (TIME) for effective therapy. *Nat Med*. (2018) 24:541–50. doi: 10.1038/s41591-018-0014-x

22. Nigam M, Mishra AP, Deb VK, Dimri DB, Tiwari V, Bungau SG, et al. Evaluation of the association of chronic inflammation and cancer: Insights and implications. *Biomed Pharmacother*. (2023) 104:115015. doi: 10.1016/j.biopha.2023.115015

23. Hu W, Pasare C. Location: tissue-specific regulation of immune responses. *J Leukoc Biol*. (2013) 94:409–21. doi: 10.1189/jlb.0413207

24. Rivera A, Siracusa MC, Yap GS, Gause WC. Innate cell communication kick-starts pathogen-specific immunity. *Nat Immunol*. (2016) 17:356–63. doi: 10.1038/ni.3375

25. Watanabe S, Alexander M, Misharin AV, Budinger GRS. The role of macrophages in the resolution of in-flammation. *J Clin Invest*. (2019) 129:2619–28. doi: 10.1172/JCI124615

26. Bulfone-Paus S, Nilsson G, Draber P, Blank U, Levi-Schaffer F. Positive and negative signals in mast cell ac-tivation. *Trends Immunol*. (2017) 38:657–67. doi: 10.1016/j.it.2017.01.008

27. Wright HL, Moots RJ, Bucknall RC, Edwards SW. Neutrophil function in inflammation and inflammatory disease. *Rheumatology*. (2010) 49:1618–31. doi: 10.1093/rheumatology/keq045

28. Kumar R, Clermont G, Vodovotz Y, Chow CC. The dynamic of acute inflammation. *J Theor Biol*. (2004) 230:145–55. doi: 10.1016/j.jtbi.2004.04.044

29. Medzhitov R. Origin and physiological roles of inflammation. *Nature*. (2008) 454:428–35. doi: 10.1038/nature07201

30. Savill JS, Wyllie AH, Henson JE, Walport MJ, Henson PM, Haslett C. Macrophage phagocytosis of aging neutrophils in inflammation. Programmed cell death in the neutrophil leads to its recognition by macrophages. *J Clin Invest*. (1989) 83:865–75. doi: 10.1172/JCI113970

31. Rossi AG, Sawatzky DA, Walker A, Ward C, Sheldrake TA, Riley NA, et al. Cyclin-dependent kinase inhibitors enhance the resolution of inflammation by promoting inflammatory cell apoptosis. *Nat Med*. (2006) 12:1056–64. doi: 10.1038/nm1468

32. Gilroy DW, Lawrence T, Perretti M, Rossi AG. Inflammatory resolution: new opportunities for drug dis-covery. *Nat Rev Drug Disco*. (2004) 3:401–16. doi: 10.1038/nrd1383

33. Serhan CN. The resolution of inflammation: the devil in the flask and in the details. *FASEB J*. (2011) 25:1441–8. doi: 10.1096/fj.11-0502ufm

34. Yang YM, Kim SY, Seki E. Inflammation and liver cancer: Molecular mechanisms and thearpeutic targets. *Semin Liver Dis*. (2019) 39:26–42. doi: 10.1055/s-0038-1676806

35. van Weverwijk' A, de Visser E. Mechanisms driving the immunoregulatory function of cancer cells. *Nat Rev Cancer*. (2023) 23:193–215. doi: 10.1038/s41568-022-00544-4

36. Hirata Y, Noorani A, Song S, Wang L, Ajani JA. Early-stage gastric adenocarcinoma: clinical and molecular landscapes. *Nat Rev Clin Oncol*. (2023) 20:453–69. doi: 10.1038/s41571-023-00767-w

37. Alsina M, Arrazubi V, Diez M, Tabernero J. Current developments in gastric cancer: from molecular profiling to treatment strategy. *Nat Rev Gastroenterol Hepatol*. (2023) 20:155–70. doi: 10.1038/s41575-022-00703-w

38. Lei Z-N, Teng Q-X, Tian Q, Chen W, Xie Y, Wu K, et al. Signaling pathways and therapeutic interventions in gastric cancers. *Signal Transduct Target Ther*. (2022) 7:358. doi: 10.1038/s41392-022-01190-w

39. Huang P, Gao W, Fu C, Wang M, Li Y, Chu B, et al. Clinical functional proteomics of intracellular signaling in pancreatic cancer. *Nature*. (2025) 637:726–35. doi: 10.1038/s41586-024-08225-y

40. Le Cosquer G, Maulat C, Bournet C, Cordelier P, Buscail E, Buscail L. Pancreatic cancer in chronic pan-creatitis: pathogenesis and diagnostic approach. *Cancers*. (2023) 15:761. doi: 10.3390/cancers15030761

41. Kim HS, Gweon T-G, Park SH, Kim TH, Kim CW, Chang JH. Incidence and risk of pancreatic cancer in patients with chronic pancreatitis: defining the optimal subgroup for surveillance. *Nature*. (2023) 13:106. doi: 10.1038/s41598-022-26411-8

42. Swidnicha-Siergiejko AK, Gomez-Chou SB, Cruz-Monseratte Z, Deng D, liu Y, Huang H. Chronic inflam-mation initiates multiple forms of K-Ras-independent mouse pancreatic cancer in the absence of TP53. *On-cogene*. (2017) 36:3149–58. doi: 10.1038/onc.2016.461

43. Robles AI, Traverso G, Zhang M, Roberts NJ, Khan MA, Joseph C, et al. Whole-exome sequencing analysis of inflammatory bowel disease-associated colorectal cancers. *Gastroenterology*. (2016) 150:931–43. doi: 10.1053/j.gastro.2015.12.036

44. Yaeger R, Shah MA, Miller VA, Kelsen JR, Wang K, Heins ZJ, et al. Genomic alterations observed in colitis-associated colorectal cancers and vary by type of inflammatory bowel disease. *Gastroenterology*. (2016) 151:278–287, e6. doi: 10.1053/j.gastro.2016.04.001

45. Hanna DN, Smith PM, Novitskly SV, Washington MK, Zi J, Weaver CJ, et al. SMAD4 suppresses colitis-associated carcinoma through inhibition of CCL20/CCR6-mediated inflammation. *Gastroenterology*. (2022) 163:1334–50. doi: 10.1053/j.gastro.2022.07.016

46. Zou D, Xu T. Construction and validation of a colon cancer prognostic model based on tumor mutation burden-related genes. *Nature*. (2024) 14:2867. doi: 10.1038/s41598-024-53257-z

47. Ringelhan M, Pfister D, O'Conner T, Pikarsky E, Hei-Kenwalder M. The immunology of hepatocellular carcinoma. *Nat Immunol*. (2018) 19:222–32. doi: 10.1038/s41590-018-0044-z

48. Sharma S, Le Guillou D, Chen JY. Cellular stress in the pathogenesis of nonalcoholic steatohepatitis and liver fibrosis. *Nat Rev Gastroenetrol Hepatol*. (2023) 20:662–78. doi: 10.1038/s41575-023-00832-w

49. Liovet JM, Willoughby CE, Singal AG, Greten TF, Helkinwalder M, El-Serag HB, et al. Nonalcoholic steatohepatitis-related hepatocellular carcinoma: pathogenesis and treatment. *Nat Rev Gas-troenterol Hepatol*. (2023) 20:487–503. doi: 10.1038/s41575-023-00754-7

50. Akkız H, Taskın E, Karaoğullarından U, Delik A, Kuran S, Kutlu O. The influence of RS738409 148M pol-ymorphism of patatin-like phospholipase domain containing 3 gene on the susceptibility of non-alcoholic fatty liver disease. *Medicine*. (2021) 19:e25893. doi: 10.1097/MD.0000000000025893

51. Hammerich L, Tacke F. Hepatic inflammatory response in liver fibrosis. *Nat Rev Gastroenterol Hepatol*. (2023) 20:633–46. doi: 10.1038/s41575-023-00807-x

52. Pinyol R, Torrecilla S, Wang H, Montironi C, Pique-Gilli M, Torres-Martin M, et al. Molecular characterization of hepatocellular carcinoma in patients with non-alcoholic steatohepatitis. *J Hepatol*. (2021) 75:865–78. doi: 10.1016/j.jhep.2021.04.049

53. Foerster F, Gaining SJ, Müller L, Galle PR. NAFLD-driven HCC: Safety and efficacy of current and emerging treatment options. *J Hepatol*. (2022) 76:446–57. doi: 10.1016/j.jhep.2021.09.007

54. Maderacke I, Filliol A, Affo S, Nair A, Hernandez C, Sun Q, et al. The purinergic P2Y14 receptorlinks hepatocyte death to hepatic stellate cell activation and fibrogenesis in the liver. *Sci Transl Med*. (2022) 14:eab5795. doi: 10.1126/scitranslmed.abe5795

55. Knorr J, Wree A, Tacke FS, Feldstein AE. The NLRP3 inflammasome in alcoholic and nonalcoholic steato-hepatitis. *Semin Liver Dis*. (2020) 40:298–306. doi: 10.1055/s-0040-1708540

56. McHedlidze T, Waldner M, Zopf S, Walker J, Rankin AL, Schuchmann M, et al. Interleukin-33 dependent innate lymphoid cells mediate hepatic fibrosis. *Immunity*. (2013) 39:357–71. doi: 10.1016/j.immuni.2013.07.018

57. Sica A, Lazzeri M. Specialization determines outcomes in inflammation and cancer. *Nat Immunol*. (2023) 24:1399–401. doi: 10.1038/s41590-023-01592-0

58. Hsu CL, Schnabi B. The gut-liver axis and gut microbiota in health and liver disease. *Nat Rev Microbiol*. (2023) 21:719–33. doi: 10.1038/s41579-023-00904-3

59. Fan Y, Pedersen O. Gut microbiota in human metabolic health and disease. *Nat Rev Microbiol*. (2021) 19:56–71. doi: 10.1038/s41579-020-0433-9

60. Schulthess J, Pandey S, Capitani M, Rue-Albrecht KC, Arnold I, Franchini F, et al. The short chain fatty acid butyrate imprints an antimicrobi-alprogram in macrophages. *Immunity*. (2019) 50:432–445.e7. doi: 10.1016/j.immuni.2018.12.018

61. Schwabe RF, Greten TF. Gut microbiome in HCC – Mechansisms, diagnosis and therapy. *J Hepatol*. (2020) 72:230–8. doi: 10.1016/j.jhep.2019.08.016

62. Luther J, Garber JJ, Khalili H, Dave M, Bale SS, Jindal R, et al. Hepatic injury in nonalcoholic steatohepatitis contributes to altered intestinal permeability. *Cell Mol Gastroenterol Hepatol*. (2015) 1:222–32. doi: 10.1016/j.jcmgh.2015.01.001

63. Chang CS, Chen GH, Lien HC, Yeh HZ. Small intestine dysmotility and bacterial overgrowth in cirrhotic patients with spontenous bacterial peritonitis. *Hepatology*. (1998) 28:1187–90. doi: 10.1002/hep.510280504

64. Kakiyama G, Pandak WM, Gillevet PM, Hylemon PB, Heuman DM, Daita K, et al. Modulation of the fecal bile acid profile by gut microbiota in cirrhosis. *J Hepatol*. (2013) 58:949–55. doi: 10.1016/j.jhep.2013.01.003

65. Ren Z, Li A, Jiang J, Zhou L, Yu Z, Lu H, et al. Gut microbiome analysis as a tool towards targeted non-invasive biomarkers for early hepatocellular carcinoma. *Gut*. (2019) 68:1014–23. doi: 10.1136/gutjnl-2017-315084

66. Ma C, Han M, Heinrich B, Fu Q, Zhang Q, Sandhu M, et al. Gut microbiome-mediated bile acid metabolism regulates liver cancer via NKT cells. *Science*. (2018) 360:531. doi: 10.1126/science.aan5931

67. Yu LX, Yan HX, Liu Q, Yang W, Wu HP, Dong W, et al. Endotoxin accumulation prevents carcinogen-induced apoptosis and promotes liver tumorigenesis in rodents. *Hepatology*. (2010) 52:1322–33. doi: 10.1002/hep.23845

68. Tijhuils AE, Johnson SC, McClelland SE. The emerging links between chromosomal instability (CIN), me-tastasis, inflammation and tumor immunity. *Mol Cytogenet*. (2019) 12:17. doi: 10.1186/s13039-019-0429-1

69. Xu M, Zhao X, Wen X, Qu X. Unveiling the role of KRAS in tumor immune microenvironment. *Biomed Pharmacother*. (2024) 171:116058. doi: 10.1016/j.biopha.2023.116058

70. Pereira F, Ferreira A, Reis CA, Sousa MJ, Olivera MJ, Preto A. KRAS as a modulator of the inflammatory tumor microenvironment: therapeutic implications. *Cells*. (2022) 11:398. doi: 10.3390/cells11030398

71. Pylayeva-Gupta Y, Lee KE, Hajdu CH, Miller G, Bar-Sagi D. Oncogenic Kras-induced GM-CSF production promotes the development of pancreatic neoplasia. *Cancer Cell*. (2012) 21:836–47. doi: 10.1016/j.ccr.2012.04.024

72. Cheng H, Fan K, Luo G, Fan Z, Yang C, Huang Q, et al. KrasG12D mutation contributes to regulatory T cell conversation through activation of the MEK/ERK pathway in pancreatic cancer. *Cancer Lett*. (2019) 446:103–11. doi: 10.1016/j.canlet.2019.01.013

73. Liao W, Overman MJ, Boutin AT, Shang X, Zhao DI, Dey P, et al. KRAS-IRF2 axis drives immune suppression and immune therapy resistance in colorectal cancer. *Cancer Cell*. (2019) 35:559–72. doi: 10.1016/j.ccell.2019.02.008

74. Hoare M, Ito Y, Kang TW, Weekes MP, Matheson NJ, Patten DA, et al. NOTCH1 mediates a switch between two distinct secretomes during senescence. *Nat Cell Biol*. (2016) 18:979–92. doi: 10.1038/ncb3397

75. Kumagal S, Koyama S, Nishikawa H. Antitumor immunity regulated by aberrant ERBB family signalling. *Nat Rev Cancer*. (2021) 21:181–7. doi: 10.1038/s41568-020-00322-0

76. Hermann F, Lehr HA, Drexler I, Sutter G, Hengstler J, Wollscheid U, et al. HER-2/neu-mediated regu-lation of component s of the MHC class I antigen-processing pathway. *Cancer Res*. (2004) 64:215–20. doi: 10.1158/0008-5472.can-2522-2

77. Park S, Jiang Z, Mortenson ED, Deng L, Radkevich-Brown O, Yang X, et al. The therapeutic effect of anti-HER2/neu-antibody depends on both innate and adaptive immunity. *Cancer Cell*. (2010) 18:160–70. doi: 10.1016/j.ccr.2010.06.014

78. Pilley S, Rodriguez TA, Vousten KH. Mutant p53 in cell-cell interactions. *Genes Dev*. (2021) 35:433–48. doi: 10.1101/gad.347542.120

79. Wellenstein MD, Coffelt SB, Duits DEM, van Miltenburg MH, Slagter M, de Rink I, et al. Loss of p53 triggers WNT-dependent systemic inflammation to drive breast cancer metastasis. *Nature*. (2019) 572:538–42. doi: 10.1038/s41586-019-1450-6

80. Chen X, Zhang T, Su W, Dou Z, Zhao D, Jin X, et al. Mutant p53 in cancer: from molecular mechanism to therapeutic modulation. *Cell Death Dis*. (2022) 13:974. doi: 10.1038/s41419-022-05408-1

81. Turizo-Smith AD, Cordoba-Hernandez S, Mejia-Guarnizo LV, Monroy-Camacho PS, Rodiriquez-Garcia JA. Inflammation and cancer: friend or foe? *Front Pharmacol*. (2024) 15:1385479. doi: 10.3389/fphar.2024.1385479

82. Parrales A, Iwakuma T. Targeting oncogenic mutant p53 for cancer therapy. *Front Oncol*. (2015) 5:288. doi: 10.3389/fonc.2015.00288

83. Blagih J, Zani F, Chakravarty P, Hennequart M, Pilley S, Hobor S, et al. Cancer-specific loss of p53 leads to modulation of myeloid and T cell responses. *Cell Rep*. (2020) 30:481–96. doi: 10.1016/j.celrep.2019.12.028

84. Lujambio A, Akkari L, Simon J, Grace D, Tscharganeh DF, Bolden JE, et al. Non-cell-autonomous tumor suppression by p53. *Cell*. (2013) 153:449–60. doi: 10.1016/j.cell.2013.03.020

85. Cooks T, Pateras IS, Jenkins LM, Patel KM, Robles AI, Morris J, et al. Mutant p53 cancers reprogram macrophages to tumor supporting macrophages via exosomal miR-1246. *Nat Commun*. (2018) 9:771. doi: 10.1038/s41467-018-03224-w

86. Kao K-C, Vilbois S, Tsai C-H, Ho P-C. Metabolic communication in the tumor-immune microenvironment. *Nat Microbiol*. (2022) 24:1574–83. doi: 10.1038/s41556-022-01002-x

87. Courvan EMC, Parker RR. Hypoxia and inflammation induce synergistic transcriptome turnover in macropgahes. *Cell Rep*. (2024) 43:114452. doi: 10.1016/j.celrep.2024.114452

88. Mello AM, Ngodup T, Lee Y, Donahue KL, Li J, Rao A, et al. Hypoxia promotes an inflammatory phenotype of fibroblasts in pancreatic cancer. *Oncogenesis*. (2022) 11:56. doi: 10.1038/s41389-022-00434-2

89. Viola A, Munari F, Sanchez-Rodriguez R, Scolaro T, Castegna A. The metabolic signature of macrophage responses. *Front Immunol*. (2019) 10:1946. doi: 10.3389/fimmu.2019.01462

90. Yu Y-R, Imrichova H, Wang H, Chao T, Xiao Z, Gao M, et al. Disturbed mitochondrial dynamics in CD8+ T TILs reinforce T cell exhaustion. *Nat Immunol*. (2020) 21:1540–51. doi: 10.1038/s41590-020-0793-3

91. Doedens AI, Phan AT, Stradner MH, Fujimoto JK, Nguyen JV, Yang E, et al. Hypox-ia-inducible factors enhance the effector responses of CD8+ T cells to persistent antigen. *Nat Immunol*. (2013) 14:1173–82. doi: 10.1038/ni.2714

92. Murray PJ, Allen JE, Biswas SK, Fisher EA, Gilray DW, Goerdt S, et al. Macrophage activation and polarization: nomenclature and experimental guidelines. *Immunity*. (2014) 41:14–20. doi: 10.1016/j.immuni.2014.06.008

93. Bouer R, Meyer SP, Kloss KA, Gueurero Ruiz VM, Reuscher S, Zhou Y, et al. Functional RNA dynamics are progressively Governed by RNA Destabilization During the Adaptation to Chronic Hypoxia. *Int J Mol Sci*. (2022) 23:5824. doi: 10.3390/ijms23105824

94. Grivennikov SI, Wang K, Mucida D, Stewart CA, Schnabi B, Jauch D, et al. Adenoma-linked barrier defects and microbial products drive IL-23/IL-17-mediated tumor growth. *Nature*. (2012) 491:254–8. doi: 10.1038/nature11465

95. Akkız H. Emerging role of cancer-associated fibroblast in the pathogenesis and treatment of hepatocellular carcinoma. *Int J Mol Sci*. (2023) 24:3941. doi: 10.3390/ijms24043941

96. Kim J, Bae JS. Tumor-associated macrophages and neutrophils in tumor microenvironment. *Mediators In-flamm*. (2016) 2016:6058147. doi: 10.1155/2016/6058147

97. Shu Y, Qin M, Song Y, Tang Q, Huang Y, Shen F, et al. M2 polarization of tumor-associated macrophages is dependent on integrin β3 via peroxisome proliferator-activated receptor-γ up-regulation in breast cancer. *Immunology*. (2020) 160:345–56. doi: 10.1111/imm.v160.4

98. Wang M, Chen S, He X, Wei X. Targeting inflammation as cancer therapy. *J Hematol Oncol*. (2024) 17:13. doi: 10.1186/s13045-024-01528-7

99. Lewis CE, Pollard JW. Distinct role of macrophages in different tumor microenvironments. *Cancer Res*. (2006) 66:605–12. doi: 10.1158/0008-5472.CAN-05-4005

100. Bied M, Ho WW, Bieriot C. Roles of macrophages in tumor development: a spatiotemporal perspective. *Cell Mol Immunol*. (2023) 20:983–92. doi: 10.1038/s41423-023-01061-6

101. Kennedy L. Tilting the scales: Sirtuin 1 favors proinflammatory macrophage response via inflammasome signaling and metabolic reprogramming. *Cell Mol Gastroenterol Hepatol*. (2022) 13:1261–2. doi: 10.1016/j.jcmgh.2022.01.011

102. Baer JM, Zuo C, Kang L-I, de la Lastra AL, Borcherding NC, Knolhoff BL, et al. Fibrosis induced by resident macrophages has divergent roles in pancreas inflammatory injury and PDAC. *Nat Immunol*. (2023) 24:1443–57. doi: 10.1038/s41590-023-01579-x

103. Bleriot C, Dunsmore G, Alanso-Curbela D, Ginhoux F. A temporal perpective for tumor-associated mac-rophage identities and functions. *Cancer Cell*. (2024) 42:747–58. doi: 10.1016/j.ccell.2024.04.002

104. Mantovani A, Allavena P, Marchesi F, Garlanda C. Macrophages as tools and targets in cancer therapy. *Nat Rev*. (2022) 21:799–820. doi: 10.1038/s41573-022-00520-5

105. Vonderlin J, Chavakis T, Sieweke M, Tackle F. The multifaced roles of macrophages in NAFLD pathogenesis. *Cell Mol Gastroenterol Hepatol*. (2023) 15:1311–24. doi: 10.1016/j.jcmgh.2023.03.002

106. Carnevale S, Di Caglie I, Grieco G, Rigatelli A, Bonavita E, Jeillons S. Neutrophil diversity in inflammation and cancer. *Front Immunol*. (2024) 14:1180810. doi: 10.3389/fimmu.2023.1180810

107. Del Prete A, Salvi V, Sariani A, Lattranchi M, Sozio F, Bosisşo D, et al. Dendritic cell subsets in cancer immunity and tumor antigen sensing. *Cell Mol Immunol*. (2023) 20:432–47. doi: 10.1038/s41423-023-00990-6

108. Catanzaro E, Beltron-Viseedo M, Galluzi L, Krysko DV. Immunogenicity of cell death and cancer immunity with immune checkpoint inhibitors. *Nat Cell Mol Immunol*. (2025) 22:24–39. doi: 10.1038/s41423-024-01245-8

109. Wu Y, Yi M, Niu Q and Wu K. Myeloid-derived suppressor cells: an emerging target for anticancer immunothjerapy. *Mol Cancer*. (2022) 21:184. doi: 10.1186/s12943-022-01657-y

110. Thommen DS, Schumacher TN. T cell dysfunction in cancer. *Cancer Cell*. (2018) 33:547–62. doi: 10.1016/j.ccell.2018.03.012

111. Crespo J, Sun H, Welling TH, Tian Z, Zou W. T cell anergy, exhaustion, senescence, and stemness in the tumor microenvironment. *Curr Opin Immunol*. (2013) 25:214–21. doi: 10.1016/j.coi.2012.12.003

112. Knutson KL, Disis ML. Tumor-antigen specific T helper cells in cancer immunity and immunotherapy. *Cancer Immunol Immunother*. (2005) 54:721–8. doi: 10.1007/s00262-004-0653-2

113. Koh C-H, Lee S, Kwak M, Kim B-S, Chung Y. CD8 T-cell subsets: heterogeneity, functions, and therapeutic potential. *Exp Mol Med*. (2023) 55:2287–99. doi: 10.1038/s12276-023-01105-x

114. Seo W, Jerin C, Nishikawa H. Transcriptional regulatory network for the establishment of CD8+ T cell ex-haustion. *Exp Mol Med*. (2021) 53:202–9. doi: 10.1038/s12276-021-00568-0

115. Vignali PDA, DePeaux K, Watson MJ, Ye C, Ford BR, Lontos K, et al. Hypoxia drives CD39-dependent suppressor function in exhausted T cells to limit antitumor immunity. *Nat Immunol*. (2023) 24:267–79. doi: 10.1038/s41590-022-01379-9

116. Chow A, Perica K, Klebanoff CA, Wolchok JD. Clinical implications of T cell exhaustion for cancer immu-notherapy. *Nat Rev Clin Oncol*. (2022) 19:775–92. doi: 10.1038/s41571-022-00689-z

117. Wouters MCA, Nelson BH. Prognostic significance of tumor-infiltrating B cells and plasma cells in human cancer. *Clin Cancer Res*. (2018) 24:6125–35. doi: 10.1158/1078-0432.CCR-18-1481

118. Jin K, Quian C, Lin C, Liu B. Cyclooxygenase-2-prostaglandin E2 pathway: A key player in tumor-associated immune cells. *Front Oncol*. (2023) 13:1099811. doi: 10.3389/fonc.2023.1099811

119. Bell CR, Pelly VS, Moeini A, Chiang S-C, Flanagan E, Bromley CP, et al. Chenotherapy-induced COX-2 upregulation by cancer cells defines their inflammatory properties and limits the efficacy of chemoimmunotherapy combinations. *Nat Commun*. (2022) 13:2063. doi: 10.1038/s41467-022-29606-9

120. Gomez-Valenzuela F, Escobbar E, Perez-Tomas R, Montecinos VP. The inflammatory profile of the tumor microenvironment, orchestrated by cyclooxygenase-2, promotes epithelial-mesenchymal transition. *Front Oncol*. (2021) 11:686792. doi: 10.3389/fonc.2021.686792

121. Kahnt AS, Hafner A-K, Steinhibber D. The role of human 5-Lipoxygenase (5-LO) in carcinogenesis – a question of canonical and non-canonical functions. *Oncogene*. (2024) 43:1319–27. doi: 10.1038/s41388-024-03016-1

122. Zamora A, Nougue M, Verdue L, Balzan E, Drala-Nicolau T, Benuzzi E, et al. 15-Lioxygenase promotes resolution of inflammation in lymphedema by controlling Treg cell function through IFN-β. *Nat Commun*. (2024) 15:221. doi: 10.1038/s41467-023-43554-y

123. Kazan HH, Urfali-Mamatoglu C, Yalcin GD, Bulut O, Sezer A, Banerjee U. 15-LOX-1 has diverse roles in the resensitization of resistant cancer lines to doxorubicin. *J Cell Physiol*. (2020) 235:4965–78. doi: 10.1002/jcp.v235.5

124. Xue C, Yao Q, Gu X, Shi Q, Yuan X, Chu Q, et al. Evolving cognition of the JAK-STAT signaling pathway: autoimmune disorders and cancer. *Signal Transduct Target Ther*. (2023) 8:204. doi: 10.1038/s41392-023-01468-7

125. Hu X, Li J, Fu M, Zhao X, Wang W. The JAK/STAT signaling pathway: from bench to clinic. *Signal Transduct Target Ther*. (2021) 6:402. doi: 10.1038/s41392-021-00791-1

126. Hu Y, Dong Z, Liu K. Unraveling the complexity of STAT3 in cancer: molecular understnading and drug discovery. *J Exp Clin Cancer Res*. (2024) 43:23. doi: 10.1186/s13046-024-02949-5

127. Qadir J, S-y W, Yuan H, Yang BB. CircRNAs regulate the crosstalk between inflammation and tumorigenesis: The bilateral association and molecular mechanisms. *Mol Ther*. (2023) 31:1514–35. doi: 10.1016/j.ymthe.2022.12.005

128. Zhong X, Ott M, Sharma, Balakrishnan A. MicroRNA-107 – a small RNA with a big impact on cytokinesis in hepatocellular carcinoma. *J Hepatol*. (2025) 82:414–6. doi: 10.1016/j.jhep.2024.09.045

129. Strasser A, Vaux DL. Cell death in the origin and treatment of cancer. *Mol Cell*. (2020) 78:1045–56. doi: 10.1016/j.molcel.2020.05.014

130. Galluzi L, Kepp O, Hett E, Kroemer MM. Immunological cell death in cancer: concept and therapeutic implications. *J Trans Med*. (2023) 21:162. doi: 10.1186/s12967-023-04017-6

131. Wu X, Cao J, Wan X, Du S. Programmed cell death in hepatocellular carcinoma: mechanisms and therapeutic perspective. *Nature*. (2024) 10:356. doi: 10.1038/s41420-024-02116-x

132. Tong X, Tang R, Xiao M, Xu J, Wang W, Zhang B, et al. Targeting cell death pathways for cancer therapy: recent developments in necroptosis, pyroptosis, ferroptosis, and cuproptosis research. *J Hematol Oncol*. (2022) 15:174. doi: 10.1186/s13045-022-01392-3

133. Liu S, Wang W, Hu S, Jia B, Tuo B, Sun H, et al. Radiotherapy remodels the tumor microenvironment for enhancing immunotehrapeutic sensitivity. *Nature*. (2023) 14:679. doi: 10.1038/s41419-023-06211-2

134. Galluzi L, Gulibbaud E, Schmidt D, Kroemer G, Marincola FM. Targeting immunologenic cell deat stress and death for cancer therapy. *Nat Rev*. (2024) 23:445–60. doi: 10.1038/s41573-024-00920-9

135. Hirata E, Sahai E. Tumor microenvironment and differential responses to therapy. *Cold Spring Harb Perspect Med*. (2017) 7:026781. doi: 10.1101/cshperspect.a026781

136. Li H, Zhou L, Zhou J, Li Q, Ji Q. Underlying mechanisms and drug intervention strategies for the tumor microenvironment. *J Exp Clin Cancer Res*. (2021) 40:97. doi: 10.1186/s13046-021-01893-y

137. Rivera G, Wakelee HA. Resistance to therapy. *Cancer Treat Res*. (2016) 170:183–202. doi: 10.1007/978-3-319-40389-2_9

138. Jaffray DA. Image-guided radiotherapy: from current concept to future perpectives. *Nat Rev Clin Oncol*. (2012) 9:688–99. doi: 10.1038/nrclinonc.2012.194

139. McLoughlin M, Patin EC, Pedersen M, Wilkins A, Dillon MT, Melcher AA, et al. Inflammatory microenvironment remodeling by tumor cells after radiotherapy. *Nat Rev Cancer*. (2020) 20:203–17. doi: 10.1038/s41568-020-0246-1

140. Li M, Bhoori S, Mehta N, Mazzaferro V. Immunotherapy for hepatocellular carcinoma: The next evoluation in expanding access to liver transplantation. *J Hepatol*. (2024) 81:743–55. doi: 10.1016/j.jhep.2024.05.037

141. Rimassa L, Finn RS, Sangro B. Combination immunotherapy for hepatocellular carcinoma. *J Hepatol*. (2023) 79:506–15. doi: 10.1016/j.jhep.2023.03.003

142. Celsa C, Cabibbo G, Fulgenzi CCA, Camma C, Cortellini A, Pinato DJ. Characteristics and outcomes of immunotherapy-related liver injury in patients with hepatocellular carcinoma versus other advanced solid tumors. *J Hepatol*. (2024) 80:431–42. doi: 10.1016/j.jhep.2023.10.040

143. Meng L, Wu H, Wu J, Ding P, He J, Sang M, et al. Mechanims of immune checkpoint inhibitors: insights into the regulation of circular RNAs involved in cancer hallmarks. *Cell Death Dis*. (2024) 15:3. doi: 10.1038/s41419-023-06389-5

144. Hou J, Karin M, Sun B. Targeting cancer-promoting inflammation – have anti-inflammatory therapies come of age? *Nat Reviews/Clinical Oncol*. (2021) 18:261–78. doi: 10.1038/s41571-020-00459-9

145. Duan X-P, Qin B-D, Jio X-D, Liu K, Wang Z, Zang Y-S. New clinical trial design in precision medicine: discovery, development and direction. *Signal Transduct Target Ther*. (2024) 9:57. doi: 10.1038/s41392-024-01760-0

146. Lu S, li Y, Zhu C, Wang W, Zhou Y. Managing cancer drug resistance from the perspective of inflammation. *J Oncol*. (2022) 1:3426407. doi: 10.1155/2022/3426407

147. Rossi J-F, Lu ZY, Massart C, Levon K. Dynamic immune/inflammation precision medicine: the good and the bad inflammation in infection and cancer. *Front Immunol*. (2021) 12:595722. doi: 10.3389/fimmu.2021.595722

148. Bibbins-Domingo K, U.S. Preventive Services Task Force. Aspirin use for the primary prevention of cardiovascular disease and colorectal cancer: U.S. preventive service task force recommendation statement. *Ann Intern Med*. (2016) 164:836–45. doi: 10.7326/M16-0577

149. Simon TG, Duberg AS, Aleman S, Chung RT, Chan AT, Ludvigsson JF. Association of aspirin with hepatocellular carcinoma and liver-related mortality. *N Eng J Med*. (2020) 382:1018–28. doi: 10.1056/NEJMoa1912035

150. Lee TY, Hsu YC, Tseng HC, Yu SH, Lin JT, Wu MS. Association of daily aspirin therapy with risk of hepatocellular carcinoma in patients with chronic hepatitis B. *JAMA Intern Med*. (2019) 179:633–40. doi: 10.1001/jamainternmed.2018.8342

151. Liao X, Lochhead P, Nishihara R, Morikawa T, Kuchiba A, Yamauchi M. Aspirin use, tumor PIK3CA mutation, and colorectal cancer survival. *N Eng J Med*. (2012) 367:1596–606. doi: 10.1056/NEJMoa1207756

152. Beragnolli MM, Eagle CJ, Zauber AG, Redston M, Solomon SD, Kim K, et al. Celexoxib for the prevention of sporadic colorectal adenomas. *N Eng J Med*. (2006) 355:873–95. doi: 10.1056/NEJMoa061355

153. Yang JD, Hainaut P, Gores GJ, Amadou A, Plymoth A, Roberts LR. A global view of hepatocellular carcinoma: trends, risk, prevention and management. *Nat Rev Gastroenterol Hepatol*. (2019) 16:589–604. doi: 10.1038/s41575-019-0186-y

154. de Sanjuse S, Quint WG, Alemany L, Geraets DT, Klaustermeier JE, Lloveras B. Human Papillomavirus genetype attribution in invasive servical cancer: a retrospective cross-sectional worldwide study. *Lancet Oncol*. (2010) 11:1048–56. doi: 10.1016/S1470-2045(10)70230-8

155. Ridker PM, Brendon M, Everett M, Thuren T, MacFadyen JG, Chang WH, et al. Antiinflammatory therapy with canakinumab for atherosclerotic disease. *N Eng J Med*. (2017) 337:1119–31. doi: 10.1056/NEJMoa1707914

156. Melisi D, Garcia-Carbonero R, Macarulla T, Pezet D, Deplanque G, Fuchs M. Galunisertib and gemcitabine vs. gemcitabine for firt-line treatment of patients with unresectable pancreatic cancer. *Br J Cancer*. (2018) 119:1208–14. doi: 10.1038/s41416-018-0246-z

157. Monk JP, Phillips G, Waite R, Kuhn J, Schaaf LJ, Otterson GA, et al. Assesment of tumor necrosis factor alpha blockade on an intensive chemotherapy in cancer patients. *J Clin Oncol*. (2006) 24:1852–9. doi: 10.1200/JCO.2005.04.2838

158. Zeng Z, Jiang M, Li X, Yuan J, Zhang H. Precision medicine in inflammatory bowel disease. *Precis Clin Med*. (2023) 6. doi: 10.1093/pcmedi/pbad033

159. Casey SC, Tong L, Li Y, Do R, Walz S, Fitzgerald KN, et al. MYC regulates the antitumor immune response through CD47 and PD-L1. *Science*. (2016) 352:227–31. doi: 10.1126/science.aac9935

160. Lopez L, Morosi LG, la Terza F, Bourdely P, Rospo G, Amadio R, et al. Dendritic cell-targeted therapy expands CD8+ T cell responses to bona-fide neoantigens in lung tumors. *Nat Commun*. (2024) 15:2280. doi: 10.1038/s41467-024-46685-y

161. Smith HA, Kang YJJ. The metastasis-promoting roles of tumor-associated immune cells. *J Mol Med*. (2013) 91:411–29. doi: 10.1007/s00109-013-1021-5

162. Lopes N, Vivier E, Narni-Mancinelli E. Natural killer cells and type 1 innate lymphoid cells in cancer. *Semin Immunol*. (2023) 66:101709. doi: 10.1016/j.smim.2022.101709

163. Coenon L, Geindreau M, Ghiringbelli F, Villalba M, Bruchard M. Natural Killer cells at the frontline in the fight against cancer. *Cell Death Dis*. (2024) 15:614. doi: 10.1038/s41419-024-06976-0

164. Tian C, Wang Y, Su M, Huang Y, Zhang Y, Dou J, et al. Motility and tumor infiltration are key aspects of invariant natural killer T cell anti-tumor function. *Nat Commun*. (2024) 15:1213. doi: 10.1038/s41467-024-45208-z

165. Tabrizan P, Abdelrahim M, Schwartz M. Immunotherapy and transplantation for hepatocellular carcinoma. *J Hepatol*. (2024) 80:822. doi: 10.1016/j.jhep.2024.01.011

frontiers | Frontiers in Immunology

TYPE Original Research
PUBLISHED 27 March 2025
DOI 10.3389/fimmu.2025.1570502

Check for updates

OPEN ACCESS

EDITED BY
Xiaosheng Tan,
Rutgers, New Brunswick, United States

REVIEWED BY
Mengliu Zhu,
Chinese Academy of Medical Sciences and Peking Union Medical College, China
Yabing Nan,
Dana–Farber Cancer Institute, United States
Jin-Ming Zhang,
University of Texas Health Science Center at Houston, United States
Zilu Chen,
Rutgers, The State University of New Jersey, United States

*CORRESPONDENCE
Danke Su
sudanke33@sina.com

RECEIVED 03 February 2025
ACCEPTED 10 March 2025
PUBLISHED 27 March 2025

CITATION
Xiang T, Li H, Wang X and Su D (2025) Melanocortin-1 receptor expression as a predictive factor for postoperative outcomes in melanoma patients: a retrospective study. *Front. Immunol.* 16:1570502. doi: 10.3389/fimmu.2025.1570502

COPYRIGHT
© 2025 Xiang, Li, Wang and Su. This is an open-access article distributed under the terms of the Creative Commons Attribution License (CC BY). The use, distribution or reproduction in other forums is permitted, provided the original author(s) and the copyright owner(s) are credited and that the original publication in this journal is cited, in accordance with accepted academic practice. No use, distribution or reproduction is permitted which does not comply with these terms.

Melanocortin-1 receptor expression as a predictive factor for postoperative outcomes in melanoma patients: a retrospective study

Tian Xiang[1,2], Haiying Li[2], Xiaowei Wang[3] and Danke Su[1]*

[1]Department of Radiology, Guangxi Medical University Cancer Hospital, Guangxi Medical University, Nanning, Guangxi, China, [2]Department of Nuclear Medicine, The Second Xiangya Hospital, Central South University, Changsha, Hunan, China, [3]Department of Pathology, The Second Xiangya Hospital, Central South University, Changsha, Hunan, China

Background and objective: This study aims to explore the relationship between melanocortin-1 receptor (MC1R) expression levels and clinical pathological parameters of melanoma, as well as its potential as a prognostic biomarker.

Methods: This retrospective study included 99 melanoma patients in our hospital from June 2017 to July 2023. MC1R expression was assessed by immunohistochemistry assays. Histochemistry score (H-score) determined the level of MC1R immunohistochemistry expression in melanoma. The relationships among MC1R expression, clinical pathological parameters in melanoma patients were assessed using Chi-square and Fisher's precision probability tests. Kaplan-Meier assay and log-rank test were utilized to estimate survival curves. Potential independent factors among the enrolled patients were investigated using COX regression analysis.

Results: According to median value of H-score, 38 cases with low MC1R expression and 61 cases with high MC1R expression in melanoma tumor tissues were observed. Patients with high MC1R expression in melanoma tissues exhibited a worse prognosis compared to patients with low MC1R expression. The survival time difference was statistically significant [MC1R expression in melanoma tumor tissue (MC1RT): median DFS, 12.83 vs. 17.53 months, $\chi2$ = 5.395, P=0.0202; median OS, 16.47 vs. 21.77 months, $\chi2$ = 5.082, P=0.0243. MC1R expression in normal adjacent to melanoma tissue (MC1RN): median DFS, 12.03 vs. 14.29 months, $\chi2$ = 6.864, P=0.0088; median OS, 16.73 vs. 21.77 months, $\chi2$ = 5.649, P=0.0175]. Multivariate COX regression model analysis indicated that MC1RN, MC1RT, sex, ESR, tumor site, targeted therapy, and immunotherapy were potential prognostic factors for the DFS. Furthermore, MC1RN, MC1RT, sex, tumor site, TLN, PLN, and immunotherapy were potential prognostic factors for the OS. Calibration curve indicated the predicted probabilities of nomogram models were in accordance with the actual probabilities, and the prediction accuracy was relatively high at one year and three years following surgery. The decision clinical curve revealed that the nomogram models had better predictive performance for DFS and OS than the MC1RT or MC1RN thresholds.

Conclusions: Low MC1R expression in melanoma tumor tissues and adjacent normal tissue might be beneficial for the prognosis of melanoma patients. MC1R was a predictive factor for the prognosis of melanoma patients. Nomogram models based on MC1R demonstrated good prediction ability.

KEYWORDS

melanoma, MC1R, tumor site, immunotherapy, prognosis

Introduction

Melanoma is a common malignant tumor of skin, characterized by early metastasis and poor prognosis (1). Globally, more than 280,000 (1.6%) new cases of melanoma occur each year, with over 60,000 (0.6%) deaths due to this disease (2). Recently, the incidence rate of melanoma is increasing rapidly in China (3). Approximately one new case of melanoma occurs in every 300,000 individuals, and one out of every 500,000 deaths is due to melanoma (4). The primary treatment for melanoma is surgery that complemented by adjuvant therapy, such as chemotherapy or radiotherapy (5). The five-year survival rate for localized melanoma is 98%, with a 64% survival rate for regional metastasis, and distant metastasis exhibits a 23% survival rate (6).

Melanocortin-1 receptor (MC1R) was first cloned by the Chhajlani and Mountjoy research groups in 1992, and composed of 317 amino acids (5). MC1R is expressed in human melanoma cells, and plays a critical role in skin tone and hair color formation (7). Some studies have shown that MC1R expression is associated with the prognosis of tumors. For example, elevated expression of MC1R in colorectal cancer (CRC) is associated with microsatellite instability (MSI) (8). In Chelakkot's study, cell proliferation was significantly reduced *in vitro* and *in vivo* when the MC1R gene was knocked out (9). MC1R expression could be an auxiliary molecular marker in diagnosing esophageal squamous cell carcinoma (10). Another study also indicated that elevated MC1R expression levels were significantly associated with a lower recurrence of the free-survival rate in ovarian cancer (11).

Recently, MC1R has attracted the interest of numerous researchers as a target for melanoma. Chen's study indicated that the APT2 inhibitor ML349 increased MC1R signaling and inhibited UVB-induced melanoma formation (12). Another study shown red-hair variant of MC1R exhibited differences in the pigmentation phenotype between males and females, and patients with the red-hair MC1R variant had an increased risk of developing melanoma (13). Yang's study demonstrated that the peptide 68Ga-DOTA-GGNe CycMSHhex could specifically bind to MC1R, and the labeled peptide revealed melanoma metastases. Moreover, this peptide could bind to MC1R on the cell surface of melanoma brain metastases, indicating that this peptide exhibited excellent potential as a signal in imaging examinations of melanoma patients with brain metastases (14). However, few studies have systematically examined MC1R expression in melanomas in patients with gender, TNM stage, or tumor sites. Thus, the ability of MC1R expression to predict the survival rate for melanoma patients is still controversial.

The current study retrospectively analyzed the expression level of MC1R in melanoma patients, and evaluated the correlation between MC1R expression and clinical pathological indicators. This study also explored whether MC1R expression could serve as a prognostic biomarker for predicting prognosis for melanoma patients.

Materials and methods

Patients

Ninety-nine melanoma patients admitted to our hospital from June 2017 to July 2023 were enrolled into this retrospective analysis. The enrolled patients received surgical treatment and histological specimens were obtained. This research received approval from the ethical committee of Second Xiangya Hospital of Central South University, written informed consent was obtained from each participant.

Inclusion and exclusion criteria

Inclusion criteria included: (1) Histopathological diagnosis of melanoma; (2) Received surgical treatment and histopathological specimens were obtained; (3) A complete hematology examination, pathology, follow-up information were obtained. Exclusion criteria included: (1) Underwent anti-tumor treatment before surgery, such as chemotherapy, radiotherapy, immunotherapy; (2) Additional diseases were present, such as hypertension, diabetes, and coronary heart disease that were difficult to control; (3) Incomplete information was provided.

Tissue processing and immunohistochemistry

Melanoma tissue samples were obtained from our hospital, and fixed in formalin and embedded in paraffin, following routine

protocols. Immunohistochemistry was performed based on standard protocols as follows. (1) Paraffin removal and clearing. (2) Antigen retrieval. (3) Blocking endogenous peroxidases. (4) Serum blocking. (5) Primary antibody. MC1R antibody (ab236734, 1:200, Waltham, MA, USA) was added to the tissue sections overnight. (6) Secondary antibody. HRP-conjugated Goat Anti-Mouse IgG (H+L) (GB23301, 1:500, Wuhan, China) in a humid chamber for two hours. (7) DAB staining. The sections were rinsed, and a freshly prepared DAB colorimetric solution was added. (8) Nuclear staining. The cell nuclei in the tissue sections were stained with hematoxylin for approximately three minutes. (9) Dehydration and cover-slipping. (10) Microscopic examination. Images of the stained, cover-slipped tissue sections were assessed using Aipathwell image acquisition and analyzed.

Immunohistochemical scoring criteria for MC1R expression

Aipathwell is a digital pathological image analysis software program based on artificial intelligence learning. Histochemistry scores (H-scores) were obtained using a histological scoring method for the immunohistochemically stained tissue sections. It converted the ratio of positively stained cells and staining intensity into corresponding values to achieve a comprehensive semi-quantitative analysis of the degree and quantity of positive tissue immunostaining. The H-Score was calculated as follows: (Σ(pi×i) = weak intensity cells (%) ×1 + moderate intensity cells (%) ×2 + strong intensity cells (%) ×3. According to the scheme, **i** represented the staining intensity of the positive cells: 1) Negative = no staining, 0 point; 2) Weak positive (light yellow) = 1 point; 3) Moderately positive (brownish yellow) = 2 points; 4) Strong positive (brown) = 3 points. Pi represented the percentage of positive cells at the corresponding level. The value of H-score ranged from 0 to 300.

In the current study, we analyzed the expression level of MC1R in tumor tissues and adjacent normal tissue, respectively. These patients were divided into two groups based on the median value of H-Score. The expression level of MC1R in tumor tissues with an H-Score ≤ 6.90 indicated low expression of MC1R (38 cases), while an H-Score>6.90 indicated high MC1R expression (61 cases). Considering the MC1R expression in adjacent normal tissues, an H-Score ≤ 3.61 indicated low expression of MC1R (58 cases), and an H-Score>3.61 indicated high MC1R expression (41 cases).

Follow-up

All enrolled patients in the study were followed through telephone interviews and outpatient visits. Follow-up assessments included routine blood analysis, blood biochemistry, coagulation function, tumor markers, magnetic resonance imaging, and others. The patients were assessed every three months after surgery. In this study, disease free survival (DFS) was referred to the duration between the time from the diagnosis of melanoma at admission and the discovery of local or distant melanoma metastasis, or the date of the last visit. Overall survival (OS) was referred to the duration between the time from the diagnosis of melanoma at admission and death from any cause or the last visit.

Statistical methods

All statistical analyses were conducted using SPSS Statistics software 29.0 (IBM Corp, https://www.ibm.com/sps), as well as R software (version 4.2.2; Vienna, Austria URL: http://www.R-project.org/). The chi-square and Fisher's precision probability tests were applied to assess the relationship between MC1R and the clinical pathological characteristics of melanoma patients. The Cox proportional hazards regression model was employed to identify the underlying independent variables that were associated with DFS and OS. Kaplan-Meier method was utilized for computing the survival curves of DFS and OS, followed by a comparison using the log-rank test. In view of the multivariate COX regression analysis of the potential prognostic factors, nomograms were constructed to predict the DFS and OS in the melanoma patients. Calibration curves and decision curve analyses were used to assess the calibration and practicality of the model. $P<0.05$ was considered statistically significant.

Results

MC1R expression in melanoma patients and its relationship with prognosis

MC1R expression was detected using immunohistochemistry for the 99 melanoma patients enrolled into this study. The expression of MC1R in melanoma tumor tissues was significantly higher than that in adjacent normal tissue, and differential expression was observed in different melanoma patients (Supplementary Figure S1). The representative MC1R immunohistochemistry images of melanoma patients were performed in Figures 1A–D.

Based on the immunohistochemical staining results by H-Score, there were 38 cases with low MC1R expression and 61 cases with high MC1R expression in melanoma tumor tissues. Melanoma patients exhibiting high MC1R expression experienced a shorter survival time. The difference in survival times was statistically significant (median DFS: 12.83 months vs. 17.53 months, χ^2 = 5.395, P=0.0202; median OS: 16.47 months vs. 21.77months, χ^2 = 5.082, P=0.0243) (Figures 2A, B).

When normal tissues adjacent to melanoma sites were examined, 58 cases with low expression of MC1R and 41 cases with high MC1R expression were observed. Patients with high expression of MC1R also exhibited a shorter survival time, and the difference in survival times was statistically significant (median DFS: 12.03 months vs. 14.29 months, χ^2 = 6.864, P=0.0088; median OS: 16.73 months vs. 21.77 months, χ^2 = 5.649, P=0.0175) (Supplementary Figures S2A, B).

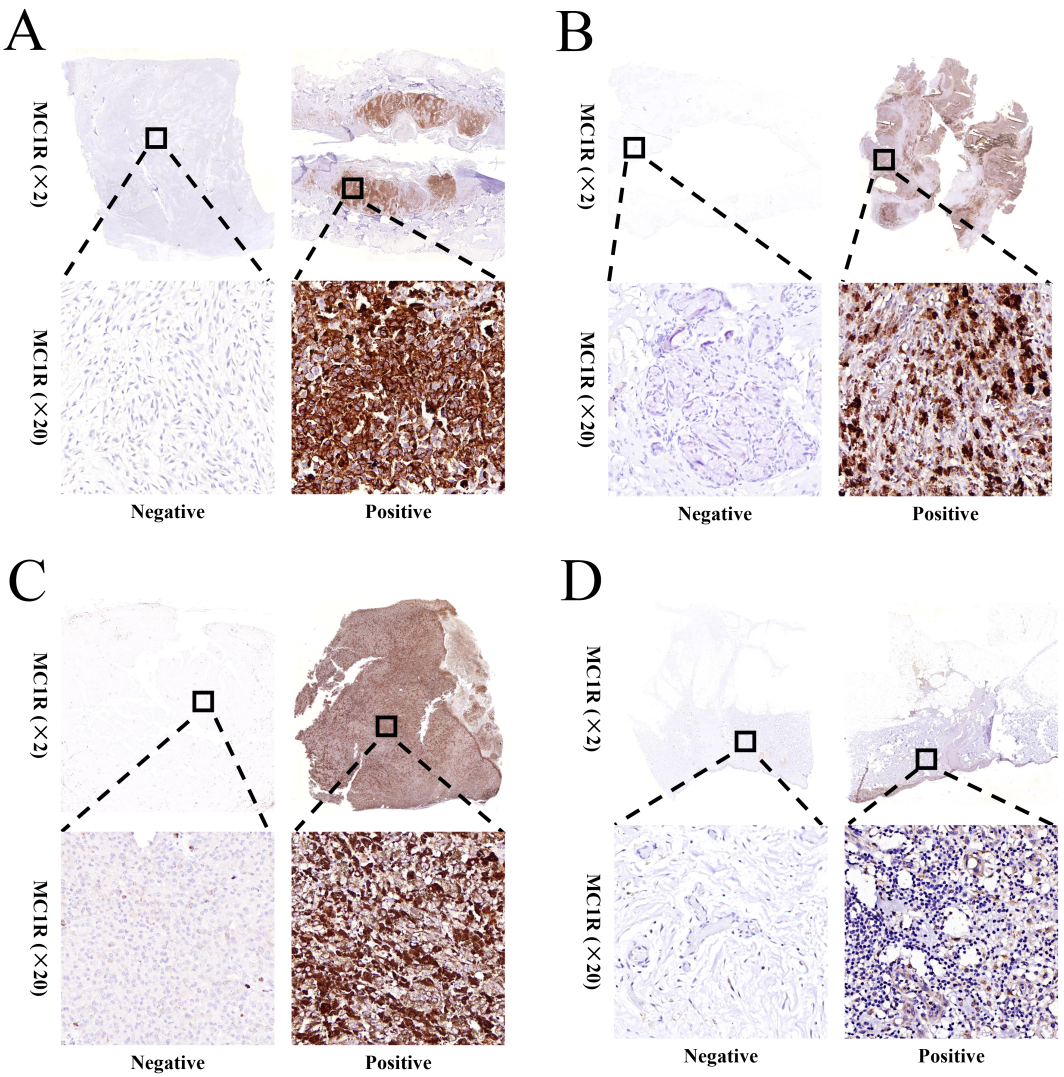

FIGURE 1
Representative images for the differential expression of MC1R in **(A)** plantar melanoma tumor tissue, **(B)** nasal melanoma tumor tissue, **(C)** ocular melanoma tumor tissue, and **(D)** dorsal surface melanoma tumor tissue.

Comparison of clinical and pathological characteristics in melanoma patients

The median age was 58 years, with an average age of 57.9 ± 13.2 years. There were 63 male patients and 36 female patients. Of all enrolled patients, 7 cases with stage I, 71 cases with stage II, 19 cases with stage III, 2 cases with stage IV, respectively. The distribution of tumor sites for melanoma was as follows: 21 cases (21.2%) of ocular choroid, 23 mucosal cases (23.2%), and 55 cases (55.6%) of acral skin. Every patient received surgical treatment. Furthermore, 16 cases (16.2%) received chemotherapy after surgery, eight cases (8.1%) received radiotherapy, 15 cases (15.2%) received targeted therapy, and 31 cases (31.3%) received immunotherapy. According to MC1R expression in melanoma tumor tissues, the expression of MC1R in melanoma tumor tissues was correlated with several factors, including family history, A/G, DBIL, and tumor site (Table 1).

The univariate analysis and multivariate analysis for potential prognostic factors in melanoma patients

Based on the univariate analysis, MC1RN (MC1R expressed in normal tissues adjacent to melanoma tissues), MC1RT (MC1R expressed in melanoma tumor tissue), sex, ESR, tumor site, targeted therapy, and immunotherapy were associated with DFS. Based on the multivariate analysis, MC1RN, MC1RT, sex, ESR, tumor site, targeted therapy, and immunotherapy were the potential prognostic factors for the DFS for melanoma (Table 2). Using univariate analysis, MC1RN, MC1RT, sex, tumor site, TLN, PLN, and immunotherapy were associated with OS. Based on multivariate analysis, MC1RN, MC1RT, sex, tumor site, TLN, PLN, and immunotherapy were the potential prognostic factors for OS for melanoma (Table 3).

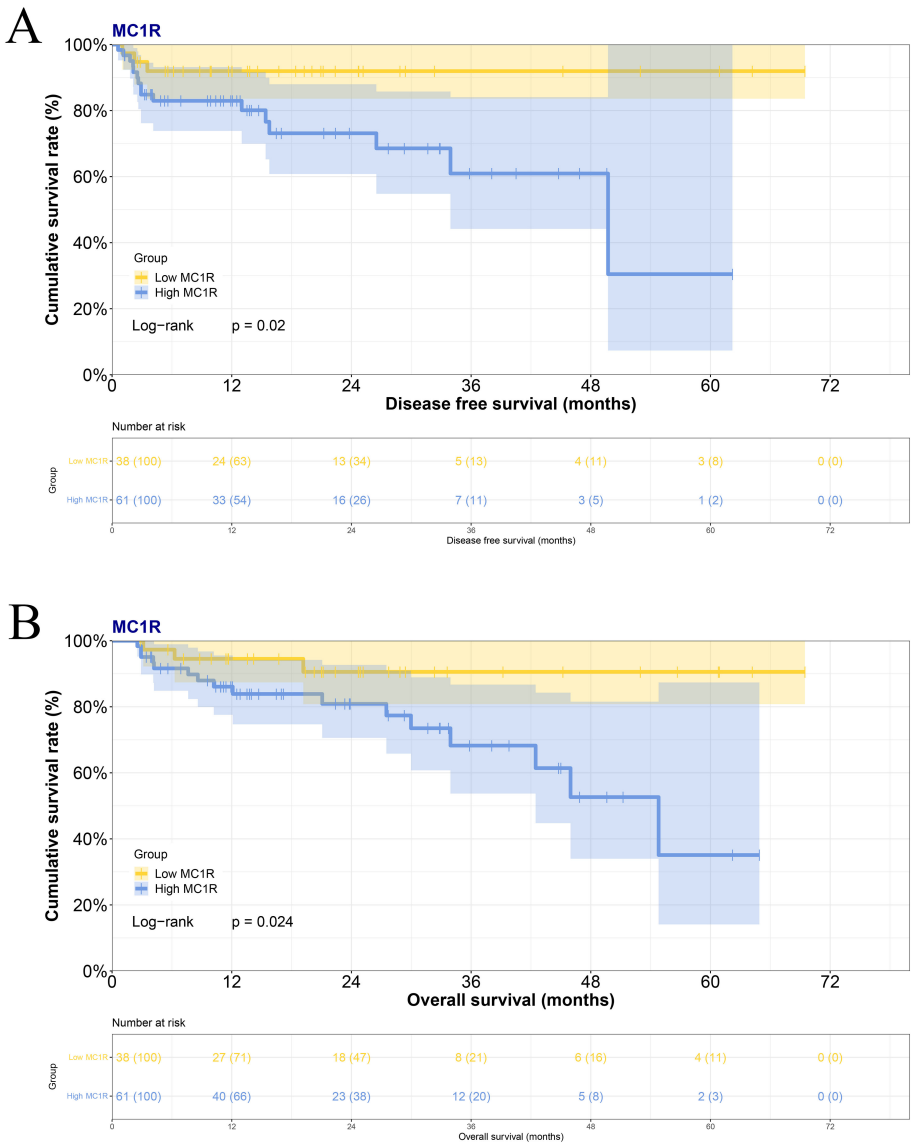

FIGURE 2
The association between MC1R expression in melanoma tumor tissues and the prognosis in melanoma patients for **(A)** DFS and **(B)** OS.

Nomogram construction and validation

For the nomogram predicting DFS, the corresponding scores were calculated based on seven factors, including MC1RN, MC1RT, sex, ESR, tumor site, targeted therapy, and immunotherapy. The scores were further summarized and projected onto the total subscale to predict the probability of the DFS for individual melanoma patients (Figure 3A). For the nomogram predicting OS, the corresponding scores were calculated based on seven factors, including MC1RN, MC1RT, sex, tumor site, TLN, PLN, and immunotherapy. These scores were further summarized and projected onto the total subscale to predict the probability of OS for individual melanoma patients (Figure 3B).

The calibration curve was used to verify the nomograms, and the results revealed that significant correlation between predictions and actual observations at one year and three years following surgery (Figures 4A–D). The decision curve analysis was used to assess the clinical application value of the nomogram model and indicated that the nomogram model predicted DFS and OS in the clinical application better than MC1RT (Figures 5A–D).

Time-dependent ROC drawing and validation

Time-dependent ROC curve analysis was used to predict the survival of melanoma patients at different times after surgery using

10.3389/fimmu.2025.1570502

TABLE 1 Clinicopathological characteristics of melanoma patients associated with the expression of MC1R in melanoma tumor tissues.

Parameters	level	Low MC1R	High MC1R	p
n		38	61	
Sex	Male	24 (63.2)	39 (63.9)	1.000
	Female	14 (36.8)	22 (36.1)	
Age	≤58	19 (50.0)	34 (55.7)	0.727
	>58	19 (50.0)	27 (44.3)	
Weight	≤60	19 (50.0)	31 (50.8)	1.000
	>60	19 (50.0)	30 (49.2)	
Height	≤1.60	17 (44.7)	28 (45.9)	1.000
	>1.60	21 (55.3)	33 (54.1)	
BMI	≤23.44	18 (47.4)	35 (57.4)	0.445
	>23.44	20 (52.6)	26 (42.6)	
Family history	Yes	6 (15.8)	1 (1.6)	0.023
	No	32 (84.2)	60 (98.4)	
ALT	≤17.65	16 (42.1)	32 (52.5)	0.426
	>17.65	22 (57.9)	29 (47.5)	
AST	≤19.50	21 (55.3)	32 (52.5)	0.948
	>19.50	17 (44.7)	29 (47.5)	
AST/ALT	≤1.10	22 (57.9)	30 (49.2)	0.524
	>1.10	16 (42.1)	31 (50.8)	
TP	≤66.55	20 (52.6)	33 (54.1)	1.000
	>66.55	18 (47.4)	28 (45.9)	
ALB	≤39.80	18 (47.4)	33 (54.1)	0.656
	>39.80	20 (52.6)	28 (45.9)	
GLO	≤26.65	26 (68.4)	30 (49.2)	0.095
	>26.65	12 (31.6)	31 (50.8)	
A/G	≤1.48	12 (31.6)	35 (57.4)	0.022
	>1.48	26 (68.4)	26 (42.6)	
TBIL	≤10.50	15 (39.5)	34 (55.7)	0.172
	>10.50	23 (60.5)	27 (44.3)	
DBIL	≤3.30	13 (34.2)	38 (62.3)	0.012
	>3.30	25 (65.8)	23 (37.7)	
TBA	≤4.55	23 (60.5)	33 (54.1)	0.675
	>4.55	15 (39.5)	28 (45.9)	
BUN	≤5.51	24 (63.2)	32 (52.5)	0.403
	>5.51	14 (36.8)	29 (47.5)	
CREA	≤67.25	18 (47.4)	34 (55.7)	0.546
	>67.25	20 (52.6)	27 (44.3)	
UA	≤325.90	18 (47.4)	36 (59.0)	0.355
	>325.90	20 (52.6)	25 (41.0)	
CO2CP	≤24.95	19 (50.0)	35 (57.4)	0.610
	>24.95	19 (50.0)	26 (42.6)	
GLU	≤4.94	19 (50.0)	34 (55.7)	0.727
	>4.94	19 (50.0)	27 (44.3)	
FDP	≤1.78	25 (65.8)	34 (55.7)	0.435
	>1.78	13 (34.2)	27 (44.3)	
INR	≤0.95	22 (57.9)	36 (59.0)	1.000
	>0.95	16 (42.1)	25 (41.0)	
Fib	≤2.88	21 (55.3)	27 (44.3)	0.391
	>2.88	17 (44.7)	34 (55.7)	
D Dimer	≤0.38	24 (63.2)	35 (57.4)	0.719
	>0.38	14 (36.8)	26 (42.6)	
AT III	≤94.40	17 (44.7)	30 (49.2)	0.823
	>94.40	21 (55.3)	31 (50.8)	
HbA1c	≤6.50	26 (68.4)	34 (55.7)	0.296
	>6.50	12 (31.6)	27 (44.3)	
ESR	≤8.00	27 (71.1)	35 (57.4)	0.248
	>8.00	11 (28.9)	26 (42.6)	
CRP	≤3.59	19 (50.0)	31 (50.8)	1.000
	>3.59	19 (50.0)	30 (49.2)	
Blood type	A	14 (36.8)	16 (26.2)	0.163
	B	10 (26.3)	24 (39.3)	
	O	14 (36.8)	17 (27.9)	
	AB	0 (0.0)	4 (6.6)	
White blood cell	≤6.10	22 (57.9)	27 (44.3)	0.266
	>6.10	16 (42.1)	34 (55.7)	
Hemoglobin	≤135.0	21 (55.3)	31 (50.8)	0.823
	>135.0	17 (44.7)	30 (49.2)	
Red blood cell	≤4.46	19 (50.0)	32 (52.5)	0.975
	>4.46	19 (50.0)	29 (47.5)	
Platelet	≤215.0	19 (50.0)	30 (49.2)	1.000
	>215.0	19 (50.0)	31 (50.8)	
Neutrophil	≤3.78	22 (57.9)	29 (47.5)	0.426

(Continued)

TABLE 1 Continued

(Continued)

10.3389/fimmu.2025.1570502

TABLE 1 Continued

Parameters	level	Low MC1R	High MC1R	p
n		38	61	
	>3.78	16 (42.1)	32 (52.5)	
Lymphocyte	≤1.72	23 (60.5)	35 (57.4)	0.921
	>1.72	15 (39.5)	26 (42.6)	
Eosinophil	≤0.12	20 (52.6)	33 (54.1)	1.000
	>0.12	18 (47.4)	28 (45.9)	
Basophil	≤0.03	25 (65.8)	45 (73.8)	0.534
	>0.03	13 (34.2)	16 (26.2)	
Monocyte	≤0.32	22 (57.9)	29 (47.5)	0.426
	>0.32	16 (42.1)	32 (52.5)	
Tumor site	Ocular choroid	2 (5.3)	19 (31.1)	0.004
	Mucosa	8 (21.1)	15 (24.6)	
	Acral skin	28 (73.7)	27 (44.3)	
T stage	T1	2 (5.3)	1 (1.6)	0.610
	T2	2 (5.3)	2 (3.3)	
	T3	5 (13.2)	12 (19.7)	
	T4	29 (76.3)	46 (75.4)	
N stage	N0	28 (73.7)	53 (86.9)	0.311
	N1	4 (10.5)	3 (4.9)	
	N2	4 (10.5)	2 (3.3)	
	N3	2 (5.3)	3 (4.9)	
M stage	M0	38 (100.0)	59 (96.7)	0.694
	M1	0 (0.0)	2 (3.3)	
TNM stage	I	3 (7.9)	4 (6.6)	0.063
	II	23 (60.5)	48 (78.7)	
	III	12 (31.6)	7 (11.5)	
	IV	0 (0.0)	2 (3.3)	
TLN	≤1	27 (71.1)	47 (77.0)	0.667
	>1	11 (28.9)	14 (23.0)	
PLN	≤0	28 (73.7)	54 (88.5)	0.103
	>0	10 (26.3)	7 (11.5)	
BRAF	Negative	5 (13.2)	13 (21.3)	0.571
	Positive	1 (2.6)	1 (1.6)	
	Unknown	32 (84.2)	47 (77.0)	
CyclinD1	Negative	0 (0.0)	6 (9.8)	0.110
	Positive	5 (13.2)	10 (16.4)	
	Unknown	33 (86.8)	45 (73.8)	
HMB45	Negative	2 (5.3)	2 (3.3)	0.833
	Positive	35 (92.1)	58 (95.1)	
	Unknown	1 (2.6)	1 (1.6)	
Ki67	Negative	0 (0.0)	1 (1.6)	0.716
	Positive	37 (97.4)	58 (95.1)	
	Unknown	1 (2.6)	2 (3.3)	
MelanA	Negative	0 (0.0)	1 (1.6)	0.653
	Positive	36 (94.7)	58 (95.1)	
	Unknown	2 (5.3)	2 (3.3)	
P16	Negative	1 (2.6)	4 (6.6)	0.370
	Positive	2 (5.3)	7 (11.5)	
	Unknown	35 (92.1)	50 (82.0)	
P53	Negative	4 (10.5)	10 (16.4)	0.511
	Positive	19 (50.0)	33 (54.1)	
	Unknown	15 (39.5)	18 (29.5)	
S100	Negative	2 (5.3)	0 (0.0)	0.079
	Positive	36 (94.7)	58 (95.1)	
	Unknown	0 (0.0)	3 (4.9)	
MITF	Negative	3 (7.9)	5 (8.2)	0.993
	Positive	11 (28.9)	17 (27.9)	
	Unknown	24 (63.2)	39 (63.9)	
Clark level	I	6 (15.8)	9 (14.8)	0.539
	II	4 (10.5)	4 (6.6)	
	III	4 (10.5)	5 (8.2)	
	IV	8 (21.1)	8 (13.1)	
	V	9 (23.7)	13 (21.3)	
	Unknown	7 (18.4)	22 (36.1)	
Blood vessel invasion	No	36 (94.7)	59 (96.7)	1.000
	Yes	2 (5.3)	2 (3.3)	
Neural invasion	No	38 (100.0)	56 (91.8)	0.180
	Yes	0 (0.0)	5 (8.2)	
Chemotherapy	No	33 (86.8)	50 (82.0)	0.719
	Yes	5 (13.2)	11 (18.0)	
Radiotherapy	No	35 (92.1)	56 (91.8)	1.000
	Yes	3 (7.9)	5 (8.2)	

(Continued)

10.3389/fimmu.2025.1570502

TABLE 1 Continued

Parameters	level	Low MC1R	High MC1R	p
n		38	61	
Targeted therapy	No	30 (78.9)	54 (88.5)	0.315
	Yes	8 (21.1)	7 (11.5)	
Immunotherapy	No	24 (63.2)	44 (72.1)	0.476
	Yes	14 (36.8)	17 (27.9)	

#BMI, body mass index; ALT, Alanine aminotransferase; AST, Aspartate aminotransferase; TP, Total protein; ALB, Albumin; GLO, Globularproteins; TBIL, Total bilirubin; DBIL, Direct bilirubin; TBA, Total bile acids; BUN, Blood urea nitrogen; CREA, Creatinine; UA, Uric acid; CO2CP, Carbon dioxide combining power; GLU, Glucose; FDP, Fibrinogen degradation products; INR, international normalized ratio; Fib, Fibrinogen; ESR, Erythrocyte sedimentation rate; CRP, C-reactive protein; TLN, Total lymph node; PLN, Positive lymph node.

MC1RT. TDROC showed that the AUROC for DFS one year after surgery was 0.595 (95% CI: 0.463-0.727). The AUROC for DFS three years after surgery was 0.652 (95% CI: 0.498-0.807). The AUROC for DFS five years after surgery was 0.836 (95% CI: 0.617-1.000) (Figures 6A, B). Furthermore, the TDROC indicated that the AUROC for OS was 0.603 (95% CI: 0.465-0.740) one year after surgery, and the AUROC for OS after surgery at three years was 0.621 (95% CI: 0.482-0.760). Finally, the AUROC for OS after surgery at five years was 0.788 (95% CI: 0.591-0.985) (Figures 6C, D).

Subgroup analysis

We investigated MC1R expression in melanoma tumor tissues from the 63 male melanoma patients. There were 24 cases in the low MC1R expression group and 39 cases in the high MC1R expression group (DFS, χ^2 = 2.3600, P=0.1245; OS, χ^2 = 1.9730, P=0.1601) (Supplementary Figure S3). Furthermore, we investigated MC1R expression in melanoma tumor tissues from the 36 female melanoma patients. There were 14 cases in the low MC1R expression group and 22 cases in the high MC1R expression group (DFS, χ^2 = 2.6460, P=0.1038; OS, χ^2 = 2.1080, P=0.1465) (Supplementary Figure S4).

We investigated MC1R expression in melanoma tumor tissues from the 31 melanoma patients who received immunotherapy. There were 14 cases in the low MC1R expression group and 17 cases in the high MC1R expression group (DFS, χ^2 = 0.4000, P=0.5271; OS, χ^2 = 0.5556, P=0.4560) (Supplementary Figure S5).

Moreover, the expression of MC1R in the melanoma tumor tissues from the acral skin group included 28 cases with low MC1R expression and 27 cases with high MC1R expression (DFS, χ^2 = 6.158, P=0.0131; OS, χ^2 = 5.490, P=0.0191) (Supplementary Figure S6).

Discussion

Melanoma is a highly malignant tumor derived from melanocytes, commonly found in the skin, as well as in mucous membranes and internal organs; it occurs more commonly in adults and is rarely observed in children (15). Melanoma can evolve from congenital or acquired benign melanocytic nevi or malignant transformation of developmental nevi (16). Compared with other solid malignant tumors, the age of death in cases of melanoma is lower and the prognosis is poor (17).

Melanocortin receptors including five types of melanocortin receptors (MC1R-MC5R) have been discovered (18). MC1R is playing a major role in skin tone and hair color formation (19). Furthermore, MC1R is related to the proliferation, invasion, migration, and metastasis of melanoma. One study demonstrated that proopiomelanocortin (POMC) could produce α-melanotropin (α-MSH), which exerts its biological functions through MC1R. α-MSH also is closely related to the promotion of tumor development, suggesting that MC1R is a promising target for tumor immunotherapy (20).

The current study analyzed the baseline characteristics of 99 melanoma patients, and utilized immunohistochemistry to detect MC1R expression and its relationship with the prognosis of these melanoma patients. We found that the expression level of MC1R in melanoma tumor tissue was higher than in adjacent normal tissue. According to the MC1R expression by H-Score, patients with high expression of MC1R in melanoma tumor tissue or adjacent normal tissue had survived shorter and worse prognosis. Kansal's study reported that reducing MC1R expression could inhibit melanoma growth (21). In Su DG's study, they demonstrated that higher MC1R expression was seen in deeper primary lesions and ulcerated lesions and was related to shorter survival in primary and metastatic tumors (22). This is generally consistent with our findings. Another study also indicated that MC1R was expressed more highly in colon tumor tissues than in adjacent tissues; MC1R was related to colon cancer prognosis, and higher expression of MC1R tended to predict a worse prognosis (23). The expression of MC1R was correlated with several factors, including family history, A/G, DBIL, and tumor site (P<0.05). In early-onset basal cell carcinoma (BCC), a family history of skin cancer was associated with an increased risk of early-onset BCC; and family history remained a strong risk factor for early-onset BCC after adjustment for MC1R genotype (24). Zhang X et al. found that the combination of N-methylation and albumin binding enhanced the labeling of MC1R-targeted radioligands for tumor uptake, which was able to overcome the adverse biological characteristics and dose limitations associated with existing single-molecule therapies, improving treatment efficacy, and demonstrating significant survival advantages in melanoma models (25).

Based on COX regression analysis, we found that MC1RN, MC1RT, sex, ESR, tumor site, targeted therapy, and immunotherapy were the potential prognostic factors for the DFS of melanoma and MC1RN, MC1RT, sex, tumor site, TLN, PLN, and immunotherapy were the potential prognostic factors for the OS of melanoma. Nomograms were assessed to evaluate and predict the survival probability of individualized melanoma patients with different DFS and OS. The nomogram models were validated using calibration curves and demonstrated a high degree of accuracy and consistency between the predicted and actual probabilities at one year and three

10.3389/fimmu.2025.1570502

TABLE 2 Univariate and multivariate COX regression model analyses for the prediction of DFS in melanoma patients.

Parameters		P	HR	95% CI		P	HR	95% CI	
				Low	High			Low	High
MC1RN	Low	0.014	1 (Ref.)			0.005	1 (Ref.)		
	High		3.380	1.282	8.910		5.552	1.684	18.303
MC1RT	Low	0.031	1 (Ref.)			0.036	1 (Ref.)		
	High		3.932	1.135	13.624		3.781	1.094	13.064
Sex	Male	0.000	1 (Ref.)			0.002	1 (Ref.)		
	Female		0.075	0.020	0.279		0.290	0.130	0.646
Age	≤58	0.239	1 (Ref.)						
	>58		0.413	0.095	1.802				
Weight	≤60	0.322	1 (Ref.)						
	>60		1.586	0.637	3.951				
Height	≤1.60	0.798	1 (Ref.)						
	>1.60		1.163	0.366	3.693				
BMI	≤23.44	0.811	1 (Ref.)						
	>23.44		1.117	0.449	2.778				
Family history	Yes	0.512	1 (Ref.)						
	No		0.456	0.044	4.758				
ALB	≤39.80	0.881	1 (Ref.)						
	>39.80		0.927	0.342	2.512				
Fib	≤2.88	0.858	1 (Ref.)						
	>2.88		1.089	0.430	2.760				
D Dimer	≤0.38	0.744	1 (Ref.)						
	>0.38		1.231	0.353	4.297				
ESR	≤8.00	0.032	1 (Ref.)			0.007	1 (Ref.)		
	>8.00		4.961	1.145	21.495		5.547	1.600	19.228
CRP	≤3.59	0.367	1 (Ref.)						
	>3.59		0.616	0.215	1.765				
Neutrophil	≤3.78	0.056	1 (Ref.)						
	>3.78		3.582	0.967	13.266				
Lymphocyte	≤1.72	0.191	1 (Ref.)						
	>1.72		2.086	0.693	6.282				
Monocyte	≤0.32	0.156	1 (Ref.)						
	>0.32		0.400	0.113	1.418				
Tumor site	Ocular choroid	0.000	1 (Ref.)			0.000	1 (Ref.)		
	Mucosa	0.000	14.475	3.848	54.449	0.000	21.377	5.326	85.811
	Acral skin	0.064	10.506	0.870	126.841	0.021	5.358	1.288	22.283
TNM stage	I	0.358	1 (Ref.)						
	II	0.462	1.356	0.134	14.324				
	III	0.744	1.553	0.016	19.465				
	IV	0.308	3.506	0.105	62.604				

(Continued)

TABLE 2 Continued

Parameters		P	HR	95% CI		P	HR	95% CI	
				Low	High			Low	High
TLN	≤1	0.088	1 (Ref.)						
	>1		4.901	0.787	30.510				
PLN	≤0	0.073	1 (Ref.)						
	>0		2.623	0.913	7.539				
Blood vessel invasion	No	0.515	1 (Ref.)						
	Yes		0.393	0.024	6.508				
Neural invasion	No	0.925	1 (Ref.)						
	Yes		1.101	0.146	8.293				
Chemotherapy	No	0.923	1 (Ref.)						
	Yes		1.075	0.246	4.700				
Radiotherapy	No	0.461	1 (Ref.)						
	Yes		1.957	0.328	11.670				
Targeted therapy	No	0.022	1 (Ref.)			0.009	1 (Ref.)		
	Yes		5.374	1.278	22.593		2.964	1.317	6.668
Immunotherapy	No	0.001	1 (Ref.)			0.000	1 (Ref.)		
	Yes		6.952	2.198	21.989		8.263	3.655	18.679

[#]MC1RN, MC1R expressed in normal tissues adjacent to melanoma tissues; MC1RT, MC1R expressed in melanoma tumor tissue; BMI, body mass index; ALB, Albumin; Fib, Fibrinogen; ESR, Erythrocyte sedimentation rate; CRP, C-reactive protein; TLN, Total lymph node; PLN, Positive lymph node.

TABLE 3 Univariate and multivariate COX regression model analyses for the prediction of OS in melanoma patients.

Parameters		P	HR	95% CI		P	HR	95% CI	
				Low	High			Low	High
MC1RN	Low	0.024	1 (Ref.)			0.040	1 (Ref.)		
	High		3.051	1.158	8.042		2.243	1.036	4.855
MC1RT	Low	0.012	1 (Ref.)			0.038	1 (Ref.)		
	High		4.737	1.402	16.005		4.309	1.083	17.145
Sex	Male	0.009	1 (Ref.)			0.026	1 (Ref.)		
	Female		0.137	0.031	0.606		0.421	0.197	0.902
Age	≤58	0.746	1 (Ref.)						
	>58		1.334	0.233	7.626				
Weight	≤60	0.425	1 (Ref.)						
	>60		1.451	0.581	3.620				
Height	≤1.60	0.155	1 (Ref.)						
	>1.60		2.372	0.721	7.809				
BMI	≤23.44	0.726	1 (Ref.)						
	>23.44		1.176	0.474	2.915				
Family history	Yes	0.512	1 (Ref.)						
	No		0.456	0.044	4.758				

(Continued)

TABLE 3 Continued

Parameters		P	HR	95% CI		P	HR	95% CI	
				Low	High			Low	High
ALB	≤39.80	0.287	1 (Ref.)						
	>39.80		1.754	0.624	4.932				
Fib	≤2.88	0.997	1 (Ref.)						
	>2.88		0.998	0.395	2.524				
D Dimer	≤0.38	0.378	1 (Ref.)						
	>0.38		0.512	0.115	2.270				
ESR	≤8.00	0.473	1 (Ref.)						
	>8.00		1.737	0.384	7.850				
CRP	≤3.59	0.928	1 (Ref.)						
	>3.59		0.959	0.389	2.365				
Neutrophil	≤3.78	0.915	1 (Ref.)						
	>3.78		1.083	0.252	4.655				
Lymphocyte	≤1.72	0.375	1 (Ref.)						
	>1.72		1.761	0.504	6.148				
Monocyte	≤0.32	0.639	1 (Ref.)						
	>0.32		0.706	0.164	3.031				
Tumor site	Ocular choroid	0.000	1 (Ref.)			0.001	1 (Ref.)		
	Mucosa	0.005	4.999	1.423	17.565	0.007	5.666	1.620	19.815
	Acral skin	0.259	0.256	0.024	2.733	0.38	1.786	0.489	6.521
TNM stage	I	0.322	1 (Ref.)						
	II	0.735	2.016	0.035	17.390				
	III	0.672	2.375	0.043	30.821				
	IV	0.188	3.387	0.214	60.484				
TLN	≤1	0.000	1 (Ref.)			0.000	1 (Ref.)		
	>1		3.541	1.704	7.357		4.639	2.019	10.659
PLN	≤0	0.040	1 (Ref.)			0.004	1 (Ref.)		
	>0		3.121	1.054	9.243		10.173	2.086	49.612
Blood vessel invasion	No	0.980	1 (Ref.)						
	Yes		1.04	0.048	22.361				
Neural invasion	No	0.962	1 (Ref.)						
	Yes		1.05	0.140	7.905				
Chemotherapy	No	0.401	1 (Ref.)						
	Yes		0.429	0.060	3.091				
Radiotherapy	No	0.358	1 (Ref.)						
	Yes		2.496	0.355	17.542				
Targeted therapy	No	0.968	1 (Ref.)						
	Yes		1.033	0.21	5.077				

(Continued)

TABLE 3 Continued

Parameters		P	HR	95% CI		P	HR	95% CI	
				Low	High			Low	High
Immunotherapy	No	0.000	1 (Ref.)			0.000	1 (Ref.)		
	Yes		11.765	3.037	45.587		5.053	2.532	10.082

[#]MC1RN, MC1R expressed in normal tissues adjacent to melanoma tissues; MC1RT, MC1R expressed in melanoma tumor tissue; BMI, body mass index; ALB, Albumin; Fib, Fibrinogen; ESR, Erythrocyte sedimentation rate; CRP, C-reactive protein; TLN, Total lymph node; PLN, Positive lymph node.

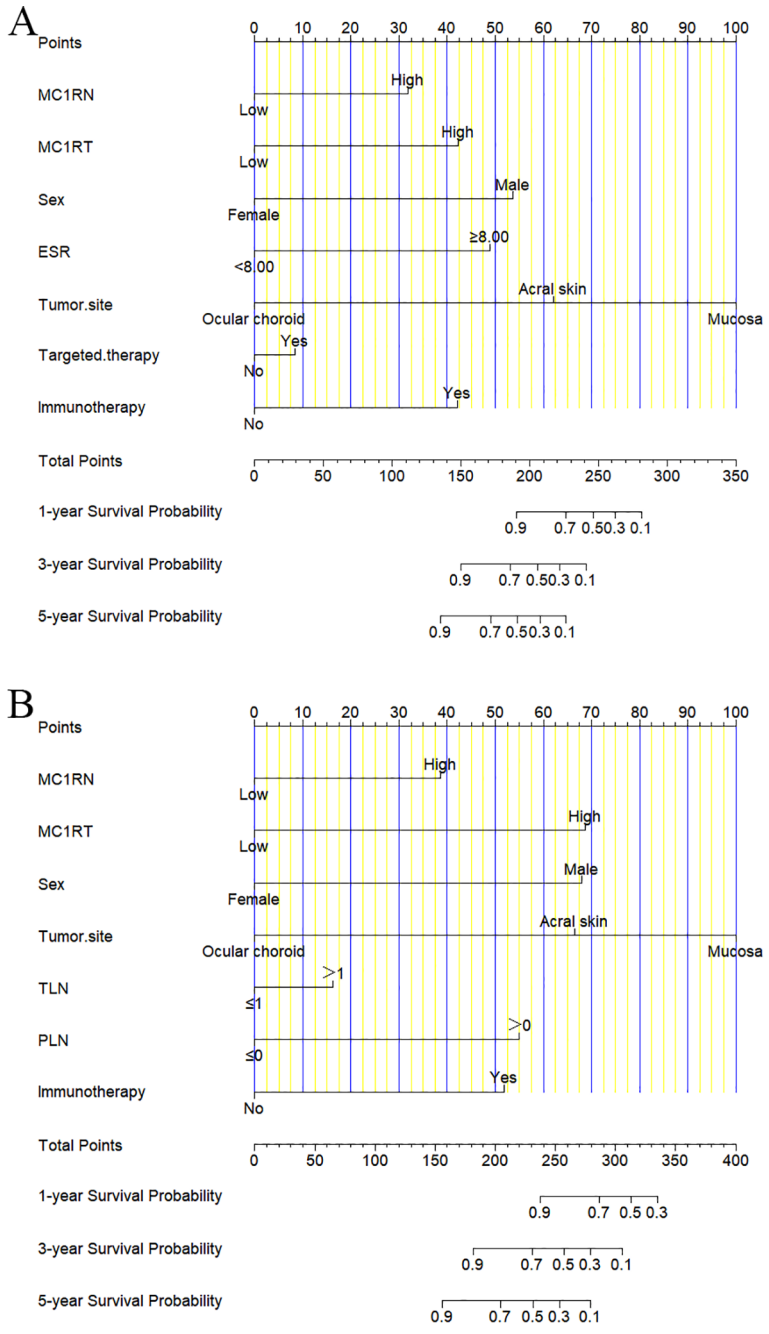

FIGURE 3
Nomograms for prognosis prediction in melanoma patients. **(A)** One-year, three-year, and five-year nomograms for prognosis prediction for DFS. **(B)** One-year, three-year, and five-year nomograms for prognosis prediction for OS.

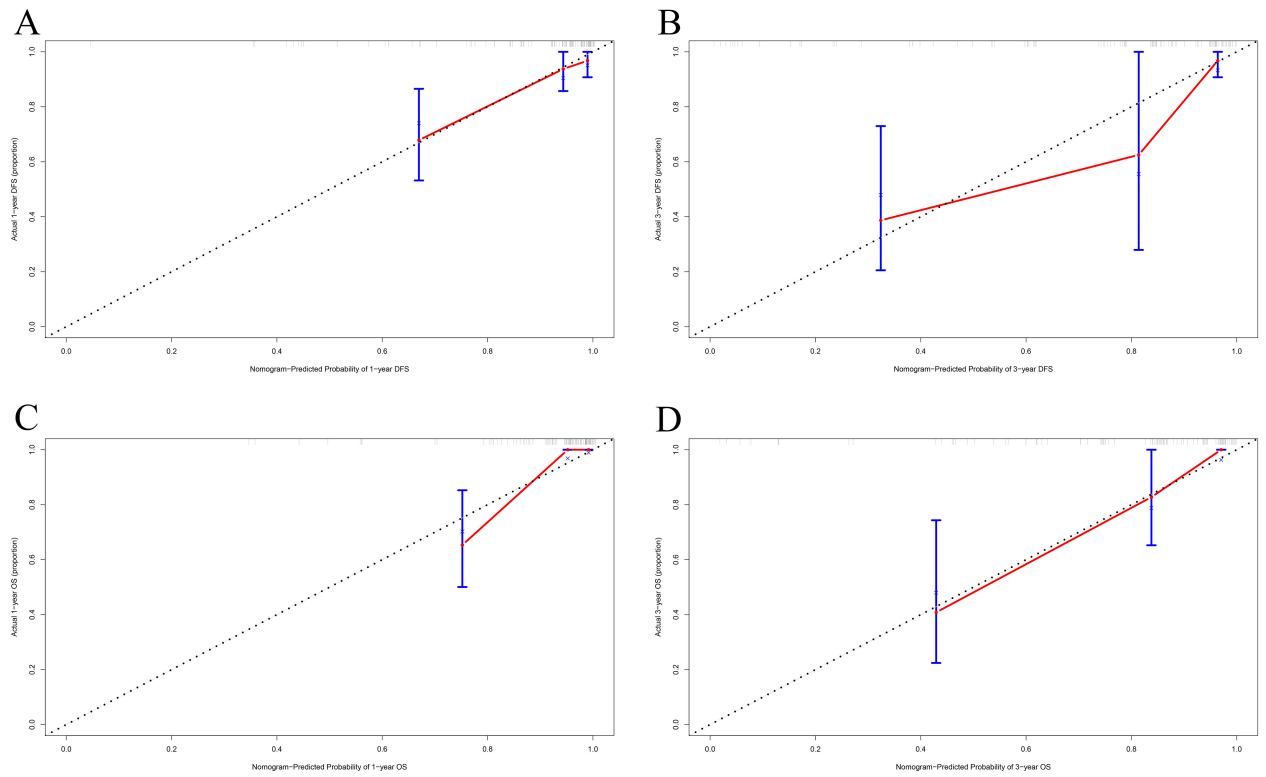

FIGURE 4
Calibration curves for nomograms in melanoma patients. **(A, B)** One-year and three-year calibration curves for nomograms for prognosis prediction for DFS. **(C, D)** One-year and three-year calibration curves for nomograms for prognosis prediction for OS.

years following surgery. The nomogram models performed better than MC1RT or MC1RN alone by decision curve analysis. We also applied time-dependent ROC curves to analyze the predictive effects of MC1RT and MC1RN on survival at different times after surgery. With the extension of survival time at any time, the area of the postoperative AUC and 95% CI gradually increased, resulting in more accurate predictions. This preliminary result indicated that the nomogram models exhibited clinical significance.

Research has shown that sex has an impact on melanoma progression, and female patients typically experience significantly better survival than male patients and younger patients perform better than older individuals (26). Our study determined that male melanoma patients experienced significantly shorter postoperative survival times than female melanoma patients. Wendt J's study demonstrated that MC1R variants contribute differently to melanoma risk in males and females, and was helpful to better classify melanoma risk factors among different sexes (13).

We also found that MC1R was related to the prognosis of melanoma patients receiving immunotherapy. However, due to the small number of melanoma patients receiving immunotherapy, there was no significant correlation between the expression of MC1R in tumor tissues and patient prognosis. A published study of 115 metastatic melanoma patients indicated that the median OS for melanoma patients receiving immunotherapy was 19.0 months, the median OS for melanoma patients receiving conventional chemotherapy was 8.0 months, and that of melanoma patients not receiving treatment was 6.0 months; the intergroup comparison revealed statistical significance (27). Another study suggested that elevated MC1R expression in human melanoma cases was associated with reduced expression of CXCL9/10/11, impaired T cell infiltration, and a poor prognosis based on the GNAS-PKA signaling pathway (28). Zhang Y's study demonstrated that the bispecific antibody combined MC1R with PD-L1 expressed on melanoma cells could enhance specific antitumor efficacy in a syngeneic B16-SIY melanoma mouse model, and increase infiltrated T cells in the tumor microenvironment (29). Ascierto et al. found that compared with a placebo group, vemurafenib provided a longer DFS survival time in patients with CD8+T cells<1% (HR: 0.56, 95% CI: 0.34-0.92) and a shorter DFS survival time in patients with CD8+T cells ≥1% (HR: 0.77, 95% CI: 0.48-1.22) (30). Furthermore, vemurafenib treatment was observed to provide a longer DFS survival time in patients with PD-L1+ immune cells <5% in tumors (HR: 0.36; 95% CI: 0.24-0.56) and a shorter DFS survival time in patients with PD-L1+ immune cells ≥5% (HR: 0.99, 95% CI: 0.58-1.69) (30). Suzuki T's study demonstrated that MT-7117 was a novel oral MC1R agonist that induces melanogenesis *in vitro* and *in vivo*, suggesting its potential application for the prevention of phototoxic reactions in patients with photodermatoses (31). Therefore, MC1R might be a potential therapeutic target for tumor immunotherapy.

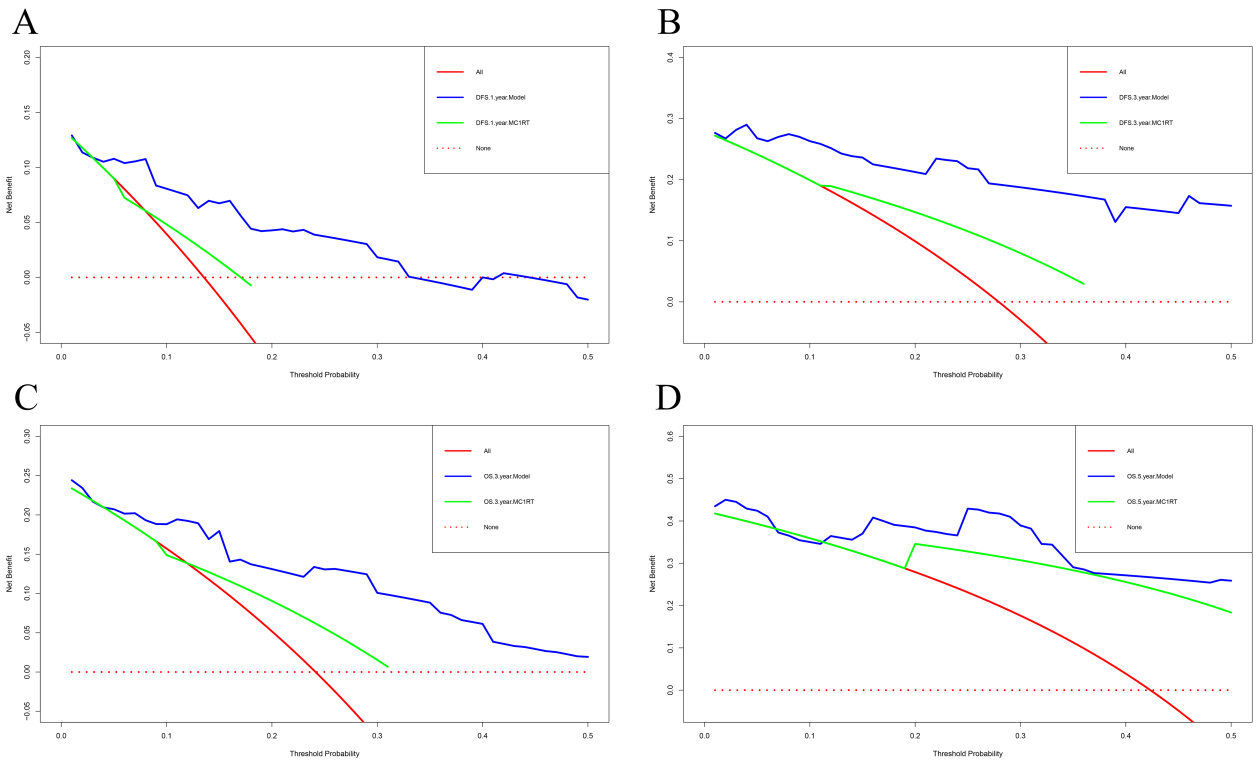

FIGURE 5
Decision curve analysis for nomograms in melanoma patients using nomogram models and MC1RT. **(A, B)** One-year and three-year decision curve analysis for nomograms for prognosis prediction for DFS. **(C, D)** Three-year and five-year decision curve analysis for nomograms for prognosis prediction for OS.

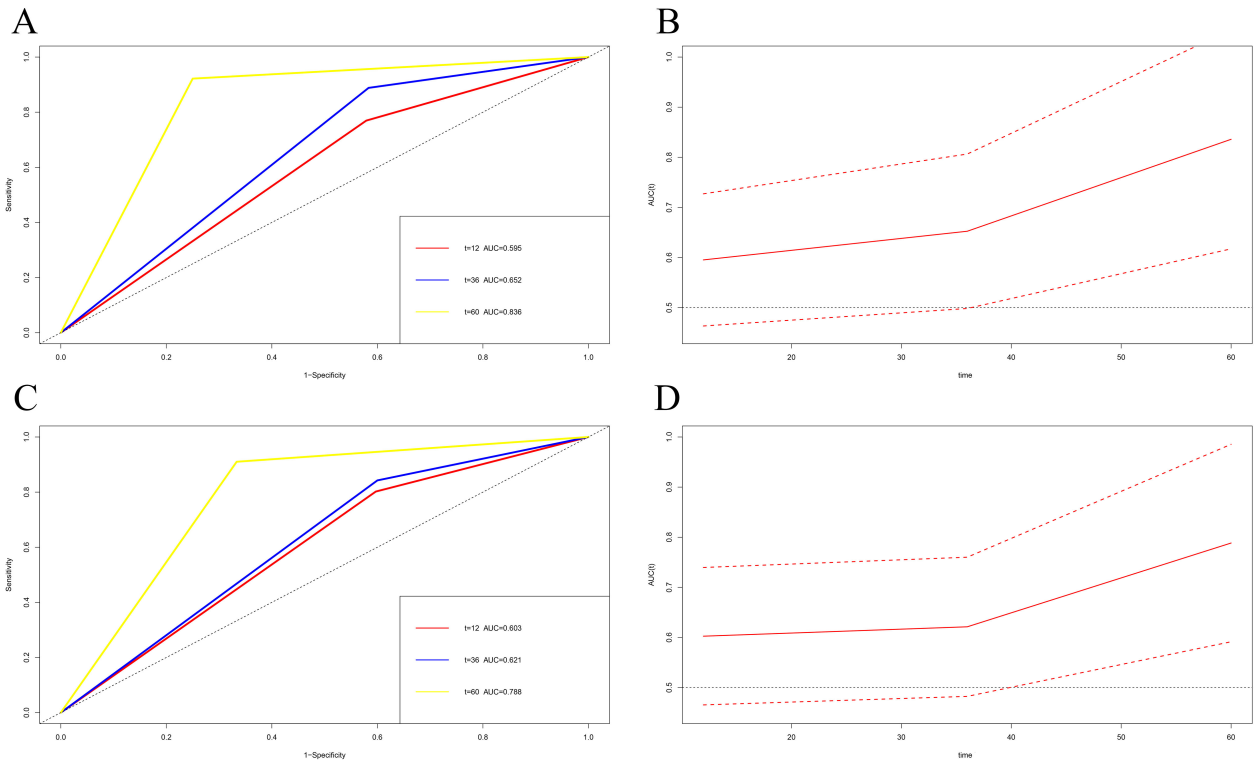

FIGURE 6
Time-dependent receiver operating characteristic (TDROC) used to analyze the area plots under the receiver operating characteristic curves (AUROCs) for MC1R expression in melanoma tumor tissues from melanoma patients after surgery and follow-up. **(A, C)** Time-dependent AUROCs for DFS and OS. **(B, D)** 95%CI changes of AUROCs for DFS and OS.

In the current study, the tumor locations included 21 cases (21.2%) of ocular choroid, 23 cases (23.2%) of mucosa, and 55 cases (55.6%) of acral skin. We conducted an in-depth analysis of the differences in the MC1R expression in melanomas of the ocular choroid, mucosa, and acral skin. Patients with high MC1R expression in melanoma had a shorter survival time in the acral skin group. Research has shown that melanoma location is related to patient prognosis (32). Patients with melanoma occurring on the skin of the limbs have a better prognosis, with a five-year survival rate of 60% for upper limb patients and 57% for lower limb patients. Patients with melanoma occurring on the head are the second most common category, with a five-year survival rate of 53%. Those with melanoma occurring on the trunk have a worse prognosis, with a five-year survival rate of 41%, and the worst five-year survival rate (20-40%) is reported for melanoma arising in the mucosa (32). A study by Tyrrell et al. reviewed the characteristics and prognosis of patients with mucosal melanoma and indicated that patients with mucosal melanoma also exhibited a poor prognosis and short survival time (33). Lian Bin et al. also analyzed the clinical and pathological characteristics of 232 patients with advanced mucosal melanoma; nasal and oral mucosa were the most common sites of melanoma, and M stage and LDH level at the time of treatment were independent prognostic factors for OS (34).

There are several limitations associated with this study. First, it was a single institution retrospective study. Our findings necessitate further prospective validation through multicenter studies involving independent patient groups. Increasing the sample size, particularly for subgroup analyses, would enhance the statistical power and reliability of the findings. Second, the expression of MC1R was only determined using immunohistochemistry, and the underlying molecular biological mechanisms have not been thoroughly investigated. Additionally, we plan to conduct molecular mechanistic investigations using *in vitro* and *in vivo* models to further elucidate the underlying mechanisms of MC1R-related effects observed in the current study, especially in MC1R activity modulate PKA signaling, immune suppression pathways. Finally, the nomogram models that were constructed need additional validation. The more patients should be enrolled to validate. And the more data collection of the enrolled patients, including clinical, pathological, and follow-up data, would improve data quality and reduce bias.

Conclusions

In summary, we analyzed the relationship between MC1R expression and melanoma, and determined that low MC1R expression in melanoma tumor tissues and adjacent normal tissue might be beneficial for the prognosis of melanoma patients. The MC1R expression was also concerned with melanoma location. An in-depth analysis of potential prognostic factors affecting melanoma, such as MC1R, tumor site, sex, and immunotherapy, also could affect the prognosis of melanoma patients.

Data availability statement

The original contributions presented in the study are included in the article/Supplementary Material. Further inquiries can be directed to the corresponding author.

Ethics statement

The studies involving humans were approved by Second Xiangya Hospital of Central South University. The studies were conducted in accordance with the local legislation and institutional requirements. The participants provided their written informed consent to participate in this study.

Author contributions

TX: Formal Analysis, Investigation, Writing – original draft, Writing – review & editing. HL: Formal Analysis, Investigation, Writing – original draft. XW: Methodology, Writing – original draft. DS: Resources, Supervision, Writing – original draft, Writing – review & editing.

Funding

The author(s) declare that no financial support was received for the research and/or publication of this article.

Conflict of interest

The authors declare that the research was conducted in the absence of any commercial or financial relationships that could be construed as a potential conflict of interest.

Generative AI statement

The author(s) declare that no Generative AI was used in the creation of this manuscript.

Publisher's note

All claims expressed in this article are solely those of the authors and do not necessarily represent those of their affiliated organizations, or those of the publisher, the editors and the reviewers. Any product that may be evaluated in this article, or claim that may be made by its manufacturer, is not guaranteed or endorsed by the publisher.

Supplementary material

The Supplementary Material for this article can be found online at: https://www.frontiersin.org/articles/10.3389/fimmu.2025.1570502/full#supplementary-material

References

1. Carvajal RD, Sacco JJ, Jager MJ, Eschelman DJ, Olofsson Bagge R, Harbour JW, et al. Advances in the clinical management of uveal melanoma. *Nat Rev Clin Oncol*. (2023) 20:99–115. doi: 10.1038/s41571-022-00714-1

2. Arnold M, Singh D, Laversanne M, Vignat J, Vaccarella S, Meheus F, et al. Global burden of cutaneous melanoma in 2020 and projections to 2040. *JAMA Dermatol*. (2022) 158:495–503. doi: 10.1001/jamadermatol.2022.0160

3. Guo W, Ren G, Sun M, Kong Y, Wang L, Bu R, et al. Expert consensus on clinical diagnosis and treatment for Chinese oral mucosal melanoma. *China J Oral Maxillofac Surg*. (2021) 19:481–8. doi: 10.19438/j.cjoms.2021.06.001

4. Wu Y, Wang Y, Wang L, Yin P, Lin Y, Zhou M. Burden of melanoma in China, 1990-2017: Findings from the 2017 global burden of disease study. *Int J Cancer*. (2020) 147:692–701. doi: 10.1002/ijc.v147.3

5. Maheshwari A, Finger PT. Laser treatment for choroidal melanoma: Current concepts. *Surv Ophthalmol*. (2023) 68:211–24. doi: 10.1016/j.survophthal.2022.05.002

6. Li Y, Li Y, Wang B, Hu C, Chen Y, Zhang G. Research progress in biological therapy for melanoma. *Chin J Gerontology*. (2022) 42:1235–9. doi: 10.3969/j.issn.1005-9202.2022.05.060

7. Chen S, Zhu B, Yin C, Liu W, Han C, Chen B, et al. Palmitoylation-dependent activation of MC1R prevents melanomagenesis. *Nature*. (2017) 549:399–403. doi: 10.1038/nature23887

8. Peng L, Chang J, Liu X, Lu S, Ren H, Zhou X. MC1R is a prognostic marker and its expression is correlated with MSI in colorectal cancer. *Curr Issues Mol Biol*. (2021) 43:1529–47. doi: 10.3390/cimb43030108

9. Chelakkot VS, Thomas K, Romigh T, Fong A, Li L, Ronen S, et al. MC1R signaling through the cAMP-CREB/ATF-1 and ERK-NFκB pathways accelerates G1/S transition promoting breast cancer progression. *NPJ Precis Oncol*. (2023) 7:85. doi: 10.1038/s41698-023-00437-1

10. Zhou X, Chang J, Peng L, Liu X, Yu F, Xu J, et al. MC1R is highly expressed in esophageal squamous cell carcinoma. *J South Med Univ*. (2022) 42:1552–9. doi: 10.12122/j.issn.1673-4254.2022.10.16

11. Ruano APC, Gadelha Guimarães AP, Braun AC, Flores BCTCP, Tariki MS, Abdallah EA, et al. Fusion cell markers in circulating tumor cells from patients with high-grade ovarian serous carcinoma. *Int J Mol Sci*. (2022) 23:14687. doi: 10.3390/ijms232314687

12. Chen S, Han C, Miao X, Li X, Yin C, Zou J, et al. Targeting MC1R depalmitoylation to prevent melanomagenesis in redheads. *Nat Commun*. (2019) 10:877. doi: 10.1038/s41467-019-08691-3

13. Wendt J, Mueller C, Rauscher S, Fae I, Fischer G, Okamoto I. Contributions by MC1R variants to melanoma risk in males and females. *JAMA Dermatol*. (2018) 154:789–95. doi: 10.1001/jamadermatol.2018.1252

14. Yang J, Xu J, Gonzalez R, Lindner T, Kratochwil C, Miao Y. 68Ga-DOTA-GGNle-CycMSHhex targets the melanocortin-1 receptor for melanoma imaging. *Sci Transl Med*. (2018) 10:eaau4445. doi: 10.1126/scitranslmed.aau4445

15. Gao X, Zhao X, Han Z. Research progress on the association of autophagy with invasion and metastasis of Malignant melanoma. *Diagnosis Ther J Dermato-Venereology*. (2024) 31:118–22. doi: 10.3969/j.issn.1674-8468.2024.02.009

16. Qiu J, Huang J, Xu S, Zhou Y, Huang P, Fu L. Progress in the treatment of Malignant melanoma of the skin. *Gansu Med J*. (2023) 42:969–71. doi: 10.15975/j.cnki.gsyy.2023.11.003

17. Wu S, Wang Y, Zheng K, Hang H, Kang J, Yu H. Prognosis and influencing factors of patients with Malignant melanoma. *Chin Gen Pract*. (2024) 27:942–7. doi: 10.12114/j.issn.1007-9572.2023.0307

18. Liu S, Pei S, Wen K, Peng A, Ma H, Huang H. MC1R-targeted NIR-II aggregation-induced emission nanoparticles for melanoma imaging. *Sci China (Materials)*. (2023) 66:4100–8. doi: 10.1007/s40843-023-2570-1

19. Yang X, Luo Z, Li J. Effect of MC1R on proliferation and apoptosis of vitiligo melanocytes. *China Med And Pharm*. (2023) 13:25–9. doi: 10.20116/j.issn2095-0616.2023.23.06

20. Xu Y, Yan J, Tao Y, Qian X, Zhang C, Yin L, et al. Pituitary hormone α-MSH promotes tumor-induced myelopoiesis and immunosuppression. *Science*. (2022) 377:1085–91. doi: 10.1126/science.abj2674

21. Kansal RG, McCravy MS, Basham JH, Earl JA, McMurray SL, Starner CJ, et al. Inhibition of melanocortin 1 receptor slows melanoma growth, reduces tumor heterogeneity and increases survival. *Oncotarget*. (2016) 7:26331–45. doi: 10.18632/oncotarget.v7i18

22. Su DG, Djureinovic D, Schoenfeld D, Marquez-Nostra B, Olino K, Jilaveanu L, et al. Melanocortin-1 receptor expression as a marker of progression in melanoma. *JCO Precis Oncol*. (2024) 8:e2300702. doi: 10.1200/PO.23.00702

23. Zhu S, Zou M, Li C, Tang Y, Luo H, Dong X. MC1R regulates T regulatory cell differentiation through metabolic reprogramming to promote colon cancer. *Int Immunopharmacol*. (2024) 138:112546. doi: 10.1016/j.intimp.2024.112546

24. Berlin NL, Cartmel B, Leffell DJ, Bale AE, Mayne ST, Ferrucci LM. Family history of skin cancer is associated with early-onset basal cell carcinoma independent of MC1R genotype. *Cancer Epidemiol*. (2015) 39:1078–83. doi: 10.1016/j.canep.2015.09.005

25. Zhang X, Chen F, Turker MZ, Ma K, Zanzonico P, Gallazzi F, et al. Targeted melanoma radiotherapy using ultrasmall 177Lu-labeled α-melanocyte stimulating hormone-functionalized core-shell silica nanoparticles. *Biomaterials*. (2020) 241:119858. doi: 10.1016/j.biomaterials.2020.119858

26. Kudura K, Basler L, Nussbaumer L, Foerster R. Sex-related differences in metastatic melanoma patients treated with immune checkpoint inhibition. *Cancers (Basel)*. (2022) 14:5145. doi: 10.3390/cancers14205145

27. Matsui Y, Sasaki J, Takatsuka S, Takenouchi T. Trends in the prognosis of metastatic melanoma in the era of targeted therapy and immunotherapy: A single-institution survey in Japan. *J Dermatol*. (2021) 48:75–9. doi: 10.1111/1346-8138.15642

28. Carlino MS, Larkin J, Long GV. Immune checkpoint inhibitors in melanoma. *Lancet*. (2021) 398:1002–14. doi: 10.1016/S0140-6736(21)01206-X

29. Zhang Y, Fang C, Wang RE, Wang Y, Guo H, Guo C, et al. A tumor-targeted immune checkpoint blocker. *Proc Natl Acad Sci U.S.A*. (2019) 116:15889–94. doi: 10.1073/pnas.1905646116

30. Ascierto PA, Lewis KD, Di Giacomo AM, Demidov L, Mandalà M, Bondarenko I, et al. Prognostic impact of baseline tumour immune infiltrate on disease-free survival in patients with completely resected, BRAFv600 mutation-positive melanoma receiving adjuvant vemurafenib. *Ann Oncol*. (2020) 31:153–9. doi: 10.1016/j.annonc.2019.10.002

31. Suzuki T, Kawano Y, Matsumoto A, Kondo M, Funayama K, Tanemura S, et al. Melanogenic effect of dersimelagon (MT-7117), a novel oral melanocortin 1 receptor agonist. *Skin Health Dis*. (2021) 2:e78. doi: 10.1002/ski2.78

32. Wu X, Feng Y, Zeng C, Wang M. Analysis of prognostic factors for survival in patients with head and neck mucosal melanoma. *J Clin Otorhinolaryngolgy Head Neck Surg*. (2020) 34:647–51. doi: 10.13201/j.issn.2096-7993.2020.07.017

33. Tyrrell H, Payne M. Combatting mucosal melanoma: recent advances and future perspectives. *Melanoma Manag*. (2018) 5:MMT11. doi: 10.2217/mmt-2018-0003

34. Lian B, Zheng N, Chi Z, Zhou L, Sheng X, Si L, et al. Curative effect of the 1st line and the 2nd line therapies for the 232 patients with advanced mucosal melanoma and factors effecting prognosis of the patients. *Chin J Cancer Biother*. (2017) 24:253–8. doi: 10.3872/j.issn.1007-385X.2017.03.007

frontiers | Frontiers in Immunology

TYPE Review
PUBLISHED 02 April 2025
DOI 10.3389/fimmu.2025.1572821

Check for updates

OPEN ACCESS

EDITED BY
Qingyu Luo,
Dana–Farber Cancer Institute, United States

REVIEWED BY
Xiaowei Wu,
Dana–Farber Cancer Institute, United States
Kang Wang,
Karolinska Institutet (KI), Sweden
Jinghui Geng,
University of California, Santa Cruz, United States

*CORRESPONDENCE
Tao Yan
yantao@cicams.ac.cn;
blizzardyt@163.com
Yi-bo Gao
yibgao@126.com
Shuang Ma
1025085193@qq.com

†These authors have contributed equally to this work and share first authorship

RECEIVED 07 February 2025
ACCEPTED 03 March 2025
PUBLISHED 02 April 2025

CITATION
Ma S, Lu Y, Sui S, Yang J-s, Fu B-b, Tan P-x, Chai Y, Lv J, Kong L, Wu X, Gao Y-b and Yan T (2025) Unraveling the triad of immunotherapy, tumor microenvironment, and skeletal muscle biomechanics in oncology. *Front. Immunol.* 16:1572821. doi: 10.3389/fimmu.2025.1572821

COPYRIGHT
© 2025 Ma, Lu, Sui, Yang, Fu, Tan, Chai, Lv, Kong, Wu, Gao and Yan. This is an open-access article distributed under the terms of the Creative Commons Attribution License (CC BY). The use, distribution or reproduction in other forums is permitted, provided the original author(s) and the copyright owner(s) are credited and that the original publication in this journal is cited, in accordance with accepted academic practice. No use, distribution or reproduction is permitted which does not comply with these terms.

Unraveling the triad of immunotherapy, tumor microenvironment, and skeletal muscle biomechanics in oncology

Shuang Ma[1*†], Ying Lu[1†], Shang Sui[2†], Jia-shuo Yang[3†], Bing-bing Fu[3†], Pei-xin Tan[3†], Yicheng Chai[1†], Jiaqi Lv[1], Lingyu Kong[1], Xiaolin Wu[4], Yi-bo Gao[5*] and Tao Yan[3*]

[1]School of Information Science and Engineering, Shenyang Ligong University, Shenyang, China, [2]St. John's Kilmarnock School, Breslau, ON, Canada, [3]Department of Anesthesiology, National Cancer Center/National Clinical Research Center for Cancer/Cancer Hospital, Chinese Academy of Medical Sciences and Peking Union Medical College, Beijing, China, [4]School of Mathematics and Statistics, Liaoning University, Shenyang, China, [5]Department of Oral and Maxillofacial Surgery, Taikang Bybo Dental, Beijing, China

The intricate interaction between skeletal muscle biomechanics, the tumor microenvironment, and immunotherapy constitutes a pivotal research focus oncology. This work provides a comprehensive review of methodologies for evaluating skeletal muscle biomechanics, including handheld dynamometry, advanced imaging techniques, electrical impedance myography, elastography, and single-fiber experiments to assess muscle quality and performance. Furthermore, it elucidates the mechanisms, applications, and limitations of various immunotherapy modalities, including immune checkpoint inhibitors, adoptive cell therapy, cancer vaccines, and combined chemoimmunotherapy, while examining their effects on skeletal muscle function and systemic immune responses. Key findings indicate that although immunotherapy is effective in augmenting antitumor immunity, it frequently induces muscle-related adverse effects such as weakness, fatigue, or damage, primarily mediated by cytokine release and immune activation. This work underscores the significance of immune niches within the tumor microenvironment in influencing treatment outcomes and proposes strategies to optimize therapy through personalized regimens and combinatorial approaches. This review highlights the need for further research on the formation of immune niches and interactions muscle-tumor. Our work is crucial for advancing the efficacy of immunotherapy, reducing adverse effects, and ultimately improving survival rates and quality of life of patients with cancer.

KEYWORDS

tumor microenvironment, immunotherapy, immune checkpoint inhibitors, immune niches, skeletal muscle biomechanics

1 Introduction

Cancer remains a major global public health concern and poses a severe threat to human health (1). Chemotherapy has long been the cornerstone of cancer treatment, plays a crucial role in inhibiting tumor cell growth (2). However, despite its anticancer effects, it also induces a series of significant side effects, among which the adverse impact on skeletal muscle function has increasingly become a research focus. Numerous clinical studies have shown that approximately 30–50% of cancer patients experience a significant decline in skeletal muscle function after undergoing chemotherapy, with an even higher proportion among elderly patients (3). This decline is primarily manifested as a reduction in muscle mass, primarily due to the direct toxic effects of chemotherapy drugs on muscle tissue, a phenomenon unrelated to the tumor response to treatment (4). The loss of muscle mass not only severely weakens patients' physical mobility and quality of daily life but may also lead to decreased chemotherapy tolerance, exacerbated drug toxicity reactions, and even a negative impact on overall survival rates. For example, studies on chemotherapy in patients with advanced lung cancer have demonstrated a strong correlation between post-chemotherapy muscle loss and poor treatment outcomes (3). Patients with significant muscle loss exhibit substantially lower hemoglobin levels and a markedly increased risk of disease progression (5). Similarly, in patients with metastatic colorectal cancer, the muscle area decreased by an average of 6.1% during chemotherapy. Among patients with a muscle reduction ≥ 9%, the survival rates were significantly lower than those who experienced less muscle loss.

Recently, immunotherapy has emerged as a promising strategy for cancer treatment. Immune checkpoint inhibitors (ICIs) block inhibitory receptors such as CTLA-4, PD-1, and PD-L1 on immune cells, effectively activating the immune system to attack tumor cells (6). These agents have demonstrated remarkable efficacy in treating melanoma, lung cancer, and various other malignancies (7). Conversely, adoptive cell immunotherapy entails harvesting immune cells (e.g., T cells or NK cells) from a patient or donor, expanding and modifying them *in vitro*, and reinfusing them to enhance antitumor immunity. This approach has led to groundbreaking progress in the treatment of hematologic malignancies (8). Tumor vaccines aim to stimulate the body's specific antitumor immune response (9). Some vaccines have shown significant success in preventing cervical cancer, and their potential applications in cancer treatment are being explored in clinical trials (10). However, while these immunotherapies effectively combat tumors, they may also affect skeletal muscle to varying degrees. For example, immune checkpoint inhibitors can cause immune-related adverse events affecting the musculoskeletal system; adoptive cell immunotherapy may trigger cytokine release syndrome, disrupting muscle cell metabolism and function; and tumor vaccines may lead to muscle fatigue, soreness, and other discomfort in some patients (6). Moreover, the integration of chemotherapy and immunotherapy is gaining prominence in the clinical practice (11). This therapeutic approach combines the cytotoxic effects of chemotherapy on tumor cells with immunotherapy immune activation of immunotherapy to synergistically enhance anticancer efficacy (12). In practice, the cytotoxicity of chemotherapeutic drugs and the immune response induced by immunotherapy can interact, further exacerbating skeletal muscle damage (13). For example, certain chemotherapeutic drugs can induce immunogenic cell death in tumors, promote immune cell activation, and intensify muscle damage (14). Moreover, the inflammatory response triggered by immunotherapy combined with the muscle toxicity of chemotherapy drugs can further aggravate muscle dysfunction (15).

Given the complex impact of immunotherapy and chemotherapy on skeletal muscle function, as well as their critical role in cancer treatment, in-depth research on their underlying mechanisms, comprehensive assessment of muscle function changes, and explore effective countermeasures (16). This study systematically examined the relationship between chemotherapy, immunotherapy, and skeletal muscle function, provided a detailed analysis of the associated mechanisms, evaluated the advantages and limitations of existing assessment methods, and discussed future research directions (17). The ultimate goal is to establish a solid theoretical foundation and practical guidance for protecting and improving skeletal muscle function during cancer treatment, thereby enhancing treatment outcomes and quality of life in patients with cancer (18).

2 Effects of immunotherapy and chemotherapy on tumor microenvironment, muscle cells, and inflammation

2.1 Mechanisms of immunotherapy in the tumor microenvironment

The tumor microenvironment forms a complex network. This network is intricately linked to immunotherapy (19). In this microenvironment, there are various immune cells and associated cellular components. They interact dynamically with tumor cells. As shown in Figure 1, natural killer (NK) cells induce cytotoxicity in tumor cells by releasing perforin and granzyme, while M2-type tumor-associated macrophages (TAMs) influenced by cytokines such as transforming growth factor-beta (TGF-β) and interleukin-10 (IL-10), and interact with tumor cells to promote i (20). Dendritic cells (DCs) capture tumor antigens and activate T cells, which play a crucial role in antigen presentation within tumor immunity (21). Regulatory T cells (Tregs) secrete TGF-β and IL-10 to suppress immune responses, whereas myeloid-derived suppressor cells (MDSCs) also release these inhibitory cytokines and induce dendritic cell apoptosis. CD8+ T cells recognize major histocompatibility complex (MHC) class I molecules on the surface of tumor cells via T cell receptors (TCRs) to induce tumor cell cytotoxicity. However, interactions between programmed death receptor-1 (PD-1) and its ligand (PD-L1), as well as tumor cell-derived exosomes, lead to T-cell exhaustion. Additionally, fibroblasts can differentiate into cancer-associated

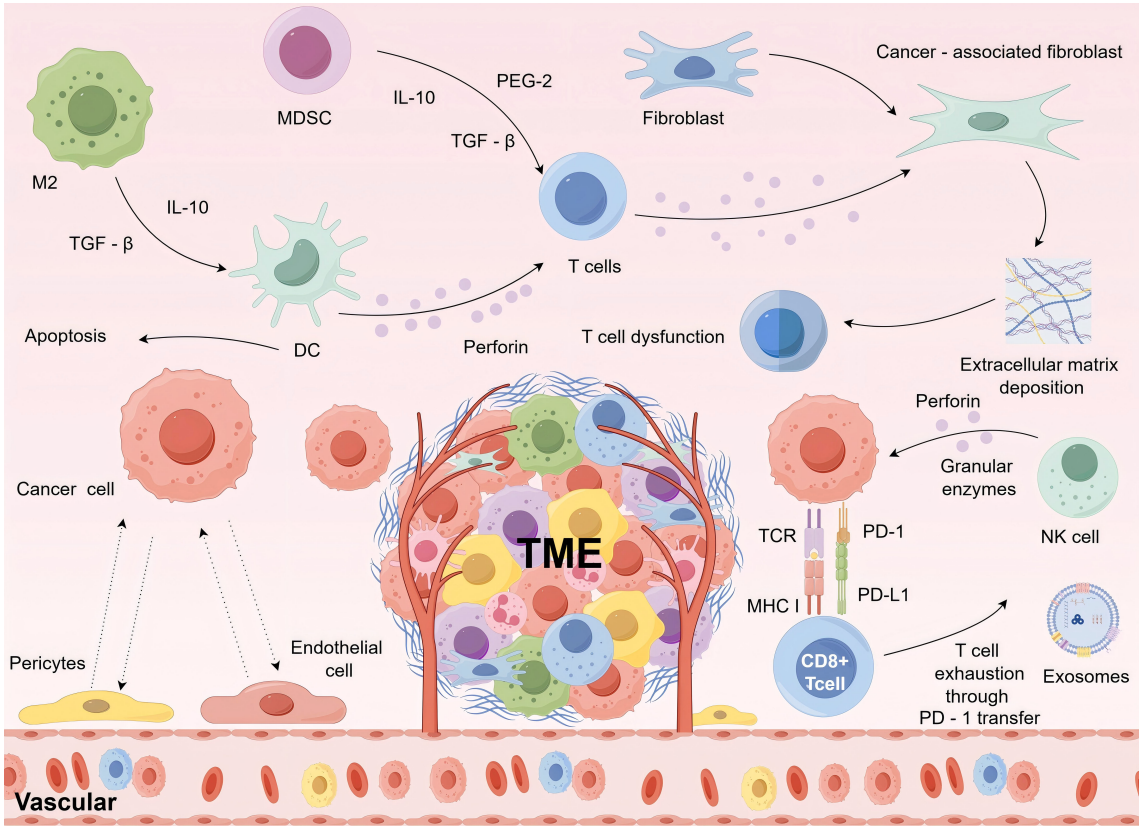

FIGURE 1
Interactions between immune cells and tumor cells in the tumor microenvironment.

fibroblasts (CAFs), contributing to extracellular matrix deposition, which further impairs T-cell function (22). This intricate interplay not only governs tumor growth, metastasis, and response to therapy but also indirectly affects the metabolism and function of normal tissues, such as skeletal muscle, through various pathways (23). Immunotherapy plays a central role in the vast ecosystem of tumor treatment. Strategies, such as ICIs targeting CTLA-4, PD-1, and PD-L1, as well as CAR-T cell therapy, aim to reprogram the immune system to better recognize and eliminate tumor cells (24). In the tumor microenvironment, immune cells undergo significant alterations (25). The activation, proliferation, and differentiation of T cells are tightly regulated, while macrophages, under tumor-derived signals, polarize into proinflammatory M1 or anti-inflammatory M2 phenotypes, dynamically shifting their cytokine production profile (26). IL-6 and TNF-α have intricate roles in polarization of immune cells.IL-6 enhances the inflammatory response by activating the STAT3 signaling pathway to promote Th17 cell differentiation and inhibit Treg cell generation.TNF-α, working together with IL-6, enhances Th17 cell polarization, worsening the immune inflammatory condition (27). This combined effect in the tumor microenvironment can contribute to immune cell dysfunction and help tumor cells evade the immune system.Conversely, in specific situations, IL-6 and TNF-α can show opposing effects. For example, TNF-α often promotes macrophages to polarize into the M1 phenotype, which has anti-tumor properties.Nonetheless, elevated levels of IL-6 might prevent M1 macrophages from polarizing and encourage their transformation into the M2 phenotype, which supports tumor growth. An imbalance in this opposing effect could affect the ability of immune cells to fight tumors within the tumor microenvironment (28). Cytokines such as IFN-γ and TNF-α travel through the bloodstream or paracrine pathways to reach skeletal muscle cells. IFN-γ binds to receptors on skeletal muscle cell surfaces, triggering the JAK-STAT signaling pathway. During this process, phosphorylated STAT proteins translocate into the nucleus, bind to the promoter regions of specific genes, and upregulate the expression of proteases, such as caspase-3, which degrade muscle proteins. In the JAK-STAT pathway, IFN-γ activates receptor-associated JAK kinases when it binds to its receptor (29).These JAK kinases have tyrosine kinase activity and, when activated, add phosphate groups to specific tyrosine residues on the receptor.The phosphorylated tyrosine residues act as docking sites for STAT proteins, which use their SH2 domains to bind to these residues and are then phosphorylated by JAK kinases. Phosphorylated STAT proteins form dimers, changing their shape and allowing them to penetrate the nucleus. After entering the nucleus, the dimerized STAT proteins attach to specific DNA sequences located in the promoter regions of target genes, including the Gamma Interferon Activation Sequence (GAS), which attracts transcription-related cofactors like RNA polymerase to start downstream gene transcription, thus controlling gene expression and affecting cellular functions (30).

This disrupts the balance between muscle protein synthesis and degradation, ultimately leading to muscle atrophy. TNF-α also interferes with the insulin signaling pathways. Under normal conditions, insulin binds to its receptor and activates insulin receptor substrate (IRS) proteins, initiating the PI3K-AKT pathway, which promotes glucose uptake in muscle cells (31). TNF-α activates the MAPK pathway, causing phosphorylation-induced inactivation of IRS proteins, blocking insulin signal transmission, and reducing glucose uptake by muscle cells, leading to metabolic dysregulation. The effects of IL-6 and TNF-α on muscles are significant (32). IL-6 can trigger the ubiquitin proteasome system in skeletal muscle cells, promoting muscle protein breakdown of muscle proteins and results in muscle wasting. Moreover, IL-6 hinders the growth and specialization of muscle satellite cells, impacting muscle repair and regeneration. TNF-α not only disrupts insulin signaling pathways affecting muscle metabolism but also works with IL-6 to boost muscle protein breakdown and hinder muscle repair. Research indicates a strong link between high serum levels of IL-6 and TNF-α in cancer patients and a decline in muscle strength and mass (33). Moreover, IL-6 and TNF-α can disrupt muscle contraction by altering calcium ion balance in muscle cells, causing fatigue and weakness. Abnormal angiogenesis and extracellular matrix remodeling within the tumor microenvironment are also closely linked to skeletal muscle alterations (34). Tumor angiogenesis is a complicated process that includes multiple angiogenic factors and signaling pathways (35). Vascular endothelial growth factor (VEGF) plays a crucial role in tumor angiogenesis, as tumor cells release significant quantities of VEGF to encourage endothelial cell growth, movement, and lumen creation, thus aiding in the development of tumor blood vessels. At the same time, the angiopoietin (Ang) family and fibroblast growth factors (FGF), among others, are also involved in this process (36). The newly developed blood vessels display irregular structures and functions, with incomplete vessel walls and heightened permeability, supplying nutrients and oxygen to tumor cells while also facilitating tumor cell metastasis. Irregularities in tumor blood vessels impact the penetration of immune cells into tumor tissues, changing the immune status of the tumor microenvironment. For example, increased vascular permeability may hinder immune cells from exiting the bloodstream, thereby diminishing their ability to destroy tumor cells. The disorganized growth of the tumor vasculature not only nourishes the tumor but also deprives the surrounding tissues of nutrients, placing skeletal muscle under ischemic and hypoxic conditions. Under such microenvironmental stress, skeletal muscle mitochondria experience oxidative phosphorylation dysfunction, reducing ATP production and shifting metabolism toward anaerobic glycolysis, leading to lactic acid accumulation (37). This disrupts the intracellular pH and ion homeostasis, ultimately impairing muscle cell metabolic functions. Additionally, when stimulated by tumor-derived signals, stromal cells such as fibroblasts secrete extracellular matrix (ECM) components including collagen and fibronectin, which undergo abnormal expression and deposition (38). Collagen, fibronectin, laminin, proteoglycans, and other components make up the ECM, a vital element of the tumor microenvironment. Through different mechanisms, tumor cells and cancer-associated fibroblasts (CAFs) can change the composition and structure of the ECM.As tumors progress, collagen fibers released by CAFs are crosslinked and remodeled, resulting in stiffer ECM. The alteration in stiffness influences the ability of tumor cells to migrate, enhancing their invasion and spread (39). Modifications in the ECM also impact immune cell function. For instance, irregular ECM can disrupt the adhesion and movement of immune cells, hindering their ability to identify and destroy tumor cells. Certain elements of the ECM can engage with receptors on immune cell surfaces, modulating their activation and cytokine release, thereby affecting the immune condition of the tumor microenvironment (40). These changes, mediated by integrin receptors, affect cytoskeletal structures and mechanotransduction signaling within skeletal muscle cells, further influencing cell migration, proliferation, and differentiation (41).Tumor blood vessels and the extracellular matrix are closely linked. Irregular tumor angiogenesis influences ECM remodeling, and alterations in the ECM can impact the stability and function of tumor blood vessels. For instance, the ECM surrounding tumor blood vessels can stabilize and support them, while an abnormal ESubstances released by tumor blood vessels can influence the production and breakdown of the ECM, while ECM components can engage with receptors on endothelial cell surfaces, impacting angiogenesis and vessel performance (40). This interaction affects not just tumor growth and metastasis but also significantly alters immune cell function within the tumor microenvironment, contributing to its complexity.

Studies on prostate cancer bone metastasis have identified BHLHE22 as a key transcription factor that is highly expressed in tumor cells (42). BHLHE22 interacts with PRMT5 to form a transcriptional complex that binds to the CSF2 promoter, initiating its transcription. CSF2, an important cytokine, recruits a large number of immunosuppressive neutrophils and monocytes into the tumor microenvironment (43). These immunosuppressive cells secrete arginase-1 (Arg-1) and other immunosuppressive factors that inhibit T-cell activation and proliferation, reduce the number of CD4+ and CD8+ T cells, and impair their function (44). This promotes bone metastasis of tumor cells and creates a strongly immunosuppressive microenvironment (45). This indicates that in prostate cancer bone metastasis, a BHLHE22-PRMT5-CSF2-mediated immunosuppressive pathway exists, which interacts with immune cells in the tumor microenvironment and jointly influences tumor progression and metastasis (46). This further exacerbates its impact on normal physiological functions, including potential interference with skeletal muscle metabolism and function (47). In soft-tissue sarcomas, researchers have discovered that the transcriptional co-activator YAP1 plays a significant role in tumor cells. YAP1 promotes the deposition of collagen VI (COLVI) in the tumor microenvironment (48). COLVI interacts with collagen I (COLI) to remodel the extracellular matrix (ECM) (49). Specifically, COLVI directly modifies the architecture of COLI fibers, altering their physical properties and subsequently affecting the function of CD8+ T cells in the tumor microenvironment (50). COLVI induces CD8+ T-cell dysfunction, characterized by upregulation of inhibitory receptor expression, decreased proliferation, and reduced cytotoxic function (51). In contrast, COLI enhances CD8 + T-cell function and serves as a tumor suppressor to some extent (52). This discovery reveals

that in soft tissue sarcomas, tumor cells influence immune cell function by regulating ECM components, thereby shaping a tumor-friendly immune escape microenvironment. Such alterations in the tumor microenvironment (TME) may indirectly affect the microenvironment of skeletal muscle cells by affecting local nutrient transport and metabolic waste clearance, potentially influencing skeletal muscle metabolism and function (53). Researchers constructed various genetically engineered mouse models of multiple myeloma and found that the MAPK-MYC pathway plays a critical role in disease progression (54).The activation of MYC correlates with tumor progression rate and affects immune cell infiltration and function within the tumor microenvironment. In rapidly progressing models, studies have identified a high prevalence of activated/exhausted CD8 + T cells and a reduced population of immunosuppressive regulatory T cells (Tregs). In slow progressing models, they found lower CD8+ T-cell infiltration and more Tregs, which suppressed immune responses (55). Single-cell transcriptomics and functional experiments demonstrated that the CD8+/Treg ratio could serve as an important predictor ICB therapy response. In untreated smoldering multiple myeloma patients, a high CD8+/Treg ratio is associated with early disease progression (56). In patients with newly diagnosed multiple myeloma patients undergoing Len/Dex treatment, this ratio was correlated with early relapse (57). In ICB-resistant multiple myeloma models, increasing CD8+ T-cell cytotoxicity or depleting Tregs reverses immune therapy resistance and prolongs disease control (58). These findings indicate that in multiple myeloma, the genetic characteristics of tumor cells and their interaction with immune cells in the tumor microenvironment jointly determine disease progression and response to immunotherapy (59). This alteration in the immune microenvironment may also indirectly influence skeletal muscle physiology by modulating the skeletal muscle cell energy metabolism and protein synthesis (60).There are significant commonalities in the interactions between tumor cells and immune cells among these cancers. Tregs play a role in the immunosuppressive process in prostate cancer, soft tissue sarcomas, and multiple myeloma (61). In bone metastasis of prostate cancer, Tregs secrete inhibitory cytokines that can suppress T cell activation and proliferation. Tregs can also dampen the immune response enabling tumor cells to escape immune surveillance. In multiple myeloma, variations in Treg quantity and activity are closely associated with disease progression. Simultaneously, CD8+ T cells, which are crucial effector cells in anti-tumor immunity, have a significant impact on these cancers. When functioning properly, they can identify and destroy tumor cells, but their abilities are suppressed by the tumor microenvironment. For instance, modifications in the tumor microenvironment of soft tissue sarcomas can cause CD8+ T cells to function less effectively (53). The progression of multiple myeloma and the effectiveness of immunotherapy are also impacted by the infiltration and functional status of CD8+ T cells. The key regulatory molecules and signaling pathways vary noticeably between different types of cancer. In the context of prostate cancer, BHLHE22 and PRMT5 assemble a transcriptional complex that initiates CSF2 transcription, which then attracts many immunosuppressive neutrophils and monocytes, promoting the tumor's metastasis to the bones. In soft tissue sarcomas, YAP1 is a significant transcriptional co-activator. It encourages collagen VI deposition, alters the extracellular matrix, and specifically hinders CD8+ T cell functions, fostering an immune-escape environment for tumor cells (53). The regulation of multiple myeloma is mainly through the MAPK-MYC pathway. The activation of this pathway influences immune cell infiltration and function, with the CD8+ T cell to Treg ratio being crucial for disease progression and immunotherapy response. In skeletal muscle injury and regeneration, regulatory T cells (Tregs) are essential for modulating macrophage polarization, promoting muscle satellite cell proliferation and differentiation, and suppressing excessive inflammation (62). Tregs facilitate the conversion of M1-type (proinflammatory) macrophages into M2-type (anti-inflammatory) macrophages, which, in turn, secrete growth factors and cytokines like TGF-β, promoting muscle repair and regeneration (63). Tregs secrete amphiregulin (Areg), which acts directly on muscle satellite cells, stimulating their proliferation and differentiation, and thereby accelerating muscle repair (64). By inhibiting excessive inflammation, Tregs prevent further damage to skeletal muscle cells (65). In some muscular diseases, such as Duchenne muscular dystrophy (DMD), Tregs help suppress type I inflammatory responses, reduce muscle damage and inflammation, and slow disease progression (66). This suggests that Tregs play an essential role in maintaining skeletal muscle homeostasis and in promoting injury repair (67). Their proper function may have potential therapeutic applications in mitigating muscle-related side effects during cancer treatment, such as reducing chemotherapy- or immunotherapy-induced muscle atrophy or dysfunction (67).

2.2 Effects of immunotherapy and immunochemotherapy on muscles

With the widespread application of immunotherapy in clinical oncology, its combination with chemotherapy has become increasingly common, with the aim of merging the cytotoxic effects of chemotherapy on tumor cells with immunotherapy immune modulation, achieving a synergistic antitumor response (68). However, while enhancing antitumor efficacy, this combination therapy also has adverse effects on skeletal muscles. Chemotherapeutic agents exert cytotoxic effects that significantly affect the skeletal muscle (6). For example, doxorubicin can enter skeletal muscle cells through passive diffusion or active transport mechanisms, intercalate into DNA, interfere with DNA replication and transcription, and induce the production of large amounts of reactive oxygen species (ROS). This damages the membranes of mitochondria and other organelles, leading to mitochondrial dysfunction, reduced ATP production, and energy crisis within the cell (69). Cisplatin primarily forms adducts with DNA, blocks DNA repair and transcription, and triggers a series of toxic

reactions such as the initiation of apoptosis (70). During this process, muscle cell mitochondria release damage-associated molecular patterns (DAMPs) including mitochondrial DNA and HMGB1 (71). These molecules are recognized by pattern recognition receptors (PRRs), such as Toll-like receptors (TLRs) on innate immune cells, thereby activating the innate immune system and triggering an inflammatory response (72).

During immunotherapy, T cells are massively activated. They proliferate and differentiate into effector T cells that infiltrate tumors. At this time, immune dysregulation may occur, leading to a cytokine storm (73) The massive release of cytokines such as IFN-γ, TNF-α, and IL-6 not only attacks tumor cells but also indirectly damages skeletal muscle cells. At the molecular level, IFN-γ can activate the ubiquitin-proteasome system, upregulating the expression of proteolytic enzymes related to actin and myosin degradation and leading to their breakdown (74). Additionally, IFN-γ can induce post-translational modifications that alter the structure and function of actin and myosin, thereby altering their kinetic properties and impairing muscle contraction (74). TNF-α can interfere with calcium regulation by activating membrane calcium channels and disrupting intracellular calcium homeostasis, leading to abnormal intracellular calcium ion concentration (75). This disruption damages the excitation-contraction coupling, resulting in impaired muscle contraction and relaxation. In clinical studies, skeletal muscle function has been assessed in cancer patients undergoing immunochemotherapy (76). In a study of non-small cell lung cancer patients, muscle force began to decline significantly around the second or third week of treatment (77). Assessments using grip strength tests and lower limb muscle force measurements revealed that the average grip strength decreased by approximately 15-20%, whereas the maximal contraction force of the lower limbs was reduced by 20-25% (78). In terms of exercise endurance, the six-minute walk distance decreased by 100-150 meters compared to the pre-treatment levels (79). Similar findings were observed in studies on patients with breast cancer, in which progressive muscle fatigue and limited physical activity were noted during treatment (80). As the number of treatment cycles increases, skeletal muscle dysfunction becomes more pronounced, characterized by muscle atrophy and a continuous decline in muscle strength (81). These findings further confirm the adverse effects of immunochemotherapy on skeletal muscle, severely affecting patients' quality of life and treatment tolerance (82). In the realm of clinical practice, achieving a balance between effective therapy and skeletal muscle protection is highly important for patients. Prior to initiating immunotherapy, it is essential to conduct a thorough evaluation of patients, which should encompass detailed tests of muscle tests, a review of medical history (with a focus on muscle-related conditions), and assessments of physical health (83). Individualized treatment plans should be developed based on the evaluation results. In cases of patients with compromised muscle function or muscle disorders, the dosage of immunotherapy drugs may be adjusted, or drugs that have a lesser effect on muscles can be selected. Throughout the treatment, consistently check the patients' muscle function indicators, including muscle strength and endurance, while also keeping an eye on relevant serum markers like creatine kinase (84).

2.3 Effect of drugs on muscle cells

Chemotherapeutic agents widely used in cancer treatment include cyclophosphamide, doxorubicin (DOX), and 5-fluorouracil (5-FU), all of which may alter muscle cell function at their final destination, including skeletal muscle contraction-relaxation properties (85). As an alkylating agent, cyclophosphamide acts on the bone marrow, bladder, lungs, and heart, and prolongs muscle paralysis through pseudocholinesterase inhibition. DOX, apart from its cardiotoxic effects, may induce muscle dysfunction, tending to cause persistent fatigue and weakness even after treatment (86). Drugs such as DOX can cause oxidative stress, resulting in increased ROS levels and disturbance of the redox balance in the muscle cells (87). Oxidative stress ultimately leads to mitochondrial damage, resulting in mitochondrial dysfunction (47). In this regard, energy metabolism and calcium homeostasis in the muscle cells can be disrupted. In addition, chemotherapy can induce structural and functional changes in the mitochondria, including swelling and rupture, vacuolization of the sarcoplasmic reticulum, inhibition of ATPase, and increased intracellular calcium concentrations, thus interfering with contraction and relaxation (88). As a result, metabolic pathways are progressively disturbed, thereby producing less ATP necessary for muscle contraction and leading to decreased strength and endurance (89).

Clinical trials that considered metabolic changes after chemotherapy in cancer patients showed significant losses in both muscle mass and strength (90). For example, trials in post-gastrectomy patients have suggested that adjuvant chemotherapy might further deteriorate lean body mass loss, which again negatively affects the patient's functional ability, quality of life, drug efficacy, and recovery (91). The effects of chemotherapy on skeletal muscle depend on the mode of administration, dose, and patient variables (92). For example, studies conducted on healthy mice treated with single or multiple doses of docetaxel did not show significant changes in muscle strength, implying that additional research is required to explain the impact of chemotherapy on the muscles (93).

Chemotherapeutic drugs can affect various metabolic pathways that directly or indirectly affect skeletal muscle function. For instance, the CAF regimen widely used in breast cancer, which includes cyclophosphamide, doxorubicin, and 5-fluorouracil, can induce muscle catabolism through oxidative stress associated with DOX metabolism in both liver and muscle tissues (94). Similarly, S-1, which is widely used in adjuvant therapy for gastric cancer, facilitates the loss of muscle mass through mechanisms that could implicate toxic metabolites arising during its metabolism, thereby acting directly on the muscle. The rate of drug clearance influences the duration and extent of exposure of the skeletal muscle to chemotherapy. Therefore, individual variability in genetic and physiological factors leads to variability in clearance (95). Therefore, similar regimens may affect the skeletal muscle of

different patients (96). Studies conducted on this issue have estimated a decline in clearance following chemotherapy, which prolongs the retention time of the drug and enhances catabolism and dysfunction. Chemotherapeutic drugs are primarily cleared by metabolic enzymes (3). These enzymes exhibit different activities and expression levels, which are influenced by chemotherapeutic drugs (97). Recently, new targeted chemotherapy drugs have been developed, showing distinct benefits in precise cancer therapy, but their possible effects on muscles have increasingly become a focus. PARP inhibitors work against cancer by blocking poly(ADP-ribose) polymerase (PARP), which in turn disrupts the DNA repair process in cancer cells. Research indicates that PARP inhibitors might influence the energy metabolism within muscle cells (98). In studies with mice, prolonged use of PARP inhibitors leads to reduced ATP levels in muscle tissue, which impacts normal muscle contraction. PARP inhibitors might disrupt the function of mitochondria in muscle cells, affecting the respiratory chain and leading to decreased ATP production. PARP inhibitors might influence the redox equilibrium in muscle cells, resulting in the buildup of reactive oxygen species (ROS), which can initiate oxidative stress responses and harm muscle cells. Antibody-drug conjugates (ADCs) are a new type of targeted chemotherapy that combines monoclonal antibodies, cytotoxic agents, and linkers to accurately deliver toxic drugs to cancer cells (99). Although ADCs improve anticancer effectiveness and minimize toxicity to healthy tissues, their effects on muscles should not be ignored. Clinical research has shown that some patients receiving ADCs report symptoms like muscle weakness and fatigue. Small-molecule inhibitors aimed at the epidermal growth factor receptor (EGFR) have been documented to potentially impact the proliferation and differentiation of muscle cells, in addition to inhibiting tumor cell growth. Laboratory studies have indicated that EGFR inhibitors might disrupt the EGFR signaling pathway in muscle satellite cells, hindering the activation and differentiation of satellite cells, which impacts the muscles' ability to repair and regenerate (100). This results in a complex regulatory feedback mechanism. Some studies suggest that chemotherapy drugs induce or inhibit the activity of certain enzymes that affect drug metabolism and clearance, and may also alter muscle biomechanics (101).

2.4 Immune system and inflammatory response

During the progression of various diseases, the immune system and inflammatory responses are intricately intertwined and mutually influential, profoundly altering disease trajectories and outcomes (102). These processes also play a significant role in skeletal muscle function, with cytokine storms often serving as the key factors (Figure 2). Cytokine storms present with a wide range of clinical manifestations, including pneumonia, respiratory distress, and pulmonary edema in the lungs; hepatomegaly, liver failure, liver injury, and elevated liver enzymes in the liver; kidney failure and acute renal dysfunction in the kidneys; coagulation abnormalities, cytopenia, anemia, leukocytosis, vasodilatory shock, and spontaneous bleeding in the vascular system; aphasia, seizures, delirium, and altered consciousness in the nervous system; tachycardia, hypotension, and cardiomyopathy in the heart; arthritis and joint pain associated with rheumatic diseases; diarrhea, nausea, ascites, and vomiting in the digestive system; and edema and rashes in the skin. In fibrotic diseases, excessive extracellular matrix (ECM) deposition and impaired degradation are central pathological features. Inflammatory responses trigger the release of cytokines, including TGF-β, TNF-α, and the IL family, which activate fibroblasts, promote epithelial-mesenchymal transition (EMT), endothelial-mesenchymal transition (EndoMT), and mesothelial-mesenchymal transition (MMT), and promote the excessive generation of myofibroblasts. This results in excessive ECM production, which disrupts the skeletal muscle microenvironment (103).

In systemic autoimmune fibrotic diseases, such as systemic sclerosis (SSc), excessive autoantibody production and abnormal activation of immune cells(e.g., T cells, B cells, and macrophages) drive tissue infiltration. Imbalances in T-cell subsets, such as increased secretion of Th2 cytokines that promote fibroblast activation and extracellular matrix (ECM) deposition, and Th17 cells producing IL-17 to amplify inflammation, induce tissue damage, suppress regulatory T (Treg) cell function, and exacerbate autoimmune responses and fibrosis (104). Macrophages polarize into the M1 and M2 subtypes. M1 macrophages drive early inflammation, whereas M2 macrophages secrete TGF-β and PDGF in the later fibrotic stages, promoting myofibroblast differentiation and ECM synthesis, thereby accelerating fibrosis (105). In liver fibrosis, activated macrophages undergo phenotypic shifts and release cytokines that activate stellate cells, thereby inducing excessive ECM deposition (106). Systemic immune dysregulation and chronic inflammation further impair skeletal muscle protein metabolism and function (107). During tumor progression, the tumor microenvironment (TME) maintains a chronic inflammatory state (19). Immune cells such as tumor-associated macrophages (TAMs) and neutrophils secrete cytokines that promote tumor cell proliferation and migration (108). TAMs polarized to the M2 phenotype release TGF-β and VEGF, thereby suppressing antitumor immunity, whereas tumor cells produce immunosuppressive molecules such as PD-L1 to deactivate T cells and facilitate immune escape (109). For example, chronic intestinal inflammation in colorectal cancer increases tumor risk and immunosuppressive TME weaken immune surveillance. During cancer therapy, particularly immunotherapy, systemic immune hyperactivation may trigger a cytokine storm. Overproduction of cytokines such as IFN-γ, TNF-α, and IL-6 indirectly damages skeletal muscle cells; IFN-γ activates the ubiquitin-proteasome system, degrading actin and myosin, whereas TNF-α disrupts excitation-contraction coupling and impairs muscle function (15). Cytokine storms also elevate serum levels of TNF-α and IL-6, inducing protein breakdown, suppressing synthesis, and hindering muscle fiber regeneration, thereby forming a vicious cycle (110). Chemotherapeutic drugs, such as S-1, further activate immune cells, alter cytokine profiles, and disrupt skeletal muscle metabolism. Prolonged inflammation exacerbates muscle fiber damage. Although immunotherapies (e.g., checkpoint inhibitors

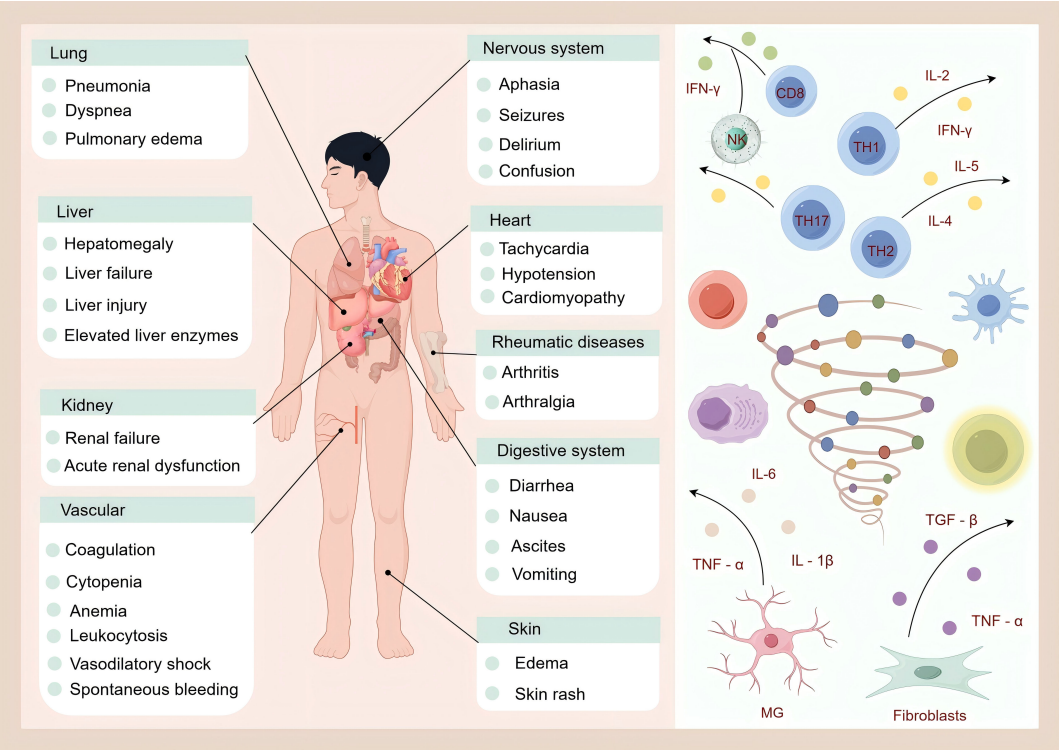

FIGURE 2
Cytokine storm and its clinical manifestations.

and CAR-T) show efficacy, adverse effects, such as cytokine storms (common in CAR-T therapy), may worsen skeletal muscle injury and compromise treatment outcomes. In neurodegenerative diseases such as Alzheimer's disease (AD), activated microglia initiate neuroinflammation by releasing cytokines (IL-1β, IL-6, and TNF-α), leading to neuronal damage, Aβ plaque accumulation, and tau hyperphosphorylation. Peripheral T-cell infiltration into the brain may alter microglial function and Aβ metabolism, thereby accelerating disease progression. Neurological disorders affect skeletal muscle via neuromuscular junctions or neuroendocrine pathways, causing atrophy and weakness (111). Cytokine storms can amplify neuroinflammation and muscle damage, thereby complicating disease management. In osteoporosis, bidirectional interactions exist between the immune system and skeletal muscles (112). Postmenopausal osteoporosis (PMOP), age-related osteoporosis, and diabetic osteoporosis involve estrogen deficiency, aging, and hyperglycemia, which alter immune cell function, elevate proinflammatory cytokines, stimulate osteoclastogenesis, and disrupt T-cell balance (112). Altered bone structure and biomechanics in osteoporosis modify mechanical loading on muscles, leading to long-term atrophy and functional decline. Muscle-derived factors also regulate bone metabolism by interacting with the immune and inflammatory pathways. Cytokine storms may further destabilize immune homeostasis, intensify inflammation, and accelerate bone loss and muscle damage. Immune and inflammatory responses are intricately linked to skeletal muscle in multiple diseases. Cytokine storms exacerbate disease complexity and severity and negatively affect muscle function. A deeper understanding of these interactions is critical for developing effective therapies and improving patient prognosis (113).

3 Methods and tools for assessing skeletal muscle biomechanics

3.1 Methods for evaluating skeletal muscle biomechanics

3.1.1 Assessment of muscle force

Initial screening can be performed using Manual Muscle Testing (MMT), which is convenient, but highly subjective. To obtain more objective data, a hand-held dynamometer (HHD) can be used to measure maximal voluntary isometric strength such as knee extension muscular force (114). Additionally, leg power devices can be used to assess lower limb muscular force by providing quantifiable data and highly reliable results. To study variations in muscle force with speed, a length-tension instrument (ID) can accurately capture force variation curves across the full range of motion, thereby facilitating a deeper understanding of muscle function (115).

In addition to direct strength measurements, other techniques such as percutaneous muscle biopsy have also been used to assess muscle biomechanical properties. Under local anesthesia, a muscle

sample was extracted from the vastus lateralis of the thigh and promptly placed in a culture dish containing paraffin oil. The sample was then kept on a 10°C ice pack to preserve freshness and physiological activity. Subsequently, it underwent cutting and chemical peeling to isolate individual fiber segments, which were then treated in a relaxing solution at 4°C for 24 h to complete the chemical peeling process (116). Following treatment, the fiber segments were stored at -20°C to maintain bioactivity and structural integrity for further experimentation. On the day of the experiment, the fibers were treated in a relaxing solution containing 0.5% Brij-58 for 30 min to enhance permeability and then mounted onto an experimental apparatus (Figure 3A) equipped with a high-precision force sensor and a DC torque motor. This setup simulates physiological muscle contraction and relaxation by measuring the force generated during contraction or stretching, respectively. During testing, fibers were exposed to various Ca2+ concentrations to establish the "force-Ca2+ relationship," and the data were analyzed using GraphPad Prism 6 software for Hill curve fitting to determine the pCa50 and Hill coefficients. Additionally, the impact of DTDP-GSH complexes on fiber Ca2+ sensitivity was assessed by exposing the fibers to 100μM DTDP solution for 5 min, followed by 2 min in 5 mM GSH solution, and recording the changes in pCa50 (Figure 3E) (117). Relaxation tests in activation solutions containing specific Ca2+ concentrations involved introducing a rapid relaxation step via the servomotor once the peak steady-state force was achieved (Figure 3B), simulating mechanical changes in the muscle during rapid contraction or extension, and recording data at the peak force (Figure 3C). The force response in the rapid release phase was divided into four stages (Figure 3F) to evaluate instantaneous response and recovery capabilities. The instantaneous stiffness and time required for the force to reach half-maximal (t1/2) were calculated to quantify the mechanical properties of the fibers (Figure 3D). These experiments were repeated for different relaxation lengths to ensure consistent measurement. Through this series of experiments, comprehensive data on muscle fiber mechanical properties such as instantaneous stiffness and unloaded shortening velocity were obtained, offering valuable insights into the mechanical behavior of muscle fibers (118).

3.1.2 Assessment of muscle mass

A single-fiber experiment is a method for assessing muscle quality and function at the muscle-cell level. The direct measurement of the mechanical properties of individual muscle fibers eliminates the influence of the nervous system, tendons, and extracellular matrix. This method allows researchers to directly evaluate the function of myofibrillar proteins, providing a more precise understanding of the mechanical changes in muscles, which are essential indicators of muscle quality (119). MRI and DXA are two of the most valuable non-invasive imaging modalities that provide complete information on the quality and distribution of muscles (Figure 3G) (120). Using magnetic fields and radio waves, MRI generates highly detailed images of muscles, which allows for quantitative volume measurement and observation of internal structural changes. The technology behind DXA discrimination of fat and muscle, and the process of measuring bone mineral content in body tissues, involves emitting two X-ray beams at varying energy levels and assessing their absorption after passing through the body. These two techniques will enable determination of the effects of chemotherapy on the biomechanical properties of skeletal muscles.

3.1.3 Assessment of muscle performance

Physiological and biochemical tests at the single-fiber level are powerful tools for comprehensively assessing muscle efficiency and functional status. To investigate the mechanisms underlying muscle performance, researchers have applied single-fiber techniques, that is, isolated and fixed muscle fibers with great precision. Using high-precision force sensors and fine-tuned motors, they simulated the natural state of human muscles, conducted isotonic contraction experiments to measure the force-velocity relationship, and applied the hyperbolic Hill equation to calculate the absolute and normalized powers of the fibers (Figure 3H) (121). Furthermore, measurements of the peak force, unloaded shortening velocity, residual force enhancement, and residual force depression have allowed researchers to unmask muscle responses to a prior contraction history. Passive elasticity measurements include the stretching of fibers of various lengths to measure muscle stiffness and elasticity. The relaxation distance was plotted based on the time of unloaded shortening for different activation and release lengths (Figure 3I). Finally, the peak power was calculated by measuring the force generated at the maximum contraction speed, and muscle calcium sensitivity was evaluated by changing the concentration of calcium ions. Thus, all the above-mentioned parameters provide a full understanding of the dynamics of the muscle, along with its activation efficiency (122).

3.1.4 Assessment of muscle stiffness

Mechanomyography (MMG) examines dynamic muscle stiffness by measuring the natural oscillation frequency and damping ratio of muscles in response to short mechanical stimulation. Owing to its ease, low cost, and minimal dependence on technical expertise, this technique has been widely applied in clinical and research settings. Myotonometry has special applications in the assessment of muscle stiffness variations under distinct conditions of muscle contraction (123). For example, muscle stiffness can increase after eccentric exercise, which indicates the degree of muscle damage. Myotonometry can monitor and quantify these changes in muscle stiffness in real time and therefore provide an indication of the degree of muscle damage and recovery. Myotonometry demonstrated high internal consistency, ensuring stability and reproducibility during the assessment. However, some influencing factors must be considered when this device is put into practical use (124). For example, the muscle composition, length, cross-sectional area, and selection of measurement points for different subjects may affect the evaluation results. Therefore, when conducting myotonometric assessments, these variables should be strictly controlled to ensure the accuracy of evaluation results.

Shear wave elastography is an advanced non-invasive ultrasound technology with unique advantages in the

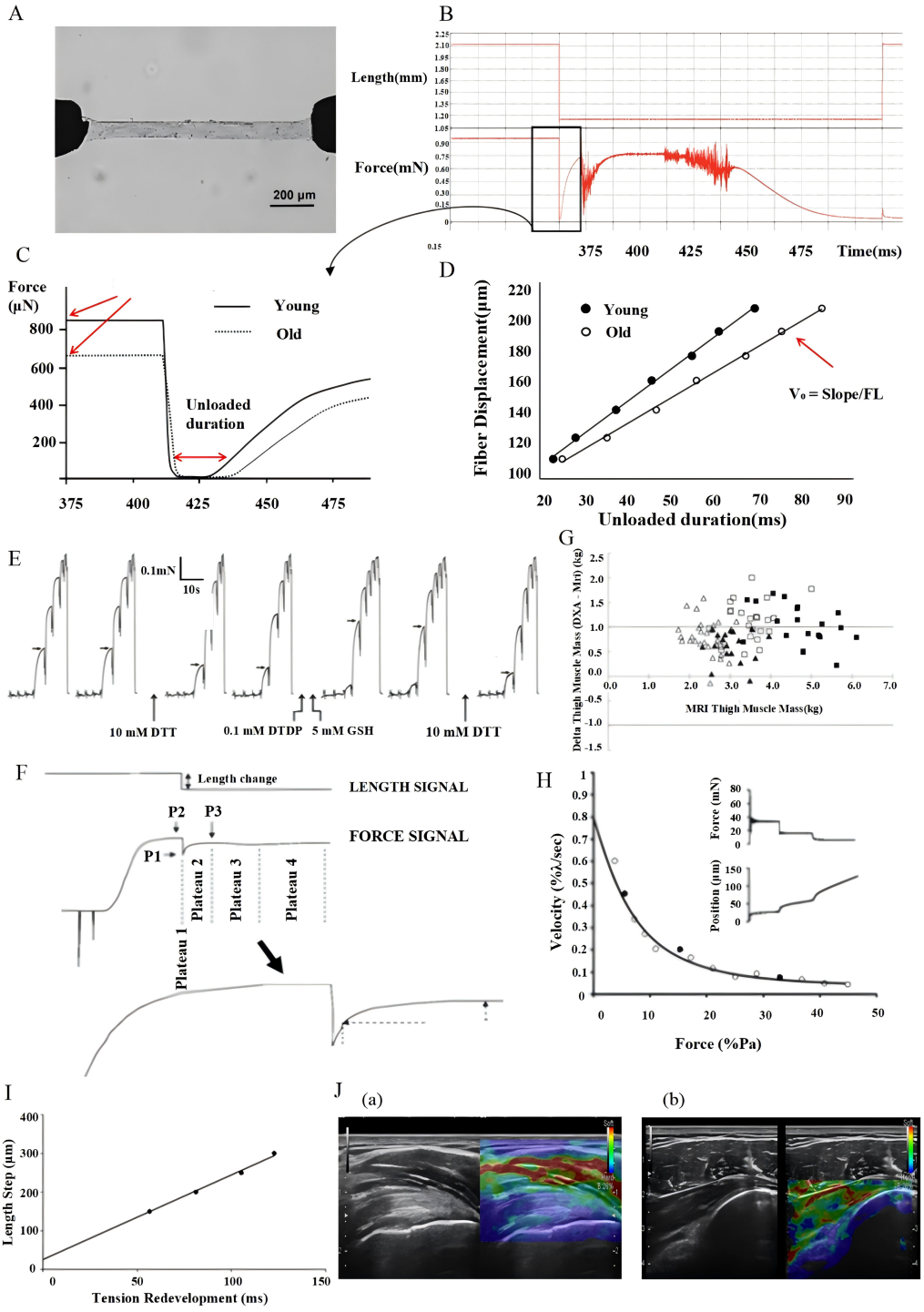

FIGURE 3
Diagram of percutaneous muscle biopsy experiment. **(A)** Image of the permeabilized fiber connected to a force transducer and servo motor. **(B)** Relaxation testing of the activation solution. **(C)** Duration of unloading after the peak force was achieved. **(D)** Unloaded shortening velocity. **(E)** Force response of vastus lateralis fibers exposed to DTT and DTDP-GSH. **(F)** Phases experienced by isometrically activated fibers during rapid length release. **(G)** Bland-Altman plot showing thigh muscle mass determined by MRI on the x-axis. **(H)** Isotonic contraction experiments, measuring force-velocity relationship. **(I)** Shortening velocity after fiber unloading. **(J)** Strain ultrasound elastography of the supraspinatus tendon (a), infraspinatus tendon, and posterior capsule (b).

measurement of biomechanical properties, especially muscle stiffness, in skeletal muscles (125). This technology is divided into two main types: static shear wave elastography (SSE) and dynamic shear wave elastography (SWE). The SSE measures the strain variation induced by external compressive pressure to provide qualitative information on tissue hardness (Figure 3J). SWE employs an acoustic radiation force to generate and propagate shear waves within tissues, which in turn measures the speed of

propagation of shear waves to quantify the hardness of tissues. This provides much detail and objectivity in the analysis of mechanical properties. During the measurement of muscle hardness, SWE is more sensitive and accurate than SSE. SWE can directly quantify the propagation speed of shear waves, which is linearly related to tissue stiffness. Therefore, it reflects the precise mechanical status of muscles (125).

3.2 Tools for assessing muscle function

3.2.1 Imaging technologies

Imaging technologies play a critical role in evaluating the impact of chemotherapy on the biomechanical properties of skeletal muscles. These technologies enable visual observation and quantification of structural changes, fiber orientation, and tissue characteristics of the muscles (126). Ultrasound imaging techniques, including A-mode, B-mode, and M-mode, offer a relatively economical and portable method for the real-time monitoring of muscle function (Figure 4A). A-mode ultrasound creates images based on the relationship between echo intensity and time, is commonly used for measuring muscle thickness, and generates two-dimensional images through transducer scanning, providing a visual view of muscle fibers and connective tissues, which is highly suitable for clinical muscle analysis (Figure 4B). In contrast, M-mode displays echoes of moving structures and is often applied in cardiac muscle assessments. Despite the advantages of ultrasound imaging, such as being non-invasive and allowing real-time monitoring, it has a limited field of view, high operator dependency, and insufficient penetration.

Magnetic Resonance Imaging (MRI), with its high-resolution and multi-contrast imaging capabilities, plays an essential role in evaluating muscle morphology, structure, and function (127). MRI can provide detailed cross-sectional images of muscles, helping researchers understand muscle fiber types, fat infiltration, and muscle injuries, making it a powerful tool for assessing muscle mass and health (128). However, MRI is expensive, complex, and often requires prolonged cooperation, which makes it unsuitable for all patients.

Elastography assesses tissue stiffness by measuring its response to mechanical pressure, thereby providing information complementary to traditional anatomical imaging (Figure 4C). Strain elastography and shear wave elastography quantitatively assessed tissue stiffness through tissue displacement and shear wave propagation speed, respectively, to understand the functional changes in the muscle (Figure 4D) (129). Clinically, elastography is widely used for disease diagnosis in multiple organs, helping doctors determine the nature of nodules or masses by evaluating the tissue stiffness. Although elastography has the advantage of being non-invasive, it is technically complex, quantitative analysis is challenging, and is yet to be widely adopted in routine clinical examinations.

3.2.2 Electrical impedance myography

Electrical impedance myography (EIM) was used to evaluate muscle function. The EIM measures muscle electrical impedance by

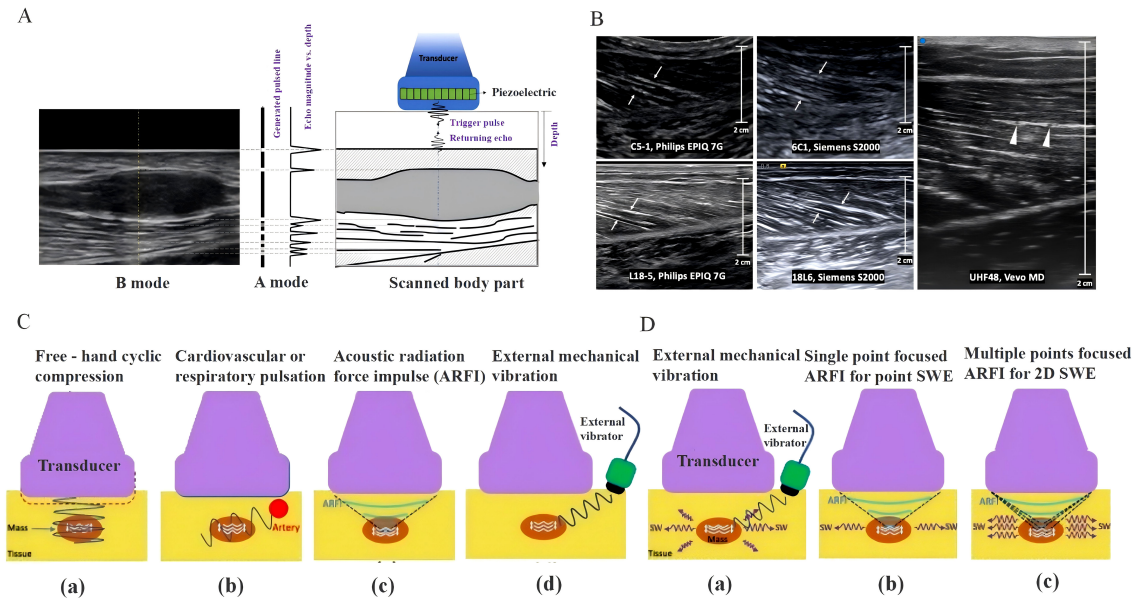

FIGURE 4
(A) Illustration of data generation in A- and B-mode ultrasound imaging. **(B)** Longitudinal B-mode ultrasound image of the medial gastrocnemius muscle of a healthy volunteer. **(C)** Diagram of strain ultrasound techniques, including freehand cyclic compression (a), internal organ pulsation from the heart and lungs (b), acoustic radiation force impulse (c), and external source vibration (d). **(D)** Schematic of shear-wave elastography techniques, including external mechanism vibration (a), single-point focused acoustic radiation force impulse (b), and multi-point focused acoustic radiation force impulse (c).

the application of low-intensity, multi-frequency alternating current to the muscle, and provides a quick, non-invasive, and relatively inexpensive means to evaluate muscle mass and health. The technical principle of EIM is based on the impedance characteristics of the muscles to electric current. The EIM reflects the microscopic structure and functional state of the muscle by analyzing how the current propagates through the muscle (130). The advantage of this technology is that it uses low-intensity current that is harmless to the body. The testing process is quick and convenient because the current is constrained within the muscle tissue and shuns low-resistance pathways such as major blood vessels and arteries.

Unlike whole-body BIA, EIM is unaffected by individual hydration levels. In addition, the results from the EIM measurements are related to the biomechanical properties of the muscle, such as the capacity for force generation, which may make the EIM one of the most valuable tools for evaluating the impact of chemotherapy on muscles. Nevertheless, some of the advantages of the EIM include its limitations. For example, EIM depend on the skin and subcutaneous fat layer; further research is required to address these issues. However, the ability to grade the deeper muscles remains unexplored. However, EIM is a low-cost technology that is more accessible and therefore becomes an assessment tool with much value in both the clinical and research realms compared to costly imaging modalities, such as MRI (130).

4 Immunotherapy and tumor microenvironment in clinical oncology

Immunotherapy has become a cornerstone of cancer treatment, with the dynamic development of diverse treatment modalities presents unprecedented opportunities coupled with clinical challenges. This article systematically delineates the principal mechanisms of action characterizing contemporary immunotherapeutic interventions, evaluates their translational applications in neoplastic diseases, and critically examines persistent obstacles using proposed resolution strategies (131).

4.1 Immune checkpoint inhibitor

ICIs enhance immune activation by blocking inhibitory receptors, such as CTLA-4 and PD-1/PD-L1, enabling immune cells to target and attack tumor cells (Figure 5A) (24). To prevent the immune system from becoming overactive, immune checkpoints serve as regulatory mechanisms that maintain balance under normal circumstances. Immune checkpoints are often used by tumor cells to escape immune system attacks. ICIs inhibit molecules like CTLA-4, PD-1, or PD-L1, freeing the immune system from suppression and activating immune cells to boost the anti-tumor response (132). In cases of melanoma and non-small cell lung cancer, these inhibitors can increase patient survival and boost their quality of life. Pembrolizumab, a PD-1 inhibitor, has demonstrated significant efficacy in melanoma treatment in clinical studies. A large-scale clinical trial reported an objective response rate (ORR) of approximately 40%, with some patients experiencing a significant extension in survival and others achieving progression-free survival (PFS) exceeding five years (133). ICIs, either as monotherapy or in combination with chemotherapy, have become the standard first-line treatment for patients with advanced non-small cell lung cancer (NSCLC), especially in cases with elevated PD-L1 expression. A multicenter, randomized controlled trial found that patients receiving ICIs combined with chemotherapy had a median overall survival (OS) of approximately six months compared to those receiving chemotherapy alone. Additionally, the risk of disease progression is reduced by approximately 40%, which significantly improves patient prognosis (134). However, ICIs are not without risks and may cause immune-related adverse effects, particularly those affecting the skeletal muscle system. The cytotoxic effects of chemotherapy can damage skeletal muscle, and this damage may be exacerbated by inflammation induced by immunotherapy. For example, cyclophosphamide can penetrate muscle cells, causing DNA cross-linking damage and disrupting intracellular calcium homeostasis, thereby impairing normal muscle function (133). Simultaneously, inflammation triggered by immunotherapy leads to the release of various inflammatory cytokines, and when combined with the direct cytotoxic effects of chemotherapy, can further disrupt muscle structure and function, aggravating muscle damage. Clinically, approximately 30% of patients develop varying degrees of muscle symptoms, commonly including muscle pain, which can present as dull, stabbing, or throbbing pain, predominantly affecting the proximal limb muscles such as the shoulders and hips. Additionally, patients frequently experience muscle weakness, making basic activities, such as combing hair or standing up from a chair, difficult and severely impacting daily life. In clinical practice, a comprehensive pre-treatment evaluation of a patient's medical history, particularly any history of autoimmune diseases or muscle disorders, along with a detailed physical examination, including muscle strength tests and joint mobility assessments, is crucial in predicting the risk of adverse reactions (135). During treatment, muscle function assessments should be conducted regularly (every 2-4 weeks), and key biomarkers, such as serum creatine kinase (CK) and lactate dehydrogenase (LDH), should be closely monitored along with careful observation of muscle symptoms. If a patient develops muscle-related adverse effects, mild cases may be managed by temporary discontinuation of ICIs and administration of nonsteroidal anti-inflammatory drugs (NSAIDs), such as ibuprofen, to alleviate pain and inflammation, while closely monitoring symptom progression. In severe cases, where muscle weakness significantly impairs mobility or CK levels rise beyond five times the normal upper limit, immediate cessation of ICI treatment is necessary and corticosteroid therapy (e.g., prednisone) should be initiated (136). Once symptoms improve, the decision to resume ICI therapy or adjust the dosage should be made based on a comprehensive evaluation of the patient's condition.

4.2 Adoptive cell immunotherapy

Adoptive cell immunotherapy involves harvesting immune cells, including T cells and natural killer (NK) cells, from the

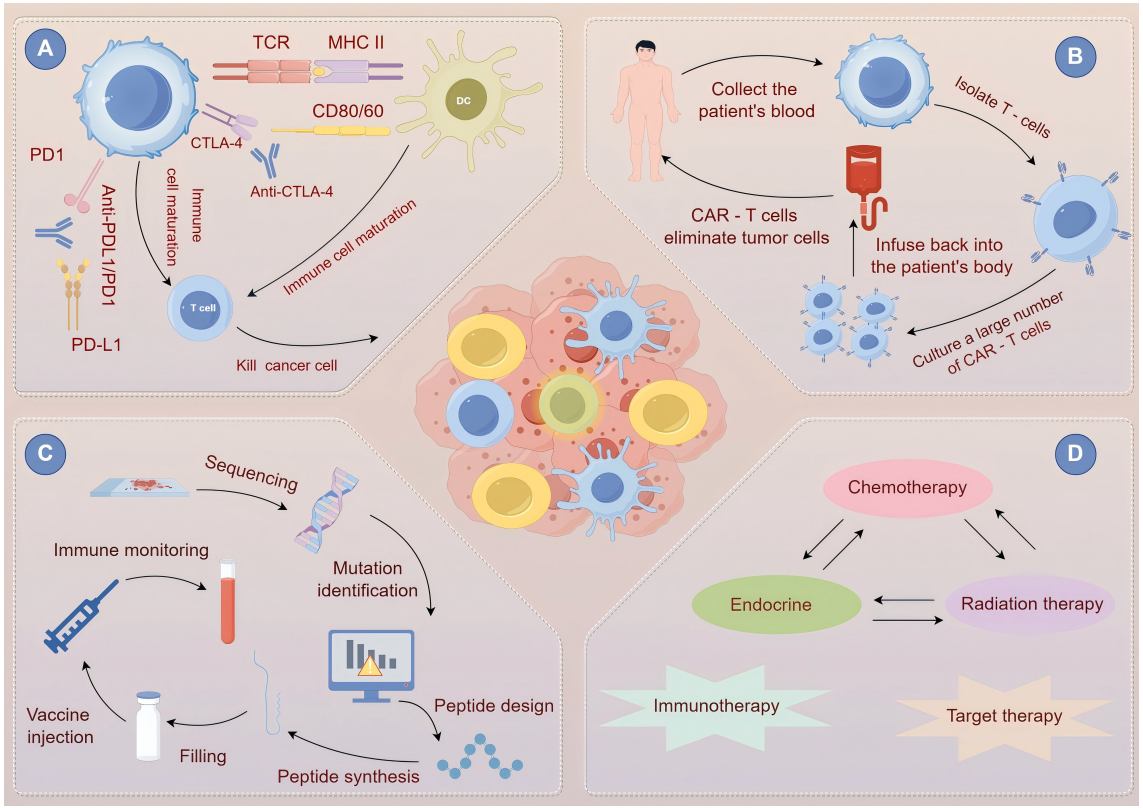

FIGURE 5
Principles and interrelationships of various cancer treatment strategies. **(A)** immune checkpoint inhibitor therapy. **(B)** Chimeric Antigen Receptor T-Cell (CAR-T) therapy. **(C)** Cancer Vaccine Therapy. **(D)** Combined Chemotherapy and Immunotherapy.

patient or donor, expanding and modifying them *in vitro*, and then reinfusing them into the patient to enhance the body's antitumor immune response (137). Various factors control the survival of immune cells in the body, with the condition of the cells being crucial. *In vitro* expansion and modification procedures can impact the expression of surface molecules and the internal signaling pathways within these cells. Taking T cells as an example, the activated costimulatory molecule CD28 can initiate a series of intracellular signal transduction pathways, promote the expression of anti-apoptoticroteins such as Bcl-2inhibit apoptosis, and prolong the survival time of T cells (138). The survival of immune cells is greatly influenced by the *in vivo* microenvironment, which contains various cytokines in the tumor microenvironment. IL-2 and IL-15 are cytokines that connect with specific receptors on immune cells, initiating pathways like JAK-STAT and delivering survival signals to these cells. Crucial interactions occur between immune cells and tumor cells, as well as with tumor-associated stromal cells. Inhibitory factors such as TGF-β, secreted by tumor cells, can impede immune cell survival. In specific scenarios, tumor-associated macrophages can affect the survival of immune cells by either cytokine secretion or direct contact. The expansion of immune cells within the body is contingent upon the combined stimulation from multiple signals. The initiation of T cell proliferation is largely due to the interaction between the T-cell receptor (TCR) and the antigen-peptide-MHC complex on tumor cells, which activates signaling pathways such as PLC-γ and Ras-MAPK (139). Following the activation of the PLC-γ pathway, there is an increase in intracellular calcium ion concentration, which activates calcineurin and facilitates the activation of the NFAT transcription factor, thereby regulating gene expression linked to cell proliferation. The Ras-MAPK pathway triggers protein kinases, encourages the expression of proteins related to the cell cycle, and allows T cells to begin proliferating. Besides the TCR signal, the costimulatory signal is essential. For instance, the interaction between CD28 and CD80/CD86 can boost the proliferation capacity of T cells. Cytokines are also crucial in the proliferation of immune cells. Immune cell proliferation can be promoted by cytokines like IL-2, IL-7, and IL-15. IL-2 engages with its receptor on immune cells, activating the JAK-STAT pathway and leading to cell growth. For immune cells to perform their roles, they must first migrate to tumor tissues, a pAdhesion molecules, including integrins like α4β1 and αLβ2, and selectins like L-selectin, are expressed on the surfaces of immune cells. Tumor tissues release chemokines such as CCL2 and CCL5. Process reliant on adhesion molecules and chemokine receptors on their surfaces (140). Chemokine receptors like CCR2 and CCR5 on immune cell surfaces bind specifically to chemokines, triggering intracellular signaling, that leads to cell polarization and movement towards higher chemokine concentrations. The relationship between immune cells and vascular endothelial cells is also highly

significant. The binding of adhesion molecules on immune cells to ligands on vascular endothelial cells allows immune cells to adhere to the vascular endothelium. Afterward, immune cells move through the spaces between endothelial cells to infiltrate the tumor tissue. Chimeric Antigen Receptor T-cell (CAR-T) therapy has achieved remarkable success in the treatment of hematological malignancies (Figure 5B). CAR-T cell therapy is a customized form of immunotherapy that employs genetic engineering to connect a single-chain antibody targeting tumor-associated antigens with a T-cell activation domain, creating a chimeric antigen receptor (CAR). The patient's T cells are then modified to include the gene that encodes CAR (141). These altered T cells are capable of identifying antigens on tumor cell surfaces, which activates their killing function and allows them to target tumor cells specifically. The process starts by collecting T cells from the patient, and then introducing the CAR gene into these T cells *in vitro* using retroviral or lentiviral vectors. These CAR-T cells are grown and multiplied *in vitro* to achieve a therapeutic scale. Ultimately, the patient receives the re-infused expanded CAR-T cells. These cells will identify and attach to specific antigens on the surface of tumor cells in a living organism, triggering the T cells' killing mechanism (73). Discharge cytotoxic agents like perforin and granzymes to directly eliminate tumor cells, while also releasing cytokines to attract and activate other immune cells, thus boosting the body's antitumor immune response. In the treatment of relapsed/refractory acute lymphoblastic leukemia (ALL), CAR-T therapy has shown a complete remission rate of 70-90% (142). A multicenter study on relapsed/refractory ALL in over 100 patients reported that approximately 75% of patients achieved complete remission, with a median remission duration of 12 months. In addition to its effectiveness in treating ALL, CAR-T cell therapy has demonstrated considerable promise in addressing other blood cancers. For example, in treating relapsed or refractory non-Hodgkin's lymphoma, several clinical studies have demonstrated that CAR-T cell therapy can greatly enhance patient remission and survival rates (143). Research has shown that CAR-T cell therapy can lead to an objective remission rate of 50%-70% in non-Hodgkin's lymphoma patients, with some experiencing long-term remission. CAR-T cell therapy offers new hope for multiple myeloma patients by targeting specific antigens on myeloma cells, effectively destroying them and enhancing the patient's health. Currently, a range of CAR-T cell therapies aimed at different blood-related cancers are in ongoing development and clinical testing, seeking to boost treatment success and lower the risk of negative reactions (144). In the coming years, CAR-T cell therapy is likely to emerge as a significant approach for managing hematological cancers. At the same time, as technology keeps progressing, CAR-T cell therapy is also being applied to treat solid tumors. For instance, certain research efforts have tried to integrate CAR-T cell therapy with ICIs to alleviate immune suppression within the tumor microenvironment and boost the antitumor effectiveness of CAR-T cells. These investigations open up new possibilities and potential for using CAR-T cell therapy in the treatment of solid tumors (145). CRS, or cytokine release syndrome, is a severe reaction that might occur during immunotherapy, notably in adoptive cell immunotherapy. A significant release of cytokines occurs when a large number of immune cells are quickly activated. The large buildup of these cytokines leads to widespread inflammatory responses, including symptoms like high fever, low blood pressure, and rapid heart rate (146). In extreme situations, it may cause respiratory failure, shock, and multiple organ dysfunction, putting the patient's life at risk and affecting the immunotherapy process and treatment results. However, during treatment, reinfused immune cells may trigger cytokine release syndrome (CRS); approximately 60-80% of patients undergoing CAR-T therapy for ALL experience CRS to varying degrees (142). In an observational study of 50 patients receiving CAR-T therapy, approximately 30% developed mild CRS, primarily presenting with low-grade fever and fatigue that was alleviated with supportive care. Approximately 20% of patients experience moderate CRS, characterized by fever, hypotension, and tachycardia, requiring medical intervention and close monitoring (142). Approximately 10% of patients develop severe CRS with life-threatening hypotension and respiratory failure, necessitating immediate admission to the intensive care unit for emergency treatment. During CRS, many cytokines are released, some of which negatively affect the metabolism and function of skeletal muscle. For example, IL-6 activates the ubiquitin-proteasome system in skeletal muscle cells, accelerating muscle protein degradation and leading to the loss of muscle mass loss. IFN-γ can inhibit respiratory chain complex activity in the mitochondria, reducing ATP production and resulting in muscle fatigue and weakness (142). Before administering adoptive cell immunotherapy, comprehensive assessment of the patient's physical condition, cardiopulmonary function, and muscle function is essential. Patients with pre-existing muscle disorders or functional impairments require careful risk-benefit analysis before proceeding with treatment. During therapy, close monitoring of serum cytokine levels (such as IL-6, IFN-γ, and TNF-α) should be conducted daily, along with regular muscle strength assessments (e.g., grip strength and lower limb push strength) and endurance evaluations (e.g., the six-minute walk test). Additionally, tracking the symptoms of muscle pain and fatigue is crucial. If CRS occurs and affects skeletal muscle function, its severity should be classified and appropriate interventions should be implemented. Mild CRS (temperature < 38°C, no organ dysfunction) requires supportive care, fluid and electrolyte supplementation, and close monitoring of the disease progression. Moderate CRS (temperature 38°C-39°C, mild organ dysfunction) requires supportive care combined with low-dose corticosteroids, such as dexamethasone (147). Severe CRS (temperature >39°C, severe organ dysfunction) requires the immediate administration of high-dose corticosteroids (e.g., methylprednisolone) and cytokine antagonists (e.g., tocilizumab). Conducting a thorough and systematic evaluation of the patient is crucial before starting adoptive cell immunotherapy. Assessing the patient's basic physical state and cardiopulmonary function is essential, along with evaluating muscle function. A detailed analysis must be conducted for patients with pre-existing muscle disorders or functional impairments. Some studies are currently

trying to reduce the risk of CRS by using cytokine antagonists as a preventive strategy (148). In certain clinical trials, administering monoclonal antibodies like tocilizumab before treatment can successfully inhibit IL-6 receptor signaling, thereby decreasing the occurrence and intensity of CRS. When CRS happens, it must be promptly assessed based on its severity. For mild cases, supportive care and close monitoring of disease progression are essential, and early moderate muscle activity might be considered (149). For moderate CRS, physical therapy techniques can be implemented alongside supportive care and low-dose corticosteroids. For instance, using hot compresses and massages can alleviate muscle pain and tiredness while enhancing blood flow and muscle metabolism. For severe CRS, active muscle rehabilitation therapy should accompany the use of high-dose corticosteroids and cytokine antagonists. Once the patient's condition is stable, gradually implementing progressive resistance training and aerobic exercise can aid in restoring muscle function. Throughout rehabilitation, it's crucial to keep a close eye on the patient's muscle strength, endurance, and physical function metrics, and to promptly modify the rehabilitation plan based on their recovery progress (150). Concurrently, muscle rehabilitation programs such as progressive resistance training and aerobic exercise should be implemented to facilitate muscle function recovery (151).

4.3 Cancer vaccine

Cancer vaccines aim to stimulate the body's specific antitumor immune response by introducing tumor-associated antigens to activate the immune system (Figure 5C). The HPV vaccine, known for its strong efficacy in preventing cervical cancer, continues to be a focus of research and development. Researchers are examining new HPV vaccine formulations and regimens, including long-acting protection mechanisms to decrease the number of doses required (152). Vaccination approaches for different age demographics and those with distinct immune profiles are being improved concurrently to increase the vaccine's effectiveness and universality. From a clinical perspective, the HPV vaccine is expected to be increasingly important in the prevention of other cancers related to HPV, such as anal and oropharyngeal cancers. As awareness of the HPV vaccine increases and its coverage broadens, its role in preventing related cancers will be more clearly demonstrated worldwide (153).Clinical trials have shown that the gp100 peptide vaccine for melanoma has some anti-tumor activity, but challenges remain. Scientists are striving to enhance it in terms of research and development. For instance, they are integrating it with other immunotherapy drugs to improve the immune response. Combining the gp100 peptide vaccine with ICIs is anticipated to disrupt the tumor's immune evasion and enhance treatment outcomes. Additionally, the use of genetic engineering technology is improving the antigen design of vaccines, enabling a more precise activation of the immune system against tumor cells. If the present challenges are addressed, therapeutic cancer vaccines could become a highly promising treatment option for those with advanced melanoma in clinical settings. These vaccines are vital components of a complete treatment plan, contributing to longer survival and better quality of life for patients (154). The success of the HPV vaccine in preventing cervical cancer serves as a model for cancer vaccine application (155). A large-scale population study with a long-term follow-up of thousands of women found that HPV vaccination significantly reduced the incidence of cervical cancer by approximately 80%. Several therapeutic vaccines have been actively explored in clinical trials for cancer treatment (156). For example, the gp100 peptide vaccine for melanoma has demonstrated antitumor activity in clinical trials, inducing specific T-cell responses in melanoma patients to inhibit tumor growth. In a clinical trial involving 50 patients with melanoma, approximately 30% of patients experienced tumor shrinkage after receiving the gp100 peptide vaccine, with 10% showing a reduction of more than 30% in tumor size. However, some patients may develop muscle fatigue, soreness, and other discomforts after vaccination. Clinical trials have reported that approximately 25% of patients experience such symptoms, usually appearing 1-3 days post-vaccination and lasting 3-7 days (157). These effects are believed to be related to the indirect impact of vaccine-induced immune responses on skeletal muscle (158). Upon immune system activation, immune cells release cytokines and immune mediators, which may affect the energy metabolism and ion balance of muscle cells. For instance, TNF-α can alter the sodium-potassium pump activity in muscle cells, leading to abnormal ion concentrations and causing muscle soreness, whereas IFN-γ can inhibit key enzymes in the glycolytic pathway of muscle cells, reducing ATP production and resulting in muscle fatigue. Further research is required to investigate the relationship between cancer vaccines and skeletal muscle function. On one hand Advanced technologies, such as single-cell sequencing and proteomics, can be used to analyze molecular changes in muscle cells induced by vaccine immune responses and to identify key signaling pathways and molecular targets (159). In an experiment using single-cell sequencing to study the effects of cancer vaccines on muscle cells, significant changes in gene expression related to these responses were observed, with the upregulation of genes associated with inflammation and downregulation of genes involved in energy metabolism, potentially correlating with muscle fatigue and soreness. Based on these research findings, vaccine design can be optimized by selecting tumor-associated antigens with higher immunogenicity and specificity, using novel delivery systems such as nanotechnology to improve antigen presentation efficiency, and adjusting vaccine dosage and administration intervals to enhance antitumor efficacy while minimizing adverse effects on skeletal muscles (160).

4.4 Combined chemotherapy and immunotherapy

Combined chemotherapy and immunotherapy is a highly regarded strategy in cancer treatment that aims to integrate the direct cytotoxic effects of chemotherapy on tumor cells with the immunomodulatory effects of immunotherapy to achieve

synergistic enhancement and improve therapeutic outcomes (Figure 5D). However, this combination therapy involves complex mechanisms that require comprehensive assessment of multiple factors during implementation (161). From a mechanistic perspective, certain chemotherapeutic agents possess unique properties that enhance the efficacy of immunotherapy. For example, oxaliplatin and cyclophosphamide can induce immunogenic cell death (ICD) in tumor cells, prompting them to release tumor-associated antigens and damage-associated molecular patterns (DAMPs) (162). These molecules attract and activate immune cells, promote their infiltration into tumor tissues, and enhance the ability of immunotherapy to recognize and attack tumor cells.

A study in tumor-bearing mice demonstrated that tumor growth was significantly suppressed in the combination therapy group (chemotherapy and immunotherapy) (163). By day 14 of treatment, tumor volume was reduced by approximately 50% compared to that in the immunotherapy-only group, and immune cell infiltration in tumor tissues was notably increased, providing strong evidence that chemotherapy can amplify the immune response to inhibit tumor growth more effectively; however, combination therapy also presents challenges (164). Given these challenges, the development of personalized combination therapy regimens is crucial. First, comprehensive patient assessment should be conducted, including age, physical condition, underlying diseases (such as diabetes and cardiovascular diseases), tumor type, and stage (165). For elderly patients or those in poor physical condition, considering their lower treatment tolerance, chemotherapy doses should be appropriately reduced, less toxic immunotherapy agents should be selected, or the treatment sequence should be adjusted to minimize adverse effects. A study on elderly patients with lung cancer compared standard-dose combination therapy with low-dose chemotherapy and immunotherapy (166). The results showed that patients in the low-dose chemotherapy and immunotherapy groups had significantly fewer adverse reactions, whereas survival rates were comparable to those in the standard-dose group, highlighting the importance of personalized treatment adjustments. Second, treatment combinations should be selected based on tumor type and characteristics (11). ICIs, alone or in combination with targeted therapy, often yield optimal results for melanoma. In contrast, for lung cancer, treatment should be tailored based on PD-L1 expression levels. Patients with high PD-L1 expression may benefit more from immune checkpoint inhibitor monotherapy or combination with chemotherapy (167). For example, in non-small cell lung cancer (NSCLC), pembrolizumab (PD-1 inhibitor) combined with chemotherapy has been shown to significantly improves progression-free survival (PFS) and overall survival (OS) in non-small cell lung cancer (NSCLC). This is because high PD-L1 expression allows tumor cells to evade immune surveillance more effectively, whereas pembrolizumab blocks the PD-1/PD-L1 pathway, restoring immune system activity against tumor cells (168). Combined chemotherapy then directly kills tumor cells, achieving a synergistic therapeutic effect, and the sequence of drug administration plays a key role in optimizing the therapeutic outcomes.

For some solid tumors, administering chemotherapy first to induce the release of tumor antigens, followed by immunotherapy, can enhance the ability of immune cells to recognize and attack tumor cells, thereby activating the immune system more effectively (169). In contrast, for certain hematologic malignancies, simultaneous administration of chemotherapy and immunotherapy may yield superior results. In lymphoma treatment, concurrent use of chemotherapy and immunotherapy has been shown to enhance tumor clearance rates and improve response durability (170). This may be due to the rapid growth and proliferation of hematologic tumor cells, making the simultaneous administration of both therapies more effective in suppressing tumor progression. Furthermore, immunotherapy can increase tumor sensitivity to chemotherapy, further improving the treatment efficacy. By precisely adjusting treatment parameters, combined chemotherapy and immunotherapy can maximize their complementary advantages, enhance antitumor efficacy while minimizing skeletal muscle damage, and improve quality of life and treatment tolerance, ultimately offering better therapeutic prospects for cancer patients (171).

5 Limitation of immunotherapy and future prospect

Immunotherapy has made significant progress in the field of cancer treatment and has brought new hope to many cancer patients; however, it also has several limitations. For example, immunotherapy can have negative effects on skeletal muscles by disrupting normal function. ICIs can cause muscle-related symptoms in approximately 30% of patients, including muscle pain, which often affects proximal limb muscles such as the shoulders and hips, with varying pain intensities (172). Additionally, muscle weakness is common and significantly affects daily activities and the quality of life. Adoptive cell immunotherapy may trigger cytokine release syndrome (CRS), with 60-80% of patients undergoing CAR-T therapy for acute lymphoblastic leukemia (ALL) experiencing CRS to varying degrees. During CRS, cytokines such as IL-6 activate the ubiquitin-proteasome system in skeletal muscle cells, accelerating muscle protein degradation and leading to muscle mass loss. IFN-γ inhibits the mitochondrial respiratory chain complex activity, reducing ATP production, which results in muscle fatigue and weakness. Cancer vaccines may also cause muscle-related side effects in some patients (173). Approximately 25% of vaccine recipients experience muscle fatigue and soreness, typically appearing 1-3 days post-vaccination and lasting 3-7 days. These effects are believed to be linked to immune responses that affect energy metabolism and ion balance of muscle cells. For instance, TNF-α alters Na+/K+ pump activity, leading to ion imbalance and muscle soreness, whereas IFN-γ suppresses key glycolytic enzymes, reducing ATP production, and causing muscle fatigue. The efficacy

of immunotherapy varies significantly among patients and is influenced by factors, such as tumor microenvironment complexity, genetic background, and immune system status. For instance, in multiple myeloma, interactions between tumor cells and immune cells in the tumor microenvironment affect disease progression and the response to immunotherapy. Differences in immune cell infiltration and function among patients make it difficult to standardize treatment plans, thereby increasing the clinical challenges. Immunotherapy may also cause various immune-related adverse effects (irAEs) beyond its impact on skeletal muscles, affecting multiple organ systems (174). Excessive immune activation can trigger a cytokine storm, leading to a massive release of cytokines such as IFN-γ, TNF-α, and IL-6, which not only indirectly damages skeletal muscle cells but also elevates systemic inflammatory cytokine levels, induces protein degradation, inhibits protein synthesis, and impairs muscle fiber regeneration and repair, ultimately forming a vicious cycle. Furthermore, immunotherapy may cause or exacerbate autoimmune diseases. For instance, ICIs have been linked to thyroid dysfunction, pneumonia, and other complications, affecting overall patient health and increasing treatment risks and complexities (175). Some patients develop resistance to immunotherapy over time, leading to diminished efficacy or treatment failure. Resistance to ICIs has been observed in cancers such as melanoma and lung cancer, where tumor cells can evade immune system attacks through mechanisms such as upregulation of immunosuppressive molecules or alteration of the tumor microenvironment, ultimately limiting the long-term effectiveness of immunotherapy and posing significant clinical challenges in overcoming resistance. Research in the future could address immunotherapy resistance by focusing on three key aspects. To start, devise innovative combination therapies. Look into more precise combinations of immunotherapy with targeted therapy, like integrating drugs based on specific gene mutations in tumors (176). Also, the integration of immunotherapy with novel technologies like oncolytic virotherapy promises to enhance treatment effectiveness in melanoma. Secondly, boost initiatives to discover new targets through the use of advanced technologies for analyzing the molecular features of tumor and immune cells. Create medications targeting new areas such as tumor-specific glycoproteins or molecules that regulate the immune system, which can prevent tumors from evading the immune system and boost the immune response against tumors. Thirdly, investigate tumor heterogeneity through multi-omics analysis to grasp its connection with immunotherapy resistance. Choose tailored immunotherapy medications and combinations according to the specific traits of a person's tumor (177). In breast cancer, for instance, personalized treatments can enhance patient survival and provide novel methods to combat resistance. Moreover, the high cost of immunotherapy imposes a significant financial burden on patients and the healthcare system (178). The cost of certain novel ICIs and CAR-T cell therapies ranges from hundreds of thousands to millions of yuan, making them unaffordable for many patients and limiting their widespread clinical application. Moreover, immunotherapy often requires long-term administration, further increasing treatment costs and posing serious challenges to the allocation of healthcare resources (179).

6 Conclusion

Our work provides an in-depth exploration of the complex interactions within the tumor microenvironment, focusing on the formation of immune niches, their underlying mechanisms, and therapeutic potential. There are intricate interactions between immunotherapy, the tumor microenvironment, and the biomechanics of skeletal muscle. Despite its effectiveness in cancer treatment, immunotherapy adversely affects skeletal muscle. Muscle-related symptoms can occur in about 30% of patients treated with ICIs (180). Muscle discomfort is a potential side effect of cancer vaccines in some patients. Also, alterations in the tumor microenvironment influence skeletal muscle metabolism and function through various pathways. The tumor microenvironment is a dynamic ecosystem in which immune cells, tumor cells, and stromal cells interact, forming distinct immune niches (181). These niches play a critical role in shaping the immune response against tumors and are key factors in the success of immunotherapy. A thorough exploration of the mechanisms behind immune niche formation can aid in creating more effective immunotherapy strategies. For instance, improving anti-tumor immune responses by aiming at specific parts of immune niches or merging different immunotherapy methods to surpass the restrictions imposed by immune niches (182). Natural killer (NK) cells, macrophages, dendritic cells, and T cells are major participants in the tumor microenvironment. NK cells release perforin and granzymes to kill tumor cells, whereas macrophages can polarize into M1 or M2 phenotypes. M1 macrophages exhibit proinflammatory and antitumor properties, whereas M2 macrophages often promote tumor growth. Dendritic cells are key mediators of antigen presentation, activating T cells to recognize and attack tumor cells. Additionally, regulatory T cells (Tregs) and myeloid-derived suppressor cells (MDSCs) produce immunosuppressive cytokines, inhibit immune responses, and facilitate tumor immune evasion (21). This intricate network of interactions contributes to the formation of unique immune niches with distinct immunological characteristics. Several factors can influence the formation of immune niches: cancer-associated fibroblasts (CAFs) release extracellular matrix components, modifying the physical and chemical properties of the microenvironment, thereby influencing immune cell infiltration and function (183). Tumor-derived factors, such as cytokines and chemokines, recruit immune cells to specific locations and shape the localized immune microenvironment. Moreover, genetic and epigenetic changes in tumor cells regulate their interactions with immune cells, further sculpting immune niches. Understanding the mechanisms underlying the immune niche formation has important therapeutic implications. Immunotherapies, such as ICIs, adoptive cell therapy, and cancer vaccines, aim to modulate the immune system to target tumors. However, their efficacy is closely linked to the immune niches within the tumor microenvironment. For example, ICIs block inhibitory receptors on immune cells; however,

their effectiveness may be limited by immunosuppressive immune niches (184). Similarly, adoptive cell therapies, such as CAR-T cell therapy, may rely on the tumor microenvironment's capacity to support the survival and function of transferred immune cells. Cancer vaccines designed to stimulate immune responses against tumor-associated antigens may also face challenges in terms of immunosuppressive niches. By conducting comprehensive research on immune niche formation in the tumor microenvironment, we can develop more effective immunotherapy strategies. This includes targeting specific components of immune niches to enhance antitumor immune responses, such as blocking immunosuppressive signals or promoting recruitment and activation of antitumor immune cells. Combining different immunotherapies or integrating immunotherapy with other treatment modalities (e.g., chemotherapy) may help overcome the limitations imposed by immune niches and ultimately improve patient outcomes (185). In conclusion, research on immune niche formation within the tumor microenvironment is a rapidly evolving field with tremendous potential for improving cancer treatment. Additional research is required to fully understand the complex mechanisms at play and to apply these insights to develop more effective clinical therapies, ultimately improving cancer patient survival and quality of life (186).

Author contributions

SM: Funding acquisition, Project administration, Writing – review & editing. YL: Writing – original draft. SS: Investigation, Writing – original draft. JY: Formal Analysis, Investigation, Writing – review & editing. BF: Formal Analysis, Investigation, Writing – review & editing. PT: Investigation, Formal Analysis, Writing – review & editing. YC: Writing – original draft, Investigation. JL: Writing – original draft. LK: Writing – review & editing, Formal Analysis. XW: Writing – review & editing, Supervision. YG: Funding acquisition, Writing – review & editing. TY: Funding acquisition, Project administration, Writing – review & editing.

Funding

The author(s) declare that financial support was received for the research and/or publication of this article. This work was supported by the National Key R&D Program of China (Grant No. 2023YFB4705500) and the National Natural Science Foundation of China (No. 2022JC2K01, No. 82073327), the CAMS Innovation Fund for Medical Sciences (Nos. CIFMS, 2022-I2M-C&T-B-061, 2021-I2M-1-066), Beijing Hope Run Special Fund of the Cancer Foundation of China (Nos. LC2021A18, LC2022B06), Doctoral Research Start-up Fund of Shenyang University of Technology(Grant Nos. 1010147001258); Liaoning Provincial Department of Education Basic Research Project Youth Project (Grant Nos.JYTQN2023051).

Conflict of interest

The authors declare that the research was conducted in the absence of any commercial or financial relationships that could be construed as a potential conflict of interest.

Generative AI statement

The author(s) declare that no Generative AI was used in the creation of this manuscript.

Publisher's note

All claims expressed in this article are solely those of the authors and do not necessarily represent those of their affiliated organizations, or those of the publisher, the editors and the reviewers. Any product that may be evaluated in this article, or claim that may be made by its manufacturer, is not guaranteed or endorsed by the publisher.

References

1. Ashir A, Jerban S, Barrere V, Wu Y, Shah SB, Andre MP, et al. Skeletal muscle assessment using quantitative ultrasound: A narrative review. *Sensors (Basel)*. (2023) 23:4763. doi: 10.3390/s23104763

2. Santucci C, Carioli G, Bertuccio P, Malvezzi M, Pastorino U, Boffetta P, et al. Progress in cancer mortality, incidence, and survival: a global overview. *Eur J Cancer Prev*. (2020) 29:367–81. doi: 10.1097/CEJ.0000000000000594

3. Anand U, Dey A, Chandel AKS, Sanyal R, Mishra A, Pandey DK, et al. Cancer chemotherapy and beyond: Current status, drug candidates, associated risks and progress in targeted therapeutics. *Genes Dis*. (2023) 10:1367–401. doi: 10.1016/j.gendis.2022.02.007

4. Yin L, Li N, Jia W, Wang N, Liang M, Yang X, et al. Skeletal muscle atrophy: From mechanisms to treatments. *Pharmacol Res*. (2021) 172:105807. doi: 10.1016/j.phrs.2021.105807

5. Yoshimura Y, Nagano F, Matsumoto A, Shimazu S, Shiraishi A, Kido Y, et al. Low hemoglobin levels are associated with compromised muscle health: Insights from a post-stroke rehabilitation cohort. *Geriatr Gerontol Int*. (2024) 24:305–11. doi: 10.1111/ggi.14834

6. Wang M, Yu F, Zhang Y. Present and future of cancer nano-immunotherapy: opportunities, obstacles and challenges. *Mol Cancer*. (2025) 24:26. doi: 10.1186/s12943-024-02214-5

7. Desai I, Thakur S, Pagariya P. Current advances in immunotherapy for cancer. *Oral Oncol Rep*. (2024) 12:100652. doi: 10.1016/j.oor.2024.100652

8. Imai Y. Novel treatment strategies for hematological Malignancies in the immunotherapy era. *Int J Hematol*. (2024) 120:3–5. doi: 10.1007/s12185-024-03793-1

9. Cao S, Jia W, Zhao Y, Liu H, Cao J, Li Z. A recent perspective on designing tumor vaccines for tumor immunology. *Int Immunopharmacol*. (2024) 142:113090. doi: 10.1016/j.intimp.2024.113090

10. Rathod S, Potdar J, Gupta A, Sethi N, Dande A. Empowering women's health: insights into HPV vaccination and the prevention of invasive cervical cancer. *Cureus*. (2023) 15:e49523. doi: 10.7759/cureus.49523

11. Liu B, Zhou H, Tan L, Siu KTH, Guan X-Y. Exploring treatment options in cancer: tumor treatment strategies. *Signal Transduct Target Ther*. (2024) 9:175. doi: 10.1038/s41392-024-01856-7

12. Kirchhammer N, Trefny MP, Auf der Maur P, Läubli H, Zippelius A. Combination cancer immunotherapies: Emerging treatment strategies adapted to the tumor microenvironment. *Sci Transl Med*. (2022) 14:eabo3605. doi: 10.1126/scitranslmed.abo3605

13. Rached L, Laparra A, Sakkal M, Danlos F-X, Barlesi F, Carbonnel F, et al. Toxicity of immunotherapy combinations with chemotherapy across tumor

indications: Current knowledge and practical recommendations. *Cancer Treat Rev*. (2024) 127:102751. doi: 10.1016/j.ctrv.2024.102751

14. Zhai J, Gu X, Liu Y, Hu Y, Jiang Y, Zhang Z. Chemotherapeutic and targeted drugs-induced immunogenic cell death in cancer models and antitumor therapy: An update review. *Front Pharmacol*. (2023) 14:1152934. doi: 10.3389/fphar.2023.1152934

15. Bhol NK, Bhanjadeo MM, Singh AK, Dash UC, Ojha RR, Majhi S, et al. The interplay between cytokines, inflammation, and antioxidants: mechanistic insights and therapeutic potentials of various antioxidants and anti-cytokine compounds. *Biomed Pharmacother*. (2024) 178:117177. doi: 10.1016/j.biopha.2024.117177

16. Klassen P, Schiessel DL, Baracos VE. Adverse effects of systemic cancer therapy on skeletal muscle: myotoxicity comes out of the closet. *Curr Opin Clin Nutr Metab Care*. (2023) 26:210–8. doi: 10.1097/MCO.0000000000000922

17. Ganesan P, Sekaran S, Ramasamy P, Ganapathy D. Systematic analysis of chemotherapy, immunotherapy, and combination therapy in Head and Neck Squamous Cell Carcinoma (HNSCC) clinical trials: Focusing on overall survival and progression-free survival outcomes. *Oral Oncol Rep*. (2024) . 12:100673. doi: 10.1016/j.oor.2024.100673

18. Mendoza J, Hampton E, Singleton L. A theoretical and practical approach to quality improvement education. *Curr Probl Pediatr Adolesc Health Care*. (2023) 53:101459. doi: 10.1016/j.cppeds.2023.101459

19. Desai SA, Patel VP, Bhosle KP, Nagare SD, Thombare KC. The tumor microenvironment: shaping cancer progression and treatment response. *J Chemother*. (2025) 37:15–44. doi: 10.1080/1120009X.2023.2300224

20. Zhao Y, Shen M, Wu L, Yang H, Yao Y, Yang Q, et al. Stromal cells in the tumor microenvironment: accomplices of tumor progression? *Cell Death Dis*. (2023) 14:587. doi: 10.1038/s41419-023-06110-6

21. Del Prete A, Salvi V, Soriani A, Laffranchi M, Sozio F, Bosisio D, et al. Dendritic cell subsets in cancer immunity and tumor antigen sensing. *Cell Mol Immunol*. (2023) 20:432–47. doi: 10.1038/s41423-023-00990-6

22. Liu Q, Guan Y, Li S. Programmed death receptor (PD-)1/PD-ligand (L)1 in urological cancers: the "all-around warrior" in immunotherapy. *Mol Cancer*. (2024) 23:183. doi: 10.1186/s12943-024-02095-8

23. El-Tanani M, Rabbani SA, Babiker R, Rangraze I, Kapre S, Palakurthi SS, et al. Unraveling the tumor microenvironment: Insights into cancer metastasis and therapeutic strategies. *Cancer Lett*. (2024) 591:216894. doi: 10.1016/j.canlet.2024.216894

24. Meng L, Wu H, Wu J, Ding Pa, He J, Sang M, et al. Mechanisms of immune checkpoint inhibitors: insights into the regulation of circular RNAS involved in cancer hallmarks. *Cell Death Dis*. (2024) 15:3. doi: 10.1038/s41419-023-06389-5

25. Ikeda H, Kawase K, Nishi T, Watanabe T, Takenaga K, Inozume T, et al. Immune evasion through mitochondrial transfer in the tumour microenvironment. *Nature*. (2025) 638:225–36. doi: 10.1038/s41586-024-08439-0

26. Ma S, Ming Y, Wu J, Cui G. Cellular metabolism regulates the differentiation and function of T-cell subsets. *Cell Mol Immunol*. (2024) 21:419–35. doi: 10.1038/s41423-024-01148-8

27. Harbour SN, DiToro DF, Witte SJ, Zindl CL, Gao M, Schoeb TR, et al. T H 17 cells require ongoing classic IL-6 receptor signaling to retain transcriptional and functional identity. *Sci Immunol*. (2020) 5:eaaw2262. doi: 10.1126/sciimmunol.aaw2262

28. Beyranvand Nejad E, Labrie C, van Elsas MJ, Kleinovink JW, Mittrücker H-W, Franken KLMC, et al. IL-6 signaling in macrophages is required for immunotherapy-driven regression of tumors. *JITC*. (2021) 9:e002460. doi: 10.1136/jitc-2021-002460

29. Hu X, li J, Fu M, Zhao X, Wang W. The JAK/STAT signaling pathway: from bench to clinic. *STTT*. (2021) 6:402. doi: 10.1038/s41392-021-00791-1

30. Mitchell TJ, John. Signal transducer and activator of transcription (STAT) signalling and T-cell lymphomas. *Int Immunol*. (2005) 114:301–12. doi: 10.1038/s41392-021-00791-1

31. Shi D, Tao J, Man S, Zhang N, Ma L, Guo L, et al. Structure, function, signaling pathways and clinical therapeutics: The translational potential of STAT3 as a target for cancer therapy. *Biochim Biophys Acta Rev Cancer*. (2024) 1879:189207. doi: 10.1016/j.bbcan.2024.189207

32. Pedersen BK, Steensberg A, Schjerling P. Muscle-derived interleukin-6: possible biological effects. *J Physiol*. (2001) 536:329–37. doi: 10.1111/j.1469-7793.2001.0329c

33. Guirao JJ, Cabrera CM, Jiménez N, Rincón L, Urra JM. High serum IL-6 values increase the risk of mortality and the severity of pneumonia in patients diagnosed with COVID-19. *Mol Immunol*. (2020) 128:64–8. doi: 10.1016/j.molimm.2020.10.006

34. Wang Y, Ye R, Fan L, Zhao X, Li L, Zheng H, et al. A TNF-α blocking peptide that reduces NF-κB and MAPK activity for attenuating inflammation. *Bioorg Med Chem*. (2023) 92:117420. doi: 10.1016/j.bmc.2023.117420

35. Lugano R, Ramachandran M, Dimberg A. Tumor angiogenesis: causes, consequences, challenges and opportunities. *CMLS*. (2019) 77:1745–70. doi: 10.1007/s00018-019-03351-7

36. Aspriţoiu VM, Stoica I, Bleotu C, Diaconu CC. Epigenetic regulation of angiogenesis in development and tumors progression: potential implications for cancer treatment. *Front Cell Dev Biol*. (2021) 9:689962. doi: 10.3389/fcell.2021.689962

37. Awad NS, Salkho NM, Abuwatfa WH, Paul V, AlSawaftah NM, Husseini GA. Tumor vasculature vs tumor cell targeting: Understanding the latest trends in using functional nanoparticles for cancer treatment. *OpenNano*. (2023) 11:100136. doi: 10.1016/j.onano.2023.100136

38. Deguchi H, Yamashita T, Hiramoto N, Otsuki Y, Mukai A, Ueno M, et al. Intracellular pH affects mitochondrial homeostasis in cultured human corneal endothelial cells prepared for cell injection therapy. *Sci Rep*. (2022) 12:6263. doi: 10.1038/s41598-022-10176-1

39. Yang D, Liu J, Qian H, Zhuang Q. Cancer-associated fibroblasts: from basic science to anticancer therapy. *EMM*. (2023) 55:1322–32. doi: 10.1038/s12276-023-01013-0

40. Kolesnikoff N, Chen C-H, Samuel Michael S. Interrelationships between the extracellular matrix and the immune microenvironment that govern epithelial tumour progression. *Clin Sci*. (2022) 136:361–77. doi: 10.1042/CS20210679

41. Kanchanawong P, Calderwood DA. Organization, dynamics and mechanoregulation of integrin-mediated cell–ECM adhesions. *Nat Rev Mol Cell Biol*. (2023) 24:142–61. doi: 10.1038/s41580-022-00531-5

42. Li S, Kang Y, Zeng Y. Targeting tumor and bone microenvironment: Novel therapeutic opportunities for castration-resistant prostate cancer patients with bone metastasis. *Biochim Biophys Acta Rev Cancer*. (2024) 1879:189033. doi: 10.1016/j.bbcan.2023.189033

43. Yin C, Wang Y, Lin Q, Lin K, Du H, Lang C, et al. BHLHE22 drives the immunosuppressive bone tumor microenvironment and associated bone metastasis in prostate cancer. *J Immunother Cancer*. (2023) 11:e005532. doi: 10.1136/jitc-2022-005532

44. Martinenaite E, Lecoq I, Aaboe-Jørgensen M, Ahmad SM, Perez-Penco M, Glöckner HJ, et al. Arginase-1-specific T cells target and modulate tumor-associated macrophages. *J Immunother Cancer*. (2025) 13:e009930. doi: 10.1136/jitc-2024-009930

45. Zarrer J, Taipaleenmäki H. The osteoblast in regulation of tumor cell dormancy and bone metastasis. *J Bone Oncol*. (2024) 45:100597. doi: 10.1016/j.jbo.2024.100597

46. Maji S, Kumar A, Emdad L, Fisher PB, Das SK. Chapter Seven - Molecular landscape of prostate cancer bone metastasis. *Adv Cancer Res*. (2024) 161:321–65. doi: 10.1016/bs.acr.2024.04.007

47. Chen S, Li Q, Shi H, Li F, Duan Y, Guo Q. New insights into the role of mitochondrial dynamics in oxidative stress-induced diseases. *Biomedicine Pharmacotherapy*. (2024) 178:117084. doi: 10.1016/j.biopha.2024.117084

48. Fan W, Jurado-Arjona J, Alanis-Lobato G, Péron S, Berger C, Andrade-Navarro MA, et al. The transcriptional co-activator Yap1 promotes adult hippocampal neural stem cell activation. *EMBO J*. (2023) 42:e110384. doi: 10.15252/embj.2021110384

49. Naba A. Mechanisms of assembly and remodelling of the extracellular matrix. *Nat Rev Mol Cell Biol*. (2024) 25:865–85. doi: 10.1038/s41580-024-00767-3

50. Siri M, Vázquez-Dávila M, Sotelo Guzman C, Bidan CM. Nutrient availability influences E. coli biofilm properties and the structure of purified curli amyloid fibers. *NPJ Biofilms Microbiomes*. (2024) 10:143. doi: 10.1038/s41522-024-00619-0

51. Zhu W, Li Y, Han M, Jiang J. Regulatory mechanisms and reversal of CD8(+)T cell exhaustion: A literature review. *Biol (Basel)*. (2023) 12:541. doi: 10.3390/biology12040541

52. Zhu C, Liu C, Wu Q, Sheng T, Zhou R, Ren E, et al. Remolding the tumor microenvironment by bacteria augments adoptive T cell therapy in advanced-stage solid tumors. *Signal Transduct Target Ther*. (2024) 9:307. doi: 10.1038/s41392-024-02028-3

53. Jumaniyazova E, Lokhonina A, Dzhalilova D, Kosyreva A, Fatkhudinov T. Immune cells in the tumor microenvironment of soft tissue sarcomas. *Cancers (Basel)*. (2023) 15:5760. doi: 10.3390/cancers15245760

54. Maura F, Coffey DG, Stein CK, Braggio E, Ziccheddu B, Sharik ME, et al. The Vk*MYC Mouse Model recapitulates human multiple myeloma evolution and genomic diversity. *bioRxiv*. (2023) 27:2023.07.25.550482. doi: 10.1101/2023.07.25.550482

55. Li J, Dong T, Wu Z, Zhu D, Gu H. The effects of MYC on tumor immunity and immunotherapy. *Cell Death Discovery*. (2023) 9:103. doi: 10.1038/s41420-023-01403-3

56. Sun Y, Yinwang E, Wang S, Wang Z, Wang F, Xue Y, et al. Phenotypic and spatial heterogeneity of CD8(+) tumour infiltrating lymphocytes. *Mol Cancer*. (2024) 23:193. doi: 10.1186/s12943-024-02104-w

57. Kulig P, Łuczkowska K, Machaliński B, Baumert B. Deep hematologic response to RD treatment in patients with multiple myeloma is associated with overexpression of IL-17R in CD138+ plasma cells. *Sci Rep*. (2024) 14:23559. doi: 10.1038/s41598-024-74558-3

58. Supimon K, Sangsuwannukul T, Luangwattananun P, Yenchitsomanus PT. Enhanced cytotoxicity in multiple myeloma via T cells armed with bispecific T cell engager targeting B-cell maturation antigen on cancer cells and CD3 on T cells. *Int Immunopharmacol*. (2024) 143:113480. doi: 10.1016/j.intimp.2024.113480

59. Yang Y, He J, Zheng G, Han X, Nie Y, Sun L, et al. Study on the molecular genetic characteristics of multiple myeloma patients in China. *Blood*. (2024) 144:6816. doi: 10.1182/blood-2024-202862

60. Liu Y, Zhao Y, Song H, Li Y, Liu Z, Ye Z, et al. Metabolic reprogramming in tumor immune microenvironment: Impact on immune cell function and therapeutic implications. *Cancer Lett*. (2024) 597:217076. doi: 10.1016/j.canlet.2024.217076

61. Zhang A, Fan T, Liu Y, Yu G, Li C, Jiang Z. Regulatory T cells in immune checkpoint blockade antitumor therapy. *Mol Cancer*. (2024) 23:251. doi: 10.1186/s12943-024-02156-y

62. Chen Z, Lan H, Liao Z, Huang J, Jian X, Hu J, et al. Regulatory T cells-centered regulatory networks of skeletal muscle inflammation and regeneration. *Cell Biosci*. (2022) 12:112. doi: 10.1186/s13578-022-00847-x

63. Vilbois S, Xu Y, Ho P-C. Metabolic interplay: tumor macrophages and regulatory T cells. *Trends Cancer*. (2024) 10:242–55. doi: 10.1016/j.trecan.2023.11.007

64. Becker M, Joseph SS, Garcia-Carrizo F, Tom RZ, Opaleva D, Serr I, et al. Regulatory T cells require IL6 receptor alpha signaling to control skeletal muscle function and regeneration. *Cell Metab*. (2023) 35:1736–51.e1737. doi: 10.1016/j.cmet.2023.08.010

65. Wu J, Ren B, Wang D, Lin H. Regulatory T cells in skeletal muscle repair and regeneration: recent insights. *Cell Death Dis*. (2022) 13:680. doi: 10.1038/s41419-022-05142-8

66. Lemos JP, Tenório LPG, Mouly V, Butler-Browne G, Mendes-da-Cruz DA, Savino W, et al. T cell biology in neuromuscular disorders: a focus on Duchenne Muscular Dystrophy and Amyotrophic Lateral Sclerosis. *Front Immunol*. (2023) 14:1202834. doi: 10.3389/fimmu.2023.1202834

67. Wan R, Liu S, Feng X, Luo W, Zhang H, Wu Y, et al. The Revolution of exosomes: From biological functions to therapeutic applications in skeletal muscle diseases. *J Orthop Translat*. (2024) 45:132–9. doi: 10.1016/j.jot.2024.01.001

68. Vafaei S, Zekiy AO, Khanamir RA, Zaman BA, Ghayourvahdat A, Azimizonuzi H, et al. Combination therapy with immune checkpoint inhibitors (ICIs); a new frontier. *Cancer Cell Int*. (2022) 22:2. doi: 10.1186/s12935-021-02407-8

69. Zong Y, Li H, Liao P, Chen L, Pan Y, Zheng Y, et al. Mitochondrial dysfunction: mechanisms and advances in therapy. *Signal Transduct Target Ther*. (2024) 9:124. doi: 10.1038/s41392-024-01839-8

70. Romani AMP. Cisplatin in cancer treatment. *Biochem Pharmacol*. (2022) 206:115323. doi: 10.1016/j.bcp.2022.115323

71. Bryant JD, Lei Y, VanPortfliet JJ, Winters AD, West AP. Assessing mitochondrial DNA release into the cytosol and subsequent activation of 1Innate immune-related pathways in mammalian cells. *Curr Protoc*. (2022) 2:e372. doi: 10.1002/cpz1.372

72. Ma M, Jiang W, Zhou R. DAMPs and DAMP-sensing receptors in inflammation and diseases. *Immunity*. (2024) 57:752–71. doi: 10.1016/j.immuni.2024.03.002

73. Ahmed H, Mahmud AR, Siddiquee MFR, Shahriar A, Biswas P, Shimul MEK, et al. Role of T cells in cancer immunotherapy: Opportunities and challenges. *CPT*. (2023) 1:116–26. doi: 10.1016/j.cpt.2022.12.002

74. Ng CT, Fong LY, Abdullah MNH. Interferon-gamma (IFN-γ): Reviewing its mechanisms and signaling pathways on the regulation of endothelial barrier function. *Cytokine*. (2023) 166:156208. doi: 10.1016/j.cyto.2023.156208

75. Li C, Liu S, Lu X, Tao F. TNFα Enhances calcium influx by interacting with AMPA receptors in the spinal dorsal horn neurons. *Mol Neurobiol*. (2023) 60:18–25. doi: 10.1007/s12035-022-03062-4

76. Dawson JK, Kang D-W, Barnes O, Wilson RL, Norris MK, Dieli-Conwright CM. Efficacy of resistive exercise on skeletal muscle-related outcomes in cancer survivors: a systematic review protocol. *Systematic Rev*. (2022) 11:252. doi: 10.1186/s13643-022-02130-z

77. Soria-Comes T, Climent-Gregori M, Maestu-Maiques I, Inchaurraga-Álvarez I, Cuenca-Martínez F, Cauli O, et al. Effect of a physical exercise intervention on physical function parameters and blood analytical changes in lung cancer survivors: A feasibility study. *Clin Pract*. (2024) 14:2202–16. doi: 10.3390/clinpract14050173

78. Tatangelo T, Muollo V, Ghiotto L, Schena F, Rossi AP. Exploring the association between handgrip, lower limb muscle strength, and physical function in older adults: A narrative review. *Exp Gerontol*. (2022) 167:111902. doi: 10.1016/j.exger.2022.111902

79. Cazzoletti L, Zanolin ME, Dorelli G, Ferrari P, Dalle Carbonare LG, Crisafulli E, et al. Six-minute walk distance in healthy subjects: reference standards from a general population sample. *Respir Res*. (2022) 23:83. doi: 10.1186/s12931-022-02003-y

80. Ackah M, Barakou I, Abonie US, Hettinga FJ. Adherence to exercise in breast cancer survivors during and after active treatment: A systematic review and meta-analysis. *JSAMS Plus*. (2024) 4:100071. doi: 10.1016/j.jsampl.2024.100071

81. Kubat GB, Bouhamida E, Ulger O, Turkel I, Pedriali G, Ramaccini D, et al. Mitochondrial dysfunction and skeletal muscle atrophy: Causes, mechanisms, and treatment strategies. *Mitochondrion*. (2023) 72:33–58. doi: 10.1016/j.mito.2023.07.003

82. Fujiwara Y, Horita N, Adib E, Zhou S, Nassar AH, Asad ZUA, et al. Treatment-related adverse events, including fatal toxicities, in patients with solid tumours receiving neoadjuvant and adjuvant immune checkpoint blockade: a systematic review and meta-analysis of randomised controlled trials. *Lancet Oncol*. (2024) 25:62–75. doi: 10.1016/S1470-2045(23)00524-7

83. Taube JM, Akturk G, Angelo M, Engle EL, Gnjatic S, Greenbaum S, et al. Society for Immunotherapy of Cancer (SITC) Pathology Task Force. The Society for Immunotherapy of Cancer statement on best practices for multiplex immunohistochemistry (IHC) and immunofluorescence (IF) staining and validation. *J Immunother Cancer*. (2020) 8:e000155. doi: 10.1136/jitc-2019-000155

84. Lee EC, Fragala MS, Kavouras SA, Queen RM, Pryor JL, Casa DJ. Biomarkers in sports and exercise: tracking health, performance, and recovery in athletes. *J Strength Cond Res*. (2017) 31:2920–37. doi: 10.1519/JSC.0000000000002122

85. Alotayk LI, Aldubayan MA, Alenezi SK, Anwar MJ, Alhowail AH. Comparative evaluation of doxorubicin, cyclophosphamide, 5-fluorouracil, and cisplatin on cognitive dysfunction in rats: Delineating the role of inflammation of hippocampal neurons and hypothyroidism. *Biomed Pharmacother*. (2023) 165:115245. doi: 10.1016/j.biopha.2023.115245

86. Rajput SK, Singh S. Chapter 45 - The influence of alkylating agent on environment: Cyclophosphamide. In: *Hazardous Chemicals* (2025) Elsevier Inc. p. 629–43. doi: 10.1016/B978-0-323-95235-4.00061-X

87. Shi S, Chen Y, Luo Z, Nie G, Dai Y. Role of oxidative stress and inflammation-related signaling pathways in doxorubicin-induced cardiomyopathy. *Cell Commun Signal*. (2023) 21:61. doi: 10.1186/s12964-023-01077-5

88. Zhou Q, Cao T, Li F, Zhang M, Li X, Zhao H, et al. Mitochondria: a new intervention target for tumor invasion and metastasis. *Mol Med*. (2024) 30:129. doi: 10.1186/s10020-024-00899-4

89. Castro-Guarda M, Evans RD. Human metabolism: metabolic pathways and clinical aspects. *Surg (Oxford)*. (2025) 43:6–15. doi: 10.1016/j.mpsur.2022.01.004

90. Teng T, Shi H, Fan Y, Guo P, Zhang J, Qiu X. Metabolic responses to the occurrence and chemotherapy of pancreatic cancer: biomarker identification and prognosis prediction. *Sci Rep*. (2024) 14:6938. doi: 10.1038/s41598-024-56737-4

91. Ren L, Fu Y, Wang Z, Ma C, Ahn S, Meng Q. Effectiveness of the CANCER-AIMS intervention on nutritional status and symptom management in patients with gastric cancer following gastrectomy: A randomized controlled trial. *Int J Nurs Stud*. (2024) 159:104873. doi: 10.1016/j.ijnurstu.2024.104873

92. Schaeffers AWMA, Scholten HA, van Beers MA, Meussen BW, Smid EJ, van Gils CH, et al. The effect of skeletal muscle mass on dose-limiting toxicities during (chemo) radiotherapy in patients with head and neck cancer: A systematic review and meta-analysis. *Oral Oncol*. (2024) 157:106978. doi: 10.1016/j.oraloncology.2024.106978

93. Salian SR, Daddangadi A, Predheepan D, Bhagat Amonkar DD, Pandya RK, Laxminarayana SLK, et al. Comparison of large single and small multiple doses of cyclophosphamide exposure in mice during early prepubertal age on fertility outcome. *Sci Rep*. (2024) 14:31042. doi: 10.1038/s41598-024-82264-3

94. Bai R, Meng Y, Cui J. Therapeutic strategies targeting metabolic characteristics of cancer cells. *Crit Rev Oncol Hematol*. (2023) 187:104037. doi: 10.1016/j.critrevonc.2023.104037

95. Webster AK, Phillips PC. Epigenetics and individuality: from concepts to causality across timescales. *Nat Rev Genet*. (2025). doi: 10.1038/s41576-024-00804-z

96. Wang X, Wang L, Wu Y, Cai M, Wang L. Effect of different exercise interventions on grip strength, knee extensor strength, appendicular skeletal muscle index, and skeletal muscle index strength in patients with Sarcopenia: A meta-analysis of randomized controlled trials. *Diseases*. (2024) 12:71. doi: 10.3390/diseases12040071

97. Kamran SH, Rehman K, Akash MSH, Khan A, Laher I. Chapter 12 - Impact of physiological factors on drug-metabolizing enzymes: From function to regulation. *Biochem Drug Metabolizing Enzymes*. (2022), p. 281–304. doi: 10.1016/B978-0-323-95120-3.00003-8

98. Bondar D, Karpichev Y. Poly(ADP-ribose) polymerase (PARP) inhibitors for cancer therapy: advances, challenges, and future directions. *Biomolecules*. (2024) 14:269. doi: 10.3390/biom14101269

99. Aggarwal D, Yang J, Salam MA, Sengupta S, Al-Amin MY, Mustafa S, et al. Antibody-drug conjugates: the paradigm shifts in the targeted cancer therapy. *Front Immunol*. (2023) 14:1203073. doi: 10.3389/fimmu.2023.1203073

100. Zubair T, Bandyopadhyay D. Small molecule EGFR inhibitors as anti-cancer agents: discovery, mechanisms of action, and opportunities. *Int Int J Mol Sci*. (2024) 24:2651. doi: 10.3390/ijms24032651

101. Luo Z, Eichinger KM, Zhang A, Li S. Targeting cancer metabolic pathways for improving chemotherapy and immunotherapy. *Cancer Lett*. (2023) 575:216396. doi: 10.1016/j.canlet.2023.216396

102. Hu T, Liu CH, Lei M, Zeng Q, Li L, Tang H, et al. Metabolic regulation of the immune system in health and diseases: mechanisms and interventions. *Signal Transduct Target Ther*. (2024) 9:268. doi: 10.1038/s41392-024-01954-6

103. Riyaz Tramboo S, Elkhalifa AME, Quibtiya S, Ali SI, Nazir Shah N, Taifa S, et al. The critical impacts of cytokine storms in respiratory disorders. *Heliyon*. (2024) 10: e29769. doi: 10.1016/j.heliyon.2024.e29769

104. Abraham D, Lescoat A, Stratton R. Emerging diagnostic and therapeutic challenges for skin fibrosis in systemic sclerosis. *Mol Aspects Med*. (2024) 96:101252. doi: 10.1016/j.mam.2024.101252

105. Zhang W, Wang M, Ji C, Liu X, Gu B, Dong T. Macrophage polarization in the tumor microenvironment: Emerging roles and therapeutic potentials. *Biomed Pharmacother*. (2024) 177:116930. doi: 10.1016/j.biopha.2024.116930

106. Wang Z, Du K, Jin N, Tang B, Zhang W. Macrophage in liver Fibrosis: Identities and mechanisms. *Int Immunopharmacol*. (2023) 120:110357. doi: 10.1016/j.intimp.2023.110357

107. Wu K, Shieh J-s, Qin L, Guo JJ. Mitochondrial mechanisms in the pathogenesis of chronic inflammatory musculoskeletal disorders. *Cell Biosci*. (2024) 14:76. doi: 10.1186/s13578-024-01259-9

108. Basak U, Sarkar T, Mukherjee S, Chakraborty S, Dutta A, Dutta S, et al. Tumor-associated macrophages: an effective player of the tumor microenvironment. *Front Immunol*. (2023) 14:1295257. doi: 10.3389/fimmu.2023.1295257

109. Zhang Y, Zhang X, Meng Y, Xu X, Zuo D. The role of glycolysis and lactate in the induction of tumor-associated macrophages immunosuppressive phenotype. *Int Immunopharmacol*. (2022) 110:108994. doi: 10.1016/j.intimp.2022.108994

110. Yang P, Zeng Y, Yang F, Peng X, Hu Y, Tan X. Transmembrane TNF-α as a novel biomarker for the diagnosis of cytokine storms in a mouse model of multiple organ failure. *Inflammation*. (2023) 46:359–69. doi: 10.1007/s10753-022-01738-6

111. Zeng J, Liao Z, Yang H, Wang Q, Wu Z, Hua F, et al. T cell infiltration mediates neurodegeneration and cognitive decline in Alzheimer's disease. *Neurobiol Dis*. (2024) 193:106461. doi: 10.1016/j.nbd.2024.106461

112. Yao Y, Cai X, Chen Y, Zhang M, Zheng C. Estrogen deficiency-mediated osteoimmunity in postmenopausal osteoporosis. *Med Res Rev*. (2024) 45:561–75. doi: 10.1002/med.22081

113. Hiti L, Markovič T, Lainscak M, Farkaš Lainščak J, Pal E, Mlinarič-Raščan I. The immunopathogenesis of a cytokine storm: The key mechanisms underlying severe COVID-19. *Cytokine Growth Factor Rev*. (2025) 11:316–29. doi: 10.1016/j.cytogfr.2024.12.003

114. Morin M, Duchesne E, Bernier J, Blanchette P, Langlois D, Hébert LJ. What is known about muscle strength reference values for adults measured by hand-held dynamometry: A scoping review. *Arch Rehabil Res Clin Translation*. (2022) 4:100172. doi: 10.1016/j.arrct.2021.100172

115. Luis I, Afschrift M, Gutierrez-Farewik EM. Experiment-guided tuning of muscle–tendon parameters to estimate muscle fiber lengths and passive forces. *Sci Rep*. (2024) 14:14652. doi: 10.1038/s41598-024-65183-1

116. Gu Y, Lv J, Gouda M, Zhu Y, He Y, Chen J. Using pectinase enzymatic peeling for obtaining high-quality Huyou (Citrus changshanensis) segments. *J Food Compost Anal*. (2024) 125:105706. doi: 10.1016/j.jfca.2023.105706

117. Lin H, Wang L, Jiang X, Wang J. Glutathione dynamics in subcellular compartments and implications for drug development. *Curr Opin Chem Biol*. (2024) 81:102505. doi: 10.1016/j.cbpa.2024.102505

118. Liu F, Wang M, Ma Y. Multiscale modeling of skeletal muscle to explore its passive mechanical properties and experiments verification. *Math Biosci Eng*. (2022) 19:1251–79. doi: 10.3934/mbe.2022058

119. Wang H, Yang Z, Yang H, Xue J, Li Y, Wang S, et al. Comparative study on the rheological properties of myofibrillar proteins from different kinds of meat. *LWT*. (2022) 153:112458. doi: 10.1016/j.lwt.2021.112458

120. Banks KP, Farrell MB, Gunther RS, McWhorter NE, Byerly DW, Peacock JG. Improving DXA quality by avoiding common technical and diagnostic pitfalls: part 1. *J Nucl Med Technol*. (2023) 51:167–75. doi: 10.2967/jnmt.122.264885

121. Schuchert P, Karimi A. High-precision control of a robotic arm using frequency-based data-driven methods. *Control Eng Pract*. (2025) 155:106175. doi: 10.1016/j.conengprac.2024.106175

122. Garcia-Retortillo S, Romero-Gómez C, Ivanov PC. Network of muscle fibers activation facilitates inter-muscular coordination, adapts to fatigue and reflects muscle function. *Commun Biol*. (2023) 6:891. doi: 10.1038/s42003-023-05204-3

123. Lukas K, Gutschmidt K, Schoser B, Wenninger S. Evaluation of myotonometry for myotonia, muscle stiffness and elasticity in neuromuscular disorders. *J Neurol*. (2023) 270:5398–407. doi: 10.1007/s00415-023-11867-z

124. Muñoz Esquivel K, Gillespie J, Kelly D, Condell J, Davies R, McHugh C, et al. Factors influencing continued wearable device use in older adult populations: quantitative study. *JMIR Aging*. (2023) 6:e36807. doi: 10.2196/36807

125. Stiver ML, Mirjalili SA, Agur AMR. Measuring shear wave velocity in adult skeletal muscle with ultrasound 2-D shear wave elastography: A scoping review. *Ultrasound Med Biol*. (2023) 49:1353–62. doi: 10.1016/j.ultrasmedbio.2023.02.005

126. Ali Z, Hamdoun A, Alattaya A. Advances in radiological techniques for cancer diagnosis: A narrative review of current technologies. *Health Nexus*. (2024) 2:43–56. doi: 10.61838/kman.hn.2.1.6

127. Feinberg DA, Beckett AJS, Vu AT, Stockmann J, Huber L, Ma S, et al. Next-generation MRI scanner designed for ultra-high-resolution human brain imaging at 7 Tesla. *Nat Methods*. (2023) 20:2048–57. doi: 10.1038/s41592-023-02068-7

128. Engelke K, Chaudry O, Gast L, Eldib MAB, Wang L, Laredo J-D, et al. Magnetic resonance imaging techniques for the quantitative analysis of skeletal muscle: State of the art. *J Orthop Translat*. (2023) 42:57–72. doi: 10.1016/j.jot.2023.07.005

129. Wu H, Zhang S, Wang C, Yan Y. Comparing the accuracy between shear wave elastography and strain elastography in the diagnosis of breast tumors: Systematic review and meta-analysis. *Med (Baltimore)*. (2022) 101:e29139. doi: 10.1097/MD.0000000000029139

130. Xu P, Zhou J, Chen ZD, Yang X, Yan H, Vasić ŽL, et al. Advancements and challenges in electrical impedance myography (EIM): A comprehensive overview of technology development, applications in sports health, and future directions. *IEEE J microw*. (2024) 4:605–25. doi: 10.1109/JMW.2024.3427710

131. Song Y, Li J, Wu Y. Evolving understanding of autoimmune mechanisms and new therapeutic strategies of autoimmune disorders. *Signal Transduct Target Ther*. (2024) 9:263. doi: 10.1038/s41392-024-01952-8

132. Alturki NA. Review of the immune checkpoint inhibitors in the context of cancer treatment. *JCM*. (2023) 12:4301. doi: 10.3390/jcm12134301

133. Bei W, Dong S, Liu G, Lin L, Jiang Y, Lu N, et al. Efficacy and safety of re-challenging PD-1 inhibitors in second-line treatment in metastatic nasopharyngeal carcinoma previously treated with chemotherapy and PD-1 inhibitors. *Cancer Manag Res*. (2024) 16:771–80. doi: 10.2147/CMAR.S460716

134. Zhang X, Dai X, Liu A, Sun M, Cong L, Liang J, et al. Efficacy, safety, and biomarker analysis of first-line immune checkpoint inhibitors with chemotherapy versus chemotherapy for advanced gastric cancer: a multicenter, retrospective cohort study. *BMC Med*. (2024) 22:585. doi: 10.1186/s12916-024-03801-5

135. Peart P. Clinical history taking. *Clinics Integrated Care*. (2022) 10:100088. doi: 10.1016/j.intcar.2021.100088

136. Higuchi T, Ide T, Fujino T, Tohyama T, Nagatomi Y, Nezu T, et al. Clinical characteristics and predictive biomarkers of intensive care unit-acquired weakness in patients with cardiogenic shock requiring mechanical circulatory support. *Sci Rep*. (2025) 15:3535. doi: 10.1038/s41598-025-87381-1

137. Laskowski TJ, Biederstädt A, Rezvani K. Natural killer cells in antitumour adoptive cell immunotherapy. *Nat Rev Cancer*. (2022) 22:557–75. doi: 10.1038/s41568-022-00491-0

138. Frauwirth KA, Thompson CB. Activation and inhibition of lymphocytes by costimulation. *JCI*. (2002) 109:295–9. doi: 10.1172/JCI14941

139. Courtney AH, Lo W-L, Weiss A. TCR signaling: mechanisms of initiation and propagation. *TiBS*. (2018) 43:108–23. doi: 10.1016/j.tibs.2017.11.008

140. Ozga AJ, Chow MT, Luster AD. Chemokines and the immune response to cancer. *Immunity*. (2021) 54:859–74. doi: 10.1016/j.immuni.2021.01.012

141. Khan SH, Choi Y, Veena M, Lee JK, Shin DS. Advances in CAR T cell therapy: antigen selection, modifications, and current trials for solid tumors. *Front Immunol*. (2025) 15:1489827. doi: 10.3389/fimmu.2024.1489827

142. Ho M, Zanwar S, Paludo J. Chimeric antigen receptor T-cell therapy in hematologic Malignancies: Successes, challenges, and opportunities. *Eur J Haematol*. (2023) 112:197–210. doi: 10.1111/ejh.14074

143. Foster C, Kuruvilla J. Treatment approaches in relapsed or refractory peripheral T-cell lymphomas. *F1000Research*. (2022) 9:F1000. doi: 10.12688/f1000research.22257.1

144. Wang J-Y, Wang L. CAR-T cell therapy: Where are we now, and where are we heading? *Blood Sci*. (2023) 5:237–48. doi: 10.1097/BS9.0000000000000173

145. Kankeu Fonkoua LA, Sirpilla O, Sakemura R, Siegler EL, Kenderian SS. CAR T cell therapy and the tumor microenvironment: Current challenges and opportunities. *Mol Ther Oncolytics*. (2022) 25:69–77. doi: 10.1016/j.omto.2022.03.009

146. Jarczak D, Nierhaus A. Cytokine storm—Definition, causes, and implications. *Int J Mol Sci*. (2022) 23:11740. doi: 10.3390/ijms231911740

147. Kang HX, Ma JY, Su YY, Kang S, Feng BJ, Feng XB, et al. Risk factors of temperature increase after cytoreductive surgery combined with hyperthermic intraperitoneal chemotherapy. *Front Oncol*. (2023) 13:1120499. doi: 10.3389/fonc.2023.1120499

148. Radtke KK, Bender BC, Li Z, Turner DC, Roy S, Belousov A, et al. Clinical pharmacology of cytokine release syndrome with T-cell–engaging bispecific antibodies: current insights and drug development strategies. *Clin Cancer Res*. (2025) 31:245–57. doi: 10.1158/1078-0432.CCR-24-2247

149. Pearson RM, Casey LM, Hughes KR, Miller SD, Shea LD. *In vivo* reprogramming of immune cells: Technologies for induction of antigen-specific tolerance. *Advanced Drug Delivery Rev*. (2017) 114:240–55. doi: 10.1016/j.addr.2017.04.005

150. Preede L, Soberg HL, Dalen H, Nyquist A, Jahnsen R, Saebu M, et al. Rehabilitation goals and effects of goal achievement on outcome following an adapted physical activity-based rehabilitation intervention. *Patient Preference Adherence*. (2021) 15:1545–55. doi: 10.2147/PPA.S311966

151. Canli U, Aldhahi MI. The physiological and physical benefits of two types of concurrent training: a randomized controlled trial. *BMC Sports Sci Med Rehabilitation*. (2024) 16:8. doi: 10.1186/s13102-023-00798-x

152. Kamolratanakul S, Pitisuttithum P. Human papillomavirus vaccine efficacy and effectiveness against cancer. *Vaccines*. (2021) 9:1413. doi: 10.3390/vaccines9121413

153. Chido-Amajuoyi OG, Jackson I, Yu R, Shete S. Declining awareness of HPV and HPV vaccine within the general US population. *Hum Vaccines Immunotherapeutics*. (2022) 17:420–7. doi: 10.1080/21645515.2020.1783952

154. Rémy V, Zöllner Y, Heckmann U. Vaccination: the cornerstone of an efficient healthcare system. *JMAHP*. (2015) 3:3. doi: 10.3402/jmahp.v3.27041

155. Pathak P, Pajai S, Kesharwani H. A review on the use of the HPV vaccine in the prevention of cervical cancer. *Cureus*. (2022) 14:e28710. doi: 10.7759/cureus.28710

156. Fan T, Zhang M, Yang J, Zhu Z, Cao W, Dong C. Therapeutic cancer vaccines: advancements, challenges and prospects. *Signal Transduct Target Ther*. (2023) 8:450. doi: 10.1038/s41392-023-01674-3

157. Tayebi A, Samimisedeh P, Jafari Afshar E, Mahmoudnia S, Milan N, Ayati A, et al. Neuromuscular diseases associated with COVID-19 vaccines: a systematic review and pooled analysis of 258 patients. *BMC Neurol*. (2023) 23:437. doi: 10.1186/s12883-023-03486-y

158. Cao Q, Fang H, Tian H. mRNA vaccines contribute to innate and adaptive immunity to enhance immune response *in vivo*. *Biomaterials*. (2024) 310:122628. doi: 10.1016/j.biomaterials.2024.122628

159. Wu X, Yang X, Dai Y, Zhao Z, Zhu J, Guo H, et al. Single-cell sequencing to multi-omics: technologies and applications. *biomark Res*. (2024) 12:110. doi: 10.1186/s40364-024-00643-4

160. Niu G, Wang H, Zhai Y, Zhou B, Kang Y, Pei Z, et al. Nanotechnology-based in *situ* cancer vaccines: Mechanisms, design, and recent advances. *Nano Today*. (2024) 56:102286. doi: 10.1016/j.nantod.2024.102286

161. Morales-Durán N, León-Buitimea A, Morones-Ramírez JR. Unraveling resistance mechanisms in combination therapy: A comprehensive review of recent advances and future directions. *Heliyon*. (2024) 10:e27984. doi: 10.1016/j.heliyon.2024.e27984

162. O'Dowd PD, Sutcliffe DF, Griffith DM. Oxaliplatin and its derivatives – An overview. *Coord Chem Rev*. (2023) 497:215439. doi: 10.1016/j.ccr.2023.215439

163. Hao M, Zhou Y, Chen S, Jin Y, Li X, Xue L, et al. Spatiotemporally controlled T-cell combination therapy for solid tumor. *Adv Sci*. (2024) 11:2401100. doi: 10.1002/advs.202401100

164. El-Serafi I, Steele S. Cyclophosphamide pharmacogenomic variation in cancer treatment and its effect on bioactivation and pharmacokinetics. *Adv Pharmacol Sci*. (2024) 2024:4862706. doi: 10.1155/2024/4862706

165. Puccetti M, Pariano M, Schoubben A, Giovagnoli S, Ricci M. Biologics, theranostics, and personalized medicine in drug delivery systems. *Pharmacol Res*. (2024) 201:107086. doi: 10.1016/j.phrs.2024.107086

166. Ouyang G, Liu Y, Liu J, Huang L, Luo F, Li L. Efficacy and safety of reduced-dose chemotherapy plus immunotherapy in patients with lung squamous cell carcinoma: A real-world observational study. *Cancer Med*. (2023) 12:18679–90. doi: 10.1002/cam4.6478

167. Wang Y, Han H, Zhang F, Lv T, Zhan P, Ye M, et al. Immune checkpoint inhibitors alone vs immune checkpoint inhibitors—combined chemotherapy for NSCLC patients with high PD-L1 expression: a network meta-analysis. *Br J Cancer*. (2022) 127:948–56. doi: 10.1038/s41416-022-01832-4

168. Lin X, Kang K, Chen P, Zeng Z, Li G, Xiong W, et al. Regulatory mechanisms of PD-1/PD-L1 in cancers. *Mol Cancer*. (2024) 23:108. doi: 10.1186/s12943-024-02023-w

169. Wang W, Liu Y, He Z, Li L, Liu S, Jiang M, et al. Breakthrough of solid tumor treatment: CAR-NK immunotherapy. *Cell Death Discovery*. (2024) 10:40. doi: 10.1038/s41420-024-01815-9

170. Duell J, Westin J. The future of immunotherapy for diffuse large B-cell lymphoma. *Int J Cancer*. (2025) 156:251–61. doi: 10.1002/ijc.35156

171. Liu J, Yu Y, Liu C, Gao C, Zhuang J, Liu L, et al. Combinatorial regimens of chemotherapeutic agents: A new perspective on raising the heat of the tumor immune microenvironment. *Front Pharmacol*. (2022) 13:1035954. doi: 10.3389/fphar.2022.1035954

172. Kong X, Zhang J, Chen S, Wang X, Xi Q, Shen H, et al. Immune checkpoint inhibitors: breakthroughs in cancer treatment. *Cancer Biol Med*. (2024) 21:451–72. doi: 10.20892/j.issn.2095-3941.2024.0055

173. Chen F, Fu J, Feng H. IL-6 promotes muscle atrophy by increasing ubiquitin-proteasome degradation of muscle regeneration factors after cerebral infarction in rats. *Neuromolecular Med*. (2025) 27:3. doi: 10.1007/s12017-024-08825-x

174. Qiu L, Yang Z, Jia G, Liang Y, Du S, Zhang J, et al. Clinical significance and immune landscape of a novel immune cell infiltration-based prognostic model in lung adenocarcinoma. *Heliyon*. (2024) 10:e33109. doi: 10.1016/j.heliyon.2024.e33109

175. Illouz F, Briet C, Rodien P. Immune checkpoint inhibitor-related thyroid dysfunction. *Ann Endocrinol*. (2023) 84:346–50. doi: 10.1016/j.ando.2023.03.005

176. Vanneman M, Dranoff G. Combining immunotherapy and targeted therapies in cancer treatment. *Nat Rev Cancer*. (2012) 12:237–51. doi: 10.1038/nrc3237

177. Barbari C, Fontaine T, Parajuli P, Lamichhane N, Jakubski S, Lamichhane P, et al. Immunotherapies and combination strategies for immuno-oncology. *Int J Mol Sci*. (2020) 21:5009. doi: 10.3390/ijms21145009

178. Liang I, Tay DL, Kirchhoff AC, Schwanke G, Ellington L, Pisu M, et al. Financial toxicity of total cancer care immunotherapy patients and caregivers: impacts of COVID-19 pandemic and inflation. *Support Care Cancer*. (2024) 32:790. doi: 10.1007/s00520-024-09007-y

179. Dailah HG, Hommdi AA, Koriri MD, Algathlan EM, Mohan S. Potential role of immunotherapy and targeted therapy in the treatment of cancer: A contemporary nursing practice. *Heliyon*. (2024) 10:e24559. doi: 10.1016/j.heliyon.2024.e24559

180. Choi J, Lee SY. Clinical characteristics and treatment of immune-related adverse events of immune checkpoint inhibitors. *Immune Netw*. (2020) 20:e9. doi: 10.4110/in.2020.20.e9

181. Goenka A, Khan F, Verma B, Sinha P, Dmello CC, Jogalekar MP, et al. Tumor microenvironment signaling and therapeutics in cancer progression. *Cancer Commun (Lond)*. (2023) 43:525–61. doi: 10.1002/cac2.12416

182. Zhang L, Zhou C, Zhang S, Chen X, Liu J, Xu F, et al. Chemotherapy reinforces anti-tumor immune response and enhances clinical efficacy of immune checkpoint inhibitors. *Front Oncol*. (2022) 12:939249. doi: 10.3389/fonc.2022.939249

183. Zhang H, Yue X, Chen Z, Liu C, Wu W, Zhang N, et al. Define cancer-associated fibroblasts (CAFs) in the tumor microenvironment: new opportunities in cancer immunotherapy and advances in clinical trials. *Mol Cancer*. (2023) 22:159. doi: 10.1186/s12943-023-01860-5

184. He S, Zheng L, Qi C. Myeloid-derived suppressor cells (MDSCs) in the tumor microenvironment and their targeting in cancer therapy. *Mol Cancer*. (2025) 24:5. doi: 10.1038/s41392-021-00670-9

185. Butterfield LH, Najjar YG. Immunotherapy combination approaches: mechanisms, biomarkers and clinical observations. *Nat Rev Immunol*. (2024) 24:399–416. doi: 10.1038/s41577-023-00973-8

186. Shin AE, Giancotti FG, Rustgi AK. Metastatic colorectal cancer: mechanisms and emerging therapeutics. *Trends Pharmacol Sci*. (2023) 44:222–36. doi: 10.1016/j.tips.2023.01.003

frontiers | Frontiers in Immunology

TYPE Original Research
PUBLISHED 07 April 2025
DOI 10.3389/fimmu.2025.1539616

Check for updates

OPEN ACCESS

EDITED BY
Xiaosheng Tan,
Rutgers, United States

REVIEWED BY
Xiaowei Wu,
Dana–Farber Cancer Institute, United States
Jin-Ming Zhang,
University of Texas Health Science Center at Houston, United States
Jingcheng Zhu,
University of Pennsylvania, United States

*CORRESPONDENCE
Na Zhou
zhouna@qdu.edu.cn
Xiaochun Zhang
zxc9670@qdu.edu.cn

RECEIVED 04 December 2024
ACCEPTED 18 March 2025
PUBLISHED 07 April 2025

CITATION
Lan H, Liu H, Hou H, Zhang C, Zhu J, Zhou N and Zhang X (2025) Combination of anlotinib with immunotherapy enhanced both anti-angiogenesis and immune response in high-grade serous ovarian cancer.
Front. Immunol. 16:1539616.
doi: 10.3389/fimmu.2025.1539616

COPYRIGHT
© 2025 Lan, Liu, Hou, Zhang, Zhu, Zhou and Zhang. This is an open-access article distributed under the terms of the Creative Commons Attribution License (CC BY). The use, distribution or reproduction in other forums is permitted, provided the original author(s) and the copyright owner(s) are credited and that the original publication in this journal is cited, in accordance with accepted academic practice. No use, distribution or reproduction is permitted which does not comply with these terms.

Combination of anlotinib with immunotherapy enhanced both anti-angiogenesis and immune response in high-grade serous ovarian cancer

Hongwei Lan[1], Hui Liu[2], Helei Hou[3], Chuantao Zhang[3], Jingjuan Zhu[1], Na Zhou[1*] and Xiaochun Zhang[1*]

[1]Precision Medicine Center of Oncology, The Affiliated Hospital of Qingdao University, Qingdao, Shandong, China, [2]Department of Clinical Laboratory, Qingdao Women's and Children's Hospital, Qingdao, Shandong, China, [3]Department of Oncology, The Affiliated Hospital of Qingdao University, Qingdao, Shandong, China

Background: High-grade serous ovarian cancer (HGSOC) poses significant treatment challenges due to frequent recurrence and resistance to conventional therapies. Combination of anlotinib with immunotherapy have showed promise in various cancers, but its impact on HGSOC remains to be fully elucidated.

Methods: A retrospective analysis was performed on 36 HGSOC patients treated with anlotinib-based therapies, including both monotherapy and combination treatment with anti-PD-L1/anti-PD-1 antibody (aPD-L1/aPD-1). Peripheral blood mononuclear cell-derived patient-derived xenograft (PBMC-PDX) model was established from drug-resistant recurrent HGSOC patient-derived tumor cells, and single-cell RNA sequencing (scRNA-seq) was conducted to dissect the TME following treatment with anlotinib, anlotinib + aPD-L1 and anlotinib + aPD-1.

Results: Clinical analysis revealed a disease control rate (DCR) of 71.43% for anlotinib monotherapy, which improved to 100% when combined with aPD-L1/aPD-1. In PBMC-PDX models, treatment evaluation showed that anlotinib decreased tumor volume, an effect further enhanced by its combination with aPD-L1. scRNA-seq analysis demonstrated that anlotinib reduced the proportions of myofibroblastic cancer-associated fibroblasts and $ESM1^+$ endothelial cells, resulting in decreased angiogenesis. The combination of anlotinib and aPD-L1 further amplified these effects, promoting $CD8^+$ T cell infiltration and reversing T cell exhaustion, whereas anlotinib + aPD-1 showed limited efficacy in this regard. Additionally, anlotinib + immunotherapy induced a shift toward M1 polarization of myeloid cells, enhanced anti-tumor activity, and inhibited immune escape. Cell-cell communication analysis revealed reduced APP-CD74 signaling and increased CD99-CD99 signaling, which might contribute to immune activation.

Conclusion: The combination of anlotinib and aPD-L1 effectively modulates the HGSOC tumor microenvironment by inhibiting angiogenesis, enhancing immune infiltration, and reversing T cell exhaustion.

KEYWORDS

high-grade serous ovarian cancer, patient-derived xenograft model, anlotinib, immunotherapy, single-cell RNA sequencing

1 Introduction

Ovarian cancer remains a significant global health challenge, with approximately 314,000 new cases diagnosed and 207,000 deaths annually—of which high-grade serous ovarian cancer (HGSOC) accounts for over 80% (1, 2). Despite decades of research and therapeutic advancements, the cornerstone treatment for HGSOC—surgical intervention followed by platinum-based chemotherapy—faces substantial hurdles, including high recurrence rates and the eventual development of resistance. Consequently, the 5-year survival rate remains below 40% (3, 4). This therapeutic impasse has intensified the search for novel strategies, such as targeted therapies and immunotherapies, to overcome the limitations of current standard care.

Anlotinib is a novel oral multi-targeted tyrosine kinase inhibitor (TKI) that exerts antitumor effects primarily by inhibiting angiogenesis and targeting pathways involved in tumor growth and survival (5). Initially approved for the treatment of recurrent, locally advanced, or metastatic non-small cell lung cancer (NSCLC) (6), anlotinib has demonstrated promising efficacy in clinical trials for medullary thyroid carcinoma and soft tissue sarcoma (7, 8). Emerging studies have reported that anlotinib exhibits favorable antitumor activity and acceptable safety profiles in ovarian cancer (9, 10), with several clinical trials currently underway. Notably, combinations of anlotinib with other therapies—including chemotherapy, immunotherapy, and radiotherapy—have shown enhanced anticancer effects compared to monotherapy (11, 12). However, limited research on the roles of anlotinib and anti-PD-L1/anti-PD-1 antibody (aPD-L1/aPD-1) within the ovarian cancer tumor microenvironment (TME) has left their clinical efficacy and underlying mechanisms unclear, hindering broader clinical application and regulatory approval.

This study comprehensively evaluates the therapeutic effects of anlotinib in drug-resistant recurrent HGSOC, both as a monotherapy and in combination with aPD-L1/aPD-1. By analyzing real-world clinical treatment data, constructing an HGSOC Peripheral blood mononuclear cell-derived patient-derived xenograft (PBMC-PDX) model, and performing single-cell sequencing (scRNA-seq), this research assesses the changes in the HGSOC TME and the underlying mechanisms, aiming to provide a deeper understanding and more effective treatment strategies for drug-resistant HGSOC.

2 Methods

2.1 Patient selection and evaluation criteria

We conducted a retrospective study of patients with HGSOC who received anlotinib-based therapy at our institution between January 2020 and July 2024. Inclusion criteria required a confirmed diagnosis of HGSOC, an Eastern Cooperative Oncology Group (ECOG) performance status of 0–2, completion of at least three cycles of anlotinib treatment, and availability of comprehensive medical records. Clinical data were collected through medical chart reviews and patient follow-ups. All treatments were administered in accordance with relevant clinical guidelines and drug protocols. PD-L1 expression levels were assessed by immunohistochemistry using the PD-L1 22C3 antibody. PD-L1 positivity was defined as a tumor proportion score (TPS) or a combined positive score (CPS) greater than 1%. Tumor staging prior to treatment was determined according to the guidelines of the 8th edition of the American Joint Committee on Cancer (AJCC). Treatment responses were evaluated radiologically using the Response Evaluation Criteria in Solid Tumors (RECIST) version 1.1.

2.2 Obtaining and processing of HGSOC sample

With approval from the Ethics Committee of Qingdao University Affiliated Hospital and after obtaining informed consent, we collected a 700 mL sample of malignant ascites from a patient diagnosed with advanced HGSC. The cancer had metastasized to the liver, peritoneum, pelvis, and multiple lymph nodes. The patient had previously undergone tumor debulking surgery, followed by multiple times of adjuvant chemotherapy. Despite these interventions, the disease progressed, evidenced by increasing tumor size and ascites, leading to a diagnosis of progressive disease (PD). Genetic profiling revealed a TP53 mutation, MYC amplification, a low tumor mutational burden of 7.1 mut/Mb, microsatellite stability, and low PD-L1 expression (TPS < 1%). No mutations in BRCA1 or BRCA2 were detected. Written informed consent was obtained from the patient for the publication of any potentially identifiable images or data included in this article.

2.3 Construction of PBMC-PDX models

To generate the PDX model, ascitic fluid was processed in a biosafety cabinet. The fluid was centrifuged at 500 × g for 5 minutes to pellet the cells. After discarding the supernatant, red blood cell lysis buffer was added, followed by a 5-minute incubation at room temperature. The remaining cells were washed twice with phosphate-buffered saline (PBS) and centrifuged. The enriched tumor cells were then resuspended in pre-chilled PBS. A 1:1 mixture of Matrigel and tumor cell suspension was prepared, and the cells were subsequently injected subcutaneously into NOD/SCID/IL2Rγ(NSG) mice. Tumor growth was monitored at regular intervals, with volumes calculated using the formula:

$$V = \frac{Length \times Width^2}{2}$$

Upon reaching an appropriate size, a portion of the tumor was excised for pathological assessment to ensure consistency with the original tumor type. The established PDX model was then maintained in NSG mice for further experiment. To mimic a fully intact immune microenvironment, PBMCs (Miaoshun Biotechnology Co., Shanghai, China) were administered intravenously at a dose of 0.2 mL containing 5×10^6 cells per mouse. Flow cytometry (FACS) analysis confirmed the successful establishment of the PBMC-PDX model, which was then used for subsequent drug efficacy assessments.

2.4 Drugs

Anlotinib was purchased from Chia Tai Tianqing Pharmaceutical Group Co. (Lianyungang, China). The PD-L1-specific antibody atezolizumab (1200 mg/20 mL) was purchased from Roche (Basel, Switzerland). The PD-1-specific antibody toripalimab (240 mg/5 mL) was purchased from Suzhou Zhenhe Biomedical Pharmaceutical Co. (Suzhou, China).

2.5 Animal study

Female NSG mice (6–8 weeks old, 18–20 g) were obtained from Shanghai Model Organisms Center, Inc. (Shanghai, China). Mice were housed in a specific pathogen-free environment in individually ventilated cages under controlled conditions of temperature (20–26 °C), humidity (40–70%), and a 12-hour light/dark cycle. Three mice were housed per cage (dimensions: 325 mm × 210 mm × 180 mm) with sterilized corn cob bedding that was replaced twice weekly. Mice had ad libitum access to food and water; the feed was sterilized by Co-60 irradiation, and the water was sterilized under high pressure, both replenished twice weekly. Tumor-bearing mice were euthanized when they exhibited severe deterioration in condition or when tumors reached an average volume of 2,000 mm^3. At the conclusion of the study, all mice were euthanized. All experimental procedures adhered to the guidelines of the Institutional Animal Care and Use Committee (IACUC) and received prior approval.

2.6 Fluorescence-activated cell sorting

Fluorescence-Activated Cell Sorting (FACS) analysis was carried out using an Attune® NxT Acoustic Focusing Cytometer (Life Technologies, CA, USA). The antibodies employed included: APC-conjugated anti-human CD45, APC/Cy7-conjugated anti-human CD8, PE-conjugated anti-human CD3, PE-conjugated anti-human CD56 from Biolegend (CA, USA), and BV421-conjugated anti-human CD45, BB515-conjugated anti-human CD3, and BV605-conjugated anti-human CD4 from BD Biosciences (NJ, USA).

Blood samples from treated PBMC-PDX model mice were divided into seven tubes (100 µL each), processed as follows: 1) Blank control, 2) CD45 single stain (5 µL anti-human CD45 antibody), 3) CD3 single stain (5 µL anti-human CD3 antibody), 4) CD4 single stain (5 µL anti-human CD4 antibody), 5) CD8 single stain (5 µL anti-human CD8 antibody), 6) CD56 single stain (5 µL anti-human CD56 antibody), and 7) a mixture of 5 µL each of CD45, CD3, CD4, CD8, and CD56 antibodies. The gating strategy used was R1: total cells, R2: single cells, R3: CD45+ cells, R4: CD45+CD3+ cells, R5: CD4+ cells, R6: CD8+ cells, and R7: CD45+CD56+ cells.

2.7 Single-cell RNA sequencing and analysis

Tumor tissues were cut into 1-2 mm^3 fragments and digested using the SoloTM Tumor Dissociation Kit (Sinotech Genomics, JZ-SC-58201) for 60 minutes at 37°C. The resulting single-cell suspension was filtered through a 40 µm strainer and kept on ice until further single-cell transcriptome analysis. The digestion was halted with RPMI-1640.

The single-cell transcriptome analysis followed the protocol of the BD Rhapsody system (BD Biosciences, CA). The cells were first stained with calcein AM and Draq7 for accurate determination of cell concentration and viability using the BD Rhapsody™ Scanner. They were then loaded into a microwell cartridge, followed by an excess loading of cell capture beads. After cell lysis with lysis buffer, the beads were retrieved and washed to prepare for reverse transcription.

Using the BD Rhapsody cDNA Kit (BD Biosciences, Cat. No. 633773) and BD RhapsodyTM WTA Amplification Kit (BD Biosciences, Cat. No. 633801), a cDNA library with cell labels and UMI information was created based on the microbead-captured single-cell transcriptome. Sequencing was carried out in PE150 mode (paired-end 150 bp reads) on the NovaSeq platform. The raw sequencing data were processed through the BD Rhapsody Whole Transcriptome Assay Analysis Pipeline (v1.8), which includes quality filtering, read and molecule annotation, and putative cell identification. The GRCh38 genome was used as the reference for this pipeline.

For subsequent clustering analysis and visualization, R software (v4.3.0) (13) and the Seurat R package (v5.0.3) (14) were employed. Cells with over 25% mitochondrial UMI or fewer than 500 UMI or 200 genes were excluded. The gene expression matrix was normalized according to the total cellular UMI count, and 2000 highly variable features were selected for PCA after data scaling based on UMI counts. The first 50 principal components were then used for clustering at a resolution of 0.6, utilizing t-SNE or UMAP algorithms. To visualize gene expression in each cluster, feature plots, violin plots, and heatmaps were generated.

Cluster-specific markers were identified through the FindAllMarkers function using the Wilcoxon test, with a threshold of log2-fold change > 0.25 and min. pct > 0.25. Each cluster was annotated with canonical marker genes from prior literature to unbiasedly identify the cell types in the filtered and combined datasets. Gene Ontology (GO) functional enrichment was performed using the ClusterProfiler R package (v4.4.4) (15), while Hallmark and KEGG pathway enrichment analyses were conducted using the GSVA (v1.50.5) (16) and msigdbr (v7.5.1) (17) R packages. SCENIC (v1.3.1) (18) was employed for transcription factor analysis, and CellChat (v1.6.1) (19) was utilized for cell-cell communication analysis. Pseudotime trajectory analysis was carried out using the Monocle2 R package (v2.18.0) (20) and CytoTRACE (v0.3.3) (21). The CHPF algorithm was applied to identify hypoxic states in cells (22).

2.8 Spatial transcriptome analysis and prognosis analysis

Spatial transcriptome data for HGSOC were obtained from the GSE211956 dataset (23). Quality control and subsequent analyses were performed using standard protocols provided by the Seurat package. Kaplan-Meier analysis of NR3C1 expression and patient prognosis after aPD-L1/aPD-1 treatment, were conducted using data from the Kaplan-Meier Plotter database (24).

2.9 Immunohistochemistry and immunofluorescence

Tumor tissues were fixed in 4% paraformaldehyde, dehydrated in graded ethanol, and embedded in paraffin. Sections (5 μm) were deparaffinized, rehydrated, and rinsed with PBS. For immunohistochemistry, antigen retrieval was performed using Tris-EDTA buffer (pH 9.0) at 95°C for 10 minutes. Sections were incubated with rabbit anti-human CD8 alpha antibody (1:1000, Abcam) or anti-human PD-L1 antibody (1:800, Invitrogen), followed by detection with the HRP/DAB IHC Detection Kit (Abcam) according to the manufacturer's instructions. Rabbit IgG isotype control (Cell Signaling Technology) was used as a negative control.

For immunofluorescence, tumor sections were incubated with anti-CD31 antibody (1:500, Servicebio Technology), followed by incubation with fluorophore-conjugated secondary antibodies (1:1000, Servicebio Technology).

2.10 Statistical analysis

Data are presented as the mean ± SEM. Statistical analyses of gene expression or module scores among groups used either the Mann–Whitney test or an unpaired two-tailed Student's t-test, with p-values reported where relevant. Multiple-testing correction for differentially expressed genes was implemented by the corresponding R packages. Genes with adjusted p-values< 0.05 were considered significant. Correlation analyses employed the R function cor.test with Pearson's method. Differential expression in pseudotime or cell-type trajectories used negative binomial models with q-values< 0.01 indicating significance. GSVA was performed with the ssgsea method on normalized gene expression data. Most of code and statistical computations were done primarily in R, with some steps handled in Python and GraphPad Prism. Statistical significance was defined as a $P< 0.05$.

3 Results

3.1 Clinical characteristics and treatment response of patients receiving anlotinib-based treatments

Based on the inclusion and exclusion criteria, 36 refractory HGSOC patients who received anlotinib treatment were selected (Supplementary Figure S1). The median age was 66 years, with the majority presenting at advanced stages: 55.56% were at stage IV and 30.56% at stage III. Among these patients, only 10 underwent PD-L1 testing, of whom 70% were PD-L1 positive (representing 19.44% of the total cohort). P53 mutation testing was performed on 24 patients, revealing that 75% (18 out of 24) harbored P53 mutations. These findings align with prior studies, indicating a high prevalence of PD-L1 positivity and P53 mutations in HGSOC (25, 26). Patients received different anlotinib regimens: 38.89% underwent monotherapy, and 16.67% received anlotinib combined with immunotherapy. Notably, anlotinib was predominantly used in patients who had relapsed or were refractory to platinum-based therapy, with 50% initiating anlotinib at the fourth line of treatment or beyond. The most common side effects were rash and fatigue, both managed symptomatically without treatment interruption. Only one patient discontinued anlotinib due to gastrointestinal bleeding (Table 1).

The overall disease control rate (DCR) was 75% (95% CI: 58.93–86.25), and the objective response rate (ORR) was 8.33% (95% CI: 2.87–21.83). In the monotherapy group, the DCR was 71.43% (95% CI: 45.35–88.28) with an ORR of 14.29% (95% CI: 4.01–39.94). In contrast, the combination immunotherapy group achieved a DCR of 100% (95% CI: 60.97–100) and an ORR of 16.67% (95% CI: 3.01–56.35). At the time of the final follow-up, the median progression-free survival (PFS) was 7.5 months (range: 2–34.9 months), while

TABLE 1 Demographic and baseline characteristics of the HGSOC patients received anlotinib-based treatments.

Characteristics	Value(N=36)
Median age(range)-year	66 (44-87)
Stage-no. (%)	
I	1 (2.78%)
II	4 (11.11%)
III	11 (30.56%)
IV	20 (55.56%)
PD-L1 status-no. (%)	
Positive	7 (19.44%)
Negative	3 (8.33%)
Not available	26 (72.22%)
P53 status-no. (%)	
Mutation	18 (50.00%)
Wild	6 (16.67%)
Not available	12 (33.33%)
Anlotinib therapy strategy-no. (%)	
Mono-therapy	14 (38.89%)
+ Targeted therapy	
Olaparib	7 (19.44%)
Niraparib	4 (11.11%)
+ Immunotherapy	
Sintilimab	3 (8.33%)
Pembrolizumab	1 (2.78%)
Atezolizumab	1 (2.78%)
Durvalumab	1 (2.78%)
+ Chemotherapy	3 (8.33%)
+ Chemotherapy & Targeted therapy (Niraparib)	2 (5.56%)
The line of anlotinib therapy -no. (%)	
2	7 (19.44%)
3	11 (30.56%)
4	8 (22.22%)
5	6 (16.67%)
≥6	4 (11.11%)
Adverse effect -no. (%)	
Rash (G1,2; G2,1)	3 (8.33%)
Fatigue	3 (8.33%)
Hemorrhage	1 (2.78%)
Congestion	1 (2.78%)
Hypertension	1 (2.78%)

(Continued)

TABLE 1 Continued

the median overall survival (OS) had not yet been reached. The monotherapy group had a median PFS of 6.5 months (range: 2–12.91 months), compared to 8.7 months (range: 2.1–20.6 months) in the combination immunotherapy group (Figure 1). These findings are consistent with those reported for anlotinib and its combination with immune checkpoint inhibitors (ICIs) in advanced NSCLC, where combination therapy achieved higher DCRs and longer PFS compared to monotherapy (27, 28).

These findings suggest that anlotinib, particularly in combination with immunotherapy, holds therapeutic potential for recurrent or refractory HGSOC. However, given the lack of approved indications for anlotinib or ICIs in HGSOC, clinical trials remain challenging. Thus, constructing PDX model was the most feasible approach to further evaluate this combination therapy in a preclinical setting.

3.2 Establishment and treatment of the immunocompetent patient-derived xenograft model

PDX models largely retain the characteristics of the parental tumors and exhibit high similarity between samples, making them more suitable for drug testing than traditional cell lines (29). To establish the PDX model, tumor cells were isolated from the malignant ascites of a refractory HGSOC patient who had relapsed after multiple lines of platinum-based chemotherapy. These cells were processed and subcutaneously injected into immunodeficient NSG mice (Methods) (Figure 2A). Pathological analysis confirmed that the transplanted tumor was HGSOC and closely resembled the parent tumor, with serial transplantation demonstrating stable passaging capability (Figure 2B).

To construct an immunocompetent PDX model, human PBMCs were subsequently injected into the PDX models (Methods). Twenty models were randomly and equally divided into four groups. The experimental groups received either anlotinib monotherapy, anlotinib combined with aPD-L1or aPD-1 (Supplementary Table S1). The results indicated that anlotinib monotherapy initially decreased tumor volume but showed progression during the final week of the experiment. In contrast, the combination of anlotinib with aPD-L1 resulted in a more pronounced and sustained reduction in tumor volume, along with a significant decrease in tumor weight. However, the combination of anlotinib with aPD-1 exhibited a less apparent reduction in tumor volume (Figures 2C–E). Despite the random grouping

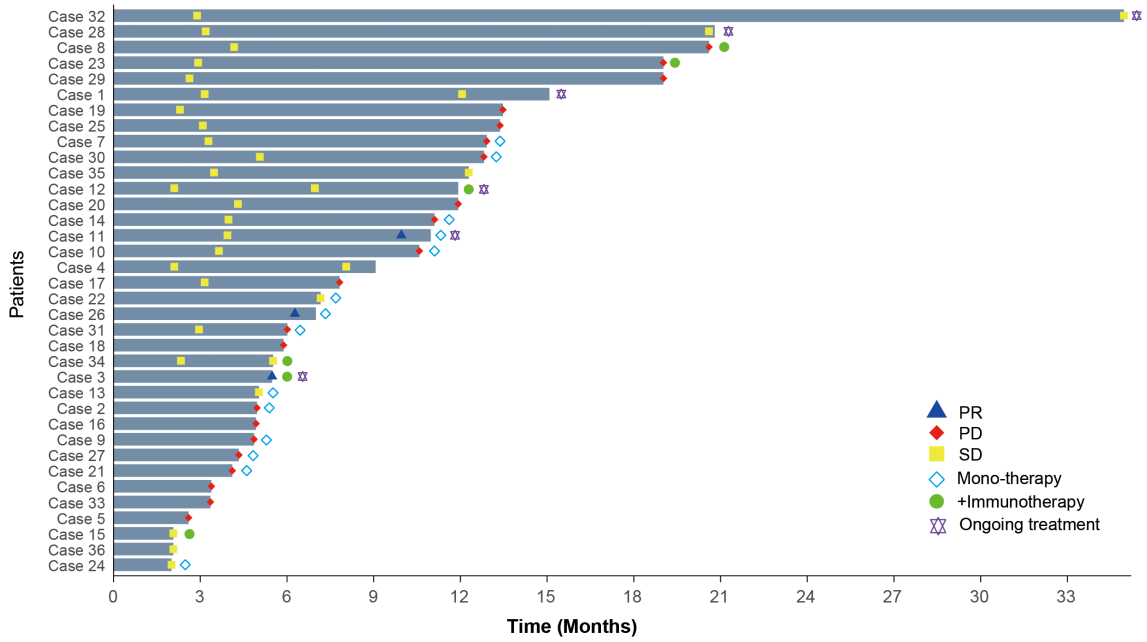

FIGURE 1
Treatment duration and clinical responses in HGSOC patients receiving anlotinib-based therapies. PR, Partial response; PD, Progressive disease; SD, Stable disease.

resulting in the anlotinib + aPD-1 group having a slightly higher initial body weight than the other groups, none of these treatments led to significant changes in the body weight of the models (Figure 2F).

Given the observed differences between the effects of AL + aPD-1 and AL + aPD-L1, we sought to uncover the cellular and molecular mechanisms underlying these discrepancies. scRNA-seq was employed to comprehensively analyze changes in the TME and evaluate the mechanisms by which this combination therapy exerts its antitumor effects in HGSOC.

3.3 Single-Cell RNA sequencing reveals cellular composition of HGSOC tumor microenvironment

Eight tumor samples were collected and processed for scRNA-seq using standard protocols (Methods). After quality control, batch effect correction, and dimensionality reduction clustering (Supplementary Figures S2A, B), we identified a total of 19 distinct cell clusters (Supplementary Figure S2C). Through pearson correlation analysis and marker gene expression profiling, these clusters were categorized into epithelial cells, myeloid cells, T cells, fibroblasts, endothelial cells, and $CDO1^+$ cells (Figures 3A–C). Epithelial cells constituted the largest proportion, accounting for 52.6% of the total cells, followed by myeloid cells at 28.7% and T cells at 16.2%. The stromal cell population was primarily composed of fibroblasts and endothelial cells (Figure 3D, Supplementary Figure S2D). The epithelial cells exhibited high expression of EPCAM, KRT19, and KRT18; myeloid cells were marked by elevated expression of CD68, C1QA, and S100A9. T cells were characterized by high levels of CD2, CD3D, and CD3E, while fibroblasts showed strong expression of COL1A1 and COL1A2. Endothelial cells were identified by high expression of VWF and PECAM1. Additionally, $CDO1^+$ cells displayed elevated expression of CDO1, PPARG, and FABP4 (Figure 3E). Additionally, IHC results confirmed the absence of B cells and NK cells in the model (Supplementary Figure S2E).

3.4 Combination of anlotinib and immunotherapy alters tumor cell heterogeneity

To further explore tumor cell heterogeneity, we conducted an in-depth analysis of the epithelial cell population. Using inferCNV analysis, we discovered that nearly all epithelial cells exhibited malignancy (Figure 4A), which may be facilitated by the comprehensive extraction of tumor tissues from the PBMC-PDX model. Dimensionality reduction and clustering further divided these tumor cells into nine subtypes (Epc1–Epc9) (Figure 4B), each with distinct gene expression profile (Supplementary Figure S3A). Based on biological characteristics, these epithelial cells were categorized into three main types: C1 cells, primarily consisting of proliferative groups (Epc1, Epc2, Epc3); C2 cells, associated with drug metabolism (Epc4, Epc9); and C3 cells, mainly related to hypoxia (Epc5, Epc6, Epc7, Epc8) (Figure 4C). Utilizing seven hypoxia-related genes identified through the CHPF algorithm, we further classified the cells into hypoxic and non-hypoxic types, confirming the hypoxic phenotype of C3 (Figure 4D–F).

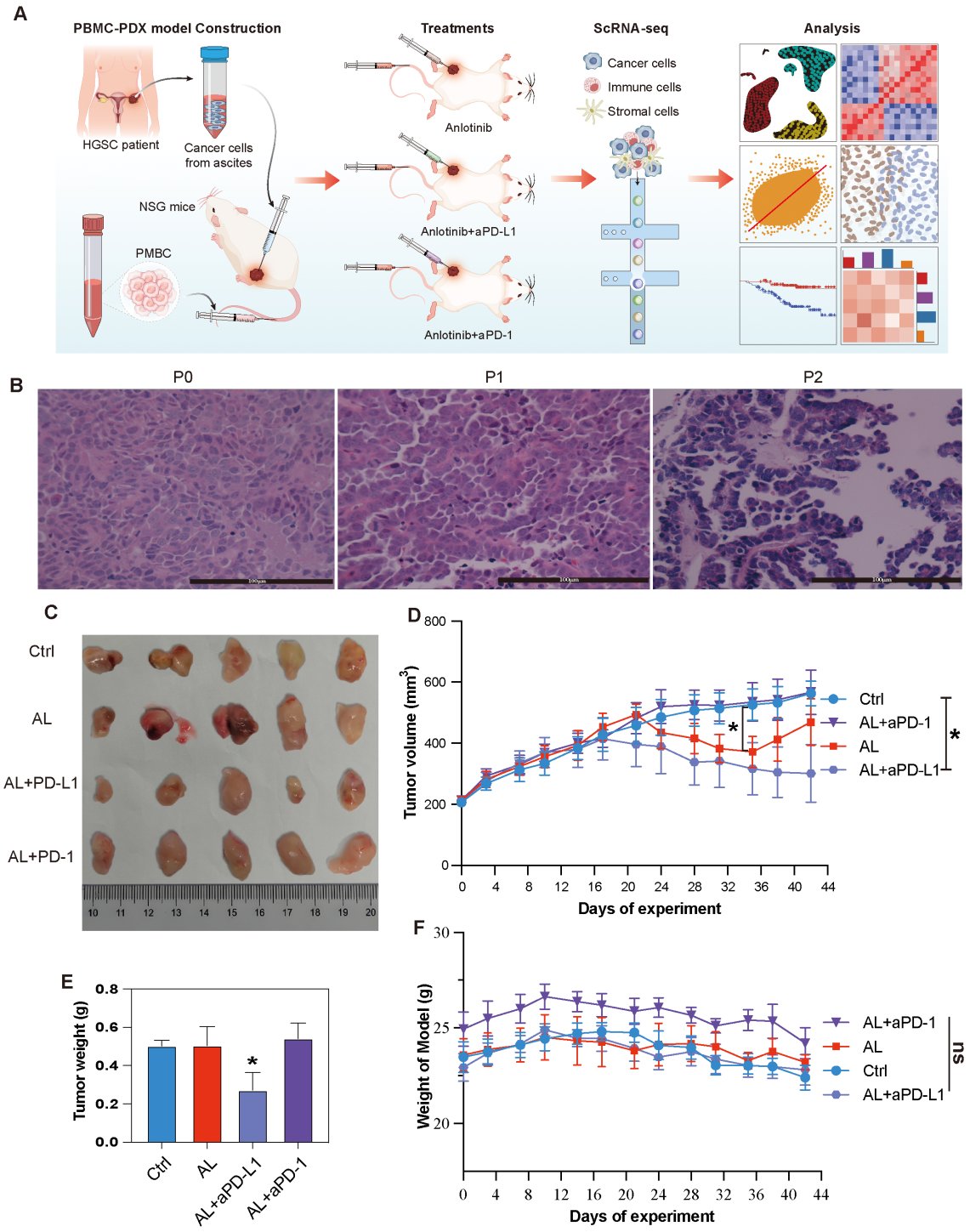

FIGURE 2
Establishment and treatment of HGSOC PBMC-PDX models. **(A)** Schematic representation of the study design and analytical workflow. **(B)** HE staining of the patient tumor (primary tumor) and the first and second passages of the PDX model. **(C)** Representative tumor tissue samples from different PBMC-PDX groups. **(D)** Changes in tumor volume over time among different groups. **(E)** Comparison of tumor weights among different groups at the end of the study. **(F)** Body weight variations of PBMC-PDX model mice among different groups. * indicates P< 0.05, ** indicates P< 0.01, *** indicates P< 0.001, and ns means no significant (applied to all subsequent figures).

Pseudotime analysis indicated that C1 cells possessed higher differentiation potential, allowing them to proliferate and develop into C2 and C3 cells, whereas C3 cells exhibited the lowest differentiation potential. Genes such as CAV2 played crucial roles in this developmental trajectory (Figure 4G, S3B). The biological differences among C1, C2, and C3 cells were governed by specific transcription factor regulons. Specifically, the E2F family of proliferative transcription factors, known to play a key role in cell

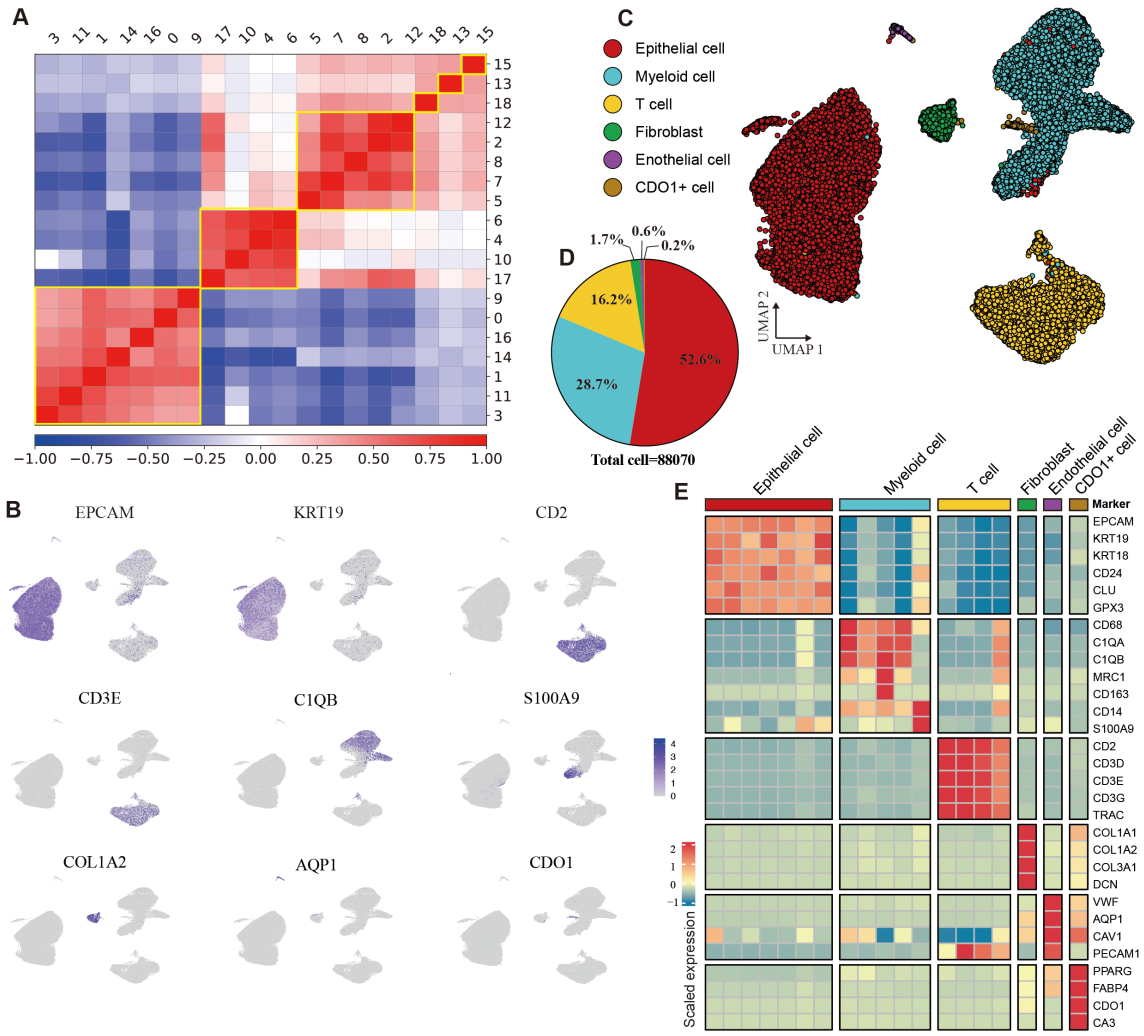

FIGURE 3
Identification of cell types in the HGSOC tumor microenvironment. **(A)** Heatmap depicting the Pearson correlation coefficients among identified cell clusters. **(B)** Uniform Manifold Approximation and Projection (UMAP) visualization of cells colored by the expression levels of marker genes. **(C)** UMAP plot illustrating the main cell types identified in the tumor microenvironment (TME). **(D)** Pie chart displaying the proportion of different cell types within the dataset. **(E)** Heatmap showing gene expression profiles across six cell types. See also Supplementary Figure S2.

cycle progression and proliferation, displayed markedly higher activity and expression in C1 cells, while ATF4 and ATF6, transcription factors related to hypoxia, were significantly upregulated in C3 cells (Supplementary Figures S3C, D).

After treatment with anlotinib, there was a reduction in the tumor cell proportion, and the combination of anlotinib with aPD-L1 further decreased this proportion. Conversely, the combination of anlotinib with aPD-1 led to an increase in tumor cell proportion (Figure 4H), corroborating previous animal experiments that demonstrated the therapeutic efficacy of anlotinib in HGSOC and the enhanced effect when combined with aPD-L1, while anlotinib + aPD-1 showed no significant antitumor activity.

Additionally, the various treatment regimens differentially influenced the composition of tumor cells. Specifically, anlotinib significantly reduced the proportion of C1 cells while increasing the proportion of C3 cells, with the combination of aPD-L1 amplifying this effect, suggesting that anlotinib+aPD-L1 exhibited enhanced effects in inhibiting tumor cell proliferation and promoting anti-angiogenesis. Notably, although the combination of anlotinib with aPD-1 did not yield significant therapeutic benefits, it did result in a reduction in the C1 cell proportion and an increase in C3 cells to a certain degree (Figure 4H).

Anlotinib treatment also led to a reduction in the expression of the E2F transcription factor family, suggesting that its antitumor effects may be mediated through both the suppression of cell proliferation and anti-angiogenesis. Surprisingly, the combination of anlotinib with aPD-L1 markedly increased the expression of ATF4 and ATF6 (Supplementary Figure S3E), suggesting its enhanced anti-angiogenesis capability.

Further analysis revealed that hypoxia can drive tumor cells to acquire enhanced invasive, metastatic, and angiogenic capabilities while simultaneously promoting tumor cell apoptosis (Figure 4I). Following treatment with anlotinib or anlotinib + aPD-L1, tumor

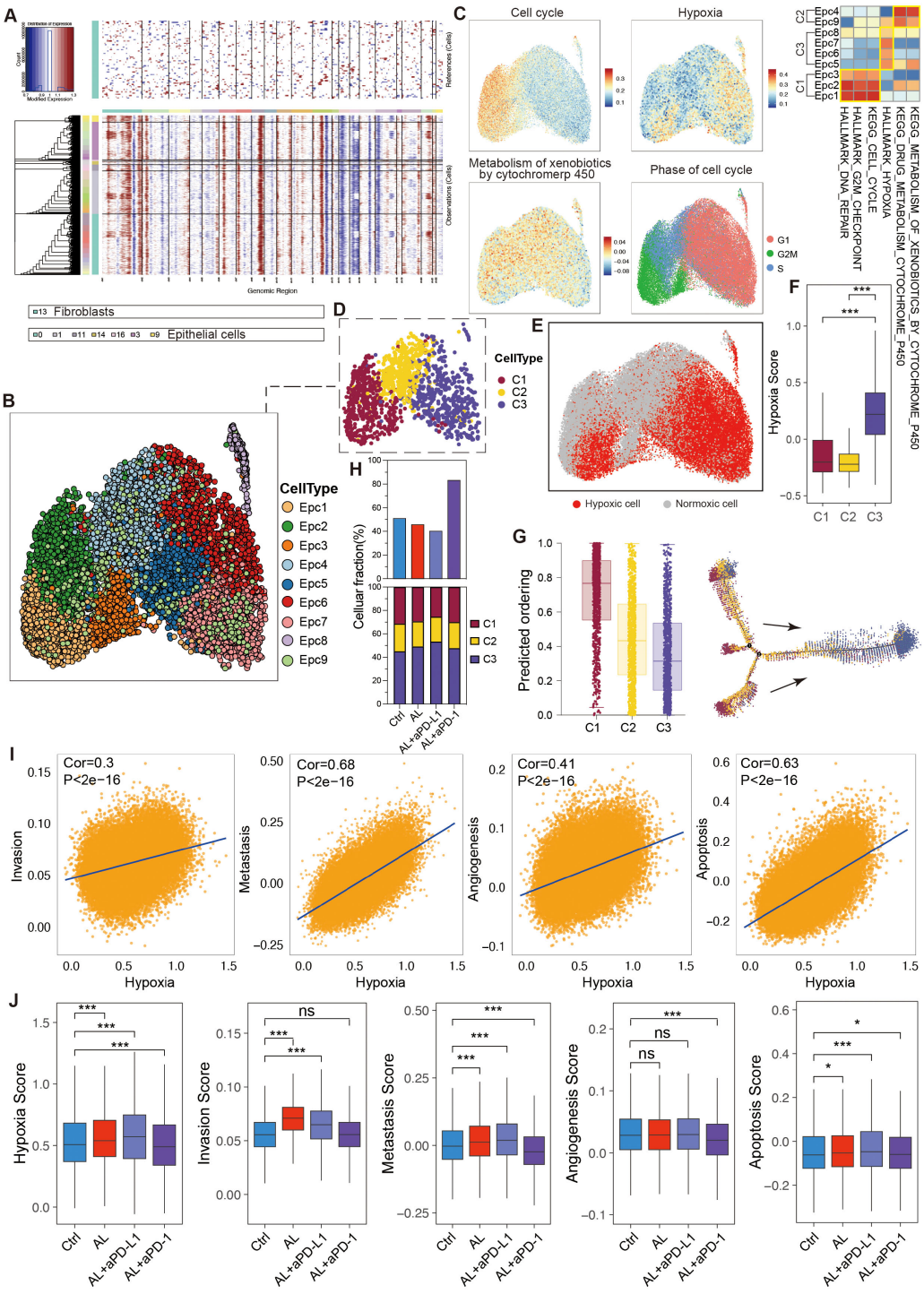

FIGURE 4
Heterogeneity and variation of epithelial cells in the HGSOC TME. **(A)** Hierarchical heatmap from InferCNV analysis displaying large-scale copy number variations (CNVs) in epithelial cells. **(B)** UMAP visualization illustrating the clustering of epithelial cell subtypes. **(C)** UMAP and corresponding heatmap depicting enriched signaling pathways across epithelial cell subtypes. **(D)** Classification of epithelial cell subtypes into three main cell types based on their biological characteristics. **(E, F)** Confirmation of the hypoxic status of epithelial cells using the CPHF algorithm. **(G)** Pseudotime trajectory analysis of epithelial cell subtypes. **(H)** Proportions of epithelial cells and their sub-types across different groups. **(I)** Analysis of the relationship between tumor cell hypoxia and invasion, metastasis, angiogenesis, and apoptosis. **(J)** Comparison of hypoxia, invasion, metastasis, angiogenesis, and apoptosis score in tumor cells following different treatments. See also Supplementary Figure S3.

cells exhibited increased hypoxia and apoptosis, accompanied by enhanced invasive potential (Figure 4J).

3.5 Combination of anlotinib and immunotherapy targets stromal cells to inhibit angiogenesis

Cancer-associated fibroblasts (CAFs) are critical components of the TME, playing pivotal roles in tumor progression and treatment response. In this study, we identified six CAF clusters (Clusters 0–6) through dimensionality reduction analysis and marker genes expression (Supplementary Figures S4A, B). These clusters were categorized as follows: inflammatory CAFs (iCAFs), mainly associated with IL6-JAK-STAT3 signaling and TNFA-signaling-via-NFKB pathways (Clusters 0 and 2); myofibroblastic CAFs (myCAFs), expressing ACTA2, ACTG2, and POSTN, primarily involved in pathways such as angiogenesis, VEGF signaling, epithelial-mesenchymal transition (EMT), and hypoxia (Cluster 4); extracellular matrix CAFs (eCAFs), linked to WNT/β-catenin signaling and MYC targets (Cluster 3); and antigen-presenting CAFs (apCAFs), which involved in antigen presentation and the interferon response immune pathway (Clusters 5 and 1) (Figures 5A–C). Through pseudotime analysis, we identified seven distinct developmental states of CAFs (Supplementary Figure S4C). eCAFs exhibited the highest differentiation potential and were primarily located at the initial stages of development, possessing the ability to differentiate into myCAFs and apCAFs under specific conditions (Figures 5D, E, Supplementary Figure S4D). iCAFs were present across nearly all developmental stages, with genes such as CD24, CCL7, and PTEN influencing these developmental trajectories (Supplementary Figure S4E, F). Interestingly, we found that hypoxia within the TME mainly impacted tumor cells, while CAFs remained largely unaffected (Figures 5F, G). This observation raises the possibility that CAFs may maintain their oxygen supply by influencing angiogenesis, highlighting their potential role in TME angiogenesis. However, further experimental evidence is required to validate this hypothesis and elucidate the underlying mechanisms.

Following treatment with anlotinib or anlotinib + aPD-1, the proportion of CAFs decreased, whereas it increased in the anlotinib + aPD-L1 group (Figure 5H, Supplementary Figure S4G). Both anlotinib and anlotinib+ aPD-L1 significantly reduced the proportion of myCAFs, with the lowest levels observed in the anlotinib +aPD-L1 group (Figure 5I). Consequently, anlotinib + aPD-L1 treatment led to the lowest angiogenic capacity in CAFs, followed by anlotinib, with no significant changes observed in the anlotinib+ aPD-1 group (Figure 5J).

Endothelial cells (ECs) were divided into four sub-types based on gene expression profiles (Figures 5K, L), displaying varying levels of differentiation and distinct functional heterogeneity. $ESM1^+$ ECs were capable of differentiating into $PAK2^+$ ECs and $RPL19^+$ ECs, eventually developing into $CD74^+$ ECs (Figure 5M, S4H). $ESM1^+$ ECs were highly enriched in angiogenesis-related pathways—such as VEGF, PI3K-AKT-mTOR, TGFβ, and coagulation signaling—endowing them with the strongest angiogenic capacity. In contrast, $CD74^+$ ECs showed the lowest enrichment in these pathways, resulting in the weakest angiogenic capacity (Supplementary Figures S4I, J). In both the anlotinib + aPD-L1 and anlotinib + aPD-1 groups, the proportion of endothelial cells decreased, particularly the $ESM1^+$ ECs, leading to the decreasing angiogenic capacity of endothelial cells (Figures 5N, O, Supplementary Figure S4K). Immunofluorescence staining showed that anlotinib and anlotinib + aPD-L1 treatment significantly reduced blood vessel numbers and made vessel structures more regular (Figure 5P).

In conclusion, anlotinib appears to inhibit angiogenesis in the TME primarily by reducing the proportion of myCAFs. The addition of aPD-L1 enhances this effect, as evidenced by a further reduction in the proportions of myCAFs and $ESM1^+$ ECs, thereby significantly limiting angiogenesis and affecting the oxygen supply to tumor cells. While CAFs seem unaffected by hypoxia in this context, the mechanisms underlying their oxygen supply and potential preferential access to vascular resources warrant further investigation.

3.6 Treatment effects on T cell subtypes: reversal of exhaustion and enhanced recruitment

To further assess the impact of anlotinib combined with aPD-L1/aPD-1 on tumor-infiltrating lymphocytes (TILs) within the TME, we conducted an in-depth analysis of T cells.

Based on specific marker expression, T cells were categorized into ten distinct subtypes, predominantly expressing either CD8A or CD4 genes, while a subset lacking CD4, CD8, and other specific markers but expressing CD3D and CD3E was defined as "T cell" (Figure 6A, Supplementary Figure S5A). Among the $CD4^+$ cells, we identified subtypes including exhausted helper T cells (Texh_CD4), regulatory T cells (Treg), naive/memory T cells (T naive/memory_CD4), activated T cells (Tactivated_CD4), and cycling T cells (Tcycling_CD4) (Figure 6B). T cycling_CD4 cells exhibited strong proliferative and differentiation potential, capable of maturing into other $CD4^+$ subtypes. In contrast, Texh_CD4 cells were at a terminal differentiation stage, exhibiting progressively exhausted functions (Supplementary Figures S5B, C). Within the $CD8^+$ T cell population, we identified three subtypes: exhausted cytotoxic T cells (Texh_CD8), naive/effector cytotoxic T cells (Tnaive/effector_CD8), and proliferating T cells (Tcycling_CD8) (Figure 6B). Among these, Tcycling_CD8 cells can differentiate into Tnaive/effector_CD8 cells. Under conditions of chronic antigen exposure, these effector cells may eventually transition into terminally exhausted Texh_CD8 cells (Supplementary Figures S5D, E). This developmental trajectory aligns with the differentiation patterns and biological roles of various T cell subtypes, with exhausted cells representing a dysfunctional state characterized by reduced effector functions and altered responsiveness (30, 31).

Strangely, PD-1 (PDCD1) expression was relatively low in Texh_CD8 cells, despite high expression of other exhaustion markers such as LAG3, TIGIT, and HAVCR2. In contrast,

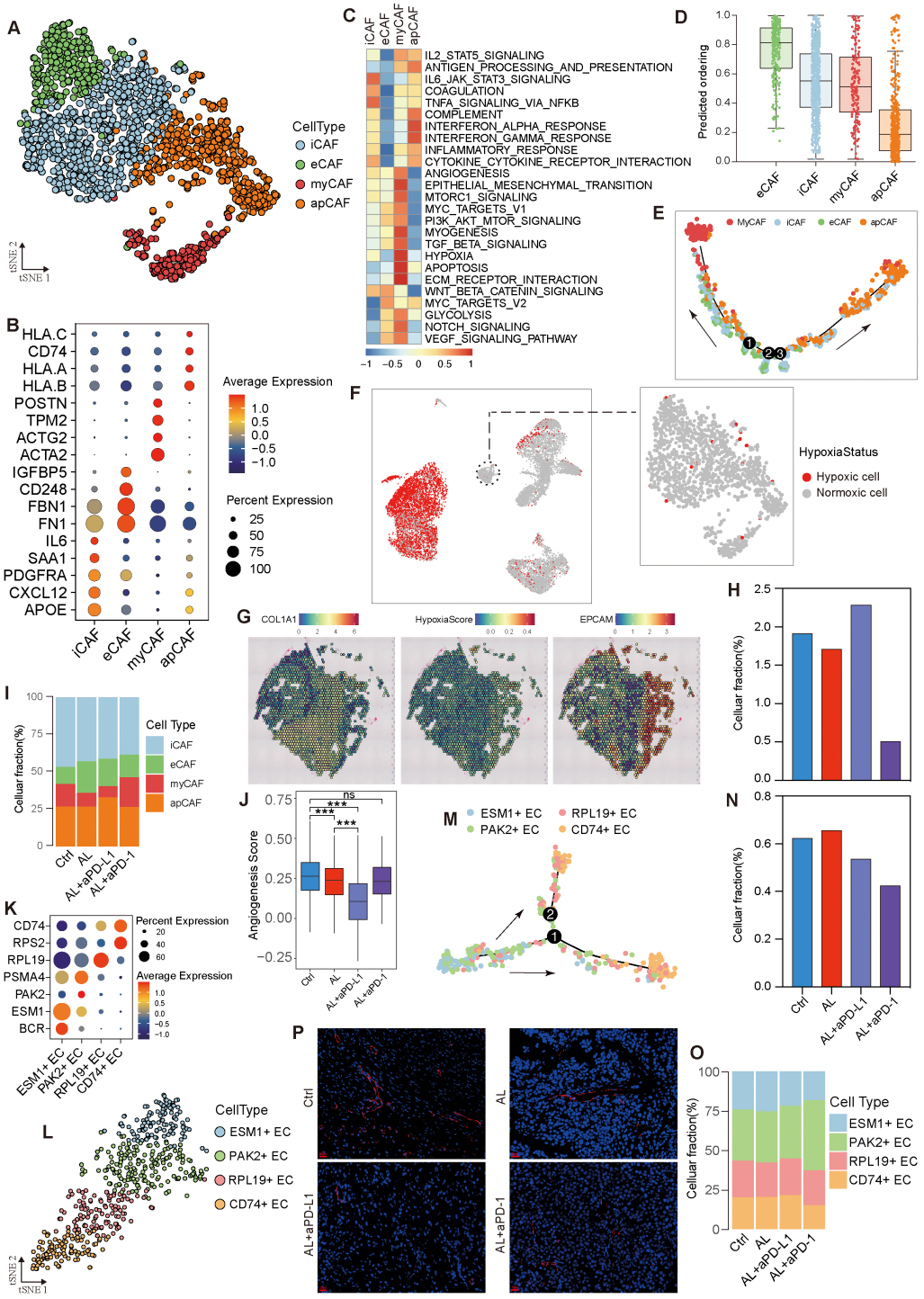

FIGURE 5
Heterogeneity and variation of stromal cells in the HGSOC TME. **(A)** t-SNE visualization of fibroblasts. **(B)** Dot plot depicting marker gene expression across fibroblast subtypes. **(C)** Enrichment analysis of fibroblast subtypes. **(D)** Analysis of differentiation levels in fibroblast subtypes. **(E)** Pseudotime trajectory analysis of epithelial subtypes. **(F)** Hypoxia status of fibroblasts. **(G)** Spatial transcriptome analysis confirming the hypoxia status of HGSOC cells and fibroblasts. **(H, I)** Variation in fibroblasts and fibroblast subtypes across different groups. **(J)** Angiogenesis capability across different groups. **(K)** Dot plot showing marker gene expression in endothelial subtypes. **(L)** t-SNE visualization of endothelial cells. **(M)** Pseudotime trajectory analysis of endothelial cell subtypes. **(N, O)** Variation in endothelial cells and endothelial cell subtypes across different groups. **(P)** Representative CD31 immunofluorescence (red) showing blood vessels in different groups. See also Supplementary Figure S4.

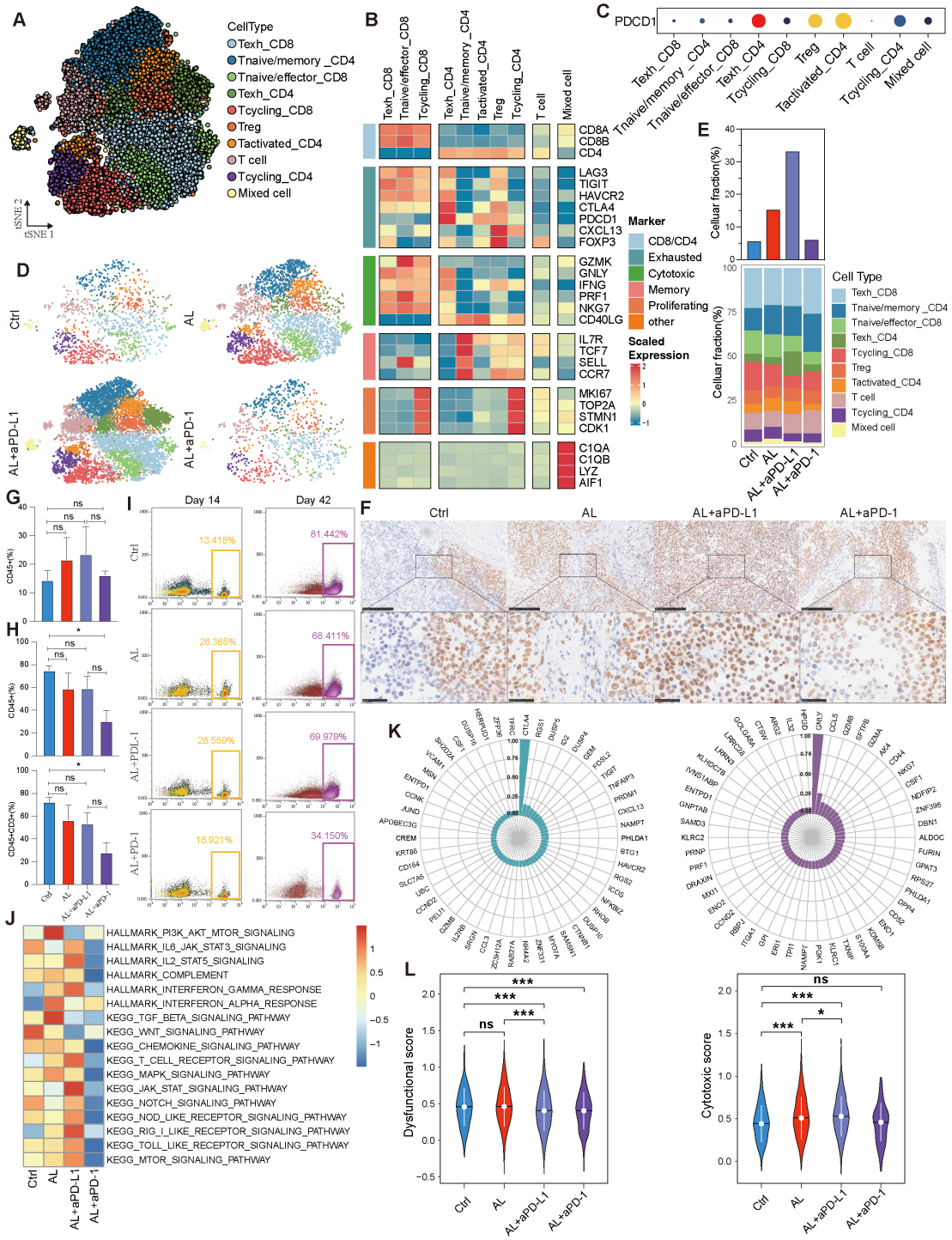

FIGURE 6
T lymphocytes variation across different treatment groups. **(A)** t-SNE visualization of T lymphocytes. **(B)** Expression levels of status-associated genes across T lymphocyte subtypes. **(C)** Expression of PDCD1 in T lymphocyte subtypes. **(D, E)** Variation in T lymphocytes and their subtypes across different groups. **(F)** Immunohistochemistry of CD8A across different groups. **(G)** Variation in CD45+ cells across different groups at day 14. **(H)** Variation in CD45+ and CD45+CD3+ cells across different groups at day 42. **(I)** Variation in CD45+ cells across different groups at days 14 and 42. **(J)** Immune-related pathway enrichment analysis across different groups. **(K)** Pearson correlation analysis of the top 50 genes related to the dysfunctional gene CTLA4 and the cytotoxic gene GNLY. **(L)** Comparison of dysfunctional and cytotoxic scores across different groups. See also Supplementary Figure S5.

Texh_CD4, Treg, and Tactivated_CD4 cells exhibited higher levels of PD-1 expression (Figures 6B, C), while HGSOC tumor cells displayed low PD-L1 (or CD274) expression level (Supplementary Figures S5F, G). Additionally, we observed an increase in T lymphocytes within the TME following treatment, with the most pronounced elevation in the anlotinib + aPD-L1 group, whereas the anlotinib + aPD-1 group demonstrated a more modest rise (Figures 6D, E). Immunohistochemistry confirmed that the anlotinib + aPD-L1 group exhibited higher levels of $CD8^+$ TILs, a factor closely associated with the efficacy of immunotherapy (Figure 6F). To investigate the cause of the differential TIL levels, we analyzed peripheral blood from the PBMC-PDX models. At the onset of treatment, all three treatment groups exhibited higher levels of $CD45^+$ immune cells compared to control group (Figures 6G, I). However, by the end of treatment, the proportions of both $CD45^+$ and $CD3^+$ cells were lower across all treatment groups than in controls (Figure 6H, I, Supplementary Figure S5H). The observed decrease in peripheral blood immune cells, coupled with the increase in TME T cells, strongly suggests T cell migration from peripheral blood to the TME, consistent with the characteristics of the PBMC-PDX model.

The efficacy of ICIs is closely related not only to the quantity of $CD8^+$ TILs but also to their functional state. We found that treatment with anlotinib or anlotinib + aPD-L1 decreased the proportion of Texh_CD8 cells, whereas the Texh_CD8 population increased in the anlotinib + aPD-1 group (Figure 6E). Furthermore, both anlotinib and anlotinib + aPD-L1 treatments significantly enhanced the inflammatory response within the TME and promoted immune activation (Figure 6J). To further validate this observation, we analyzed the top 50 genes associated with the exhaustion marker CTLA4 and the cytotoxic marker GNLY, calculating and comparing the exhaustion and cytotoxic scores of $CD8^+$ TILs (Figure 6K). The analysis revealed that both dysfunctinal and cytotoxic score increased in the anlotinib treatment group, indicating that anlotinib promotes the infiltration of $CD8^+$ T cells into the TME—including both exhausted and non-exhausted cells—but does not reverse the exhausted state of existing Texh_$CD8^+$ cells (Figure 6L). In contrast, dysfunctional score decreased and cytotoxic score increased in the anlotinib + aPD-L1 (Figure 6L), suggesting the reactivation of exhausted $CD8^+$ TILs. Additionally, following anlotinib + aPD-L1 treatment, the Texh_CD8 subtype exhibited an increase in downregulated genes, while the Tnaive/effector_CD8 subtype showed a significant increase in upregulated genes, further supporting the potential reversal of $CD8^+$ T cell exhaustion (Supplementary Figure S5I). Moreover, IF results demonstrated that the number and proportion of $CD8^+GZMB^+$ T cells were higher in the anlotinib + aPD-L1 group compared to both the control and anlotinib monotherapy groups (Supplementary Figure S6A–C).

Summarily, anlotinib increases TIL levels, establishing a foundation for improved ICI efficacy. The combination of anlotinib + aPD-L1 achieved superior therapeutic outcomes by facilitating stronger T cell recruitment and exhausted $CD8^+$ T cell reactivation.

3.7 Combination of anlotinib and immunotherapy induced modulation of myeloid cell polarization and anti-tumor activity

Myeloid cells constitute another significant component within the TME. We categorized these myeloid cells into nine distinct subtypes based on dimensionality reduction clustering and gene expression profiling (Figures 7A, B). Except for M09, all other subtypes expressed macrophage markers such as CD68, C1QB, S100A9, and AIF1, suggesting that they are tumor-associated macrophages (TAMs) (Supplementary Figure S7A). Among these, M01_SPP1 and M08_S100A9 were the most prevalent (Supplementary Figure S7B). These subtypes exhibited varying levels of differentiation. M05_CDK1, which demonstrated the highest proliferative and differentiation potential, occupied the starting point of the developmental trajectory and had the ability to differentiate into various subtypes (Figure 7C, Supplementary Figure S7C). This differentiation followed multiple developmental branches, highlighting the significant heterogeneity within the myeloid population. M08_S100A9, with the lowest differentiation potential, was positioned at the terminal stage of these trajectories (Figure 7C, Supplementary Figure S7D). Moreover, these subtypes exhibited distinct biological roles: M01 was associated with angiogenesis, M04 was primarily involved in antigen presentation, and M07, M08, and M09 were enriched in immune and inflammation-related pathways (Figure 7D).

Following treatment, the proportion of myeloid cells decreased, particularly in the anlotinib + aPD-L1 group, coupled with an increase in M01 cells. Both the anlotinib and anlotinib + aPD-1 groups saw a significant rise in the proportion of M01 cells, enhancing the angiogenic capacity of tumor-associated macrophages (TAMs). In contrast, the M01 population remained relatively stable in the anlotinib + aPD-L1 group, along with a diminished angiogenic potential (Figures 7E, F, Supplementary Figure S7E).

To further delineate the inflammatory states of myeloid cells after different treatments, we calculated M1 and M2 polarization scores using specific gene sets. The data indicated that M07, M08, and M09 exhibited higher M1 polarization scores, while M03 had the highest M2 polarization score (Figure 7G). After treatment, M1 polarization increased, with the most notable rise in the anlotinib group, whereas M2 polarization scores decreased in the anlotinib + aPD-L1 and anlotinib + aPD-1 groups (Figure 7H). These treatments also enhanced antigen-presenting capability and inhibited immune escape (Supplementary Figure S7E), indicating a promotion of pro-inflammatory and anti-tumor activity within the myeloid cells in the TME. Additionally, myeloid cells displayed more upregulated than downregulated genes after anlotinib + aPD-L1 treatment, with the M01 subtype showing the most prominent changes, suggesting that the treatment may regulate myeloid cells to promote pro-inflammatory and anti-tumor effects (Supplementary Figure S7F).

Additionally, these therapies induced significant changes in transcription factor regulon activity. In the anlotinib + aPD-L1 group, the activity of regulons such as EP300, NR3C1, BCLAF1, and FOSB, which participate in DNA damage response, immune

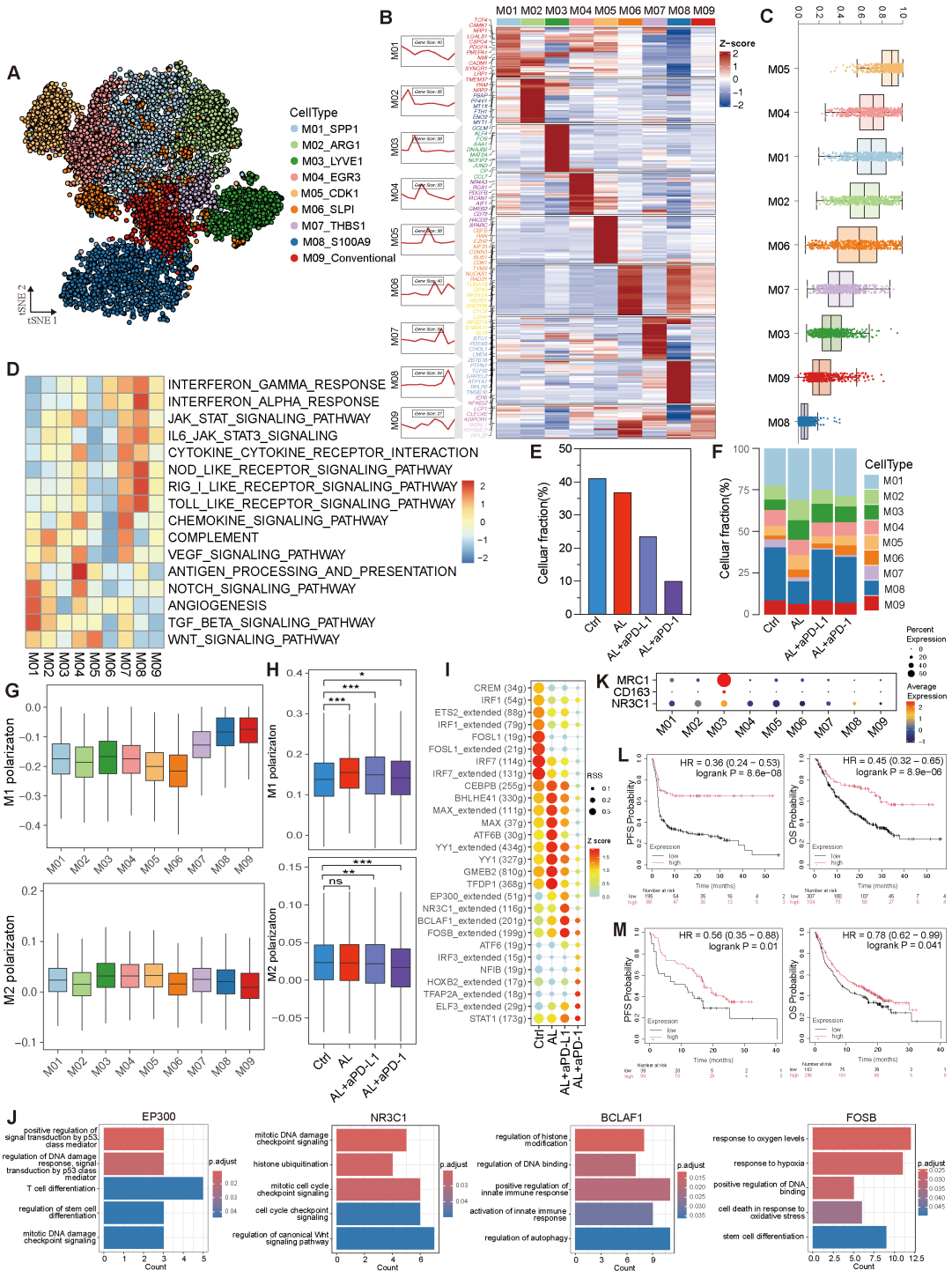

FIGURE 7
Variation of myeloid cells after treatments in HGSOC TME. **(A)** t-SNE visualization of myeloid cell subtypes. **(B)** Expression profile of myeloid cell subtypes. **(C)** Analysis of differentiation levels in myeloid cell sub-types. **(D)** Pathway enrichment analysis of myeloid cell subtypes. **(E, F)** Variation in myeloid cells and myeloid cell subtypes across different groups. **(G)** M1 and M2 polarization of myeloid cell subtypes. **(H)** Comparison of M1 and M2 polarization of myeloid cells across different groups. **(I)** Activity and regulon specificity scores of transcription factors across different groups. **(J)** GO BP enrichment of transcription factor in the anlotinib + aPD-L1 group. **(K)** Co-expression of NR3C1 with CD163 and MRC1. **(L, M)** Kaplan-Meier plots showing the correlation between NR3C1 expression and progression-free survival (PFS) and overall survival (OS) in cancer patients treated with aPD-1 **(L)** and aPD-L1 **(M)**, with data sourced from the Kaplan-Meier Plotter database. See also Supplementary Figure S7.

regulation, stress adaptation mechanisms, and response to hypoxia, were notably elevated (Figures 7I, J). Interestingly, NR3C1 was co-expressed with MRC1 and CD163 in M03 cells (Figure 7K), suggesting that NR3C1 may play a role in inhibiting immune-mediated tumor cell killing. We further analyzed NR3C1 in pan-cancer patients receiving aPD-L1/aPD-1 therapy and found that NR3C1 expression was positively correlated with both PFS and OS (Figures 7L, M). This discrepancy may stem from a shift in NR3C1's role after immunotherapy.

In conclusion, anlotinib treatment enhances the tumor-killing ability of immune cells and suppresses immune escape via regulating myeloid cells, while the combination of anlotinib with aPD-L1 or aPD-1 further amplifies these anti-tumor effects.

3.8 Alterations in cell-to-cell communication networks after anlotinib-based treatments

To investigate alterations in intercellular communication signals following treatment, we conducted a comprehensive cell-to-cell communication analysis. Compared to the control group, treatment with anlotinib led to an increased number of cell communications; however, the intensity of these interactions was reduced. This reduction may be attributed to decreased activity in certain ligand–receptor pairs (Supplementary Figure S8A). Notably, anlotinib promoted increased communication between CAFs and tumor cells, while interactions between $CD8^+$ T cells and other cell types diminished (Figure 8A). In contrast, after treatment with anlotinib + aPD-L1, although the overall number and intensity of cell communications decreased further, communication involving $CD8^+$ T cells increased significantly, which didn't happen when treated with anlotinib + aPD-1 (Figure 8A).

We further identified that the APP–CD74 ligand–receptor pair (LRP) primarily mediated communication between tumor cells and immune cells. Additionally, MDK–NCL/SDC2/SDC4 interactions played a central role in CAF interactions with other cells, while CD99–CD99 interactions were widely involved in communications between immune cells and tumor cells (Figure 8B, Supplementary Figure S8B). These LRPs form the core components of the APP, CD99, and MK signaling pathways, respectively (Figures 8C, E, Supplementary Figure S8C).

Following treatment, the number of MK signaling interactions remained relatively unchanged. However, communication through the APP signaling pathway was significantly reduced (Supplementary Figure S8D). In the APP pathway, tumor cells primarily acted as signal senders, with immune cells (T cells and myeloid cells) serving as primary receivers, and CAFs also playing a vital role (Figure 8C). After treatment with anlotinib, signal output from myeloid cells decreased, and CAFs transitioned from being signal receivers to signal senders. Following treatment with anlotinib combined with aPD-L1 or aPD-1, APP signaling was further diminished, while interactions between $CD8^+$ T cells and tumor cells increased (Figure 8D). Conversely, the CD99 signaling pathway was significantly upregulated after treatment (Supplementary Figure S8D). Although CAFs contributed to this pathway, their involvement in communications was relatively minor (Figure 8E). In the control group, CD99 signaling predominantly occurred between $CD4^+$ and $CD8^+$ T cells and tumor cells. After anlotinib treatment, interactions among M01–M07 myeloid cells, $CD4^+$ and $CD8^+$ T cells, and C1 and C2 tumor cells increased notably.

This trend persisted in the anlotinib + aPD-L1 group. However, the changes in CD99 signaling were less pronounced in the anlotinib+ aPD-1 group (Figure 8F). These results suggest that anlotinib and its combination with aPD-L1 may enhance CD99 signaling between myeloid cells, T cells, and tumor cells, thereby improving immune-mediated tumor destruction and leading to better therapeutic outcomes. The observed changes in APP, CD74, and CD99 expression across different treatment groups further support these findings (Figure 8G).

4 Discussion

In this study, we systematically evaluated the potential efficacy of the anlotinib, and its combination with aPD-1/aPD-L1 in the treatment of HGSOC. Through clinical patient data, HGSOC derived PBMC-PDX models, and scRNA analysis, we found that anlotinib monotherapy exhibited anti-tumor effects, while the combination with aPD-L1 significantly enhanced anti-angiogenic effects, improved T-cell infiltration, and effectively reversed immune evasion. These findings are visually summarized in Supplementary Figure S9, which illustrates the dynamic changes in key cell populations within the TME. This combination strategy offers a new approach for HGSOC treatment, especially in situations where the current immune therapies show limited efficacy, and thus displays broad clinical potential.

From real-world data that anlotinib monotherapy achieved a 71.43% DCR and a median PFS of 6.5 months in patients with recurrent or refractory HGSOC. In particular, the combination with aPD-L1/aPD-1 achieved a DCR of 100%, with a prolonged PFS of 8.7 months. The combination of anlotinib and aPD-L1/aPD-1 has demonstrated synergistic antitumor effects across various cancer types (28, 32), even in other refractory cancers and triple-negative breast cancer, which is also classified as "cold tumor" (33, 34). While limited studies have reported on the efficacy and safety of this combination therapy in HGSOC, conclusive results and in-depth analyses remain lacking (35), and several clinical trials are still ongoing (36). These has contributed to the fact that anlotinib combination with aPD-L1/aPD-1 have not yet been approved for use in HGSOC.

We further validated the effects of the treatment by constructing PBMC-PDX models. The results showed that the combination of anlotinib and aPD-L1 significantly delayed tumor growth, exhibiting more pronounced anti-tumor effects compared to monotherapy. ScRNA also confirmed that anlotinib + aPD-L1 further reduced the proportion of tumor cells compared to anlotinib alone.

10.3389/fimmu.2025.1539616

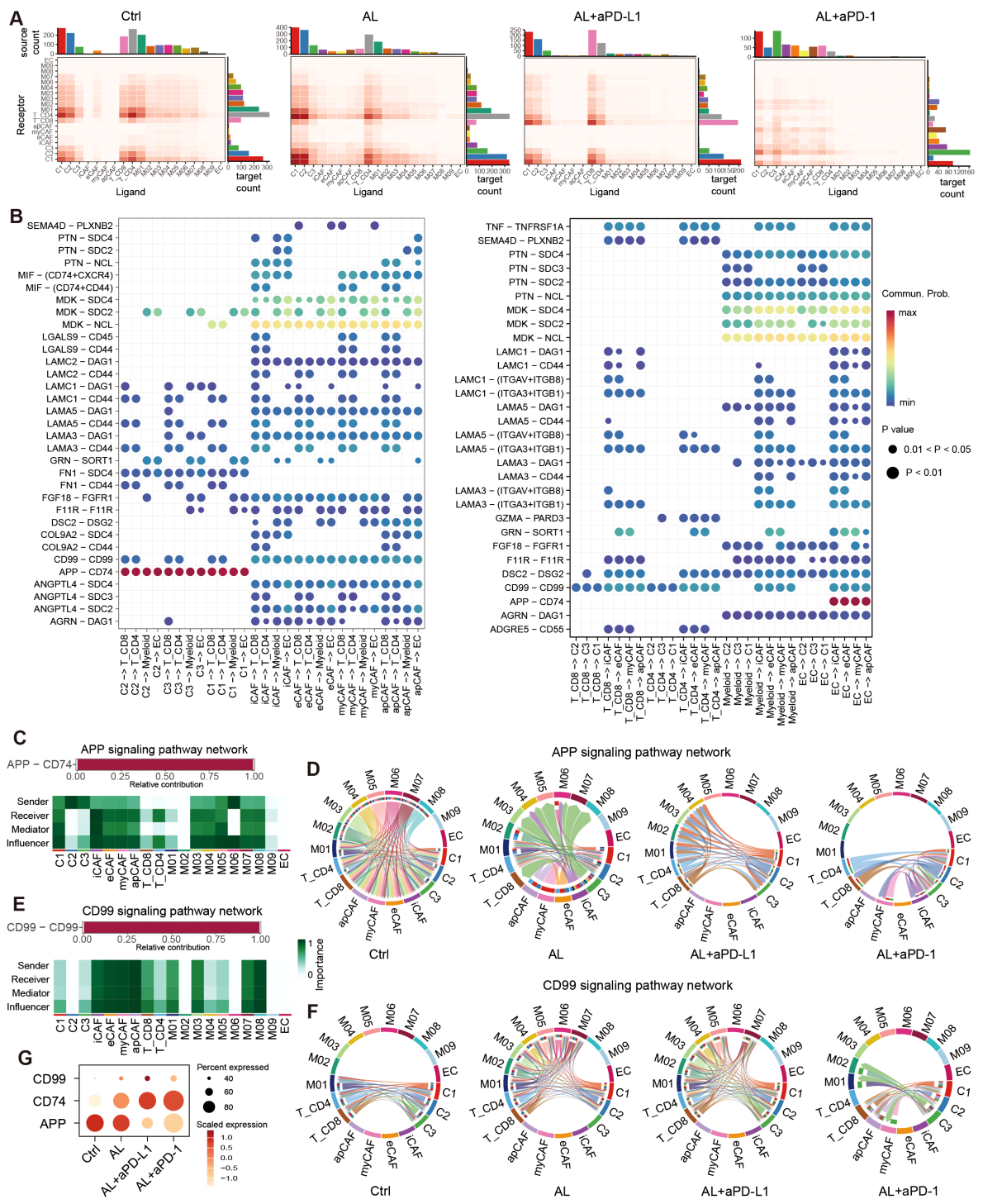

FIGURE 8
Cell-cell communication in the HGSOC TME. **(A)** Heatmap showing the number of total potential ligand–receptor pairs between different cell types in each group obtained with CellChat. The bar plot represents the sum of a column or row. **(B)** Dot plot showing the main significant ligand-receptor pairs between tumor cells, fibroblast and T cells, myeloid cells, endothelial cells. The dot color and size represent the calculated communication probability and p-values. p-values are computed from a one-sided permutation test. **(C)** The L-R paired APP signaling include, and the relative importance of cell types in APP signaling. **(D)** Chord plot showing the variation of APP signaling in different groups. **(E)** The L-R paired CD99 signaling include, and the relative importance of cell types in CD99 signaling. **(F)** Chord plot showing the variation of CD99 signaling in different groups. **(F)** Dot plot showing the expression of APP, CD74, CD99. See also Supplementary Figure S8.

Regarding the mechanisms, anlotinib treatment increased hypoxia and apoptosis in tumor tissue while reducing the proportion of proliferating cells. Additionally, it decreased the expression and activity of the proliferation-associated E2F transcription factor, which is primarily linked to cell cycle regulation and tumor proliferation. These findings suggest that anlotinib inhibits both tumor cell proliferation and angiogenesis, aligning with observations from previous studies (9, 37). Interestingly, we found that aPD-L1 enhanced anlotinib's pro-apoptotic effects and further increased hypoxia levels, as indicated by elevated expression and activity of ATF4 and ATF6, transcription factors associated with hypoxic conditions (38). This intensified hypoxia may result from increased immune cell infiltration and activation, leading to greater oxygen consumption or immune-mediated vascular disruption, thereby reducing oxygen supply (39, 40).

In the present study, we found that anlotinib's inhibition of angiogenesis was primarily associated with myCAFs, a subtype originally identified in pancreatic ductal adenocarcinoma but less studied in HGSOC (41–44). The reduction in myCAF populations following anlotinib or anlotinib + aPD-L1 treatment significantly impaired HGSOC's angiogenic capacity, leading to pronounced hypoxia in tumor cells. Interestingly, while tumor cells experienced hypoxia after treatment, CAFs did not, suggesting that CAFs may maintain their oxygen supply by modulating blood vessel formation, possibly through localized angiogenesis or spatial proximity to functional vasculature.

Endothelial cells (ECs) are another major target of anlotinib (45). Specifically, we identified $ESM1^+$ ECs as the primary endothelial cell population driving angiogenesis in the HGSOC TME, with their functional decline closely associated with reduced angiogenic capacity after treatment. Conversely, the proportion of $CD74^+$ ECs increased following combination therapy, potentially indicating a shift in endothelial cell states that further inhibits angiogenesis.

In addition to its effects on tumor and stromal cells, anlotinib also improved the immunosuppressive microenvironment by significantly increasing T cell and $CD8^+$ T cell infiltration, likely achieved through vascular normalization. Anlotinib's anti-angiogenic properties reduce abnormal tumor vasculature and promote vascular normalization, thereby alleviating high interstitial fluid pressure and increasing vascular permeability. These changes facilitate the migration of immune cells, particularly cytotoxic $CD8^+$ T cells, into the TME, as similarly reported in studies on lung cancer and hepatocellular carcinoma (46–48).

However, anlotinib monotherapy was unable to reverse the exhausted state of $CD8^+$ T cells. In contrast, anlotinib combined with aPD-L1 not only enhanced $CD8^+$ T cell infiltration but also improved the functional state of these exhausted cells, suggesting that this combination therapy enhances both the quantity and cytotoxic activity of $CD8^+$ T cells, making them more effective at eliminating tumor cells. This indicates that while vascular normalization facilitates immune cell infiltration into the tumor microenvironment, the reactivation of exhausted T cells primarily depends on immune checkpoint blockade, such as aPD-L1, rather than on vascular normalization alone. Furthermore, VEGF/VEGFR-targeted therapy not only reduces abnormal vasculature but also alleviates the immunosuppressive effects of VEGF, creating a microenvironment conducive to immune cell activity, while PD-L1 blockade directly restores T cell effector functions (49, 50). These complementary mechanisms underlie the synergistic effect of the combination therapy.

Conversely, anlotinib combined with aPD-1 did not produce a similar effect on T cells. Our analysis showed that PD-1 expression was primarily on Tregs and low on $CD8^+$ T cells, suggesting that aPD-1 therapy may preferentially target PD-1-expressing Tregs. This interaction could enhance the suppressive activity of Tregs, potentially contributing to the limited efficacy observed with anlotinib and aPD-1, thus explaining why the anlotinib and aPD-L1 combination demonstrated superior outcomes (51–53).

Recent studies align with our findings, supporting the efficacy of combined anti-angiogenic and immune checkpoint therapies. For instance, the Phase 3 IMpower150 trial demonstrated that atezolizumab combined with bevacizumab/chemotherapy achieved strong anticancer activity and manageable side effects in NSCLC (54). Similarly, the combination of anti-angiogenic therapy and immunotherapy showed superior tumor reduction in renal cell carcinoma and hepatocellular carcinoma (47, 55). Sequential therapy was also explored in NSCLC, where initiating anti-angiogenic therapy after immune checkpoint blockade showed better outcomes than concurrent or reverse sequencing (56). Mechanistically, anti-angiogenic therapy normalizes tumor vasculature, improving cytotoxic TILs and reducing interstitial fluid pressure. This normalization enhances immune cell access to the TME, creating conditions favorable for ICIs to reactivate exhausted T cells and boost antitumor immunity (57–59). Additionally, anti-angiogenic therapies downregulate immunosuppressive factors and reverse endothelial cell deactivation, further augmenting the effects of ICIs (60).

Myeloid cells also exhibited substantial changes post-treatment. Anlotinib, alone or in combination with aPD-L1/aPD-1, significantly increased the M1 polarization score while reducing the M2 polarization score when combined with aPD-L1/aPD-1. Additionally, anlotinib or its combinations enhanced myeloid cells' antigen-presenting capability and inhibited immune escape. These immunomodulatory effects on both T cells and myeloid cells indicate that anlotinib can reshape the immunosuppressive TME in HGSOC, potentially improving responsiveness to aPD-L1. Study in neuroblastoma demonstrated that anlotinib could reprogram an immunosuppressive TME into an immunostimulatory environment, curbing tumor growth and preventing systemic immunosuppression, while in lung cancer, it was shown to inhibit M2 polarization of TAMs through the AKT/mTORC1 and Pparδ pathways (61, 62).

Further analysis suggested that the effects of anlotinib, both alone and combined with aPD-L1, on the immune microenvironment may be mediated through inhibition of APP signaling and enhancement of CD99 signaling. APP signaling transmits inhibitory signals that suppress the phagocytic activity

of tumor-associated macrophages (TAMs) (63) and reduces immune activity within the TME, allowing tumor cells to evade immune surveillance and promote tumor progression (64, 65). In contrast, CD99 signaling may enhance T cell cytotoxicity and induce tumor cell apoptosis (66, 67). Given the limited studies on APP-CD74 and CD99-CD99 signaling in HGSOC, further research is required to clarify their specific roles in the TME.

In conclusion, this study demonstrated the therapeutic potential of anlotinib combined with aPD-L1/aPD-1 in HGSOC. Anlotinib combination with aPD-L1 effectively inhibits angiogenesis, suppresses tumor cell proliferation, and transforms cold tumors into hot tumors by enhancing TIL infiltration, reactivates exhausted TILs, and fosters a tumor-killing environment, showing strong synergistic effects compare to anlotinib monotherapy. To our knowledge, this is the first study to utilize scRNA-seq to evaluate the efficacy and underlying mechanisms of anlotinib combined with aPD-L1/aPD-1 therapy in HGSOC. These findings lay a promising foundation for advancing precision treatment strategies in refractory HGSOC.

Although neither anlotinib nor aPD-L1 is currently approved for HGSOC, the manageable toxicity and preclinical efficacy observed suggest that this therapy could be safely implemented in clinical trials, which has been implemented in other solid tumors recently (48, 68–70). Based on our findings and relevant reports, potential biomarkers for patient stratification include PD-L1 expression, TMB levels, the CD8+ TIL/Treg ratio, the M1/M2 myeloid cell ratio, and tertiary lymphoid structures, all of which reflect an immunostimulatory TME (68). Future clinical trials could incorporate these biomarkers to identify subgroups most likely to benefit, to advance precision treatments for refractory HGSOC.

While this study provides promising insights, several limitations remain.

First, the small sample size (n=36) limits the generalizability of the findings, large-scale clinical trials are essential for further validation. We will continue to collect relevant cases to increase the reliability of the results. Second, this study utilized a single PDX model to evaluate the effects of anlotinib combined with immunotherapy, which limits the generalizability of the findings. Additionally, the small sample size may introduce statistical bias, and the lack of functional immune assays, such as cytotoxicity tests or cytokine secretion analysis, limits the mechanistic understanding of immune responses. Furthermore, the absence of longitudinal measurements precludes capturing the dynamic changes during treatment. To address these limitations, we are constructing additional PDX models from diverse HGSOC patient samples, incorporating functional assays like cytotoxicity tests and cytokine profiling, and designing longitudinal studies to monitor treatment effects over time. These efforts aim to enhance the robustness and translational potential of our findings.

Additionally, although we demonstrated the therapeutic efficacy of anlotinib combined with aPD-L1, the combination of anlotinib with aPD-1 showed comparatively poorer outcomes. This discrepancy between the effects of AL + aPD-1 and AL + aPD-L1 prompted us to further investigate the underlying mechanisms. Our findings revealed several potential explanations: (1) PD-1 (PDCD1) expression was predominantly localized to Tregs and $CD4^+$ T cells, and the use of aPD-1 may have inadvertently enhanced Treg-mediated immunosuppression, contributing to immune evasion. (2) AL + aPD-1 was less effective than AL + aPD-L1 in promoting M1 polarization of myeloid cells, though the precise mechanism remains unclear. (3) AL + aPD-1 demonstrated a reduced ability to recruit T cells into the TME compared to AL + aPD-L1, potentially due to broader immunoregulatory effects of aPD-L1 on TME composition. These findings suggest that PD-1 and PD-L1 inhibitors might exert distinct regulatory effects on immune cells within the TME, resulting in differential therapeutic outcomes.

Several important questions remain to be addressed: Is this unique pattern of PD-1 (PDCD1) expression (predominantly in Tregs and $CD4^+$ T cells) a common feature in HGSOC? Could this expression pattern underlie the poor response of HGSOC to immune checkpoint inhibitors? Addressing these questions in future studies will help to clarify the role of PD-1 and PD-L1 pathways in modulating the immune microenvironment of HGSOC and guide the development of more effective therapeutic strategies.

Moreover, addressing resistance remains another critical challenge for future investigations. Tumors may adapt to anti-angiogenic therapy by upregulating alternative pro-angiogenic pathways or through ECM deposition, which hinders immune cell infiltration and drug delivery (71, 72). For ICIs, resistance mechanisms include T cell exhaustion, alternative immune checkpoints, or immunosuppressive activity from Tregs, MDSCs, and TAMs (73). Overcoming these challenges may require combining therapies targeting compensatory angiogenic pathways, hypoxia-related factors, or sequential immune checkpoint blockades. Additionally, given that platinum-based chemotherapy remains the standard treatment for HGSOC and most anlotinib use in this study occurred after ≥3 lines of prior treatment, future research will focus on evaluating concurrent or sequential combinations of chemotherapy, anti-angiogenic therapy, and immunotherapy to optimize strategies and improve patient outcomes.

Data availability statement

The scRNA-seq data presented in the study are deposited in the Genome Sequence Archive repository (https://ngdc.cncb.ac.cn/gsa), accession number CRA024166.

Ethics statement

The use of human samples was approved by the Ethics Committee of Qingdao University Affiliated Hospital and after obtaining informed consent. All experimental procedures adhered to the guidelines of the Institutional Animal Care and Use

Committee (IACUC) and received prior approval. Written informed consent was obtained from the patient for the publication of any potentially identifiable images or data included in this article.

Author contributions

HWL: Writing – original draft. HL: Writing – original draft. HH: Writing – original draft. CZ: Writing – original draft. JZ: Writing – original draft. NZ: Writing – review & editing. XZ: Writing – review & editing.

Funding

The author(s) declare that financial support was received for the research and/or publication of this article. This work was supported by the Shandong Provincial Natural Science Foundation (ZR2022MH048 to Xiaochun Zhang), the National Natural Science Foundation of China (82272693 to Na Zhou), Qilu Health Leading Talents Training Project (Na Zhou), and the Wu Jieping Medical Foundation (320.6750.2022-22-62 to Na Zhou).

Acknowledgments

We thank the reviewers and editors for their valuable comments.

Conflict of interest

The authors declare that the research was conducted in the absence of any commercial or financial relationships that could be construed as a potential conflict of interest.

Generative AI statement

The author(s) declare that no Generative AI was used in the creation of this manuscript.

Publisher's note

All claims expressed in this article are solely those of the authors and do not necessarily represent those of their affiliated organizations, or those of the publisher, the editors and the reviewers. Any product that may be evaluated in this article, or claim that may be made by its manufacturer, is not guaranteed or endorsed by the publisher.

Supplementary material

The Supplementary Material for this article can be found online at: https://www.frontiersin.org/articles/10.3389/fimmu.2025.1539616/full#supplementary-material

References

1. Sideris M, Menon U, Manchanda R. Screening and prevention of ovarian cancer. *Med J Aust*. (2024) 220:264–74. doi: 10.5694/mja2.52227

2. Sung H, Ferlay J, Siegel RL, Laversanne M, Soerjomataram I, Jemal A, et al. Global cancer statistics 2020: GLOBOCAN estimates of incidence and mortality worldwide for 36 cancers in 185 countries. *CA Cancer J Clin*. (2021) 71:209–49. doi: 10.3322/caac.21660

3. Ghisoni E, Imbimbo M, Zimmermann S, Valabrega G. Ovarian cancer immunotherapy: turning up the heat. *Int J Mol Sci*. (2019) 20:2927. doi: 10.3390/ijms20122927

4. Ghoneum A, Almousa S, Warren B, Abdulfattah AY, Shu J, Abouelfadl H, et al. Exploring the clinical value of tumor microenvironment in platinum-resistant ovarian cancer. *Semin Cancer Biol*. (2021) 77:83–98. doi: 10.1016/j.semcancer.2020.12.024

5. Shen G, Zheng F, Ren D, Du F, Dong Q, Wang Z, et al. Anlotinib: a novel multi-targeting tyrosine kinase inhibitor in clinical development. *J Hematol Oncol*. (2018) 11:120. doi: 10.1186/s13045-018-0664-7

6. Han B, Li K, Wang Q, Zhang L, Shi J, Wang Z, et al. Effect of anlotinib as a third-line or further treatment on overall survival of patients with advanced non-small cell lung cancer: the ALTER 0303 phase 3 randomized clinical trial. *JAMA Oncol*. (2018) 4:1569–75. doi: 10.1001/jamaoncol.2018.3039

7. Li D, Chi Y, Chen X, Ge M, Zhang Y, Guo Z, et al. Anlotinib in locally advanced or metastatic medullary thyroid carcinoma: A randomized, double-blind phase IIB trial. *Clin Cancer Res*. (2021) 27:3567–75. doi: 10.1158/1078-0432.CCR-20-2950

8. Xu B, Pan Q, Pan H, Li H, Li X, Chen J, et al. Anlotinib as a maintenance treatment for advanced soft tissue sarcoma after first-line chemotherapy (ALTER-S006): a multicentre, open-label, single-arm, phase 2 trial. *EClinicalMedicine*. (2023) 64:102240. doi: 10.1016/j.eclinm.2023.102240

9. Ji Y, Li X, Qi Y, Zhao J, Zhang W, Qu P. Anlotinib exerts inhibitory effects against cisplatin-resistant ovarian cancer *in vitro* and *in vivo*. *Molecules*. (2022) 27:8873. doi: 10.3390/molecules27248873

10. Shen W, Jing C, Tian W, Zhang W, Ren Y, Shan B, et al. Anlotinib in patients with recurrent platinum resistant/refractory ovarian cancer: a prospective, single arm, phase II study. *Int J Gynecol Cancer*. (2023) 33:1764–70. doi: 10.1136/ijgc-2023-004777

11. Liu G, Feng Y, Li J, Deng T, Yin A, Yan L, et al. A novel combination of niraparib and anlotinib in platinum-resistant ovarian cancer: Efficacy and safety results from the phase II, multi-center ANNIE study. *EClinicalMedicine*. (2022) 54:101767. doi: 10.1016/j.eclinm.2022.101767

12. Huang S, Sheng G, Lv Q, Li Y, Meng Q, Gao X, et al. Efficacy and safety of combined anlotinib-oral etoposide treatment for patients with platinum-resistant ovarian cancer. *J Gynecol Oncol*. (2024) 35:e100. doi: 10.3802/jgo.2024.35.e100

13. Clarke ZA, Andrews TS, Atif J, Pouyabahar D, Innes BT, MacParland SA, et al. Tutorial: guidelines for annotating single-cell transcriptomic maps using automated and manual methods. *Nat Protoc*. (2021) 16(6):2749–64. doi: 10.1038/s41596-021-00534-0

14. Hao Y, Hao S, Andersen-Nissen E, Mauck WM 3rd, Zheng S, Butler A, et al. Integrated analysis of multimodal single-cell data. *Cell*. (2021) 184:3573–3587.e29. doi: 10.1016/j.cell.2021.04.048

15. Wu T, Hu E, Xu S, Chen M, Guo P, Dai Z, et al. clusterProfiler 4.0: A universal enrichment tool for interpreting omics data. *Innovation (Camb)*. (2021) 2:100141. doi: 10.1016/j.xinn.2021.100141

16. Hänzelmann S, Castelo R, Guinney J. GSVA: gene set variation analysis for microarray and RNA-seq data. *BMC Bioinf*. (2013) 14:7. doi: 10.1186/1471-2105-14-7

17. Liberzon A, Birger C, Thorvaldsdóttir H, Ghandi M, Mesirov JP, Tamayo P. The Molecular Signatures Database (MSigDB) hallmark gene set collection. *Cell Syst*. (2015) 1:417–25. doi: 10.1016/j.cels.2015.12.004

18. Aibar S, González-Blas CB, Moerman T, Huynh-Thu VA, Imrichova H, Hulselmans G, et al. SCENIC: single-cell regulatory network inference and clustering. *Nat Methods*. (2017) 14:1083–6. doi: 10.1038/nmeth.4463

19. Jin S, Guerrero-Juarez CF, Zhang L, Chang I, Ramos R, Kuan CH, et al. Inference and analysis of cell-cell communication using CellChat. *Nat Commun*. (2021) 12:1088. doi: 10.1038/s41467-021-21246-9

20. Bray NL, Pimentel H, Melsted P, Pachter L. Near-optimal probabilistic RNA-seq quantification. *Nat Biotechnol*. (2016) 34:525–7. doi: 10.1038/nbt.3519

21. Gulati GS, Sikandar SS, Wesche DJ, Manjunath A, Bharadwaj A, Berger MJ, et al. Single-cell transcriptional diversity is a hallmark of developmental potential. *Science*. (2020) 367:405–11. doi: 10.1126/science.aax0249

22. Zhang Y, Zhang B, Lv C, Zhang N, Xing K, Wang Z, et al. Single-cell RNA sequencing identifies critical transcription factors of tumor cell invasion induced by hypoxia microenvironment in glioblastoma. *Theranostics*. (2023) 13:3744–60. doi: 10.7150/thno.81407

23. Denisenko E, de Kock L, Tan A, Beasley AB, Beilin M, Jones ME, et al. Spatial transcriptomics reveals discrete tumour microenvironments and autocrine loops within ovarian cancer subclones. *Nat Commun*. (2024) 15:2860. doi: 10.1038/s41467-024-47271-y

24. Győrffy B. Integrated analysis of public datasets for the discovery and validation of survival-associated genes in solid tumors. *Innovation (Camb)*. (2024) 5:100625. doi: 10.1016/j.xinn.2024.100625

25. Jovanović L, Janković R, Ćirković A, Jović M, Janjić T, Djuričić S, et al. PD-L1 expression in different segments and histological types of ovarian cancer according to lymphocytic infiltrate. *Medicina (Kaunas)*. (2021) 57:1309. doi: 10.3390/medicina57121309

26. Saleh A, Perets R. Mutated p53 in HGSC-from a common mutation to a target for therapy. *Cancers (Basel)*. (2021) 13:3465. doi: 10.3390/cancers13143465

27. Shao L, Wang W, Song Z, Zhang Y. The efficacy and safety of anlotinib treatment for advanced lung cancer. *Onco Targets Ther*. (2019) 12:6549–54. doi: 10.2147/OTT.S205674

28. Wang P, Fang X, Yin T, Tian H, Yu J, Teng F. Efficacy and safety of anti-PD-1 plus anlotinib in patients with advanced non-small-cell lung cancer after previous systemic treatment failure-A retrospective study. *Front Oncol*. (2021) 11:628124. doi: 10.3389/fonc.2021.628124

29. Invrea F, Rovito R, Torchiaro E, Petti C, Isella C, Medico E. Patient-derived xenografts (PDXs) as model systems for human cancer. *Curr Opin Biotechnol*. (2020) 63:151–6. doi: 10.1016/j.copbio.2020.01.003

30. Wherry EJ. T cell exhaustion. *Nat Immunol*. (2011) 12:492–9. doi: 10.1038/ni.2035

31. Franco F, Jaccard A, Romero P, Yu YR, Ho PC. Metabolic and epigenetic regulation of T-cell exhaustion. *Nat Metab*. (2020) 2:1001–12. doi: 10.1038/s42255-020-00280-9

32. Xu Q, Wang J, Sun Y, Lin Y, Liu J, Zhuo Y, et al. Efficacy and safety of sintilimab plus anlotinib for PD-L1-positive recurrent or metastatic cervical cancer: A multicenter, single-arm, prospective phase II trial. *J Clin Oncol*. (2022) 40:1795–805. doi: 10.1200/JCO.21.02091

33. Han Y, Wang J, Sun T, Ouyang Q, Li J, Yuan J, et al. Predictive biomarkers of response and survival following immunotherapy with a PD-L1 inhibitor benmelstobart (TQB2450) and antiangiogenic therapy with a VEGFR inhibitor anlotinib for pretreated advanced triple negative breast cancer. *Signal Transduct Target Ther*. (2023) 8:429. doi: 10.1038/s41392-023-01672-5

34. Qin BD, Jiao XD, Wang Z, Liu K, Wu Y, Ling Y, et al. Pan-cancer efficacy and safety of anlotinib plus PD-1 inhibitor in refractory solid tumor: A single-arm, open-label, phase II trial. *Int J Cancer*. (2023) 153:815–25. doi: 10.1002/ijc.v153.4

35. Li XY, Rao Y, Sun B, Mao XM. Efficacy and safety of anlotinib combined with PD-1 blockades for patients with previously treated epithelial ovarian cancer: A retrospective study. *Int J Gen Med*. (2022) 15:3977–89. doi: 10.2147/IJGM.S352536

36. Lan CY, Zhao J, Yang F, Xiong Y, Li R, Huang Y, et al. Anlotinib combined with TQB2450 in patients with platinum-resistant or -refractory ovarian cancer: A multi-center, single-arm, phase 1b trial. *Cell Rep Med*. (2022) 3:100689. doi: 10.1016/j.xcrm.2022.100689

37. Zhu Y, Wang X, Chen Z, Zhou L, Di X, Fan P, et al. Anlotinib suppressed ovarian cancer progression via inducing G2/M phase arrest and apoptosis. *J Clin Med*. (2022) 12:162. doi: 10.3390/jcm12010162

38. Martin R, Nora M, Anna L, Olivia P, Leif B, Gunilla WT, et al. Altered hypoxia-induced cellular responses and inflammatory profile in lung fibroblasts from COPD patients compared to control subjects. *Respir Res*. (2024) 25:282. doi: 10.1186/s12931-024-02907-x

39. Kuo HY, Khan KA, Kerbel RS. Antiangiogenic-immune-checkpoint inhibitor combinations: lessons from phase III clinical trials. *Nat Rev Clin Oncol*. (2024) 21:468–82. doi: 10.1038/s41571-024-00886-y

40. Huinen ZR, Huijbers EJM, van Beijnum JR, Nowak-Sliwinska P, Griffioen AW. Anti-angiogenic agents - overcoming tumour endothelial cell anergy and improving immunotherapy outcomes. *Nat Rev Clin Oncol*. (2021) 18:527–40. doi: 10.1038/s41571-021-00496-y

41. Fang Z, Meng Q, Xu J, Wang W, Zhang B, Liu J, et al. Signaling pathways in cancer-associated fibroblasts: recent advances and future perspectives. *Cancer Commun (Lond)*. (2023) 43:3–41. doi: 10.1002/cac2.12392

42. Elyada E, Bolisetty M, Laise P, Flynn WF, Courtois ET, Burkhart RA, et al. Cross-species single-cell analysis of pancreatic ductal adenocarcinoma reveals antigen-presenting cancer-associated fibroblasts. *Cancer Discovery*. (2019) 9:1102–23. doi: 10.1158/2159-8290.CD-19-0094

43. Geng X, Chen H, Zhao L, Hu J, Yang W, Li G, et al. Cancer-associated fibroblast (CAF) heterogeneity and targeting therapy of CAFs in pancreatic cancer. *Front Cell Dev Biol*. (2021) 9:655152. doi: 10.3389/fcell.2021.655152

44. Launonen IM, Vähärautio A, Färkkilä A. The emerging role of the single-cell and spatial tumor microenvironment in high-grade serous ovarian cancer. *Cold Spring Harb Perspect Med*. (2023) 13:a041314. doi: 10.1101/cshperspect.a041314

45. Xie C, Wan X, Quan H, Zheng M, Fu L, Li Y, et al. Preclinical characterization of anlotinib, a highly potent and selective vascular endothelial growth factor receptor-2 inhibitor. *Cancer Sci*. (2018) 109:1207–19. doi: 10.1111/cas.13536

46. Luo J, Cheng K, Ji X, Gao C, Zhu R, Chen J, et al. Anlotinib enhanced CD8(+) T cell infiltration via induction of CCL5 improves the efficacy of PD-1/PD-L1 blockade therapy in lung cancer. *Cancer Lett*. (2024) 591:216892. doi: 10.1016/j.canlet.2024.216892

47. Song F, Hu B, Liang XL, Cheng JW, Wang CG, Wang PX, et al. Anlotinib potentiates anti-PD1 immunotherapy via transferrin receptor-dependent CD8(+) T-cell infiltration in hepatocellular carcinoma. *Clin Transl Med*. (2024) 14:e1738. doi: 10.1002/ctm2.v14.8

48. Zhang C, Chu T, Wang Q, Cheng Y, Zhang Y, Wang R, et al. Enhancement of anti-PD-L1 antibody plus anlotinib efficacy due to downregulation of PD-L1 in the micro-conduit endothelium within the tumor: a randomized double-blind trial. *Cancer Biol Med*. (2024) 21:951–62. doi: 10.20892/j.issn.2095-3941.2023.0423

49. Fukumura D, Kloepper J, Amoozgar Z, Duda DG, Jain RK. Enhancing cancer immunotherapy using antiangiogenics: opportunities and challenges. *Nat Rev Clin Oncol*. (2018) 15:325–40. doi: 10.1038/nrclinonc.2018.29

50. Apte RS, Chen DS, Ferrara N. VEGF in signaling and disease: beyond discovery and development. *Cell*. (2019) 176:1248–64. doi: 10.1016/j.cell.2019.01.021

51. Kumagai S, Koyama S, Itahashi K, Tanegashima T, Lin YT, Togashi Y, et al. Lactic acid promotes PD-1 expression in regulatory T cells in highly glycolytic tumor microenvironments. *Cancer Cell*. (2022) 40:201–218.e9. doi: 10.1016/j.ccell.2022.01.001

52. Kumagai S, Togashi Y, Kamada T, Sugiyama E, Nishinakamura H, Takeuchi Y, et al. The PD-1 expression balance between effector and regulatory T cells predicts the clinical efficacy of PD-1 blockade therapies. *Nat Immunol*. (2020) 21:1346–58. doi: 10.1038/s41590-020-0769-3

53. Kamada T, Togashi Y, Tay C, Ha D, Sasaki A, Nakamura Y, et al. PD-1(+) regulatory T cells amplified by PD-1 blockade promote hyperprogression of cancer. *Proc Natl Acad Sci U.S.A*. (2019) 116:9999–10008. doi: 10.1073/pnas.1822001116

54. Reck M, Mok TSK, Nishio M, Jotte RM, Cappuzzo F, Orlandi F, et al. Atezolizumab plus bevacizumab and chemotherapy in non-small-cell lung cancer (IMpower150): key subgroup analyses of patients with EGFR mutations or baseline liver metastases in a randomised, open-label phase 3 trial. *Lancet Respir Med*. (2019) 7:387–401. doi: 10.1016/S2213-2600(19)30084-0

55. Bickley LJ, Yang YH, Jackson-Spence F, Toms C, Sng C, Flanders L, et al. Systemic therapies and primary tumour downsizing in renal cell carcinoma: a real-world comparison of anti-angiogenic and immune checkpoint inhibition regimens. *World J Urol*. (2024) 42:442. doi: 10.1007/s00345-024-05133-8

56. Lin QX, Song WW, Xie WX, Deng YT, Gong YN, Liu YR, et al. Sequential treatment of anti-PD-L1 therapy prior to anti-VEGFR2 therapy contributes to more significant clinical benefits in non-small cell lung cancer. *Neoplasia*. (2025) 59:101077. doi: 10.1016/j.neo.2024.101077

57. Lee WS, Yang H, Chon HJ, Kim C. Combination of anti-angiogenic therapy and immune checkpoint blockade normalizes vascular-immune crosstalk to potentiate cancer immunity. *Exp Mol Med*. (2020) 52:1475–85. doi: 10.1038/s12276-020-00500-y

58. Zhu S, Zhang T, Zheng L, Liu H, Song W, Liu D, et al. Combination strategies to maximize the benefits of cancer immunotherapy. *J Hematol Oncol*. (2021) 14:156. doi: 10.1186/s13045-021-01164-5

59. Xu Q, Shao D. Leveraging the synergy between anti-angiogenic therapy and immune checkpoint inhibitors to treat digestive system cancers. *Front Immunol*. (2024) 15:1487610. doi: 10.3389/fimmu.2024.1487610

60. Wu M, Huang Q, Xie Y, Wu X, Ma H, Zhang Y, et al. Improvement of the anticancer efficacy of PD-1/PD-L1 blockade via combination therapy and PD-L1 regulation. *J Hematol Oncol*. (2022) 15:24. doi: 10.1186/s13045-022-01242-2

61. Su Y, Luo B, Lu Y, Wang D, Yan J, Zheng J, et al. Anlotinib induces a T cell-inflamed tumor microenvironment by facilitating vessel normalization and enhances the efficacy of PD-1 checkpoint blockade in neuroblastoma. *Clin Cancer Res*. (2022) 28:793–809. doi: 10.1158/1078-0432.CCR-21-2241

62. Zou BK, Jiang HH, Liu HY, Lu J, Qiang HP, Lu MF, et al. Anlotinib combined with anti-PD1 potentiates anti-tumor immunity via immunogenic cell death and macrophage reprogramming. *Advanced Ther*. (2023) 6:2300141. doi: 10.1002/adtp.202300141

63. Ma C, Chen J, Ji J, Zheng Y, Liu Y, Wang J, et al. Therapeutic modulation of APP-CD74 axis can activate phagocytosis of TAMs in GBM. *Biochim Biophys Acta Mol Basis Dis*. (2024) 1870:167449. doi: 10.1016/j.bbadis.2024.167449

64. Chen G, Wang W, Wei X, Chen Y, Peng L, Qu R, et al. Single-cell transcriptomic analysis reveals that the APP-CD74 axis promotes immunosuppression and progression of testicular tumors. *J Pathol*. (2024) 264:250–69. doi: 10.1002/path.v264.3

65. Ma R, Zhou X, Zhai X, Wang C, Hu R, Chen Y, et al. Single-cell RNA sequencing reveals immune cell dysfunction in the peripheral blood of patients with highly aggressive gastric cancer. *Cell Prolif.* (2024) 57:e13591. doi: 10.1111/cpr.13591

66. Yu F, Liu G, Zhang H, Wang X, Wu Z, Xu Q, et al. Cell adhesion molecule CD99 in cancer immunotherapy. *Curr Mol Med.* (2023) 23:1028–36. doi: 10.2174/1566524023666221007143513

67. Husak Z, Dworzak MN. CD99 ligation upregulates HSP70 on acute lymphoblastic leukemia cells and concomitantly increases NK cytotoxicity. *Cell Death Dis.* (2012) 3:e425. doi: 10.1038/cddis.2012.164

68. Tan Z, Wu Y, Fan Z, Gao T, Guo W, Bai C, et al. Anlotinib plus TQB2450, a PD-L1 antibody, in patients with advanced alveolar soft part sarcoma: A single-arm, phase II trial. *Clin Cancer Res.* (2024) 30:5577–83. doi: 10.1158/1078-0432.CCR-24-2444

69. Du Y, Dai J, Mao L, Wei X, Bai X, Chen L, et al. Phase Ib study of anlotinib in combination with anti-PD-L1 antibody (TQB2450) in patients with advanced acral melanoma. *J Eur Acad Dermatol Venereol.* (2024) 38:93–101. doi: 10.1111/jdv.19467

70. Wang J, Sun T, Ouyang Q, Han Y, Xu B. A phase Ib study of TQB2450 plus anlotinib in patients with advanced triple-negative breast cancer. *iScience.* (2023) 26:106876. doi: 10.1016/j.isci.2023.106876

71. Haibe Y, Kreidieh M, El Hajj H, Khalifeh I, Mukherji D, Temraz S, et al. Resistance mechanisms to anti-angiogenic therapies in cancer. *Front Oncol.* (2020) 10:221. doi: 10.3389/fonc.2020.00221

72. Liu ZL, Chen HH, Zheng LL, Sun LP, Shi L. Angiogenic signaling pathways and anti-angiogenic therapy for cancer. *Signal Transduct Target Ther.* (2023) 8:198. doi: 10.1038/s41392-023-01460-1

73. Schoenfeld AJ, Hellmann MD. Acquired resistance to immune checkpoint inhibitors. *Cancer Cell.* (2020) 37:443–55. doi: 10.1016/j.ccell.2020.03.017

frontiers | Frontiers in Immunology

TYPE Original Research
PUBLISHED 08 April 2025
DOI 10.3389/fimmu.2025.1532306

Check for updates

OPEN ACCESS

EDITED BY
Qingyu Luo,
Dana–Farber Cancer Institute, United States

REVIEWED BY
Xiaowei Wu,
Dana–Farber Cancer Institute, United States
Yabing Nan,
Dana–Farber Cancer Institute, United States

*CORRESPONDENCE
Jidong Gao
ab168@cicams.ac.cn
Shuangjiu Hu
HShuangjiu@163.com
Zhihua Chen
czh19821127@163.com

†These authors have contributed equally to this work

RECEIVED 21 November 2024
ACCEPTED 17 March 2025
PUBLISHED 08 April 2025

CITATION
Zhang W, Yang C, Lu Y, Tang C, Zhao M, Wang Z, Gao J, Hu S and Chen Z (2025) Cancer-associated fibroblasts gene signature: a novel approach to survival prediction and immunotherapy guidance in colon cancer.
Front. Immunol. 16:1532306.
doi: 10.3389/fimmu.2025.1532306

COPYRIGHT
© 2025 Zhang, Yang, Lu, Tang, Zhao, Wang, Gao, Hu and Chen. This is an open-access article distributed under the terms of the Creative Commons Attribution License (CC BY). The use, distribution or reproduction in other forums is permitted, provided the original author(s) and the copyright owner(s) are credited and that the original publication in this journal is cited, in accordance with accepted academic practice. No use, distribution or reproduction is permitted which does not comply with these terms.

Cancer-associated fibroblasts gene signature: a novel approach to survival prediction and immunotherapy guidance in colon cancer

Wenbing Zhang[1†], Chi Yang[2†], Ye Lu[3,4†], Chenling Tang[5], Mengyu Zhao[1], Zhaohui Wang[1], Jidong Gao[3,4*], Shuangjiu Hu[1*] and Zhihua Chen[5*]

[1]Department of General Surgery, Anqing First People's Hospital of Anhui Medical University, Anqing, China, [2]Department of General Surgery, QingPu Branch of Zhongshan Hospital Affiliated to Fudan University, QingPu District Central Hospital Shanghai, No. 1158, Gong Yuan Dong Road, Shanghai, China, [3]Department of Breast Surgical Oncology, National Cancer Center/National Clinical Research Center for Cancer/Cancer Hospital, Chinese Academy of Medical Sciences and Peking Union Medical College, Beijing, China, [4]Department of Breast Surgical Oncology, National Cancer Center/National Clinical Research Center for Cancer/Cancer Hospital & Shenzhen Hospital, Chinese Academy of Medical Sciences and Peking Union Medical College, Shenzhen, China, [5]The First People's Hospital of Taicang City, Taicang Affiliated Hospital of Soochow University, Suzhou, Jiangsu, China

Background: Fibroblasts can regulate tumour development by secreting various factors. For COAD survival prediction and CAFs-based treatment recommendations, it is critical to comprehend the heterogeneity of CAFs and find biomarkers.

Methods: We identified fibroblast-associated specific marker genes in colon adenocarcinoma by single-cell sequencing analysis. A fibroblasts-related gene signature was developed, and colon adenocarcinoma patients were classified into high-risk and low-risk cohorts based on the median risk score. Additionally, the impact of these risk categories on the tumor microenvironment was evaluated. The ability of CAFGs signature to assess prognosis and guide treatment was validated using external cohorts. Ultimately, we verified MAN1B1 expression and function through *in vitro* assays.

Results: Relying on the bulk RNA-seq and scRNA-seq data study, we created a predictive profile with 11 CAFGs. The profile effectively differentiated survival differences among cohorts of colon adenocarcinoma patients. The nomogram further effectively predicted the prognosis of COAD patients, with low-risk patients having a better prognosis. A higher immune infiltration rate and lower IC50 values of anticancer drugs were significant in the high-risk group. In cellular experiments, Following MAN1B1 knockdown, in cell assays, the colony formation, migration, and invasion ability of HCT116 and HT29 cell lines decreased.

Conclusion: Our CAFG signature provides important insights into the role of CAF cells in influencing COAD prognosis. It may also serve as a guide for selecting immunotherapy options and predicting chemotherapy responses in COAD patients.

KEYWORDS

colon adenocarcinoma, cancer-associated fibroblasts, signature, tumor immune microenvironment, MAN1B1

1 Introduction

Colon adenocarcinoma (COAD) is a heterogeneous neoplastic disease characterized by diverse stromal cell population infiltration. The progression of COAD is driven by the accumulation of oncogenic mutations and the dynamic interactions within the tumor microenvironment (TME) (1, 2). The TME, comprising non-epithelial cells and extracellular matrix components, plays a critical role in tumor development and therapy resistance. However, the traditional pathological staging system often fails to accurately predict patient outcomes, highlighting the need for more reliable prognostic models (3). Such models are essential for assessing patient risk drug sensitivity and guiding personalized immunotherapy and chemotherapy regimens.

TME includes a variety of non-cancerous cells, with cancer-associated fibroblasts (CAFs) being the most important and common type (4). CAFs can regulate blood vessel production and cell metabolism, subsequently driving tumors' onset and transfer (5, 6). CAFs promote tumor immunosuppression through interactions with immune cells in the tumor immune microenvironment (7). Despite their importance, CAFs exhibit considerable heterogeneity, which is reflected in the diversity of their subpopulation markers. Commonly used markers such as αSMA and FAP are not exclusive to CAFs, as they are also expressed in pericytes and fibroblastic reticular cells (8, 9). This underscores the need to identify specific markers for CAFs to enable targeted therapeutic strategies for COAD.

Recent advances in single-cell RNA sequencing (scRNA-seq) have provided new insights into the heterogeneity of CAFs across various cancers, revealing potential therapeutic targets. By integrating single-cell and bulk RNA-seq analyses, we identified 11 CAF-related genes that may serve as promising targets for COAD treatment. Further *in vitro* experiments confirmed the expression of MAN1B1 in COAD cells, suggesting its potential as a therapeutic target. This study explores the functional roles of these genes and their implications for COAD therapy.

2 Materials and methods

2.1 Data collection

We selected 23 tumour samples by downloading scRNA-seq data of GSE132465 via the GEO database. RNA-seq data in FPKM format and survival information for 430 TCGA-COAD cases were retrieved from the UCSC Xena platform (https://gdc.xenahubs.net). The normalized FPKM values were converted into TPM and further transformed using log2 (TPM+1) conversion. We also obtained normalized gene expression profiles and clinical details from the GEO database of 177 cases in the GSE17536 dataset and 171 cases in the GSE159216 dataset, averaging the values if a gene matched multiple probes.

2.2 Single-cell RNA-sequence analysis

The 'Seurat' toolkit (version 4.3.0) in R was used to standardize the scRNA-seq data's downstream processing (10). For the scRNA-seq dataset, each gene must be expressed in at least three cells, with no less than 200 genes per cell. Furthermore, the amount of mitochondria was kept to less than 14%. The LogNormalize method was used for data normalization. After performing PCA, we employed UMAP, a non-linear dimensionality reduction technique. Subsequently, clustering was conducted using the 'FindNeighbors' function with a dimensionality parameter set to 1, followed by the 'FindClusters' function with parameters dim set to 20 and resolution set to 0.2 (11). Subsequently, we identified the marker genes unique to each cluster by utilizing the 'FindAllMarkers' function, setting a threshold of an absolute log2 fold change (FC) of at least 0.5 and requiring a minimum cell population percentage of 0.25 (minpct = 0.25) for each cluster. Following this, we employed the 'SingleR' tool (version 1.10.0) to annotate the cell types based on the identified markers (12).

2.3 GO and KEGG pathway examination

To investigate the biological functions and pathways associated with CAFs-related key genes, we utilized the R tools org.Hs.eg.db (version 3.15.0) and clusterProfiler (version 4.9.0). GO functional enrichment evaluation was performed to identify differences and similarities across BP (Biological Process), CC (Cellular Component), and MF (Molecular Function) categories. Furthermore, an enrichment analysis of KEGG pathways was carried out to highlight the most prevalent pathways.

2.4 Creating and validating a predictive gene signature correlated with CAFs

We developed a prognostic model for COAD by identifying CAF marker genes from scRNA-seq data. We identified genes significantly correlated with overall survival (OS) through univariate Cox regression ($P<0.05$). To refine the model, we employed LASSO Cox regression with the glmnet package (version 4.1-6)and followed with multivariate Cox regression (13, 14). The risk score was calculated as the aggregate of the products obtained by multiplying gene expressions by their respective coefficients. We employed the timeROC package (version 0.4) to evaluate the model's predictive accuracy and further validated its performance in separate cohorts.

2.5 Development of nomogram

We initially conducted univariate and multivariate Cox regression analyses on clinical and risk factors to develop a nomogram tool for clinical use. Factors with $p<0.05$ in the multivariate Cox analysis were selected to generate the column-line diagram for predicting COAD prognosis with the rms package (version 6.5-0). The final nomogram was developed based on CAF characteristics, M stage, and patient age. Its predictive performance and accuracy were then assessed through ROC and calibration curves to confirm reliability.

2.6 Immune infiltration analysis

The ESTIMATE technique was used to assess stromal and immune cell infiltration levels. RNA sequencing data from the TCGA-COAD cohort were analyzed using the ESTIMATE computational method to generate stromal, immune, estimate, and tumor purity scores. Wilcoxon tests were conducted to compare these scores across different risk groups. Fibroblast infiltration levels were determined through the Microenvironmental Cell Population Counting (MCP-counter) algorithm, utilizing the MCP-counter package (version 1.2-0) (15). The infiltration levels of 28 immune cell types were measured through single-sample Gene Set enrichment analysis (ssGSEA) (16). To evaluate the disparities in immune checkpoint blockade responses between the two groups, we employed the 'ggpubr' software package (version 0.6.0).

2.7 Identification of CAFs relevant mutations and analysis of drug sensitivity

Somatic mutation information of COAD patients was obtained from the TCGA repository. For each person, the rates of genetic mutations and the lengths of exons were determined. To compare mutations across various risk categories, waterfall plots were created utilizing the 'maftools' R package and visual representations of tumor mutational burden (TMB) values. The Wilcoxon test assessed the differences in TMB values between these categories. K-M analysis was used to examine OS variations between the two groups. Additionally, the chemotherapy response of COAD individuals was analyzed using the Genomics of Drug Sensitivity in Cancer (GDSC) database (17). The "pRRophetic" package (18) was employed to estimate the 50% maximal inhibitory concentration (IC50) to evaluate chemotherapy sensitivity.

2.8 TIMER database analysis

MAN1B1 expression in COAD and adjacent normal tissues were examined through the TIMER database, which includes 10,897 samples from 32 distinct cancer types. The DiffExp module was employed to evaluate MAN1B1 expression in a pan-cancer context.

2.9 Cell culture, transfection and reverse transcription-quantitative PCR

The COAD cell lines, HCT116 and HT29, were acquired from the Chinese Cell Culture Collection and cultured in RPMI 1640 medium supplemented with 10% fetal bovine serum (FBS) and 100 units per milliliter of penicillin-streptomycin. MAN1B1 knockdown was confirmed by qRT-PCR. Cells treated with NC, siMAN1B1-1, and siMAN1B1-2 to inhibit MAN1B1 expression were used in subsequent experiments (19). Supplementary Table S1 contains the primer sequences.

2.10 Colony formation assay

Four hundred transfected cells were cultured in 6-well plates for approximately 14 days. The samples underwent fixation with 4% paraformaldehyde for 15 minutes, which was succeeded by a 20-minute staining process using Crystal Violet (Solarbio, China). Following the staining, the cells were allowed to air-dry at room temperature, and then the cell count in each well was determined.

2.11 Wound healing assay

After plating the transfected cells into 6-well plates, then cultured in a cell incubator until achieving 95% confluence. A straight line was then drawn using a sterile 200 μL pipette tip. Then, carefully wash away any detached cells and debris with PBS. Subsequently, the cells were moved into a cell growth medium devoid of serum. Finally, Image J was used to estimate the breadth of the scratches after pictures were taken at the same location at 0 and 48 hours.

2.12 Transwell experiment

Transwell experiments were employed to evaluate cell invasion and migration. Treated cells were placed in the upper chamber in 200 μl of medium without serum, with 5×10^4 cells per well. The upper chamber was coated with Matrigel solution to evaluate invasive and migratory capacity, while the lower chamber contained 700 μl of complete medium. Photographs and counts of the successfully moving cells were taken.

2.13 Statistical analysis

The data are presented as the mean ± standard deviation. To evaluate the differences between groups, a Student's t-test was applied, and all experiments were conducted at least three times. The statistical analyses used GraphPad Prism version 9.1.1 and R version 4.1.1.

3 Result

3.1 Single cell RNA-seq analysis

Quality control preprocessing of scRNA-seq data was conducted according to appropriate metrics, and the quality control results are shown in Supplementary Figure S1. 47285. High quality cell samples were isolated from 23 COAD tissues screened for subsequent further examination. Following data normalization, we chose the 2000 most variable genes (Figure 1A). Dimensionality reduction was executed employing the PCA technique (Figure 1B), and the 20 most significant PCs with $p< 0.05$ were selected for additional examination (Figure 1C). We successfully classified the cells into 15 distinct clusters based on

the top 20 major components and identified 5356 differentially expressed marker genes across these clusters, which are listed in Supplementary Table S2. The heatmap illustrates the expression values of the five most significant marker genes within every cluster (Figure 1D). The IMAP technique also represented the multi-dimensional scRNA sequencing data (Figure 1E). We annotated the cell subpopulations using the "SingleR" package as recognized cell types (Figure 1F). The main cell categories include T cells, epithelial cells, NK cells, B cells, DCs, fibroblasts, and endothelial cells, with cluster 6 identified as the fibroblasts subpopulation. Finally, we identified 1025 significant expression marker genes of COAD-associated fibroblasts based on a threshold adjPval < 0.05.

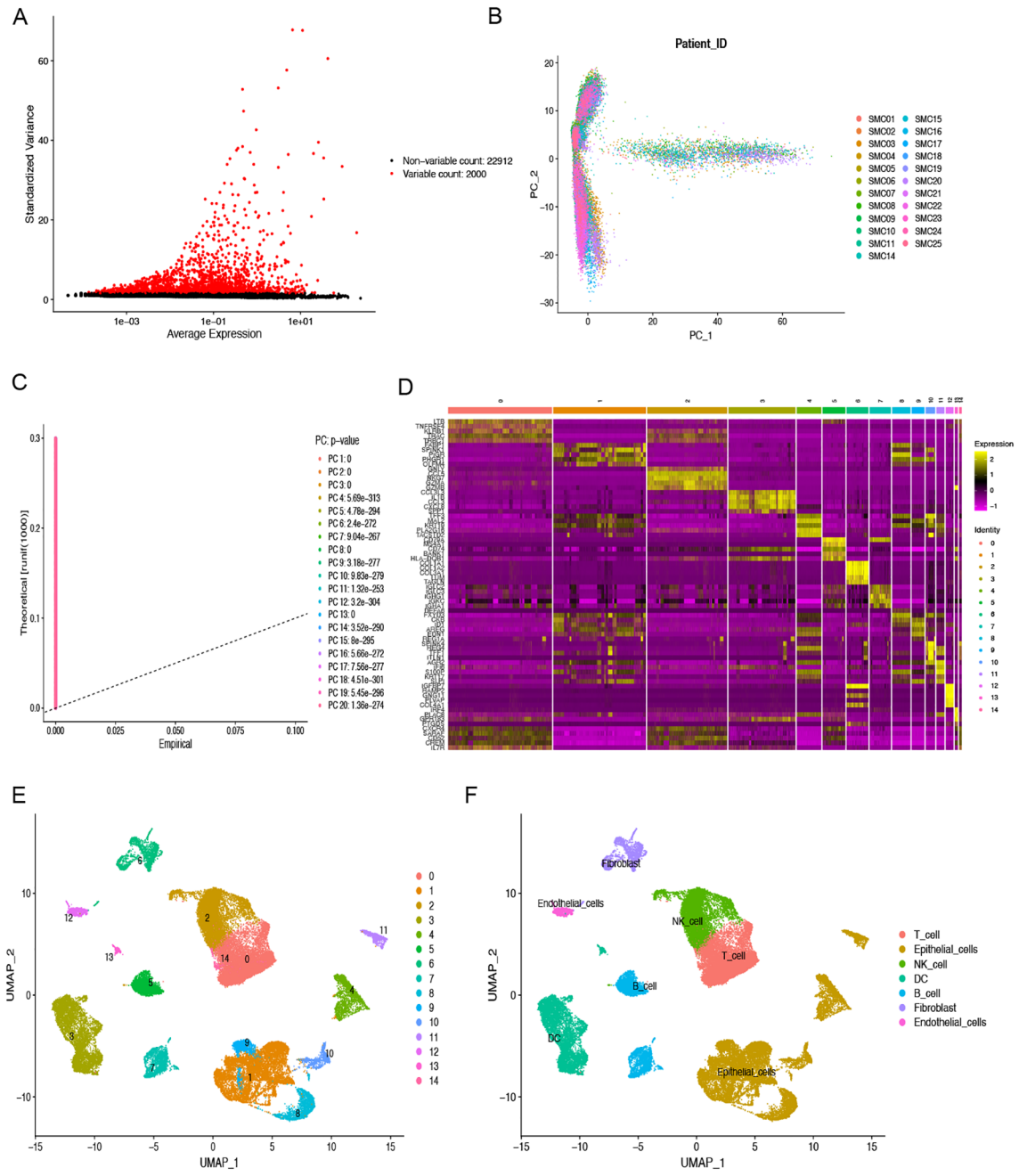

FIGURE 1
scRNA-seq analysis to identify fibroblasts marker genes. **(A)** The top 2000 highly variable genes are highlighted in red dots. **(B)** PCA was used to decrease dimensionality. **(C)** The top 20 PCs were identified with the P-value < 0.05. **(D)** The heatmap indicated the relative gene expression of 15 clusters. Genes with high expression are depicted in yellow, whereas genes with low expression are highlighted in purple. **(E)** Fifteen clusters were visualized using the UMAP technique. **(F)** Cell subpopulations identified by marker genes. Different color areas represent different cells.

3.2 Functional assessment of GO and KEGG of fibroblasts-associated genes

GO and KEGG functional assessments were conducted to investigate the functions and pathways of fibroblasts-associated genes. Figure 2A displays the 10 most significantly enriched GO terms. For BP, the enriched terms included "extracellular structural organization," "extracellular matrix organization," and "external encapsulating structure organization." In the CC category, genes were enriched in "collagen-containing extracellular matrix," "focal adhesion," and "cell-substrate junction." MF terms were primarily associated with "actin binding," "extracellular matrix structural constituent," and "cadherin binding." Additionally, the top 20 enriched KEGG pathways were displayed in Figure 2B, which included pathways such as "PI3K-Akt signaling pathway," "focal adhesion," "proteoglycans in cancer," "regulation of actin cytoskeleton," "ECM-receptor interaction," "protein digestion and absorption," "tight junction," "adherens junction," "leukocyte transendothelial migration," and "gap junction."

3.3 CAFGs signature construction and verification

A Cox proportional hazards analysis was performed on CAF marker genes in the TCGA-COAD dataset, identifying 144 genes with P<0.05. Following this, LASSO Cox regression analysis (Figures 3A, B) was conducted on the genes, resulting in the selection of 11 prognostic genes with significant non-zero coefficients (Figure 3C). Risk Score =(-0.66451*CTNNA1 expression)+(0.25692*HSPA1A expression)+(0.72129*P4HA1 expression)+(-0.72811*PPP2CB expression)+(0.85761*MAN1B1 expression)+(-0.74474*LRRC59 expression)+(1.17154*CCPS7A expression)+(0.52996*SLC9A3R2 expression)+(1.21188*RAB7A expression) +(-0.92288*CAMTA1 expression)+(-0.39307*WIPI1 expression). Among the 11 identified prognostic genes, six (HSPA1A, P4HA1, MAN1B1, CCPS7A, SLC9A3R2, and RAB7A) were classified as risk-associated genes (HR > 1), while CTNNA1, PPP2CB, LRRC59, CAMTA1, and WIPI1 were regarded as protective genes (HR < 1). The CAFG risk score was calculated for each person by leveraging these genes. Subsequently, the TCGA-COAD, GSE17536, and GSE159216 cohorts were separated into low-risk and high-risk groups based on the median risk scores. Studies revealed that individuals belonging to the low-risk group showed better OS outcomes in comparison to those in the high-risk group (TCGA, HR = 3.272, 95% CI: 2.008-5.332, P < 0.001; GSE159216, HR = 1.924, 95% CI: 1.197-3.092, P = 0.031; GSE17536, HR = 1.496, 95% CI: 1.708-2.075, P = 0.005, Figures 3D-F). The distribution and scatter plot of CAFGs risk score showed that as risk score grew, OS declined while mortality increased (Figures 3G-I). The AUC of the 1-, 3-, and 5-year TCGA-COAD cohorts were 0.762, 0.796, and 0.852, respectively. In the GSE159216 cohort, the 1-, 3-, and 5-year AUCs were 0.660, 0.588, and 0.599. The AUC of the GSE17536 were 0.913, 0.635, and 0.587, respectively (Figures 3J-L). The CAFG signature model demonstrated an effective and dependable method for forecasting OS in COAD patients.

3.4 CAFGs signature is an independent prognostic indicator

In the TCGA-COAD cohort, univariate and multivariate Cox regression analyses were performed to evaluate whether the

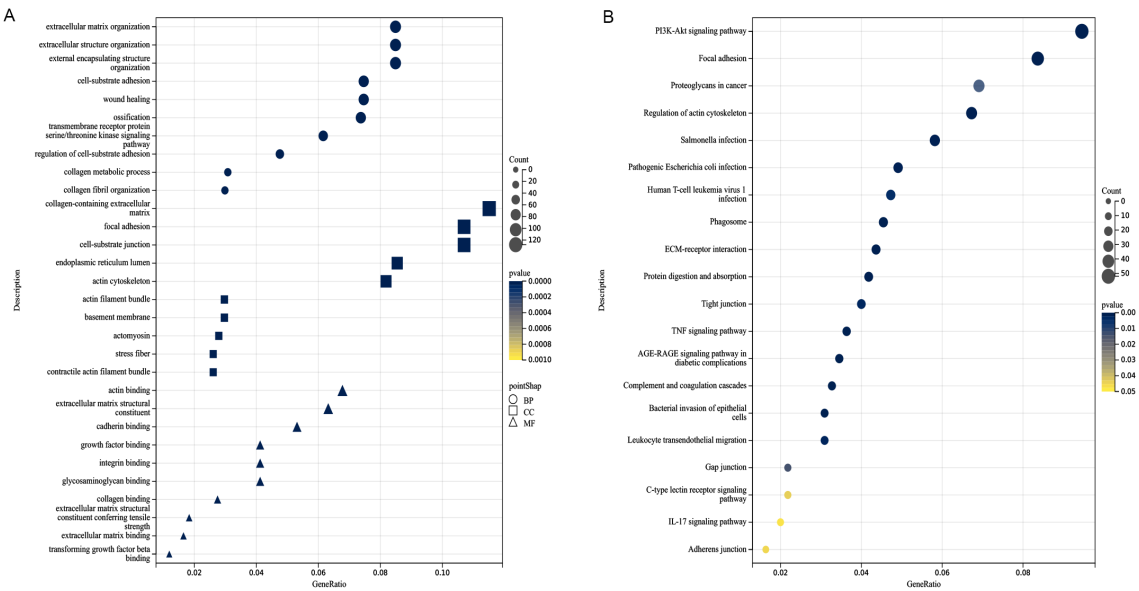

FIGURE 2
Analysis of functional enrichment. **(A)** Function enrichment analysis based on BP, CC, and MF, three different viewpoints. **(B)** The top 20 pathways of KEGG analysis. The darker the color, the smaller the P value, and the larger the shape, the larger the number.

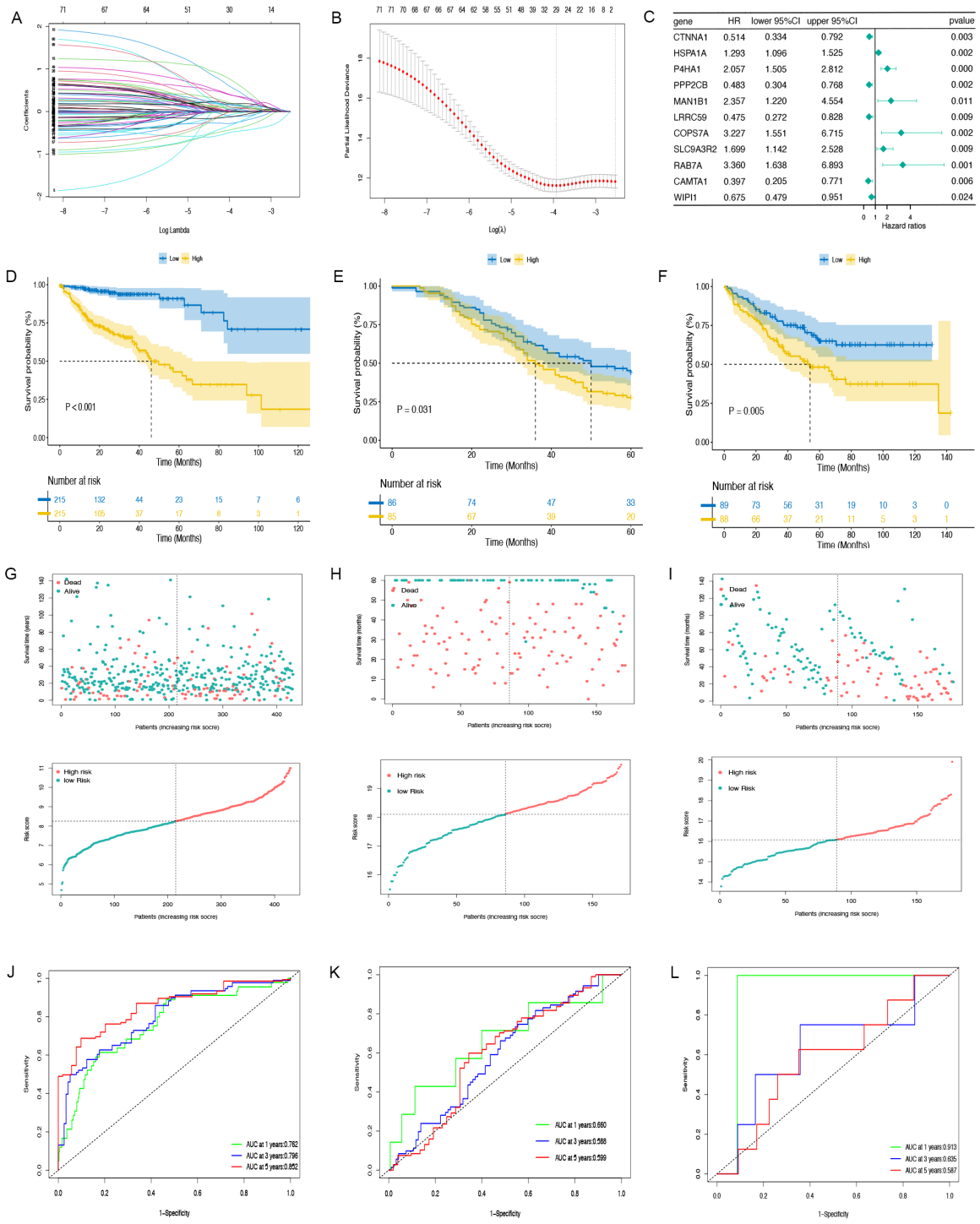

FIGURE 3
The prognostic model is constructed and validated. **(A, B)** LASSO regression analysis. **(C)** Multivariate Cox regression results are plotted in a forest. **(D–F)** The Kaplan-Meier curves in TCGA-COAD, GSE159216 and GSE17536 cohorts. **(G–I)** Distribution of CAFGs risk score and scatter plot of the OS of each patient in TCGA-COAD, GSE159216 and GSE17536 cohorts, respectively. **(J–L)** The AUC at 1-, 3-, and 5-years of prognostic models in TCGA-COAD, GSE159216 and GSE17536 cohorts.

prognostic relevance of CAFGs-associated gene signature was autonomous of factors like age, gender, and TNM stage. As shown in Figures 4A, B, both analyses confirmed that the CAFGs signature is an independent prognostic indicator. By utilizing the risk scores calculated by the Cox regression coefficients for the 11 genes associated with CAFs, combined with clinical attributes like age and M stage from the TCGA-COAD dataset, a nomogram was constructed to predict the 1-, 3-, and 5-year OS rates for COAD patients (Figure 4C). We assessed the discriminatory power of the nomogram using ROC and the AUC for the CAFGs risk grouping

model was 0.77 (Figure 4D). To assess the reliability of the risk model, we calculated the area beneath the time-dependent ROC curve for OS. The AUC values were 0.820, 0.786, and 0.815 for the one-year, three-year, and five-year predictions (Figure 4E). The calibration curve demonstrated that the model's OS predictions aligned with the dataset's outcomes (Figure 4F).

3.5 Tumour immune infiltration

Differences in the expression levels of the stroma score, estimate score, immune score, and tumor purity were identified across the low-risk and high-risk groups (Figures 5A-D). Using the MCPcounter algorithm, the abundance of 10 cell categories,

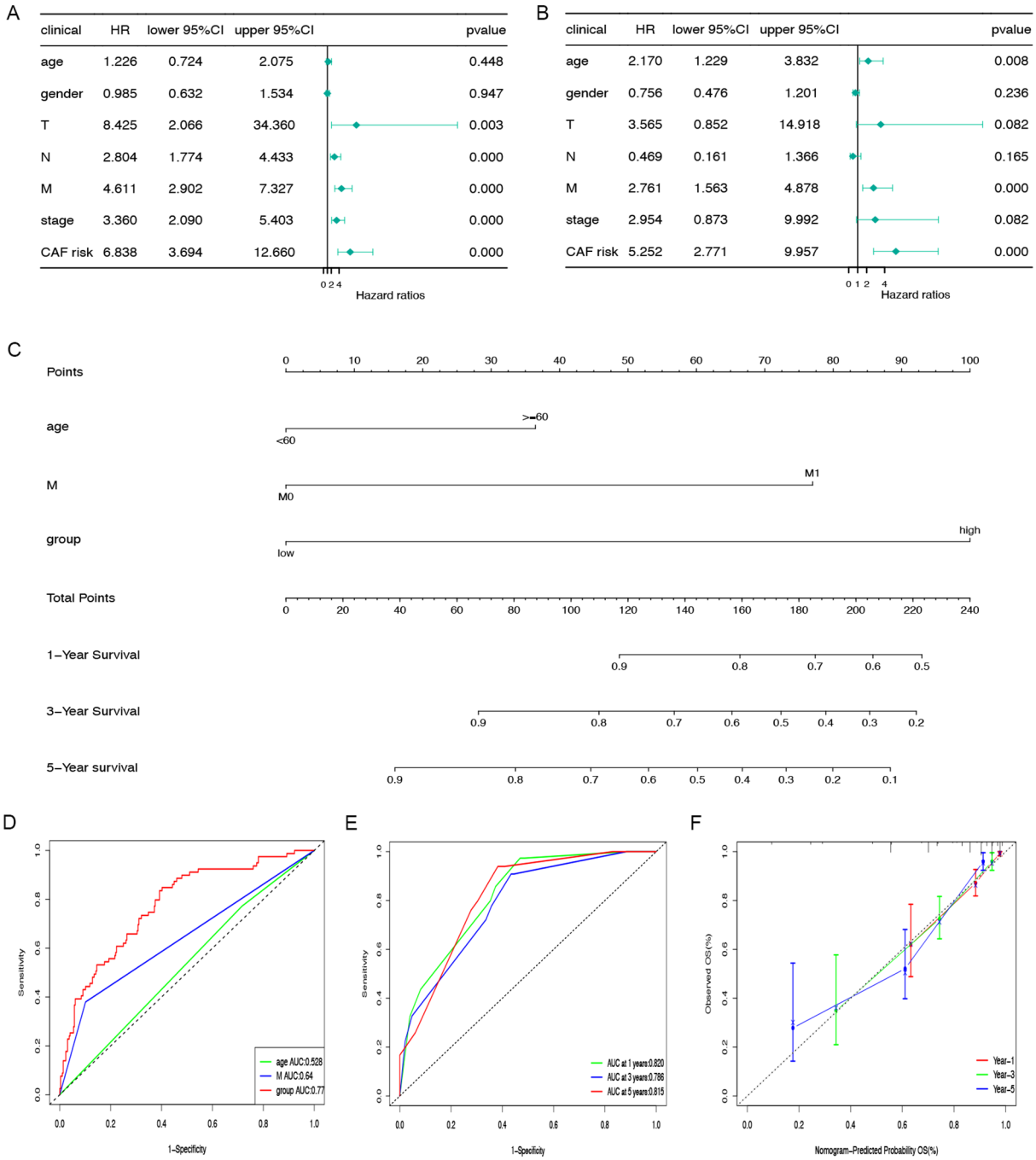

FIGURE 4
Nomogram construction and evaluation. The correlations between OS and CAFGs risk scores and other clinical indicators in TCGA-COAD populations were examined using univariate **(A)** and multivariate **(B)** Cox regression analyses. **(C)** The nomogram was applied to predict the 1-, 3-, and 5-year OS and the total score on the bottom scale implies the probability of OS. **(D)** ROC curves to evaluate the age, M stage and CAFGs risk group accuracy for predicting in patients. **(E)** ROC curves to evaluate the nomogram accuracy for predicting 1-, 3-, and 5-year OS in patients. **(F)** Calibration curves of the nomogram for predicting survival rates at 1-, 3-, and 5- years.

comprising eight immune cells, endothelial cells and fibroblasts, were compared between these two groups (Figure 5E), revealing a significantly higher prevalence of fibroblasts in the high-risk group. Additionally, results from the ssGSEA algorithm showed that central memory CD4+ T cells, NK cells, and macrophages showed higher expression in the high-risk group (Figure 5F). Given the importance of immune checkpoint inhibitors (ICIs) in immunotherapy, we analyzed the expression of eight common ICI-related genes in both groups. The analysis showed that PDCD1, PDCD1LG2, TIGIT, and HAVCR2 were more highly expressed in the high-risk group (Figure 5G). These results indicate that individuals in the high-risk group might be better candidates for ICI therapy.

3.6 Evaluation of somatic mutations and TMB analysis

Figure 6A illustrates the comprehensive genetic alteration landscape of COAD. In addition, somatic mutation interactions were detected, as shown in Figure 6B, where most genes had co-occurring mutations. In both the low-risk and high-risk categories, APC, TP53, and TTN emerged as the most commonly mutated genes (Figures 6C, D). Additionally, an analysis of TMB across groups revealed no substantial differences (P = 0.49) (Figure 6E). The K-M analysis indicated that the outcome of the low TMB group was better than that of the high TMB group (P=0.038) (Figure 6F). Notably, following the integration with our model, the outcome of the high-risk + high TMB group was considerably worse than that of the low-risk + low TMB group (Figure 6G).

3.7 Response to drug sensitivity predicted by CAFG signature

Additionally, the differences in IC50 levels of chemotherapy drugs between the low-risk and high-risk groups in the TCGA-COAD cohort were investigated (Figures 7A-E). The analysis

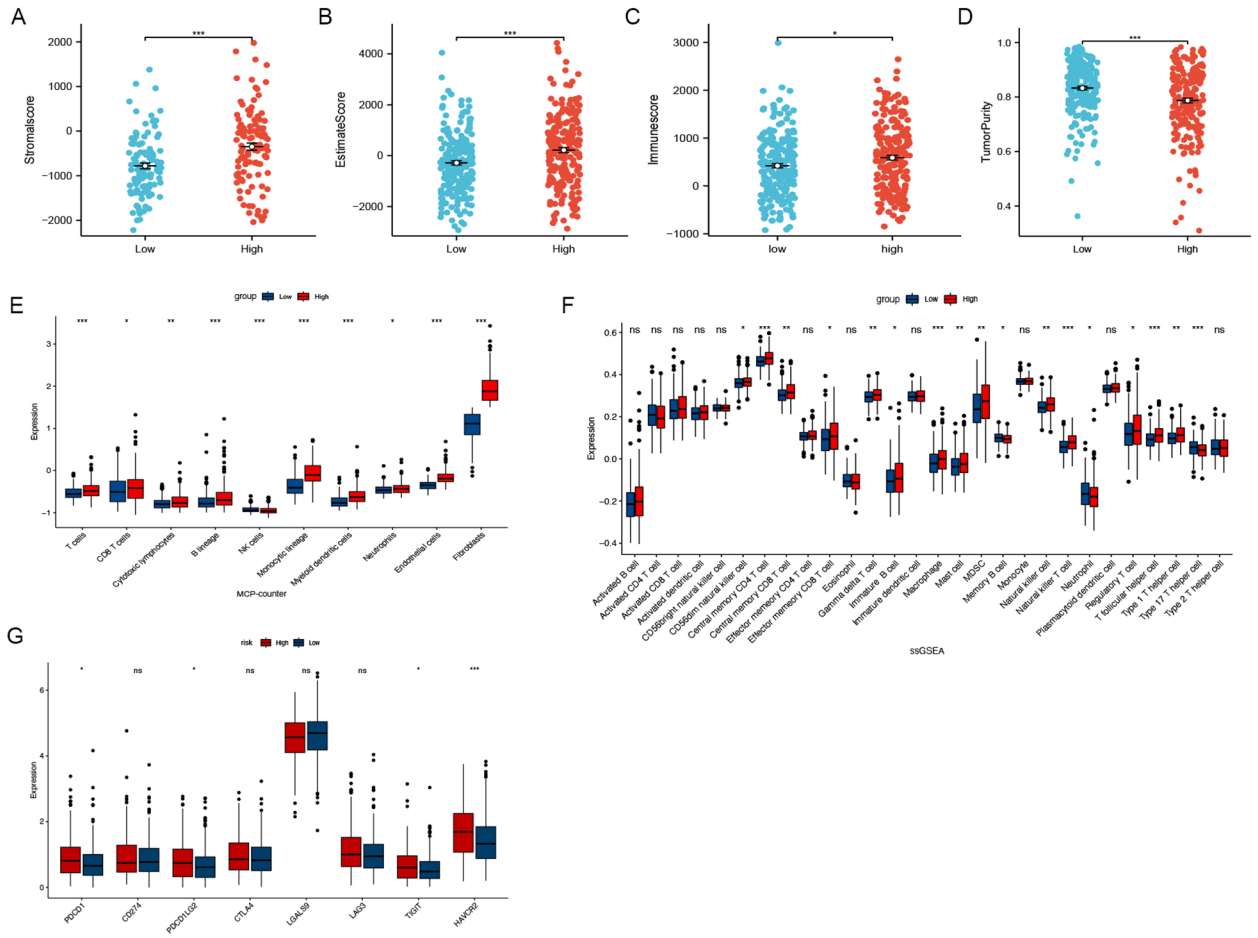

FIGURE 5
Immune infiltration analysis. **(A-D)** Different expression levels of stroma score, estimate score, immune score and tumour purity between the low- and high-risk groups. **(E)** The MCPcounter algorithm estimated the expression levels of ten different cell types, including fibroblasts. **(F)** The association of CAFGs risk score with 28 tumor-infiltrating immune cells. **(G)** Differential expression levels of the immune checkpoint-related genes between low- and high-risk groups. (ns, no significance, *P < 0.05, **P < 0.01, ***P < 0.001).

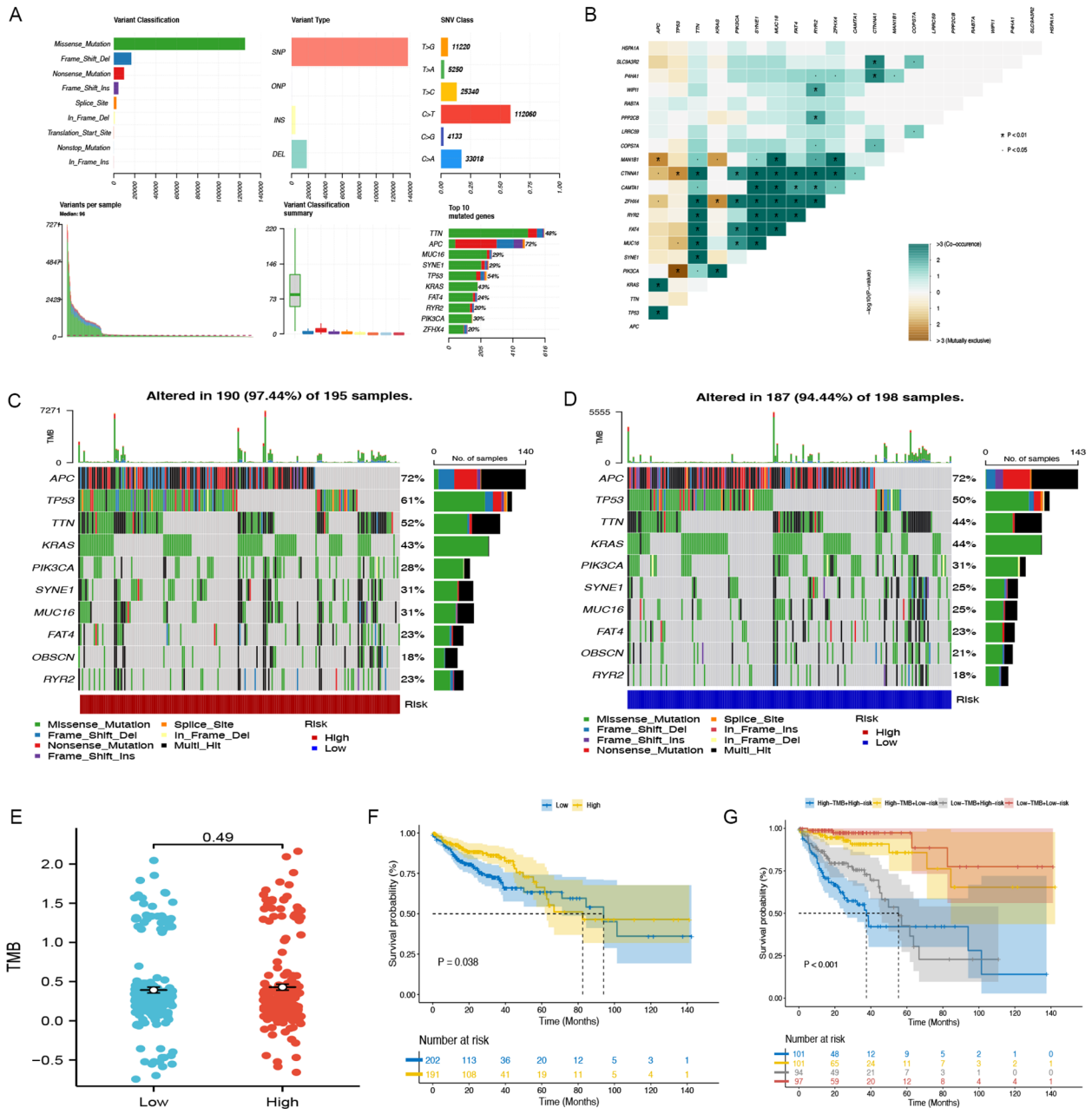

FIGURE 6
Somatic mutation in TCGA-COAD. **(A)** The general mutation profile. Different colors indicate different mutations. **(B)** Interaction relationship of major mutation genes. **(C)** The high-risk group's gene mutation frequency. **(D)** The low-risk group's gene mutation frequency. **(E)** Variations in TMB expression levels between groups. **(F)** The Kaplan-Meier curve between low- and high-TMB groups. **(G)** Kaplan-Meier analysis curves for patients categorized by TMB and CAFGs risk group.

revealed that individuals in the low-risk category had higher IC50 values for anticancer drugs such as gemcitabine, gefitinib, docetaxel, camptothecin, and sorafenib. Comparable findings were noted in the GSE17536 (Figures 7F-J) and GSE159216 (Figures 7K-O) validation cohorts. These results indicate that the CAFG signature could be a useful predictor for selecting appropriate anticancer drugs in COAD treatment.

3.8 Tumor-suppressive effects of MAN1B1 knockdown

Figure 8A, which examined MAN1B1 expression levels across different malignancies, demonstrates that MAN1B1 mRNA expression was considerably greater in COAD samples than in normal samples. We used siRNAs to knock down MAN1B1

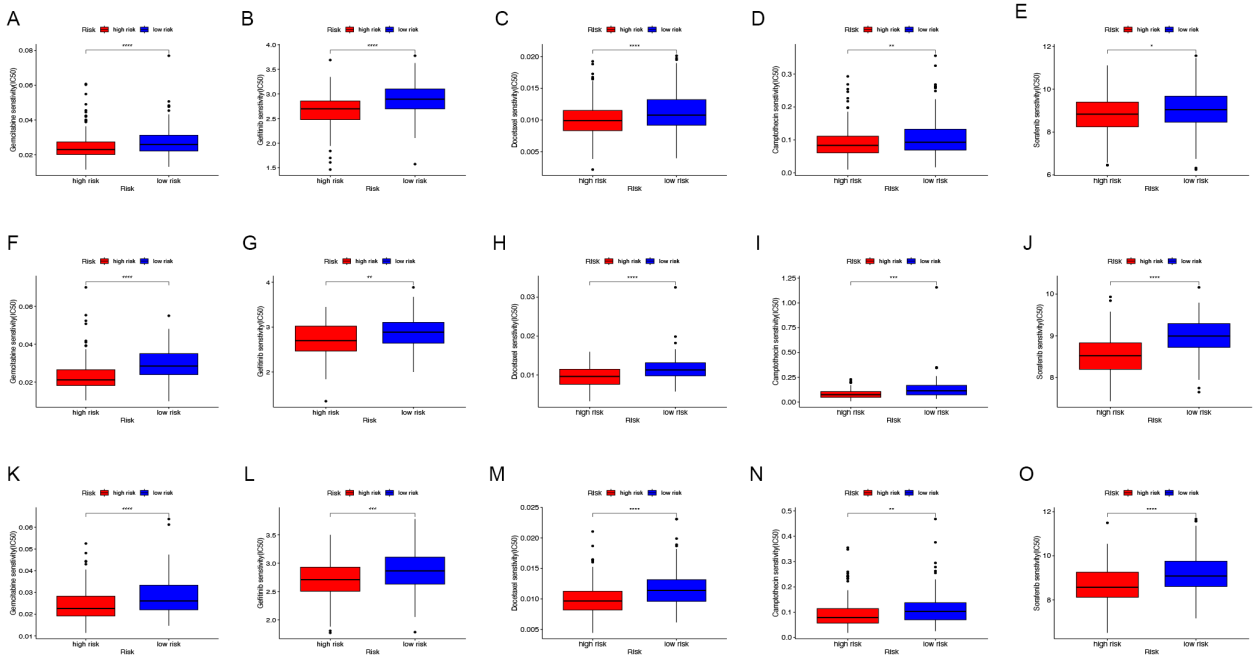

FIGURE 7
Drug sensitivity assessment. In the TCGA-COAD **(A-E)**, GSE17536 **(F-J)** and GSE159216 **(K-O)** cohorts, the IC50 values of Gemcitabine **(A, F, K)**, Gefitinib **(B, G, L)**, Docetaxel **(C, H, M)**, Camptothecin **(D, I, N)**, and Sorafenib **(E, J, O)** were compared between low-risk and high-risk groups. (*P < 0.05, **P < 0.01, ***P < 0.001, ****P < 0.0001).

expression in HCT116 and HT29 cells during *in vitro* experiments, and qRT-PCR confirmed this (Figure 8B). Colony formation experiments were conducted to evaluate the proliferative capacity of COAD cells. The findings indicated that the colony formation rate in the MAN1B1 knockdown group was significantly lower than the control group (Figures 8C, D). To additionally explore the impact of MAN1B1 on cell invasion and migration, transwell and wound healing assays were conducted. The data revealed that reducing MAN1B1 expression reduced cells' invasion and migration capabilities (Figures 8E-I). Our results demonstrate that inhibiting MAN1B1 expression markedly suppresses COAD cell proliferation.

4 Discussion

CAFs constitute the most prevalent cell type in connective tissue, and their origin and function remain difficult to determine. Due to their phenotypic and functional heterogeneity, there is currently a lack of clear biomarkers (4, 20, 21). CAFs experience epigenetic modifications, releasing secretory factors that affect tumor angiogenesis, immune responses, and metabolism. Through intricate interactions with other cells, they actively contribute to tumor advancement (22, 23). Targeting specific CAF subtypes or converting CAFs into normal fibroblasts or anti-tumor phenotypes may offer therapeutic advantages for patients. However, in clinical practice, it is not always necessary to eliminate or reprogram CAFs. Blocking the signaling pathways from CAFs can also effectively achieve positive clinical outcomes. For example, targeting CXCL12 to antagonize the development of pancreatic cancer associated with FAP-expressing cancer-associated fibroblasts (24, 25). Nevertheless, the clinical application of CAFs in COAD presents challenges, prompting us to explore new CAF indicators. Analyzing the single-cell genome dataset, we identified a specific fibroblasts subset and developed a robust 11 CAFGs-related profile. The profile can predict prognosis, evaluate stromal components in the tumor microenvironment, and assess treatment responsiveness in COAD patients. Cox regression analyses established the CAFGs profile as an independent predictor of OS. To enhance its predictive precision and support clinical utility, we created and tested a nomogram incorporating age, M stage, and the CAFGs profile to forecast OS. The reliability of this model was confirmed through ROC and calibration curves, emphasizing its potential for clinical application. We also screened for chemotherapeutic drugs sensitive to high-risk populations, including gemcitabine, gefitinib, docetaxel, cephalexin, and sorafenib. These findings suggest that our model is reliable in predicting COAD prognosis and informing treatment decisions.

The tumor microenvironment and immunotherapy are crucial factors in the progression and treatment of COAD. Multiple studies have revealed the dynamic changes among various cell types and their interactions inside the COAD microenvironment through single-cell RNA sequencing and spatial transcriptomics technologies (26–29). Fibroblasts, as a key element of the tumor microenvironment, exhibit heterogeneity essential in regulating the tumor's immune environment (30). Cancer-associated fibroblasts expressing MMP14 within the tumor immune microenvironment could be a promising therapeutic option in advancing stage III COAD (31). Our findings indicate that infiltration levels of

10.3389/fimmu.2025.1532306

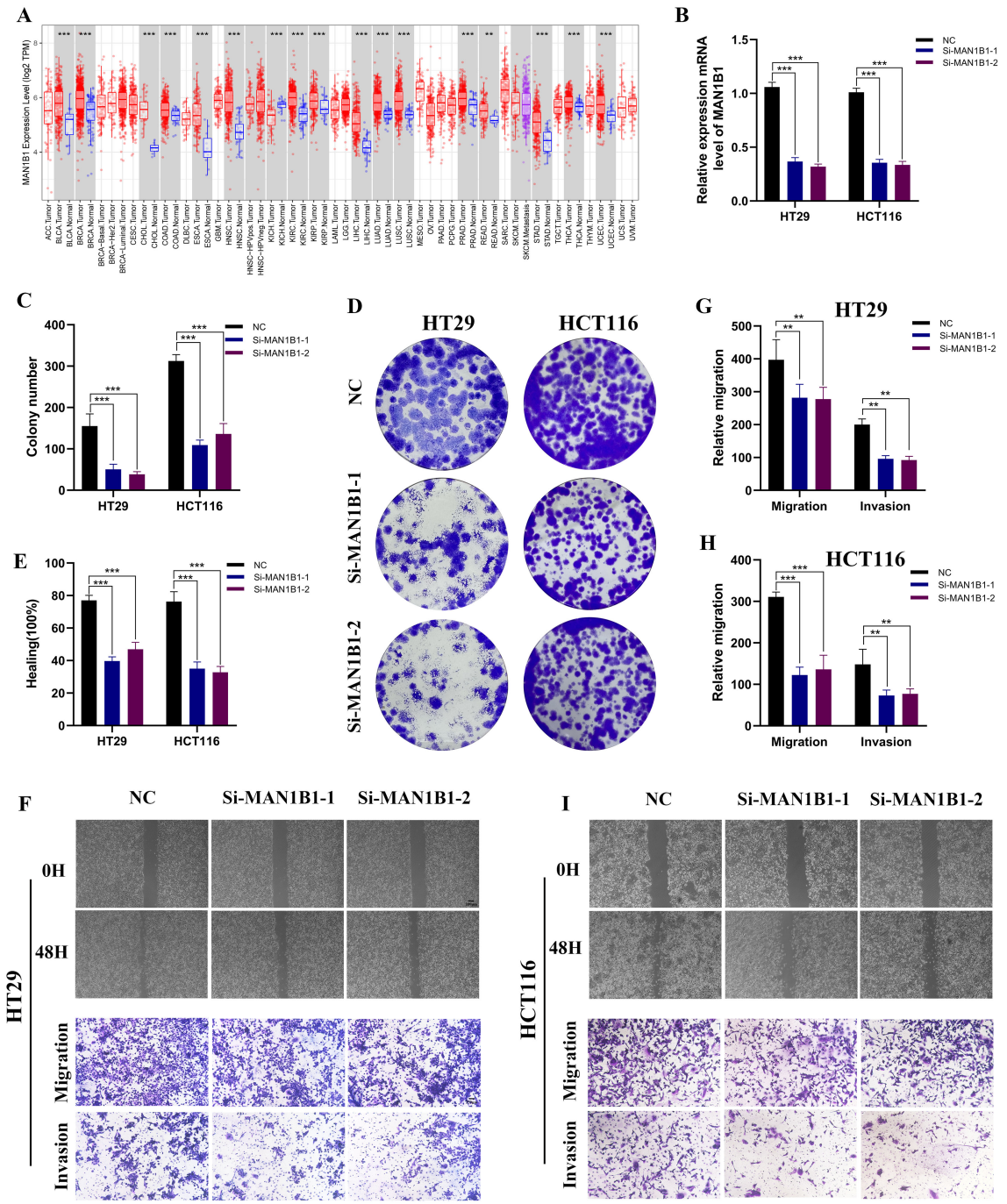

FIGURE 8
The impact of MAN1B1 in HCT116 and HT29. **(A)** The mRNA expression level of MAN1B1 in pan malignancies. **(B)** Following MAN1B1 knockdown, qRT-PCR showed a reduction in MAN1B1 expression. **(C, D)** As demonstrated by the cell colony formation experiment, cell proliferation was suppressed. **(E-I)** The capacity for invasion and migration dramatically reduced following the MAN1B1 knockdown. (**P < 0.01, ***P < 0.001).

immunosuppressive cells within the tumor tissues of high-risk COAD patients are significantly increased, including CD8 T cells, regulatory T cells, and tumor-associated macrophages. TAMs attract regulatory T cells (Tregs) by secreting the chemokine CCL2, establishing an immunosuppressive microenvironment in COAD (32, 33). Conversely, high-risk COAD patients have fewer NK cells in their tumor microenvironment. NK cells function as cytotoxic innate lymphocytes that kill tumor targets and coordinate immune responses through cytokines and chemokines (34, 35). Combining cetuximab with IL-2 and IL-15 boosts the cytotoxic activity of NK cells against COAD cell lines (36). We observed a notable increase in the expression of various immune checkpoint genes in the high-risk subgroup relative to the low-risk group, including PDCD1, PDCD1LG2 (PD-L1), TIGIT, and HAVCR2.

The overexpression of PD-L1 can reduce the cytolytic function of T cells, thereby greatly enhancing tumor progression (37). The anti-PD-1/PD-L1 interaction has proven effective in COAD immunotherapy (38). Based on our findings, COAD patients in the high-risk group could be more suitable candidates for immune checkpoint blockade treatment.

MAN1B1, a newly identified tumor-associated gene, encodes a class I alpha-1,2-mannosidase. Alterations in this gene are known to result in autosomal-recessive intellectual disability (39–41). Studies suggest MAN1B1 as a potential cancer therapy target, promoting bladder cancer progression and linked to poor outcomes (42). Hepatitis B virus facilitates liver cancer development by increasing MAN1B1 expression (43). A separate study indicated that miR-125b regulates liver cancer formation by targeting the product of the MAN1B1 gene (44). MAN1B1 was identified as a harmful predictor, highly expressed in most malignant tumors. *In vitro* studies showed that MAN1B1 knockdown reduced COAD cell growth and colony formation. Furthermore, cell migration and invasion capabilities were significantly diminished. These results suggest that MAN1B1 may contribute to the onset and advancement of COAD. Nonetheless, this research has certain constraints. Further validation of the CAFGs signature in larger, independent clinical cohorts to confirm its prognostic accuracy and clinical utility. Additionally, mechanistic studies are needed, particularly its interactions with stromal and immune cells in the tumor microenvironment. Finally, exploring the combination of CAFGs-based therapies with existing treatments, such as immune checkpoint inhibitors, could provide synergistic benefits and improve outcomes for COAD patients.

5 Conclusion

In this research, we developed and confirmed a CAFGs-related signature, a prognostic marker for individuals with COAD. Additionally, we showcased MAN1B1's role in colon adenocarcinoma via *in vitro* assays, suggesting its suitability as a potential target for COAD therapeutics. These results offer valuable insights for studies on anti-CAFs therapies, especially for individuals unresponsive to existing treatment strategies.

Data availability statement

The original contributions presented in the study are included in the article/Supplementary Material, further inquiries can be directed to the corresponding author/s.

Ethics statement

Ethical approval was not required for the studies on humans in accordance with the local legislation and institutional requirements because only commercially available established cell lines were used.

Author contributions

WZ: Conceptualization, Funding acquisition, Validation, Visualization, Writing – original draft, Writing – review & editing. CY: Investigation, Methodology, Supervision, Validation, Writing – original draft, Writing – review & editing. YL: Formal analysis, Supervision, Validation, Writing – original draft, Writing – review & editing. CT: Data curation, Formal analysis, Methodology, Writing – original draft, Writing – review & editing. MZ: Formal analysis, Methodology, Validation, Writing – original draft, Writing – review & editing. ZW: Data curation, Methodology, Software, Writing – original draft, Writing – review & editing. JG: Formal analysis, Supervision, Validation, Writing – original draft, Writing – review & editing. SH: Formal analysis, Validation, Visualization, Writing – original draft, Writing – review & editing. ZC: Project administration, Validation, Visualization, Writing – original draft, Writing – review & editing.

Funding

The author(s) declare that financial support was received for the research and/or publication of this article. This study was supported by the Youth Science Foundation Project of Anhui Medical.

Conflict of interest

The authors declare that the research was conducted in the absence of any commercial or financial relationships that could be construed as a potential conflict of interest.

Generative AI statement

The author(s) declare that no Generative AI was used in the creation of this manuscript.

Publisher's note

All claims expressed in this article are solely those of the authors and do not necessarily represent those of their affiliated organizations, or those of the publisher, the editors and the reviewers. Any product that may be evaluated in this article, or claim that may be made by its manufacturer, is not guaranteed or endorsed by the publisher.

Supplementary material

The Supplementary Material for this article can be found online at: https://www.frontiersin.org/articles/10.3389/fimmu.2025.1532306/full#supplementary-material

References

1. Li J, Ma X, Chakravarti D, Shalapour S, DePinho RA. Genetic and biological hallmarks of colorectal cancer. *Genes Dev.* (2021) 35:787–820. doi: 10.1101/gad.348226.120

2. Wang M, Zhao J, Zhang L, Wei F, Lian Y, Wu Y, et al. Role of tumor microenvironment in tumorigenesis. *J Cancer.* (2017) 8:761–73. doi: 10.7150/jca.17648

3. Chen K, Collins G, Wang H, Toh JWT. Pathological features and prognostication in colorectal cancer. *Curr Oncol.* (2021) 28:5356–83. doi: 10.3390/curroncol28060447

4. Luo H, Xia X, Huang LB, An H, Cao M, Kim GD, et al. Pan-cancer single-cell analysis reveals the heterogeneity and plasticity of cancer-associated fibroblasts in the tumor microenvironment. *Nat Commun.* (2022) 13:6619. doi: 10.1038/s41467-022-34395-2

5. Sewell-Loftin MK, Bayer SVH, Crist E, Hughes T, Joison SM, Longmore GD, et al. Cancer-associated fibroblasts support vascular growth through mechanical force. *Sci Rep.* (2017) 7:12574. doi: 10.1038/s41598-017-13006-x

6. Valencia T, Kim JY, Abu-Baker S, Moscat-Pardos J, Ahn CS, Reina-Campos M, et al. Metabolic reprogramming of stromal fibroblasts through P62-mtorc1 signaling promotes inflammation and tumorigenesis. *Cancer Cell.* (2014) 26:121–35. doi: 10.1016/j.ccr.2014.05.004

7. Mao X, Xu J, Wang W, Liang C, Hua J, Liu J, et al. Crosstalk between cancer-associated fibroblasts and immune cells in the tumor microenvironment: new findings and future perspectives. *Mol Cancer.* (2021) 20:131. doi: 10.1186/s12943-021-01428-1

8. Yamamoto Y, Kasashima H, Fukui Y, Tsujio G, Yashiro M, Maeda K. The heterogeneity of cancer-associated fibroblast subpopulations: their origins, biomarkers, and roles in the tumor microenvironment. *Cancer Sci.* (2023) 114:16–24. doi: 10.1111/cas.15609

9. Biffi G, Tuveson DA. Diversity and biology of cancer-associated fibroblasts. *Physiol Rev.* (2021) 101:147–76. doi: 10.1152/physrev.00048.2019

10. Cao Y, Fu L, Wu J, Peng Q, Nie Q, Zhang J, et al. Integrated analysis of multimodal single-cell data with structural similarity. *Nucleic Acids Res.* (2022) 50:e121. doi: 10.1093/nar/gkac781

11. Becht E, McInnes L, Healy J, Dutertre CA, Kwok IWH, Ng LG, et al. Dimensionality reduction for visualizing single-cell data using umap. *Nat Biotechnol.* (2018). doi: 10.1038/nbt.4314

12. Aran D, Looney AP, Liu L, Wu E, Fong V, Hsu A, et al. Reference-based analysis of lung single-cell sequencing reveals a transitional profibrotic macrophage. *Nat Immunol.* (2019) 20:163–72. doi: 10.1038/s41590-018-0276-y

13. Simon N, Friedman J, Hastie T, Tibshirani R. Regularization paths for cox's proportional hazards model via coordinate descent. *J Stat Softw.* (2011) 39:1–13. doi: 10.18637/jss.v039.i05

14. Chen W, Kang Y, Sheng W, Huang Q, Cheng J, Pei S, et al. A new 4-gene-based prognostic model accurately predicts breast cancer prognosis and immunotherapy response by integrating wgcna and bioinformatics analysis. *Front Immunol.* (2024) 15:1331841. doi: 10.3389/fimmu.2024.1331841

15. Zhong H, Chang L, Pei S, Kang Y, Yang L, Wu Y, et al. Senescence-related genes analysis in breast cancer reveals the immune microenvironment and implications for immunotherapy. *Aging (Albany NY).* (2024) 16:3531–53. doi: 10.18632/aging.205544

16. Li Z, Pei S, Wang Y, Zhang G, Lin H, Dong S. Advancing predictive markers in lung adenocarcinoma: A machine learning-based immunotherapy prognostic prediction signature. *Environ Toxicol.* (2024) 39:4581–93. doi: 10.1002/tox.24284

17. Yang W, Soares J, Greninger P, Edelman EJ, Lightfoot H, Forbes S, et al. Genomics of drug sensitivity in cancer (Gdsc): A resource for therapeutic biomarker discovery in cancer cells. *Nucleic Acids Res.* (2013) 41:D955–61. doi: 10.1093/nar/gks1111

18. Geeleher P, Cox N, Huang RS. Prrophetic: an R package for prediction of clinical chemotherapeutic response from tumor gene expression levels. *PloS One.* (2014) 9:e107468. doi: 10.1371/journal.pone.0107468

19. Li Y, Cai H, Yang J, Xie X, Pei S, Wu Y, et al. Decoding tumor heterogeneity in uveal melanoma: basement membrane genes as novel biomarkers and therapeutic targets revealed by multi-omics approaches for cancer immunotherapy. *Front Pharmacol.* (2023) 14:1264345. doi: 10.3389/fphar.2023.1264345

20. Kalluri R. The biology and function of fibroblasts in cancer. *Nat Rev Cancer.* (2016) 16:582–98. doi: 10.1038/nrc.2016.73

21. Melchionna R, Trono P, Di Carlo A, Di Modugno F, Nisticò P. Transcription factors in fibroblast plasticity and caf heterogeneity. *J Exp Clin Cancer Res.* (2023) 42:347. doi: 10.1186/s13046-023-02934-4

22. Chen Y, McAndrews KM, Kalluri R. Clinical and therapeutic relevance of cancer-associated fibroblasts. *Nat Rev Clin Oncol.* (2021) 18:792–804. doi: 10.1038/s41571-021-00546-5

23. Öhlund D, Elyada E, Tuveson D. Fibroblast heterogeneity in the cancer wound. *J Exp Med.* (2014) 211:1503–23. doi: 10.1084/jem.20140692

24. Sahai E, Astsaturov I, Cukierman E, DeNardo DG, Egeblad M, Evans RM, et al. A framework for advancing our understanding of cancer-associated fibroblasts. *Nat Rev Cancer.* (2020) 20:174–86. doi: 10.1038/s41568-019-0238-1

25. Feig C, Jones JO, Kraman M, Wells RJ, Deonarine A, Chan DS, et al. Targeting cxcl12 from fap-expressing carcinoma-associated fibroblasts synergizes with anti-pd-L1 immunotherapy in pancreatic cancer. *Proc Natl Acad Sci U.S.A.* (2013) 110:20212–7. doi: 10.1073/pnas.1320318110

26. Bruni D, Angell HK, Galon J. The immune contexture and immunoscore in cancer prognosis and therapeutic efficacy. *Nat Rev Cancer.* (2020) 20:662–80. doi: 10.1038/s41568-020-0285-7

27. Qi J, Sun H, Zhang Y, Wang Z, Xun Z, Li Z, et al. Single-cell and spatial analysis reveal interaction of fap(+) fibroblasts and spp1(+) macrophages in colorectal cancer. *Nat Commun.* (2022) 13:1742. doi: 10.1038/s41467-022-29366-6

28. Zhang Q, Liu Y, Wang X, Zhang C, Hou M, Liu Y. Integration of single-cell rna sequencing and bulk rna transcriptome sequencing reveals a heterogeneous immune landscape and pivotal cell subpopulations associated with colorectal cancer prognosis. *Front Immunol.* (2023) 14:1184167. doi: 10.3389/fimmu.2023.1184167

29. Xiao J, Yu X, Meng F, Zhang Y, Zhou W, Ren Y, et al. Integrating spatial and single-cell transcriptomics reveals tumor heterogeneity and intercellular networks in colorectal cancer. *Cell Death Dis.* (2024) 15:326. doi: 10.1038/s41419-024-06598-6

30. Davidson S, Coles M, Thomas T, Kollias G, Ludewig B, Turley S, et al. Fibroblasts as immune regulators in infection, inflammation and cancer. *Nat Rev Immunol.* (2021) 21:704–17. doi: 10.1038/s41577-021-00540-z

31. Makutani Y, Kawakami H, Tsujikawa T, Yoshimura K, Chiba Y, Ito A, et al. Contribution of mmp14-expressing cancer-associated fibroblasts in the tumor immune microenvironment to progression of colorectal cancer. *Front Oncol.* (2022) 12:956270. doi: 10.3389/fonc.2022.956270

32. Qian BZ, Pollard JW. Macrophage diversity enhances tumor progression and metastasis. *Cell.* (2010) 141:39–51. doi: 10.1016/j.cell.2010.03.014

33. Wang H, Tian T, Zhang J. Tumor-associated macrophages (Tams) in colorectal cancer (Crc): from mechanism to therapy and prognosis. *Int J Mol Sci.* (2021) 22(16):8470. doi: 10.3390/ijms22168470

34. Vivier E, Nunès JA, Vély F. Natural killer cell signaling pathways. *Science.* (2004) 306:1517–9. doi: 10.1126/science.1103478

35. Maia A, Tarannum M, Lérias JR, Piccinelli S, Borrego LM, Maeurer M, et al. Building a better defense: expanding and improving natural killer cells for adoptive cell therapy. *Cells.* (2024) 13(5):451. doi: 10.3390/cells13050451

36. Rocca YS, Roberti MP, Juliá EP, Pampena MB, Bruno L, Rivero S, et al. Phenotypic and functional dysregulated blood nk cells in colorectal cancer patients can be activated by cetuximab plus il-2 or il-15. *Front Immunol.* (2016) 7:413. doi: 10.3389/fimmu.2016.00413

37. Iwai Y, Ishida M, Tanaka Y, Okazaki T, Honjo T, Minato N. Involvement of pd-L1 on tumor cells in the escape from host immune system and tumor immunotherapy by pd-L1 blockade. *Proc Natl Acad Sci U.S.A.* (2002) 99:12293–7. doi: 10.1073/pnas.192461099

38. Xiao Y, Freeman GJ. The microsatellite instable subset of colorectal cancer is a particularly good candidate for checkpoint blockade immunotherapy. *Cancer Discovery.* (2015) 5:16–8. doi: 10.1158/2159-8290.Cd-14-1397

39. Rymen D, Peanne R, Millón MB, Race V, Sturiale L, Garozzo D, et al. Man1b1 deficiency: an unexpected cdg-ii. *PloS Genet.* (2013) 9:e1003989. doi: 10.1371/journal.pgen.1003989

40. Rafiq MA, Kuss AW, Puettmann L, Noor A, Ramiah A, Ali G, et al. Mutations in the alpha 1,2-mannosidase gene, man1b1, cause autosomal-recessive intellectual disability. *Am J Hum Genet.* (2011) 89:176–82. doi: 10.1016/j.ajhg.2011.06.006

41. Van Scherpenzeel M, Timal S, Rymen D, Hoischen A, Wuhrer M, Hipgrave-Ederveen A, et al. Diagnostic serum glycosylation profile in patients with intellectual disability as a result of man1b1 deficiency. *Brain.* (2014) 137:1030–8. doi: 10.1093/brain/awu019

42. Wang HF, Wu JH, Gai JW, Yang SQ, Ma QT, Ma HS, et al. Man1b1 is associated with poor prognosis and modulates proliferation and apoptosis in bladder cancer. *Gene.* (2018) 679:314–9. doi: 10.1016/j.gene.2018.09.022

43. You H, Zhang N, Yu T, Ma L, Li Q, Wang X, et al. Hepatitis B virus X protein promotes man1b1 expression by enhancing stability of grp78 via trim25 to facilitate hepatocarcinogenesis. *Br J Cancer.* (2023) 128:992–1004. doi: 10.1038/s41416-022-02115-8

44. Pan S, Cheng X, Chen H, Castro PD, Ittmann MM, Hutson AW, et al. Ermani is a target of mir-125b and promotes transformation phenotypes in hepatocellular carcinoma (Hcc). *PloS One.* (2013) 8:e72829. doi: 10.1371/journal.pone.0072829

frontiers | Frontiers in Immunology

TYPE Review
PUBLISHED 02 May 2025
DOI 10.3389/fimmu.2025.1580108

Check for updates

OPEN ACCESS

EDITED BY
Xiaosheng Tan,
Rutgers, United States

REVIEWED BY
Xin Luo,
University of Texas MD Anderson Cancer Center, United States
Yanjun Gao,
George Washington University, United States
Lida Zhu,
Santec, Japan

*CORRESPONDENCE
Tao Yan
yantao@cicams.ac.cn;
blizzardyt@163.com
Yi Liu
931160913@qq.com
Shuang Ma
1025085193@qq.com

†These authors have contributed equally to this work and share first authorship

RECEIVED 20 February 2025
ACCEPTED 14 April 2025
PUBLISHED 02 May 2025

CITATION
Ma S, Zhao G, Sui S, Chen X, Wu L, Wang T, Xu W, Lu Z, Wang A, Wu X, Wu J, Liu Y and Yan T (2025) Tumor microenvironment and immune-related myositis: addressing muscle wasting in cancer immunotherapy. *Front. Immunol.* 16:1580108. doi: 10.3389/fimmu.2025.1580108

COPYRIGHT
© 2025 Ma, Zhao, Sui, Chen, Wu, Wang, Xu, Lu, Wang, Wu, Wu, Liu and Yan. This is an open-access article distributed under the terms of the Creative Commons Attribution License (CC BY). The use, distribution or reproduction in other forums is permitted, provided the original author(s) and the copyright owner(s) are credited and that the original publication in this journal is cited, in accordance with accepted academic practice. No use, distribution or reproduction is permitted which does not comply with these terms.

Tumor microenvironment and immune-related myositis: addressing muscle wasting in cancer immunotherapy

Shuang Ma[1*†], Guangyu Zhao[1†], Shang Sui[2†], Xiankai Chen[3†], Linxin Wu[4†], Taihang Wang[4†], Wanying Xu[1†], Zhijiao Lu[5†], Andong Wang[1], Xiaolin Wu[6], Jiaxuan Wu[1], Yi Liu[7*] and Tao Yan[4*]

[1]School of Information Science and Engineering, Shenyang Ligong University, Shenyang, China, [2]St. John's Killmarnock School, Waterloo Region, ON, Canada, [3]Department of Thoracic Surgery, National Cancer Center/National Clinical Research Center for Cancer/Cancer Hospital, Chinese Academy of Medical Sciences and Peking Union Medical College, Beijing, China, [4]Department of Anesthesiology, National Cancer Center/National Clinical Research Center for Cancer/Cancer Hospital, Chinese Academy of Medical Sciences and Peking Union Medical College, Beijing, China, [5]Department of Radiology, Sun Yat-sen Memorial Hospital of Sun Yat-sen University, Guangzhou, China, [6]School of Mathematics and Statistics, Liaoning University, Shenyang, China, [7]Department of Anesthesiology, Shanxi Province Cancer Hospital/Shanxi Hospital Affiliated to Cancer Hospital, Chinese Academy of Medical Sciences/Cancer Hospital Affiliated to Shanxi Medical University, Beijing, China

Cancer immunotherapy, which leverages the immune system to target neoplastic cells, has undergone significant transformation in recent. However, immunotherapy may have negative effects on skeletal muscle function, causing muscle wasting and functional decline in cancer patients. In this study, we review the mechanisms by which immunotherapy influences skeletal muscle, focusing on immune-related myositis, inflammation, and metabolic alterations within the tumor microenvironment (TME). The key methodologies, including biomechanical assessment techniques such as electrical impedance myography and ultrasound imaging, are discussed to provide valuable insights into process that maintain muscle integrity and function in patients receiving immunotherapy. Moreover, the dual effects of immunotherapy on tumor suppression and muscle damage are described, revealing the significance of inflammatory cytokines, immune checkpoints, and metabolic disturbances within the TME. Importantly, we propose combination therapies integrating immunotherapy and nutritional interventions or anti-inflammatory interventions as potential approaches for mitigating muscle wasting. This study highlights the need for deeper investigations to optimize immunotherapy and improve its efficacy in preserving muscle health, thereby improving patient outcomes and quality of life.

KEYWORDS

cancer immunotherapy, tumor microenvironment, skeletal muscle, inflammatory cytokines, muscle wasting

1 Introduction

Cancer is a leading cause of mortality worldwide and recent advances have led to the discovery of new therapeutic approaches. Although conventional treatments such as surgery, radiotherapy, and chemotherapy can significantly improve survival rates of cancers patients (1), these treatments are often associated with substantial adverse side effects, particularly skeletal muscle dysfunction. In recent years, new discoveries in the field of immunotherapy have revolutionized cancer treatment strategies (2). By harnessing the patient's immune system to enhance tumor cell recognition and elimination, immunotherapy offers possess significant potential to treat complex diseases, but immune-related adverse events need to be addressed. For instance, patients undergoing immunotherapy often present with pronounced alterations in skeletal muscle function (3), such as immune-related myositis and, in some cases, myasthenia gravis. Although immunotherapy may cause some skeletal muscle damage, it has the following significant advantages over traditional therapies: a. Lower cytotoxicity: Immunotherapy mainly attacks tumor cells by activating or regulating the immune system rather than directly damaging cells, so it causes less direct damage to normal tissues and has lower cytotoxicity. b. Persistent immune memory: Immunotherapy can induce persistent immune memory, allowing patients to maintain long-term immune surveillance of tumors after treatment, which is not possible with traditional therapies. c. Better specificity: Immunotherapy generally has higher specificity and can more accurately identify and attack tumor cells, thereby reducing the impact on normal cells (4). Among these, PD-1/PD-L1 inhibitor therapy and CAR-T cell therapy will be the focus of this review. In light of the diverse immune-related adverse events associated with immunotherapy, this review specifically concentrates on immune-related myositis. Myositis represents one of the more prevalent and clinically significant muscle-related adverse events, characterized by inflammation and necrosis of muscle fibers, which culminates in muscle weakness and functional decline (5). Although other immune-related neuromuscular complications, such as myasthenia gravis, are also of considerable importance, myositis has been selected as the primary focus due to its higher incidence and its direct impact on muscle integrity and patient quality of life. A comprehensive understanding of the mechanisms and clinical manifestations of myositis is essential for the development of effective management strategies aimed at mitigating muscle toxicity and enhancing patient outcomes (6). Skeletal muscle functions as the principal effector organ for locomotor activity and plays a critical role in metabolic and immune regulation (7). Cancer progression and prolonged treatment often lead to muscle impairment, cachexia, and functional decline (8, 9). These advances have not only significantly improved patients' survival rates and quality of life, but also opened up new avenues for cancer treatment.

Cytotoxic pharmacological interventions, which are crucial to cancer treatment, induce dual-spectrum myocyte perturbations (both immediate and secondary) during neoplastic targeting (10). Contemporary investigations have shown that chemoimmunotherapeutic regimens not only elicit oxidative stress-mediated impairment of myocyte bioenergetic capacity but also accelerate myofibrillar catabolism by inducing pro-inflammatory cytokine cascades (11). Tumor environment (TME) is a major factor influencing cancer therapy (12). The TME actively facilitates tumor growth, metastasis, immune evasion, drug resistance, and therapeutic responsiveness and is defined as the complex milieu comprising non-neoplastic cells, extracellular matrix components, and signaling molecules surrounding tumor cells (12). Immunotherapy modulates the TME by altering the balance between immunostimulatory and immunosuppressive cells, thereby amplifying anti-tumor immunity (13). However, these modalities are associated with immune-mediated adverse events, particularly immunogenic myopathies, characterized by interleukin-driven multisystem cytokine dysregulation that propagates myocellular damage, culminating in the diminution of both oncological response metrics and patient-reported outcome measures (14). This pathophysiological interplay necessitates further investigations into immunotherapy-associated myocellular remodeling mechanisms (15), particularly the TME crosstalk dynamics, to develop musculoskeletal interventions that concurrently improve patient treatment while also ameliorating cancer survivorship trajectories (16). Therefore, it is particularly important to deeply explore the mechanism of the impact of immunotherapy on skeletal muscle function.

In recent year, several studies are increasingly studying the iatrogenic potential of immunotherapeutic modalities (17, 18), particularly their propensity to elicit myopathic sequelae through complex pathophysiological mechanisms (19). Researchers have directed their efforts to develop cytoprotective interventions, including immunoregulatory cell modulation, metabolic network reprogramming, and precision dosing that improve the musculoskeletal toxicity profiles of immuno-oncological agents (13). The iatrogenic manifestations of such patients extend beyond mere sarcopenic alterations, to include occurrence of systemic immunotolerance that undermines anti-tumor surveillance (20). Consequently, it is crucial to explore the bidirectional crosstalk between immunotherapeutic agents, the TMEal niche, and clarify their collective effect on myocellular homeostasis to improve the prognosis of patients (21).

In this review, we systematically examined the effects of immunotherapy on skeletal muscle function and its associated mechanisms (Figure 1). Initially, we investigated the mechanisms by which immunotherapy triggers immune-related adverse events (e.g.immune-mediated myositis) and systemic inflammatory responses that disrupt skeletal muscle biology and lead to muscle atrophy, cachexia, and functional decline. Subsequently, we evaluated the performance of currently used biomechanical assessment techniques to detect skeletal muscle injury, emphasizing their utility in monitoring immunotherapy-related muscular dysfunction. Finally, we discussed the bidirectional crosstalk between immunotherapy and the TME, particularly how immune checkpoint blockade (e.g., PD-1/PD-L1 inhibition) disrupts tumor immune evasion while causing unintended side effects on skeletal muscle homeostasis. Strategies for enhancing

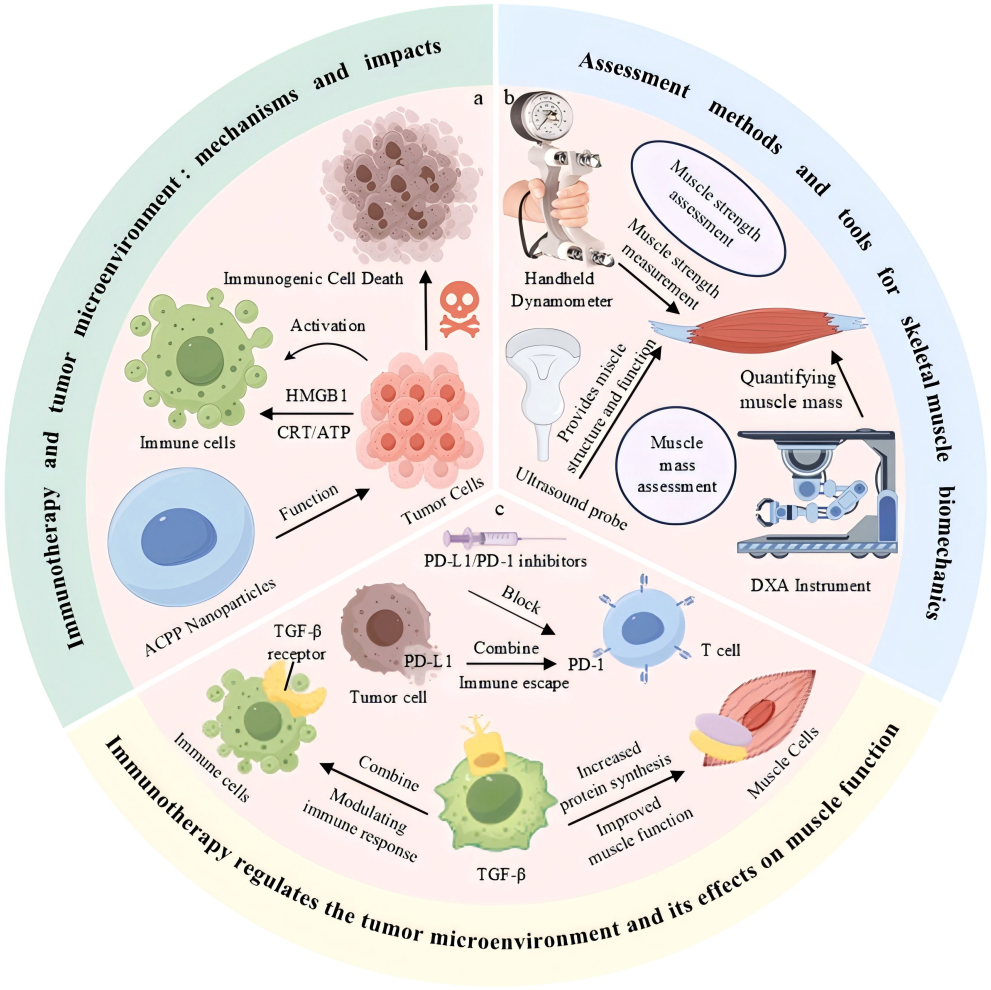

FIGURE 1
Immunotherapy modulates the tumor microenvironment and influences skeletal muscle function. **(a)** Immune activation and tumor cell death mediated by immunogenic signals. **(b)** Common tools for skeletal muscle strength and mass assessment. **(c)** Immunotherapeutic blockade of PD-1/PD-L1 and TGF-β pathways enhances immune response and improves muscle function

immunotherapy protocols, such as the temporal modulation of dosing, combination with anti-inflammatory agents, and precise targeting of TME components, have been proposed to prevent muscle toxicity while also enhancing anti-tumor efficacy.

2 Immunotherapy-mediated modulation of the TME and skeletal muscle function

2.1 Regulation of the TME by immunotherapy

In recent years, immunotherapy has emerged as a significant advancement in the treatment of tumors. This therapeutic approach functions by recognizing and targeting tumor cells through the activation or modulation of the patient's own immune system. Central to this process are the immune checkpoints PD-1 (programmed death receptor-1) and its ligand PD-L1, which play a crucial role in the regulation of T cell immune activity. Tumor cells frequently evade immune detection by overexpressing PD-L1, thereby suppressing T cell proliferation and function. Inhibitors of the PD-1/PD-L1 pathway counteract this evasion by blocking the interaction between PD-1 and PD-L1, thereby restoring T cell activity and enhancing anti-tumor immune responses, which has led to a marked improvement in the survival rates of patients with various malignant tumors (22). Additionally, CTLA-4 (cytotoxic T lymphocyte-associated protein 4) represents another pivotal immune checkpoint molecule. Inhibitors targeting CTLA-4 bind to this molecule on the surface of T cells, disrupting its interaction with CD80 and CD86 on antigen-presenting cells. This disruption enhances T cell activation and proliferation, thereby promoting robust anti-tumor immune responses (23). Chimeric antigen receptor T cell (CAR-T) therapy represents a pioneering advancement in cellular therapy. This approach

involves the genetic modification of a patient's T cells to express chimeric antigen receptors (CARs), which are designed to specifically target antigens on the surface of tumor cells, thereby augmenting the T cells' capacity to identify and eradicate malignant cells. CAR-T cell therapy has demonstrated substantial efficacy in the management of hematological malignancies; however, its application in the treatment of solid tumors is hindered by challenges such as immunosuppression within the TME (24). These immunotherapeutic strategies modulate the immune system through various mechanisms, offering novel prospects and methodologies for cancer treatment.

Recently, immunotherapy has shown great potential to treat cancer, by enhancing anti-tumor immune responses and modulating immune cell function within the TME (2, 19). The TME not only contains tumor cells but also immune cells, stromal cells, vasculature, extracellular matrix, and various signaling molecules (25). The intricate interactions among these components influence the tumor growth, metastasis, and immune evasion (25, 26). Immunotherapy aims to modify these elements to regulate the immune microenvironment, thereby enhancing the ability of the immune system to recognize and eliminate tumor cells (27). For instance, it significantly improves anti-tumor responses by activating immune cells, particularly T cells and natural killer (NK) cells, which enhances cancer treatment efficacy (28). Beside modulating conventional immune checkpoint inhibitors such as PD-1/PD-L1 inhibitors, immunotherapies that target specific immunosuppressive cells within the TME are increasingly recognized as promising therapeutic strategies (29). For instance, polymorphonuclear myeloid-derived suppressor cells (PMN-MDSCs) are involved in the regulation of immune suppression within the TME, facilitating immune evasion by inhibiting anti-tumor functions of immune cells (30). This, in turn, promotes tumor progression and metastasis. Therefore, targeting immunosuppressive cells to neutralize their effects within the TME is proposed as an alternative approach for improving immunotherapy research (31).

Metabolic reprogramming of tumor and immune cells is increasingly studies in recent years (32). Tumor cells often alter their metabolic pathways characterized by increased consumption of glucose, amino acids, and lipids to sustain their proliferation (33). Metabolic reprogramming within the TME not only supports tumor cell survival, growth, and metastasis but also affects immune cell function (34). For example, metabolic alterations in the TME can decrease immune cell activity by disrupting glycolysis in T cells, thereby reducing their anti-tumor capacity and fostering immune tolerance (34, 35). This indicates that modulating these metabolic pathways may be a novel therapeutic approach to enhancing immune responses and improving immunotherapy outcomes.

Long non-coding RNAs (lncRNAs) play major regulatory roles in the TME (36). Research has indicated that they influence immune cell function by modulating immune checkpoint expression, to alter immune cell-mediated anti-tumor activity and tumor progression (36, 37). The expression levels of lncRNAs affect the immune evasion, immunosuppression, and therapeutic responses in cancer (37). Consequently, the specific lncRNAs that modulate anti-tumor immune responses are being studies to provide modalities for patient treatment.

In summary, immunotherapy enhances anti-tumor immune responses by modulating immune cell composition, function, and metabolic characteristics within the TME (38). Therefore, research need to identify molecular targeting approaches to optimize the efficacy of immunotherapy. For instance, integrating immunotherapy with metabolic reprogramming, immunosuppressive cell targeting, and lncRNA regulation can promote the implementation of personalized, precise, and highly effective treatment strategies for patients with cancer.

2.2 Mechanistic interplay between immunotherapy and the TME

2.2.1 Immune checkpoint modulation

Immunotherapy significantly enhances anti-tumor immune responses by activating immune cells, inhibiting immune escape pathways, regulating cytokines, and remodeling the immunosuppressive microenvironment (39). However, these mechanisms may also lead to immune-related side effects, especially on skeletal muscle. While attacking tumor cells, T cells and NK cells activated by immunotherapy may mistakenly identify skeletal muscle cells as targets, triggering an inflammatory response (40, 41). In addition, the systemic inflammatory response and cytokine release induced by immunotherapy can aggravate muscle protein breakdown and mitochondrial dysfunction, affecting muscle function (42). Immune checkpoint inhibitors, including PD-1/PD-L1 and CTLA-4 inhibitors, have demonstrated significant efficacy in restoring immunological function and counteracting tumor immune evasion (43). These inhibitors specifically augment the tumoricidal potential of T cells by disrupting co-inhibitory signaling pathways, thereby achieving sustained clinical remission across various malignancies (43). Nonetheless, therapeutic resistance is prevalent among a substantial subset of patients, attributed to the emergence of immunologically "cold" tumor phenotypes. These phenotypes are characterized by inadequate infiltration of cytotoxic T-lymphocytes and impaired immune synapse formation within the TME (44). Research indicates that patients receiving PD-1 inhibitors may experience a higher incidence of immune-related myositis compared to those undergoing conventional therapies. Additionally, immune checkpoint inhibitors may modulate cellular senescence by facilitating the clearance of senescent cells, thereby diminishing the release of the senescence-associated secretory phenotype (SASP), which can indirectly confer beneficial effects on skeletal muscle function (45).

As depicted in Figure 2, Immunotherapy, while modulating the TME, also influences the process of cellular senescence, thereby exerting an indirect impact on skeletal muscle function (46). Cellular senescence can be categorized into two types: transient and permanent (47, 48). In transient senescence, normal cells enter a senescent state following damage or oncogenic stress (49), during

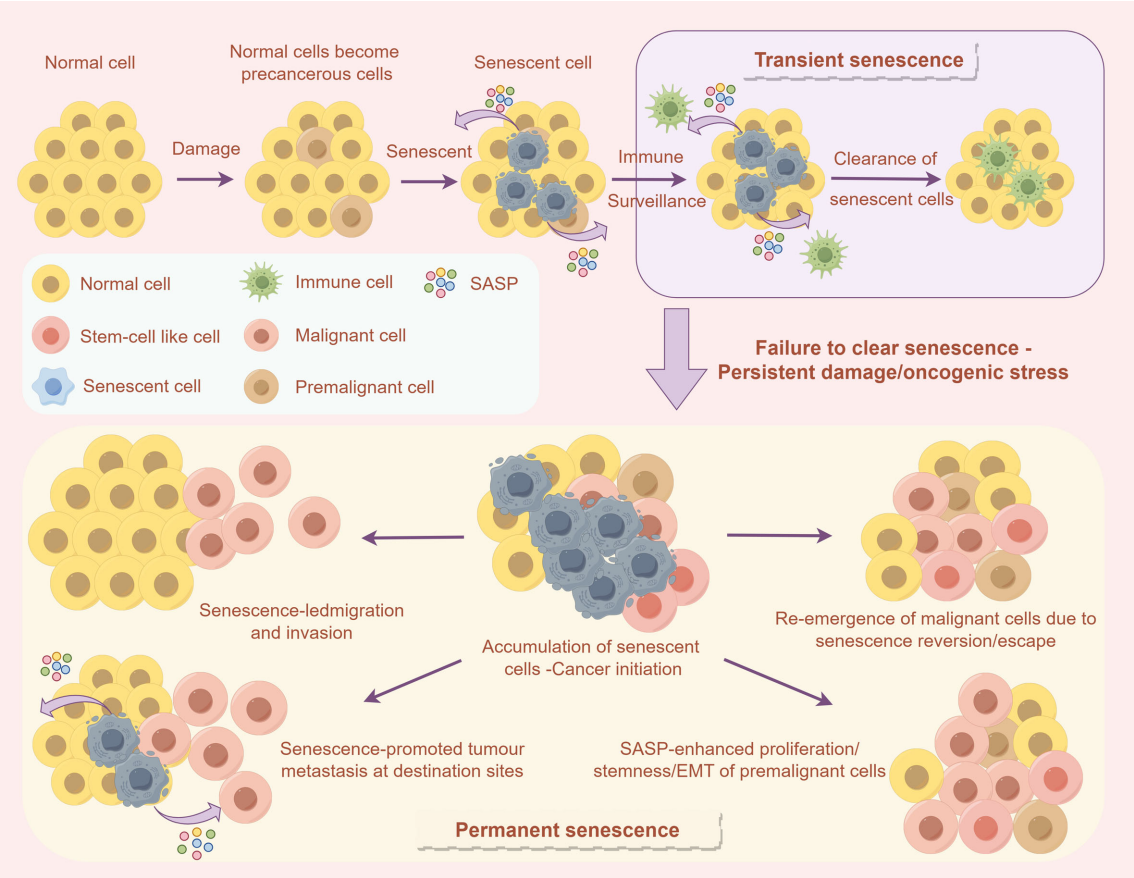

FIGURE 2
The influence of cellular senescence on the TME and immune response. The upper section describes how normal cells can enter a temporary senescent state following damage, subsequently being removed through immune surveillance. Conversely, the lower section explains that if senescent cells are not efficiently cleared, they may accumulate as a result of sustained damage or oncogenic stress. This accumulation can result in permanent senescence, thereby facilitating tumor initiation, invasion, and metastasis.

which the immune surveillance mechanism can eliminate these senescent cells, thereby maintaining tissue homeostasis (50). However, immunotherapy may disrupt this process (51). For instance, immune checkpoint inhibitors might indirectly facilitate the clearance of senescent cells and reduce the release of the senescence-associated secretory phenotype (SASP) by enhancing the immune system's attack on tumor cells, thus mitigating its adverse effects on muscle function (49, 51). Conversely, the inflammatory response induced by immunotherapy may expedite cellular senescence, elevate SASP secretion, and further impair muscle health (52). Consequently, comprehending the dual effects of immunotherapy on cellular senescence is crucial for thoroughly evaluating its impact on skeletal muscle function and for providing a foundation to optimize treatment strategies (53).

2.2.2 Cytokine-driven mechanisms

Immunotherapy-activated T cells and NK cells can mistakenly target skeletal muscle causing inflammation. Cytokines and chemokines have been shown to stimulate muscle cell apoptosis and protein breakdown, while also activating pathways like NF-κB and JAK-STAT to boost the secretion of inflammatory factors, creating a feedback loop that worsens muscle inflammation. Tumor necrosis factor-alpha (TNF-α) activates the NF-κB pathway, increasing muscle protein breakdown, while IFN-γ enhances the immune cell activity via activating the JAK-STAT pathway, which aggravates inflammation (54). The inflammatory response elicited by immunotherapy can activate downstream signaling cascades, notably the NF-κB pathway, which subsequently enhances the expression of proinflammatory cytokines, including TNF-α and IL-6. These cytokines exacerbate muscle protein catabolism and impair the regenerative capacity of muscle stem cells, leading to reduced muscle function (55). Clinical evidence from patients undergoing treatment with immune checkpoint inhibitors indicates that elevated cytokine levels are associated with an increased incidence of muscle weakness and fatigue. Management strategies, such as monitoring inflammatory markers and adjusting treatment regimens, can assist in mitigating these adverse effects (56).

2.2.3 Metabolic alterations

The impact of immunotherapy on skeletal muscle function is complex and involves a sophisticated interaction between

inflammatory and metabolic pathways (26). The inflammatory response induced by immunotherapy can activate downstream signaling cascades, such as the NF-κB pathway, which subsequently promotes the expression of proinflammatory cytokines, including TNF-α and IL-6. These cytokines not only intensify muscle protein catabolism but also impair the regenerative capacity of muscle stem cells, resulting in diminished muscle function (4). Metabolic disturbances within the TME further aggravate these effects by disrupting energy homeostasis and impairing contractile performance through the induction of oxidative stress and mitochondrial dysfunction in myofibers (57). Tumor cells frequently modify their metabolic pathways, which is evidenced by an increased uptake of glucose, amino acids, and lipids to support their proliferation (58). This metabolic reprogramming within the TME not only facilitates tumor cell survival, growth, and metastasis but also influences immune cell function. For example, metabolic changes in the TME can impair immune cell activity by disrupting glycolysis in T cells, thereby diminishing their anti-tumor efficacy and promoting immune tolerance (35). Nutritional interventions, such as high-protein diets and omega-3 fatty acids, may mitigate these metabolic effects and promote muscle health. Furthermore, the gut microbiota plays a pivotal role in modulating systemic inflammation and immune responses, presenting novel therapeutic opportunities to maintain muscle health during immunotherapy (59).

2.3 Comparison of the effects of immunotherapy and chemotherapy on skeletal muscle

Immunotherapy and chemotherapy represent two principal modalities in cancer treatment, each exerting distinct impacts on skeletal muscle function. Chemotherapeutic agents predominantly influence skeletal muscle via direct cytotoxic effects, culminating in muscle atrophy and diminished functionality (60). For instance, specific chemotherapeutic agents, including cyclophosphamide, doxorubicin, and docetaxel, affect muscle cells through various mechanisms, resulting in muscle weakness, fatigue, and atrophy. These agents may induce muscle protein degradation and mitochondrial dysfunction through pathways involving oxidative stress, inflammatory responses, and direct cellular damage. Immunotherapy augments the anti-tumor response by modulating the immune system; however, it may concurrently induce immune-related adverse effects and impair skeletal muscle function (61). Specifically, immune checkpoint inhibitors, such as PD-1/PD-L1 inhibitors, reinstate the immune system's capacity to identify tumors by obstructing the pathways utilized by tumor cells to evade immune surveillance. Nonetheless, this method of immune system activation can result in immune-related myositis, thereby affecting muscle function (62). Furthermore, the inflammatory response and metabolic alterations induced by immunotherapy may detrimentally impact skeletal muscle, leading to muscle protein degradation and mitochondrial dysfunction.

In contrast to chemotherapy, the impact of immunotherapy on skeletal muscle is primarily associated with the modulation and activation of the immune system. The engagement of immune cells and the subsequent release of inflammatory mediators can exert direct or indirect effects on the metabolism and structural integrity of muscle cells, thereby influencing muscle function (63). For instance, immunotherapy may alter muscle strength and endurance by elevating proinflammatory cytokine levels and facilitating the catabolism of muscle proteins. Specifically, the administration of immune checkpoint inhibitors can result in the hyperactivation of T cells and NK cells, which may erroneously target skeletal muscle cells, thereby initiating inflammatory responses and causing muscle damage. The impact of immunotherapy on skeletal muscle likely encompasses the modulation of muscle stem cells, such as satellite cells, which are crucial for muscle repair and regeneration following injury (64). Immunotherapy may influence the reparative and regenerative capabilities of muscles by altering the activity of these stem cells. For instance, immune checkpoint inhibitors may modify the microenvironment surrounding muscle stem cells, thereby affecting their proliferation and differentiation, which in turn could influence the restoration of muscle function (65).

Furthermore, the systemic inflammatory response induced by immunotherapy may indirectly impact skeletal muscle. Persistent inflammatory conditions can result in enhanced muscle protein catabolism and suppression of muscle protein synthesis, thereby exacerbating muscle atrophy and functional deterioration (66). This systemic effect may be particularly pronounced in patients undergoing prolonged immunotherapy. In clinical practice, the concurrent use of immunotherapy and chemotherapy necessitates careful consideration of their potential impacts on skeletal muscle function (67). A comprehensive understanding of the distinct mechanisms by which these treatments affect skeletal muscle is crucial for the development of more effective intervention strategies. Such understanding can aid in minimizing muscle toxicity and enhancing both the quality of life and treatment tolerance for patients (68). Future research should focus on investigating the long-term effects of immunotherapy and chemotherapy on skeletal muscle, as well as on formulating protective measures to optimize integrated treatment regimens.

In summary, immunotherapy and chemotherapy exert distinct mechanisms of action on skeletal muscle function, yet both can result in a deterioration of muscle performance. In clinical practice, it is imperative to thoroughly consider these effects. By designing and monitoring treatment plans judiciously, it is possible to mitigate damage to skeletal muscle, thereby enhancing therapeutic outcomes and improving patients' quality of life (69).

2.4 Effects of immunotherapy on muscle function: clinical evidence and mechanism discussion

Immunotherapy has achieved substantial advancements in the treatment of tumors; however, its impact on muscle function has

increasingly garnered scholarly attention. Clinical studies and case reports offer valuable insights into immunotherapy-induced muscle dysfunction and elucidate its potential mechanisms (70). In recent years, numerous clinical investigations have examined the effects of immunotherapy on muscle function. For instance, a retrospective study involving patients with non-small cell lung cancer found that approximately 15% of patients experienced varying degrees of muscle weakness and fatigue following treatment with PD-1 inhibitors, with 5% exhibiting more severe symptoms that impaired their daily activities (71). Additionally, a prospective cohort study reported that around 20% of melanoma patients receiving CTLA-4 inhibitors developed immune-related myositis, with 10% necessitating the suspension or discontinuation of treatment. In a clinical trial involving patients with renal cell carcinoma, approximately 12% of those treated with PD-1/PD-L1 inhibitors experienced symptoms of muscle weakness and fatigue, with 3% necessitating hospitalization (72). These findings indicate that immunotherapy-induced muscle dysfunction presents with a notable incidence and severity in clinical settings.

In clinical practice, there is a growing body of evidence documenting cases of muscle dysfunction induced by immunotherapy. For instance, a case series study identified five patients undergoing treatment with PD-1/PD-L1 inhibitors, three of whom exhibited progressive muscle weakness and atrophy, while two developed severe inflammatory myopathy (73). Muscle biopsies from these patients revealed significant inflammatory cell infiltration and necrosis within muscle fibers, suggesting that immunotherapy may directly target muscle tissue through immune system activation. Additionally, a separate case report describes a patient who underwent CAR-T cell therapy and subsequently experienced severe muscle atrophy and dysfunction, accompanied by a systemic inflammatory response (74). The muscle biopsy of this patient demonstrated extensive CD8+ T cell infiltration in muscle fibers, indicating that immunotherapy might directly affect muscle tissue by activating specific immune cells. These case reports underscore the potential risks associated with immunotherapy on muscle function, particularly in the context of long-term treatment.

Muscle dysfunction induced by immunotherapy is characterized by several underlying mechanisms. Firstly, immune checkpoint inhibitors play a crucial role by potentially misidentifying muscle cells as targets, thereby activating T cells and natural killer (NK) cells and initiating an inflammatory response (4). Secondly, the systemic inflammatory response elicited by immunotherapy can contribute to muscle weakness and atrophy through increased muscle protein degradation and mitochondrial dysfunction. Lastly, immunotherapy may exacerbate muscle dysfunction by impairing the activity of muscle stem cells, known as satellite cells, thus inhibiting muscle repair and regeneration (75). These mechanisms align with clinical observations of muscle dysfunction, such as weakness and atrophy, underscoring the multifaceted impact of immunotherapy on muscle function.

Data from clinical studies and case reports demonstrate a strong correlation with the aforementioned mechanisms. For instance, the infiltration of inflammatory cells and the presence of necrosis observed in muscle biopsies align with the effects of immune checkpoint inhibitors in activating T cells. Furthermore, the degradation of muscle proteins and mitochondrial dysfunction are consistent with the mechanisms underlying the systemic inflammatory response. These findings offer a theoretical foundation for the development of intervention strategies aimed at mitigating muscle toxicity associated with immunotherapy.

3 Assessment of skeletal muscle biomechanics

3.1 Evaluation of muscle strength

Conventional methods for evaluating muscle strength include the use of handheld and hydraulic dynamometers (76). A portable dynamometermeasures muscular strength by quantifying the force generated during maximal voluntary contractions (77). Grip strength assessments are also frequently performed using a hydraulic dynamometer specifically designed to evaluate forearm and hand grip strength, based on the principle of force measurement.

Although macro-assessment techniques can provide important parameters during testing, they do not sufficiently capture more complex changes within the muscles. To address these limitations, microscopic assessment methods such as dermatomechanical fiber testing have been proposed to obtain a more comprehensive understanding of muscle function (78, 79). To investigate the relationship between muscle fiber contraction force and calcium ion concentration, desmosomal fibers were subjected to a series of solutions with varying calcium ion concentrations (Figure 3A) (83). The collected data were subsequently fitted to Hill equations using GraphPad Prism software to calculate the calcium ion concentration (pCa50) and Hill coefficient (h) that produced the half-maximal force (Figure 3B) (83). The characteristic force-velocity and force-power curves for skeletal muscle behavior are presented in Figure 3C (84). PCa50 represents the negative logarithm of the calcium ion concentration required to elicit a half-maximal force, whereas the Hill coefficient reflects the steepness of the curve, indicating muscle sensitivity to changes in calcium ions. By analyzing the pCa50 and Hill coefficients to evaluate the mechanical properties of muscle fibers, these tests provided key insights into the specific effects of chemotherapy on muscle fiber characteristics. Various muscle function assessment techniques and their applications are shown in Table 1.

3.2 Evaluation of muscle mass

Traditional methods for assessing muscle mass primarily rely on imaging techniques that provide comprehensive information about muscle volume and density (84, 92). For instance, the Dual-Energy X-ray Absorptiometry (DXA) is a commonly used non-invasive approach for quantifying whole-body and regional muscle

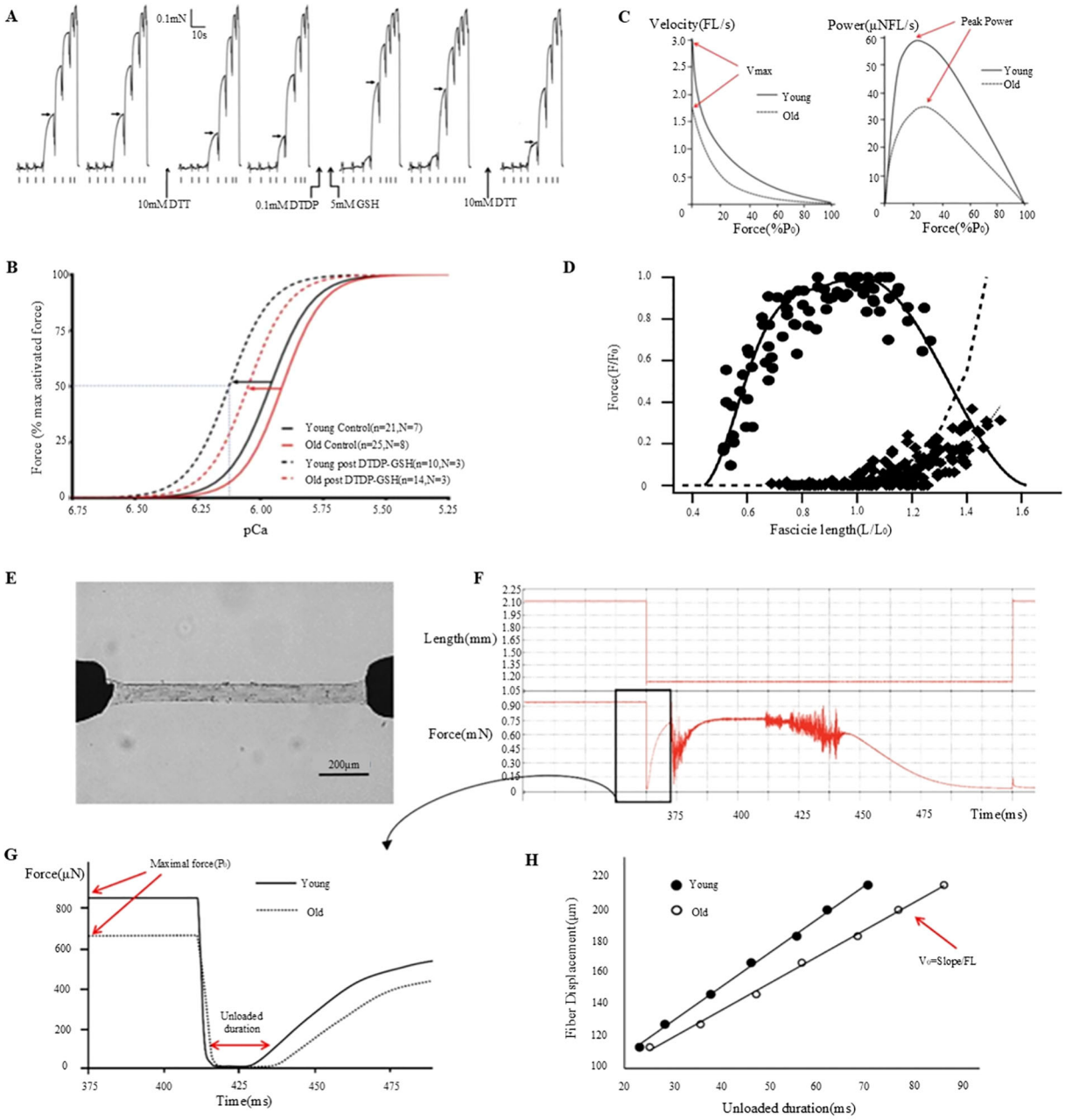

FIGURE 3
Muscle fiber mechanics and function: effects of DTT, DTDP, and GSH and age-related changes. **(A)** Investigation of the effects of DTT, DTDP, and GSH on the calcium sensitivity of the contractile apparatus in type II lateral femoral muscle fibers in elderly individuals (80). **(B)** Analysis of pCa50 and Hill coefficient values derived from Hill curves, based on the mean of individual fit values to the force-pCa relationship, plotted before (control) and after S-glutathionylation treatment for each type II muscle fiber in both young and elderly subjects (80). **(C)** Examination of the relationship between muscle velocity and force during isotonic contraction (81). **(D)** Assessment of the *in vivo* force-length relationship of the human soleus muscle (82). **(E)** Description of the experimental setup, which includes permeabilized fibers connected to a force transducer and servomotor (81). **(F)** Outline of the experimental procedure involving the transfer of fibers to an activation solution for relaxation testing (81). **(G)** Comparative analysis of the maximum force (Po) and no-load duration in type-I fibers of young and elderly subjects (81). **(H)** Quantification of the no-load duration across various relaxation lengths (81).

mass (84, 87). This technique can potentially differentiate muscle, fat, and bone tissues by contrasting X-ray absorption at various energy levels. DXA scans specifically measure muscle mass in appendages serving as important diagnostic indicators of sarcopenia (84, 93). The advantages of DXA include ease of administration, rapid scanning, and capability to capture muscle mass data from multiple bodily sites. Alternatively, Computed Tomography (CT) and Magnetic Resonance Imaging (MRI) offer higher resolution assessments of muscle mass, providing detailed insights into muscle anatomy and composition (94). These modalities facilitate the analysis of localized muscle alterations, including muscle atrophy or fat infiltration. In addition, CT and

TABLE 1 Principles, advantages and disadvantages of muscle assessment techniques.

Technology	Principle	Advantages	Limitations	References
Handheld Dynamometer	Measures force generated during maximal voluntary contraction	Portable, easy to use	Cannot capture complex internal muscle changes	(85)
Hydraulic Dynamometer	Specifically designed to assess forearm and hand muscle strength	High accuracy, reliable	Heavy, not easily portable	(80)
Skin Mechanical Fiber Testing	Stimulates muscle fibers using solutions with varying calcium ion concentrations	Directly reflects muscle contraction characteristics	Complex technique, requires specialized equipment	(86)
Dual-Energy X-ray Absorptiometry (DXA)	Measures muscle mass using X-ray absorption differences	High accuracy, comprehensive	Radiation exposure, high cost	(87)
Computed Tomography (CT)	Evaluates muscle volume and density using X-ray imaging	High resolution, detailed images	Radiation exposure, high cost	(88)
Magnetic Resonance Imaging (MRI)	Uses magnetic fields and radio waves to image muscle structures	No radiation, high soft tissue contrast	High cost, not suitable for patients with metal implants	(89)
Bioelectrical Impedance Analysis (BIA)	Measures muscle mass by assessing electrical current flow through the body	Portable, cost-effective	Accuracy affected by various factors	(81)
Ultrasound Imaging	Uses sound waves to monitor muscle structure and function in real-time	Non-invasive, real-time monitoring	Operator-dependent	(82)
Magnetic Resonance Elastography (MRE)	Combines MRI and vibration technology to assess muscle stiffness and elasticity	High precision, non-invasive	Expensive equipment, complex technology	(90)
Electrical Impedance Myography (EIM)	Measures muscle electrical impedance properties at different frequencies	Portable, cost-effective	Limited specificity, affected by external factors	(91)

MRI provide precise and high-resolution imaging data of muscle tissue. Bioelectrical Impedance Analysis (BIA) is used to quantify muscle mass by assessing the passage of electrical currents through the human body (95). In principle, it works on the fact that muscle and fat tissues exhibit conductivities distinct from those of electrical currents. Although BIA is easy to administer and is cost-effective, its accuracy is significantly influenced by the hydration status and operator proficiency. Although macro-assessment techniques provide a rapid overall evaluation during testing, they do not effectively capture deeper muscular alterations. To address these limitations, microscopic assessment techniques that utilize isolated permeable single-muscle fiber samples to examine the fundamental mechanical attributes of skeletal muscles have been proposed (96). Permeability fibers offer direct insights into the functionality of contractile proteins (such as myosin, actin, and other myosins) when activated at peak calcium concentrations (97). Measurements such as the maximum force (Po), specific force (force adjusted for cross-sectional area), and no-load shortening velocity (Vo) indicate the active mechanical properties of single muscle fibers. In Figure 3D, the essential procedures and measurements acquired through this method are detailed (84). Figure 3E depicts the experimental setup of the permeabilized fibers connected to a force sensor and servomotor (84). Figure 3F illustrates the process of transferring the fibers to an activation solution for relaxation testing (84). Figure 3G compares the maximum force (Po) and no-load duration (the time required for tension to re-establish itself) for young and old Type I fibers (84). Figure 3H shows the no-load durations measured at different relaxation lengths from which the no-load shortening velocity (Vo) was calculated (84).

Therefore, macro-level techniques for assessing muscle mass are advantageous for preliminary evaluation whereas microscopic methods provide a more comprehensive understanding of muscle functions and characteristics. This has been confirmed by studies investigating the effects of sarcopenia and aging on skeletal muscles, where microscopic assessments have demonstrated superior efficacy (84).

Integrating macro- and micro-measurements can help researcher obtain a more comprehensive understanding of muscle function across diverse movement patterns. Specifically, combining alterations in muscle fiber length, as quantified through ultrasound imaging, with joint kinematic data obtained via motion capture technology, can effectively reveal muscle function during specific movements, making it ideal for application in exercise training, rehabilitation therapy, and biomechanical research. The comprehensive nature of these measurements not only enhances our understanding of the muscular function in various athletic and daily activities, but also provides important ideas for improving muscle performance through targeted training or therapeutic interventions (Figure 3D) (84). This holistic methodology provides insights into the intricacies of muscle function and the scope of applications (84).

3.3 Evaluation of muscle function

Ultrasound imaging is a non-invasive, real-time assessment tool that is extensively utilized to assess muscle function (98, 99). This imaging technique offers various modes for evaluating muscle

structure and function, including A-mode, B-mode, M-mode, and Doppler mode. The A-mode or amplitude mode is a pioneering ultrasound imaging technique (17, 98, 99). It measures and displays the intensity of reflections from tissue interfaces using a single beam of sound (Figure 4A) (99). Although it is primarily to assess tissue thickness and locate reflective interfaces, A-mode ultrasound, although less commonly applied in clinical practice, it is used in specific scenarios. On the other hand, the B-mode, or Brightness mode, ultrasound imaging is the most frequently used modality (101). It can display muscle structure and morphology by generating grayscale images. In this mode, ultrasound waves are reflected as they pass through tissues, producing distinct gray values that correspond to the tissue density and structural characteristics (Figures 4B, D) (17, 99). M-mode, or Motion mode, ultrasound imaging is utilized to assess muscle activity during movement (17, 98, 99). It captures and displays the real-time trajectory of muscle

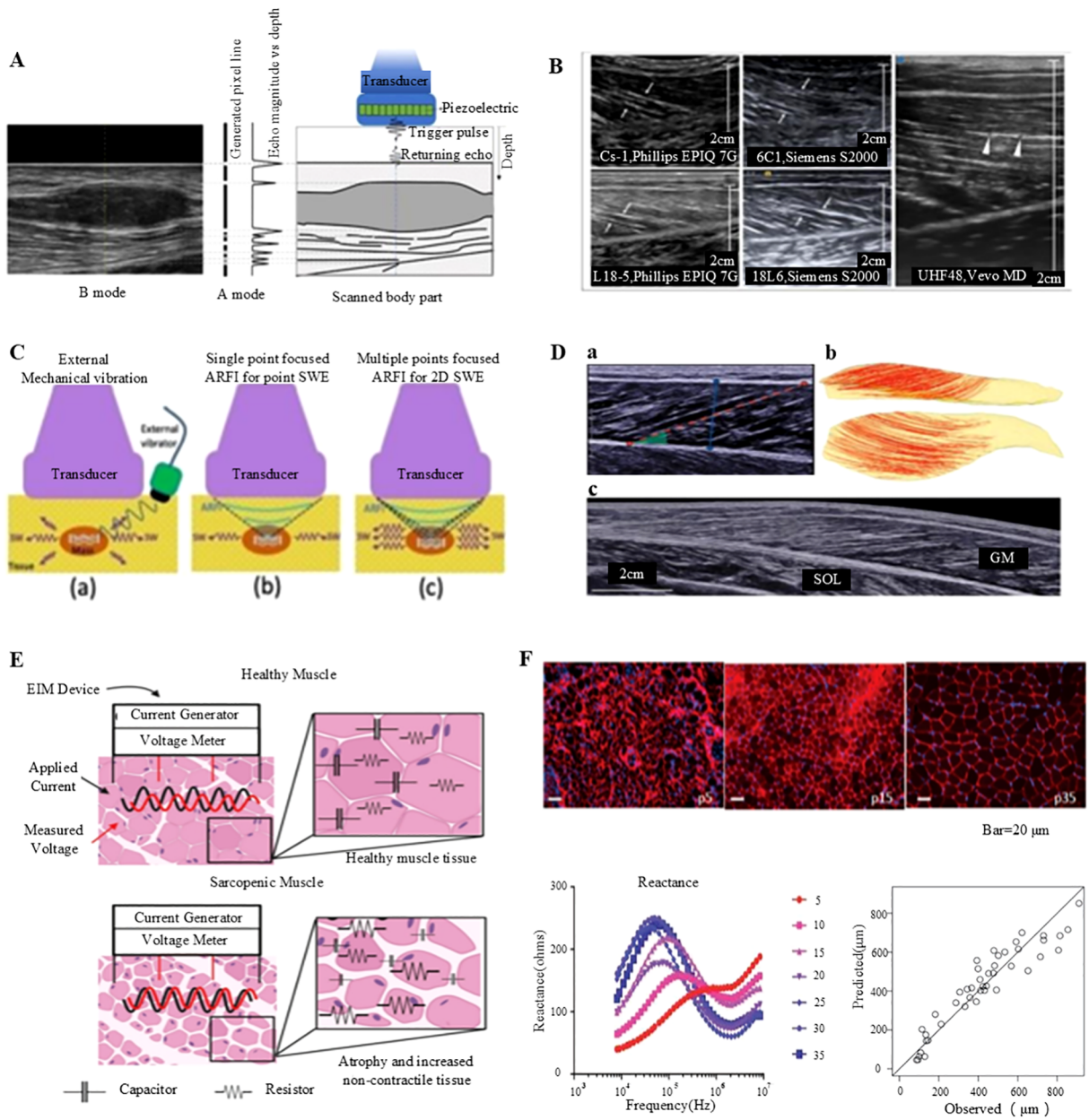

FIGURE 4
Non-invasive assessment of muscle function: ultrasound imaging and electrical impedance myography. **(A)** Generation of A- and B-mode ultrasonography (98). **(B)** Longitudinal B-mode ultrasound imaging of the medial gastrocnemius muscle in a healthy volunteer (98). **(C)** B-mode ultrasound imaging of the gastrocnemius muscle conducted with a linear transducer (98). **(D)** Comprehensive analysis of the medial gastrocnemius muscle (GM) utilizing ultrasonography: **(a)** B-mode ultrasound imaging performed with a linear transducer, **(b)** Diffusion tensor imaging (DTI) fiber reconstruction of the GM, and **(c)** Extended field-of-view ultrasound imaging of the GM (99). **(E)** Conceptual illustration of impedance measurements in healthy versus sarcopenic muscles, highlighting increased non-contractile tissue and reduced myocyte size (100). **(F)** Illustration of employing electrical impedance myography (EIM) data to predict muscle fiber size (100).

motion, making it particularly suitable for cardiac ultrasound and for evaluating muscle contractile function. Doppler-mode ultrasound imaging can assess blood flow by quantifying the shift in the frequency of the ultrasonic waves (102). This technique allows clinicians to identify and measure blood flow velocity and direction, providing important details regarding muscle blood supply and detecting vascular abnormalities. In ultrasound images, normal muscle tissue exhibits a homogeneous structure with moderate echogenicity, well-aligned fibers, and distinct continuous reflections of myofascial and fascial tissues (103). Any abnormalities such as muscle atrophy, fibrosis, or inflammation can be detected based on variations in echo characteristics (104).

The MRI technique is recognized as the definitive method for evaluating skeletal muscle mass and composition (68). This imaging modality provides highly precise and reproducible analysis of muscle volume and fat infiltration. The primary applications of MRI in skeletal muscle research are as follows.

3.3.1 Structural imaging

MRI generates high-resolution images of muscle structures, providing detailed visualization of muscle fiber arrangement and tissue status (68).

3.3.2 Magnetic resonance elastography

MRE uses MRI data to assess the tissue elasticity. Through the application of vibrations and measurement of the resultant displacements, MRE estimates the shear wave velocity and elasticity of the tissue, facilitating assessment of the muscle stiffness and elasticity (68).

Elastography is a technique employed to evaluate tissue stiffness and elasticity, classified into two main types. Quasi-static elastography measures tissue deformation in response to externally applied pressure, making it suitable for assessing the stiffness of superficial tissues (105). Conversely, dynamic elastography utilizes acoustic waves to determine the shear wave velocity within a tissue, and by analyzing this wave velocity, the tissue's modulus of elasticity can be obtained (106). This method provides a more precise assessment of the elastic properties of the deeper tissues. Elastography has several applications in skeletal muscle research, including evaluation of muscle stiffness, modulus of elasticity, and muscle damage (99, 106). In a previous study, shear wave elastography was employed to assess stiffness changes in rotator cuff tendinopathy, demonstrating a strong correlation with the MRI findings (Figure 4C) (99).

Electrical Impedance Myography (EIM) is a non-invasive assessment technique used to examine the muscle tissue structure and function based on the electrical impedance (107). It allows high-resolution and portable monitoring of muscle mass, adipose tissue content, and overall muscle health. In clinical practice, ultrasound imaging and EIM are the common modalities for assessing muscle function which is principally due to their non-invasive nature, real-time capabilities, and high-resolution data (100). The EIM technology employs parameters, such as resistance, reactance, and phase angle, vary with the frequency of the input current, providing important insights into the structure and integrity of the muscle (Figure 4E) (100). For instance, the EIM measurements of muscle fiber atrophy indicate increased resistance and decreased reactance values within a specific frequency range, accompanied with elevated fat infiltration which reduce resistance and decreases anisotropy ratios (108). Moreover, high glycogen accumulation and vacuole formation elevate both resistance and reactance values at high frequencies. Despite its numerous advantages, the EIM has certain limitations, including the need for highly standardized measurement techniques and it is mainly applicable for superficial muscle measurements. Thus, further technical advancements are necessary to optimize its performance in deeper muscles (Figure 4F) (100). Notwithstanding these limitations, the EIM is considered a robust tool for evaluating skeletal muscle health, owing to its rapid, cost-effective, portable, and user-friendly properties.

4 Impact of immunotherapy and immune microenvironment in tumor treatment

4.1 Application of immune checkpoint inhibitors

Programmed cell death protein 1 (PD-1) and its ligand, programmed death-ligand 1 (PD-L1), serve as pivotal immune checkpoints that regulate T cell immune responses (109). Tumor cells can circumvent immune detection by upregulating PD-L1 expression, which interacts with PD-1 on T cells, thereby suppressing T cell proliferation and effector functions (110). Inhibitors targeting the PD-1/PD-L1 axis disrupt this interaction, thereby restoring T cell activity and augmenting anti-tumor immune responses (Figure 5A). These immune checkpoint inhibitors not only induce apoptosis in tumor cells but also contribute to the modulation of immune homeostasis, suppression of chronic inflammation, and improvement of patient survival rates (111). In addition to their direct anti-tumor effects, PD-1/PD-L1 inhibitors have been shown to mitigate cancer-associated cachexia, a syndrome marked by significant muscle and fat loss that adversely affects quality of life and treatment tolerance (83, 112). These inhibitors achieve this by reducing the secretion of pro-inflammatory mediators and diminishing the activity of immunosuppressive cells, such as regulatory T cells and M2-type macrophages, thereby alleviating muscle atrophy (22). PD-1/PD-L1 inhibitors contribute to the improvement of the TME by modulating the metabolic activities of tumor-associated macrophages and enhancing the supply of oxygen and nutrients (22, 113). Specifically, these inhibitors can induce the polarization of macrophages from the M2 phenotype, which is associated with tumor promotion, to the M1 phenotype, which exhibits anti-tumor properties, thereby reducing immune suppression and mitigating muscle wasting (114). Furthermore, PD-1/PD-L1 inhibitors have the potential to preserve skeletal muscle mass by enhancing nutrient metabolism and promoting protein synthesis in patients with tumors (115). Evidence suggests that inhibition of the PD-1/PD-

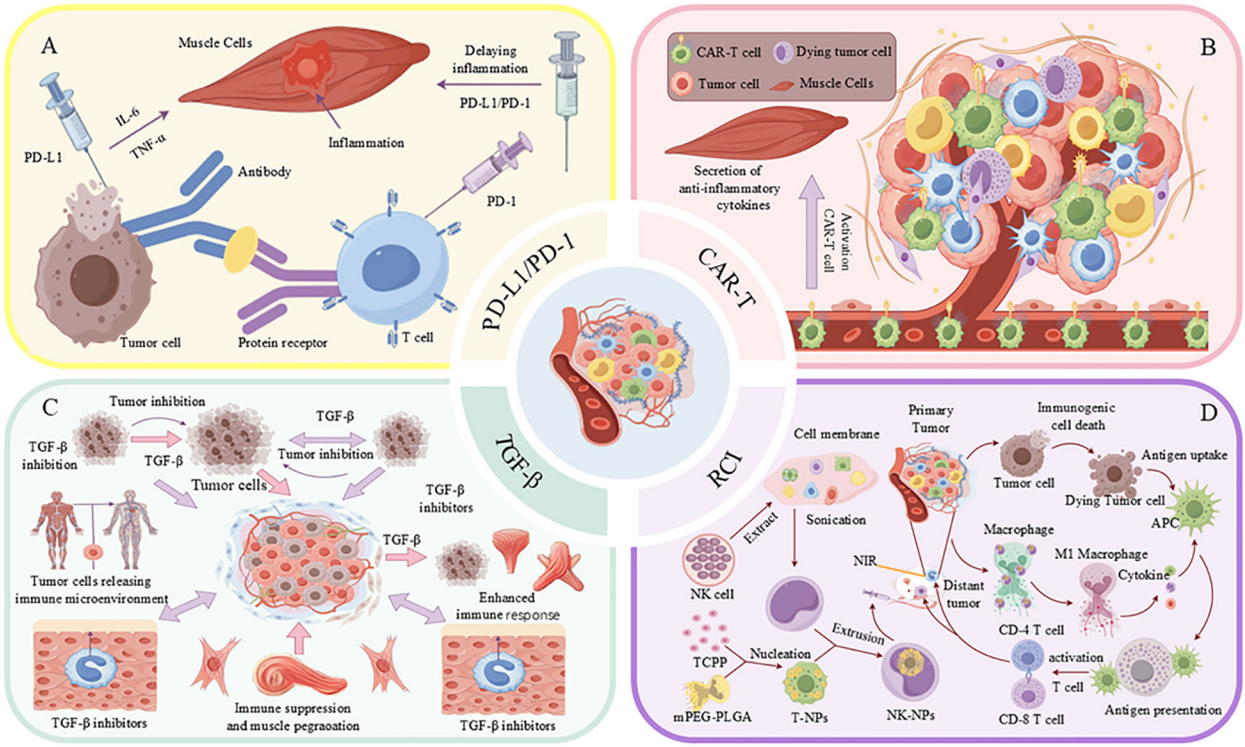

FIGURE 5
Strategies for combined treatment of tumors with immunotherapy and the TME. **(A)** Tumor cells impede the immune response through the interaction of PD-L1 with PD-1 on T-cells, while simultaneously inducing inflammation via the secretion of TNF-α and IL-6. **(B)** CAR-T cells contribute to the tumor microenvironment (TME) by secreting anti-inflammatory cytokines and activating M1-type macrophages. **(C)** Inhibition of TGF-β enhances the immune response and suppresses tumor growth. **(D)** The activation of immune cells through the application of nanoparticles, such as T-NPs and NK-NPs, in conjunction with near-infrared (NIR) light irradiation, facilitates anti-tumor immune responses.

L1 pathway can suppress muscle protein degradation pathways, including the ubiquitin-proteasome system and autophagy-lysosome systems, thus preventing muscle loss (116). Recent studies show that PD-1/PD-L1 inhibitors improve skeletal muscle function. A retrospective study found a 20% reduction in muscle wasting in non-small cell lung cancer patients treated with PD-1 inhibitors compared to those on conventional chemotherapy (117). Additionally, a prospective study reported improved muscle strength and a 30% decrease in severe muscle weakness in melanoma patients using these inhibitors. These benefits, which include anti-inflammatory effects and enhanced nutrient metabolism, suggest that PD-1/PD-L1 inhibitors help maintain muscle integrity and function (117, 118). Continued research is essential to further elucidate these mechanisms and optimize the therapeutic application of PD-1/PD-L1 inhibitors, potentially expanding their role in cancer treatment.

CTLA-4 inhibitors play a pivotal role in cancer immunotherapy by activating effector T cells to mitigate tumor-induced immunosuppression (119). These inhibitors function by binding to CTLA-4 on T cells, thereby preventing its interaction with CD80 and CD86 on antigen-presenting cells. This blockade facilitates the restoration of T cell activation and proliferation, thereby augmenting the anti-tumor immune response (120). Additionally, CTLA-4 inhibitors have the capacity to selectively deplete tumor-infiltrating regulatory T cells, a process mediated by macrophages with Fcγ receptors within the TME. Their efficacy in melanoma treatment is partly attributed to the elimination of Tregs (119). Clinical evidence substantiates the beneficial impact of CTLA-4 inhibitors on skeletal muscle function. A prospective study involving melanoma patients treated with ipilimumab, a CTLA-4 inhibitor, reported a 25% enhancement in muscle strength and a 15% reduction in symptoms of muscle wasting compared to those receiving standard therapy (120, 121). Additionally, a retrospective analysis of patients with advanced renal cell carcinoma indicated that individuals treated with CTLA-4 inhibitors exhibited decreased levels of pro-inflammatory cytokines, such as IL-6 and TNF-α, alongside improved muscle mass, as assessed by DXA (122). These findings imply that CTLA-4 inhibitors not only augment anti-tumor immunity but also ameliorate muscle wasting by attenuating systemic inflammation and enhancing metabolic homeostasis. The underlying mechanisms of these benefits include the depletion of immunosuppressive regulatory Tregs and the restoration of balanced immune responses, which collectively contribute to the preservation of muscle integrity and function (123). Furthermore, these inhibitors demonstrate potential in mitigating muscle wasting induced by inflammatory factors present in the TME (124). This modulation of the immune system not only addresses excessive immune reactions but also

maintains immune tolerance. In summary, CTLA-4 inhibitors enhance anti-tumor effects and provide novel strategies for managing muscle wasting in cancer therapy.

4.2 Association of CAR-T cell therapy with the treatment of tumor-induced muscle damage

CAR-T therapy demonstrates significant efficacy in the treatment of hematological malignancies; however, its application in solid tumors is impeded by the immunosuppressive TME (125, 126). This TME not only obstructs CAR-T cell functionality but also exacerbates cancer-related cachexia, a leading cause of mortality among patients with solid tumors (127). Pro-inflammatory cytokines, such as IL-6, TGF-β, and TNF-α, present within the TME, are implicated in the induction of muscle atrophy and dysfunction. Clinical evidence suggests that CAR-T cell therapy may inadvertently exacerbate muscle wasting in patients with solid tumors. A retrospective analysis of individuals with advanced colorectal cancer undergoing CAR-T therapy reported a 30% incidence of muscle weakness and atrophy, accompanied by elevated levels of pro-inflammatory cytokines, including IL-6 and TNF-α (128). In contrast, a preclinical study indicated that modifying CAR-T cells to secrete anti-inflammatory cytokines, such as IL-10, reduced muscle inflammation and preserved muscle function in murine models. These findings underscore the dual impact of CAR-T therapy on skeletal muscle, highlighting the necessity for strategies that mitigate muscle toxicity while enhancing anti-tumor efficacy (129). To enhance the effectiveness of CAR-T therapy and mitigate muscle damage, strategies have been proposed, including the engineering of CAR-T cells for prolonged persistence and the secretion of anti-inflammatory cytokines (Figure 5B), as well as the combination of CAR-T therapy with IL-6 inhibitors, TGF-β blockers, or metabolic regulators. Preclinical investigations indicate that targeting TGF-β can alleviate muscle wasting and enhance the anti-tumor efficacy of CAR-T cells (130–132). Current research endeavors focus on optimizing these strategies to improve both oncological outcomes and muscle health, thereby potentially enhancing patient survival and quality of life (133).

4.3 Modulation of the tumour microenvironment to improve muscle function

4.3.1 Anti-TGF-β therapy

The TGF-β is a major cytokine involved in the regulation of various biological processes, including cell growth, differentiation, apoptosis and immune regulation (134). However, in the TME, high TGF-β expression promotes tumor progression, immunosuppression, and treatment resistance (135). Studies have shown that TGF-β not only promotes tumor cell growth and metastasis, but also inhibits the body's immune surveillance function via multiple mechanisms, allowing tumor cells to evade immune attack (136). TGF-β promotes the expansion and accumulation of immunosuppressive cells (e.g., regulatory T cells, Tregs, and myeloid-derived suppressor cells, MDSCs), leading to the suppression of anti-tumor activity of effector T cells (137). This immunosuppressive effect reduces the ability of the immune system to eliminate tumor cells (Figure 5C). In addition, TGF-β can activate cancer-associated fibroblasts and induce extracellular matrix remodeling, leading to establishment of a conducive environment that favors tumor growth while preventing immune cell infiltration (138). Studies have shown that TGF-β can promote angiogenesis and increase the blood supply to tumor tissues, generating more oxygen and nutrients needed for tumor growth and metastasis. In addition, TGF-β increases the viability of tumor cells by regulating their metabolic pathways and promoting immune escape by altering energy metabolism.

Considering that TGF-β is an important component of the tumour microenvironment, its inhibition can be a promising therapeutic strategy. Inhibition of TGF-β improves the efficacy of immune checkpoint inhibitors, and overexpression of TGF-β expression causes tolerance to immune checkpoint inhibitors (for example, PD-1/PD-L1 and CTLA-4 antibodies), and that inhibition of TGF-β can reverse this tolerance, thereby increasing the response rate to immunotherapy (139). In addition, TGF-β inhibition enhances the Tregs and MDSCs accumulation as well as the anti-tumor activity of CD8+ T cells, resulting in enhanced TME and improved immune response (140). TGF-β inhibition also reduces the cancer cells invasiveness and metastatic potential to distant organs. When combined with other therapeutic approaches (e.g., radiotherapy, chemotherapy, and targeted therapies), TGF-β inhibitors exhibit synergistic effects, improving the overall therapeutic effect (141). Besides its role in cancer therapy, TGF-β inhibition can potentially address cancer-related muscle atrophy (cancer cachexia). In cancer patients, TGF-β was found to prevent loss of muscle mass and function by accelerating the degradation of muscle proteins through activation of the ubiquitin-proteasome pathway (UPS) and autophagy-lysosomal pathways. TGF-β inhibition suppressed the signalling of the pathways, slowing down muscle loss. Overexpression of TGF-β inhibits the proliferation and differentiation of muscle stem cells (satellite cells), decreasing their capacity for repair. TGF-β inhibition inhibits satellite cells and promotes muscle regeneration and repair. Elevated TGF-β expression was reported to be associated with chronic inflammation, which exacerbated muscle wasting (142). Other studies have reported that TGF-β inhibition can reduce the secretion of pro-inflammatory factors in the muscles, improving muscle function. TGF-β inhibition not only enhanced the anti-tumor immune response but also indirectly improved muscle health, improve the physical status and quality of life for patients. Therefore, high expression of TGF-β in the TME not only promotes cancer progression but also exacerbates muscle wasting. These findings indicate that anti-TGF-β therapy can treat cancer as well as cancer-related muscle atrophy. A combination of immunotherapy, chemotherapy, or targeted therapy, TGF-β inhibitors can provide better treatment effects, while preventing the decline in muscle function. Further clinical studies are needed to optimize TGF-β inhibition strategies to promote personalized

cancer treatment. Besides its use in cancer therapy, TGF-β inhibition can potentially improve cancer-related muscle wasting (cancer cachexia). Patients with cancer often experience loss of muscle mass and function, and TGF-β plays an important role in this process (142). TGF-β has been shown to accelerate the degradation of muscle proteins through the activation of the UPS and autophagy-lysosomal pathways, ultimately resulting in muscle atrophy. Inhibiting TGF-β activity mitigates the activation of these pathways, thereby decelerating muscle loss. Furthermore, research indicates that elevated levels of TGF-β suppress the proliferation and differentiation of muscle stem cells, known as satellite cells, which impairs the muscle repair process. The inhibition of TGF-β can restore the functionality of satellite cells, thereby facilitating muscle regeneration and repair. Additionally, high TGF-β expression is frequently correlated with chronic inflammation, which further exacerbates muscle wasting. By inhibiting TGF-β, the levels of pro-inflammatory factors within the muscle can be reduced, leading to improved muscle function. Notably, TGF-β inhibition not only enhances the anti-tumor immune response but also indirectly promotes muscle health, thereby enabling patients to maintain a better physical condition and quality of life. Moreover, elevated TGF-β expression within the TME not only facilitates cancer progression but also contributes to muscle wasting. Consequently, anti-TGF-β therapy emerges as a significant approach in cancer treatment and may represent a novel strategy for improving cancer-related muscle deterioration.

4.3.2 Targeting the muscle-tumor connection

Tumors negatively impact muscle function through the secretion of various factors, notably TNF-α, which contributes to muscle atrophy and dysfunction (143). TNF-α is a key pro-inflammatory cytokine implicated in muscle degradation across a range of diseases. In the context of cancer cachexia, elevated TNF-α levels facilitate muscle protein degradation and the consequent loss of muscle mass. Furthermore, TNF-α exacerbates muscle degradation by interacting with its receptor and activating several downstream signaling pathways, including the NF-κB pathway (144). Pharmacological interventions targeting TNF-α and its signaling pathways, such as TNF inhibitors, have demonstrated potential in delaying muscle wasting in preclinical studies. These agents mitigate the inflammatory response by inhibiting TNF-α activity, thereby decelerating muscle protein breakdown and the progression of muscle atrophy. Nonetheless, despite promising outcomes in animal models, the clinical efficacy of TNF inhibitors remains inconsistent, potentially due to individual variability and the complexity of the disease (145). Other cytokines, including interleukin-6 (IL-6), play a significant role in muscle wasting. Empirical evidence suggests that IL-6 exacerbates muscle wasting by exerting deleterious effects on muscle tissue. In addition to TNF-α inhibitors, alternative anti-inflammatory strategies, such as IL-6 inhibitors and TGF-β blockers, present promising approaches for alleviating muscle wasting. IL-6, a pro-inflammatory cytokine, has been demonstrated to contribute to muscle atrophy by facilitating protein degradation and hindering muscle regeneration (146). Transforming growth factor-beta (TGF-β), recognized for its involvement in immune evasion and fibrosis, also promotes muscle wasting by enhancing the activity of proteasome systems (147). Targeting these cytokines may reduce muscle protein degradation and enhance muscle function. In conclusion, a comprehensive approach is essential for addressing the interplay between muscle and tumor, which involves targeting pro-inflammatory cytokines such as TNF-α, IL-6, and TGF-β, in conjunction with nutritional interventions aimed at supporting muscle health. Future research should prioritize the optimization of these strategies to enhance clinical efficacy and improve patient outcomes.

4.4 Combination therapy

4.4.1 Radiotherapy with immunomodulators

The mechanism of action of radiotherapy in cancer treatment extends beyond the direct cytotoxic effects on tumor cells, incorporating the enhancement of the immune response through the release of tumor antigens (148) This immunostimulatory effect primarily arises from radiotherapy-induced immunogenic cell death (ICD), which is marked by the emission of damage-associated molecular patterns (DAMPs) and tumor antigens. These elements are capable of activating both innate and adaptive immune responses, thereby facilitating the immune system's recognition and elimination of tumor cells. Furthermore, radiotherapy can augment the anti-tumor immune response by modifying the TME, promoting the infiltration and activation of immune cells (149). Combining radiotherapy with immunomodulators can further mitigate tumor- and treatment-induced systemic inflammation and muscle damage. For instance, the integration of radiotherapy with immune checkpoint inhibitors may produce a synergistic effect, enhancing the anti-tumor immune response and potentially improving clinical treatment outcomes (150). This combination therapy not only facilitates the immunogenic demise of tumor cells but also augments their capacity to identify and eradicate tumors through the activation of immune cells, including T cells and NK cells. Moreover, radiotherapy can bolster tumor-specific immunity by eliciting an acute inflammatory response, thereby enhancing therapeutic efficacy. As illustrated in Figure 5D, radiotherapy can potentiate the immune system via near-infrared (NIR) light irradiation by activating nanoparticles that encapsulate components derived from tumor cell membranes or NK cell membranes, which mimic tumor antigens and further stimulate the immune response (151). These nanoparticles amplify the immune system's assault on tumors by promoting the activation of immune cells and inflammatory responses within the TME.

Radiotherapy also promotes the polarization of macrophages from the immunosuppressive M2 type to the anti-tumor M1 type, thereby enhancing the anti-tumor immune response in the TME (152). In conclusion, radiotherapy not only controls tumors through direct cytotoxic effects but also enhances systemic anti-tumor immune responses through complex immunomodulatory mechanisms. The understanding and application of such

mechanisms provide a theoretical basis for the combination of radiotherapy and immunotherapy, which may offer new hope for cancer treatment. By studying the interaction between radiotherapy and immunomodulators in detail, we can develop more effective cancer treatment protocols that not only control the growth and spread of tumors but also improve the quality of life and prognosis of patients.

4.4.2 Integrating immunotherapy with nutrition

Malnutrition and tumor-induced metabolic disorders are significant factors contributing to the decline in muscle function among cancer patients. Cancer cachexia, marked by ongoing muscle degeneration and dysfunction, is a common and debilitating condition (153). Studies have emphasized the impact of inflammation and oxidative stress in disrupting the pathways of muscle protein synthesis and degradation, resulting in muscle wasting (154). In response to this issue, nutritional interventions are increasingly being recognized for their potential to mitigate these adverse effects. High-protein diets play a critical role in supplying the amino acids required for muscle protein synthesis, thereby mitigating the catabolic effects associated with cancer and its treatment. Certain amino acids, notably leucine, have been demonstrated to activate the mTOR pathway, which is vital for facilitating muscle growth and preventing atrophy (155). Additionally, omega-3 fatty acids, present in fish oil, enhance this strategy by diminishing the production of pro-inflammatory cytokines such as TNF-α and IL-6, which are involved in muscle protein degradation. Research suggests that omega-3 supplementation can enhance muscle function and alleviate fatigue in cancer patients undergoing immunotherapy (156). The integration of immunotherapy with specific nutritional strategies presents a synergistic approach to improving treatment outcomes. For instance, the combination of immune checkpoint inhibitors with high-protein diets and omega-3 fatty acids has the potential to enhance anti-tumor immune responses and promote muscle health (157). This approach not only fortifies the immune system but also mitigates the inflammatory burden associated with muscle wasting.

Additional anti-inflammatory supplements, such as curcumin and green tea extract, may contribute to improved muscle health by inhibiting NF-κB signaling, thereby mitigating inflammation and oxidative stress in muscle tissue (158). Considering the diverse nutritional status and metabolic requirements of cancer patients, it is essential to develop individualized nutritional plans based on metabolic profiling and inflammatory markers to optimize treatment efficacy and minimize adverse effects (157). Future research should focus on examining the long-term effects of integrating immunotherapy with nutritional interventions. Clinical trials are necessary to establish standardized protocols for nutritional support in cancer patients undergoing immunotherapy. Investigating the role of gut microbiota in modulating immune responses and muscle health offers a novel avenue for intervention (157). In conclusion, the integration of immunotherapy with nutritional interventions represents a promising strategy for enhancing treatment efficacy and improving patient quality of life. By addressing both the tumor and its effects on muscle health, these combined approaches aim to achieve improved clinical outcomes in cancer management.

5 Challenges and future directions

In recent years, immunotherapy has made remarkable progress in the treatment of tumors, particularly in the regulation of the TME. However, this field still faces several challenges that limit its widespread application and therapeutic effects. Moreover, the impact of immunotherapy on skeletal muscle and its potential role in muscle preservation or damage during cancer treatment remain underexplored, necessitating further investigation (75).

First, the complexity and diversity of the TME severely restrict the efficacy of immunotherapy. The TME contains a variety of cellular components, cytokines, blood vessels, and stroma that interact to create an environment that supports tumor growth and metastasis while suppressing immune responses (159). For example, hypoxia is a prominent feature of the TME, and studies have shown that it not only affects the metabolism and growth of tumor cells but also facilitates immune escape, which severely weakens the efficacy of immunotherapy. A hypoxic environment enhances tumor immune evasion by promoting the accumulation of immunosuppressive cells (e.g., Tregs and MDSCs) and inducing the expression of immune checkpoints. Therefore, modulation of the hypoxic microenvironment has become an important strategy for improving immunotherapy efficacy. Additionally, recent evidence suggests that hypoxia and inflammation in the TME may also contribute to muscle wasting in cancer patients (159). Chronic systemic inflammation and immune dysregulation associated with immunotherapy could exacerbate skeletal muscle atrophy, further impairing patients' quality of life and treatment outcomes.

The introduction of nanotechnology offers new solutions to address these challenges. Nanomaterials have unique physicochemical properties that allow them to play a crucial role in targeted drug delivery and TME modulation. They can enhance the efficacy of immunotherapy by improving drug targeting and penetration (160). In particular, nanomaterials can improve the response rate of immunotherapy by penetrating tumor tissues, targeting tumor cells, and reducing immunosuppressive factors in the TME. Additionally, nanotechnology can be used to carry immunomodulators, such as immune activators, cytokines, or immune checkpoint inhibitors, which directly enhance immune cell function and enable the immune system to recognize and attack tumor cells more effectively. These advances highlight the great potential of nanotechnology in improving immunotherapy, particularly for cancer treatment (70). However, the effects of nanotechnology-based immunotherapy on skeletal muscle remain unclear. Given that systemic immune activation can lead to muscle inflammation and oxidative stress, nanomaterials must be carefully designed to minimize unintended adverse effects on muscle tissue while maintaining their anti-tumor efficacy.

Despite progress in immunotherapy and TME modulation, many pressing issues still need to be addressed. One major challenge is the effective combination of immunotherapy with other therapeutic approaches (e.g., chemotherapy, radiotherapy, or targeted therapies) to achieve a more integrated treatment effect. Combining different therapeutic strategies can exploit their respective strengths, overcome the limitations of single therapies, and improve treatment efficacy and tolerability (70). Additionally, immune escape and drug resistance remain significant hurdles. Tumor cells evade immune surveillance by constantly altering surface markers and inducing an immunosuppressive microenvironment, which not only leads to immunotherapy failure but also contributes to tumor recurrence and metastasis. Overcoming these immune escape mechanisms and restoring the anti-tumor function of the immune system remains a critical area of current research. Moreover, cancer-induced muscle loss, or cachexia, remains a major challenge in cancer treatment. Immunotherapy-induced cytokine release may exacerbate muscle protein degradation pathways, leading to further muscle atrophy (161). Therefore, strategies to mitigate muscle loss, such as incorporating anti-inflammatory agents, exercise interventions, or metabolic modulators alongside immunotherapy, warrant further investigation.

In terms of emerging therapeutic approaches, CAR-T cell therapy has shown great potential. By genetically engineering patients' T cells to express CARs, these modified T cells can specifically recognize and kill tumor cells expressing certain antigens (162). However, the application of CAR-T cell therapy in solid tumors is limited by the immunosuppressive nature of the TME. To overcome this, researchers have developed several strategies, such as genetically modifying CAR-T cells to enhance their survival and anti-tumor activity within the TME. For instance, CAR-T cells can be engineered to secrete anti-inflammatory cytokines (e.g., TGF-β), which not only boost the anti-tumor immune response but also protect muscle tissue from inflammatory damage. Additionally, combining CAR-T cell therapy with other treatments like IL-6 inhibitors, TGF-β blockers, or metabolic modulators can simultaneously improve muscle mass and function (131). Preclinical studies have demonstrated that targeting TGF-β can reduce muscle wasting and enhance the anti-tumor effect of CAR-T cells in mouse models of malignant disease. This suggests that by modulating key factors in the TME, muscle function can be protected and restored while enhancing CAR-T cell therapy efficacy.

Another emerging area is the development of novel immune checkpoint modulators. Beyond the well-studied PD-1/PD-L1 and CTLA-4 inhibitors, new inhibitors targeting other immune checkpoints such as TIM-3 and LAG-3 are under development. These novel inhibitors hold promise for overcoming resistance to existing immunotherapies and could be effective in treating different types of cancer (120). Furthermore, combining multiple immune checkpoint inhibitors has shown promising results, as blocking several inhibitory pathways at once can more comprehensively activate the immune system and enhance the intensity and durability of the anti-tumor immune response.

In terms of combination strategies, the integration of immunotherapy with anti-inflammatory treatments offers a new avenue for reducing muscle damage. Nonsteroidal anti-inflammatory drugs (NSAIDs) and selective COX-2 inhibitors can reduce muscle inflammation and injury by inhibiting inflammatory responses (163). For example, using NSAIDs in patients receiving immune checkpoint inhibitors has been shown to significantly decrease the incidence and severity of immune-related myositis. Moreover, nutritional interventions during immunotherapy have shown potential for muscle protection. Diets rich in omega-3 fatty acids and high-quality proteins can enhance muscle anti-inflammatory capacity and regenerative potential, reducing muscle atrophy. Clinical trials have indicated that such nutritional support can improve muscle strength and quality of life in patients undergoing immunotherapy.

New interventions such as gene editing technology are also being explored to optimize immunotherapy and protect muscle function (164). Using tools like CRISPR/Cas9, researchers can precisely modify immune cells to enhance their anti-tumor activity while reducing toxicity to normal tissues. For example, T cells can be edited to delete genes that may cause autoimmune reactions or to insert genes that enhance their ability to recognize and target tumors (165). Additionally, gene editing can be applied to regulate inflammatory and apoptotic pathways within muscle cells, thereby reducing muscle injury caused by immunotherapy.

The combination of immunotherapy and exercise intervention is another emerging research direction. Regular exercise can increase muscle strength and endurance, improve muscle metabolism, and reduce immunotherapy-related muscle toxicity (84). Research has shown that exercise can activate anti-inflammatory signaling pathways in muscles, reducing the production of inflammatory cytokines while promoting muscle protein synthesis and mitochondrial function recovery. This combined approach not only helps maintain and enhance muscle function but also improves patients' tolerance and adherence to immunotherapy (84, 166).

In conclusion, the combination of immunotherapy with TME modulation holds promise for cancer treatment by enhancing therapeutic efficacy and overcoming tumor drug resistance. However, further research is needed to optimize treatment protocols and address existing technical challenges. A deeper understanding of the interplay between immunotherapy and skeletal muscle health is crucial for developing more comprehensive treatment strategies that target tumors while preserving muscle function. Looking ahead, the integration of nanotechnology, immunotherapy, and muscle-protective interventions may be a key direction for achieving breakthroughs in cancer therapy while minimizing adverse effects on muscle tissue.

6 Conclusion

This study investigates the mechanisms through which immunotherapy influences skeletal muscle function in cancer patients, with a particular emphasis on the interaction between

immunotherapy and TME and its impact on the biological properties of skeletal muscle. While immunotherapy suppresses tumor growth by activating the immune system, it can also induce immune-related adverse effects, notably detrimental impacts on skeletal muscle (28). Specifically, immunotherapy may impair skeletal muscle function by triggering immune-associated myositis and systemic inflammatory responses, which can result in muscle mass loss and functional decline, especially in cancer patients. The TME plays a pivotal role in immunotherapy by modulating the immune response and anticancer efficacy through the regulation of immune cells and metabolic activities (167). Alterations in the TME can exacerbate skeletal muscle wasting through mechanisms such as chronic inflammation. The inflammatory response elicited by immunotherapy is closely linked to muscle wasting, and cachexia—a cancer-associated muscle wasting condition—may be more prevalent in patients undergoing immunotherapy (168). This paper also examines current biomechanical methodologies for evaluating the impact of immunotherapy on skeletal muscle and suggests strategies to mitigate the associated damage by targeting immunosuppressive cells and implementing metabolic reprogramming to enhance therapeutic efficacy. Future research should prioritize minimizing the adverse effects of immunotherapy on skeletal muscles to improve patient quality of life and clinical outcomes. In conclusion, while immunotherapy has introduced significant advancements in cancer treatment, its impact on skeletal muscle warrants greater attention. Subsequent studies should aim to enhance the therapeutic benefits of immunotherapy while mitigating its detrimental effects on skeletal muscle, thereby offering a more holistic treatment approach for cancer patients.

Author contributions

SM: Funding acquisition, Project administration, Writing – review & editing. GZ: Writing – original draft. SS: Writing – original draft, Investigation. XC: Writing – original draft. LW: Project administration, Writing – review & editing. TW: Writing – original draft, Formal Analysis. WX: Writing – original draft. ZL: Writing – original draft. AW: Writing – original draft. XW: Writing – review & editing, Supervision. JW: Writing – original draft. YL: Writing – review & editing. TY: Funding acquisition, Project administration, Writing – review & editing.

Funding

The author(s) declare that financial support was received for the research and/or publication of this article. This work was supported by the National Key R&D Program of China (Grant No. 2023YFB4705500), National Natural Science Foundation of China (Nos. 2022JC2K01, No. 82073327), CAMS Innovation Fund for Medical Sciences (Nos. CIFMS, 2022-I2M-C&T-B-061, 2021-I2M-1-066), Beijing Hope Run Special Fund of the Cancer Foundation of China (Nos. LC2021A18, LC2022B06), Doctoral Research Start up Fund of Shenyang University of Technology(Grant Nos. 1010147001258); Liaoning Provincial Department of Education Basic Research Project Youth Project (Grant Nos.JYTQN2023051).

Conflict of interest

The authors declare that the research was conducted in the absence of any commercial or financial relationships that could be construed as a potential conflict of interest.

Generative AI statement

The author(s) declare that no Generative AI was used in the creation of this manuscript.

Publisher's note

All claims expressed in this article are solely those of the authors and do not necessarily represent those of their affiliated organizations, or those of the publisher, the editors and the reviewers. Any product that may be evaluated in this article, or claim that may be made by its manufacturer, is not guaranteed or endorsed by the publisher.

References

1. Liu B, Zhou H, Tan L. Exploring treatment options in cancer: Tumor treatment strategies. *Signal Transduct Target Ther.* (2024) 9:175. doi: 10.1038/s41392-024-01856-7

2. Hsu CY, Pallathadka H, Jasim SA, Rizaev J, Olegovich BD, Hjazi A, et al. Innovations in cancer immunotherapy: A comprehensive overview of recent breakthroughs and future directions. *Crit Rev Oncol Hematol.* (2025) 206:104588. doi: 10.3390/jcm13216537

3. Casagrande S, Sopetto GB, Bertalot G, Bortolotti R, Racanelli V, Caffo O, et al. Immune-related adverse events due to cancer immunotherapy: immune mechanisms and clinical manifestations. *Cancers (Basel).* (2024) 16:1440. doi: 10.3390/cancers16071440

4. Amy HN, Diana MM, An TN, Eduardo B. Immunotherapy-related skeletal muscle weakness in cancer patients: a case series. *Case Reports.* (2021) 10:2359–65. doi: 10.21037/apm-20-454

5. Jiahua L, Zichao C, Yaqun L, Wenjie Z, JiBiao W, Zhen Z. PD-1/PD-L1 checkpoint inhibitors in tumor immunotherapy. *Front Pharmacol.* (2021) 12:731798. doi: 10.3389/fphar.2021.731798

6. Ingrid EL, Manabu F, Jiri V, Rohit A, Marie H, Lisa C, et al. Idiopathic inflammatory myopathies. *Nat Rev Dis Prime.* (2021) 7:86. doi: 10.1038/s41572-021-00321-x

7. Mukund K, Subramaniam S. Skeletal muscle: A review of molecular structure and function, in health and disease. *Wiley Interdiscip Rev Syst Biol Med.* (2020) 12:1462. doi: 10.1002/wsbm.1462

8. Shorter E, Engman V, Lanner JT. Cancer-associated muscle weakness - From triggers to molecular mechanisms. *Mol Aspects Med.* (2024) 97:101260. doi: 10.1016/j.mam.2024.101260

9. Siddiqui JA, Pothuraju R, Jain M, Batra SK, Nasser MW. Advances in cancer cachexia: Intersection between affected organs, mediators, and pharmacological

interventions. *Biochim Biophys Acta Rev Cancer*. (2020) 1873:188359. doi: 10.1016/j.bbcan.2020.188359

10. Huang KB, Wang FY, Lu Y, Yang LM, Long N, Wang SS, et al. Cu(II) complex that synergistically potentiates cytotoxicity and an anti-tumor immune response by targeting cellular redox homeostasis. *Proc Natl Acad Sci U S A*. (2024) 121:e240466812. doi: 10.1073/pnas.240466812

11. Li S, Liu Y, Zhang X, Liu Y, Si L, Jiang S, et al. Multi-pathway oxidative stress amplification via controllably targeted nanomaterials for photoimmunotherapy of tumors. *J Nanobiotechnol*. (2025) 23:33. doi: 10.1186/s12951-025-03116-4

12. Desai SA, Patel VP, Bhosle KP, Nagare SD, Thombare KC. The tumor microenvironment: shaping cancer progression and treatment response. *J Chemother*. (2025) 37:15–44. doi: 10.1080/1120009X.2023.2300224

13. Luri-Rey C, Teijeira Á, Wculek SK, de Andrea C, Herrero C, Lopez-J A, et al. Cross-priming in cancer immunology and immunotherapy. *Nat Rev Cancer*. (2025) 25:249–73. doi: 10.1038/s41568-024-00785-5

14. Wu Y, Luo J, Duan L. Pathogenic mechanisms of disease in idiopathic inflammatory myopathies: autoantibodies as clues. *Front Immunol*. (2024) 15:1439807. doi: 10.3389/fimmu.2024.1439807

15. Acosta-Alvear D, Harnoss JM, Walter P, Ashkenazi A. Homeostasis control in health and disease by the unfolded protein response. *Nat Rev Mol Cell Biol*. (2024) 26:193–212. doi: 10.1038/s41580-024-00794-0

16. Dong Y, Yuan H, Ma G, Gao H. Bone-muscle crosstalk under physiological and pathological conditions. *Cell Mol Life Sci*. (2024) 81:310. doi: 10.1007/s00018-024-05331-y

17. Dick TJM, Hug F. Advances in imaging for assessing the design and mechanics of skeletal muscle in *vivo*. *J Biomech*. (2023) 155:111640. doi: 10.1016/j.jot.2023.07.005

18. Khan M, Make AV, Jain S. The evolution of cancer immunotherapy. *Vaccines (Basel)*. (2021) 9:614. doi: 10.3390/vaccines9060614

19. Patel AA. Recent advances in immunotherapy in cancer treatment. *Cell Mol Biol (Noisy-le-grand)*. (2024) 70:89–99. doi: 10.14715/cmb/2024.70.5.13

20. Ali SR, Nkembo AT, Tipparaju SM, Ashraf M, Xuan W. Sarcopenia: recent advances for detection, progression, and metabolic alterations along with therapeutic targets. *Can J Physiol Pharmacol*. (2024) 102:697–708. doi: 10.1139/cjpp-2024-0201

21. Zhang SW, Wang H, Ding XH, Xiao YL, Shao ZM, You C, et al. Bidirectional crosstalk between therapeutic cancer vaccines and the tumor microenvironment: Beyond tumor antigens. *Fundam Res*. (2023) 3:1005–24. doi: 10.1016/j.fmre.2022.03.009

22. Shen S, Hong Y, Huang J, Qu X, Sooranna SR, Lu S, et al. Targeting PD-1/PD-L1 in tumor immunotherapy: Mechanisms and interactions with host growth regulatory pathways. *Cytokine Growth Factor Rev*. (2024) 79:16–28. doi: 10.1016/j.cytogfr.2024.08.001

23. Xiaoyu Z, Hanbing C, Shao YF, Ryan DC, Kaiyuan T, Medha M, et al. CTLA-4 tail fusion enhances CAR-T anti-tumor immunity. *Nat Immunol*. (2023) 24:1499–510. doi: 10.1038/s41590-023-01571-5

24. Xiaomin Z, Lingling Z, Hui Z, Shanshan C, Yang X. CAR-T cell therapy in hematological Malignancies: current opportunities and challenges. *Front Immunol*. (2022) 13:927153. doi: 10.3389/fimmu.2022.927153

25. De Visser KE, Joyce JA. The evolving tumor microenvironment: From cancer initiation to metastatic outgrowth. *Cancer Cell*. (2023) 41:374–403. doi: 10.1016/j.ccell.2023.02.016

26. El-Tanani M, Rabbani SA, Babiker R, Rangraze I, Kapre S, Palajurthi SS, et al. Unraveling the tumor microenvironment: Insights into cancer metastasis and therapeutic strategies. *Cancer Lett*. (2024) 591:216894. doi: 10.1016/j.canlet.2024.216894

27. Wang M, Yu F, Zhang Y. Present and future of cancer nano-immunotherapy: opportunities, obstacles and challenges. *Mol Cancer*. (2025) 24:26. doi: 10.1186/s12943-024-02214-5

28. Chen Y, Zhou Q, Jia Z, Cheng N, Zhang S, Chen W, et al. Enhancing cancer immunotherapy: Nanotechnology-mediated immunotherapy overcoming immunosuppression. *Acta Pharm Sin B*. (2024) 14:3834–54. doi: 10.1016/j.apsb.2024.05.032

29. Xu M, Li S. The opportunities and challenges of using PD-1/PD-L1 inhibitors for leukemia treatment. *Cancer Lette*. (2024) 593:216969. doi: 10.1016/j.canlet

30. Campanell R, Carolei A, Catarsi P, Abba C, Boveri E, Paulli M, et al. Circulating polymorphonuclear myeloid-derived suppressor cells (PMN-MDSCs) have a biological role in patients with primary myelofibrosis. *Cancers (Basel)*. (2024) 16:2556. doi: 10.3390/cancers16142556

31. Jin Y, Huan Y, Ren H, Hang H, Lai C, Wang W, et al. Nano-enhanced immunotherapy: Targeting the immunosuppressive tumor microenvironment. *Biomaterials*. (2024) 305:122463. doi: 10.1016/j.biomaterials

32. Liu Y, Zhao Y, Song H, Li Y, Liu Z, Ye Z, et al. Metabolic reprogramming in tumor immune microenvironment: Impact on immune cell function and therapeutic implications. *Cancer Lett*. (2024) 597:217076. doi: 10.1016/j.canlet.2024.217076

33. Martínez-Reyes I, Chandel NS. Cancer metabolism: looking forward. *Nat Rev Cancer*. (2021) 21:669–80. doi: 10.1038/s41568-021-00378-6

34. Arner EN, Rathmell JC. Metabolic programming and immune suppression in the tumor microenvironment. *Cancer Cell*. (2023) 41:421–33. doi: 10.1016/j.ccell.2023.01.009

35. Wang J, He Y, Hu F, Hu C, Sun Y, Yang K, et al. Metabolic reprogramming of immune cells in the tumor microenvironment. *Int J Mol Sci*. (2024) 25:12223. doi: 10.3390/ijms252212223

36. Wang K, Lu Y, Li H, Zhang J, Ju J, Ouyang M. Role of long non-coding RNAs in metabolic reprogramming of gastrointestinal cancer cells. *Cancer Cell Int*. (2024) 24:15. doi: 10.1186/s12935-023-03194-0

37. Qu C, Cui H, Xiao S, Dong L, Lu Q, Zhang L, et al. The landscape of immune checkpoint-related long non-coding RNAs core regulatory circuitry reveals implications for immunoregulation and immunotherapy responses. *Commun Biol*. (2024) 7:327. doi: 10.1038/s42003-024-06004-z

38. Dai E, Zhu Z, Wahed S, Qu Z, Storkus WJ, Gou ZS. Epigenetic modulation of anti-tumor immunity for improved cancer immunotherapy. *Mol Cancer*. (2021) 20:171. doi: 10.1186/s12943-021-01464-x

39. Yang W, Feng Z, Lai X, Li J, Cao Z, Jiang F, et al. Calcium nanoparticles target and activate T cells to enhance anti-tumor function. *Nat Commun*. (2024) 15:10095. doi: 10.1038/s41467-024-54402-y

40. Liu J, Bai Y, Li Y, Li X, Luo K. Reprogramming the immunosuppressive tumor microenvironment through nanomedicine: an immunometabolism perspective. *EBioMedicine*. (2024) 107:105301. doi: 10.1016/j.ebiom.2024.105301

41. Wang DR, Wu XL, Sun YL. Therapeutic targets and biomarkers of tumor immunotherapy: response versus non-response. *Signal Transduct Target Ther*. (2022) 7:331. doi: 10.1038/s41392-022-01136-2

42. Baharom F, Hermans D, Delamarre L, Seder RA. Vax-Innate: improving therapeutic cancer vaccines by modulating T cells and the tumour microenvironment. *Nat Rev Immunol*. (2025) 25:195–211. doi: 10.1038/s41577-024-01091-9

43. Qian S, Zhenya H, Cong Z, Liangliang W, Zhiqiang H, Ding M. Immune checkpoint therapy for solid tumours clinical dilemmas and future trends. *Signal Transduct Target Ther*. (2023) 8:320. doi: 10.1038/s41392-023-01522-4

44. Besan HA, Bassam RA, Eyad E. Resistance mechanisms to immune checkpoint inhibitors updated insights. *Mol Cancer*. (2025) 24:20. doi: 10.1186/s12943-024-02212-7

45. Boshi W, Jin H, Jennifer HE, Marco D. The senescence-associated secretory phenotype and its physiological and pathological implications. *Nat Rev Mol Cell Biol*. (2024) 25:958–78. doi: 10.1038/s41580-024-00727-x

46. Dong Z, Luo Y, Yuan Z, Tian Z, Jin T, Xu F. Cellular senescence and SASP in tumor progression and therapeutic opportunities. *Mol Cancer*. (2024) 23:181. doi: 10.1186/s12943-024-02096-7

47. Roger L, Tomas F, Gire V. Mechanisms and regulation of cellular senescence. *Int J Mol Sci*. (2021) 22:13173. doi: 10.3390/ijms222313173

48. Domen A, Deben C, Verswyvel J, Flieswasser T, Prenen H, Peeters M, et al. Cellular senescence in cancer: clinical detection and prognostic implications. *J Exp Clin Cancer Res*. (2022) 41:360. doi: 10.1186/s13046-022-02555-3

49. Iltis C, Moskalevska I, Debiesse A, Seguin L, Fissoun C, Cernera L, et al. A ganglioside-based immune checkpoint enables senescent cells to evade immunosurveillance during aging. *Nat Aging*. (2025) 5:219–36. doi: 10.1038/s43587-024-00776-z

50. Shmulevich R, Krizhanovsky V, Senescence C, Damage DNA. and metabolism. *Antioxid Redox Signal*. (2021) 34:324–34. doi: 10.1089/ars.2020.8043

51. Ming X, Yang Z, Huang Y, Wang Z, Zhang Q, Lu C, et al. A chimeric peptide promotes immune surveillance of senescent cells in injury, fibrosis, tumorigenesis and aging. *Nat Aging*. (2025) 5:28–47. doi: 10.1038/s43587-024-00750-9

52. Hwang HJ, Kang D, Shin J, Jung J, Ko S, Jung KH, et al. Therapy-induced senescent cancer cells contribute to cancer progression by promoting ribophorin 1-dependent PD-L1 upregulation. *Nat Commun*. (2025) 16:353. doi: 10.1038/s41467-024-54132-1

53. Yasuda T, Wang Y. Immune therapeutic strategies for the senescent tumor microenvironment. *Br J Cancer*. (2025) 132:237–44. doi: 10.1038/s41416-024-02865-7

54. Ruolan L, Liyuan P, Li Z, Zhao H, Chengwei Z, Canhua H. Oxidative stress in cancer immunotherapy: molecular mechanisms and potential applications. *Antioxid (Basel)*. (2022) 11:853. doi: 10.3390/antiox11050853

55. Megha KB, Joseph X, Akhil V, Mohanan PV. Cascade of immune mechanism and consequences of inflammatory disorders. *Phytomedicine*. (2021) 91:153712. doi: 10.1016/j.phymed.2021.153712

56. Qi Z, Jialing C, Nana T, Xuejuan Z, Minyan Z, Lirong M, et al. Characterising immune-related adverse events in different types of cancer among Chinese patients receiving immune checkpoint inhibitors. *Sci Rep*. (2024) 14:30983. doi: 10.1038/s41598-024-82105-3

57. Kunz HE, Lanza IR. Age-associated inflammation and implications for skeletal muscle responses to exercise. *Exp Gerontol*. (2023) 177:112177. doi: 10.1016/j.exger.2023.112177

58. Muhamma T, Can HJ, Ning L. Altered metabolism in cancer: insights into energy pathways and therapeutic targets. *Mol Cancer*. (2024) 23:203. doi: 10.1186/s12943-024-02119-3

59. Muhammad LR, Syed TH, Subia J, Wajiha F, Madiha F. Nutritional interventions in depression: The role of vitamin D and omega-3 fatty acids in neuropsychiatric health. *Clin Nutrition*. (2025) 45:270–80. doi: 10.1016/j.clnu.2025.01.009

60. Elena C, Elena B, Laura R, Ornella C, Annamaria DL, Antonio T. et al, cisplatin-induced skeletal muscle dysfunction: mechanisms and counteracting therapeutic strategies. *Int J Mol Sci*. (2020) 21:1242. doi: 10.3390/ijms21041242

61. Yibin L, Yifu S, Yaochuan Z, Xiaodong L, Liang K, Sheng H. New insights on anti-tumor immunity of CD8(+) T cells: cancer stem cells, tumor immune microenvironment and immunotherapy. *J Transl Med*. (2025) 23:341. doi: 10.1186/s12967-025-06291-y

62. Durre A, Samreen Z, Niti S, Monal T, Jai KC, Sufian Z. Exploring immune checkpoint inhibitors: Focus on PD-1/PD-L1 axis and beyond. *Pathol Res Pract*. (2025) 269:155864. doi: 10.1016/j.prp.2025.15586

63. Danping Z, Timur L, Eran E. Inflammasome activation and regulation: toward a better understanding of complex mechanisms. *Cell Discov*. (2020) 6:36. doi: 10.1038/s41421-020-0167-x

64. Brandon NV, Angela EM, James AC. The impact of immune cells on the skeletal muscle microenvironment during cancer cachexia. *Front Physiol*. (2020) 11:1037. doi: 10.3389/fphys.2020.01037

65. Lingjiao M, Haotian W, Jiaxiang W, Ping'an D, Jinchen H, Meixiang S, et al. Mechanisms of immune checkpoint inhibitors: insights into the regulation of circular RNAS involved in cancer hallmarks. *Cell Death Dis*. (2024) 15:3. doi: 10.1038/s41419-023-06389-5

66. Emily EH, Stefan MP, Christopher NB, Maya AF, Nancy RR. Divergent roles of inflammation in skeletal muscle recovery from injury. *Front Physiol*. (2020) 11:87. doi: 10.3389/fphys.2020.00087

67. Layal R, Ariane L, Madona S, François X, Fabrice B, Franck C, et al. Toxicity of immunotherapy combinations with chemotherapy across tumor indications: Current knowledge and practical recommendations. *Cancer Treat Rev*. (2024) 127:102751. doi: 10.1016/j.ctrv.2024.102751

68. Yin L, Li N, Jia W, Wang N, Liang M, Yang X, et al. Skeletal muscle atrophy: From mechanisms to treatments. *Pharmacol Res*. (2021) 172:105807. doi: 10.1016/j.phrs.2021.105807

69. Lorenzo G, Juliette H, Aitziber B, Laurence Z, Guido K. Immunostimulation with chemotherapy in the era of immune checkpoint inhibitors. *Nat Rev Clin Oncol*. (2020) 17:725–41. doi: 10.1038/s41571-020-0413-z

70. Indrajit D, Saee T, Pradeep P. Current advances in immunotherapy for cancer. *Oncol Reports*. (2024) 12:100652. doi: 10.1016/j.oor.2024.100652

71. Florent FR, Deepa K, Pierre F. Treatment patterns and outcomes in patients with non-small cell lung cancer. *Heliyon*. (2024) 10:e40147. doi: 10.1016/j.heliyon.2024.e40147

72. Mohammadsaleh J, Omid Y, Mohammda SK, Sara S, Hamidreza J, Azam M, et al. Clinical potential of PD-1/PD-L1 blockade therapy for renal cell carcinoma (RCC): a rapidly evolving strategy. *Cancer Cell Int*. (2022) 22:401. doi: 10.1186/s12935-022-02816-3

73. Xian K, Peng L, Chuanxin L, Yuzhu G, Yuying Y, Yuying P, et al. A combination of PD–1/PD–L1 inhibitors: The prospect of overcoming the weakness of tumor immunotherapy (Review). *Mol Med Rep*. (2021) 23:362. doi: 10.3892/mmr.2021.12001

74. Qi Z, Xiajian Z, Bo L, Yicheng Z, Yi X. Case report: Sandwich therapy of CAR-T combined with ASCT: Sequential CAR-T cell therapy with ASCT after remission with CAR-T therapy caused long-term survival in a patient with relapsed/refractory Burkitt's lymphoma with TP53 mutations. *Front Immunol*. (2023) 14:1127868. doi: 10.3389/fimmu.2023.1127868

75. Deng Y, Zhao L, Huang X, Zeng Y, Xiong Z, Zuo M. Contribution of skeletal muscle to cancer immunotherapy: A focus on muscle function, inflammation, and microbiota. *Nutrition*. (2023) 105:111829. doi: 10.1016/j.nut.2022.111829

76. Morin M, Duchesne E, Bernier J, Blanchette P, Langlois D, Hebert LJ. What is known about muscle strength reference values for adults measured by hand-held dynamometry: A scoping review. *Arch Rehabil Res Clin Transl*. (2022) 4:100172. doi: 10.1016/j.arrct.2021.100172

77. Bakers JNE, Van Den Berg LH, Ajeks TG, Holleman MJ, Verhoeven J, Beelen A, et al. Portable fixed dynamometry: towards remote muscle strength measurements in patients with motor neuron disease. *J Neurol*. (2021) 268:1738–46. doi: 10.1007/s00415-020-10366-9

78. Garcia-Retortillo S, Romero-Gómez C, Ivanov PC. Network of muscle fibers activation facilitates inter-muscular coordination, adapts to fatigue and reflects muscle function. *Commun Biol*. (2023) 6:891. doi: 10.1038/s42003-023-05204-3

79. Rockenfeller R, Gunther M, Gunther SL. Muscle active force-length curve explained by an electrophysical model of interfilament spacing. *Biophys J*. (2022) 121:1823–55. doi: 10.1016/j.bpj.2022.04.019

80. Blättler M, Bizzini M, Schaub G, Monn S, Barrué-Belou S, Oberhofer K, et al. Assessment of hip abductor and adductor muscle strength with fixed-frame dynamometry: Considerations on the use of bilateral and unilateral tasks. *Phys Ther Sport*. (2024) 70:22–8. doi: 10.1016/j.ptsp.2024.08.004

81. Mariana GB, Carlota M, Manuel LC, Nuno P, Teresa S, Antti M, et al. Bioelectrical impedance analysis (BIA) for the assessment of body composition in oncology: A scoping review. *Nutrients*. (2023) 15:4792. doi: 10.3390/nu15224792

82. Andrej Š, Ján B, Veronika B, Adrián K, David T, Alexander L. Current limitations of intraoperative ultrasound in brain tumor surgery. *Front Oncol*. (2021) 11:659048. doi: 10.3389/fonc.2021.659048

83. Setiawan T, Sari IN, Wijaya YT, Julianto NM, Muhammad JA, Lee H, et al. Cancer cachexia: molecular mechanisms and treatment strategies. *J Hematol Oncol*. (2023) 16:54. doi: 10.1186/s13045-023-01454-0

84. Roberts TJ, Dick TJM. What good is a measure of muscle length? The how and why of direct measurements of skeletal muscle motion. *J Biomech*. (2023) 157:111709. doi: 10.1016/j.jbiomech.2023.111709

85. Miller JD, Cabarkapa D, Miller AJ, Frazer LL, Templin TN, Elison TD, et al. Novel 3D force sensors for a cost-effective 3D force plate for biomechanical analysis. *Sensors (Basel)*. (2023) 23:4437. doi: 10.3390/s23094437

86. Alberini R, Spagnoli A, Sadeghnia MJ, Skallerud B, Terzano M, Holzapfel G. Second harmonic generation microscopy, biaxial mechanical tests and fiber dispersion models in human skin biomechanics. *Acta Biomater*. (2024) 185:266–80. doi: 10.1016/j.actbio.2024.07.026

87. Slart RHJA, Marija P, Dalal SA, Alberto B, Oliver B, Pauline C, et al. Updated practice guideline for dual-energy X-ray absorptiometry (DXA). *Eur J Nucl Med Mol Imag*. (2025) 52:539–63. doi: 10.1007/s00259-024-06912-6

88. Salim AS, Sara B, Marjorie V, Yoad Y, Klaus E, Loic B, et al. First experience with a whole-body spectral photon-counting CT clinical prototype. *Invest Radiol*. (2023) 58:459–71. doi: 10.1097/RLI.0000000000000965

89. Fritz S, Claus CP, Patrick K, Haidara A, Gabriel K, Fabian S, et al. 1.5 vs 3 tesla magnetic resonance imaging: A review of favorite clinical applications for both field strengths-part 1. *Invest Radiol*. (2021) 56:680–91. doi: 10.1097/RLI.0000000000000812

90. Jing G, Lynn JS, Karl HH, Ingolf S. MR elastography in cancer. *Invest Radiol*. (2023) 58:578–86. doi: 10.1097/RLI.0000000000000971

91. Tetsuaki H, Fuqiang Z, Rina B, Takeshi H, Ryosuke K, Kazunori S, et al. Electrical impedance myography detects dystrophin-related muscle changes in mdx mice. *Skelet Muscle*. (2023) 13:19. doi: 10.1186/s13395-023-00331-1

92. Sabatino A, Sola KH, Brismar TB, Lindholm B, Stenvinkel P, Avesani CM. Making the invisible visible: imaging techniques for assessing muscle mass and muscle quality in chronic kidney disease. *Clin Kidney J*. (2024) 17:sfae028. doi: 10.1093/ckj/sfae028

93. Zhao R, Li X, Jiang Y, Su N, Li J, Kang L, et al. Evaluation of appendicular muscle mass in sarcopenia in older adults using ultrasonography: A systematic review and meta-analysis. *Gerontology*. (2022) 68:1174–98. doi: 10.1159/000525758

94. Mccarthy C, Tinsley GM, Bosy-Westphal A, Müller MJ, Shepherd J, Gallagher D, et al. Total and regional appendicular skeletal muscle mass prediction from dual-energy X-ray absorptiometry body composition models. *Sci Rep*. (2023) 13:2590. doi: 10.1038/s41598-023-29827-y

95. Enji K, Sumin K, Yong WK, Hunkyu S, Moohyun K, Won GC, et al. Electrical stimulation for therapeutic approach. *Interdiscip Med*. (2023) 1:e20230003. doi: 10.1002/INMD.20230003

96. Ma P, Li C, Rahaman MM, Yao Y, Zhang J, Zou S, et al. A state-of-the-art survey of object detection techniques in microorganism image analysis: from classical methods to deep learning approaches. *Artif Intell Rev*. (2023) 56:1627–98. doi: 10.1007/s10462-022-10209-1

97. Davidson MD, Prendergast ME, Ban E, Xu KL, Mickel G, Mensah P, et al. Programmable and contractile materials through cell encapsulation in fibrous hydrogel assemblies. *Sci Adv*. (2021) 7:eabi8157. doi: 10.1126/sciadv.abi8157

98. Mcgee SL, Hargreaves M. Exercise adaptations: molecular mechanisms and potential targets for therapeutic benefit. *Nat Rev Endocrinol*. (2020) 16:495–505. doi: 10.1038/s41574-020-0377-1

99. Ren J, Li J, Chen S, Liu Y, Ta D. Unveiling the potential of ultrasound in brain imaging: Innovations, challenges, and prospects. *Ultrasonics*. (2025) 145:107465. doi: 10.1016/j.ultras.2024.107465

100. Sanchez B, Martinsen OG, Freeborn TJ, Furse CM. Electrical impedance myography: A critical review and outlook. *Clin Neurophysiol*. (2021) 132:338–44. doi: 10.1016/j.clinph.2020.11.014

101. Ashir A, Jerban S, Barrere V, Wu Y, Shah SB, Andre MP, et al. Skeletal muscle assessment using quantitative ultrasound: A narrative review. *Sensors (Basel)*. (2023) 23:4763. doi: 10.3390/s23104763

102. Sebastian JA, Strohm EM, Baranger J, Villemain O, Kolios MC, Simmons CA. Assessing engineered tissues and biomaterials using ultrasound imaging: *In vitro* and *in vivo* applications. *Biomaterials*. (2023) 296:122054. doi: 10.1016/j.biomaterials.2023.122054

103. Wang PJF, Feng Y. Flexible Doppler ultrasound device for the monitoringof blood flow velocity. *Sci Adv*. (2021) 7:eabi9283. doi: 10.1126/sciadv.abi9283

104. Paris MT, Mourtzakis M. Muscle composition analysis of ultrasound images: A narrative review of texture analysis. *Ultrasound Med*. (2021) 47:880–95. doi: 10.1016/j.ultrasmedbio.2020.12.012

105. Engelke K, Chaudry O, Gast L, Eldib MA, Wang L, Laredo JD, et al. Magnetic resonance imaging techniques for the quantitative analysis of skeletal muscle: State of the art. *J Orthop Translat*. (2023) 42:57–72. doi: 10.1016/j.jot.2023.07.005

106. Bou Matar O, Pernod P. Chapter 14 - Ultrasound elastography: *in vivo* assessment of tissue stiffness. In: *Biomechanics of the Female Reproductive System: Breast and Pelvic Organs*. Computational Intelligence in Healthcare Applications Academic Press (2023). p. 357–76. doi: 10.1016/B978-0-12-823403-7.00027-0

107. Kamezawa C, Cramer A, Krull W, Yashiro W, Hyodo K, Gupta R. Dynamic X-ray elastography using a pulsed photocathode source. *Sci Rep*. (2021) 11:24128. doi: 10.1038/s41598-021-03221-y

108. Clark BC, Rutkove S, Lupton EC, Pandilla CJ, Arnold WD. Potential utility of electrical impedance myography in evaluating age-related skeletal muscle function deficits. *Front Physiol*. (2021) 12:666964. doi: 10.3389/fphys.2021.666964

109. Moro T, Brightwel CR, Volpi E, Rasmussen BB, Fry CS. Resistance exercise training promotes fiber type-specific myonuclear adaptations in older adults. *J Appl Physiol*. (2020) 128:795–804. doi: 10.1152/japplphysiol.00723.2019

110. Parvez A, Choudhary F, Mudgal P, Khan R, Qureshi KA, Farooqi H, et al. PD-1 and PD-L1: architects of immune symphony and immunotherapy breakthroughs in cancer treatment. *Front Immunol*. (2023) 14:1296341. doi: 10.3389/fimmu.2023.1296341

111. Lee D, Cho M, Kim E, Sen Y, Cha JH. PD-L1: From cancer immunotherapy to therapeutic implications in multiple disorders. *Mol Ther*. (2024) 32:4235–55. doi: 10.1016/j.ymthe.2024.09.026

112. Kapoor G, Prakash S, Jaiswal V, Singh AK. Chronic inflammation and cancer: key pathways and targeted therapies. *Cancer Invest*. (2025) 43:1–23. doi: 10.1080/07357907.2024.2437614

113. Strati A, Adamopoulos C, Kotsantis I, Psyrri A, Lianidou E, Papavassiliou AG. Targeting the PD-1/PD-L1 signaling pathway for cancer therapy: focus on biomarkers. *Int J Mol Sci*. (2025) 26:1235. doi: 10.3390/ijms26031235

114. Ghebremedhin A, Athavale D, Zhang Y, Yao X, Balch C, Song S. Tumor-associated macrophages as major immunosuppressive cells in the tumor microenvironment. *Cancers (Basel)*. (2024) 16:3410. doi: 10.3390/cancers16193410

115. Gassner T, Chittilappilly C, Pirich T, Neuditschko B, Hackner K, Lind J, et al. Favorable impact of PD1/PD-L1 antagonists on bone remodeling: an exploratory prospective clinical study and ex vivo validation. *J Immunother Cancer*. (2024) 12:e008669. doi: 10.1136/jitc-2023-008669

116. Wu Q, Jiang L, Li SC, He QJ, Yang B, Cao J. Small molecule inhibitors targeting the PD-1/PD-L1 signaling pathway. *Acta Pharmacol Sin*. (2021) 42:1–9. doi: 10.1038/s41401-020-0366-x

117. Alessio C, Federico B, Pierpaolo P, Davide B, Pietro DM, Nicola T, et al. Weighing the role of skeletal muscle mass and muscle density in cancer patients receiving PD-1/PD-L1 checkpoint inhibitors: a multicenter real-life study. *Sci Rep*. (2020) 10:1456. doi: 10.1038/s41598-020-58498-2

118. Ting TW, Xiu XL, Gao YC, Jun Y, Jing X, Chen JL. Muscle strength trajectories and outcomes in critically ill patients: A prospective multicentre cohort study. *Intens Crit Care Nurs*. (2025) 88:103934. doi: 10.1016/j.iccn.2024.103934

119. Navid S, Dana RT, Aram D, Daniele G, Raheleh R, Yong L. CTLA-4 in regulatory T cells for cancer immunotherapy. *Cancers (Basel)*. (2021) 13:1440. doi: 10.3390/cancers13061440

120. Binbin C, Jinke L, Yao X, Changshan S, Jianjun C, Chuxiao S. Small molecule inhibitors targeting PD-L1, CTLA4, VISTA, TIM-3, and LAG3 for cancer immunotherapy (2020–2024). *Eur J Med Chem*. (2025) 283:117141. doi: 10.1016/j.ejmech.2024.117141

121. Elin A, Kari J, Oddbjørn S, Christian K, Oluf H, Jarle K, et al. Ipilimumab in a real-world population: A prospective Phase IV trial with long-term follow-up. *Int J Cancer*. (2022) 150:100–11. doi: 10.1002/ijc.33768

122. Matteo S, Sebastiano B, Zin WM, Marco M, R obeto I, Martin P, et al. Real-world outcome of patients with advanced renal cell carcinoma and intermediate- or poor-risk international metastatic renal cell carcinoma database consortium criteria treated by immune-oncology combinations: differential effectiveness by risk group? *Eur Urol Oncol*. (2024) 7:102–11. doi: 10.1016/j.euo.2023.07.003

123. Oliver G, Obiageli VN, Qian C, Eva M. Mechanisms underlying immunosuppression by regulatory cells. *Front Immunol*. (2024) 15:1328193. doi: 10.3389/fimmu.2024.1328193

124. Jigang D, Ying Q, Sha S. Low-dose radiation improves tumor immune microenvironment, enhancing the effects of anti-CTLA-4 therapy. *Iran J Immunol*. (2025) 22:2825. doi: 10.22034/iji.2025.103258.2825

125. Beatrice S, Sharad K, Maria FB. Chimeric antigen receptor (CAR) T-cell therapy: Harnessing extracellular vesicles for enhanced efficacy. *Pharmacol Res*. (2024) 208:107352. doi: 10.1016/j.phrs.2024.107352

126. Karan K, Venu GP, Teresa SK. Key chemokines direct migration of immune cells in solid tumors. *Cancer Gene Ther*. (2022) 29:10–21. doi: 10.1038/s41417-021-00303-x

127. Oliver FB. Tumor metabolism as a factor affecting diversity in cancer cachexia. *Am J Physiol Cell Physiol*. (2025) 328:C908–c920. doi: 10.1152/ajpcell.00677.2024

128. Kewen Q, Guangyao L, Shuyi Z, Wenya F, Tian Li, Jian Z. CAR-T-cell products in solid tumors: Progress, challenges, and strategies. *Interdiscip Med*. (2024) 2:e20230047. doi: 10.1002/INMD.20230047

129. Rohit S. Beyond the CAR T cells: TIL therapy for solid tumors. *Immune Netw*. (2024) 24:e16. doi: 10.4110/in.2024.24.e16

130. Lei P, Giacomo S, Luojia Y, Liqun Z, Sidi C. CAR-T and CAR-NK as cellular cancer immunotherapy for solid tumors. *Cell Mol Immunol*. (2024) 21:1089–108. doi: 10.1038/s41423-024-01207-0

131. Ugur U, Sofia C, Carl HJ. CAR T cell combination therapies to treat cancer. *Cancer Cell*. (2024) 42:1319–25. doi: 10.1016/j.ccell.2024.07.002

132. Yan T, Fan T, Dandan P, Ye Z, Huashan S. TGF-beta signal transduction: biology, function and therapy for diseases. *Mol Biomed*. (2022) 3:45. doi: 10.1186/s43556-022-00109-9

133. Kexin A, Bowen L, Xiaomei C, Chuxin H, Liping Y, Weiya Z, et al. Optimizing CAR-T cell therapy for solid tumors: current challenges and potential strategies. *J Hematol Oncol*. (2024) 17:105. doi: 10.1186/s13045-024-01625-7

134. Chia ZJ, Cao YN, Little PJ, Kamato D. Transforming growth factor-beta receptors: versatile mechanisms of ligand activation. *Acta Pharmacol Sin*. (2024) 45:1337–48. doi: 10.1038/s41401-024-01235-6

135. Wang X, Eichhorn PJA, Thiery JP. TGF-beta, EMT, and resistance to anticancer treatment. *Semin Cancer Biol*. (2023) 97:1–11. doi: 10.1016/j.semcancer.2023.10.004

136. Hourani T, Sharma A, Luwor RB, Achuthan AA. Transforming growth factor-beta in tumor microenvironment: Understanding its impact on monocytes and macrophages for its targeting. *Int Rev Immunol*. (2025) 44:82–97. doi: 10.1080/08830185.2024.2411998

137. Li K, Shi H, Zhang B, Ou X, Ma Q, Chen Y, et al. Myeloid-derived suppressor cells as immunosuppressive regulators and therapeutic targets in cancer. *Signal Transduct Target Ther*. (2021) 7:362. doi: 10.1038/s41392-021-00670-9

138. Chandra JB, Sarkar S, Rout L, Mandal M. The transformation of cancer-associated fibroblasts: Current perspectives on the role of TGF-β in CAF mediated tumor progression and therapeutic resistance. *Cancer Lette*. (2021) 520:222–32. doi: 10.1016/j.canlet.2021.08.002

139. Tschernia NP, Gulley JL. Tumor in the crossfire: inhibiting TGF-beta to enhance cancer immunotherapy. *BioDrugs*. (2022) 36:153–80. doi: 10.1007/s40259-022-00521-1

140. Zhang A, Fan T, Liu Y, Yu G, Li C, Jiang Z. Regulatory T cells in immune checkpoint blockade anti-tumor therapy. *Mol Cancer*. (2024) 23:251. doi: 10.1186/s12943-024-02156-y

141. Huang CY, Chung CL, Hu TH, Chen J, Liu PF, Chen CL. Recent progress in TGF-β inhibitors for cancer therapy. *BioMed Pharmacother*. (2021) 134:111046. doi: 10.1016/j.biopha.2020.111046

142. Francesco G, Anissa T, Majid E, Asiman D, Dilani GG, Cécile P, et al. TGFβ signaling curbs cell fusion and muscle regeneration. *Nat Commun*. (2021) 12:750. doi: 10.1038/s41467-020-20289-8

143. Jang DI, Lee AH, Shin HY, Song HR, Park JH, Kang TB, et al. The role of tumor necrosis factor alpha (TNF-alpha) in autoimmune disease and current TNF-alpha inhibitors in therapeutics. *Int J Mol Sci*. (2021) 22:2719. doi: 10.3390/ijms22052719

144. Van Loo G, Bertrand MJM. Death by TNF: a road to inflammation. *Nat Rev Immunol*. (2023) 23:289–303. doi: 10.1038/s41577-022-00792-3

145. Yang J, Yang L, Wang Y, Huai L, Shi B, Zhang D, et al. Interleukin-6 related signaling pathways as the intersection between chronic diseases and sepsis. *Mol Med*. (2025) 31:34. doi: 10.1186/s10020-025-01089-6

146. Igor José Dos Santos N, da Silve-Júnior EF. TNF-α Inhibitors from natural compounds: an overview, CADD approaches, and their exploration for anti-inflammatory agents. *Comb Chem High Throughput Screen*. (2022) 25:2317–40. doi: 10.2174/1386207324666210715165943

147. Frangogiannis N. Transforming growth factor-β in tissue fibrosis. *J Exp Med*. (2020) 217:e20190103. doi: 10.1084/jem.20190103

148. Jin Y, Jiang J, Mao W, Bai M, Chen Q, Zhu J. Treatment strategies and molecular mechanism of radiotherapy combined with immunotherapy in colorectal cancer. *Cancer Lett*. (2024) 591:216858. doi: 10.1016/j.canlet.2024

149. Luo H, Ma W, Chen Q, Yang Z, Dai Y. Radiotherapy-activated tumor immune microenvironment: Realizing radiotherapy-immunity combination therapy strategies. *Nano Today*. (2023) 53:102042. doi: 10.1016/j.nantod.2023.102042

150. Guanli Y, Zhen Z, Chengxin L. Efficacy and safety of combining radiotherapy with immune checkpoint inhibitors in patients with advanced non-small cell lung cancer: a real-world study. *Immunopharmacol Immunotoxicol*. (2024) 46:861–71. doi: 10.1080/08923973.2024.2415121

151. Nakajima K, Ogawa M. Near-infrared photoimmunotherapy and anticancer immunity. *Int Immunol*. (2024) 36:57–64. doi: 10.1093/intimm/dxad042

152. Zhang W, Wang M, Ji C, Liu X, Gu B, Dong T. Macrophage polarization in the tumor microenvironment: Emerging roles and therapeutic potentials. *BioMed Pharmacother*. (2024) 177:116930. doi: 10.1016/j.biopha.2024.116930

153. Arends J. Malnutrition in cancer patients: Causes, consequences and treatment options. *Eur J Surg Oncol*. (2024) 50:107074. doi: 10.1016/j.ejso.2023.107074

154. Haß U, Kochlik B, Herpich C, Rudloff S, Norman K. Effects of an omega-3 supplemented, high-protein diet in combination with vibration and resistance exercise on muscle power and inflammation in old adults: A pilot randomized controlled trial. *Nutrients*. (2022) 14:4274. doi: 10.3390/nu14204274

155. Vellai T. How the amino acid leucine activates the key cell-growth regulator mTOR. *Nature*. (2021) 596:192–4. doi: 10.1038/d41586-021-01943-7

156. Zhang X, Li H, Lv X, Hu L, Li W, Zi M, et al. Impact of diets on response to immune checkpoint inhibitors (ICIs) therapy against tumors. *Life (Basel)*. (2022) 12:409. doi: 10.3390/life12030409

157. Peng Y, Ao M, Dong B, Jiang Y, Yu L, Chen Z, et al. Anti-inflammatory effects of curcumin in the inflammatory diseases: status, limitations and countermeasures. *Drug Des Devel Ther*. (2021) 15:4503–25. doi: 10.2147/DDDT.S327378

158. Atef ME, Hanem E, Ahmed A, Marisol F, Ramy KAS. The role of the tumor microenvironment (TME) in advancing cancer therapies: immune system interactions, tumor-infiltrating lymphocytes (TILs), and the role of exosomes and inflammasomes. *Int J ecular Sci*. (2025) 26:2716. doi: 10.3390/ijms26062716

159. Fatma K, Hasret T, Arif EC, Seda NT. Nanomedicine: How nanomaterials are transforming drug delivery, bio-imaging, and diagnosis. *Next Nanotechnol*. (2025) 7:100129. doi: 10.1016/j.nxnano.2024.100129

160. Quan L, Yanhong D, Jianye F, Meng Q, Zhe S, Dickson A, et al. Nano-immunotherapy: Unique mechanisms of nanomaterials in synergizing cancer immunotherapy. *Nano Today*. (2021) 36:101023. doi: 10.1016/j.nantod.2020.101023

161. Deep S, Brian S, Lindsay S. Cytokine release syndrome and cancer immunotherapies - historical challenges and promising futures. *Front Immunol*. (2023) 14:1190379. doi: 10.3389/fimmu.2023.1190379

162. Anna M, Kevin PL, Sai R. Engineering next-generation chimeric antigen receptor-T cells: recent breakthroughs and remaining challenges in design and screening of novel chimeric antigen receptor variants. *Curr Opin Biotechnol*. (2024) 90:103223. doi: 10.1016/j.copbio.2024.103223

163. Mohsen A, Sander B, Klaus-Dieter W, Thomas W, Kristian W. Non-steroidal anti-inflammatory drugs: recent advances in the use of synthetic COX-2 inhibitors. *RSC Med Chem*. (2022) 13:471–96. doi: 10.1039/d1md00280e

164. Tao L, Yazhuo W, Yuchen Z, Yufei Y, Jiaying C, Jiansong H, et al. Leveraging CRISPR gene editing technology to optimize the efficacy, safety and accessibility of CAR T-cell therapy. *Leukemia*. (2024) 12:2517–43. doi: 10.1038/s41375-024-02444-y

165. Xiaoying C, Shuhan Z, Yonghao Z, Xuepei Z. CRISPR–Cas9 applications in T cells and adoptive T cell therapies. *Cell Mol Biol Lett*. (2024) 29:52. doi: 10.1186/s11658-024-00561-1

166. Débora da LS, Alexandra L. Exercise-induced immune system response: Anti-inflammatory status on peripheral and central organs. *Biochim Biophys Acta Mol Basis Dis*. (2020) 10:165823. doi: 10.1016/j.bbadis.2020.165823

167. Perucca A, Llonin AG, Benach OM, Hallopeau C, Rivas EI, Linares J, et al. Micro Immune Response On-chip (MIRO) models the tumour-stroma interface for immunotherapy testing. *Nat Commun*. (2025) 16:1279. doi: 10.1038/s41467-025-56275-1

168. Dougan M, Luoma AM, Dougan SK, Wuchepfenning KW. Understanding and treating the inflammatory adverse events of cancer immunotherapy. *Cell*. (2021) 184:1575–88. doi: 10.1016/j.cell.2021.02.011

frontiers | Frontiers in Oncology

TYPE Review
PUBLISHED 21 May 2025
DOI 10.3389/fonc.2025.1598934

Check for updates

OPEN ACCESS

EDITED BY
Xiaosheng Tan,
Rutgers, United States

REVIEWED BY
Minglu Yan,
University of Texas Southwestern Medical Center, United States
Yan Wang,
University of Texas Medical Branch at Galveston, United States
Xue Yang,
University of Texas MD Anderson Cancer Center, United States

*CORRESPONDENCE
Yanlin Chen
chenyl_doctor@163.com

†These authors have contributed equally to this work

RECEIVED 24 March 2025
ACCEPTED 30 April 2025
PUBLISHED 21 May 2025

CITATION
Li M, Li Q, Zou C, Huang Q and Chen Y (2025) Application and recent advances in conventional biomarkers for the prognosis of papillary thyroid carcinoma.
Front. Oncol. 15:1598934.
doi: 10.3389/fonc.2025.1598934

COPYRIGHT
© 2025 Li, Li, Zou, Huang and Chen. This is an open-access article distributed under the terms of the Creative Commons Attribution License (CC BY). The use, distribution or reproduction in other forums is permitted, provided the original author(s) and the copyright owner(s) are credited and that the original publication in this journal is cited, in accordance with accepted academic practice. No use, distribution or reproduction is permitted which does not comply with these terms.

Application and recent advances in conventional biomarkers for the prognosis of papillary thyroid carcinoma

Muzi Li[1,2†], Qiong Li[1,2†], Cancan Zou[1,2], Qin Huang[1,2] and Yanlin Chen[1,2*]

[1]Department of Pathology, Women and Children's Hospital of Chongqing Medical University (Chongqing Health Center for Women and Children), Chongqing, China, [2]National Health Commission (NHC) Key Laboratory of Birth Defects and Reproductive Health, Chongqing, China

Cancer remains one of the most common and deadliest diseases worldwide. Among endocrine neoplasms, the incidence of thyroid malignancies has been rising in recent years. Papillary thyroid carcinoma (PTC), the most frequently observed histological subtype of thyroid cancer (THCA), typically yields favorable clinical outcomes for affected individuals. However, this has raised concerns about the overdiagnosis and underdetermination of the prognostic factors in PTC cases. As a result, researchers now advocate for patient stratification and tailored therapeutic approaches for PTC cases, with the goal of minimizing unnecessary surgical procedures and radioiodine treatments. These treatments can lead to clinical complications and impose avoidable physiological and psychological stress on patients. Multiple prognostic biomarkers have been identified for PTC, which play a critical role in predicting outcomes and informing treatment decisions. This review examines both established molecular tools and recent advancements in the determination of prognosis in in papillary thyroid carcinoma.

KEYWORDS

papillary thyroid carcinoma, BRAF V600E, TERT, Ras, CD147, tumor microenvironment, ctDNA, microRNA

1 Introduction

Among thyroid malignancies, papillary thyroid carcinoma (PTC) is the most common histopathological subtype of thyroid malignancy, accounting for approximately 85-90% of all diagnosed cases (1, 2). Most PTC patients exhibit disease progression similar to benign neoplasms, with minimal mortality, low recurrence rates, and excellent long-term survival outcomes. Limited lymphatic and distant organ involvement further contributes to favorable prognosis observed in many PTC cases (3–5). However, approximately 15-20% (6, 7) of patients experience disease recurrence, persistence, or mortality (8). With PTC incidence steadily rising throughout the past decade, prognostic classification has become increasingly important for therapeutic decision-making, including the evaluation of active surveillance versus surgical management options.

According to the 2022 World Health Organization classification of thyroid neoplasms, multiple histologic subtypes of PTC are recognized, including classic, hypercellular, and follicular varieties. Each subtype may exhibit either encapsulated or infiltrative growth patterns Notably (9), follicular PTC—particularly its encapsulated variant—shares certain pathologic characteristics with follicular thyroid cancer (FTC). Currently, surgical intervention combined with radioiodine therapy remains the primary effective treatment approach for diverse PTC subtypes (10–12). Given the generally favorable outcomes for most PTC patients. Therefore, it is important to distinguish between patients who require active treatment or those who do not. Conventional clinicopathological prognostic indicators have limitations in accurately predicting individual PTC patient outcomes. As a result, a deeper understanding of molecular and transcriptomic profiles may lead to the development of new risk stratification frameworks, facilitating prognostic assessment. This analysis explores both conventional and newly identified biomarkers linked to PTC outcomes, with the aim of developing applicable risk stratification models for integration into clinical practice.

2 Conventional biomarkers of PTC prognosis

2.1 BRAF V600E mutation in PTC

Tumor-associated BRAF gene mutations were first identified in 2002 (13). Subsequently, researchers have gradually characterized over 40 distinct BRAF mutations. Pathologies involving activating BRAF alterations predominantly affect codon 600, yielding V600E (Figure 1) mutations, while alternative BRAF-associated conditions exhibit K601E (Figure 1) mutations or manifest as minor in-frame insertions, deletions, or structural rearrangements (14, 15). Thyroid malignancies commonly harbor BRAF mutations (16–19). These genomic abnormalities are commonly observed in PTC, poorly differentiated thyroid carcinoma (PDTC), and anaplastic thyroid carcinoma (ATC), while being notably absent in follicular thyroid cancer (FTC), medullary thyroid carcinoma (MTC), and non-malignant thyroid growths.

Within PTC, BRAF alterations represent the most prevalent genetic alteration, occurring in approximately 36-69% of cases (20, 21). Scientific evidence suggests the BRAF gene encodes a serine/threonine kinase, which acts as an immediate downstream mediator of RAS. Moreover, BRAF promotes continuous kinase activity via MEK and ERK phosphorylation, leading to the tumorigenic activation of the mitogen-activated protein kinase (MAPK) signaling pathway (Figure 2A). Somatic activating BRAF mutations are found across various malignancies, notably melanoma (prevalence approaching 70%), and colorectal and ovarian cancers (approximately 15%). According to reports, these mutations promote carcinogenic MAPK pathway activation by disrupting essential interactions that normally preserve the inactive state of the enzyme. Specifically, this genetic alteration interferes with the hydrophobic bonds linking activation loop segments with ATP-binding domain elements, thereby breaking the inactive configuration and creating new molecular interactions that activate the kinase, resulting in persistent enzymatic activity (14, 15). BRAFV600E transfection induces persistent ERK

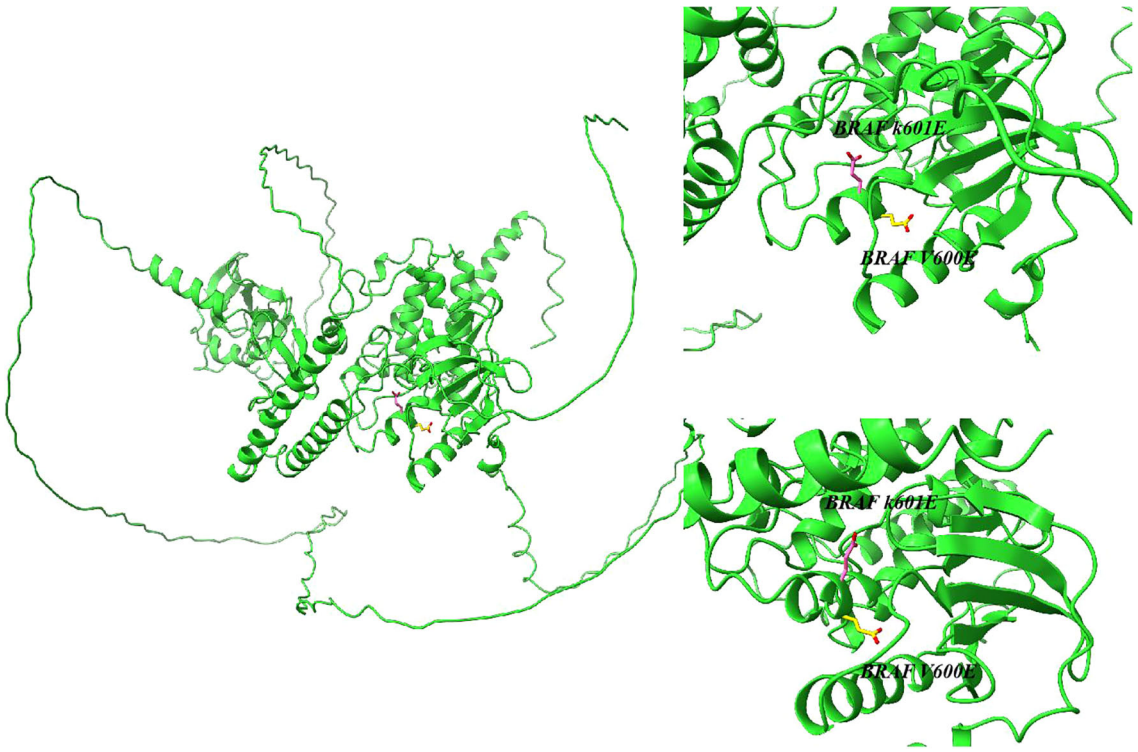

FIGURE 1
Structure of the serine/threonine kinase encoded by the BRAF K601E and BRAF V600E gene predicted by AlphaFold.

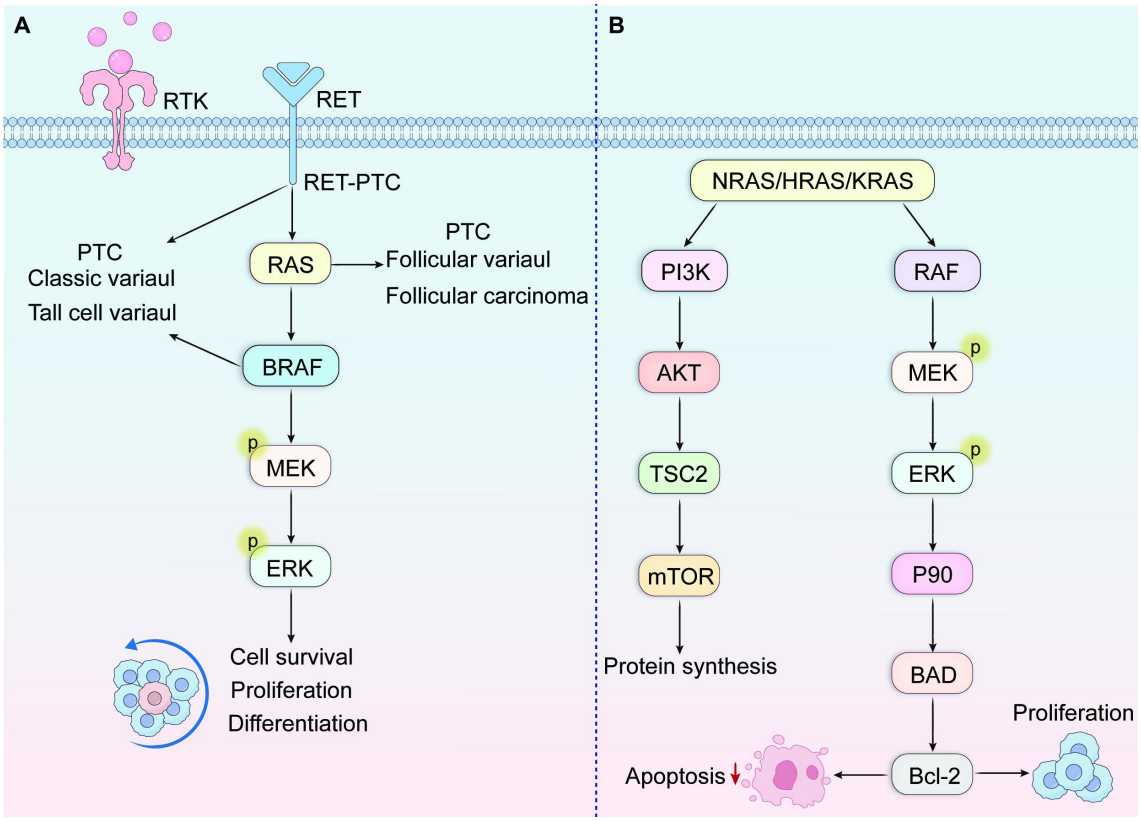

FIGURE 2
(A) MAPK signaling pathway. This pathway binds to growth factors and receptor tyrosine kinase RTK, thereby activating the phosphorylation cascade of RAS, BRAF, MEK, and ERK. **(B)** RAS activation subsequently initiates downstream signaling cascades, predominantly the Raf-MAPK and PI3K-AKT pathways.

phosphorylation, along with elevated translational activity within NIH3T3 cellular models (22).

2.2 TERT

2.2.1 TERT mutations in PTC

As the catalytic component of telomerase responsible for preserving terminal DNA sequences, telomerase reverse transcriptase (TERT) is typically not expressed in most normal human somatic cells, a phenomenon considered crucial for malignancy prevention. In contrast, numerous malignancies exhibit enhanced TERT gene expression through various molecular mechanisms. Predominantly, mutations in the core promoter region of the TERT gene (TERT-p mutations) facilitate cellular immortalization, fundamental characteristic of neoplastic transformation. Cancer-associated TERT-p mutations were first documented in scientific literature during 2013 (23, 24). Comprehensive genomic sequencing examination of melanoma specimens revealed two frequently occurring somatic alterations within the TERT promoter region: mutually exclusive heterozygous cytosine-to-thymine substitutions positioned 124 and 146 base pairs upstream from the translation initiation codon (25). These genetic variants are designated as chr5:1,295,228 C > T (C228T) and chr5:1,295,250 C > T (C250T), respectively, according to human genome reference assembly 19 (hg19) coordinates. Scholars have proposed a biphasic mechanism underlying the contribution of TERT promoter (TERT-p) mutations to oncogenesis (26). Initially, mutations in TERT-p enhance telomerase activity; however, this enhancement only delays cellular aging rather than completely preventing telomere shortening. Subsequently, critically shortened telomeres accumulate, leading to genomic instability, which further elevates TERT expression and ultimately supports cellular proliferative. Indeed, tumors harboring TERT-p mutations exhibit shorter telomeres compared to those in normal tissues (26).

Research has identified TERT-p mutations across various thyroid cancer types, with particularly high frequency in aggressive histological subtypes, such as poorly differentiated thyroid cancer (PDTC) and anaplastic thyroid carcinoma (A TC) (27, 28). These genetic alterations occur across all four principal follicular cell-derived thyroid neoplasms— PTC, FTC, PDTC, and ATC—with predominance in the more aggressive PDTC and ATC variants. Notably, such mutations remain absent in MTC originating from parafollicular C cells. Within PTC specifically, TERT promoter mutations occur in approximately 10% of cases. Recent evidence has established TERT promoter mutations as dependable markers of poor prognosis, supporting their inclusion in clinical management guidelines for thyroid malignancies.

2.2.2 Clinical outcomes and pathological processes in papillary thyroid carcinoma harboring concurrent BRAF V600E and TERT promoter alterations

Extensive studies have established a link between BRAF V600E mutations and increased tumor aggressiveness, including higher rates of recurrence and disease-specific mortality in PTC patients. Similar correlations with adverse clinicopathological parameters have been observed in melanoma (29–32), colorectal neoplasms, and glial tumors. Likewise, TERT promoter mutations are associated with aggressive disease features, such as increased recurrence risk and disease-specific mortality in PTC, as well as greater malignant potential in melanoma, glioma, and urothelial cancers (33). Notably, substantial correlations have been identified between BRAF V600E and TERT promoter genetic changes, with especially frequent simultaneous presence detected in papillary thyroid carcinomas and skin melanomas. While each genetic alteration independently affects cancer prognosis, their simultaneous presence is associated with significantly more aggressive clinical and pathological characteristics. Such features encompass lymph node involvement, remote metastatic spread, higher tumor stages, disease recurrence, and increased mortality specific to PTC among affected individuals. A comprehensive PTC meta-analysis revealed 7.7% prevalence (145/1892 cases) of concurrent BRAF V600E and TERT promoter mutations. Similarly, in melanoma, this mutational co-occurrence correlates with increased tumor dimensions, elevated mitotic indices, lymphatic involvement, ulceration, treatment resistance, heightened recurrence risk, and melanoma-specific mortality (34, 35). Together, this evidence indicates that coexisting BRAF V600E and TERT promoter mutations synergistically drive tumor progression and enhance malignant behavior in papillary thyroid carcinoma.

Research conducted by Liu and colleagues (36) confirmed a potent synergistic interaction, in which concurrent mutations upregulate TERT expression via the BRAF V600E → MAPK pathway → FOS → GABP → TERT signaling cascade (Figure 3). This mechanistic discovery sheds light on the molecular basis underlying the synergistic oncogenic potential observed when BRAF V600E and TERT promoter mutations coexist. The activated BRAF V600E/MAPK pathway facilitates the formation of GABP transcriptional complexes, thereby enhancing their recruitment to and transcriptional activation of mutated TERT promoter regions. Specifically, investigations identified GABPB—the catalytic subunit of the GABP complex, rather than GABPA (the DNA-binding subunit)—as a critical downstream effector within the BRAF V600E/MAPK signaling cascade. effector significantly enhances GABPB transcriptional expression, thereby driving GABP complex formation and subsequently potentiating TERT expression. TERT expression is strongly promoted. Evidence also shows that both MYC and FOS transcription factors interact with the 5'-untranslated region (5'-UTR) of GABPB. Furthermore, BRAF V600E/MAPK signaling promotes FOS phosphorylation, strengthening its binding capacity to GABPB 5′-UTR, which in turn amplifies GABPB expression and

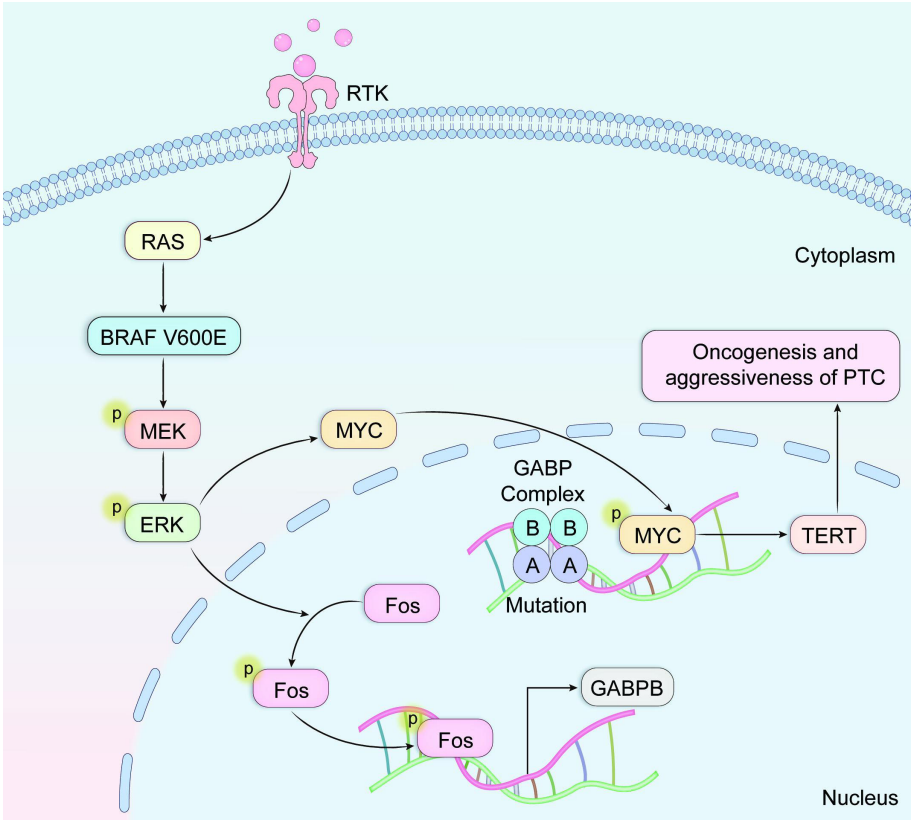

FIGURE 3
The activated BRAF V600E/MAPK pathway facilitates assembly of transcriptional GABP complexes, subsequently enhancing their recruitment to and transcriptional activation of mutated TERT promoter regions.

activating mutant TERT. FOS-dependent stimulation of GABP transcription via the activated BRAF V600E/MAPK pathways augments mutant TERT promoter activity by promoting the recruitment of conventional RNA polymerase complexes. This mechanism enables mutation-specific regulation of TERT transcription. However, TERT expression can also be regulated independently of TERT promoter status; specifically, BRAF V600E/MAPK signaling can elevate TERT levels through MYC without requiring TERT promoter mutations, even in the absence of TERT promoter mutations, although this effect is comparatively weaker than the promoter-dependent pathway. Consequently, the BRAF V600E/MAPK pathway demonstrates dual regulatory capacity over TERT expression, operating through both mutation-dependent and mutation-independent mechanisms. Within this synergistic model, BRAF V600E mutations primarily enhance cellular proliferative, while TERT promoter mutations mainly contribute to cellular immortalization and survival.

Radioiodine (RAI) therapy constitutes the conventional systemic intervention for differentiated thyroid carcinoma (DTC) presenting with advanced, persistent, recurrent, or metastatic characteristics. Therapeutic responsiveness to RAI administration fundamentally determines clinical outcomes. BRAFV600E mutations demonstrate established correlations with radioiodine refractoriness (RAI-R) through MAPK pathway hyperactivation, which induces cellular dedifferentiation and consequently impairs sodium-iodide symporter (NIS) expression and functionality. Several studies have also confirmed the association of TERT-p mutations with RAI-R (25, 30, 37–40). The clinical significance of this association has been independently validated across diverse geographical cohorts, encompassing both Asian and Western patient populations. Notably, concurrent BRAF V600E and TERT promoter mutations demonstrate significantly stronger predictive capacity for radioiodine refractoriness compared with either mutation occurring independently. Despite relatively limited sample sizes in existing studies, TERT promoter mutations demonstrate remarkably high positive predictive value for therapeutic resistance with the predominant majority of TERT-mutated cases exhibiting radioiodine refractoriness. Furthermore, these genetic alterations demonstrate strong associations with impaired radioiodine uptake capacity (41–44). Conversely, TERT promoter mutation status demonstrates limited sensitivity as a predictive biomarker, evidenced by numerous radioiodine-refractory cases occurring in the absence of these genetic alterations. This observation strongly suggests the existence of alternative molecular mechanisms contributing to therapeutic resistance. Current evidence indicates TERT promoter mutations occur in approximately 24.2-45.5% of radioiodine-refractory cases, representing a significant but incomplete proportion of therapy-resistant patients.

2.3 RAS mutations

The RAS proto-oncogene family encompasses three structurally conserved membrane-anchored proteins: NRAS, HRAS, and KRAS, which function as critical molecular switches in signal transduction pathways. Under physiological conditions, RAS activation occurs through guanine nucleotide exchange specifically GDP displacement by GTP facilitated by Grb2/SOS adapter protein complexes. This activation subsequently initiates downstream signaling cascades, predominantly the Raf-MAPK and PI3K-AKT pathways (Figure 2B). Such integrated signal transduction systems control multiple vital cellular functions encompassing cell division, specialization, longevity, and metabolic operations (45–47). Specific missense mutations affecting critical codons within RAS genes—particularly codons 12, 13, and 61 in NRAS and HRAS—impair intrinsic GTPase activity necessary for RAS protein inactivation. Consequently, these alterations result in constitutive pathway activation and unregulated downstream signaling. This cancer-promoting process participates in the development of various human tumors, such as pancreatic ductal adenocarcinoma, colorectal cancer, non-small cell pulmonary carcinoma, and differentiated thyroid tumors. Specifically in papillary thyroid carcinoma, RAS gene aberrations appear most frequently within the follicular variant histological pattern.

RAS mutants demonstrate distinctive patterns of downstream pathway activation. Within tumor tissues, research has identified KRAS mutants primarily activating the MAPK pathway, whereas NRAS mutants predominantly amplify PI3K-AKT pathway signaling. Among PTC cases, RAS genomic modifications display reciprocal exclusivity with BRAF mutations (48), indicating functional similarity between RAS and BRAF alterations, while suggesting BRAF mutations can autonomously influence PTC development. Production of aberrant RAS proteins triggers continuous activation of downstream signaling cascades, disturbing cellular equilibrium and fostering abnormal proliferation, compromised differentiation, and heightened survival mechanisms.

Beyond their distinctive function within the PI3K/AKT signaling cascade, RAS gene alterations may simultaneously appear with EIF1AX mutations in patients diagnosed with papillary thyroid carcinoma. In advanced eukaryotic organisms, the process of translation initiation operates under strict control of both cap binding mechanisms and the 43S pre-initiation complexes (PIC). The assembly of PIC requires the ternary complex (EIF2-GTP-tRNAi(Met)) to be incorporated onto the 40S ribosomal subunit. EIF1A, a constituent of PIC, derives from genes located on human chromosomes X and Y, specifically EIF1AX and EIF1AY. According to a previous study (49), protein translation initiation necessitates the complex containing EIF1AX as an essential element. Follicular PTC commonly exhibits isolated alterations within the EIF1AX gene. However, progressive disease stages tend to manifest simultaneous genetic changes affecting both EIF1AX and RAS genes. The literature (25, 37, 50) indicates that C-terminal splice site alterations (A113splice) in EIF1AX appear exclusively in thyroid malignancies, whereas N-terminal structural domain modifications can be detected across various neoplasms, including uveal melanoma. Research investigation 149 examining EIF1AX (A113splice) variants across multiple laboratory and animal models reveals their capacity to substantially elevate mutation frequencies. Experimental systems both outside and within living organisms showed that A113splice variants can collaborate with cancer-causing RAS to accelerate thyroid malignancy development. The prevalent EIF1AX-A113Splice alteration, frequently linked with

carcinogenic RAS in thyroid neoplasms, stimulates TF4 production, subsequently triggering widespread protein generation through GADD34-mediated removal of phosphate groups from EIF2α. Additionally, altered EIF1AX, functioning cooperatively with malignancy-driving RAS, enhanced C-MYC protein durability. CMYC and TF4 cooperated to induce transcription of amino acid transporter proteins, and the resulting amino acid flux activated MTOR signaling. These specific mutations may be therapeutically inconvenient (e.g., for MEK, BRD4, and mTOR inhibition).

2.4 RET/PTC rearrangement

Initially described by Fusco and colleagues (38), chromosomal rearrangement of RET was first documented in papillary thyroid carcinoma. Positioned at chromosomal locus 10q11.2, the ancestral RET proto-oncogene encodes a transmembrane receptor possessing tyrosine kinase functionality that modulates cellular differentiation and growth mechanisms. Scientific investigations have discovered four separate ligands to date: glial-derived neurotrophic factor (GDN), neurotrophin (NRTN), artemin (ARTN), and persephin (PSPN). These ligands collectively stimulate RET activity via interactions with their respective co-receptor molecules. Expression of RET protein occurs primarily in thyroid par bone or C cells, while scientific consensus regarding its presence in follicular cells of the thyroid continues to be debated.

RET/PTC-associated oncogenic activity emerges through specific chromosomal alterations wherein RET's C-terminal kinase domain becomes joined with both promoter regions and N-terminal segments from disparate genetic elements (39).

The transformation of the cancer patient's condition into a genetic disorder linked to the presence of the RET/PTC kinase is triggered by a series of genomic events. These events involve the fusion of the C-terminus of the kinase with the N-terminal sequences of the regulatory elements. In addition, the development of the disorder allows the inappropriate expression of the receptor in the tissue of the thyroid. The fusion of the two components allows the creation of a chimeric oncoprotein that can interact with the SHC articulin adapter proteins. This activity then activates the RAS-RAF-MAPK pathway. According to the scientific literature, there are no fewer than 13 different variants of the RET/PTC rearrangement (40). These genomic alterations exhibit remarkable specificity, appearing predominantly in papillary thyroid carcinoma cases. RET/PTC1 and RET/PTC3 predominate among these genomic alterations, constituting in excess of 90% of documented rearrangement cases (51). Inversions occurring centrally within chromosome 10q generate both RET/PTC1 and RET/PTC3 oncogenes, wherein RET undergoes fusion with activator genes—CCDC6 (alternatively designated H4) and NCOA4 (alternatively termed ELE1 or RFG), respectively. The RET/PTC rearrangement is more frequent in patients less than 45 years of age. Notably elevated frequencies of this rearrangement appear in pediatric papillary thyroid carcinoma patients and individuals with radiation exposure history (47). Research examining pediatric cohorts revealed associations between RET/PTC1 and classical papillary thyroid carcinoma morphology, while solid variant PTC tumors demonstrated greater prevalence of RET/PTC3 rearrangements (39). Micropapillary thyroid carcinomas likewise exhibit substantial RET/PTC rearrangement rates, indicating these genomic alterations likely represent initiating molecular events during papillary thyroid carcinogenesis. Transgenic murine models have established that thyroid-specific expression of RET/PTC1 oncogenes triggers characteristic morphological alterations consistent with PTC development (51). Previously mentioned investigations confirm that detection of RET/PTC rearrangements within RNA isolates from thyroid nodule aspirates provides valuable diagnostic information as one criterion for PTC identification. However, false positive results occasionally occur in certain benign nodular conditions, while accumulated evidence suggests patients harboring RET/PTC-positive PTC predominantly manifest non-aggressive disease without progression to poorly differentiated thyroid malignancies.

2.5 Association of traditional biomarkers with clinicopathologic features

Studies have shown that mutations in BRAF and mutations in TERT p are significantly associated with clinicopathologic features of PTC, such as distant metastasis, many metastases in lymph nodes, and advanced development (52, 53). Lee and Tufano et al. conducted a meta-analysis of 26 studies including 1168 and 2470 patients with PTC (54, 55). They reported that BRAF mutations were associated with histologic subtypes, the presence of distant metastases in papillary thyroid carcinoma, and a higher clinical stage, even though the same results were initially published in a meta-analysis by Tufano et al. in Korea. Xing et al. reported the association of BRAF mutations with high recurrence and mortality rates in a large multicenter study, except for the progressive stage and malignant development in patients with PTC, and tiny PTCs (less than 1 cm in diameter) have also been shown to have BRAF mutations, which have been suggested to be an early stage of PTC or a contributing factor to tumorigenesis (56–59). However, in Chen's study (60), double mutations in BRAF and TERT p were also significantly associated with clinicopathologic features, and as the prevalence of PTC increased, at least 30% of PTC patients had BRAFV600E mutations, of which approximately 10% also had TERTp mutations.The coexistence of BRAFV600E and TERTp mutations strongly predicted a poor prognosis, while The coexistence of BRAFV600E and TERTp mutations strongly predicts poor prognosis, and TERTp is an independent predictor over BRAF. And as older men are more likely to have double mutations, testing for double genes is also recommended for older men.

In Nasirden's study (61), we found that all patients with TERT p mutations underwent total thyroidectomy, which provides a new perspective on the value of preoperative molecular mutation testing for decision-making on the scope of surgery.TERTp mutations have received widespread attention in recent years, and in addition to their prognostic value, TERTp mutations help determine the significance of surgical scope, prophylactic lymph

node dissection, dose of radioiodine therapy, and many other clinical issues, and more high-quality evidence is needed to guide clinical practice. Therefore, the coexistence of the two mutations greatly exacerbates tumorigenesis, metastasis, and lymph node metastasis in PTC, and it has been demonstrated that the two-gene mutations have the following prognostic or therapeutic aggressiveness ranking for PTC patients: BRAF + TERT+ > BRAF - TERT+ > BRAF + TERT- (60).

Despite the overall low mortality rate in PTC patients, our analysis showed that patients with BRAFV600E or TERTp mutations had a poorer prognosis and higher tumor aggressiveness, and that patients carrying dual mutations were significantly associated with recurrence, stage III/IV, and disease-free survival. Patients with double mutations had a 5.85-fold higher risk of aggressiveness and a 31.2-fold higher risk of advanced TNM stage compared to double wild type (62).

RET/PTC1 (CCDC6-RET) and RET/PCT3 (NCOA4-RET) account for 90% of RET rearrangements in patients with PTC. a large cohort study published in 2014 reported mutation rates of 6.8%-10%.RET/PTC mutations are also significantly associated with clinicopathologic features, and they are more likely to occur in younger patients with multifocal lesions and distant metastases (63). Therefore, regardless of the clinical stage, especially when treating patients with recurrent metastases, dual gene testing for RET and BRAF should be performed. Statistical analysis showed that BRAF-positive patients tended to develop lymph node metastasis. In addition, patients with bilateral tumors had a relatively high frequency of BRAF mutations. On the contrary, patients with positive RET status were more likely to be associated with distant metastasis. Moreover, among patients with RET fusion, the number of patients with T4 stage was significantly increased (64).

Whereas RAS mutations are more likely to occur with follicular PTC, studies have shown that RAS is more likely to occur in patients with PTC who have a relatively good prognosis and most of whom have not developed lymph node metastasis and progressed to advanced stages. If preoperative testing of the RAS gene is performed, a better understanding of the extent of lymph node dissection can be obtained (65).

3 Recent advances in PTC prognostic biomarkers

3.1 CD147 protein levels and genomic instability

CD147 protein,also known as matrix metalloproteinase-inducible protein or extracellular matrix metalloproteinase inducer (EMMPRIN), is a key component of the extracellular matrix metalloproteinase family and plays a crucial role in various cancer progression mechanisms. CD147, a member of the immunoglobulin superfamily, predominantly mediates intercellular interactions and signaling processes, with a structural organization comprising extracellular, transmembrane, and intracellular domains. Functionally, CD147 plays a critical role in regulating tumor biology through multiple mechanisms, including apoptotic pathway modulation via interactions with Bax (66). The interaction of CD147 with various molecules such as integrins and glycoproteins facilitates the modulation of cellular adhesion and migratory capabilities. CD147 activates multiple signal transduction pathways, notably the MAPK/ERK and PI3K/Akt cascades, thereby promoting increased cell proliferation and survival. CD147 expression is elevated in numerous neoplasms, showing a strong correlation with tumor cell invasiveness and metastatic potential. PTC exhibits a significant association between heightened CD147 expression levels and increased tumor aggressiveness, as well as poorer clinical outcomes. There has been considerable scientific interest in the interrelationship between CD147 and chromosomal instability (CIN). CIN, characterized by alterations in chromosome number and structure, is a key feature of tumorigenesis across various malignancies. Studies have shown that CD147 may affect CIN through multiple pathways, including the regulation of cell cycle, DNA damage repair, genome maintenance and other processes.

CIN is a critical feature in the pathogenesis and progression of malignancies, typically presenting as structural and numerical chromosomal aberrations (66, 67). By modulating the expression and function of repair-associated proteins, CD147 disrupts DNA damage repair mechanisms, consequently promoting CIN. Through its modulatory impact on critical checkpoint regulators including p53 and CHK1, CD147 disrupts proper cell cycle advancement and exacerbates CIN. These functions of CD147 are mediated through a large, sometimes overlapping, number of molecular pathways: it transduces signals from upstream molecules or ligands, such as cyclophilin A (CyPA), CD98, and S100A9; activates a range of downstream molecules and pathways, including matrix metalloproteinases (MMPs)-2,3,9, hypoxia-inducible factor (HIF)-1/2a, PI3K/Akt/mTOR/HIF-1a, ATM/ATR/p53; and also regulates monocarboxylate, fatty acid, and amino acid transport proteins (68). And disruption of TP53 has been suggested as an important mechanism to promote CIN propagation *in vitro* and in mouse modeling experiments. Therefore, Elevated CD147 levels potentially augment genomic mutation frequency while additionally promoting CIN through mechanisms involving inflammatory processes and oxidative stress responses. CIN Influence on Recurrence-Free Intervals among PTC Patients. Disease-free survival serves as a key clinical outcome measure, documenting the timespan patients maintain absence of disease recurrence or progression after therapeutic intervention. Scientific studies have demonstrated significant associations between CIN and patient survival trajectories, suggesting that subjects displaying CIN-associated alterations may encounter heightened probability of disease recurrence or progression compared to those without such genetic changes.

Alterations in genetic material, such as duplications, deletions, rearrangements, and additions, constitute chromosomal abnormalities that can disrupt cellular function, thereby promoting neoplastic

transformation (69–71). Previous research has identified 676 genes within chromosome 22q, with specific deletions in this region correlating with developmental disorders, neoplasms, and increased vulnerability to various pathological conditions. The repressor gene MYO18B, situated on the long arm of chromosome 22, is a widely studied genetic variant whose absence appears instrumental in ovarian and colorectal carcinogenesis (72, 73). Patients with PTC frequently exhibit Ch22q deletions and the loss of genetic material from this chromosome's long arm, which harbors the MYO18B gene, may significantly impact patient outcomes. It has been demonstrated that the incidence of chromosomal abnormalities is higher in intermediate- and high-risk patients, whereas no abnormal chromosomal changes are detected in low-risk patients. Such findings indicate that individuals with chromosomal instability typically exhibit with more aggressive disease characteristics and worse prognostic outcomes compared to those maintaining chromosomal integrity (Figure 4). Additionally, patients with chromosomal instability tend to develop larger tumors than those with normal chromosomal profiles. Furthermore, CD147 positivity correlates with increased susceptibility to advanced thyroid malignancies, including hypo-differentiated and undifferentiated variants, while simultaneously predisposing to chromosomal instability—establishing CD147 as a novel prognostic indicator for papillary thyroid carcinoma.

3.2 Tumor microenvironment

Comprising malignant cells along with adjacent immune cells, fibroblasts, glial elements, inflammatory mediators, extracellular matrix, and peritumoral vasculature, the tumor microenvironment represents a complex biological ecosystem. Growing evidence suggests that the tumor microenvironment significantly influences neoplastic initiation, growth, invasiveness, and additional pathological mechanisms. Within this complex milieu, immune cellular components exhibit particularly strong associations with cancer progression and clinical outcomes. These elements function as key mediators in immune editing processes, initially providing surveillance and suppressive functions during early carcinogenesis, yet potentially facilitating immune evasion as the malignancy evolves.

Macrophages are the predominant immune cell population within tumor microenvironments and are categorized into three distinct subtypes based on phenotypic and functional characteristics: M0, M1, and M2 (74, 75). M0 macrophages persist in an undifferentiated and dormant condition until exposed to specific polarization stimuli that induce their transformation into functionally specialized M1 or M2 phenotypes. The M1 phenotype exhibits pro-inflammatory properties that enhance immune responses and impede neoplastic advancement, whereas M2 macrophages acts oppositely by facilitating carcinogenesis and malignant progression, thus establishing these distinct macrophage populations as key determinants of tumor behavior. Research indicates that macrophages infiltrating PTC primarily demonstrate M2 polarization (76), playing a significant role in PTC dedifferentiation and facilitating tumor immune evasion processes. 13,23 Additionally, studies have shown that the M0/M2 macrophage infiltration ratios in papillary thyroid carcinoma is significantly higher than those in non-neoplastic thyroid tissue, correlating positively with TNM classification. Conversely, M1 macrophage infiltration is reduced in malignant tissues compared to normal counterparts, exhibiting inverse correlation with TNM parameters. Therefore, it can be concluded that M1 macrophages predominantly infiltrate PTC, the patient is likely to have low-risk PTC, whereas when M0 and M2

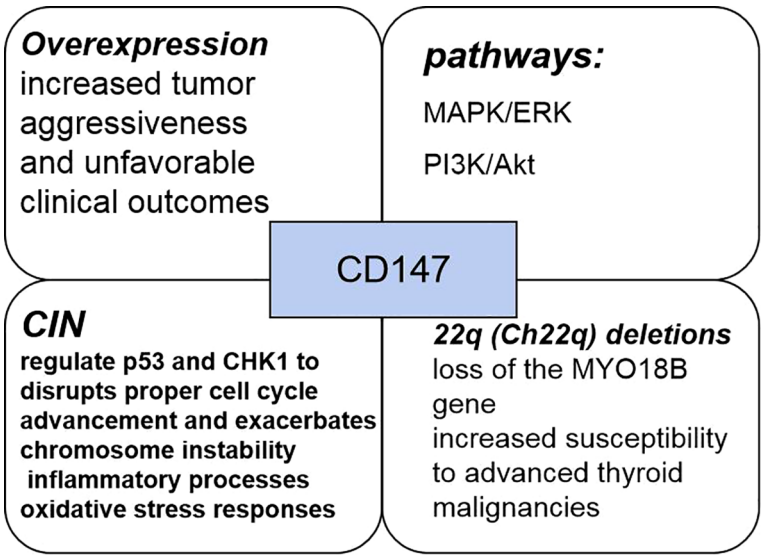

FIGURE 4
The pathways, mechanisms, and clinical features of CD147 in PTC.

macrophages are more abundant, the patient is likely to have high-risk PTC.

Within the neoplastic milieu, lymphocytes represent another critical immune cell population deserving substantial attention. Antigen-specific CD4+ T cells differentiate into specialized CD4+ memory T cell subsets that maintain immunological memory (76–78). Upon secondary antigenic stimulation, CD4+ T cells undergo multiplication and develop into a specific CD4+ T cell subpopulation targeting the pathogen.27,28 Studies have shown that the higher the infiltration ratio of CD4+ memory T cells versus CD8+ T cells in tumor tissues, the lower the risk of PTC. In contrast, a higher ratio of γδ T cell infiltration suggests a higher risk of PTC. Immune cell correlation analysis reveal interactions between macrophages and lymphocytes within the PTC microenvironment. The presence of M1 macrophages is positively associated with infiltration patterns of CD8 + T cells, CD4+ memory T cells, and follicular helper T lymphocytes. Conversely, M2 macrophage abundance demonstrates inverse correlations with these same lymphocyte populations. Therefore, a high percentage of infiltration by M1 macrophages, CD4+ memory T cells, follicular helper T cells, and CD8+ T cells represents low-risk PTC. In contrast, an excessive percentage of infiltration by M0 macrophages, M2 macrophages, and γδ T cells represents high-risk PTC (79).

Through protein-protein interaction network analysis, Li identified pivotal immune-related genes within the neoplastic microenvironment—namely CXCL5, CSF2, ICAM1, CD40LG, and CXCL12—highlighting their associations with both immunological evasion mechanisms and TNM classification parameters (80, 81). Granulocyte-macrophage colony-stimulating factor (CSF2), a hematopoietic growth factor governing myeloid lineage development from precursor cells50, exhibits strong associations with poor clinical outcomes in various cancer types (82). In addition, CSF2 maintains close functional relationships with antigen-presenting cells—specifically dendritic cells and macrophages—within the tumor microenvironment (TME), substantially influencing disease progression and patient outcomes. ICAM1, a transmembrane glycoprotein belonging to the immunoglobulin superfamily, plays essential roles in cellular adhesion, transendothelial leukocyte migration toward inflammatory sites, and lymphocyte activation. These functions consequently modulate neoplastic invasion and metastatic dissemination capacities. The chemokines CXCL5, CCL19, and CCL17 are members of the chemotactic cytokine family closely associated with tumoral angiogenesis. Upon receptor-ligand interaction, these signaling molecules promote malignant progression through various downstream pathways. Existing literature has demonstrated that chemokines CXCL5, CCL19, and CCL17 function as significant mediators in the advancement of diverse malignancies (83, 84). Survival analyses reveal significant prognostic correlations between CD40LG expression and papillary thyroid carcinoma outcomes. Furthermore, bioinformatic interrogation of TCGA dataset indicates potential tumor-suppressive role for this gene in thyroid malignancy. CD40LG ligand (CD40LG), a member of the tumor necrosis factor (TNF) gene superfamily, functions as a cytokine that specifically engages CD40 receptor. This CD40LG-CD40 interaction directly inhibits the proliferation of CD40-expressing neoplastic cells and simultaneously activates immune-mediated tumor suppression through indirect mechanisms (85).

Three immune cell types (M1 macrophages, CD4+ memory T cells, and CD8+ T cells) have been identified to be closely associated with low-risk PTC. In contrast, three immune cell types (M0 macrophages, M2 macrophages, and γδ T cells) and six immune-related genes (CSF2, CXCL5, CCL17, ICAM1, CCL19, and CD40LG) have been identified to be closely associated with high-risk PTC. Based on these associations, it was hypothesized that these cells and genes could be used as biomarkers to predict the prognosis of PTC. Their combined evaluation could help distinguish between high-risk and low-risk subtypes of the disease.

3.3 ctDNA and microRNA

ctDNA is derived from DNA fragments found in body fluids including urine, blood and cerebrospinal fluid (86). ctDNA is a very small DNA molecule that can be obtained almost exclusively from tumor cells, and it can be released from tumor cells into the bloodstream through a variety of mechanisms (e.g., apoptosis, necrosis, and secretion) (87, 88). Genetic changes in ctDNA include heterozygosity, mutations, methylation, and copy number alterations (89), which make it a potential biomarker for possible diagnostic treatments. In addition, ctDNA levels are affected by disease severity or disease progression and can vary according to disease progression, site and changes in tumor biology (90). Previous studies have shown that detection of ctDNA is helpful in diagnosing and monitoring cancer patients (91, 92). In addition, the short half-life of ctDNA (less than two hours) makes it possible to monitor tumors in real time. All these findings are sufficient to prove that ctDNA is a potential biomarker for diagnosing tumors and determining their prognosis (93).

Chung et al. (94) found that BRAF mutations could be detected in the circulating DNA of 21% of patients with PTC, whereas mutations in this gene were not present in benign patients. lan et al. (95) found that the detection rate of ctDNA was considerably higher in PTC with distant metastases (DM) than in PTC without DM, and that the rate of detection was correlated with the aggressiveness and the size of the tumor. In addition, ctDNA levels appeared to fluctuate more rapidly with disease status than conventional markers, suggesting that ctDNA may also be one of the biomarkers with therapeutic utility for PTC.

MicroRNA (miRNA) is a class of small RNA molecules that play an important role in the regulation of gene expression in cells. It is a short RNA fragment of about 20 to 22 nucleotides in length. These molecules are crucial in post-transcriptional regulation of gene expression. miRNAs can affect processes such as tumor progression, angiogenesis, invasion and metastasis. Therefore, studying miRNAs in cancer can provide valuable information

about tumor biology and possible therapeutic opportunities or biomarkers for cancer diagnosis and monitoring. Several studies have demonstrated the role of miRNA-based analysis in distinguishing high-risk tumor mutations (96)

Some studies have revealed that various miRNAs can serve as biomarkers for the diagnosis of PTC, such as miR-223-3p, miR-34-5p, miR182-5p, miR-146b-5p, miR-29a, miR-223-5p, miR-16-2-3p, miR-34a-5p, miR-346, miR-10a-5p, miR-485-3p, miR-4433a-5p和 mir-5189-3p。. In addition, studies have shown that certain miR-31 and miR-21 (e.g., miR-31 and miR-21) can help distinguish between different types of thyroid cancer (e.g., PTC and FTC).MiR-145 has also been identified as a potent marker of increased malignancy in PTC, while miR-6879-5p and miR-6774-3p are diagnostic of lymph node metastasis in PTC, and on the other hand early detection of the presence of recurrence potential in thyroid cancer is crucial. Studies have shown that miRNAs play a role in metastasis and recurrence of PTC. Specific concentrations of exosomal miRNAs (e.g., miR-29a) are associated with recurrence of PTC. In addition, miR-146b and miR-222 can be used as recurrence markers in PTC (93).

Recent studies have evaluated the expression of patient-specific miRNAs in PTC. These miRNAs may serve as useful markers for predicting the likelihood of cancer recurrence after initial treatment. Their early detection in treated patients could help identify those at higher risk of recurrence and allow for more effective and personalized interventions (97).

4 Conclusions

Strong advances in molecular research have greatly expanded our understanding of PTC even further and have led to a broader understanding of biomarkers of PTC prognosis and can be used to improve the treatment modalities for patients with PTC through biomarker expression (Figure 5, Table 1).This review provides traditional as well as novel biomarkers that predict the prognosis

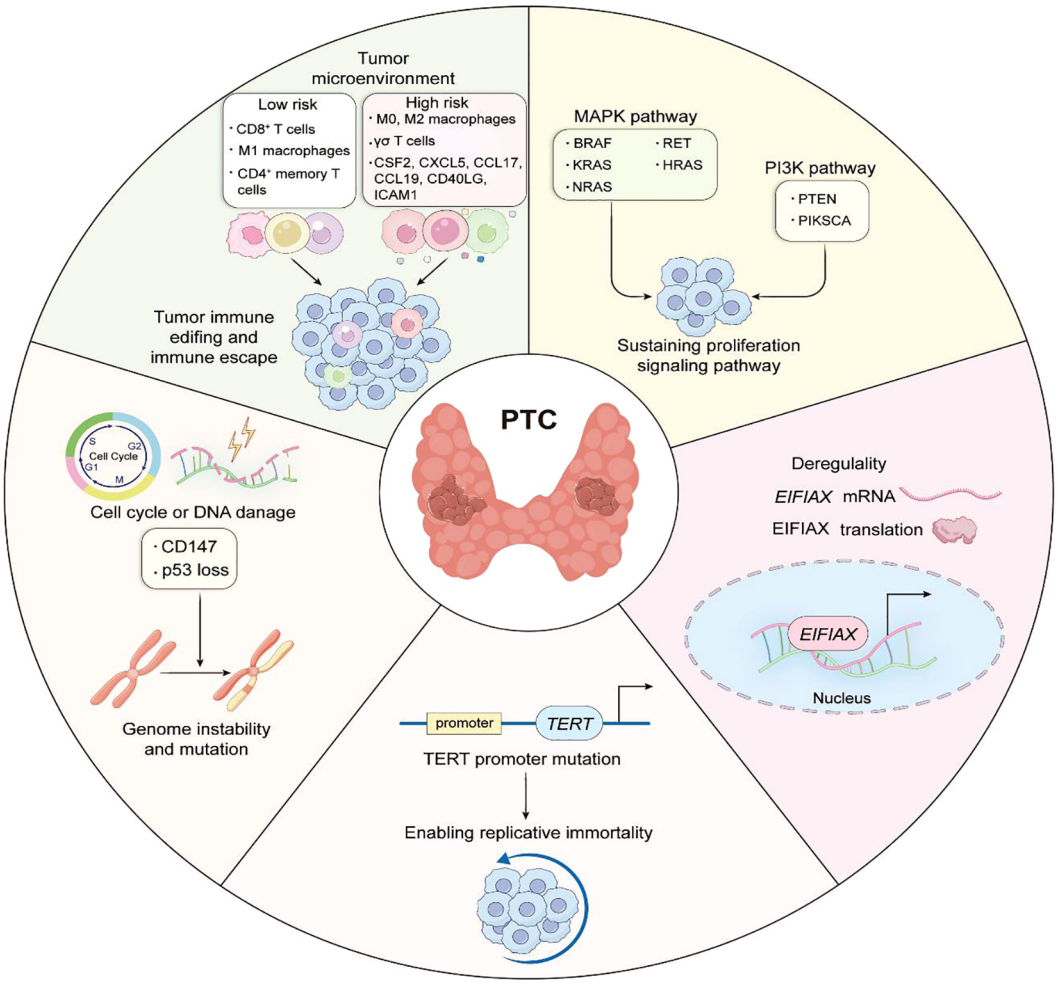

FIGURE 5
The role of biomarkers in the prognosis of papillary thyroid carcinoma.

TABLE 1 Biomarkers associated with prognosis in PTC.

Biomarkers	Signaling Pathway/mechanism	Clinical significance		References
BRAF V600E	*BRAF V600E/MAPK*	*High recurrence* *Higher mortality rate* *Worse prognosis*	*BRAF + TERT+ > BRAF − TERT+ > BRAF + TERT−*	(52–59)
TERT	*BRAF V600E → MAPK → FOS → GABP → TERT*	*RAI-R* *Poor prognosis* *Increased aggressiveness*		(25, 30, 37–40, 61)
RAS	*Raf-MAPK* *PI3K-AKT*	*Follicular PTC* *Good prognosis*		(48, 65)
RET/PTC	*RAS-RAF-MAPK*	*Prevalent in younger individuals* *multifocal lesions* *distant metastases*		(40, 63, 64)
CD147	*PI3K/Akt/mTOR/HIF-1aATM/ATR/p53*	*CIN* *Poor prognosis* *Larger tumor size*		(68–71)
ctDNA	*apoptosis* *necrosis* *secretion*	*BRAF V600E* *Distant Metastasis* *Tumor Size*		(86–90, 93–95)
microRNA	*Post transcriptional gene expression regulation*	*Diagnosis of Thyroid Cancer Types* *Recurrence* *High Risk*		(93, 96, 97)
Tumor Microenvironment	*Tumor immune editing*	*Distinguish between low-risk and high-risk PTC*		(74–85)

of PTC and can be detected by single or multiple genes and cells, for example, mutations in the BRAF and TERT genes imply increased tumor aggressiveness and refractoriness to radioiodine therapy, mutations in the BRAF and RET genes imply an increase in the TMN stage, and mutations in the RAS imply a more favorable The previous traditional biomarkers are already in use in the clinic, and the detection of these genes at the time of thyroid puncture not only provides a basis for an uncertain diagnosis, but also suggests a surgical approach and postoperative treatment. The detection of new biomarkers, including the expression of CD147, which implies increased aggressiveness and chromosomal instability in PTC, and the detection of macrophages and T-cells and their associated immune-expressed genes, which can be used to categorize patients into those with low-risk and high-risk PTC, have not yet been used in the clinic. However, this immunohistochemistry is not specific and has no significance for the diagnosis of PTC, but it has a guiding significance for the potential prognosis of PTC patients, and further experiments and investigations are needed to determine whether there is any correlation with the traditional biomarkers, and the detection of the tumor microenvironment is relatively more complicated, and the current detection of the tumor microenvironment not only consumes more consumables and funds (98), but also leads to inaccurate results, and some studies have shown that the heterogeneity of the tumor can lead to inaccurate results. The tumor heterogeneity can also lead to inaccurate results, and some studies have proved that the tumor microenvironment may be a solution to overcome drug resistance and improve the prognosis of patients (99), but this requires a large number of experiments to prove the research. We know that ctDNA and microRNA are biomarkers with great potential in diagnosing and determining the prognosis of PTC. However, ctDNA and microRNA have very small fragments that are difficult to extract in blood, and it is unstable and easily degraded by various enzymes. Therefore, the analysis of ctDNA and microRNA requires highly sensitive and specific techniques. In recent years, detection strategies for ctDNA and microRNA have become more sophisticated (100). Several techniques are available for analyzing ctDNA, including concentration-based detection and structure-based detection (mutation, methylation). Based on the detection principle, they can be categorized into two types: QPCR and NGS. however, the former can identify only a few known mutations, whereas the latter, although it can identify a large amount of mutation data, must be tested on a large number of samples each time, which makes it difficult to implement within many hospitals.

The combined use of biomarkers has been increasingly used in clinical practice, but with the increase in morbidity, it is crucial to choose a more appropriate treatment for patients to achieve better therapeutic efficacy and longer-term survival. Whether it is possible to combine new biomarkers with traditional biomarkers, whether there is a link between them, and how to better utilize them in

clinical practice to guide the prognosis of patients are all worthy of further clinical research. deserve further clinical research.

Author contributions

ML: Writing – original draft, Writing – review & editing, Methodology, Investigation, Conceptualization. QL: Writing – review & editing, Investigation, Resources, Supervision. CZ: Writing – review & editing, Supervision, Investigation. QH: Writing – review & editing, Supervision, Data curation. YC: Writing – review & editing, Conceptualization, Supervision.

Funding

The author(s) declare that financial support was received for the research and/or publication of this article. We are thankful for grants from Chongqing Medical University Future Medicine Youth Innovation Program (W 0181), and the Cultivation Fund of the Chongqing Health Center for Women and Children (No. 2021YJMS01).

Conflict of interest

The authors declare that the research was conducted in the absence of any commercial or financial relationships that could be construed as a potential conflict of interest.

Generative AI statement

The author(s) declare that no Generative AI was used in the creation of this manuscript.

Publisher's note

All claims expressed in this article are solely those of the authors and do not necessarily represent those of their affiliated organizations, or those of the publisher, the editors and the reviewers. Any product that may be evaluated in this article, or claim that may be made by its manufacturer, is not guaranteed or endorsed by the publisher.

References

1. Hundahl SA, Cady B, Cunningham MP, Mazzaferri E, Mckee RF, Rosai J, et al. Initial results from a prospective cohort study of 5583 cases of thyroid carcinoma treated in the United States during 1996. u.s. and german thyroid cancer study group. an american college of surgeons commission on cancer patient care evaluation study. *Cancer*. (2015) 89:202–17. doi: 10.1002/1097-0142(20000701)89:1<202::AID-CNCR27>3.0.CO;2-A

2. Davies L, Welch HG. Increasing incidence of thyroid cancer in the United States, 1973-2002. *Jama*. (2006) 295:2164–7. doi: 10.1001/jama.295.18.2164

3. Aschebrook-Kilfoy B, Ward MH, Sabra MM, Devesa SS. Thyroid cancer incidence patterns in the United States by histologic type, 1992–2006. *Thyroid*. (2011) 21(2):125–34. doi: 10.1089/thy.2010.0021

4. Cho BY, Choi HS, Park YJ, Lim JA, Ahn HY, Lee EK, et al. Changes in the clinicopathological characteristics and outcomes of thyroid cancer in Korea over the past four decades. *Thyroid Off J Am Thyroid Assoc*. (2013) 23:797–804. doi: 10.1089/thy.2012.0329

5. La Vecchia C, Malvezzi M, Bosetti C, Garavello W, Bertuccio P, Levi F, et al. Thyroid cancer mortality and incidence: a global overview. *Int J Cancer J Int Du Cancer*. (2015) 136:2187–95. doi: 10.1002/ijc.v136.9

6. Loh KC, Greenspan FS, Gee L, Miller TR, Yeo PP. Pathological tumor-node-metastasis (pTNM) staging for papillary and follicular thyroid carcinomas: a retrospective analysis of 700 patients. *J Clin Endocrinol Metab*. (1997) 82:3553–62. doi: 10.1210/jcem.82.11.4373

7. Liu C, Chen T, Liu Z. Associations between BRAF(V600E) and prognostic factors and poor outcomes in papillary thyroid carcinoma: a meta-analysis. *World J Surg Oncol*. (2016) 14:241. doi: 10.1186/s12957-016-0979-1

8. Oh CM, Kong HJ, Kim E, Kim H, Jung KW, Park S, et al. National epidemiologic survey of thyroid cancer (NEST) in korea. *Epidemiol Health*. (2018) 40:e2018052. doi: 10.4178/epih.e2018052

9. Lobo J, Ohashi R, Amin MB, Berney DM, Compérat EM, Cree IA, et al. WHO 2022 landscape of papillary and chromophobe renal cell carcinoma. *Histopathology*. (2022) 81:426–38. doi: 10.1111/his.14700

10. Ramirez AT, Gibelli B, Tradati N, Giugliano G, Zurlo V, Grosso E, et al. Surgical management of thyroid cancer. *Expert Rev Anticancer Ther*. (2007) 7:1203–14. doi: 10.1586/14737140.7.9.1203

11. Smallridge RC, Copland JA. Anaplastic thyroid carcinoma: pathogenesis and emerging therapies. *Clin Oncol*. (2010) 22:486–97. doi: 10.1016/j.clon.2010.03.013

12. Are C, Shaha AR. Anaplastic thyroid carcinoma: biology, pathogenesis, prognostic factors, and treatment approaches. *Ann Surg Oncol*. (2006) 13:453–64. doi: 10.1245/ASO.2006.05.042

13. Davies H, Bignell GR, Cox C, Stephens P, Edkins S, Clegg S, et al. Davies h, bignell gr, cox c et al.mutations of the braf gene in human cancer. *nature*. (2002) 417:949–54. doi: 10.1038/nature00766

14. Garnett MJ, Marais R. Guilty as charged: b-raf is a human oncogene. *Cancer Cell*. (2004) 6:313–9. doi: 10.1016/j.ccr.2004.09.022

15. Soares P, Trovisco V, Rocha AS, Lima J, Castro P, Preto A, et al. Braf mutations and ret[[sol]]ptc rearrangements are alternative events in the etiopathogenesis of ptc. *Oncogene*. (2003) 22:4578. doi: 10.1038/sj.onc.1206706

16. Kim SK, Song KH, Lim SD, Lim YC, Yoo YB, Kim JS, et al. Clinical and pathological features and the braf(v600e) mutation in patients with papillary thyroid carcinoma with and without concurrent hashimoto thyroiditis. *Thyroid Off J Am Thyroid Assoc*. (2009) 19:137. doi: 10.1089/thy.2008.0144

17. Namba H, Nakashima M, Hayashi T, Hayashida N, Maeda S, Rogounovitch TI, et al. Clinical implication of hot spot braf mutation, v599e, in papillary thyroid cancers. . *J Clin Endocrinol Metab*. (2003) 9):4393–7. doi: 10.1210/jc.2003-030305

18. Scheffel RS, Dora JM, Maia AL. BRAF mutations in thyroid cancer. *Current opinion in oncology*. (2022) 34:9–18. doi: 10.1097/CCO.0000000000000797

19. Chung JH. Braf and tert promoter mutations: clinical application in thyroid cancer. *Endocrine J*. (2020) 67(6):577–84. doi: 10.1507/endocrj.EJ20-0063

20. Nikiforova MN, Kimura ET, Gandhi M, Biddinger PW, Knauf JA, Basolo F, et al. BRAF mutations in thyroid tumors are restricted to papillary carcinomas and anaplastic or poorly differentiated carcinomas arising from papillary carcinomas. *J Clin Endocrinol Metab*. (2003) 88:5399–404. doi: 10.1210/jc.2003-030838

21. Kimura ET, Nikiforova MN, Zhu Z, Knauf JA, Fagin JA. High prevalence of braf mutations in thyroid cancer: genetic evidence for constitutive activation of the ret/ptc-ras-braf signaling pathway in papillary thyroid carcinoma1. *Cancer Res*. (2003) 63:1454–7. doi: 10.1016/j.jacc.2011.10.507

22. Mitsutake N. Conditional brafv600e expression induces dna synthesis, apoptosis, dedifferentiation, and chromosomal instability in thyroid pccl3 cells. *Cancer Res*. (2005) 65:2465–73. doi: 10.1158/0008-5472.CAN-04-3314

23. Huang FW, Hodis E, Xu MJ, Kryukov GV, Garraway LA. Highly recurrent tert promoter mutations in human melanoma. *Science*. (2013) 339(6122):957–9. doi: 10.1126/science.1229259

24. Horn S, Adina FI, Rachakonda PS, Fischer C, Sucker A, Gast A, et al. Tert promoter mutations in familial and sporadic melanoma. *Science*. (2013) 339:959–61. doi: 10.1126/science.1230062

25. Landa I., Cabanillas M. E.. Genomic alterations in thyroid cancer: biological and clinical insights. *Nat Rev Endocrinol*. (2024) 20:93–110. doi: 10.1038/s41574-023-00920-6

26. Chiba K, Lorbeer FK, Shain AH, McSwiggen DT, Schruf E, Oh A, et al. Mutations in the promoter of the telo-merase gene TERT contribute to tumorigenesis by a two-step mechanism. *Science*. (2017) 357:1416–20. doi: 10.1126/science.aao0535

27. Landa I, Ganly I, Chan TA, Mitsutake N, Matsuse M, Ibrahimpasic T, et al. Frequent somatic tert promoter mutations in thyroid cancer: higher prevalence in advanced forms of the disease. *J Clin Endocrinol Metab*. (2013) 98(9):E1562–6. doi: 10.1210/jc.2013-2383

28. Liu X, Bishop J, Shan Y, Pai S, Liu D, Murugan AK, et al. Highly prevalent tert promoter mutations in aggressive thyroid cancers. *Endocrine Related Cancer*. (2013) 20:603–10. doi: 10.1530/ERC-13-0210

29. Safaee Ardekani G, Jafarnejad SM, Tan L, Saeedi A, Li G, Toland AE. The prognostic value of braf mutation in colorectal cancer and melanoma: a systematic review and meta-analysis. *PloS One*. (2012) 7:e47054. doi: 10.1371/journal.pone.0047054

30. Thomas NE, Edmiston SN, Alexander A, Groben PA, Parrish E, Kricker A, et al. Association between nras and braf mutational status and melanoma-specific survival among patients with higher-risk primary melanoma. *JAMA Oncol*. (2015) 1:359. doi: 10.1001/jamaoncol.2015.0493

31. Dahiya S, Haydon DH, Alvarado D. Brafv600e mutation is a negative prognosticator in pediatric ganglioglioma. *Acta Neuropathologica*. (2013) 125:901–10. doi: 10.1007/s00401-013-1120-y

32. Summers MG, Smith CG, Maughan TS, Kaplan R, Cheadle JP. Braf and nras locus specific variants have different outcomes on survival to colorectal cancer. *Clin Cancer Res*. (2017) 23:2742–9. doi: 10.1158/1078-0432.CCR-16-1541

33. Griewank KG, Rajmohan M, Anton PBJ, Bastian S, Elisabeth L, Miriam P, et al. Tert promoter mutation status as an independent prognostic factor in cutaneous melanoma. *J Natl Cancer Inst*. (2014) 106:dju246. doi: 10.1093/jnci/dju246

34. Nagore E, Heidenreich B, Rachakonda S, Garcia-Casado Z, Requena C, Soriano V, et al. Tertpromoter mutations in melanoma survival. *Int J Cancer*. (2016) 139(1):75–84. doi: 10.1002/ijc.v139.1

35. Macerola E, Loggini B, Giannini R, Garavello G, Giordano M, Proietti A, et al. Coexistence of tert promoter and braf mutations in cutaneous melanoma is associated with more clinicopathological features of aggressiveness. *Virchows Archiv*. (2015) 467:177–84. doi: 10.1007/s00428-015-1784-x

36. Liu R, Zhang T, Zhu G, Xing M. Regulation of mutant tert by braf v600e/map kinase pathway through fos/gabp in human cancer. *Nat Commun*. (2018) 9:579. doi: 10.1038/s41467-018-03033-1

37. Kunstman JW, Christofer JC, Gerald G, Brown TC, Adam S, Healy JM, et al. Characterization of the mutational landscape of anaplastic thyroid cancer via whole-exome sequencing. *Hum Mol Genet*. (2015) 8):2318–29. doi: 10.1093/hmg/ddu749

38. Fusco A, Grieco M, Santoro M, Berlingieri MT, Pilotti S, Pierotti MA, et al. A new oncogene in human thyroid papillary carcinomas and their lymph-nodal metastases. *Nature*. (1987) 328:170–2. doi: 10.1038/328170a0

39. Nikiforov YE. Ret/ptc rearrangement in thyroid tumors. *Endocrine Pathol*. (2002) 13:3–16. doi: 10.1385/EP:13:1:03

40. Cristina R, Rossella E. Ret/ptc translocations and clinico-pathological features in human papillary thyroid carcinoma. *Front Endocrinol*. (2012) 3. doi: 10.3389/fendo.2012.00054

41. Chakravarty D, Santos E, Ryder M, Knauf JA, Fagin JA. Small-molecule mapk inhibitors restore radioiodine incorporation in mouse thyroid cancers with conditional braf activation. *J Clin Invest*. (2011) 121:4700–11. doi: 10.1172/JCI46382

42. Nagarajah J, Le M, Knauf JA, Ferrandino G, Fagin JA. Sustained erk inhibition maximizes responses of brafv600e thyroid cancers to radioiodine. *J Clin Invest*. (2016) 126:4119. doi: 10.1172/JCI89067

43. Lamartina L, Anizan N, Dupuy C, Leboulleux S, Schlumberger M. Redifferentiation-facilitated radioiodine therapy in thyroid cancer. *Endocrine Related Cancer*. (2021) 28:T179–91. doi: 10.1530/ERC-21-0024

44. Van Nostrand D, Veytsman I, Kulkarni K, Heimlich L, Burman KD. Redifferentiation of differentiated thyroid cancer: clinical insights from a narrative review of literature. *Thyroid: Off J Am Thyroid Assoc*. (2023) 33(6):674–81. doi: 10.1089/thy.2022.0632

45. Moura MM, Cavaco BM, Leite V. Ras proto-oncogene in medullary thyroid carcinoma. *Endocrine-related Cancer*. (2015) 22:R235. doi: 10.1530/ERC-15-0070

46. Paulson VA, Shivdasani P, Angell TE, Cibas ES, Krane JF, Lindeman NI, et al. Noninvasive follicular thyroid neoplasm with papillary-like nuclear features accounts for more than half of "carcinomas" harboring ras mutations. *Thyroid*. (2017) 27:506–11. doi: 10.1089/thy.2016.0583

47. Abdullah MI, Junit SM, Ng KL, Jayapalan JJ, Karikalan B, Hashim OH. Papillary thyroid cancer: genetic alterations and molecular biomarker investigations. *Int J Med Sci*. (2019) 16:450–60. doi: 10.7150/ijms.29935

48. Haigis KM, Kendall KR, Yufang W, Ann C, Haigis MC, Glickman JN, et al. Differential effects of oncogenic K-Ras and N-Ras on proliferation, differentiation and tumor progression in the colon. *Nature genetics* (2018) 40(5):600–8. doi: 10.1038/ng.115.

49. Kilic E, Koopmans A, Yavuzyigitoglu S, Vaarwater J, Klein JD. Sf3b1 and eif1ax mutations in uveal melanoma: a protective factor, or not? *Acta Ophthalmologica*. (2015) 92(s253):0–0. doi: 10.1111/j.1755-3768.2014.4246.x

50. Landa I, Ibrahimpasic T, Boucai L, Sinha R, Fagin JA. Genomic and transcriptomic hallmarks of poorly differentiated and anaplastic thyroid cancers. *J Clin Invest*. (2016) 126:1052. doi: 10.1172/JCI85271

51. Cortés JMR, Zerón HM. Genetics of Thyroid Disorders. *Folia medica*. (2019) 61:172–9. doi: 10.2478/folmed-2018-0078

52. Kim TH, Park YJ, Lim JA, Ahn HY, Lee EK, Lee YJ, et al. The association of the BRAF(V600E) mutation with prognostic factors and poor clinical outcome in papillary thyroid cancer: a meta-analysis. *Cancer: A J Am Cancer Soc*. (2012) 118:1764–73. doi: 10.1002/cncr.26500

53. Lee JI, Jang HW, Kim SW, Kim JW, Oh YL, Chung JH. Brafv600e mutation in fine-needle aspiration aspirates: association with poorer prognostic factors in larger papillary thyroid carcinomas. *Head Neck*. (2013) 35(4):548–53. doi: 10.1002/hed.22997

54. Lee JH, Lee ES, Kim YS. Clinicopathologic significance ofbraf v600e mutation in papillary carcinomas of the thyroid. *Cancer*. (2007) 110:38–46. doi: 10.1002/cncr.v110:1

55. Tufano RP, Teixeira GV, Bishop J, Carson KA, Xing M. Braf mutation in papillary thyroid cancer and its value in tailoring initial treatment: a systematic review and meta-analysis. *Medicine*. (2012) 91:274–86. doi: 10.1097/MD.0b013e31826a9c71

56. Park YJ, Kim YA, Lee YJ, Kim SH, Park SY, Kim KW, et al. Papillary microcarcinoma in comparison with larger papillary thyroid carcinoma in brafv600e mutation, clinicopathological features, and immunohistochemical findings. *Head Neck*. (2010) 32:38–45. doi: 10.1002/hed.21142

57. Jung CK, Im SY, Kang YJ, Lee H, Jung ES, Kang CS, Bae JS, et al. Mutational patterns and novel mutations of the braf gene in a large cohort of Korean patients with papillary thyroid carcinoma. *Thyroid: Off J Am Thyroid Assoc*. (2012) 22(8):791–7. doi: 10.1089/thy.2011-0123

58. de Biase D, Cesari V, Visani M, Casadei GP, Cremonini N, Gandolfi G, et al. High-sensitivity braf mutation analysis: braf v600e is acquired early during tumor development but is heterogeneously distributed in a subset of papillary thyroid carcinomas. *J Clin Endocrinol Metab*. (2014) 99:E1530–8. doi: 10.1210/jc.2013-4389

59. Guan H, Ji M, Bao R, Yu H, Wang Y, Hou P, et al. Association of high iodine intake with the t1799a braf mutation in papillary thyroid cancer. *J Clin Endocrinol Metab*. (2009) 5):1612–7. doi: 10.1210/jc.2008-2390

60. Chen B, Shi Y, Xu Y, Zhang J. The predictive value of coexisting BRAFV600E and TERT promoter mutations on poor outcomes and high tumour aggressiveness in papillary thyroid carcinoma: A systematic review and meta-analysis. *Clin Endocrinol*. (2021) 94:731–42. doi: 10.1111/cen.14316

61. Nasirden A, Saito T, Fukumura Y, Hara K, Akaike K, Kurisaki-Arakawa A, et al. In Japanese patients with papillary thyroid carcinoma, TERT promoter mutation is associated with poor prognosis, in contrast to BRAF ^{V600E} mutation. *Virchows Archiv: an Int J Pathol*. (2016) 469:687–96. doi: 10.1007/s00428-016-2027-5

62. Ding Z, Tao X, Deng X, Guo B, Kang J, Wu B, et al. Genetic analysis and clinicopathologic features of locally advanced papillary thyroid cancers: a prospective observational study. *J Cancer Res Clin Oncol*. (2023) 149:6303–13. doi: 10.1007/s00432-022-04541-w

63. Uno D, Endo K, Yoshikawa T, Hirai N, Kobayashi E, Nakanishi Y, et al. Correlation between gene mutations and clinical characteristics in papillary thyroid cancer: a retrospective analysis of BRAF mutations and RET rearrangements. *Thyroid Res*. (2024) 17:21. doi: 10.1186/s13044-024-00209-4

64. Wang Q, Yu B, Zhang S, Wang D, Xiao Z, Meng H, et al. Papillary thyroid carcinoma: correlation between molecular and clinical features. *Mol diagnosis Ther*. (2024) 28:601–9. doi: 10.1007/s40291-024-00721-1

65. Haghzad T, Khorsand B, Razavi SA, Hedayati M. A computational approach to assessing the prognostic implications of BRAF and RAS mutations in patients with papillary thyroid carcinoma. *Endocrine*. (2024) 86:707–22. doi: 10.1007/s12020-024-03911-3

66. Zhou Y, Fang J, Chi Y, Wu L, Chen W, Xiao R, et al. Cd147 protein molecule expression and chromosomal instability in the pathogenesis and prognosis of thyroid cancer. *Int J Biol Macromolecules*. (2024) 276(Pt 2):133944. doi: 10.1016/j.ijbiomac.2024.133944

67. De' Angelis GL, Bottarelli L, Azzoni C, De' Angelis N, Leandro G, Di Mario F, et al. Microsatellite instability in colorectal cancer. *Acta bio-medica: Atenei Parmensis*. (2018) 89:97–101. doi: 10.23750/abm.v89i9-S.7960

68. Nyalali AMK, Leonard AU, Xu Y, Li H, Zhou J, Zhang X, et al. CD147: an integral and potential molecule to abrogate hallmarks of cancer. *Front Oncol*. (2023) 13:1238051. doi: 10.3389/fonc.2023.1238051

69. Sansregret L, Vanhaesebroeck B, Swanton C. Determinants and clinical implications of chromosomal instability in cancer. Nature reviews. *Clin Oncol*. (2018) 15:139–50. doi: 10.1038/nrclinonc.2017.198

70. Yoo SK, Song YS, Lee EK, Hwang J, Kim HH, Jung G, et al. Integrative analysis of genomic and transcriptomic characteristics associated with progression of aggressive thyroid cancer. *Nat Commun*. (2019) 10:2764. doi: 10.1038/s41467-019-10680-5

71. Ye LP, Mao XL, Zhou XB, Wang Y, Xu SW, He SQ, et al. Cost-effective low-coverage whole-genome sequencing assay for the risk stratification of gastric cancer. *World J gastrointestinal Oncol*. (2022) 14:690–702. doi: 10.4251/wjgo.v14.i3.690

72. Qian S, Xie F, Zhao H, Jiang T, Sang Y, Ye W, et al. Detection of chromosomal instability using ultrasensitive chromosomal aneuploidy detection in the diagnosis of precancerous lesions of gastric cancer. *Front Genet*. (2024) 15:1359231. doi: 10.3389/fgene.2024.1359231

73. Girish V, Lakhani AA, Thompson SL, Scaduto CM, Brown LM, Hagenson RA, et al. Oncogene-like addiction to aneuploidy in human cancers. *Sci (New York N.Y.).* (2023) 381:eadg4521. doi: 10.1126/science.adg4521

74. Behnes CL, Bremmer F, Hemmerlein B, Strauss A, Ströbel P, Radzun HJ. Tumor-associated macrophages are involved in tumor progression in papillary renal cell carcinoma. *Virchows Archiv: an Int J Pathol.* (2014) 464:191–6. doi: 10.1007/s00428-013-1523-0

75. Zhang Q, Li H, Mao Y, Wang X, Zhang X, Yu X, et al. Apoptotic SKOV3 cells stimulate M0 macrophages to differentiate into M2 macrophages and promote the proliferation and migration of ovarian cancer cells by activating the ERK signaling pathway. *Int J Mol Med.* (2020) 45:10–22. doi: 10.3892/ijmm.2019.4408

76. Liu Q, Sun Z, Chen L. Memory T cells: strategies for optimizing tumor immunotherapy. *Protein Cell.* (2020) 11:549–64. doi: 10.1007/s13238-020-00707-9

77. Fu C, Jiang A. Dendritic cells and CD8 T cell immunity in tumor microenvironment. *Front Immunology.* (2018) 9:3059. doi: 10.3389/fimmu.2018.03059

78. Wang B, Hu J, Zhang J, Zhao L. Radiation therapy regulates TCF-1 to maintain CD8+T cell stemness and promotes anti-tumor immunotherapy. *Int immunopharmacology,107.* (2022) 107:108646. doi: 10.1016/j.intimp.2022.108646

79. Chatzopoulos K, Kotoula V, Manoussou K, Markou K, Vlachtsis K, Angouridakis N, et al. Tumor infiltrating lymphocytes and CD8+ T cell subsets as prognostic markers in patients with surgically treated laryngeal squamous cell carcinoma. *Head Neck Pathol.* (2020) 14:689–700. doi: 10.1007/s12105-019-01101-6

80. Li X, Jian J, Zhang A, Xiang JM, Huang J, Chen Y. The role of immune cells and immune related genes in the tumor microenvironment of papillary thyroid cancer and their significance for immunotherapy. *Sci Rep.* (2024) 14:18125. doi: 10.1038/s41598-024-69187-9

81. Lee BS, Jang JY, Seo C, Kim CH. Crosstalk between head and neck cancer cells and lymphatic endothelial cells promotes tumor metastasis via CXCL5-CXCR2 signaling. *FASEB journal: Off Publ Fed Am Societies Exp Biol.* (2021) 35:e21181. doi: 10.1096/fj.202001455R

82. Xu Z, Zhang Y, Xu M, Zheng X, Lin M, Pan J, et al. Demethylation and overexpression of CSF2 are involved in immune response, chemotherapy resistance, and poor prognosis in colorectal cancer. *OncoTargets Therapy.* (2019) 12:11255–69. doi: 10.2147/OTT.S216829

83. Gao Y, Guan Z, Chen J, Xie H, Yang Z, Fan J, et al. CXCL5/CXCR2 axis promotes bladder cancer cell migration and invasion by activating PI3K/AKT-induced upregulation of MMP2/MMP9. *Int J Oncol.* (2015) 47:690–700. doi: 10.3892/ijo.2015.3041

84. Peng C, Zhou K, An S, Yang J. The effect of CCL19/CCR7 on the proliferation and migration of cell in prostate cancer. *Tumour biology: J Int Soc Oncodevelopmental Biol Med.* (2015) 36:329–35. doi: 10.1007/s13277-014-2642-1(Retraction published Tumour Biol)

85. Kuhn NF, Purdon TJ, van Leeuwen DG, Lopez AV, Curran KJ, Daniyan AF, et al. CD40 ligand-modified chimeric antigen receptor T cells enhance antitumor function by eliciting an endogenous antitumor response. *Cancer Cell.* (2019) 35:473–488.e6. doi: 10.1016/j.ccell.2019.02.006

86. Shields MD, Chen K, Dutcher G, Patel I, Pellini B. Making the rounds: exploring the role of circulating tumor DNA (ctDNA) in non-small cell lung cancer. *Int J Mol Sci.* (2022) 23:9006. doi: 10.3390/ijms23169006

87. Yoon HJ, Kozminsky M, Nagrath S. Emerging role of nanomaterials in circulating tumor cell isolation and analysis. *ACS nano.* (2014) 8:1995–2017. doi: 10.1021/nn5004277

88. Sánchez-Herrero E, Serna-Blasco R, Robado de Lope L, González-Rumayor V, Romero A, Provencio M. Circulating Tumor DNA as a Cancer Biomarker: An Overview of Biological Features and Factors That may Impact on ctDNA Analysis. *Front Oncol.* (2022) 12:943253. doi: 10.3389/fonc.2022.943253

89. Caputo V, Ciardiello F, Corte CMD, Martini G, Troiani T, Napolitano S. Diagnostic value of liquid biopsy in the era of precision medicine: 10 years of clinical evidence in cancer. *Explor targeted anti-tumor Ther.* (2023) 4:102–38. doi: 10.37349/etat

90. Corcoran RB, Chabner BA. Application of cell-free DNA analysis to cancer treatment. *New Engl J Med.* (2018) 379:1754–65. doi: 10.1056/NEJMra1706174

91. Tan L, Sandhu S, Lee RJ, Li J, Callahan J, Ftouni S, et al. Prediction and monitoring of relapse in stage III melanoma using circulating tumor DNA. *Ann oncology: Off J Eur Soc Med Oncol.* (2019) 30:804–14. doi: 10.1093/annonc/mdz048

92. de Abreu AR, Op de Beeck K, Laurent-Puig P, Taly V, Benhaim L. The position of circulating tumor DNA in the clinical management of colorectal cancer. *Cancers.* (2023) 15:1284. doi: 10.3390/cancers15041284

93. Wang W, Zheng Z, Lei J. CTC, ctDNA, and exosome in thyroid cancers: A review. *Int J Mol Sci.* (2023) 24:13767. doi: 10.3390/ijms241813767

94. Chuang TC, Chuang AY, Poeta L, Koch WM, Califano JA, Tufano RP. Detect able BRAF mutation in serum DNA samples from patients with papillary thyroid carcinomas. *Head Neck.* (2010) 32:229–34. doi: 10.1002/hed.21178

95. Lan X, Bao H, Ge X, Cao J, Fan X, Zhang Q, et al. Genomic landscape of metastatic papillary thyroid carcinoma and novel biomarkers for predicting distant metastasis. *Cancer Sci.* (2020) 111:2163–73. doi: 10.1111/cas.v111.6

96. Zhang H, Duan HL, Wang S, Liu Y, Ding GN, Lin RX. Epigenetic signature associated with thyroid cancer progression and metastasis. *Semin Cancer Biol.* (2022) 83:261–8. doi: 10.1016/j.semcancer.2021.03.026

97. Jiang K, Li G, Chen W, Song L, Wei T, Li Z, et al. Plasma Exosomal miR-146b-5p and miR-222-3p are Potential Biomarkers for Lymph Node Metastasis in Papillary Thyroid Carcinomas. *OncoTargets Ther.* (2020) 13:1311–9. doi: 10.2147/OTT.S231361

98. Elhanani O, Ben-Uri R, Keren L. Spatial profiling technologies illuminate the tumor microenvironment. *Cancer Cell.* (2023) 41:404–20. doi: 10.1016/j.ccell.2023.01.010

99. Wu T, Dai Y. Tumor microenvironment and therapeutic response. *Cancer Lett.* (2017) 387:61–8. doi: 10.1016/j.canlet.2016.01.043

100. Cendrowicz E, Sas Z, Bremer E, Rygiel TP. The role of macrophages in cancer development and therapy. *Cancers.* (2021) 13:1946. doi: 10.3390/cancers13081946

frontiers | Frontiers in Oncology

TYPE Original Research
PUBLISHED 21 May 2025
DOI 10.3389/fonc.2025.1586307

Check for updates

OPEN ACCESS

EDITED BY
Xiaosheng Tan,
Rutgers, United States

REVIEWED BY
Qi Wang,
Auburn University, United States
Xiang Yu,
Rutgers, The State University of New Jersey, United States
Yanjun Gao,
George Washington University, United States
Juan Wang,
Northwestern University, United States

*CORRESPONDENCE
Wensheng Liu
lwsdoct@aliyun.com

RECEIVED 02 March 2025
ACCEPTED 28 April 2025
PUBLISHED 21 May 2025

CITATION
Yang H, Wei L, Qian J and Liu W (2025) Multifactorial risk stratification for central lymph node metastasis in papillary thyroid carcinoma: a predictive model integrating clinical and tumor characteristics.
Front. Oncol. 15:1586307.
doi: 10.3389/fonc.2025.1586307

COPYRIGHT
© 2025 Yang, Wei, Qian and Liu. This is an open-access article distributed under the terms of the Creative Commons Attribution License (CC BY). The use, distribution or reproduction in other forums is permitted, provided the original author(s) and the copyright owner(s) are credited and that the original publication in this journal is cited, in accordance with accepted academic practice. No use, distribution or reproduction is permitted which does not comply with these terms.

Multifactorial risk stratification for central lymph node metastasis in papillary thyroid carcinoma: a predictive model integrating clinical and tumor characteristics

Huaiyu Yang, Liyuan Wei, Jiaxin Qian and Wensheng Liu*

Department of Head and Neck Surgical Oncology, National Cancer Center,National Clinical Research Center for Cancer, Cancer Hospital, Chinese Academy of Medical Sciences and Peking Union Medical College, Beijing, China

Background: With the increasing prevalence of papillary thyroid carcinoma PTC) and advancements in auxiliary examination technology, the holistic detection rate of malignant thyroid nodules, particularly small ones, continues to rise. However, there remains controversy surrounding the optimal treatment for PTC, and a crucial factor influencing treatment decisions is the status of central lymph node metastasis (CLNM). There is a lack of research on the relationship between clinical laboratory results and tumor characteristics observed during surgery and CLNM status. Therefore, our research aims to systematically explore the risk factor of CLNM in patients with PTC.

Methods: We systematically gathered and analyzed clinical features and pathological data of 2,435 PTC patients who underwent surgery. After variable screening, the selected variables were included in logistic regression analysis, and a Nomogram prediction model was constructed according to the analysis results. To investigate the risk factors for CLNM in patients with PTC.

Result: This study included a total of 2,435 patients diagnosed with PTC, among whom 933 patients were confirmed as CLNM by postoperative pathology. Univariate and multivariate regression analysis identified age, serum TRAb levels, calcification, multifocality, extrathyroidal invasion, tumor size, and tumor location as risk factors associated with CLNM. The prediction model based on these risk factors demonstrated robust accuracy with an AUC of 0.76. Clinical decision curve analysis indicated that aside from a small range of low threshold probabilities, intervening based on the model's predictions can yield greater clinical benefit.

Conclusion: Key risk factors for CLNM in PTC patients include young age, high serum thyrotropin receptor antibody (TR-Ab) levels, calcification, multifocality,

extrathyroidal extension, larger tumor size, and tumor location in the middle or lower poles of the thyroid. The clinical prediction model established based on these critical risk factors can provide a more accurate reference standard for clinical decision-making in practice.

KEYWORDS

papillary thyroid carcinoma, central lymph node metastasis, risk factor (RF), Nomogram model, retrospective study

1 Introduction

Thyroid cancer, predominantly papillary thyroid carcinoma (PTC), constitutes the most prevalent endocrine malignancy globally, accounting for over 90% of cervical region neoplasms in head and neck oncology as defined by the World Health Organization (WHO) classification of endocrine tumors (1), with PTC being the most prevalent type of pathology. The gradually incremental incidence of thyroid malignancies, along with advancements in imaging techniques, has resulted in a higher detection rate of PTC, particularly in cases involving small foci (2). At present, surgical intervention remains the primary treatment modality for PTC (3). The prevailing strategy for managing regional lymph nodes involves preventive lymph node dissection (PLND), which facilitates the removal of both macroscopic and microscopic metastatic foci (4), thereby contributing to precise clinical staging. However, retrospective studies have shown that approximately 30–80% of PTC patients undergoing PLND have pathologically confirmed lymph node metastases (5). Furthermore, this procedure significantly increases the incidence of short-term and permanent postoperative complications, including hypocalcemia, recurrent laryngeal nerve paralysis, and transient parathyroid dysfunction (6, 7). Consequently, the preoperative identification of high-risk PTC patients with central lymph node metastasis (CLNM) is of paramount importance. This study systematically compiles prevalent clinical characteristics, examines risk factors associated with CLNM, develops a predictive model, and assesses its efficacy in determining CLNM risk. The objective of this model is to furnish clinicians with a meaningful tool to assess the CLNM status of PTC patients, thereby enhancing the precision of clinical decision.

2 Materials and methods

2.1 Patient population

This retrospective cohort study included patients diagnosed with PTC who underwent thyroid lobectomy or total thyroidectomy with PLND at the Department of Head and Neck Surgery, Cancer Hospital of the Chinese Academy of Medical Sciences (CICAMS), between January 1, 2015, and December 1, 2022.The inclusion criteria encompassed: a) patients with an initial diagnosis of PTC confirmed through preoperative, core needle biopsy pathology, aspiration cytology, and postoperative pathology; and b) patients who underwent thyroid lobectomy accompanied by PLND, with comprehensive preoperative ultrasound and thyroid function assessment, and postoperative pathological record. And the exclusion criteria encompassed the following: a) individuals with a prior history of neck radiotherapy or other malignancies; b) individuals exhibiting preoperative thyroid function test results indicative of hyperthyroidism or hypothyroidism; c) individuals with a history of partial thyroidectomy or other thyroid-related surgical procedures; d) individuals whose preoperative biopsy pathology revealed lateral neck lymph node metastasis. Finally, 2,435 patients satisfied the criteria, comprising 933 patients with CLNM, and 1,502 patients no-CLNM. Subsequently, Randomly divided the patients into training cohort (1,948) and validation cohort (487) following an 8:2 distribution ratio. The process for patient enrollment is shown in Figure 1. The experimental scheme was designed in accordance with the ethical principles of the Helsinki Declaration and authorized by the Ethics Committee of the Cancer Hospital, Chinese Academy of Medical Sciences.

2.2 Baseline data information

We systematically collected data from patients included in the study, encompassing basic demographic information, laboratory test results, thyroid ultrasound findings, surgical methods, surgical records, and postoperative pathological outcomes. The demographic data comprise age, BMI, and sex. Laboratory indicators include consequence of thyroid-stimulating hormone (TSH), thyroglobulin (Tg), thyrotropin receptor antibodies (TR-Ab), and thyroglobulin antibodies (TG-Ab) levels. The thyroid ultrasound findings provided a comprehensive assessment of primary tumor site, including the nodule localization and the number of thyroid nodules, calcification, extrathyroidal extension (ETE), and tumor diameter. Multifocality was characterized by the detection of two or more thyroid nodules via ultrasound, which were later pathologically confirmed as PTC (8). Tumor size was determined by measuring the maximum diameter of the nodule on ultrasound, with these measurements subsequently corroborated through pathological analysis.

To ensure the consistency of image quality, all preoperative ultrasound images were completed by the same grade of

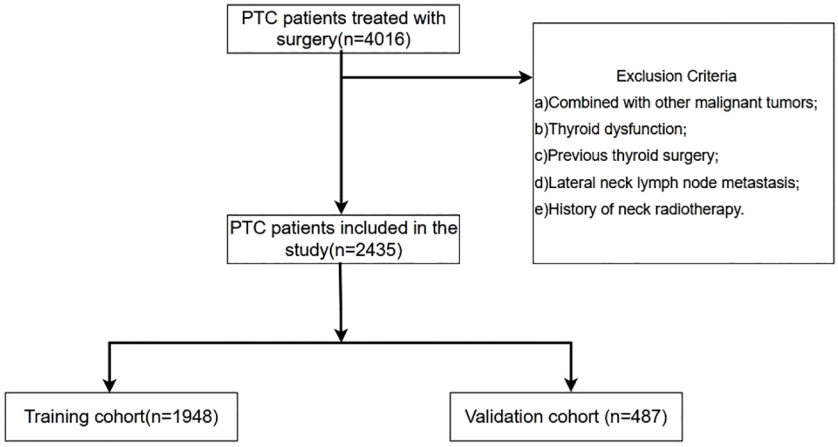

FIGURE 1
Schematic diagram of the procedure for inclusion and exclusion of patients in this study. A total of 4016 PTC patients were consecutively reviewed in this study. According to the prespecified inclusion and exclusion criteria, 2435 PTC patients were finally included in this study. According to the ratio of 8:2, they were randomly divided into training set (1948 cases) and validation set (487 cases).

sonographer with reference to the Chinese version of Thyroid Imaging Reporting and Data System (C-TIRADS), and calibrated by a senior chief sonographer. In this study, the classification criteria for thyroid nodule location by sonographers and surgeons was based on the tripartition of the thyroid gland lobe. The description of thyroid nodule location in preoperative ultrasound reports and surgical records of PTC patients was reviewed completely, and the specific results were recorded for subsequent statistical analysis of this study. In the data analysis phase, we used Kappa coefficient to evaluate the inter-rater reliability of tumor localization between surgeons and radiologists. The results showed that the inter-rater reliability of tumor localization between surgeons and radiologists was 0.880 ($p < 0.0001$, 95%CI 0, 862 to 0.899). The Kappa coefficient was greater than 0.8, indicating excellent correlation between the two sets of data. The anatomical location of thyroid nodules, including the upper pole, middle pole, lower pole and isthmus, and the degree of extrathyroidal extension observed during the operation were recorded.

The complete collection of postoperative pathological information should include the following: the histopathological subtype of papillary thyroid carcinoma (classic variant, diffuse sclerosing variant, follicular variant, tall cell variant, etc.); whether the tumor exhibits multifocal growth and the specific number of tumor foci; the maximum diameter of the primary tumor (in millimeters); surrounding tissue invasion such as the thyroid capsule, trachea, or recurrent laryngeal nerve; the presence of coexisting chronic thyroiditis; and whether ipsilateral CLNM is present, along with the number of metastatic lymph nodes.

All enrolled patients' surgical records were retrieved through the HIS system. After verifying the completeness of the surgical documentation, intraoperative findings from PTC patients meeting the inclusion criteria were collected. This included the lobe of the thyroid gland where the primary tumor was located (upper pole, middle third, lower pole, or isthmus), the presence of extrathyroidal extension (ETE), and the extent of such invasion.

2.3 Statistical analysis

All statistical analyses applied in our study were conducted utilizing R software (version 4.4.0), with statistical significance established at p-value less than 0.05. Categorical data were expressed as percentage, while continuous variables were reported as means ± SD or medians (interquartile range, 1 and 3) after the primary analysis, depending on the normality of the variables. Collinearity among variables was assessed using a correlation coefficient matrix, variance inflation factor (VIF), and tolerance. Variables were screened based on collinearity diagnostics and subsequently included in univariable logistic regression analysis to calculate odds ratios (OR). After screening, these variables were incorporated into a multivariable logistic analysis. And then utilizing these selected variables developed clinical prediction model for CLNM. The receiver operating characteristic curve (ROC) and the area under the curve(AUC), decision curve analysis (DCA) and calibration curve were adopted to verify the performance of the prediction model.

3 Results

3.1 Demographic and clinical profiles at enrollment

Our study gathered data from 2,435 patients with PTC, comprising1,502 patients without CLNM and 933 patients with CLNM. A summary of the clinical data characteristics for both groups is presented in Table 1.

10.3389/fonc.2025.1586307

TABLE 1 Clinical baseline characteristics of total patients cohort.

Variables	Total (n = 2435)	No-CLNM (n = 1502)	CLNM (n = 933)	*P*
Age	43.74 ± 10.09	45.47 ± 10.07	40.94 ± 9.48	**<.001**
Weight	67.12 ± 12.94	67.43 ± 13.15	66.62 ± 12.60	0.133
Height	164.17 ± 13.87	163.58 ± 10.50	165.12 ± 17.97	**0.008**
Diameter (ultrasound)	8.62 ± 4.51	7.50 ± 3.73	10.42 ± 5.05	**<.001**
Diameter (pathology)	7.34 ± 4.11	6.32 ± 3.51	8.98 ± 4.46	**<.001**
Tg	45.29 ± 129.06	43.88 ± 145.61	47.57 ± 96.28	0.555
TR-Ab	0.45 ± 0.37	0.42 ± 0.31	0.49 ± 0.46	**<.001**
TG-Ab	122.39 ± 408.36	126.58 ± 407.33	115.60 ± 410.24	0.578
BMI	31.50 ± 135.58	30.45 ± 122.09	33.18 ± 154.92	0.630
Sex, n(%)				**0.002**
female	1734 (71.21)	1104 (73.50)	630 (67.52)	
male	701 (28.79)	398 (26.50)	303 (32.48)	
Calcification, n(%)				**<.001**
No	1323 (54.33)	975 (64.91)	348 (37.30)	
Yes	1112 (45.67)	527 (35.09)	585 (62.70)	
Multifocal (ultrasound), n(%)				**<.001**
Multifocal	447 (18.36)	232 (15.45)	215 (23.04)	
Unifocal	1988 (81.64)	1270 (84.55)	718 (76.96)	
Diameter group-1, n(%)				**<.001**
>7mm	1275 (52.36)	606 (40.35)	669 (71.70)	
≤7mm	1160 (47.64)	896 (59.65)	264 (28.30)	
Diameter group-2, n(%)				**<.001**
>10mm	590 (24.23)	236 (15.71)	354 (37.94)	
≤10mm	1845 (75.77)	1266 (84.29)	579 (62.06)	
ETE (ultrasound), n(%)				**<.001**
Negative	2303 (94.58)	1379 (91.81)	924 (99.04)	
Positive	132 (5.42)	123 (8.19)	9 (0.96)	
Bilateral/Unilateral, n(%)				**<.001**
Bilateral	575 (23.61)	443 (29.49)	132 (14.15)	
Unilateral	1860 (76.39)	1059 (70.51)	801 (85.85)	
Lobes, n(%)				**<.001**
Bilateral	575 (23.61)	443 (29.49)	132 (14.15)	
Isthmus	24 (0.99)	20 (1.33)	4 (0.43)	
Lift	846 (34.74)	493 (32.82)	353 (37.83)	
Right	990 (40.66)	546 (36.35)	444 (47.59)	
Location, n(%)				0.156
Lower	436 (19.34)	254 (18.53)	182 (20.61)	
Middle	1228 (54.48)	769 (56.09)	459 (51.98)	

(Continued)

TABLE 1 Continued

Variables	Total (n = 2435)	No-CLNM (n = 1502)	CLNM (n = 933)	*P*
Upper	590 (26.18)	348 (25.38)	242 (27.41)	
Age group-1, n(%)				**<.001**
≤40	830 (34.09)	403 (26.83)	427 (45.77)	
>40	1605 (65.91)	1099 (73.17)	506 (54.23)	
Age group-2, n(%)				**<.001**
≤45	1335 (54.83)	708 (47.14)	627 (67.20)	
>45	1100 (45.17)	794 (52.86)	306 (32.80)	
Multifocal (pathology), n(%)				**<.001**
Unifocal	1850 (75.98)	1222 (81.36)	628 (67.31)	
Multifocal	585 (24.02)	280 (18.64)	305 (32.69)	
Number of nodules, n(%)				**<.001**
1	1856 (76.22)	1228 (81.76)	628 (67.31)	
2	364 (14.95)	183 (12.18)	181 (19.40)	
3	215 (8.83)	91 (6.06)	124 (13.29)	
ETE (pathology), n(%)				**<.001**
Negative	1053 (43.33)	745 (49.60)	308 (33.19)	
Capsular	324 (13.33)	203 (13.52)	121 (13.04)	
Extracapsular	1053 (43.33)	554 (36.88)	499 (53.77)	

The meaning of the bold values indicated that there were clear statistical differences in the variable in different central lymph node metastasis status groups of papillary thyroid carcinoma ($p < 0.05$).

We used the `createDataPartition()` function in the R package `caret` to randomly divide the total dataset into a training set (1,948 cases) and a validation set (487 cases). Based on the outcome variable (lymph node metastasis status) as the basis for stratification, the proportion parameter for the training set was set to $p = 0.8$. The random seed was fixed at 1234 to ensure the repeatability of the results. In the training cohort, there were 743 patients diagnosed with CLNM and 1,205 patients without CLNM. Similarly, in the validation cohort, 190 patients were identified as having CLNM and 297 patients were identified as having no CLNM. After dividing the training set and the validation set, the balance analysis of the data between the training set and the validation set was carried out. The results showed that, Apart from the number of tumor foci identified through ultrasound and subsequently confirmed by postoperative pathology, There were no significant differences in other clinical and pathological features between the two groups. Summary of the clinical data characteristics for both groups is presented in Table 2.

3.2 Relation between clinicopathological features of PTC and CLNM in all patient cohort

In this study, CLNM was identified in 933 patients (38.30%) with PTC. A comprehensive pre-analysis of all patients revealed a noteworthy association between CLNM and multiple factors, including age ($p < 0.01$), maximum tumor diameter ($p < 0.01$), serum TR-Ab levels ($p < 0.01$), sex ($p < 0.01$), calcification ($p < 0.01$), multifocality ($p < 0.01$), the number of tumor foci ($p < 0.01$) and extrathyroidal invasion ($p < 0.01$) observed via ultrasound, tumor location ($p < 0.01$), and ETE ($p < 0.01$). correspondingly, no significant correlations were observed regarding weight, BMI, serum triglyceride (Tg) levels, serum TG-antibody (TG-Ab) levels, or the laterality of the tumor ($p > 0.05$).

Building on previous studies (9), we classified the maximum tumor diameter using thresholds of >7 mm and >10 mm. Significant differences in CLNM rates were observed between these groups. The >10 mm threshold (OR: 3.75, 95% CI: 3.14–4.47) exhibited superior accuracy and specificity than the >7 mm threshold. Detailed results are presented in Table 3.

3.3 Univariate logistic regression analysis of clinicopathological predictors for CLNM in a training cohort

Based on the comprehensive statistical analysis of the full cohort of participants, the correlation coefficient matrix (correlation coefficient value less than 0.8. Table 4), variance inflation factor (VIF value less than 5) and tolerance were used to diagnose the collinearity between the variables (Table 5). Combined with clinical experience, the collinearity factor was removed from the training using principal

10.3389/fonc.2025.1586307

TABLE 2 Baseline characteristics of the patients of training and validation cohort.

Variables	Total (n = 2435)	Validation cohort (n = 487)	Training cohort (n = 1948)	*P*
Age	43.74 ± 10.09	43.85 ± 9.83	43.71 ± 10.16	0.773
Weight	67.12 ± 12.94	67.27 ± 12.81	67.09 ± 12.98	0.777
Height	164.17 ± 13.87	164.07 ± 12.63	164.20 ± 14.16	0.860
Diameter(ultrasound)	8.62 ± 4.51	8.61 ± 4.50	8.62 ± 4.52	0.986
Diameter(pathology)	7.34 ± 4.11	7.39 ± 4.29	7.33 ± 4.06	0.745
Tg	45.29 ± 129.06	45.32 ± 125.28	45.28 ± 130.11	0.995
TR-Ab	0.45 ± 0.37	0.45 ± 0.39	0.45 ± 0.37	0.893
TG-Ab	122.39 ± 408.36	104.87 ± 312.39	127.08 ± 430.39	0.345
BMI	31.50 ± 135.58	35.93 ± 174.86	30.39 ± 123.83	0.420
Sex, n(%)				0.840
female	1734 (71.21)	345 (70.84)	1389 (71.30)	
male	701 (28.79)	142 (29.16)	559 (28.70)	
Age group-1, n(%)				0.831
≤40	830 (34.09)	164 (33.68)	666 (34.19)	
>40	1605 (65.91)	323 (66.32)	1282 (65.81)	
Age group-2, n(%)				1.000
≤45	1335 (54.83)	267 (54.83)	1068 (54.83)	
>45	1100 (45.17)	220 (45.17)	880 (45.17)	
Calcification, n(%)				0.887
No	1323 (54.33)	266 (54.62)	1057 (54.26)	
Yes	1112 (45.67)	221 (45.38)	891 (45.74)	
Multifocal(ultrasound), n(%)				**0.030**
Unifocal	1988 (81.64)	381 (78.23)	1607 (82.49)	
Multifocal	447 (18.36)	106 (21.77)	341 (17.51)	
Diameter group-1, n(%)				0.224
≤7mm	1160 (47.64)	244 (50.10)	916 (47.02)	
>7mm	1275 (52.36)	243 (49.90)	1032 (52.98)	
Diameter group-2, n(%)				0.723
≤10mm	1845 (75.77)	366 (75.15)	1479 (75.92)	
>10mm	590 (24.23)	121 (24.85)	469 (24.08)	
ETE(ultrasound), n(%)				0.325
Negative	2303 (94.58)	465 (95.48)	1838 (94.35)	
Positive	132 (5.42)	22 (4.52)	110 (5.65)	
Bilateral/Unilateral, n(%)				0.340
Unilateral	1860 (76.39)	364 (74.74)	1496 (76.80)	
Bilateral	575 (23.61)	123 (25.26)	452 (23.20)	
Lobes, n(%)				0.798
Lift	846 (34.74)	163 (33.47)	683 (35.06)	

(Continued)

TABLE 2 Continued

Variables	Total (n = 2435)	Validation cohort (n = 487)	Training cohort (n = 1948)	*P*
Right	990 (40.66)	196 (40.25)	794 (40.76)	
Isthmus	24 (0.99)	5 (1.03)	19 (0.98)	
Bilateral	575 (23.61)	123 (25.26)	452 (23.20)	
Location, n(%)				0.063
Upper	436 (19.34)	73 (15.94)	363 (20.21)	
Medium	1228 (54.48)	251 (54.80)	977 (54.40)	
Lower	590 (26.18)	134 (29.26)	456 (25.39)	
Multifocal(pathology), n(%)				**0.033**
Unifocal	1850 (75.98)	352 (72.28)	1498 (76.90)	
Multifocal	585 (24.02)	135 (27.72)	450 (23.10)	
Number of nodules, n(%)				0.053
1	1856 (76.22)	351 (72.07)	1505 (77.26)	
2	364 (14.95)	87 (17.86)	277 (14.22)	
3	215 (8.83)	49 (10.06)	166 (8.52)	
ETE (pathology), n(%)				0.710
Negative	1053 (43.33)	217 (44.56)	836 (43.03)	
Capsular	324 (13.33)	60 (12.32)	264 (13.59)	
Extracapsular	1053 (43.33)	210 (43.12)	843 (43.39)	

The meaning of the bold values indicated that there were clear statistical differences in the variable in different central lymph node metastasis status groups of papillary thyroid carcinoma ($p < 0.05$).

component analysis. Variables with $p < 0.05$ were included in subsequent analyses. The findings revealed that, within the training cohort, the following were identified as potential risk factors for CLNM: male (OR: 1.33, 95% CI: 1.12–1.60), calcification (OR: 3.11, 95% CI: 2.62–3.69), multifocality (OR: 1.64, 95% CI: 1.33–2.02), ETE (ultrasound) (OR: 3.45, 95% CI: 2.38–5.00), and tumor location in the mid-thyroid (OR: 1.41, 95% CI: 1.09–1.83),lower pole (OR: 1.64, 95% CI: 1.33–2.02), ET(intraoperative) (OR: 1.82, 95% CI: 1.51–2.19), maximum tumor diameter ($p < 0.001$), high level serum TR-Ab ($p < 0.01$), and younger age ($p < 0.01$) were identified as potential risk factors of CLNM.

The results of multivariate regression analysis suggested that the presence of calcification (OR: 1.99, 95% CI: 1.57–2.53), maximum tumor diameter exceeding 10 mm (OR: 3.55, 95% CI: 2.76–4.56), ETE (OR: 2.54, 95% CI: 1.52–4.24), tumor localization in the mid-thyroid region (OR: 1.95, 95% CI: 1.46–2.62) and lower pole (OR: 2.09, 95% CI: 1.45–3.00), younger patient age, and high serum TR-Ab levels ($p < 0.01$) were identified as independent risk factors for CLNM in patients with PTC. Detailed results are presented in Table 6, and the forest plots of the results of the multivariate analysis are shown in Figure 2.

3.4 Construction and evaluation of nomogram prediction model

Utilizing the outcomes of logistic analyses, we constructed a Nomogram prediction model to predict the CLNM status of PTC patients by including the variables screened earlier (Figure 3). ROC, calibration curves, and DCA were used to verify the multidimensional effectiveness of the constructed Nomogram model.

The ROC constructed in the training cohort is shown in Figure 4, and the AUC was 0.76(95%CI: 0.74-0.79). To evaluate the generalizability and robustness of the model, The validation cohort, consisting of 487 patients, demonstrated robust discriminatory performance with an AUC of 0.77 (95% CI: 0.72-0.81). The consistency between the predicted probability of the model and the actual observed probability was evaluated by the calibration curve (Figure 5). The results showed that the predicted risk and the true risk were distributed along the 45° diagonal for both the training and validation cohorts. and the Hosmer-Lemeshow (HL) test was used to evaluate the fit between the observed values and the predicted values of the model, and the p value of the HL test was 0.99, indicating that there was no significant difference between the predicted values of the model and the true values, and the model fit was good. In addition, the mean absolute error (MAE) of the calibration curve was 0.07 by 1000 Bootstrap resampling, which further verified the high prediction accuracy and calibration consistency of the model. For robustness validation, DCA was performed to assess the clinical applicability of the nomogram, In the DCA, the clinical benefit curves of prophylactic central lymph node dissection for all patients and those without central lymph node dissection were delineated. Subsequently, the clinical benefit curves of prophylactic central lymph node dissection for PTC patients with different risks of

TABLE 3 Univariate logistic regression analysis of total patients cohort.

Variables	*P*	OR (95%CI)
Age	**<.001**	0.95 (0.95 ~ 0.96)
Weight	0.134	1.00 (0.99 ~ 1.00)
Height	**0.015**	1.01 (1.01 ~ 1.02)
Diameter(ultrasound	**<.001**	1.17 (1.15 ~ 1.20)
Diameter(pathology)	**<.001**	1.18 (1.16 ~ 1.21)
Tg	0.556	1.00 (1.00 ~ 1.00)
TR-Ab	**<.001**	1.57 (1.24 ~ 1.99)
TG-Ab	0.579	1.00 (1.00 ~ 1.00)
BMI	0.632	1.00 (1.00 ~ 1.00)
Sex		
female		1.00 (Reference)
male	**0.002**	1.33 (1.12 ~ 1.60)
Calcification		
No		1.00 (Reference)
Yes	**<.001**	3.11 (2.62 ~ 3.69)
Multifocal		
Unifocal		1.00 (Reference)
Multifocal	**<.001**	1.64 (1.33 ~ 2.02)
Number of nodules (ultrasound)		
1		1.00 (Reference)
≥2	**<.001**	0.42 (0.31 ~ 0.56)
Diameter group-1		
≤7mm		1.00 (Reference)
>7mm	**<.001**	3.28 (2.71 ~ 3.97)
Diameter group-2		
≤10mm		1.00 (Reference)
>10mm	**<.001**	3.75 (3.14 ~ 4.47)
ETE (ultrasound)		
Negative		1.00 (Reference)
Positive	**<.001**	3.45 (2.38 ~ 5.00)
Bilateral/Unilateral		
Unilateral		1.00 (Reference)
Bilateral	0.072	0.84 (0.69 ~ 1.02)
Thyroid gland lobe		
Lift		1.00 (Reference)
Right	0.929	0.99 (0.82 ~ 1.20)
Isthmus	0.156	0.51 (0.20 ~ 1.29)
Bilateral	0.088	0.83 (0.66 ~ 1.03)
Location		
Upper		1.00 (Reference)
Medium	**<.001**	1.64 (1.33 ~ 2.02)
Lower	**0.010**	1.41 (1.09 ~ 1.83)
ETE-1(intraoperative)		
Negative		1.00 (Reference)
Capsular	**<.001**	1.59 (1.27 ~ 1.99)
Extracapsular	**<.001**	2.32 (1.74 ~ 3.09)
ETE-2(intraoperative)		
Negative		1.00 (Reference)
Positive	**<.001**	1.82 (1.51 ~ 2.19)
Multifocal(pathology)		
Unifocal		1.00 (Reference)
Multifocal	**<.001**	2.12 (1.76 ~ 2.56)
Number of nodules (pathology)		
1		1.00 (Reference)
2	**<.001**	1.93 (1.54 ~ 2.43)
≥3	**<.001**	2.66 (2.00 ~ 3.55)
ETE (pathology)		
Negative		1.00 (Reference)
Capsular	**0.006**	1.44 (1.11 ~ 1.87)
Extracapsular	**<.001**	2.18 (1.82 ~ 2.61)

(Continued)

TABLE 3 Continued

The meaning of the bold values indicated that there were clear statistical differences in the variable in different central lymph node metastasis status groups of papillary thyroid carcinoma ($p < 0.05$).

lymph node metastasis, according to this prediction model, were compared with the aforementioned curves. The clinical value of the model was evaluated. The results confirmed that, except for a small range of low threshold probabilities, if the risk of CLNM in a particular PTC patient lies between the DCA curve and the other two control curves, the clinical benefit of prophylactic central lymph node dissection for this selected PTC patient is higher (Figure 6). Moreover, the clinical benefit interval of the Nomogram model covered most clinical decision-making scenarios, suggesting its applicability in different risk stratification.

4 Discussion

Thyroid cancer is the most common malignancy of the endocrine system, with PTC representing the most frequently occurring histological subtype. Surgical intervention constitutes the primary therapeutic modality for PTC, largely due to the favorable survival prognosis and the absence of specific

TABLE 4 Matrix table of correlation coefficients based on the full cohort of PTC patients.

Pearson correlation coefficients																		
	Status	Age	Weight	Height	Tg	TR-Ab	TG-Ab	BMI	Sex	Calcification	Multifocal	Diameter	Diametergroup-1	ETE	Unilateral/ bilateral	Gland lobe	Location	ETE (intraoperative)
Status	1																	
Age	-0.232**	1																
Weight	-0.019	0.016	1															
Height	0.056*	-0.169**	0.422**	1														
Tg	0.010	0.006	0.011	-0.020	1													
TR-Ab	0.071**	-0.085**	-0.007	0.039	-0.015	1												
TG-Ab	-0.046	0.044	-0.066**	0.005	-0.053*	0.159**	1											
BMI	0.012	0.004	-0.007	-0.738**	-0.009	-0.026	-0.016	1										
Sex	0.087**	-0.127**	0.564**	0.507**	-0.018	0.022	-0.106**	-0.034	1									
Calcification	0.284**	-0.154**	0.014	0.074**	0.027	0.020	0.048*	-0.056*	0.073**	1								
Multifocal	-0.132**	0.027	-0.069**	-0.018	-0.045	-0.047	0.008	-0.050*	-0.045	-0.081**	1							
Diameter	0.303**	-0.111**	-0.019	0.062*	0.046	0.023	-0.015	-0.045	0.039	0.318**	-0.103**	1						
Diameter group-1	0.217**	-0.105**	0.017	0.073**	0.040	0.007	-0.019	-0.035	0.052*	0.213**	-0.119**	0.810**	1					
ETE	-0.190**	0.123**	0.073**	-0.005	0.038	0.037	-0.011	-0.012	0.022	-0.126**	0.071**	-0.323**	-0.139**	1				
Unilateral/ bilateral	0.184**	-0.024	-0.021	0.026	0.001	-0.015	0.035	-0.041	0.012	0.262**	0.156**	0.534**	0.308**	-0.450**	1			
Gland lobe	0.175**	-0.039	-0.011	0.044	-0.011	-0.011	0.030	-0.043	0.017	0.232**	0.136**	0.486**	0.286**	-0.413**	0.919**	1		
Location	-0.021	-0.007	-0.032	-0.025	-0.027	-0.031	0.030	0.024	-0.001	-0.010	0.075**	0.063*	0.061*	-0.056*	0.067**	0.046	1	
ETE (intraoperative)	0.012	0.035	0.013	-0.014	-0.009	-0.029	-0.005	0.035	0.019	0.054*	-0.106**	-0.127**	-0.144**	0.070**	-0.012	0.014	-0.071**	1

* p<0.05 ** p<0.01.

10.3389/fonc.2025.1586307

TABLE 5 Collinearity diagnosis (VIF value and tolerance) based on data from all PTC patients.

Diagnostic results of collinearity		
Variables	VIF value	Tolerance
Age	1.208	0.828
Weight	1.817	0.550
Height	5.849	0.171
Tg	1.015	0.985
TR-Ab	1.051	0.952
TG-Ab	1.071	0.934
BMI	4.097	0.244
Sex	2.219	0.451
Calcification	1.222	0.818
Multifocal	1.163	0.860
Diameter	4.331	0.231
Diametergroup-1	3.219	0.311
ETE	1.387	0.721
Unilateral/bilateral	7.501	0.133
Gland lobe	6.549	0.153
Location	1.024	0.977
ETE (intraoperative)	1.072	0.933

postoperative adjuvant therapies (10), iodine-131 therapy is predominantly reserved for PTC patients exhibiting distant metastases (11). Consequently, achieving complete resection is imperative in the management of PTC. Although guidelines pertaining to the surgical approach for primary PTC are continuously evolving, the management of regional lymph nodes remains inconsistent (12),with PLND currently being the main recommendation. While PLND facilitates comprehensive lymph node clearance, it concurrently elevates the risk of postoperative complications, including recurrent laryngeal nerve injury and transient hypocalcemia (13). Prior research has documented varying incidences of CLNM following PLND (14). Consequently, we propose that evaluating the likelihood of CLNM through preoperative assessments and intraoperative observations to identify high-risk PTC patients for PLND represents a viable clinical strategy. This approach seeks to enhance surgical precision and reduce postoperative complications.

In this study, we utilized logistic regression analyses to identify independent variables included in the study after removing the high collinearity variables. Univariate analysis indicated no statistical differences in weight, height, and BMI between different CLNM status groups.

Some previous studies have suggested that lymph node metastasis in PTC patients has a significant gender preference, and male patients are more likely to have CLNM and lateral lymph node metastasis (LLNM) (15, 16), and suggest that for male patients, Physical examination and imaging evaluation of cervical lymph node status should be emphasized before operation (17). The possible mechanisms include the high expression of androgen receptor in male PTC tissues and the promotion of tumor cell invasion through MAPK/ERK pathway. The infiltration abundance of regulatory T cells (Tregs, Foxp3+) in the tumor microenvironment of male patients is higher, indicating stronger immunosuppression, and male patients tend to have M2 macrophage polarization. All the above mechanisms suggest that the tumor of male PTC patients is more aggressive. However, some studies believe that estrogen is a strong stimulator of malignant thyroid nodules, and female PTC patients are often accompanied by multifocal lesions and a higher rate of lymph node metastasis (18). However, in this study, males do not exhibit a higher likelihood of CLNM compared to females. While univariate analysis and clinical experience suggest that males under 40 show a high risk of CLNM, we attempted to include gender as a variable in our nomogram model to more fully explore the relationship between gender and the risk of central lymph node metastasis in PTC patients. However, it did not show robust predictive significance. Therefore, the

TABLE 6 Univariate and multivariate logistic regression analysis of training cohort.

Variables	Univariate		Multivariate	
	P	OR (95%CI)	P	OR (95%CI)
Age	**<.001**	0.95 (0.95 ~ 0.96)	**<.001**	0.95 (0.94 ~ 0.97)
TR-Ab(IUml)	**<.001**	1.59 (1.21 ~ 2.08)	**0.048**	1.40 (1.01 ~ 1.95)
Sex				
female		1.00 (Reference)		1.00 (Reference)
male	**0.019**	1.27 (1.04 ~ 1.55)	0.759	1.04 (0.81 ~ 1.35)
Calcification				
No		1.00 (Reference)		1.00 (Reference)
Yes	**<.001**	3.12 (2.58 ~ 3.77)	**<.001**	1.99 (1.57 ~ 2.53)
Multifocal				
Unifocal		1.00 (Reference)		1.00 (Reference)
Multifocal	**<.001**	1.62 (1.28 ~ 2.05)	0.169	1.24 (0.91 ~ 1.68)
Diameter-group,				
≤10mm		1.00 (Reference)		1.00 (Reference)
>10mm	**<.001**	3.78 (3.10 ~ 4.60)	**<.001**	3.55 (2.76 ~ 4.56)
ETE				
Negative		1.00 (Reference)		1.00 (Reference)
Positive	**<.001**	2.85 (1.88 ~ 4.30)	**<.001**	2.54 (1.52 ~ 4.24)
Location				
Upper		1.00 (Reference)		1.00 (Reference)
Medium	**<.001**	1.64 (1.30 ~ 2.08)	**<.001**	1.95 (1.46 ~ 2.62)
Lower	**0.010**	1.47 (1.10 ~ 1.97)	**<.001**	2.09 (1.45 ~ 3.00)

The meaning of the bold values indicated that there were clear statistical differences in the variable in different central lymph node metastasis status groups of papillary thyroid carcinoma ($p < 0.05$).

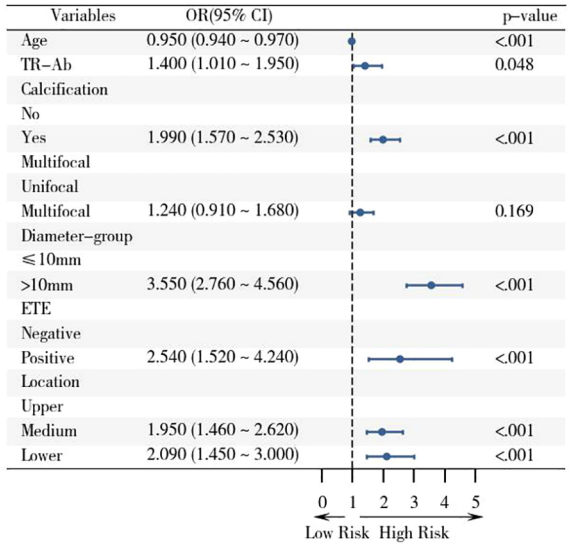

FIGURE 2
Forest plot of risk factors associated with CLNM in the training cohort based on logistic regression analysis with 95% confidence intervals. The screened variables were included in the logistic regression analysis, and the OR value and 95% CI of the multivariate analysis were displayed with the aid of the forest plot.

influence of gender on CLNM in PTC patients still needs to be further studied in a larger patient cohort.

4.1 Age

Some studies have verified that age is a significant predictive factor of CLNM and the rate of CLNM was higher in younger patients (19), our research yielded similar result. Reviewing previous studies, we categorized patients based on age <40 (20) and age <45 (21, 22). The results revealed that PTC patients younger than 40 had a higher incidence of CLNM (51.45% vs. 46.97%) compared to those categorized by age <45. Including different age group criteria in the analysis, we found that using <40 years as a cutoff displayed a more robust predictive value (OR: 1.74, 95% CI: 1.33–2.27) compared to age <45 (OR: 1.60, 95% CI: 1.23–2.09). These results confirm that younger PTC patients are more likely to experience CLNM, with age 40 potentially being a more accurate cutoff than age 45.

4.2 Primary tumor characteristics

Ultrasound features serve as the principal method for evaluating the characteristics of thyroid tumors and the condition of regional lymph nodes (23). In this study, we examined the influence of ultrasound features on CLNM in patients with PTC. Univariate analysis demonstrated associations between CLNM and factors such as tumor location, calcification, the number of tumor foci, and ETE. Further multivariate analysis indicated that tumor situated in the middle or lower poles, calcification, multifocality, and ETE emerged as significant independent predictor of CLNM in PTC patients.

In contrast to tumors located in the upper pole, PTC patients with tumors in the middle and lower poles exhibited a higher rate of CLNM (24) (upper pole vs. middle pole OR: 1.64, 95% CI: 1.33–2.02; upper pole vs. lower pole OR: 1.59, 95% CI: 1.09–1.83). Calcification is a common characteristic of PTC, and before formulating the strategy of clinical data collection, we defined granular and microcalcifications as pathological calcifications, while the large coarse calcifications with clear edges were classified as physiological calcifications (25). Multivariate analysis

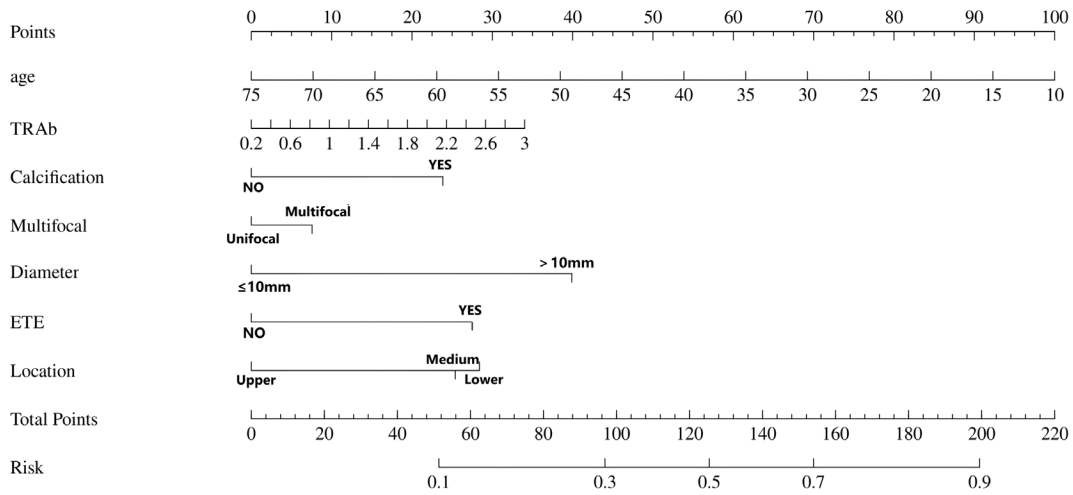

FIGURE 3
The Nomogram prediction model for the risk of central lymph node metastasis. In this predictive model, "Points" denote the weighted scores assigned to each risk factor (e.g., calcification, ETE) associated with CLNM based on their clinical status. For individual cases, clinicians calculate the "Total Points" by summing the individual scores corresponding to the patient's specific clinical parameters within this nomogram model. This cumulative score is then projected onto the "Risk" axis to quantitatively estimate the probability of CLNM occurrence. ETE, extrathyroidal extension; location, Location of thyroid nodules (upper pole, middle pole, lower pole).

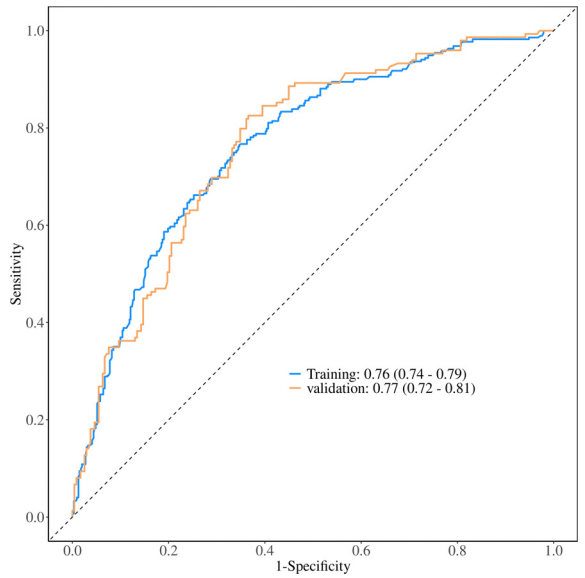

FIGURE 4
Comparative ROC curve analysis of the nomogram prediction model in training and validation cohorts.

demonstrated that PTC patients with pathological calcifications demonstrated an elevated probability of occurrence CLNM compared to those without calcifications or with physiological calcifications (OR: 3.11, 95% CI: 2.62–3.69). This is consistent with the previous results regarding calcification and high TNM stage PTC (26).

Current research suggests that extrathyroidal invasion increases the rate of CLNM (27, 28). Our study compared the relationship between CLNM and whether PTC tumor foci invaded the thyroid capsule. The results confirmed that extrathyroidal extension is associated with a higher likelihood of CLNM (OR: 3.45, 95% CI: 2.38–5.00). Additionally, we examined the influence of the relationship between intraoperative tumor foci and the thyroid capsule regarding regional lymph node metastasis. The findings indicate that both simple invasion of the thyroid capsule (OR: 1.59, 95% CI: 1.27–1.99) and tumor breach the thyroid capsule (OR: 2.32, 95% CI: 1.74–3.09) increase the likelihood of regional lymph node metastasis. Moreover, tumor breach the thyroid capsule also heightens the CLNM rate compared to simple capsule invasion (OR: 1.46, 95% CI: 1.01–2.28) (29).

Tumor size has been demonstrated to be relevant to CLNM (30), and larger tumors generally exhibiting more aggressive

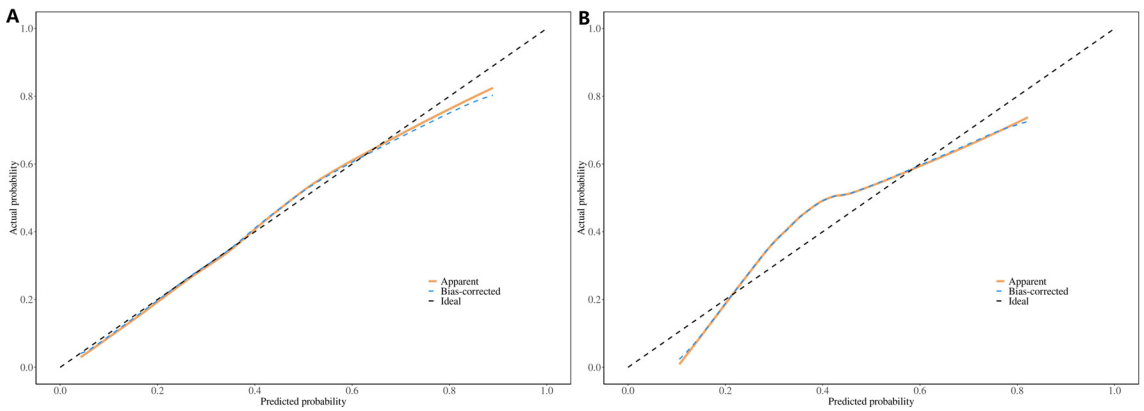

FIGURE 5
Calibration curves of the Nomogram prediction model: **(A)** Training Cohort (Left Panel), **(B)** Validation Cohort (Right Panel).

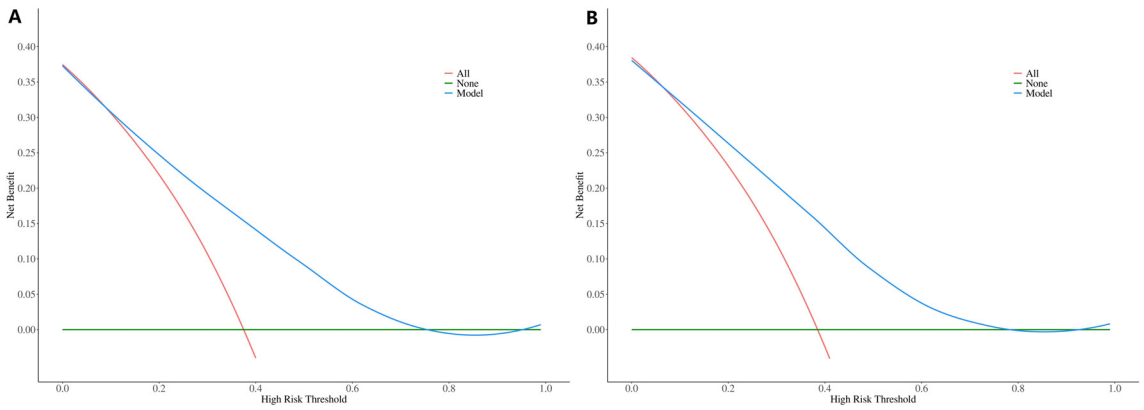

FIGURE 6
DCA curves of the Nomogram prediction model: **(A)** Training Cohort (Left Panel), **(B)** Validation Cohort (Right Panel).

behavior (31). In the TNM staging of PTC, The diameter of the tumor less than or equal to 2 centimeters is classified as T1. However, with advancements in ultrasound detection accuracy and the growing frequency of routine check-ups, the detectable rate of small thyroid tumors has increased, thereby reducing the clinical significance of the traditional staging standard. The T1a/T1b classification has demonstrated greater precision in guiding the clinical management PTC (32).In our research, we did not observe significant differences between the tumor sizes measured by ultrasound with the actual size of pathological samples obtained after surgical resection, suggesting that the tumor sizes measured by ultrasound can be reliably utilized in predictive analyses. Consistent with numerous studies, we categorized primary tumors according to T1a staging. Our results indicated that PTC patients with tumors larger than 10 mm experience a heightened risk of CLNM compared to those classified as T1a. However, some researchers propose that a cutoff of 7 mm may offer a more precise threshold for assessing this risk (33). In our study, employing 7 mm as a grouping criterion did not show any significant clinical advantage in regression analyses or enhance the predictive capability of the model.

4.3 Tumor multifocality

Previous studies have revealed that multifocality increases the possibility of CLNM (34). In our study, patients with multifocal PTC exhibited a higher rate of CLNM. We define multifocality as the presence of two or more tumor foci and further categorize it into two foci and three or more foci. The comparison revealed that patients with two tumor foci had a higher CLNM rate (OR: 1.61, 95% CI: 1.19–2.18) compared to unifocal PTC. However, patients with ≥3 tumor foci did not demonstrate a significantly higher lymph node metastasis rate (OR: 0.73, 95% CI: 0.78–1.73), possibly due to the small sample size of this group (165/2,435, 6.78%). In our predictive model, we included the maximum tumor diameter as a variable, using the largest tumor focus for multifocal cases. To further elucidate the relationship between number of tumor foci and CLNM, we compared the maximum diameters among different groups. The results indicated no statistically significant differences in maximum tumor diameters across the groups (unifocal vs. bifocal: 10.04 vs. 9.78, p=0.735; unifocal vs. ≥3 foci: 10.04 vs. 11.35, p=0.155; bifocal vs. ≥3 foci: 9.78 vs. 11.35, p=0.118). Overall, although multifocal lesions demonstrated a higher rate of CLNM compared with unifocal lesions, further research involving larger cohorts is essential to establish whether three or more foci significantly elevate the risk of CLNM.

4.4 Thyroid function

Previous studies have suggested that serum thyroid hormone levels do not have a clear correlation with the progression of PTC or CLNM (35). However, the relationship between thyroid-related autoantibodies and PTC or CLNM remains unclear (36). Some research indicates that PTC patients with concurrent chronic lymphocytic thyroiditis are more likely to present with multifocal, bilateral thyroid lesions and lymph node metastasis (37). Our findings did not show significant differences in serum thyroglobulin (Tg) levels and thyroglobulin antibody (Tg-Ab) levels between different CLNM status groups (p>0.05). Notably, the CLNM group had higher thyroid receptor antibody levels(TR-Ab) (0.48 ± 0.43) compared to the CLNM(-) group (0.42 ± 0.28) (p=0.004). Through multivariate analysis, serum thyroid receptor antibody levels were identified as a significant risk factor for CLNM in patients with PTC (38). These findings offer valuable insights for preoperative decision-making.

In this study, we utilized demographic characteristics, ultrasound features, and thyroid function results to develop a nomogram prediction model of CLNM, and the Area Under the Curve (AUC) was 0.76. Previous studies utilizing CT or PET features reported AUCs of 0.730 and 0.75 for predicting CLNM in patients with PTC (39, 40), suggesting that our model exhibits enhanced differentiation capability for CLNM. Moreover, in comparison to those studies, the clinical features we selected are more readily accessible, providing greater socioeconomic relevance while preserving clinical predictive accuracy.

This study has certain limitations. First, although our model showed consistent predictive accuracy in the validation cohort, the model was derived from a single-center study and lacked external validation from other hospitals. which may limit the reliability and representativeness of the findings. The results of single-center studies are susceptible to institution-specific factors (e.g.,equipment models and practice norms), and only represent the disease characteristics and treatment patterns of a specific institution or region. The internal validity of the findings is high, but the external validity is low. In addition, our center is one of the top cancer treatment centers in China, The department of imaging diagnosis, pathology and head and neck surgery have more experience in the diagnosis and treatment of PTC patients compared with other medical centers, and the detection rate of different primary tumor characteristics is higher. Differences in imaging and clinical testing capabilities across patient populations and medical centers may limit the generalizability of this model. Future studies should further expand the sample size and conduct studies in medical centers with different imaging and pathological diagnostic capabilities and surgical treatment levels to enhance the generalizability of the results. Additionally, because BRAF V600E mutation status was not routinely tested at our institution, corresponding clinical data could not be collected, and BRAF V600E mutation status could not be included in this study as an independent variable, which may limit the accuracy and generalizability of our conclusions. Subsequent studies should further explore the impact of BRAF V600E mutation status on the risk of CLNM in PTC patients, especially by integrating multi-omics data and clinical covariates.

In conclusion, our study revealed key risk factors for CLNM in PTC patients, including younger age, elevated serum TR-Ab levels, calcification, multifocality, extrathyroidal invasion, larger tumor

size, and tumors located in the mid-thyroid region and lower pole of the thyroid. The nomogram model we developed provides valuable clinical insights for surgeons, enabling the formulation of more tailored surgical strategies for PTC patients, which may significantly improve patient outcomes.

Data availability statement

The original contributions presented in the study are included in the article/supplementary material. Further inquiries can be directed to the corresponding author.

Ethics statement

The studies involving humans were approved by The ethics committee of the Cancer Hospital, Chinese Academy of Medical Sciences. The studies were conducted in accordance with the local legislation and institutional requirements. Written informed consent for participation was not required from the participants or the participants' legal guardians/next of kin in accordance with the national legislation and institutional requirements.

Author contributions

HY: Data curation, Formal Analysis, Investigation, Methodology, Software, Writing – original draft, Writing – review & editing, Validation. LW: Data curation, Resources, Software, Writing – review & editing. JQ: Data curation, Methodology, Software, Writing – review & editing, Validation. WL: Conceptualization, Supervision, Validation, Writing – review & editing.

Funding

The author(s) declare that no financial support was received for the research and/or publication of this article.

Conflict of interest

The authors declare that the research was conducted in the absence of any commercial or financial relationships that could be construed as a potential conflict of interest.

Generative AI statement

The author(s) declare that no Generative AI was used in the creation of this manuscript.

Publisher's note

All claims expressed in this article are solely those of the authors and do not necessarily represent those of their affiliated organizations, or those of the publisher, the editors and the reviewers. Any product that may be evaluated in this article, or claim that may be made by its manufacturer, is not guaranteed or endorsed by the publisher.

References

1. Yuan L, Ma L, Xue H, Song S. Relationship between the upregulation of Notch1 signaling and the clinical characteristics of patients with papillary thyroid carcinoma in East Asia: a systematic review and meta-analysis. *Cancer Cell Int*. (2019) 19:5. doi: 10.1186/s12935-018-0723-8

2. Lubitz CC, Sadow PM, Daniels GH, Wirth LJ. Progress in treating advanced thyroid cancers in the era of targeted therapy. *Thyroid*. (2021) 31:1451–62. doi: 10.1089/thy.2020.0962

3. Wang F, Zhao S, Shen X, Zhu G, Liu R, Viola D, et al. BRAF V600E confers male sex disease-specific mortality risk in patients with papillary thyroid cancer. *J Clin Oncol*. (2018) 36:2787–95. doi: 10.1200/JCO.2018.78.5097

4. Wang Z, Chang Q, Zhang H, Du G, Li S, Liu Y, et al. A clinical predictive model of central lymph node metastases in papillary thyroid carcinoma. *Front Endocrinol (Lausanne)*. (2022) 13:856278. doi: 10.3389/fendo.2022.856278

5. Zhao Y, Shi W, Dong F, Wang X, Lu C, Liu C. Risk prediction for central lymph node metastasis in isolated isthmic papillary thyroid carcinoma by nomogram: A retrospective study from 2010 to 2021. *Front Endocrinol (Lausanne)*. (2022) 13:1098204. doi: 10.3389/fendo.2022.1098204

6. Dolcetti V, Lori E, Fresilli D, Del Gaudio G, Di Bella C, Pacini P, et al. US evaluation of topical hemostatic agents in post-thyroidectomy. *Cancers (Basel)*. (2023) 15(9):2644. doi: 10.3390/cancers15092644

7. Buckle T, Hensbergen AW, van Willigen DM, Bosse F, Bauwens K, Pelger RCM, et al. Intraoperative visualization of nerves using a myelin protein-zero specific fluorescent tracer. *EJNMMI Res*. (2021) 11:50. doi: 10.1186/s13550-021-00792-9

8. Woo J, Kwon H. Optimal surgical extent in patients with unilateral multifocal papillary thyroid carcinoma. *Cancers (Basel)*. (2022) 14(2):432. doi: 10.3390/cancers14020432

9. Cheng P, Xiang Y, Chen E, Zou Z, Zhang X. Papillary thyroid microcarcinoma with synchronous asymptomatic advanced esophageal squamous cell carcinoma: A case report and review of the literature. *Oncol Lett*. (2015) 9:731–4. doi: 10.3892/ol.2014.2748

10. Jeong S, Lee SG, Kim H, Lee G, Park S, Kim IK, et al. Simultaneous expression of long non-coding RNA FAL1 and extracellular matrix protein 1 defines tumour behaviour in young patients with papillary thyroid cancer. *Cancers (Basel)*. (2021) 13 (13):3223. doi: 10.3390/cancers13133223

11. Du W, Shi X, Fang Q, Zhang X, Liu S. Feasibility of apatinib in radioiodine-refractory differentiated thyroid carcinoma. *Front Endocrinol (Lausanne)*. (2022) 13:768028. doi: 10.3389/fendo.2022.768028

12. Adam MA, Pura J, Goffredo P, Dinan MA, Hyslop T, Reed SD, et al. Impact of extent of surgery on survival for papillary thyroid cancer patients younger than 45 years. *J Clin Endocrinol Metab*. (2015) 100:115–21. doi: 10.1210/jc.2014-3039

13. Robinson TJ, Thomas S, Dinan MA, Roman S, Sosa JA, Hyslop T. How many lymph nodes are enough? Assessing the adequacy of lymph node yield for papillary thyroid cancer. *J Clin Oncol*. (2016) 34:3434–9. doi: 10.1200/JCO.2016.67.6437

14. Chen P, Cai X, Mu G, Duan Y, Jing C, Yang Z, et al. Supramolecular nanofibers co-loaded with dabrafenib and doxorubicin for targeted and synergistic therapy of differentiated thyroid carcinoma. *Theranostics*. (2023) 13:2140–53. doi: 10.7150/thno.82140

15. Ahn JE, Lee JH, Yi JS, Shong YK, Hong SJ, Lee DH, et al. Diagnostic accuracy of CT and ultrasonography for evaluating metastatic cervical lymph nodes in patients with thyroid cancer. *World J Surg*. (2008) 32:1552–8. doi: 10.1007/s00268-008-9588-7

16. Tao L, Zhou W, Zhan W, Li W, Wang Y, Fan J. Preoperative prediction of cervical lymph node metastasis in papillary thyroid carcinoma via conventional and contrast-enhanced ultrasound. *J Ultrasound Med*. (2020) 39:2071–80. doi: 10.1002/jum.v39.10

17. Zhou SL, Guo YP, Zhang L, Deng T, Xu ZG, Ding C, et al. Predicting factors of central lymph node metastasis and BRAF(V600E) mutation in Chinese population with papillary thyroid carcinoma. *World J Surg Oncol*. (2021) 19:211. doi: 10.1186/s12957-021-02326-y

18. Kumar A, Klinge CM, Goldstein RE. Estradiol-induced proliferation of papillary and follicular thyroid cancer cells is mediated by estrogen receptors alpha and beta. *Int J Oncol*. (2010) 36:1067–80. doi: 10.3892/ijo_00000588

19. Sezer A, Celik M, Yilmaz Bulbul B, Can N, Tastekin E, Ayturk S, et al. Relationship between lymphovascular invasion and clinicopathological features of papillary thyroid carcinoma. *Bosn J Basic Med Sci*. (2017) 17:144–51. doi: 10.17305/bjbms.2017.1924

20. Xu SY, Yao JJ, Zhou W, Chen L, Zhan WW. Clinical characteristics and ultrasonographic features for predicting central lymph node metastasis in clinically node-negative papillary thyroid carcinoma without capsule invasion. *Head Neck*. (2019) 41:3984–91. doi: 10.1002/hed.v41.11

21. Mao J, Zhang Q, Zhang H, Zheng K, Wang R, Wang G. Risk factors for lymph node metastasis in papillary thyroid carcinoma: A systematic review and meta-analysis. *Front Endocrinol (Lausanne)*. (2020) 11:265. doi: 10.3389/fendo.2020.00265

22. Yan B, Hou Y, Chen D, He J, Jiang Y. Risk factors for contralateral central lymph node metastasis in unilateral cN0 papillary thyroid carcinoma: A meta-analysis. *Int J Surg*. (2018) 59:90–8. doi: 10.1016/j.ijsu.2018.09.004

23. Andrioli M, Carzaniga C, Persani L. Standardized ultrasound report for thyroid nodules: the endocrinologist's viewpoint. *Eur Thyroid J*. (2013) 2:37–48. doi: 10.1159/000347144

24. So YK, Kim MJ, Kim S, Son YI. Lateral lymph node metastasis in papillary thyroid carcinoma: A systematic review and meta-analysis for prevalence, risk factors, and location. *Int J Surg*. (2018) 50:94–103. doi: 10.1016/j.ijsu.2017.12.029

25. Pyo JS, Kang G, Kim DH, Park C, Kim JH, Sohn JH. The prognostic relevance of psammoma bodies and ultrasonographic intratumoral calcifications in papillary thyroid carcinoma. *World J Surg*. (2013) 37:2330–5. doi: 10.1007/s00268-013-2107-5

26. Bai Y, Zhou G, Nakamura M, Ozaki T, Mori I, Taniguchi E, et al. Survival impact of psammoma body, stromal calcification, and bone formation in papillary thyroid carcinoma. *Mod Pathol*. (2009) 22:887–94. doi: 10.1038/modpathol.2009.38

27. Zheng X, Peng C, Gao M, Zhi J, Hou X, Zhao J, et al. Risk factors for cervical lymph node metastasis in papillary thyroid microcarcinoma: a study of 1,587 patients. *Cancer Biol Med*. (2019) 16:121–30. doi: 10.20892/j.issn.2095-3941.2018.0125

28. Vasileiadis I, Karakostas E, Charitoudis G, Stavrianaki A, Kapetanakis S, Kouraklis G, et al. Papillary thyroid microcarcinoma: clinicopathological characteristics and implications for treatment in 276 patients. *Eur J Clin Invest*. (2012) 42:657–64. doi: 10.1111/j.1365-2362.2011.02633.x

29. Kamaya A, Tahvildari AM, Patel BN, Willmann JK, Jeffrey RB, Desser TS. Sonographic detection of extracapsular extension in papillary thyroid cancer. *J Ultrasound Med*. (2015) 34:2225–30. doi: 10.7863/ultra.15.02006

30. Ma B, Wang Y, Yang S, Ji Q. Predictive factors for central lymph node metastasis in patients with cN0 papillary thyroid carcinoma: A systematic review and meta-analysis. *Int J Surg*. (2016) 28:153–61. doi: 10.1016/j.ijsu.2016.02.093

31. Chai W, Ye F, Zeng L, Li Y, Yang L. HMGB1-mediated autophagy regulates sodium/iodide symporter protein degradation in thyroid cancer cells. *J Exp Clin Cancer Res*. (2019) 38:325. doi: 10.1186/s13046-019-1328-3

32. Fei Y, Wang B, Yao X, Wu J. Factors associated with occult lateral lymph node metastases in patients with clinically lymph node negative papillary thyroid carcinoma: a systematic review and meta-analysis. *Front Endocrinol (Lausanne)*. (2024) 15:1353923. doi: 10.3389/fendo.2024.1353923

33. Heng Y, Yang Z, Cao P, Cheng X, Tao L. Lateral involvement in different sized papillary thyroid carcinomas patients with central lymph node metastasis: A multi-center analysis. *J Clin Med*. (2022) 11(17):4975. doi: 10.3390/jcm11174975

34. Wang Z, Qu L, Chen Q, Zhou Y, Duan H, Li B, et al. Deep learning-based multifeature integration robustly predicts central lymph node metastasis in papillary thyroid cancer. *BMC Cancer*. (2023) 23:128. doi: 10.1186/s12885-023-10598-8

35. Wang L, Chen J, Yuan X, Wang J, Sun L, Jiang J, et al. Lymph node metastasis of papillary thyroid carcinoma in the context of Hashimoto's thyroiditis. *BMC Endocr Disord*. (2022) 22:12. doi: 10.1186/s12902-021-00923-2

36. Fiore E, Latrofa F, Vitti P. Iodine, thyroid autoimmunity and cancer. *Eur Thyroid J*. (2015) 4:26–35. doi: 10.1159/000371741

37. Liu Y, Lv H, Zhang S, Shi B, Sun Y. The impact of coexistent hashimoto's thyroiditis on central compartment lymph node metastasis in papillary thyroid carcinoma. *Front Endocrinol (Lausanne)*. (2021) 12:772071. doi: 10.3389/fendo.2021.772071

38. Kitahara C.M., K.R.F. D, Jørgensen JOL, Cronin-Fenton D, Sørensen HT. Benign thyroid diseases and risk of thyroid cancer: A nationwide cohort study. *J Clin Endocrinol Metab*. (2018) 103:2216–24. doi: 10.1210/jc.2017-02599

39. Peng Y, Zhang ZT, Wang TT, Wang Y, Li CH, Zuo MJ, et al. Prediction of central lymph node metastasis in cN0 papillary thyroid carcinoma by CT radiomics. *Acad Radiol*. (2023) 30:1400–7. doi: 10.1016/j.acra.2022.09.002

40. Kim BS, Kim SJ, Kim IJ, Pak K, Kim K. Factors associated with positive F-18 flurodeoxyglucose positron emission tomography before thyroidectomy in patients with papillary thyroid carcinoma. *Thyroid*. (2012) 22:725–9. doi: 10.1089/thy.2011.0031

frontiers | Frontiers in Oncology

TYPE Mini Review
PUBLISHED 29 May 2025
DOI 10.3389/fonc.2025.1605085

Check for updates

OPEN ACCESS

EDITED BY
Xiaosheng Tan,
Rutgers, United States

REVIEWED BY
Hao Zhang,
Chongqing Medical University, China
Zheng Liu,
Xiangtan Central Hospital, China
Yanjun Gao,
George Washington University, United States
Yaping Li,
Yale University, United States

*CORRESPONDENCE
Qijun Zhang
zhangqijun8354@163.com
Haixia Shi
haixia.0101@163.com

†These authors have contributed equally to this work

RECEIVED 02 April 2025
ACCEPTED 12 May 2025
PUBLISHED 29 May 2025

CITATION
Chen C, Chen J, Zhang Y, Zhang Q and Shi H (2025) Senescence-associated secretory phenotype in lung cancer: remodeling the tumor microenvironment for metastasis and immune suppression.
Front. Oncol. 15:1605085.
doi: 10.3389/fonc.2025.1605085

COPYRIGHT
© 2025 Chen, Chen, Zhang, Zhang and Shi. This is an open-access article distributed under the terms of the Creative Commons Attribution License (CC BY). The use, distribution or reproduction in other forums is permitted, provided the original author(s) and the copyright owner(s) are credited and that the original publication in this journal is cited, in accordance with accepted academic practice. No use, distribution or reproduction is permitted which does not comply with these terms.

Senescence-associated secretory phenotype in lung cancer: remodeling the tumor microenvironment for metastasis and immune suppression

Chen Chen[1†], Ji Chen[1†], Yanling Zhang[1], Qijun Zhang[2*] and Haixia Shi[3*]

[1]Department Traditional of Chinese Medicine (TCM), Shanghai Pudong New Area Pulmonary Hospital, Shanghai, China, [2]Department of Oncology, Integrated Traditional Chinese and Western Medicine Hospital of Shanghai Minhang District, Shanghai, China, [3]Department of Traditional Chinese Medicine, Shanghai Ninth People's Hospital, Shanghai Jiao Tong University School of Medicine, Shanghai, China

Cellular senescence exerts dual roles in lung cancer pathogenesis: initially suppressing tumorigenesis via p53/p21/p16-mediated cell cycle arrest, but promoting malignancy through the senescence-associated secretory phenotype (SASP). SASP secretes cytokines, proteases, and growth factors, reshaping the tumor microenvironment (TME) to drive immune evasion, metastasis, and therapy resistance. NF-κB activation induces APOBEC3B mutagenesis and PD-L1 overexpression, while mTOR signaling enhances glycolysis and OXPHOS to fuel tumor growth. Clinically, telomere attrition, p16/p21 expression, and SASP components serve as prognostic biomarkers. Therapeutic strategies target senescent cells and SASP. Future directions focus on single-cell multi-omics to decode senescence heterogeneity, spatially controlled drug delivery, and therapies targeting senescence-immune-metabolic crosstalk. By unraveling senescence's dual regulatory mechanisms, this review highlights precision approaches to overcome resistance and improve lung cancer outcomes.

KEYWORDS

cellular senescence, lung cancer, SASP, therapy resistance, precision medicine

1 Introduction

Lung cancer remains the leading cause of global cancer mortality and the most prevalent malignant tumor, with adenocarcinoma constituting its predominant histological subtype (1). According to GLOBOCAN 2020 statistics, there were over 2.2 million new cases of lung cancer worldwide, accounting for 11.4% of all cancer cases. The number of deaths was approximately 1.79 million, representing 18% of the total cancer mortality. Among them, lung adenocarcinoma is the most common subtype of non-small cell lung cancer, accounting for

about 40%–50% of NSCLC cases, with a higher incidence in women and non-smokers (2). As the most common form of non-small cell lung cancer (NSCLC), lung adenocarcinoma (LUAD) arises from malignant transformation of bronchial glandular cells, pathologically defined by glandular differentiation patterns and mucin-producing cellular architecture (3, 4). Distinct from other NSCLC subtypes, LUAD predominantly originates in peripheral lung structures including distal airways and alveoli, exhibiting characteristic histomorphological patterns such as acinar, papillary, micropapillary, and invasive mucinous adenocarcinoma (5). Clinical presentation often involves nonspecific respiratory symptoms—persistent cough, hemoptysis, dyspnea, and chest pain—frequently accompanied by constitutional manifestations like unexplained weight loss and fatigue (6). Its indolent early-stage progression explains why 20–30% of cases are incidentally detected through routine chest imaging (X-ray/CT), while over 60% present with locally advanced or metastatic disease at diagnosis (7). Epidemiologically, LUAD accounts for 40–50% of global lung cancer diagnoses, displaying unique demographic patterns: increased incidence in never-smokers, female predominance, higher prevalence in Asian populations, and elevated urban versus rural rates, potentially reflecting differential air pollution exposure (8). These epidemiological shifts, coupled with rising adenocarcinoma incidence rates, position LUAD as a critical driver of lung cancer's persistent mortality burden (9). Despite the advancements in targeted therapies and immunotherapies that have significantly improved survival outcomes for some patients, the overall five-year survival rate for lung cancer remains below 20% (10). Particularly in advanced lung adenocarcinoma, issues such as drug resistance, recurrence, and immune evasion continue to pose significant challenges in clinical treatment, underscoring the urgent need to elucidate their molecular mechanisms and explore novel therapeutic strategies.

Molecular pathogenesis of LUAD centers on dysregulation of proliferative signaling cascades mediated by driver mutations (11). Epidermal growth factor receptor (EGFR) mutations represent the most prevalent oncogenic drivers, occurring in 10–50% of cases depending on population ethnicity and smoking status (12). Mutant EGFR acquires ligand-independent tyrosine kinase activity, constitutively activating downstream effectors including mitogen-activated protein kinase/extracellular signal-regulated kinase (MAPK/ERK, pro-survival signaling), phosphatidylinositol 3-kinase/protein kinase B (PI3K/AKT, anti-apoptotic signaling), and janus kinase/signal transducer and activator of transcription (JAK/STAT, proliferative/invasive regulation) pathways (13). Concurrently, PI3K/AKT/mTOR pathway hyperactivation promotes tumor metabolism and survival through enhanced glucose utilization and protein synthesis (14). Wnt/β-catenin signaling aberrations further contribute by sustaining cancer stem cell populations and apoptotic resistance (15). Moreover, kirsten rat sarcoma viral oncogene (KRAS) mutations, rearranged during transfection gene (RET) fusions, and ROS proto-oncogene 1 (ROS1) rearrangements represent pivotal oncogenic drivers in LUAD. KRAS mutations constitute the most prevalent driver mutation in EGFR-negative LUAD, notably with the smoking-associated KRAS G12C subtype predominating, accounting for around 13% of all NSCLC cases. By activating multiple downstream signaling pathways, including MAPK, PI3K/AKT, and RalGDS, KRAS mutations facilitate tumor proliferation, migration, and immune evasion (16). RET fusions predominantly occur in younger LUAD patients who are either non-smokers or light smokers, with an incidence rate of approximately 1–2%, and they are closely linked with accelerated tumor progression. RET fusions frequently result in fusion proteins with partner genes such as kinesin family member 5B (KIF5B) or coiled-coil domain containing 6 (CCDC6), thereby activating the MAPK and STAT pathways. As highly selective RET inhibitors, Selpercatinib and Pralsetinib have demonstrated remarkable objective response rates and favorable safety profiles in advanced RET fusion-positive LUAD, subsequently being incorporated into the recommended first-line treatment regimens (17). ROS1 fusion proteins propel tumor progression by engaging signaling pathways including PI3K/AKT and JAK/STAT. Crizotinib stands as the first approved targeted therapeutic for ROS1-rearranged NSCLC, demonstrating an efficacy rate exceeding 70% (18).

Similarly, epigenetic mechanisms, including DNA methylation, histone modifications and the dysregulation of non-coding RNAs (such as microRNAs and long non-coding RNAs), play pivotal roles in the initiation and progression of lung adenocarcinoma (19), while epigenetic dysregulation via abnormal DNA methylation, histone modifications, and non-coding RNA expression (miR-21 overexpression and lncRNA HOTAIR dysregulation) drives malignant transformation without altering genomic sequences (20).

The biological continuum of aging intersects critically with LUAD pathogenesis through cellular senescence mechanisms. Aging involves progressive functional decline across organ systems, mediated by hallmarks including genomic instability, telomere attrition, epigenetic drift, and mitochondrial dysfunction (21, 22). Cellular senescence—a permanent cell-cycle arrest triggered by oncogenic stress, DNA damage, or tumor suppressor activation—exerts context-dependent tumor-modulating effects (23). While initially tumor-suppressive by halting malignant transformation, senescent cells develop a senescence-associated secretory phenotype (SASP) (24), releasing inflammatory cytokines (IL-6, IL-8), growth factors (TGF-β), and proteases that remodel the tumor microenvironment (TME) (25). SASP components induce paracrine senescence in adjacent cells, recruit immunosuppressive myeloid cells, and paradoxically promote angiogenesis and metastasis through TME modulation (26, 27).

Emerging evidence positions senescence as a dual-axis regulator in LUAD progression (28). Lin et al. developed a 16-gene senescence-related signature (SRS) demonstrating that SASP-mediated immune microenvironment remodeling predicts immunotherapy response and survival outcomes (29). Complementary transcriptomic analyses of 278 senescence-associated genes revealed distinct senescence subtypes correlated with differential immune infiltration patterns in LUAD (30). These findings illuminate senescence as a dynamic interface between tumor biology and immune regulation, offering novel therapeutic targets—particularly for immunotherapy-resistant LUAD subtypes where SASP factors may mediate immune evasion. This review aims to systematically summarize the current understanding of cellular senescence in lung adenocarcinoma, with an emphasis on its dual roles in both tumor suppression and

promotion. We particularly focus on the SASP and how it impacts tumor progression, immune modulation, and therapy resistance. Additionally, we discuss potential therapeutic opportunities and challenges in this context.

2 Association of cellular senescence with lung cancer

2.1 Telomere attrition

Telomere attrition serves as a critical nexus between cellular aging and lung carcinogenesis, driving chromosomal instability while paradoxically influencing tumor-suppressive and oncogenic pathways (31). Telomeres—terminal chromosomal regions composed of repetitive TTAGGG sequences and stabilized by shelterin protein complexes (TRF1/TRF2, TPP1)—prevent aberrant DNA repair by masking chromosomal ends from damage recognition systems (32). In somatic cells, the end-replication problem results in progressive telomere shortening (50–200 bp per division), culminating in replicative senescence when critical length thresholds (Hayflick limit) are breached; This triggers DNA damage response (DDR) activation through ataxia-telangiectasia mutated/ATM and rad3-related (ATM/ATR) kinases, stabilizing p53 to induce p21-mediated cell cycle arrest—a fundamental tumor-suppressive mechanism (33).

Contrasting this protective role, 85–90% of lung cancers exhibit pathological telomerase reactivation via telomerase reverse transcriptase (TERT, catalytic subunit) overexpression and telomerase RNA component (TERC, RNA template) dysregulation, enabling replicative immortality; Reactivation mechanisms include recurrent TERT promoter mutations (C228T/C250T) and epigenetic remodeling of telomere maintenance genes (34). Paradoxically, despite telomerase activity, lung tumors frequently display ongoing telomere attrition, generating chromosomal fusions and breakage-fusion-bridge cycles that amplify oncogenic signaling through PI3K/AKT and RAS-MAPK pathways while enhancing immune evasion via programmed death protein 1 (PD-L1)/PD-1 axis upregulation (35). Telomere attrition can elicit a persistent DNA damage response, thereby activating the ATM/ATR-checkpoint kinase 1 (CHK1) pathway and facilitating immune surveillance evasion by upregulating PD-L1 expression, ultimately promoting tumor cell immune tolerance and progression (36). Telomere disruption and the consequent loss of telomere-binding protein functionality can also activate cell survival signaling via the PI3K/AKT pathway, thereby enhancing tumor cell adaptability to oxidative stress and nutrient-poor conditions (37, 38). Clinically, leukocyte telomere length demonstrates bidirectional associations with lung adenocarcinoma risk: longer telomeres in peripheral blood correlate with heightened susceptibility, potentially reflecting inherited telomere maintenance defects or accelerated age-related shortening (39, 40). Mechanistically, while elongated telomeres can delay replicative senescence and extend the proliferative lifespan of somatic cells, they may also elevate the risk of accumulating genetic and epigenetic alterations under carcinogenic exposures, such as tobacco smoke, thereby increasing the potential for oncogenesis (41). Elongated telomeres are frequently accompanied by increased telomerase activity, which not only maintains chromosomal stability but also interacts with oncogenic pathways, such as MYC and TERT promoter mutations (42). This dual role positions telomere dynamics as both a biomarker and therapeutic target. Emerging strategies include TERT promoter inhibition using oligonucleotide antagonists such as GRN163L, telomerase splicing modulation through NOVA1-dependent alternative splicing blockade, and senescence-targeted therapies that combine senolytics (navitoclax) with SASP pathway inhibitors to mitigate pro-tumorigenic microenvironment effects, all of which represent promising approaches to advance lung cancer treatment (Shown in Figure 1) (43).

2.2 Carcinogenic effects of DNA damage and mutation accumulation

The accumulation of DNA damage and mutations constitutes a pivotal carcinogenic mechanism, driven by structural genomic alterations from endogenous sources—including replication errors and oxidative stress—and exogenous environmental carcinogens such as ultraviolet radiation and chemical agents (44).Unrepaired DNA lesions induce oncogenic transformation through point mutations, gene amplifications, or chromosomal translocations, which activate proto-oncogenes via gain-of-function mutations or inactivate tumor suppressors through loss of heterozygosity and epigenetic silencing (45). Compromised DNA repair pathways further amplify genomic instability: for example, breast cancer susceptibility gene 1/2(BRCA1/2) mutations disrupt homologous recombination (HR) repair, forcing reliance on error-prone mechanisms like non-homologous end joining, thereby accelerating oncogenic mutation accrual, while mismatch repair (MMR) deficiencies propagate microsatellite instability (46). Deficiency in HR repair serves as a principal driver of genomic instability across various tumor types. In LUAD, TP53 and KRAS mutations are intricately associated with defects in HR repair mechanisms. The loss of TP53 function compromises DNA damage checkpoint control, thereby synergistically promoting genomic instability and increased reliance on HR pathways. Conversely, KRAS mutations elevate ROS levels, thereby intensifying DNA damage stress and compelling tumor cells to rely more heavily on residual HR mechanisms for survival (47, 48). On the other hand, while MMR deficiencies are relatively uncommon in LUAD, their presence often results in a high tumor mutational burden (TMB), facilitating neoantigen formation and increasing sensitivity to immune checkpoint inhibitors (ICIs). The loss of function in core MMR genes such as muts homolog 2 (MSH2) and muts homolog 1 (MSH1) can lead to the upregulation of PD-L1 expression while activating the cyclic GMP-AMP synthase-stimulator of interferon genes (cGAS-STING) pathway, thereby inducing IFN-γ signaling to enhance tumor immunogenicity (49). PARP inhibitors obstruct the repair of single-strand breaks, thereby compelling cells to rely on the HR pathway to rectify DNA damage. Consequently, in tumor cells harboring BRCA1/2 mutations, where HRR function is

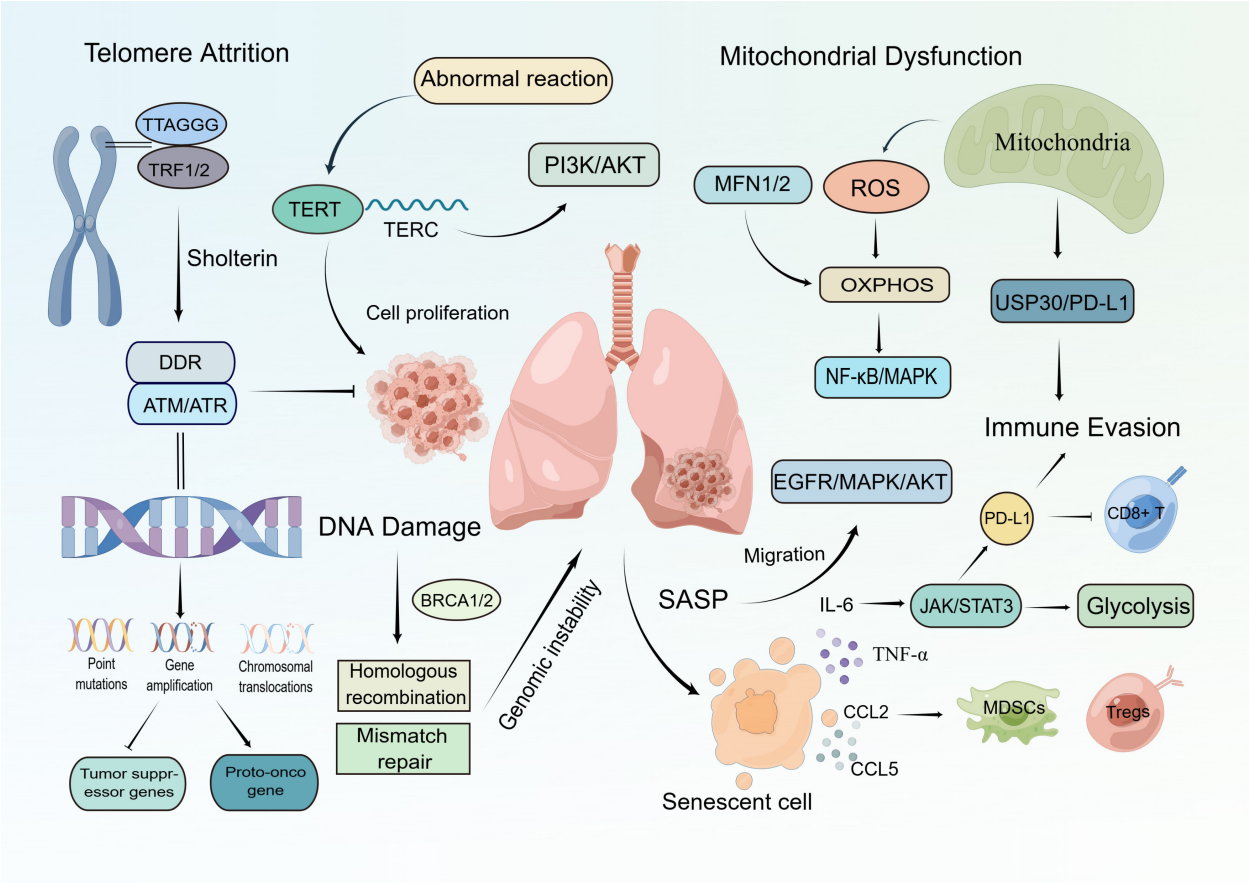

FIGURE 1
The Role of Cellular Senescence in Lung Cancer Progression. This figure illustrates the biological network through which cellular senescence drives lung cancer progression. (1)Telomere Attrition: Shortening of TTAGGG sequences and TRF1/2 imbalance disrupts Shelterin complex protection, activating ATM/ATR-mediated DDR. This induces genomic instability, leading to oncogene activation (EGFR, KRAS) and tumor suppressor inactivation (BRCA1/2); (2)DNA Damage: Defective homologous recombination repair (BRCA1/2) and mismatch repair (MMR) accelerate malignant clonal evolution; (3)Mitochondrial Dysfunction: MFN1/2 abnormalities elevate ROS, activating NF-κB/MAPK pathways to enhance cancer cell migration. Simultaneously, increased OXPHOS supports cancer stem cell survival; (4)Immune Evasion: ROS and PD-L1 suppress $CD8^+$ T cell function, while USP30-mediated glycolytic reprogramming further weakens antitumor immunity; (5)Senescence-Associated Secretory Phenotype (SASP): Senescent cells secrete IL-6, TNF-α, and CCL2/5, recruiting MDSCs and Tregs to create an immunosuppressive microenvironment. This synergizes with EGFR/MAPK/AKT signaling to promote tumor growth and metastasis.

compromised, the action of PARP inhibitors leads to the accumulation of DNA damage, triggering apoptosis—a phenomenon known as "synthetic lethality" (50).

Emerging approaches focus on replication stress mitigation using ATR/CHK1 inhibitors to bypass therapy resistance, alongside novel agents disrupting DNA damage tolerance pathways, collectively advancing precision oncology paradigms that capitalize on repair pathway dysregulation (51, 52). ATR and CHK1 are key kinases within the DDR network, primarily responding to replication stress and single-stranded DNA (ssDNA) damage. In LUAD, frequent mutations in genes such as TP53, KRAS, and ATM result in increased reliance of tumor cells on the ATR/CHK1 pathway (53). Ceralasertib (AZD6738), an ATR kinase inhibitor, markedly increases apoptosis, induces G2/M arrest, and enhances p21 expression while reducing CDC2 levels in SNU478 and SNU869 cell lines, demonstrating enhanced antitumor activity when combined with paclitaxel (54, 55). Prexasertib (LY2606368) is a substrate ATP competitive selective inhibitor of CHK1 and checkpoint kinase 2 (CHK2). In a phase I clinical trial involving patients with advanced squamous cell carcinoma, prexasertib monotherapy exhibited notable antitumor activity, with some patients achieving disease control after 3 months (56).

2.3 Mitochondrial dysfunction and cancer cell metabolism

Mitochondrial dysfunction drives cancer metabolic reprogramming by enabling survival advantages through energy metabolism remodeling, oxidative stress modulation, apoptosis evasion, and anabolic precursor synthesis (57). Although the Warburg effect historically dominated cancer metabolism paradigms, recent studies demonstrate that oxidative phosphorylation (OXPHOS) sustains the survival of therapy-resistant tumor subpopulations and metastatic cancer stem cells (58)—a phenomenon exemplified by

glioblastoma stem cells that maintain immortality through mitochondrial fusion-mediated OXPHOS enhancement and NAD+ metabolic rewiring (59).This metabolic plasticity underpins therapeutic challenges, as lung cancers with elevated OXPHOS activity exhibit immunotherapy resistance, prompting the development of precision strategies like the OXPHOS inhibitor IACS-010759 to target refractory malignancies (60).

Mitochondrial reactive oxygen species (ROS) exhibit context-dependent oncogenic roles: mtDNA mutations or electron transport chain defects induce ROS overproduction, activating nuclear factor kappa-B (NF-κB) and MAPK pathways to drive lung cancer metastasis (61), while pharmacologic ROS modulation exerts antitumor effects. For instance, metformin suppresses ROS via complex I inhibition to sensitize tumors to chemotherapy, whereas pro-oxidant therapies exploit ROS overload to eliminate cancer stem cells (62). Parallel mechanisms involve mitochondrial regulation of apoptosis—overexpression of anti-apoptotic BCL-2 proteins (e.g., in lymphomas and breast cancers) blocks cytochrome c-mediated apoptosome activation, a vulnerability successfully targeted by the BCL-2 inhibitor venetoclax (63).

Mitochondrial metabolism plays a pivotal regulatory role in shaping the tumor immune microenvironment (TIME), significantly influencing immune evasion and antitumor immune responses (64). Tumor cells, by enhancing oxidative phosphorylation (OXPHOS) and aerobic glycolysis metabolism, accelerate nutrient consumption and produce lactate, leading to glucose and oxygen scarcity in TIME and the formation of an acidic microenvironment. This suppresses $CD8^+$ effector T cell activity and promotes the expansion of regulatory T cells (Tregs) and myeloid-derived suppressor cells (MDSCs), creating an immunosuppressive niche (65). On the other hand, the proliferation and sustained functionality of effector and memory $CD8^+$ T cells depend on mitochondrial OXPHOS and the tricarboxylic acid cycle (TCA). Mitochondrial dysfunction, such as loss of membrane potential and accumulation of reactive oxygen species (ROS), can lead to T cell exhaustion, closely related to the upregulation of immune checkpoint molecules like PD-1 (66). Therefore, targeting mitochondrial metabolism to remodel TIME and enhance T cell-mediated immune responses has become a key research direction in tumor immunotherapy. For instance, inhibiting pyruvate dehydrogenase kinase (PDK) can enhance TCA activity, promote acetyl-CoA production, and lead to increased histone acetylation, thereby boosting PD-L1 expression on tumor cells (67). In a triple-negative breast cancer (TNBC) mouse model, combined treatment with metformin and PD-1 antibodies significantly inhibited tumor growth and metastasis, increased $CD8^+$ T cell infiltration, and reduced PD-L1 expression, indicating synergistic antitumor effects of the combination (68).

2.4 Promoting role of SASP in the carcinogenic microenvironment

The senescence-associated secretory phenotype (SASP) drives tumor progression through a multifaceted molecular network—comprising cytokines (IL-6, IL-8), chemokines (CXCL1, CCL2), proteases (MMPs), and growth factors (VEGF, TGF-β)—that remodels the tumor microenvironment (TME) into a pro-carcinogenic niche (69). SASP components directly amplify tumor proliferation and invasion: EREG/EGFR signaling activation via the MAPK/AKT axis mediates chemotherapy-induced progression in prostate cancer (70), while MMP1 and MMP3 degrade extracellular matrix (ECM) components to facilitate glioblastoma and lung cancer metastasis (71). Concurrently, SASP reprograms cancer metabolism; IL-6-induced STAT3 activation shifts energy production toward glycolysis while suppressing oxidative phosphorylation (OXPHOS), thereby fueling rapid tumor growth (72).

immune evasion (73). In KRAS-mutant lung cancer, senescent macrophages secrete CCL2 to recruit MDSCs, while IL-10 and TGF-β polarize tumor-associated macrophages (TAMs) toward an immunosuppressive M2 phenotype, crippling cytotoxic T cell activity (74). This immunosuppressive axis is reinforced by PD-L1 upregulation: IL-6 and VEGF activate PD-L1 expression on tumor cells, impairing NK cell function and $CD8^+$ T cell-mediated cytotoxicity (75). Beyond immune modulation, SASP reshapes the stromal architecture by inducing fibrotic barriers. Cancer-associated fibroblasts (CAFs) secrete collagen and fibronectin under SASP influence, while lysyl oxidase (LOX)-mediated ECM crosslinking increases tissue stiffness, activating integrin-FAK signaling to accelerate metastasis and confer therapy resistance (76).

2.5 Regulation of immune evasion and inflammatory response by senescence

Cellular senescence orchestrates immune evasion and chronic inflammation in lung cancer through SASP-mediated immunosuppression and mitochondrial dysfunction (28).SASP-derived pro-inflammatory cytokines (IL-6, IL-8, TNF-α) and chemokines (CCL2, CXCL1) directly suppress antitumor immunity: IL-6 activates JAK/STAT3 signaling to upregulate PD-L1 expression on tumor cells and dendritic cells, inducing $CD8^+$ T cell exhaustion (77). This mechanism corroborated by the 30% higher PD-L1 expression prevalence in elderly lung cancer patients compared to younger counterparts (78). Chemokine-driven immunosuppression is exemplified in KRAS-mutant lung cancer, where senescent cells recruit MDSCs and regulatory Tregs via CCL2 secretion, establishing an immune-privileged niche (79).

Senescent lung cancer cells further sabotage immune function through mitochondrial hijacking. Mutant mitochondria are transferred to T cells via tunneling nanotubes (TNTs), reducing T cell oxidative phosphorylation activity by 60% while activating the USP30-PD-L1 axis to amplify immune evasion—a process demonstrating direct crosstalk between metabolic dysfunction and checkpoint signaling (80). Concurrently, senescence-associated chronic inflammation fuels tumor progression through genomic destabilization: apolipoprotein B mRNA editing enzyme catalytic subunit 3B (APOBEC3B)-mediated cytosine deamination elevates mutation burden (2.5-fold higher in elderly patients) while NF-κB activation sustains pro-tumorigenic cytokine release (81).

Therapeutic inhibition of NF-κB in aged preclinical models reduces lung tumor volume by 70%, underscoring the pathway's centrality in senescence-driven malignancy (82). Collectively, these mechanisms drive immune surveillance failure and aggressive progression within the senescent lung cancer microenvironment (Shown in Table 1).

3 Cellular senescence and lung cancer-related signaling pathways

3.1 Dual Roles of the p53/p21/p16 Signaling Pathway

The p53/p21/p16 axis exerts context-dependent tumor-suppressive and oncogenic effects in lung cancer through dynamic molecular crosstalk. Canonically, wild-type p53 activates p21 (cyclin dependent kinase Inhibitor 1A, CDKN1A) to enforce G1/S cell cycle arrest, enabling DNA repair or apoptosis initiation (83). This mechanism impaired in ~50% of lung cancers harboring TP53 mutations (84). Mutant p53 acquires oncogenic functions via epigenetic remodeling, including senescence-associated heterochromatin foci (SAHF) formation, which derepresses MYC transcription while silencing the cyclin dependent kinase Inhibitor 2A (CDKN2A) locus encoding p16 (85).

The p21 demonstrates paradoxical roles contingent on p53 status. In p53-wildtype tumors, p21-mediated CDK2/4 inhibition enhances chemotherapy response (86). Conversely, mutant p53 redirects p21 to upregulate RAD21, promoting homologous recombination repair and cisplatin resistance (87). Microenvironmental cues further modulate p21 activity: EGFR-STAT3 signaling phosphorylates p21 to induce its cytoplasmic translocation, where the p21/STAT3 complex activates AKT-mTOR signaling to drive metastasis (88).

The p16 (CDKN2A) inactivation—primarily through promoter hypermethylation—represents a hallmark of lung cancer progression, enabling cell cycle dysregulation via CDK4/6-RB pathway activation (89). Paradoxically, p16 loss upregulates telomerase (hTERT) to immortalize tumor cells, whereas its overexpression induces senescence, highlighting its dual regulatory capacity (90). Clinically, p16/p21 co-expression patterns predict immunotherapy efficacy: NSCLC patients with low p16 expression exhibit elevated PD-L1 levels but paradoxically inferior responses to PD-1 inhibitors, suggesting p16 loss primes an immune-evasive phenotype resistant to checkpoint blockade (91). These findings underscore the pathway's complexity as a therapeutic determinant in lung cancer.

3.2 Cross-talk of NF-κB in lung cancer and cellular senescence

The NF-κB pathway functions as a molecular nexus linking cellular senescence to lung cancer progression through dual pro-survival and pro-inflammatory mechanisms. In senescent cells, DNA damage triggers ATM/ATR kinase activation, which phosphorylates the IKK complex to degrade IκBα, enabling nuclear translocation of the p65/p50 heterodimer—a prerequisite for SASP factor transcription (IL-6, IL-8, MMP9) that fosters a tumor-promoting inflammatory niche (92). Lung cancer cells amplify this cascade autonomously via TNF-α and HMGB1 secretion, creating a self-reinforcing NF-κB activation loop (93).

TABLE 1 Mechanisms of the impact of cellular senescence on lung cancer.

Senescence Mechanism	Mechanisms	Impact on Lung Cancer	Signaling Pathways/ Molecules	Therapeutic Strategies
Telomere Attrition	Telomere attrition activates DNA damage response, inducing replicative senescence; telomerase reactivation bypasses senescence, enabling tumor immortality.	Promotes chromosomal instability; activates oncogenic pathways PI3K/AKT, RAS-MAPK; enhances immune evasion via PD-L1/PD-1 axis.	p53/p21; ATM/ATR; TERT promoter mutations	Telomerase inhibitors; TERT mutation-targeting drugs
DNA Damage and Mutation Accumulation	Endogenous/exogenous DNA damage leads to mutations in oncogenes or tumor suppressor inactivation.	Drives malignant transformation; induces APOBEC3B-mediated mutations;.	BRCA1/2; PARP; ATM/ATR	PARP inhibitors; immune checkpoint inhibitors; ATR/CHK1 inhibitors.
Mitochondrial Dysfunction	Impaired mitophagy causes ROS accumulation; OXPHOS supports therapy-resistant cancer stem cells; metabolic reprogramming.	Promotes metastasis; suppresses T cell function; enhances chemoresistance.	mTOR; HIF-1α; BCL-2 family	OXPHOS inhibitors; Metformin (glycolysis suppression); BCL-2 inhibitor.
SASP Secretion	SASP secretes IL-6, IL-8, MMPs and TGF-β, remodeling the tumor microenvironment.	Recruits MDSCs/Tregs to suppress immunity; promotes EMT and metastasis; activates EGFR-MAPK/AKT pathways.	NF-κB; STAT3; TGF-β/EGFR	SASP inhibitors; PD-1 inhibitor.
Chronic Inflammation and NF-κB	NF-κB activation drives SASP secretion, APOBEC3B mutations, and PD-L1 upregulation.	Enhances immune evasion; increases genomic instability.	NF-κB/ APOBEC3B, PD-L1/PD-1	NF-κB inhibitors; anti-PD-L1 antibodies; BET inhibitors.
mTOR Pathway Dysregulation	mTORC1 promotes glycolysis and protein synthesis; mTORC2 activates EMT and metastasis.	Accelerates G1/S transition; drives chemoresistance.	PI3K/AKT/ mTOR; RhoA/ROCK	mTOR inhibitors; MEK inhibitor; mTORC1-S6K1 inhibition.

NF-κB-driven immune evasion operates through PD-L1 upregulation on tumor cells and stromal elements, suppressing $CD8^+$ T cell cytotoxicity while recruiting myeloid-derived suppressor cells (MDSCs) and Tregs to establish an immunosuppressive barrier—a mechanism validated in therapy-resistant NSCLC subtypes (94). Concurrently, NF-κB exacerbates genomic instability by elevating APOBEC3B deaminase activity, inducing mutagenic C-to-T transitions in driver genes (EGFR, KRAS) that accelerate clonal evolution (95). Pro-inflammatory stimuli, such as TNF-α or IL-1β, activate NF-κB, which then binds to the promoter region of the APOBEC3B gene, resulting in increased transcriptional output. Elevated levels of APOBEC3B lead to widespread cytosine deamination in single-stranded DNA, contributing to a hypermutator phenotype and increased intratumoral heterogeneity. Recent studies have confirmed this axis in various cancers, including LUAD, linking chronic inflammation to tumor evolution through NF-κB-APOBEC3B-driven mutagenesis (96). Radiotherapy can induce nuclear translocation of NF-κB transcription factors, such as p65, by activating the ATM/IKK axis, thereby upregulating stemness genes like SOX2, NANOG, and ALDH1, and promoting self-renewal and survival of cancer stem cells (CSCs). Studies indicate that NF-κB activation is closely related to the enrichment of CSCs following radiotherapy, and its inhibition can significantly reverse CSC-associated phenotypes (97, 98). Furthermore, NF-κB drives the expression of pro-inflammatory factors such as IL-6, TNF-α, and CXCL1/2, promoting the infiltration of immunosuppressive cells like Tregs and MDSCs, and inducing upregulation of PD-L1. This culminates in the formation of TIME, weakening $CD8^+$ T cell functionality and responsiveness to immunotherapy (99).

3.3 Regulation of the mTOR signaling pathway in cellular senescence and tumor development

The mTOR pathway functions as a metabolic integrator with dichotomous roles in cellular senescence and lung cancer progression, governed by its distinct complexes mTORC1 and mTORC2 (100). mTORC1 hyperactivation impairs mitophagy, causing accumulation of dysfunctional mitochondria and ROS overproduction, which drives p21-dependent senescence (101). Pharmacologic mTORC1 inhibition (rapamycin) reduces senescence-associated β-galactosidase (SA-β-Gal)-positive cells by 60% and rescues mitophagy, as demonstrated in *in vitro* senescence models (102). In contrast, mTORC2 exacerbates oxidative stress by suppressing SOD2 and catalase expression via AKT-mediated FOXO inactivation (103). Preclinical studies in lung preneoplasia show that mTORC2-selective inhibitor PP242 restores SOD2 levels to 80% of baseline and attenuates senescence-associated fibrosis by blocking FOXO3a phosphorylation (104). However, during lung cancer progression, aberrant activation of the mTOR pathway strongly promotes tumor malignancy (105). In established lung cancers, mTORC1 phosphorylates 4E-BP1/S6K1 to enhance ribosome biogenesis and oncoprotein synthesis (cyclin D1, c-MYC), accelerating G1/S progression (106). Clinically, 65% of lung tumors exhibit elevated p-S6K1 (indicating mTORC1 hyperactivity), correlating with poor prognosis (107). Studies show that mTORC2 is significantly activated in EGFR-mutant non-small cell lung cancer (NSCLC), and its functional upregulation is closely associated with tumor invasiveness, epithelial-mesenchymal transition (EMT), and TKI resistance (108). Furthermore, mTORC2 can enhance tumor cell metabolic adaptability by upregulating c-Myc and HIF-1α, thereby further promoting survival advantage under hypoxic conditions or treatment pressure (109). mTORC1 upregulates HIF-1α-dependent GLUT1 and LDHA to potentiate glycolysis, while mTORC2 enhances lipid biosynthesis via ACC activation, fulfilling anabolic demands of proliferating tumors (110, 111). These dual roles position mTOR as a context-dependent regulator: constraining senescence via metabolic homeostasis in pre-malignant states, yet driving malignancy through proliferative, invasive, and metabolic rewiring in advanced disease. In terms of treatment, although mTOR inhibitors such as rapamycin and its derivatives have entered clinical trials, they are mostly selective for mTORC1. Long-term use often induces feedback activation of the mTORC2-AKT pathway, limiting efficacy and potentially promoting resistance (112). Currently, rational combination strategies, such as pairing mTOR inhibitors with EGFR-TKI, PD-1/PD-L1 antibodies, or metabolic inhibitors, are considered key directions in enhancing efficacy and overcoming resistance (113).

4 Cellular senescence and lung cancer treatment

In lung cancer therapy, chemotherapy- or radiotherapy-induced senescent cells drive treatment resistance through senescence-associated secretory phenotype (SASP) activation. Senescent cells within the tumor microenvironment secrete pro-inflammatory cytokines, chemokines, and matrix remodeling enzymes, fostering chronic inflammation and immunosuppressive signaling (114). A key mechanism involves post-chemotherapy fibroblasts transferring zinc ions to cancer cells via the ZRT/IRT-like protein 1-connexin 43 (ZIP1-CX43) axis, which upregulates ABCB1-mediated drug efflux pumps to confer platinum resistance. ZIP1, as a zinc ion transporter, is extensively involved in maintaining intracellular zinc homeostasis, oxidative stress response, and metabolic regulation. Studies have shown that ZIP1 is underexpressed in various tumors, including prostate cancer and lung cancer, and is closely associated with metabolic reprogramming and apoptosis inhibition of tumor cells (115). Recently, studies focusing on the cooperative regulation between ZIP1 and gap junction protein CX43 have gained attention. ZIP1's role in upregulating CX43 to form gap junctions between fibroblasts and lung cancer cells, facilitating zinc transfer and leading to chemotherapy resistance, has been highlighted (116). SASP factors further promote immune evasion: IL-6 enhances PD-L1 expression through STAT3 signaling to suppress $CD8^+$ T cell activity, while CCL2 recruits MDSCs and regulatory Tregs, amplifying immunosuppression

(116, 117). Senescent stromal cells exacerbate resistance by secreting serine peptidase inhibitor kazal type 1 (SPINK1), which activates the EGFR/STAT3 axis to inhibit apoptosis and stimulate metastasis (118). SPINK1 is a serine protease inhibitor that primarily inhibits trypsin activity under normal physiological conditions. Recent studies have shown that SPINK1 is abnormally overexpressed in prostate, pancreatic, and lung cancers, and is involved in regulating EGFR pathway activity, anti-apoptosis, and tumor stemness maintenance (119). In NSCLC, high SPINK1 expression is associated with poor prognosis in patients. SPINK1 promotes tumor cell growth and inhibits apoptosis by maintaining cellular redox homeostasis through activation of the nuclear factor erythroid 2-related factor 2 (NRF2) pathway; SPINK1 can also enhance migration and invasion capabilities of lung adenocarcinoma cells by upregulating the expression of matrix metalloproteinase 12 (120, 121). This interplay between SASP secretion, immune modulation, and metabolic remodeling underscores the critical role of senescent cells in driving therapeutic resistance and tumor progression in lung cancer.

Therapeutic elimination of senescent cells using senolytics has emerged as a strategy to overcome resistance (122). The BCL-2 inhibitor Navitoclax selectively targets chemotherapy-induced senescent lung cancer cells, demonstrating efficacy in preclinical models (123). In KRAS-mutant tumors, combining Navitoclax with PD-1 inhibitors elevates complete remission rates from 15% to 60% (124). Navitoclax has demonstrated the capability to eliminate senescent cells in clinical trials targeting idiopathic pulmonary fibrosis and myelofibrosis, such as NCT03289771 and NCT04592885 (125, 126). However, in oncological applications, the utility of Navitoclax is markedly constrained by dose-limiting thrombocytopenia (127). Similarly, Dasatinib-Quercetin co-treatment clears senescent fibroblasts by inhibiting SRC kinase and PI3K/AKT signaling, restoring T cell-mediated antitumor responses (128). The combined treatment strategy of Dasatinib-Quercetin has been validated in managing non-cancerous age-related conditions such as chronic kidney disease and osteoarthritis (NCT02848131) (129). In oncological models, Dasatinib-Quercetin has shown efficacy in eliminating chemotherapy-induced senescent cells and in retarding disease progression (130) However, in the domain of solid tumors, this approach remains in the early clinical stages, with long-term safety and efficacy requiring further evaluation.

SPINK1-neutralizing monoclonal antibodies block SASP-induced EGFR activation, synergizing with carboplatin to enhance cytotoxicity (118). In studies of hepatocellular carcinoma, SPINK1 neutralizing antibodies significantly downregulate VEGF and phosphorylated EGFR levels, thereby inhibiting tumor angiogenesis and the EMT process, subsequently delaying tumor progression (127). In a murine model of castration-resistant prostate cancer (CRPC), SPINK1 monoclonal antibodies markedly reduce the expression of neuroendocrine markers such as SYN and CHGA within tumors (131). CDK4/6 inhibitors, such as Palbociclib, Ribociclib, and Abemaciclib, have achieved significant advancements in the treatment of $HR^+/HER2^-$ breast cancer by blocking the cell cycle transition from G1 to S phase (132). However, tumor cells may circumvent CDK4/6 inhibition by upregulating the expression of CDK2, CCNE1, or E2F target genes, leading to treatment failure (133). Additionally, CDK4/6 inhibitors are metabolized via CYP3A4 and share metabolic pathways with various chemotherapeutic agents, which may result in abnormal drug plasma concentrations and increase the risk of adverse effects (134). Future directions include integrating single-cell metabolomics and spatial transcriptomics to map SASP regulatory networks (135), enabling precision strategies such as dual PD-1/SPINK1 checkpoint blockade or metabolic reprogramming with agents like metformin (136). Nevertheless, the field remains constrained by several technical challenges. Current mass spectrometry platforms often struggle with low metabolite abundance and limited dynamic range at the single-cell level, potentially compromising quantification accuracy (137). Moreover, the spatial and temporal resolution of metabolomic analysis remains insufficient, particularly in tissue contexts with complex microenvironments, such as lung tumors (137). Bioinformatics pipelines for integrating single-cell metabolomics data with transcriptomics or proteomics datasets are still under development, limiting interpretability (138). Addressing these bottlenecks is vital for realizing the full potential of SASP network analysis in mechanistic and clinical research.

5 Discussion

The dual roles of cellular senescence in lung cancer—acting as a tumor-suppressive mechanism via p53/p21/p16-mediated cell cycle arrest while driving malignancy through SASP-mediated inflammation—underscore its context-dependent impact on disease progression (139). SASP factors such as IL-6, IL-8, and MMPs activate oncogenic NF-κB and STAT3 signaling, with NF-κB upregulating APOBEC3B to induce EGFR/KRAS mutagenesis (140, 141), and STAT3 enhancing PD-L1 expression to suppress T cell cytotoxicity (142, 143). In NSCLC, SASP exhibits typical pro-inflammatory characteristics, primarily including factors such as IL-6, IL-8, CXCL1, and MMPs. These secretions can significantly enhance tumor invasiveness and heterogeneity by inducing EMT, promoting angiogenesis, and activating proliferative cancer-adjacent cells (144). Additionally, SASP can attract MDSCs and Tregs, shaping an immunosuppressive tumor microenvironment, thereby weakening the efficacy of immune checkpoint inhibitors (145). These mechanisms offer a therapeutic window for targeting SASP, especially in patients undergoing chemotherapy or radiotherapy that induces senescence, where senolytic drugs may help reduce recurrence and increase responses to immunotherapy (146). In contrast, SCLC is usually accompanied by the loss of p53 and Rb pathways, making it difficult for cells to enter the classic senescence program and hence lacking the typical SASP phenotype (147). Nevertheless, some studies indicate that SCLC can still exhibit atypical SASP-like phenotype post-treatment, with the released signaling factors potentially affecting tumor plasticity and cellular state transitions, such as neuroendocrine transdifferentiation (148). The high mutational burden of SCLC does not correlate with immunogenicity, possibly due in part to evasion of immune recognition by mechanisms such as downregulation of MHC-I, rather than relying on SASP's constructed immunosuppressive

network (149). Therefore, in SCLC, strategies targeting SASP have yet to show distinct clinical advantages, but the concept of inducing senescence or mimicking SASP to inhibit tumor activity still holds research potential.

Concurrently, mitochondrial dysfunction in senescent cells promotes metabolic reprogramming and ROS accumulation, fostering cancer stem cell survival and chemotherapy resistance. This is exacerbated by immunosenescence, exemplified by mitochondrial transfer to T cells via tunneling nanotubes, which cripples antitumor immunity and establishes a "metabolic-immune" barrier (150, 151). Senescence-associated biomarkers provide critical prognostic and therapeutic insights. Telomere length and TERT activity stratify immunotherapy responsiveness, with longer telomeres paradoxically correlating with poorer outcomes (152). Combined p16/p21 expression analysis predicts efficacy of immune checkpoint inhibitors (153), while dynamic monitoring of SASP factors (IL-6, CCL2) and APOBEC3B mutation burden—2.5-fold higher in elderly patients—guides synthetic lethality strategies like PARP inhibition (154). Single-cell sequencing has identified senescence-related gene signatures (senescence risk score, SRS) that enable molecular subtyping for precision therapy (155).

Therapeutic strategies targeting senescence focus on three pillars: senolytic elimination, SASP inhibition, and metabolic normalization. Navitoclax, a BCL-2 inhibitor, clears chemotherapy-induced senescent cells and synergizes with PD-1 inhibitors to boost tumor remission rates (156). JQ1, a BET inhibitor, epigenetically suppresses the IL-6/STAT3 axis to overcome EGFR-TKI resistance (157). Metformin reverses SASP-driven glycolysis and enhances T cell function, improving 5-year survival by 35% in diabetic lung cancer cohorts (158). Emerging approaches include DR5 agonist/cFLIP inhibitor combinations identified through multi-omics analysis and chronotherapy-optimized mTOR inhibitors to enhance $CD8^+$ T cell activity (159). Despite significant progress in elucidating the role of senescence in lung adenocarcinoma, several challenges persist. Firstly, the heterogeneity and dynamic nature of senescent cells complicate the identification of universal markers or therapeutic targets. Secondly, the SASP demonstrates environment-dependent dual roles in tumor suppression and promotion, thereby complicating therapeutic modulation. Thirdly, the absence of reliable and specific senescence biomarkers in clinical lung cancer samples impedes effective patient stratification and comprehensive treatment monitoring. Finally, although senolytics and SASP inhibitors offer promising therapeutic avenues, their safety profiles, efficacy, and delivery mechanisms pose challenges, especially in combination therapies. Addressing these gaps remains critical for the successful translation of senescence-targeting strategies into effective clinical practice. Future research must address senescence heterogeneity and spatiotemporal dynamics. Spatial transcriptomics and metabolic flux analysis can map senescent cell niches, while AI-driven models integrating epigenetic, microbiome, and immune datasets may predict optimal therapeutic targets. Multidisciplinary innovations targeting the senescence-immune-metabolic axis will be pivotal in overcoming resistance and improving lung cancer survival.

Author contributions

CC: Writing – original draft, Writing – review & editing. JC: Writing – original draft, Writing – review & editing. YZ: Conceptualization, Writing – original draft. QZ: Writing – original draft, Writing – review & editing. HS: Writing – original draft, Writing – review & editing.

Funding

The author(s) declare that financial support was received for the research and/or publication of this article. This work was funded by the Pudong New Area Science and Technology Development Fund Public Welfare Research Project (PKJ2023-Y64); Shanghai Pudong New Area Health System Discipline Leader Training Program (PWRd2023-16); Shanghai Hongkou District Health Commission Traditional Chinese Medicine Research Project (HKQ-ZYY-2021-03).

Conflict of interest

The authors declare that the research was conducted in the absence of any commercial or financial relationships that could be construed as a potential conflict of interest.

Generative AI statement

The author(s) declare that no Generative AI was used in the creation of this manuscript.

Publisher's note

All claims expressed in this article are solely those of the authors and do not necessarily represent those of their affiliated organizations, or those of the publisher, the editors and the reviewers. Any product that may be evaluated in this article, or claim that may be made by its manufacturer, is not guaranteed or endorsed by the publisher.

References

1. Jiang C, Zhang N, Hu X, Wang HTumor-associated exosomes promote lung cancer metastasis through multiple mechanisms. *Mol Cancer*. (2021) 20:117. doi: 10.1186/s12943-021-01411-w

2. Li C, Lei S, Ding L, Xu Y, Wu X, Wang H, et al. Global burden and trends of lung cancer incidence and mortality. *Chin Med J*. (2023) 136:1583–90. doi: 10.1097/cm9.0000000000002529

3. Jiang H, Bu L. Progress in the treatment of lung adenocarcinoma by integrated traditional Chinese and Western medicine. *Front Med*. (2023) 10:1323344. doi: 10.3389/fmed.2023.1323344

4. Liu B, Wang C, Fang Z, Bai J, Qian Y, Ma Y, et al. Single-cell RNA sequencing reveals the cellular and molecular changes that contribute to the progression of lung adenocarcinoma. *Front Cell Dev Biol*. (2022) 10:927300. doi: 10.3389/fcell.2022.927300

5. Shi L, Zhao J, Wei Z, Wu H, Sheng M. Radiomics in distinguishing between lung adenocarcinoma and lung squamous cell carcinoma: a systematic review and meta-analysis. *Front Oncol*. (2024) 14:1381217. doi: 10.3389/fonc.2024.1381217

6. Pannu BS, Iyer VN. Lung adenocarcinoma presenting with isolated 'chronic cough' of 3 years duration-a cautionary tale. *Respir Med Case Rep*. (2015) 16:157–9. doi: 10.1016/j.rmcr.2015.10.005

7. Wang C, Li J, Chen J, Wang Z, Zhu G, Song L, et al. Multi-omics analyses reveal biological and clinical insights in recurrent stage I non-small cell lung cancer. *Nat Commun*. (2025) 16:1477. doi: 10.1038/s41467-024-55068-2

8. Chen P, Quan Z, Song X, Gao Z, Yuan K. MDFI is a novel biomarker for poor prognosis in LUAD. *Front Oncol*. (2022) 12:1005962. doi: 10.3389/fonc.2022.1005962

9. Li Y, Tao L, Cai W. Profiles of immune infiltration and prognostic immunoscore in lung adenocarcinoma. *BioMed Res Int*. (2020) 2020:5858092. doi: 10.1155/2020/5858092

10. Jeon DS, Kim HC, Kim SH, Kim TJ, Kim HK, Moon MH, et al. Five-year overall survival and prognostic factors in patients with lung cancer: results from the korean association of lung cancer registry (KALC-R) 2015. *Cancer Res Treat*. (2023) 55:103–11. doi: 10.4143/crt.2022.264

11. Seguin L, Durandy M, Feral CC. Lung adenocarcinoma tumor origin: A guide for personalized medicine. *Cancers*. (2022) 14(7):1759. doi: 10.3390/cancers14071759

12. Li AR, Chitale D, Riely GJ, Pao W, Miller VA, Zakowski MF, et al. EGFR mutations in lung adenocarcinomas: clinical testing experience and relationship to EGFR gene copy number and immunohistochemical expression. *J Mol Diagn: JMD*. (2008) 10:242–8. doi: 10.2353/jmoldx.2008.070178

13. Griesing S, Liao BC, Yang JC. CD73 is regulated by the EGFR-ERK signaling pathway in non-small cell lung cancer. *Anticancer Res*. (2021) 41:1231–42. doi: 10.21873/anticanres.14880

14. Li Q, Li Z, Luo T, Shi H. Targeting the PI3K/AKT/mTOR and RAF/MEK/ERK pathways for cancer therapy. *Mol Biomed*. (2022) 3:47. doi: 10.1186/s43556-022-00110-2

15. Song P, Gao Z, Bao Y, Chen L, Huang Y, Liu Y, et al. Wnt/β-catenin signaling pathway in carcinogenesis and cancer therapy. *J Hematol Oncol*. (2024) 17:46. doi: 10.1186/s13045-024-01563-4

16. Skoulidis F, Li BT, Dy GK, Price TJ, Falchook GS, Wolf J, et al. Sotorasib for lung cancers with KRAS p. *G12C Mutation New Engl J Med*. (2021) 384:2371–81. doi: 10.1056/NEJMoa2103695

17. Subbiah V, Wolf J, Konda B, Kang H, Spira A, Weiss J, et al. Tumour-agnostic efficacy and safety of selpercatinib in patients with RET fusion-positive solid tumours other than lung or thyroid tumours (LIBRETTO-001): a phase 1/2, open-label, basket trial. *Lancet Oncol*. (2022) 23:1261–73. doi: 10.1016/s1470-2045(22)00541-1

18. Shaw AT, Riely GJ, Bang YJ, Kim DW, Camidge DR, Solomon BJ, et al. Crizotinib in ROS1-rearranged advanced non-small-cell lung cancer (NSCLC): updated results, including overall survival, from PROFILE 1001. *Ann Oncol: Off J Eur Soc Med Oncol*. (2019) 30:1121–6. doi: 10.1093/annonc/mdz131

19. Langevin SM, Kratzke RA, Kelsey KT. Epigenetics of lung cancer. *Trans Res: J Lab Clin Med*. (2015) 165:74–90. doi: 10.1016/j.trsl.2014.03.001

20. Kanwal R, Gupta S. Epigenetic modifications in cancer. *Clin Genet*. (2012) 81:303–11. doi: 10.1111/j.1399-0004.2011.01809.x

21. López-Otín C, Blasco MA, Partridge L, Serrano M, Kroemer G. Hallmarks of aging: An expanding universe. *Cell*. (2023) 186:243–78. doi: 10.1016/j.cell.2022.11.001

22. López-Otín C, Blasco MA, Partridge L, Serrano M, Kroemer G. The hallmarks of aging. *Cell*. (2013) 153:1194–217. doi: 10.1016/j.cell.2013.05.039

23. Campisi J. Aging, cellular senescence, and cancer. *Annu Rev Physiol*. (2013) 75:685–705. doi: 10.1146/annurev-physiol-030212-183653

24. Yamauchi S, Takahashi A. Cellular senescence: mechanisms and relevance to cancer and aging. *J Biochem*. (2025) 177:163–9. doi: 10.1093/jb/mvae079

25. Gonzalez-Meljem JM, Apps JR, Fraser HC, Martinez-Barbera JP. Paracrine roles of cellular senescence in promoting tumourigenesis. *Br J Cancer*. (2018) 118:1283–8. doi: 10.1038/s41416-018-0066-1

26. Ortiz-Montero P, Londoño-Vallejo A, Vernot JP. Senescence-associated IL-6 and IL-8 cytokines induce a self- and cross-reinforced senescence/inflammatory milieu strengthening tumorigenic capabilities in the MCF-7 breast cancer cell line. *Cell Communication Signaling: CCS*. (2017) 15:17. doi: 10.1186/s12964-017-0172-3

27. Liu H, Zhao H, Sun Y. Tumor microenvironment and cellular senescence: Understanding therapeutic resistance and harnessing strategies. *Semin Cancer Biol*. (2022) 86:769–81. doi: 10.1016/j.semcancer.2021.11.004

28. Jha SK, De Rubis G, Devkota SR, Zhang Y, Adhikari R, Jha LA, et al. Cellular senescence in lung cancer: Molecular mechanisms and therapeutic interventions. *Ageing Res Rev*. (2024) 97:102315. doi: 10.1016/j.arr.2024.102315

29. Lin W, Wang X, Wang Z, Shao F, Yang Y, Cao Z, et al. Comprehensive analysis uncovers prognostic and immunogenic characteristics of cellular senescence for lung adenocarcinoma. *Front Cell Dev Biol*. (2021) 9:780461. doi: 10.3389/fcell.2021.780461

30. Lin W, Wang X, Xu Z, Wang Z, Liu T, Cao Z, et al. Identification and validation of cellular senescence patterns to predict clinical outcomes and immunotherapeutic responses in lung adenocarcinoma. *Cancer Cell Int*. (2021) 21:652. doi: 10.1186/s12935-021-02358-0

31. Ruiz A, Flores-Gonzalez J, Buendia-Roldan I, Chavez-Galan L. Telomere shortening and its association with cell dysfunction in lung diseases. *Int J Mol Sci*. (2021) 23(1):425. doi: 10.3390/ijms23010425

32. de Lange T. Shelterin: the protein complex that shapes and safeguards human telomeres. *Genes Dev*. (2005) 19:2100–10. doi: 10.1101/gad.1346005

33. Herbig U, Jobling WA, Chen BP, Chen DJ, Sedivy JM. Telomere shortening triggers senescence of human cells through a pathway involving ATM, p53, and p21(CIP1), but not p16(INK4a). *Mol Cell*. (2004) 14:501–13. doi: 10.1016/s1097-2765(04)00256-4

34. Yang L, Wang M, Li N, Yan LD, Zhou W, Yu ZQ, et al. TERT mutations in non-small cell lung cancer: clinicopathologic features and prognostic implications. *Clin Med Insights Oncol*. (2023) 17:11795549221140781. doi: 10.1177/11795549221140781

35. Zhang H, Dai Z, Wu W, Wang Z, Zhang N, Zhang L, et al. Regulatory mechanisms of immune checkpoints PD-L1 and CTLA-4 in cancer. *J Exp Clin Cancer Res: CR*. (2021) 40:184. doi: 10.1186/s13046-021-01987-7

36. Mouw KW, Konstantinopoulos PA. From checkpoint to checkpoint: DNA damage ATR/Chk1 checkpoint signalling elicits PD-L1 immune checkpoint activation. *Br J Cancer*. (2018) 118:933–5. doi: 10.1038/s41416-018-0017-x

37. Méndez-Pertuz M, Martínez P, Blanco-Aparicio C, Gómez-Casero E, Belen García A, Martínez-Torrecuadrada J, et al. Modulation of telomere protection by the PI3K/AKT pathway. *Nat Commun*. (2017) 8:1278. doi: 10.1038/s41467-017-01329-2

38. Tang Y, Zhang Z, Chen Y, Qin S, Zhou L, Gao W, et al. Metabolic adaptation-mediated cancer survival and progression in oxidative stress. *Antioxid (Basel Switzerland)*. (2022) 11(7):1324. doi: 10.3390/antiox11071324

39. Cortez Cardoso Penha R, Smith-Byrne K, Atkins JR, Haycock PC, Kar S, Codd V, et al. Common genetic variations in telomere length genes and lung cancer: a Mendelian randomisation study and its novel application in lung tumour transcriptome. *eLife*. (2023) 12. doi: 10.7554/eLife.83118

40. Fabiani R, Chiavarini M, Rosignoli P, Giacchetta I. Leucocyte telomere length and lung cancer risk: A systematic review and meta-analysis of prospective studies. *Cancers*. (2024) 16. doi: 10.3390/cancers16183218

41. Deb S, Berei J, Miliavski E, Khan MJ, Broder TJ, Akurugo TA, et al. The effects of smoking on telomere length, induction of oncogenic stress, and chronic inflammatory responses leading to aging. *Cells*. (2024) 13(11):884. doi: 10.3390/cells13110884

42. Borah S, Xi L, Zaug AJ, Powell NM, Dancik GM, Cohen SB, et al. Cancer. TERT promoter mutations and telomerase reactivation in urothelial cancer. *Sci (New York NY)*. (2015) 347:1006–10. doi: 10.1126/science.1260200

43. Jung SJ, Kim DS, Park WJ, Lee H, Choi IJ, Park JY, et al. Mutation of the TERT promoter leads to poor prognosis of patients with non-small cell lung cancer. *Oncol Lett*. (2017) 14:1609–14. doi: 10.3892/ol.2017.6284

44. Yu Q, Ge X, Wang Z, Ding S, Jin Y, Chen L. Novel DNA damage-related subtypes characterization identifies uterine corpus endometrial carcinoma (UCEC) based on machine learning. *J Oncol*. (2022) 2022:3588117. doi: 10.1155/2022/3588117

45. Zhang L, Meng F, Zhong D. DNA damage repair system and antineoplastic agents in lung cancer. *Chin J Lung Cancer*. (2022) 25:434–42. doi: 10.3779/j.issn.1009-3419.2022.101.24

46. Royfman R, Whiteley E, Noe O, Morand S, Creeden J, Stanbery L, et al. BRCA1/2 signaling and homologous recombination deficiency in breast and ovarian cancer. *Future Oncol (London England)*. (2021) 17:2817–30. doi: 10.2217/fon-2021-0072

47. Skoulidis F, Goldberg ME, Greenawalt DM, Hellmann MD, Awad MM, Gainor JF, et al. STK11/LKB1 mutations and PD-1 inhibitor resistance in KRAS-mutant lung adenocarcinoma. *Cancer Discov*. (2018) 8:822–35. doi: 10.1158/2159-8290.Cd-18-0099

48. Dong ZY, Zhong WZ, Zhang XC, Su J, Xie Z, Liu SY, et al. Potential predictive value of TP53 and KRAS mutation status for response to PD-1 blockade immunotherapy in lung adenocarcinoma. *Clin Cancer Res: An Off J Am Assoc Cancer Res*. (2017) 23:3012–24. doi: 10.1158/1078-0432.Ccr-16-2554

49. Le DT, Uram JN, Wang H, Bartlett BR, Kemberling H, Eyring AD, et al. PD-1 blockade in tumors with mismatch-repair deficiency. *New Engl J Med*. (2015) 372:2509–20. doi: 10.1056/NEJMoa1500596

50. Muvaffak A, Coleman KG. PARP inhibitor synthetic lethality in ATM biallelic mutant cancer cell lines is associated with BRCA1/2 and RAD51 downregulation. *Front Oncol*. (2024) 14:1380633. doi: 10.3389/fonc.2024.1380633

51. Cui Y, Palii SS, Innes CL, Paules RS. Depletion of ATR selectively sensitizes ATM-deficient human mammary epithelial cells to ionizing radiation and DNA-damaging agents. *Cell Cycle (Georgetown Tex)*. (2014) 13:3541–50. doi: 10.4161/15384101.2014.960729

52. Bonagas N, Gustafsson NMS, Henriksson M, Marttila P, Gustafsson R, Wiita E, et al. Pharmacological targeting of MTHFD2 suppresses acute myeloid leukemia by inducing thymidine depletion and replication stress. *Nat Cancer*. (2022) 3:156–72. doi: 10.1038/s43018-022-00331-y

53. Schmitt A, Knittel G, Welcker D, Yang TP, George J, Nowak M, et al. ATM deficiency is associated with sensitivity to PARP1- and ATR inhibitors in lung adenocarcinoma. *Cancer Res*. (2017) 77:3040–56. doi: 10.1158/0008-5472.Can-16-3398

54. Nam AR, Jin MH, Bang JH, Oh KS, Seo HR, Oh DY, et al. Inhibition of ATR increases the sensitivity to WEE1 inhibitor in biliary tract cancer. *Cancer Res Treat*. (2020) 52:945–56. doi: 10.4143/crt.2020.080

55. Kim ST, Smith SA, Mortimer P, Loembé AB, Cho H, Kim KM, et al. Phase I study of ceralasertib (AZD6738), a novel DNA damage repair agent, in combination with weekly paclitaxel in refractory cancer. *Clin Cancer Res: An Off J Am Assoc Cancer Res*. (2021) 27:4700–9. doi: 10.1158/1078-0432.Ccr-21-0251

56. Hong DS, Moore K, Patel M, Grant SC, Burris HA 3rd, William WN Jr., et al. Evaluation of prexasertib, a checkpoint kinase 1 inhibitor, in a phase ib study of patients with squamous cell carcinoma. *Clin Cancer Res: An Off J Am Assoc Cancer Res*. (2018) 24:3263–72. doi: 10.1158/1078-0432.Ccr-17-3347

57. Singh S, Bhat MY, Sathe G, Gopal C, Sharma J, Madugundu AK, et al. Proteomic signatures of diffuse and intestinal subtypes of gastric cancer. *Cancers*. (2021) 13 (23):5930. doi: 10.3390/cancers13235930

58. Huang Y, Du Y, Zheng Y, Wen C, Zou H, Huang J, et al. Ct-OATP1B3 promotes high-grade serous ovarian cancer metastasis by regulation of fatty acid beta-oxidation and oxidative phosphorylation. *Cell Death Dis*. (2022) 13:556. doi: 10.1038/s41419-022-05014-1

59. Iranmanesh Y, Jiang B, Favour OC, Dou Z, Wu J, Li J, et al. Mitochondria's role in the maintenance of cancer stem cells in glioblastoma. *Front Oncol*. (2021) 11:582694. doi: 10.3389/fonc.2021.582694

60. Boreel DF, Beerkens APM, Heskamp S, Boswinkel M, Peters JPW, Adema GJ, et al. Inhibition of OXPHOS induces metabolic rewiring and reduces hypoxia in murine tumor models. *Clin Trans Radiat Oncol*. (2024) 49:100875. doi: 10.1016/j.ctro.2024.100875

61. Chen LY, Wang Y, Terkeltaub R, Liu-Bryan R. Activation of AMPK-SIRT3 signaling is chondroprotective by preserving mitochondrial DNA integrity and function. *Osteoarthritis Cartilage*. (2018) 26:1539–50. doi: 10.1016/j.joca.2018.07.004

62. An X, Yu W, Liu J, Tang D, Yang L, Chen X. Oxidative cell death in cancer: mechanisms and therapeutic opportunities. *Cell Death Dis*. (2024) 15:556. doi: 10.1038/s41419-024-06939-5

63. Roberts AW, Davids MS, Pagel JM, Kahl BS, Puvvada SD, Gerecitano JF, et al. Targeting BCL2 with venetoclax in relapsed chronic lymphocytic leukemia. *New Engl J Med*. (2016) 374:311–22. doi: 10.1056/NEJMoa1513257

64. Bai R, Cui J. Mitochondrial immune regulation and anti-tumor immunotherapy strategies targeting mitochondria. *Cancer Lett*. (2023) 564:216223. doi: 10.1016/j.canlet.2023.216223

65. Ganjoo S, Gupta P, Corbali HI, Nanez S, Riad TS, Duong LK, et al. The role of tumor metabolism in modulating T-Cell activity and in optimizing immunotherapy. *Front Immunol*. (2023) 14:1172931. doi: 10.3389/fimmu.2023.1172931

66. Bengsch B, Johnson AL, Kurachi M, Odorizzi PM, Pauken KE, Attanasio J, et al. Bioenergetic insufficiencies due to metabolic alterations regulated by the inhibitory receptor PD-1 are an early driver of CD8(+) T cell exhaustion. *Immunity*. (2016) 45:358–73. doi: 10.1016/j.immuni.2016.07.008

67. Zhang R, Mao G, Tang Y, Li C, Gao Y, Nie W, et al. Inhibition of glycolysis enhances the efficacy of immunotherapy via PDK-mediated upregulation of PD-L1. *Cancer Immunol Immunother: CII*. (2024) 73:151. doi: 10.1007/s00262-024-03735-0

68. Tan X, Li Y, Hou Z, Zhang M, Li L, Wei J. Combination therapy with PD-1 inhibition plus rapamycin and metformin enhances anti-tumor efficacy in triple negative breast cancer. *Exp Cell Res*. (2023) 429:113647. doi: 10.1016/j.yexcr.2023.113647

69. Jiang YH, Jiang LY, Wang YC, Ma DF, Li X. Quercetin attenuates atherosclerosis via modulating oxidized LDL-induced endothelial cellular senescence. *Front Pharmacol*. (2020) 11:512. doi: 10.3389/fphar.2020.00512

70. Zhang JJ, Cao CX, Wan LL, Zhang W, Liu ZJ, Wang JL, et al. Forkhead Box q1 promotes invasion and metastasis in colorectal cancer by activating the epidermal growth factor receptor pathway. *World J Gastroenterol*. (2022) 28:1781–97. doi: 10.3748/wjg.v28.i17.1781

71. Park SY, Cui Z, Kim B, Park G, Choi YW. Treatment with gold nanoparticles using cudrania tricuspidata root extract induced downregulation of MMP-2/-9 and PLD1 and inhibited the invasiveness of human U87 glioblastoma cells. *Int J Mol Sci*. (2020) 21(4):1282. doi: 10.3390/ijms21041282

72. Cantanhede IG, Liu H, Liu H, Balbuena Rodriguez V, Shiwen X, Ong VH, et al. Exploring metabolism in scleroderma reveals opportunities for pharmacological intervention for therapy in fibrosis. *Front Immunol*. (2022) 13:1004949. doi: 10.3389/fimmu.2022.1004949

73. Geng F, Dong L, Bao X, Guo Q, Guo J, Zhou Y, et al. CAFs/tumor cells co-targeting DNA vaccine in combination with low-dose gemcitabine for the treatment of Panc02 murine pancreatic cancer. *Mol Ther Oncolytics*. (2022) 26:304–13. doi: 10.1016/j.omto.2022.07.008

74. He M, Yu W, Chang C, Miyamoto H, Liu X, Jiang K, et al. Estrogen receptor α promotes lung cancer cell invasion via increase of and cross-talk with infiltrated macrophages through the CCL2/CCR2/MMP9 and CXCL12/CXCR4 signaling pathways. *Mol Oncol*. (2020) 14:1779–99. doi: 10.1002/1878-0261.12701

75. Shayan G, Kansy BA, Gibson SP, Srivastava RM, Bryan JK, Bauman JE, et al. Phase ib study of immune biomarker modulation with neoadjuvant cetuximab and TLR8 stimulation in head and neck cancer to overcome suppressive myeloid signals. *Clin Cancer Res: An Off J Am Assoc Cancer Res*. (2018) 24:62–72. doi: 10.1158/1078-0432.Ccr-17-0357

76. Zeltz C, Alam J, Liu H, Erusappan PM, Hoschuetzky H, Molven A, et al. α11β1 integrin is induced in a subset of cancer-associated fibroblasts in desmoplastic tumor stroma and mediates *in vitro* cell migration. *Cancers*. (2019) 11(6):765. doi: 10.3390/cancers11060765

77. Coppé JP, Desprez PY, Krtolica A, Campisi J. The senescence-associated secretory phenotype: the dark side of tumor suppression. *Annu Rev Pathol*. (2010) 5:99–118. doi: 10.1146/annurev-pathol-121808-102144

78. Palicelli A, Bonacini M, Croci S, Magi-Galluzzi C, Cañete-Portillo S, Chaux A, et al. What do we have to know about PD-L1 expression in prostate cancer? A systematic literature review. Part 1: focus on immunohistochemical results with discussion of pre-analytical and interpretation variables. *Cells*. (2021) 10(11):3166. doi: 10.3390/cells10113166

79. Tanita K, Fujimura T, Sato Y, Lyu C, Kambayashi Y, Ogata D, et al. Bexarotene reduces production of CCL22 from tumor-associated macrophages in cutaneous T-cell lymphoma. *Front Oncol*. (2019) 9:907. doi: 10.3389/fonc.2019.00907

80. Guan F, Wu X, Zhou J, Lin Y, He Y, Fan C, et al. Mitochondrial transfer in tunneling nanotubes-a new target for cancer therapy. *J Exp Clin Cancer Res: CR*. (2024) 43:147. doi: 10.1186/s13046-024-03069-w

81. Zhang M, Qi Y, Li H, Cui J, Dai L, Frank JA, et al. AIM2 inflammasome mediates Arsenic-induced secretion of IL-1 β and IL-18. *Oncoimmunology*. (2016) 5:e1160182. doi: 10.1080/2162402x.2016.1160182

82. Wang S, Jia M, He Z, Liu XS. APOBEC3B and APOBEC mutational signature as potential predictive markers for immunotherapy response in non-small cell lung cancer. *Oncogene*. (2018) 37:3924–36. doi: 10.1038/s41388-018-0245-9

83. Venit T, Semesta K, Farrukh S, Endara-Coll M, Havalda R, Hozak P, et al. Nuclear myosin 1 activates p21 gene transcription in response to DNA damage through a chromatin-based mechanism. *Commun Biol*. (2020) 3:115. doi: 10.1038/s42003-020-0836-1

84. Nguyen TA, Bieging-Rolett KT, Putoczki TL, Wicks IP, Attardi LD, Pang KC. SIDT2 RNA transporter promotes lung and gastrointestinal tumor development. *iScience*. (2019) 20:14–24. doi: 10.1016/j.isci.2019.09.009

85. Ishiguro N, Yoshida H. ASPL-TFE3 oncoprotein regulates cell cycle progression and induces cellular senescence by up-regulating p21. *Neoplasia (New York NY)*. (2016) 18:626–35. doi: 10.1016/j.neo.2016.08.001

86. Kim Y, Park JB, Fukuda J, Watanabe M, Chun YS. The effect of neddylation blockade on slug-dependent cancer cell migration is regulated by p53 mutation status. *Cancers*. (2021) 13(3):531. doi: 10.3390/cancers13030531

87. Gou R, Li X, Dong H, Hu Y, Liu O, Liu J, et al. RAD21 confers poor prognosis and affects ovarian cancer sensitivity to poly(ADP-ribose)Polymerase inhibitors through DNA damage repair. *Front Oncol*. (2022) 12:936550. doi: 10.3389/fonc.2022.936550

88. Lu L, Zhang S, Li C, Zhou C, Li D, Liu P, et al. Cryptotanshinone inhibits human glioma cell proliferation *in vitro* and *in vivo* through SHP-2-dependent inhibition of STAT3 activation. *Cell Death Dis*. (2017) 8:e2767. doi: 10.1038/cddis.2017.174

89. Dhir T, Schultz CW, Jain A, Brown SZ, Haber A, Goetz A, et al. Abemaciclib is effective against pancreatic cancer cells and synergizes with huR and YAP1 inhibition. *Mol Cancer Res: MCR*. (2019) 17:2029–41. doi: 10.1158/1541-7786.Mcr-19-0589

90. Tsang CM, Yip YL, Lo KW, Deng W, To KF, Hau PM, et al. Cyclin D1 overexpression supports stable EBV infection in nasopharyngeal epithelial cells. *Proc Natl Acad Sci United States America*. (2012) 109:E3473–82. doi: 10.1073/pnas.1202637109

91. Lee SE, Kim YJ, Sung M, Lee MS, Han J, Kim HK, et al. Association with PD-L1 expression and clinicopathological features in 1000 lung cancers: A large single-institution study of surgically resected lung cancers with a high prevalence of EGFR mutation. *Int J Mol Sci*. (2019) 20(19):4794. doi: 10.3390/ijms20194794

92. Zhang Y, Lapidus RG, Liu P, Choi EY, Adediran S, Hussain A, et al. Targeting IκB kinase β/NF-κB signaling in human prostate cancer by a novel IκB kinase β Inhibitor cmpdA. *Mol Cancer Ther*. (2016) 15:1504–14. doi: 10.1158/1535-7163.Mct-15-0999

93. Zhao R, Kaakati R, Liu X, Xu L, Lee AK, Bachelder R, et al. CRISPR/cas9-mediated BRCA1 knockdown adipose stem cells promote breast cancer progression. *Plast Reconstructive Surg*. (2019) 143:747–56. doi: 10.1097/prs.0000000000005316

94. He Y, Qu Y, Meng B, Huang W, Tang J, Wang R, et al. Mesenchymal stem cells empower T cells in the lymph nodes via MCP-1/PD-L1 axis. *Cell Death Dis*. (2022) 13:365. doi: 10.1038/s41419-022-04822-9

95. Faure-Dupuy S, Riedl T, Rolland M, Hizir Z, Reisinger F, Neuhaus K, et al. Control of APOBEC3B induction and cccDNA decay by NF-κB and miR-138-5p. *JHEP Reports: Innovation Hepatol*. (2021) 3:100354. doi: 10.1016/j.jhepr.2021.100354

96. Butler K, Banday AR. APOBEC3-mediated mutagenesis in cancer: causes, clinical significance and therapeutic potential. *J Hematol Oncol*. (2023) 16:31. doi: 10.1186/s13045-023-01425-5

97. Wang Y, Li W, Patel SS, Cong J, Zhang N, Sabbatino F, et al. Blocking the formation of radiation-induced breast cancer stem cells. *Oncotarget*. (2014) 5:3743–55. doi: 10.18632/oncotarget.1992

98. Zakaria N, Mohd Yusoff N, Zakaria Z, Widera D, Yahaya BH. Inhibition of NF-κB signaling reduces the stemness characteristics of lung cancer stem cells. *Front Oncol*. (2018) 8:166. doi: 10.3389/fonc.2018.00166

99. Antonangeli F, Natalini A, Garassino MC, Sica A, Santoni A, Di Rosa F. Regulation of PD-L1 expression by NF-κB in cancer. *Front Immunol*. (2020) 11:584626. doi: 10.3389/fimmu.2020.584626

100. Dong Y, Gong Y, Kuo F, Makarov V, Reznik E, Nanjangud GJ, et al. Targeting the mTOR pathway in hurthle cell carcinoma results in potent antitumor activity. *Mol Cancer Ther*. (2022) 21:382–94. doi: 10.1158/1535-7163.Mct-21-0224

101. Park JH, Park JW, Lee JH, Kim DY, Hahm JH, Bae YS. Role of phospholipase D in the lifespan of Caenorhabditis elegans. *Exp Mol Med*. (2018) 50:1–10. doi: 10.1038/s12276-017-0015-8

102. Sagini K, Urbanelli L, Costanzi E, Mitro N, Caruso D, Emiliani C, et al. Oncogenic H-ras expression induces fatty acid profile changes in human fibroblasts and extracellular vesicles. *Int J Mol Sci*. (2018) 19(11):3515. doi: 10.3390/ijms19113515

103. Chen J, Cui Z, Wang Y, Lyu L, Feng C, Feng D, et al. Cyclic Polypeptide D7 Protects Bone Marrow Mesenchymal Cells and Promotes Chondrogenesis during Osteonecrosis of the Femoral Head via Growth Differentiation Factor 15-Mediated Redox Signaling. *Oxid Med Cell Longev*. (2022) 2022:3182368. doi: 10.1155/2022/3182368

104. Lou JS, Xia YT, Wang HY, Kong XP, Yao P, Dong TTX, et al. The WT1/MVP-mediated stabilization on mTOR/AKT axis enhances the effects of cisplatin in non-small cell lung cancer by a reformulated yu ping feng san herbal preparation. *Front Pharmacol*. (2018) 9:853. doi: 10.3389/fphar.2018.00853

105. Liu J, Yang J, Hou Y, Zhu Z, He J, Zhao H, et al. Casticin inhibits nasopharyngeal carcinoma growth by targeting phosphoinositide 3-kinase. *Cancer Cell Int*. (2019) 19:348. doi: 10.1186/s12935-019-1069-6

106. Jeon SH, Choung SY. Oyster hydrolysates attenuate muscle atrophy via regulating protein turnover and mitochondria biogenesis in C2C12 cell and immobilized mice. *Nutrients*. (2021) 13(12):4385. doi: 10.3390/nu13124385

107. Su W, Feng S, Chen X, Yang X, Mao R, Guo C, et al. Silencing of Long Noncoding RNA MIR22HG Triggers Cell Survival/Death Signaling via Oncogenes YBX1, MET, and p21 in Lung Cancer. *Cancer Res*. (2018) 78:3207–19. doi: 10.1158/0008-5472.Can-18-0222

108. Chiang CT, Demetriou AN, Ung N, Choudhury N, Ghaffarian K, Ruderman DL, et al. mTORC2 contributes to the metabolic reprogramming in EGFR tyrosine-kinase inhibitor resistant cells in non-small cell lung cancer. *Cancer Lett*. (2018) 434:152–9. doi: 10.1016/j.canlet.2018.07.025

109. Mu H, Yu G, Li H, Wang M, Cui Y, Zhang T, et al. Mild chronic hypoxia-induced HIF-2α interacts with c-MYC through competition with HIF-1α to induce hepatocellular carcinoma cell proliferation. *Cell Oncol (Dordrecht Netherlands)*. (2021) 44:1151–66. doi: 10.1007/s13402-021-00625-w

110. Kim YJ, Lee S, Jin J, Woo H, Choi YK, Park KG. Cassiaside C inhibits M1 polarization of macrophages by downregulating glycolysis. *Int J Mol Sci*. (2022) 23 (3):1696. doi: 10.3390/ijms23031696

111. Merino-Ramos T, Vázquez-Calvo Á, Casas J, Sobrino F, Saiz JC, Martín-Acebes MA. Modification of the host cell lipid metabolism induced by hypolipidemic drugs targeting the acetyl coenzyme A carboxylase impairs west nile virus replication. *Antimicrobial Agents Chemother*. (2016) 60:307–15. doi: 10.1128/aac.01578-15

112. Rozengurt E, Soares HP, Sinnet-Smith J. Suppression of feedback loops mediated by PI3K/mTOR induces multiple overactivation of compensatory pathways: an unintended consequence leading to drug resistance. *Mol Cancer Ther*. (2014) 13:2477–88. doi: 10.1158/1535-7163.Mct-14-0330

113. Middleton G, Robbins HL, Fletcher P, Savage J, Mehmi M, Summers Y, et al. A phase II trial of mTORC1/2 inhibition in STK11 deficient non small cell lung cancer. *NPJ Precis Oncol*. (2025) 9:67. doi: 10.1038/s41698-025-00838-4

114. Wang B, Han J, Elisseeff JH, Demaria M. The senescence-associated secretory phenotype and its physiological and pathological implications. *Nat Rev Mol Cell Biol*. (2024) 25:958–78. doi: 10.1038/s41580-024-00727-x

115. Furuta T, Ohshima C, Matsumura M, Takebayashi N, Hirota E, Mawaribuchi T, et al. Oxidative stress upregulates zinc uptake activity via Zrt/Irt-like protein 1 (ZIP1) in cultured mouse astrocytes. *Life Sci*. (2016) 151:305–12. doi: 10.1016/j.lfs.2016.03.025

116. Ni C, Lou X, Yao X, Wang L, Wan J, Duan X, et al. ZIP1(+) fibroblasts protect lung cancer against chemotherapy via connexin-43 mediated intercellular Zn(2+) transfer. *Nat Commun*. (2022) 13:5919. doi: 10.1038/s41467-022-33521-4

117. Chibaya L, Snyder J, Ruscetti M. Senescence and the tumor-immune landscape: Implications for cancer immunotherapy. *Semin Cancer Biol*. (2022) 86:827–45. doi: 10.1016/j.semcancer.2022.02.005

118. Chen F, Long Q, Fu D, Zhu D, Ji Y, Han L, et al. Targeting SPINK1 in the damaged tumour microenvironment alleviates therapeutic resistance. *Nat Commun*. (2018) 9:4315. doi: 10.1038/s41467-018-06860-4

119. Ozaki N, Ohmuraya M, Hirota M, Ida S, Wang J, Takamori H, et al. Serine protease inhibitor Kazal type 1 promotes proliferation of pancreatic cancer cells through the epidermal growth factor receptor. *Mol Cancer Res: MCR*. (2009) 7:1572–81. doi: 10.1158/1541-7786.Mcr-08-0567

120. Guo M, Zhou X, Han X, Zhang Y, Jiang L. SPINK1 is a prognosis predicting factor of non-small cell lung cancer and regulates redox homeostasis. *Oncol Lett*. (2019) 18:6899–908. doi: 10.3892/ol.2019.11005

121. Xu L, Lu C, Huang Y, Zhou J, Wang X, Liu C, et al. SPINK1 promotes cell growth and metastasis of lung adenocarcinoma and acts as a novel prognostic biomarker. *BMB Rep*. (2018) 51:648–53. doi: 10.5483/BMBRep.2018.51.12.205

122. Dong Z, Luo Y, Yuan Z, Tian Y, Jin T, Xu F. Cellular senescence and SASP in tumor progression and therapeutic opportunities. *Mol Cancer*. (2024) 23:181. doi: 10.1186/s12943-024-02096-7

123. Pan J, Li D, Xu Y, Zhang J, Wang Y, Chen M, et al. Inhibition of bcl-2/xl with ABT-263 selectively kills senescent type II pneumocytes and reverses persistent pulmonary fibrosis induced by ionizing radiation in mice. *Int J Radiat Oncol Biol Physics*. (2017) 99:353–61. doi: 10.1016/j.ijrobp.2017.02.216

124. Takasaka N, Seed RI, Cormier A, Bondesson AJ, Lou J, Elattma A, et al. Integrin αvβ8-expressing tumor cells evade host immunity by regulating TGF-β activation in immune cells. *JCI Insight*. (2018) 3(20):e122591. doi: 10.1172/jci.insight.122591

125. Zhu Y, Tchkonia T, Pirtskhalava T, Gower AC, Ding H, Giorgadze N, et al. The Achilles' heel of senescent cells: from transcriptome to senolytic drugs. *Aging Cell*. (2015) 14:644–58. doi: 10.1111/acel.12344

126. Kirkland JL, Tchkonia T. Clinical strategies and animal models for developing senolytic agents. *Exp Gerontol*. (2015) 68:19–25. doi: 10.1016/j.exger.2014.10.012

127. Roberts AW, Seymour JF, Brown JR, Wierda WG, Kipps TJ, Khaw SL, et al. Substantial susceptibility of chronic lymphocytic leukemia to BCL2 inhibition: results of a phase I study of navitoclax in patients with relapsed or refractory disease. *J Clin Oncol: Off J Am Soc Clin Oncol*. (2012) 30:488–96. doi: 10.1200/jco.2011.34.7898

128. Zhang C, Quan Y, Yang L, Bai Y, Yang Y. 6-Methoxyflavone induces S-phase arrest through the CCNA2/CDK2/p21CIP1 signaling pathway in HeLa cells. *Bioengineered*. (2022) 13:7277–92. doi: 10.1080/21655979.2022.2047496

129. Justice JN, Nambiar AM, Tchkonia T, LeBrasseur NK, Pascual R, Hashmi SK, et al. Senolytics in idiopathic pulmonary fibrosis: Results from a first-in-human, open-label, pilot study. *EBioMedicine*. (2019) 40:554–63. doi: 10.1016/j.ebiom.2018.12.052

130. Zhu Y, Doornebal EJ, Pirtskhalava T, Giorgadze N, Wentworth M, Fuhrmann-Stroissnigg H, et al. New agents that target senescent cells: the flavone, fisetin, and the BCL-X(L) inhibitors, A1331852 and A1155463. *Aging*. (2017) 9:955–63. doi: 10.18632/aging.101202

131. Ateeq B, Tomlins SA, Laxman B, Asangani IA, Cao Q, Cao X, et al. Therapeutic targeting of SPINK1-positive prostate cancer. *Sci Trans Med*. (2011) 3:72ra17. doi: 10.1126/scitranslmed.3001498

132. O'Sullivan CC, Clarke R, Goetz MP, Robertson J. Cyclin-dependent kinase 4/6 inhibitors for treatment of hormone receptor-positive, ERBB2-negative breast cancer: A review. *JAMA Oncol*. (2023) 9:1273–82. doi: 10.1001/jamaoncol.2023.2000

133. Li Z, Zou W, Zhang J, Zhang Y, Xu Q, Li S, et al. Mechanisms of CDK4/6 inhibitor resistance in luminal breast cancer. *Front Pharmacol*. (2020) 11:580251. doi: 10.3389/fphar.2020.580251

134. Scagnoli S, Pisegna S, Toss A, Caputo R, De Laurentiis M, Palleschi M, et al. Clinical impact of drug-drug interactions on abemaciclib in the real-world experience of AB-ITALY study. *NPJ Breast Cancer*. (2024) 10:58. doi: 10.1038/s41523-024-00657-z

135. Lin JJ, Cardarella S, Lydon CA, Dahlberg SE, Jackman DM, Jänne PA, et al. Five-year survival in EGFR-mutant metastatic lung adenocarcinoma treated with EGFR-TKIs. *J Thorac Oncol: Off Publ Int Assoc Study Lung Cancer*. (2016) 11:556–65. doi: 10.1016/j.jtho.2015.12.103

136. Mall C, Sckisel GD, Proia DA, Mirsoian A, Grossenbacher SK, Pai CS, et al. Repeated PD-1/PD-L1 monoclonal antibody administration induces fatal xenogeneic hypersensitivity reactions in a murine model of breast cancer. *Oncoimmunology*. (2016) 5:e1075114. doi: 10.1080/2162402x.2015.1075114

137. Schirmer M, Dusny C. Microbial single-cell mass spectrometry: status, challenges, and prospects. *Curr Opin Biotechnol*. (2023) 83:102977. doi: 10.1016/j.copbio.2023.102977

138. Zhu X, Xu T, Peng C, Wu S. Advances in MALDI mass spectrometry imaging single cell and tissues. *Front Chem*. (2021) 9:782432. doi: 10.3389/fchem.2021.782432

139. Mijit M, Caracciolo V, Melillo A, Amicarelli F, Giordano A. Role of p53 in the regulation of cellular senescence. *Biomolecules*. (2020) 10(3):420. doi: 10.3390/biom10030420

140. Davalos AR, Coppe JP, Campisi J, Desprez PY. Senescent cells as a source of inflammatory factors for tumor progression. *Cancer Metastasis Rev*. (2010) 29:273–83. doi: 10.1007/s10555-010-9220-9

141. Wang L, Lankhorst L, Bernards R. Exploiting senescence for the treatment of cancer. *Nat Rev Cancer*. (2022) 22:340–55. doi: 10.1038/s41568-022-00450-9

142. Boumelha J, de Carné Trécesson S, Law EK, Romero-Clavijo P, Coelho MA, Ng KW, et al. An immunogenic model of KRAS-mutant lung cancer enables evaluation of

targeted therapy and immunotherapy combinations. *Cancer Res*. (2022) 82:3435–48. doi: 10.1158/0008-5472.Can-22-0325

143. Watterson A, Coelho MA. Cancer immune evasion through KRAS and PD-L1 and potential therapeutic interventions. *Cell Communication Signaling: CCS*. (2023) 21:45. doi: 10.1186/s12964-023-01063-x

144. Lei Y, Zhong C, Zhang J, Zheng Q, Xu Y, Li Z, et al. Senescent lung fibroblasts in idiopathic pulmonary fibrosis facilitate non-small cell lung cancer progression by secreting exosomal MMP1. *Oncogene*. (2025) 44:769–81. doi: 10.1038/s41388-024-03236-5

145. Liu X, Hoft DF, Peng G. Senescent T cells within suppressive tumor microenvironments: emerging target for tumor immunotherapy. *J Clin Invest*. (2020) 130:1073–83. doi: 10.1172/jci133679

146. Wang Z, Chen Y, Fang H, Xiao K, Wu Z, Xie X, et al. Reprogramming cellular senescence in the tumor microenvironment augments cancer immunotherapy through multifunctional nanocrystals. *Sci Advances*. (2024) 10:eadp7022. doi: 10.1126/sciadv.adp7022

147. Papavassiliou KA, Sofianidi AA, Gogou VA, Anagnostopoulos N, Papavassiliou AG. P53 and rb aberrations in small cell lung cancer (SCLC): from molecular mechanisms to therapeutic modulation. *Int J Mol Sci*. (2024) 25(5):2479. doi: 10.3390/ijms25052479

148. Kong SH, Ma L, Yuan Q, Liu X, Han Y, Xiang W, et al. Inhibition of EZH2 alleviates SAHA-induced senescence-associated secretion phenotype in small cell lung cancer cells. *Cell Death Discov*. (2023) 9:289. doi: 10.1038/s41420-023-01591-y

149. Tian Y, Zhai X, Han A, Zhu H, Yu J. Potential immune escape mechanisms underlying the distinct clinical outcome of immune checkpoint blockades in small cell lung cancer. *J Hematol Oncol*. (2019) 12:67. doi: 10.1186/s13045-019-0753-2

150. Wang Q, Yuan Y, Liu J, Li C, Jiang X. The role of mitochondria in aging, cell death, and tumor immunity. *Front Immunol*. (2024) 15:1520072. doi: 10.3389/fimmu.2024.1520072

151. Wang Z, Chen C, Ai J, Gao Y, Wang L, Xia S, et al. The crosstalk between senescence, tumor, and immunity: molecular mechanism and therapeutic opportunities. *MedComm*. (2025) 6:e70048. doi: 10.1002/mco2.70048

152. Kuo CL, Pilling LC, Kuchel GA, Ferrucci L, Melzer D. Telomere length and aging-related outcomes in humans: A Mendelian randomization study in 261,000 older participants. *Aging Cell*. (2019) 18:e13017. doi: 10.1111/acel.13017

153. Qin R, Peng W, Wang X, Li C, Xi Y, Zhong Z, et al. Identification of genes related to immune infiltration in the tumor microenvironment of cutaneous melanoma. *Front Oncol*. (2021) 11:615963. doi: 10.3389/fonc.2021.615963

154. Suzuki K, Tange M, Yamagishi R, Hanada H, Mukai S, Sato T, et al. SMG6 regulates DNA damage and cell survival in Hippo pathway kinase LATS2-inactivated Malignant mesothelioma. *Cell Death Discov*. (2022) 8:446. doi: 10.1038/s41420-022-01232-w

155. Yang C, Pang Y, Huang Y, Ye F, Chen X, Gao Y, et al. Single-cell transcriptomics identifies premature aging features of TERC-deficient mouse brain and bone marrow. *GeroScience*. (2022) 44:2139–55. doi: 10.1007/s11357-022-00578-4

156. González-Gualda E, Pàez-Ribes M, Lozano-Torres B, Macias D, Wilson JR3rd, González-López C, et al. Galacto-conjugation of Navitoclax as an efficient strategy to increase senolytic specificity and reduce platelet toxicity. *Aging Cell*. (2020) 19:e13142. doi: 10.1111/acel.13142

157. Yeo MK, Kim Y, Lee DH, Chung C, Bae GE. Cosuppression of NF-κB and AICDA overcomes acquired EGFR-TKI resistance in non-small cell lung cancer. *Cancers*. (2022) 14(12):2940. doi: 10.3390/cancers14122940

158. An T, Zhang Z, Li Y, Yi J, Zhang W, Chen D, et al. Integrin β1-mediated cell Cell adhesion augments metformin-induced anoikis. *Int J Mol Sci*. (2019) 20(5):1161. doi: 10.3390/ijms20051161

159. Zhao N, Guo M, Wang K, Zhang C, Liu X. Identification of pan-cancer prognostic biomarkers through integration of multi-omics data. *Front Bioengineering Biotechnol*. (2020) 8:268. doi: 10.3389/fbioe.2020.00268

frontiers | Frontiers in Oncology

TYPE Review
PUBLISHED 04 June 2025
DOI 10.3389/fonc.2025.1581951

Check for updates

OPEN ACCESS

EDITED BY
Weiling Li,
Dalian Medical University, China

REVIEWED BY
Liewei Wen,
Jinan University, China
Xinghua Yu,
Zhejiang University, China

*CORRESPONDENCE
Huiping Liu
1074983953@qq.com

RECEIVED 23 February 2025
ACCEPTED 29 April 2025
PUBLISHED 04 June 2025

CITATION
Liu W, Jing Y, Chen Y, Sun H, Xu W, Liang R, Liu W, Zhang Z and Liu H (2025) Research progress on the cross-regulation between ferroptosis and immunogenic cell death in tumor micro-environment.
Front. Oncol. 15:1581951.
doi: 10.3389/fonc.2025.1581951

COPYRIGHT
© 2025 Liu, Jing, Chen, Sun, Xu, Liang, Liu, Zhang and Liu. This is an open-access article distributed under the terms of the Creative Commons Attribution License (CC BY). The use, distribution or reproduction in other forums is permitted, provided the original author(s) and the copyright owner(s) are credited and that the original publication in this journal is cited, in accordance with accepted academic practice. No use, distribution or reproduction is permitted which does not comply with these terms.

Research progress on the cross-regulation between ferroptosis and immunogenic cell death in tumor micro-environment

Weitao Liu[1], Yichen Jing[1], Yang Chen[2], Han Sun[1], Wenbo Xu[1], Ruihan Liang[1], Wanglin Liu[1], Zengyu Zhang[1,3] and Huiping Liu[1]*

[1]Hunan Provincial Key Laboratory of Traditional Chinese Medicine Oncology, Hunan University of Traditional Chinese Medicine, Changsha, Hunan, China, [2]Department of Foreign Languages, University of Chinese Academy of Sciences, Beijing, China, [3]Research Center for Clinical Medicine, Jinshan Hospital Affiliated to Fudan University, Shanghai,, China

Ferroptosis and immunogenic cell death, as two unique forms of cell death, have attracted extensive attention in the biomedical field. Recent studies have shown the synergistic effect of ICD and ferroptosis in the tumor microenvironment, where tumor cells undergo immunogenic cell death and release immunogenic molecules, such as DAMPs, to recruit and activate immune cells and promote adaptive immune responses. At the same time, molecules such as lipid peroxides produced by ferroptosis may also enhance the anti-tumor activity of immune cells. In addition, the synergistic use of ferroptosis and ICD in combination with novel protocols such as biomaterials and nanotechnology has demonstrated promising anti-tumor effects. This article reviews the cross-regulatory mechanism of ferroptosis and ICD in the tumor microenvironment, and explores the related biological effects between immune cells and ferroptosis, and the potential application of the two in the treatment of cancer. At the same time, we put forward insights into the solution of the existing problems in the combination of ferroptosis and ICD, as well as new ideas and development directions for future cancer treatment.

KEYWORDS

ferroptosis, cross regulation, tumor microenvironment, immunogenic cell death (ICD), damage associated molecular pattern molecules (DAMPS)

1 Introduction to ferroptosis

Tumor micro-environment (TME) refers to a comprehensive environment in which the occurrence, growth and metastasis of tumor are closely related to the internal and external environment of tumor cells. Tumor microenvironment affects tumor cell metabolism, immunity and therapeutic effect, and plays a core role in tumor occurrence and development

(1). Although the research on tumor microenvironment has made remarkable progress, there are still some limitations. For example, the understanding of the interaction mechanism between various components in tumor microenvironment is still not deep enough, and the targeted therapy methods for tumor microenvironment still need to be explored and optimized (2). In recent years, Ferroptosis and immunogenic cell death (ICD), as two unique ways of cell death, have attracted wide attention in the biomedical field. Ferroptosis and immunotherapy have shown great potential in the field of cancer treatment (3). Inducing ferroptosis and targeting immune cells are new strategies for cancer treatment (4). Ferroptosis is characterized by the accumulation of a large number of lipid peroxide products, especially phospholipid hydroperoxide, which will destroy the integrity of cell membrane and eventually lead to cell death. And it is a unique form of cell death because its mechanism is significantly different from the traditional cell death pathway (5). It has been proved that it is closely related to the occurrence, development and metastasis of tumors, and its potential application value in anti-tumor therapy is increasingly prominent. ICD is a special mode of cell death (6). By releasing DAMPs, antigen presenting cells (such as dendritic cells, calreticulin (CRT) and heat shock protein (HSPs)) can be recruited and adaptive immune response of T cells can be activated, so as to induce tumor cell death and establish immune memory. This way of death plays an important role in the treatment of tumor cancer, because it can promote the recognition and clearance of tumor cells and enhance the anti-tumor immune response (7). Recent studies have shown that ferroptosis and ICD have a synergistic effect in tumor microenvironment. Molecules such as lipid peroxide produced by ferroptosis may also enhance the anti-tumor activity of immune cells. Ferroptosis treats tumors through iron metabolism, lipid metabolism and amino acid metabolism, and also has some effects on the function and activity of immune cells in tumor microenvironment (8). Ferroptosis can regulate ICD through T cells, B cells, neutrophils and macrophages in tumor microenvironment. ICD not only inhibits tumor cells, but also has certain influence on tumor microenvironment (9). When tumor cells experience ICD, they will release immunogenic molecules, such as DAMPs, recruit and activate immune cells, and promote adaptive immune response. CD8+ T cells in immune cells promote ferroptosis of tumor cells through interferon-γ (IFN-γ), forming positive feedback and enhancing anti-tumor effect (10). The metabolism and polarization of T cells and macrophages affect ferroptosis. The molecular mechanism of cross-regulation of ferroptosis and ICD provides a new potential target for tumor treatment. It is beneficial to the implementation of clinical combined treatment strategies such as the combination of ferroptosis inducer and ICD inducer, and provides more effective choices for the treatment of cancer. In this paper, the cross-dialogue mechanisms between ferroptosis and ICD in tumor microenvironment are systematically summarized, and the biological effects associated with ferroptosis in immune cells are deeply discussed, and the potential application prospects of these mechanisms in the field of cancer treatment are further analyzed. By targeting the molecular mechanism of ferroptosis and ICD, we can provide ideas for developing new anti-tumor drugs and treatment schemes, improve the therapeutic effect of tumors and reduce side effects.

1.1 The concept of ferroptosis

Ferroptosis is a unique form of iron-dependent cell death, which is caused by excessive accumulation of lipid peroxide on the cell membrane (5). Since its first discovery in 2012, it has attracted wide attention because of its unique cellular characteristics and its potential role in cancer treatment (11). Different from apoptotic cells, iron-dead cells show the characteristics of cell membrane rupture, bubbling, mitochondrial volume reduction, intima density increase, crista reduction or disappearance, adventitia rupture and so on (12). And release DAMPs (13). Its core regulatory mechanism includes the axis of solute carrier family 7 member 11(SLC7A11)- glutathione-GPX4 and the endosome sorting complex ESCRT-III which is necessary for transport (14). SLC7A11 participates in the reverse transport of cystine/glutamic acid in cells, and generates glutathione (GSH), which is an important antioxidant in cells, and reduces lipid peroxide through GPX4 to protect cells from ferroptosis (15). Inhibition of SLC7A11 or GPX4 activity will lead to GSH depletion and lipid peroxidation accumulation (16), causing ferroptosis. In the process of ferroptosis, the mechanism of endosome sorting complex endosomal sorting complex required for transport (ESCRT)-III, which is necessary for transport, participates in limiting plasma membrane damage (14).

Studies have shown that ferroptosis is closely related to iron, lipid and amino acid metabolism. Loss of iron metabolized ferroportin (FPN) and reactive oxygen species (ROS) (17). Deletion of PLs, peroxidation of PLS in lipid metabolism (18). The chemical substances arachidonic acid and adrenal acid (AdA), amino acid metabolized GPX4 inactivation and glutathione depletion are all important factors of ferroptosis. In addition, ferroptosis also affects inflammatory reaction and tumor growth *in vivo*. Many small molecular drugs such as eRAStin (SLC7A11 inhibitor) and RSL3 (GPX4 inhibitor) can specifically induce ferroptosis, especially for cancer cells carrying mutant ras oncogene (19).

Its specific mechanism remains to be further studied. Generally speaking, ferroptosis, as a unique form of cell death, has great potential in tumor treatment. In-depth study of its regulatory mechanism and its interaction with the immune system is expected to provide new ideas for cancer treatment.

1.1.1 Iron metabolism

Iron is an important element for life activities and participates in many life regulation processes. Ferroptosis, that is, iron-dependent cell death, is closely related to iron metabolism disorder. *In vivo*, Free Fe^{3+} in blood forms a complex with extracellular transferrin (Tf) and binds to transferrin receptor 1 (TfR1) on cell membrane (20), enters cells through endocytosis, and Fe is reduced to Fe by iron reductase (such as Six-Transmembrane Epithelial Antigen of Prostate 3 (STEAP3)) (21). After that, Fe^{2+} was transported to the cytosol by divalent metal ion transporter 1 (DMT1). In the cytosol, most Fe^{2+} is released to the outside of the cell through FPN1 or stored by ferritin. However, when FPN is missing or ferritin function is abnormal, it will cause iron metabolism imbalance, which will lead to intracellular iron

overload, lead to excessive Fe^{2+} entering the unstable iron pool (LIP) in the cytosol, generate a large number of ROS through Fenton reaction, destroy lipid peroxidation, and eventually lead to ferroptosis (22).

Therefore, iron chelating agents and nitrogen oxides can inhibit Fenton reactions, such as deferoxamine (DFO) and TEMPO, thus interrupting ferroptosis (23). In addition, the mutation or abnormal expression of genes related to iron metabolism may also affect the sensitivity of ferroptosis pathway. For example, iron response element binding protein 2 (IRB2), a key regulator of iron metabolism, can participate in PUFA peroxidation, reducing the sensitivity of cells to ferroptosis, and inhibiting IRB2 can inhibit ferroptosis (24).

In addition, ferritin autophagy is a process regulated by autophagy-related (ATG) proteins, which is related to the interaction between autophagy and lysosomes, and nuclear receptor coactivator 4(NCOA4) is its special molecule. During the autophagy of ferritin, ferritin combines with NCOA4 through FTH1 subunit to form a complex. After that, the double-walled autophagy membrane contains ferritin -NCOA4 complex, forming a completely closed structure and transferring to lysosomes, where ferritin degrades and releases iron. When iron metabolism is disordered or ATG expression is abnormal, iron autophagy mediated by NCOA4 can induce ferroptosis by degrading ferritin and inducing iron overload (25).

Hypoxia can also affect iron metabolism. Hypoxia leads to the increase of erythropoietin (EPO) and serum TF, which eventually leads to abnormal iron metabolism, thus promoting ferroptosis. In addition, hypoxia can enhance the level of HIF-1 and promote the concentration of transferrin to regulate ferroptosis (23).

1.1.2 Lipid metabolism

Lipid metabolism plays a central role in ferroptosis. Lipid peroxidation is a process in which ROS oxidizes biofilm after oxidative stress is enhanced, and it is a key factor driving cell death (26). There are two ways to trigger lipid peroxidation: non-enzymatic or enzymatic. Enzymes mean that lipid peroxidation can occur through lipoxygenase (LOX), cyclooxygenase (COX) and cytochrome P450 (CYP). Non-enzymatic means that lipid peroxidation can occur in a non-enzymatic way through free radical-induced peroxidation, autooxidation and photodegradation (25).

The accumulation of polyunsaturated fatty acids (PUFA) is considered as a sign of ferroptosis (27). Because PUFA is the site of oxidative lipid damage, it is a necessary substance to perform ferroptosis. There are a lot of PUFA in the cell membrane, which are esterified by acyl-CoA synthetase long chain family member 4 (ACSL4), modified by lysophosphatidylcholine acyltransferase 3 (LPCAT3) and integrated into cell membrane phospholipids. These lipids are easily attacked by free radicals. For example, PUFA in lipid membrane is highly sensitive to oxidative stress, which can react with ROS and induce lipid peroxidation to form L-ROS, while high concentration of L-ROS will trigger oxidative stress in cells and lead to oxidative damage. Lipid peroxides are extremely destructive to cells, because they will destroy the thickness, permeability and structure of membrane bilayers. Lipid peroxidation occurs and lipid hydroperoxide (PL-OOH) is generated, which leads to membrane damage and ferroptosis (25, 28, 29). Studies have shown that exogenous monounsaturated fatty acids (MUFA) can inhibit the accumulation of lipid ROS on plasma membrane and replace PUFA on plasma membrane, thus effectively inhibiting ferroptosis (30, 31). In addition, studies have shown that phosphatidylethanolamine (PE) is the key phospholipid to induce cell ferroptosis. PE is involved in biosynthesis and reconstruction by ACSL4 and lysophosphatidylcholine acyltransferase 3 (LPCAT3), which can activate PUFA and affect its transmembrane characteristics (31, 32).

At the same time, the decomposition products of lipid peroxide, including 4- hydroxynonenal (HNE) and malondialdehyde (MDA), will also damage the cell process, because they form adducts with protein and DNA, thus affecting the normal function of cells (30).

1.1.3 Amino acid metabolism

The occurrence of ferroptosis is closely related to the depletion of intracellular GSH and the failure of antioxidant enzyme GPX4. System Xc-, as the reverse transport protein of cystine/glutamic acid, is very important for amino acid metabolism.

System Xc- a heterodimer composed of two subunits, SLC3A2 and SLC7A11, can transport cystine into cells and release glutamic acid out of cells. In the cell, cystine is first reduced to cysteine, and then enters the cell with the help of transporter SLC7A11 to participate in the synthesis of GSH, thus enhancing the activity of GPX4, the main antioxidant enzyme. When Xc- is inhibited, the concentration of intracellular cysteine decreases, which limits the synthesis speed of GSH, increases the level of intracellular ROS, leads to the accumulation of lipid peroxide, and finally leads to ferroptosis. Therefore, the function of system Xc- has a direct impact on GSH level and GPX4 activity (33, 34). Based on this, we can develop drugs that can inhibit or promote ferroptosis, such as cisplatin, which inhibits the activity of GPX4 (35). In addition, amino acid metabolism also involves other pathways related to ferroptosis. For example, some amino acids can regulate ferroptosis by affecting the production of ROS or the activity of antioxidant enzymes, such as cysteine as GSH raw material (36).

1.2 The pathway of ferroptosis

1.2.1 GSH-GPX4 pathway

The fundamental cause of ferroptosis is the imbalance of redox balance between oxidant and antioxidant, which is driven by the abnormal expression and activity of various redox enzymes in the process of producing free radicals and lipid oxidation products or detoxification. When the antioxidant system can't withstand iron overload, excessive ROS will attack sensitive fatty acids, trigger peroxidation, destroy the integrity of cell membrane, increase oxidative stress *in vivo*, and destroy DNA, protein and lipids, thus aggravating lipid metabolism disorder and further causing ferroptosis (37). At the same time, LPO produced by lipid peroxidation, such as malondialdehyde and 4- hydroxynonenal, can induce lipid peroxidation of phospholipid-containing cell

membrane, and then induce ferroptosis (38, 39). GPX4 can reduce the amount of ROS, reduce phospholipid hydrogen peroxide (PL-OOH) to phospholipid hydroxylate, maintain the redox state of GSH, prevent the accumulation of lipid reactive oxygen species, and then regulate the occurrence of ferroptosis. When GPX4 activity is lost or its function is impaired, ROS accumulation leads to lipid peroxidation, which in turn leads to ferroptosis (39, 40). Therefore, regulating the levels of GPX4 and GSH can change the occurrence and development of ferroptosis. Glutathione is the most abundant reducing agent, which affects the biogenesis of iron and sulfur clusters, and is also an auxiliary factor of many enzymes (including GPX and glutathione S transferase) (41).

1.2.2 NADPH-FSP1-CoQ10 pathway

NADPH-FSP1-CoQ10 pathway is another key anti-ferroptosis pathway. The N-terminal of FSP1 contains myristic acylation domain, which has the function of lipid modification, enriching it in plasma and reducing the sensitivity of cells to ferroptosis (42). Previous studies have confirmed that FSP1 is a nicotinamide-adenine dinucleotide phosphate (NADP-)-dependent coenzyme Q (CoQ) oxidoreductase, which can be used as an electron carrier and a fat-soluble antioxidant (43). Recent studies have found that FSP1 and GPX4 cooperate to inhibit ferroptosis by directly regulating the antioxidant system of non-mitochondrial coenzyme Q10 (44).

According to Doll et al.' s research, overexpression of apoptosis-inducing factor Mitochondrial Associated 2(AIFM2, also known as FSP1) can reverse ferroptosis induced by GPX4 inhibition, which indicates that FSP1 has nothing to do with the mechanism of GPX4 (42). Therefore, the combined inhibition of FSP1 and GPX4 is expected to be an effective strategy for the treatment of ferroptosis-related diseases.

1.2.3 P62-Keap1-Nrf2 signal transduction pathway

Other molecular signal pathways related to ferroptosis, including p62-Keap1-Nrf2 signal transduction pathway, bind to Kelch-like ECH-related protein 1(Keap1) under oxidative stress, and remain inactive through ubiquitination in proteasome, and then release Nrf2 from the coupled Keap1 protein and transfer to the nucleus (45). Its core lies in that the nuclear factor erythroid 2-related factor 2(Nrf2) has antioxidant function and can participate in the regulation of ferroptosis (11, 45). Sun and his team's research confirmed that p62-Keap1-Nrf2 signal transduction pathway has antioxidant effect on ferroptosis of hepatocellular carcinoma cells, which mainly depends on the localization mechanism of p62 as autophagy receptor, and activates Nrf2 by inactivating Keap1 (46). Nrf2 prevented ferroptosis under the mediation of NQO1, family oxygenase -1 (HO-1) and ferritin heavy chain (FTH1) (5), which indicated that ferroptosis was indirectly related to autophagy. It has been reported that p53 down-regulates the expression of SLC7A11 to conduct metal-dependent apoptosis signals and affect Xc- system, thus inhibiting the ferroptosis process. It has been found that the activation of p53 will reduce the antioxidant capacity of cells, leading to ferroptosis, which can be reversed by the treatment of ferritin -1 (Fer-1) (47). It can be seen that Nrf2 regulates the antioxidant reaction and its interaction with autophagy, while p53 regulates ferroptosis by regulating SLC7A11 expression and ROS metabolism.

Ferroptosis involves many molecules and signal pathways, and these mechanisms provide a new perspective and strategy for studying cell death and treating diseases related to ferroptosis.

1.3 Ferroptosis reagent

1.3.1 Ferroptosis Inducer

1.3.1.1 Targets small molecules and drug inducers of iron metabolism and lipid metabolism

Compared with normal cells, tumor cells are more dependent on iron, so they are highly sensitive to ferroptosis. This process can also be induced by drugs that modulate lipid and iron metabolism. For example, Withaferin A and FINO2 induce ferroptosis by inhibiting GPX4 and changing iron metabolism, respectively (48, 49). In addition, Song et al. showed that temozolomide (TMZ) could induce ferroptosis in glioblastoma cells through DMT1-dependent pathway (50). In addition, t-BuOOH-induced cell death can be saved by intercellular contact through the Hippo pathway (51). Nanomaterials partially loaded with iron can also cause ferroptosis in tumor cells (52). The recently discovered inducer, MMRi62, has been shown to induce the degradation of ferritin heavy chain, thus promoting ferroptosis (50). In the treatment of hepatocellular carcinoma, sorafenib, as an FDA-certified anticancer drug, can induce ferroptosis in the presence of ACSL4 acyl-CoA synthetase long chain family member 4 (53). Especially, the intervention of sorafenib will directly affect the metabolic pathway of lipid ROS production in cells. T-BuOOH can directly affect the level of lipid ROS, leading to DNA damage, oxidative stress and mitochondrial membrane potential imbalance, and its mechanism involves the oxidation of cardiolipin. Cardiolipin oxidation inhibitors XJB-5–131 and JP4–039 can reverse this process (53).

1.3.1.2 Targets small molecules and drug inducers of GSH/GPX4 axis and FSP1/CoQ related pathways

Some tumors have failed the pathway of sulfur transfer due to mutation or apparent modification, so tumor cells are highly dependent on System Xc- for cystine uptake, and System Xc- has become an important target of anti-tumor drugs (54, 55). Erastin can effectively inhibit the growth of cervical cancer and ovarian cancer cells by regulating the formation and oxidation of GSH (56). In addition, Erastin also consumes GSH and leads to degradation of GPX4 (12, 57). Sorafenib, an anti-tumor drug approved by FDA, promotes the occurrence of ferroptosis in cells by inhibiting the function of System Xc- (58). Buthionine sulfoximine (BSO) inhibits the activity of glutamyl-cysteine ligase and blocks the production of GSH, thus inhibiting the growth of breast tumors in mice (59) and enhancing the chemosensitivity of melanoma and glioma (60, 61). RSL3 is the most commonly used GPX4 inhibitor, which can effectively promote ferroptosis in fibrosarcoma and multiple cell models (56). NDP4928 is an ferroptosis enhancer (62), and its cytotoxicity is significantly improved when it is combined with RSL3 or BSO. The target of NDP4928 is FSP1, which binds to and

inhibits FSP1, and defines the ferroptosis pathway induced by GSH inhibition (63). FOIN56 is a multi-effect inducer, which not only induces ferroptosis by degrading GPX4, but also induces ferroptosis by combining with squalene synthase (SQS) and consuming CoQ (64). Statins are formulated into therapeutic nanoparticles (65), which can inhibit the synthesis of CoQ10 by blocking HMGCR in mevalonate pathway and trigger ferroptosis after reducing CoQ (66). As shown in Table 1.

1.3.2 Ferroptosis inhibitor

1.3.2.1 Small-molecule inhibitors that reduce the ferroptosis

Iron chelating agents, such as DFO and dexrazoxane (DXZ), can selectively target intracellular Fe^{2+} and prevent ROS produced by Fenton reaction, thus achieving the effect of inhibiting ferroptosis (67, 68). DXZ is approved by FDA for DIC treatment of cancer patients, which can relieve heart dysfunction by inhibiting ferroptosis. In addition, there are other iron ion chelating agents, such as DFA1, BMS536924 and purine analog 2, which show higher efficiency and lower side effects in inhibiting ferroptosis. At the same time, there are ferroptosis inhibitors that directly reduce the level of Fe^{2+}, such as YL 939, which can reduce the iron level in intracellular LIP by regulating ferritin expression and ferritin phagocytosis, thus inhibiting ferroptosis. According to the research of YANG W et al. (69), this compound can effectively inhibit cell death and inflammatory infiltration in acetaminophen-induced liver injury model. Hirata et al. (70) synthesized a class of compounds containing N,N- dimethylaniline structure, targeting secondary endosomes and lysosomes, and inhibiting ferroptosis by reducing Fe^{2+}. Among them, GIF-2–114 and GIF-2 197-r), the two compounds with the highest activity, have the same neuroprotective ability as Fer-1 on cell death induced by glutamate and Erastin at sub-nano molar concentration. Ferristatin II can promote the degradation of TfR1, interfere with Tf-mediated iron delivery, and has also been proved to inhibit ferroptosis (71), which provides a new strategy for the treatment of various nervous system diseases. Fang et al. (72) found a kind of ferroptosis inhibitor 9a targeting NCOA4. By binding with NCOA4, it destroyed the protein-protein interaction between NCOA4 and FTH1, blocked iron autophagy dependent on NCO A4, and reduced Fe^{2+} in intracellular LIP, thus inhibiting ferroptosis.

1.3.2.2 As a small molecular inhibitor for reducing lipid peroxide

The first ferroptosis inhibitor, Fer 1, was found by Qualcomm screening, which can quickly react with peroxy free radicals in cells and block the amplification of chain reaction in lipid peroxidation, thus inhibiting ferroptosis (73). Lip-1 is a spiroquinoxaline amine derivative with the same mechanism as Fer-1. Because of its good absorption and distribution, ferroptosis can be effectively inhibited at a lower dose (74). α -tocopherol (α-TOH) is the most bioactive form of vitamin E, and it is also an effective ferroptosis inhibitor. The reactivity of its analogue THNs is 100 times higher than that of Fer 1 and Lip-1 in organic solution, but its ferroptosis inhibitory activity in cells is similar to that of them (75).

1.3.2.3 Small-molecule inhibitors affecting the GSH/GPX 4 axis

β-mercaptoethanol (m-ME) has an ferroptosis inhibitory effect in System Xc-it can prevent the cell from being blocked in the process of cystine uptake (34). In this process, β-ME reacts with cystine to generate mixed disulfide, which is transmitted to cells through system L, and cystine is rapidly generated, thus accelerating the generation of GPX4 (76). Increasing the expression of GPX4 can effectively resist ferroptosis, which is regulated by selenium (Se) and can be achieved by activating transcription factors TFAP2c (transcription factor activating protein 2γ) and Sp1 (specific protein 1). However, TFAP2c may be affected by transcription inhibitors, and cells with low GPX4 level cannot be protected by Se (77). Partner-mediated autophagy can induce the degradation of GPX4, but triterpenoid 2-amino -5- chloro -N, 3- dimethylbenzamide (CDDO) can inhibit the degradation of GPX4 by inhibiting molecular chaperone HSP90, thus preventing cells from ferroptosis (78). A new diphenyl butene inhibitor compound 3f discovered by Fang et al. (79) can inhibit ferroptosis by increasing the level of FSP1 protein. In addition, many natural antioxidants, such as 43 kinds of curcumin, 26 kinds of baicalin, 44 kinds of resveratrol and 45 kinds of sulforaphane (80), have been proved to have the activity of inhibiting ferroptosis because of their polyphenol structure. As shown in Table 2.

2 Introduction of immunogenic cell death

2.1 The concept of an immunogenic cell death

Immunogenic cell death is a regulatory programmed cell death pattern specially designed to activate the adaptive immune response of syngeneic hosts with sound immune function (81). The function of ICD is to trigger adaptive immune response, trigger stress response of organelles and cells, and finally lead to apoptosis (82). Molecules released by dying or stressed cells, such as ATP, HMGB1, CRT and proinflammatory cytokines, can all be used as adjuvants or danger signals of the immune system, and such signals are collectively called DAMPs (83). The release of DAMPs is a remarkable feature of ICD. When DAMPs are exposed to the extracellular membrane or released to the extracellular matrix in a specific time and space, it can combine with its corresponding pattern recognition receptors (PRR), such as TLR, NLRs, RLRs, etc., so as to deliver immune stimulation signals, stimulate downstream signal transduction pathways, start cell cascade reactions, and attract antigen-presenting cells. For example, when TLR4 recognizes HMGB1, it will activate MyD88 signal pathway. RIG-I-like receptor can activate interferon regulatory factor IRF 3/7 after recognizing viral RNA; NOD-like receptors promote the release of IL-1β and IL-18 by forming inflammatory corpuscles (84), further stimulate the proliferation and activation of T lymphocytes, greatly enhance their anti-tumor benefits, and finally trigger innate and adaptive immune responses, resulting in strong and lasting anti-cancer immunity (85–89).

TABLE 1 Ferroptosis inducer form.

Medicine	Mechanism	Experimental model	Related genes	Cite
Withaferin	Inhibit GPX4 activity, degrade heme and increase iron content.	Human neuroblastoma cells IMR-32 and SK-N-SH	CPX4	Song Q et al. (50)
FINO2	Inhibiting GPX4 and ferric oxide	Human fibrosarcoma cell HT-1080, human immortalized skin tissue cell BJeLR.	CPX4	Faust D et al. (51)
Temozolomide (TMZ)	Decreased the expression of Nrf2 and HO-1, and up-regulated DMT1.	Human glioblastoma cell line TG905	DMT1, SQLE, GPX4	Song Q et al. (50)
Iron-based nanomaterials	Inhibition of tumor growth by Fenton reaction	MMTV-PyMT (mouse breast tumor virus-T antigen in polyoma) breast cancer cells	TfR1、FPN1、HO-1	Chen M et al. (54), Geppert M et al. (239)
Sorafenib	Inhibition system Xc enhances intracellular iron content.	Hepatocellular carcinoma (HCC) tissue	SLC711, STAT3,MCL1	Dhiman P et al. (55)
Erastin	Inhibition of System Xc-, interference with cystine uptake, decrease of GSH and increase of lipid peroxidation level.	Human cervical cancer cell Hela, human ovarian cancer cell COV362	p53	Xiong Y et al. (59), Wu H et al. (60)
Buthionine sulfoxide imine (BSO)	Inhibit the activity of glutamyl-cysteine ligase and block the production of GSH.	Neuroblastoma cell line	p53,GPX4,ATM	Cunningham A et al. (244), Yoshioka et al. (63), Chen X et al. (64)
RSL3	Cysteine binding to GPX4 active site inhibits GPX4 activity.	Human fibrosarcoma cell HT-1080 and nude mice transplanted tumor model	GPX4,SLC711,SLC3A2	Tang R et al. (52)
Statins	Inhibit GPX4	Triple negative breast cancer (TNBC) cells	GPX4	MILLÁN M et al. (68)
FIN56	Inhibit GPX4;; Combined with squalene synthase (SQS), CoQ is consumed.	Four kinds of engineered BJ cell lines, 143B cells (osteosarcoma), Calu-1 cells (lung adenocarcinoma) and HT-1080 cells (fibrosarcoma).	SLC7A11 GPX4 FSP1	Deepa S et al. (67), Costa I et al. (245)

2.1.1 ICD antigenicity of ICD

In the process of ICD, antigenicity plays a key role, which determines whether the dead cells can be effectively recognized by the host immune system and the efficiency of triggering immune response. Antigenicity mainly comes from four aspects: 1. Bacterial and viral infection: Infection by pathogens (such as viruses and bacteria) can lead to the production of a large number of antigenic determinants. Microbial proteins are not covered by central tolerance, and their epitopes are highly antigenic, which can bind to host T cell receptor (TCR) and initiate immune response (90, 91). 2. Tumor cell mutation: Most human tumors are not driven by active virus infection, but malignant cells are often accompanied by an increase in gene mutation rate during immune escape (92, 93). These mutations include non-sense point mutation, insertion deletion and so on, which lead to the exposure of new tumor antigen (TNA). TNA is quite different from its own epitope structure, and some of them are similar to microbial epitopes, which can effectively trigger ab initio immune response. In addition, cancer cells also express some tumor-associated antigens (TAA), such as CD19, CD20, PMEL and MLANA (94, 95). These antigens also exist in healthy tissues, but due to incomplete central tolerance, they can still trigger immune response under the background of strong adjuvant. 3. Post-translational modification (PTM): antigenic determinants can also be produced by PTM, such as phosphorylation, acetylation, glycosylation, etc (96). These modifications can change the structure of protein and produce new epitopes, which may not be covered by central tolerance, so they can trigger immune response under certain conditions. 4. Endogenous retroviruses: Normal cell genomes contain a large number of endogenous retroviruses, which are usually dormant under physiological conditions. However, under stress conditions, these viruses may be activated and express antigen proteins, giving healthy cells certain ICD capabilities (97, 98). ICD process is an immune response triggered by cell death. The key is that DAMPs released after cell death can stimulate immune cells such as antigen presenting cells (APC) and T cells, leading to programmed cell death. Therefore, if we can inhibit the activation or function of immune cells, or block the release pathway of DAMPs (such as HMGB1 and ATP), it is expected to weaken the immune response caused by ICD. For example, by inhibiting the three key genes LY96, BCL2 and IFNGR1 in SAP and using antagonists of immune checkpoint inhibitors, it may be helpful to control the activation of T cells, thus reducing the impact of immune response on ICD (99). However, due to the variety of DAMPs and the complex mechanism of action, the research on inhibitors of DAMPs release is still in the primary stage. It is expected that with the in-depth understanding of the release mechanism of DAMPs, such inhibitors are expected to become new therapeutic strategies.

In addition, cytokines involved in ICD (such as IFN-γ and IL-1β) and death receptors on the cell surface (such as FAS and TNFR) can also be used as key factors affecting the immune effect (100, 101).

2.1.2 ICD adjuvant nature of ICD

Adjuvant is another key aspect in ICD process, which determines whether dying cells can effectively recruit and APC, and then start adaptive immune response. Adjuvant properties are mainly provided by DAMPs, including ATP, HMGB1, CRT, HSPs and so on (82). These molecules are released or exposed to the cell surface during cell death. These molecules are released or exposed during cell death and are recognized by the immune system as "danger signals".

2.1.2.1 DAMPs mechanism of DAMPS

2.1.2.1.1 ATP

ATP, as a cell energy carrier, is released to the outside of the cell during ICD, and serves as a "find-me" signal to recruit DC and macrophages to the tumor area to promote the infiltration of immune cells. Its release mechanism includes autophagy dependence and ERS induction. ATP-loaded vesicles are released in a autophagy-dependent manner through Pannexin channels. In ERS state, ATP release may be related to the activation of PERK/eIF2α signaling pathway (102). The main function of ATP is to recruit and activate immune cells. By binding to DC and P2RY2 receptor on the surface of macrophages, ATP promotes the infiltration of many myeloid cells into tumor areas (103). In addition, it can activate NLRP3 inflammatory corpuscles in DC, promote the secretion of IL-1β and IL-18, and activate CD8+ T cells and γδT cells (104).

2.1.2.1.2 HMGB1

As a kind of DAMP, HMGB1 has immune stimulation. HMGB1 released from the nucleus to the extracellular matrix binds to TLR4 on the surface of DC, which enhances the processing and cross-presentation of antigen by DC and activates the specific T cell immune response (84). The release mechanism includes active release and passive release. Active release is the exocytosis pathway mediated by specific lysosomal vesicles, or active release in the process of cell death mediated by caspase-1/caspase-11; Passive release is the late stage of apoptosis, and the permeability of cell membrane increases, which leads to the passive release of HMGB1 to the extracellular space (105).

2.1.2.1.3 CRT

As an "eat-me" signal, CRT promotes the phagocytosis of apoptotic cells by macrophages. CRT is a Ca-binding protein resident in endoplasmic reticulum (ER), which is involved in protein folding, ER homeostasis and MHC class I molecule assembly (106). During ICD, CRT is transferred from ER to the surface of cell membrane, which promotes the phagocytosis of apoptotic cells by immune cells. CRT has the functions of phagocytosis signal and antigen presentation, and interacts with CD91 and TLR4 on DC surface to drive macrophages to phagocytize apoptotic cells (82, 107). The release mechanism includes ERS induction and vesicle transport. ERS-induced translocation of CRT is caused by ER stress (ERS) activating unfolded protein reaction (UPR). Under the interaction of SNARE and SNAP23/25, CRT translocates to cell membrane through exocytosis (108); As for vesicle transport, CRT binds to vesicle or plasma membrane-related proteins, and transports from ER to Golgi apparatus in the form of vesicles, and then transports to cell membrane (109).

TABLE 2 Ferroptosis inhibitor form.

Medicine	Mechanism	Experimental model	Related genes	Cite
Iron chelating agent	It can selectively target Fe2+ in cells and prevent ROS produced by Fenton reaction.	Middle cerebral artery occlusion (MCAO) model in rats	GPX4, ACSL4,	Kosyakovsky J et al. (246), MILLÁN M et al. (68)
YL 939	Regulate ferritin expression and ferritin phagocytosis, and reduce the iron level in intracellular LIP.	Acetaminophen-induced liver injury model	PHB2	Wang Y et al. (74)
Ferristatin II	Promote the degradation of TfR1 and interfere with Tf-mediated iron delivery.	Mouse TBI model	TfR1, 、 Tf	Wang Y et al. (74)
9a	Destroy the interaction between NCOA4-FTH1 protein and protein to reduce the amount of bioavailable intracellular ferrous iron.	Rat model of ischemic stroke	NCOA4-FTH1	Fang et al. (72)
Fer-1	Quickly react with peroxy free radicals in cells to block the amplification of chain reaction in lipid peroxidation.	Cell models of Huntington's disease (HD), periventricular leukomalacia (PVL) and renal dysfunction	SLC711,GPX4	Li Z et al. (247)
Lip-1	ROS produced by lipid peroxidation	Mouse melanoma cells	EGRI,SLC711,GPX4	Bao C et al. (248)
β-MErcaptoethanol (β-me)	Increase GPX4 expression.	Mouse lymphoma L1210 cells	Transcription factors TFAP2c, HSP90,	Fang Y et al. (79), Gu Y et al. (80)
Novel diphenyl butene inhibitor compound 3f	Increase FSP1 protein level	Rat model of ischemic stroke	FSP1	Fang et al. (79)

2.1.2.1.4 HSPs

HSPs not only protect cells from damage, but also combine with damaged protein to form immune response complex and activate immune cells. HSPs are molecular chaperones activated under stress, including HSP60, HSP70, HSP90, etc., which play a key role in the survival of cells in environmental stress injury. In the process of ICD, HSPs will be translocated to the cell membrane or passively released to the outside of the cell as immunostimulating molecules. HSPs has two main functions. First of all, HSPs can be used as an immune adjuvant, combined with damaged protein, to enhance the recognition and presentation of antigens by DC (110). Secondly, HSPs can promote phagocytosis, and HSPs on cell membrane, as an "eat-me" signal, promote phagocytosis of apoptotic cells by immune cells. The release mechanism of HSPs includes ERS induction and passive release. In ERS state, HSPs may participate in the process of apoptosis through Fas/caspase8 pathway and be exposed on the cell membrane (111), while HSPs may be passively released into extracellular matrix during cell death.

2.2 Immunogenic cell death pathway

2.2.1 ROS-based endoplasmic reticulum stress-related pathway activation

ERS, as a comprehensive stress response, is closely related to ICD. Under ERS condition, unfolded protein reaction (UPR) is activated, which mainly activates protein kinase R-like endoplasmic reticulum kinase (PERK) through glucose regulatory protein 78(GRP78)/binding protein (BiP). PERK further phosphorylates eukaryotic translation initiation factor 2α(eIF2α), thus promoting the translation of activated transcription factor 4(ATF4) and inducing the expression of CCAAT enhancer binding protein homologous protein (CHOP). This process will then activate the expression of apoptotic proteins such as BAX, PUMA and BAK downstream, and complete the cell stress response program (112). However, some drugs such as 4-phenylbutyric acid (4-PBA) can inhibit endoplasmic reticulum stress response, which may inhibit ICD induced by ERS (113).

Overexpression of ERS and ROS is considered to be a common feature of ICD, and ICD inducers that can induce strong ERS are classified as type II inducers. Compared with other inducers, type ii inducer has stronger inducing effect, and wogonin is one of them, which can induce ERS by inducing ROS, and then induce ICD. In this process, PRK/PEKR/eIF2α, as the upstream signal of PI3K/AKT activation, can induce the release of DAMPs and activate DCs to participate in the generation of ICD (114). In addition, cardiac glycoside ICD inducers such as oleanolide can also trigger ERS by blocking Na^+/Ca^{2+} exchange, which will enrich and promote ROS production in mitochondria, thus activating the PERK/eIF2α/ATF4/CHOP pathway and inducing ICD (115). According to the current reports, ERS-related PEKR/eIF2α/ATF4 pathway based on ROS may be the most critical upstream pathway for ICD induction.

2.2.2 Inducing ICD-related pathway activation based on regulated cell death

Cell death is the basis of ICD generation. At this time, RCD-related pathways play the role of repeaters in the process of ICD generation. At present, the research on the death pathway of ICD mainly focuses on the classical pathway of apoptosis. For example, brucine can inhibit autophagy by regulating ERK/mTOR/p70S6K pathway, and further trigger ICD (116). PI3K/AKT acts as the downstream response pathway of eIF2α in the process of inducing ICD by wogonin (114). Resveratrol promotes apoptosis and autophagy by inhibiting NGFR/AMPK/mTOR pathway, thus inducing ICD (117). Cinobufagin induces ICD through the upstream STAT pathway (118). Apoptosis is the most common death form of ICD. However, in recent years, new RCD forms such as autophagy, scorching death, ferroptosis and necrotizing apoptosis have also been confirmed in ICD research. The same drug can even trigger ICD through multiple forms of death. For example, shikonin, as a proteasome inhibitor, can activate receptor and mitochondrial mediated apoptosis pathway by targeting granzyme A (GzmsA), thus triggering ICD. In addition, shikonin can mediate ferritin phagocytosis by regulating aspartate aminotransferase (GOT), and then induce ICD (119, 120). Necrotic apoptosis is considered to be a highly immunogenic way of death, and enhanced autophagy is usually accompanied by necrosis. It is found that shikonin can stimulate RIPK1 and RIPK3-dependent necrosis and directly promote the up-regulation of DAMPs through autophagy, in which ROS accumulation and NF-κB pathway activation may be the main mechanisms of cell necrotizing apoptosis (121). Coke death is due to the perforation of gasdermins (GSDMs), which destroys the continuity of cell membrane. This death mode is more conducive to the release of DAMPs such as HMGB1 than apoptosis, and has a natural pro-inflammatory advantage. When ferroptosis occurs, ferrous ions will start liposome peroxidation through Fenton reaction, which will lead to the accumulation of ROS in cells, thus it is easier to induce strong ERS. The discovery of immunogenic ferroptosis broadens the concept of immunogenic cell death at present and opens up new possibilities for cancer treatment.

2.3 Immunogenic cell death drugs

2.3.1 ICD application of ICD activator

2.3.1.1 Chemotherapy and radiotherapy

The main form of ICD is apoptosis, but recently, new RCD methods such as autophagy, coke death, ferroptosis and necrotizing apoptosis have gradually emerged. The reason is that such drugs as adriamycin and daunorubicin can not only directly inhibit the synthesis of DNA and RNA, kill tumor cells, but also induce ICD in tumor cells. In this process, tumor cells will release DAMPs (such as HMGB1, ATP, CRT, etc.), which can be used as signals of "eat me" and "find me" to attract and activate DCs and other immune cells, thus triggering adaptive immune response.

Oxaliplatin, another platinum drug, induces tumor cell apoptosis by forming DNA adducts and triggers ICD. Similarly, the ICD induced by oxaliplatin is accompanied by the release of DAMPs, which further enhances the anti-tumor immune response.

Other chemotherapeutic drugs, such as cyclophosphamide and paclitaxel, can induce ICD to some extent and improve the anti-

tumor effect, although their mechanisms of action are different. Radiotherapy directly damages the DNA of tumor cells through high-energy rays, leading to cell death. Radiotherapy can not only kill tumor cells directly, but also induce ICD and release DAMPs, thus activating the immune system. At present, the combined application of radiotherapy and immunotherapy has become a research hotspot, aiming at enhancing the effect of immunotherapy through ICD induced by radiotherapy.

2.3.1.2 Immunocheckpoint inhibitors for immunotherapy drugs

Although PD-1/PD-L1 inhibitor cannot directly activate ICD function, it can effectively alleviate immunosuppression and improve the body's ability to recognize and remove antigens caused by ICD (122). With the assistance of chemotherapy or radiotherapy, these inhibitors can significantly enhance the anti-tumor effect. In addition, tumor vaccine is also a good choice. This vaccine is based on tumor-specific antigen and can stimulate human specific immune response. When vaccine-induced T cells encounter tumor cells that trigger ICD, their ability to recognize and eliminate these cells will be greatly improved.

2.3.1.3 Emerging treatment technologies

Photodynamic therapy (PDT): PDT is a non-invasive treatment method, which uses photosensitizer and light with specific wavelength to destroy tumor cells. Photosensitizers accumulate in tumor cells and are activated by light with a specific wavelength, and then generate singlet oxygen and other ROS, which destroy the membrane structure, protein and DNA of tumor cells and cause cell death. The production of reactive oxygen species can also trigger endoplasmic reticulum stress. Endoplasmic reticulum stress can lead to tumor cell apoptosis or other forms of programmed cell death. In the process of cell death, tumor cells will release DAMPs, such as CRT and HMGB1. These DAMPs can be recognized by peripheral immune cells and activate anti-tumor immune response. Therefore, PDT not only directly destroys the tumor cells in the irradiated area, but also activates the immune system of the body, recognizes and attacks distant tumor cells that are not directly affected by PDT, and achieves systemic anti-tumor immune effect. This treatment method shows great potential in the field of cancer treatment because of its advantages of high efficiency, strong selectivity and stimulating immune system.

CAR-T cell therapy: CAR-T cell therapy is a kind of cell therapy. Through genetic engineering technology, T cells of patients are transformed to express chimeric antigen receptor (CAR) which can recognize the surface antigen of tumor cells, so as to accurately target and destroy cancer cells (123). CAR-T cell therapy can not only directly kill tumor cells, but also indirectly activate the immune system by releasing cytokines. OV, as a new treatment method, can induce ICD (124–126). OV has the ability to cooperate with CAR-T cells to help them overcome many obstacles in solid tumors. Firstly, OV can release dangerous signals through ICD, reverse tumor immunosuppression, and make CAR-T cells expand, activate and recruit in TME (127). Secondly, the selective directional lysis function of OV on tumor cells leads to the lysis of infected tumor cells and the subsequent release of TAA, which triggers tumor-specific immune response and prevents tumor from escaping due to antigen deletion or antigen heterogeneity. Finally, therapeutic transgene can be inserted into OV, which is expected to enhance the effector ability of T cells (128).

2.3.2 ICD application of ICD inhibitors

In some autoimmune diseases or organ transplant rejection, immunomodulatory drugs can be used to suppress excessive immune response, including ICD-induced immune response. By reducing or eliminating the stressors that can induce ICD, such as chemotherapy drugs, radiotherapy and virus infection, the incidence of ICD can be reduced. For example, using drugs to change the tumor microenvironment leads to the loss of immunosuppression and immune monitoring, which leads to the disorder of ICD (129). Hypoxia is a key factor in tumor microenvironment, which promotes immunosuppression through various mechanisms. For example, the anaerobic respiration of cells increases under anoxic conditions, which leads to the accumulation of lactic acid and forms an acidic environment, which is not conducive to the function of cytotoxic T lymphocytes (CTL) and reduces the toxicity of natural killer cells (NK cells) (130, 131). In addition, hypoxia also promotes the formation of tumor neovascularization, enhances the invasion of tumor cells, and damages the function of T cells in many ways, such as glucose deprivation, extracellular adenosine accumulation and enhanced expression of immune checkpoints (130, 132). Finally, hypoxia can also promote the survival of tumor cells by inhibiting the expression of apoptotic genes and supporting autophagy (129). Therefore, drugs aimed at hypoxic tumor microenvironment can be used to improve immune environment. However, the application of these drugs requires strict control of indications and contraindications to avoid unnecessary damage to patients. As shown in Table 3.

3 Cross-regulation

3.1 Ferroptosis regulates immunogenic cell death

3.1.1 Immunogenicity of ferroptosis

3.1.1.1 Difference and experimental evidence of early and late ferroptosis

The immunogenicity of ferroptosis in the process of cell death shows obvious stage dependence, mainly because the release stage of DAMPs in the process of cell ferroptosis will affect the immunogenicity of cancer cells. In the immunogenicity of ferroptosis, the release of DAMPs such as ATP and HGMB1 is very important. Because of the different DAMPs content in different stages of ferroptosis in cancer cells, the immunogenicity is different. Early ferroptosis cells released a large number of DAMPs such as ATP and HMGB1, These molecules act as immune-activating "alarm signals" that activate the NF-κB signaling pathway by binding to purine-sensitive receptors (such as P2X7) and pattern recognition receptors (such as TLR4) on the surface of dendritic

cells (DCs), which significantly stimulate the proliferation, activation and immune effect of DCs, thus triggering an efficient adaptive immune response (133). However, due to the depletion of key DAMPs, among which the extracellular enzymes CD39/CD73 degrade ATP to adenosine, which inhibits T cell function through the A2A receptor, and immunosuppressive factors such as TGF-β accumulate, the immunogenicity of late iron-dead cells is weakened, and it is difficult to effectively activate the immune response (134).

Efimova (135) et al. found that the cell proliferation and activation induced by ferroptosis was time-dependent with immune effect, and was closely related to the release of ATP and HMGB1 in tumor cells. They interfered with the function of purinergic receptors by oxidizing ATP (oxiATP), the 2', 3'- dialdehyde derivative of ATP, and successfully regulated the functions of DAMPs such as extracellular ATP by inhibiting P2X7 (136–138). Related experiments have proved that in MCA205 cells at the early stage of ferroptosis, if these purinergic receptors are blocked after being induced by RSL3 for a period of time, the ability of cells to resist re-attack will be obviously weakened (138–140). These findings emphasize the important role of ATP in the immune response triggered by early iron-dead cancer cells, and the remarkable immunogenicity potential of early iron-dead cells. In addition, photodynamic therapy has also been proved to further promote the release of DAMPs and enhance the anti-tumor immune response by inducing ferroptosis.

In general, the sequential release of DAMPs during ferroptosis constitutes the molecular basis of its immunogenicity. The explosive release of DAMPs in the early stage provides the necessary starting signal for activating antitumor immunity, while the depletion of DAMPs in the late stage leads to a decline in immunogenicity. This finding provides an important theoretical basis for the development of tumor immunotherapy strategies based on the regulation of ferroptosis timing, especially in terms of optimizing the ICD process to enhance antitumor immune responses.

3.1.1.2 Promoting effect of characteristic substances of ferroptosis (lipid peroxides) on ICD

Lipid peroxidation products can lead to various types of RCD, such as ferroptosis, apoptosis, and immunogenic cell death. Lipid peroxides not only act as passive byproducts but also serve as active mediators that regulate cell death pathways and influence disease pathogenesis. The promotional role of lipid peroxides in ICD has opened new avenues for targeted therapies against tumors, which can regulate lipid peroxidation to prevent or treat diseases characterized by abnormal cell death (141).

The accumulation of lipid peroxides leads to oxidative damage of cell membranes, disrupting their structural and functional integrity, and serves as an important initiating step in promoting ICD. In this process, lipid peroxides attack unsaturated fatty acids in cell membranes, generating lipid free radicals and peroxides, which trigger a chain reaction causing widespread damage to cell membranes. This increases cell membrane permeability, leading to abnormal exchange of substances between the intracellular and extracellular environments, and leakage of cellular contents such as ATP and HMGB1—DAMPs—into the extracellular environment. This triggers an immunogenic response, activates the immune system, and promotes the occurrence of ICD (142). Additionally, lipid peroxidation reactions produce large amounts of ROS. ROS not only further exacerbate lipid peroxidation reactions but also cause oxidative damage to other macromolecules within cells, such as proteins and DNA, leading to cellular dysfunction and cell death (142). Increased ROS levels can also activate multiple signaling pathways associated with ICD, such as the NF-κB pathway. Activation of NF-κB promotes the expression of pro-inflammatory genes, releases pro-inflammatory cytokines, further enhances immunogenicity, and drives the progression of ICD (143). For example, 4-hydroxy-2-nonenal (4-HNE), a product of lipid peroxidation, can upregulate Fas expression, activate caspase-3,This then triggers apoptosis, a form of the ICD (144).

Lipid peroxides can also promote mitochondrial membrane permeability by oxidatively modifying key molecules on the mitochondrial membrane, such as cardiolipin, thereby releasing cytochrome C and activating downstream apoptotic signaling pathways (145). Lipid peroxides can regulate the expression of immune-related molecules, such as by modulating the expression of thioredoxin-interacting protein (Txnip) to influence the redox state within cells, thereby regulating the survival and function of immune cells (146). In Th17 cells, the accumulation of lipid peroxides can upregulate Txnip expression, inhibit the activity of the antioxidant protein thioredoxin (Trx), further increase ROS levels, form a positive feedback loop, and accelerate Th17 cell death, a process that may be related to ICD (147, 148). In addition, the accumulation of lipid peroxides in lysosomes leads to oxidative damage to the lysosomal membrane, increasing lysosomal membrane permeability (LMP) and causing lysosomal hydrolases such as cathepsin B to be released into the cytoplasm. These hydrolases can degrade various proteins and organelles within cells, disrupting normal cell function and triggering ICD (149).

3.1.2 Regulation of ferroptosis on immunogenic cells

3.1.2.1 T cells

Ferroptosis, a form of iron-dependent lipid peroxidation-driven programmed cell death, plays a dual role in T cell anti-tumor immunity. The survival, expansion, and effector function of CD8+ T cells, a core effector cell population in anti-tumor immunity, are precisely regulated by GPX4. GPX4 uses reduced GSH to reduce toxic lipid peroxides (such as phosphatidylethanolamine hydroperoxide, PE-OOH) to non-toxic lipid alcohols through the selenocysteine residue in its active center, thereby maintaining cell membrane stability and blocking the ferroptosis process (150, 151). This catalytic process involves two key steps: First, the selenolate group (-SeH) of GPX4 reacts with PE-OOH to form a selenoic acid intermediate (-SeOH), while reducing PE-OOH to PE-OH; then, two molecules of GSH provide electrons to reduce the selenoic acid intermediate to -SeH, which ultimately produces oxidized glutathione (GSSG) and water (15). In follicular helper T cells (Tfh), GPX4 deficiency leads to the destruction of mitochondrial cristae structure, accumulation of lipid ROS, and subsequent ferroptosis, which ultimately weakens the germinal center response and antibody affinity maturation. It is noteworthy that

TABLE 3 Application related forms of ICD.

Genes/axes/ compounds/drugs	Mechanism	Related genes/pathways	Cite
Wogonin	Induce ROS to trigger ERS, and then induce ICD.	PRK/PEKR/eIF2α	Xie Y et al. (11)
Oleanolide	Blocking Na+/Ca2+ exchange can trigger ERS, promote the production of ROS, and then induce ICD.	PERK/eIF2α/ATF4/CHOP	Tang Z-Y, et al. (249)
resveratrol	Promote apoptosis and autophagy, thus inducing ICD.	NGFR/AMPK/mTOR	Farras M et al. (76)
Cinobufagin	Inducing ICD	Upstream STAT pathway	Liang D et al. (12)
alkannin	Activate receptor and mitochondrial mediated apoptosis pathway, thus triggering ICD.	Regulating aspartate aminotransferase (GOT) to mediate ferritin phagocytosis; Stimulate RIPK1 and RIPK3-dependent necrosis and up-regulate DAMPs; ROS accumulation, NF-κB pathway activation	Tang D et al. (14) Zhang W et al. (15)
Adriamycin, daunorubicin	Directly inhibit the synthesis of DNA and RNA, kill tumor cells, and induce ICD in tumor cells.	Tumor cells release DAMPs	Lei G et al. (5)
Oxaliplatin	The formation of DNA adducts induces apoptosis of tumor cells and triggers ICD.	Tumor cells release DAMPs	Xie Y et al. (11) Tang Z-Y et al. (249)
Chemotherapeutic drugs such as cyclophosphamide and paclitaxel.	Inducing ICD can improve the anti-tumor effect and promote the apoptosis of tumor cells.	DAMPs, PGE_2, STAT3	Zhao Y et al. (28)
PD-1/PD-L1 inhibitor	Relieve immunosuppression and improve the body's ability to recognize and remove antigens produced by ICD.	Suppression immune checkpoint	Farras M et al. (76)
Drugs for relieving tumor hypoxia microenvironment	Improve the tumor hypoxia microenvironment and promote the normal running of immune cell function	The anaerobic respiration of tumor cells increases and lactic acid accumulates, which damages the function of immune cells; Tumor neovascularization enhances the invasion of tumor cells	Song L et al. (250)
4- phenylbutyric acid (4-PBA)	Inhibition of endoplasmic reticulum stress response, thereby inhibiting ICD induced by ERS	ROS-based endoplasmic reticulum stress-related pathway	Rellmann Y et al. (251)
adenosine	Inhibit the function of various anti-tumor immune cells and enhance the activity of immunosuppressed cells.	Adenosine -A2AR	Bao W D et al. (17), Song L et al. (250)

The purpose of using bold numerical values: References for ICD-related mechanisms and pathways.

selenium, an essential component of the active center of GPX4, can upregulate GPX4 expression through selenite or selenomethionine (Se-Met). Yao (150) et al. confirmed that Se-Met supplementation can increase the survival rate of GPX4-deficient Tfh cells by about 35%, and increase the antibody titer of influenza-vaccinated mice by 2–3 times, revealing the protective effect of the "selenium-GPX4 axis" on T cell function.

There is significant heterogeneity in the effects of ferroptosis on T cell subsets: CD8+ T cells are highly sensitive to GPX4 inhibitors (such as RSL3), and low doses of the drug can induce ferroptosis; however, regulatory T cells (Tregs) rely on GPX4 to resist oxidative stress after activation. Cheng et al. used the Foxp3YFP-Cre Gpx4FL/FL mouse model and found that GPX4-specific deletion in Tregs leads to lipid peroxide accumulation and triggers ferroptosis, accompanied by an increase in the proportion of Th17 cells and an enhanced anti-tumor immune response (151). This difference is due to significant differences in their metabolic characteristics: Tregs generate NADPH through the fatty acid oxidation (FAO) pathway (dependent on malate dehydrogenase and IDH1), maintaining a high GSH/GSSG ratio to resist lipid peroxidation. In addition, Tregs highly express glutaminase (GLS), which provides active support for GPX4 through glutamine metabolism. In contrast, CD8+ T cells rely on glycolysis for energy, and their rapid proliferation leads to an increase in the proportion of polyunsaturated fatty acids (such as arachidonic acid and adrenic acid) in membrane phospholipids. In addition, the insufficient amount of NADPH produced by glycolysis makes it difficult to effectively neutralize lipid peroxidation damage (152), which makes them significantly more sensitive to GPX4 inhibitors than Tregs.

In addition to GPX4, multiple molecules are involved in regulating T cell ferroptosis. The CD36 receptor, which is highly expressed on the surface of CD8+ T cells, promotes lipid droplet formation and increases the content of PUFAs in membrane phospholipids by mediating the uptake of palmitic acid and arachidonic acid, ultimately inducing ferroptosis (122). Targeting CD36 or supplementing with GSH precursors (such as N-acetylcysteine) can significantly increase the survival rate of CD8+ T cells, making them potential protective strategies. ACSL4

promotes the integration of PUFA into membrane phospholipids by catalyzing the esterification of PUFA to generate PUFA-CoA, making CD8+ T cells 2–3 times more sensitive to GPX4 inhibitors (152). It is worth noting that the immunomodulatory effect of ferroptosis is not limited to T cells themselves. For example, OTUD1 in colorectal cancer cells promotes iron uptake mediated by TfR1 by stabilizing iron response element binding protein 2 (IREB2), which exacerbates ROS production and induces ferroptosis. Metabolites such as HMGB1 and glutamate released by dead cells can reshape the immune microenvironment through a dual mechanism (153): HMGB1 binds to TLR4 on the surface of DCs, activates the NF-κB pathway to promote DC maturation and MHC molecule expression, and then activates tumor antigen-specific CD8+ T cells; glutamate indirectly promotes DC migration by regulating metabolic balance, and directly recruits tumor-reactive T cells as a chemokine factor, ultimately shifting the ratio of effector T cells/regulatory T cells in the tumor microenvironment towards the pro-inflammatory direction.

Additionally, under the stimulation of DAMPs, T cell responses exhibit a dual-track regulatory mechanism. First, DAMPs (such as HMGB1 and ATP) exert their effects through indirect activation of PRR signaling networks. Specifically, DAMPs stimulate TLR4 and NLRP3 inflammasome receptors on the surface of antigen-presenting cells such as dendritic cells, triggering upregulation of co-stimulatory molecules CD80/CD86 and secretion of cytokines such as interleukin-12 (IL-12) and interleukin-6 (IL-6), thereby creating a pro-inflammatory microenvironment that enhances T cell activation. A classic example is HMGB1 inducing Th1 cell differentiation through the TLR4 pathway, thereby enhancing antitumor immune effects (Tang et al., 2010) (154). Second, some DAMPs (such as HSP70) can directly act on the TLR2/4 receptors on the surface of T cells, regulating T cell function through a dual mechanism—promoting the proliferation of effector T cells while inhibiting the immunosuppressive activity of regulatory T cells (Tregs). This direct regulatory mechanism has demonstrated unique advantages in tumor immunotherapy (Wang et al., 2016) (155). This multi-level interaction pattern reveals the complex network of DAMPs in the regulation of immune homeostasis.

However, ferroptosis has significant bidirectional effects on immune system regulation: on the one hand, inducing Tregs ferroptosis can relieve immunosuppression and significantly enhance effector T cell activity; on the other hand, excessive activation of CD8+ T cell ferroptosis can lead to a decline in their antitumor function. This contradiction is particularly prominent in the clinical application of GPX4 inhibitors: although these drugs can enhance the immune response by clearing Tregs, their toxic effects on CD8+ T cells limit their efficacy (151, 152, 156). Key issues that need to be urgently addressed include: how to use the metabolic differences between T cell subsets (e.g., Tregs rely on FAO and CD8 + T cells rely on glycolysis) to design selective regulation strategies; the safety and efficacy of selenium supplements or CD36 inhibitors in tumor immunotherapy still need to be verified in large-scale clinical trials. Although studies have explored the therapeutic regimen of selenium compounds combined with PD-1 antibodies, the molecular mechanism still needs to be further analyzed, which provides an important research direction for the development of precise ferroptosis regulation strategies.

3.1.2.2 B cells

Ferroptosis, an iron-dependent lipid peroxidation-driven form of programmed cell death, exhibits unique subset-specific effects in B cell immunoregulation. The functional heterogeneity of B lymphocytes is derived from their subset-specific biological characteristics: B cells can be divided into two major subsets, B1 and B2, based on differences in CD5 expression, and B2 cells are further subdivided into marginal zone (MZ) B cells and follicular (Fo) B cells (157). B1 cells participate in the innate immune response by rapidly secreting natural antibodies, but lack the ability to form memory cells. MZ B cells are located in the marginal zone of the spleen and are responsible for capturing circulating antigens in the blood to initiate an early immune response. Fo B cells reside in lymphoid follicles and mediate long-term immune memory by participating in germinal center responses. It is noteworthy that these subsets have significant differences in their sensitivity to oxidative stress: B1 and MZ B cells have high expression of key enzymes involved in lipid synthesis, such as acetyl-coenzyme A carboxylase (ACC) and fatty acid synthase (FASN), resulting in elevated levels of ROS in the cells, and are therefore highly dependent on GPX4 to maintain redox homeostasis (158). GPX4 binds to reduced GSH through its selenocysteine residue and catalyzes the reduction of lipid peroxides, converting the peroxyl bond into a non-toxic hydroxyl radical, thereby maintaining the stability of cell membrane lipids (159). In the absence of GPX4, the chain reaction of lipid peroxidation gets out of control, and free iron ions generate hydroxyl radicals through the Fenton reaction, leading to the destruction of cell membrane integrity. Relevant studies have shown that in GPX4 knockout models of B1 and MZ B cells, malondialdehyde (MDA) levels were significantly elevated, accompanied by increased cell membrane permeability, ultimately leading to increased cell mortality and impaired antibody secretion (160). In contrast, Fo B cells showed greater tolerance to GPX4 deficiency due to the antioxidant defense mechanism that depends on the thioredoxin system (consisting of Trx, TrxR, and NADPH). This system uses TrxR to reduce Trx with NADPH, which maintains the reduced state of intracellular proteins through disulfide bond exchange, thereby maintaining cell survival in the event of a GPX4 functional defect (161). This difference in antioxidant strategies between subpopulations provides an important molecular target for the targeted regulation of B cell immune responses.

In pathological microenvironments, the differences in ferroptosis susceptibility of B cell subsets significantly affect the anti-tumor immune response. In ovarian cancer, for example, oxidative stress in the tumor microenvironment leads to the accumulation of lipid peroxides (such as 4-hydroxy nonenal, HNE) by depleting GSH and activating 5-LOX, selectively inducing ferroptosis of B1 and MZ B cells (160). In addition, relevant studies have shown that the expression level of GPX4 in B1/MZ B cells in tumor tissue from liver cancer patients is

significantly lower than that in normal tissue, while the expression of 5-LOX is significantly higher (162). Mechanistic studies have shown that oxidative stress further upregulates 5-LOX expression by activating the Nrf2 signaling pathway, forming a vicious cycle of "oxidative stress-lipid peroxidation", which leads to impaired humoral immune function and the expansion of myeloid-derived suppressor cells (MDSCs), thereby promoting tumor immune escape (160).

The regulatory effect of ferroptosis in B-cell lymphoma shows significant subtype specificity. The germinal center B-cell-like (GCB) subtype of diffuse large B-cell lymphoma (DLBCL) is highly sensitive to the ferroptosis inducer dimethyl fumarate (DMF) due to low GPX4 expression and high 5-LOX expression (163). DMF inhibits GPX4 activity by reducing the GSH/GSSG ratio and forms a positive feedback loop with 5-LOX, which synergistically increases lipid peroxidation levels by 3–5 times and significantly induces tumor cell death. In contrast, the activated B-cell-like (ABC) subtype is resistant to ferroptosis, but DMF can enhance the killing effect of chemotherapeutic drugs by inhibiting the NF-κB and STAT3 signaling pathways and significantly downregulating the expression of the anti-apoptotic protein BCL-2. Gene expression profiling analysis shows that the expression of GPX4 and genes related to GSH synthesis in the GCB subtype is significantly lower than that in the ABC subtype, while the expression of BCL-2 in the ABC subtype is significantly higher. This molecular characteristic provides a basis for the development of subtype-specific treatment strategies (164, 165).

Under the stimulation of DAMPs, B cell responses exhibit a bidirectional characteristic of both effector and regulatory functions. On the one hand, B cells enhance humoral immune responses through pattern recognition mechanisms. For example, endogenous DAMPs (such as DNA fragments and uric acid crystals) can directly activate TLR9 receptors and NLRP3 inflammasome signaling pathways in B cells (166), driving B cells to differentiate into plasma cells and significantly enhancing the secretion of antibodies such as IgG and IgM. Specifically, mitochondrial DNA (mtDNA) as a DAMP can induce autoantibody production through the TLR9 pathway (Caielli et al., 2016) (167), revealing the triggering role of endogenous molecules in autoimmune responses. On the other hand, B cells also exhibit immune regulatory functions, responding specifically to protein-based DAMPs such as S100A8/A9 and secreting anti-inflammatory cytokines such as IL-10 to form a negative feedback regulatory loop, effectively suppressing excessive inflammatory responses (Shen et al., 2014) (168). This dual response pattern reflects the multidimensional role of B cells in DAMPs-mediated immune homeostasis regulation.

Although ferroptosis shows great potential in B cell immunomodulation and tumor therapy, the current treatment of DLBCL still faces significant challenges: the sensitivity of the GCB subtype to ferroptosis and the resistance of the ABC subtype create a therapeutic dilemma. This difference stems from the essential differences in metabolic characteristics and signaling pathways: the redox imbalance of the GCB subtype makes it vulnerable to ferroptosis, while the high expression of BCL-2 in the ABC subtype gives it an anti-apoptotic survival advantage. Solving this dilemma requires the development of precision targeting strategies, such as nanomedicine delivery systems based on surface markers of B cell subsets (such as CD10 and MUM1), which can achieve selective drug delivery by targeting specific surface antigens on tumor-associated B cells, thereby reducing damage to normal B cell subsets (169). In addition, the combination of ferroptosis inducers and BCL-2 inhibitors may be an effective strategy for overcoming subtype differences. By simultaneously targeting the ferroptosis pathway and anti-apoptotic mechanisms, the killing effect on both GCB and ABC subtypes is synergistically enhanced, thereby improving the overall treatment effect of DLBCL.

3.1.2.3 Neutrophile

The core mechanism of ferroptosis is uncontrolled lipid peroxidation, and the key regulatory hub is the GSH metabolic system, in which GPX4 plays a vital role. GPX4 catalyzes the reduction of lipid peroxides through selenocysteine (Sec) in its active center, as follows: LOOH+2GSH→GPX4LOH+GSSG+H2O LOOH+2GSHGPX4LOH+GSSG+H2O

The selenol group (-SeH) of selenocysteine is directly involved in electron transfer and is 100 times more catalytically efficient than regular cysteine (15). In PMN-MDSCs (polymorphonuclear myeloid-derived suppressor cells), downregulated GPX4 expression and dysfunction of System Xc^- (cystine/glutamate antiporter) lead to GSH depletion, which triggers a chain reaction of lipid peroxidation (170). For example, RSL3 inhibits the activity of GPX4 by covalently binding to its Sec residue (171), while Erastin blocks System Xc^-, further exacerbating GSH depletion. Lipid peroxidation products such as oxidized phosphatidylethanolamine (PEox) generate hydroxyl radicals through the Fenton reaction, which directly damage cell membrane integrity and release toxic aldehydes (such as malondialdehyde, MDA) (172).

Immunosuppression is mediated by multiple mechanisms, including peroxidation of PUFAs to generate PEox and prostaglandin E2 (PGE2). PEox activates Toll-like receptor 4 (TLR4), induces NF-κB-dependent PD-L1 expression, and directly inhibits CD8+ T cell function (173). PGE2 promotes the secretion of IL-10 and TGF-β by PMN-MDSCs and inhibits T cell proliferation by binding to EP2/EP4 receptors (174). Fatty acid transport protein 2 (FATP2) promotes arachidonic acid (AA) uptake and enhances the supply of lipid peroxidation substrates (175). In a FATP2 knockout mouse model, AA uptake by PMN-MDSCs was significantly reduced, resulting in decreased PEox levels and partial restoration of T cell activity (175).

The tumor microenvironment (TME) enhances the ferroptosis sensitivity of PMN-MDSCs through multiple pathways. Hypoxia stabilizes HIF-1α, which binds to the hypoxia response element (HRE) of the GPX4 promoter to inhibit GPX4 transcription (176). Tumor cells competitively uptake cystine through high expression of SLC7A1, which leads to impaired GSH synthesis in PMN-MDSCs (177). At the same time, IL-6 and TNF-α secreted by TAMs (tumor-associated macrophages) promote ROS accumulation through NOX2 activation, forming a vicious cycle of oxidative stress-ferroptosis (178). Iron-dead PMN-MDSCs highly express CD71 (transferrin receptor 1) on their surface, which transmits inhibitory signals

through interactions with T cells and releases TGF-β and oxidized lipids, synergistically suppressing anti-tumor immunity (179).

Under the stimulation of DAMPs, the response of neutrophils exhibits dual characteristics of rapid response and effect amplification: on the one hand, DAMPs (such as IL-1α and ATP) activate endothelial cells, promoting the release of chemokines such as CXCL8, forming concentration gradients to guide neutrophils to migrate directionally to the injury site. Simultaneously, they directly activate the intracellular NADPH oxidase system, triggering a burst of ROS, thereby executing pathogen clearance functions (McDonald et al., 2010) (180); on the other hand, specific DAMPs (such as mitochondrial DNA and HMGB1) can stimulate neutrophils to initiate programmed cell death mechanisms, releasing extracellular traps (NETs) composed of chromatin and granular proteins. Although these reticular structures can effectively capture and inactivate pathogens, excessive activation may lead to damage to surrounding tissues (Jorch et al., 2017) (181), demonstrating the precise regulation of neutrophil function by DAMPs in acute inflammatory responses.

However, ferroptosis regulation also presents contradictions and challenges in treatment. The ferroptosis inhibitor liproxstatin-1 can reduce the immunosuppression of PMN-MDSCs, but protect tumor cells from ferroptosis, leading to an increased risk of metastasis (170). The GSH synthesis enhancer N-acetylcysteine (NAC) can restore the GSH level of PMN-MDSCs, but high doses may induce oxidative stress (182). Current solutions include targeted delivery systems, such as CD66b antibody-conjugated nanoparticles for the selective delivery of RSL3 to PMN-MDSCs; and metabolic-specific interventions, such as inhibiting CPT1A (a key enzyme in fatty acid oxidation) in PMN-MDSCs to block NADPH regeneration and enhance ferroptosis sensitivity (170). In terms of clinical application, the GPX4 agonist selenomethionine (Se-Met) upregulates GPX4 expression in a liver cancer model, and in combination with a PD-1 antibody, it significantly improves the complete response rate (CR) (183).

In summary, ferroptosis constructs an immunosuppressive network in PMN-MDSCs through the GSH depletion-GPX4 inactivation-oxidative lipid accumulation axis, providing a theoretical basis for the development of "ferroptosis-immunometabolism" dual-targeted therapy.

3.1.2.4 Macrophage

The core mechanism of ferroptosis involves the dual effects of "danger signal" release and metabolic reprogramming, which regulate the remodeling of the macrophage inflammatory and polarized phenotype to reshape the tumor immune microenvironment. Lipid mediators (such as SAPE-OOH) and DAMPs such as HMGB1 and ATP released from ferroptotic cells can be used as "find me" and "eat me" specific signals to activate the macrophage immune response through pattern recognition receptors (PRRs) (184). HMGB1 activates the MyD88/TRIF-dependent NF-κB pathway by binding to the RAGE and TLR2/4 receptors, which promotes the synthesis and release of core inflammatory mediators such as IL-6 and TNF-α by macrophages (185): IL-6 activates and maintains the inflammatory response, promotes T cell proliferation and differentiation, and enhances the immune response; TNF-α has antitumor activity, induces apoptosis of tumor cells, promotes infiltration of inflammatory cells, and enhances the killing of tumor cells by immune cells (186). KRAS mutant protein and HMGB1 synergistically induce macrophage polarization to M1 type through the STING pathway, enhancing antitumor immunity (187); while SAPE-OOH directly binds to TLR2 on the surface of macrophages, enhancing the phagocytic clearance of ferroptotic cells (188). In addition, ferroptosis can induce the expression of various inflammation-related genes such as CCL2 and CCL7, thereby promoting the recruitment and chemotaxis of macrophages.

It is worth noting that the immunomodulatory effect of DAMPs is bidirectional: in hepatocellular carcinoma, HMGB1 promotes CD8+ T cell infiltration through the STING pathway, and its high expression is positively correlated with patient survival (189); however, in acute inflammation models, excessive release of HMGB1 can activate caspase-1 through the AIM2 inflammasome, promote the maturation and release of IL-1β and IL-18, and exacerbate tissue damage (190). Iron-killed tumor cells may release specific proteins (such as those encoded by the K-RasG12D gene) that are mediated by RAGE, which polarizes macrophages to the M2 phenotype through the signal transducer and activator of transcription 3 (STAT3) fatty acid oxidation pathway (187); at the same time, under certain conditions (intervention of ferroptosis inducers or KRAS mutation), 8-hydroxyguanine (8-OHG) released from iron-killed cells induces macrophages to secrete pro-inflammatory factors such as IL-6 by activating the STING pathway, promoting the infiltration of TAMs and M2 polarization (187), and forming an inflammatory environment that is conducive to tumor growth.

In the tumor microenvironment, ferroptosis drives macrophage phenotype conversion through metabolic reprogramming. KRAS mutant proteins activate mTORC1 through the RAF-MEK-ERK pathway, promote glycolysis (upregulation of HK2 and LDHA) and DNA methylation (mediated by DNMT1), and induce M2 polarization (187, 191). 8-hydroxyguanine (8-OHG) activates the cGAS-STING-IRF3 axis, which significantly increases IFN-β secretion and promotes M1 polarization. This polarization regulation is dynamically affected by microenvironmental factors: hypoxia inhibits GPX4 transcription through HIF-1α, which enhances ferroptosis sensitivity (192); tumor cells with high SLC7A11 expression block macrophage glutathione synthesis by competitively consuming cystine (177); TAMs secrete IL-6/TNF-α to activate NOX2, which exacerbates ROS accumulation and forms a positive feedback loop of "oxidative stress-ferroptosis" (187).

Additionally, macrophages exhibit synergistic characteristics of dynamic phenotypic conversion and functional remodeling in response to DAMPs: during the acute injury phase, DAMPs (such as high-mobility group box protein B1 and adenosine triphosphate) activate the Toll-like receptor 4/P2X7 receptor pathway, which in turn activates the NF-κB and NLRP3 inflammasome, driving macrophages toward M1 polarization and the secretion of pro-inflammatory factors such as interleukin-1β(IL-1β) and tumor necrosis factor-α (TNF-α), thereby establishing an efficient

pathogen clearance mechanism (Gong et al., 2020) (86). In the chronic injury microenvironment, DAMPs such as fibrinogen induce the expression of arginase 1 (Arg1) and IL-10 through the integrin signaling pathway, promoting the conversion of macrophages toward the M2 phenotype to support tissue repair (Wynn et al., 2013) (193). Furthermore, DAMPs such as calretinin significantly enhance macrophage phagocytic activity through "eat me" signals such as CD91, accelerating the clearance of apoptotic cells to maintain tissue homeostasis (Gardai et al., 2005) (194).This multimodal response mechanism enables macrophages to precisely regulate between immune defense and tissue repair based on the type and duration of DAMPs.

The new delivery system shows clinical potential against the double-edged sword effect of ferroptosis therapy. Sorafenib nanoparticles wrapped in platelet membranes can specifically target TAMs, resulting in a significant decrease in the M2/M1 ratio in a pancreatic cancer model (187, 195). Exosomes modified with an antibody against CD206 deliver dimethyl fumarate (DMF) to M2 macrophages, reducing the incidence of hepatotoxicity (196). The combination of low-dose RSL3 and a PD-1 antibody significantly increased the complete response rate in melanoma (197) Notably, ferroptosis-induced immunoregulation involves epigenetic regulation: inhibition of apolipoprotein C1 (APOC1) can downregulate GPX4 activity (198), promote HMGB1 release through the MCP-UFM1-PIR axis, activate the HMGB1-RAGE-NF-κB signaling cascade (199), effectively trigger immunogenic ferroptosis, ultimately induce macrophage polarization towards the M1 type and enhance antigen presentation capacity, and produce a synergistic anti-tumor effect with PD-1 antibodies.

Current research focuses on precisely regulating the temporal and spatial effects of ferroptosis: selectively protecting normal tissue macrophages by selenomethionine to enhance the sensitivity of TAMs to ferroptosis; developing ferritin/iron transporter regulators to intervene in the balance of M1-M2 polarization; and using magnetic nanoparticles to target and induce the repolarization of M2 to M1 phenotype. These strategies aim to break through the core contradiction of ferroptosis therapy—how to induce immunosuppressive M2 macrophage ferroptosis while avoiding tissue damage caused by excessive activation of pro-inflammatory M1 type—and provide a new paradigm for solid tumor immunotherapy.

3.2 Immune cell death regulation ferroptosis

3.2.1 Influence of immune microenvironment on ferroptosis

Immune microenvironment (TME) plays a key role in the development of tumor, and it can regulate the ferroptosis of tumor cells in many ways. Since lipid peroxidation is one of the signs of ferroptosis and is highly correlated with lipid metabolism, lipid metabolism is an important medium for ferroptosis. Intracellular fatty acids (FA) mainly come from blood and lymphatic vessels, and the level of FA is precisely regulated by the cellular conditions and external stimuli. FA oxidation is an important energy source for cancer cells. TME can affect the utilization of lipid by cancer cells through the interaction with adjacent substrates. According to this concept, lipid metabolism can regulate tumor hypoxia environment by activating hypoxia inducible factor (HIF) (200). However, in the process of tumor development, tumor cells may release some FA into TME, thus affecting the function of infiltrating immune cells, such as the transition from TAM to M2 phenotype. In addition, when lipids accumulate in DC, the antigen presenting function of DC is impaired, which further leads to the impairment of T cell response and anti-tumor immunity. Therefore, lipid metabolism is an important regulator of TME and ferroptosis of tumor cells (201). It is reported that prostaglandin E2(PGE2) can change the condition of TME by inhibiting the functions of NK cells, cytotoxic T cells and conventional type 1 dendritic cells (cDC1), which can further affect lipid metabolism (202).

In addition, related studies have found that there may be an endogenous trigger of ferroptosis in tumor cells-cystine limitation (203). That is, the degradation of cysteine induced by cyst(e)inase treatment will lead to ferroptosis of tumor cells, which is due to the decrease of GSH and the increase of ROS (204). The metabolic activity of tumor can also affect the changes of TME, and immune escape can be achieved by inhibiting the function of T cells (205, 206). The results show that the metabolic response triggered by T cells can affect the terminal fate of tumor cells. Therefore, improving the metabolism related to ferroptosis in tumor is expected to improve the effect of tumor immunotherapy and new insights.

3.2.2 The interaction mechanism and treatment strategy of the tumor immune microenvironment and ICD

TIME dynamically regulates the initiation and effector phases of ICD through a complex immunosuppressive network, acting as a key barrier to limit the anti-tumor immune response. In tumors with low immune infiltration (i.e., "cold tumors") or immune exclusion, the immunosuppressive properties of TIME significantly impair the efficiency of ICD. This is manifested by insufficient infiltration of antigen-presenting cells (APCs), which results in the failure to effectively capture DAMPs (e.g., ATP, HMGB1) released by dying tumor cells, thereby inhibiting cross-presentation of antigens and activation of cytotoxic T lymphocytes (CTLs) (82). In addition, co-inhibitory receptors highly expressed in TIME (e.g., CTLA-4, TIM-3) directly block APC recognition of "eat me" signals (e.g., calreticulin) by binding HMGB1 or phosphatidylserine (82). Metabolic reprogramming further exacerbates immunosuppression, such as the conversion of extracellular ATP to adenosine mediated by the CD39/CD73 axis, which not only inhibits CTL function but also promotes T cell exhaustion by activating the adenosine A2A receptor (ADORA2A) (207).

Despite the multiple suppressive factors in TIME, ICD can be activated by the release of DAMPs to activate an adaptive immune response. The specific mechanisms include: DAMPs can activate dendritic cells (DCs) to remodel the immune response network and

coordinate multidimensional antitumor immune effects (208). When DAMPs, such as HMGB1 and ATP, bind to pattern recognition receptors (PRRs) on the surface of DCs (e.g., TLR and NLRP3), they trigger DC maturation, enhance antigen processing and presentation capabilities (86), and promote the secretion of proinflammatory factors such as IL-12 and TNF-α, as well as CCR7-mediated lymph node homing. Activated DCs directly activate CD8+ T cells through the MHC-costimulatory signaling axis, inducing their differentiation into cytotoxic T lymphocytes (CTLs) (10), and regulate the polarization of CD4+ T cell subsets (e.g., Th1/Th17/Treg) to adapt to the demands of the immune microenvironment (154). In addition, DCs drive B cell differentiation into plasma cells through the secretion of BAFF/APRIL and cell contact-dependent signals, promoting the production of high-affinity antibodies (166, 167). They also release CXCL8/GM-CSF to recruit neutrophils and enhance their phagocytic and NET formation abilities (181). Exosome-mediated antigen information exchange and IFN-γ signal transduction between DCs and macrophages further amplify the proinflammatory and antigen-presenting functions of M1-type macrophages (193). This cascade reaction initiated by the DAMPs-DC axis not only strengthens the synergistic effects of innate and adaptive immunity but also provides a theoretical framework for DC-targeted vaccine design or combined immune checkpoint blockade therapy (209). For example, CRT and other DAMPs can be used to enhance the efficacy of DC vaccines, or IL-10 signaling can be blocked to reverse the immunosuppressive microenvironment, thereby optimizing the anti-tumor immune response (210).

In addition, ATP drives DC maturation and recruits CTLs to the tumor site by binding to the purine receptor P2RX7; and HMGB1 activates Toll-like receptor 4 (TLR4) to enhance pro-inflammatory signaling to accelerate the ICD process (207). However, the inhibitory factors in TIME (such as IL-10 and TGF-β1) and the functional defects of immature DCs lead to a 30%-50% decrease in antigen cross-presentation efficiency (211). To break through this bottleneck, a combined intervention strategy has emerged: Shikonin (SHK) and curcumin (CUR) form a self-delivering nanosystem (chitosan-polyethylene glycol nanoparticles, CS-PEG NPs) that synergistically induces endoplasmic reticulum stress and Ca^{2+} homeostasis imbalance, which significantly increases the release of DAMPs, thereby increasing DC maturation and significantly increasing the infiltration density of CTLs in the core region of the tumor (from 5% to 20%) (211), Thus reversing the immunosuppression mediated by regulatory T cells (Tregs) and myeloid-derived suppressor cells (MDSCs). DMAPs remodel the tumor immune microenvironment by inducing immunogenic cell death. Under stress, tumor cells release DAMP molecules (CRT, HMGB1, ATP, and type I IFN). CRT acts as an "eat-me" signal to promote antigen-presenting cells to phagocytose tumor antigens; HMGB1 enhances dendritic cell maturation through TLR4; ATP activates the NLRP3 inflammasome to drive CD8+ T cell activation; type I IFN enhances NK cell killing function through the cGAS-STING pathway while inhibiting Treg activity, thereby reversing immune suppression and restoring the body's antitumor capacity. These combined effects indicate that DMAPs have significant antitumor potential in TIME remodeling (212, 213).

The dynamic interaction between TIME and ICDs not only serves as a barrier to immunotherapy, but also provides potential targets for the development of new combination therapies. When ICDs are used in combination with immune checkpoint inhibitors (ICIs), the neoantigens they release, together with DAMPs, provide a dual "antigen-adjuvant" signal, while anti-PD-1/CTLA-4 antibodies form a triple "antigen-adjuvant-unblocking of inhibition" effect by relieving the inhibitory state of T cells (85). For example, irreversible electroporation (IRE) significantly alleviates the immunosuppressive microenvironment of pancreatic cancer by disrupting the integrity of tumor cell membranes, increasing the release of DAMPs such as HMGB1, and downregulating PD-L1 expression (108). Paclitaxel nanocarriers convert "cold tumors" into highly immunoinfiltrated "hot tumors" by inhibiting STAT3 phosphorylation and polarizing M2 tumor-associated macrophages (TAMs) to the proinflammatory M1 phenotype, increasing the infiltration of CTLs from 15% to 45% (108). The above studies have shown that targeting key TIME nodes such as DAMP release, metabolic reprogramming, and immune checkpoints can effectively enhance the efficacy of ICD. Future research needs to further elucidate the impact of TIME heterogeneity on ICD and develop combined delivery systems with temporal and spatial control characteristics to overcome immunosuppressive networks. As shown in Figure 1.

3.2.3 The tumor microenvironment bidirectionally regulates ferroptosis and immunogenic cell death through metabolic stress, hypoxia, and cytokine networks

3.2.3.1 Threshold effect of metabolic stress

Nutritional deprivation in the TME synergistically regulates ferroptosis and (ICD through multidimensional mechanisms. Cysteine competitive depletion inhibits GSH synthesis, leading to inactivation of GPX4 and driving lipid peroxidation-dependent ferroptosis; this process is exacerbated under glucose deprivation conditions due to AMPK-mediated fatty acid oxidation (FAO) pathway activation, forming a positive feedback loop of lipid peroxidation substrate accumulation (Kshattry et al., 2019; Liu et al., 2021) (202, 204). Concurrently, nutritional deprivation triggers endoplasmic reticulum stress (ERS), promoting the surface exposure of calretin (CRT) via the unfolded protein response (UPR), thereby enhancing the immunogenicity of tumor cell ICD (Garg et al., 2012) (208). However, when nutritional deprivation exceeds a critical threshold, ATP synthesis impairment leads to insufficient release of DAMPs, inhibiting antigen cross-presentation by dendritic cells (DCs), and ultimately weakening the immune activation efficacy of ICD (Krysko et al., 2012) (214). This dynamic equilibrium suggests that the intensity of metabolic stress is a key determinant of the direction of tumor immune editing.

3.2.3.2 Spatiotemporal regulation of hypoxia signals

Hypoxia differentially regulates ferroptosis and ICD through the HIF signaling pathway. At the level of ferroptosis, hypoxia inhibits lipid peroxidation through a dual mechanism: 1) HIF-1α/2α upregulates PLIN2, a lipid droplet-associated protein, forming a physical barrier to isolate peroxidation reaction substrates (Zou et al., 2020) (215); 2) IDH1/2-dependent reverse TCA cycle activates the NADPH-GSH antioxidant system, enhancing reducing power reserves (He et al.,

2024) (200). The regulation of ICD is time-dependent: acute hypoxia promotes HMGB1/ATP release through mitochondrial ROS bursts, enhancing DC antigen presentation function (Semenza et al., 2012) (216); chronic hypoxia significantly reduces CD8+ T cell infiltration through HIF-1α-mediated immunosuppressive metabolic reprogramming, blocking the immune effects of ICD (Noman et al., 2014) (217). This spatiotemporal heterogeneity reveals the dynamic regulatory nature of hypoxia in tumor immune escape.

3.2.3.3 Immunometabolic regulation of cytokine networks

The cytokine profile in the TME precisely regulates the interaction between ferroptosis and ICD by shaping the pro-inflammatory/anti-inflammatory balance. Pro-inflammatory factors such as IFN-γ weaken GSH synthesis by downregulating the cystine transporter SLC7A11, thereby enhancing ferroptosis sensitivity (Wang et al., 2020) (10); TNF-α releases DAMPs such as HMGB1 through necroptotic apoptosis, forming synergistic immune activation with ICD (Vandenabeele et al., 2022) (209). In contrast, the immune-suppressive factor TGF-β enhances antioxidant defense through the Smad3/GPX4 pathway (Tang et al., 2021) (19), while IL-10 blocks immune surveillance by inhibiting DC maturation (Vegran et al., 2011) (210). Notably, the IL-6/JAK2/STAT3 pathway exhibits bidirectional regulation: it promotes the accumulation of PUFAs by activating fatty acid synthase (FASN), thereby increasing the risk of ferroptosis, while simultaneously inhibiting CRT exposure to weaken the immunogenicity of ICD (Johnson et al., 2020) (201). This multi-layered cytokine interaction network provides a theoretical basis for combined therapeutic strategies targeting the TME.

3.2.4 Regulatory role of immune cells

3.2.4.1 Neutrophil granulocyte

Tumor-associated neutrophils (TANs) regulate ferroptosis in tumor cells through multiple mechanisms. Their direct mechanisms of action include iron overload mediated by NETosis and oxidative damage by myeloperoxidase (MPO). TANs promote lipid peroxidation driven by the Fenton reaction by forming neutrophil extracellular traps (NETs), releasing DNA-histone complexes and capturing free iron in the microenvironment, thereby increasing local iron concentration by 2–3 times. In addition, MPO secreted by TANs can catalyze the production of hypochlorous acid (HOCl) from H_2O_2 and Cl^-, which directly oxidizes tumor cell membrane lipids, resulting in a 4-fold increase in lipid peroxidation and accelerating the ferroptosis process. In glioblastoma (GBM), TANs deliver MPO to tumor cells through cell membrane fusion or exosomes, stimulating a significant increase in lipid peroxidation markers such as MDA. This process is driven by DAMPs released by tumor necrosis: for example, HMGB1 recruits neutrophils to the necrotic area by activating the TLR4/NF-κB pathway, forming a positive feedback loop of "necrosis-DAMP-TAN infiltration" that further amplifies the ferroptosis effect (218, 219).

In addition to direct oxidative damage, TAN also indirectly affects the ferroptosis process by regulating iron metabolism. Under neuropathological conditions, impaired activity of peroxisome proliferator-activated receptor γ (PPARγ) can inhibit lactoferrin (Ltf) transcription, leading to increased free iron concentrations and increased lipid peroxidation levels in neurons, thereby exacerbating ferroptosis. This mechanism suggests that TAN may regulate tumor cell iron homeostasis by secreting iron-binding proteins such as Ltf. However, in a high-sugar microenvironment (such as a diabetes-related tumor), TAN Ltf secretion is inhibited by the ROS-JNK pathway, and its specific regulatory network still needs to be further analyzed (219). It is worth noting that the role of TAN is significantly tissue- and microenvironment-specific: for example, in breast cancer, TAN upregulates the expression of the ferroptosis-sensitive gene ACSL4 through CXCR2 signaling, which significantly increases the response rate of tumor cells to ferroptosis inducers (220).

In summary, TAN is involved in the ferroptosis molecular network through multiple pathways such as NETosis, MPO delivery, and iron metabolism regulation. Its function is dynamically regulated by the concentration of DAMPs, metabolic status, and cell-cell interactions. Future research needs to reveal the precise mechanism of TAN heterogeneity and its spatiotemporal interaction with ferroptosis, in order to provide theoretical support for novel anti-tumor strategies targeting the TAN-ferroptosis axis.

3.2.4.2 T cell

In the tumor microenvironment, T cells regulate tumor cell ferroptosis through multidimensional molecular mechanisms. CD8+ T cells are the core effector cells that drive ferroptosis: after immune checkpoint inhibitors (such as anti-PD-L1 and anti-CTLA4) activate CD8+ T cells, IFN-γ they secrete binds to the tumor cell membrane receptor IFNGR1/2, activating the JAK-STAT1 signaling pathway. Phosphorylated STAT1 enters the nucleus and directly inhibits the cystine/glutamate antiporter system $Xc^{=-}$ (composed of SLC7A11 and SLC3A2), resulting in a 60%-80% reduction in GSH synthesis and a 3-5-fold increase in lipid peroxidation levels due to impaired GPX4 activity (219, 221). At the same time, STAT1 forms a complex with interferon regulatory factor 1 (IRF1), upregulates ACSL4, and promotes the integration of polyunsaturated fatty acids (such as arachidonic acid) into the phospholipids of tumor cell membranes, significantly increasing lipid peroxidation sensitivity (156, 219). In addition, the granule enzyme B released by CD8+ T cells inactivates GPX4 by cleaving its C-terminal domain and degrades ferroptosis suppressor protein 1 (FSP1), resulting in a collapse of the tumor cell's antioxidant defense system (222).

In contrast, regulatory T cells (Treg) inhibit the ferroptosis process through antagonistic mechanisms. Treg highly express GPX4 to maintain their own antioxidant capacity: GPX4 deficiency leads to increased accumulation of intracellular lipid peroxides and ferroptosis, thereby relieving immunosuppression of effector T cells (219). In addition, Treg limit the synthesis of GSH in effector T cells and tumor cells by competing for cystine and glutamine in the tumor microenvironment. For example, in a melanoma model, Treg infiltration significantly reduced tumor cell SLC7A11 expression, leading to resistance to ferroptosis (219).

The metabolic status of T cells and their sensitivity to ferroptosis are characterized by bidirectional regulation. Tumor-infiltrating CD8+ T cells mediate the uptake of oxidized lipids (such

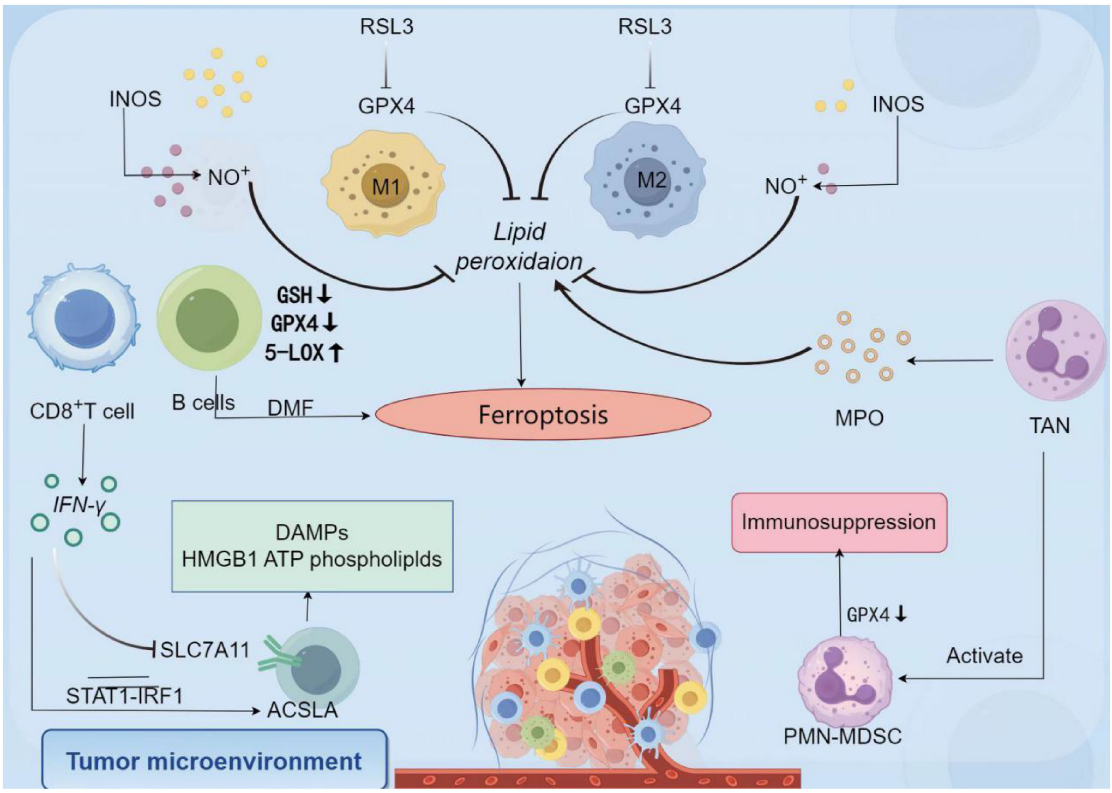

FIGURE 1
Schematic diagram of cross-regulation of ferroptosis and immunogenic cell death in tumor microenvironment. (In the tumor microenvironment, ferroptosis and immunogenic death are cross-regulated through complex mechanisms. In the core pathway of ferroptosis, RSL3 can regulate the GPX4 levels of M1 and M2 macrophages, causing lipid peroxidation and thus promoting ferroptosis. The specific mechanism is as follows: M1 macrophages highly express INOS, which catalyzes the production of a large amount of NO, which promotes lipid peroxidation—a core process of ferroptosis—thereby promoting ferroptosis of tumor cells; M2 macrophages have low expression of INOS and produce little NO, which makes it difficult to effectively induce lipid peroxidation and inhibit ferroptosis. Meanwhile, DMF further promotes lipid peroxidation by reducing intracellular GSH and GPX4 levels and upregulating 5-LOX, which strengthens the ferroptosis process. In terms of immunogenic death, tumor cells release DAMPs such as HMGB1 and ATP when undergoing ferroptosis, and these molecules can activate the immune response. For example, IFN-γ secreted by CD8+ T cells regulates SLC7A11 and ACSL4 through the STAT1-IRF1 pathway, which not only affects ferroptosis-related metabolism but also promotes immune activation. The cross-regulatory network between the two is manifested in many ways. On the one hand, immune cells are involved in the regulation of ferroptosis. M1 and M2 macrophages affect lipid peroxidation through GPX4, thereby regulating the occurrence of ferroptosis. Neutrophil-derived substances such as MPO are also involved in the ferroptosis process. On the other hand, ferroptosis affects the immune microenvironment. Ferroptosis-related signals such as GPX4 downregulation can activate immunosuppressive cells such as PMN-MDSC, leading to immunosuppression. The release of DAMPs, on the other hand, activates the immune response, forming a two-way regulation of "ferroptosis-immune activation-microenvironment remodeling" that ultimately affects tumor development). (Created by Figdraw).

as oxysterols) through CD36, leading to increased intracellular lipid peroxide accumulation and inducing autophagic ferroptosis, which significantly reduces their antitumor activity. Inhibition of CD36 or overexpression of GPX4 can significantly increase the survival rate of CD8+ T cells (122, 222). It is noteworthy that CD8+ T cells are significantly more sensitive to GPX4 inhibition than tumor cells: ACSL4 knockdown significantly reduces ferroptotic cell death, while FSP1 overexpression provides protection through the CoQ10 regeneration pathway (156).

Based on the above mechanism, combined therapeutic strategies targeting the T cell-ferroptosis axis have shown clinical potential: radiotherapy synergizes with immunity, and radiotherapy-induced ATM activation synergistically inhibits SLC7A11 expression with IFN-γ released by CD8+ T cells, significantly increasing lipid peroxidation levels and thus significantly enhancing the therapeutic effect of ferroptosis (223); immune checkpoint inhibitors combined with ferroptosis inducers, anti-PD-1 combined with ACSL4 agonists (such as RSL3), upregulate ACSL4 through the STAT1-IRF1 pathway, making tumor cells more sensitive to T cell-mediated ferroptosis (219); photodynamic therapy (PDT) and immune memory, hemoglobin iron combined with PDT activate CD8+ T cells to release IFN-γ to induce ferroptosis, while the nano photosensitizer MAR releases tumor-associated antigens (TAAs) through ferroptosis, which increases the maturation rate of dendritic cells (DCs) and forms long-lasting anti-tumor immune memory (222, 224).

However, about 30% of tumor cells escape ferroptosis through SLC7A11 overexpression, leading to the failure of immunotherapy. Targeting the ferroptosis resistance pathway (e.g., in combination with the FSP1 inhibitor iFSP1) can reverse drug resistance and

significantly improve the treatment response rate (219, 222). Future research should focus on the dynamic interaction mechanism between T cell metabolic reprogramming and ferroptosis in order to develop more effective combination treatment strategies.

3.2.4.3 Macrophage

Macrophages are directly involved in the process of ferroptosis by regulating iron homeostasis. When red blood cells are abnormally increased or damaged, the macrophage surface receptor natural resistance-associated macrophage protein 1 (Nramp1) mediates red blood cell phagocytosis. After lysosomal digestion, heme oxygenase-1 (HO-1) breaks down heme to release free iron ions (Fe^{2+}). Fe^{2+} produces ROS through the Fenton reaction, which increases lipid peroxidation levels by 2–3 times, thereby triggering ferroptosis in target cells (225–227). In addition, IL-6 regulates iron metabolism by activating the JAK-STAT3/BMP/SMAD pathway: after bone morphogenetic protein 6 (BMP6) binds to the membrane receptor, it induces phosphorylation of SMAD1/5/8 and upregulates hepcidin expression, resulting in the internalization and degradation of the iron transporter FPN, which exponentially increases the amount of intracellular iron accumulation, further exacerbating ferroptosis (228–230).

Macrophage polarization has a bidirectional regulatory effect on ferroptosis. M1 macrophages secrete TNF-α in response to LPS/IFN-γ stimulation, activate the NF-κB/MAPK pathway, upregulate NADPH oxidase 4 (NOX4), significantly increase ROS production, and inhibit the expression of the cystine/glutamate antiporter system Xc^- (SLC7A11/SLC3A2) and GPX4, significantly enhancing ferroptosis sensitivity (221, 231). However, M1 macrophages highly express inducible nitric oxide synthase (iNOS), which catalyzes the production of nitric oxide (NO), and inhibit 15-LOX activity, thereby reducing lipid peroxidation levels and conferring ferroptosis resistance (232, 233). M2 macrophages activate the STAT6 pathway in response to IL-4/IL-13, upregulate ferritin to store free iron, and secrete TGF-β1. Smad3 signaling inhibits the function of the tumor cell system Xc^-, leading to a decrease in GSH synthesis and a doubling of the lipid peroxidation marker MDA level (221, 234, 235).

There is a significant synergistic effect between immune microenvironment remodeling and ferroptosis. Ferroptosis inducers (such as erastin) or nanoparticles (Fe_3O_4-SAS@PLT) can reverse the M2 polarization of tumor-associated macrophages (TAMs) and promote their conversion to the M1 phenotype, resulting in a significant increase in TNF-α and IL-12 secretion, respectively, and a significant improvement in the immunosuppressive microenvironment (222, 236). IL-6 regulates the polarization direction in a concentration-dependent manner: low concentrations activate STAT3 to induce M2 polarization, while high concentrations drive M1 polarization through STAT1, thereby regulating the ferroptosis process (237). In addition, extracellular vesicles released by M1 macrophages carry miR-140-5p, which targets and inhibits the stability of SLC7A11 mRNA in cardiomyocytes, inducing ferroptosis. Ferric citrate, on the other hand, antagonizes ferroptosis by activating the Nrf2 signal, promoting its nuclear translocation and binding to the antioxidant response element (ARE) in the GPX4 promoter region, which exponentially upregulates GPX4 expression (221).

Targeting macrophages in disease treatment strategies has made progress. In non-alcoholic steatohepatitis (NASH), Kupffer cells (KCs) in the liver are polarized to the M1 phenotype, which enhances lipid uptake, increases the level of free fatty acids in hepatocytes, and increases the accumulation of ROS, ultimately exacerbating ferroptosis (238). Inhibiting the TGF-β1/γ-glutamyl transpeptidase 1 (GGT1) axis in TAMs can significantly reduce iron-mediated hepatocyte death (227). In tumor therapy, engineered magnetic microspheres induce TAMs polarization to the M1 phenotype through the TLR4/NF-κB pathway, which reduces the expression of SLC7A11 in tumor cells and thus increases ferroptosis sensitivity (234). Nanoparticles that synergize with iron metabolism (such as chitosan-arabinogalactan/iron complexes CSAA/Fe@PPI) significantly enhance the ferroptosis effect by delivering exogenous $Fe^{3+}$and inducing ferroptin autophagy, which increases the level of the LIP in cells and the lipid peroxidation marker 4-HNE (239).

Although the ferroptosis axis targeting macrophages shows therapeutic potential, key issues still need to be addressed: developing nanoscale vectors with spatiotemporally specific regulation (such as pH or ROS-responsive), precisely regulating iron release and macrophage polarization; elucidating the ferroptosis escape mechanism caused by SLC7A11 overexpression or GPX4 mutation; exploring the impact of macrophage heterogeneity (such as the $TREM2^+$ subset) on ferroptosis regulation and optimizing combined immunotherapy strategies. As shown in Figure 2.

In the tumor microenvironment, the interaction between ferroptosis and immune-competent cell death (ICD) has opened up a new frontier in cancer immunotherapy. Ferroptosis induces tumor cell death through lipid peroxidation, accompanied by the release of immune-stimulatory signals (such as ATP and HMGB1), forming a synergistic effect with ICD. This significantly enhances tumor antigen presentation and activates anti-tumor immune responses. This mechanism not only reshapes the immunosuppressive state of the tumor microenvironment but also provides key targets for breaking immune tolerance and improving the efficacy of immunotherapy.

In preclinical studies, several combination therapy strategies have achieved breakthrough progress and demonstrated significant potential for translation into clinical applications. The combination of ursolic acid and sorafenib inhibits SLC7A11 and reduces GSH synthesis, while significantly increasing lipid peroxidation levels, inducing ferroptosis in cells, and reversing drug resistance in liver cancer cells, thereby exhibiting significant antitumor activity and providing a new therapeutic strategy for tumor treatment. Zero-valent iron nanoparticles (ZVI-NP) can target and enhance the degradation of nuclear factor-E2-related factor 2 (NRF2), inducing ferroptosis in lung cancer cells through the Fenton reaction (with MDA levels increasing exponentially), while polarizing M2-type tumor-associated macrophages (TAMs) to M1-type and reducing the infiltration of regulatory T cells (Tregs) by half. This approach inhibits angiogenesis and weakens the self-renewal capacity of cancer cells, demonstrating great potential as a next-generation cancer therapy that reduces side effects and enhances efficacy (240,

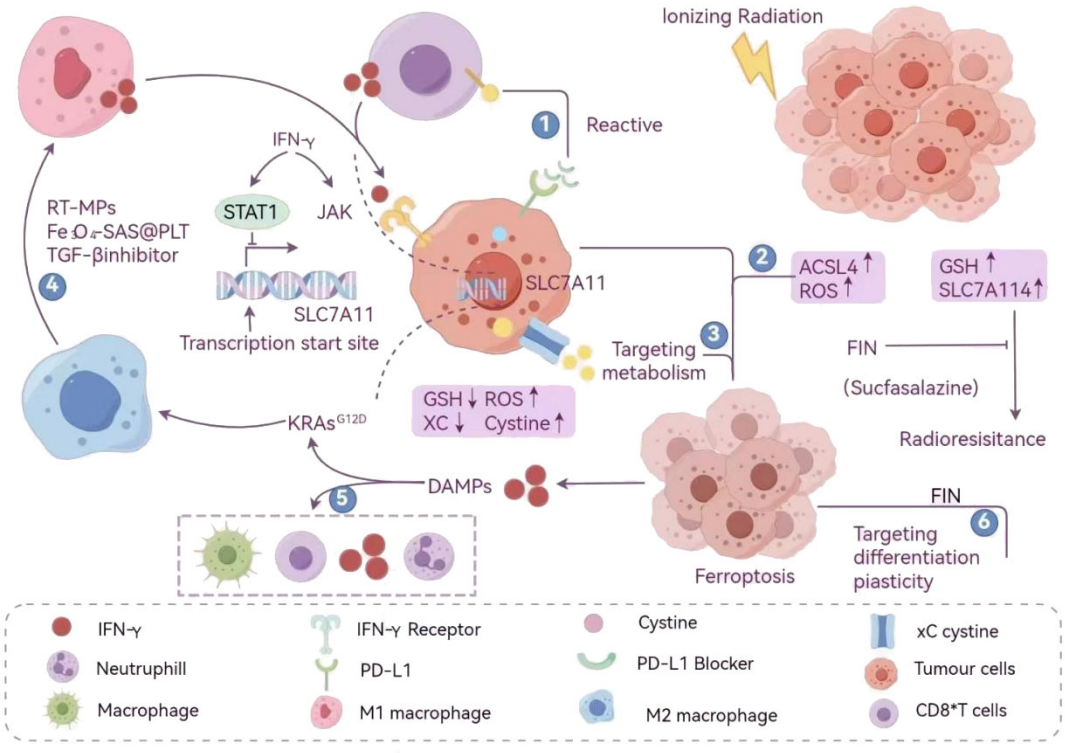

FIGURE 2
Comprehensive schematic diagram of cross-regulation of ferroptosis and immunogenic cell death. (Ionizing radiation activates the ferroptosis core pathway by triggering ROS bursts and lipid peroxidation: on the one hand, it upregulates ACSL4, which promotes the integration of PUFAs into cell membrane phospholipids and enhances oxidative sensitivity; on the other hand, it inhibits cystine/glutamate antiporter (system Xc^-, composed of SLC7A11/SLC3A2), which leads to a decrease in GSH synthesis and loss of GPX4 activity, ultimately triggering ferroptosis. Radiation-induced tumor cell death releases DAMPs, such as ATP and HMGB1, which initiate antigen presentation and recruit CD8+ T cells to form an adaptive immune response. At the level of the immune microenvironment, ionizing radiation and the ferroptosis inducer PIN (sulfasalazine) can have a synergistic effect: IFN-γ inhibits SLC7A11 expression through the JAK-STAT1 signaling pathway, blocking the antioxidant defense of tumor cells; at the same time, the STAT1-IRF1 complex upregulates ACSL4, amplifying the lipid peroxidation effect and significantly increasing ferroptosis sensitivity. M1 macrophages secrete pro-inflammatory factors driven by IFN-γ to activate anti-tumor immunity; and PD-L1 blockers can relieve the inhibition of tumor cells on T cells and enhance the killing function of CD8+ T cells. Neutrophils release free iron and myeloperoxidase (MPO) through NETosis, directly oxidizing the tumor cell membrane and accelerating the process of ferroptosis. The comprehensive treatment strategy is a combination of RT-MPs, Fe_3O_4-SAS@PLT, TGF-β inhibitors, and other methods to regulate immune cells such as M2 macrophages and CD8+ T cells. By targeting metabolic plasticity and differentiation plasticity, a comprehensive anti-tumor mechanism of radiation combined with immune activation and ferroptosis induction is formed). (Created by Figdraw).

241). In addition, liposomes containing prostaglandin 1 (LLI) activated systemic immune responses by inhibiting neutrophil ferroptosis and inducing intracellular cell death (ICD) in tumor cells, resulting in a significant reduction in the volume of distant metastatic lesions.

However, ferroptosis still faces multiple challenges in clinical application. Tumor heterogeneity leads to significant differences in the sensitivity of different cancer types to ferroptosis: gastric cancer is resistant due to low ACSL4 expression levels, while liver cancer is more sensitive due to high SLC7A11 expression levels. Immune cells also face heterogeneity issues: tissue-resident memory T cells (TRMs) often exhibit time-dependent heterogeneity in TRM exhaustion in late-stage tumors due to persistent antigen and TCR stimulation; depending on the distance from the tumor site, TRMs tend to increase in number with proximity, and TRMs can promote or inhibit the progression of different tumor types, exhibiting spatial heterogeneity (242). The immunosuppressive properties of the tumor microenvironment (TME) further limit its efficacy: regulatory T cells (Tregs) suppress ferroptosis by consuming cysteine and secreting IL-10, while tumor cells escape through the Nrf2 pathway by upregulating GPX4 and FSP1. In addition, ferroptosis inducers (such as Erastin) have low bioavailability and may cause liver and kidney damage (significant elevation of transaminases), highlighting the urgent need for the development of precise delivery systems. Similarly, immune cells exhibit varying sensitivity to ferroptosis inducers and interact with tumor cells, posing challenges such as selecting the appropriate inducer type and optimal dose, and developing treatment regimens that evolve with the tumor cycle. Overcoming these challenges is essential for the successful application of ferroptosis and ICD in tumor therapy.

Ferroptosis can activate antigen-presenting cells by releasing DAMP-related molecules, induce immune responses, and trigger anti-tumor immune memory through ICD. However, ferroptic death can also impair the function of immune effector cells, thereby affecting the efficacy of immune responses. Inflammatory factors activated by ICD and ROS produced by stress can promote the development of ferroptic death in tumor cells, thereby achieving anti-tumor effects. Based on the complex regulatory mechanisms of the two, many new therapies have emerged. Numerous novel combined strategies have emerged. Copper-based nanoparticles (HCuSPE@TSL-tlyp-1) induce ferroptosis through the Fenton reaction and release TLR7/8 agonists to activate dendritic cells (DCs), resulting in a significant increase in IFN-γ secretion and an increase in the proportion of CD8+ T cell infiltration. Manganese-based layered double hydroxide (Mn-LDH) nanosheets enhance IFN-γ secretion by activating the STING pathway, synergistically promoting ferroptosis and immune response, and prolonging mouse survival. Dynamic treatment regimens such as pH-responsive nanocarriers (CSAA/Fe@PPI) can precisely increase local tumor iron concentration while avoiding systemic toxicity. Immunotherapy combined with ferroptosis inducers is also one of the novel treatment strategies. Studies have shown that Erastin can reverse the M2 polarization of tumor-associated macrophages (TAMs) and promote their conversion to the M1 phenotype, significantly increasing TNF-α secretion to remodel the immunosuppressive microenvironment (222); BNP@R + L + aPDL1 (benzoic acid ester-functionalized nanoparticles loaded with RSL-3 + laser therapy + anti-PD-L1 antibody) can promote IFN-γ secretion in tumor tissues, inhibit the expression of endogenous SLC3A2 and SLC7A11, leading to a significant accumulation of ROS and lipid peroxides in tumor tissues, thereby promoting ferroptosis in cancer cells and increasing CD8 + T cell infiltration and DC cell maturation to reduce tumor cell metastasis and promote their ICD-mediated death (243).

The current experimental direction and design can focus on solving the problems faced by combined treatment of ferroptosis and ICD. Combined treatment faces the challenge of biological toxicity: ferroptosis can kill normal cells, while ICD may trigger cytokine storms and autoimmune diseases in patients. Faced with the problem of biological toxicity, the experimental direction can be to develop a targeted delivery system based on the tumor microenvironment response. By using nanocarriers to transport drugs, drugs can be released when stimulated by the acidic tumor microenvironment, achieving stimulatory targeted delivery and verifying its targeting *in vivo* and *in vitro*. Tumor heterogeneity causes differences in treatment effects, which is also a challenge for combined treatment: different tumor types may have huge differences in sensitivity to ferroptosis and ICD. The experimental direction can be to find the best inducers for different types of tumors and achieve personalized treatment plans according to the actual condition of patients. Through the design of multi-omics analysis of the molecular differences between sensitive and resistant cells, specific target verification can be carried out, and combined therapy using different inducers can be used for *in vivo* and *in vitro* experiments to find "subtyping-targeted" personalized combination therapies suitable for different tumors. Future research and development efforts can focus on two main directions: analyzing the molecular networks regulating ferroptosis in immune cells (such as TAMs and Tregs) within the tumor microenvironment (TME); and conducting precision clinical trials based on biomarkers (such as ACSL4 and SLC7A11). Despite numerous challenges, the synergistic role of ferroptosis and immune cell death (ICD) has opened up new dimensions for tumor treatment, and its successful translation will depend on the close integration of in-depth exploration of mechanisms and technological innovation.

Document search

1. Literature sources: PubMed (biomedical literature database), Web of Science (SCIE, Science Citation Index Expanded), Embase (biomedical and pharmacological literature database), Chinese Biomedical Literature Database (CBM), China National Knowledge Infrastructure (CNKI); the search period focused on January 1, 2019 to March 15, 2025. The language was limited to Chinese and English literature to ensure data homogeneity.
2. Search method: In order to more comprehensively search for literature that meets the criteria, a cross-search was conducted using keywords. The Chinese search terms were: (ferroptosis) AND (immunogenic cell death OR immune cell OR immunotherapy). The English search terms were: ferroptosis; ((Immunogenic cell death OR ICD) OR immune cell OR T cell OR B cell OR (neutrophile granulocyte OR neutrophil) OR (macrophage OR macrophagocyte Or megalophage); Tumor microenvironment, etc. The search strategy used a combination of subject terms (such as MeSH terms) and free terms, and Boolean operators (AND/OR/NOT) were used to construct an accurate search formula. The search syntax was adjusted for the characteristics of different databases (such as truncation characters in PubMed and synonym expansion in CNKI).
3. The initial search yielded a total of 9,411 relevant literature citations. Two researchers independently performed a preliminary screening of the titles and abstracts of all retrieved documents, and then read the full text of the documents screened in the first round to conduct a second screening based on the inclusion criteria, while recording the reasons for rejection. Duplicate citations were removed: all retrieved citations were imported into NoteExpress software for duplicate checking, and 8,731 were removed after deduplication. 7,966 were excluded in the first round of screening, and 765 were retained in the first round of screening.

(Preliminary screening: According to the exclusion criteria and inclusion criteria, the titles and abstracts of the retrieved entries are initially read to eliminate ineligible literature such as conference papers, technical reports, evaluation studies, and diseases that do not match.)

Secondary screening: According to the exclusion and inclusion criteria, the full text of the obtained literature was carefully read,

and 514 articles that did not meet the inclusion criteria were excluded, and finally 251 articles that met the inclusion criteria were obtained. Inclusion criteria: The research content focuses on the cross-regulatory mechanism of ferroptosis and immunogenic cell death in the tumor microenvironment. The types of research include: basic experiments (cell or animal models) to reveal the molecular pathways of their interaction; clinical studies (such as cohort studies, RCTs) to explore the efficacy of combination therapy (such as ferroptosis inducers + immunotherapy); and mechanistic studies to analyze the effects of ferroptosis on the immune microenvironment (such as T cell infiltration and immune checkpoint expression). The types of literature are original research papers (Articles), reviews, meta-analyses, clinical studies, mechanistic studies, etc., and conference abstracts, reviews, and case reports are excluded. Exclusion criteria: The research subjects are non-tumor diseases (such as neurodegenerative diseases); the research content is not related to the tumor microenvironment; the data is incomplete or there are significant methodological deficiencies (such as insufficient sample size and no statistical analysis).Then, using specific data collection forms, the researchers extracted relevant data from each study, including basic information about the article (first author, year of publication, journal name, and type of study); the experimental model of the research design (e.g., cellular animal model or patient), interventions (e.g., erastin-induced ferroptosis, anti-PD-1 antibody therapy); key regulators of the core mechanism [e.g., Glutathione peroxidase 4 (GPX4), SLC7A11, adenosine triphosphate (ATP) release), signal pathways (e.g., nuclear factor-κB (NF-κB), mitogen-activated protein kinase (MAPK)]; and the main findings of ferroptosis's promotion/inhibition of immunogenic cell death, remodeling effect on the tumour microenvironment, and synergistic effect of combination therapy, as well as the limitations of the experimental model (e.g., lack of clinical verification) and unresolved scientific questions.

Meta-analysis results showed that ferroptosis promotes immunogenic cell death by releasing damage-associated molecular patterns (DAMPs) (e.g., ATP, HMGB1). GPX4 is a central node of ferroptosis and immune regulation, and its low expression is associated with immune activation.

Author contributions

WL: Conceptualization, Funding acquisition, Writing – original draft, Writing – review & editing. YJ: Writing – original draft, Writing – review & editing. YC: Writing – original draft, Writing – review & editing. HS: Conceptualization, Writing – original draft, Writing – review & editing. WX: Conceptualization, Writing – original draft, Writing – review & editing. RL: Writing – original draft, Writing – review & editing, Conceptualization. WLL: Writing – original draft, Writing – review & editing. ZZ: Writing – original draft, Writing – review & editing. HL: Writing – original draft, Writing – review & editing, Funding acquisition, Supervision.

Funding

The author(s) declare that financial support was received for the research and/or publication of this article. National Innovation and Entrepreneurship Training Program for College Students (S202410541090), National Innovation and Entrepreneurship Program for College Students Training Program (S202410541010), Key research funds at the university level of Hunan Traditional Chinese Medicine (2024BKS095), key guidance topics for research projects of the Hunan Health Commission (202305017379), major research funds for high-level health personnel in Hunan (R2023168), Hunan University Student Innovation and Equity Training Program (202210541117), Hunan Natural Science Fund (2022JJ30035), Key topics guided by research projects of the Hunan Health Commission (202305017379), The Hunan Department of Education's Scientific Research Key Project (21A0233).

Conflict of interest

The authors declare that the research was conducted in the absence of any commercial or financial relationships that could be construed as a potential conflict of interest.

Generative AI statement

The author(s) declare that no Generative AI was used in the creation of this manuscript.

Publisher's note

All claims expressed in this article are solely those of the authors and do not necessarily represent those of their affiliated organizations, or those of the publisher, the editors and the reviewers. Any product that may be evaluated in this article, or claim that may be made by its manufacturer, is not guaranteed or endorsed by the publisher.

References

1. Lei X, Lei Y, Li JK, Du WX, Li RG, Yang J, et al. Immune cells within the tumor microenvironment: Biological functions and roles in cancer immunotherapy. *Cancer Lett*. (2020) 470:126–33. doi: 10.1016/j.canlet.2019.11.009

2. Bejarano L, Jordão MJC, Joyce JA. Therapeutic targeting of the tumor microenvironment. *Cancer Discovery*. (2021) 11:933–59. doi: 10.1158/2159-8290.CD-20-1808

3. Xiao FP, Wang WH, Jia B, Luo YB, Xiong LJ, Wu DM, et al. Effects of ferroptosis-related genes on microenvironment and prognosis in hepatocellular carcinoma. *J Cancer Control Treat*. (2024) 37:649–57. doi: 10.3969/j.issn.1674-0904.2024.08.003

4. Casares N, Pequignot MO, Tesniere A, Ghiringhelli F, Roux S, Chaput N, et al. Caspase-dependent immunogenicity of doxorubicin-induced tumor cell death. *J Exp Med*. (2005) 202:1691–701. doi: 10.1084/jem.20050915

5. Lei G, Zhuang L, Gan B. Targeting ferroptosis as a vulnerability in cancer. *Nat Rev Cancer*. (2022) 22:381–96. doi: 10.1038/s41568-022-00459-0

6. Ahmed A, Tait SWG. Targeting immunogenic cell death in cancer. *Mol Oncol*. (2020) 14:2994–3006. doi: 10.1002/1878-0261.12851

7. Galluzzi L, Buqué A, Kepp O, Zitvogel L, Kroemer G. Immunogenic cell death in cancer and infectious disease. *Nat Rev Immunol*. (2017) 17:97–111. doi: 10.1038/nri.2016.107

8. Han X, Xie YH, Park JH. Study on targeted ferroptosis in tumor microenvironment. *J Mudanjiang Med Univ*. (2024) 45:125–8. doi: 10.13799/j.cnki.mdjyxyxb.2024.01.014

9. Li Y, Liao W, Liu F, Ma L, Qian X. Study on new mechanism of antitumor Chinese medicine based on immunogenic cell death. *J Oncol Chin Med*. (2023) 5:86–94. doi: 10.19811/j.cnki.ISSN2096-6628.2023.07.014

10. Wang W, Green M, Choi JE, Gijón M, Kennedy PD, Johnson JK, et al. CD8+ T cells regulate tumour ferroptosis during cancer immunotherapy. *Nature*. (2019) 569:270–4. doi: 10.1038/s41586-019-1170-y

11. Xie Y, Hou W, Song X, Yu Y, Huang J, Sun X, et al. Ferroptosis: process and function. *Cell Death Differ*. (2016) 23:369–79. doi: 10.1038/cdd.2015.158

12. Liang D, Minikes AM, Jiang X. Ferroptosis at the intersection of lipid metabolism and cellular signaling. *Mol Cell*. (2022) 82:2215–27. doi: 10.1016/j.molcel.2022.03.022

13. Lyu Y, Wang T, Huang S, Zhang Z. Mitochondrial damage-associated molecular patterns and metabolism in the regulation of innate immunity. *J Innate Immun*. (2023) 15:665–79. doi: 10.1159/000533602

14. Tang D, Kroemer G. Ferroptosis. *Curr Biol*. (2020) 30:R1292–7. doi: 10.1016/j.cub.2020.09.068

15. Zhang W, Liu Y, Liao Y, Zhu C, Zou Z. GPX4, ferroptosis, and diseases. *Biomedicine Pharmacotherapy*. (2024) 174:116512. doi: 10.1016/j.biopha.2024.116512

16. Xu L, Liu Y, Chen X, Zhong H, Wang Y. Ferroptosis in life: To be or not to be. *Biomedicine Pharmacotherapy*. (2023) 159:114241. doi: 10.1016/j.biopha.2023.114241

17. Bao W-D, Pang P, Zhou X-T, Hu F, Xiong W, Chen K, et al. Loss of ferroportin induces memory impairment by promoting ferroptosis in Alzheimer's disease. *Cell Death Differ*. (2021) 28:1548–62. doi: 10.1038/s41418-020-00685-9

18. Lin D, Gold A, Kaye S, Atkinson JR, Tol M, Sas A, et al. Arachidonic acid mobilization and peroxidation promote microglial dysfunction in Aβ Pathology. *J Neurosci*. (2024) 44:e0202242024. doi: 10.1523/JNEUROSCI.0202-24.2024

19. Tang D, Chen X, Kang R, Kroemer G. Ferroptosis: molecular mechanisms and health implications. *Cell Res*. (2021) 31:107–25. doi: 10.1038/s41422-020-00441-1

20. Shao M, Qi K, Wang L, Yu X, Zhang Q, Yu L, et al. E3 ubiquitin ligase CHIP interacts with transferrin receptor 1 for degradation and promotes cell proliferation through inhibiting ferroptosis in hepatocellular carcinoma. *Cell Signalling*. (2024) 118:111148. doi: 10.1016/j.cellsig.2024.111148

21. Dick CF, De Moura Guimarães L, Carvalho-Kelly LF, Cortes AL, Da Silva Lara Morcillo L, Da Silva Sampaio L, et al. A ferric reductase of Trypanosoma cruzi (TcFR) is involved in iron metabolism in the parasite. *Exp Parasitol*. (2020) 217:107962. doi: 10.1016/j.exppara.2020.107962

22. He Y-J, Liu X-Y, Xing L, Wan X, Chang X, Jiang H-L. Fenton reaction-independent ferroptosis therapy via glutathione and iron redox couple sequentially triggered lipid peroxide generator. *Biomaterials*. (2020) 241:119911. doi: 10.1016/j.biomaterials.2020.119911

23. Gao X, Hu W, Qian D, Bai X, He H, Li L, et al. The mechanisms of ferroptosis under hypoxia. *Cell Mol Neurobiol*. (2023) 43:3329–41. doi: 10.1007/s10571-023-01388-8

24. Chen H, Wang C, Liu Z, He X, Tang W, He L, et al. Ferroptosis and its multifaceted role in cancer: mechanisms and therapeutic approach. *Antioxidants*. (2022) 11:1504. doi: 10.3390/antiox11081504

25. Rochette L, Dogon G, Rigal E, Zeller M, Cottin Y, Vergely C. Lipid peroxidation and iron metabolism: two corner stones in the homeostasis control of ferroptosis. *IJMS*. (2022) 24:449. doi: 10.3390/ijms24010449

26. Yu Z, He S, Tan L. Ferroptosis and tumor drug resistance. *Chem Life*. (2024) 44:710–8. doi: 10.13488/j.smhx.20230712

27. Dierge E, Debock E, Guilbaud C, Corbet C, Mignolet E, Mignard L, et al. Peroxidation of n-3 and n-6 polyunsaturated fatty acids in the acidic tumor environment leads to ferroptosis-mediated anticancer effects. *Cell Metab*. (2021) 33:1701–15.e5. doi: 10.1016/j.cmet.2021.05.016

28. Zhao Y, Li Y, Zhang R, Wang F, Wang T, Jiao Y. The role of erastin in ferroptosis and its prospects in cancer therapy. *Onco Targets Ther*. (2020) 13:5429–41. doi: 10.2147/OTT.S254995

29. Uyeda M, Duarte GHB, De Piloto Fernandes AMA, Contesini FJ, Messias MCF, De Santis GKD, et al. Bio-synthesized sardine oil concentrate alters the composition of hepatic lipids in rats: A lipidomic approach. *Food Res Int*. (2020) 130:108874. doi: 10.1016/j.foodres.2019.108874

30. Mortensen MS, Ruiz J, Watts JL. Polyunsaturated fatty acids drive lipid peroxidation during ferroptosis. *Cells*. (2023) 12:804. doi: 10.3390/cells12050804

31. Wang S, Bai X, Cao Q, Liu Y, Hu H, Zhu Y. Research progress of regulating mechanism and traditional Chinese medicine intervention of iron lipid metabolic disorder based on ferroptosis. *Herald Med*. (2024) 43:1816–21. doi: 10.3870/j.issn.1004-0781.2024.11.019

32. Stockwell BR. Ferroptosis turns 10: Emerging mechanisms, physiological functions, and therapeutic applications. *Cell*. (2022) 185:2401–21. doi: 10.1016/j.cell.2022.06.003

33. Lai B, Wu CH, Wu CY, Luo SF, Lai JH. Ferroptosis and autoimmune diseases. *Front Immunol*. (2022) 13:916664. doi: 10.3389/fimmu.2022.916664

34. Liu J, Kang R, Tang D. Signaling pathways and defense mechanisms of ferroptosis. *FEBS J*. (2022) 289:7038–50. doi: 10.1111/febs.16059

35. Luo L, Wang Z, Liu Y, Jia S, Chen H, Jiang X, et al. Mechanisms of ferroptosis and research progress on anticancer nanopreparations. *Shandong Chem Industry*. (2024) 53:105–107,110. doi: 10.19319/j.cnki.issn.1008-021x.2024.08.050

36. Zhang X, Zhao Z, Zhang W, Li F, Zhou S, Zhao Z. Effects of methionine restriction on the proliferation, apoptosis, and ferroptosis of osteosarcoma cells. *Prog Modern Biomedicine*. (2024) 24:1608–1613,1638. doi: 10.13241/j.cnki.pmb.2024.09.002

37. Salnikow K. Role of iron in cancer. *Semin Cancer Biol*. (2021) 76:189–94. doi: 10.1016/j.semcancer.2021.04.001

38. Zhu X, Xu Y, Lu Y, Dong X, Lu Y. Research progress of ferroptosis and the inhibitors. *Chin J Modern Appl Pharm*. (2024) 41:1–12. doi: 10.13748/j.cnki.issn1007-7693.20232168

39. Zhang C, Liu X, Jin S, Chen Y, Guo R. Ferroptosis in cancer therapy: a novel approach to reversing drug resistance. *Mol Cancer*. (2022) 21:47. doi: 10.1186/s12943-022-01530-y

40. Huang C, Fan M, Shi X. Traditional Chinese medicine in prevention and treatment of depression based on ferroptosis theory: a review. *Chin J Exp Traditional Med Formulae*. (2024) 31:307–14. doi: 10.13422/j.cnki.syfjx.20241242

41. Hu W, Liang K, Zhu H, Zhao C, Hu H, Yin S. Ferroptosis and its role in chronic diseases. *Cells*. (2022) 11:2040. doi: 10.3390/cells11132040

42. Rodencal J, Kim N, He A, Li VL, Lange M, He J, et al. Sensitization of cancer cells to ferroptosis coincident with cell cycle arrest. *Cell Chem Biol*. (2024) 31:234–48.e13. doi: 10.1016/j.chembiol.2023.10.011

43. Nakamura T, Hipp C, Santos Dias Mourão A, Borggräfe J, Aldrovandi M, Henkelmann B, et al. Phase separation of FSP1 promotes ferroptosis. *Nature*. (2023) 619:371–7. doi: 10.1038/s41586-023-06255-6

44. Doll S, Freitas FP, Shah R, Aldrovandi M, Da Silva MC, Ingold I, et al. FSP1 is a glutathione-independent ferroptosis suppressor. *Nature*. (2019) 575:693–8. doi: 10.1038/s41586-019-1707-0

45. Lee DH, Park JS, Lee YS, Han J, Lee D-K, Kwon SW, et al. SQSTM1/p62 activates NFE2L2/NRF2 via ULK1-mediated autophagic KEAP1 degradation and protects mouse liver from lipotoxicity. *Autophagy*. (2020) 16:1949–73. doi: 10.1080/15548627.2020.1712108

46. Ulasov AV, Rosenkranz AA, Georgiev GP, Sobolev AS. Nrf2/Keap1/ARE signaling: Towards specific regulation. *Life Sci*. (2022) 291:120111. doi: 10.1016/j.lfs.2021.120111

47. Liu Y, Su Z, Tavana O, Gu W. Understanding the complexity of p53 in a new era of tumor suppression. *Cancer Cell*. (2024) 42:946–67. doi: 10.1016/j.ccell.2024.04.009

48. Bayır H, Dixon SJ, Tyurina YY, Kellum JA, Kagan VE. Ferroptotic mechanisms and therapeutic targeting of iron metabolism and lipid peroxidation in the kidney. *Nat Rev Nephrol*. (2023) 19:315–36. doi: 10.1038/s41581-023-00689-x

49. Gaschler MM, Andia AA, Liu H, Csuka JM, Hurlocker B, Vaiana CA, et al. FINO2 initiates ferroptosis through GPX4 inactivation and iron oxidation. *Nat Chem Biol*. (2018) 14:507–15. doi: 10.1038/s41589-018-0031-6

50. Song Q, Peng S, Sun Z, Heng X, Zhu X. Temozolomide drives ferroptosis via a DMT1-dependent pathway in glioblastoma cells. *Yonsei Med J*. (2021) 62:843. doi: 10.3349/ymj.2021.62.9.843

51. Faust D, Wenz C, Holm S, Harms G, Greffrath W, Dietrich C. Cell–cell contacts prevent t-BuOOH-triggered ferroptosis and cellular damage *in vitro* by regulation of intracellular calcium. *Arch Toxicol*. (2024) 98:2953–69. doi: 10.1007/s00204-024-03792-5

52. Tang R, Xu J, Zhang B, Liu J, Liang C, Hua J, et al. Ferroptosis, necroptosis, and pyroptosis in anticancer immunity. *J Hematol Oncol*. (2020) 13:110. doi: 10.1186/s13045-020-00946-7

53. Feng J, Lu P, Zhu G, Hooi SC, Wu Y, Huang X, et al. ACSL4 is a predictive biomarker of sorafenib sensitivity in hepatocellular carcinoma. *Acta Pharmacol Sin*. (2021) 42:160–70. doi: 10.1038/s41401-020-0439-x

54. Chen M, Zhu J-Y, Mu W-J, Guo L. Cysteine dioxygenase type 1 (CDO1): Its functional role in physiological and pathophysiological processes. *Genes Dis*. (2023) 10:877–90. doi: 10.1016/j.gendis.2021.12.023

55. Dhiman P, Bharadwaj B, Veena P, Rajendiran S. Polymorphisms in vitamin B12 and folate metabolising genes and their association with adverse pregnancy outcome: secondary analysis of a population based case control study. *J Obstetrics Gynaecology*. (2022) 42:962–7. doi: 10.1080/01443615.2021.1979948

56. Liang Y, Wang Y, Zhang Y, Ye F, Luo D, Li Y, et al. HSPB1 facilitates chemoresistance through inhibiting ferroptotic cancer cell death and regulating NF-κB signaling pathway in breast cancer. *Cell Death Dis.* (2023) 14:434. doi: 10.1038/s41419-023-05972-0

57. Qiao Y, Su M, Zhao H, Liu H, Wang C, Dai X, et al. Targeting FTO induces colorectal cancer ferroptotic cell death by decreasing SLC7A11/GPX4 expression. *J Exp Clin Cancer Res.* (2024) 43:108. doi: 10.1186/s13046-024-03032-9

58. Yang X, Chen Y, Guo J, Li J, Zhang P, Yang H, et al. Polydopamine nanoparticles targeting ferroptosis mitigate intervertebral disc degeneration via reactive oxygen species depletion, iron ions chelation, and GPX4 ubiquitination suppression. *Advanced Sci.* (2023) 10:2207216. doi: 10.1002/advs.202207216

59. Xiong Y, Yong Z, Zhao Q, Hua A, Wang X, Chen X, et al. Hydroxyethyl starch-based self-reinforced nanomedicine inhibits both glutathione and thioredoxin antioxidant pathways to boost reactive oxygen species-powered immunotherapy. *Biomaterials.* (2024) 311:122673. doi: 10.1016/j.biomaterials.2024.122673

60. Wu H, Liu Q, Shan X, Gao W, Chen Q. ATM orchestrates ferritinophagy and ferroptosis by phosphorylating NCOA4. *Autophagy.* (2023) 19:2062–77. doi: 10.1080/15548627.2023.2170960

61. Tasu J-P, Tougeron D, Rols M-P. Irreversible electroporation and electrochemotherapy in oncology: State of the art. *Diagn Interventional Imaging.* (2022) 103:499–509. doi: 10.1016/j.diii.2022.09.009

62. Du Y, Guo Z. Recent progress in ferroptosis: inducers and inhibitors. *Cell Death Discovery.* (2022) 8:501. doi: 10.1038/s41420-022-01297-7

63. Yoshioka H, Kawamura T, Muroi M, Kondoh Y, Honda K, Kawatani M, et al. Identification of a small molecule that enhances ferroptosis via inhibition of ferroptosis suppressor protein 1 (FSP1). *ACS Chem Biol.* (2022) 17:483–91. doi: 10.1021/acschembio.2c00028

64. Chen X, Kang R, Kroemer G, Tang D. Broadening horizons: the role of ferroptosis in cancer. *Nat Rev Clin Oncol.* (2021) 18:280–96. doi: 10.1038/s41571-020-00462-0

65. Yang J, Jia Z, Zhang J, Pan X, Wei Y, Ma S, et al. Metabolic intervention nanoparticles for triple-negative breast cancer therapy via overcoming FSP1-mediated ferroptosis resistance. *Adv Healthcare Materials.* (2022) 11:2102799. doi: 10.1002/adhm.202102799

66. Liang D, Deng L, Jiang X. A new checkpoint against ferroptosis. *Cell Res.* (2020) 30:3–4. doi: 10.1038/s41422-019-0258-0

67. Deepa S, Mamta S-K, Anitha A, Senthilkumaran B. Exposure of carbon nanotubes affects testis and brain of common carp. *Environ Toxicol Pharmacol.* (2022) 95:103957. doi: 10.1016/j.etap.2022.103957

68. Millán M, DeGregorio-Rocasolano N, Pérez de la Ossa N, Reverté S, Costa J, Giner P, et al. Targeting pro-oxidant iron with deferoxamine as a treatment for ischemic stroke: safety and optimal dose selection in a randomized clinical trial. *Antioxidants.* (2021) 10:1270. doi: 10.3390/antiox10081270

69. Yang W, Mu B, You J, Tian C, Bin H, Xu Z, et al. Non-classical ferroptosis inhibition by a small molecule targeting PHB2. *Nat Commun.* (2022) 13:7473. doi: 10.1038/s41467-022-35294-2

70. Hirata Y, Tsunekawa Y, Takahashi M, Oh-hashi K, Kawaguchi K, Hayazaki M, et al. Identification of novel neuroprotective N,N-dimethylaniline derivatives that prevent oxytosis/ferroptosis and localize to late endosomes and lysosomes. *Free Radical Biol Med.* (2021) 174:225–35. doi: 10.1016/j.freeradbiomed.2021.08.015

71. Cheng Y, Qu W, Li J, Jia B, Song Y, Wang L, et al. an Iron Uptake Inhibitor, Exerts Neuroprotection against Traumatic Brain Injury via Suppressing Ferroptosis. *ACS Chem Neurosci.* (2022) 13:664–75. doi: 10.1021/acschemneuro.1c00819

72. Fang Y, Chen X, Tan Q, Zhou H, Xu J, Gu Q. Inhibiting ferroptosis through disrupting the NCOA4–FTH1 interaction: A new mechanism of action. *ACS Cent Sci.* (2021) 7:980–9. doi: 10.1021/acscentsci.0c01592

73. Zhou Q, Meng Y, Li D, Yao L, Le J, Liu Y, et al. Ferroptosis in cancer: from molecular mechanisms to therapeutic strategies. *Sig Transduct Target Ther.* (2024) 9:55. doi: 10.1038/s41392-024-01769-5

74. Wang Y, Zhang M, Bi R, Su Y, Quan F, Lin Y, et al. ACSL4 deficiency confers protection against ferroptosis-mediated acute kidney injury. *Redox Biol.* (2022) 51:102262. doi: 10.1016/j.redox.2022.102262

75. Cheng H, Feng D, Li X, Gao L, Tang S, Liu W, et al. Iron deposition-induced ferroptosis in alveolar type II cells promotes the development of pulmonary fibrosis. *Biochim Biophys Acta (BBA) - Mol Basis Dis.* (2021) 1867:166204. doi: 10.1016/j.bbadis.2021.166204

76. Farràs M, Román R, Camps M, Miret J, Martínez Ó, Pujol X, et al. Heavy chain dimers stabilized by disulfide bonds are required to promote *in vitro* assembly of trastuzumab. *BMC Mol Cell Biol.* (2020) 21:2. doi: 10.1186/s12860-019-0244-x

77. Wang P, Huang Y, Sun B, Chen H, Ma Y, Liu Y, et al. Folic acid blocks ferroptosis induced by cerebral ischemia and reperfusion through regulating folate hydrolase transcriptional adaptive program. *J Nutr Biochem.* (2024) 124:109528. doi: 10.1016/j.jnutbio.2023.109528

78. Dixon SJ, Olzmann JA. The cell biology of ferroptosis. *Nat Rev Mol Cell Biol.* (2024) 25:424–42. doi: 10.1038/s41580-024-00703-5

79. Fang Y, Tan Q, Zhou H, Gu Q, Xu J. Discovery of novel diphenylbutene derivative ferroptosis inhibitors as neuroprotective agents. *Eur J Medicinal Chem.* (2022) 231:114151. doi: 10.1016/j.ejmech.2022.114151

80. Gu Y, Li Y, Wang J, Zhang L, Zhang J, Wang Y. Targeting ferroptosis: Paving new roads for drug design and discovery. *Eur J Medicinal Chem.* (2023) 247:115015. doi: 10.1016/j.ejmech.2022.115015

81. Aguilera A, Klemenčič M, Sueldo DJ, Rzymski P, Giannuzzi L, Martin MV. Cell death in cyanobacteria: current understanding and recommendations for a consensus on its nomenclature. *Front Microbiol.* (2021) 12:631654. doi: 10.3389/fmicb.2021.631654

82. Galluzzi L, Vitale I, Warren S, Adjemian S, Agostinis P, Martinez AB, et al. Consensus guidelines for the definition, detection and interpretation of immunogenic cell death. *J Immunother Cancer.* (2020) 8:e000337. doi: 10.1136/jitc-2019-000337

83. Demuynck R, Efimova I, Naessens F, Krysko DV. Immunogenic ferroptosis and where to find it? *J Immunother Cancer.* (2021) 9:e003430. doi: 10.1136/jitc-2021-003430

84. Tavalaee M, Rahmani M, Drevet JR, Nasr-Esfahani MH. The NLRP3 inflammasome: molecular activation and regulation in spermatogenesis and male infertility; a systematic review. *Basic Clin Androl.* (2022) 32:8. doi: 10.1186/s12610-022-00157-9

85. Fucikova J, Kepp O, Kasikova L, Petroni G, Yamazaki T, Liu P, et al. Detection of immunogenic cell death and its relevance for cancer therapy. *Cell Death Dis.* (2020) 11:1013. doi: 10.1038/s41419-020-03221-2

86. Gong T, Liu L, Jiang W, Zhou R. DAMP-sensing receptors in sterile inflammation and inflammatory diseases. *Nat Rev Immunol.* (2020) 20:95–112. doi: 10.1038/s41577-019-0215-7

87. Lai J-J, Cruz FM, Rock KL. Immune sensing of cell death through recognition of histone sequences by C-type lectin-receptor-2d causes inflammation and tissue injury. *Immunity.* (2020) 52:123–35.e6. doi: 10.1016/j.immuni.2019.11.013

88. Monterrubio-Ledezma F, Navarro-García F, Massieu L, Mondragón-Flores R, Soto-Ponce LA, Magaña JJ, et al. Rescue of mitochondrial function in Hutchinson-Gilford progeria syndrome by the pharmacological modulation of exportin CRM1. *Cells.* (2023) 12:275. doi: 10.3390/cells12020275

89. VanPortfliet JJ, Chute C, Lei Y, Shutt TE, West AP. Mitochondrial DNA release and sensing in innate immune responses. *Hum Mol Genet.* (2024) 33:R80–91. doi: 10.1093/hmg/ddae031

90. Primorac D, Vrdoljak K, Brlek P, Pavelić E, Molnar V, Matišić V, et al. Adaptive immune responses and immunity to SARS-CoV-2. *Front Immunol.* (2022) 13:848582. doi: 10.3389/fimmu.2022.848582

91. Møller SH, Hsueh P-C, Yu Y-R, Zhang L, Ho P-C. Metabolic programs tailor T cell immunity in viral infection, cancer, and aging. *Cell Metab.* (2022) 34:378–95. doi: 10.1016/j.cmet.2022.02.003

92. Mansur MB, deSouza NM, Natrajan R, Abegglen LM, Schiffman JD, Greaves M. Evolutionary determinants of curability in cancer. *Nat Ecol Evol.* (2023) 7:1761–70. doi: 10.1038/s41559-023-02159-w

93. Ma L, Wang L, Khatib SA, Chang C-W, Heinrich S, Dominguez DA, et al. Single-cell atlas of tumor cell evolution in response to therapy in hepatocellular carcinoma and intrahepatic cholangiocarcinoma. *J Hepatol.* (2021) 75:1397–408. doi: 10.1016/j.jhep.2021.06.028

94. Li J, Li J, Peng Y, Du Y, Yang Z, Qi X. Dendritic cell derived exosomes loaded neoantigens for personalized cancer immunotherapies. *J Controlled Release.* (2023) 353:423–33. doi: 10.1016/j.jconrel.2022.11.053

95. Liu W, Tang H, Li L, Wang X, Yu Z, Li J. Peptide-based therapeutic cancer vaccine: Current trends in clinical application. *Cell Proliferation.* (2021) 54:e13025. doi: 10.1111/cpr.13025

96. Taylor S, Isobe S, Cao A, Contrepois K, Benayoun BA, Jiang L, et al. Endogenous retroviral elements generate pathologic neutrophils in pulmonary arterial hypertension. *Am J Respir Crit Care Med.* (2022) 206:1019–34. doi: 10.1164/rccm.202102-0446OC

97. Geis FK, Goff SP. Silencing and transcriptional regulation of endogenous retroviruses: an overview. *Viruses.* (2020) 12:884. doi: 10.3390/v12080884

98. Wang MM, Koskela SA, Mehmood A, Langguth M, Maranou E, Figueiredo CR. Epigenetic control of CD1D expression as a mechanism of resistance to immune checkpoint therapy in poorly immunogenic melanomas. *Front Immunol.* (2023) 14:1152228. doi: 10.3389/fimmu.2023.1152228

99. Wang Z, Liu J, Wang Y, Guo H, Li F, Cao Y, et al. Identification of key biomarkers associated with immunogenic cell death and their regulatory mechanisms in severe acute pancreatitis based on WGCNA and machine learning. *IJMS.* (2023) 24:3033. doi: 10.3390/ijms24033033

100. Hänggi K, Ruffell B. Cell death, therapeutics, and the immune response in cancer. *Trends Cancer.* (2023) 9:381–96. doi: 10.1016/j.trecan.2023.02.001

101. Calvillo-Rodríguez KM, Lorenzo-Anota HY, Rodríguez-Padilla C, Martínez-Torres AC, Scott-Algara D. Immunotherapies inducing immunogenic cell death in cancer: insight of the innate immune system. *Front Immunol.* (2023) 14:1294434. doi: 10.3389/fimmu.2023.1294434

102. Lombardi M, Gabrielli M, Adinolfi E, Verderio C. Role of ATP in extracellular vesicle biogenesis and dynamics. *Front Pharmacol.* (2021) 12:654023. doi: 10.3389/fphar.2021.654023

103. Guo Y, Zhang H, Lv Z, Du Y, Li D, Fang H, et al. Up-regulated CD38 by daphnetin alleviates lipopolysaccharide-induced lung injury via inhibiting MAPK/NF-κB/NLRP3 pathway. *Cell Commun Signal.* (2023) 21:66. doi: 10.1186/s12964-023-01041-3

104. Fu J, Wu H. Structural mechanisms of NLRP3 inflammasome assembly and activation. *Annu Rev Immunol*. (2023) 41:301–16. doi: 10.1146/annurev-immunol-081022-021207

105. DeWulf B, Minsart L, Verdonk F, Kruys V, Piagnerelli M, Maze M, et al. High mobility group box 1 (HMGB1): potential target in sepsis-associated encephalopathy. *Cells*. (2023) 12:1088. doi: 10.3390/cells12071088

106. Kielbik M, Szulc-Kielbik I, Klink M. Calreticulin—Multifunctional chaperone in immunogenic cell death: potential significance as a prognostic biomarker in ovarian cancer patients. *Cells*. (2021) 10:130. doi: 10.3390/cells10010130

107. Ruan H, Leibowitz BJ, Zhang L, Yu J. Immunogenic cell death in colon cancer prevention and therapy. *Mol Carcinogenesis*. (2020) 59:783–93. doi: 10.1002/mc.23183

108. Asadzadeh Z, Safarzadeh E, Safaei S, Baradaran A, Mohammadi A, Hajiasgharzadeh K, et al. Current approaches for combination therapy of cancer: the role of immunogenic cell death. *Cancers*. (2020) 12:1047. doi: 10.3390/cancers12041047

109. Khalaji A, Yancheshmeh FB, Farham F, Khorram A, Sheshbolouki S, Zokaei M, et al. Don't eat me/eat me signals as a novel strategy in cancer immunotherapy. *Heliyon*. (2023) 9:e20507. doi: 10.1016/j.heliyon.2023.e20507

110. Li D-Y, Liang S, Wen J-H, Tang J-X, Deng S-L, Liu Y-X. Extracellular HSPs: the potential target for human disease therapy. *Molecules*. (2022) 27:2361. doi: 10.3390/molecules27072361

111. Liu Z, Xiong J, Gao S, Zhu MX, Sun K, Li M, et al. Ameliorating cancer cachexia by inhibiting cancer cell release of Hsp70 and Hsp90 with omeprazole. *J cachexia sarcopenia Muscle*. (2022) 13:636–47. doi: 10.1002/jcsm.12851

112. Dong Y-F, Zhang J, Zhou J-H, Xiao Y-L, Pei W-J, Liu H-P. Mitochondrial-associated endoplasmic reticulum membrane interference in ovarian cancer (Review). *Oncol Rep*. (2024) 52:112. doi: 10.3892/or.2024.8771

113. Dai Z, Huang Q, Hu Q, Wu H, Pan Y, Deng Z, et al. Mechanisms of immunogenic cell death induced by octyl ester derivative of ginsenoside Rh2 in hepatocellular carcinoma cells based on endoplasmic reticulum stress. *Chin J Immunol*. (2024) 40:767–771,779. doi: 10.3969/j.issn.1000-484X.2024.04.016

114. Abhishek K, Das S, Kumar A, Kumar A, Kumar V, Saini S, et al. Leishmania donovani induced Unfolded Protein Response delays host cell apoptosis in PERK dependent manner. *PloS Negl Trop Dis*. (2018) 12:e0006646. doi: 10.1371/journal.pntd.0006646

115. Li X, Zheng J, Chen S, Meng F, Ning J, Sun S. Oleandrin, a cardiac glycoside, induces immunogenic cell death via the PERK/elF2α/ATF4/CHOP pathway in breast cancer. *Cell Death Dis*. (2021) 12:314. doi: 10.1038/s41419-021-03605-y

116. Ishimwe N, Wei P, Wang M, Zhang H, Wang L, Jing M, et al. Autophagy impairment through lysosome dysfunction by brucine induces immunogenic cell death (ICD). *Am J Chin Med*. (2020) 48:1915–40. doi: 10.1142/S0192415X20500962

117. Li J, Fan Y, Zhang Y, Liu Y, Yu Y, Ma M. Resveratrol induces autophagy and apoptosis in non-small-cell lung cancer cells by activating the NGFR-AMPK-mTOR pathway. *Nutrients*. (2022) 14:2413. doi: 10.3390/nu14122413

118. Li F. *Study on the role of Cinobufotalin-mediated immune activation in suppressing bladder cancer*. Changchun, China: Jilin University (2021). doi: 10.27162/d.cnki.gjlin.2021.002471

119. Wu J, Li X, Zhang Q, Li J, Cui R, Li X. Differential effects of intra-RMTg infusions of pilocarpine or 4-DAMP on regulating depression- and anxiety-like behaviors. *Behav Brain Res*. (2024) 462:114833. doi: 10.1016/j.bbr.2023.114833

120. Li X, Su Y, Xu Y, Hu T, Lu X, Sun J, et al. Adipocyte-specific hnrnpa1 knockout aggravates obesity-induced metabolic dysfunction via upregulation of CCL2. *Diabetes*. (2024) 73:713–27. doi: 10.2337/db23-0609

121. Li W, Fu H, Fang L, Chai H, Gao T, Chen Z, et al. Shikonin induces ferroptosis in multiple myeloma via GOT1-mediated ferritinophagy. *Front Oncol*. (2022) 12:1025067. doi: 10.3389/fonc.2022.1025067

122. Ma X, Xiao L, Liu L, Ye L, Su P, Bi E, et al. CD36-mediated ferroptosis dampens intratumoral CD8+ T cell effector function and impairs their antitumor ability. *Cell Metab*. (2021) 33:1001–12.e5. doi: 10.1016/j.cmet.2021.02.015

123. Sterner RC, Sterner RM. CAR-T cell therapy: current limitations and potential strategies. *Blood Cancer J*. (2021) 11:69. doi: 10.1038/s41408-021-00459-7

124. Mannion J, Gifford V, Bellenie B, Fernando W, Ramos Garcia L, Wilson R, et al. A RIPK1-specific PROTAC degrader achieves potent antitumor activity by enhancing immunogenic cell death. *Immunity*. (2024) 57:1514–32.e15. doi: 10.1016/j.immuni.2024.04.025

125. Ma R, Li Z, Chiocca EA, Caligiuri MA, Yu J. The emerging field of oncolytic virus-based cancer immunotherapy. *Trends Cancer*. (2023) 9:122–39. doi: 10.1016/j.trecan.2022.10.003

126. Scepankova H, Galante D, Espinoza-Suaréz E, Pinto CA, Estevinho LM, Saraiva J. High hydrostatic pressure in the modulation of enzymatic and organocatalysis and life under pressure: A review. *Molecules*. (2023) 28:4172. doi: 10.3390/molecules28104172

127. Hamad A, Yusubalieva GM, Baklaushev VP, Chumakov PM, Lipatova AV. Recent developments in glioblastoma therapy: oncolytic viruses and emerging future strategies. *Viruses*. (2023) 15:547. doi: 10.3390/v15020547

128. Evgin L, Vile RG. Parking CAR T cells in tumours: oncolytic viruses as valets or vandals? *Cancers*. (2021) 13:1106. doi: 10.3390/cancers13051106

129. Galluzzi L, Guilbaud E, Schmidt D, Kroemer G, Marincola FM. Targeting immunogenic cell stress and death for cancer therapy. *Nat Rev Drug Discovery*. (2024) 23:445–60. doi: 10.1038/s41573-024-00920-9

130. Liu YQ. *Study on immune regulation and tumor therapeutic effects of polydopamine-based materials*. Shanghi, China: Tongji University (2022). doi: 10.27372/d.cnki.gtjsu.2022.000657

131. Chen Z, Bian H, Yang X. Remodeling homeostasis of tumor microenvironment to suppress tumor progression. *J Air Force Med Univ*. (2024) 45:723–31. doi: 10.13276/j.issn.2097-1656.2024.07.002

132. Chen Z, Han F, Du Y, Shi H, Zhou W. Hypoxic microenvironment in cancer: molecular mechanisms and therapeutic interventions. *Sig Transduct Target Ther*. (2023) 8:70. doi: 10.1038/s41392-023-01332-8

133. Bersuker K, Hendricks JM, Li Z, Magtanong L, Ford B, Tang PH, et al. The CoQ oxidoreductase FSP1 acts parallel to GPX4 to inhibit ferroptosis. *Nature*. (2019) 575:688–92. doi: 10.1038/s41586-019-1705-2

134. Idris M, Alves MM, Hofstra RMW, Mahe MM, Melotte V. Intestinal multicellular organoids to study colorectal cancer. *Biochim Biophys Acta (BBA) - Rev Cancer*. (2021) 1876:188586. doi: 10.1016/j.bbcan.2021.188586

135. Efimova I, Catanzaro E, van der Meeren L, Turubanova VD, Hammad H, Mishchenko TA, et al. Vaccination with early ferroptotic cancer cells induces efficient antitumor immunity. *J Immunother Cancer*. (2020) 8:e001369. doi: 10.1136/jitc-2020-001369

136. Birmpilis AI, Paschalis A, Mourkakis A, Christodoulou P, Kostopoulos IV, Antimissari E, et al. Immunogenic cell death, DAMPs and prothymosin α as a putative anticancer immune response biomarker. *Cells*. (2022) 11:1415. doi: 10.3390/cells11091415

137. Zheng M, Kanneganti T. The regulation of the ZBP1-NLRP3 inflammasome and its implications in pyroptosis, apoptosis, and necroptosis (PANoptosis). *Immunol Rev*. (2020) 297:26–38. doi: 10.1111/imr.12909

138. Herrera SA, Günther Pomorski T. Reconstitution of ATP-dependent lipid transporters: gaining insight into molecular characteristics, regulation, and mechanisms. *Bioscience Rep*. (2023) 43:BSR20221268. doi: 10.1042/BSR20221268

139. Takahara T, Nakamura S, Tsuzuki T, Satou A. The immunology of DLBCL. *Cancers*. (2023) 15:835. doi: 10.3390/cancers15030835

140. Richter K, Amati A-L, Padberg W, Grau V. Negative regulation of ATP-induced inflammasome activation and cytokine secretion by acute-phase proteins: A mini review. *Front Pharmacol*. (2022) 13:981276. doi: 10.3389/fphar.2022.981276

141. Flores-Romero H, Ros U, García-Sáez AJ. A lipid perspective on regulated cell death. In: *International Review of Cell and Molecular Biology*. Amsterdam, Netherlands: Elsevier (2020). p. 197–236. doi: 10.1016/bs.ircmb.2019.11.004

142. Zheng Y, Sun J, Luo Z, Li Y, Huang Y. Emerging mechanisms of lipid peroxidation in regulated cell death and its physiological implications. *Cell Death Dis*. (2024) 15:859. doi: 10.1038/s41419-024-07244-x

143. Wang T, Duan R, Li Z, Zhang B, Jiang Q, Jiang L, et al. Lipid metabolism analysis reveals that DGAT1 regulates Th17 survival by controlling lipid peroxidation in uveitis. *JCI Insight*. (2025) 10:e184072. doi: 10.1172/jci.insight.184072

144. Oltean T, Lippens L, Lemeire K, De Tender C, Vuylsteke M, Denys H, et al. Association of cell death markers with tumor immune cell infiltrates after chemo-radiation in cervical cancer. *Front Oncol*. (2022) 12:892813. doi: 10.3389/fonc.2022.892813

145. Lidman M, Pokorná Š, Dingeldein APG, Sparrman T, Wallgren M, Šachl R, et al. The oxidized phospholipid PazePC promotes permeabilization of mitochondrial membranes by Bax. *Biochim Biophys Acta (BBA) - Biomembranes*. (2016) 1858:1288–97. doi: 10.1016/j.bbamem.2016.03.003

146. Xiao L, Xian M, Zhang C, Guo Q, Yi Q. Lipid peroxidation of immune cells in cancer. *Front Immunol*. (2024) 14:1322746. doi: 10.3389/fimmu.2023.1322746

147. Deng J, Pan T, Liu Z, McCarthy C, Vicencio JM, Cao L, et al. The role of TXNIP in cancer: a fine balance between redox, metabolic, and immunological tumor control. *Br J Cancer*. (2023) 129:1877–92. doi: 10.1038/s41416-023-02442-4

148. Abimannan T, Peroumal D, Parida JR, Barik PK, Padhan P, Devadas S. Oxidative stress modulates the cytokine response of differentiated Th17 and Th1 cells. *Free Radical Biol Med*. (2016) 99:352–63. doi: 10.1016/j.freeradbiomed.2016.08.026

149. Saimoto Y, Kusakabe D, Morimoto K, Matsuoka Y, Kozakura E, Kato N, et al. Lysosomal lipid peroxidation contributes to ferroptosis induction via lysosomal membrane permeabilization. *Nat Commun*. (2025) 16:3554. doi: 10.1038/s41467-025-58909-w

150. Yao Y, Chen Z, Zhang H, Chen C, Zeng M, Yunis J, et al. Selenium–GPX4 axis protects follicular helper T cells from ferroptosis. *Nat Immunol*. (2021) 22:1127–39. doi: 10.1038/s41590-021-00996-0

151. Xu C, Sun S, Johnson T, Qi R, Zhang S, Zhang J, et al. The glutathione peroxidase Gpx4 prevents lipid peroxidation and ferroptosis to sustain Treg cell activation and suppression of antitumor immunity. *Cell Rep*. (2021) 35:109235. doi: 10.1016/j.celrep.2021.109235

152. Watson MJ, Vignali PDA, Mullett SJ, Overacre-Delgoffe AE, Peralta RM, Grebinoski S, et al. Metabolic support of tumour-infiltrating regulatory T cells by lactic acid. *Nature*. (2021) 591:645–51. doi: 10.1038/s41586-020-03045-2

153. Song J, Liu T, Yin Y, Zhao W, Lin Z, Yin Y, et al. The deubiquitinase OTUD1 enhances iron transport and potentiates host antitumor immunity. *EMBO Rep*. (2021) 22:e51162. doi: 10.15252/embr.202051162

154. Tang D, Kang R, Cheh C-W, Livesey KM, Liang X, Schapiro NE, et al. HMGB1 release and redox regulates autophagy and apoptosis in cancer cells. *Oncogene*. (2010) 29:5299–310. doi: 10.1038/onc.2010.261

155. Wang Y, Gao W, Shi X, Ding J, Liu W, He H, et al. Chemotherapy drugs induce pyroptosis through caspase-3 cleavage of a gasdermin. *Nature*. (2017) 547:99–103. doi: 10.1038/nature22393

156. Drijvers JM, Gillis JE, Muijlwijk T, Nguyen TH, Gaudiano EF, Harris IS, et al. Pharmacologic screening identifies metabolic vulnerabilities of CD8+ T cells. *Cancer Immunol Res*. (2021) 9:184–99. doi: 10.1158/2326-6066.CIR-20-0384

157. Lechner M, Engleitner T, Babushku T, Schmidt-Supprian M, Rad R, Strobl LJ, et al. Notch2-mediated plasticity between marginal zone and follicular B cells. *Nat Commun*. (2021) 12:1111. doi: 10.1038/s41467-021-21359-1

158. Muri J, Thut H, Bornkamm GW, Kopf M. B1 and marginal zone B cells but not follicular B2 cells require Gpx4 to prevent lipid peroxidation and ferroptosis. *Cell Rep*. (2019) 29:2731–2744.e4. doi: 10.1016/j.celrep.2019.10.070

159. Pei J, Pan X, Wei G, Hua Y. Research progress of glutathione peroxidase family (GPX) in redoxidation. *Front Pharmacol*. (2023) 14:1147414. doi: 10.3389/fphar.2023.1147414

160. Maslanka J, Torres G, Londregan J, Goldman N, Silberman D, Somerville J, et al. Loss of B1 and marginal zone B cells during ovarian cancer. *Cell Immunol*. (2024) 395–396:104788. doi: 10.1016/j.cellimm.2023.104788

161. Li X, Zhang B, Yan C, Li J, Wang S, Wei X, et al. A fast and specific fluorescent probe for thioredoxin reductase that works via disulphide bond cleavage. *Nat Commun*. (2019) 10:2745. doi: 10.1038/s41467-019-10807-8

162. Guerriero E, Capone F, Accardo M, Sorice A, Costantini M, Colonna G, et al. GPX4 and GPX7 over-expression in human hepatocellular carcinoma tissues. *Eur J Histochem*. (2015) 59:283–8. doi: 10.4081/ejh.2015.2540

163. Schmitt A, Xu W, Bucher P, Grimm M, Konantz M, Horn H, et al. Dimethyl fumarate induces ferroptosis and impairs NF-κB/STAT3 signaling in DLBCL. *Blood*. (2021) 138:871–84. doi: 10.1182/blood.2020009404

164. Ashkenazi A, Fairbrother WJ, Leverson JD, Souers AJ. From basic apoptosis discoveries to advanced selective BCL-2 family inhibitors. *Nat Rev Drug Discovery*. (2017) 16:273–84. doi: 10.1038/nrd.2016.253

165. Luo W, Adamska JZ, Li C, Verma R, Liu Q, Hagan T, et al. SREBP signaling is essential for effective B cell responses. *Nat Immunol*. (2023) 24:337–48. doi: 10.1038/s41590-022-01376-y

166. Leadbetter EA, Rifkin IR, Hohlbaum AM, Beaudette BC, Shlomchik MJ, Marshak-Rothstein A. Chromatin–IgG complexes activate B cells by dual engagement of IgM and Toll-like receptors. *Nature*. (2002) 416:603–7. doi: 10.1038/416603a

167. Caielli S, Athale S, Domic B, Murat E, Chandra M, Banchereau R, et al. Oxidized mitochondrial nucleoids released by neutrophils drive type I interferon production in human lupus. *J Exp Med*. (2016) 213:697–713. doi: 10.1084/jem.20151876

168. Shen P, Fillatreau S. Antibody-independent functions of B cells: a focus on cytokines. *Nat Rev Immunol*. (2015) 15:441–51. doi: 10.1038/nri3857

169. Bora A, Sarmah D, Rather MA, Mandal M, Karak N. Nanocomposite of starch, gelatin and itaconic acid-based biodegradable hydrogel and ZnO/cellulose nanofiber: A pH-sensitive sustained drug delivery vehicle. *Int J Biol Macromolecules*. (2024) 256:128253. doi: 10.1016/j.ijbiomac.2023.128253

170. Kim R, Hashimoto A, Markosyan N, Tyurin VA, Tyurina YY, Kar G, et al. Ferroptosis of tumour neutrophils causes immune suppression in cancer. *Nature*. (2022) 612:338–46. doi: 10.1038/s41586-022-05443-0

171. Eaton JK, Furst L, Ruberto RA, Moosmayer D, Hilpmann A, Ryan MJ, et al. Selective covalent targeting of GPX4 using masked nitrile-oxide electrophiles. *Nat Chem Biol*. (2020) 16:497–506. doi: 10.1038/s41589-020-0501-5

172. Sparvero LJ, Tian H, Amoscato AA, Sun W, Anthonymuthu TS, Tyurina YY, et al. Direct mapping of phospholipid ferroptotic death signals in cells and tissues by gas cluster ion beam secondary ion mass spectrometry (GCIB-SIMS). *Angew Chem Int Ed*. (2021) 60:11784–8. doi: 10.1002/anie.202102001

173. Han L, Bai L, Qu C, Dai E, Liu J, Kang R, et al. PPARG-mediated ferroptosis in dendritic cells limits antitumor immunity. *Biochem Biophys Res Commun*. (2021) 576:33–9. doi: 10.1016/j.bbrc.2021.08.082

174. Lou X, Gao D, Yang L, Wang Y, Hou Y. Endoplasmic reticulum stress mediates the myeloid-derived immune suppression associated with cancer and infectious disease. *J Transl Med*. (2023) 21:1. doi: 10.1186/s12967-022-03835-4

175. Kudo K, Yanagiya R, Hasegawa M, Carreras J, Miki Y, Nakayama S, et al. Unique lipid composition maintained by extracellular blockade leads to prooncogenicity. *Cell Death Discovery*. (2024) 10:221. doi: 10.1038/s41420-024-01971-y

176. Huang X, Lin K, Chen W, Zhang D, Khan M, Ye X, et al. Modulation of the local angiotensin II: Suppression of ferroptosis and radiosensitivity in nasopharyngeal carcinoma via the HIF-1α-HILPDA axis. *Radiother Oncol*. (2025) 203:110686. doi: 10.1016/j.radonc.2024.110686

177. Yan Y, Teng H, Hang Q, Kondiparthi L, Lei G, Horbath A, et al. SLC7A11 expression level dictates differential responses to oxidative stress in cancer cells. *Nat Commun*. (2023) 14:3673. doi: 10.1038/s41467-023-39401-9

178. Dilly S, Romero M, Solier S, Feron O, Dessy C, Slama Schwok A. Targeting M2 macrophages with a novel NADPH oxidase inhibitor. *Antioxidants*. (2023) 12:440. doi: 10.3390/antiox12020440

179. Derynck R, Turley SJ, Akhurst RJ. TGFβ biology in cancer progression and immunotherapy. *Nat Rev Clin Oncol*. (2021) 18:9–34. doi: 10.1038/s41571-020-0403-1

180. McDonald B, Pittman K, Menezes GB, Hirota SA, Slaba I, Waterhouse CCM, et al. Intravascular danger signals guide neutrophils to sites of sterile inflammation. *Science*. (2010) 330:362–6. doi: 10.1126/science.1195491

181. Jorch SK, Kubes P. An emerging role for neutrophil extracellular traps in noninfectious disease. *Nat Med*. (2017) 23:279–87. doi: 10.1038/nm.4294

182. Zhong L, Liu Z, Zhou X, Song S, Weng G, Wen Y, et al. Expansion of PMN-myeloid derived suppressor cells and their clinical relevance in patients with oral squamous cell carcinoma. *Oral Oncol*. (2019) 95:157–63. doi: 10.1016/j.oraloncology.2019.06.004

183. Ni X, Lu Y, Li M, Liu Y, Zhang M, Sun F, et al. Application of Se-Met to CdTe QDs significantly reduces toxicity by modulating redox balance and inhibiting apoptosis. *Ecotoxicology Environ Saf*. (2023) 267:115614. doi: 10.1016/j.ecoenv.2023.115614

184. Gong C, Ji Q, Wu M, Tu Z, Lei K, Luo M, et al. Ferroptosis in tumor immunity and therapy. *J Cell Mol Medi*. (2022) 26:5565–79. doi: 10.1111/jcmm.17529

185. Kang R, Chen R, Zhang Q, Hou W, Wu S, Cao L, et al. HMGB1 in health and disease. *Mol Aspects Med*. (2014) 40:1–116. doi: 10.1016/j.mam.2014.05.001

186. Lee J-W, Park J-W, Shin N-R, Park S-Y, Kwon O-K, Park HA, et al. Picrasma quassiodes (D. Don) Benn. attenuates lipopolysaccharide (LPS)-induced acute lung injury. *Int J Mol Med*. (2016) 38:834–44. doi: 10.3892/ijmm.2016.2669

187. Dai E, Han L, Liu J, Xie Y, Zeh HJ, Kang R, et al. Ferroptotic damage promotes pancreatic tumorigenesis through a TMEM173/STING-dependent DNA sensor pathway. *Nat Commun*. (2020) 11:6339. doi: 10.1038/s41467-020-20154-8

188. Luo X, Gong H-B, Gao H-Y, Wu Y-P, Sun W-Y, Li Z-Q, et al. Oxygenated phosphatidylethanolamine navigates phagocytosis of ferroptotic cells by interacting with TLR2. *Cell Death Differ*. (2021) 28:1971–89. doi: 10.1038/s41418-020-00719-2

189. Zhang L, Han J, Wu H, Liang X, Zhang J, Li J, et al. The association of HMGB1 expression with clinicopathological significance and prognosis in hepatocellular carcinoma: a meta-analysis and literature review. *PloS One*. (2014) 9:e110626. doi: 10.1371/journal.pone.0110626

190. Zhang H, Luo J, Alcorn JF, Chen K, Fan S, Pilewski J, et al. AIM2 inflammasome is critical for influenza-induced lung injury and mortality. *J Immunol*. (2017) 198:4383–93. doi: 10.4049/jimmunol.1600714

191. Xiao H, Du X, Tao Z, Jing N, Bao S, Gao W, et al. Taurine inhibits ferroptosis mediated by the crosstalk between tumor cells and tumor-associated macrophages in prostate cancer. *Advanced Sci*. (2024) 11:2303894. doi: 10.1002/advs.202303894

192. Yang Z, Su W, Wei X, Qu S, Zhao D, Zhou J, et al. HIF-1α drives resistance to ferroptosis in solid tumors by promoting lactate production and activating SLC1A1. *Cell Rep*. (2023) 42:112945. doi: 10.1016/j.celrep.2023.112945

193. Wynn TA, Chawla A, Pollard JW. Macrophage biology in development, homeostasis and disease. *Nature*. (2013) 496:445–55. doi: 10.1038/nature12034

194. Gardai SJ, McPhillips KA, Frasch SC, Janssen WJ, Starefeldt A, Murphy-Ullrich JE, et al. Cell-Surface Calreticulin Initiates Clearance of Viable or Apoptotic Cells through trans-Activation of LRP on the Phagocyte. *Cell*. (2005) 123:321–34. doi: 10.1016/j.cell.2005.08.032

195. Chen L, Zhou Z, Hu C, Maitz MF, Yang L, Luo R, et al. Platelet membrane-coated nanocarriers targeting plaques to deliver anti-CD47 antibody for atherosclerotic therapy. *Research*. (2022) 2022:9845459. doi: 10.34133/2022/9845459

196. Humphries F, Shmuel-Galia L, Ketelut-Carneiro N, Li S, Wang B, Nemmara VV, et al. Succination inactivates gasdermin D and blocks pyroptosis. *Science*. (2020) 369:1633–7. doi: 10.1126/science.abb9818

197. Zou H, Li T. Research progress of PD-1/PD-L1 checkpoint inhibitors in (Neo) adjuvant therapy for Malignant melanoma. *Cancer Res Prev Treat*. (2020) 47:141–6. doi: 10.3971/j.issn.1000-8578.2020.19.0945

198. Hao X, Zheng Z, Liu H, Zhang Y, Kang J, Kong X, et al. Inhibition of APOC1 promotes the transformation of M2 into M1 macrophages via the ferroptosis pathway and enhances anti-PD1 immunotherapy in hepatocellular carcinoma based on single-cell RNA sequencing. *Redox Biol*. (2022) 56:102463. doi: 10.1016/j.redox.2022.102463

199. Li G, Liao C, Chen J, Wang Z, Zhu S, Lai J, et al. Targeting the MCP-GPX4/HMGB1 axis for effectively triggering immunogenic ferroptosis in pancreatic ductal adenocarcinoma. *Advanced Sci*. (2024) 11:2308208. doi: 10.1002/advs.202308208

200. He Q, Yu T, Chen J, Liang J, Lin D, Yan K, et al. Enhancement of *de novo* lipogenesis by the IDH1 and IDH2-dependent reverse TCA cycle maintains the growth and angiogenic capacity of bone marrow-derived endothelial progenitor cells under hypoxia. *Free Radical Biol Med*. (2024) 213:327–42. doi: 10.1016/j.freeradbiomed.2024.01.028

201. Johnson AM, Kleczko EK, Nemenoff RA. Eicosanoids in cancer: new roles in immunoregulation. *Front Pharmacol*. (2020) 11:595498. doi: 10.3389/fphar.2020.595498

202. Liu Y, Duan C, Dai R, Zeng Y. Ferroptosis-mediated crosstalk in the tumor microenvironment implicated in cancer progression and therapy. *Front Cell Dev Biol*. (2021) 9:739392. doi: 10.3389/fcell.2021.739392

203. Ping Y, Shan J, Qin H, Li F, Qu J, Guo R, et al. PD-1 signaling limits expression of phospholipid phosphatase 1 and promotes intratumoral CD8+ T cell ferroptosis. *Immunity*. (2024) 57:2122–39.e9. doi: 10.1016/j.immuni.2024.08.003

204. Kshattry S, Saha A, Gries P, Tiziani S, Stone E, Georgiou G, et al. Enzyme-mediated depletion of l-cyst(e)ine synergizes with thioredoxin reductase inhibition for suppression of pancreatic tumor growth. *NPJ Precis Onc*. (2019) 3:16. doi: 10.1038/s41698-019-0088-z

205. Barros LF, Schirmeier S, Weber B. The astrocyte: metabolic hub of the brain. *Cold Spring Harb Perspect Biol*. (2024) 16:a041355. doi: 10.1101/cshperspect.a041355

206. Deretic V. Autophagy in inflammation, infection, and immunometabolism. *Immunity*. (2021) 54:437–53. doi: 10.1016/j.immuni.2021.01.018

207. Xiong X, Zhao J, Su R, Liu C, Guo X, Zhou S. Double enhancement of immunogenic cell death and antigen presentation for cancer immunotherapy. *Nano Today*. (2021) 39:101225. doi: 10.1016/j.nantod.2021.101225

208. Garg AD, Nowis D, Golab J, Vandenabeele P, Krysko DV, Agostinis P. Immunogenic cell death, DAMPs and anticancer therapeutics: An emerging amalgamation. *Biochim Biophys Acta (BBA) - Rev Cancer*. (2010) 1805:53–71. doi: 10.1016/j.bbcan.2009.08.003

209. Vandenabeele P, Galluzzi L, Vanden Berghe T, Kroemer G. Molecular mechanisms of necroptosis: an ordered cellular explosion. *Nat Rev Mol Cell Biol*. (2010) 11:700–14. doi: 10.1038/nrm2970

210. Végran F, Apetoh L, Ghiringhelli F. Th9 cells: A novel CD4 T-cell subset in the immune war against cancer. *Cancer Res*. (2015) 75:475–9. doi: 10.1158/0008-5472.CAN-14-2748

211. Yan C, Zhao Y, Liu X, Jiang Y, Li Q, Yang L, et al. Self-delivery nanobooster to enhance immunogenic cell death for cancer chemoimmunotherapy. *ACS Appl Mater Interfaces*. (2024) 16:33169–81. doi: 10.1021/acsami.4c06149

212. Li Z, Lai X, Fu S, Ren L, Cai H, Zhang H, et al. Immunogenic cell death activates the tumor immune microenvironment to boost the immunotherapy efficiency. *Advanced Sci*. (2022) 9:2201734. doi: 10.1002/advs.202201734

213. Zhang Z, Li X, Wang Y, Wei Y, Wei X. Involvement of inflammasomes in tumor microenvironment and tumor therapies. *J Hematol Oncol*. (2023) 16:24. doi: 10.1186/s13045-023-01407-7

214. Krysko DV, Garg AD, Kaczmarek A, Krysko O, Agostinis P, Vandenabeele P. Immunogenic cell death and DAMPs in cancer therapy. *Nat Rev Cancer*. (2012) 12:860–75. doi: 10.1038/nrc3380

215. Zou Y, Palte MJ, Deik AA, Li H, Eaton JK, Wang W, et al. A GPX4-dependent cancer cell state underlies the clear-cell morphology and confers sensitivity to ferroptosis. *Nat Commun*. (2019) 10:1617. doi: 10.1038/s41467-019-09277-9

216. Semenza GL. Hypoxia-inducible factors in physiology and medicine. *Cell*. (2012) 148:399–408. doi: 10.1016/j.cell.2012.01.021

217. Noman MZ, Buart S, Romero P, Ketari S, Janji B, Mari B, et al. Hypoxia-inducible miR-210 regulates the susceptibility of tumor cells to lysis by cytotoxic T cells. *Cancer Res*. (2012) 72:4629–41. doi: 10.1158/0008-5472.CAN-12-1383

218. Zhao C, Yu D, He Z, Bao L, Feng L, Chen L, et al. Endoplasmic reticulum stress-mediated autophagy activation is involved in cadmium-induced ferroptosis of renal tubular epithelial cells. *Free Radical Biol Med*. (2021) 175:236–48. doi: 10.1016/j.freeradbiomed.2021.09.008

219. Zeng L, Yang K, Yu G, Hao W, Zhu X, Ge A, et al. Advances in research on immunocyte iron metabolism, ferroptosis, and their regulatory roles in autoimmune and autoinflammatory diseases. *Cell Death Dis*. (2024) 15:481. doi: 10.1038/s41419-024-06807-2

220. Yee PP, Wei Y, Kim S-Y, Lu T, Chih SY, Lawson C, et al. Neutrophil-induced ferroptosis promotes tumor necrosis in glioblastoma progression. *Nat Commun*. (2020) 11:5424. doi: 10.1038/s41467-020-19193-y

221. Xu S, Min J, Wang F. Ferroptosis: an emerging player in immune cells. *Sci Bull*. (2021) 66:2257–60. doi: 10.1016/j.scib.2021.02.026

222. Sun LL, Linghu DL, Hung MC. Ferroptosis: a promising target for cancer immunotherapy. *Am J Cancer Res*. (2021) 11:5856–63.

223. Hong T, Lei G, Chen X, Li H, Zhang X, Wu N, et al. PARP inhibition promotes ferroptosis via repressing SLC7A11 and synergizes with ferroptosis inducers in BRCA-proficient ovarian cancer. *Redox Biol*. (2021) 42:101928. doi: 10.1016/j.redox.2021.101928

224. Xu T, Ma Y, Yuan Q, Hu H, Hu X, Qian Z, et al. Enhanced ferroptosis by oxygen-boosted phototherapy based on a 2-in-1 nanoplatform of ferrous hemoglobin for tumor synergistic therapy. *ACS Nano*. (2020) 14:3414–25. doi: 10.1021/acsnano.9b09426

225. Urrutia PJ, Bórquez DA, Núñez MT. Inflaming the brain with iron. *Antioxidants*. (2021) 10:61. doi: 10.3390/antiox1001006

226. Delaby C, Rondeau C, Pouzet C, Willemetz A, Pilard N, Desjardins M, et al. Subcellular localization of iron and heme metabolism related proteins at early stages of erythrophagocytosis. *PloS One*. (2012) 7:e42199. doi: 10.1371/journal.pone.0042199

227. Lu K, Dong S, Xia T, Mao L. Kupffer Cells Degrade14 C-Labeled Few-Layer Graphene to14 CO2 in Liver through Erythrophagocytosis. *ACS Nano*. (2021) 15:396–409. doi: 10.1021/acsnano.0c07452

228. Han F, Li S, Yang Y, Bai Z. Interleukin-6 promotes ferroptosis in bronchial epithelial cells by inducing reactive oxygen species-dependent lipid peroxidation and disrupting iron homeostasis. *Bioengineered*. (2021) 12:5279–88. doi: 10.1080/21655979.2021.1964158

229. Xiao X, Xu Y, Moschetta GA, Yu Y, Fisher AL, Alfaro-Magallanes VM, et al. BMP5 contributes to hepcidin regulation and systemic iron homeostasis in mice. *Blood*. (2023) 142:1312–22. doi: 10.1182/blood.2022019195

230. Billesbølle CB, Azumaya CM, Kretsch RC, Powers AS, Gonen S, Schneider S, et al. Structure of hepcidin-bound ferroportin reveals iron homeostatic mechanisms. *Nature*. (2020) 586:807–11. doi: 10.1038/s41586-020-2668-z

231. Shyam R, Ogando DG, Choi M, Liton PB, Bonanno JA. Mitochondrial ROS induced lysosomal dysfunction and autophagy impairment in an animal model of congenital hereditary endothelial dystrophy. *Invest Ophthalmol Vis Sci*. (2021) 62:15. doi: 10.1167/iovs.62.12.15

232. Zhang B, Yang Y, Yi J, Zhao Z, Ye R. Hyperglycemia modulates M1/M2 macrophage polarization via reactive oxygen species overproduction in ligature-induced periodontitis. *J Periodontal Res*. (2021) 56:991–1005. doi: 10.1111/jre.12912

233. Wan C, Sun Y, Tian Y, Lu L, Dai X, Meng J, et al. Irradiated tumor cell–derived microparticles mediate tumor eradication via cell killing and immune reprogramming. *Sci Adv*. (2020) 6:eaay9789. doi: 10.1126/sciadv.aay9789

234. Winn BA, Devkota L, Kuch B, MacDonough MT, Strecker TE, Wang Y, et al. Bioreductively activatable prodrug conjugates of combretastatin A-1 and combretastatin A-4 as anticancer agents targeted toward tumor-associated hypoxia. *J Nat Prod*. (2020) 83:937–54. doi: 10.1021/acs.jnatprod.9b00773

235. Sarode P, Zheng X, Giotopoulou GA, Weigert A, Kuenne C, Günther S, et al. Reprogramming of tumor-associated macrophages by targeting β-catenin/FOSL2/ARID5A signaling: A potential treatment of lung cancer. *Sci Adv*. (2020) 6:eaaz6105. doi: 10.1126/sciadv.aaz6105

236. Jiang Q, Wang K, Zhang X, Ouyang B, Liu H, Pang Z, et al. Platelet membrane-camouflaged magnetic nanoparticles for ferroptosis-enhanced cancer immunotherapy. *Small*. (2020) 16:2001704. doi: 10.1002/smll.202001704

237. Zwicker C, Bujko A, Scott CL. Hepatic macrophage responses in inflammation, a function of plasticity, heterogeneity or both? *Front Immunol*. (2021) 12:690813. doi: 10.3389/fimmu.2021.690813

238. Wang H, Li L, Li Y, Li Y, Sha Y, Wen S, et al. Intravital imaging of interactions between iNKT and kupffer cells to clear free lipids during steatohepatitis. *Theranostics*. (2021) 11:2149–69. doi: 10.7150/thno.51369

239. Geppert M, Himly M. Iron oxide nanoparticles in bioimaging – an immune perspective. *Front Immunol*. (2021) 12:688927. doi: 10.3389/fimmu.2021.688927

240. Hsieh C-H, Hsieh H-C, Shih F-H, Wang P-W, Yang L-X, Shieh D-B, et al. An innovative NRF2 nano-modulator induces lung cancer ferroptosis and elicits an immunostimulatory tumor microenvironment. *Theranostics*. (2021) 11:7072–91. doi: 10.7150/thno.57803

241. Niu X, Chen L, Li Y, Hu Z, He F. Ferroptosis, necroptosis, and pyroptosis in the tumor microenvironment: Perspectives for immunotherapy of SCLC. *Semin Cancer Biol*. (2022) 86:273–85. doi: 10.1016/j.semcancer.2022.03.009

242. Shang Y, He Y, Zhang X, He W, Hua H, Ye F, et al. Optimization of immunotherapy strategies based on spatiotemporal heterogeneity of tumour-associated tissue-resident memory T cells. *Immunology*. (2025) 175:123–262. doi: 10.1111/imm.13924

243. Song R, Li T, Ye J, Sun F, Hou B, Saeed M, et al. Acidity-activatable dynamic nanoparticles boosting ferroptotic cell death for immunotherapy of cancer. *Advanced Materials*. (2021) 33:2101155. doi: 10.1002/adma.202101155

244. Cunningham A, Oudejans LL, Geugien M, Pereira-Martins DA, Wierenga ATJ, Erdem A, et al. The nonessential amino acid cysteine is required to prevent ferroptosis in acute myeloid leukemia. *Blood Adv*. (2024) 1:56–69. doi: 10.1182/bloodadvances.2023010786

245. Costa I, Barbosa DJ, Benfeito S, Silva V, Chavarria D, Borges F, et al. Molecular mechanisms of ferroptosis and their involvement in brain diseases. *Pharmacol Ther*. (2023) 244:108373. doi: 10.1016/j.pharmthera.2023.108373

246. Kosyakovsky J, Fine J, Frey W, Hanson L. Mechanisms of intranasal deferoxamine in neurodegenerative and neurovascular disease. *Pharmaceuticals*. (2021) 14:95. doi: 10.3390/ph14020095

247. Li Z, Lange M, Dixon SJ, Olzmann JA. Lipid quality control and ferroptosis: from concept to mechanism. *Annu Rev Biochem*. (2024) 93:499–528. doi: 10.1146/annurev-biochem-052521-033527

248. Bao C, Liu C, Liu Q, Hua L, Hu J, Li Z, et al. Corrigendum to "Liproxstatin-1 alleviates LPS/IL-13-induced bronchial epithelial cell injury and neutrophilic asthma in mice by inhibiting ferroptosis" [Int. Immunopharmacol. 109 (2022) 108770. *Int Immunopharmacol*. (2023) 115:109482. doi: 10.1016/j.intimp.2022.109482

249. Tang Z-Y, Li Y, Tang Y-T, Ma X-D, Tang Z-Y. Anticancer activity of oleanolic acid and its derivatives: Recent advances in evidence, target profiling and mechanisms of action. *Biomedicine Pharmacotherapy*. (2022) 145:112397. doi: 10.1016/j.biopha.2021.112397

250. Song L, Hao Y, Wang C, Han Y, Zhu Y, Feng L, et al. Liposomal oxaliplatin prodrugs loaded with metformin potentiate immunotherapy for colorectal cancer. *J Controlled Release*. (2022) 350:922–32. doi: 10.1016/j.jconrel.2022.09.013

251. Rellmann Y, Gronau I, Hansen U, Dreier R. 4-phenylbutyric acid reduces endoplasmic reticulum stress in chondrocytes that is caused by loss of the protein disulfide isomerase ERp57. *Oxid Med Cell Longevity*. (2019) 2019:1–12. doi: 10.1155/2019/6404035

frontiers | Frontiers in Immunology

TYPE Original Research
PUBLISHED 06 June 2025
DOI 10.3389/fimmu.2025.1610267

Check for updates

OPEN ACCESS

EDITED BY
Qingyu Luo,
Dana–Farber Cancer Institute, United States

REVIEWED BY
Yanting Chen,
Duke University, United States
Yihang Qi,
Harvard Medical School, United States
Yuxuan Xue,
The University of Hong Kong, Hong Kong SAR, China

*CORRESPONDENCE
Tao Yan
yantao@cicams.ac.cn;
blizzardyt@163.com
Yi Liu
931160913@qq.com
Li Sun
ykyzlyysunli@126.com

†These authors have contributed equally to this work and share first authorship

RECEIVED 11 April 2025
ACCEPTED 16 May 2025
PUBLISHED 06 June 2025

CITATION
Tan P-x, Wu L-x, Ma S, Wei S-j, Wang T-h, Wang B-c, Fu B-b, Yang J-s, Zhao Q, Sun L, Liu Y and Yan T (2025) Impact of postoperative depression and immune-inflammatory biomarkers on the prognosis of patients with esophageal cancer receiving minimally invasive esophagectomy: a retrospective cohort study based on a Chinese population.
Front. Immunol. 16:1610267.
doi: 10.3389/fimmu.2025.1610267

COPYRIGHT
© 2025 Tan, Wu, Ma, Wei, Wang, Wang, Fu, Yang, Zhao, Sun, Liu and Yan. This is an open-access article distributed under the terms of the Creative Commons Attribution License (CC BY). The use, distribution or reproduction in other forums is permitted, provided the original author(s) and the copyright owner(s) are credited and that the original publication in this journal is cited, in accordance with accepted academic practice. No use, distribution or reproduction is permitted which does not comply with these terms.

Impact of postoperative depression and immune-inflammatory biomarkers on the prognosis of patients with esophageal cancer receiving minimally invasive esophagectomy: a retrospective cohort study based on a Chinese population

Pei-xin Tan[1†], Lin-xin Wu[1†], Shuang Ma[2†], Shi-jing Wei[1†], Tai-hang Wang[1†], Bing-chen Wang[3†], Bing-bing Fu[1†], Jia-shuo Yang[1†], Qing Zhao[4,5], Li Sun[6*], Yi Liu[7*] and Tao Yan[1*]

[1]Department of Anesthesiology, National Cancer Center/National Clinical Research Center for Cancer/Cancer Hospital, Chinese Academy of Medical Sciences and Peking Union Medical College, Beijing, China, [2]School of Information Science and Engineering, Shenyang Ligong University, Shenyang, China, [3]Department of Hepatobiliary Surgery, National Cancer Center/National Clinical Research Center for Cancer/Cancer Hospital, Chinese Academy of Medical Sciences and Peking Union Medical College, Beijing, China, [4]Department of Diagnostic Radiology, National Cancer Center/National Clinical Research Center for Cancer/Cancer Hospital, Chinese Academy of Medical Sciences and Peking Union Medical College, Beijing, China, [5]Department of Radiology, Shanxi Province Cancer Hospital/Shanxi Hospital Affiliated to Cancer Hospital, Chinese Academy of Medical Sciences/Cancer Hospital Affiliated to Shanxi Medical University, Taiyuan, China, [6]Department of Anesthesiology, Shenzhen Samii Medical Centre, The Fourth People's Hospital of Shenzhen, Shenzhen, China, [7]Department of Anesthesiology, Shanxi Province Cancer Hospital/Shanxi Hospital Affiliated to Cancer Hospital, Chinese Academy of Medical Sciences/Cancer Hospital Affiliated to Shanxi Medical University, Taiyuan, China

Background: Patients with esophageal cancer (EC) frequently experience depression following neoadjuvant therapy and surgery, a condition that may trigger systemic inflammation, suppress antitumor immunity, and alter immune-inflammatory pathways in the tumor microenvironment (TME), potentially contributing to residual tumor progression and theoretically worsening patient prognosis. This study aimed to investigate the interrelationship between depression and prognosis in patients with EC, with a focus on immune-inflammatory biomarkers.

Methods: This single-center retrospective trial was conducted at the National Cancer Center/Cancer Hospital of the Chinese Academy of Medical Sciences. A total of 319 patients who underwent minimally invasive esophagectomy between November 2023 and December 2024 were enrolled. Least absolute shrinkage and selection operator (LASSO) regression in combination with multivariate Cox and logistic regression were employed to identify the main impact indicators of relapse-free survival (RFS) and depression. The developed predictive model was

evaluated using calibration plots, receiver operating characteristic (ROC) curves, and decision curve analysis (DCA). Internal validation was carried out using a 7:3 data split.

Results: LASSO and Cox regression identified clinical stage (hazard ratio [HR] =2.472, P=0.003), the preoperative systemic inflammatory index (SII, HR=1.001, P<0.001), and depression severity (HR=2.398, P=0.004) as independent predictors of RFS. Based on these variables, a predictive model for RFS was constructed utilizing multivariate logistic regression and visualized as a nomogram. The model demonstrated good discriminative ability, with the areas under the ROC curves (AUCs) of 0.826 (6 months) and 0.773 (12 months) in the training set and 0.817 (6 months) and 0.789 (12 months) in the validation set. The incidence of postoperative depression in the study cohort was 28.2%, with chronic postsurgical pain identified as the sole independent risk factor for depression.

Conclusion: This study revealed that preoperative immune-inflammatory biomarkers and postoperative depression significantly affect patient prognosis after minimally invasive esophagectomy. Our work has also provided new insight into the individualized and comprehensive management of patients with EC, underscoring the necessity for comprehensive psychosocial interventions alongside conventional anticancer therapies to optimize clinical endpoints.

KEYWORDS

esophageal cancer, prognosis, depression, immune-inflammatory biomarkers, predictive model

1 Introduction

According to the 2024 GLOBOCAN report, esophageal cancer (EC) ranks 7th in terms of global cancer-related mortality and remains one of the most prevalent malignant tumors, with a 5-year survival rate ranging from 10% to 30% after diagnosis (1, 2). In 2022, there were approximately 511,000 new cases of EC worldwide, resulting in an estimated 445,000 deaths. Notably, China accounts for more than 50% of the global burden, with 346,000 new cases and 323,000 deaths (1, 3). With advancements in endoscopic surgery techniques, minimally invasive esophagectomy (MIE) has emerged as the primary treatment for EC and substantially improves patient survival. Nevertheless, given the highly traumatic nature of the procedure, prolonged postoperative recovery period, and increased rate of postoperative complications, patients with EC usually suffer from poor postoperative quality of life and long-term health outcomes (4–10).

Depression is a major complication among postoperative patients with cancer (5). The postoperative depression rate among patients with breast cancer might exceed 30% (11), and a recent meta-analysis revealed that depression might predict breast cancer mortality (12). In the case of lung cancer, the morbidity rates of patients with newly developed depression after thoracoscopic surgery and open thoracotomy are 12.4% and 16.1%, respectively (13). Patients with EC also experience a relatively high incidence of depression, with rates of approximately 20% preoperatively and 27% at 6 months and 32% at 12 months postoperatively (14). These statistics underscore the considerable psychological burden faced by patients with cancer throughout the continuum of care.

In addition to the well-documented psychological burden of depression, emerging evidence suggests that its pathophysiology may be intertwined with systemic inflammatory processes (15). Systemic inflammation can modulate the comorbidity of depression and impact tumor progression through neuroimmune pathways (16) and the tumor microenvironment (TME) (17). Conversely, inflammatory mediators such as tumor necrosis factor-α (TNF-α), interleukin-1β (IL-1β) and IL-6 can be released in response to psychological stress and surgical injury and can cross the blood-brain barrier and induce the upregulation of corticotropin-releasing factor (CRF) (18). Concurrently, these inflammatory signals cause dysfunction of the reward circuit (19), which further exacerbates emotional disorders, thereby creating a vicious cycle.

The relationship between postoperative depression and cancer prognosis has attracted increasing attention, with recent investigations emphasizing the role of underlying inflammatory mechanisms (20) and advances in the biopsychosocial model (21).

MIE involves significant surgical trauma, complex multimodal therapies, and extended recovery periods, all of which impose considerable biological and psychological stress on patients. EC exhibits a lower prevalence outside Asia, and the evidence linking depression to survival outcomes remains limited (5, 22). In light of this gap, we conducted a retrospective analysis to evaluate the association between depression and relapse-free survival (RFS) and to explore the potential role of perioperative immune-inflammatory biomarkers in mediating this association.

2 Materials and methods

2.1 Patient selection

In this retrospective cohort study, we enrolled patients with EC at the National Cancer Center/Cancer Hospital of the Chinese Academy of Medical Sciences from November 2023 to December 2024. Participants were included based on the following criteria: (1) pathological diagnosis of esophageal adenocarcinoma (EAC), esophageal squamous cell carcinoma (ESCC), or esophageal adenosquamous carcinoma; (2) underwent MIE; (3) at least 3 months of postoperative follow-up with complete follow-up data available; and (4) at least 18 years of age and capable of understanding the study objectives to comply with the follow-up procedures.

The exclusion criteria were as follows: (1) the presence of distant metastasis (defined as M1 stage according to the 8th edition of the AJCC TNM classification) or concomitant malignant tumors before esophagectomy; (2) a history of chronic pain (defined as pain persisting for more than 3 months, including chronic low back pain, arthritis-related pain, or neuropathic pain) or a preoperative diagnosis of a mental disorder (including major depressive disorder, generalized anxiety disorder, bipolar disorder, or schizophrenia); (3) the presence of severe infection, hematologic disease, or autoimmune disease; and (4) incomplete clinical data or a follow-up duration of less than 3 months.

Ethics approval was received from the Institutional Ethics Committee of Cancer Hospital (Approval Number: 25/110-5056). All data were extracted from the database of the clinical electronic medical records system. Medical ethical principles were strictly observed during the research process to ensure patient privacy and data confidentiality, and all data were used only for analysis and reports in this study.

2.2 Data acquisition

Data on population characteristics and clinical aspects, including age, sex, height, weight, body mass index (BMI), history of neoadjuvant therapy, tumor type, clinical stage, tumor differentiation, postoperative adjuvant therapy, and other relevant data, were retrieved from the clinical electronic medical records system. Postoperative pathology results were assessed through pathological reports (ypTNM by the American Joint Committee on Cancer, 8th edition) (23). Hematologic parameters, including neutrophils (NEU) count, lymphocytes (LYM) count, monocytes (MONO) count, albumin (ALB) level, C-reactive protein (CRP) level, and platelets (PLT) count, were collected preoperatively and one week postoperatively. Immune-inflammatory biomarkers were processed using the following calculations: (1) systemic immune-inflammation index (SII) =PLT×NEU/LYM; (2) systemic inflammation response index (SIRI) =NEU×MONO/LYM; (3) neutrophil-to-lymphocyte ratio (NLR) =NEU/LYM; (4) inflammatory burden index (IBI) =CRP×NEU/LYM; (5) pan-immune-inflammation value (PIV) =NEU×MONO×PLT/LYM; (6) CRP-to-albumin ratio (CAR) =CRP/ALB; (7) CRP-to-lymphocyte ratio (CLR) =CRP/LYM; (8) lymphocyte-to-monocyte ratio (LMR) =LYM/MONO; and (9) CRP-albumin-lymphocyte (CALLY) index =ALB×LYM/(CRP×10).

2.3 Follow-up

All patients received postoperative follow-up through outpatient visits or telephone conversations, with assessments conducted every three months. The follow-up period lasted from the date of surgery to March 30, 2025, or until all-cause mortality. We defined the RFS as the interval from surgery to confirmed disease recurrence. Recurrence or metastasis was diagnosed based on pathologic examination or imaging modalities with diagnostic value, including computed tomography (CT), magnetic resonance imaging (MRI), bone scintigraphy and others.

A psychiatrist with specialized expertise evaluated the patient's postoperative depression using the Patient Health Questionnaire (PHQ-9) (Supplementary Table 1). Follow-up visits were conducted between 9:00 AM and 10:00 AM at 3 months postoperatively to ensure the homogeneity of the follow-up data. The overall score of nine items (each rated on a scale of 0–3) was calculated, with higher scores indicating a greater level of depression (24, 25). The total PHQ-9 total score ranges from 0 to 27 (scores of 0–4 are classified as nondepression; scores of 5–9 are classified as mild depression; and scores of ≥10 are classified as moderate-to-severe depression) (26, 27).

An experienced anesthesiologist assessed postoperative pain using the numeric rating scale (NRS) (28) at 48 h and 3 months after surgery. Pain that emerged or intensified following surgical procedures, persisted for more than 3 months, and was confined to the surgical area was regarded as chronic postsurgical pain (CPSP), as defined by the International Association of the Study of Pain (29).

2.4 Statistical analysis

The datasets used in the study were analyzed using R software (version 4.2.1; R Foundation for Statistical Computing) and IBM SPSS Statistics 26.0 software. The tidyverse package (version 1.3.1) in R was deployed for multiple imputations to handle missing data. The caret package (versions 6.0-90) was used to randomly assign

patients to a 7:3 split, with 70% in the training set and 30% in the validation set for internal validation. Data with a normal distribution are presented as the mean ± standard deviation. To compare two groups, Student's t-test was employed, and three or more groups were compared using one-way ANOVA. Data that did not adhere to the normal distribution are presented as the median (quartile range). Comparisons between two groups were performed with the Wilcoxon rank sum test, and comparisons among three or more groups were performed with the Kruskal-Wallis test. Count data are expressed as frequencies (%), and differences were assessed via the χ^2 test or Fisher's exact test.

We employed the R language ggplot2 package to draw survival curves (version 3.4.0) and the R language survival package to perform the log-rank test (version 3.5-7). The variables were subsequently screened using the least absolute shrinkage and selection operator (LASSO) and cross-validated with 10-fold partitioning. LASSO regression was selected for variable screening because it is particularly effective in handling high-dimensional data and multicollinearity while preventing model overfitting, which aligns well with the characteristics of our dataset. We determined the optimal regularization parameter λ by performing 10-fold cross-validation and selecting the largest λ value within one standard error of the minimum cross-validation error (λ1se). The glmnet package (version 4.1-4) was used to conduct the LASSO regression. Multivariate Cox regression analysis was used to evaluate the independent effects of multiple variables on survival and control for the effects of other confounding factors. The hazard ratio (HR) was calculated for each predictive factor, along with the corresponding 95% confidence interval (CI). To construct a predictive model, multivariate logistic regression was applied to the variables that had been screened previously. The model was then visualized by constructing a nomogram for RFS. To determine the effectiveness of the model, the receiver operating characteristic (ROC) curve was drawn, and the areas under the ROC curves (AUCs) were computed. In addition, the accuracy of its prediction and clinical utility were further evaluated by employing calibration curves and decision curve analysis (DCA). The analysis and figures were obtained using the proc (v1.18.0), rms (v6.3-0), and rmda (v1.6.0) packages. A P value less than 0.05 was regarded as statistically significant unless otherwise noted.

3 Results

Based on the inclusion criteria, 354 patients were enrolled from the initial 824 patients, 35 of whom were excluded for meeting exclusion criteria, including other surgical procedures (due to distant metastasis or other malignancies), surgical contradictions (due to perioperative infection, blood disease, or autoimmune disease), or loss to follow-up. Ultimately, the analysis included 319 patients. Figure 1 illustrates the criteria for including or excluding patients who underwent surgery for EC between November 2023 and December 2024. For further analysis, these patients were split into two categories: 224 for training and 95 for validation.

3.1 Baseline demographics

To confirm the consistency of the significant baseline characteristics, comparisons were made between the baseline variables of the training and validation sets. There were 95 patients in the validation set and 224 in the training set, with an allocation ratio of 3:7. According to the statistical test results, the baseline features of the patients in the validation and training sets did not differ significantly in any other way except for the status of proficient mismatch repair (pMMR) (P=0.004, Table 1).

3.2 Identification of independent prognostic factors

We used the maximum selection rank statistics method to perform LASSO regression analysis to screen for key variables associated with RFS in patients with EC (results in Figures 2A, B; λ1se=3). LASSO regression identified clinical stage, preoperative SII, and depression severity as key factors affecting RFS.

These elements were subsequently incorporated into the multivariate Cox regression analysis. The clinical stage, preoperative SII, and depression severity independently predicted RFS in patients with EC. The RFS was significantly associated with clinical stage (P=0.003), and the mortality risk increased approximately 2.47-fold for each additional clinical stage (HR=2.472, 95% CI: 1.365-4.476). Among the various immune-inflammatory biomarkers considered, the SII was selected as the key predictor for RFS. The P value of the preoperative SII was less than 0.001, and for each additional unit of preoperative SII, the risk of relapse slightly increased (HR=1.001, 95% CI: 1–1.002). Depression severity was also significantly associated with RFS (P=0.004). The relapse risk in patients with severe depression was 2.4 times greater than that in patients with mild depression (HR=2.398, 95% CI: 1.333–4.316). The results were shown in Figure 2C.

We determined the optimal cutoff point of the preoperative systemic inflammatory index (pre-SII) to be 913.95 based on the maximally selected rank statistics. Patients were classified into a low pre-SII group or a high pre-SII group in accordance with this threshold (Figure 3A). A further log-rank test revealed that the SII was a significant influencing factor for RFS, and compared with that of the low pre-SII group, the RFS of the high pre-SII group was substantially lower (P<0.0001; Figure 3B). With increasing clinical stage, the RFS of patients was notably reduced, and the difference was highly statistically significant (P<0.0001; Figure 3C). Patients with varying severities of depression showed that those with severe depression had the poorest RFS, with statistically significant differences (P=0.0025; Figure 3D). Other factors were not significantly associated with patient RFS.

3.3 Design and confirmation of the predictive model

Using the independent predictors from the multivariate Cox regression, a logistic regression model was formulated to estimate

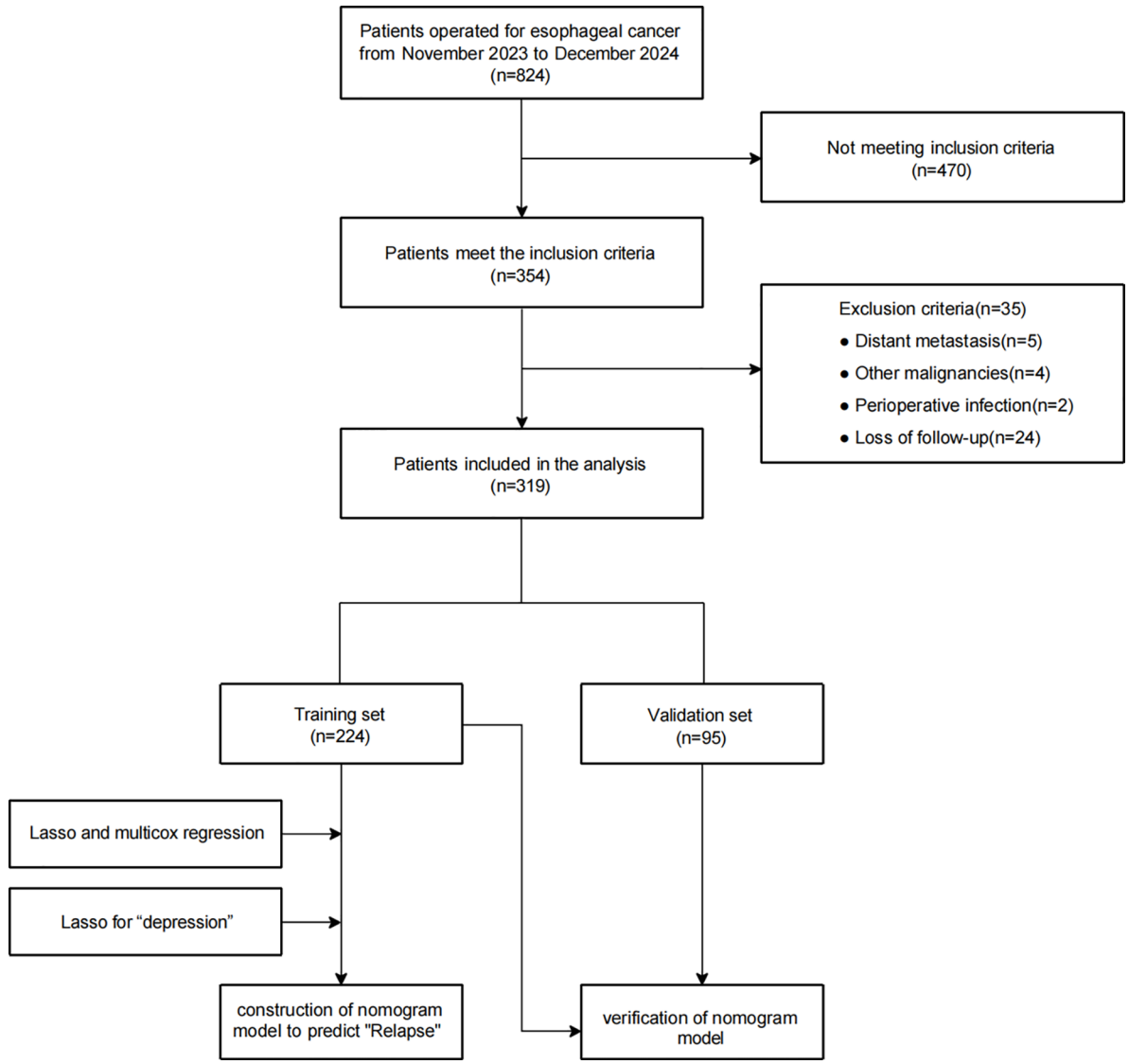

FIGURE 1
Inclusion and exclusion flow chart.

RFS risk. The nomogram in Figure 4A illustrates the predictive model for estimating patient survival probability at 6 months and 12 months following surgery. The performance of the model was measured by the ROC curve, with the training set's 6-month and 12-month prediction AUCs being 0.826 (95% CI: 0.716–0.936) and 0.773 (95% CI: 0.656–0.891), respectively (Figure 4B). In the validation set, the AUCs for the 6-month and 12-month predictions were 0.817 (95% CI: 0.540–1.000) and 0.789 (95% CI: 0.582–0.996), respectively (Figure 4E). The calibration plots of the model for 6-month prediction in the training set are shown in Figure 4C, and the calibration plots of the model for 12-month prediction in the validation set are shown in Figure 4F, indicating that the nomogram was closely aligned with the observed postoperative recurrence outcomes. Further evaluation of the nomogram graph was conducted using decision curve analysis (DCA), as shown in Figures 4D,G. The model curves were higher than the baselines within a certain range in the training set (Figure 4D), especially within the threshold probability interval of 10% to 60%. Although the overall net benefit value was slightly lower in the validation set (Figure 4G), the model curves were still higher than the baselines of "Treat All" and "Treat None" between the 5% and 50% intervals, indicating that the model has good generalizability for external data and has certain clinical decision-making value. Our recently created nomogram can successfully differentiate between patients at high and low risk and has good discrimination capacity in both the training and validation categories, suggesting that the clinical stage, preoperative SII, and depression severity are key risk factors for EC recurrence.

3.4 Identification of independent influencing factors of depression

In the present study, the postoperative survival outcomes of patients were systematically evaluated, and the importance of

10.3389/fimmu.2025.1610267

TABLE 1 Statistical test results of training set and validation set.

Characteristic	Whole population (n=319)	Training cohort (n=224)	Validation cohort (n=95)	P value
Sex [a]				0.431
Female	43 (13.5)	28 (12.5)	15 (15.8)	
Male	276 (86.5)	196 (87.5)	80 (84.2)	
Age [b]	63.2 ± 7.6	63.2 ± 7.8	63.2 ± 7.1	0.983
BMI [b]	23.4 ± 3.1	23.3 ± 3.2	23.7 ± 2.9	0.243
Neoadjuvant chemotherapy [a]				0.870
No	72 (22.6)	50 (22.3)	22 (23.2)	
Yes	247 (77.4)	174 (77.7)	73 (76.8)	
Neoadjuvant immunotherapy [a]				0.629
No	107 (33.5)	77 (34.4)	30 (31.6)	
Yes	212 (66.5)	147 (65.6)	65 (68.4)	
Neoadjuvant radiotherapy [a]				0.773
No	278 (87.1)	196 (87.5)	82 (86.3)	
Yes	41 (12.9)	28 (12.5)	13 (13.7)	
Pathological response [a]				0.760
non-neoadjuvant therapy	224 (70.2)	160 (71.4)	64 (67.4)	
pCR	47 (14.7)	32 (14.3)	15 (15.8)	
Non-pCR	48 (15)	32 (14.3)	16 (16.8)	
Chemotherapy cycles [a]				0.962
0 cycles	74 (23.2)	52 (23.2)	22 (23.2)	
1–3 cycles	194 (60.8)	137 (61.2)	57 (60)	
≥ 4 cycles	51 (16)	35 (15.6)	16 (16.8)	
Nausea [a]				0.177
No	296 (92.8)	205 (91.5)	91 (95.8)	
Yes	23 (7.2)	19 (8.5)	4 (4.2)	
Dizzy [a]				0.440
No	282 (88.4)	196 (87.5)	86 (90.5)	
Yes	37 (11.6)	28 (12.5)	9 (9.5)	
NRS (at rest) [a]				0.135
Mild pain	299 (93.7)	207 (92.4)	92 (96.8)	
Moderate-high pain	20 (6.3)	17 (7.6)	3 (3.2)	
NRS (during activity) [a]				0.881
Mild pain	240 (75.2)	168 (75)	72 (75.8)	
Moderate-high pain	79 (24.8)	56 (25)	23 (24.2)	
PDL1 positivity [a]				0.673
(-)	247 (77.4)	172 (76.8)	75 (78.9)	
(+)	72 (22.6)	52 (23.2)	20 (21.1)	

(Continued)

TABLE 1 Continued

Characteristic	Whole population (n=319)	Training cohort (n=224)	Validation cohort (n=95)	P value
pMMR [a]				0.004
No	289 (90.6)	196 (87.5)	93 (97.9)	
Yes	30 (9.4)	28 (12.5)	2 (2.1)	
Pathology [a]				0.621
Non-ESCC	36 (11.3)	24 (10.7)	12 (12.6)	
ESCC	283 (88.7)	200 (89.3)	83 (87.4)	
Differentiation [a]				0.699
poorly differentiated	131 (41.1)	95 (42.4)	36 (37.9)	
moderately differentiated	153 (48)	103 (46)	50 (52.6)	
well-differentiated	14 (4.4)	11 (4.9)	3 (3.2)	
Intraepithelial Neoplasia	21 (6.6)	15 (6.7)	6 (6.3)	
Clinical stage [a]				0.323
I+II	142 (44.5)	99 (44.2)	43 (45.3)	
III	157 (49.2)	108 (48.2)	49 (51.6)	
IV	20 (6.3)	17 (7.6)	3 (3.2)	
Preoperative SII [c]	409.1 (279.5, 628.3)	406.8 (283.6, 615.3)	419.7 (266.1, 648.6)	0.564
Preoperative SIRI [c]	0.9 (0.6, 1.3)	0.9 (0.6, 1.3)	0.9 (0.6, 1.2)	0.864
Preoperative NLR [c]	2.2 (1.6, 3.2)	2.2 (1.6, 3.3)	2.3 (1.5, 3)	0.941
Preoperative PIV [c]	165.3 (100.7, 268.2)	165.1 (100.1, 264.8)	170.6 (102.9, 273.5)	0.902
Preoperative IBI [c]	3.1 (1.3, 8.6)	3.1 (1.2, 9.8)	3 (1.4, 7.7)	0.548
Preoperative CAR [c]	0 (0, 0.1)	0 (0, 0.1)	0 (0, 0.1)	0.431
Preoperative CLR [c]	1 (0.4, 3.6)	1.1 (0.3, 4.4)	1 (0.4, 1.9)	0.647
Preoperative LMR [c]	3.9 (2.9, 5.2)	3.9 (2.9, 5.3)	3.9 (2.8, 5.1)	0.782
Preoperative CALLY [c]	4.3 (1.8, 10.7)	4.1 (1.6, 10.3)	4.4 (2.4, 11.7)	0.259
Postoperative SII [c]	914.1 (663.9, 1364.6)	939.7 (686.6, 1360.5)	900.5 (617.7, 1347.2)	0.582
Postoperative SIRI [c]	2 (1.4, 3.3)	2.1 (1.4, 3.4)	1.9 (1.3, 3.2)	0.292
Postoperative NLR [c]	4.6 (3.4, 6.8)	4.7 (3.4, 6.8)	4.3 (3.2, 6.6)	0.430
Postoperative PIV [c]	431.2 (263.8, 701.5)	444 (269.5, 724.5)	398 (259.6, 591.1)	0.326
Postoperative IBI [c]	27 (12.3, 53.7)	29.3 (12.9, 53.9)	21.2 (11.4, 44)	0.090
Postoperative CAR [c]	0.1 (0.1, 0.3)	0.2 (0.1, 0.3)	0.1 (0.1, 0.3)	0.136
Postoperative CLR [c]	5.3 (2.8, 10.5)	5.5 (3.1, 11.1)	4.6 (2.5, 9.2)	0.196
Postoperative LMR [c]	2.3 (1.7, 3.1)	2.3 (1.7, 3)	2.4 (1.7, 3.3)	0.515
Postoperative CALLY [c]	0.1 (0, 0.1)	0.1 (0, 0.1)	0.1 (0, 0.2)	0.237
Distance from incisors [a]				0.906
Upper	136 (42.6)	97 (43.3)	39 (41.1)	
Middle	168 (52.7)	117 (52.2)	51 (53.7)	
Lower	15 (4.7)	10 (4.5)	5 (5.3)	

(Continued)

TABLE 1 Continued

Characteristic	Whole population (n=319)	Training cohort (n=224)	Validation cohort (n=95)	P value
Postoperative chemotherapy [a]				0.316
No	212 (66.5)	145 (64.7)	67 (70.5)	
Yes	107 (33.5)	79 (35.3)	28 (29.5)	
Postoperative immunotherapy [a]				0.765
No	228 (71.5)	159 (71)	69 (72.6)	
Yes	91 (28.5)	65 (29)	26 (27.4)	
Postoperative radiotherapy [a]				0.052
No	286 (89.7)	196 (87.5)	90 (94.7)	
Yes	33 (10.3)	28 (12.5)	5 (5.3)	
Depression severity [a]				0.413
Nondepressed	229 (71.8)	157 (70.1)	72 (75.8)	
Mild depressed	79 (24.8)	60 (26.8)	19 (20)	
Moderate-to-severe depressed	11 (3.4)	7 (3.1)	4 (4.2)	
CPSP [a]				0.767
No	222 (69.6)	157 (70.1)	65 (68.4)	
Yes	97 (30.4)	67 (29.9)	30 (31.6)	

[a]Data are n (%) and are compared by χ^2 test.
[b]Data are mean ± standard deviation and are compared by Student's t test.
[c]Data are median (interquartile range) and are compared by Mann-Whitney U test.
Abbreviations: BMI, body mass index; pCR, pathological complete response; pMMR, proficient mismatch repair; ESCC, esophageal squamous cell carcinoma; SII, systemic immune-inflammation index; SIRI, systemic inflammation response index; NLR, neutrophil-to-lymphocyte ratio; PIV, pan-immune-inflammation value; IBI, inflammatory burden index; CAR, C-reactive protein to albumin ratio; CLR, C-reactive protein to lymphocyte ratio; LMR, lymphocyte to monocyte ratio; CALLY, CRP-albumin-lymphocyte index.

variables such as clinical stage, inflammatory indicators, and psychological state in prognosis prediction was revealed by constructing a multivariate nomogram model. On this basis, this study focused on the prediction and analysis of postoperative depression. Among the 319 analyzed patients, 90 experienced postoperative depression (28.2%), with 79 (24.8%) classified as mild and 11 (3.4%) as moderate-to-severe based on follow-up assessments (Table 1). To identify the main factors influencing postoperative depression in patients with EC, we used the maximum selection rank statistics method to perform LASSO regression analysis. According to the outcomes, CPSP was the only independent risk factor for depression that was identified (results in Figures 5A, B; λ1se=1), precluding the possibility of a predictive model.

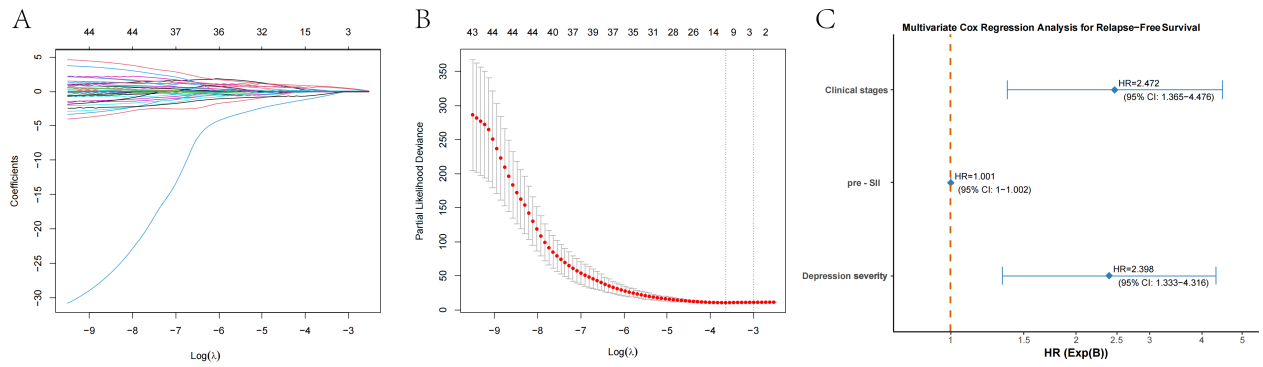

FIGURE 2
LASSO regression and multivariate Cox regression for prognostic factors in patients with esophageal cancer. **(A)** LASSO regression plot showing the relationship between the logarithm of the penalty parameter [Log (λ)] and the coefficients of selected prognostic variables. **(B)** Partial likelihood deviance plot from LASSO regression, illustrating the fit of the model as the Log (λ) changes. **(C)** Multivariate Cox regression analysis for relapse-free survival (RFS), showing the hazard ratios (HR) for clinical stage, the preoperative systemic inflammatory index (pre-SII), and depression severity. The HR values with 95% confidence intervals (CI) are provided for each factor.

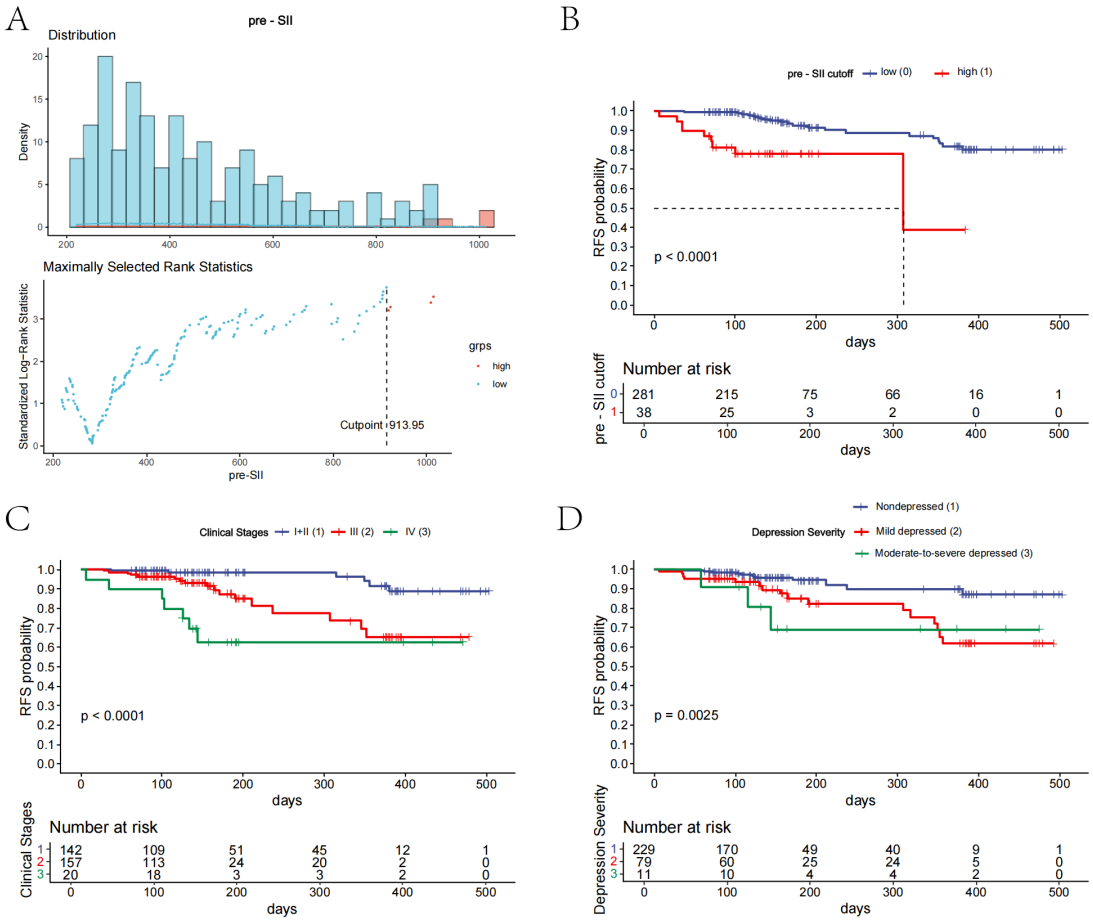

FIGURE 3
Kaplan-Meier curves for prognostic factors in patients with esophageal cancer. **(A)** The distribution of the preoperative systemic inflammatory index (pre-SII) and the optimal cutoff value of 913.95 were determined using maximally selected rank statistics. **(B)** Kaplan-Meier curve illustrating the relapse-free survival (RFS) for patients with a preoperative SII above or below the established cutoff value. **(C)** Kaplan-Meier curve showing the RFS for patients stratified by clinical stage. **(D)** Kaplan-Meier curve showing the RFS for patients categorized by depression severity.

4 Discussion

This study retrospectively analyzed the correlation between depression and RFS in patients with EC and further explored the predictive value of several popular immune-inflammatory biomarkers. The results demonstrated that clinical stage, preoperative SII, and depression severity were independent prognostic factors for RFS. The predictive model, constructed based on these factors, demonstrated strong discrimination and calibration for predicting 6-month and 12-month recurrence across the training and validation cohorts, with DCA confirming its clinical utility. These findings underscore the critical prognostic value of inflammatory biomarkers alongside depression.

Consistent with earlier studies (30–33), we found that the preoperative SII was an independent factor for RFS, further confirming that inflammatory markers can be used as effective predictors of prognosis in patients with EC. A large prospective cohort study revealed that the SII was more strongly associated with cancer risk than other inflammatory markers, such as the NLR and the LMR (34). Recent studies have demonstrated that the SII, calculated as the platelet count × neutrophil count/lymphocyte count, reflects systemic immune-inflammatory conditions and is linked to both the morbidity and overall mortality of patients with cancer (35, 36). Neutrophils can promote metastasis from the primary tumor site by promoting the escape of cancer cells into the vasculature and escorting circulating tumor cells to enable cell cycle progression (37, 38). Similarly, platelets actively participate in every stage of tumorigenesis, including tumor growth, tumor cell extravasation, and metastasis (39). Conversely, both T lymphocytes and B lymphocytes are critical in the antitumor immune response (40, 41). Thus, a higher SII suggests a dominance of tumor-promoting inflammation over immune surveillance, which is correlated with a worse prognosis. Similar to a previous report, which identified a preoperative SII ≤916.6 as a favorable prognostic indicator in patients with advanced ESCC (24), an SII ≤913.95 was associated with significantly prolonged RFS in patients with EC. In addition to the SII, several other immune-inflammatory biomarkers have also been used to predict the prognosis of different types of tumors in previous studies. The CALLY index has been reported to be a positive indicator of long-term survival in patients with EC

10.3389/fimmu.2025.1610267

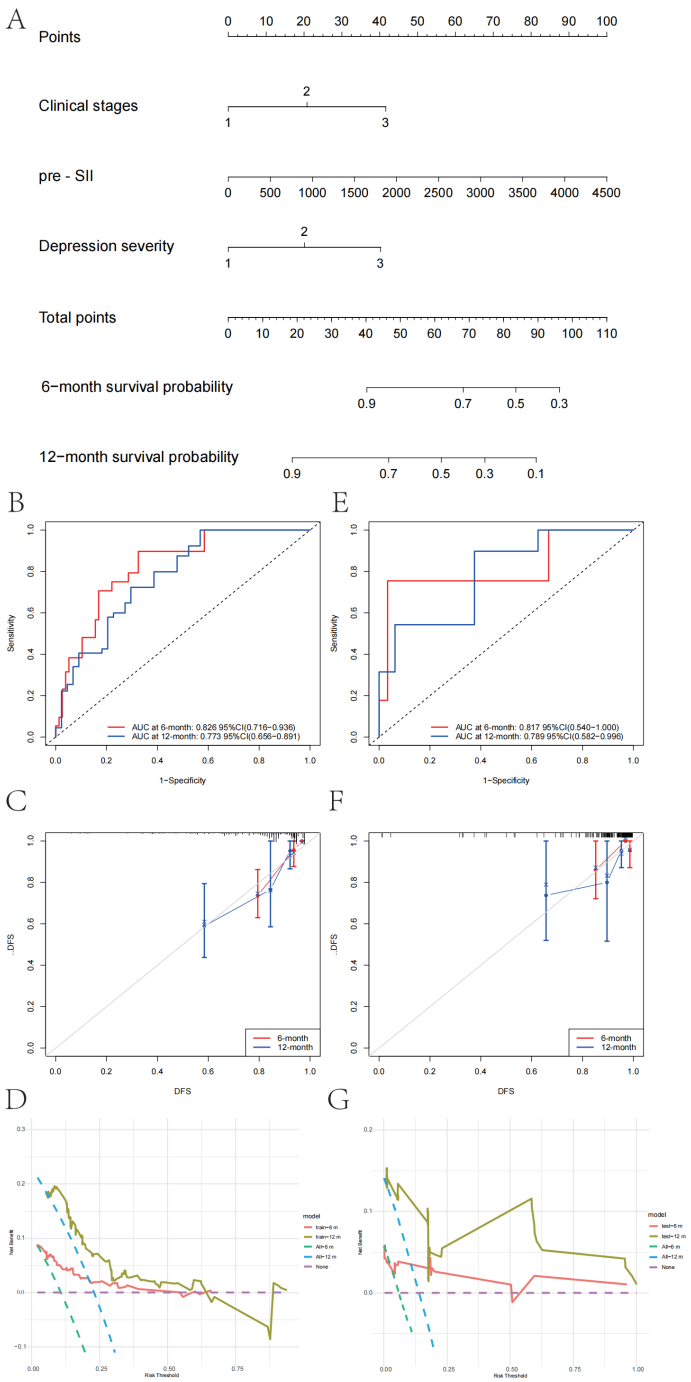

FIGURE 4
Nomogram and performance evaluation for prognosis prediction in patients with esophageal cancer. **(A)** Nomogram for predicting the 6-month and 12-month survival probabilities of patients with esophageal cancer. The total points are calculated based on the clinical stage, preoperative systemic inflammatory index (pre-SII), and depression severity. **(B)** Receiver operating characteristic (ROC) curve for the 6-month and 12-month survival predictive models in the training set. **(C)** Calibration curve for the 6-month and 12-month survival predictive models in the training set, showing the agreement between the predicted and observed survival probabilities. **(D)** Decision curve analysis (DCA) for the 6-month and 12-month survival models in the training set, evaluating the net clinical benefit of using the model at different threshold probabilities. **(E)** ROC curve for the 6-month and 12-month survival predictive models in the validation set. **(F)** Calibration curve for the 6-month and 12-month survival predictive models in the validation set, demonstrating model calibration. **(G)** DCA for the 6-month and 12-month survival models in the validation set was performed to assess the net clinical benefit of the model for decision-making.

(42). Additionally, a higher CLR has also been reported to be related to negative outcomes in patients with colorectal and pancreatic cancers (43). Moreover, a multicenter prospective study revealed that the IBI is the most effective systemic inflammatory marker for predicting the outcome of non-small cell lung cancer, and patients with higher IBI levels had a notably poorer prognosis than individuals with lower IBI levels did (44). However, these factors did not correlate with prognosis in patients with EC in this study.

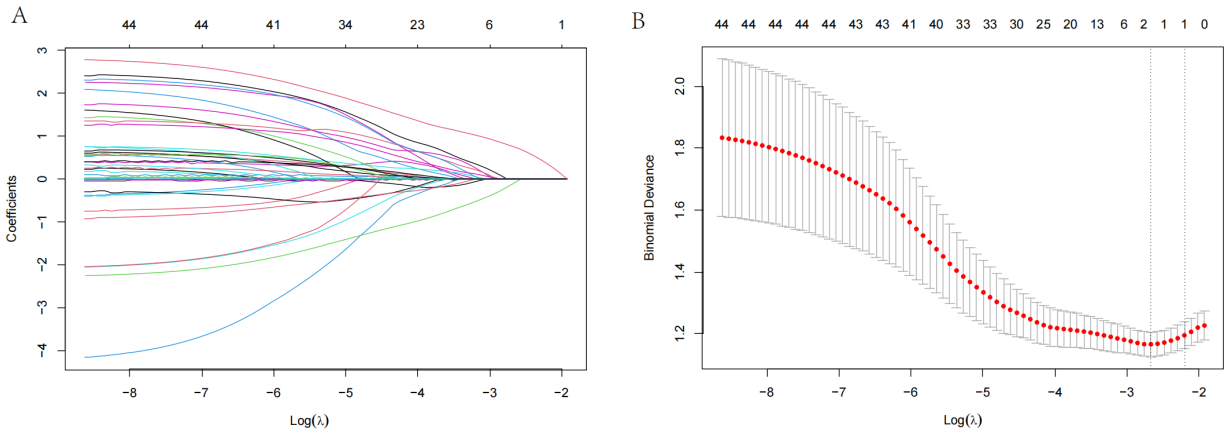

FIGURE 5
LASSO regression analysis for postoperative depression in patients with esophageal cancer. **(A)** LASSO regression plot showing the relationship between the logarithm of the penalty parameter [Log (λ)] and the coefficients of the selected variables for depression. **(B)** Partial likelihood deviance plot from LASSO regression, illustrating the fit of the model as the Log (λ) changes.

This discrepancy may be attributed to the heterogeneity of cancer-related inflammatory pathways.

MIE involves significant surgical trauma, complex multimodal therapies, and a long recovery period, and is often associated with chronic pain, all of which put physical and psychological stress on the patient and predispose them to depression. From a clinical perspective, the prevalence of depression reportedly ranges from 27% to 44% among patients with EC within one year of diagnosis (45). The incidence of postoperative depression in this study was 28.2%, which is in line with previously reported rates. Postoperative depression is known to significantly impair quality of life after MIE (46, 47), but its impact on recurrence remains limited. Luo et al. reported that comorbid anxiety and depression independently predicted nutritional impairment and were correlated with significantly inferior survival outcomes compared to nondistressed counterparts in patients with EC during the peri-radiotherapy period (48). The interplay among primary tumor progression, side effects of neoadjuvant therapies and surgery, and depression-induced appetite disturbance may synergistically contribute to malnutrition and poor prognosis through distinct biological pathways (49, 50). From a basic research perspective, depression and EC share commonalities in terms of systemic inflammation and immune dysregulation, suggesting a potentially shared pathogenesis. First, inflammatory cytokines play a prominent role in both conditions. Depression has been linked to elevated levels of cytokines, including TGF-β1, IL-1β and IL-6 (51, 52). These proinflammatory cytokines are also enriched in the TME, contributing to immune suppression and correlating with poor outcomes in patients with ESCC (53, 54). Second, immune cell dysregulation is a hallmark of both depression and EC (55). Elevated serum myeloid-derived suppressor cell (MDSC) expression has been demonstrated in patients with EC, reinforcing the role of these cells in disease progression (56). They not only promote tumor immune escape by decreasing the neutralizing function of T cells (57) but also may be implicated in chronic low-grade systemic inflammation and immune dysfunction in depression (58). Third, immune-inflammatory proteins such as CRP and immune-checkpoint proteins are also involved in depression and EC. Depression and EC were found to be correlated with CRP levels exceeding 10 mg/L (46) and with elevated serum expression, respectively (59). Another classic immune-inflammatory protein is programmed cell death protein 1 (PD-1), which is expressed on the membranes of T-cells and inhibits immune responses by binding to programmed cell death ligand 1 (PD-L1) on cancer cells (53, 60). Patients with EC with increased PD-L1 levels may face a poor prognosis (61, 62). The PD-1/PD-L1 pathway is also dysregulated in patients with depression, leading to reduced immune surveillance and the persistence of inflammatory responses (55). Notably, the immune-inflammatory response affects tumor progression through elevated cytokines, immune–cell dysregulation, and immune–checkpoint activation, which together function as an interconnected cascade. A recent review highlighted that MDSCs, as key immune-suppressive cells, contribute to immune tolerance in the TME by secreting cytokines (such as IL-6 and TGF-β) and upregulating PD-L1 expression, which together inhibit the T-cell-mediated antitumor response and worsen patient prognosis. Simultaneously, tumor-secreted proinflammatory cytokines stimulate myeloid progenitor cells in the bone marrow, leading to their differentiation into MDSCs and recruitment to the tumor site, thereby forming a malignant feedback loop (63). Although the immune-inflammatory response is closely linked to depression, the precise mechanisms involved remain unclear. Future prospective studies should combine mental assessments with corresponding real-time serological data to elucidate the specific mechanism between depression and inflammation and pave the way for a novel scientific issue: whether improvements in mental health could improve prognosis through immune-inflammatory pathways in patients with EC.

Given the relationship between depression and cancer progression, this study also analyzed the risk factors for postoperative depression. LASSO regression identified CPSP as the sole significant factor. Emerging evidence suggests that CPSP is

commonly accompanied by depression (64). On the other hand, prolonged depression may enhance central sensitization via long-term potentiation (LTP), potentially exacerbating acute pain after surgery and shifting pain from acute to chronic (65). Given this bidirectional relationship, integrating psychosocial interventions and postoperative pain management may be crucial in optimizing clinical outcomes in patients with EC. Notably, the relationship between postoperative pain and oncological outcomes has increasingly become a focus of research. The National Comprehensive Cancer Network (NCCN) guidelines report that chronic pain is strongly associated with worsened quality of life and prognosis in patients with tumors (66). Furthermore, acute perioperative pain can exacerbate surgical stress responses by increasing sympathetic nervous system activation and neuroendocrine activity, thereby suppressing natural killer (NK) cell cytotoxicity (67). As pivotal antitumor immune effectors, reduced NK cell activity may facilitate the evasion of compromised immunosurveillance by circulating tumor cells, consequently increasing the risk of recurrence and metastasis. While this study did not identify significant associations between postoperative pain and RFS, this does not preclude potential effects within specific patient subgroups. Future longitudinal studies should prioritize clarifying the mechanistic links between CPSP, depression and tumor progression.

The reliability of the prognostic model for RFS was also verified in this study. The prognostic model in patients with EC demonstrated good discriminatory ability, with AUC values of 0.826 and 0.773 for 6-month and 12-month prediction in the training set and 0.817 and 0.789 in the validation set, respectively. Calibration and DCA analyses revealed high accuracy and clinical decision-making value, with the model offering substantial net clinical benefit. This study provides a tool for prognostic evaluation in patients with EC, highlighting the importance of combining psychological interventions with regular follow-up care for oncology treatment in clinical practice.

There are several limitations that we must mention. First, it is a retrospective analysis with a certain degree of selection bias. The data come from a single hospital, which may limit their generalizability. A multicenter, large-sample prospective study for the external validation of our model will be conducted in the future. Second, immune-inflammatory factors and some specific biomarkers at the follow-up time points were unable to be assessed due to the retrospective nature of our study. Larger-scale prospective research is needed to explore the dynamic changes in immune-inflammatory factors and their interactions with psychological health. Finally, although our study fills a gap in research on depression and postoperative survival in patients with EC, the mechanisms linking depression with the prognosis of EC still require further exploration through basic research.

5 Conclusion

This study reveals a close relationship between depression, the preoperative SII and the prognosis of patients with EC. Establishing a reliable prognostic model can assist clinicians in identifying high-risk groups for EC recurrence. These findings provide novel insights for future research to elucidate the specific interaction mechanism of psychiatric comorbidities and prognosis in patients with EC, with the goal of developing targeted therapies.

Data availability statement

The datasets analyzed contain information that could be used to identify the individuals included, therefore are not uploaded as Supplementary Material. The datasets can be obtained from the corresponding authors upon reasonable request. Requests to access these datasets should be directed to TY, blizzardyt@163.com.

Ethics statement

The studies involving humans were approved by the Ethics Committee of the Cancer Hospital of the Chinese Academy of Medical Sciences. The studies were conducted in accordance with the local legislation and institutional requirements. The human samples used in this study were acquired from a by-product of routine care. Written informed consent for participation was not required from the participants or the participants' legal guardians/next of kin in accordance with the national legislation and institutional requirements.

Author contributions

P-XT: Writing – original draft, Investigation, Data curation, Conceptualization, Writing – review & editing. L-XW: Data curation, Conceptualization, Writing – review & editing, Investigation. SM: Writing – review & editing, Funding acquisition, Methodology, Software, Formal analysis. S-JW: Conceptualization, Investigation, Writing – review & editing, Data curation. T-HW: Writing – review & editing, Conceptualization, Investigation, Formal analysis, Methodology. B-CW: Visualization, Software, Methodology, Formal analysis, Writing – review & editing. B-BF: Data curation, Writing – review & editing, Investigation, Conceptualization. J-SY: Data curation, Conceptualization, Investigation, Writing – review & editing. QZ: Resources, Funding acquisition, Writing – review & editing. LS: Validation, Writing – review & editing, Supervision, Project administration. YL: Writing – review & editing, Supervision, Validation, Project administration. TY: Resources, Project administration, Validation, Supervision, Methodology, Writing – review & editing.

Funding

The author(s) declare that financial support was received for the research and/or publication of this article. Support for this work was received from the Youth program of Beijing Natural Science

Foundation (7244398), the Fundamental Research Program of Shanxi Province (202403021211143), the Liaoning Provincial Department of Education Basic Research Project Youth Project (Grant Nos. JYTQN2023051), the Bethune Charitable Foundation (BCF, kqxs-2024-A-02), and the National Science and Technology Major Project of China (Innovation 2030, Development and Application of Liquid Biopsy in Therapeutic Decision-Making for Solid Tumors. 2024ZD0533300).

Acknowledgments

We thank the enrolled esophageal cancer patients and all the medical staff in our study.

Conflict of interest

The authors declare that the research was conducted in the absence of any commercial or financial relationships that could be construed as a potential conflict of interest.

Generative AI statement

The author(s) declare that no Generative AI was used in the creation of this manuscript.

Publisher's note

All claims expressed in this article are solely those of the authors and do not necessarily represent those of their affiliated organizations, or those of the publisher, the editors and the reviewers. Any product that may be evaluated in this article, or claim that may be made by its manufacturer, is not guaranteed or endorsed by the publisher.

Supplementary material

The Supplementary Material for this article can be found online at: https://www.frontiersin.org/articles/10.3389/fimmu.2025.1610267/full#supplementary-material

References

1. Bray F, Laversanne M, Sung H, Ferlay J, Siegel RL, Soerjomataram I, et al. Global cancer statistics 2022: globocan estimates of incidence and mortality worldwide for 36 cancers in 185 countries. *CA: Cancer J Clin*. (2024) 74:229–63. doi: 10.3322/caac.21834

2. Herskovic A, Russell W, Liptay M, Fidler MJ, Al-Sarraf M. Esophageal carcinoma advances in treatment results for locally advanced disease: review. *Ann Oncology: Off J Eur Soc Med Oncol*. (2012) 23:1095–103. doi: 10.1093/annonc/mdr433

3. Xia C, Dong X, Li H, Cao M, Sun D, He S, et al. Cancer statistics in China and United States, 2022: profiles, trends, and determinants. *Chin Med J*. (2022) 135:584–90. doi: 10.1097/CM9.0000000000002108

4. Bennett AE, O'Neill L, Connolly D, Guinan E, Boland L, Doyle S, et al. Perspectives of esophageal cancer survivors on diagnosis, treatment, and recovery. *Cancers (Basel)*. (2020) 13:100. doi: 10.3390/cancers13010100

5. Housman B, Flores R, Lee D-S. Narrative review of anxiety and depression in patients with esophageal cancer: underappreciated and undertreated. *J Thorac Dis*. (2021) 13:3160–70. doi: 10.21037/jtd-20-3529

6. Hu L-Y, Ku F-C, Wang Y-P, Shen C-C, Hu Y-W, Yeh C-M, et al. Anxiety and depressive disorders among patients with esophageal cancer in Taiwan: A nationwide population-based study. *Supportive Care Cancer: Off J Multinational Assoc Supportive Care Cancer*. (2015) 23:733–40. doi: 10.1007/s00520-014-2403-0

7. Ma Y, Wu H, Wei X, Yang Y, Xu Z, Chen Y. Comparison of different pain management strategies during the perioperative period of esophageal squamous cell carcinoma: A retrospective cohort study. *Perioperative Med (London England)*. (2025) 14:2. doi: 10.1186/s13741-024-00488-3

8. Müller-Stich BP, Probst P, Nienhüser H, Fazeli S, Senft J, Kalkum E, et al. Meta-analysis of randomized controlled trials and individual patient data comparing minimally invasive with open oesophagectomy for cancer. *Br J Surg*. (2021) 108:1026–33. doi: 10.1093/bjs/znab278

9. Wikman A, Ljung R, Johar A, Hellstadius Y, Lagergren J, Lagergren P. Psychiatric morbidity and survival after surgery for esophageal cancer: A population-based cohort study. *J Clin Oncology: Off J Am Soc Clin Oncol*. (2015) 33:448–54. doi: 10.1200/JCO.2014.57.1893

10. Yang Y, Han C, Xing X, Qin Z, Wang Q, Lan L, et al. Effects of postoperative complications on overall survival following esophagectomy: A meta-analysis using the restricted mean survival time analysis. *Thorac Cancer*. (2025) 16:e70011. doi: 10.1111/1759-7714.70011

11. Pilevarzadeh M, Amirshahi M, Afsargharehbagh R, Rafiemanesh H, Hashemi SM, Balouchi A. Global prevalence of depression among breast cancer patients: A systematic review and meta-analysis. *Breast Cancer Res Treat*. (2019) 176:519–33. doi: 10.1007/s10549-019-05271-3

12. Wang X, Wang N, Zhong L, Wang S, Zheng Y, Yang B, et al. Prognostic value of depression and anxiety on breast cancer recurrence and mortality: A systematic review and meta-analysis of 282,203 patients. *Mol Psychiatry*. (2020) 25:3186–97. doi: 10.1038/s41380-020-00865-6

13. O'Gara B, Espinosa Leon JP, Robinson K, Schaefer M, Talmor D, Fischer M. New onset postoperative depression after major surgery: an analysis from a national claims database. *BJA Open*. (2023) 8:100223. doi: 10.1016/j.bjao.2023.100223

14. Hellstadius Y, Lagergren J, Zylstra J, Gossage J, Davies A, Hultman CM, et al. A longitudinal assessment of psychological distress after oesophageal cancer surgery. *Acta Oncol*. (2017) 56:746–52. doi: 10.1080/0284186x.2017.1287945

15. Cash E, Albert C, Palmer I, Polzin B, Kabithe A, Crawford D, et al. Depressive symptoms, systemic inflammation, and survival among patients with head and neck cancer. *JAMA Otolaryngol Head Neck Surg*. (2024) 150:405–13. doi: 10.1001/jamaoto.2024.0231

16. Li M, She K, Zhu P, Li Z, Liu J, Luo F, et al. Chronic pain and comorbid emotional disorders: neural circuitry and neuroimmunity pathways. *Int J Mol Sci*. (2025) 26:436. doi: 10.3390/ijms26020436

17. Ma S, Lu Y, Sui S, Yang JS, Fu BB, Tan PX, et al. Unraveling the triad of immunotherapy, tumor microenvironment, and skeletal muscle biomechanics in oncology. *Front Immunol*. (2025) 16:1572821. doi: 10.3389/fimmu.2025.1572821

18. Rouwette T, Vanelderen P, Roubos EW, Kozicz T, Vissers K. The amygdala, a relay station for switching on and off pain. *Eur J Pain (London England)*. (2012) 16:782–92. doi: 10.1002/j.1532-2149.2011.00071.x

19. Borsook D, Linnman C, Faria V, Strassman AM, Becerra L, Elman I. Reward deficiency and anti-reward in pain chronification. *Neurosci Biobehav Rev*. (2016) 68:282–97. doi: 10.1016/j.neubiorev.2016.05.033

20. McFarland DC, Saracino RM, Miller AH, Breitbart W, Rosenfeld B, Nelson C. Prognostic implications of depression and inflammation in patients with metastatic lung cancer. *Future Oncol*. (2021) 17:183–96. doi: 10.2217/fon-2020-0632

21. Bolton D. A revitalized biopsychosocial model: core theory, research paradigms, and clinical implications. *Psychol Med*. (2023) 53:7504–11. doi: 10.1017/s0033291723002660

22. Zhu H, Wang Z, Deng B, Mo M, Wang H, Chen K, et al. Epidemiological landscape of esophageal cancer in asia: results from globocan 2020. *Thorac Cancer*. (2023) 14:992–1003. doi: 10.1111/1759-7714.14835

23. Sudo N, Ichikawa H, Muneoka Y, Hanyu T, Kano Y, Ishikawa T, et al. Clinical utility of yptnm stage grouping in the 8th edition of the american joint committee on cancer tnm staging system for esophageal squamous cell carcinoma. *Ann Surg Oncol*. (2021) 28:650–60. doi: 10.1245/s10434-020-09181-3

24. Mufson L, Morrison C, Shea E, Kluisza L, Robbins R, Chen Y, et al. Screening for depression with the phq-9 in young adults affected by hiv. *J Affect Disord*. (2022) 297:276–82. doi: 10.1016/j.jad.2021.10.037

25. Negeri ZF, Levis B, Sun Y, He C, Krishnan A, Wu Y, et al. Accuracy of the patient health questionnaire-9 for screening to detect major depression: updated systematic review and individual participant data meta-analysis. *BMJ (Clinical Res ed)*. (2021) 375: n2183. doi: 10.1136/bmj.n2183

26. Levis B, Benedetti A, Thombs BD. Accuracy of patient health questionnaire-9 (Phq-9) for screening to detect major depression: individual participant data meta-analysis. *Bmj*. (2019) 365:l1476. doi: 10.1136/bmj.l1476

27. Sun Y, Fu Z, Bo Q, Mao Z, Ma X, Wang C. The reliability and validity of phq-9 in patients with major depressive disorder in psychiatric hospital. *BMC Psychiatry*. (2020) 20:474. doi: 10.1186/s12888-020-02885-6

28. Khan JS, Sessler DI, Chan MTV, Wang CY, Garutti I, Szczeklik W, et al. Persistent incisional pain after noncardiac surgery: an international prospective cohort study. *Anesthesiology*. (2021) 135:711–23. doi: 10.1097/ALN.0000000000003951

29. Moloney NA, Pocovi NC, Dylke ES, Graham PL, De Groef A. Psychological Factors Are Associated with Pain at All Time Frames after Breast Cancer Surgery: A Systematic Review with Meta-Analyses. *Pain Med (Malden Mass)*. (2021) 22:915–47. doi: 10.1093/pm/pnaa363

30. Dong Y, Wang F, Deng J, Tong T, Chen X, Wu L, et al. Prognostic value of serum inflammatory markers in patients with esophageal squamous cell carcinoma undergoing surgery: A two-center retrospective cohort study. *BMC Cancer*. (2025) 25:213. doi: 10.1186/s12885-025-13600-7

31. Feng J, Wang L, Yang X, Chen Q. Clinical significance of preoperative cally index for prognostication in patients with esophageal squamous cell carcinoma undergoing surgery. *Sci Rep*. (2024) 14:713. doi: 10.1038/s41598-023-51109-w

32. Yang M, Lin S-Q, Liu X-Y, Tang M, Hu C-L, Wang Z-W, et al. Association between C-reactive protein-albumin-lymphocyte (Cally) index and overall survival in patients with colorectal cancer: from the investigation on nutrition status and clinical outcome of common cancers study. *Front Immunol*. (2023) 14:1131496. doi: 10.3389/fimmu.2023.1131496

33. Zhang H, Lin J, Huang Y, Chen Y. The systemic immune-inflammation index as an independent predictor of survival in patients with locally advanced esophageal squamous cell carcinoma undergoing neoadjuvant radiotherapy. *J Inflammation Res*. (2024) 17:4575–86. doi: 10.2147/JIR.S463163

34. Nøst TH, Alcala K, Urbarova I, Byrne KS, Guida F, Sandanger TM, et al. Systemic inflammation markers and cancer incidence in the uk biobank. *Eur J Epidemiol*. (2021) 36:841–8. doi: 10.1007/s10654-021-00752-6

35. Li Y, Yu M, Yang M, Yang J. The association of systemic immune-inflammation index with incident breast cancer and all-cause mortality: evidence from a large population-based study. *Front Immunol*. (2025) 16:1528690. doi: 10.3389/fimmu.2025.1528690

36. Lu W, Gong Y, Liu L, Zhang Y, Tian X, Liu H. Association of systemic immune-inflammatory index with all-cause and cancer mortality in americans aged 60 years and older. *Front Aging*. (2025) 6:1502746. doi: 10.3389/fragi.2025.1502746

37. Bald T, Quast T, Landsberg J, Rogava M, Glodde N, Lopez-Ramos D, et al. Ultraviolet-radiation-induced inflammation promotes angiotropism and metastasis in melanoma. *Nature*. (2014) 507:109–13. doi: 10.1038/nature13111

38. Szczerba BM, Castro-Giner F, Vetter M, Krol I, Gkountela S, Landin J, et al. Neutrophils escort circulating tumour cells to enable cell cycle progression. *Nature*. (2019) 566:553–7. doi: 10.1038/s41586-019-0915-y

39. Haemmerle M, Stone RL, Menter DG, Afshar-Kharghan V, Sood AK. The platelet lifeline to cancer: challenges and opportunities. *Cancer Cell*. (2018) 33:965–83. doi: 10.1016/j.ccell.2018.03.002

40. Downs-Canner SM, Meier J, Vincent BG. Serody JS. *B Cell Funct Tumor Microenvironment. Annu Rev Immunol*. (2022) 40:169–93. doi: 10.1146/annurev-immunol-101220-015603

41. Tan X, Zhao X, Hu Z, Jiang D-S, Ma Z, Sun L, et al. Targeting Setdb1 in T cells induces transplant tolerance without compromising antitumor immunity. *Nature Communications*. (2025) 16:4534. doi: 10.1038/s41467-025-58841-z

42. Jia P, Shen F, Zhao Q, Wu X, Sun K, Wang X, et al. Association between C-reactive protein-albumin-lymphocyte index and overall survival in patients with esophageal cancer. *Clin Nutr (Edinburgh Scotland)*. (2025) 45:212–22. doi: 10.1016/j.clnu.2024.12.032

43. Fan Z, Luo G, Gong Y, Xu H, Qian Y, Deng S, et al. Prognostic value of the C-reactive protein/lymphocyte ratio in pancreatic cancer. *Ann Surg Oncol*. (2020) 27:4017–25. doi: 10.1245/s10434-020-08301-3

44. Xie H, Ruan G, Wei L, Deng L, Zhang Q, Ge Y, et al. The inflammatory burden index is a superior systemic inflammation biomarker for the prognosis of non-small cell lung cancer. *J Cachexia Sarcopenia Muscle*. (2023) 14:869–78. doi: 10.1002/jcsm.13199

45. Bergquist H, Ruth M, Hammerlid E. Psychiatric morbidity among patients with cancer of the esophagus or the gastro-esophageal junction: A prospective, longitudinal evaluation. *Dis Esophagus*. (2007) 20:523–9. doi: 10.1111/j.1442-2050.2007.00741.x

46. Du J, Kang Z, Zhao Z, Wu H, Chen Y, Zhang C, et al. Analysis of the effect of ivor-lewis esophagectomy and mckeown esophagectomy on perioperative anxiety and depression in patients with esophageal cancer. *Eur J Cancer Prev*. (2024) 33:200–7. doi: 10.1097/cej.0000000000000850

47. Edmondson J, Hunter J, Bakis G, O'Connor A, Wood S, Qureshi AP. Understanding post-esophagectomy complications and their management: the early complications. *J Clin Med*. (2023) 12:7622. doi: 10.3390/jcm12247622

48. Luo F, Lu Y, Chen C, Chang D, Jiang W, Yin R. Analysis of the risk factors for negative emotions in patients with esophageal cancer during the peri-radiotherapy period and their effects on malnutrition. *Int J Gen Med*. (2023) 16:6137–50. doi: 10.2147/IJGM.S444255

49. Boyle E, Elliott JA. Novel nutrition strategies in gastric and esophageal cancer. *Expert Rev Gastroenterol Hepatol*. (2025) 19:89–104. doi: 10.1080/17474124.2025.2457444

50. Kroemer NB, Opel N, Teckentrup V, Li M, Grotegerd D, Meinert S, et al. Functional connectivity of the nucleus accumbens and changes in appetite in patients with depression. *JAMA Psychiatry*. (2022) 79:993–1003. doi: 10.1001/jamapsychiatry.2022.2464

51. Black C, Miller BJ. Meta-analysis of cytokines and chemokines in suicidality: distinguishing suicidal versus nonsuicidal patients. *Biol Psychiatry*. (2015) 78:28–37. doi: 10.1016/j.biopsych.2014.10.014

52. Haapakoski R, Mathieu J, Ebmeier KP, Alenius H, Kivimäki M. Cumulative meta-analysis of interleukins 6 and 1β, tumour necrosis factor α and C-reactive protein in patients with major depressive disorder. *Brain Behav Immun*. (2015) 49:206–15. doi: 10.1016/j.bbi.2015.06.001

53. Zhang XJ, Yu Y, Zhao HP, Guo L, Dai K, Lv J. Mechanisms of tumor immunosuppressive microenvironment formation in esophageal cancer. *World J Gastroenterol*. (2024) 30:2195–208. doi: 10.3748/wjg.v30.i16.2195

54. Zheng Y, Li Y, Tang B, Zhao Q, Wang D, Liu Y, et al. Il-6-induced cd39 expression on tumor-infiltrating nk cells predicts poor prognosis in esophageal squamous cell carcinoma. *Cancer Immunol Immunother*. (2020) 69:2371–80. doi: 10.1007/s00262-020-02629-1

55. Yu S, Li W, Tang L, Fan X, Yao S, Zhang X, et al. Depression in breast cancer patients: immunopathogenesis and immunotherapy. *Cancer Lett*. (2022) 536:215648. doi: 10.1016/j.canlet.2022.215648

56. Gabitass RF, Annels NE, Stocken DD, Pandha HA, Middleton GW. Elevated myeloid-derived suppressor cells in pancreatic, esophageal and gastric cancer are an independent prognostic factor and are associated with significant elevation of the th2 cytokine interleukin-13. *Cancer Immunol Immunother*. (2011) 60:1419–30. doi: 10.1007/s00262-011-1028-0

57. Budhwar S, Verma P, Verma R, Rai S, Singh K. The yin and yang of myeloid derived suppressor cells. *Front Immunol*. (2018) 9:2776. doi: 10.3389/fimmu.2018.02776

58. Bauer ME, Teixeira AL. Neuroinflammation in mood disorders: role of regulatory immune cells. *Neuroimmunomodulation*. (2021) 28:99–107. doi: 10.1159/000515594

59. Groblewska M, Mroczko B, Sosnowska D, Szmitkowski M. Interleukin 6 and C-reactive protein in esophageal cancer. *Clin Chim Acta*. (2012) 413:1583–90. doi: 10.1016/j.cca.2012.05.009

60. Ma S, Wu J, Liu Z, He R, Wang Y, Liu L, et al. Quantitative characterization of cell physiological state based on dynamical cell mechanics for drug efficacy indication. *J Pharm Anal*. (2023) 13:388–402. doi: 10.1016/j.jpha.2023.03.002

61. Ohigashi Y, Sho M, Yamada Y, Tsurui Y, Hamada K, Ikeda N, et al. Clinical significance of programmed death-1 ligand-1 and programmed death-1 ligand-2 expression in human esophageal cancer. *Clin Cancer Res*. (2005) 11:2947–53. doi: 10.1158/1078-0432.Ccr-04-1469

62. Ma S, Zhang X, Dang D, Wang W, Wang Y, Liu L, et al. Dynamic characterization of single cells based on temporal cellular mechanical properties. *IEEE Trans Nanobioscience*. (2023) 22:19–27. doi: 10.1109/tnb.2021.3136198

63. Lasser SA, Ozbay Kurt FG, Arkhypov I, Utikal J, Umansky V. Myeloid-derived suppressor cells in cancer and cancer therapy. *Nat Rev Clin Oncol*. (2024) 21:147–64. doi: 10.1038/s41571-023-00846-y

64. Hassett AL, Marshall E, Bailey AM, Moser S, Clauw DJ, Hooten WM, et al. Changes in anxiety and depression are mediated by changes in pain severity in patients undergoing lower-extremity total joint arthroplasty. *Regional Anesth Pain Med*. (2018) 43:14–8. doi: 10.1097/AAP.0000000000000682

65. Chapman CR, Vierck CJ. The transition of acute postoperative pain to chronic pain: an integrative overview of research on mechanisms. *J Pain*. (2017) 18:359. doi: 10.1016/j.jpain.2016.11.004

66. Swarm RA, Paice JA, Anghelescu DL, Are M, Bruce JY, Buga S, et al. Adult cancer pain, version 3.2019, nccn clinical practice guidelines in oncology. *J Natl Compr Canc Netw*. (2019) 17:977–1007. doi: 10.6004/jnccn.2019.0038

67. Moorthy A, Eochagáin AN, Buggy DJ. Can acute postoperative pain management after tumour resection surgery modulate risk of later recurrence or metastasis? *Front Oncol*. (2021) 11:802592. doi: 10.3389/fonc.2021.802592

frontiers | Frontiers in Immunology

TYPE Original Research
PUBLISHED 12 June 2025
DOI 10.3389/fimmu.2025.1604394

Check for updates

OPEN ACCESS

EDITED BY
Xiaosheng Tan,
Rutgers, United States

REVIEWED BY
Zunsong Hu,
University of Tennessee Health Science Center (UTHSC), United States
Jin-Ming Zhang,
University of Texas Health Science Center at Houston, United States
Kang Yu,
National Institute of Arthritis and Musculoskeletal and Skin Diseases (NIH), United States
Shunian Xiang,
Admera Health, United States

*CORRESPONDENCE
Xuejun Sun
sunxy@mail.xjtu.edu.cn
Zhengshui Xu
xuzhengshui@xjtu.edu.cn

†These authors have contributed equally to this work

RECEIVED 01 April 2025
ACCEPTED 27 May 2025
PUBLISHED 12 June 2025

CITATION
Ye C, Chen X, Chen Z, Liu S, Kong R, Lin W, Zhu M, Sun X and Xu Z (2025) Comprehensive analysis of single-cell and bulk RNA sequencing data reveals an EGFR signature for predicting immunotherapy response and prognosis in pan-cancer. *Front. Immunol.* 16:1604394. doi: 10.3389/fimmu.2025.1604394

COPYRIGHT
© 2025 Ye, Chen, Chen, Liu, Kong, Lin, Zhu, Sun and Xu. This is an open-access article distributed under the terms of the Creative Commons Attribution License (CC BY). The use, distribution or reproduction in other forums is permitted, provided the original author(s) and the copyright owner(s) are credited and that the original publication in this journal is cited, in accordance with accepted academic practice. No use, distribution or reproduction is permitted which does not comply with these terms.

Comprehensive analysis of single-cell and bulk RNA sequencing data reveals an EGFR signature for predicting immunotherapy response and prognosis in pan-cancer

Changchun Ye[1,2†], Xiaoya Chen[2†], Zilu Chen[2], Shiyuan Liu[1], Ranran Kong[1], Wenhao Lin[2], Minxia Zhu[3], Xuejun Sun[2*] and Zhengshui Xu[1*]

[1]Department of Thoracic Surgery, The Second Affiliated Hospital of Xi'an Jiaotong University, Xi'an, Shaanxi, China, [2]Department of General Surgery, The First Affiliated Hospital of Xi'an Jiaotong University, Xi'an, Shaanxi, China, [3]Department of Thoracic Surgery, The First Affiliated Hospital of Wenzhou Medical University, Wenzhou, Zhejiang, China

Introduction: Immune checkpoint inhibitors (ICIs) have changed the paradigm of cancer treatment, but their effectiveness in some patients with epidermal growth factor receptor (EGFR) mutations is unsatisfactory. Therefore, it is necessary to develop a new biomarker for combined immunotherapy strategies to maximize the clinical benefits.

Methods: We collected and investigated 34 pan-cancer scRNA-Seq cohorts from The Cancer Genome Atlas (TCGA) and 10 bulk RNA-Seq cohorts utilizing multiple machine learning (ML) algorithms to identify and verify a representative EGFR-related gene signature (EGFR.Sig) as a predictive biomarker for immunotherapy response. Core genes were identified as Hub-EGFR.Sig to predict the prognosis of cancers and to understand the crosstalk between EGFR and the tumor immune microenvironment (TIME).

Results: EGFR.Sig can accurately predict the ICI response with an AUC of 0.77, demonstrating superior predictive performance compared to previously established signatures. Twelve core genes in EGFR.Sig were identified as Hub-EGFR.Sig, of which 4 immune resistance genes were previously verified in different CRISPR cohorts. Notably, the prognosis most related to Hub-EGFR.Sig was bladder cancer, which can be divided into two clusters with different responses to immunotherapy based on Hub-EGFR.Sig.

Discussion: We developed a promising pan-cancer signature based on EGFR-related genes to serve as a biomarker for immunotherapy response and survival outcome prediction. Furthermore, core genes were identified for future targeting, which will pave the way for improving the effect of immunotherapy in the context of combination immunotherapies.

KEYWORDS

immune checkpoint inhibitors (ICIs), epidermal growth factor receptor (EGFR), pan-cancer, scRNA-seq, immunotherapy response

1 Introduction

Immunotherapy with immune checkpoint inhibitors (ICIs) has innovatively expanded the field of cancer treatment and conferred substantial clinical benefits to patients over the past decade (1, 2). Since approved for clinical use, ICIs targeting humanized cytotoxic T lymphocyte antigen 4 (CTLA4), programmed cell death 1 (PD-1) or PD-1 ligand 1 (PD-L1) have been used to treat an ever-growing list of malignant tumors, such as melanoma, lung cancers, head and neck squamous cell cancer, bladder cancer (BLCA), and gastro-esophageal cancer (3). However, only a subset of patients respond to ICIs (4). Hence, the advancement of strategies for accurately predicting ICI response and improving understanding of resistance mechanisms to optimize ICI regimens is paramount (2, 5, 6). All of the above highlight the importance of identifying and developing predictive biomarkers for an ICI response.

Epidermal growth factor receptor (EGFR), which is widely distributed on the surface of epithelial cells in various tissues of mammals, is studied as one of the most well-known kinase receptors in the mechanism of tumorigenesis (7). The robust signaling of EGFR in the activation of prosurvival and antiapoptotic pathways can promote tumorigenesis, proliferation and invasiveness (8–10). Consequently, therapies targeting EGFR have advanced precision oncology. There are currently dozens of EGFR-targeting drugs for various tumors according to the updated directory of the FDA (11), such as gefitinib for the first-line treatment of non-small cell lung cancer (NSCLC) (12) and erdafitinib, which was first approved for urothelial carcinoma (UC) (13), and the drug catalogue is in continuous iteration (7). Therefore, EGFR may have the potential to be a powerful predictive biomarker for ICI response.

Currently, the crosstalk between immunotherapy and EGFR has received increasing attention (14, 15). Several clinical trials in NSCLC have suggested that most EGFR-mutated NSCLC shows a poor response to anti-PD-1/PD-L1 treatment (16–18). Initial results indicated that this phenomenon may be related to the interplay between EGFR and the immune environment, such as weakening immunogenicity through low PD-L1 expression, low $CD8^+$ tumor-infiltrating lymphocytes, and low tumor mutational burden (TMB); however, the specific mechanism is unclear (7, 16). Therefore, there is an urgent need for relevant research to comprehensively understand the relationship between EGFR and the tumor immunotherapy response in pan-cancer.

Compared with the traditional study of biomarkers based on the average genetic spectrum of many different cell populations in tumor tissue, the advent of single-cell RNA sequencing (scRNA-Seq) makes it possible to dissect gene expression in the single-cell dimension of malignant tumors, which enables us to identify more accurate and higher performance gene signatures as biomarkers (19). In the present study, we revealed the potential relationship between EGFR and immunotherapy response in two scRNA-Seq cohorts of patients treated with ICI therapy. Subsequently, we conducted a comprehensive analysis of 34 pan-cancer scRNA-Seq and 10 bulk RNA-Seq cohorts to identify a representative EGFR-related gene signature (EGFR.Sig). Furthermore, we extensively investigated and verified the predictive effectiveness of EGFR.Sig for immunotherapy response and identified hub genes in EGFR.Sig (Hub-EGFR.Sig) with the help of multiple machine learning (ML) algorithms to explore the relationship between EGFR and cancer prognosis. Finally, the prognosis of BLCA was found to be most significantly associated with Hub-EGFR.Sig and was analyzed in depth. Our findings more convincingly emphasize the potential of EGFR as a promising biomarker for predicting tumor immunotherapy response and prognosis across multiple cancer types.

2 Materials and methods

2.1 Data download

A total of 36 EGFR-related genes were obtained through the Gene Set Enrichment Analysis database (GSEA, https://www.gsea-msigdb.org/gsea, Supplementary Table S1). Gene set variation analysis (GSVA) can transform the expression matrix of genes into gene sets among different samples to evaluate the results of gene set enrichment (20). According to GSVA, the expression scores of EGFR-related gene sets in the datasets could be obtained.

To research the relationship between EGFR and the immunotherapy response of cancer cells, two scRNA–Seq ICI cohorts with definite curative effects were downloaded from the Gene

Expression Omnibus (GEO, https://www.ncbi.nlm.nih.gov/geo) database. One was a melanoma cohort (GSE115978, 33 patient samples, 7186 cells) for analysis (21), and the other was an independent basal cell carcinoma (BCC) cohort (GSE123813, 10 patient samples, 43640 cells) for verification (22).

To construct EGFR.Sig in pan-cancer, 34 scRNA-Seq datasets including 345 patients and 663760 cells were collected from the Tumor Immune Single-cell Hub (TISCH, http://tisch.comp-genomics.org/) portal (23). The TISCH database employs multiple integrated methodologies for comprehensive single-cell annotation within the tumor microenvironment. The datasets covered 17 cancer types, namely, BCC, breast cancer (BRCA), cholangiocarcinoma (CHOL), colorectal cancer (CRC), lower grade glioma (LGG), head and neck cancer (HNSC), liver hepatocellular carcinoma (LIHC), medulloblastoma (MB), Merkel cell carcinoma (MCC), multiple myeloma (MM), neuroendocrine tumor (NET), NSCLC, ovarian serous cystadenocarcinoma (OV), pancreatic adenocarcinoma (PAAD), skin cutaneous melanoma (SKCM), stomach adenocarcinoma (STAD), and uveal melanoma (UVM).

To explore the potential association between EGFR.Sig and the immune response, the transcriptome data of a TCGA pan-cancer cohort comprising 30 different cancer types were downloaded from the UCSC XENA (https://xenabrowser.net) data portal (24). Our analysis excluded some cancer types mainly composed of immune cells, including diffuse large B-cell lymphoma (DLBC), acute myeloid leukemia (LAML) and thymoma (THYM) (25). All downloaded sample data met the following criteria: (a) patients had mRNA expression data and clinical data, (b) patients had completed standardized diagnosis and treatment, including surgery, chemotherapy, and radiotherapy, and (c) survival data were available for patients with survival times greater than 30 days.

TMB was retrieved from cBioPortal (https://www.cbioportal.org) (26, 27). The intratumor heterogeneity (ITH) data were from published research by Thorsson et al. (28). These data were used to analyze the correlation between EGFR.Sig and TMB or ITH.

Ten ICI RNA-Seq cohorts with clinical information were systematically collected to construct a prediction model and subsequent survival analysis. These cohorts included 5 SKCM cohorts (Hugo 2016 (29), Liu 2019 (30), Gide 2019 (31), Riaz 2017 (32) and Van Allen 2015 (33, 34)), 2 urothelial carcinoma (UC) cohorts (Mariathasan 2018 (35), Synder 2017 (36)), 1 glioblastoma (GBM) cohort (Zhao 2019 (37)), 1 gastric cancer (GC) cohort (Kim 2018 (38)) and 1 renal cell carcinoma (RCC) cohort (Braun 2020 (39)). All included cohort samples were collected prior to immunotherapy treatment. For the same patient with multiple tissue samples, an earlier sample was selected, and each patient was counted as one case. After using COMPAT to eliminate the batch effect of different cohorts, the Braun 2020 RCC, Mariathasan 2018 UC, Liu 2019 SKCM, Gide 2019 SKCM and Riaz 2017 SKCM datasets were merged into a large dataset (n=772) according to a previously reported method (40). The combined dataset was randomly divided into a training set (80%, n=618) and a validation set (20%, n=154). In addition, Hugo 2016 SKCM, Synder 2017 UC and Zhao 2019 GBM were used as independent verification sets to evaluate the predictive value of the model.

The workflow is presented in Figure 1.

2.2 ScRNA-Seq data analysis

All scRNA-Seq data analyses and integrations were performed using R software Seurat v4.0.6. Based on the current mainstream practice in the field of scRNA-Seq of tumor tissues, we set strict quality control thresholds, excluding cells with less than 300 genes in a single cell and cells with more than 20% of mitochondrial genes (41). The data normalization and standardization of each sample were achieved by principal component analysis (PCA), and the batch differences between samples were achieved by the "harmony" package. The annotation of major cell types was performed based on well-established canonical marker genes from the TISCH database and relevant literature (23). Detailed procedures can refer to the TISCH portal website (http://tisch.comp-genomics.org/documentation/). Then, we reduced the dimension and visualized the scRNA-Seq data by the uniform manifold approximation and projection (UMAP) algorithm. The R "FindAllMarkers" package was used to identify differentially expressed genes between different cell types. Genes with a $\log_2$-fold change ($\log_2$FC) ≥1 and a false discovery rate (FDR) <1e-05 were considered differentially upregulated genes for each cell subtype (23). For malignant tumor cells, Spearman correlation analysis was used to discover the relationship between EGFR-related gene expression and EGFR scores in 34 scRNA-Seq datasets.

2.3 Evaluation of clinical efficacy

The main index of clinical outcomes was the objective response rate (ORR). ORR of all cohorts was assessed with the use of Response Evaluation Criteria in Solid Tumors (RECIST) version 1.1, except Hugo 2016, which was assessed with the immune-related RECIST (irRECIST) (42). According to the response status, patients with complete response (CR) and partial response (PR) were grouped as responders (R), while those with stable disease (SD) and progressive disease (PD) were considered nonresponders (NR). Moreover, TN represents treatment-naive patients.

2.4 Machine learning and prediction model construction

Eight common ML algorithms were used to train and adjust prediction models of ICI response based on EGFR.Sig. For the support vector machine (SVM), naive bayes (NB), random forest (RF), k-nearest neighbors (KNN), Adaptive Boosting (AdaBoost), logistic regression model (Logistic) and boosted logistic regression (LogiBoost) algorithms, fivefold cross-validation was used for hyperparameter tuning to optimize the performance of the model

10.3389/fimmu.2025.1604394

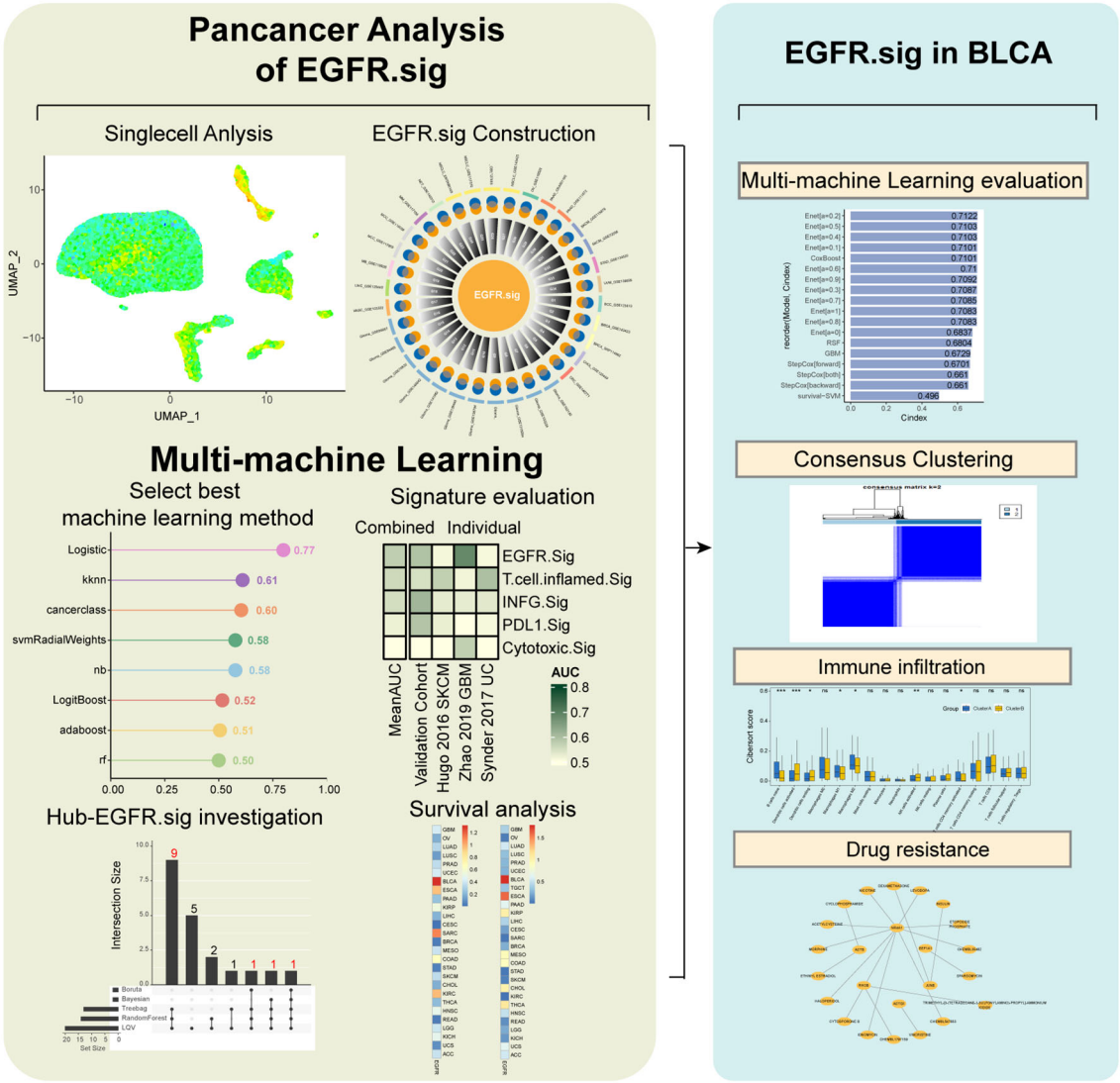

FIGURE 1
Workflow of this study.

(43). To ensure robustness, we repeated the optimization process 10 times using different random seeds for each single resampling (44). For cancer class algorithms, which do not require parameters, we directly used the entire training set to train the model. The receiver operating characteristic (ROC) curve and the area under the curve (AUC) were used to evaluate the sensitivity and specificity of the models. The analyses were performed using R packages including caret (v6.0-93), randomForest (v4.7-1.1), e1071 (v1.7-13), nnet (v7.3-18), and adabag (v4.2). Finally, the models constructed with the above algorithms were analyzed by the validation set to screen out the efficacy prediction model in pan-cancer immunotherapy. Furthermore, we compared the predictive efficiency of gene signatures in our study and other previously reported ICI response pan-cancer biomarkers, including INFG.Sig (45), T.cell.inflamed.Sig (45), PDL1.Sig (46) and Cytotoxic.Sig (47)(Supplementary Table S2).

To further screen the core EGFR-related immune efficacy genes, we used 5 ML algorithms, namely, Wrapper, learning vector quantization (LQV), RF, bagged decision tree and Bayesian, for the training set to analyze the important role of EGFR-related genes in immunotherapy. The random forest method was configured with 500 decision trees. The Wrapper method employed stepwise feature selection, while the Bayesian approach utilized a naïve Bayes classifier. Both LQV and bagged decision trees adopted the default parameters from the R caret package. For each model, gene importance was ranked based on feature importance scores (e.g., mean decrease in accuracy for random forest, selection frequency for Wrapper, etc.). Finally, the genes that made sense in at least three algorithms were selected as the hub EGFR-related gene signature (Hub-EGFR.Sig).

To explore the relationship between Hub-EGFR.Sig and the prognosis of cancer patients, we constructed Hub-EGFR.Sig-related prediction models with a total of 18 algorithm models using 5 ML algorithms, namely, elastic network (Enet), random survival forest (RSF), generalized boosted regression modelling (GBM), stepwise Cox and survival support vector machine (Survival-SVM). For the

Enet model, we tested alpha values ranging from 0 to 1 with increments of 0.1, ultimately selecting the optimal model with alpha=0.2. For the RSF, we configured the following parameters: number of trees (n.tree)=1000, node size (nodesize)=10, splitting rule=logrank test, and proximity calculation using inbag samples. The GBM was implemented with these specifications: number of trees (n.tree)=10000, interaction depth=3, minimum observations in terminal nodes (n.minobsinnode)=10, and shrinkage=0.001. The Stepwise Cox regression was performed with 1000 steps, while the Survival-SVM used gamma.mu=1 as its key parameter. All model algorithms were based on leave-one-out cross-validation, and the prediction performance of the models was evaluated by Harrell's concordance index (C-index). The optimal algorithm was selected by comparing the C-index values of different ML algorithms.

2.5 CRISPR analysis

To explore potential therapeutic targets based on EGFR.Sig, seven published CRISPR screening studies covering melanoma, breast, colon, and renal cancer cell lines were collected, namely, Freeman 2019 (48), Kearney 2018 (49), Manguso 2017 (50), Pan 2018 (51), Patel 2017 (52), Vredevoogd 2019 (53), and Lawson 2020 (54). According to the model cell lines and treatment conditions, these seven CRISPR studies were divided into 17 datasets that evaluated the individual effects of each gene knockout on tumor immunity (40). Data were utilized to identify genes that were more likely to influence the response to immunotherapy across different cancer cell lines.

Generally, the first step of CRISPR screening is to conduct genome-wide CRISPR–Cas9 knockout across various cancer cells. Then, the cells are either cocultured with cytotoxic lymphocytes (CTLs) *in vitro* or implanted in immunodeficient/immunocompetent mice *in vivo*. Finally, ten RNA sequences are used to estimate the sgRNA abundance of the genes studied. By calculating the log-fold changes in sgRNA readings between gene knockout cell lines and control groups, we can understand the effect of gene knockout on cancer under the pressure of CTLs or antitumor immunity (54). This study invokes the normalized z scores from log-fold changes to eliminate the batch effect and compare genes in different CRISPR datasets. The genes were sorted from low to high according to their average z scores across the 17 datasets. The top-ranked genes have lower average z scores, and the lower z scores indicate a better immune response after gene knockout, so these genes were identified as immune resistance genes. Referring to previous studies, the proportion of the first 6% top-ranked immune resistance genes in EGFR.Sig and other published ICI response signatures (CRMA.Sig (55), LRRC15.CAF.Sig (56), IMS.Sig (57), TcellExc.Sig (21), ImmmunCells.Sig (58)) was compared (40).

2.6 Survival analysis

We used 1000 iterations of 10-fold cross-validation LASSO-Cox for dimensionality reduction screening. Each patient's risk score was computed by summing the products of expression levels of selected Hub-EGFR.Sig genes and their corresponding LASSO-Cox regression coefficients, following the formula: risk score = (β_1 × expression of gene$_1$) + (β_2 × expression of gene$_2$) +… + (β_n × expression of gene$_n$). The cancer patients were divided into a high-risk group and a low-risk group according to the median score to explore the relationship between Hub-EGFR.Sig and prognosis in pan-cancer by Kaplan–Meier (K–M) survival analysis. The "survival" package of R was used to perform survival analyses. Disease-specific survival (DSS) and progression-free interval (PFI) were used in the survival analysis of this study because they can well reflect the effectiveness of clinical treatment (59). We also analyzed the Spearman correlation and drew the correlation heatmap of DSS or PFI through the "cowplot" package and verified it by the "GOSemSim" package.

2.7 Molecular subtype identification and characteristic analysis

Consensus clustering using the "ConsensusClusterPlus" package was conducted to identify different populations with EGFR functional phenotypes in BLCA based on Hub-EGFR.Sig. Principal coordinate analysis (PCoA) was used to verify the results of consensus clustering. The immunotherapy response of BLCA patients in different clusters was predicted by Tumor Immune Dysfunction and Exclusion (TIDE, http://tide.dfci.harvard.edu), which is a widely recognized program for evaluating the prognosis of ICI therapy (60, 61). The R "ggpubr" package was used to draw a bar graph of immunotherapy response between different clusters. From Genomic Data Commons (GDC, https://portal.gdc.cancer.gov), we obtained the mutation information of TCGA datasets and analyzed the characteristics with the "maftools" packet. To systematically identify pathway-level alterations associated with the observed mutational profiles, we first identified significantly differentially mutated genes (q-value < 0.1) with high mutation frequencies between two clusters. These selected genes were then subjected to pathway enrichment analysis through hypergeometric testing against two comprehensive pathway databases: the Hallmark gene sets from MSigDB (https://www.gsea-msigdb.org/gsea/msigdb) and the Reactome database (https://reactome.org/). All analyses were performed using the clusterProfiler R "clusterProfiler" package, with statistical significance of pathway enrichment determined after Benjamini-Hochberg multiple testing correction (FDR < 0.05). Moreover, the Drug Gene Interaction database (DGIdb) was used to predict the mutant gene druggability of different subtypes.

2.8 Immune cell infiltration analysis

The infiltration of immune cells in the TIME was evaluated by CIBERSORT (https://cibersort.stanford.edu/) and single-sample gene set enrichment analysis (ssGSEA). For CIBERSORT, we first uploaded gene expression data to the CIBERSORT portal and then evaluated the infiltration of immune cells in samples based on the gene expression features of 22 known immune cell subtypes (62).

For ssGSEA, the enrichment scores calculated by ssGSEA were used to express the relative abundance of immune cell infiltration in each sample. Finally, we used the "ggplot2" and "pheatmap" packages to present the results.

2.9 Network regulation and interaction analysis

We searched the regulatory relationship and network interaction of Hub-EGFR.Sig in the miRTarBase v8.0 (https://mirtarbase.cuhk.edu.cn/) and ENCODE (https://www.encodeproject.org/) databases, and the mRNA–miRNA and mRNA-TF network information was collected. Then, we predicted the interaction between proteins corresponding to the key genes through the online database STRING (https://string-db.org). All interactive networks were visualized with Cytoscape software.

2.10 Cells and cell culture

Human ureteral epithelial immortalized cell line SV-HUC-1 and human bladder cancer cell line 5637 were purchased from Wuhan Servicebio Technology Co., Ltd (Wuhan, China). Cells were cultured in a 37°C, 5% CO_2 incubator using special media purchased from Servicebio, Inc. (GZ12301, GZ11703).

2.11 Western blotting

Total protein was obtained with RIPA lysis buffer (P0013B, Beyotime, Shanghai, China). BCA Protein Assay Kit (P0012, Beyotime, Shanghai, China) was employed to measure protein concentration. Proteins were subjected to SDS-page for separation and then transferred to PVDF membranes (0.22 μm, Millipore). 5% milk blocking buffer (P30500, NCM Biotech, Soochow, China) was used to block nonspecific binding sites. The membranes were incubated with specific primary antibodies overnight at 4°C. Subsequently, washed membranes were incubated with corresponding secondary antibodies for 1 h at room temperature. ECL Chemiluminescence kit was purchased from Mishu Biotechnology (MI00607B, Xi 'an, China). The primary antibodies included ABCA7(YP-mAb-05349, UpingBio, China), HOOK2 (YP-mAb-10034, UpingBio, China), VMP1 (F1488, Selleck, China), JUNB (F0578, Selleck, China), ACTG1(YP-mAb-06774, UpingBio, China), RHOB (YP-mAb-16239, UpingBio, China). The second antibodies included goat anti-mouse IgG-HRP (abs20039, Absin, China) and goat anti-rabbit IgG-HRP (abs20040, Absin, China).

2.12 The Human Protein Atlas analysis

The Human Protein Atlas (HPA, https://www.proteinatlas.org/) is a human proteome atlas database containing information on the protein distribution of human tissues and cells. To analyze the differential expression of ABCA7, HOOK2, VMP1, JUNB, ACTG1 and RHOB at the protein level, we downloaded immunohistochemical images of bladder tumor tissues with their corresponding normal tissues from HPA.

2.13 Statistical analysis

All data processing and analysis were performed with R software (version 4.0.2). For comparisons of continuous variables between the two groups, the statistical significance of normally distributed variables was estimated with an independent Student's t test, and differences between variables that were not normally distributed were analysed with the Mann–Whitney U test (i.e., the Wilcoxon rank-sum test). The chi-square test or Fisher's exact test was used to compare and analyze the statistical significance between the two groups of categorical variables. $P<0.05$ was used as the criterion for significantly different results if there were no special notes.

3 Results

3.1 Relationship between EGFR-related genes and tumor immunotherapy efficacy

Two scRNA-Seq GEO datasets with clear efficacy of tumor immunotherapy were downloaded to evaluate the relationship between EGFR-related genes and tumor immunotherapy outcomes. After quality control, 33 samples were included in the GSE115978 cohort (melanoma, TN=16, NR=16, R=1), and 10 patients were included in the GSE123813 cohort (BCC, NR=4, R=6). First, we comprehensively presented the distribution of EGFR scores (defined as the ssGSEA-derived enrichment score of the EGFR gene set) among single-cell samples and found that the distribution was uneven (Figures 2A, B). Considering the presence of different cell types in tumor tissues, we marked these cells and found that they could be roughly divided into three categories: immune cells, stromal cells and malignant cells (Figures 2C, D). Then, we investigated the differences in EGFR scores among different cell subtypes. The results demonstrate a statistically significant difference in EGFR scores between malignant and immune cells (Figures 2E, F). This discrepancy was particularly pronounced in the GSE123813 dataset, where malignant cells demonstrated significantly elevated EGFR scores while immune cells showed markedly lower scores (mean=0.89 vs 0.47, Figure 2F). Subsequent analysis revealed that the EGFR scores of patients in GSE115978 who were untreated or did not respond to immunotherapy were higher than those of patients who responded to immunotherapy ($P < 0.001$, Figure 2G). Similar results were also observed in GSE123813 ($P < 0.001$, Figure 2H). These results indicated that the EGFR-related genes may have a potential connection with the response to immunotherapy in cancer patients.

3.2 Development of EGFR.Sig based on pan-cancer scRNA-Seq analysis

As there were differences in the EGFR scores of cancer patients with different immunotherapy responses, we hypothesized that the

10.3389/fimmu.2025.1604394

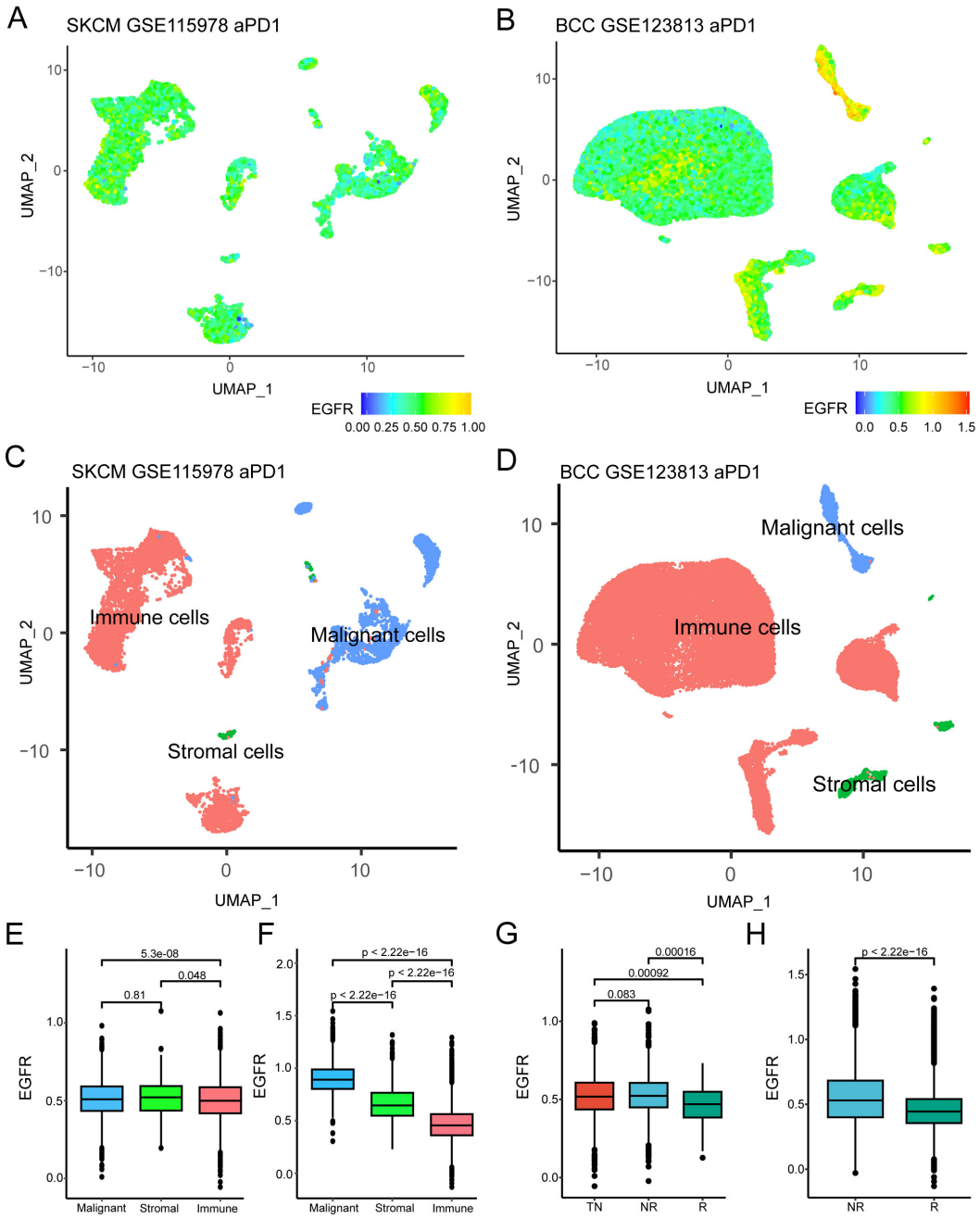

FIGURE 2
Relationship between EGFR related genes and immunotherapy efficacy. **(A, B)** UMAP plot of EGFR related genes scores in GSE115978 and GSE123813. **(C, D)** UMAP plot of different cell subtypes in GSE115978 and GSE123813. **(E, F)** Differences in EGFR related gene scores among different cell subtypes in GSE115978 and GSE123813 (Wilcoxon test). **(G, H)** EGFR related genes scores of patients with different immunotherapy responses in GSE115978 and GSE123813(Wilcoxon test). Abbreviation: SKCM, skin cutaneous melanoma; BCC, basal cell carcinoma; NR, non-responders; R, responders; TN, treatment naïve patients.

evaluation of EGFR.Sig expression levels could predict the efficacy of immunotherapy to some extent. Therefore, 34 pan-cancer scRNA-Seq datasets were included to screen important EGFR-related genes for EGFR.Sig (Figure 3A). First, Spearman correlation was performed to analyze the relationship between EGFR-related genes and EGFR scores in malignant tumor cells across 34 scRNA-Seq datasets. If there was a positive correlation (Spearman R > 0.2 and FDR < 0.05), the gene was labelled Gx. Then, genes highly expressed in malignant tumor cells were screened and marked as Gy (logFC ≥ 0.5 and FDR < 0.05). Gn was generated by the intersection of Gx and Gy in each dataset to identify the upregulated genes in specific tumors that were positively related to EGFR. For example, Gx and Gy were screened out in the first scRNA-Seq dataset, and their common genes make up G1. Finally, the geometric mean of Spearman R was calculated, and genes with a geometric mean R > 0.4 (moderate to strong correlation) in G1-G34

10.3389/fimmu.2025.1604394

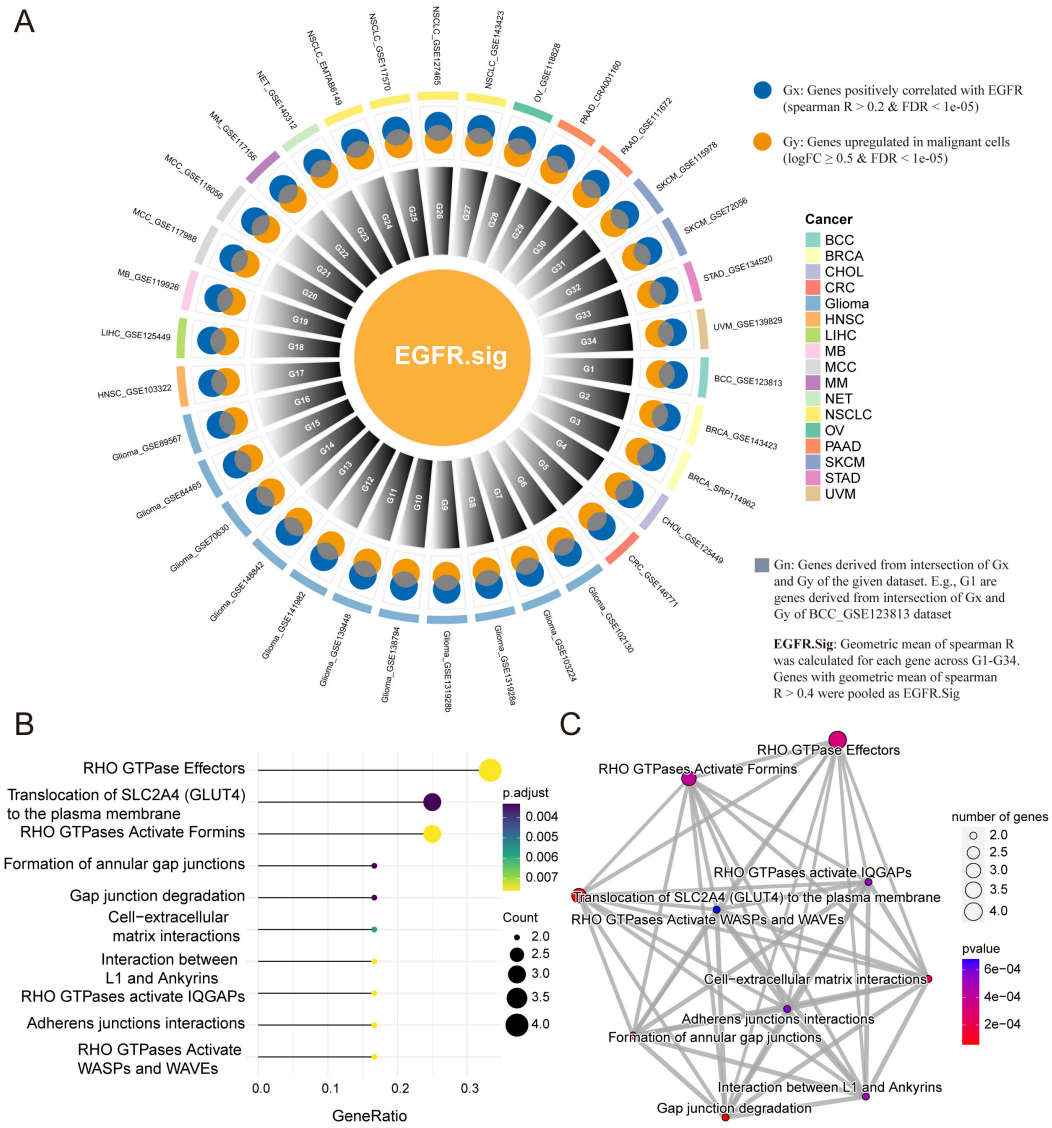

FIGURE 3
Development of EGFR related gene signature and enrichment analysis. **(A)** Circle diagram depicting the development of EGFR.Sig. **(B)** Top 10 enriched Reactome pathways of genes in EGFR.Sig. **(C)** The network of enriched Reactome pathways of EGFR.Sig. The colored dots indicate the corresponding pathway, the size of the dots indicates the number of enriched genes in the pathway, and the depth of the color indicates the *P* value.

were merged as EGFR.Sig (Supplementary Table S3). Furthermore, we investigated the biological functions of EGFR.Sig. The EGFR.Sig enrichment pathways mainly included RHO GTPase effectors, translocation of SLC2A4 and RHO GTPases activating formins (Figure 3B), and there were interrelations and interaction networks among these functional pathways (Figure 3C).

3.3 Potential link between EGFR.Sig and immune suppression across cancers

To further explore the relationship between EGFR.Sig and the effect of cancer immunotherapy, we comprehensively analysed the correlation between EGFR.Sig and 75 immune-related genes previously published in the pan-cancer TCGA cohort (Supplementary Table S4) (28). A generally correlation between EGFR.Sig and most of the immune-related genes across 30 different cancers was observed (Figure 4A). Then, we evaluated the CIBERSORT infiltration abundance of immune cells in the TIME across TCGA pan-cancer cohort. The results demonstrated that EGFR.Sig was negatively correlated with the infiltration of various immune-promoting cells, including $CD8^+$ T cells, NK cells and macrophages, in different cancer types (Figure 4B). Next, we analysed the hallmark pathways associated with EGFR.Sig in the TCGA pan-cancer dataset by calculating Spearman correlation coefficients between EGFR.Sig expression and the enrichment scores (obtained by ssGSEA calculations) of each hallmark pathway. In our analysis, we observed that EGFR.Sig showed a positive correlation with certain immune-related biological

10.3389/fimmu.2025.1604394

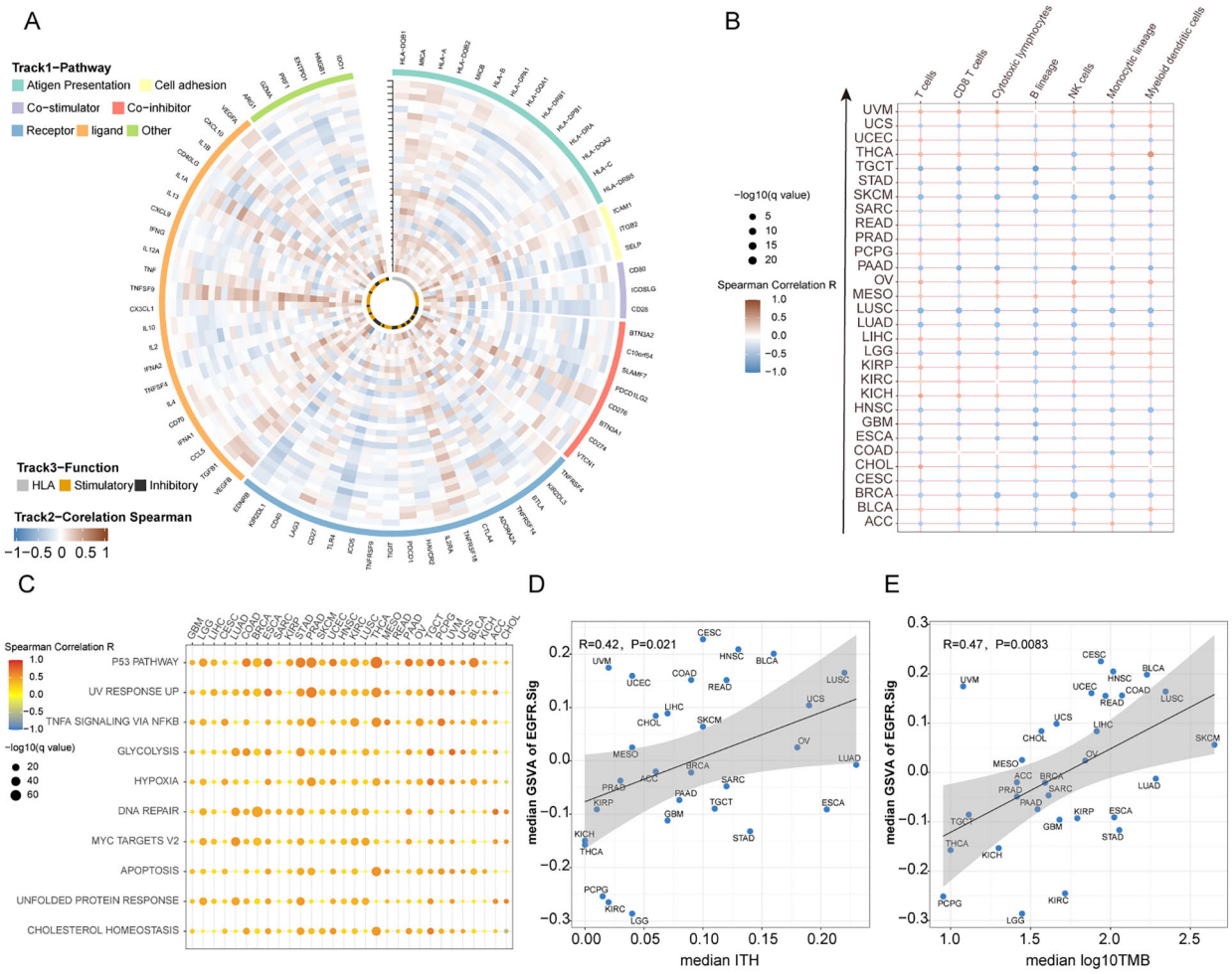

FIGURE 4
Potential links between EGFR.Sig and immune resistance in pan-cancer. **(A)** Circos plot depicting the correlation between the expression levels of EGFR.Sig and immune related genes in pan-cancer. Types of cancer from inner to outer rings refer to the y-axis of plot **(B)** B. Heatmap depicting the correlation between EGFR.Sig and the infiltration of immune cells across multiple cancer types. **(C)** Correlation between EGFR.Sig and hallmark pathways. **(D)** Correlation between median EGFR.Sig score and median ITH score across cancer types. **(E)** Correlation between median EGFR score and median TMB score across cancer types.

pathways (e.g., P53, UV response up and DNA repair pathway) (Figure 4C) (63–65). Furthermore, the relationship between EGFR.Sig and ITH, which is a stem-related trait associated with tumor immunosuppression (66), was analysed. Similarly, ITH was positively correlated with EGFR.Sig in pan-cancer (R = 0.42, $P = 0.021$, Figure 4D). Moreover, the TMB, a well-known molecular marker related to immunotherapy efficacy, was also detected to have a similar positive association with EGFR.Sig (R = 0.47, $P = 0.0083$, Figure 4E). In summary, EGFR.Sig was observed to be negatively correlated with the tumor immune response.

3.4 Immune response prediction by EGFR.Sig

To effectively predict the immunotherapy response of cancer patients through EGFR.Sig, bulk RNA-Seq cohorts with clear immunotherapy response information were identified and assessed. The cohorts were divided into a training set (n = 618) and a validation set (n = 154). First, we used eight ML algorithms to construct and optimize prediction models for immunotherapy efficacy and verified the models by ROC. By comparing the AUCs of different algorithm models, we found that the logistic regression model had better predictive efficiency than the other algorithms, with an AUC of 0.77 (Figures 5A, B). Then, we compared the predictive performance of EGFR.Sig with that of previously published gene signatures in another independent validation set to validate the superiority of EGFR.Sig. The results demonstrated that that EGFR.Sig exhibited superior predictive performance compared to other published gene signatures in the Zhao 2019 GBM cohort, while maintaining consistently robust predictive power relative to existing signatures across multiple independent validation cohorts (Figure 5C, Supplementary Table S2). As revealed in the heatmap, the average AUC of EGFR.Sig ranked at the top of the published gene signatures (Figure 5D), which indicated a better ability

10.3389/fimmu.2025.1604394

of EGFR.Sig to predict the immunotherapy response, especially for the Zhao 2019 GBM cohort. Taken together, the EGFR.Sig predictive models developed with the logistic regression algorithm can effectively predict the response of cancer patients to immunotherapy.

3.5 Screening potential therapeutic targets associated with EGFR.Sig

Seven CRISPR cohorts including 17 CRISPR datasets were systematically collected to further explore potential therapeutic targets, and 22505 knockout genes with immune response data were ranked according to the average z scores. Lower z-scores indicate that gene knockout enhances tumor cell susceptibility to immune-mediated killing. Therefore, the top genes were considered immune resistance genes, while those at the bottom were considered immune sensitive genes (Figure 5E). Then, we calculated the proportion of the first 6% top-ranked genes in EGFR.Sig and other published ICI response signatures. The results showed that there were four top 6% CRISPR genes, which accounted for 12.5% of EGFR.Sig, and the proportion of immune resistance genes (6% top-ranked genes) in EGFR.Sig was much higher than that of other gene signatures (Figure 5F). The four identified immune resistance genes were MAT2A, JUNB, C12orf57

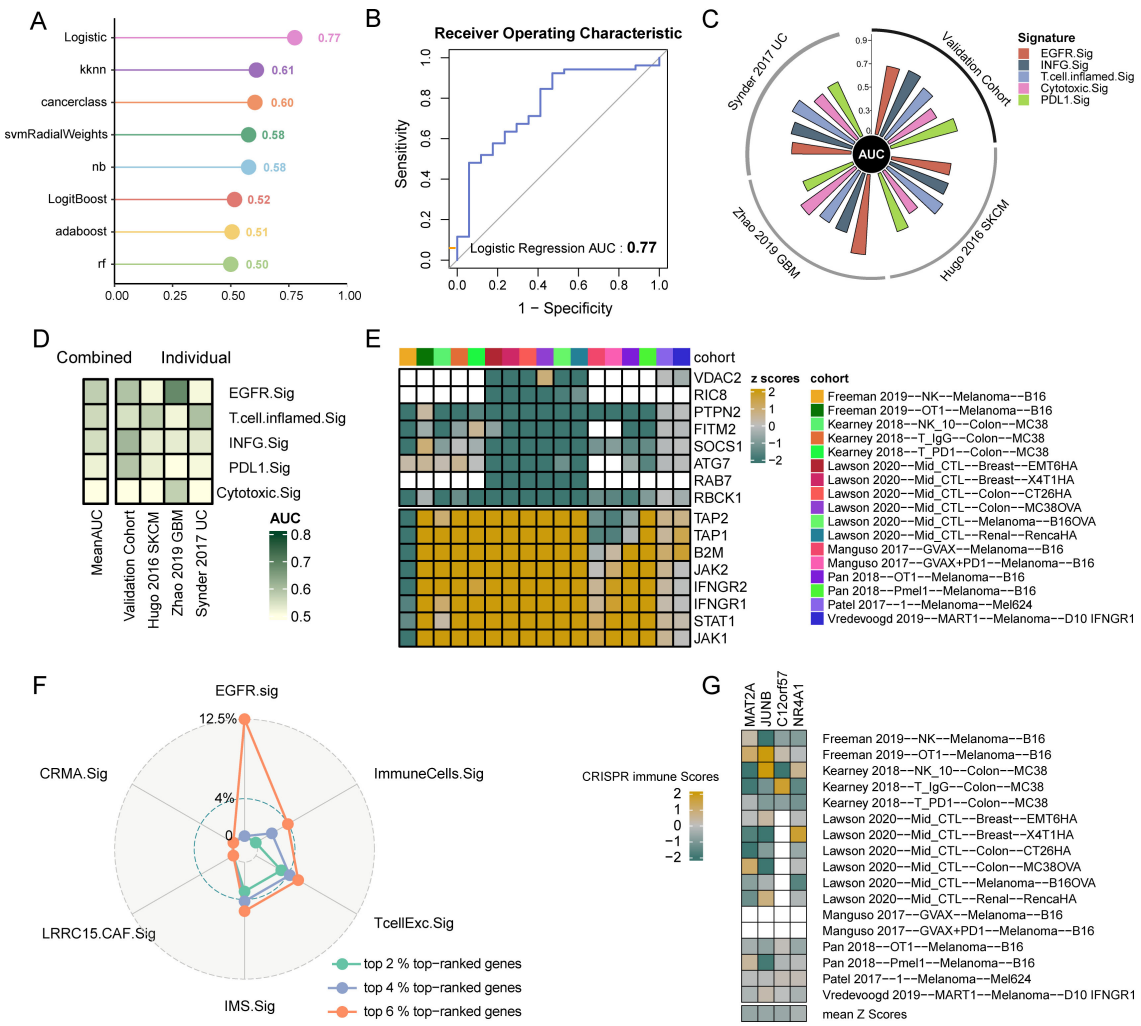

FIGURE 5
Predictive value to immunotherapy and potential therapeutic targets of EGFR.Sig. **(A)** AUC of the prediction models constructed by eight ML algorithms in the validation set. **(B)** ROC plot of Logistic regression algorithm. **(C)** The performance of immune response signatures in independent external validation set. The vertical axis indicated AUC values. The independent external validation set comprises three different cohorts including Hugo 2016 SKCM, Zhao 2019 GBM and Synder 2017 UC. **(D)** The predictive value of immune response signatures. The signatures are ordered by mean AUC from top to bottom. **(E)** Genes ranking at top and bottom according to their average z-scores across 17 CRISPR datasets. Top-ranked (bottom-ranked) genes associated with immune resistance (sensitive) and the anti-tumor immune response is better (worse) after knockout. Blank squares indicate the missing values of gene data in the corresponding cohorts. **(F)** Comparing the percentage of top-ranked genes among immune response signatures. **(G)** The z-scores of the four screened EGFR.Sig genes in the different CRISPR datasets. CRISPR immune scores represent the average normalized z-score of each gene across 17 CRISPR datasets. AUC, area under the curve; Sig, signature.

10.3389/fimmu.2025.1604394

and NR4A1, which were verified in the CRISPR dataset and were thought to promote antitumor immunotherapy after knockout (Figure 5G). Therefore, these genes may be meaningful targets in synergy with immunotherapy for cancer patients.

3.6 Identification of prognostic genes in EGFR.Sig

To further screen the core genes in EGFR.Sig and explore its relationship with the prognosis of cancer patients, five ML algorithms were used to analyze the importance of genes for tumor immunotherapy response in the training set (Supplementary Figures S1A-E). The genes determined to be most closely related to tumor immunotherapy efficacy in at least three algorithms were ABCA7, ACTB, ACTG1, C12orf57, EEF1A1, HOOK2, JUNB, MAT2A, NR4A1, RHOB, SEMA4B and VMP1 (Supplementary Figure S1F), and they were considered the hub genes comprising Hub-EGFR.Sig (Figure 6A). Furthermore, cancer patients in the total ICI cohorts were divided into two subgroups according to the risk scores of Hub-EGFR.Sig (Figures 6B, C), and Hub-EGFR.Sig gene expression varied between the two groups (Figure 6D). To understand the relationship between Hub-EGFR.Sig and the immunotherapy prognosis of pan-cancer, PFI were calculated, and the results indicated that patients with higher scores of Hub-EGFR.Sig had a worse prognosis in the training set (P = 0.045, Figure 6E). As expected, similar results were also observed in the verification set (P = 0.041, Figure 6F).

3.7 Protein interaction networks of Hub-EGFR.Sig

In the above combined ICI treatment cohort, we investigated the expression of immunogenic death (ICD)-related genes that are closely related to the efficacy of immunotherapy (67). The

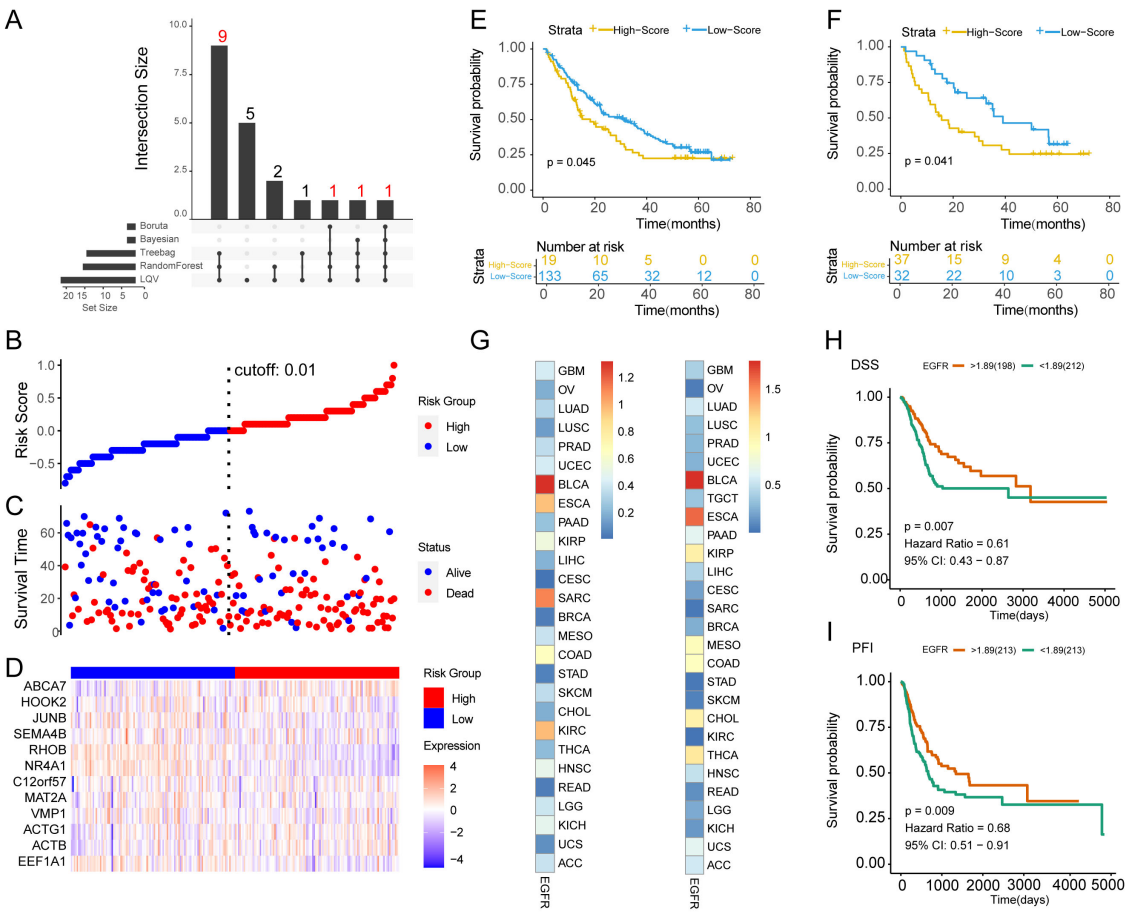

FIGURE 6
Identification of the Hub-EGFR.Sig and survival analysis in pan-cancer. **(A)** Intersection of the core genes in 5 different ML algorithms. **(B)** Distribution of patients according to the Hub-EGFR.Sig risk score from low to high. Patients were divided into high and low risk groups with 0.01 as the best cutoff value. **(C)** Survival time and status distribution of patients in high and low risk groups. **(D)** Heatmap of Hub-EGFR.Sig expression in high and low risk groups. **(E, F)** K-M survival analysis of the high and low risk groups in the training set and validation set (Log-rank test). **(G)** The relationship between Hub-EGFR.Sig and DSS or PFI in different cancers. The p values in the figure are converted, and the darker the colour means the lower the *P* value. **(H, I)** DSS and PFI of high and low Hub-EGFR.Sig score groups in bladder cancer (Log-rank test). DSS, disease specific survival; PFI, progression free interval.

expression of 13 ICD-related genes showed significant differences between the R and NR cancer patients treated with ICIs. Among them, BAX, CALR, FOXP3, HSP90AA1, IFNB1, IL6, PIK3CA and TLR4 were highly expressed in the NR group, while CXCR3, EIF2AK3, ENTPD1, IFNG and PRF1 were highly expressed in the R group (Supplementary Figures S2A-M). To further analyze the interaction between Hub-EGFR.Sig and ICD genes, we constructed PPI networks using the STRING database. Finally, we obtained a regulatory network of 38 nodes with a wide range of connections (Supplementary Figure S2N), which reflected the universal and close relationship of Hub-EGFR.Sig and ICD in the immune response of pan-cancer. In addition, we constructed the mRNA–miRNA network and mRNA-TF network to reveal potentially regulated molecules of Hub-EGFR.Sig. There were 49 interactions, including 11 genes in Hub-EGFR.Sig and 17 miRNAs from the miRTarBase v8.0 database (Supplementary Figure S2O). Among them, EEF1A1 interacted with 11 miRNAs, MAT2A and ACTB interacted with 6 miRNAs, and RHOB interacted with 5 miRNAs, showing the most common connection. Similarly, the constructed mRNA-TF network included 98 interactions, which consisted of all the Hub-EGFR.Sig genes and 14 TFs from the ENCODE database (Supplementary Figure S2P). The Hub-EGFR.Sig genes that interacted most widely with TFs were ABCA7, HOOK2, and JUNB, which interacted with all 14 TFs, and NR4A1, which interacted with 10 TFs. In summary, these findings provide an important reference for future studies on the regulatory mechanism of Hub-EGFR.Sig in cancer immunotherapy.

3.8 Landscape of Hub-EGFR.Sig in pan-cancer

We systematically reviewed the Hub-EGFR.Sig scores in TCGA pan-cancer datasets. As expected, Hub-EGFR.Sig presented stable enrichment scores across multiple cancer types, of which LUAD, LUSC and BLCA showed higher scores (Supplementary Figure S3A). In addition, various immune cells in the TIME, such as CD4 memory T cells, M2 macrophages and resting mast cells, were negatively correlated with Hub-EGFR.Sig in most types of cancer, while follicular helper T cells, active mast cells, eosinophils and plasma cells were positively correlated (Supplementary Figure S3B). Then, the correlation between Hub-EGFR.Sig and microsatellite instability (MSI) was analysed in pan-cancer samples. The results suggested that there was a positive correlation between Hub-EGFR.Sig and MSI in most cancer types but a negative correlation in adrenocortical carcinoma and pancreatic cancer (Supplementary Figure S3C). Furthermore, we analysed the correlation between the 12 genes in Hub-EGFR.Sig and MSI (Supplementary Figure S3D). The results showed that C17orf57 and SEMA4B were positively correlated with MSI, while RHOB presented a negative correlation in colon cancer. In BLCA, HOOK2 and ABCA7 were positively correlated with MSI, while SEMA4B and EEF1A1 were negatively correlated. Moreover, SEMA4B and HOOK2 were significantly associated with MSI in more than 10 cancers. In summary, Hub-EGFR.Sig plays an important role in the TIME of pan-cancer, but there is heterogeneity in different types of cancer.

3.9 Relationship between Hub-EGFR.Sig and prognosis in different tumor types

Considering the heterogeneous function of Hub-EGFR.Sig in pan-cancer, we subsequently performed survival analysis across tumor types. Correlation analysis demonstrated that the relationship between Hub-EGFR.Sig and DSS or PFI varied in different cancers (Figure 6G). Notably, Hub-EGFR.Sig showed the closest correlation with BLCA both in DSS (HR = 0.61, P = 0.007, Figure 6H) and PFI (HR = 0.68, P = 0.009, Figure 6I). Next, we comprehensively evaluated the 12 genes in Hub-EGFR.Sig and found that the expression levels of 6 genes had a significant effect on both the DSS and PFI of BLCA patients (Supplementary Figures S4A-X). In the results of K–M analysis, higher expression of ABCA7 (Supplementary Figures S4A, B), HOOK2 (Supplementary Figures S4K, L), JUNB (Supplementary Figures S4M, N), RHOB (Supplementary Figures S4S, T), and VMP1 (Supplementary Figures S4W, X) indicated better survival viability, while higher expression of ACTG1 was associated with poorer survival (Supplementary Figures S4C, D). Altogether, there is a significant association between Hub-EGFR.Sig and the prognosis of BLCA.

3.10 Prognostic model construction, subtype distinction and immune cell infiltration of BLCA based on Hub-EGFR.Sig

In the TCGA-BLCA dataset, we applied 5 ML algorithms and a total of 18 algorithm models to construct a prognostic model based on Hub-EGFR.Sig. The C-index indicated that Hub-EGFR.Sig in most of the prognostic models had a satisfactory performance in predicting the prognosis of BLCA, among which the Enet[a=0.2] algorithm had the best prediction performance (C-index = 0.7122, Figure 7A). Then, we conducted consensus clustering to identify the Hub-EGFR.Sig-related BLCA subtypes. With a consensus matrix of k = 2, patients could be divided into two distinct subgroups named Cluster A and Cluster B (Figure 7B). The stability of consensus clustering was validated by PCoA (Figure 7C). Further exploration revealed that patients in Cluster B were more likely to benefit from immunotherapy predicted by TIDE (Figure 7D). Next, ssGSEA was used to evaluate the differences in immune cell infiltration between the two clusters (Supplementary Table S5). Except for CD56-bright natural killer cells, which had no significance, the results demonstrated that the levels of all the other immune cells in Cluster A patients were higher than those in Cluster B patients (Figure 7E). We further calculated the correlation between Hub-EGFR.Sig and the content of immune cells separately, and the results showed that most of the Hub-EGFR.Sig genes were significantly correlated with the infiltration of immune cells

10.3389/fimmu.2025.1604394

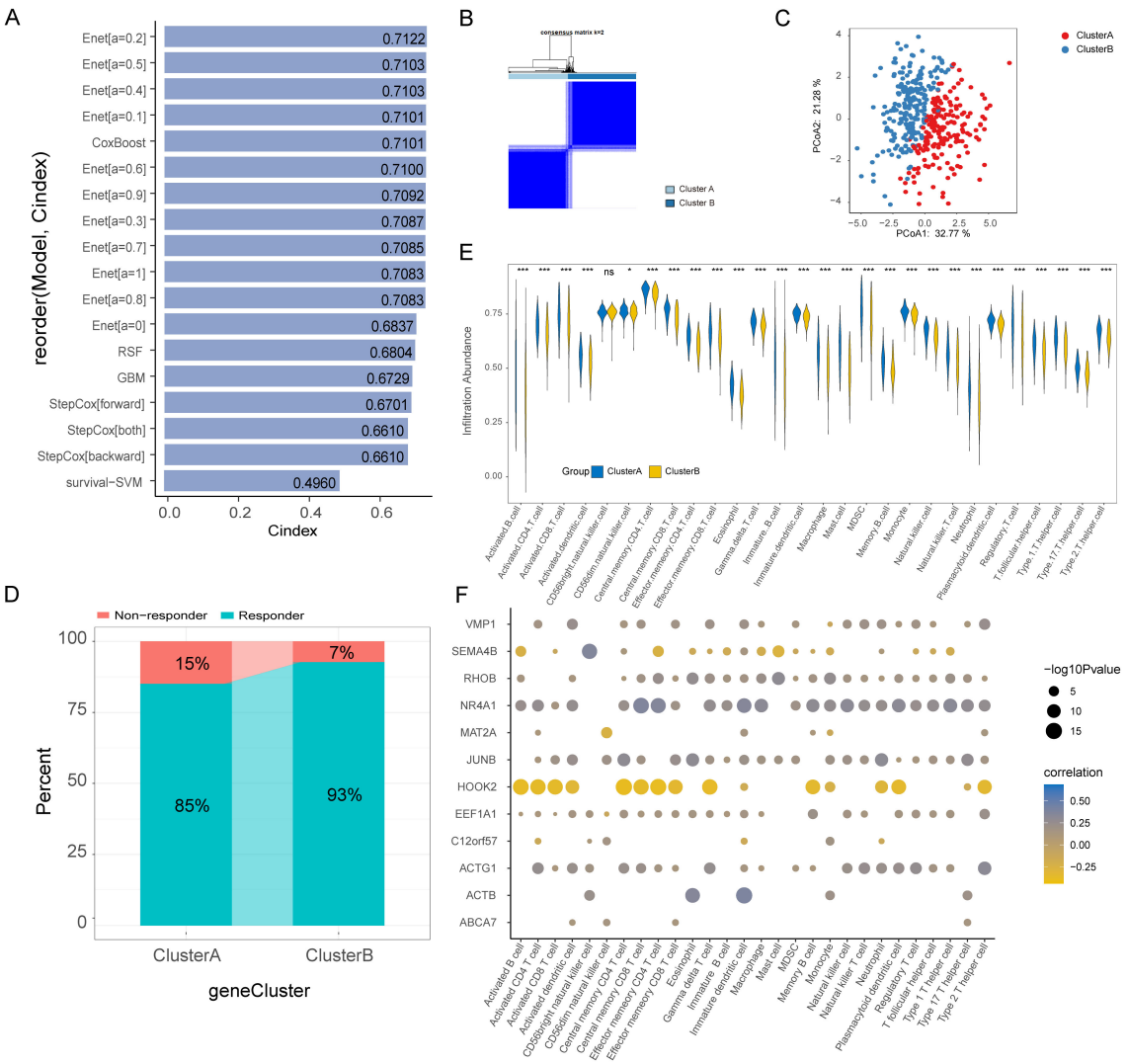

FIGURE 7
Prognostic model, molecular subtypes and immune cells infiltration (ssGSEA) of bladder cancer based on Hub-EGFR.Sig. **(A)** C-index of the 18 ML algorithm models based on Hub-EGFR.Sig to predict the prognosis of patients in BLCA. **(B)** Consensus cluster analysis of patients in BLCA. **(C)** PCoA analysis of patients in BLCA. **(D)** Immunotherapy response predicted by TIDE in two clusters of BLCA. **(E)** Immune cell infiltration in the two Hub-EGFR.Sig subtypes patients of BLCA. Student's t-test, **P*<0.05, ***P*<0.01, ****P*<0.001 and ns means no significant. **(F)** Correlation analysis between genes in Hub-EGFR.Sig and immune cell abundance in BLCA.

(Figure 7F). Among them, HOOK2 was negatively correlated with the abundance of most immune cells, while NR4A1, JUNB and ACTG1 were positively associated with the abundance of immune cells, and their correlation intensities were all above 0.25. CIBERSORT was also utilized to evaluate the infiltration status of 22 immune cells (Supplementary Figure S5A). The results showed that the infiltration abundance of naive B cells, M1 macrophages, M2 macrophages and activated memory $CD4^+$ T cells in Cluster A patients was significantly higher than that in Cluster B patients, while the infiltration abundance of dendritic cells and NK cells in Cluster B patients was significantly higher than that in Cluster A patients (Supplementary Figure S5B). Heatmap presented the immune cell infiltration abundance of different clusters in BLCA (Supplementary Figure S5C). Correlation analysis demonstrated that some genes in Hub-EGFR.Sig were related to the infiltration of immune cells in BLCA. For example, SEMA4B was negatively correlated with the content of naive B cells (r = -0.3, $P < 0.001$, Supplementary Figure S5D), ACTB was positively related to M1 macrophages (r = 0.29, $P < 0.001$, Supplementary Figure S5E) and activated memory $CD4^+$ T cells (r = 0.38, $P < 0.001$, Supplementary Figure S5F), while HOOK2 was negatively correlated with activated memory $CD4^+$ T cells (r = -0.26, $P < 0.001$, Supplementary Figure S5G).

3.11 Hub-EGFR.Sig-associated mutation characteristics and drug sensitivity analysis

To screen drugs to potentially combine with immunotherapy strategies for BLCA, we further investigated the mutation

10.3389/fimmu.2025.1604394

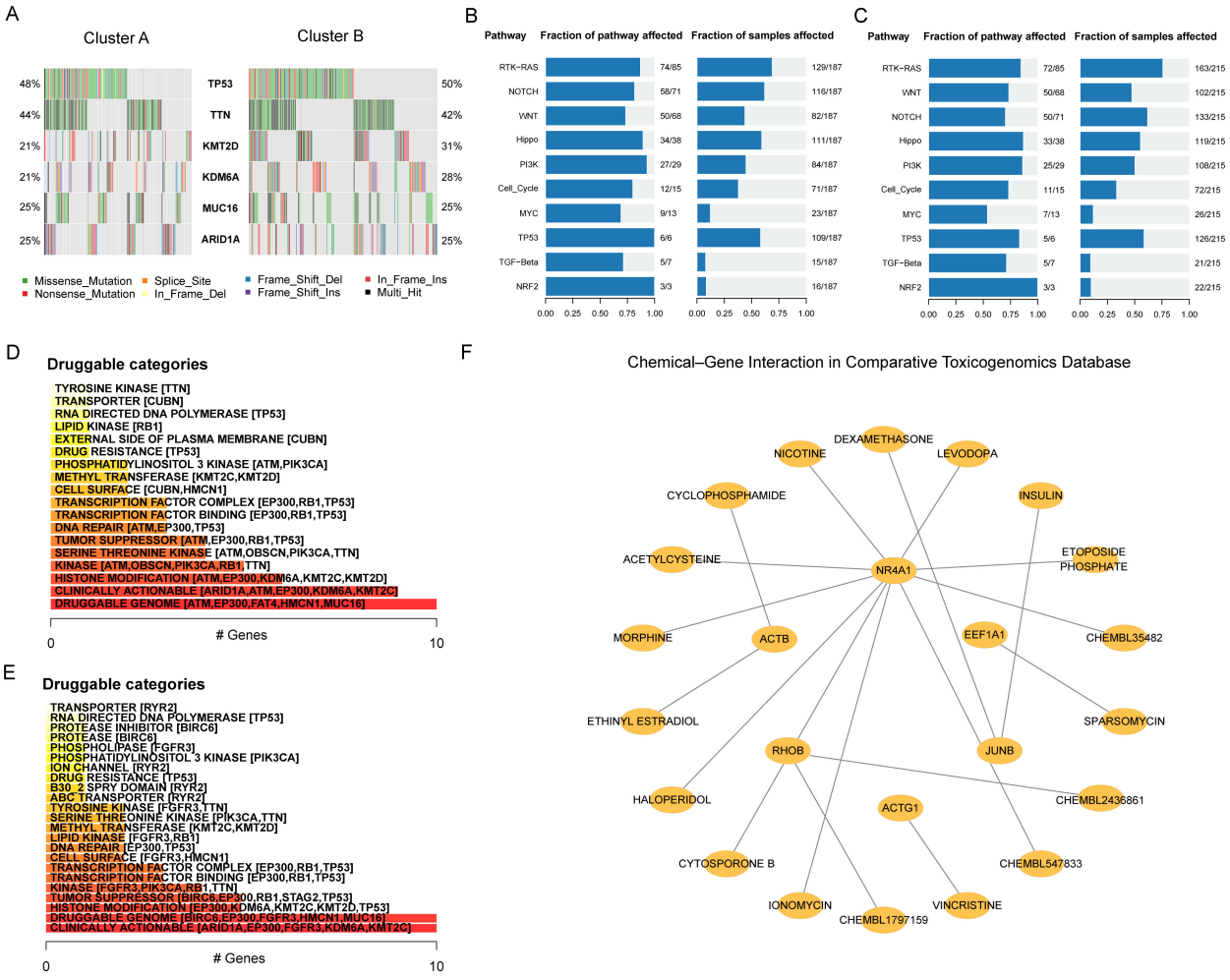

FIGURE 8
Hub-EGFR.Sig associated mutation characteristics and drug sensitivity analysis. **(A)** Mutant genes landscape in the two Hub-EGFR.Sig subtypes of BLCA. **(B, C)** Biological functions pathways affected by mutations in Cluster A and Cluster B. **(D, E)** Categories of potentially druggable genes in Cluster A and Cluster B. The horizontal axis is the gene counting in the category. Following each category are the top 5 genes in parentheses, and all are shown if less than 5 genes in the category. **(F)** Drug-gene interaction network of Hub-EGFR.Sig and potentially sensitive drugs in BLCA. Nodes without interaction have been removed.

characteristics in patients with BLCA. TP53, TTN, KMT2D, KDM6A, MUC16, and ARID1A were found to have high mutation frequencies in both clusters (Figure 8A). Among them, the mutation frequencies of TP53 were the highest, which were 48% in Cluster A and 50% in Cluster B. Moreover, the mutation frequencies of KMT2D and KDM6A were higher in Cluster B than in Cluster A. For the biological function changes caused by mutations, the top pathways were the RTK-RAS, NOTCH and WNT signaling pathways in Cluster A (Figure 8B) and RTK-RAS, WNT and NOTCH signaling pathways in Cluster B (Figure 8C). Next, we analysed the druggability drug-gene interaction of the mutant genes in the two clusters through the DGIdb database. The results indicated that the most likely druggable category in Cluster A was the Druggable Genome, in which the first five potential druggable genes were ATM, EP300, FAT4, HMCN1 and MUC16 (Figure 8D). The most druggable category in Cluster B was Clinically Actionable, which contained ARID1A, EP300, FGFR3, KDM6A and MT2C as the first five potential druggable genes (Figure 8E). Finally, the Comparative Toxicogenomics Database (CTD) was used to identify potentially effective drugs or molecular compounds for Hub-EGFR.Sig in BLCA. The drug-gene interaction network demonstrated that 5 Hub-EGFR.Sig genes were in the interactive network, and 18 drugs or molecular compounds, including etoposide phosphate, sparsomycin and vincristine, had effects on them in BLCA to varying degrees (Figure 8F). Although more clinical trials are needed, these findings provide important clues for the future development of therapeutic drugs for BLCA.

3.12 Validation of key protein expression levels

To investigate the protein expression profiles of six genes (ABCA7, HOOK2, JUNB, RHOB, VMP1, and ACTG1) that

10.3389/fimmu.2025.1604394

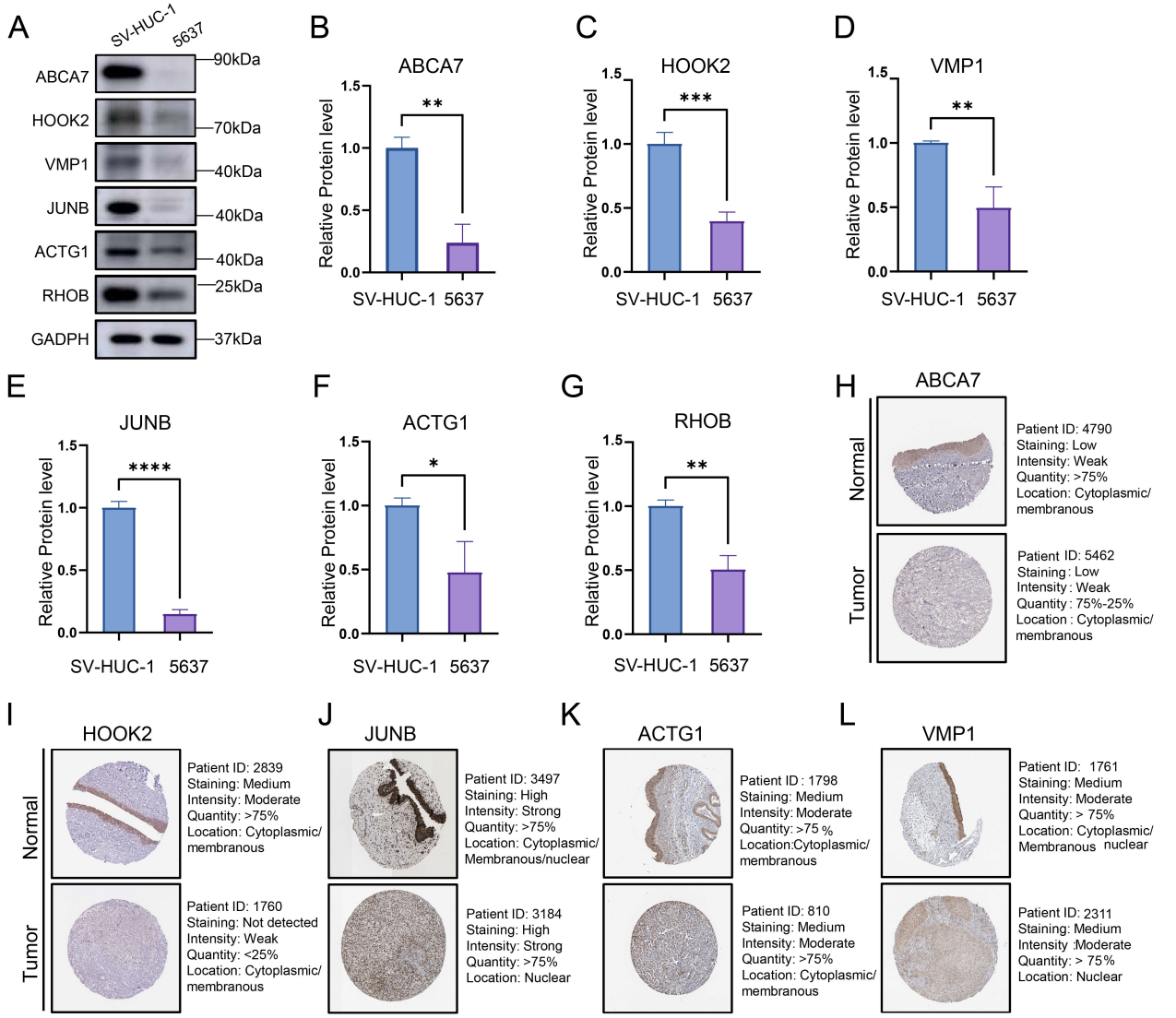

FIGURE 9
(A) Representative Western blot images showing the protein expression levels of six bladder cancer prognosis-associated genes. **(B-G)** Quantification of protein expression levels from three independent Western blot experiments. Data represent mean ± SD of triplicate measurements normalized to GAPDH. Statistical significance was determined by Student's t-test, **P*<0.05, ***P*<0.01, ****P*<0.001, *****P*<0.0001. **(H-L)** The protein expression levels of ABCA7, HOOK2, VMP1, JUNB and ACTG1 in normal tissues and bladder cancers from HPA database.

significantly impact both DSS and PFI in bladder cancer patients, we conducted Western blot analyses using SV-HUC-1 and 5637 cell lines. The results demonstrated significantly lower protein expression levels of these genes in bladder cancer cell lines compared to normal epithelial cell lines (Figures 9A-G). Subsequently, we further analyzed the expression patterns of these six genes in tumor tissue samples from patients using the HPA database. With the exception of RHOB, whose expression profile requires further clarification, the differential expression of the remaining proteins between bladder cancer and normal tissues was consistent with our analytical results (Figures 9H-L). Collectively, this study not only reveals the potential of these genes as novel pan-cancer therapeutic targets but also provides a theoretical foundation for precise prognostic stratification and biomarker-driven clinical management of BLCA patients.

4 Discussion

Resistance to tumor immunotherapy is a critical challenge hindering the beneficial treatment of cancer patients (2, 68). The heterogeneous response to immunotherapy across cancer types aggravates the need for biomarker research to optimize clinical selection and maximize survival benefits (69, 70). The high mutation frequency of EGFR in various human cancers inspired the hypothesis that EGFR could serve as a potential biomarker; however, the deterministic interaction relationship and mechanism between EGFR and TIME has not been fully reported (7, 71). Here, we utilized scRNA-Seq data of ICI cohorts to demonstrate the potential negative relationship between the EGFR scores of individual malignant cells and the response to immunotherapy.

Subsequently, the interaction analysis of scRNA-Seq and bulk RNA-Seq in pan-cancer identified EGFR.Sig and confirmed this phenomenon. Notably, EGFR.Sig showed better predictive performance for immunotherapy response than previously published gene signatures. Based on multiple ML algorithms, we identified Hub-EGFR.Sig and found that it had an extensive relationship with the TIME and prognosis in pan-cancer. Focusing on BLCA, we further investigated the complex connection of Hub-EGFR.Sig and molecular typing, immune cell infiltration and drug sensitivity screening.

In this study, a generally negative relationship between EGFR scores and immunotherapy response was observed. This phenomenon that patients with most EGFR mutation have generally low response to ICIs is the most widespread concern in NSCLC (72–74). We excluded the interference of other cells in tumor tissues at the single-cell level and found that patients who responded to ICI treatment had lower EGFR scores. To further investigate the immune resistance of patients with high EGFR scores in pan-cancer, we developed EGFR.Sig based on the interactive analysis of 34 scRNA-Seq cohorts. The genes in EGFR.Sig are mainly enriched in pathways related to Rho GTPase effectors, which hold critical positions in multiple immune signal transducers serving as Ras homology (RHO) GTPases (75). Similar to other members of the small GTPase superfamily, Rho GTPase effectors have been reported to promote tumor immune evasion through MAPK- and β-catenin-related pathways (76). Therefore, we comprehensively screened the immune molecular landscape of EGFR.Sig across various cancers. As expected, results demonstrated that EGFR.Sig is positively correlated with most immune inhibitory genes and pathways but negatively correlated with antitumor immune cells in the TIME. Moreover, there is a strongly positive correlation between EGFR.Sig and ITH, which is consistent with previous studies (77, 78). For the commonly recognized ICI biomarker TMB, a previous explanation owed the lack of therapeutic effect in patients with EGFR mutations to its low expression (7, 79). However, failure to respond to ICIs still exists in many patients with a high TMB (80), which may lead to our observation of a positive correlation between EGFR.Sig and TMB. Altogether, the association between EGFR.Sig and tumor immunosuppression suggests its potential to serve as a predictive biomarker of immunotherapy.

Subsequently, multiple ML algorithms confirmed the capability of EGFR.Sig as a new predictive biomarker for ICI response. Compared with the previously published gene signatures, EGFR.Sig has better generalization and achieved an overall favorable performance in the independent verification set. In addition to these advantages, EGFR is widely recognized as one of the primary clinical targets for tumor therapy (7). The approval and ongoing clinical trials of various drugs have significantly enhanced the potential for future combined therapies to improve the response to immunotherapy. Moreover, the percentage of genes verified by *in vivo* and *in vitro* experiments in the CRISPR datasets proved the reliability of EGFR.Sig, in which MAT2A, JUNB, NR4A1 and C12orf57 were screened for combined strategies to overcome immune resistance. The increased expression of MAT2A (methionine adenosyltransferase 2A gene) in various cancers, including liver cancer, CRC, and gastric cancer, is recognized as a therapeutic target due to its role in regulating cell growth (81–84). Recent research has also found that the deletion of MAT2A mediated by CRISPR–Cas9 restricted the growth of hepatocellular carcinoma in mice by inhibiting T-cell exhaustion, which may be a potential strategy to enhance the ICI response of HCC (85). Moreover, JUNB (JunB proto-oncogene) and NR4A1 (nuclear receptor subfamily 4 group A member 1 gene) can also regulate the functional state of T cells in the TIME, serving as targets of tumor immunotherapy (86, 87). C12orf57 (chromosome 12 open reading frame 57) is found in the interactome atlas of receptor tyrosine kinase, although there are have been few more detailed studies to date (88). These studies suggest that the in-depth study of EGFR.Sig will contribute to the development of new strategies to strengthen tumor immunotherapy.

Furthermore, genes that are most critical to the immunotherapy response in EGFR.Sig were identified as Hub-EGFR.Sig. The above 4 genes screened by CRISPR are all in Hub-EGFR.Sig, and most of the other Hub-EGFR.Sig genes have also been reported to hold a position in the treatment of tumors. For example, RHOB (Ras homologue family member B gene) acts as a tumor suppressor most of the time, unlike other members of the Ras homologue family (89). RHOB can not only limit EGFR signal transduction on the cell surface (90) but also participate in antitumor immunity, such as antigen presentation and T-cell activation (89, 91). In our investigation, we also discovered that RHOB exhibited significant upregulation within the low-risk group of Hub-EGFR.Sig. Our Western blot analyses and HPA validation concordantly confirmed this expression pattern. In contrast, ABCA7 (ATP binding cassette subfamily A member 7) was expressed at a relatively higher level in the high-risk group. A recent study has shown that the inhibition of RHOB by hsa-miR-3178 can increase the expression of ABC transporter proteins through the PI3K/Akt pathway, which finally leads to the resistance of pancreatic cancer to gemcitabine (92). The antagonistic role of RHOB and ABCA7 in cancer reveals that there are complex interactions among Hub-EGFR.Sig, which was also confirmed in our subsequent miRNA–mRNA and TF-mRNA interactive network analysis. Notably, the Hub-EGFR.Sig risk scoring model integrates weighted contributions from multiple genes rather than relying on extreme expression changes of any single gene. This integrative approach more effectively captures the global biological characteristics of EGFR-related signaling and enhances the model's robustness against technical variability and biological heterogeneity. Overall, Hub-EGFR.Sig encompasses a set of characteristic EGFR-related genes that play a vital role in determining the efficacy of immunotherapy, so it holds great potential as a novel and significant therapy target and prognostic biomarker.

In general, our study found that cancer patients with higher Hub-EGFR.Sig risk scores presented poorer DSS and PFI in pan-cancer. Elevated EGFR levels have a particularly strong association with the survival outlook of many cancers (93). Specific to individual cancer types, LUAD and LUSC have relatively high Hub-EGFR.Sig scores among cancers, and ample evidence has

confirmed that EGFR tyrosine kinase inhibitors indeed prolong the PFS of NSCLC patients (94, 95). EGFR signal transduction also usually promotes the progression of BLCA (96, 97). However, the positive prognosis correlation of BLCA with Hub-EGFR.Sig observed in this study was not consistent with that in pan-cancer, although both DSS and PFI in BLCA showed the strongest association with Hub-EGFR.Sig. This observed heterogeneity primarily stems from differences in tumor microenvironment composition, molecular subtypes, MSI status, and variable responses to immunotherapy. Therefore, clinical interpretation of Hub-EGFR.Sig as a biomarker requires careful consideration of both the specific cancer type and underlying molecular context. Further investigation revealed that there were different correlations of Hub-EGFR.Sig with MSI across different cancer types. The relatively high Hub-EGFR.Sig score of BLCA was similar to that of LUAD and LUSC, while there was no significant correlation between Hub-EGFR.Sig and MSI in BLCA. MSI is observed at varied frequencies within malignant tumors, and its presence can serve as a predictor for cancer response to specific treatments, particularly immunotherapy (98, 99). Crosstalk between MSI affects the prognosis of tumors (100, 101), which may partly explain this phenomenon. Second, our study utilized DSS and PFI to better reflect the impact of immune therapy on the prognosis of BLCA (59). As we all know, BLCA is one of several tumors that responds positively to ICI treatment (102, 103). Our Hub-EGFR.Sig recognition by multiple ML algorithms was based on the importance of genes for immunotherapy, and deep analysis revealed that most of the genes in Hub-EGFR.Sig could independently affect the prognosis of BLCA. Thus, BLCA patients with higher Hub-EGFR.Sig scores may have better DSS and PFI in our study. Notably, our study was based on the transcriptional level analysis of EGFR-related genes. Tumor EGFR status can be evaluated by more than a dozen different methods, and the inconsistency in detection can lead to different results, which increases the variability between studies (93). In summary, Hub-EGFR.Sig can be used as a predictive biomarker for cancers despite the heterogeneity in various tumors.

Finally, we found that BLCA patients can be clustered into two subtypes according to Hub-EGFR.Sig, and there were some differences in the response of the two clusters to immunotherapy. Further comparing the infiltration of immune cells revealed an obvious difference in the TIME between the two clusters, which could be an important reason for the inconsistent response to immunotherapy. Although the continuous and complex crosstalk between multiple interrelated immune cells and tumors in BLCA still needs to be better characterized (104), several studies have confirmed that immune cell-related gene signatures can predict the clinical response of BLCA patients (105, 106). These findings reveal the possibility of targeted regulation of EGFR signaling combined with immunotherapy in the treatment of BLCA, which has rarely been reported in previous studies. By developing a new combination therapy, the response rate of immunotherapy can be improved (102, 107). The Hub-EGFR.Sig may serve as a valuable theoretical foundation for screening potential novel therapeutic targets, developing precision combination therapies, and formulating personalized treatment regimens. Therefore, we further screened the potentially available drugs for tumor immune regulation based on Hub-EGFR.Sig. These drugs included antineoplastic drugs such as etoposide phosphate, sparsomycin and vincristine, which will contribute to the design of new combined cancer treatment strategies.

Certainly, our research has several limitations. First, this study primarily depended on transcriptomic data, whether scRNA-Seq or bulk RNA-Seq, which may have technically heterogeneous. To investigate the relationship between EGFR and cancer cell immunotherapy response, we included two scRNA-Seq ICI cohorts with clear clinical outcomes from the GEO database. We noted that these two cohorts differed in their single-cell building and sequencing processes, resulting in different numbers of patients and cells in each group. In response to possible technical heterogeneity, stringent quality control measures were taken, including the exclusion of low-quality cells and normalization of the different datasets. Batch effect correction was performed before downstream analyses. In addition, screening of EGFR.Sig genes was based on the integration and cross-validation of multiple cohorts and multiple ML algorithms, thereby minimizing the impact of technical bias in any single dataset. This approach ensured the robustness and generalization ability of the identified EGFR-related signature genes. Moreover, the selection of data and the lack of information on the retrospective pan-cancer cohorts may have a potential impact on our results. We employed well-established normalization and batch correction approaches, including the Harmony package for single-cell data and the COMPAT tool for bulk RNA-Seq datasets, to ensure the reliability of downstream analyses. While these methods effectively address major technical variations, we acknowledge that certain potential biases may require development of more sophisticated statistical approaches for comprehensive detection in future studies. Finally, although multiple ML algorithms were used and many published cohorts were included to develop and verify EGFR.Sig, it will be necessary to verify this signature in future experiments and clinical validation studies.

5 Conclusion

In conclusion, our research offers novel insights into EGFR linked to immunotherapy response and prognosis in pan-cancer. Using multiple ML algorithms based on interactive analysis of scRNA-Seq and bulk RNA-Seq data, we successfully devised an improved predictive biomarker for immunotherapy and identified Hub-EGFR.Sig to explore the heterogeneity of different cancer prognoses. Focusing on BLCA, we investigated its interaction with molecular typing, TIME and drug sensitivity screening. The present study provides a potential pan-cancer targeting strategy related to clinical treatment for precision oncology, which will help to improve tumor immunotherapy and benefit patients.

Data availability statement

The original contributions presented in the study are included in the article/Supplementary Material. Further inquiries can be directed to the corresponding authors.

Ethics statement

Ethical approval was not required for the studies on humans in accordance with the local legislation and institutional requirements because only commercially available established cell lines were used.

Author contributions

CY: Data curation, Formal analysis, Writing – original draft, Writing – review & editing. XC: Conceptualization, Data curation, Software, Supervision, Validation, Writing – review & editing. ZC: Investigation, Methodology, Project administration, Validation, Writing – review & editing. SL: Funding acquisition, Project administration, Resources, Supervision, Writing – review & editing. RK: Conceptualization, Data curation, Formal analysis, Funding acquisition, Writing – review & editing. WL: Investigation, Methodology, Software, Writing – review & editing. MZ: Data curation, Formal analysis, Validation, Writing – review & editing. XS: Data curation, Resources, Supervision, Project administration, Writing – review & editing. ZX: Funding acquisition, Methodology, Project administration, Supervision, Data curation, Resources, Writing – review & editing.

Funding

The author(s) declare that financial support was received for the research and/or publication of this article. This work was funded by grants from the National Natural Science Foundation of China (Grant Serial Number: 82303811, 82373002), the Natural Science Basic Research Program of Shaanxi (Grant serial number: 2023-JC-QN-0840) and the Key Research and Development Projects of Shaanxi Province (Grant serial numbers: 2023-YBSF-359).

Acknowledgments

We would like to thank the staff members of the TCGA Research Network, the cBioPortal, the UCSC Xena data portal, the TISCH data portal, and all the authors for making their valuable research data public. Thanks to Dr. Weichao Dan for his guidance and assistance in the selection of cell lines.

Conflict of interest

The authors declare that the research was conducted in the absence of any commercial or financial relationships that could be construed as a potential conflict of interest.

Generative AI statement

The author(s) declare that no Generative AI was used in the creation of this manuscript.

Publisher's note

All claims expressed in this article are solely those of the authors and do not necessarily represent those of their affiliated organizations, or those of the publisher, the editors and the reviewers. Any product that may be evaluated in this article, or claim that may be made by its manufacturer, is not guaranteed or endorsed by the publisher.

Supplementary material

The Supplementary Material for this article can be found online at: https://www.frontiersin.org/articles/10.3389/fimmu.2025.1604394/full#supplementary-material

References

1. Wang Y, Wang M, Wu HX, Xu RH. Advancing to the era of cancer immunotherapy. *Cancer Commun (Lond).* (2021) 41:803–29. doi: 10.1002/cac2.12178

2. Robert C. A decade of immune-checkpoint inhibitors in cancer therapy. *Nat Commun.* (2020) 11:3801. doi: 10.1038/s41467-020-17670-y

3. Gong J, Chehrazi-Raffle A, Reddi S, Salgia R. Development of PD-1 and PD-L1 inhibitors as a form of cancer immunotherapy: a comprehensive review of registration trials and future considerations. *J Immunother Cancer.* (2018) 6:8. doi: 10.1186/s40425-018-0316-z

4. Kong J, Ha D, Lee J, Kim I, Park M, Im SH, et al. Network-based machine learning approach to predict immunotherapy response in cancer patients. *Nat Commun.* (2022) 13:3703. doi: 10.1038/s41467-022-31535-6

5. Havel JJ, Chowell D, Chan TA. The evolving landscape of biomarkers for checkpoint inhibitor immunotherapy. *Nat Rev Cancer.* (2019) 19:133–50. doi: 10.1038/s41568-019-0116-x

6. Tan X, Zhao X, Hu Z, Jiang D-S, Ma Z, Sun L, et al. Targeting Setdb1 in T cells induces transplant tolerance without compromising antitumor immunity. *Nat Commun.* (2025) 16:4534. doi: 10.1038/s41467-025-58841-z

7. Levantini E, Maroni G, Del Re M, Tenen DG. EGFR signaling pathway as therapeutic target in human cancers. *Semin Cancer Biol.* (2022) 85:253–75. doi: 10.1016/j.semcancer.2022.04.002

8. Gamez-Belmonte R, Mahapatro M, Erkert L, Gonzalez-Acera M, Naschberger E, Yu Y, et al. Epithelial presenilin-1 drives colorectal tumour growth by controlling EGFR-COX2 signalling. *Gut.* (2023) 72:1155–66. doi: 10.1136/gutjnl-2022-327323

9. Lei ZN, Teng QX, Tian Q, Chen W, Xie Y, Wu K, et al. Signaling pathways and therapeutic interventions in gastric cancer. *Signal Transduct Target Ther.* (2022) 7:358. doi: 10.1038/s41392-022-01190-w

10. Kang J, Chun J, Hwang JS, Pan C, Li J, Boese AC, et al. EGFR-phosphorylated GDH1 harmonizes with RSK2 to drive CREB activation and tumor metastasis in EGFR-activated lung cancer. *Cell Rep.* (2022) 41:111827. doi: 10.1016/j.celrep.2022.111827

11. Roskoski R Jr. Properties of FDA-approved small molecule protein kinase inhibitors: A 2023 update. *Pharmacol Res.* (2023) 187:106552. doi: 10.1016/j.phrs.2022.106552

12. Lu S, Dong X, Jian H, Chen J, Chen G, Sun Y, et al. AENEAS: A randomized phase III trial of aumolertinib versus gefitinib as first-line therapy for locally advanced or metastaticNon-small-cell lung cancer with EGFR exon 19 deletion or L858R mutations. *J Clin Oncol*. (2022) 40:3162–71. doi: 10.1200/JCO.21.02641

13. Markham A. Erdafitinib: first global approval. *Drugs*. (2019) 79:1017–21. doi: 10.1007/s40265-019-01142-9

14. Kang JJ, Ko A, Kil SH, Mallen-St Clair J, Shin DS, Wang MB, et al. EGFR pathway targeting drugs in head and neck cancer in the era of immunotherapy. *Biochim Biophys Acta Rev Cancer*. (2023) 1878:188827. doi: 10.1016/j.bbcan.2022.188827

15. Yang L, He YT, Dong S, Wei XW, Chen ZH, Zhang B, et al. Single-cell transcriptome analysis revealed a suppressive tumor immune microenvironment in EGFR mutant lung adenocarcinoma. *J Immunother Cancer*. (2022) 10(2):e003534. doi: 10.1136/jitc-2021-003534

16. Qiao M, Jiang T, Liu X, Mao S, Zhou F, Li X, et al. Immune checkpoint inhibitors in EGFR-mutated NSCLC: dusk or dawn? *J Thorac Oncol*. (2021) 16:1267–88. doi: 10.1016/j.jtho.2021.04.003

17. Rittmeyer A, Barlesi F, Waterkamp D, Park K, Ciardiello F, von Pawel J, et al. Atezolizumab versus docetaxel in patients with previously treated non-small-cell lung cancer (OAK): a phase 3, open-label, multicentre randomised controlled trial. *Lancet*. (2017) 389:255–65. doi: 10.1016/S0140-6736(16)32517-X

18. Herbst RS, Baas P, Kim DW, Felip E, Pérez-Gracia JL, Han JY, et al. Pembrolizumab versus docetaxel for previously treated, PD-L1-positive, advanced non-small-cell lung cancer (KEYNOTE-010): a randomised controlled trial. *Lancet*. (2016) 387:1540–50. doi: 10.1016/S0140-6736(15)01281-7

19. Hwang B, Lee JH, Bang D. Single-cell RNA sequencing technologies and bioinformatics pipelines. *Exp Mol Med*. (2018) 50:1–14. doi: 10.1038/s12276-018-0071-8

20. Hänzelmann S, Castelo R, Guinney J. GSVA: gene set variation analysis for microarray and RNA-seq data. *BMC Bioinf*. (2013) 14:7. doi: 10.1186/1471-2105-14-7

21. Jerby-Arnon L, Shah P, Cuoco MS, Rodman C, Su MJ, Melms JC, et al. A cancer cell program promotes T cell exclusion and resistance to checkpoint blockade. *Cell*. (2018) 175:984–97.e24. doi: 10.1016/j.cell.2018.09.006

22. Yost KE, Satpathy AT, Wells DK, Qi Y, Wang C, Kageyama R, et al. Clonal replacement of tumor-specific T cells following PD-1 blockade. *Nat Med*. (2019) 25:1251–9. doi: 10.1038/s41591-019-0522-3

23. Sun D, Wang J, Han Y, Dong X, Ge J, Zheng R, et al. TISCH: a comprehensive web resource enabling interactive single-cell transcriptome visualization of tumor microenvironment. *Nucleic Acids Res*. (2021) 49:D1420–d30. doi: 10.1093/nar/gkaa1020

24. Goldman MJ, Craft B, Hastie M, Repečka K, McDade F, Kamath A, et al. Visualizing and interpreting cancer genomics data via the Xena platform. *Nat Biotechnol*. (2020) 38:675–8. doi: 10.1038/s41587-020-0546-8

25. Chen YT, Shen JY, Chen DP, Wu CF, Guo R, Zhang PP, et al. Identification of cross-talk between m(6)A and 5mC regulators associated with onco-immunogenic features and prognosis across 33 cancer types. *J Hematol Oncol*. (2020) 13:22. doi: 10.1186/s13045-020-00854-w

26. Gao J, Aksoy BA, Dogrusoz U, Dresdner G, Gross B, Sumer SO, et al. Integrative analysis of complex cancer genomics and clinical profiles using the cBioPortal. *Sci Signal*. (2013) 6:pl1. doi: 10.1126/scisignal.2004088

27. Cerami E, Gao J, Dogrusoz U, Gross BE, Sumer SO, Aksoy BA, et al. The cBio cancer genomics portal: an open platform for exploring multidimensional cancer genomics data. *Cancer Discov*. (2012) 2:401–4. doi: 10.1158/2159-8290.CD-12-0095

28. Thorsson V, Gibbs DL, Brown SD, Wolf D, Bortone DS, Ou Yang TH, et al. The immune landscape of cancer. *Immunity*. (2018) 48:812–30.e14. doi: 10.1016/j.immuni.2018.03.023

29. Hugo W, Zaretsky JM, Sun L, Song C, Moreno BH, Hu-Lieskovan S, et al. Genomic and transcriptomic features of response to anti-PD-1 therapy in metastatic melanoma. *Cell*. (2016) 165:35–44. doi: 10.1016/j.cell.2016.02.065

30. Liu D, Schilling B, Liu D, Sucker A, Livingstone E, Jerby-Arnon L, et al. Integrative molecular and clinical modeling of clinical outcomes to PD1 blockade in patients with metastatic melanoma. *Nat Med*. (2019) 25:1916–27. doi: 10.1038/s41591-019-0654-5

31. Gide TN, Quek C, Menzies AM, Tasker AT, Shang P, Holst J, et al. Distinct immune cell populations define response to anti-PD-1 monotherapy and anti-PD-1/anti-CTLA-4 combined therapy. *Cancer Cell*. (2019) 35:238–55.e6. doi: 10.1016/j.ccell.2019.01.003

32. Riaz N, Havel JJ, Makarov V, Desrichard A, Urba WJ, Sims JS, et al. Tumor and microenvironment evolution during immunotherapy with nivolumab. *Cell*. (2017) 171:934–49.e16. doi: 10.1016/j.cell.2017.09.028

33. Van Allen EM, Miao D, Schilling B, Shukla SA, Blank C, Zimmer L, et al. Genomic correlates of response to CTLA-4 blockade in metastatic melanoma. *Science*. (2015) 350:207–11. doi: 10.1126/science.aad0095

34. Van Allen EM, Miao D, Schilling B, Shukla SA, Blank C, Zimmer L, et al. Erratum for the Report "Genomic correlates of response to CTLA-4 blockade in metastatic melanoma. *Science*. (2016) 352(6283):aaf8264. doi: 10.1126/science.aaf8264

35. Mariathasan S, Turley SJ, Nickles D, Castiglioni A, Yuen K, Wang Y, et al. TGFβ attenuates tumour response to PD-L1 blockade by contributing to exclusion of T cells. *Nature*. (2018) 554:544–8. doi: 10.1038/nature25501

36. Snyder A, Nathanson T, Funt SA, Ahuja A, Buros Novik J, Hellmann MD, et al. Contribution of systemic and somatic factors to clinical response and resistance to PD-L1 blockade in urothelial cancer: An exploratory multi-omic analysis. *PloS Med*. (2017) 14:e1002309. doi: 10.1371/journal.pmed.1002309

37. Zhao J, Chen AX, Gartrell RD, Silverman AM, Aparicio L, Chu T, et al. Immune and genomic correlates of response to anti-PD-1 immunotherapy in glioblastoma. *Nat Med*. (2019) 25:462–9. doi: 10.1038/s41591-019-0349-y

38. Kim ST, Cristescu R, Bass AJ, Kim KM, Odegaard JI, Kim K, et al. Comprehensive molecular characterization of clinical responses to PD-1 inhibition in metastatic gastric cancer. *Nat Med*. (2018) 24:1449–58. doi: 10.1038/s41591-018-0101-z

39. Braun DA, Hou Y, Bakouny Z, Ficial M, Sant' Angelo M, Forman J, et al. Interplay of somatic alterations and immune infiltration modulates response to PD-1 blockade in advanced clear cell renal cell carcinoma. *Nat Med*. (2020) 26:909–18. doi: 10.1038/s41591-020-0839-y

40. Zhang Z, Wang ZX, Chen YX, Wu HX, Yin L, Zhao Q, et al. Integrated analysis of single-cell and bulk RNA sequencing data reveals a pan-cancer stemness signature predicting immunotherapy response. *Genome Med*. (2022) 14:45. doi: 10.1186/s13073-022-01050-w

41. Osorio D, Cai JJ. Systematic determination of the mitochondrial proportion in human and mice tissues for single-cell RNA-sequencing data quality control. *Bioinformatics*. (2021) 37:963–7. doi: 10.1093/bioinformatics/btaa751

42. Eisenhauer EA, Therasse P, Bogaerts J, Schwartz LH, Sargent D , Ford R, et al. New response evaluation criteria in solid tumours: revised RECIST guideline (version 1.1). *Eur J Cancer*. (2009) 45:228–47. doi: 10.1016/j.ejca.2008.10.026

43. Vougas K, Sakellaropoulos T, Kotsinas A, Foukas GP, Ntargaras A, Koinis F, et al. Machine learning and data mining frameworks for predicting drug response in cancer: An overview and a novel in silico screening process based on association rule mining. *Pharmacol Ther*. (2019) 203:107395. doi: 10.1016/j.pharmthera.2019.107395

44. Sammut SJ, Crispin-Ortuzar M, Chin SF, Provenzano E, Bardwell HA, Ma W, et al. Multi-omic machine learning predictor of breast cancer therapy response. *Nature*. (2022) 601:623–9. doi: 10.1038/s41586-021-04278-5

45. Ayers M, Lunceford J, Nebozhyn M, Murphy E, Loboda A, Kaufman DR, et al. IFN-γ-related mRNA profile predicts clinical response to PD-1 blockade. *J Clin Invest*. (2017) 127:2930–40. doi: 10.1172/JCI91190

46. Topalian SL, Hodi FS, Brahmer JR, Gettinger SN, Smith DC, McDermott DF, et al. Safety, activity, and immune correlates of anti-PD-1 antibody in cancer. *N Engl J Med*. (2012) 366:2443–54. doi: 10.1056/NEJMoa1200690

47. Rooney MS, Shukla SA, Wu CJ, Getz G, Hacohen N. Molecular and genetic properties of tumors associated with local immune cytolytic activity. *Cell*. (2015) 160:48–61. doi: 10.1016/j.cell.2014.12.033

48. Freeman AJ, Vervoort SJ, Ramsbottom KM, Kelly MJ, Michie J, Pijpers L, et al. Natural killer cells suppress T cell-associated tumor immune evasion. *Cell Rep*. (2019) 28:2784–94.e5. doi: 10.1016/j.celrep.2019.08.017

49. Kearney CJ, Vervoort SJ, Hogg SJ, Ramsbottom KM, Freeman AJ, Lalaoui N, et al. Tumor immune evasion arises through loss of TNF sensitivity. *Sci Immunol*. (2018) 3(23):eaar3451. doi: 10.1126/sciimmunol.aar3451

50. Manguso RT, Pope HW, Zimmer MD, Brown FD, Yates KB, Miller BC, et al. *In vivo* CRISPR screening identifies Ptpn2 as a cancer immunotherapy target. *Nature*. (2017) 547:413–8. doi: 10.1038/nature23270

51. Pan D, Kobayashi A, Jiang P, Ferrari de Andrade L, Tay RE, Luoma AM, et al. A major chromatin regulator determines resistance of tumor cells to T cell-mediated killing. *Science*. (2018) 359:770–5. doi: 10.1126/science.aao1710

52. Patel SJ, Sanjana NE, Kishton RJ, Eidizadeh A, Vodnala SK, Cam M, et al. Identification of essential genes for cancer immunotherapy. *Nature*. (2017) 548:537–42. doi: 10.1038/nature23477

53. Vredevoogd DW, Kuilman T, Ligtenberg MA, Boshuizen J, Stecker KE, de Bruijn B, et al. Augmenting immunotherapy impact by lowering tumor TNF cytotoxicity threshold. *Cell*. (2020) 180:404–5. doi: 10.1016/j.cell.2020.01.005

54. Lawson KA, Sousa CM, Zhang X, Kim E, Akthar R, Caumanns JJ, et al. Functional genomic landscape of cancer-intrinsic evasion of killing by T cells. *Nature*. (2020) 586:120–6. doi: 10.1038/s41586-020-2746-2

55. Shukla SA, Bachireddy P, Schilling B, Galonska C, Zhan Q, Bango C, et al. Cancer-germline antigen expression discriminates clinical outcome to CTLA-4 blockade. *Cell*. (2018) 173:624–33.e8. doi: 10.1016/j.cell.2018.03.026

56. Dominguez CX, Müller S, Keerthivasan S, Koeppen H, Hung J, Gierke S, et al. Single-cell RNA sequencing reveals stromal evolution into LRRC15(+) myofibroblasts as a determinant of patient response to cancer immunotherapy. *Cancer Discov*. (2020) 10:232–53. doi: 10.1158/2159-8290.CD-19-0644

57. Cui C, Xu C, Yang W, Chi Z, Sheng X, Si L, et al. Ratio of the interferon-γ signature to the immunosuppression signature predicts anti-PD-1 therapy response in melanoma. *NPJ Genom Med*. (2021) 6:7. doi: 10.1038/s41525-021-00169-w

58. Xiong D, Wang Y, You M. A gene expression signature of TREM2(hi) macrophages and γδ T cells predicts immunotherapy response. *Nat Commun*. (2020) 11:5084. doi: 10.1038/s41467-020-18546-x

59. Liu J, Lichtenberg T, Hoadley KA, Poisson LM, Lazar AJ, Cherniack AD, et al. An integrated TCGA pan-cancer clinical data resource to drive high-quality survival outcome analytics. *Cell*. (2018) 173:400–16.e11. doi: 10.1016/j.cell.2018.02.052

60. Fu J, Li K, Zhang W, Wan C, Zhang J, Jiang P, et al. Large-scale public data reuse to model immunotherapy response and resistance. *Genome Med*. (2020) 12:21. doi: 10.1186/s13073-020-0721-z

61. Jiang P, Gu S, Pan D, Fu J, Sahu A, Hu X, et al. Signatures of T cell dysfunction and exclusion predict cancer immunotherapy response. *Nat Med*. (2018) 24:1550–8. doi: 10.1038/s41591-018-0136-1

62. Newman AM, Steen CB, Liu CL, Gentles AJ, Chaudhuri AA, Scherer F, et al. Determining cell type abundance and expression from bulk tissues with digital cytometry. *Nat Biotechnol*. (2019) 37:773–82. doi: 10.1038/s41587-019-0114-2

63. Guo G, Cui Y. New perspective on targeting the tumor suppressor p53 pathway in the tumor microenvironment to enhance the efficacy of immunotherapy. *J Immunother Cancer*. (2015) 3:9. doi: 10.1186/s40425-015-0053-5

64. Damiani E, Ullrich SE. Understanding the connection between platelet-activating factor, a UV-induced lipid mediator of inflammation, immune suppression and skin cancer. *Prog Lipid Res*. (2016) 63:14–27. doi: 10.1016/j.plipres.2016.03.004

65. Jiang M, Jia K, Wang L, Li W, Chen B, Liu Y, et al. Alterations of DNA damage response pathway: Biomarker and therapeutic strategy for cancer immunotherapy. *Acta Pharm Sin B*. (2021) 11:2983–94. doi: 10.1016/j.apsb.2021.01.003

66. Miranda A, Hamilton PT, Zhang AW, Pattnaik S, Becht E, Mezheyeuski A, et al. Cancer stemness, intratumoral heterogeneity, and immune response across cancers. *Proc Natl Acad Sci U S A*. (2019) 116:9020–9. doi: 10.1073/pnas.1818210116

67. Galluzzi L, Buqué A, Kepp O, Zitvogel L, Kroemer G. Immunogenic cell death in cancer and infectious disease. *Nat Rev Immunol*. (2017) 17:97–111. doi: 10.1038/nri.2016.107

68. Sharma P, Siddiqui BA, Anandhan S, Yadav SS, Subudhi SK, Gao J, et al. The next decade of immune checkpoint therapy. *Cancer Discov*. (2021) 11:838–57. doi: 10.1158/2159-8290.CD-20-1680

69. Sharma P, Goswami S, Raychaudhuri D, Siddiqui BA, Singh P, Nagarajan A, et al. Immune checkpoint therapy-current perspectives and future directions. *Cell*. (2023) 186:1652–69. doi: 10.1016/j.cell.2023.03.006

70. Morad G, Helmink BA, Sharma P, Wargo JA. Hallmarks of response, resistance, and toxicity to immune checkpoint blockade. *Cell*. (2021) 184:5309–37. doi: 10.1016/j.cell.2021.09.020

71. Sigismund S, Avanzato D, Lanzetti L. Emerging functions of the EGFR in cancer. *Mol Oncol*. (2018) 12:3–20. doi: 10.1002/mol2.2018.12.issue-1

72. Yoshida H, Kim YH, Ozasa H, Nagai H, Sakamori Y, Tsuji T, et al. Nivolumab in non-small-cell lung cancer with EGFR mutation. *Ann Oncol*. (2018) 29:777–8. doi: 10.1093/annonc/mdx745

73. Yamada T, Hirai S, Katayama Y, Yoshimura A, Shiotsu S, Watanabe S, et al. Retrospective efficacy analysis of immune checkpoint inhibitors in patients with EGFR-mutated non-small cell lung cancer. *Cancer Med*. (2019) 8:1521–9. doi: 10.1002/cam4.2019.8.issue-4

74. Hastings K, Yu HA, Wei W, Sanchez-Vega F, DeVeaux M, Choi J, et al. EGFR mutation subtypes and response to immune checkpoint blockade treatment in non-small-cell lung cancer. *Ann Oncol*. (2019) 30:1311–20. doi: 10.1093/annonc/mdz141

75. El Masri R, Delon J. RHO GTPases: from new partners to complex immune syndromes. *Nat Rev Immunol*. (2021) 21:499–513. doi: 10.1038/s41577-021-00500-7

76. Chaker M, Minden A, Chen S, Weiss RH, Chini EN, Mahipal A, et al. Rho GTPase effectors and NAD metabolism in cancer immune suppression. *Expert Opin Ther Targets*. (2018) 22:9–17. doi: 10.1080/14728222.2018.1413091

77. Kunimasa K, Hirotsu Y, Miyashita Y, Goto T, Amemiya K, Mochizuki H, et al. Multiregional sequence revealed SMARCA4 R1192C mutant clones acquired EGFR C797S mutation in the metastatic site of an EGFR-mutated NSCLC patient. *Lung Cancer*. (2020) 148:28–32. doi: 10.1016/j.lungcan.2020.07.035

78. Yang F, Wang Y, Li Q, Cao L, Sun Z, Jin J, et al. Intratumor heterogeneity predicts metastasis of triple-negative breast cancer. *Carcinogenesis*. (2017) 38:900–9. doi: 10.1093/carcin/bgx071

79. Lin A, Wei T, Meng H, Luo P, Zhang J. Role of the dynamic tumor microenvironment in controversies regarding immune checkpoint inhibitors for the treatment of non-small cell lung cancer (NSCLC) with EGFR mutations. *Mol Cancer*. (2019) 18:139. doi: 10.1186/s12943-019-1062-7

80. Ready N, Hellmann MD, Awad MM, Otterson GA, Gutierrez M, Gainor JF, et al. First-line nivolumab plus ipilimumab in advanced non-small-cell lung cancer (CheckMate 568): outcomes by programmed death ligand 1 and tumor mutational burden as biomarkers. *J Clin Oncol*. (2019) 37:992–1000. doi: 10.1200/JCO.18.01042

81. Li C, Gui G, Zhang L, Qin A, Zhou C, Zha X. Overview of methionine adenosyltransferase 2A (MAT2A) as an anticancer target: structure, function, and inhibitors. *J Med Chem*. (2022) 65:9531–47. doi: 10.1021/acs.jmedchem.2c00395

82. Li JT, Yang H, Lei MZ, Zhu WP, Su Y, Li KY, et al. Dietary folate drives methionine metabolism to promote cancer development by stabilizing MAT IIA. *Signal Transduct Target Ther*. (2022) 7:192. doi: 10.1038/s41392-022-01017-8

83. Chen H, Xia M, Lin M, Yang H, Kuhlenkamp J, Li T, et al. Role of methionine adenosyltransferase 2A and S-adenosylmethionine in mitogen-induced growth of human colon cancer cells. *Gastroenterology*. (2007) 133:207–18. doi: 10.1053/j.gastro.2007.03.114

84. Zhang T, Zheng Z, Liu Y, Zhang J, Zhao Y, Liu Y, et al. Overexpression of methionine adenosyltransferase II alpha (MAT2A) in gastric cancer and induction of cell cycle arrest and apoptosis in SGC-7901 cells by shRNA-mediated silencing of MAT2A gene. *Acta Histochem*. (2013) 115:48–55. doi: 10.1016/j.acthis.2012.03.006

85. Hung MH, Lee JS, Ma C, Diggs LP, Heinrich S, Chang CW, et al. Tumor methionine metabolism drives T-cell exhaustion in hepatocellular carcinoma. *Nat Commun*. (2021) 12:1455. doi: 10.1038/s41467-021-21804-1

86. Liu X, Wang Y, Lu H, Li J, Yan X, Xiao M, et al. Genome-wide analysis identifies NR4A1 as a key mediator of T cell dysfunction. *Nature*. (2019) 567:525–9. doi: 10.1038/s41586-019-0979-8

87. Katagiri T, Yamazaki S, Fukui Y, Aoki K, Yagita H, Nishina T, et al. JunB plays a crucial role in development of regulatory T cells by promoting IL-2 signaling. *Mucosal Immunol*. (2019) 12:1104–17. doi: 10.1038/s41385-019-0182-0

88. Salokas K, Liu X, Öhman T, Chowdhury I, Gawriyski L, Keskitalo S, et al. Physical and functional interactome atlas of human receptor tyrosine kinases. *EMBO Rep*. (2022) 23:e54041. doi: 10.15252/embr.202154041

89. Zaoui K, Duhamel S. RhoB as a tumor suppressor: It's all about localization. *Eur J Cell Biol*. (2023) 102:151313. doi: 10.1016/j.ejcb.2023.151313

90. Kazerounian S, Gerald D, Huang M, Chin YR, Udayakumar D, Zheng N, et al. RhoB differentially controls Akt function in tumor cells and stromal endothelial cells during breast tumorigenesis. *Cancer Res*. (2013) 73:50–61. doi: 10.1158/0008-5472.CAN-11-3055

91. Samuelsson M, Potrzebowska K, Lehtonen J, Beech JP, Skorova E, Uronen-Hansson H, et al. RhoB controls the Rab11-mediated recycling and surface reappearance of LFA-1 in migrating T lymphocytes. *Sci Signal*. (2017) 10(509): eaai8629. doi: 10.1126/scisignal.aai8629

92. Gu J, Huang W, Wang X, Zhang J, Tao T, Zheng Y, et al. Hsa-miR-3178/RhoB/PI3K/Akt, a novel signaling pathway regulates ABC transporters to reverse gemcitabine resistance in pancreatic cancer. *Mol Cancer*. (2022) 21:112. doi: 10.1186/s12943-022-01587-9

93. Nicholson RI, Gee JM, Harper ME. EGFR and cancer prognosis. *Eur J Cancer*. (2001) 37 Suppl 4:S9–15. doi: 10.1016/S0959-8049(01)00231-3

94. Soria JC, Ohe Y, Vansteenkiste J, Reungwetwattana T, Chewaskulyong B, Lee KH, et al. Osimertinib in untreated EGFR-mutated advanced non-small-cell lung cancer. *N Engl J Med*. (2018) 378:113–25. doi: 10.1056/NEJMoa1713137

95. Han JY, Park K, Kim SW, Lee DH, Kim HY, Kim HT, et al. First-SIGNAL: first-line single-agent iressa versus gemcitabine and cisplatin trial in never-smokers with adenocarcinoma of the lung. *J Clin Oncol*. (2012) 30:1122–8. doi: 10.1200/JCO.2011.36.8456

96. Ying X, Liu B, Yuan Z, Huang Y, Chen C, Jiang X, et al. METTL1-m(7) G-EGFR/EFEMP1 axis promotes the bladder cancer development. *Clin Transl Med*. (2021) 11: e675. doi: 10.1002/ctm2.v11.12

97. Daizumoto K, Yoshimaru T, Matsushita Y, Fukawa T, Uehara H, Ono M, et al. A DDX31/mutant-p53/EGFR axis promotes multistep progression of muscle-invasive bladder cancer. *Cancer Res*. (2018) 78:2233–47. doi: 10.1158/0008-5472.CAN-17-2528

98. Baretti M, Le DT. DNA mismatch repair in cancer. *Pharmacol Ther*. (2018) 189:45–62. doi: 10.1016/j.pharmthera.2018.04.004

99. Luchini C, Bibeau F, Ligtenberg MJL, Singh N, Nottegar A, Bosse T, et al. ESMO recommendations on microsatellite instability testing for immunotherapy in cancer, and its relationship with PD-1/PD-L1 expression and tumour mutational burden: a systematic review-based approach. *Ann Oncol*. (2019) 30:1232–43. doi: 10.1093/annonc/mdz116

100. Taieb J, Svrcek M, Cohen R, Basile D, Tougeron D, Phelip JM. Deficient mismatch repair/microsatellite unstable colorectal cancer: Diagnosis, prognosis and treatment. *Eur J Cancer*. (2022) 175:136–57. doi: 10.1016/j.ejca.2022.07.020

101. Lin A, Zhang J, Luo P. Crosstalk between the MSI status and tumor microenvironment in colorectal cancer. *Front Immunol*. (2020) 11:2039. doi: 10.3389/fimmu.2020.02039

102. Tran L, Xiao JF, Agarwal N, Duex JE, Theodorescu D. Advances in bladder cancer biology and therapy. *Nat Rev Cancer*. (2021) 21:104–21. doi: 10.1038/s41568-020-00313-1

103. Flaig TW, Spiess PE, Abern M, Agarwal N, Bangs R, Boorjian SA, et al. NCCN guidelines® Insights: bladder cancer, version 2.2022. *J Natl Compr Canc Netw*. (2022) 20:866–78. doi: 10.6004/jnccn.2022.0041

104. Schneider AK, Chevalier MF, Derré L. The multifaceted immune regulation of bladder cancer. *Nat Rev Urol*. (2019) 16:613–30. doi: 10.1038/s41585-019-0226-y

105. Chen X, Xu R, He D, Zhang Y, Chen H, Zhu Y, et al. CD8(+) T effector and immune checkpoint signatures predict prognosis and responsiveness to immunotherapy in bladder cancer. *Oncogene*. (2021) 40:6223–34. doi: 10.1038/s41388-021-02019-6

106. Oh DY, Kwek SS, Raju SS, Li T, McCarthy E, Chow E, et al. Intratumoral CD4 (+) T cells mediate anti-tumor cytotoxicity in human bladder cancer. *Cell*. (2020) 181:1612–25.e13. doi: 10.1016/j.cell.2020.05.017

107. Zhu S, Ma AH, Zhu Z, Adib E, Rao T, Li N, et al. Synergistic antitumor activity of pan-PI3K inhibition and immune checkpoint blockade in bladder cancer. *J Immunother Cancer*. (2021) 9(11):e002917. doi: 10.1136/jitc-2021-002917

frontiers | Frontiers in Oncology

TYPE Original Research
PUBLISHED 24 June 2025
DOI 10.3389/fonc.2025.1564826

Check for updates

OPEN ACCESS

EDITED BY
Ying Luo,
University of Texas Southwestern Medical Center, United States

REVIEWED BY
Xin Xu,
Evozyne, Inc., United States
Fu Gao,
Yale University, United States
Xinmiao Meng,
Yale University, United States

*CORRESPONDENCE
Chang-Bin Yang
xbbyang@fmmu.edu.cn

†These authors have contributed equally to this work

RECEIVED 22 January 2025
ACCEPTED 03 June 2025
PUBLISHED 24 June 2025

CITATION
Ning W, Yang Y-R, Wu C-X, Hou Y, Liu Z-W and Yang C-B (2025) CHMP6 as a novel prognostic biomarker in bladder cancer: insights from a comprehensive cell death-related gene risk model.
Front. Oncol. 15:1564826.
doi: 10.3389/fonc.2025.1564826

COPYRIGHT
© 2025 Ning, Yang, Wu, Hou, Liu and Yang. This is an open-access article distributed under the terms of the Creative Commons Attribution License (CC BY). The use, distribution or reproduction in other forums is permitted, provided the original author(s) and the copyright owner(s) are credited and that the original publication in this journal is cited, in accordance with accepted academic practice. No use, distribution or reproduction is permitted which does not comply with these terms.

CHMP6 as a novel prognostic biomarker in bladder cancer: insights from a comprehensive cell death-related gene risk model

Wei Ning[1†], Yan-Ru Yang[2†], Chen-Xu Wu[3], Yue Hou[1], Zhi-Wei Liu[1] and Chang-Bin Yang[1*]

[1]Medical Innovation Center, Air Force Medical University, Xi'an, China, [2]Department of Pathology, the First Affiliated Hospital of Air Force Medical University, Xi'an, China, [3]School of Life Information Science and Technology, ShanghaiTech University, Shanghai, China

Introduction: Bladder cancer (BLCA) is a prevalent and aggressive disease characterized by substantial molecular heterogeneity, complicating its diagnosis and treatment. Existing therapies, including surgery and chemotherapy, often lack specificity. Alterations in cell death mechanisms, such as ferroptosis, cuproptosis, and immunogenic cell death, significantly impact cancer progression and prognosis.

Methods: We analyzed gene expression data from TCGA and GEO. Cox regression analyses generated a prognostic risk score model incorporating LIPT1, ACSL5, and CHMP6. This model successfully stratified BLCA patients into different risk categories and was validated through survival analysis, immune infiltration, mutation burden assessment, drug sensitivity predictions, and single-cell analysis. The high-risk group was linked to differentiation processes, developmental stages, and active metabolic pathways.

Results: Experimental validation highlighted CHMP6's role in enhancing BLCA cell survival and migration by regulating the cell cycle. The model's prognostic relevance was further supported by drug sensitivity and immune metrics. These results provide valuable insights into potential biomarkers and therapeutic targets for BLCA treatment.

Discussion: The CHMP6 protein promotes BLCA cell survival and invasive migration through modulation of the cell cycle.

KEYWORDS

CHMP6, BLCA, CDRI, ICD, ferroptosis

1 Introduction

Bladder cancer is the second most common malignant tumor of the urinary system globally, with an annual incidence rate exceeding 540,000 cases and a mortality rate of approximately 200,000 deaths per year. It ranks as the ninth most prevalent malignant tumor and the thirteenth leading cause of cancer-related deaths worldwide (1, 2). Currently, the standard treatment for bladder cancer involves surgical resection followed by chemotherapy (3). However, the selection of chemotherapy agents remains largely at the discretion of the treating physician (4). Furthermore, the anticipated length of survival has a significant influence on the selection of active or conservative treatment options for patients (5). Currently, there are numerous prognostic categories for bladder cancer, including the Uromol-2016 classification (6), the Van-Kessel classification (7), the Seiler classification (8), and others. However, the substantial heterogeneity of bladder cancer poses a significant challenge in molecular classification. Consequently, an enhanced insight into the regulatory mechanisms driving the onset and progression of bladder cancer, the identification of molecular markers for prognostication, and the discovery of novel biological targets for targeted therapy are crucial for advancing the prevention and treatment of bladder cancer.

Molecular alterations that affect the mechanisms of cell death are frequently observed in the development of cancer. These alterations permit malignant cells to evade the effects of intrinsic death signals (9). Nevertheless, an increasing body of evidence suggests that there are multiple alternative mechanisms that coordinate various death pathways. Ferroptosis is an iron-dependent form of programmed cell death, marked by uncontrolled peroxidation of phospholipids. The occurrence of this process is primarily contingent upon the elevation of phospholipid-containing polyunsaturated fatty acid chains (pufa-pl), metabolite reactive oxygen species (ROS), and iron accumulation (10). Several studies have shown a relationship between ferroptosis-related genes and cancer prognosis (11, 12). Additionally, Cuproptosis is a unique form of programmed cell death that distinguishes itself from other well-defined cell death processes, the regulatory process is directly connected to mitochondrial metabolism (13). Several studies have established a strong association between copper death-related genes and the onset and progression of cancer (14, 15). Immunogenic cell death (ICD) is a type of tumor cell death induced by the stress caused by certain chemotherapeutics, radiotherapy and oncolytic viruses (16). Many literatures have confirmed that immunogenic death-related genes have great prognostic value (17, 18). While ferroptosis, cuproptosis, and ICD have been extensively studied as independent cell death modalities, their interplay in the prognosis of bladder cancer remains unexplored.

This study holds a novel research perspective on comprehensive cell death mechanisms, with the objective of identifying new molecular markers for bladder cancer prognosis based on a comprehensive cell death model, utilising readily accessible resources in the clinical setting. Additionally, the study aims to elucidate the mechanism through which comprehensive cell death affects the development of bladder cancer. By examining clinical tumour samples, this project would elucidate aspects such as tumour heterogeneity, mutation map, drug sensitivity, and other factors related to comprehensive cell death mechanisms. This would provide a novel perspective on the efficacy of comprehensive death-related oncogene targeted therapy and the advancement of novel therapeutic approaches.

Abbreviations: CDRI, comprehensive cell death gene risk model; BLCA, bladder cancer.

2 Materials and methods

2.1 Bulk RNA-seq analysis

2.1.1 Dataset collection

Gene expression profiles and clinical data of bladder cancer patients were sourced from the Cancer Genome Atlas (TCGA) database (https://portal.gdc.cancer.gov/). We also consulted to obtain information on ferroptosis, cuproptosis, and immunogenic death-related genes (Supplementary Table S1). Furthermore, gene expression profiles and clinical data of the GSE31684, GSE32548 and GSE32894 datasets were acquired from the Gene Expression Omnibus (GEO) database (https://www.ncbi.nlm.nih.gov/geo/).

2.1.2 Prognostic risk characteristics construction

Firstly, the "edger" (19) was employed to analyse the discrepancy between BLCA samples and normal samples. Genes with a log2 fold change (log2fc) greater than 1 and a false discovery rate (FDR) below 0.05 were regarded as differentially expressed. Subsequently, the intersection analysis with comprehensive death-related genes was conducted to ascertain the differential comprehensive death-related genes. Then the univariate Cox regression analysis was employed to identify comprehensive death-related genes associated with overall survival (OS) in patients with BLCA. To identify comprehensive death-related genes that independently influence the prognosis of BLCA, We conducted a multivariate Cox regression on the selected genes. The correlation coefficient between each gene was calculated. A comprehensive mortality prognostic risk score for BLCA was constructed, and a formula was established as follows:

$$\begin{aligned} RiskScore = {} & coef(LIPT1) * \exp(LIPT1) \\ & + coef(ACSL5) * exp(ACSL5) \\ & + coef(CHMP6) * \exp(CHMP6) \end{aligned}$$

2.1.3 Survival analysis

A survival analysis was conducted on various subgroups of BLCA and TCGA comprehensive death risk scores for other cancer types. The R packages "survival" and "survminer" (20) were employed to generate Kaplan-Meier curves.

2.1.4 Enrichment analysis of high and low risk groups

The R packages "edgeR" and "ggplot2" (21) were utilized for the analysis and visualization of differentially expressed protein-coding genes across the distinct risk groups. To further explore the potential biological functions, We performed GSEA, GO enrichment, and KEGG pathway analysis. The R packages "msigdbr" (22), "fgsea" (23), "clusterProfiler" (24) were used to generate the enrichment results.

2.1.5 Analysis of immune infiltration

The tumour tissue transcriptome data underwent quantitative transformation via "CIBERSORT" (25), xCell (26) and TIMER (27) analysis, allowing the assessment of human immune cell subsets. Immune cell profiles were compared between high-risk and low-risk groups to assess tumor microenvironment differences. The Wilcoxon test was applied to identify significant variations in immune cell infiltration and associated functional characteristics between the two groups.

2.1.6 Somatic variant analysis

Somatic mutation data, derived from whole exome sequencing of the TCGA-BLCA dataset. The mutation annotation format (MAF) files, containing information on single nucleotide variants, were analyzed using the "maftools" R package (28).

2.1.7 Pharmacological response assessment

The "pRRophetic" package (29) was employed to evaluate the response of each sample to a range of pharmacological agents. The Wilcoxon test was used to assess drug sensitivity differences between the two groups.

2.2 Single cell data analysis

Three single cell datasets, GSE135337, GSE129845 and GSE277524, were collected from GEO database. Single-cell data were analyzed using the "Seurat" R package (30). The expression matrix was filtered using the criteria: ncount_rna > 200, nfeature_rna< 5000, and percent_MT< 5 to exclude overexpressed and low-quality cells. Principal component analysis (PCA) and UMAP dimensionality reduction were performed to cluster the cells, followed by annotation using cluster-specific marker genes. Cell trajectory analysis by Monocle2 (31) package.

2.3 Experimental validation protocols

2.3.1 Clinical samples

Primary BLCA tissue samples were obtained from 54 patients who underwent surgery at Xijing Hospital, Air Force Military Medical University (Xi'an, China) between 2019 and 2024. All clinical samples adhered to the Clinical International Staging Guidelines and the Declaration of Helsinki. Informed consent was obtained from all participants. Clinicopathologic information was collected from surgical records and pathology reports. The local ethics committee approved all operations done in this research (ethics approval number: K202201-04).

2.3.2 Cell line cultivation and transfection

The human bladder cancer cell lines 5637 and T24 were obtained from Procell Life Science and Technology (Wuhan, China). 5637 cells were cultured in RPMI 1640 medium (PM150110) supplemented with 10% fetal bovine serum (164210-500), 100 units/mL of penicillin, and 100 units/mL of streptomycin sulfate, and incubated at 37°C in a humidified incubator with 5% CO2. T24 cells were maintained in MEM medium (PM150410) supplemented with 10% fetal bovine serum (164210-500), 100 units/mL of penicillin, and 100 units/mL of streptomycin sulfate, and cultured under standard conditions. CHMP6 knockdown (KD) and control (NC) lentiviruses were obtained from GeneChem (Shanghai, China). Transfection was performed following the manufacturer's instructions, and transfection efficiency was verified through Western blotting and RT-PCR analysis.

2.3.3 Immunohistochemistry and H-score

Surgical specimens were fixed in paraformaldehyde and embedded in paraffin. The blocks were sliced into 4-μm sections and mounted on slides. Slides were baked at 37°C overnight, deparaffinized in xylene, rehydrated in alcohol, acid repaired, and treated with 3% hydrogen peroxide to block peroxidase activity. The sections were incubated with anti-CHMP6 antibody (Catalog No: 31838-2, SAB, USA) at 4°C for ≥12 hours after being blocked with phosphate-buffered saline (PBS) containing 5% bovine serum albumin for 30 minutes. Protein-antibody complexes were detected and developed using standard rapid EnVision technology (Dako, Denmark). The tissue sections were counterstained with hematoxylin, mounted, and observed under a microscope for imaging.

Immunoreactivity was graded as follows: 0 = absence of staining, 1 + = weak cytoplasmic staining, and 2+ = intense cytoplasmic staining. Two experienced researchers independently evaluated the immunohistochemically stained sections. Samples were classified into high expression (2+) and low expression (1+ and 0) groups according to the staining intensity. H scores were calculated using the formula: H score = 1 × (percentage of 1+ stained cells) + 2 × (percentage of 2+ stained cells) + 3 × (percentage of 3+ stained cells), with a range from 0 to 300.

2.3.4 Western blotting assay

Cells were harvested by scraping or grinding, and proteins were extracted for analysis by Western blotting. Anti-CHMP6 antibodies (31838-2, SAB, Nanjing, China; PA5-145901, Invitrogen, USA), anti-LIPT1 antibody (PA5-57064, Invitrogen, USA), and anti-β-tubulin antibody (1:2000, CST, USA) were used to detect the target proteins. The original image is provided in the Supplementary Information.

2.3.5 RT-PCR

RNAiso Plus (TAKARA, Shiga-ken, Japan) was used to extract

total RNA, which was subsequently analyzed by reverse transcription-PCR with the SYBR Green II kit (TAKARA, Shiga-ken, Japan). The expression levels of target genes' mRNA were normalized to the ACTN gene. Thermal cycling conditions included 45 cycles: 15 s at 95°C, 5 s at 95°C, and 30 s at 60°C.

2.3.6 Cell viability assay

BLCA cell proliferation was assessed *in vitro* using the Cell Counting Kit-8 (YEASEN, China). Cells were seeded in 96-well plates at a density of 2×10^3 cells per well, with a final volume of 100 µL. The plates were incubated for a period of time at 37°C with 5% CO_2. Next, 10 µL of CCK-8 solution was added to each well, and after 1–4 hours of incubation, absorbance at 450 nm was measured using a microplate reader.

2.3.7 Cell permeabilization assay

Transwell chambers (8-µm pores, Corning, Lowell, MA, USA) were positioned on 24-well culture plates (REF3524, Corning, Lowell, MA, USA). Matrigel (356234, BD, USA) was mixed with serum-free medium and added to the chambers. A 200 µL serum-free cell suspension (3.5×10^4cells) was added to the upper chamber, and 500 µL of cell suspension to the lower chamber. After 24 hours, cells that had invaded into the lower chamber were fixed with anhydrous ethanol, stained with crystal violet, and air-dried. Images were captured in three random fields using an inverted microscope (200× magnification), and the number of cells was counted.

2.3.8 Scratch wound test

5637 cells were cultured to 80%-90% confluence, and a straight-line "scratch" was created using a 200-µL pipette tip to form a cell-free area. The cells were then incubated in serum-free medium for 24–48 hours, and cell migration was observed under a microscope.

2.3.9 Annexin V/PI staining

5637 cells were digested with EDTA-free trypsin and then centrifuged at 500 × g for 5 minutes to terminate digestion. The supernatant was discarded, and the cells were washed twice with PBS. For every $1 \times 10_5$ cells, they were resuspended in 500 µL of cell staining buffer (typically PBS containing 1%-3% BSA or FBS). Next, 2-5 µL of PI/Annexin V-FITC staining solution (final PI concentration of 0.5 mg/mL) was added to each sample. The cells were incubated for 10-15 minutes, washed twice with PBS, and then analyzed by flow cytometry. The original image is provided in the Supplementary Information.

3 Results

3.1 Defining multiple cell death genes associated with BLCA prognosis

The initial analysis of the TCGA database revealed significant differences between BLCA cancer samples and corresponding paracancerous samples (Figure 1A; Supplementary Table S2). By intersecting with the three cell death related gene sets, it was observed that the three cell death related genes showed no significant difference between cancer tissues and adjacent tissues (Figure 1B; Supplementary Figure S1A–C), indicating that the cell death activity would not be affected by cancer. Univariate Cox survival analysis was performed on three cell death-related genes to identify those associated with the prognosis of BLCA patients. This analysis revealed that a total of 25 cell death-related genes had a significant impact on the prognosis (Figure 1C; Supplementary Table S3). Multivariate Cox analysis of these prognostic genes identified three genes that were significantly associated with prognosis. The overall p-value for the likelihood ratio test of the model is 2e-11. Among them, chmp6 is a risk factor, while lipt1 and ACSL5 are protective factors (Figure 1D). However, no marked differences in the expression of these three genes were observed between cancerous and adjacent tissues (Supplementary Figure S1D-F), suggesting that the prognosis of our patients may not be solely driven by cancer-related factors.

3.2 Evaluating the effect of CDRI model on prognosis

A comprehensive death gene risk model (CDRI) was constructed using the genes CHMP6, LIPT1, and ACSL5. Subsequently, cancer patients were divided into high-risk and low-risk groups using CDRI scores (-3.003, 2.369) with a threshold of 0.522 (Supplementary Table S4; Supplementary Table S5). The prognosis of the high-risk group was markedly inferior to that of the low-risk group (Figure 2A). The same trend was observed in additional BLCA datasets upon validation (Figure 2B; Supplementary Figure S2). To investigate the potential of the CDRI model for pan-cancer prognosis prediction, we extended the model to encompass additional cancer types. Our analysis demonstrated that the prognosis of the high-risk group in TCGA-UECE, TCGA-LIHC, TCGA-MESO and TCGA-ACC was considerably poorer than the low-risk group (Figures 2C–F). Previous literature also confirmed that knockout of chmp6 gene would make pancreatic cancer cells and liver cancer cells more sensitive to ferroptosis (32). Our results indicate that the area under the curve for predicting the 1-year, 3-year, and 5-year survival rates of BLAD patients is all above 0.7 (Supplementary Figure S3A; Supplementary Table S6). Similar results were observed in the validation cohort (Supplementary Figure S3B–F). These results indicate that the CDRI model could potentially act as a prognostic biomarker for pan-cancer.

In addition, we compared the CDRI model with Peng's model (33) and Bo's model (34), and found that the AUC of the CDRI model was better than that of the Peng's model at one, three, and five years. Although the AUC of the CDRI model was comparable to that of the Bo's model on the TCGA dataset, the performance of the CDRI model was much better than that of the Bo's model on the GSE32548 and GSE32894 datasets. In addition, the Bo's model uses seven gene features, while the CDRI model only uses three gene features. These results indicate that the CDRI model could potentially act as a prognostic biomarker for pan-cancer.

10.3389/fonc.2025.1564826

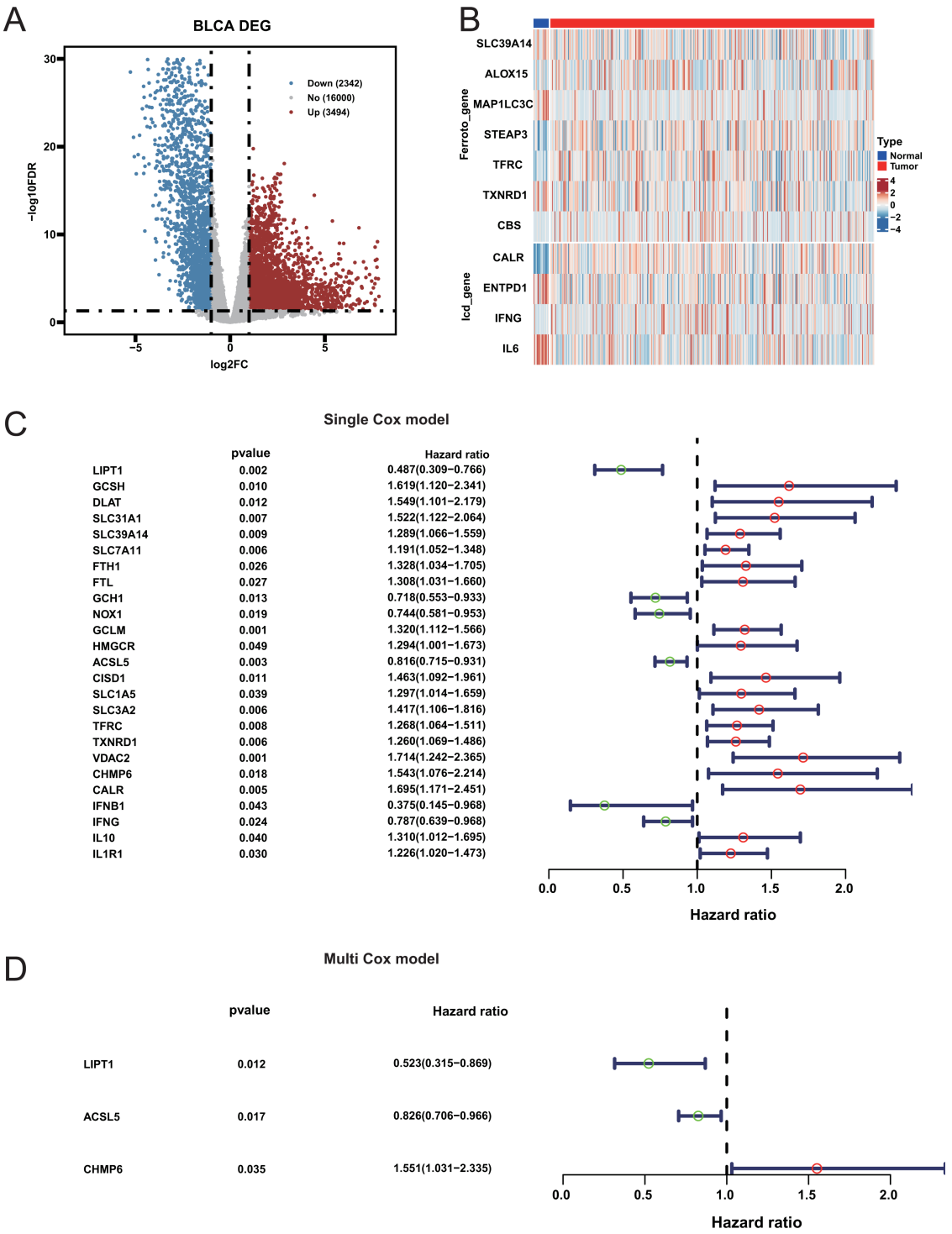

FIGURE 1
Differential expression and prognostic significance of genes in bladder cancer. **(A)** Volcano Plot of Differentially Expressed Genes between bladder cancer and normal samples. **(B)** Heatmap of Ferroptosis and Immunogenic Cell Death-Related Genes. **(C)** Forest Plot of Univariate Cox Analysis: Hazard ratios and 95% confidence intervals for genes significantly associated with bladder cancer prognosis from univariate Cox analysis. **(D)** Forest Plot of Multivariate Cox Analysis.

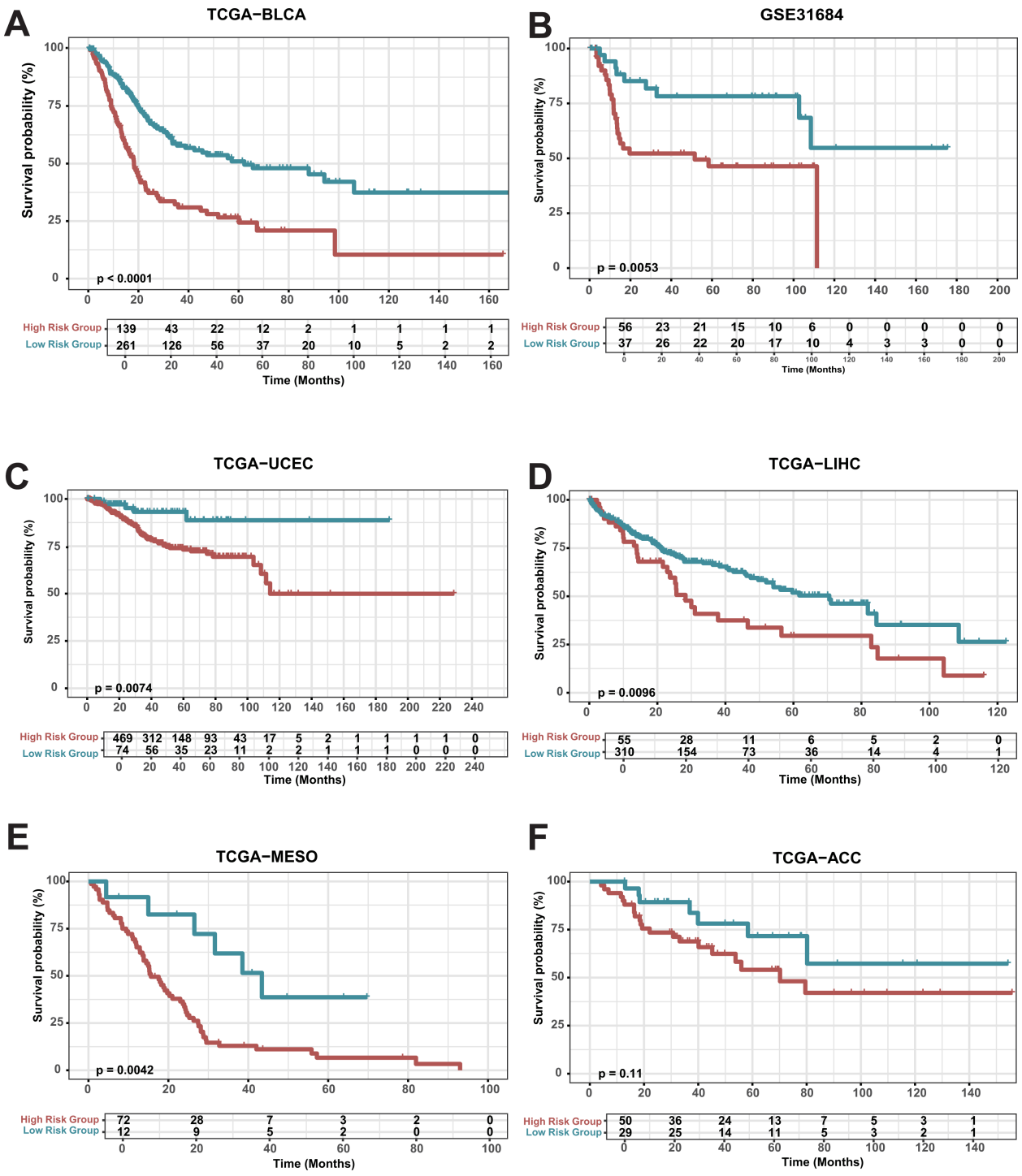

FIGURE 2
Survival analysis of risk groups **(A)** Overall Survival in TCGA-BLCA: Kaplan-Meier survival curves for high-risk and low-risk groups in bladder cancer (TCGA-BLCA). **(B-E)** Kaplan-Meier survival curves for GSE31684, TCGA-LIHC, TCGA-MESO, TCGA-UCEC, and TCGA-ACC.

3.3 Research on the mechanism of CDRI model

To further explore the mechanism behind the CDRI model, we first carried out a comparative assessment between the two groups. Subsequently, our analysis showed that the differences between two groups were predominantly associated with biological processes related to differentiation and development, as well as molecular functions linked to serine peptidase activity (Figure 3A). Earlier research has demonstrated that serine peptidase is involved in regulating biological processes related to tumor development (35). KEGG pathway enrichment analysis further indicated that the differences between

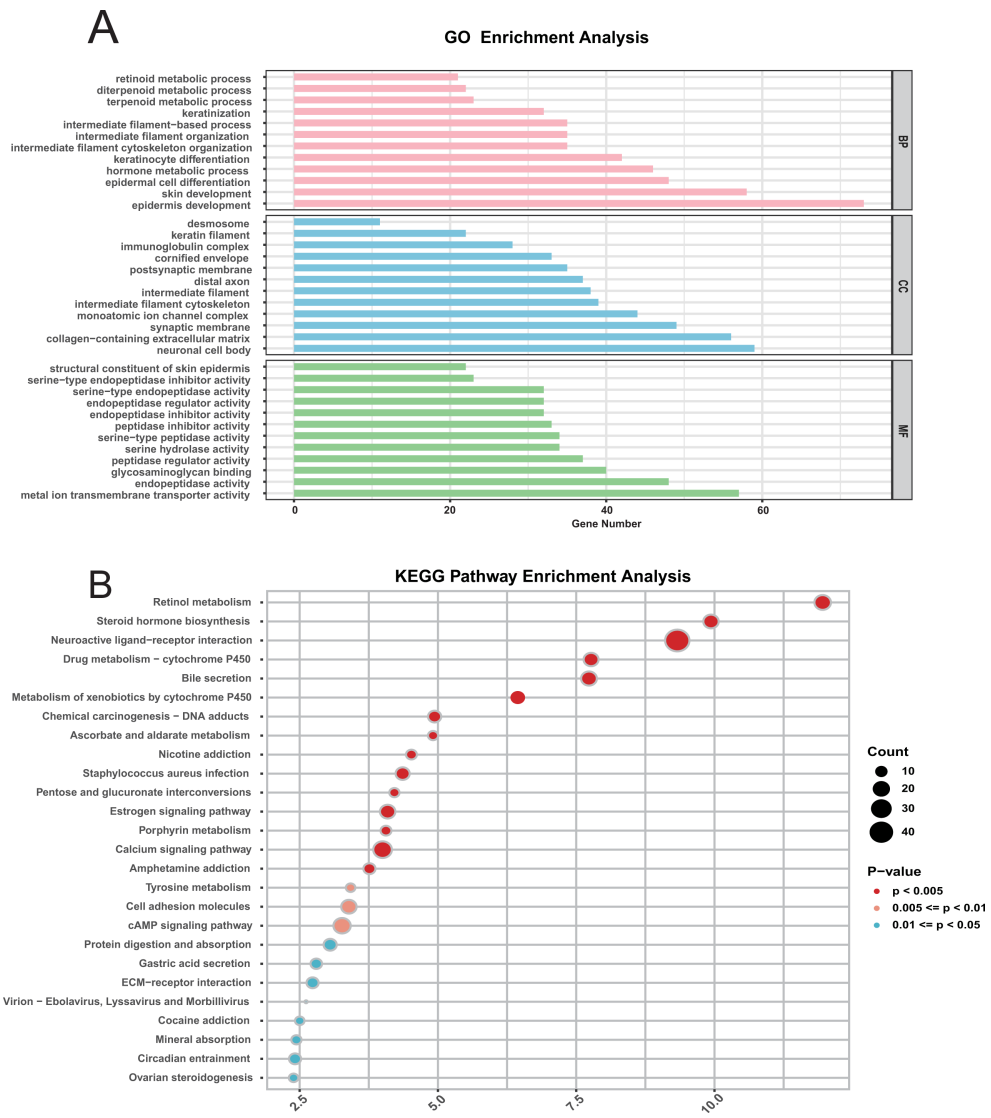

FIGURE 3
Functional enrichment analysis of differentially expressed genes in bladder cancer. **(A)** GO Pathway Enrichment Analysis: Enriched Gene Ontology (GO) terms for differentially expressed genes include biological processes (BP), cellular components (CC), and molecular functions (MF). **(B)** KEGG Pathway Enrichment Analysis.

two groups were primarily enriched in metabolic pathways, including the cAMP signaling pathway (Figure 3B). This pathway is also involved in cancer proliferation and progression (36).

3.4 Comparison of the tumor immune microenvironment between two groups

To determine whether discrepancies exist in the tumor immune landscape between two groups, we estimated the proportions of 22 immune cell types (Figure 4A). No significant correlation was observed among the 22 immune cell types (Figure 4C), indicating that there was no mixing between cell types. Additionally, there was no significant difference in the proportion of most immune cells between the two groups (Figure 4B; Supplementary Figure S4), indicating that the difference in prognosis between the two groups was not caused by the proportion of immune cells. The estimated score further indicated no discernible difference in immune scores between the two groups (Figure 4D). However, the stromal score in the high-risk group was significantly higher than that in the low-risk group, indicating greater tumor purity in the high-risk group. We speculate that the prognosis of patients may be mainly affected by the purity of tumor, rather than by the composition of immune cells.

3.5 Comparison of mutation characteristics between two groups

We analyzed the mutation profiles of the two groups to evaluate potential differences in tumor mutation burden. The number of

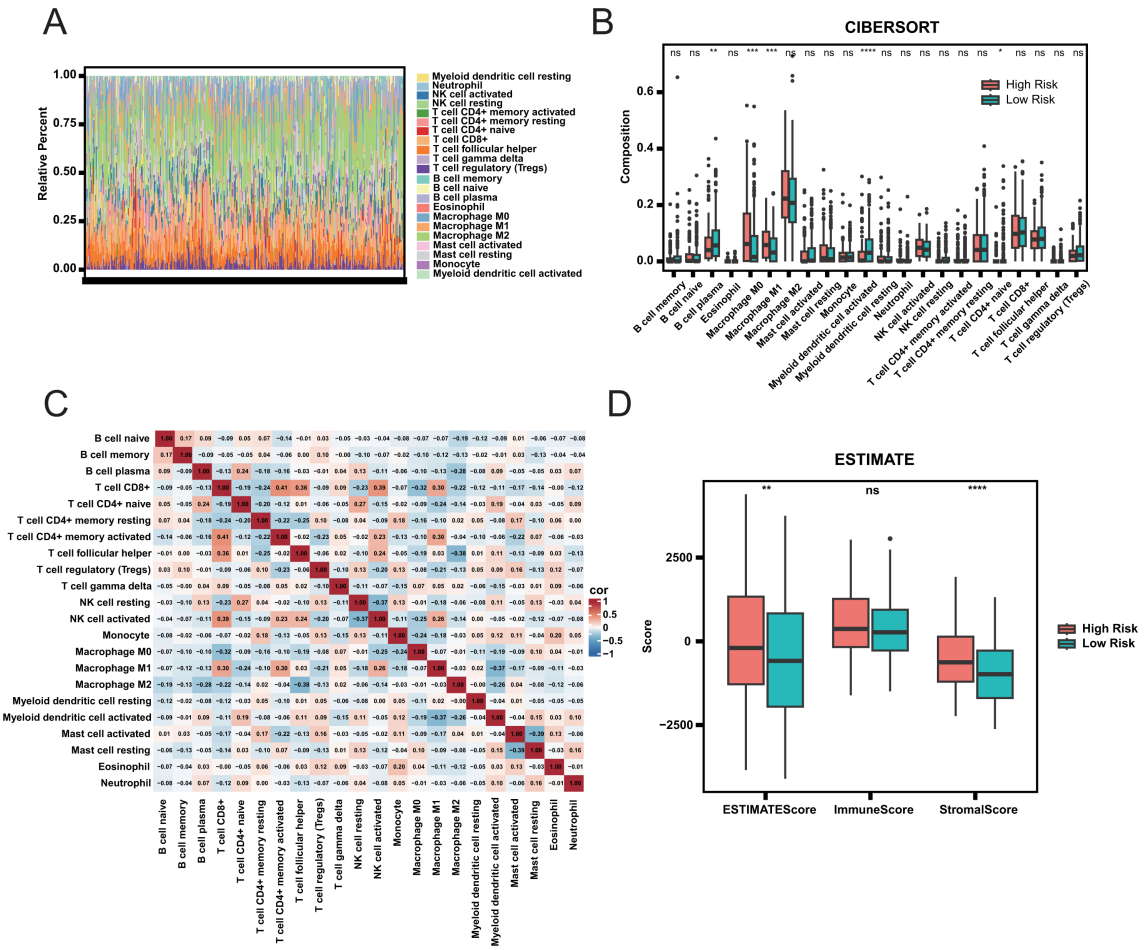

FIGURE 4
Immune infiltration and tumor microenvironment analysis. **(A)** Relative Abundance of Immune Cell Types in High and Low Risk Groups. **(B)** Comparison of Immune Cell Composition Between High and Low Risk Groups. Statistical significance is indicated by ns (not significant), * (adjust.p< 0.05), ** (adjust.p< 0.01), *** (adjust.p< 0.001), and **** (adjust.p< 0.0001). **(C)** Correlation Heatmap of Immune Cell Types. **(D)** ESTIMATE Scores Comparison Between High and Low Risk Groups.

mutations in high-risk group was higher than that in low-risk group (Figures 5A, B). But the mutation distribution pattern is similar between the two groups (Figures 5C, D). The tumor mutation burden (TMB) of high-risk group was lower than that of low-risk group (Figures 5E-F). Additionally, the TMB in both groups was higher than in other cancers (Supplementary Figure S5). Previous studies have demonstrated that patients with higher TMB tend to have prolonged survival following immune checkpoint inhibitor (ICI) therapy (37). It also confirmed the correctness of our prognosis classification.

3.6 Assessment of drug sensitivity in high-risk and low-risk groups

To guide clinical treatment for two groups, we calculated the sensitivity of each sample to various drug types, including chemotherapy agents, targeted therapies, and immune modulators. The sensitivity of high-risk group and low-risk group to drugs is different (Figure 6A). These findings can guide medication administration for patients in different risk groups. Additionally, a significant correlation exists between the risk score and drug sensitivity (Figure 6B), It shows that our CDRI model can be used to guide patients' medication. Notably, a higher proportion of patients in the low-risk group achieved a complete treatment response compared to the high-risk group (Supplementary Figure S6). Recapitulation of known molecular subtypes within our prognostic groups biologically corroborates the classification logic.

3.7 Evaluation of the prognostic impact of CDRI combined with other scoring systems

To assess the combined effect of CDRI and other evaluation scores on prognosis, we investigated the impact of TMT and $CXCR5^{+}CD8^{+}$ scores in both two groups. In the high-risk group, a higher TMT score was associated with a poorer prognosis (Figures 7A, B), while a higher $CXCR5^{+}CD8^{+}$ score correlated with a more favorable prognosis (Figures 7C, D). The TIDE score in the high-risk group was significantly higher than in the low-risk group, indicating a greater level of tumor immune escape in the former (Figure 7E). However, the

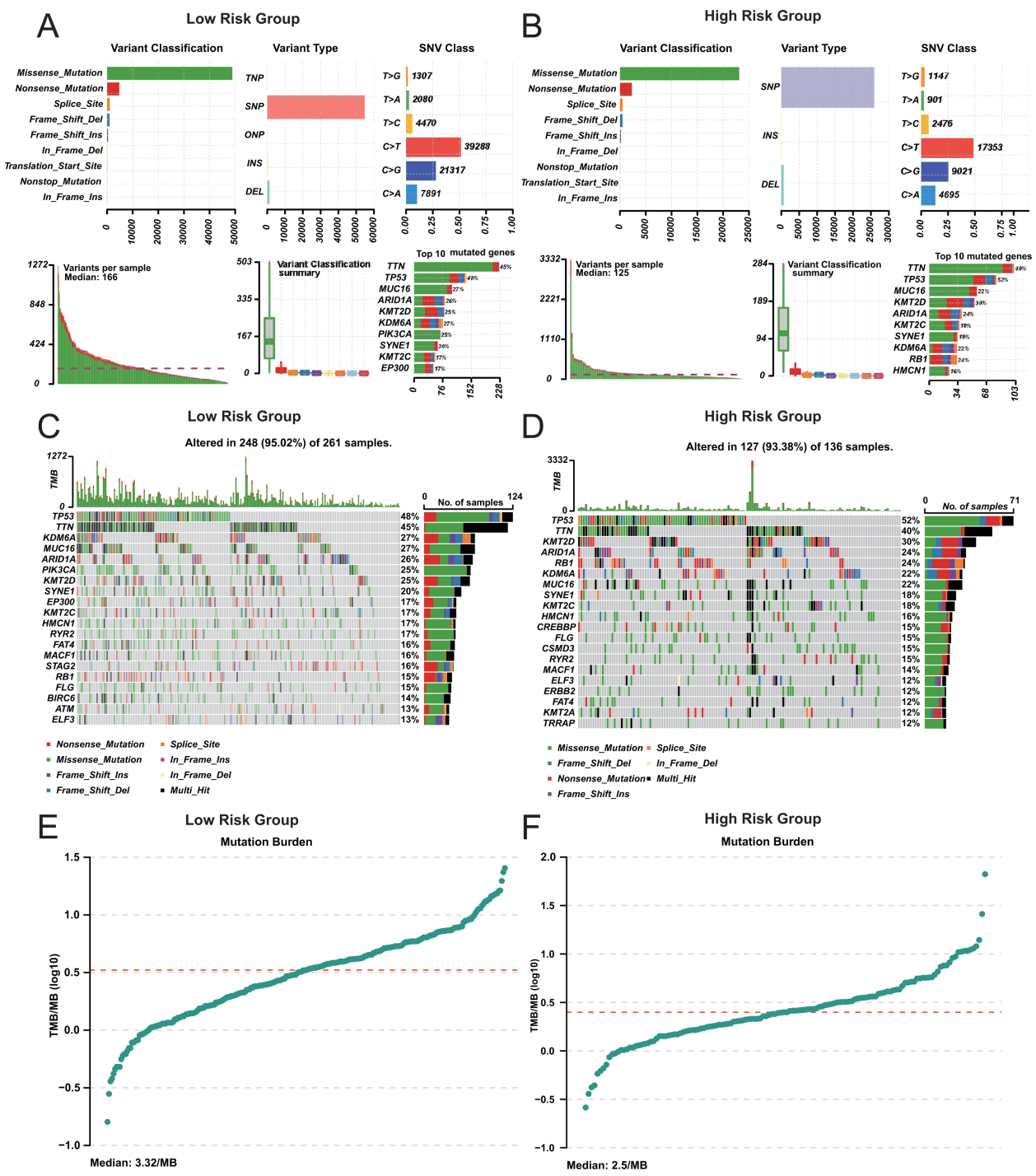

FIGURE 5
Mutation analysis in risk groups. **(A, B)** Mutation Summary in Risk Group. Variant classification and type distribution. **(C, D)** Mutation Landscape in Risk Group. **(E, F)** Tumor Mutation Burden (TMB) in Risk Group.

TIDE score in both the two groups had no significant impact on patient prognosis (Supplementary Figure S7). Additionally, no difference in the prognosis of TIL between the two groups (Figure 7F; Supplementary Figure S8), suggesting comparable levels of tumor-infiltrating lymphocytes in both groups. This finding supports our previous conclusion that the prognostic differences between the two groups may not be solely driven by immune cell infiltration.

3.8 Validating the mechanism of CDRI effect based on single cell data

To validate the conclusions proposed in our study at the cellular level, we conducted cluster analysis on single-cell RNA sequencing data from seven bladder cancer patients. Following cell annotation, the dataset was classified into six distinct cell types

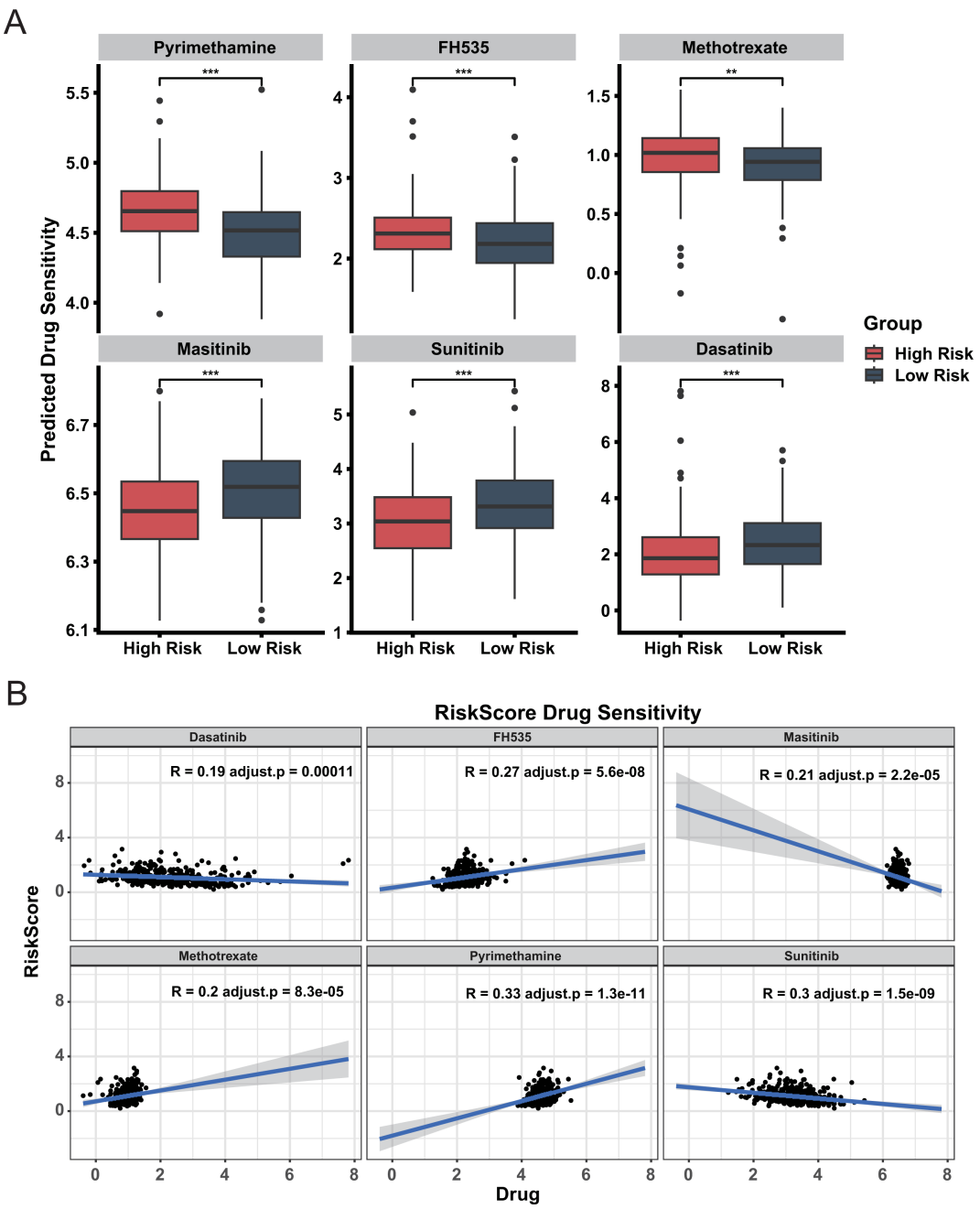

FIGURE 6
Drug sensitivity analysis in high and low risk groups. **(A)** Predicted Drug Sensitivity. Boxplots compare predicted drug sensitivity between high risk and low risk groups. Statistical significance is indicated by ** (adjust.p< 0.01) and *** (adjust.p< 0.001). **(B)** Correlation between Drug Sensitivity and Risk Score.

(Figure 8A), with epithelial cells representing the predominant population. The marker genes for each cell type were highly specific (Figure 8B). Notably, we observed that CHMP6 were highly expressed in fibroblasts and endothelial (Figure 8C), with relatively low expression in immune cells. Additionally, we found that CHMP6 expression was particularly elevated during the G1 phase, a critical phase for cell proliferation (Figure 8D). We also observed consistent trends in other data sets (Supplementary Figure S9). Further analysis indicated that the expression levels of these three genes did not significantly change during the differentiation process (Figure 8E). These results provide additional evidence for our hypothesis that the prognostic differences in the samples are primarily determined by tumor purity.

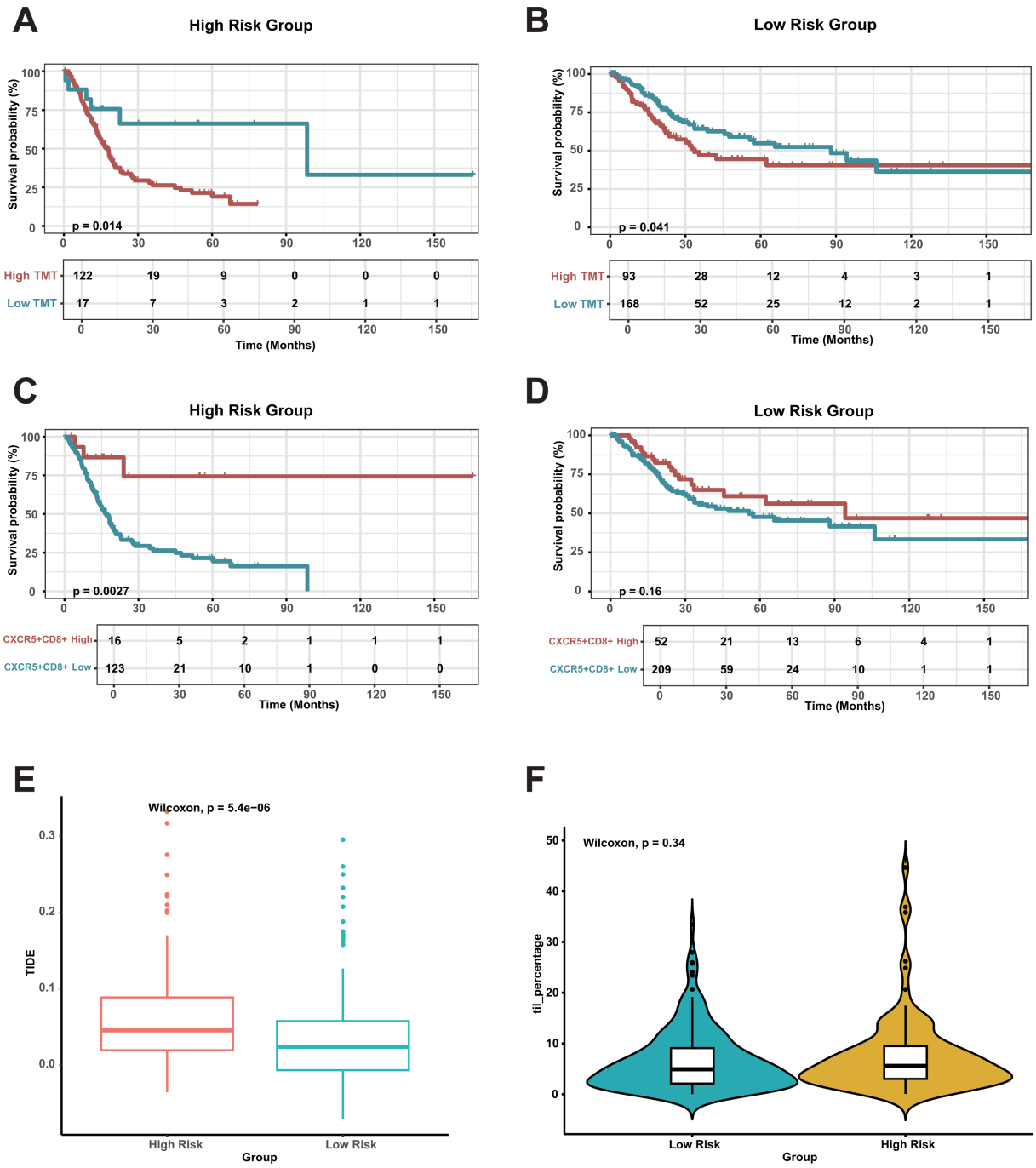

FIGURE 7
Survival analysis and immune cell impact in risk groups. **(A, B)** Overall Survival Based on Tumor Mutation Burden (TMB) in risk Group. **(C, D)** Overall Survival Based on $CXCR5^{+}CD8^{+}$ T Cells in risk Group. **(E)** Comparing TIDE scores between the risk groups. **(F)** Comparing TILs between the risk groups.

3.9 CHMP6 protein enhances BLCA cell survival and invasive migration by regulating the cell cycle

We investigated the cytoplasmic expression of CHMP6, ACSL5, and LIPT1 in 54 cases of BLCA using immunohistochemical analysis. In comparison to the corresponding noncancerous tissues, the protein levels of CHMP6 and ACSL5 were more highly expressed in cancerous tissues (Figures 9A, B) and were mainly localized in the cytoplasm and cell membranes, whereas LIPT1 was expressed at a lower level in both cancerous and paracancerous tissues (Figure 9C). In Figure 9D, we examined the expression levels of CHMP6, ACSL5,

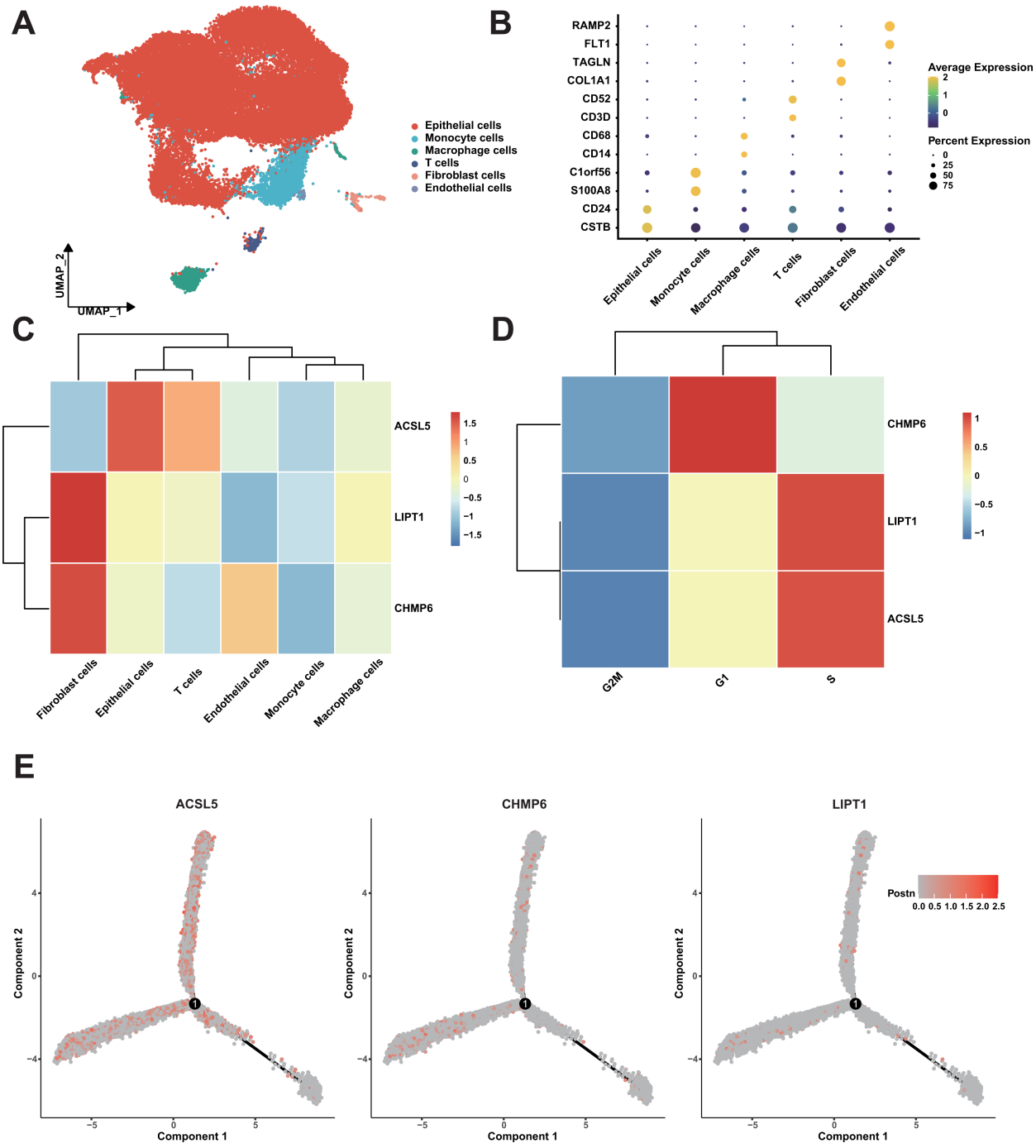

FIGURE 8
Single-Cell RNA sequencing analysis of bladder cancer samples. **(A)** UMAP Plot of cell types. **(B)** Dot plot of cell types. **(C)** Heatmap of expression of three genes in cell types. **(D)** Heatmap of expression of three genes in cell phase. **(E)** The expression distribution of three genes in the trajectory of cell differentiation.

CDK2, CHMP5, Cyclin A proteins in 5637 and T24 cell lines, in which ACSL5 protein expression was lower compared to CHMP6, which was consistent with what we observed in immunohistochemistry. We constructed CHMP6 knockdown human bladder cancer cell lines and utilized WB and Q-pcr techniques for validation at the protein level and RNA level (Figures 9D-F), and in the cell lines with CHMP6 knockdown, we found that ACSL5 protein levels were elevated. CDK2, CHMP6 and Cyclin A protein levels were weakened (Figure 9E). We selected 5637-shCHMP6#2 with higher knockdown efficiency for subsequent experiments. It was found by Annexin V/PI staining that more early apoptosis and late apoptosis were exhibited in 5637-shCHMP6#2 cells (Figure 9G). By analyzing the cell cycle with flow cytometry, we found that 5637-shCHMP6#2 cells showed significant S-phase block (Figure 9H). Through the scratch assay, We observed a

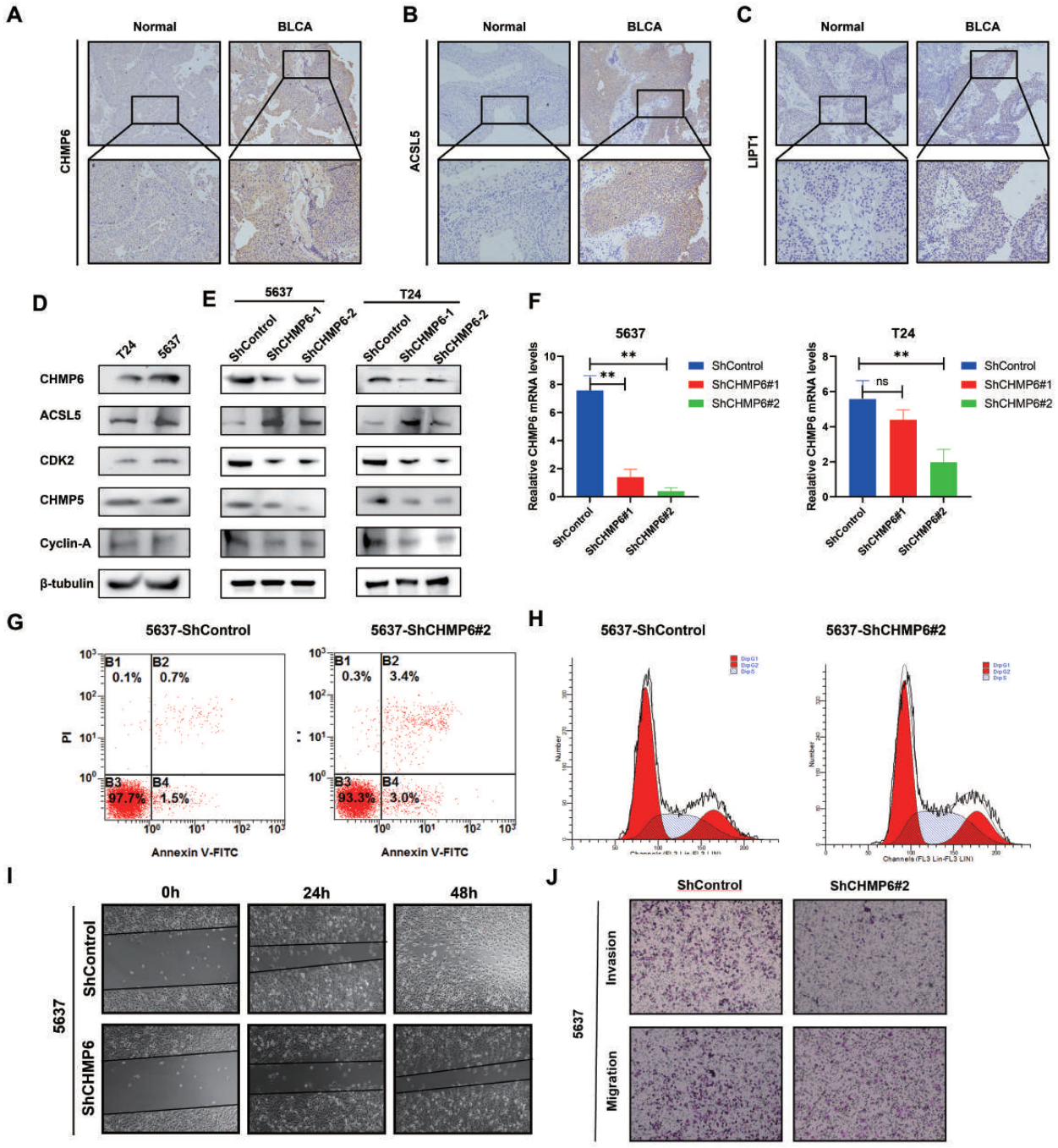

FIGURE 9
Validation of CHMP6 through *in vitro* methods. **(A-C)** Immunohistochemical Staining: Immunohistochemical analysis of CHMP6, ACSL5, and LIPT1 in BLCA tissues. **(D)** Protein Expression Levels: Expression of CHMP6 and ACSL5 proteins in 5637 and T24 cell lines. **(E)** Western Blot (WB) Analysis: Detection of CHMP6 protein knockdown in 5637 and T24 cell lines, along with ACSL5 expression. **(F)** RNA Knockdown Efficiency: Validation of CHMP6 knockdown efficiency at the RNA level in 5637 and T24 cell lines. **(G)** Apoptosis Assay: Assessment of early and late apoptosis in 5637-shControl and 5637-shCHMP6#2 cells. **(H)** Cell Cycle Analysis: Flow cytometry analysis of the cell cycle in 5637-shControl and 5637-shCHMP6#2 cells. **(I)** Migration Assay: Scratch assay to evaluate the migration ability of 5637-shControl and 5637-shCHMP6#2 cells. **(J)** Invasion and Migration Assay: Transwell assay to assess invasion and migration capabilities of 5637-shControl and 5637-shCHMP6#2 cells. ns (not significant) and ** (adjust.p < 0.01).

significant reduction in the migration ability of 5637-shCHMP6#2 cells (Figure 9I). In the Transwell assay, CHMP6 knockdown significantly decreased the cells' invasive and migratory abilities (Figure 9J).

4 Discussion

The findings of this study highlight the significant prognostic role of genes involved in programmed cell death in bladder cancer. Univariate and multivariate Cox analyses further underscore the prognostic value of cell death genes. The consistency of results across the multiple datasets enhances the study's credibility and suggests the widespread relevance of cell death-related genes across various cancer types. Immune infiltration and estimation analyses highlight the complex role of the tumor microenvironment, particularly the variations in tumor purity and stromal invasion levels. Mutation analysis suggests that a higher mutation load in the low-risk group may correlate with a more favorable prognosis. Drug sensitivity analysis may also provide practical implications for personalized treatment in clinical practice. Experimental data indicate that CHMP6 may promote the survival and invasive migration of BLCA cells by modulating the cell cycle.

Although this study offers valuable insights, several limitations must be recognized. First, the data predominantly come from public databases, such as TCGA and GEO, which may introduce sample selection bias. Furthermore, heterogeneity across datasets could affect the interpretation and generalizability of the findings. Lastly, although several prognostic genes have been identified, their underlying mechanisms and pathways warrant further investigation in future research.

Future research should consider the following directions. First, new experimental methods are needed to validate the function and mechanism of the identified genes at the single-cell level (38–40). Second, expanding the sample size, particularly to include individuals from diverse racial and geographical backgrounds, would help assess the generalizability of the findings. Exploring the transcriptional mechanism of chmp6 in paracancerous tissues and tumors will provide direction for the study of bladder cancer treatment. Additionally, integrating various data sources and analytical techniques could strengthen the reliability and broader applicability of the results. Finally, the drug sensitivity analysis in this study may serve as a valuable resource for designing clinical trials of relevant drugs, aiding in the evaluation of their potential for personalized bladder cancer treatment.

5 Conclusions

In this study, we developed a comprehensive death gene risk model (CDRI) based on cell death-related genes. Additionally, Our analysis indicates that the prognosis in cancer samples is mainly related to tumor purity. The CHMP6 protein promotes BLCA cell survival and invasive migration through modulation of the cell cycle. Our findings deepen the molecular understanding of bladder cancer and offer potential biomarkers and therapeutic targets to improve patient prognosis.

Data availability statement

The data presented in the study are deposited in the GEO repository, accession number GSE32548, GSE32894, GSE31684, GSE129845, GSE277524, GSE135337. The data presented in the study are deposited in the TCGA repository, accession number TCGA-BLCA, TCGA-UCEC, TCGA-LIHC, TCGA-MESO, TCGA-ACC.

Ethics statement

The studies involving humans were approved by Medical Ethics Committee of Tangdu Hospital, the FourthMilitary Medical University of the People's Liberation Army. The studies were conducted in accordance with the local legislation and institutional requirements. The participants provided their written informed consent to participate in this study.

Author contributions

WN: Conceptualization, Data curation, Formal analysis, Writing – original draft. CW: Conceptualization, Investigation, Writing – original draft. YY: Data curation, Formal analysis, Writing – original draft. YH: Validation, Visualization, Writing – review & editing. ZL: Supervision, Writing – review & editing. CY: Methodology, Supervision, Validation, Writing – review & editing.

Funding

The author(s) declare that no financial support was received for the research and/or publication of this article.

Acknowledgments

We thank Analysis & Testing Laboratory for Life Sciences and Medicine of Air Force Medical University for Support.

Conflict of interest

The authors declare that the research was conducted in the absence of any commercial or financial relationships that could be construed as a potential conflict of interest.

Generative AI statement

The author(s) declare that no Generative AI was used in the creation of this manuscript.

Publisher's note

All claims expressed in this article are solely those of the authors and do not necessarily represent those of their affiliated organizations, or those of the publisher, the editors and the reviewers. Any product that may be evaluated in this article, or claim that may be made by its manufacturer, is not guaranteed or endorsed by the publisher.

Supplementary material

The Supplementary Material for this article can be found online at: https://www.frontiersin.org/articles/10.3389/fonc.2025.1564826/full#supplementary-material

SUPPLEMENTARY FIGURE S1
Analysis of Differential Gene Expression and Specific Gene Expression Levels. **(A)** Intersection of Differentially Expressed Genes and Copper-Related Genes. Bar plot shows the intersection sizes of upregulated and downregulated genes with copper-related genes. The set size indicates the total number of genes in each category. **(B)** Intersection of Differentially Expressed Genes and Ferroptosis-Related Genes. **(C)** Intersection of Differentially Expressed Genes and Immunogenic Cell Death (ICD)-Related Genes. **(D)** ACSL5 Expression in Normal and Tumor Samples. Box plot shows the expression levels of ACSL5 in normal and tumor samples. Expression is measured in log2(TPM + 1). **(E)** CHMP6 Expression in Normal and Tumor Samples. **(F)** LIPT1 Expression in Normal and Tumor Samples.

SUPPLEMENTARY FIGURE S2
Performance of CDRI model in independent validation dataset. **(A)** The performance of CDRI model in GSE32548 dataset, the left figure is the survival KM curve, and the right figure is the ROC of CDRI model. **(B)** The performance of CDRI model in GSE32894 dataset, the left figure is the survival KM curve, and the right figure is the ROC of CDRI model.

SUPPLEMENTARY FIGURE S3
ROC of CDRI model in multiple datasets.

SUPPLEMENTARY FIGURE S4
Comparison of immune cell proportion estimated by various methods. **(A)** Comparison of immune cell proportion in different risk groups estimated by xCell method. **(B)** Comparison of immune cell proportion in different risk groups estimated by TIMER method. **(C)** Comparison of immune cell proportion in different risk groups estimated by EPIC method. **(D)** Comparison of immune cell proportion in different risk groups estimated by QUANTISEQ method. **(E)** Comparison of different active states of T cells.

SUPPLEMENTARY FIGURE S5
Tumor Mutation Burden Across Various Cancer Types.

SUPPLEMENTARY FIGURE S6
Treatment Response Comparison Between High and Low Risk Groups.

SUPPLEMENTARY FIGURE S7
Survival Analysis Based on Tumor Immune Dysfunction and Exclusion (TIDE) Score.

SUPPLEMENTARY FIGURE S8
Comparison of Immune Infiltration Between High and Low Risk Groups.

SUPPLEMENTARY FIGURE S9
Specific enrichment of genes in cell type and cell cycle. The left figure shows the expression of three genes in different cell types, and the right figure shows the expression of three genes in different cell cycles.

SUPPLEMENTARY TABLE S1
Three kinds of cell death related genes.

SUPPLEMENTARY TABLE S2
Different results of different groups.

SUPPLEMENTARY TABLE S3
Results of univariate Cox analysis.

SUPPLEMENTARY TABLE S4
Grouping results of samples.

SUPPLEMENTARY TABLE S5
Baseline characteristics of different group patient.

SUPPLEMENTARY TABLE S6
C_index of CDRI model on different datasets.

References

1. Antoni S, Ferlay J, Soerjomataram I, Znaor A, Jemal A, Bray F. Bladder cancer incidence and mortality: A global overview and recent trends. *Eur Urol*. (2017) 71:96–108. doi: 10.1016/j.eururo.2016.06.010

2. Ferlay J, Soerjomataram I, Ervik M, Dikshit R, Eser S, Rebelo M, et al. GLOBOCAN 2012 v1.0, cancer incidence and mortality worldwide: IARC cancer base no. 11 [Internet. *Int Agency Res Cancer Lyon*. (2014).

3. Compérat E, Amin MB, Cathomas R, Choudhury A, Santis M, Kamat A, et al. Current best practice for bladder cancer: a narrative review of diagnostics and treatments. *Lancet*. (2022) 400:1712–21. doi: 10.1016/S0140-6736(22)01188-6

4. Alifrangis C, McGovern U, Freeman A, Powles T, Linch M. Molecular and histopathology directed therapy for advanced bladder cancer. *Nat Rev Urol*. (2019) 16:465–83. doi: 10.1038/s41585-019-0208-0

5. Caffo O, Veccia A, Fellin G, Russo L, Mussari S, Galligioni E. Trimodality treatment in the conservative management of infiltrating bladder cancer: a critical review of the literature. *Crit Rev Oncol Hematol*. (2013) 86:176–90. doi: 10.1016/j.critrevonc.2012.09.011

6. Hedegaard J, Lamy P, Nordentoft I, Algaba F, Høyer S, Ulhøi BP, et al. Comprehensive transcriptional analysis of early-stage urothelial carcinoma. *Cancer Cell*. (2016) 30:27–42. doi: 10.1016/j.ccell.2016.05.004

7. van Kessel KEM, van der Keur KA, Dyrskjøt L, Algaba F, Welvaart NYC, Beukers W, et al. Molecular markers increase precision of the european association of urology non-muscle-invasive bladder cancer progression risk groups. *Clin Cancer Res*. (2018) 24:1586–93. doi: 10.1158/1078-0432.CCR-17-2719

8. Seiler R, Gibb EA, Wang NQ, Oo HZ, Lam HM, van Kessel KE, et al. Divergent biological response to neoadjuvant chemotherapy in muscle-invasive bladder cancer. *Clin Cancer Res*. (2019) 25:5082–93. doi: 10.1158/1078-0432.CCR-18-1106

9. Pentimalli F, Grelli S, Di Daniele N, Melino G, Amelio I. Cell death pathologies: targeting death pathways and the immune system for cancer therapy. *Genes Immun*. (2019) 20:539–54. doi: 10.1038/s41435-018-0052-x

10. Jiang X, Stockwell BR, Conrad M. Ferroptosis: mechanisms, biology and role in disease. *Nat Rev Mol Cell Biol*. (2021) 22:266–82. doi: 10.1038/s41580-020-00324-8

11. Bruedigam C, Porter AH, Song A, Vroeg In de Wei G, Stoll T, Straube J, et al. Imetelstat-mediated alterations in fatty acid metabolism to induce ferroptosis as a therapeutic strategy for acute myeloid leukemia. *Nat Cancer*. (2024) 5:47–65. doi: 10.1038/s43018-023-00653-5

12. Schwab A, Rao Z, Zhang J, Gollowitzer A, Siebenkäs K, Bindel N, et al. Zeb1 mediates EMT/plasticity-associated ferroptosis sensitivity in cancer cells by regulating lipogenic enzyme expression and phospholipid composition. *Nat Cell Biol*. (2024) 26:1470–81. doi: 10.1038/s41556-024-01464-1

13. Tsvetkov P, Coy S, Petrova B, Dreishpoon M, Verma A, Abdusamad M, et al. Copper induces cell death by targeting lipoylated TCA cycle proteins. *Science*. (2022) 375:1254–61. doi: 10.1126/science.abf0529

14. Wu C, Tan J, Wang X, Qin C, Long W, Pan Y, et al. Pan-cancer analyses reveal molecular and clinical characteristics of cuproptosis regulators. *Imeta*. (2022) 2(1):e68. doi: 10.1002/imt2.68

15. Bu F, Li X, Zhao Y, Bai L, Zhang S, Min L. Pan-cancer patterns of cuproptosis markers reveal biologically and clinically relevant cancer subtypes. *biomark Res*. (2023) 11:13. doi: 10.1186/s40364-022-00446-5

16. Kroemer G, Galassi C, Zitvogel L, Galluzzi L. Immunogenic cell stress and death. *Nat Immunol*. (2022) 23:487–500. doi: 10.1038/s41590-022-01132-2

17. Kang X, Zhang Y, Song J, Wang L, Li W, Qi J, et al. A photo-triggered self-accelerated nanoplatform for multifunctional image-guided combination cancer immunotherapy. *Nat Commun*. (2023) 14:5216. doi: 10.1038/s41467-023-40996-2

18. Yang Y, Gu Z, Tang J, Zhang M, Yang Y, Song H, et al. MnO(2) nanoflowers induce immunogenic cell death under nutrient deprivation: enabling an orchestrated cancer starvation-immunotherapy. *Adv Sci (Weinh)*. (2021) 8:2002667. doi: 10.1002/advs.202002667

19. Chen Y, Chen L, Lun ATL, Baldoni PL, Smyth GK. edgeR v4: powerful differential analysis of sequencing data with expanded functionality and improved support for small counts and larger datasets. *Nucleic Acids Res*. (2025) 53(2):gkaf018. doi: 10.1093/nar/gkaf018

20. Therneau TM, Grambsch PM. Modeling survival data: extending the cox model. (2000).

21. Wickham H. *ggplot2: Elegant Graphics for Data Analysis*. New York: Springer International Publishing (2016). Available online at: https://ggplot2.tidyverse.org.

22. Subramanian A, Tamayo P, Mootha VK, Mukherjee S, Ebert BL, Gillette MA, et al. Gene set enrichment analysis: a knowledge-based approach for interpreting genome-wide expression profiles. *Proc Natl Acad Sci USA*. (2005) 102(43):15545–50. doi: 10.1073/pnas.0506580102

23. Korotkevich G, Sukhov V, Budin N, Shpak B, Artyomov MN, Sergushichev A. Fast gene set enrichment analysis. *bioRxiv*. (2021) 060012. doi: 10.1101/060012

24. Wu T, Hu E, Xu S, Chen M, Guo P, Dai Z, et al. clusterProfiler 4.0: A universal enrichment tool for interpreting omics data. *Innovation (Camb)*. (2021) 2:100141. doi: 10.1016/j.xinn.2021.100141

25. Newman AM, Liu CL, Green MR, Gentles AJ, Feng W, Xu Y, et al. Robust enumeration of cell subsets from tissue expression profiles. *Nat Methods*. (2015) 12:453–7. doi: 10.1038/nmeth.3337

26. Aran D. Cell-type enrichment analysis of bulk transcriptomes using xCell. In: Boegel S, editor. *Bioinformatics for Cancer Immunotherapy: Methods and Protocols*. Springer US, New York, NY (2020). p. 263–76.

27. Li T, Fu J, Zeng Z, Cohen D, Li J, Chen Q, et al. TIMER2.0 for analysis of tumor-infiltrating immune cells. *Nucleic Acids Res*. (2020) 48(W1):W509–14. doi: 10.1093/nar/gkaa407

28. Mayakonda A, Lin DC, Assenov Y, Plass C, Koeffler HP. Maftools: efficient and comprehensive analysis of somatic variants in cancer. *Genome Res*. (2018) 28:1747–56. doi: 10.1101/gr.239244.118

29. Geeleher P, Cox N, Huang RS. pRRophetic: an R package for prediction of clinical chemotherapeutic response from tumor gene expression levels. *PloS One*. (2014) 9:e107468. doi: 10.1371/journal.pone.0107468

30. Hao Y, Stuart T, Kowalski MH, Choudhary S, Hoffman P, Hartman A, et al. Dictionary learning for integrative, multimodal and scalable single-cell analysis. *Nat Biotechnol*. (2024) 42:293–304. doi: 10.1038/s41587-023-01767-y

31. Qiu X, Mao Q, Tang Y, Wang L, Chawla R, Pliner HA, et al. Reversed graph embedding resolves complex single-cell trajectories. *Nat Methods*. (2017) 14:979–82. doi: 10.1038/nmeth.4402

32. Dai E, Meng L, Kang R, Wang X, Tang D. ESCRT-III–dependent membrane repair blocks ferroptosis. *Biochem Biophys Res Commun*. (2020) 522:415–21. doi: 10.1016/j.bbrc.2019.11.110

33. Xing P, Jiang Z, Liu Y. Construction and validation of a gene signature related to bladder urothelial carcinoma based on immune gene analysis. *BMC Cancer*. (2022) 22:926. doi: 10.1186/s12885-022-09794-9

34. Hu B, Zhao T, Li Y, Li K, Shen L, Zhu Q, et al. Identification of E3 ubiquitin ligase-based molecular subtypes and prognostic signature regarding prognosis and immune landscape in bladder cancer. *Cancer Cell Int*. (2025) 25:70. doi: 10.1186/s12935-025-03703-3

35. Ji C, Sun L-S, Xing F, Niu N, Gao H-L, Dai J-W, et al. HTRA3 is a prognostic biomarker and associated with immune infiltrates in gastric cancer. *Front Oncol*. (2020) 10. doi: 10.3389/fonc.2020.603480

36. Zhang H, Liu Y, Liu J, Chen J, Wang J, Hua H, et al. cAMP-PKA/EPAC signaling and cancer: the interplay in tumor microenvironment. *J Hematol Oncol*. (2024) 17:5. doi: 10.1186/s13045-024-01524-x

37. Valero C, Lee M, Hoen D, Wang J, Nadeem Z, Patel N, et al. The association between tumor mutational burden and prognosis is dependent on treatment context. *Nat Genet*. (2021) 53:11–5. doi: 10.1038/s41588-020-00752-4

38. Liu Y, DiStasio M, Su G, Asashima H, Enninful A, Qin X, et al. High-plex protein and whole transcriptome co-mapping at cellular resolution with spatial CITE-seq. *Nat Biotechnol*. (2023) 41:1405–9. doi: 10.1038/s41587-023-01676-0

39. Zhang D, Rubio Rodríguez-Kirby LA, Lin Y, Song M, Wang L, Wang L, et al. Spatial dynamics of mammalian brain development and neuroinflammation by multimodal tri-omics mapping. *bioRxiv*. (2024). doi: 10.1101/2024.07.28.605493

40. Baysoy A, Tian X, Zhang F, Renauer P, Bai Z, Shi H, et al. Spatially Resolved *in vivo* CRISPR Screen Sequencing via Perturb-DBiT. *bioRxiv*. (2024). doi: 10.1101/2024.11.18.624106

Frontiers in Immunology

Explores novel approaches and diagnoses to treat immune disorders.

The official journal of the International Union of Immunological Societies (IUIS) and the most cited in its field, leading the way for research across basic, translational and clinical immunology.

Discover the latest Research Topics

See more →

Frontiers

Avenue du Tribunal-Fédéral 34
1005 Lausanne, Switzerland
frontiersin.org

Contact us

+41 (0)21 510 17 00
frontiersin.org/about/contact